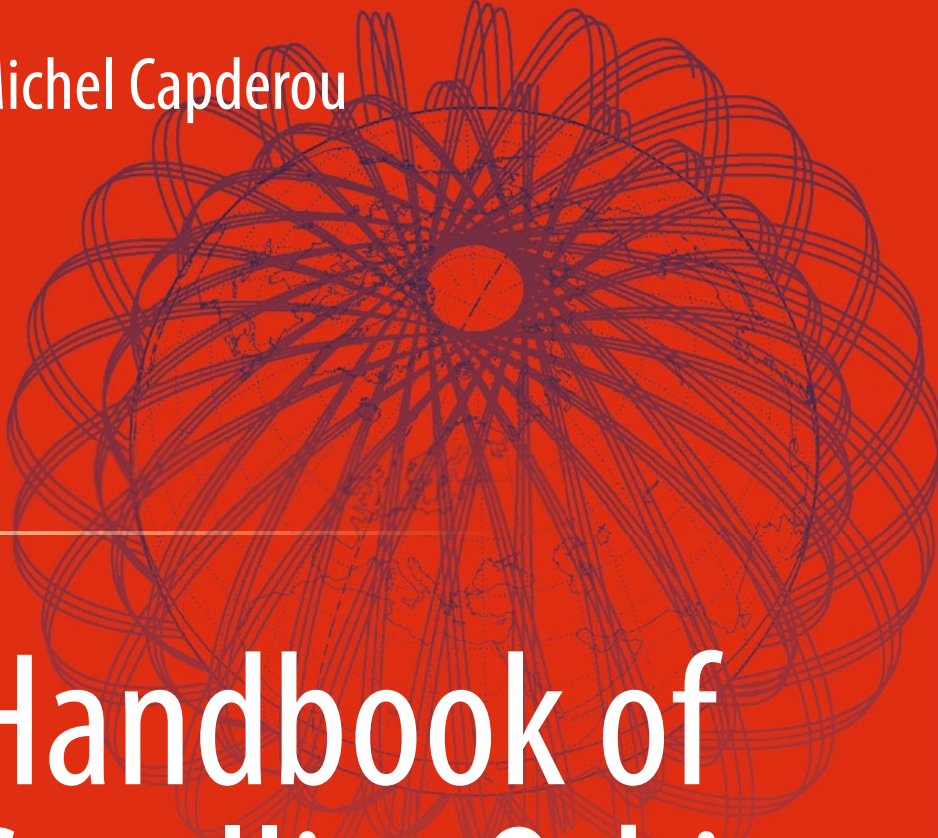


Michel Capderou



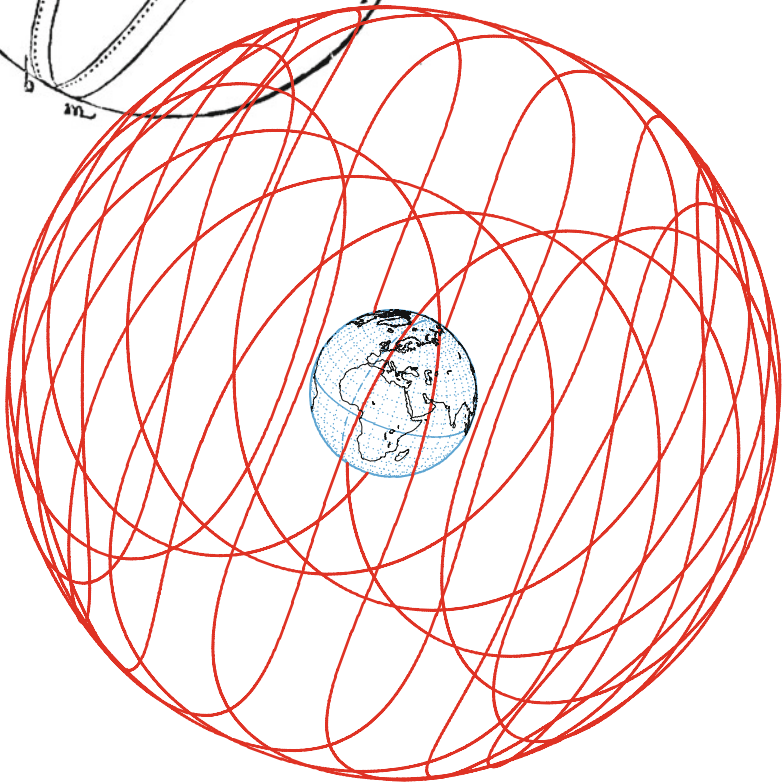
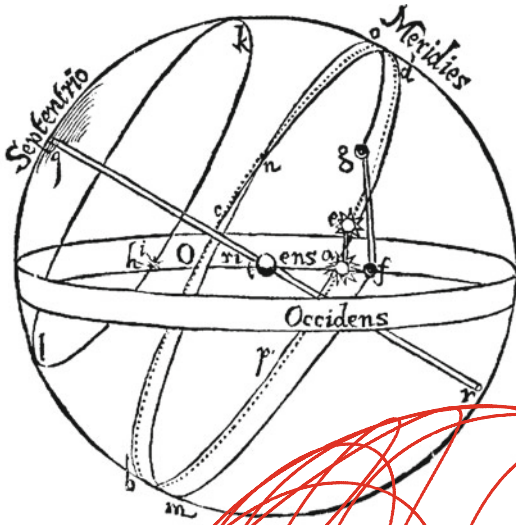
# Handbook of Satellite Orbits

From Kepler to GPS

 Springer

# Handbook of Satellite Orbits





From Kepler to GPS

Michel Capderou

# Handbook of Satellite Orbits

From Kepler to GPS

Translated by Stephen Lyle

Foreword by Charles Elachi, Director, NASA Jet Propulsion  
Laboratory, California Institute of Technology,  
Pasadena, California, USA

 Springer

Michel Capderou  
Université Pierre et Marie Curie  
Paris, France

ISBN 978-3-319-03415-7      ISBN 978-3-319-03416-4 (eBook)  
DOI 10.1007/978-3-319-03416-4  
Springer Cham Heidelberg New York Dordrecht London

Library of Congress Control Number: 2014930341

© Springer International Publishing Switzerland 2014

This work is subject to copyright. All rights are reserved by the Publisher, whether the whole or part of the material is concerned, specifically the rights of translation, reprinting, reuse of illustrations, recitation, broadcasting, reproduction on microfilms or in any other physical way, and transmission or information storage and retrieval, electronic adaptation, computer software, or by similar or dissimilar methodology now known or hereafter developed. Exempted from this legal reservation are brief excerpts in connection with reviews or scholarly analysis or material supplied specifically for the purpose of being entered and executed on a computer system, for exclusive use by the purchaser of the work. Duplication of this publication or parts thereof is permitted only under the provisions of the Copyright Law of the Publisher's location, in its current version, and permission for use must always be obtained from Springer. Permissions for use may be obtained through RightsLink at the Copyright Clearance Center. Violations are liable to prosecution under the respective Copyright Law.

The use of general descriptive names, registered names, trademarks, service marks, etc. in this publication does not imply, even in the absence of a specific statement, that such names are exempt from the relevant protective laws and regulations and therefore free for general use.

While the advice and information in this book are believed to be true and accurate at the date of publication, neither the authors nor the editors nor the publisher can accept any legal responsibility for any errors or omissions that may be made. The publisher makes no warranty, express or implied, with respect to the material contained herein.

Printed on acid-free paper

Springer is part of Springer Science+Business Media ([www.springer.com](http://www.springer.com))

# Foreword

Since the dawn of the space age with the launch of Sputnik 1 and Explorer 1, orbital mechanics became a major discipline in space exploration. This book reflects many years of research and teaching in this field by Michel Capderou. It is a comprehensive and modern treatment of the theory of orbital mechanics, its application, and current day samples of how it is used in the field. In that sense, it is not just a textbook for classroom-style lectures; it is truly a handbook for practitioners.

It is full of fascinating historical information and references that intrigue the readers to follow the anecdotes and details on how this particular discipline evolved from the collective genius of giants in mathematics, physics and astronomy such as Tycho Brahe, Kepler, Newton, Galileo, Lagrange, Laplace, Gauss, Poincaré and Einstein. This story telling not only makes reading interesting but also challenges the readers to understand the fundamentals used by these giants before the advent of computers.

Most classroom-style textbook would skip intermediate steps in the derivation of equations or refer the readers to the original papers or textbooks. This book provides sufficient intermediate steps so readers with basic freshman mathematics can follow the logical steps. Its treatment of geodesy, geopotential and perturbation methods connects theory to physical measurements and observables. The chapter on Orbit and Mission is unique in that it provides a comprehensive survey of how theory is applied to real-life missions. It connects this discipline to science and inspires the reader to appreciate how a satellite orbit provides a special vantage point for conducting scientific measurements. Orbital mechanics is not just about getting into space, but it is integral to the measurement technique such as altimetry, radar topography, radio occultation, interferometry and gravity field through radiometric observables. The comprehensive treatment on designing an orbit for systematic ground track control and target point visibility is unique. In the past, practitioners had to conduct a literature search and examine multiple publications. Its treatment on GPS begs the reader to further explore the world of precision orbit determination, timing and terrestrial reference frame. The book is sprinkled with stories of much innovative use of “tricks” in orbital mechanics such as frozen orbit, sun-synchronicity, aerobraking, libration point and Lissajous orbits, and gravity assist that enables missions like Voyager Grand Tour, Galileo, Cassini-

Huygens and tours of their satellites. This book has superb illustrations and graphics enhanced by colorful photographs.

Since the flight of Explorer 1, JPL prides itself in pioneering techniques in orbital mechanics and its applications to carry out NASA's mission in space-borne observation of our Earth; in fly-by, orbiting and landing of planetary bodies and their satellites; in astronomical telescopes that can observe our galaxy and the early Universe. We continue to recruit the best and the brightest graduates in this discipline from universities around the world, who understand not only the physics and mathematics of orbital mechanics but also its applications of real-life missions. The *Handbook of Satellite Orbits: From Kepler to GPS* is exactly what is needed for all graduates of this discipline.

Michel Capderou's book is an essential treatise in orbital mechanics for all students, lecturers and practitioners in this field, as well as other aerospace systems engineers.

Charles Elachi

*Director*

NASA Jet Propulsion Laboratory

California Institute of Technology

Pasadena, CA, USA

# Preface

Of all the fields of modern science and technology, space exploration is the one that most clearly displays the following fundamental contrast: on the one hand, its theoretical basis is underpinned by long-established, historically tested and almost immutable, one might even say timeless, principles; on the other, the whole field of space science is undergoing meteoric technological evolution, with exponential growth, bringing with it a broad mix of commercial, political and ideological considerations. And so we have come from Kepler to GPS.

Regarding the “immutable foundations”, we know that the notion of geopotential or the solution of Lagrange’s equations is no easy matter. We just hope that, with teaching experience among the ingredients, we have succeeded in presenting these issues in a sufficiently clear and interesting way. To illustrate unbridled technological progress, we supply a wealth of examples.

The book falls into six main parts:

- The first part, consisting of Chaps. 1–3, is devoted to geodesy. We begin with the ellipse and its geometrical properties and work our way to the Earth’s gravitational potential and the geoid.
- The second part, Chaps. 4–8, focuses on the motion of the satellite, working from the ideal, Keplerian case to the real, perturbed case.
- The third part, Chaps. 9–11, takes us into the actual running and functioning of satellites, discussing their missions and the ways that orbits are designed to fulfil those missions. We consider some novel issues, such as the constant of Sun-synchronicity  $k_h$  and, for recurrent satellites, the constant  $\kappa$  and the index  $\Phi$ . Abundant illustrations are provided, always relating to past, present or future space programmes.

- The fourth part, Chaps. 12 and 13, considers the instruments carried aboard the satellite from a geometrical point of view. We begin with the different ways of observing the Earth from a satellite, then move on to sampling, i.e. the conditions under which a given point on the Earth can view the satellite, considering the viewing angle and frequency of visibility.
- We then devote the whole of Chap. 14 to GPS. This navigation system, entirely satellite-based, appeals to almost all branches of modern physics.
- In the final part, Chaps. 15 and 16, we leave the confines of our own planet to apply all these theories first to Mars, then to the other planets of the Solar System, and even to the natural satellites of those planets, around which artificial satellites may gravitate.

★

The orbit and sampling software *Ixion* forms the backbone of this book. We first developed it as a teaching tool for an M.Sc. in climatology and space observation, and also in the research context, as an aid to understanding issues of orbital elements, satellite–pixel–Sun configuration, and so on, which arise when processing the data transmitted to us by our satellites. But once the accuracy of *Ixion* had been proven in the context of real data, by the confrontation with pixels, one might say, we extended it to all types of orbit and included some didactic features that would make it accessible and useful to a broader audience.

The software *Ixion* has since been used for preliminary studies of orbital strategy, as it is known, which serve to match orbital elements in the best possible way to the physical phenomena we need to observe. Among the orbits studied in this context, we cite the French–Indian satellite Megha-Tropiques and the planned Mars missions Premier-07 and MEMO. *Ixion* is often used by our colleagues for calibration and validation campaigns in the field, as for the satellites Calipso, MetOp-A and -B, Megha-Tropiques, and others.

*Ixion/Web* is the part of *Ixion* that is now accessible online. Our mapping software *Atlas* has been coupled with *Ixion* to produce graphical representations of orbits and their ground tracks. We hope the maps it produces will be pleasant and useful to the reader. They should provide a refreshing change to the deeply saddening lack of cartographic imagination and the striking flatness of the projections generally used in this field.

We have selected many examples among experiments that are familiar to us, such as the CERES and ScaRaB instruments and the Megha-Tropiques satellite. They may appear to be over-represented in the book, but perhaps it is better to stick to the things we know best!

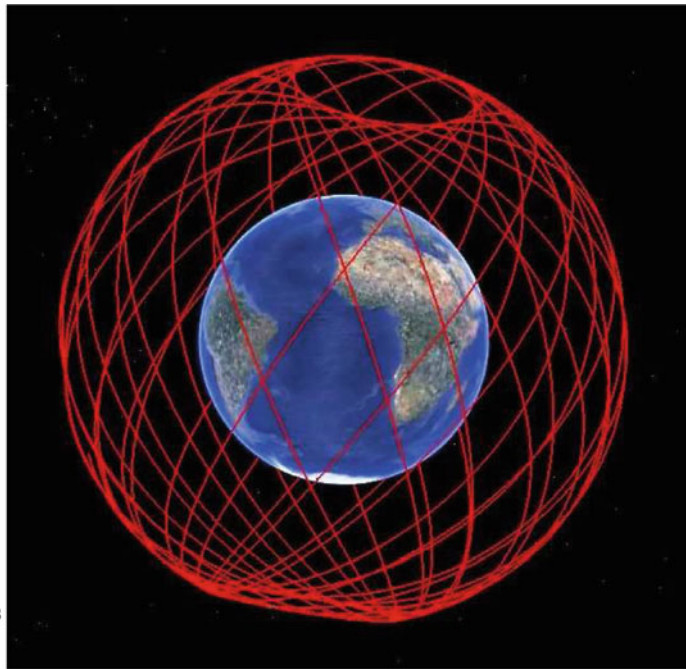
Because this book focuses on space mechanics and the geometry of observation, with all its concomitants, such as spatiotemporal sampling, there is no consideration at all of the satellite as a technological object. There is not one word about the launch vehicles or the functioning of the onboard instruments, apart from the geometric aspect of the swath in the latter case, since this is directly relevant to our purpose.



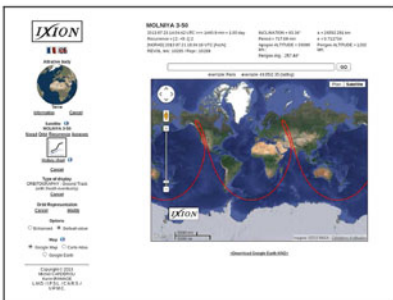
By concentrating in this way on the orbits, we have made every effort to prove or at least explain all the formulas used. This may look somewhat austere, so we have tried to brighten things up with plenty of examples and illustrations. The examples will show the reader some rather unexpected orbits, while the photographs will demonstrate the level of accuracy achieved today in images acquired by satellite-borne instruments.

To liven up the whole discussion, we have also included many references to historical aspects, even presenting several pages of the books that founded celestial mechanics and discussing some of those early results which leave us in admiration. And so we have come from Kepler to GPS.

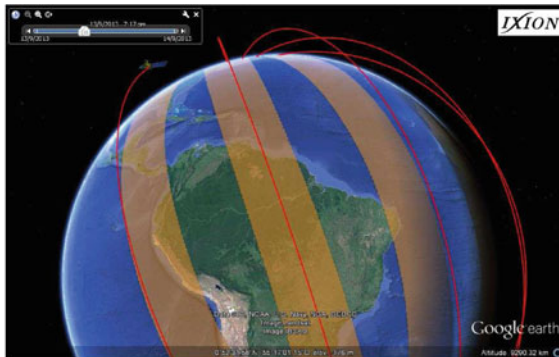
With that, let me wish you a good trip into space . . . and into time.



© 2013 Google  
 © 2013 Tele Atlas



Screen captures. *Ixion/*Web, the online *Ixion* software



Screen captures. *Ixion/WeB*, the online *Ixion* software (continued)

## Acknowledgements

This work was accomplished in the context of my teaching at the University of Pierre and Marie Curie (UPMC, Paris) and my research at the *Laboratoire de météorologie dynamique* (LMD), whose director, Vincent Cassé, I would like to thank. The LMD is a research unit depending on the *Centre national de la recherche scientifique* (CNRS) and four institutes of higher education, namely, the UPMC, the *Ecole Polytechnique*, the *Ecole normale supérieure* (ENS) and the *Ecole nationale des Ponts et chaussées* (ENPC).

I am particularly grateful to Jacques Lefrère, François Forget and Florent Deleflie for their comments and criticisms during the preparation of this book. Their advice was invaluable and I extend my warmest gratitude to them. I would also like to thank Rémy Roca, Olivier Chomette, Patrick Raberanto and the whole team at Megha-Tropiques, as well as Karim Ramage, webmaster for *Ixion/WeB*, my colleagues at the university and the CNRS, François Barlier, Pierre Briole, Nicole Capitaine, Xavier Collilieux, Michel Desbois, Albert Hertzog, Robert Kandel, Richard Kerner, Richard Marchand, Patrick Rocher, Jérôme Sirven and Aymeric Spiga.

I am grateful for the trust shown to me by the publisher Springer, and in particular by Nathalie Huilleret in Paris and Harry Blom and Jennifer Satten in New York.

And last but not least, my thanks to Stephen Lyle who translated this book: *bravo et merci!*

Palaiseau, France

Michel Capderou

## Ἰξίων

The figure from Greek mythology known as Ixion was not, if the truth be told, a particularly savoury one. The King of the Lapiths, he behaved in a decidedly reprehensible manner on the day of his wedding, causing his future father-in-law to fall into a burning pit so that he would not have to pay the dowry.

This act was considered the ultimate crime, for it broke all the rules of hospitality, and indeed, it was reproved by all the gods but one. The only deity who would agree to purify Ixion for the murder was Zeus, a connoisseur when it came to perjury and other misdemeanours. Zeus even felt some compassion for this strong-minded king, inviting him to Olympus and offering him hospitality. As an exceptional sign of friendship, he bade him drink ambrosia, which made him immortal.

Ixion admired Zeus' antics and escapades and, encouraged by the atmosphere of familiarity in the Olympian realm, began to covet Zeus' own wife Hera. But this was where he overstepped the mark! The king of the gods cried out: "A little respect for one's host!" As a punishment, he bound him to a fiery wheel which whirled him forever through the skies.

As he had been made immortal, the poor fellow must still be spinning around up there. One may thus consider Ixion as the first of all artificial satellites, and this is therefore the name we have chosen for our software.



*Ixion* is the orbitography and sampling software that forms the basis for this book. Since 2010, many of the features of this software have been put online in collaboration with Karim Ramage at the Institut Pierre-Simon Laplace (IPSL). This software *Ixion/Web* is perfectly operational. The orbital elements of the satellites are updated daily (NORAD data) and the calculation of the satellite trajectory is thus fully accurate. For past dates, the automatically archived NORAD data are used.

The ground track of the satellite and instrumental swath are indicated on Google Maps, providing much detail and easy consultation. Graphic representations can also be obtained on standard maps, with a choice of over a hundred cartographic projections using the software *Atlas*. Another option is 3D visualisation of the orbit with Google Earth.

At a given location, sampling tables indicate the times (day and time) of satellite overpasses for the whole month, specifying conditions of viewing such as sight angle and solar configuration. Statistical tables provide global data for the whole Earth.

*Ixion/Web* also gives orbits and sampling for the planet Mars. Satellite ground tracks are represented on Google Map Mars or conventional maps. Ground tracks of satellites orbiting other planets (Venus, Mercury, etc.) or the Moon can also be represented.

Apart from being fully operational, *Ixion/Web* has a clear pedagogical interest as an aid to understanding satellite motion in different frames, i.e. Galilean or moving with the Earth. We give here four examples of graphical representations: a 3D representation of the orbit of the satellite LAGEOS-1, a close-up of the orbital ground track of Jason-2, an orbital ground track of Molniya-3-50 and an orbital ground track of Terra with swath.

<http://climserv.ipsl.polytechnique.fr/ixion.html>

# Contents

<b>1</b>	<b>Geometry of the Ellipse</b> .....	1
1.1	Definition and Properties .....	1
1.1.1	Conic Sections .....	1
1.1.2	Definition and Properties of the Ellipse .....	2
1.1.3	Applications of the Definition .....	3
1.1.4	Demonstrating the Main Properties .....	7
1.1.5	Eccentricity and Flattening .....	13
1.2	Applications and Other Characteristics .....	17
1.2.1	Arc Length of an Ellipse .....	17
1.2.2	Radius of an Ellipse .....	19
1.2.3	Radius of Curvature of an Ellipse .....	20
<b>2</b>	<b>Geodesy</b> .....	25
2.1	Earth Ellipsoid .....	25
2.1.1	Different Definitions of Latitude .....	25
2.1.2	Cartesian Coordinates: Great Normal .....	31
2.1.3	Radius of Curvature .....	32
2.1.4	Radius of the Ellipse .....	32
2.1.5	Degrees of Latitude and Longitude .....	33
2.1.6	Meridian Arc Length .....	35
2.2	Altitude Relative to the Ellipsoid .....	37
2.2.1	Definition of Geodetic Altitude and Nadir .....	37
2.2.2	Latitude Related to Geodetic Altitude .....	37
2.2.3	Determining the Geodetic Altitude and Nadir .....	39
2.3	A Little History .....	42
2.3.1	Before the Enlightenment .....	42
2.3.2	A French Affair .....	44
2.3.3	Dynamical Geodesy .....	51
<b>3</b>	<b>Geopotential</b> .....	53
3.1	Some Preliminaries .....	53
3.1.1	Reference Systems .....	53
3.1.2	Review of Work and Potential .....	54

3.2	Gravitational Potential and Field . . . . .	56
3.2.1	Gravity . . . . .	56
3.2.2	Gauss' Theorem . . . . .	57
3.2.3	Gravity and Weight . . . . .	60
3.3	Calculating the Geopotential . . . . .	61
3.3.1	Potential Element . . . . .	61
3.3.2	Obtaining the Potential by Integration . . . . .	62
3.3.3	Spherical Harmonics . . . . .	64
3.3.4	Second Degree Expansion of the Potential . . . . .	65
3.3.5	Expanding the Potential to Higher Degrees . . . . .	68
3.4	Weight Field and Potential for the Ellipsoid . . . . .	71
3.4.1	Calculating the Field and Potential . . . . .	71
3.4.2	Weight Field at the Earth's Surface . . . . .	73
3.4.3	Clairaut's Formula . . . . .	75
3.4.4	Somigliana's Formula . . . . .	78
3.5	Geoid . . . . .	79
3.5.1	Gravity Anomalies . . . . .	79
3.5.2	Satellites and Geodesy . . . . .	79
3.5.3	Development of Geopotential Models . . . . .	83
3.5.4	Evaluation of the Geocentric Gravitational Constant . . . . .	87
3.6	Appendix: Terrestrial Reference Systems . . . . .	88
3.6.1	Celestial Reference System . . . . .	88
3.6.2	Terrestrial Reference System . . . . .	89
3.7	Appendix: Summary of Legendre Functions . . . . .	92
<b>4</b>	<b>Keplerian Motion . . . . .</b>	<b>95</b>
4.1	Central Acceleration . . . . .	95
4.1.1	General Acceleration . . . . .	95
4.1.2	Properties of Central Acceleration . . . . .	96
4.1.3	Motion with Central Acceleration . . . . .	97
4.2	Newtonian Acceleration . . . . .	99
4.2.1	Equation for the Trajectory . . . . .	99
4.2.2	Types of Trajectory . . . . .	100
4.3	Trajectory and Period for Keplerian Motion . . . . .	102
4.3.1	Definition of Keplerian Motion . . . . .	102
4.3.2	Periodic Trajectories . . . . .	102
4.3.3	Period and Mean Motion . . . . .	106
4.3.4	Relation Between Position and Time . . . . .	107
4.4	Time as a Function of Position: The Three Anomalies . . . . .	107
4.4.1	Expression for the Time and the Mean Anomaly $M$ . . . . .	108
4.4.2	Expression $t = t(\theta)$ and the True Anomaly $v$ . . . . .	108
4.4.3	Expression $t = t(r)$ and the Eccentric Anomaly $E$ . . . . .	110
4.4.4	Relating the Anomalies . . . . .	112

4.5	Position as a Function of Time: Kepler’s Problem . . . . .	115
4.5.1	Methods for Solving Kepler’s Problem . . . . .	115
4.5.2	Solution by Numerical Iteration . . . . .	115
4.5.3	Other Methods of Solution . . . . .	120
4.6	Representation of Anomalies . . . . .	122
4.6.1	Representation of Anomalies $v(M)$ and $E(M)$ . . . . .	122
4.6.2	Equation of Center . . . . .	124
4.6.3	Summary of Anomalies . . . . .	127
4.7	First Integrals of the Motion . . . . .	136
4.7.1	Conservation Laws . . . . .	136
4.7.2	Note on Energy . . . . .	139
4.8	Historical Note on Universal Attraction . . . . .	141
4.8.1	Kepler’s Laws . . . . .	141
4.8.2	Newton and the Law of Universal Attraction . . . . .	145
<b>5</b>	<b>Satellite in Keplerian Orbit . . . . .</b>	<b>149</b>
5.1	Two-Body Problem . . . . .	149
5.2	Orbital Elements . . . . .	151
5.2.1	Specifying the Satellite Orbit in Space . . . . .	151
5.2.2	Keplerian Elements . . . . .	154
5.2.3	Adapted Orbital Elements . . . . .	154
5.3	Keplerian Period . . . . .	156
5.4	Appendix: Rotation of a Solid—Euler and Cardan Angles . . . . .	159
<b>6</b>	<b>Satellite in Real (Perturbed) Orbit . . . . .</b>	<b>163</b>
6.1	Perturbing Forces . . . . .	163
6.1.1	From Ideal to Real Orbits . . . . .	163
6.1.2	Order of Magnitude of Perturbing Forces . . . . .	164
6.1.3	Potential . . . . .	164
6.1.4	Perturbations and Altitude of a Satellite . . . . .	165
6.2	Perturbative Methods: Presentation . . . . .	171
6.2.1	Orbit Propagation: Numerical and Analytical Methods . . . . .	171
6.2.2	Basic Principles . . . . .	174
6.2.3	Lagrange Brackets . . . . .	176
6.2.4	Properties of the Lagrange Bracket . . . . .	178
6.3	Perturbative Method: Solution . . . . .	179
6.3.1	Calculating the Coordinates . . . . .	179
6.3.2	Calculating the Lagrange Brackets . . . . .	182
6.3.3	Lagrange Equations . . . . .	183
6.3.4	Metric and Angular Orbital Elements . . . . .	186
6.3.5	Poorly Defined Parameters . . . . .	187
6.3.6	Delaunay Elements . . . . .	187



6.4	Perturbative Method: Results for the Geopotential up to $J_2$ . . . . .	189
6.4.1	Expression for the Perturbative Potential up to $J_2$ . . . . .	189
6.4.2	Variation of the Orbital Elements . . . . .	192
6.5	Perturbative Method: Results for General Case . . . . .	195
6.5.1	Geopotential up to $J_n$ . . . . .	195
6.5.2	Full Geopotential . . . . .	201
6.5.3	Other Forces Deriving from a Potential . . . . .	202
6.5.4	Perturbative Forces not Derived from a Potential . . . . .	202
6.5.5	Different Definitions of the Period . . . . .	203
6.6	Appendix: Atmospheric Drag . . . . .	204
6.6.1	Description of the Earth's Atmosphere . . . . .	204
6.6.2	Density of the Atmosphere . . . . .	205
6.6.3	Models of the Atmosphere . . . . .	206
6.6.4	Calculation of Atmospheric Drag: The Notion of $\Delta V$ . . . . .	207
6.6.5	Effect of Drag on the Orbit . . . . .	210
6.6.6	Simplified Calculations for an Eccentric Orbit: Air Braking . . . . .	210
6.7	Historical Note: First Determinations of the Harmonics $J_n$ . . . . .	213
6.7.1	First Satellite Determination of $J_2$ . . . . .	213
6.7.2	First Satellite Determination of $J_3$ . . . . .	214
6.7.3	First Determinations of $J_n$ up to $J_{14}$ . . . . .	215
6.8	Historical Note: Success in Calculating Perturbations . . . . .	215
6.8.1	The Delayed Return of Halley's Comet . . . . .	215
6.8.2	The Discovery of Neptune by Le Verrier . . . . .	216
6.8.3	Advance of the Perihelion of Mercury . . . . .	217
6.9	Astronomical Note: Perturbations and the Solar System . . . . .	220
6.9.1	Stability of the Solar System . . . . .	220
6.9.2	Precession of the Equinoxes . . . . .	223
6.9.3	The Earth as a Satellite . . . . .	224
6.10	Appendix: Astronomical Constants . . . . .	227
6.10.1	Systems of Units . . . . .	227
6.10.2	Astronomical Constants . . . . .	228
6.10.3	Time Scales . . . . .	228
6.11	Appendix: Gravitational Sphere of Influence . . . . .	231
6.11.1	Attraction of the Sun and Earth . . . . .	231
6.11.2	Determining the Sphere of Influence . . . . .	233
6.12	Appendix: Lagrange Points . . . . .	234
6.12.1	Restricted Three-Body Problem . . . . .	234
6.12.2	Simplified Study of Points $L_1$ and $L_2$ . . . . .	234
6.12.3	Lagrange Points and Sphere of Influence . . . . .	236
6.12.4	The Five Lagrange Points . . . . .	237
6.12.5	Lagrange Points in Astronomy . . . . .	238
6.12.6	Artificial Satellites at Lagrange Points . . . . .	239

6.13	Appendix: Spherical Trigonometry . . . . .	241
6.13.1	Gauss' Relations . . . . .	241
6.13.2	Fifteen Relations for the Spherical Triangle . . . . .	243
<b>7</b>	<b>Motion of Orbit, Earth and Sun . . . . .</b>	<b>245</b>
7.1	Motion of the Orbit . . . . .	245
7.1.1	Secular Variations: Simplified Case . . . . .	245
7.1.2	Secular Variations up to Degree 4 . . . . .	250
7.1.3	Secular Variations up to Degree $n$ . . . . .	252
7.1.4	Removing Precessional Motion . . . . .	252
7.1.5	Effective Calculation of Period and Altitude . . . . .	256
7.2	Motion of the Earth . . . . .	259
7.2.1	Motion of the Earth About the Sun . . . . .	260
7.2.2	Motion of the Earth About the Polar Axis . . . . .	261
7.2.3	Motion of the Poles . . . . .	263
7.2.4	Motion of the Orbit and Earth . . . . .	264
7.3	Apparent Motion of the Sun . . . . .	266
7.3.1	Celestial Sphere and Coordinates . . . . .	266
7.3.2	Hour Angle . . . . .	267
7.3.3	Equation of Time . . . . .	267
7.3.4	Solar Time . . . . .	272
7.3.5	Declination . . . . .	273
7.3.6	Julian Day, Julian Date . . . . .	274
7.4	Geosynchronicity . . . . .	276
7.4.1	Definition . . . . .	276
7.4.2	Calculating the Orbit . . . . .	277
7.4.3	Geostationary Satellites . . . . .	278
7.4.4	Drift of the Geostationary Orbit . . . . .	280
7.4.5	Stationkeeping . . . . .	282
7.4.6	Geosynchronous Satellites with Highly Eccentric Orbits . . . . .	289
7.5	Sun-Synchronicity . . . . .	291
7.5.1	Definition . . . . .	291
7.5.2	Constant of Sun-Synchronicity . . . . .	291
7.5.3	Calculating the Orbit: Circular Case . . . . .	292
7.5.4	Calculating the Orbit: Elliptical Case . . . . .	296
7.5.5	Sun-Synchronous Satellites . . . . .	298
7.5.6	Orbit Maintenance . . . . .	299
<b>8</b>	<b>Ground Track of a Satellite . . . . .</b>	<b>301</b>
8.1	Position of Satellite on Its Orbit . . . . .	301
8.1.1	Using Euler Angles to Describe Satellite Motion . . . . .	301
8.1.2	Position of Satellite in Cartesian Coordinates . . . . .	304
8.1.3	Position of Satellite in Spherical Coordinates . . . . .	305

8.2	Ground Track of Satellite . . . . .	305
8.2.1	Equation for Ground Track . . . . .	305
8.2.2	Maximum Attained Latitude . . . . .	306
8.3	Ground Track of Satellite in Circular Orbit . . . . .	307
8.3.1	Equation for Satellite Ground Track . . . . .	308
8.3.2	Equatorial Shift . . . . .	308
8.3.3	Apparent Inclination . . . . .	310
8.3.4	Angle Between Ground Track and a Meridian . . . . .	316
8.3.5	Velocity of a Satellite and Its Ground Track . . . . .	317
8.3.6	Eliminating Time from the Ground Track Equation . . . . .	320
8.4	Appendix: NORAD Orbital Elements . . . . .	322
8.4.1	NORAD: The Organisation . . . . .	322
8.4.2	Two-Line Element (TLE) Set Format . . . . .	323
8.4.3	Decoding the TLE . . . . .	323
8.4.4	Conditions of Use . . . . .	327
8.5	Appendix: Cartographic Projections . . . . .	329
8.5.1	Definitions and Properties . . . . .	329
8.5.2	Classifying Projections by Type or Aspect . . . . .	330
8.5.3	Description of Three Projections . . . . .	331
<b>9</b>	<b>Orbit and Mission . . . . .</b>	<b>339</b>
9.1	Classifying Orbit Types . . . . .	339
9.2	Classifying Satellites by Mission . . . . .	340
9.2.1	The First Satellites . . . . .	341
9.2.2	Satellites for Geodesy . . . . .	344
9.2.3	Earth Environment Satellites . . . . .	348
9.2.4	Satellites for Meteorology and Climate Study . . . . .	357
9.2.5	Satellites for Remote-Sensing and Surveillance . . . . .	384
9.2.6	Oceanographic Satellites . . . . .	388
9.2.7	Navigation Satellites . . . . .	390
9.2.8	Communications Satellites . . . . .	391
9.2.9	Satellites for Astronomy and Astrophysics . . . . .	408
9.2.10	Satellites for Fundamental Physics . . . . .	421
9.2.11	Technological Satellites . . . . .	424
9.2.12	Satellites with Specific Military Missions . . . . .	425
9.2.13	Manned Satellites . . . . .	428
9.2.14	Non-Scientific Satellites . . . . .	429
9.3	Appendix: Delays in Scheduling Space Missions . . . . .	430
<b>10</b>	<b>Orbit Relative to the Sun: Crossing Times and Eclipse . . . . .</b>	<b>433</b>
10.1	Cycle with Respect to the Sun . . . . .	433
10.1.1	Crossing Time . . . . .	433
10.1.2	Calculating the Cycle $C_s$ . . . . .	434

10.1.3	Cycle $C_S$ and Orbital Characteristics . . . . .	436
10.1.4	Cycle and Ascending Node Crossing Time . . . . .	448
10.2	Crossing Time for a Sun-Synchronous Satellite . . . . .	449
10.2.1	Passage at a Given Latitude . . . . .	449
10.2.2	Choice of Local Time at the Ascending Node . . . . .	454
10.2.3	Calculating the Drift in Local Crossing Time . . . . .	460
10.3	Angle Between Orbital Plane and Solar Direction . . . . .	464
10.3.1	Position of the Normal to the Orbital Plane . . . . .	464
10.3.2	Angle $\beta$ . . . . .	465
10.4	Solar Eclipse for Circular Orbits . . . . .	466
10.4.1	Duration of Solar Eclipse . . . . .	469
10.4.2	Sun-Synchronous LEO Orbit . . . . .	470
10.4.3	Dawn–Dusk Sun-Synchronous LEO Orbit . . . . .	474
10.4.4	MEO Orbit . . . . .	478
10.4.5	GEO Orbit . . . . .	478
10.5	General Conditions for Solar Eclipse . . . . .	479
10.5.1	Establishing General Eclipse Conditions . . . . .	479
10.5.2	Criterion for Eclipse . . . . .	482
<b>11</b>	<b>Orbit Relative to the Earth: Recurrence and Altitude</b> . . . . .	<b>487</b>
11.1	Recurrence Constraint . . . . .	487
11.1.1	Definition of Recurrence . . . . .	487
11.1.2	Calculating the Recurrence Cycle $C_T$ . . . . .	488
11.1.3	Recurrence Triple . . . . .	490
11.2	Recurrence of Sun-Synchronous LEO Satellites . . . . .	491
11.2.1	Method for Obtaining Recurrence . . . . .	491
11.2.2	Recurrence Module . . . . .	491
11.2.3	Recurrence Diagram . . . . .	492
11.2.4	Recurrence Defined by the Recurrence Triple . . . . .	498
11.2.5	One-Day Recurrence Cycle . . . . .	506
11.3	Recurrence for Non-Sun-Synchronous LEO Satellites . . . . .	508
11.3.1	Obtaining the Recurrence Triple . . . . .	508
11.3.2	Recurrence, Altitude, and Inclination . . . . .	512
11.4	Recurrence for MEO and HEO Satellites . . . . .	514
11.5	Recurrence Grid . . . . .	516
11.5.1	Constructing the Recurrence Grid . . . . .	516
11.5.2	Grid Interval . . . . .	517
11.5.3	Recurrence Subcycle . . . . .	520
11.5.4	Reference Grids . . . . .	524
11.5.5	Grid Points for Recurrent Satellites . . . . .	526
11.6	Maintaining a Recurrent Satellite on Orbit . . . . .	533
11.7	Recurrence Index . . . . .	536
11.7.1	Definition of Recurrence Index . . . . .	536

---

11.7.2	Perfect or Imperfect Recurrence	538
11.7.3	Applications of the Recurrence Index	538
11.7.4	Recurrence Index and Orbital Characteristics	540
11.8	Altitude Variations	542
11.8.1	Altitude and Orbital Parameters	543
11.8.2	Altitude During One Revolution	546
11.8.3	Variation of the Altitude over a Long Period	550
11.9	Frozen Orbits	551
11.9.1	Definition of a Frozen Orbit	551
11.9.2	Determining the Frozen Parameters	551
11.9.3	Altitude of a Satellite on a Frozen Orbit	554
11.10	Altitude and Atmospheric Drag	558
<b>12</b>	<b>View from the Satellite</b>	<b>561</b>
12.1	Swath of an Instrument	561
12.1.1	Local Orbital Frame	561
12.1.2	Scanning Modes	562
12.2	Swath Viewing Geometry	565
12.2.1	Definition of Angles	565
12.2.2	Relations Between Angles	567
12.2.3	Ground Swath	567
12.2.4	Latitudes Viewed and Latitude Overlap	568
12.3	Pixel Distortion	570
12.3.1	Calculating the Distortion Index	570
12.3.2	Pixel Distortion for LEO Satellites	572
12.3.3	Pixel Distortion for GEO Satellites	574
12.4	Swath Track for an LEO Satellite	576
12.4.1	Cross-track Swath	576
12.4.2	Variable-Yaw Swath	582
12.4.3	Conical Swath	585
12.4.4	Ground Track Superposition	592
12.5	View from a GEO Satellite	593
12.5.1	Simplified Geometric Conditions	593
12.5.2	Pixels and Geographic Coordinates Correspondence	604
<b>13</b>	<b>Spatiotemporal and Angular Sampling</b>	<b>613</b>
13.1	Satellite–Target Direction	614
13.1.1	Line-of-Sight Direction of the Satellite	614
13.1.2	Geostationary Satellites	618
13.1.3	Local View and Sky Plots	620
13.1.4	Visibility Window for LEO Satellites	622
13.1.5	Visibility Window for HEO Satellites	627

13.2	Target–Sun Direction . . . . .	629
13.2.1	Solar Line of Sight . . . . .	629
13.2.2	Sunrise, Sunset, and Apparent Noon . . . . .	632
13.3	Sun–Target–Satellite Configuration . . . . .	633
13.3.1	Angles Describing the Sun–Target–Satellite Configuration . . . . .	633
13.3.2	Specular Reflection (Sun Glint) . . . . .	635
13.4	Monthly Sampling Tables . . . . .	639
<b>14</b>	<b>Global Positioning Systems (GPS)</b> . . . . .	<b>653</b>
14.1	Basic Principle of GPS . . . . .	653
14.1.1	Positioning in the Ideal Case . . . . .	653
14.1.2	Positioning in Real Situations . . . . .	654
14.1.3	Determining User Velocity . . . . .	658
14.1.4	Perturbation of Signal and Measurement . . . . .	660
14.1.5	Geometric Considerations and Measurement Accuracy . . . . .	661
14.1.6	Position on Earth and Geographic Coordinates . . . . .	663
14.1.7	Differential GPS (DGPS) . . . . .	664
14.2	Navstar/GPS . . . . .	666
14.2.1	Setting up the System . . . . .	666
14.2.2	Space Segment . . . . .	667
14.2.3	Control Segment . . . . .	670
14.2.4	User Segment . . . . .	675
14.2.5	Local View . . . . .	676
14.2.6	Navstar/GPS and Other Systems . . . . .	676
14.3	Glonass . . . . .	678
14.3.1	The Three Segments . . . . .	678
14.3.2	Local View and Visibility Table . . . . .	679
14.4	Galileo . . . . .	681
14.4.1	A European Project . . . . .	681
14.4.2	The Three Segments . . . . .	684
14.5	BeiDou NS . . . . .	684
14.5.1	The Three Segments . . . . .	687
14.5.2	Beidou-1 Experimental System . . . . .	688
14.6	Augmentation Systems . . . . .	691
14.7	Regional Systems . . . . .	694
14.7.1	IRNSS . . . . .	694
14.7.2	QZSS . . . . .	694
14.8	Non-positioning Uses of GPS . . . . .	696
14.8.1	Radio Occultation . . . . .	696
14.8.2	Studying the Troposphere via the Base Stations . . . . .	698
14.8.3	Other Applications . . . . .	698

14.9	Historical Note: The First Systems . . . . .	698
14.9.1	Transit . . . . .	698
14.9.2	The Soviet System . . . . .	701
14.10	Appendix: GPS and Tectonic Plates . . . . .	702
14.11	Appendix: GPS and Relativity . . . . .	705
14.11.1	Presentation . . . . .	705
14.11.2	Proper Time Difference . . . . .	705
14.11.3	Effect Due to Orbital Eccentricity . . . . .	713
14.11.4	Sagnac Effect . . . . .	715
14.11.5	Conclusion . . . . .	717
<b>15</b>	<b>Satellites of Mars . . . . .</b>	<b>719</b>
15.1	Presenting the Planet Mars . . . . .	719
15.1.1	Mars and Space Exploration . . . . .	719
15.1.2	Geography of Mars . . . . .	726
15.2	Geodetic and Astronomical Quantities . . . . .	731
15.2.1	Geodetic Data . . . . .	731
15.2.2	Astronomical Data . . . . .	732
15.2.3	Areocentric Longitude and Martian Day . . . . .	733
15.2.4	Declination . . . . .	739
15.2.5	Equation of Time . . . . .	741
15.3	Satellite in Real Orbit . . . . .	742
15.3.1	Satellite in Keplerian Orbit . . . . .	742
15.3.2	Perturbative Accelerations . . . . .	742
15.3.3	Secular Variation of Orbital Elements . . . . .	746
15.4	Different Orbits . . . . .	748
15.4.1	Areosynchronous Satellite . . . . .	748
15.4.2	Sun-Synchronous Satellite . . . . .	752
15.5	Ground Track of a Satellite . . . . .	754
15.5.1	Representing the Ground Track . . . . .	754
15.5.2	Apparent Inclination . . . . .	761
15.5.3	Velocity of Satellite in Circular Orbit . . . . .	762
15.6	Orbit Relative to the Sun: Crossing Times and Eclipse . . . . .	763
15.6.1	Overpass Time for a Sun-Synchronous Satellite . . . . .	766
15.6.2	Eclipse Conditions . . . . .	767
15.7	Orbit Relative to Mars: Recurrence and Altitude . . . . .	773
15.7.1	Recurrence . . . . .	773
15.7.2	Altitude . . . . .	781
15.8	View from the Satellite . . . . .	782
15.8.1	Viewing Configuration and Pixel Distortion . . . . .	782
15.8.2	Swath Track for an LMO Satellite . . . . .	782
15.8.3	Image Acquisition and Apparent Inclination . . . . .	785
15.8.4	View from an SMO Satellite . . . . .	788



15.9	Spatiotemporal and Angular Sampling . . . . .	790
15.9.1	Examples of Sampling . . . . .	790
15.9.2	Sun Glint . . . . .	792
15.10	Natural Satellites . . . . .	795
15.10.1	Phobos and Deimos . . . . .	795
15.10.2	Space Exploration . . . . .	795
15.10.3	View and Sampling . . . . .	796
15.11	Historical Note: Kepler and the Planet Mars . . . . .	798
15.11.1	Calculating the Period of Revolution . . . . .	798
15.11.2	Other Calculations for the Earth and Mars . . . . .	802
<b>16</b>	<b>Satellites of Other Celestial Bodies . . . . .</b>	<b>803</b>
16.1	Planets of the Solar System . . . . .	804
16.1.1	Presenting the Planets . . . . .	804
16.1.2	Space Exploration of the Planets . . . . .	808
16.2	Geodetic and Astronomical Quantities for Planets . . . . .	816
16.2.1	Geodetic and Astronomical Data . . . . .	816
16.2.2	Satellite in Keplerian Orbit . . . . .	817
16.2.3	Geographical Maps . . . . .	821
16.3	Satellite of Planet in Real Orbit . . . . .	822
16.3.1	Perturbative Accelerations . . . . .	822
16.3.2	Classification of Satellites . . . . .	824
16.4	Ground Track for a Satellite of a Planet . . . . .	826
16.4.1	Satellites of Mercury . . . . .	827
16.4.2	Satellites of Venus . . . . .	830
16.4.3	Satellites of the Asteroid Eros . . . . .	834
16.4.4	Satellites of the Asteroids Vesta and Ceres . . . . .	838
16.4.5	Satellites of Giant Planets . . . . .	845
16.5	Natural Satellites in the Solar System . . . . .	852
16.5.1	Presentation of the Natural Satellites . . . . .	852
16.5.2	Space Exploration of Natural Satellites . . . . .	853
16.6	Geodetic and Astronomical Quantities for Natural Satellites . . . . .	853
16.6.1	Geodetic and Astronomical Data . . . . .	853
16.6.2	Satellite in Keplerian Orbit . . . . .	855
16.6.3	Geographical Maps . . . . .	855
16.7	Satellite of a Natural Satellite in Real Orbit . . . . .	856
16.7.1	Perturbative Accelerations . . . . .	856
16.7.2	Classification of Satellites . . . . .	857
16.8	Ground Track of a Satellite of a Natural Satellite . . . . .	861
16.8.1	Satellites of the Moon . . . . .	861
16.8.2	Satellites of Europa and Ganymede . . . . .	872
16.8.3	Satellites of Titan . . . . .	873
16.8.4	Satellites of Triton . . . . .	877

16.9	Appendix: The Three Planetocentric Spheres .....	877
16.9.1	Presenting the Three Spheres .....	878
16.9.2	The Case of the Four Giant Planets .....	879
16.10	Historical Note: Kepler and the Solar System .....	881
	<b>Index of <i>Astronomia Nova</i> .....</b>	<b>883</b>
	<b>Bibliography .....</b>	<b>885</b>
	<b>Index .....</b>	<b>891</b>

# Chapter 1

## Geometry of the Ellipse

We will be concerned with ellipses in two different contexts:

- The orbit of a satellite around the Earth (or the orbit of a planet around the Sun) is an ellipse.
- A cross-section of the planet Earth containing the polar axis is an ellipse.

Naturally, in both cases, this is just a first approximation. However, a preliminary study of this geometric object will prove useful before going into greater detail.

In the first case, the ellipse will be viewed as a geometrical object localised by its focus and specified by its eccentricity  $e$ . In the second, it will arise rather as a flattened circle, localised by its center and characterised by the degree of flattening  $f$ .

Ellipses can be defined in many different ways, as we shall now see. It is indeed a rich geometrical object.

### 1.1 Definition and Properties

#### 1.1.1 Conic Sections

Consider a cone  $\mathcal{C}$ , with apex  $S$ , and a plane  $\mathcal{P}$  which does not pass through  $S$ . Let  $\mathcal{P}'$  be the plane parallel to  $\mathcal{P}$  which does pass through  $S$ . There are three possible cases:

- If  $\mathcal{P}'$  lies outside the cone, the intersection of  $\mathcal{P}$  and  $\mathcal{C}$  is an ellipse.
- If  $\mathcal{P}'$  is tangent to the cone, the intersection of  $\mathcal{P}$  and  $\mathcal{C}$  is a parabola.
- If  $\mathcal{P}'$  lies within the cone, the intersection of  $\mathcal{P}$  and  $\mathcal{C}$  is a hyperbola.

In ancient times, these conic sections were viewed as a geometrical curiosity.

When he wanted to explain the orbit of Mars around the Sun, Kepler was the first to rediscover the notion of ellipse that had been so carefully enunciated by the Greek geometers. Later on, with the help of Newton's theory, astronomers were able to show that the trajectory of a body subject to a gravitational force could be not only an ellipse, but also a parabola or a hyperbola. Kepler's ellipse was thus replaced by the whole family of conic sections.

We begin by describing the many different ways of understanding conic sections.

Knowledge of this particular curve goes back at least to Ancient Greece. Menaechmus<sup>1</sup> and Apollonius of Perga<sup>2</sup> defined the ellipse as one of the family of conic sections.<sup>3</sup>

### 1.1.2 Definition and Properties of the Ellipse

In this book, we shall be interested almost exclusively in the ellipse, because of all the conic sections, only this one constitutes a periodic trajectory.

The ellipse has many properties. We may thus choose one as the definition and deduce the others from it by means of rather straightforward demonstration. In general, the first of the following is usually taken as the definition, while the others are considered as consequences.

#### Definition

[1] The ellipse is the locus of points  $M$  in the plane such that the sum of the distances  $MF$  and  $MF'$  to two fixed points  $F$  and  $F'$ , called the foci, is constant.<sup>4</sup>

---

<sup>1</sup>Menaechmus (Μέναιχος, −375 to −325), was a Greek mathematician and member of Plato's Academy. He is credited by Eratosthenes with the discovery of the conic sections, objects which arose in the so-called Delian problem, also known as doubling the cube (given a cube of volume  $a^3$ , construct another of volume  $2a^3$ ). Menaechmus sought two numbers  $x$  and  $y$  such that  $a/x = x/y = y/2a$ , which leads to  $x^3 = 2a^3$ , by finding the intersections of a parabola ( $y = x^2/a$ ) and a hyperbola ( $y = 2a^2/x$ ).

<sup>2</sup>Apollonius of Perga, a city in Pamphylia in Anatolia (Ἀπολλώνιος ὁ Περργαίος, −262 to −180) was a Greek geometer and astronomer and a student of Euclid. He wrote an eight volume work entitled *Conics*, part of which has come down to us directly in the Greek version, and part through the Arab translation. He studied the possible intersections of a cone by an arbitrary plane, classifying them into the three types of conic section which still carry the names he attributed to them.

<sup>3</sup>The word "conic" comes from the Greek *kōnikos*, an adjective derived from *kōnos* (ὁ κώνος, ον), meaning "pine cone", the fruit of certain conifers.

<sup>4</sup>A direct application of this definition can be used to draw an ellipse in what is sometimes known as the gardener's method. Two stakes are stuck in the ground, some distance  $d$  apart. A non-stretch string of length  $\ell > d$  is attached with one end at each stake. If we then hold a third stake against the string and move it in such a way that the string is always taut, this stake will trace out an ellipse with focal points at the two fixed stakes. The major axis is equal to  $\ell$  and the eccentricity is  $d/\ell$ .

## Main Properties

[2a] The ellipse is an affine transformation of a circle.

[2b] The projection of a circle on a plane is an ellipse.

[3] The ellipse is the locus of points  $M$  such that the ratio  $MF/d$  is a constant  $q$ ,  $q < 1$ , where  $F$  is a fixed point, the focus, and  $d$  is the distance between  $M$  and a fixed straight line called the directrix.

[4] The ellipse is obtained from the intersection of a cone and a plane in the case specified above.

## Other Properties

Here are a few more properties that we shall not prove here.

[5] The ellipse is the locus of the centers of circles passing through a fixed point  $F$  and tangent to a fixed circle, the director circle, with center  $F'$ .

[6] A light ray passing through one focus will reflect on the ellipse and pass through the second focus.<sup>5</sup>

[7] If the ends of a line segment of fixed length run along two perpendicular straight lines, an arbitrary point on the segment will describe an ellipse and the envelope of the segment is then an astroid.

## 1.1.3 Applications of the Definition

### Ellipse as a Geometrical Object

From the definition [1], the ellipse has a center<sup>6</sup> of symmetry  $O$ , which we shall call the center of the ellipse. Taking  $O$  as the origin for an orthonormal Cartesian frame of reference (see Fig. 1.1), the various points of interest have the following coordinates:

$$OF = \begin{pmatrix} c \\ 0 \end{pmatrix}, \quad OF' = \begin{pmatrix} -c \\ 0 \end{pmatrix}, \quad OA = \begin{pmatrix} a \\ 0 \end{pmatrix}, \quad OB = \begin{pmatrix} 0 \\ b \end{pmatrix}.$$

We use the standard terminology:

$$\begin{aligned} a &= OA, & \text{semi-major axis of the ellipse,} \\ b &= OB, & \text{semi-minor axis of the ellipse, } b \leq a, \\ c &= OF = OF', & \text{focal distance.} \end{aligned}$$

---

<sup>5</sup>The term was introduced into scientific Latin (New Latin) by Kepler in 1603, from the Latin word *focus*, *i*, which means “a place where fire is made”. A pencil of light rays passing through one focus will converge at the other, and could start a fire there. This is indeed the explanation for the name “focus” (see Fig. 1.11).

<sup>6</sup>The word “center” comes from Old French *centre*, which comes from the Latin *centrum*, *i*, meaning “compass point”, “center of a circle”, or “midpoint of an ensemble”. The word derives from the Greek *kentron*, τὸ κέντρον, *ou*, a “goad”, from the verb *κεντέω*, meaning “to prick or sting”. This is a rather rare example of a technical country word which became scientific and later assumed a very general meaning. The Latin word spread to all the Latin languages and many non-Latin ones, too.

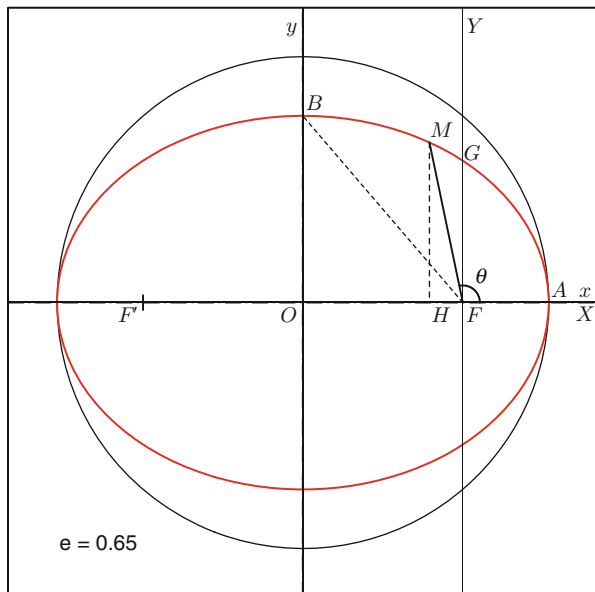


FIG. 1.1: *Ellipse and principal circle, showing the notation used for the Cartesian coordinate system (axes  $Ox, Oy$ ) and the polar coordinate system ( $r = FM$ , angle  $\theta$ ).*

Since  $c$  is always strictly less than  $a$ , we can always define a number  $e$  such that

$$c = ea, \quad \text{where } 0 \leq e < 1. \quad (1.1)$$

The real number  $e$  is the eccentricity of the ellipse.

### Equation of the Ellipse in Cartesian Coordinates Centred on $O$

Consider an orthonormal Cartesian frame of reference  $(O; x, y)$ , centered on  $O$ . The axis  $Ox$  is the straight line  $F'F$ , the focal axis. Let  $M(x, y)$  be a point on the ellipse and set

$$r = FM, \quad r' = F'M.$$

Definition [1] applied to  $M$  at  $A$  yields

$$r + r' = 2a, \quad (1.2)$$

and when  $M$  is at  $B$ , we obtain

$$b^2 = a^2 - c^2 = a^2(1 - e^2). \quad (1.3)$$

The lengths  $r$  and  $r'$  are expressed in Cartesian coordinates through their squares:

$$r^2 = (x - c)^2 + y^2 = (x - ea)^2 + y^2 , \quad (1.4)$$

$$r'^2 = (x + c)^2 + y^2 = (x + ea)^2 + y^2 , \quad (1.5)$$

and by the difference

$$r'^2 - r^2 = 4cx = 4eax . \quad (1.6)$$

Using (1.2), we obtain

$$r' - r = \frac{r'^2 - r^2}{r' + r} = 2ex ,$$

and finally the following expressions for  $r$  and  $r'$ , whose sum and difference are as given:

$$r = a - ex , \quad (1.7)$$

$$r' = a + ex . \quad (1.8)$$

Note that these expressions are very simple and do not involve any square roots.

Using (1.4) and (1.7), we then have

$$r^2 = (x - ea)^2 + y^2 = (a - ex)^2 ,$$

$$x^2 + e^2a^2 + y^2 = a^2 - e^2x^2 ,$$

$$x^2(1 - e^2) + y^2 = a^2 - e^2a^2 ,$$

whence

$$\frac{x^2}{a^2} + \frac{y^2}{a^2(1 - e^2)} = 1 , \quad (1.9)$$

or again

$$\frac{x^2}{a^2} + \frac{y^2}{b^2} = 1 , \quad (1.10)$$

which clearly reveal the role played by the semi-minor and semi-major axes.



### Equation of the Ellipse in Polar Coordinates Centred on $F$

Consider first the orthonormal Cartesian frame  $(F; X, Y)$ , centered on  $F$ , with axis  $FX$  identified with  $Ox$  and  $FY$  parallel to  $Oy$ . We then have the following relation between the abscissæ:

$$X = x - ea .$$

For a point  $M(X, Y)$  of the ellipse, (1.7) becomes

$$r = a(1 - e^2) - eX .$$

We then define the quantity

$$p = a(1 - e^2) , \tag{1.11}$$

known as the parameter or semi-latus rectum of the ellipse. It corresponds to the distance between the focus  $F$  and the point of intersection of the ellipse with the axis  $FY$  (which is the straight line with equation  $X = 0$ ). In Fig. 1.1,  $p = FG$ . Note that  $b$  is the geometric mean of  $a$  and  $p$ :

$$b^2 = ap . \tag{1.12}$$

The equation for the ellipse can once again be written very simply as

$$r = p - eX . \tag{1.13}$$

Consider polar coordinates centered on  $F$  (see Fig. 1.1). The coordinates  $r$  and  $\theta$  of an arbitrary point  $M$  are defined by

$$r = \|\mathbf{FM}\| = FM , \tag{1.14}$$

$$\theta = (\mathbf{FX}, \mathbf{FM}) . \tag{1.15}$$

The abscissa of  $M$  in Cartesian coordinates is then  $X = r \cos \theta$  and (1.13) yields

$$r = \frac{p}{1 + e \cos \theta} . \tag{1.16}$$

The equation for the ellipse in polar coordinates is thus

$$r(\theta) = \frac{a(1 - e^2)}{1 + e \cos \theta} . \tag{1.17}$$

## Note on Conic Sections

If we always define the parameter  $p$  to be the distance between the focus  $F$  and the point  $G$  at which the conic section intersects the perpendicular to the focal axis passing through  $F$ , the relation (1.16) can be used to define all the conic sections,<sup>7</sup> with the eccentricity discriminating between them:

$$\begin{cases} 0 \leq e < 1, & \text{for the ellipse,} \\ e = 1, & \text{for the parabola,} \\ e > 1, & \text{for the hyperbola.} \end{cases}$$

Note that, for  $e = 0$ , the ellipse is a circle, and if  $e \geq 1$ , the conic section extends to infinity.

### 1.1.4 Demonstrating the Main Properties

Here we deduce the main properties of the ellipse.

**Definition [1]  $\implies$  Property [2a]**

An affine transformation or affinity with axis  $\Delta$ , direction  $\delta$ , and coefficient  $k$  ( $k \neq 0$ ) is the point transformation which maps any point  $P$  in the plane

---

<sup>7</sup>Apollonius used the following three terms to characterise conic sections, inspired by the language of the Pythagoreans:

- Ellipse (ἡ ἔλλειψις, εἰς) means “lacking” or “omitted”.
- Parabola (ἡ παραβολή, ἤς) describes the action of throwing, and hence suggests a mapping, or comparison.
- Hyperbola (ἡ ὑπερβολή, ἤς) describes the action of throwing higher, hence invokes the idea of an excess.

The first term comes from εἰς, meaning “in”, and the verb λείπειν, meaning “to leave or neglect”. The last two derive from the verb βάλλειν, meaning “to throw”. The word “parabola” should not be associated with the idea of throwing something in the sense of throwing a projectile. This link between “parabola” and “throw” was described by Galileo, but was unknown to the Ancient Greeks. It is interesting to note that, taken in this order, the three terms “lacking”, “comparable”, and “in excess” associated with the conic sections correspond to the values of the eccentricity as compared to unity. In fact, Apollonius introduced the length  $p$ , the parameter of the ellipse, and calculated the areas of squares and rectangles based on this length. With modern notation, taking the focal axis as the axis  $Ox$ , with  $Oy$  perpendicular to it and the origin  $O$  at the apex of the conic section, we obtain the following relation for the parabola:

$$y^2 = 2px,$$

which means that the area of a square of side  $y$  is equal to that of a rectangle of dimensions  $2p \times x$ . For the two other conic sections, we have:

- For the ellipse,  $y^2 = 2px - (p/a)x^2$ .
- For the hyperbola,  $y^2 = 2px + (p/a)x^2$ .

In *comparison* with the parabola, it is thus the quantity  $(p/a)x^2$  which *lacks* for the ellipse and which is in *excess* for the hyperbola. The name for the conic sections was introduced by Kepler, Desargues, and Descartes, first in Latin, then in the modern European languages.



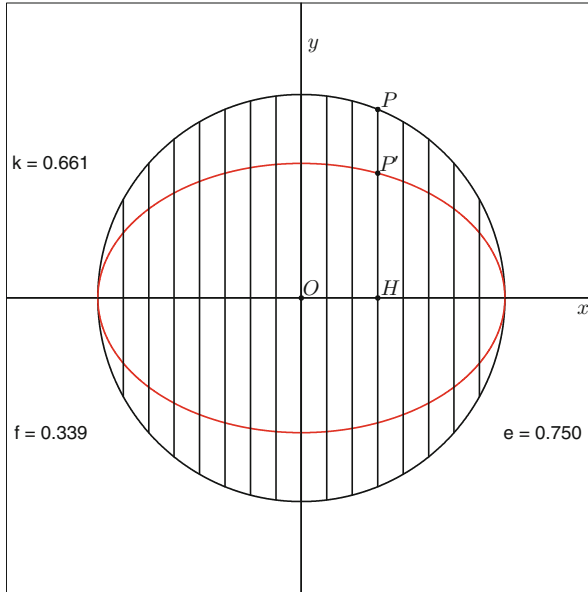


FIG. 1.3 : *Ellipse and principal circle. The ellipse is obtained from the principal circle by an affine transformation with axis  $Ox$ , direction  $Oy$ , and coefficient  $k$ .*

makes a dihedral angle  $\alpha$  with  $\mathcal{P}_1$  and passes through  $O$ . Let  $Ox$  be the axis of intersection of the two planes and  $Oy$  perpendicular to it and lying in the plane  $\mathcal{P}_2$ . For the points of the circle in  $\mathcal{P}_1$  which are projected into  $\mathcal{P}_2$ , the  $x$  coordinates remain the same, while the  $y$  coordinates are modified by a multiplicative coefficient equal to  $\cos \alpha$ . The equation of the image in  $\mathcal{P}_2$  is thus

$$\frac{x^2}{a^2} + \frac{y^2}{(a \cos \alpha)^2} = 1 ,$$

which corresponds to an affine transformation with coefficient  $k = \cos \alpha$ . This object is thus an ellipse.

**Definition [1]  $\implies$  Property [3]**

If we write  $r$  in (1.7) in the form

$$r = a - ex = e \left( \frac{a}{e} - x \right) , \quad (1.21)$$

this brings in the quantity  $a/e - x$ , which is the distance from the point  $M$ , with abscissa  $x$ , to the straight line parallel to  $Oy$  and with abscissa  $a/e$ .

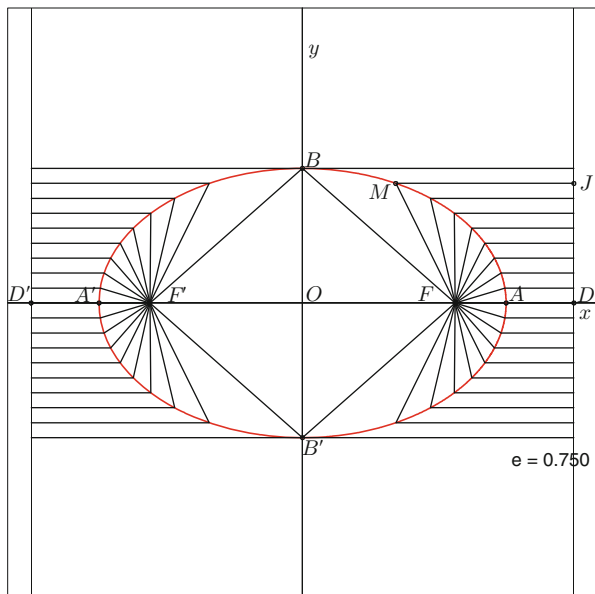


FIG. 1.4: *Ellipse and directrices.* The ellipse is the locus of points  $M$  such that the distance  $FM$  to the focus and the distance to a straight line denoted by  $d = MJ$  have constant ratio  $e$ .

Hence, with  $r = FM$  and  $a/e - x = MJ$  (see Fig. 1.4), it can be shown that the points of the ellipse are such that the ratio  $FM/MJ$  is constant and in fact equal to  $e$ :

$$\frac{FM}{MJ} = e .$$

Note that, if  $D$  is the intersection of the directrix with  $Ox$ , we have

$$OF \cdot OD = OA^2 = a^2 .$$

**Definition [1]  $\implies$  Property [4]**

The equivalence between the definition of a conic by focus and directrix and its definition as the intersection of a plane and a cone was not shown until the nineteenth century. Here we consider the ellipse and give the proof of Dandelin's theorem.<sup>8</sup>

Consider a cone with apex  $S$  and axis  $Sx$ . Consider also a plane  $\mathcal{P}$  which cuts the cone and such that the plane parallel to  $\mathcal{P}$  passing through  $S$  lies

<sup>8</sup>This theorem, proven in 1822, is also called the Dandelin–Quételet theorem, after the two Belgian mathematicians Germinal Dandelin (1794–1847) and Adolphe Quételet (1796–1841).

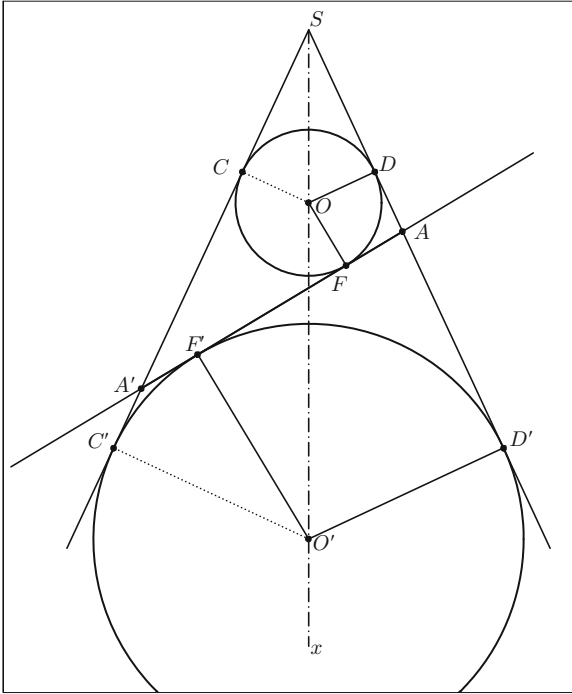


FIG. 1.5: Plane representation, in the plane  $\mathcal{T}$  perpendicular to the intersecting plane  $\mathcal{P}$ , of the cross-section of the cone of axis  $Sx$  by the plane  $\mathcal{P}$ , represented here by the straight line  $AA'$ .

outside the cone. Let  $\mathcal{T}$  be the plane perpendicular to  $\mathcal{P}$  and containing  $Sx$ . The intersection of this plane  $\mathcal{T}$  (called the plane of the page) with the cone comprises the two generators  $SA'$  and  $SA$ , while its intersection with the plane  $\mathcal{P}$  is the straight line  $AA'$ .

Consider first the view in the plane  $\mathcal{T}$ , as shown in Fig. 1.5. Among the circles tangent to the three sides of the triangle  $SAA'$ , we consider the two circles with centers lying on  $Sx$ .  $O$  is the center of the inscribed circle and the points of contact between the circle and the triangle are  $F$  on  $AA'$  and  $C$  and  $D$  on  $SA'$  and  $SA$ , respectively. Likewise, let  $O'$  be the center of the escribed circle, and let the points of contact of this circle with the triangle be  $F'$  on  $AA'$  and  $C'$  and  $D'$  on  $SA$  and  $SA'$ , respectively. Segments  $CD$  and  $C'D'$  are then parallel, each being perpendicular to the axis  $Sx$ .

We now rotate the figure about the axis  $Sx$ , but keeping the straight line  $AA'$  fixed:  $SA$  and  $SA'$  generate the cone, while the circles centered at  $O$  and  $O'$  generate two spheres inscribed within the cone. By translation, the straight line  $AA'$  generates the plane  $\mathcal{P}$  perpendicular to  $\mathcal{T}$  (see Fig. 1.6). The spheres  $O$  and  $O'$  are tangent to the plane  $\mathcal{P}$  at  $F$  and  $F'$ , and they are tangent to the cone at two parallel circles of diameter  $CD$  and  $C'D'$ , respectively.

Let  $M$  be a point on the conic section, i.e., the intersection of the given cone and the plane  $\mathcal{P}$ .  $SM$  cuts the circles  $CD$  and  $C'D'$  at  $J$  and  $J'$ , and

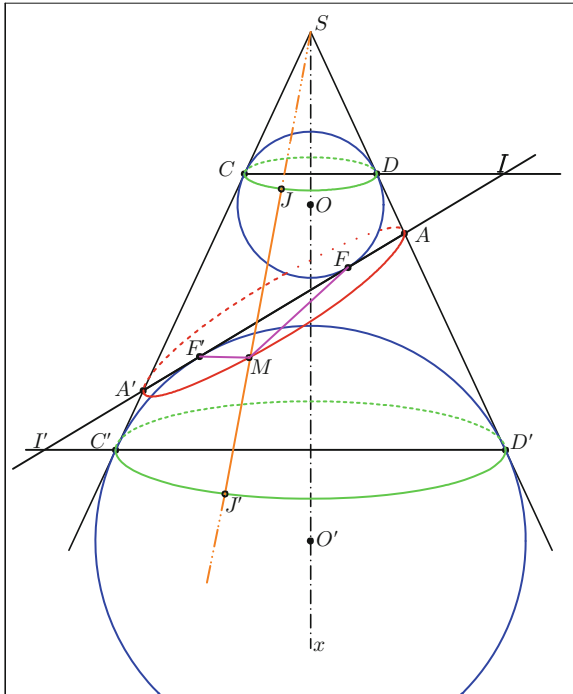


FIG. 1.6 : Three-dimensional representation of the cone of axis  $Sx$  and the intersecting plane  $\mathcal{P}$ . The curve of intersection goes through the points  $A$ ,  $A'$ , and  $M$ .

at these points, the generator  $SM$  is tangent to the spheres centered at  $O$  and  $O'$ . Since  $MF$  and  $MF'$  are tangent to the same spheres, respectively, we have:

- For the sphere centered at  $O$ ,  $MF = MJ$ .
- For the sphere centered at  $O'$ ,  $MF' = MJ'$ .

Now  $MJ + MJ' = JJ'$ , which is constant and equal to both  $CC'$  and  $DD'$ . Hence,

$$MF + MF' = \text{constant},$$

and  $M$  describes an ellipse with foci  $F$  and  $F'$ .

The plane  $\mathcal{P}$  cuts the parallel planes containing the circles  $CD$  and  $C'D'$  in straight lines perpendicular to the plane  $\mathcal{T}$ , passing through  $I$  and  $I'$ , respectively. It can be shown that these two straight lines, perpendicular to  $FF'$ , are the directrices of the ellipse.

### 1.1.5 Eccentricity and Flattening

From (1.3), the eccentricity  $e$  can be expressed in the form

$$e^2 = \frac{a^2 - b^2}{a^2} . \quad (1.22)$$

The relation between  $a$  and  $b$  can also be given in terms of the flattening  $f$ , which is defined by

$$f = \frac{a - b}{a} . \quad (1.23)$$

Note that the affine ratio  $k$  defined by (1.19) is  $k = 1 - f$ .

We immediately deduce the relationship between  $e$  and  $f$ :

$$\frac{b^2}{a^2} = 1 - e^2 = (1 - f)^2 . \quad (1.24)$$

This leads to the explicit relations

$$f = 1 - \sqrt{1 - e^2} , \quad (1.25)$$

$$e = \sqrt{f(2 - f)} . \quad (1.26)$$

Figure 1.7 shows the transformation of an ellipse with fixed semi-major axis  $a$  when  $e$  is increased in regular steps of 0.1. When instead we increase  $f$  in the same steps, the behaviour of the ellipse is very different, as shown in Fig. 1.8.

Gauss introduced the angle of eccentricity  $\epsilon$ , defined by

$$e = \sin \epsilon . \quad (1.27)$$

We may then write

$$b = a \cos \epsilon , \quad c = a \sin \epsilon , \quad p = a \cos^2 \epsilon .$$

Later we shall see how certain formulas can be made more elegant with the help of this auxiliary variable.

#### Low Eccentricities

There are many situations in which an ellipse is very close to its principal circle. In the case  $e \ll 1$ , (1.24) gives

$$e^2 \simeq 2f , \quad (1.28)$$

whence the flattening varies approximately as the square of the eccentricity.



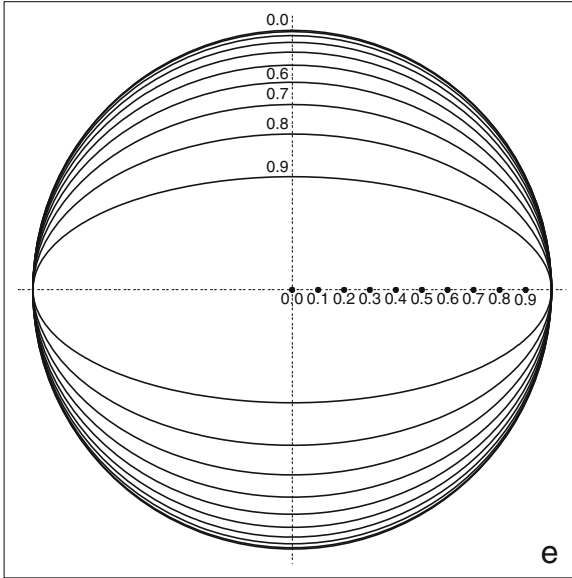


FIG. 1.7 : Ellipses with the same semi-major axis but eccentricity  $e$  varying from 0.0 to 0.9, in constant steps of 0.1. The corresponding eccentricity  $e$  is indicated on one of the two foci and on one end of the semi-minor axis. Note that the foci are regularly spaced.

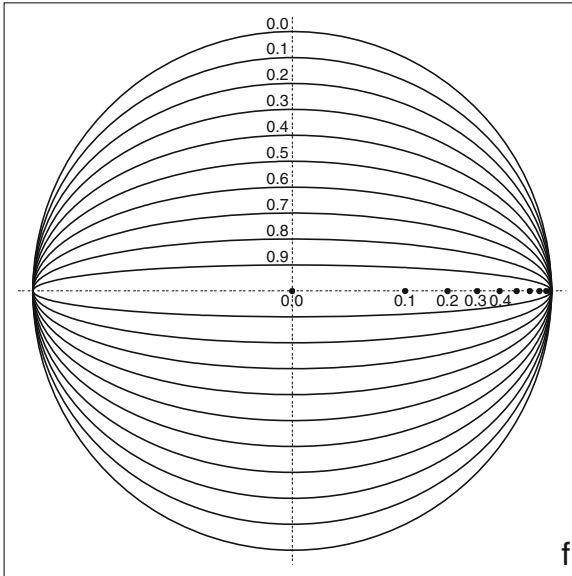


FIG. 1.8 : Ellipses with the same semi-major axis but flattening  $f$  varying from 0.0 to 0.9, in constant steps of 0.1. The corresponding flattening  $f$  is indicated on one of the two foci and on one end of the semi-minor axis. Note that the ends of the semi-minor axes are regularly spaced.

**Example 1.1** *Eccentricity and flattening for the orbit of Mars and Kepler's doubts.*

► The elliptic orbit of Mars is characterised by  $a = 1.52366$  a.u. (astronomical units) and  $e = 0.093412$ . The orbit looks almost circular:

$$b/a = \sqrt{1 - e^2} = \sqrt{0.099564} = 0.99782 \implies f = 0.0022,$$

and the relative difference between  $a$  and  $b$  is 0.22%. However, the distance between the center of the almost circular ellipse and the focus (the Sun) is significant:

$$c = ea = 0.14233 \text{ a.u.}$$

This means that the distance from Mars to the Sun varies between 1.38133 a.u. at perihelion and 1.66599 a.u. at aphelion.

In 1600, Kepler thus formulated what was to be his first law (in 1609): the orbit of Mars is circular and the Sun is not at its center. Kepler used the notion of ellipse from 1603. He later wrote:

I originally assumed that the orbits of the planets were perfect circles. This mistake cost me all the more time and effort in that it was supported by the authority of all the philosophers and was indeed quite plausible from a metaphysical point of view.

Figure 1.9 is one of Kepler's drawings, taken from *Astronomia Nova*, in which he shows the orbits of Mercury, Venus, the Earth, and Mars (relative to the Sun). They are almost circular.<sup>9</sup> However, the orbit of Mars is quite clearly off center, as is Mercury's. See also the historical note on Kepler and the planet Mars at the end of Chap. 15. ◀

**Example 1.2** *Calculating the lengths  $b$  and  $c$  for an ellipse specified by  $a$  and  $e$  in the case of the almost circular orbit of the satellite MetOp-A.*

► The ellipse representing the orbit of the satellite MetOp-A is specified by its semi-major axis  $a = 7,195,606$  m and its eccentricity  $e = 0.0011655$ . With this value of the eccentricity, we obtain

$$\sqrt{1 - e^2} = \sqrt{1 - 1.3584 \times 10^{-6}} = 1 - 0.6792 \times 10^{-6},$$

---

<sup>9</sup>To illustrate this property, V.I. Arnold suggests the following experiment in one of his books: Drop a droplet of tea close to the center of the cup. The waves will come together at the symmetric point. This is due to the definition of the foci of the ellipse, which implies that waves coming from one focus of the ellipse will converge at the other.

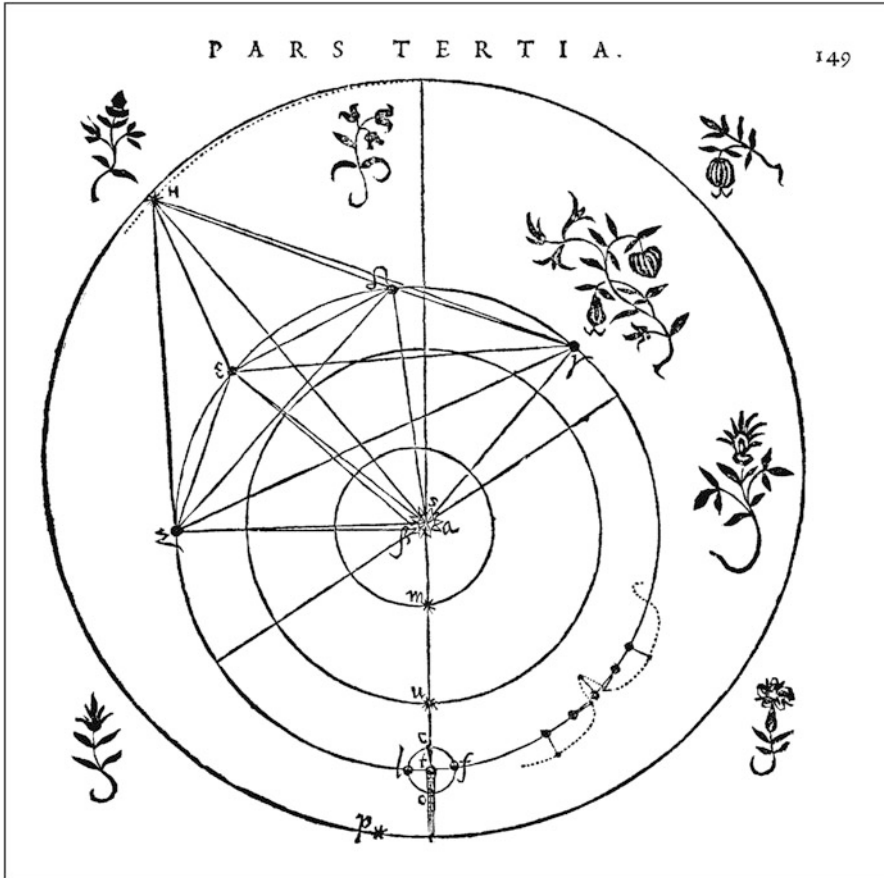


FIG. 1.9: Positions of Mars in a heliocentric frame. The planet is observed at four different dates separated by time intervals that are multiples of the sidereal period of revolution (687 days). Mars is then in the same position relative to the stars. Kepler calculated the positions of the Earth at these dates and deduced the eccentricity of the Earth orbit. He was thus able to reconstruct the orbits of all the planets. The orbit of Mars appears almost circular but significantly off center. The orbits of Mercury, Venus, and the Earth (with the Moon) are also shown. They look circular, but the Sun is not exactly at the center. It is interesting to note that the printers of the day were averse to completely white regions in drawings, so the empty parts of illustrations were systematically adorned with little flowers. J. Kepler: *Astronomia Nova*, Chap. XXVII, p. 149.

and hence  $a - b = fa = 4.9$  m. We thus obtain the following values for  $a$ ,  $b$ , and  $c$ :

$$a = 7,195,606 \text{ m}, \quad b = 7,195,601 \text{ m}, \quad c = ea = 8,386 \text{ m}.$$

In conclusion, the orbit is almost circular since the difference between  $a$  and  $b$  is only 5 m for a total of 7,200 km. However, the value of  $c$ , which measures the distance between the center of the ellipse and the focus is 8.4 km, which would be significant in any calculation of the altitude of the satellite. ◀

## 1.2 Applications and Other Characteristics

### 1.2.1 Arc Length of an Ellipse

The affine transformation of the circle  $(O; a)$  (see Fig. 1.10) with axis  $Ox$ , orthogonal direction, and ratio  $b/a$  gives the ellipse  $(O; a, b)$ . The coordinates of  $N$  on the circle and  $M$  on the ellipse can be expressed in terms of the polar angle<sup>10</sup>  $u$ , centered on  $O$ :

$$\mathbf{ON} = \begin{pmatrix} a \cos u \\ a \sin u \end{pmatrix}, \quad \mathbf{OM} = \begin{pmatrix} a \cos u \\ b \sin u \end{pmatrix}. \quad (1.29)$$

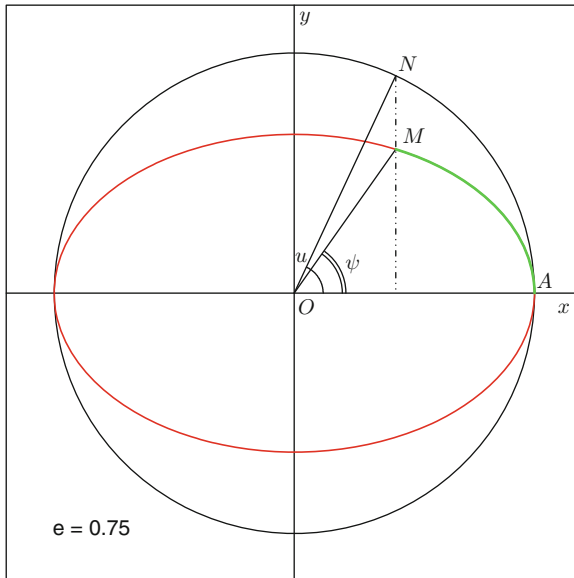


FIG. 1.10 : *Ellipse and principal circle, showing the angles  $u$  and  $\psi$  to the center and the arc  $AM$  of the ellipse.*

<sup>10</sup>This angular parameter  $u$  corresponds to the parametric (or reduced) latitude  $u$  in geodesy or Kepler's eccentric anomaly  $E$  in astronomy, as we shall see later on.

## Arc Length

To obtain the arc length of an ellipse, measured from an arbitrary origin, we first calculate the element  $ds$  of the curvilinear abscissa in terms of  $dx$  and  $dy$ :

$$ds^2 = (a^2 \sin^2 u + b^2 \cos^2 u) du^2 = a^2(1 - e^2 \cos^2 u) du^2 .$$

The arc length of the ellipse between  $A$  ( $u = 0$ ) and  $M$  ( $u = \alpha$ ) is then obtained by integration:

$$s(\alpha) = a \int_0^\alpha \sqrt{1 - e^2 \cos^2 u} du . \quad (1.30)$$

The value of  $s(\alpha)$  cannot be expressed in terms of simple analytic functions. This integral<sup>11</sup> is an incomplete elliptic integral of the second kind. It can be obtained as the limit of an infinite series.

## Perimeter of the Ellipse

The perimeter  $L$  of an ellipse is obtained as a complete elliptic integral of the second kind:

$$L = 4a \int_0^{\pi/2} \sqrt{1 - e^2 \cos^2 u} du , \quad (1.31)$$

which has no simple analytic representation. Expanding in powers of the eccentricity, we obtain Lambert's formula:

$$L = 2\pi a \left[ 1 - \left(\frac{1}{2}\right)^2 \frac{e^2}{1} - \left(\frac{1 \times 3}{2 \times 4}\right)^2 \frac{e^4}{3} - \left(\frac{1 \times 3 \times 5}{2 \times 4 \times 6}\right)^2 \frac{e^6}{5} + \dots \right] . \quad (1.32)$$

For this elliptic integral, there are several approximate formulas with varying degrees of complexity and which become more accurate as the eccentricity  $e$  decreases. The simplest approximate result is the one provided by Euler:

$$L \simeq \pi \sqrt{2(a^2 + b^2)} , \quad (1.33)$$

or again,

$$L \simeq \pi \left[ \frac{3}{2}(a + b) - \sqrt{ab} \right] . \quad (1.34)$$

---

<sup>11</sup>Such integrals are classified into three kinds. Those of the second kind have the form

$$E(\phi, k) = \int_0^\phi \sqrt{1 - k^2 \sin^2 \vartheta} d\vartheta ,$$

with parameter  $k$  such that  $0 < k^2 < 1$ . These elliptic integrals are said to be incomplete when  $\phi$  is arbitrary. When  $\phi = \pi/2$ , one speaks of complete elliptic integrals.

For greater accuracy, we may use the formulas given by Ramanujan<sup>12</sup>:

$$L \simeq \pi \left[ 3(a+b) - \sqrt{(a+3b)(3a+b)} \right],$$

or again,

$$L \simeq \pi(a+b) \left( 1 + \frac{3h}{10 + \sqrt{4-3h}} \right), \quad \text{where } h = \left( \frac{a-b}{a+b} \right)^2.$$

To first order in  $f$ , all these formulas are equivalent to

$$L \simeq \pi(a+b) = 2\pi a \left( 1 - \frac{f}{2} \right) \simeq 2\pi a \left( 1 - \frac{e^2}{4} \right), \quad (1.35)$$

which amounts to considering the ellipse as a circle with radius equal to the arithmetic mean of the two semi-axes of the ellipse.<sup>13</sup>

### 1.2.2 Radius of an Ellipse

The radius of an ellipse is the distance from an arbitrary point  $M$  on the ellipse to its center  $O$ . This radius is denoted  $R_\psi$ , since it is not constant but varies with  $\psi$ . The polar coordinates centered on  $O$  (see Fig. 1.10) are

$$R_\psi = \|\mathbf{OM}\|, \quad \psi = (\mathbf{Ox}, \mathbf{OM}).$$

The Cartesian coordinates of  $M$ , viz.,

$$\mathbf{OM} = \begin{pmatrix} x = R_\psi \cos \psi \\ y = R_\psi \sin \psi \end{pmatrix}, \quad (1.36)$$

give, using (1.10),

$$R_\psi^2 \left( \frac{\cos^2 \psi}{a^2} + \frac{\sin^2 \psi}{b^2} \right) = 1.$$

---

<sup>12</sup>*Srinivāsa Aiyangār Rāmānujan* (1887–1920) was a highly original Indian mathematician, considered as a genius in his field. He taught himself mathematics using a compendium of 6,000 theorems, most of which were given without proof. From the age of 17, and in particular during his time in England between 1913 and 1919, he established hundreds of formulas which he noted down without proof in his notebooks. His intuition and memory were astonishing. He worked on number theory, elliptic integrals, Bernoulli numbers, and so on. Ramanujan established the values of  $\pi$  and  $e$  using continued fractions, series, or extremely concise formulas.

<sup>13</sup>In the words of Kepler: “Any elliptic circumference is very close to the arithmetic mean between the circle of longest diameter and the circle of shortest diameter.” *Astronomia Nova*, Chap. LIX, p. 287. He considered only the elliptic orbits of the known bodies.

Then, in terms of the flattening  $f$ , the radius  $R_\psi$  of the ellipse is

$$R_\psi = \frac{a}{\sqrt{\cos^2 \psi + \frac{\sin^2 \psi}{(1-f)^2}}}, \quad (1.37)$$

and in terms of the eccentricity  $e$ ,

$$R_\psi = \frac{a\sqrt{1-e^2}}{\sqrt{1-e^2\cos^2\psi}}. \quad (1.38)$$

For small flattening ( $f \ll 1$ ), we have

$$R_\psi \simeq a(1 - f \sin^2 \psi), \quad \text{or} \quad R_\psi \simeq a \left( 1 - \frac{e^2}{2} \sin^2 \psi \right). \quad (1.39)$$

### 1.2.3 Radius of Curvature of an Ellipse

Any curve can be approximated near one of its points (provided it is not a cusp), over an infinitesimal interval, by a circle known as the osculating circle. Its radius  $\rho$  is the radius of curvature. The locus of the centers of these osculating circles is called the evolute of the curve. Equivalently, we may define the evolute of a plane curve as the envelope of all the normals to this curve (see Fig. 1.11). It can be shown that, at a given point, the osculating circle is unique.

Consider an ellipse specified by the angular parameter  $u$ . Let  $M$  be a point on the ellipse and  $M'$  the corresponding point on the evolute. This means that the circle of center  $M'$  and radius  $\rho = \|\mathbf{M}'\mathbf{M}\|$  is tangent to the ellipse at  $M$ . The vector  $\mathbf{M}'\mathbf{M}$  is normal to the ellipse at  $M$ .

The normal at point  $M$ , with parameter  $u$ , is written in the following way in terms of the coordinates  $X$  and  $Y$ :

$$\frac{aX}{\cos u} - \frac{bY}{\sin u} - c^2 = 0. \quad (1.40)$$

The parametric equation of the evolute is obtained by determining the two unknowns  $X$  and  $Y$  using two equations: the equation of the normal given by (1.40) and the derivative of this equation with respect to  $u$ . These can be written

$$aX \sin u - bY \cos u = c^2 \sin u \cos u,$$

$$aX \cos u + bY \sin u = c^2(\cos^2 u - \sin^2 u),$$

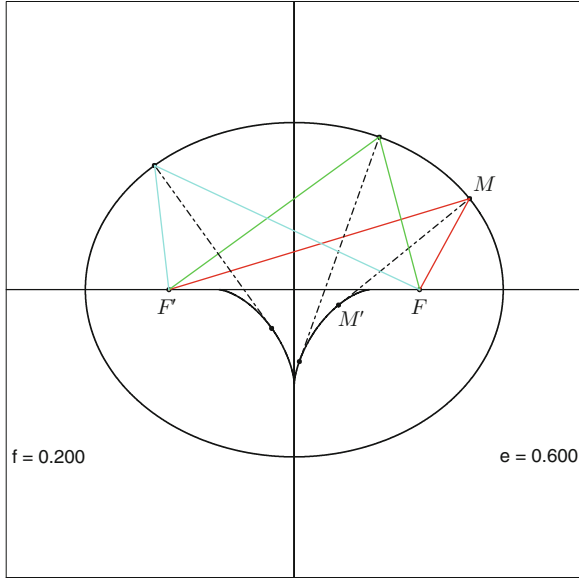


FIG. 1.11 : Radius of curvature of an ellipse.  $M$  is an arbitrary point on an ellipse with foci  $F$  and  $F'$ .  $M'$  is the center of the osculating circle of the ellipse at  $M$ . When  $M$  moves around the ellipse,  $M'$  describes the evolute of the ellipse. This diagram illustrates another property of the ellipse:  $MM'$  bisects the angle  $FMF'$ , so any ray of light passing through  $F$  will pass through  $F'$  after reflection on the ellipse.

and we obtain

$$aX = c^2 \cos^3 u, \quad bY = c^2 \sin^3 u.$$

In short, the coordinates of  $M$  and  $M'$  can be written in the form

$$\mathbf{OM} = \begin{pmatrix} a \cos u \\ b \sin u \end{pmatrix}, \quad \mathbf{OM}' = \begin{pmatrix} \frac{a^2 - b^2}{a} \cos^3 u \\ \frac{a^2 - b^2}{b} \sin^3 u \end{pmatrix}. \quad (1.41)$$

The evolute of the ellipse shown in Fig. 1.12 (upper) is the curve  $A'B'C'D'$  with four cusps. It is the affine transformation with axis  $Ox$ , direction orthogonal, and ratio  $-b/a$ , of the astroid with equation

$$\begin{pmatrix} A \cos^3 u \\ A \sin^3 u \end{pmatrix}, \quad \text{where } A = \frac{a^2 - b^2}{a} = \frac{c^2}{a} = ae^2.$$

The components of the vector  $\mathbf{MM}'$  can be calculated from (1.41):

$$\mathbf{M'M} = \begin{pmatrix} \left( a \sin^2 u + \frac{b^2}{a} \cos^2 u \right) \cos u \\ \left( b \cos^2 u + \frac{a^2}{b} \sin^2 u \right) \sin u \end{pmatrix} = (a^2 \sin^2 u + b^2 \cos^2 u) \begin{pmatrix} \frac{\cos u}{\sin u} \\ \frac{a}{b} \end{pmatrix}. \quad (1.42)$$



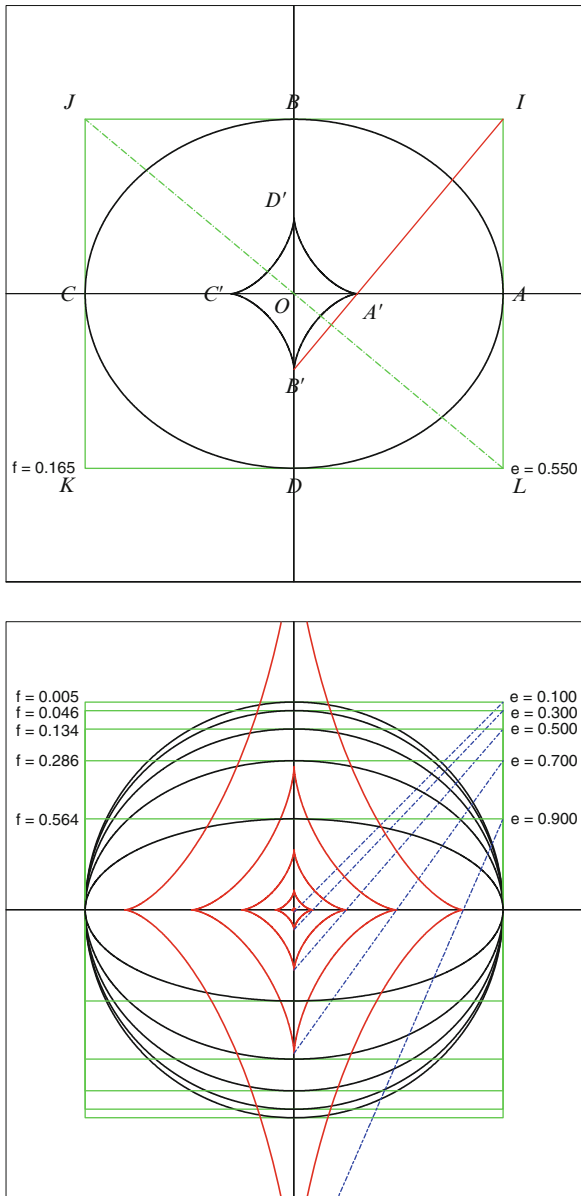


FIG. 1.12 : Relationship between an ellipse and its evolute. Upper: The straight line joining  $A'$  and  $B'$ , centers of curvature for  $A$  and  $B$ , respectively, passes through  $I$  and is perpendicular to the diagonal  $JL$  of the rectangle  $IJKL$ , a rectangle with sides  $2a$  and  $2b$ , center  $O$ , escribed on the ellipse. Lower: The same construction for different values of the eccentricity between  $e = 0.10$  and  $e = 0.90$ , in steps of  $0.20$ . The semi-major axis remains constant.

We deduce the value of the radius of curvature  $\rho = \|\mathbf{M}'\mathbf{M}\|$ :

$$\rho = \frac{(a^2 \sin^2 u + b^2 \cos^2 u)^{3/2}}{ab} . \tag{1.43}$$

We note the particular values for the points  $A'$  and  $B'$ :

$$u = 0 \implies \mathbf{OA} = \begin{pmatrix} a \\ 0 \end{pmatrix}, \quad \mathbf{OA}' = \begin{pmatrix} a^2 - b^2 \\ a \\ 0 \end{pmatrix}, \quad \mathbf{A'A} = \begin{pmatrix} b^2 \\ a \\ 0 \end{pmatrix},$$

$$u = \frac{\pi}{2} \implies \mathbf{OB} = \begin{pmatrix} 0 \\ b \end{pmatrix}, \quad \mathbf{OB}' = \begin{pmatrix} 0 \\ b^2 - a^2 \\ b \end{pmatrix}, \quad \mathbf{B'B} = \begin{pmatrix} 0 \\ a^2 \\ b \end{pmatrix}.$$

The radius of curvature varies between two extreme values:

- maximal for  $B$  and  $D$ , with  $\rho = a^2/b$ ,
- minimal for  $A$  and  $C$ , with  $\rho = b^2/a$ .

Let  $IJKL$  be the rectangle with center  $O$ , sides  $2a$  and  $2b$ , in which the ellipse is inscribed (see Fig. 1.12 upper). Using the coordinates of the various points calculated above, we obtain the following relations:

$$\frac{BI}{BB'} = \frac{b}{a}, \quad \frac{OA'}{OB'} = \frac{b}{a}, \quad \mathbf{JL} = \begin{pmatrix} +2a \\ -2b \end{pmatrix},$$

which show that:

- The straight line  $A'B'$  passes through  $I$ .
- The diagonal of the rectangle which does not pass through  $I$  is perpendicular to  $A'B'$ .

Figure 1.12 (lower) shows this property for a range of eccentricities.

# Chapter 2

## Geodesy

### 2.1 Earth Ellipsoid

#### 2.1.1 Different Definitions of Latitude

##### Spherical Coordinates

Consider an orthonormal Cartesian frame  $(O; x, y, z)$ . A point  $M$  in space can be identified by the three spherical coordinates  $r, \psi, \lambda$ , defined in the following way. We select one axis  $Oz$  and project  $M$  to  $M'$  on the plane  $xOy$  perpendicular to  $Oz$  passing through  $O$ . We then set

$$r = \|\mathbf{OM}\|, \quad \psi = (\mathbf{OM}', \mathbf{OM}), \quad \lambda = (\mathbf{Ox}, \mathbf{OM}'),$$

where the ranges of the three coordinates are

$$r \in [0, \infty), \quad \psi \in \left[-\frac{\pi}{2}, +\frac{\pi}{2}\right], \quad \lambda \in [0, 2\pi).$$

The Cartesian coordinates of the point  $M$  can be expressed as follows in terms of the spherical coordinates:

$$\mathbf{OM} = \begin{pmatrix} x = r \cos \psi \cos \lambda \\ y = r \cos \psi \sin \lambda \\ z = r \sin \psi \end{pmatrix}. \quad (2.1)$$

Now consider a sphere of radius  $R$ , centered on  $O$ . If this sphere is a representation of the (spherical) Earth, the geometric quantities defined above have geographic significance:

- $Oz$  is the *polar axis* and  $xOy$  is the *equatorial plane*.
- The distance  $r = R + h$  is often specified by the *altitude*  $h$ .
- $\psi$  is the *latitude* and  $\lambda$  is the *longitude*.



FIG. 2.1 : British stamp issued in June 1984 to commemorate the 100th anniversary of the adoption of the Greenwich Meridian as Longitude Zero for the Earth. Created by Sedley Place Design.

Latitude and longitude are quite generally defined here in spherical coordinates. Circles passing through both poles are *meridians* (loci of points of constant longitude). Circles parallel to the equatorial plane are called *parallels* (loci of points at constant latitude), and the parallel in the equatorial plane is the *equator*. The meridians are great circles, while all the parallels apart from the equator are small circles.<sup>1</sup>

We apply the following conventions:

- The polar axis is oriented from the South Pole to the North Pole.
- The meridian plane  $xOz$  serving as origin is called the *prime meridian*, *zero meridian*, or (see Fig. 2.1) *Greenwich meridian*.<sup>2</sup>
- Longitudes are measured in the right-handed trigonometric sense from  $0^\circ$  to  $360^\circ$  or from  $-180^\circ$  to  $+180^\circ$ , which gives values  $[+E/-W]$ , i.e., positive for the east and negative for the west.

<sup>1</sup>If they intersect at all, a sphere and a plane intersect in a circle. If the plane passes through the center of the sphere, the circle in question is a *great circle*, otherwise it is a *small circle*.

<sup>2</sup>When it was officially chosen as prime meridian at the International Meridian Conference, held in Washington in 1884, the meridian passing through the Royal Observatory in Greenwich was already being used in most shipping charts (the British delegate declared at the time that, in terms of sheer tonnage, 72% of world shipping trade was using charts based on Greenwich). On the other hand, when it came to land charts, there was a multitude of different zero meridians. Naturally, France used the Paris meridian set down by Cassini, which passed through the Paris Observatory. Italy referred to the meridian in Rome, Russia to the one in Pulkovo, and so on. The meridian which passes through El Hierro Island (*Isla de el Hierro*), the westernmost island of the Canaries, and hence the westernmost point known to Europe before the discovery of the Americas, had the advantage that it gave only positive longitudes at the time. It had often been used in Europe in the seventeenth and eighteenth centuries. Even in the nineteenth century it was still to be found on several maps from central Europe.

Ellipsoid	Year	$a$ (m)	$1/f$ (dimensionless)
Delambre	1810	6,375,653	334
Airy	1830	6,376,542	299.3
Everest	1830	6,377,206.4	300.8017
Bessel	1840	6,377,397.16	299.1528
Clarke I	1866	6,378,206.4	294.9787
Clarke II	1880	6,378,249.2	293.4660
Hayford International	1924	6,378,388.2	297
Krassowsky	1942	6,378,245	293.3
AIG67	1967	6,378,160	298.2471
WGS72	1972	6,378,135	298.26
GRS80	1980	6,378,137	298.257222101
WGS84	1984	6,378,137	298.257223563
GEM-T2	1990	6,378,137	298.257
EGM96	1996	6,378,136.30	298.25765
GRIM5	2000	6,378,136.46	298.25765
EIGEN	2008	6,378,136.46	298.25765
EGM2008	2008	6,378,136.46	298.25765

TABLE 2.1 : *Reference ellipsoids used in geodesy (with year of application). Changing estimates of the values of the semi-major axis  $a$  and the flattening  $f$ . The ellipsoids are divided into three chronological groups: (a) now historical ellipsoids, (b) ellipsoids from the satellite era, and (c) ellipsoids relating to geopotential models.*

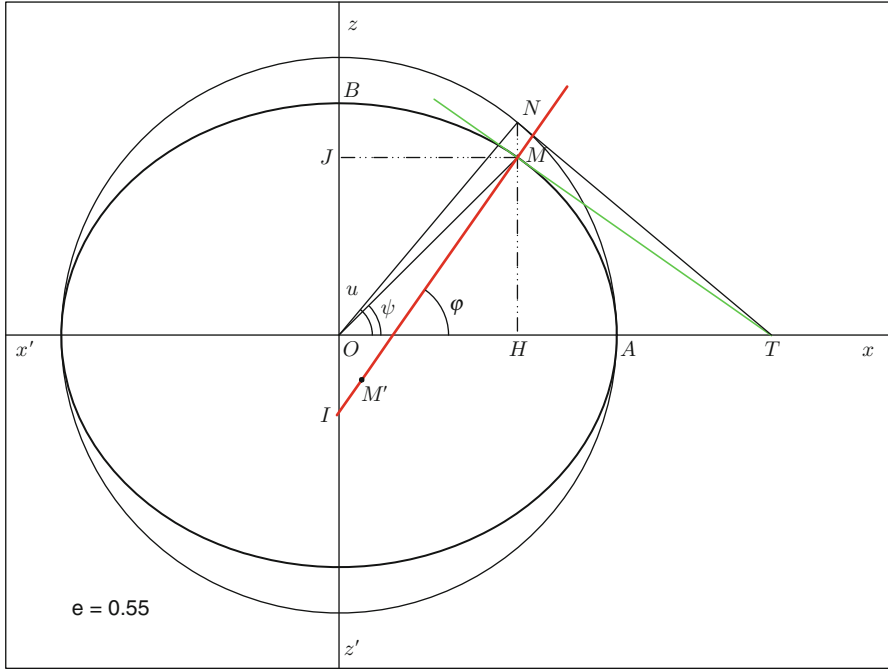
- Latitudes are measured in the right-handed trigonometric sense from  $-90^\circ$  to  $+90^\circ$ , which gives values  $[+N/-S]$ , positive for the north and negative for the south.

## Coordinates on the Ellipsoid

Let us now model the Earth as an ellipsoid of revolution, with the polar axis as the axis of revolution. Consider a point  $M$  on the surface of the ellipsoid (the notion of altitude relative to this ellipsoid will be considered later). The intersection of an arbitrary meridian plane with the ellipsoid will be an ellipse with center  $O$ . We set  $a = OA$  and  $b = OB$  (see Fig. 2.2), where  $A$  is a point on the equator and  $B$  is the North Pole. The plane  $xOz$  is the meridian plane.

The semi-major axis  $a$  is the equatorial radius  $R_e$  and the semi-minor axis  $b$  is the polar radius  $R_p$ . This ellipse, and hence also the Earth ellipsoid, is thus determined by two quantities. We choose  $a$  and the flattening  $f$  (see Table 2.1).

From the symmetry of revolution, the point  $M$  can be identified by the longitude specified on the sphere, but for the latitude, we must think again. Indeed, the latitude was obtained historically by measuring angles between the directions of carefully selected stars and the local horizontal plane (or



Latitude	Symbol	Reference direction	Angle
Geocentric	$\psi$	Center of the Earth	$\psi = (\mathbf{OA}, \mathbf{OM})$
Geodetic	$\varphi$	Normal to the ellipsoid	$\varphi = (\mathbf{OA}, \mathbf{IM})$
Geographic	$\varphi'$	Normal to the geoid	$\varphi' = (\mathbf{OA}, [\text{plumb line at } M])$
Parametric	$u$	Center of the Earth	$u = (\mathbf{OA}, \mathbf{ON})$

FIG. 2.2 : Different definitions of latitude at a point  $M$ .

the direction of a plumb line, which is perpendicular to it). In Fig. 2.2, the latitude of the point  $M$  corresponds to the angle between the sightline to the north (say, the pole star, sightline  $MN$ , parallel to the polar axis  $OB$ ) and the tangent to the ellipse at  $M$ . This angle is equal to  $\varphi = (\mathbf{OA}, \mathbf{IM})$ , angle between the normal to the ellipse and the equatorial radius, called the *geodetic latitude*.<sup>3</sup>

The *geographic latitude*, also called the *astronomical latitude*, which is measured “in the field”, takes the plumb line as reference, rather than the normal to any theoretical ellipsoid of reference. The plumb line hangs perpendicu-

<sup>3</sup>The word “geodesy” comes from the New Latin *geodesia*, as attested in the sixteenth century. This in turn came from the Greek, and in particular from the prefix *geo-*, γῆ γῆ, γῆς, meaning “the Earth” or “the country”, and *-desy*, ἡ δαίς, δαίτος, meaning “share”, in the sense of equal shares distributed at mealtimes.

lar to the equipotential surface represented by the local geoid. The difference between geodetic and geographical latitude, known as the *deviation from the vertical*, is at most 3 s of arc in regions where the geoid is particularly “uneven”. This difference must be taken into account for certain very accurate measurements that will not be considered in this book.

The *geocentric latitude*  $\psi$  at the point  $M$  is defined relative to the center of the Earth:  $\psi = (\mathbf{OA}, \mathbf{OM})$ . This angle is used in particular to specify satellite positions. The various definitions of latitude are summarised in Fig. 2.2.

To find the relation between  $\psi$  and  $\varphi$ , we introduce yet another latitude with a purely geometric role, namely the *parametric latitude*  $u$  (see Fig. 2.2). Consider the principal circle of the ellipse. The parallel to  $Oz$  passing through  $M$  cuts the principal circle at  $N$ , a point used to define the parametric latitude by  $u = (\mathbf{OA}, \mathbf{ON})$ .

The point  $M$  is obtained from  $N$  by an affine transformation with axis  $Ox$ , direction  $Oz$ , and ratio  $b/a$ . We thus have

$$\tan \psi = \frac{b}{a} \tan u . \tag{2.2}$$

The affine transformation conserves contact: it transforms the tangent to the circle at  $N$  to the tangent to the ellipse at  $M$ . These tangents cut the axis  $Ox$  at the same point  $T$ . The angle  $(\mathbf{TO}, \mathbf{TM})$  is complementary to  $\varphi$  and the angle  $(\mathbf{TO}, \mathbf{TN})$  is complementary to  $u$ . This gives

$$\tan \varphi = \frac{a}{b} \tan u . \tag{2.3}$$

We deduce the relation between the two latitudes from (2.2) and (2.3), using  $f$  or  $e$ :

$$\tan \varphi = \frac{\tan \psi}{(1 - f)^2} = \frac{\tan \psi}{1 - e^2} . \tag{2.4}$$

These three latitudes always have the same sign at any given location. Their absolute values are ordered as follows:

$$|\varphi| \geq |u| \geq |\psi| ,$$

with equality only at the equator or the poles.

For small values of the flattening ( $f \ll 1$ ), (2.4) yields

$$\tan \varphi \simeq (1 + 2f) \tan \psi .$$

Setting  $\delta\varphi = \varphi - \psi$  and expanding  $\tan(\varphi - \psi)$ , we obtain

$$\tan(\varphi - \psi) = \frac{\tan \varphi - \tan \psi}{1 + \tan^2 \psi} \simeq 2f \tan \psi \cos^2 \psi = f \sin 2\psi .$$

With these small-angle approximations, the difference between the angles becomes

$$\delta\varphi \simeq f \sin 2\psi . \tag{2.5}$$

Its maximum value  $\delta\varphi_0$ , reached when  $\varphi = \pm\pi/4$ , latitude  $45^\circ$  North or South, is equal to

$$\delta\varphi_0 = \begin{cases} f = 0.0035281 & \text{(in radians),} \\ f \times 180/\pi = 0.19210 & \text{(in degrees),} \\ f \times 3600 \times 180/\pi = 692 & \text{(in arc sec).} \end{cases} \quad (2.6)$$

**Example 2.1** For the planet Earth, calculate the difference between the equatorial and polar radii, and the maximal difference of latitude  $\delta\varphi_0$ .

► Consider the values of the Earth ellipsoid WGS84 (*World Geodetic System 1984*, revised in 2004, and updated by EGM96) given in Table 2.1. The values required here are  $R_e = a$ ,  $R_p = a(1 - f)$ , with  $f = 0.0035281$ :

$$R_e = 6,378,137.000 \text{ m}, \quad R_p = 6,356,752.314 \text{ m}.$$

The difference between the two radii is

$$\delta R = R_e - R_p = f R_e = 21.285 \text{ km}.$$

For the maximal difference in the latitude values, we obtain

$$\delta\varphi_0 = f = 3.35 \text{ mrad} = 0.19^\circ = 11' 32'' = 692'',$$

which represents a difference  $\delta\ell_0$  in the field given by

$$\delta\ell_0 \simeq R_e \delta\varphi_0 \simeq f R_e = 21.3 \text{ km}.$$

Note therefore that, as long as  $f$  is much smaller than unity, the values of  $\delta R$  and  $\delta\ell_0$  are the same, because they are equal to  $f R_e$ . ◀

From (2.4), we obtain

$$\tan(\varphi - \psi) = \frac{f_o \sin 2\varphi}{1 + f_o \cos 2\varphi} \text{ with } f_o = \frac{e^2}{2 - e^2}. \quad (2.7)$$

A more accurate expansion gives

$$\varphi - \psi = f_o \sin 2\varphi - \frac{f_o^2}{2} \sin 4\varphi + \frac{f_o^3}{3} \sin 6\varphi + \dots, \quad (2.8)$$

$$\varphi - \psi = f_o \sin 2\psi + \frac{f_o^2}{2} \sin 4\psi + \frac{f_o^3}{3} \sin 6\psi + \dots. \quad (2.9)$$

For the Earth (WGS84):

$$\delta\varphi = 692.72622 \sin 2\varphi - 1.16324 \sin 4\varphi + 0.00260 \sin 6\varphi - 0.00001 \sin 8\varphi, \quad (2.10)$$

with  $\delta\varphi = \varphi - \psi$  in arc sec.



### 2.1.2 Cartesian Coordinates: Great Normal

In a Cartesian frame  $(O; x, z)$ , it is straightforward to express the coordinates of  $M$  in terms of the latitudes  $u$  or  $\psi$ , as in (1.29) or (1.36). But the geodetic latitude  $\varphi$  has the greater practical value. We use (2.3) to express the relation between  $u$  and  $\psi$ , while bringing in the eccentricity:

$$\begin{aligned} \frac{1}{\cos^2 u} &= 1 + \tan^2 u = 1 + (1 - e^2) \tan^2 \varphi \\ &= \frac{1}{\cos^2 \varphi} - e^2 \tan^2 \varphi = \frac{1}{\cos^2 \varphi} (1 - e^2 \sin^2 \varphi), \end{aligned}$$

whence

$$a \cos u = a \cos \varphi (1 - e^2 \sin^2 \varphi)^{-1/2}.$$

Furthermore,

$$\sin u = \tan u \cos u = \frac{b}{a} \tan \varphi \cos \varphi (1 - e^2 \sin^2 \varphi)^{-1/2},$$

whence, using the relation  $b^2/a = a(1 - e^2)$ ,

$$b \sin u = a(1 - e^2) \sin \varphi (1 - e^2 \sin^2 \varphi)^{-1/2}.$$

Equation (1.29) thus gives

$$\mathbf{OM} = \begin{pmatrix} x = a \frac{\cos \varphi}{\sqrt{(1 - e^2 \sin^2 \varphi)}} \\ z = a \frac{(1 - e^2) \sin \varphi}{\sqrt{(1 - e^2 \sin^2 \varphi)}} \end{pmatrix}. \tag{2.11}$$

The normal to the ellipse at  $M$  cuts the axis  $z'Oz$  at  $I$ . In geodesy, the length  $IM$  is sometimes called the *great normal* (see Fig. 2.2). It is denoted by  $\mathcal{N}$ .

Since  $x = IM \cos \varphi$ , we deduce the value of  $\mathcal{N}$  from (2.11):

$$\mathcal{N} = \frac{a}{\sqrt{1 - e^2 \sin^2 \varphi}}, \tag{2.12}$$

and the plane Cartesian coordinates of  $M$  can be written in the form

$$\mathbf{OM} = \begin{pmatrix} x = \mathcal{N} \cos \varphi \\ z = \mathcal{N}(1 - e^2) \sin \varphi \end{pmatrix}. \tag{2.13}$$

We can now obtain the coordinates of  $I$ , where  $OI = z - \mathcal{N} \sin \varphi$ :

$$\mathbf{OI} = \begin{pmatrix} 0 \\ -\mathcal{N}e^2 \sin \varphi \end{pmatrix}. \tag{2.14}$$

The coordinates (geodetic latitude  $\varphi$ , longitude  $\lambda$ ) of  $M$  on the ellipsoid are therefore

$$\mathbf{OM} = \begin{pmatrix} x = \mathcal{N} \cos \varphi \cos \lambda \\ y = \mathcal{N} \cos \varphi \sin \lambda \\ z = \mathcal{N}(1 - e^2) \sin \varphi \end{pmatrix}. \quad (2.15)$$

### 2.1.3 Radius of Curvature

The center of the radius of curvature  $M'$  lies between  $I$  and  $M$ . We use (1.43) to calculate  $\rho$  as a function of  $\varphi$ . To begin with,

$$a^2 \sin^2 u + b^2 \cos^2 u = a^2(1 - e^2 \cos^2 u) = a^2 \frac{1 - e^2}{1 - e^2 \sin^2 \varphi},$$

whence we obtain  $\rho(\varphi)$  as

$$\rho = a \frac{1 - e^2}{(1 - e^2 \sin^2 \varphi)^{3/2}}, \quad (2.16)$$

which can also be written

$$\rho = \mathcal{N} \frac{1 - e^2}{1 - e^2 \sin^2 \varphi}. \quad (2.17)$$

For small values of the flattening, (2.16) becomes

$$\frac{\rho}{a} \simeq 1 + \left( \frac{3}{2} \sin^2 \varphi - 1 \right) e^2. \quad (2.18)$$

In this case, the radius of curvature is equal to the equatorial radius, whatever the value of  $e$ , for two values of the latitude, viz.,  $\varphi = \pm \arcsin \sqrt{2/3}$ :

$$\rho = a \iff \varphi \simeq 54.7^\circ \text{N or } 54.7^\circ \text{S}. \quad (2.19)$$

### 2.1.4 Radius of the Ellipse

The “natural” variable to use for the radius of the ellipse, denoted  $R_\psi$ , is the geocentric latitude  $\psi$ , as we saw previously [see (1.38) on p. 20]. However, if we wish to express this radius as a function of the geodetic latitude  $\varphi$ , the resulting formula is more involved:

$$R_\psi(\varphi) = a \frac{\sqrt{(1 - e^2)^2 \sin^2 \varphi + \cos^2 \varphi}}{\sqrt{1 - e^2 \sin^2 \varphi}} = \mathcal{N} \sqrt{(1 - e^2)^2 \sin^2 \varphi + \cos^2 \varphi}. \quad (2.20)$$

Note the relation obtained with the projection of  $OM$  on the axis  $Ox$ :

$$R_\psi \cos \psi = \mathcal{N} \cos \varphi. \quad (2.21)$$

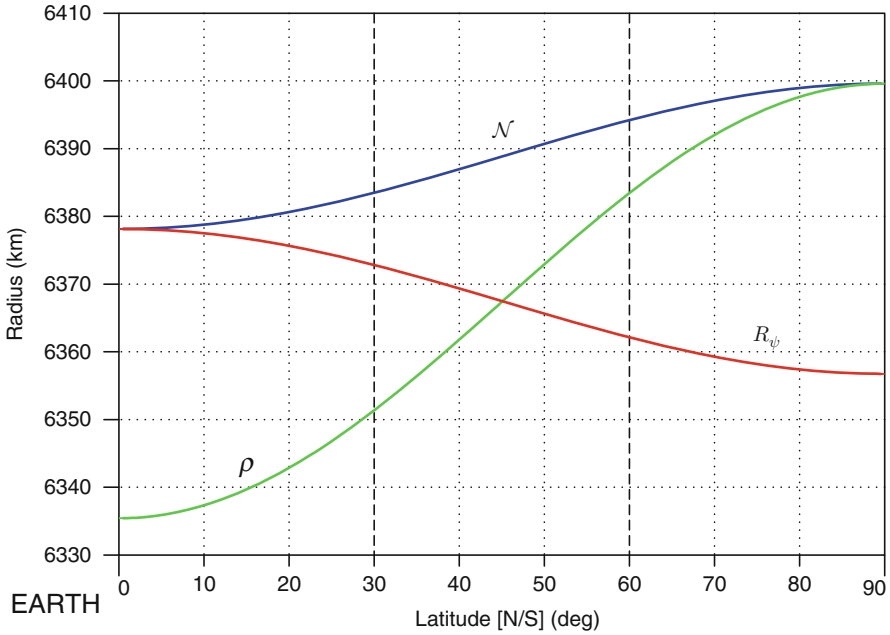


FIG. 2.3: Different radii relating to the Earth ellipsoid: radius of curvature  $\rho$  in the meridian plane, the great normal  $\mathcal{N}$ , and the radius of the ellipsoid  $R_\psi$ .

### 2.1.5 Degrees of Latitude and Longitude

#### Distance Along a Meridian or a Parallel

Let us return to the Earth ellipsoid and evaluate the distance corresponding to an infinitesimal increase in the latitude (or the longitude) along a meridian (along a parallel). Along a meridian, a change  $d\varphi$  in geodetic latitude will correspond to an elliptical arc  $dL_M$ , identified at this point with the arc of the osculating circle, or radius  $\rho_M = M'M$  [see Fig. 2.2 and (2.16) or (2.17)]:

$$dL_M = \rho_M d\varphi, \quad \text{with } \rho_M = \rho. \tag{2.22}$$

Along a parallel, a change  $d\lambda$  in longitude will correspond to a circular arc  $dL_P$  in a plane perpendicular to the polar axis, of radius  $\rho_P = JM$  [see Fig. 2.2 and (2.12)]:

$$dL_P = \rho_P d\lambda, \quad \text{with } \rho_P = \mathcal{N} \cos \varphi. \tag{2.23}$$

Figure 2.3 shows the changes in the various radii as a function of the latitude, whether it be a radius of curvature, like  $\rho$  (for  $\rho_M$ ) or  $\mathcal{N}$  (for  $\rho_P / \cos \varphi$ ), or the

Latitude $\varphi$	1° latitude $\Delta L_M$	→ $\Delta L_P / \cos \varphi$	1° longitude $\Delta L_P$	Arc $\mathcal{L}(\varphi)$	Historical $\mathcal{L}_h(\varphi)$
0	110.574	111.319	111.319	0.000	0.000
5	110.583	111.322	110.899	552.885	553.074
10	110.608	111.331	109.639	1,105.855	1,106.223
15	110.649	111.344	107.550	1,658.990	1,659.520
20	110.704	111.363	104.647	2,212.366	2,213.032
25	110.773	111.386	100.950	2,766.054	2,766.823
30	110.852	111.413	96.486	3,320.114	3,320.946
35	110.941	111.442	91.288	3,874.593	3,875.444
40	111.035	111.474	85.394	4,429.529	4,430.349
45	111.132	111.506	78.847	4,984.944	4,985.683
50	111.229	111.539	71.696	5,540.847	5,541.451
55	111.324	111.570	63.994	6,097.230	6,097.648
60	111.412	111.600	55.800	6,654.073	6,654.255
65	111.493	111.627	47.176	7,211.339	7,211.241
70	111.562	111.650	38.187	7,768.981	7,768.561
75	111.618	111.669	28.902	8,326.938	8,326.162
80	111.660	111.683	19.393	8,885.140	8,883.982
85	111.685	111.691	9.735	9,443.509	9,441.951
90	111.694	111.694	0.000	10,001.966	10,000.000

TABLE 2.2 : *One degree of latitude and longitude as a function of latitude  $\varphi$ . Reference ellipsoid: WGS84. Length  $\Delta L_M$  in km on the meridian for  $\Delta\varphi = 1$  degree of latitude. Length  $\Delta L_P$  in km on the parallel for  $\Delta\lambda = 1^\circ$  of longitude. Length  $\mathcal{L}$  of the meridian arc in km, measured from the equator. A historical value of the arc length  $\mathcal{L}_h$  is also given, using the reference ellipsoid of Delambre and Méchain which served to define the standard metre.*

radius of the ellipse, like  $R_\psi(\varphi)$ . Note also the ranges of these variations for the Earth, between the equator and the pole (all monotonic in  $[0, \pi/2]$ ):

- $\rho$  varies between  $b^2/a$  and  $a^2/b$ , i.e., between 6,335.439 and 6,399.594 km.
- $\mathcal{N}$  varies between  $a$  and  $a^2/b$ , i.e., between 6,378.137 and 6,399.594 km.
- $R_\psi$  varies between  $a$  and  $b$ , i.e., between 6,378.137 and 6,356.752 km.

### Change of One Degree

It is perhaps more meaningful to replace the infinitesimal change of angle by a change of one degree,<sup>4</sup> which remains small compared with the whole circumference. Table 2.2 gives the value  $\Delta L_M$  for the length along the meridian of an arc of  $1^\circ$  around a central value  $\varphi$  of the geodetic latitude. Likewise,  $\Delta L_P$

<sup>4</sup>In the navy, the *nautical mile* is defined as the distance equivalent to  $1'$  of arc of latitude, with the relation  $1 \text{ nautical mile} = 40 \times 10^6 / (360 \times 60) = 1\,851.851 \text{ m}$ . The second of arc is equivalent to  $1'' = 1 \text{ nm} / 60 = 30.864 \text{ m}$ . The speed is obtained directly in nautical miles per hour by spacing knots every 15.432 m (equivalent to  $0.5''$  of arc) and measuring the rate at which the knots go by for a period of 30 s (or 0.5 min).

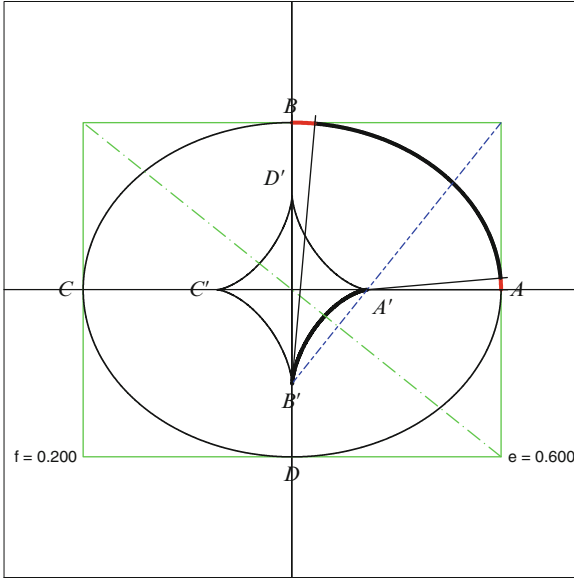


FIG. 2.4 : Length of  $1^\circ$  of latitude at the surface of the ellipsoid as a function of the latitude. Different distances correspond to equal angles, and the effect increases toward the poles. Angular difference in geodesic latitude represented in the figure:  $5^\circ$ .

is the length along the parallel  $\varphi$  of an arc of  $1^\circ$  longitude. It is interesting to compare  $\Delta L_P / \cos \varphi$  with  $\Delta L_M$  (Fig. 2.4).

### 2.1.6 Meridian Arc Length

#### Arc Length of an Ellipse

In the general case, the length of arc of the ellipse, which we denote by  $\mathcal{L}(\varphi)$ , is calculated as an incomplete elliptic integral of the second kind, as in (1.30). Such integrals are usually carried out with the help of expansions using the Wallis integrals.

For a small value of the flattening, Levallois notes that direct integration gives results that are just as accurate and which converge more quickly. Consider an element  $dL_M$  of the meridian arc:

$$dL_M = \rho d\varphi = a(1 - e^2)(1 - e^2 \sin^2 \varphi)^{-3/2} d\varphi .$$

This can be expanded as follows:

$$dL_M \simeq a(1 - e^2) \left( 1 + \frac{3}{2}e^2 \sin^2 \varphi + \frac{15}{8}e^4 \sin^4 \varphi + \frac{105}{48}e^6 \sin^6 \varphi + \dots \right) d\varphi ,$$

noting that terms in  $e^8$  and beyond, neglected here, contribute less than 1 mm in the arc length of the Earth meridian. The sine functions are linearised using the Moivre formula:

$$2 \sin^2 \varphi = 1 - \cos 2\varphi, \quad 8 \sin^4 \varphi = 3 - 4 \cos 2\varphi + \cos 4\varphi,$$

$$32 \sin^6 \varphi = 10 - 15 \cos 2\varphi + 6 \cos 4\varphi - \cos 6\varphi.$$

We thus obtain an expression for  $dL_M$  that can be integrated term by term from 0 up to the latitude  $\varphi$ :

$$\mathcal{L}(\varphi) = \int_0^\varphi dL_M. \quad (2.24)$$

The meridian arc length  $\mathcal{L}(\varphi)$  is then

$$\mathcal{L}(\varphi) \simeq a(1 - e^2)A(\varphi), \quad (2.25)$$

where

$$A(\varphi) = A_0\varphi - \frac{3}{8}A_2e^2 \sin 2\varphi + \frac{15}{256}A_4e^4 \sin 4\varphi - \frac{35}{3072}A_6e^6 \sin 6\varphi$$

and

$$A_0 = 1 + \frac{3}{4}e^2 + \frac{45}{64}e^4 + \frac{175}{256}e^6,$$

$$A_2 = 1 + \frac{5}{4}e^2 + \frac{175}{128}e^4, \quad A_4 = 1 + \frac{7}{4}e^2, \quad A_6 = 1.$$

A length of great historical importance was the quarter meridian, i.e., the arc length of the meridian from the equator to the pole:

$$\mathcal{L}\left(\frac{\pi}{2}\right) = \frac{\pi}{2}a(1 - e^2)A_0. \quad (2.26)$$

Expanding to second order in  $e$ , this yields

$$\mathcal{L}\left(\frac{\pi}{2}\right) \simeq \frac{\pi}{2}a \left(1 - \frac{e^2}{4}\right) \simeq \frac{\pi}{2}a \left(1 - \frac{f}{2}\right) = \frac{\pi}{2} \frac{a+b}{2}, \quad (2.27)$$

already given in (1.35). For the Earth,

$$e^2 \simeq 1/150 \simeq 6.7 \times 10^{-3}, \quad e^4 \simeq 1/22500 \simeq 4.4 \times 10^{-5}.$$

### Lengths of the Meridian and the Equator

The full length of the meridian  $L_M$  going right around the globe (the ellipsoid) and the full length of the equator  $L_{P/\text{equator}}$  are

$$L_M = 2\pi a(1 - e^2)A_0, \quad L_{P/\text{equator}} = 2\pi a.$$

Numerical values are given in Table 2.3.

Ellipsoid	Length of the meridian (m)	Length of the equator (m)
Delambre and Méchain (creation of the metre)	40,000,000	40,059,944
WGS84 (and current ellipsoids)	40,007,864	40,075,016

TABLE 2.3: *Lengths of the meridian and the equator. Historical values (definition of the metre) and current values, in metres.*

## 2.2 Altitude Relative to the Ellipsoid

### 2.2.1 Definition of Geodetic Altitude and Nadir

Consider a point  $S$  above the ellipsoid at a distance  $r$  from the point  $O$  at the center of the ellipsoid (see Fig. 2.5). Its longitude is  $\lambda$ . If  $S$  is identified by the geocentric latitude  $\psi = (\mathbf{Ox}, \mathbf{OS})$ , its Cartesian coordinates are, as obtained in (2.1),

$$\mathbf{OS} = \begin{pmatrix} x = r \cos \psi \cos \lambda \\ y = r \cos \psi \sin \lambda \\ z = r \sin \psi \end{pmatrix}. \quad (2.28)$$

The point  $T$  is the intersection of  $OS$  and the ellipsoid. If  $S$  is identified by the geodetic latitude  $\varphi = (\mathbf{Ox}, \mathbf{IS})$ , its Cartesian coordinates are, adapting (2.15) and denoting the great normal by  $\mathcal{N} = IS$ ,

$$\mathbf{OS} = \begin{pmatrix} x = (\mathcal{N} + h) \cos \varphi \cos \lambda \\ y = (\mathcal{N} + h) \cos \varphi \sin \lambda \\ z = [\mathcal{N}(1 - e^2) + h] \sin \varphi \end{pmatrix}, \quad (2.29)$$

where  $h = SN$  is called the *geodetic altitude* or *ellipsoidal height*, that is, the distance between the point  $S$  and the base  $N$  of the normal to the ellipsoid.

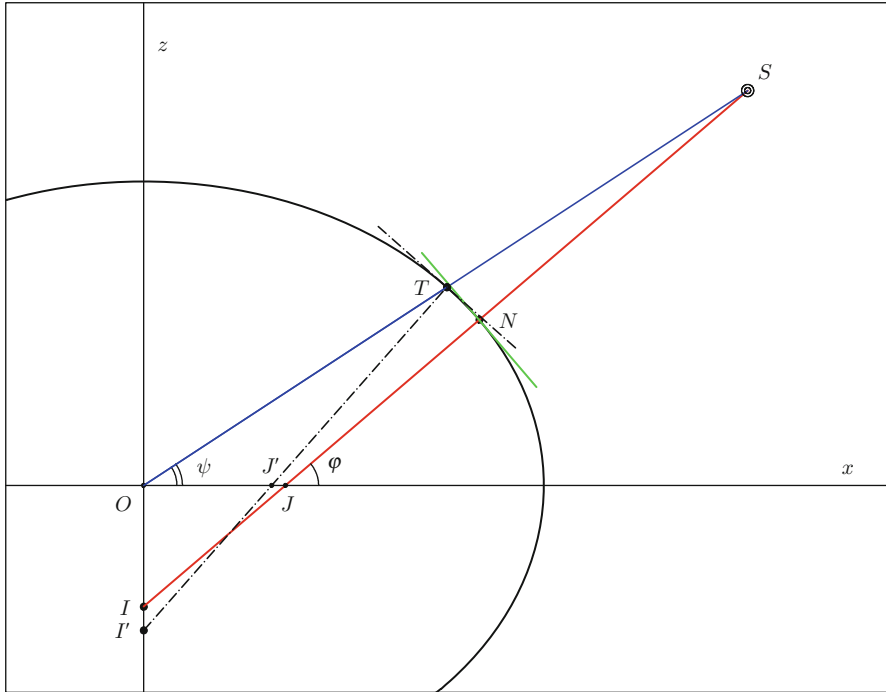
In the terminology of space mechanics,  $S$  represents a satellite,  $O$  the center of attraction (the center of the Earth),  $T$  the *ground track* (or *geocentric ground track*), and  $N$  the *nadir*<sup>5</sup> (or *geodetic ground track*, or *subsatellite point*).

### 2.2.2 Latitude Related to Geodetic Altitude

The angles used to determine these quantities are shown in Fig. 2.5. Note that, although  $\psi$  and  $\varphi$  are both related to the point  $S$ , these angles do not refer to the same point on the surface of the ellipsoid.

---

<sup>5</sup>The nadir is the direction given by the vertical, but in the downward direction. The opposite direction is the zenith. The word “nadir” comes from the Arabic *nādir*, from the root of the verb “to look towards”.



Symbol	Latitude	Latitude	Angle
$\psi$	Geocentric, of $T$	Geocentric, of $S$	$\psi = (\mathbf{Ox}, \mathbf{OS})$
$\varphi_T$	Geodetic, of $T$	–	$\varphi_T = (\mathbf{Ox}, \mathbf{I'T})$
$\psi_N$	Geocentric, of $N$	–	$\psi_N = (\mathbf{Ox}, \mathbf{ON})$
$\varphi$	Geodetic, of $N$	Geodetic, of $S$	$\varphi = (\mathbf{Ox}, \mathbf{IS})$

FIG. 2.5 : Representation of the geodetic latitude  $\varphi$  and the geocentric latitude  $\psi$  of the point  $S$ . Shown are the ground track  $T$  and the nadir  $N$ , together with the geodetic altitude or ellipsoidal height  $SN$ .

The point  $S$  is considered to be perfectly determined in space by its Cartesian coordinates  $(x, y, z)$ , or equivalently by its geocentric spherical coordinates  $(r, \psi, \lambda)$  [see (2.28)]. Regarding its geodetic coordinates  $(h, \varphi, \lambda)$ , only the longitude is easily obtained:

$$\lambda = \arctan \frac{y}{x}, \quad \text{with } \text{sign}(\lambda) = \text{sign}(y), \text{ for } [+E/-W]. \quad (2.30)$$

It is more difficult to obtain  $h$  and  $\varphi$ , bearing in mind that they are related. Let us begin by examining the relationship between the geocentric and geodetic latitudes of  $S$ . Equations (2.28) and (2.29) give

$$r \cos \psi = (\mathcal{N} + h) \cos \varphi, \quad r \sin \psi = [\mathcal{N}(1 - e^2) + h] \sin \varphi,$$



whence

$$\frac{\tan \psi}{\tan \varphi} = 1 - \frac{\mathcal{N}}{\mathcal{N} + h} e^2, \tag{2.31}$$

or again,

$$\tan \varphi = \left( 1 - \frac{e^2}{1 + h/\mathcal{N}} \right)^{-1} \tan \psi. \tag{2.32}$$

This immediately shows the limiting values of  $\varphi$ :

- For  $h = 0$ ,  $\tan \varphi = (1 - e^2)^{-1} \tan \psi \implies \varphi = \varphi_T$ .
- For  $h \rightarrow \infty$ ,  $\tan \varphi = \tan \psi \implies \varphi = \psi$ .

The geodetic latitude of  $S$  lies between the geodetic latitude of the ground track  $T$  and its geocentric latitude.

### 2.2.3 Determining the Geodetic Altitude and Nadir

The coordinates  $h$  and  $\varphi$  can be obtained iteratively, by approximation, or directly. We consider each in turn.

#### Iterative Method

Let  $P$  be the projection of  $OS$  on the equatorial plane:

$$P = \sqrt{x^2 + y^2} = (\mathcal{N} + h) \cos \varphi, \tag{2.33}$$

whence the geodetic altitude  $h$  is given by

$$h = \frac{P}{\cos \varphi} - \mathcal{N}. \tag{2.34}$$

The projection of  $OS$  on the polar axis  $Oz$  is  $z = P \tan \psi$ , and using (2.31), we have

$$\frac{z}{P} = \left( 1 - \frac{\mathcal{N}}{\mathcal{N} + h} e^2 \right) \tan \varphi,$$

and hence,

$$\varphi = \arctan \left[ \frac{z}{P} \left( 1 - \frac{e^2}{1 + h/\mathcal{N}} \right)^{-1} \right]. \tag{2.35}$$

We then proceed as shown in Table 2.4. Convergence is very fast. In fact, two or three iterations give the result to high accuracy.

◦ 0 ◦	Ellipsoid: $a = R_e$ , $e^2 = f(2 - f)$
◦ 1 ◦	Data: $x, y, z \implies P = \sqrt{x^2 + y^2}$ , $\psi = \arctan(z/P)$
◦ 2 ◦	Initialisation: $\varphi_1 = \psi$
◇ 3 ◇	Start loop $i = 1, \dots, n$
• 4 •	$N_i = a (1 - e^2 \sin^2 \varphi_i)^{-1/2}$
• 5 •	$h_i = \frac{P}{\cos \varphi_i} - N_i$
• 6 •	$\varphi_i = \arctan \left[ \frac{z}{P} \left( 1 - \frac{e^2}{1 + h_i/N_i} \right)^{-1} \right]$
• 7 •	Test $\varphi_i \mapsto \diamond 3 \diamond$ or $\diamond 8 \diamond$
◇ 8 ◇	End loop
◦ 9 ◦	Results

TABLE 2.4: Iterative method for obtaining the height  $h$  and latitude  $\varphi$  of the nadir (subsattellite point).

### Approximation Method

In the triangle  $ONS$  shown in Fig. 2.5, the angle at  $O$  (equal to  $\psi - \psi_N$ ) and the angle at  $S$  (equal to  $\varphi - \psi$ ) are both small, in fact, always less than  $0.19^\circ$  for the Earth ellipsoid. This justifies trigonometric approximations leading to the following formulas:

$$\varphi = \psi + \frac{f}{\eta} \sin 2\psi + \frac{f^2}{\eta^2} \left( 1 - \frac{\eta}{4} \right) \sin 4\psi, \quad (2.36)$$

$$\frac{h}{R_e} = (\eta - 1) + f \frac{1 - \cos 2\psi}{2} + \frac{f^2}{\eta} \left( 1 - \frac{\eta}{4} \right) \frac{1 - \cos 4\psi}{4}, \quad (2.37)$$

using the *reduced distance*  $\eta$  defined by

$$\eta = \frac{r}{a}, \quad (2.38)$$

where  $r$  is the distance  $OS$  and  $a$  the semi-major axis of the ellipsoid,<sup>6</sup> here  $a = R_e$ .

### Direct Method

The Borkowski algorithm can be used to obtain the values of  $\varphi$  and  $h$  directly. It exploits the fact that this problem reduces to a fourth order polynomial equation. This is rather difficult to solve, and indeed, much more involved than the two preceding methods, while the gain in accuracy is almost negligible. The three methods agree to within  $10^{-4}$  degrees for the angles.

<sup>6</sup>Note that  $\eta = 1$  only corresponds to  $h = 0$  in the equatorial plane for  $\psi = 0$ . If we set  $\eta = 1$  with  $\psi = \pi/2$  in (2.37), we obtain  $h/R_e = f$ , or  $h = R_e - R_p$ . At the poles, zero altitude  $h = 0$  corresponds to  $\eta = 1 - f$ .

### Some Remarks Concerning Altitude and Latitude

For a given point  $S$ , we define the difference in latitude  $\delta\varphi$  by

$$\delta\varphi = \delta\varphi(h, \psi) = \varphi - \psi. \tag{2.39}$$

We define also the difference in altitude:

$$\delta h = \delta h(h, \psi) = h' - h, \tag{2.40}$$

where  $h' = ST$  is the geocentric altitude. Since the tangent to the ellipse lies outside the ellipse,  $h'$  is always greater than  $h$  ( $h$  is the smallest distance between  $S$  and the ellipsoid).

With  $r = OS = OT + TS = R_\psi + h'$ , the relative distance  $\eta$  is equal to  $(R_\psi + h')/R_e$ . Using (1.39), we deduce that

$$\frac{h'}{R_e} = \eta - \frac{R_\psi}{R_e} = (\eta - 1) + f \frac{1 - \cos 2\psi}{2} + o(f^2). \tag{2.41}$$

Comparing (2.39) and (2.36), then (2.41) and (2.37), we see that  $\delta\varphi$  is a small quantity, proportional to  $f$ , while  $\delta h$  is another small quantity, proportional to  $f^2$ . In the triangle  $SNT$  shown in Fig. 2.5, the arc  $NT$  is almost proportional to the angle at  $S$  (equal to  $\delta\varphi$ ), hence proportional to  $f$ , whereas the difference between the sides  $SN$  and  $ST$  depends, if we write down the distances, on the square of  $f$ .

Figure 2.6 shows the dependence of the latitude difference  $\delta\varphi = \delta\varphi(h, \psi)$  on the latitude (varying from  $0^\circ$  to  $90^\circ$ ) and the altitude (varying from 0 to infinity).

**Example 2.2** *Calculating the differences  $\delta\varphi$  and  $\delta h$ , as defined above, for two satellites, one in low Earth orbit (LEO) and the other in medium Earth orbit (MEO).*

► For the low Earth orbit (LEO), we choose the satellite SPOT-5 (average height at the equator 822.3 km, inclination  $i = 98.670^\circ$ ). Results are given for latitudes in steps of  $15^\circ$ , starting from  $0^\circ$ , the extreme latitude being  $|\psi| = 180^\circ - i = 81.330^\circ$ . We give the three angles  $\psi$  (geocentric latitude of the satellite  $S$ ),  $\varphi_T$  (geodetic latitude of its ground track  $T$ ),  $\varphi$  (geodetic latitude of the nadir  $N$  and hence of the satellite  $S$ ), and also the difference  $|\delta\varphi|$ . In addition,  $h$  is the geodetic altitude and  $h'$  the geocentric altitude. The quantity  $\delta h$  is at most a few metres.

We give the corresponding results for a medium Earth orbit (MEO) satellite, choosing one component of the Navstar/GPS constellation, namely, the satellite Navstar-2RM-6 (average altitude at the equator 20,182.3 km, inclination  $i = 55.284^\circ$ ). The extreme latitude is in this case  $|\psi| = i = 55.284^\circ$ .

All the results are displayed in Table 2.5. Technical data on satellite orbits: calculations using *Ixion* with NORAD initialisation. SPOT-5, Revolution 34006, Date 2008-11-24. Navstar-2RM-6 [PRN 07], Revolution 510, Date 2008-11-22. ◀

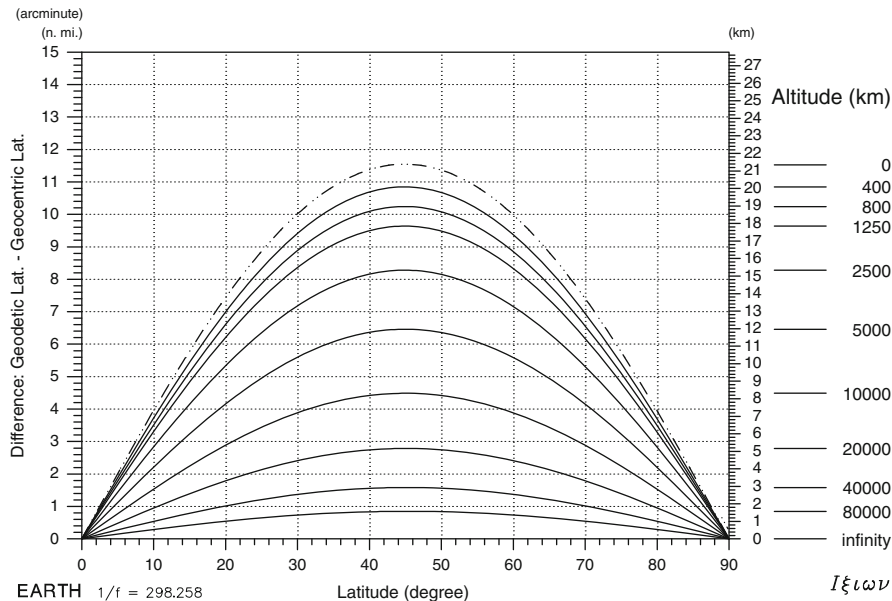


FIG. 2.6 : Latitudinal dependence of  $\delta\varphi = \varphi - \psi$ , the difference between the geodetic latitude  $\varphi$  and the geocentric latitude  $\psi$ , for a point  $S$  representing a satellite. Each curve corresponds to a specific altitude of  $S$ , indicated on the right opposite the highest point of the curve. The value of  $\delta\varphi$  is given in arc minutes (ordinate on the left) and in kilometres corresponding to the distance on the ground (right). Recall that  $1'$  of latitude = 1 nautical mile of distance. The variable on the abscissa is indicated as “latitude” because it is impossible to distinguish the two latitudes for this coordinate. For each altitude, the maximum is attained at latitude  $45^\circ$ .

## 2.3 A Little History

### 2.3.1 Before the Enlightenment

If humanity had applied the principle of Saint Thomas—seeing is believing—we would have had to wait for Gagarin before we could say “the Earth is round”. But fortunately for the human intellect, this fact has been known for a long time now, and no satellites were involved in discovering or checking it. However, as we shall see, it is mainly thanks to satellites that we have been able to refine, to a very high level of accuracy, our knowledge of the true shape of the Earth, and indeed, the shapes of other planets in the Solar System.

The oldest description of the real world that has come down to us is to be found in Homer’s *Odyssey*. The *aoidos* describes Ulysses’ return journey, with his 10 years of wandering in the Mediterranean. The whole trip can be reconstructed to establish a geographical map of the world as it was perceived

S	$\psi$ (degrees)	$\varphi_T$ (degrees)	$\varphi$ (degrees)	$ \delta\varphi $ (degrees)	$h$ (km)	$h'$ (km)	$\delta h$ (km)
L	0.000	0.000	0.000	0.000	822.011	822.011	0.000
	14.963	15.059	15.048	0.085	823.341	823.341	0.000
	29.957	30.124	30.105	0.148	827.187	827.190	0.003
	44.992	45.185	45.162	0.170	832.510	832.514	0.004
	59.987	60.153	60.134	0.147	837.849	837.851	0.002
	74.905	75.002	74.991	0.086	841.777	841.778	0.001
	81.330	81.387	81.381	0.051	842.796	842.796	0.000
	-0.022	-0.022	-0.022	0.000	822.631	822.631	0.000
	-81.330	-81.387	-81.381	0.051	843.647	843.647	0.000
M	0.000	0.000	0.000	0.000	20,240.459	20,240.459	0.000
	14.965	15.061	14.988	0.023	20,235.031	20,235.039	0.008
	29.874	30.040	29.914	0.040	20,226.316	20,226.338	0.022
	44.981	45.174	45.027	0.046	20,211.941	20,211.969	0.027
	55.284	55.464	55.327	0.043	20,184.322	20,184.346	0.023
	-0.027	-0.027	-0.027	0.000	20,124.195	20,124.195	0.000
	-55.284	-55.464	-55.327	0.043	20,208.988	20,209.010	0.023

TABLE 2.5 : Geodetic latitude  $\varphi$  and geodetic altitude  $h$  for two satellites ( $S$ ), one in an LEO orbit ( $L$ ), like SPOT-5, and the other in an MEO orbit ( $M$ ), like Navstar/GPS. Comparison with geocentric quantities  $\psi$  and  $h'$ . Refer to Fig. 2.5 for notation.

in ancient times: a flat disk, surrounded by the World Ocean, a great river encircling the world.<sup>7</sup>

Later on, the first suggestion that the Earth might be round also emanated from Greece. Philosophical theories, as put forward by Aristotle, had clearly incorporated the fact that, when a boat disappears at the horizon—first the hull, then the sail—it is because the sea surface is not flat but rounded, while this was corroborated by scientific theories supported by measurement, as presented by Eratosthenes with his comparative observation of the noonday sun in Alexandria and Syene. As far as we know by juggling with the length units of the day, the value found by this geometer–mathematician–astronomer for the Earth’s circumference was rather accurate.

From a geographical point of view, the Middle Ages represent a dark period. In fact, very dark. The Hereford *mappa mundi* shows that, by 1300, the perception of the world had barely evolved since the time of Homer—except for one significant change: Jerusalem had replaced Delphi as the center of the world. The so-called T and O maps, from *orbis terrarum*, represent the land mass as a T-shape, surrounded by an ocean O. These *mappæ mundi* reflect above all the overwhelming obscurantism of the age, founded on and serving the prevailing religion.

---

<sup>7</sup>At the exact center of this circular world was the Temple of Apollo in Delphi. The name Delphi, οἱ Δελφοί, ὦν in Greek, is closely related to the word ἡ δελφύς, ὄος, which means “womb”.

And then there was light. Or rather, the stage was lit again by the likes of Copernicus, Kepler, and Galileo. The Earth became round again, but this time it lost its place at the center of the Universe.

### 2.3.2 A French Affair

In its early stages, from 1666 (the foundation of the *Académie des Sciences*, by Colbert, under Louis XIV) up until around 1810, geodesy was a French affair, brilliantly developed by the learned assembly and its appendage, the Paris Observatory. There are really three stages in this fruitful development:

- (a) measurement of the Earth's radius,
- (b) measurement of the flattening of the Earth,
- (c) definition of the metre.

#### Picard's Measurement of the Earth

Father Jean Picard<sup>8</sup> carried out the first scientifically serious measurement of  $1^\circ$  of latitude in order to establish the radius of the Earth, which he assumed at the time to be spherical. With precision instruments, he used the method of triangulation<sup>9</sup> invented by the Dutch astronomer and mathematician Snellius. Picard measured (1669–1671)  $1^\circ$  on the meridian from Paris to Amiens (the so-called Paris meridian). More precisely, he established 13 triangles between Malvoisine to the south and Sourdon to the north, covering  $1^\circ 22'$ , with Villejuif–Juvisy as baseline.<sup>10</sup>

---

<sup>8</sup> *Jean-Félix Picard* (1620–1683) was a French astronomer and geodesist. He invented the sighting telescope with crosswires, which allowed him to carry out very accurate surveying, and in particular, levelling. Having determined the Earth's radius, as explained in the main text (*Mesure de la Terre*, 1671), he immediately communicated his result to Newton, who was thus able to check the relation between the accelerations and the squares of the distances, and thereby obtained a clear confirmation of his universal theory of gravitation. In another area, Picard was the first to carry out systematic measurements of the diameter of the solar disk. He observed its variations and sought the connection with climate change on Earth. His series of measurements between 1666 and 1682 was continued by La Hire from 1683 to 1718.

<sup>9</sup> Given a straight line distance to be measured in the field, the idea is to consider a chain of adjacent triangles along the straight line. The apices of the triangles are church towers or other features that are clearly visible from afar. The angles of these triangles are then measured, and if the length of one side is known, the lengths of the other two sides can be deduced by trigonometry. This yields the required distance. The side that is actually measured is called the *baseline*.

<sup>10</sup> In Picard's own words: "The cobbled road from the mill in Ville-Juive to the pavillion in Juvisy, a straight line with no significant unevenness, was considered ideal as baseline for this undertaking." Its length was very carefully measured in both directions by juxtaposition of *toises*. Today, this 11 km section of the D7 (previously the N7), which goes under the landing strips at Orly airport, is still very straight, apart from one or two recent urban adjustments. Each end is commemorated by a pyramidal marker stone.

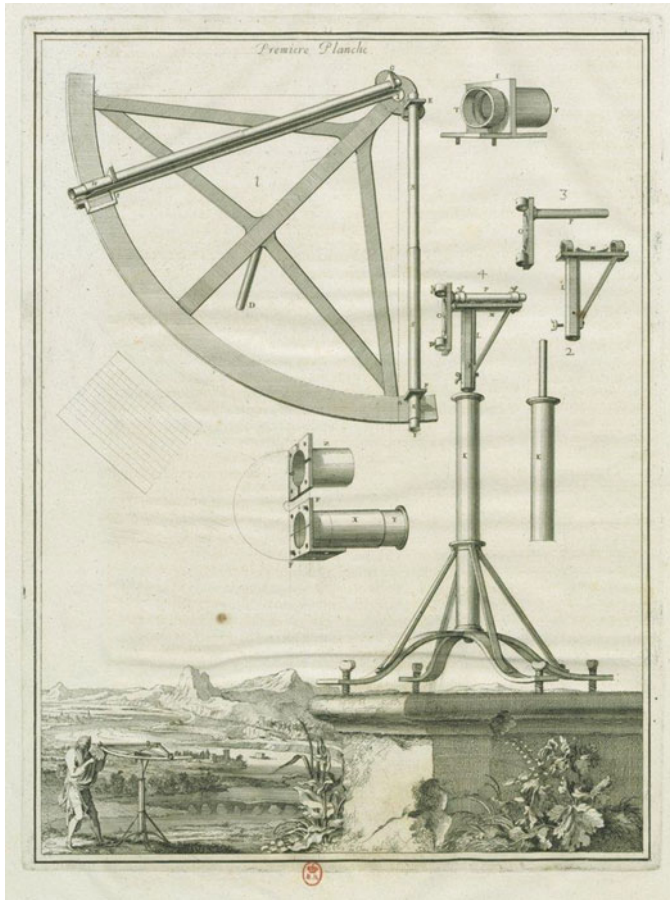


FIG. 2.7 : *Sighting and measurement instruments used for triangulation. Colour plate (p. 16) taken from La Mesure de la Terre by J. Picard, Paris, 1671.*

He found a value of 57,060 toises for  $1^\circ$  along the meridian, which corresponds to 6,372 km for the radius of the Earth. This is remarkably accurate, within 0.1% of the exact value. This is certainly due in part to the quality of the measurements (see Fig. 2.7), but also to the fact that the region measured is close to latitude  $50^\circ$ , where the radius of curvature happens to be practically equal to the radius of the Earth, as can be seen from (2.19).





FIG. 2.8 : Map of France (by Maraldi and Cassini de Thury) 1744. Detail of frontispiece. This map shows the rays observed in building up the primary triangulation network. Cartographic projection: Cassini projection.

## From Sphere to Ellipsoid

In 1672, the astronomer J. Richer was sent to French Guiana.<sup>11</sup> He noticed that the mechanical clock he had brought with him, and which had been

<sup>11</sup>As the radius of the Earth had been known since the previous year, the Academy sent Jean Richer to Cayenne to observe the parallax of Mars (the angle subtended by the Earth's diameter as viewed from Mars) in a joint effort with Picard, who had remained in Paris. By thus measuring the distance to Mars, Kepler's third law allows one to deduce the sizes of the planetary orbits. So the length scale of the whole Solar System was at this point underpinned by the Villejuif–Juvisy baseline!



scrupulously adjusted to “beat seconds” at the Paris Observatory, was losing 2 min every day (the expression *battre la seconde* in French indicates that the period is 2 s). He attributed this failing to a reduction in weight, and for him this could have only one explanation: the equator was further from the center of the Earth than Paris. He thus suggested that the Earth was flattened.

Shortly afterwards, Newton and Huygens independently showed, in 1687 and 1690, that if the Earth’s innards were more or less fluid, its daily rotation ought to transform the sphere into an ellipsoid, flattened along the polar axis. Newton obtained a value of  $f = 1/230$  by considering a uniform distribution of matter within the ellipsoid, while Huygens obtained  $f = 1/576$  by assuming that the mass of the Earth was concentrated in a central core.

In 1668, J.D. Cassini<sup>12</sup> observed the flattening phenomenon on Jupiter, which is indeed considerably flattened along the polar axis ( $f = 1/18$ ), and he measured it later for Saturn.

To measure the flattening effect on Earth, the French Academy of Sciences decided in 1683 to extend the Picard meridian to the north as far as Dunkerque and the south to Collioure, whence it would extend right across France. This

---

<sup>12</sup>The name Cassini will come up several times during this section. Indeed, there was a genuine dynasty of outstanding astronomers, often numbered with Roman numerals like the crowned heads of Europe:

- *Gian Domenico Cassini* (1625–1712), known to the French as Jean Dominique Cassini, or Cassini I, was actually of Italian origin (from Nice). He soon became famous for his work on geodesy, and especially on astronomy, with his very accurate observations of the planets Mars and Jupiter. He set up tables of the Galilean moons of Jupiter, a fundamental step in the determination of longitudes, because the eclipses of these satellites constitute instantaneous signals for an Earth-based observer. So it was really the “transfer of the century” when Louis XIV called Cassini to Paris in 1669 to entrust him with the foundation and the running of the Paris Observatory. In 1679, the observatory began to publish *La Connaissance des Temps*, a publication that is still alive today and which lists the positions of the heavenly bodies to the greatest possible accuracy. Cassini continued his observation of the moons of Jupiter, work which allowed Oläus Römer to show that the speed of light was not infinite. He also improved observations of the Moon and Saturn. This was the Cassini who gave his name to the Cassini Division of Saturn’s rings and also to the Cassini space probe, designed to explore Saturn and its environment.
- *Jacques Cassini* (1677–1756), or Cassini II, was the son of Jean Dominique. He pursued his father and Picard’s geodetic measurements, but the publication of *De la grandeur et de la figure de la Terre* (1722), in which he made a mistake over the flattening of the Earth, was later to reduce his scientific status. This was the Cassini who instigated the scientific dispute between the Cassini dynasty and Newton.
- *César François Cassini de Thury* (1714–1784), or Cassini III, was the son of Jacques. After assisting his father with his geodetic measurements, he devoted himself to cartography. See Fig. 2.8. In 1750, Louis XV asked him to map the whole of the kingdom. This is the Cassini who is remembered for the Cassini projection and the Cassini map of France.
- *Jacques Dominique Cassini* (1748–1845), or Cassini IV, was the son of César François. He was to finally publish the map of France in 1790.

From 1669 to 1793, the Cassinis ran the Paris Observatory, either officially or unofficially, each son succeeding his father.

work was carried out from 1700 to 1718 under the supervision of J. Cassini, Maraldi, and La Hire, see Fig. 2.8. Measurements implied a degree of latitude that was longer in the south than in the north. This in turn suggested an ellipsoid that was stretched along the polar axis, with  $f = -1/95$  ( $f$  is negative if  $b > a$ ), the opposite of what is shown in Fig. 2.4.

This was the beginning of a 20 year feud between supporters of Newton and those of the Cassinis: was the Earth shaped like an apple or a lemon?<sup>13</sup>

Between the north and the south of France, the change in latitude is not significant enough to be able to obtain a reliable result. On the recommendation of the French Academy of Sciences, the Count of Maurepas, Secretary of State for the Marine, sent two expeditions to the geodetic limits of the world, one polar, the other equinoctial:

- P.L.M. de Maupertuis,<sup>14</sup> A.C. Clairaut, and A. Celsius measured  $1^\circ$  in Lapland, on the frontier between Sweden and Finland, in 1736 and 1737.
- L. Godin, C.M. de la Condamine, and L. Bouguer measured  $1^\circ$  in Peru (in a region that has now become part of Ecuador), from 1736 to 1744, under very difficult conditions.

At the same time, in 1739 and 1740, Cassini de Thury and Father La Caille went back to Picard's meridian, and then from 1750 to 1754, La Caille went to the Cape of Good Hope and measured  $1^\circ$  in the southern hemisphere.

We can exploit these results to work out the flattening (see Table 2.6). Using (2.16), the ratio of two radii of curvature,  $\rho_1$  at  $\varphi_1$  and  $\rho_2$  at  $\varphi_2$ , yields

$$\frac{\rho_1}{\rho_2} = \left( \frac{1 - e^2 \sin^2 \varphi_2}{1 - e^2 \sin^2 \varphi_1} \right)^{3/2}.$$

Expanding to first order in  $e^2$ , we obtain

$$\frac{\rho_1}{\rho_2} = 1 - \frac{3}{4}e^2 (\cos 2\varphi_1 - \cos 2\varphi_2).$$

Since the ratio of the radii of curvature is equivalent to the ratio of the measurements  $\Delta L_M$  for  $1^\circ$ , and since  $e^2$  is almost equal to  $2f$ , this means that

$$f = \frac{2}{3} \frac{1 - \Delta L_{M1}/\Delta L_{M2}}{\cos 2\varphi_1 - \cos 2\varphi_2}. \quad (2.42)$$

<sup>13</sup>Traditionally, the contrast is illustrated by: mandarin or lemon? There seems to be an anachronism here, since the word "mandarin" did not appear in French until 1773.

<sup>14</sup>*Pierre Louis Moreau de Maupertuis* (1698–1759), a French physicist, led the expedition to Lapland. In so doing, he earned these two graceful lines from Voltaire:

*Vous allâtes vérifier en ces lieux pleins d'ennui  
Ce que Newton connut sans sortir de chez lui.*

[In this soulless landscape you are sure to construe  
What Newton in his college lodgings always knew.]

While there is probably no connection with this typical irony, Maupertuis subsequently published, in 1744, his famous *Principe de moindre action* (Principle of least action).



Name of degree	Latitude $\varphi$	$\Delta L_M$ (toises)	$\Delta L_M$ (km)
Lapland	+66° 20'	57,438	111.949
Paris	+49° 29'	57,074	111.239
Peru	-01° 30'	56,746	110.600
Cape	-33° 18'	57,037	111.167

TABLE 2.6 : Results found for the degree of latitude  $\Delta L_M$  between 1736 and 1754, for different values of the average latitude  $\varphi$ , in degrees [+N/-S]. The value of  $\Delta L_M$  is given in toises, together with the modern equivalent in kilometres.

If we calculate the flattening from the measurements  $(\Delta L_{M1}, \varphi_1)$  in Peru and  $(\Delta L_{M2}, \varphi_2)$  in Paris, we obtain

$$\frac{\Delta L_{M1}}{\Delta L_{M2}} = 0.99425, \quad \cos 2\varphi_1 - \cos 2\varphi_2 = 1.15506,$$

$$\implies f = \frac{2 \cdot 5.4769 \times 10^{-3}}{3 \cdot 1.15506} = 3.31696 \times 10^{-3} = \frac{1}{301}.$$

The measurement at the Cape of Good Hope was not retained. Its value was overestimated because the vertical was affected by the presence of mountains nearby.

The calculation of  $f$  using the Lapland degree gave results that differed too much to be accepted by the scientific community ( $f = 1/123$  and  $f = 1/207$ ), whereupon the Swedish Academy opted for a new expedition to Lapland in 1801, which would give  $\Delta L_M = 57,196$  toises, i.e., 0.42% less than the first measurement.

The use of (2.42) to calculate  $f$  is extremely sensitive to the accuracy of the measurements. If we assume that the latitudes  $\varphi_1$  and  $\varphi_2$  are known with certainty and the degree in Paris  $\Delta L_{M2}$  measured exactly, a relative error of 0.1% in the degree in Peru  $\Delta L_{M1}$  (or an error of just 57 toises per degree) would lead to an error of 17.3% in  $f$ . We find the following results:

- for  $\Delta L_{M1} = 56,803$  toises,  $1/f = 364.6$ ,
- for  $\Delta L_{M1} = 56,689$  toises,  $1/f = 257.0$ .



FIG. 2.9 : *Commemorating the revolution: for all time, for all peoples.*

As a result of all this state-of-the-art geodesy, France was the first country in the world to draw up a highly accurate map of its own territory, known as the Cassini map.<sup>15</sup>

### Definition of the Meter

*A tous les temps, à tous les peuples* (for all time, for all peoples, see Fig. 2.9), in the universal spirit of the French Revolution which characterised what was happening in France at the time, there was born the idea of offering humanity a single consistent system of physical units.

Since the length of a pendulum which “beats the second” is not independent of the latitude,<sup>16</sup> the Assembly decided on 30 March 1791 that the unit of length would be one ten-millionth part of the Earth meridian, based on a proposal by a committee whose members were Borda, Lagrange, Laplace, Monge, and Condorcet. The astronomers Delambre and Méchain were requested to make accurate measurements of the meridian arc from Dunkerque to Barcelona, towns separated by “9 and 2 thirds degrees” on the Paris meridian, and both situated by the sea.

<sup>15</sup>This map, already mentioned earlier, used a scale of 1/86,400 (one line for 100 toises). It comprised 182 sheets to cover the whole kingdom. Cassini de Thury used a novel projection, now called the Cassini projection, in which he plotted lines perpendicular to the Paris meridian. These lines are not parallels, i.e., they are not the loci of points at constant latitude, but great circles (for a spherical Earth). The perpendicular line passing through the Paris Observatory goes from Granville to Strasbourg. This projection is the transverse aspect of the projection known in French as the *plate-carrée* (flat square) projection.

<sup>16</sup>In a field with acceleration due to gravity equal to  $g$ , the period  $T$  of a pendulum of length  $l$  is given by  $T = 2\pi\sqrt{l/g}$  in SI units. With  $T = 2$  s, this gives  $l = g/\pi^2$  numerically. As  $g$  varies between the equator and the pole,  $l$  varies from 0.991 to 0.996 m. We note that the metre was chosen close to the length of this pendulum, whereas a doubled metre would have been close to the toise.

The process of triangulation was carried out<sup>17</sup> from June 1792 to the end of 1798,<sup>18</sup> with 115 triangles and two baselines, the Melun baseline (from Lieusaint to Melun) and the Perpignan baseline (from Salses to Vernet).

The result was proclaimed in June 1799. The quarter meridian, as calculated from these measurements, was

$$\mathcal{L}\left(\frac{\pi}{2}\right) = 5,130,740 \text{ toises,}$$

which was thus equal, by definition of the new unit of length, to

$$\mathcal{L}\left(\frac{\pi}{2}\right) = 10,000,000 \text{ m.}$$

The official conversion rate was thus fixed at

$$1 \text{ Châtelet toise} = 1.9490363 \text{ m.}$$

The law instating the metre<sup>19</sup> was signed on 10 December 1799 (19 frimaire An VIII in the revolutionary dating system).

Using Delambre and Méchain's ellipsoid ( $a = 6,375.738 \text{ m}$ ,  $1/f = 334$ ), which gives this definitive value for  $\mathcal{L}(\pi/2)$ , the last column of Table 2.2 shows the values of the meridian arc as a function of latitude. These can then be compared with current values. The relative error introduced by Delambre et Méchain is a mere 0.02%, which attests to the high quality of these measurements.<sup>20</sup>

### 2.3.3 Dynamical Geodesy

Modern geodesy begins with Clairaut. With his *Théorie de la figure de la Terre, tirée des principes de l'hydrostatique* (Theory of the Earth's shape, based on the principles of hydrostatics, 1743), he laid the foundations of dynamical geodesy: measurements of the acceleration due to gravity should be used, like the measurement of degrees of latitude, to determine the shape of the ellipsoid. The shape of the Earth depends on its rate of rotation along the polar axis and the distribution of mass within it.

---

<sup>17</sup>The angles were measured to an accuracy of  $1''$  of arc using Borda's repeating circle method, with instruments made by his assistant Lenoir.

<sup>18</sup>It was not a good time to be carrying out this kind of expedition. In the thick of the revolution, hauling strange-looking instruments to the tops of church towers or onto the battlements of castles was unnecessarily intriguing for the local populations. There were many unfortunate incidents, with material being sabotaged and surveyors arrested, among other things.

<sup>19</sup>Given the delays in completing the measurements, a provisional metre had been adopted on 1 August 1793. This metre would give  $\mathcal{L}(\pi/2) = 5,130,430$  toises.

<sup>20</sup>Once it had been determined relative to the Earth ellipsoid, the metre was then fixed by the General Conference on Weights and Measures (*Conférence Générale des Poids et Mesures* CGPM). In 1889 (the first CGPM), the metre was defined by the prototype deposited at the *Archives de France*. In 1960 (the 11th CGPM), it was defined in terms of a particular wavelength of light emitted by krypton 86. Since 1983 (the 17th CGPM), the metre has been defined relative to the speed of light (see Sect. 6.10).



FIG. 2.10 : *The Soviet Union remembers its conquest of space.*

Lagrange invented the notion of gravitational potential and was no longer satisfied to define the Earth ellipsoid by its flattening. In 1810, he expanded the gravitational potential of the Earth in spherical harmonics and the coefficients of this expansion provide a much better representation for the imperfections in the Earth's shape when compared with a sphere. The notion of the Earth's shape was then replaced by the "geoid". This is the equipotential surface which best fits the mean level of the oceans.

On 4 October 1957, Sputnik-1 was put into orbit (see the commemorative stamp in Fig. 2.10), and this marked the beginning of a new era of space geodesy.

# Chapter 3

## Geopotential

### 3.1 Some Preliminaries

#### 3.1.1 Reference Systems

Consider a reference frame centered on the Sun and with axes pointing to distant (fixed) stars. This is a *Copernican frame*, which we denote by  $\mathfrak{R}_0$ . Any frame  $\mathfrak{R}_1$  in uniform translational motion relative to  $\mathfrak{R}_0$  is a *Galilean frame*. In this kind of frame, experiment shows that Newton's second law<sup>1</sup> is perfectly satisfied:

$$\mathbf{F} = \frac{d(m\mathbf{v})}{dt}, \quad (3.1)$$

where  $\mathbf{F}$  is the force applied to a body of mass  $m$  and  $d\mathbf{v}/dt$  is the acceleration of the body.

Consider a frame  $\mathfrak{R}$  with origin at the center of the Earth and axes parallel to the axes of the frame  $\mathfrak{R}_1$ . Strictly speaking, this is not a Galilean frame, because the motion of the Earth around the Sun is neither linear nor uniform.

---

<sup>1</sup>*Isaac Newton* (1643–1727) was an English mathematician, physicist, and astronomer. In 1687, he stated his three laws of motion in *Philosophiæ Naturalis Principia Mathematica*: (1) the principle of inertia, (2) his famous second law, which says that, in a Galilean frame, the force is equal to mass times acceleration, and (3) the principle of action and reaction. It can be shown that (1) is a special case of (2) and that (3) can be deduced from (2). The fundamental second law (2) was not expressed in exactly this way by Newton. Combined with Kepler's law of elliptical orbits, the second law can be used to derive Newton's universal law of gravity [see (4.115)–(4.117)]. Newton's work dominated the eighteenth century, in mathematics (analysis, solution of equations) and in physics, especially in optics, with the publication of *Opticks*. Regarding Newton's date of birth, it is interesting to note that 25 December 1642 on the Julian calendar, which was still used in England at the time, corresponds to 4 January 1643 on the Gregorian calendar.

However, this motion is nevertheless slow, with one round trip per year, and above all, it is perfectly well known, so there is no difficulty in calculating the resulting apparent accelerations. In the following, this pseudo-Galilean frame  $\mathfrak{R}$  will be treated as a Galilean frame moving with the Earth.

In this book, we shall use two frames with origin  $O$  at the center of the Earth:

- The Galilean (pseudo-Galilean) frame  $\mathfrak{R}$  we have just defined, fixed relative to the orthonormal triad  $(O; x_G, y_G, z_G)$ , where  $Oz_G$  is the polar axis and  $Ox_G$  points in a fixed direction in space, i.e., toward a distant star. This is called an Earth-centered inertial (ECI) frame, or Earth-centered space-fixed (ECSF) frame.
- The terrestrial (non-Galilean) frame  $\mathfrak{R}_T$ , which is needed to describe fixed points on the Earth, fixed relative to the orthonormal triad  $(O; x_T, y_T, z_T)$ , where  $Oz_T = Oz_G$  is the polar axis, while  $Ox_T$  rotates with the Earth, remaining fixed in the prime meridian through Greenwich. This is called the Earth-centered Earth-fixed (ECEF) frame.

## Theory and Practice

The frames ECI and ECEF are used to set up all the equations in this book from the standpoint of space mechanics. The definitions here are theoretical and didactic. In contrast, the practical and technical realisation of these frames, denoted respectively by ICRF and ITRF, is the work of astronomers and geodesists. They are explained briefly in an appendix to this chapter (see Sect. 3.6).

### 3.1.2 Review of Work and Potential

#### Work, Force Field, Potential

The work done by a force  $\mathbf{F}$  applied at a point  $M$  is the scalar quantity

$$dW = \mathbf{F} \cdot d\mathbf{l} ,$$

where  $d\mathbf{l}$  is the displacement of the point of application of the force from  $M$  to  $M'$ . In an orthonormal frame, with  $\mathbf{F}(X, Y, Z)$  and  $d\mathbf{l}$  ( $dx, dy, dz$ ), the scalar product gives

$$dW = Xdx + Ydy + Zdz .$$

The total work done when the point of application of the force moves from  $A$  to  $B$  is

$$W = \int_A^B \mathbf{F} \cdot d\mathbf{l} .$$

A point  $M$  is said to be subjected to a force field if, throughout its domain of application, a force  $\mathbf{F}(X, Y, Z)$  can be associated with each position of the point  $M(x, y, z)$ .



If there is a function  $V(x, y, z)$  such that the components of the force  $\mathbf{F}(X, Y, Z)$  can be expressed in the form

$$X = \frac{\partial V}{\partial x}, \quad Y = \frac{\partial V}{\partial y}, \quad Z = \frac{\partial V}{\partial z},$$

throughout the region of definition, the field is said to derive from a *potential*. In this case, the force field is said to be *conservative*. Using the vector operator *gradient*, denoted by **grad** or  $\nabla$  and defined by  $dV = \mathbf{grad} V \cdot d\mathbf{l}$ , we can then write

$$\mathbf{F} = \mathbf{grad} V,$$

whence  $dW$  becomes

$$dW = \mathbf{grad} V \cdot d\mathbf{l},$$

which represents the exact differential  $dV$ :

$$dW = dV.$$

Integrating between points  $A$  and  $B$ ,

$$\int_A^B dW = W_A^B = V(B) - V(A).$$

This shows that the work done by the force in going from  $A$  to  $B$ , denoted by  $W_A^B$ , depends only on the values of the potential  $V$  at the points  $A$  and  $B$ , and not on any of the intermediate values taken along the intervening path. The function  $V$  is only defined up to an additive constant.

### Equipotential Surface

An *equipotential surface* is a surface of the form

$$V(x, y, z) = \text{constant}.$$

This has the following properties:

- No work is done by displacement on a given equipotential surface, which shows that the component of the force tangent to the surface is zero. An equipotential surface is an equilibrium surface.
- For the same reason, i.e., the fact that  $\mathbf{F} \cdot d\mathbf{l} = 0$ , the force is normal to each equipotential surface.
- Two equipotential surfaces cannot intersect, otherwise work could be done without ever leaving one of the equipotential surfaces.

## Potential Energy

The *potential energy*  $\mathcal{U}$  is defined in the following way in terms of the work done by a conservative force field on a moving point:

$$\int_A^B dW = W_A^B = \mathcal{U}(A) - \mathcal{U}(B) .$$

Hence,  $\mathcal{U} = -V$  and the relationship with  $\mathbf{F}$  is

$$\mathbf{F} = -\mathbf{grad} \mathcal{U} . \quad (3.2)$$

This expression involving the potential energy can be used to define the mechanical energy  $\mathcal{E}$  as the sum of the potential energy  $\mathcal{U}$  and the kinetic energy  $\mathcal{T}$ . Indeed, we can write  $dW$  in two different ways:

$$\begin{aligned} dW &= -d\mathcal{U} , \\ dW &= \mathbf{F} \cdot d\mathbf{l} = m \frac{d\mathbf{v}}{dt} \cdot d\mathbf{l} = d\left(\frac{1}{2}mv^2\right) = d\mathcal{T} . \end{aligned}$$

Hence,  $d\mathcal{U} + d\mathcal{T} = 0$ . For an isolated system subjected to a conservative force field, we thus establish conservation of mechanical energy:

$$\mathcal{E} = \mathcal{T} + \mathcal{U} = \text{constant} . \quad (3.3)$$

We usually set  $\mathcal{U}(\infty) = 0$ .

When  $\mathcal{E}$  is not constant, energy is dissipated and the force is said to be dissipative.

## 3.2 Gravitational Potential and Field

### 3.2.1 Gravity

The law of gravity, or universal law of gravitational attraction, established by Newton, states that two point bodies  $A$  and  $B$ , with masses  $M$  and  $m$ , respectively, will each exert an attractive force on the other that is proportional to their mass and inversely proportional to the square of the distance between them:

$$\mathbf{f}_{A \rightarrow B} = -\mathbf{f}_{B \rightarrow A} = -G \frac{Mm}{r^2} \mathbf{e}_r , \quad (3.4)$$

where  $\mathbf{f}_{A \rightarrow B}$  is the force exerted by  $A$  on  $B$  and  $\mathbf{AB} = \mathbf{r} = r\mathbf{e}_r$ . The gravitational constant  $G$  is not used as such in space mechanics. Instead, we use the *specific gravitational constant*  $\mu$ , which is the product of  $G$  and the mass of the relevant attracting body:

$$\mu = GM . \quad (3.5)$$

The relation (3.4) is symmetric. In order to distinguish the role of one of the two bodies, we may express the fact that body  $A$ , for example, creates a gravitational field to which body  $B$  is subjected. This field  $\mathbf{g}$  is such that

$$\mathbf{f}_{A \rightarrow B} = \mathbf{F} = m\mathbf{g} ,$$

or in terms of  $\mu$ ,

$$\mathbf{g} = -\frac{\mu}{r^2} \mathbf{e}_r . \quad (3.6)$$

There is a function  $\mathcal{U}$  such that

$$\mathbf{F} = -\mathbf{grad} \mathcal{U} = -\frac{\partial \mathcal{U}}{\partial r} \mathbf{e}_r ,$$

This can be obtained by integrating over  $r$ :

$$\mathcal{U} = -\int \mathbf{F} \cdot d\mathbf{r} = -m\frac{\mu}{r} , \quad \text{with } \mathcal{U}(\infty) = 0 . \quad (3.7)$$

We then introduce the quantity  $U = -\mathcal{U}/m$ . To sum up,  $\mathcal{U}$  is the *potential energy* of the mass  $m$  in this force field, the gravitational field.  $U$  is then the *gravitational potential* produced by the mass  $M$  at distance  $r$ :

$$U = \frac{\mu}{r} . \quad (3.8)$$

In astronomy and geodesy, the potential  $U$  is defined like this so that the leading term in the potential, viz.,  $\mu/r$ , is positive [see (3.28)].

### 3.2.2 Gauss' Theorem

In the last section, we obtained the field and gravitational potential produced by a point body of mass  $M$  located at  $A$  and acting on another point body of mass  $m$  at a point  $B$ . For a continuous distribution of matter, we must then carry out an integral to obtain the force exerted on  $B$ . For a given configuration, Gauss' theorem gives the result directly without the need for such an integration.

#### Proof of Gauss' Theorem

There are several ways to prove Gauss' theorem.<sup>2</sup> We shall use a method based on the idea of solid angle. We consider a closed surface  $S$ , enclosing a

---

<sup>2</sup> Carl Friedrich Gauß (1777–1855) was a German astronomer, mathematician, and physicist. He was extremely precocious and interested in astronomy from an early age. He invented a method for calculating the orbital elements of the planets (see the note about Piazzi), then developed powerful methods for handling the problems of celestial mechanics, such as the theory of least squares, in his work *Theoria motus corporum coelestium* (1809). In mathematics, he invented congruences (modulo) and studied quadratic forms, er-

volume  $\tau$ . We can thus define an inside and an outside. We then consider a surface element  $dS$  with unit normal  $\mathbf{n}$  pointing outwards. The flux of an arbitrary vector  $\mathbf{g}$  through this surface element is defined as

$$d\Phi = \mathbf{g} \cdot d\mathbf{S}, \quad \text{with } d\mathbf{S} = \mathbf{n} dS.$$

The total flux of  $\mathbf{g}$  out through the surface  $S$  is then given by the integral over the whole closed surface  $S$ , viz.,

$$\Phi = \oint_S \mathbf{g} \cdot d\mathbf{S}.$$

We consider a surface  $S$  surrounding a distribution of masses: the different points  $A_i$  are each attributed a mass  $M_i$ . The field created by each mass  $M_i$  at a point  $B$  is then

$$\mathbf{g}_i = -GM_i \frac{\mathbf{A}_i \mathbf{B}}{A_i B^3},$$

where  $\mathbf{A}_i \mathbf{B}$  is the vector from  $A_i$  to  $B$  and  $A_i B$  its length. The flux leaving  $S$  is

$$\begin{aligned} \Phi &= \oint_S \mathbf{g} \cdot d\mathbf{S} \\ &= G \oint_S \sum_i M_i \frac{\mathbf{A}_i \mathbf{P}}{A_i P^3} \cdot d\mathbf{S} \\ &= G \sum_i M_i \oint_S \frac{\mathbf{n} \cdot \mathbf{A}_i \mathbf{P}}{A_i P^3} dS, \end{aligned}$$

where  $P$  is a point running over  $S$ . Now,

$$\frac{\mathbf{n} \cdot \mathbf{A}_i \mathbf{P}}{A_i P^3} dS = \frac{dS \cos \alpha_i}{A_i P^2} = \frac{d\Sigma}{A_i P^2} = d\Omega_i,$$

where  $\alpha_i$  is the angle between the normal and  $\mathbf{A}_i \mathbf{P}$  and  $d\Sigma$  is the projection of  $dS$  on the plane perpendicular to  $\mathbf{A}_i \mathbf{P}$ . The quantity  $d\Omega_i$  is then the element of solid angle, represented by the infinitesimal cone with apex  $A_i$  and base the surface element  $dS$  (or  $d\Sigma$ , which comes to the same thing).

The integration over  $d\Omega_i$  is independent of the surface  $S$ . We thus take a sphere of center  $A_i$  and radius  $R$ . This gives

ror analysis (bell-shaped curve, 1821), regular polygons, conformal representations, spherical trigonometry, and the curvature of surfaces (1827). He revolutionised the field of geodesy by introducing and developing novel methods, and he was not afraid to go out into the field, e.g., setting up the cadastral survey of the Hanover region between 1817 and 1821. In physics, he carried out fundamental work on magnetism (*Allgemeine Theorie des Erdmagnetismus*, published in 1839), electricity (Gauss' theorem), and optics (Gaussian optics). His contemporaries called him the Prince of Mathematicians. So who was the king?

$$\Omega_i = \oint d\Omega_i = \oint \frac{d\Sigma}{R^2} = \frac{1}{R^2} \oint d\Sigma = \frac{4\pi R^2}{R^2} = 4\pi .$$

On the other hand, an external mass, i.e., with  $A_i$  outside  $S$ , produces a field whose flux through  $S$  is zero. Indeed, a cone with apex  $A_i$  standing on a surface element  $dS$  determines two opposing flux elements whose total contribution cancels, since  $d\Phi$  is a scalar whose sign depends on the scalar product.

Finally, letting  $M_{\text{int}} = \sum_{\text{int}} M_i$ , the sum of the masses contained within the surface  $S$ , the flux out of  $S$  is

$$\Phi = -4\pi G \sum_{\text{int}} M_i ,$$

and *Gauss' theorem* can be stated as follows:

$$\oint_S \mathbf{g} \cdot d\mathbf{S} = -4\pi G M_{\text{int}} . \quad (3.9)$$

For a continuous distribution of masses represented by the density  $\rho$  at each point of space,  $M_{\text{int}}$  is given by

$$M_{\text{int}} = \iiint_V \rho(\mathbf{r}) d\tau ,$$

where the triple integral extends over the whole volume  $V$ .

### Calculating the Field Using Gauss' Theorem

If the density depends only on  $r$  (the magnitude of  $\mathbf{r}$ ), i.e., if the mass distribution is spherically symmetric, the field it produces will also have spherical symmetry:

$$\mathbf{g}(r) = \|\mathbf{g}(r)\| \frac{\mathbf{r}}{r} .$$

It is then straightforward to calculate the flux. For the surface  $S$ , we choose a sphere of radius  $r$  containing all the mass  $M_{\text{int}}$ . From the symmetry, the field  $\mathbf{g}$  must be orthogonal to  $S$  at every point. Remembering that  $r$  is constant over the whole surface  $S$ , we obtain

$$\Phi = \oint_S \mathbf{g} \cdot d\mathbf{S} = \oint_S \|\mathbf{g}(r)\| \frac{\mathbf{r}}{r} \cdot \mathbf{n} dS = \|\mathbf{g}(r)\| \oint_S dS = 4\pi \|\mathbf{g}(r)\| r^2 .$$

Applying Gauss' theorem (3.9), we find that

$$4\pi \|\mathbf{g}(r)\| r^2 = -4\pi G M_{\text{int}} ,$$

whence the gravitational field  $\mathbf{g}$  is given by

$$\mathbf{g}(r) = -G M_{\text{int}} \frac{\mathbf{r}}{r^3} . \quad (3.10)$$

We thus obtain the following very important result: the field produced by a spherically symmetric mass distribution is the same as would be produced by a point mass of the same value located at the center of the spherical distribution. This property results from the fact that the forces are central and go as  $r^{-2}$ .

## Gravitational Field of the Earth

If we treat the Earth as spherical and assume that its density only depends on the distance from the center  $O$ , then at a point outside or on the surface of the Earth, and at distance  $r$  from  $O$ , the field produced there is

$$\mathbf{g}(r) = -\mu \frac{\mathbf{r}}{r^3} = -\frac{\mu}{r^2} \mathbf{e}_r, \quad \text{with } \mu = GM, \quad (3.11)$$

where  $M$  is the total mass of the Earth. In this case,  $\mu$  is called the *geocentric gravitational constant*.

### 3.2.3 Gravity and Weight

If we assume once again that the Earth is spherically symmetric and in addition that it is not moving relative to a Galilean frame, the equipotential surfaces will be concentric spheres. But as Galileo pointed out, the Earth is spinning on its axis, so a point subjected to the force of gravity will also suffer an inertial force relative to a non-Galilean frame fixed relative to the Earth. This is how the Earth's shape was transformed and flattened during its formation. Its outer envelope is an equipotential surface: its points are in equilibrium. If we ignore tides, currents, and winds, the ocean surface provides a faithful image of this equipotential surface,<sup>3</sup> and it is generally taken as the zero altitude. This geoid naturally extends beneath the continents. The surface of a motionless lake<sup>4</sup> also represents an equipotential surface, at another altitude, and the plumb line, which defines the local vertical, will be exactly perpendicular to this surface.

On such a surface, the potential  $U$  is constant. However, as mentioned above, the gravitational field is not constant on this equilibrium surface. Indeed, it is stronger at the poles than at the equator, since  $R_p < R_e$ , while the centrifugal acceleration is zero at the poles and maximal at the equator. We shall calculate the gravitational potential produced by a flattened planet, then the weight potential which takes into account the Earth's rotation. By integrating this potential, we will obtain the weight as a function of latitude.

Maupertuis was the first to make a clear terminological distinction between gravity and weight, a distinction that was subsequently taken up by D'Alembert<sup>5</sup> and Clairaut<sup>6</sup>:

---

<sup>3</sup>In 1742, MacLaurin showed that the ellipsoid of revolution spinning on its minor axis was the only geometrical shape that could meet requirements. Later, Poincaré showed that, for much faster rotation, there were other possibilities, but they are not relevant to the planets.

<sup>4</sup>The water is in equilibrium so there is no reason why it should flow from left to right, or from right to left!

<sup>5</sup>Jean le Rond d'Alembert (1717–1783) was a French mathematician, physicist, and philosopher. He published *Recherche sur la précession des équinoxes et sur la nutation de l'axe de la Terre dans le système newtonien*, in 1749. In 1743, he had stated the principle that carries his name in his *Traité de dynamique*. With Diderot, he wrote the *Encyclopédie*.

<sup>6</sup>“I make here the same distinction as M. de Maupertuis (*La Figure de la Terre déterminée*, etc.) between weight and gravity. By weight, I understand the natural force

- Gravity is the sum of the attractive effects acting on a mass according to the universal law of gravitation.
- Weight is the resultant of gravity and the action of the centrifugal acceleration due to the Earth's rotation.

In other words, gravity is the field measured in the frame  $\mathfrak{R}$ , while weight is the field measured in the frame  $\mathfrak{R}_T$ . Any body on the Earth is subjected to weight, while a satellite in orbit around the Earth is subjected to gravity.

## 3.3 Calculating the Geopotential

### 3.3.1 Potential Element

The temporal variation in the terrestrial mass distribution (due to land and ocean tides and phenomena linked to internal geophysical processes) and the variation in the direction of the Earth's axis of rotation (motion of the poles) are not taken into account here. We only consider the averaged effect of these phenomena over a given period and calculate the static geopotential produced by a fixed mass distribution (see Fig. 3.1).

Let  $O$  be the center of the Earth and  $(O; x, y, z)$  a coordinate system fixed relative to the Earth, like  $\mathfrak{R}_T$ , where  $Oz$  is the polar axis and  $(xOy)$  the equatorial plane. Let  $S$  be a point outside the Earth (the satellite). Its position is specified by the three spherical coordinates  $r, \lambda, \psi$  [see (2.28)]. The angles  $\lambda$  and  $\psi$  represent the longitude and geocentric latitude of the point  $S$ . If  $T$  is a point inside the Earth, it can also be specified by its three spherical coordinates  $\rho, \alpha, \beta$ , where  $\rho$  is the magnitude of  $OT$ ,  $\alpha$  the longitude, and  $\beta$  the geocentric latitude.

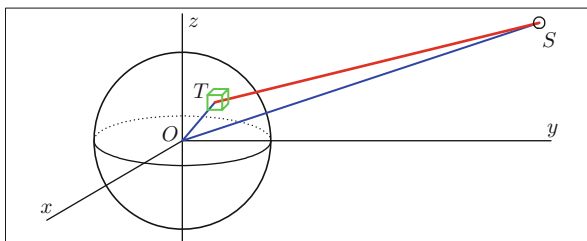


FIG. 3.1 : Obtaining the gravitational potential at a point  $S$ . The volume element of mass  $dM$  contains the point  $T$ . In the integration, it runs over the whole volume of the Earth. Each such element produces a gravitational potential  $dU$  at  $S$ . The notations for the distances are  $r = OS$ ,  $\rho = OT$ , and  $D = TS$ .

---

with which all bodies fall, and by gravity, the force with which the body would fall if the Earth's rotation were not to alter its effect and direction." Clairaut, in his introduction to *Théorie de la Figure de la Terre*.

We now have the standard relations giving components in Cartesian coordinates:

$$\frac{\mathbf{OS}}{r} = \begin{pmatrix} \cos \psi \cos \lambda \\ \cos \psi \sin \lambda \\ \sin \psi \end{pmatrix}, \quad \frac{\mathbf{OT}}{\rho} = \begin{pmatrix} \cos \beta \cos \alpha \\ \cos \beta \sin \alpha \\ \sin \beta \end{pmatrix}. \quad (3.12)$$

Let  $\theta$  be the angle between the two radial vectors, viz.,

$$\theta = (\mathbf{OS}, \mathbf{OT}),$$

so that the distance  $D$  between the two points  $S$  and  $T$  is

$$D^2 = \|\mathbf{TS}\|^2 = r^2 - 2r\rho \cos \theta + \rho^2,$$

and

$$D = D(T, S) = r \left[ 1 - 2\frac{\rho}{r} \cos \theta + \left(\frac{\rho}{r}\right)^2 \right]^{1/2}.$$

The scalar product  $\mathbf{OS} \cdot \mathbf{OT}$  yields

$$\cos \theta = \sin \psi \sin \beta + \cos \psi \cos \beta \cos(\lambda - \alpha).$$

The potential element  $dU$  produced at  $S$  by the mass element  $dM$  located at  $T$ , at a distance  $D$  from  $S$ , is given by (3.8) as

$$dU = \frac{d\mu}{D} = G \frac{dM}{D}. \quad (3.13)$$

### 3.3.2 Obtaining the Potential by Integration

The potential  $U$  we hope to calculate here is obtained by summing all the potential elements produced by the mass elements making up the mass distribution. The mass element  $dM$  is associated with the point  $T$  which ranges over the whole of the Earth:

$$U = U(S) = \int_{\text{Earth}} dU = G \int_{T \in \text{Earth}} \frac{dM(T)}{D(T, S)}. \quad (3.14)$$

The expression for  $D$  arising in the calculation of the potential is given as a function of  $\theta$  by

$$\frac{1}{D} = \frac{1}{r} \frac{1}{\sqrt{1 - 2\frac{\rho}{r} \cos \theta + \left(\frac{\rho}{r}\right)^2}}. \quad (3.15)$$

This expression can be expanded in terms of Legendre polynomials (see the appendix at the end of the chapter). The expansion converges if  $\rho/r < 1$ .



The calculation is thus valid if  $S$  remains strictly outside the sphere containing all the mass elements. We may then write

$$\frac{1}{D} = \frac{1}{r} \sum_{l=0}^{\infty} \left(\frac{\rho}{r}\right)^l P_l(\cos \theta), \quad (3.16)$$

where  $P_l$  is the  $l$ th Legendre polynomial (or Legendre polynomial of degree  $l$ ). Replacing  $\cos \theta$  by its value in terms of spherical coordinates, the angles  $\lambda$ ,  $\psi$ ,  $\alpha$ , and  $\beta$ , or more precisely  $\psi$ ,  $\beta$ , and  $\lambda - \alpha$ , we now use the Legendre addition formula:

$$\begin{aligned} P_l(\cos \theta) &= P_l(\sin \psi) \cdot P_l(\sin \beta) \\ &+ 2 \sum_{m=1}^l \frac{(l-m)!}{(l+m)!} P_{lm}(\sin \psi) P_{lm}(\sin \beta) \cos m(\lambda - \alpha), \end{aligned}$$

where  $P_{lm}$  are the associated Legendre functions. We thus obtain  $1/D$  in terms of the six spherical coordinates. Substituting this expression into (3.16), then into (3.14), and using  $R$  to denote the equatorial radius  $R_e = a$  of the Earth, we obtain:

$$\begin{aligned} U(r, \lambda, \psi) &= G \int_{\rho} \int_{\alpha} \int_{\beta} \frac{dM(\rho, \alpha, \beta)}{D(r, \lambda, \psi, \rho, \alpha, \beta)} \\ &= G \frac{1}{r} \int_{\rho=0}^R \int_{\alpha=0}^{2\pi} \int_{\beta=-\pi/2}^{\pi/2} \sum_{l=0}^{\infty} \left(\frac{\rho}{r}\right)^l \left[ P_l(\sin \psi) P_l(\sin \beta) \right. \\ &\quad + 2 \sum_{m=1}^l \frac{(l-m)!}{(l+m)!} P_{lm}(\sin \psi) \cos m\lambda P_{lm}(\sin \beta) \cos m\alpha \\ &\quad \left. + 2 \sum_{m=1}^l \frac{(l-m)!}{(l+m)!} P_{lm}(\sin \psi) \sin m\lambda P_{lm}(\sin \beta) \sin m\alpha \right] dM. \end{aligned}$$

Finally, we obtain the expression for  $U$  in terms of the associated Legendre functions  $P_{lm}$  and the coefficients  $C_{lm}$  and  $S_{lm}$ :

$$U(r, \lambda, \psi) = \frac{\mu}{r} \sum_{l=0}^{\infty} \left(\frac{R}{r}\right)^l \left[ \sum_{m=0}^l (C_{lm} \cos m\lambda + S_{lm} \sin m\lambda) P_{lm}(\sin \psi) \right], \quad (3.17)$$

with  $\mu = GM$  and  $M$  the mass of the Earth given by

$$M = \int_{\rho=0}^R \int_{\alpha=0}^{2\pi} \int_{\beta=-\pi/2}^{\pi/2} dM(\rho, \alpha, \beta),$$

and  $C_{lm}$  and  $S_{lm}$  the *harmonic coefficients* of the geopotential of degree  $l$  and order  $m$ .

In the expression (3.17), the terms for  $m = 0$  refer to the Legendre polynomial  $P_l$  and the sum from  $m = 1$  to  $m = l$  refers to the associated Legendre functions  $P_{lm}$ . The coefficients  $C_{lm}$  and  $S_{lm}$  are obtained by identifying the two formulas for  $U$ . There are two cases, depending on whether  $m$  is zero or not:

- Harmonic coefficients for  $m = 0$ ,  $C_{l0}$  and  $S_{l0}$  :

$$C_{l0} = \frac{1}{MR^l} \int_{\rho=0}^R \int_{\alpha=0}^{2\pi} \int_{\beta=-\pi/2}^{\pi/2} \rho^l P_l(\sin \beta) dM(\rho, \alpha, \beta) , \quad (3.18)$$

$$S_{l0} = 0 . \quad (3.19)$$

The coefficients  $S_{l0}$  are always zero.

- Harmonic coefficients for  $m \neq 0$ ,  $C_{lm}$  and  $S_{lm}$  :

$$C_{lm} = \frac{2}{MR^l} \frac{(l-m)!}{(l+m)!} \int_{\rho} \int_{\alpha} \int_{\beta} \rho^l P_{lm}(\sin \beta) \cos m\alpha dM \quad (3.20)$$

$$S_{lm} = \frac{2}{MR^l} \frac{(l-m)!}{(l+m)!} \int_{\rho} \int_{\alpha} \int_{\beta} \rho^l P_{lm}(\sin \beta) \sin m\alpha dM \quad (3.21)$$

The function  $U(r, \lambda, \psi)$  representing the gravitational potential of the Earth is called the *geopotential*.

### 3.3.3 Spherical Harmonics

The potential  $U$  has been given as a linear combination of spherical functions  $F_{lm}$  and  $G_{lm}$  defined by

$$\begin{aligned} F_{lm}(\lambda, \psi) &= P_{lm}(\sin \psi) \cos m\lambda , \\ G_{lm}(\lambda, \psi) &= P_{lm}(\sin \psi) \sin m\lambda . \end{aligned}$$

These can be considered as the real and imaginary parts of the functions  $H_{lm}$ , called *spherical harmonics*:

$$H_{lm}(\lambda, \psi) = e^{im\lambda} P_{lm}(\sin \psi) .$$

These functions have many mathematical properties (such as orthogonality) and there exists an extensive literature. In the present context, they can be used to give a graphical decomposition of the geopotential.

One can gain an idea of the way the spherical functions vary by plotting the points on the sphere where they vanish. To do so, the spherical harmonics are divided into three groups: the zonal harmonics, the sectorial harmonics, and the tesseral harmonics:

- Zonal harmonics. These are obtained when  $m = 0$ . In this case,

$$F_{l0} = P_{l0}(\sin \psi) = P_l(\sin \psi), \quad G_{l0} = 0, \quad H_{l0} = P_l(\sin \psi).$$

Hence,  $H_{l0}(\lambda, \psi) = H_{l0}(\psi)$  depends only on the latitude. Zonal harmonics have axial symmetry about the axis through the poles. In particular, they take into account the flattening of the Earth. They divide the Earth up along the geographic parallels.

- Sectorial harmonics. These are obtained when  $m = l$ . In this case,

$$P_{lm}(\sin \psi) = P_{ll}(\sin \psi) = \frac{(2l)!}{2^l l!} (\cos^2 \psi)^{l/2}.$$

This function of  $\psi$  is never zero, except at the poles. Hence,  $H_{ll}$  is only zero for certain values of  $\lambda$ . The sectorial harmonics only vanish on the geographic meridians and one generally gives a picture of the sphere that looks like an orange separated into segments that meet at the poles.

- Tesseral harmonics. These are obtained in all other cases. The zeros produce a kind of spherical chessboard pattern, marked out by the meridians and parallels.

### Normalised Coefficients

Geopotential models are generally expressed in terms of normalised coefficients  $C_{lm}^*$ , while the coefficients  $C_{lm}$  used above are referred to as non-normalised. The relation between  $C_{lm}^*$  and  $C_{lm}$  is

$$C_{lm}^* = \sqrt{\frac{(l+m)!}{(l-m)!(2l+1)(2-\delta_{0m})}} C_{lm}, \quad (3.22)$$

where  $\delta_{0m}$  is the Kronecker symbol, equal to 1 if  $m = 0$  or 0 if  $m \neq 0$ .

### 3.3.4 Second Degree Expansion of the Potential

To make use of these rather complex formulas, we begin by the simplest case, namely when the Earth is treated as an ellipsoid of revolution. This amounts to stopping the expansion at degree and order 2.

#### Theoretical Calculation of Coefficients

If we expand the potential  $U$  given by (3.17) up to second degree, we obtain

$$\begin{aligned}
U(r, \lambda, \psi) = \frac{\mu}{r} & \left\{ C_{00} P_0(\sin \psi) \right. \\
& + \left( \frac{R}{r} \right) \left[ C_{10} P_1(\sin \psi) + (C_{11} \cos \lambda + S_{11} \sin \lambda) P_{11}(\sin \psi) \right] \\
& + \left( \frac{R}{r} \right)^2 \left[ C_{20} P_2(\sin \psi) + (C_{21} \cos \lambda + S_{21} \sin \lambda) P_{21}(\sin \psi) \right. \\
& \quad \left. \left. + (C_{22} \cos 2\lambda + S_{22} \sin 2\lambda) P_{22}(\sin \psi) \right] \right\}. \quad (3.23)
\end{aligned}$$

The values of the first few Legendre polynomials and functions for the argument  $\sin \beta$  are as follows:

$$P_0(\sin \beta) = 1, \quad P_1(\sin \beta) = \sin \beta, \quad P_2(\sin \beta) = (3 \sin^2 \beta - 1)/2,$$

$$P_{11}(\sin \beta) = \cos \beta, \quad P_{21}(\sin \beta) = 3 \sin \beta \cos \beta, \quad P_{22}(\sin \beta) = 3 \cos^2 \beta.$$

We can now calculate the harmonic coefficients  $C_{lm}$  and  $S_{lm}$  using the four relations (3.18)–(3.21), adopting the spherical coordinates of the interior point  $T$  defined by (3.12). The coordinates of the center of gravity of the Earth are  $(x_0, y_0, z_0)$  and the components of the Earth's inertia tensor<sup>7</sup> are  $I_x$ ,  $I_{xy}$ , and so on. The results are displayed in Table 3.1.

### Case of the Earth Ellipsoid

In the case of a solid Earth, the origin of the coordinate system for expanding the geopotential is taken at the center of the Earth. We then have  $x_0 = y_0 = z_0 = 0$ , which implies that

$$C_{10} = 0, \quad C_{11} = 0, \quad S_{11} = 0.$$

If the axis  $Oz$  passes through the center of inertia, we have  $I_{xz} = I_{yz} = 0$ , which implies that

$$C_{21} = 0, \quad S_{21} = 0.$$

The most significant inhomogeneity in the terrestrial mass distribution is due to the flattening at the poles. The Earth is treated here as an ellipsoid of

---

<sup>7</sup>The moment of inertia  $I_x$  is defined by  $I_x = \iiint (y^2 + z^2) dM$ , while the product of inertia  $I_{xy}$  is defined by  $I_{xy} = \iiint xy dM$ . In the literature, the moments of inertia are often denoted by  $A = I_x$ ,  $B = I_y$ , and  $C = I_z$ , whence (3.25) and (3.26) become  $J_2 = (C - A)/MR^2$ .

$$\begin{aligned}
C_{00} &= \frac{1}{M} \int_{\rho} \int_{\alpha} \int_{\beta} dM(\rho, \alpha, \beta) = 1 \\
C_{10} &= \frac{1}{MR} \int_{\rho} \int_{\alpha} \int_{\beta} \rho \sin \beta dM(\rho, \alpha, \beta) \\
&= \frac{1}{MR} \iiint z dM = \frac{z_0}{R} \\
C_{11} &= \frac{1}{MR} \int_{\rho} \int_{\alpha} \int_{\beta} \rho \cos \beta \cos \alpha dM(\rho, \alpha, \beta) \\
&= \frac{1}{MR} \iiint x dM = \frac{x_0}{R} \\
S_{11} &= \frac{1}{MR} \int_{\rho} \int_{\alpha} \int_{\beta} \rho \cos \beta \sin \alpha dM(\rho, \alpha, \beta) \\
&= \frac{1}{MR} \iiint y dM = \frac{y_0}{R} \\
C_{20} &= \frac{1}{MR^2} \int_{\rho} \int_{\alpha} \int_{\beta} \rho^2 \frac{3 \sin^2 \beta - 1}{2} dM(\rho, \alpha, \beta) \\
&= \frac{1}{2MR^2} \iiint [3z^2 - (x^2 + y^2 + z^2)] dM \\
&= \frac{1}{2MR^2} \iiint [(x^2 + z^2) + (y^2 + z^2) - 2(x^2 + y^2)] dM \\
&= \frac{1}{2MR^2} (I_x + I_y - 2I_z) \\
C_{21} &= \frac{1}{3MR^2} \int_{\rho} \int_{\alpha} \int_{\beta} 3\rho^2 \sin \beta \cos \beta \cos \alpha dM(\rho, \alpha, \beta) \\
&= \frac{1}{MR^2} \iiint xz dM = \frac{1}{MR^2} I_{xz} \\
S_{21} &= \frac{1}{3MR^2} \int_{\rho} \int_{\alpha} \int_{\beta} 3\rho^2 \sin \beta \cos \beta \sin \alpha dM(\rho, \alpha, \beta) \\
&= \frac{1}{MR^2} \iiint yz dM = \frac{1}{MR^2} I_{yz} \\
C_{22} &= \frac{1}{12MR^2} \int_{\rho} \int_{\alpha} \int_{\beta} 3\rho^2 \cos^2 \beta \cos 2\alpha dM(\rho, \alpha, \beta) \\
&= \frac{1}{4MR^2} \iiint (x^2 - y^2) dM = \frac{1}{4MR^2} (I_y - I_x) \\
S_{22} &= \frac{1}{12MR^2} \int_{\rho} \int_{\alpha} \int_{\beta} 3\rho^2 \cos^2 \beta \sin 2\alpha dM(\rho, \alpha, \beta) \\
&= \frac{1}{2MR^2} \iiint xy dM = \frac{1}{2MR^2} I_{xy}
\end{aligned}$$

TABLE 3.1 : Harmonic coefficients  $C_{lm}$  and  $S_{lm}$  of the geopotential of degree  $l$  and order  $m$ , up to  $l = 2$ ,  $m = 2$ .

revolution with axis  $Oz$ . In this case, the axial symmetry implies that  $I_{xy} = 0$  and  $I_x = I_y$ , which in turn implies that

$$C_{22} = 0, \quad S_{22} = 0. \quad (3.24)$$

The flattening at the poles is expressed by the fact that  $I_z > I_x$ . Hence,

$$C_{20} = \frac{1}{MR^2}(I_x - I_z), \quad C_{20} < 0. \quad (3.25)$$

When we expand the geopotential to second order and with the above assumptions, the only nonzero term (apart from the leading term  $C_{00} = 1$ ) is thus the term  $C_{20}$  (which is negative). It is customary to introduce the coefficients  $J_l$  defined by<sup>8</sup>

$$J_l = -C_{l0}. \quad (3.26)$$

The geopotential is then

$$U(r, \lambda, \psi) = U(r, \psi) = \frac{\mu}{r} \left[ 1 - \left( \frac{R}{r} \right)^2 J_2 \frac{3 \sin^2 \psi - 1}{2} \right], \quad (3.27)$$

with

$$J_2 = 1.0826 \times 10^{-3}.$$

This term is dimensionless, like all the coefficients  $C_{lm}$  and  $S_{lm}$ . The value of the coefficient  $J_2$  was known for a long time from geodetic considerations (see Sect. 3.4.3), and then to very high accuracy by studying the trajectories of the first artificial satellites.

### 3.3.5 Expanding the Potential to Higher Degrees

For degrees higher than 2 and using the notation introduced above, the potential can be written

$$U(r, \lambda, \psi) = \frac{\mu}{r} \left[ 1 - \sum_{l=1}^{\infty} \left( \frac{R}{r} \right)^l J_l P_l(\sin \psi) + \sum_{l=1}^{\infty} \sum_{m=1}^l \left( \frac{R}{r} \right)^l (C_{lm} \cos m\lambda + S_{lm} \sin m\lambda) P_{lm}(\sin \psi) \right]. \quad (3.28)$$

---

<sup>8</sup>In 1958, one of the pioneers of space geodesy, Desmond King-Hele, decided to attribute the letter  $J$  to this coefficient, in homage to the British geodesist Sir Harold Jeffreys (1891–1989).

$J_n = -C_{n0}$	Value [dimensionless]
$C_{00}$	1
$J_1$	0
$J_2$	$+1,082.62652305 \times 10^{-6}$
$J_3$	$-2.53253531 \times 10^{-6}$
$J_4$	$-1.61997147 \times 10^{-6}$
$J_5$	$-0.22780140 \times 10^{-6}$
$J_6$	$+0.54066755 \times 10^{-6}$
$J_7$	$-0.36055772 \times 10^{-6}$
$J_8$	$-0.20402823 \times 10^{-6}$
$J_9$	$-0.12211470 \times 10^{-6}$
$J_{10}$	$-0.24439275 \times 10^{-6}$

TABLE 3.2 : Harmonic coefficients  $J_n$  for the geopotential, up to  $n = 10$ . Values taken from the EIGEN-6C2 model.

In the part between square brackets, there are three groups of terms:

- The first comprises only the number 1, representing the central potential.
- The second, with  $J_l$  and  $P_l$ , constitutes the contribution of the zonal harmonics [see (3.45)].
- The third, involving  $C_{lm}$ ,  $S_{lm}$ , and  $P_{lm}$ , gives the contribution of the sectorial and tesseral harmonics.

These terms  $J_l$ ,  $C_{lm}$ , and  $S_{lm}$  can only be known (except possibly for  $J_2$ ) by comparing the ellipsoid with the actual shape of the Earth, which is called the *geoid*.<sup>9</sup> To do this, weight measurements can be carried out in situ, but the best approach today is to use precise observations of the motions of artificial satellites. These points will be discussed below.

For the Earth as it really is (dropping the ellipsoid approximation), the numerical values of  $J_l$  are given in Table 3.2 (but see also Table 3.3). These coefficients are usually referred to in the literature as  $J_n$  terms. So for the geoid, the coefficients  $C_{10}$  (or  $J_1$ ),  $C_{11}$ , and  $S_{11}$  are zero, while the coefficients  $C_{21}$  and  $S_{21}$  ( $\sim 10^{-9}$ ),  $C_{22}$ , and  $S_{22}$  ( $\sim 10^{-6}$ ) are nonzero.

Regarding orders of magnitude, we see that the  $J_2$  term is about  $10^3$  times smaller than the leading term, but  $10^3$  times greater than the following coefficients. To sum up, considering the expansion of the potential given by (3.28), we observe that (see Fig. 3.2):

<sup>9</sup>When geodesists realised that the shape of the Earth was not exactly ellipsoidal, they chose to call it the *geoid* (Listing in 1873), which is tautological: it is like saying that the Earth is Earth-shaped! One sometimes sees the word *telluroid*, a disharmonious product of Latin-Greek hybridisation that is just as tautological.

Coefficient	GEM-T2	JGM-3	GRIM5-C1	GRIM5-S1
$C_{20}^*$	-484.1652998	-484.165368	-484.16511551	-484.16511551
$C_{30}^*$	0.9570331	0.957171	0.95857491	0.95857492
$C_{40}^*$	0.5399078	0.539777	0.53978784	0.53978784
$C_{50}^*$	0.0686883	0.068659	0.06726760	0.06720440
$C_{60}^*$	-0.1496092	-0.149672	-0.14984936	-0.14985240
$C_{70}^*$	0.0900847	0.090723	0.09301877	0.09311367
$C_{80}^*$	0.0483835	0.049118	0.05039091	0.05046451
$C_{90}^*$	0.0284403	0.027385	0.02628356	0.02620763
$C_{100}^*$	0.0549673	0.054130	0.05101952	0.05076191
$C_{200}^*$	0.0199685	0.018790	0.02340848	0.02342817
$C_{990}^*$			-0.00128836	-0.00001554

Coefficient	EGM96	EIGEN-CH03S	EIGEN-6C2
$C_{20}^*$	-484.165371736	-484.165562843	-484.165299956
$C_{30}^*$	0.957254174	0.957477372	0.957208401
$C_{40}^*$	0.539873864	0.539923241	0.539990490
$C_{50}^*$	0.068532348	0.068584004	0.068684705
$C_{60}^*$	-0.149957995	-0.149991332	-0.149954200
$C_{70}^*$	0.090978937	0.090539419	0.090513612
$C_{80}^*$	0.049671167	0.049295631	0.049484115
$C_{90}^*$	0.027671430	0.028093014	0.028015031
$C_{100}^*$	0.052622249	0.053699211	0.053330869
$C_{110}^*$	-0.050961371	-0.050765723	-0.507685657
$C_{120}^*$	0.037725264	0.036209032	0.036437330
$C_{130}^*$	0.042298221	0.041543398	0.041729879
$C_{140}^*$	-0.024278650	-0.022288877	-0.022669657
$C_{150}^*$	0.001479101	0.002425544	0.002192288
$C_{200}^*$	0.022238461	0.021496270	0.021558749
$C_{990}^*$	0.001478118	-0.000779156	0.002263992
$C_{22}^*$	2.439143524	2.439311853	2.439355937
$S_{22}^*$	-1.400166837	-1.400342254	-1.400284583
$C_{31}^*$	2.029988822	2.030480649	2.030499314
$S_{31}^*$	0.248513159	0.248170920	0.248199233
$C_{33}^*$	0.721072657	0.721306788	0.721274250
$S_{33}^*$	1.414356270	1.414370341	1.414373139

TABLE 3.3: Comparison between different models. Normalised zonal coefficients  $C_{i0}^*$  and other normalised coefficients  $C_{i_m}^*$  and  $S_{i_m}^*$ . All values should be multiplied by  $10^{-6}$ .

- The term of degree 0 is the leading term, causing the Keplerian motion (see below), in which the Earth is considered to be spherical and made up of homogeneous layers.



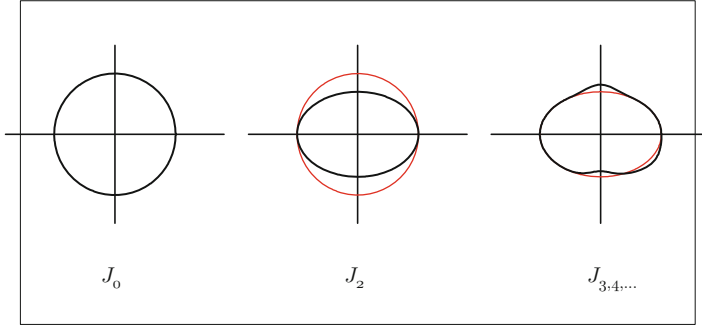


FIG. 3.2 : *Changing perception of the shape of the Earth in geodesy.* Left: *Sphere*, with  $C_{00} = -J_0 = 1$  and  $J_1 = 0$ . Center: *From the sphere to the ellipsoid of revolution*, with  $J_2$  term indicating flattening. Right: *From the ellipsoid to the geoid*, with  $J_n$  terms  $n \geq 3$ .

- The term of degree 1, which would correspond to a shift in the center of mass of the Earth away from the geometrical center, is made to vanish by choice of the coordinate origin.<sup>10</sup>
- The term of degree 2 corresponds to the flattening of the Earth when the latter is considered as an ellipsoid of revolution.
- The terms of degree 3 and higher cater for deviations between the geoid and the Earth ellipsoid.

## 3.4 Weight Field and Potential for the Ellipsoid

### 3.4.1 Calculating the Field and Potential

In order to investigate the weight field at the surface of the Earth, one has to consider the gravitational force field in a frame  $\mathfrak{R}_T$  moving with the Earth, rather than in the Galilean frame  $\mathfrak{R}$ . To obtain the relations in  $\mathfrak{R}_T$ , in addition to the acceleration as calculated in  $\mathfrak{R}$ , one must take into account the centrifugal acceleration  $a_c$  due to the Earth's rotation:

$$\mathbf{a}_c = -\varpi^2 \mathbf{J} \mathbf{M} ,$$

where  $\varpi$  is the angular speed of the Earth's rotation<sup>11</sup> and  $\mathbf{J}$  is the projection of  $\mathbf{M}$  on the polar axis, which is the point of geodetic latitude  $\varphi$  (and geocentric

<sup>10</sup>For the great majority of geopotential models,  $C_{00} = 1$  and  $C_{10}^* = 0$ . There are some exceptions, however, such as EIGEN-CHAMP03-S, with  $C_{00} = 1$  and  $C_{10}^* = -0.83390966 \times 10^{-9}$  or GRIM5-C1, with  $C_{00} = 1 - 1.14 \times 10^{-10}$  and  $C_{10}^* = 0$ .

<sup>11</sup>We use the notation  $\varpi$  only in this chapter. In subsequent chapters, we shall use the notation  $\hat{\Omega}_T$  for this quantity, and we shall explain why when the time comes. The angular speed  $\varpi$  is equal to one revolution per sidereal day, or  $\varpi = 7.292115 \times 10^{-5} \text{ rad s}^{-1}$ .

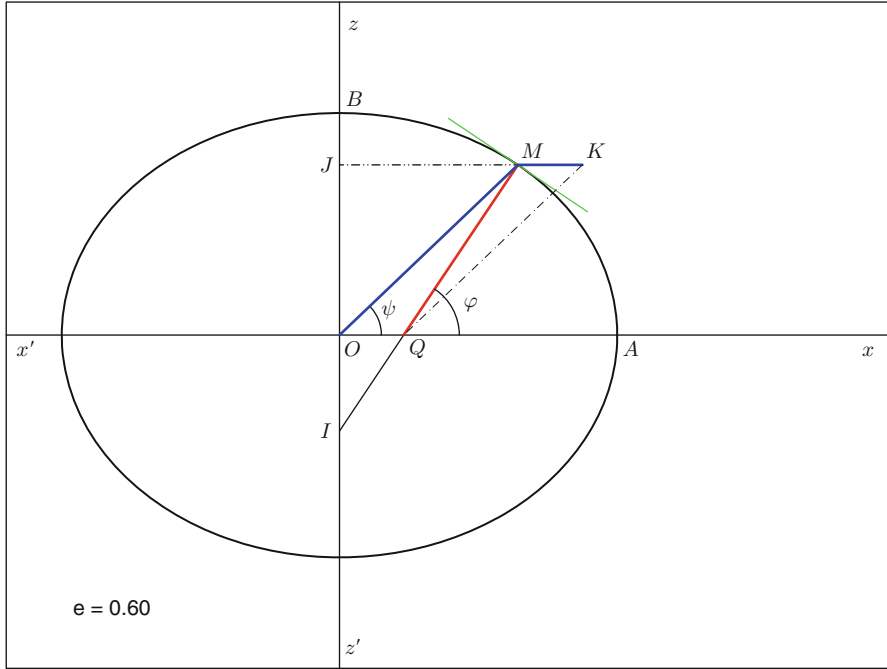


FIG. 3.3 : For a point  $M$  at the Earth's surface with geodetic latitude  $\varphi$  and geocentric latitude  $\psi$ , we represent gravity, pointing toward  $O$ , and weight, pointing toward  $I$ , normal to the ellipsoid at  $M$ .

latitude  $\psi$ ) at the Earth's surface (see Fig. 3.3). The center of the Earth is  $O$  and we set  $r = OM$ . Therefore,  $JM = r \cos \psi$ . The unit vector in the direction  $OM$  is denoted by  $\mathbf{e}_r$ .

To simplify the notation, we set

$$\mathbf{g} = \mathbf{g}_{\mathcal{R}} \quad (\text{gravity}), \quad \boldsymbol{\gamma} = \mathbf{g}_{\mathcal{R}_T} \quad (\text{weight}).$$

The rule for composition of accelerations is then

$$\text{absolute acceleration } (\mathbf{g}) = \text{relative acceleration } (\boldsymbol{\gamma}) + \text{centrifugal acceleration } (\mathbf{a}_c).$$

We obtain

$$\boldsymbol{\gamma} = \mathbf{g} + \varpi^2 \mathbf{JM}. \quad (3.29)$$

The vector  $\boldsymbol{\gamma}$  represents the weight. This is what defines the weight of a body at a given location. The weight is the vector sum of the gravity and the

centrifugal acceleration. The vector  $\mathbf{g}$  lies along  $\mathbf{OM}$ . The angle between the vector  $\boldsymbol{\gamma}$  and  $\mathbf{g}$  is very small, equal to  $\varphi - \psi$ . Its value, given by (2.5), is at most  $0.19^\circ$ . We can thus write

$$\mathbf{g} = -g\mathbf{e}_r, \quad \boldsymbol{\gamma} = -\gamma\mathbf{e}_r.$$

Projecting the expression in (3.29) onto  $\mathbf{OM}$ , we then have

$$-\gamma\mathbf{e}_r = (-g + \varpi^2 r \cos^2 \psi)\mathbf{e}_r. \quad (3.30)$$

Expressing the fields  $\mathbf{g}$  and  $\boldsymbol{\gamma}$  in terms of the respective potentials  $U$  and  $U_T$  and integrating (3.30) with respect to  $r$ , we obtain

$$U_T = U + \frac{1}{2}\varpi^2 r^2 \cos^2 \psi.$$

Cutting off the expansion of  $U$  at the second order as in (3.27), i.e., treating the geoid as an ellipsoid, we obtain

$$U_T(r, \psi) = \frac{\mu}{r} \left[ 1 - \left( \frac{R}{r} \right)^2 J_2 \frac{3 \sin^2 \psi - 1}{2} \right] + \frac{\varpi^2}{2} r^2 \cos^2 \psi. \quad (3.31)$$

The axial symmetry of the model appears through the absence of the variable  $\lambda$  (longitude) in the expression for the potential  $U_T$ .

### 3.4.2 Weight Field at the Earth's Surface

The weight field  $\boldsymbol{\gamma}$  is found by differentiating  $U_T$  along the normal to the ellipsoid. To the same order of approximation as when we identify the directions of the vectors  $\mathbf{g}$  and  $\boldsymbol{\gamma}$ , we may consider the field to be given by  $\partial U_T / \partial r$ . Its magnitude  $\gamma$  is then

$$\gamma(\psi) = \frac{\mu}{r^2} \left[ 1 - 3 \left( \frac{a}{r} \right)^2 J_2 \frac{3 \sin^2 \psi - 1}{2} \right] - \varpi^2 r \cos^2 \psi. \quad (3.32)$$

Replacing  $r$  by its value as a function of  $\psi$ , viz.,  $r = R_\psi(\psi)$  as given by (1.37), we obtain an expression for the magnitude  $\gamma(\psi)$  of the weight field at the surface of the ellipsoid as a function of the latitude alone.

The dependence of the weight field on the latitude is shown in Fig. 3.4. The latitude dependence of the gravitational field is also shown. In SI units, the gravity  $g$  varies from 9.814 at the equator to 9.832 at the pole, due to the flattening of the Earth, but this quantity is not directly measurable, because we cannot stop the Earth from rotating!

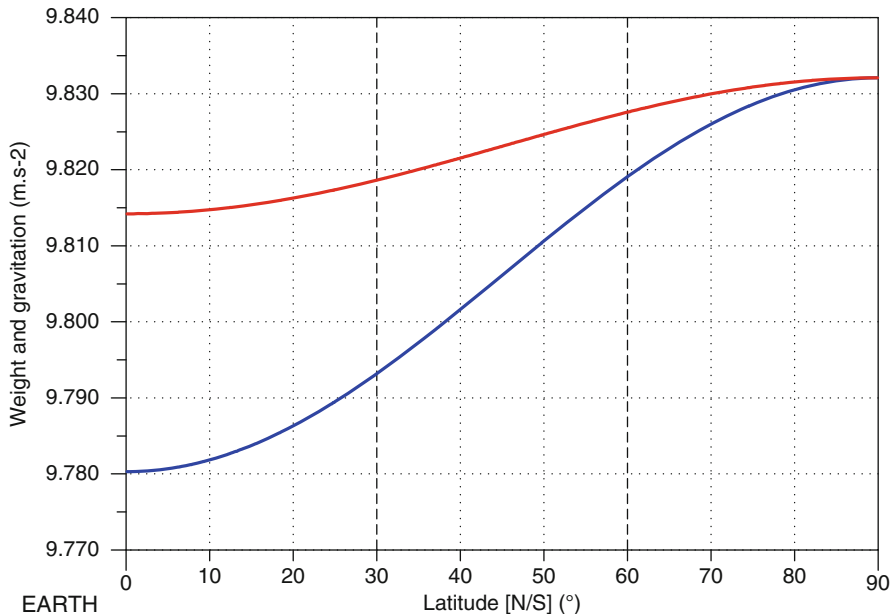


FIG. 3.4 : Dependence of the weight (lower curve) on the latitude at the surface of the ellipsoid. The upper curve shows the theoretical latitude dependence, not directly measurable, of the gravitational field. The difference between these two curves gives the value of the centrifugal acceleration.

The weight  $\gamma$ , measured experimentally,<sup>12</sup> varies from 9.780 at the equator to the same value 9.832 at the pole, because the variation caused by the Earth's rotation, which is zero at the pole, adds algebraically to the variation of  $g$ .<sup>13</sup>

<sup>12</sup>ESA's presentation of the satellite GOCE provides an interesting illustration of the levels of accuracy attained in weight measurements at a given location:

Weight =	9.8	Mass of spherical Earth
	9.81	Flattening and rotation
	9.812	Mountain and oceanic rifts
	9.8123	Internal mass distribution
	9.81234	Major river dams
	9.812345	Sea and land tides
	9.8123456	Large buildings in the neighbourhood

<sup>13</sup>Let us indulge in a little science fiction! Imagine a planet just like the Earth, but rotating faster, with angular speed  $\varpi'$ . Let us calculate the weight at the equator, assuming that the planet is spherical with radius  $R$ . From (3.32), we find

$$\gamma = \frac{\mu}{r^2} - \varpi'^2 R = \frac{\mu}{R^2} \left( 1 - \frac{\varpi'^2 R^3}{\mu} \right) = \frac{\mu}{R^2} (1 - m_a),$$

where  $m_a$  is defined below by (3.34). This term represents the contribution of the centrifugal acceleration to the weight when gravity is taken as unity. For the Earth,  $m_a = 1/288$ . If  $m_a = 1$ , the weight is zero, and all bodies at the equator on the surface find themselves

This formula for the latitude dependence of the weight field is quite accurate enough in many cases. However, if we require a more accurate formula in terms of the geodetic latitude and without approximation, we can use Somigliana's formula discussed below.

### 3.4.3 Clairaut's Formula

The  $J_2$  term in the expansion of the geopotential, which can be related to the difference in moments of inertia of the Earth about the polar axis and about an equatorial axis, as can be seen from (3.25) and (3.26), cannot be measured directly. But without waiting for the advent of the artificial satellite, it could be determined from geodetic considerations, exploiting the properties of equipotential surfaces.

#### Relation Between $J_2$ and Flattening

Clairaut<sup>14</sup> made the assumption that the Earth was in hydrostatic equilibrium in its rotation about its own axis. It follows that, for any point on the Earth's surface, taken as an ellipsoid, the potential is constant. Let us choose a point at the pole ( $r = R_p = b$ ) and a point at the equator ( $r = R_e = a$ ):

$$U_T(r = a, \psi = 0) = U_T(r = b, \psi = \pi/2) .$$

Equation (3.31) yields

$$\frac{\mu}{a} \left( 1 + \frac{1}{2} J_2 \right) + \frac{\varpi^2}{2} a^2 = \frac{\mu}{b} \left( 1 - \frac{a^2}{b^2} J_2 \right) .$$

The quantities  $f$  and  $J_2$  are much smaller than 1. Neglecting small quantities to second order, the right-hand side becomes

$$\frac{\mu}{a} (1 + f) [1 - J_2(1 + 2f)] \approx \frac{\mu}{a} (1 + f - J_2) ,$$

---

in weightless conditions. For such a fast-spinning version of Earth, we thus have  $(\varpi'/\varpi)^2 = 288$ , or  $\varpi' \approx 17\varpi$ . With such an angular speed, the day lasts 17 times less than on the real Earth, i.e., a mere 84.5 min. Furthermore, this is equal to the period of rotation of a terrestrial satellite at zero altitude, as we shall see in (5.9) of Chap. 5.

<sup>14</sup>Alexis Claude Clairaut (1713–1765) was a French astronomer and mathematician. He entered the French Academy of Sciences at the age of eighteen, after astonishing the assembly by his investigation of geometric curves. He soon turned his attention to geodesy and celestial mechanics, publishing *Théorie de la figure de la Terre tirée des principes de l'hydrostatique* in 1743. This explored the differences in the acceleration due to the weight at the poles and the equator. He then studied the three-body problem and published his *Théorie de la Lune* in 1752. He was also one of the first to investigate gravitational perturbations (see the historical note on the return of Halley's comet in Sect. 6.8.1).

which gives Clairaut's first equation:

$$J_2 = \frac{2}{3}f - \frac{1}{3}m_a, \quad (3.33)$$

where the dimensionless quantity

$$m_a = \frac{\varpi^2 a^3}{\mu} \quad (3.34)$$

is easily found to be  $m_a = 3.461 \times 10^{-3}$ . If we consider the flattening to be given by  $f = 1/298.3$ , we obtain the value of  $J_2$  to first order as

$$J_2 = 1.0814 \times 10^{-3}.$$

This is very close<sup>15</sup> to the value of  $J_2$  given in Table 3.2.

### Relation Between $J_2$ and Weight

Historically, it was the quantity  $f$  that scientists sought to calculate. That is, they hoped to determine the flattening without having to measure the Earth's meridian. They thus had to find some way of expressing  $J_2$ , and this could be done by measuring  $\gamma$ , the acceleration due to the weight, at various points on the Earth's surface. Now using (3.32), we can calculate  $\gamma = \gamma_e$  at the equator and  $\gamma = \gamma_p$  at the pole:

$$\begin{aligned} \gamma_e &= \frac{\mu}{a^2} \left( 1 + \frac{3}{2}J_2 \right) - \varpi^2 a, \\ \gamma_p &= \frac{\mu}{b^2} \left( 1 - 3\frac{a^2}{b^2}J_2 \right) \approx \frac{\mu}{a^2} (1 + 2f - 3J_2). \end{aligned}$$

Neglecting small quantities to second order, the difference gives

$$\gamma_p - \gamma_e = \frac{\mu}{a^2} \left( 2f - \frac{9}{2}J_2 \right) + \varpi^2 a.$$

Replacing  $\gamma_e$  by  $\mu/a^2$  in the small terms, since  $g = \mu/R^2$  to a first approximation, we obtain

$$\frac{\gamma_p - \gamma_e}{\gamma_e} = 2f - \frac{9}{2}J_2 + m_g,$$

---

<sup>15</sup>Carrying out the calculation to second order in the small quantities, we obtain

$$J_2 = \frac{2}{3}f - \frac{1}{3}m_b - \frac{1}{3}f^2 + \frac{2}{21}fm_b,$$

where  $m_b = \varpi^2 a^2 b / \mu = m_a(1 - f)$ . The numerical result is  $J_2 = 1.082634 \times 10^{-3}$ , implying a relative error of  $7 \times 10^{-6}$  compared with the value of  $J_2$  given in the text.

where

$$m_g = \frac{\varpi^2 a}{\gamma_e} . \quad (3.35)$$

The value of  $m_g$  is equivalent under the given approximations to that of  $m_a$  in (3.34). We set

$$\beta = \frac{\gamma_p - \gamma_e}{\gamma_e} ,$$

a dimensionless quantity which one might call the flattening of gravity. This can be accurately obtained by measuring  $\gamma$  at the equator and the pole. We thus have another relation for  $J_2$ , known as Clairaut's second equation:

$$J_2 = \frac{2}{9}(2f + m_a - \beta) . \quad (3.36)$$

### Clairaut's Formula

Comparing the two equations (3.33) and (3.36) and eliminating  $J_2$ , we obtain *Clairaut's formula*:

$$f = \frac{5}{2}m_a - \beta . \quad (3.37)$$

This formula can be used to determine  $f$  from two measurements of  $\gamma$ . Numerical calculations give

$$\gamma_e = 9.7804 \text{ ms}^{-2} , \quad \gamma_p = 9.8322 \text{ ms}^{-2} ,$$

$$\beta = 5.296 \times 10^{-3} \approx 1/189 , \quad m_a = 3.467 \times 10^{-3} \approx 1/288 ,$$

$$f = 3.373 \times 10^{-3} \approx 1/297 .$$

Given the approximations made here, this result can be considered to be highly satisfactory.

Clairaut's formula<sup>16</sup> shows that the flattening  $f$  can be determined from weight measurements, since  $\varpi$  and  $a$  are known. To obtain  $f$ , it is not necessary to know anything about the composition of matter within the ellipsoid.

---

<sup>16</sup>Clairaut was pursuing an idea of Newton and Huygens that the Earth's rotation, weight, and flattening were all related. Indeed, he formulated this idea, but not in the way discussed here. He did not use the concept of potential, invented later by Lagrange, and did not exploit the coefficient  $J_2$  in this form.

### 3.4.4 Somigliana's Formula

Equation (3.32) giving the weight field, or Clairaut's relations, are approximate results, to first order in  $f$ . The Italian geodesists Pizetti (1894) and later Somigliana (1922) were to take up the same problem in a global way. The main idea was to define a body with the shape of an ellipsoid of revolution such that the ellipsoid was itself an equipotential surface of its own field. Although the final formula looks simple and elegant, the calculation leading to it is long and arduous, and goes well beyond the scope of the present book. Somigliana's formula gives the normal weight field at the surface of the ellipsoid as a function of the geodetic latitude  $\varphi$ :

$$\gamma(\varphi) = \frac{a\gamma_e \cos^2 \varphi + b\gamma_p \sin^2 \varphi}{\sqrt{a^2 \cos^2 \varphi + b^2 \sin^2 \varphi}}, \quad (3.38)$$

where  $\gamma_e$  and  $\gamma_p$  are the values of the weight at the equator and the pole, as discussed earlier. It can also be written in the form

$$\gamma(\varphi) = \gamma_e \frac{1 + k \sin^2 \varphi}{\sqrt{1 - e^2 \sin^2 \varphi}}, \quad (3.39)$$

where

$$k = \frac{b}{a} \frac{\gamma_p}{\gamma_e} - 1 \quad (3.40)$$

is the Somigliana constant. This formula can also be given in numerical form. The values of the various terms depend to some extent on the reference ellipsoid (see Table 2.1):

- With GRS80, the values are:

$$\begin{aligned} a &= 6,378,137 \text{ m}, & b &= 6,356,752.3141 \text{ m}, \\ e^2 &= 0.00669438002290, & k &= 0.001931851353, \\ \gamma_e &= 9.7803267715 \text{ ms}^{-2}, & \gamma_p &= 9.8321863685 \text{ ms}^{-2}, \end{aligned}$$

$$\gamma(\varphi) = 9.780327 \left( 1 + 5.3024 \times 10^{-3} \sin^2 \varphi + 5.8 \times 10^{-6} \sin^2 2\varphi \right). \quad (3.41)$$

- With WGS84, the values are:

$$\gamma_e = 9.7803253359 \text{ ms}^{-2}, \quad k = 0.001931853.$$

Once above the ellipsoid, the weight  $\gamma_h(\varphi)$  at altitude  $h$  is given by a relation involving  $\gamma(\varphi)$  and  $\gamma_e$ :

$$\frac{\gamma_h(\varphi) - \gamma(\varphi)}{\gamma_e} = -2 \frac{h}{a} \left[ 1 + f + m_a + \left( -3f + \frac{5}{2} m_a \right) \sin^2 \varphi \right] + 3 \left( \frac{h}{a} \right)^2. \quad (3.42)$$



## 3.5 Geoid

### 3.5.1 Gravity Anomalies

A gravimeter can be used to measure the weight field at many points on land, and with suitable precautions, at sea. Furthermore, as we shall see in later chapters, the orbit of a satellite is sensitive to the distribution of mass in the regions it overflies. When accurately measured, the discrepancy between the theoretical position according to a given model and the actual position can be used to deduce the spherical harmonic coefficients of the geopotential. In addition to this method, used for over 40 years now, since the beginning of the space age, with ever more refined models, one should also mention altimetry measurements made by ocean satellites over the past 20 years or so.

Once the data has been processed and the transition made from weight to geopotential, the result is a map of anomalies, i.e., the difference in altitude (or equipotential surface) between the geoid and the ellipsoid. Such maps, each associated with a geopotential model, reveal ripples not exceeding a 100 m or so. Figure 3.5 shows the map resulting from the American model EGM96. The main negative anomalies are south of India ( $-105$  m), in Tibet ( $-65$  m), in the Antarctic south of New Zealand ( $-55$  m), and in the Carribean ( $-50$  m). The main positive anomalies are in New Guinea ( $+75$  m), in Iceland ( $+70$  m), and halfway between Madagascar and the Antarctic ( $+60$  m).

It should be noted that these anomalies are not correlated with the relief of the visible land mass. They are explained as manifestations of the non-uniform density of matter in the Earth's mantle.

Long-wavelength anomalies are identified by satellite, while smaller-scale anomalies are found by ground-based measurements. These anomalies are called gravity anomalies and they are measured in milliGal.<sup>17</sup>

### 3.5.2 Satellites and Geodesy

The first artificial satellite, Sputnik-1, was launched by the USSR on 4 October 1957 and only emitted a signal for three weeks.<sup>18</sup> However, by studying the trajectories of subsequent satellites,<sup>19</sup> launched shortly afterwards, the zonal coefficient  $J_2$  was determined by the Czechoslovakian geodesist E.

---

<sup>17</sup>The unit of acceleration in CGS units is the Gal in homage to Galileo. Hence,  $1 \text{ Gal} = 1 \text{ cm s}^{-2}$ . Geodesists use the milliGal,  $1 \text{ mGal} = 10^{-5} \text{ m s}^{-2}$ .

<sup>18</sup>Orbital elements for the first few revolutions are: altitude at perigee  $h_p = 228$  km, altitude at apogee  $h_a = 947$  km, inclination  $i = 65.128^\circ$ , period  $T = 96.17$  min ( $\Delta T = 1.80$  s/day), perigee on latitude  $41^\circ$  N. Last signal 26 October 1958. Reentry 4 January 1958.

<sup>19</sup>Sputnik-2 was launched on 4 November 1957. Orbital elements for the first few revolutions are:  $h_p = 225$  km,  $h_a = 1,671$  km,  $i = 65.310^\circ$ ,  $T = 103.75$  min ( $\Delta T = 3.08$  s/day), perigee on latitude  $40^\circ$  N. Reentry 14 avril 1958. Sputnik-3 was launched on 15 May 1958. Orbital elements for the first few revolutions:  $h_p = 226$  km,  $h_a = 1,881$  km,  $i = 65.188^\circ$ ,  $T = 105.95$  min ( $\Delta T = 0.75$  s/day), perigee at latitude  $45^\circ$  N. Reentry 6 April 1960.

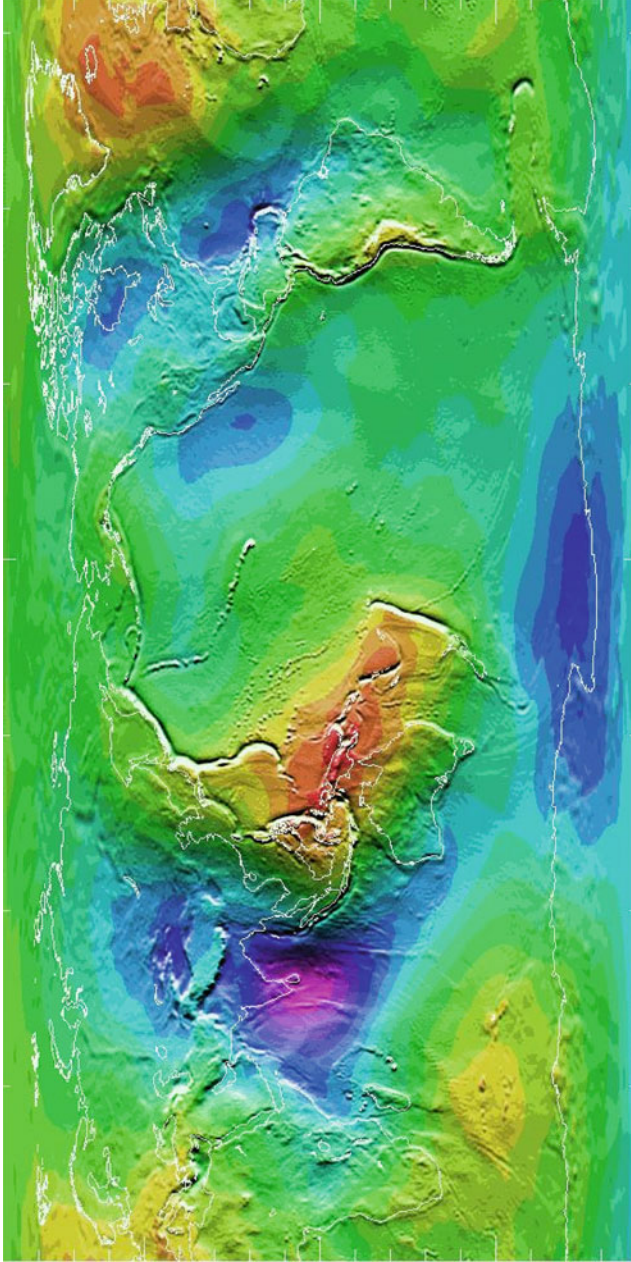


FIG. 3.5 : *Anomalies of the geoid in the EGM96 model. This map, using the plate-carrée projection, represents the anomalies of the geoid (in meters) relative to the reference ellipsoid, as described by the US model EGM96. The maximal depression ( $-105\text{ m}$ ) is south of India, while the highest point ( $+75\text{ m}$ ) is in New Guinea. Note that the relief of land masses and anomalies are not correlated, except near the Andes mountain range. Credit: The NASA GSFC and NIMA Joint Geopotential Model. NASA, NIMA, Ohio State University.*

Buchar in 1958. The value was quite close to predictions calculated from Earth-based measurements. The US satellite Vanguard-1, launched on 17 March 1958, was able to evaluate for the first time the discrepancy between the ellipsoid and the geoid. This important harmonic of degree 3 corresponds to a raising of the North Pole by 15 m above the ellipsoid and a lowering of the South Pole by the same amount.<sup>20</sup> The  $J_4$  term and a few others were subsequently established after 1960. The methods used to determine the coefficients  $J_n$  are discussed further in the historical note in Sect. 6.7.

In 1961, W. Kaula produced a complete model of degree 4, i.e., involving all the coefficients  $C_{lm}$  and  $S_{lm}$ : a sectorial harmonic, coefficient of the associated Legendre function  $P_{22}$ , accounts for an elevation of the geoid around  $165^\circ\text{E}$  and  $15^\circ\text{W}$  and a depression around  $75^\circ\text{E}$  and  $105^\circ\text{W}$ . These points mark out four equal sectors on the equator,<sup>21</sup> since we are dealing with the function  $P_{lm}$  in the case  $l = 2$  and  $m = 2$ . This point is further discussed in Sect. 7.4 on geostationary satellites (see Fig. 7.12).

Our knowledge of the Earth's gravitational potential has moved ahead very quickly since this time. Geodesists have not only taken advantage of all available satellites, but they have also sent up their own dedicated satellites.<sup>22</sup> A considerable improvement came with the advent of satellite-borne radar altimeters, which could describe the ocean surface (the geoid) relative to the orbit. The first were the US military satellites GEOS-3, Seasat, and Geosat.

Since 1980, the geopotential has been better measured above the oceans than above the continents. Subsequently, the European satellites ERS-1 and 2, followed by the French–US satellites TOPEX/Poseidon and Jason-1 and 2 have refined the measurements. The latter measure the sea level (whose mean represents the geoid) relative to the reference ellipsoid with an accuracy be-

---

<sup>20</sup>At the time, this was considered a scoop: the Earth was pear-shaped. Given the scale of these discrepancies, just 15 m compared with a radius of 6,400 km, this was perhaps slightly exaggerated!

<sup>21</sup>D. King-Hele summed this up in a little refrain of his own invention:

When you cut a slice  
 Through the polar ice  
     The Earth is like a pear.  
 But sliced along the equator  
 She looks like a potato –  
     A giant *pomme de terre*.

<sup>22</sup>Among these, the US series GEOS (Geodetic Earth Orbiting Satellite), GEOS-1 (Explorer-29), GEOS-2 (Explorer-36), PAGEOS, LAGEOS, with passive ranging (PA) or laser ranging (LA), which followed on from the satellites Echo-1 and Echo-2 (balloon-borne), ANNA-1B (Army, Navy, Nasa, Air Force, the first satellite to emit flashes), ADE-A (Atmospheric Density Explorer, Explorer-19), Beacon Explorer-1 (BE-B, Explorer-22, or S-66a, the first satellite equipped with laser reflectors), and Beacon Explorer-2 (BE-C, Explorer-27). After 1970, came the French satellites Starlette and Stella, launched in 1975 and 1993, the Japanese satellite EGP (Experimental Geodetic Payload), also called EGS-1 (Earth Geodetic Satellite or *Ajisai*, meaning “hydrangea” in Japanese), launched in 1986, and the Russian satellite Fizeau (Meteor-2-21), launched in 1993.

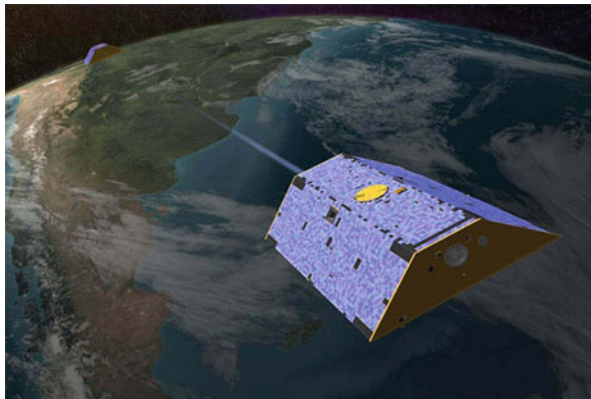


FIG. 3.6 : *Artist's view of the satellites GRACE-A and B, showing their microwave ranging system. Credit: University of Texas Center for Space Research.*

tween 2 and 3 cm. This means that the altitude of the satellite is known to even better accuracy. The quality of the altimeters used is important, but the accuracy with which the satellite orbit is established is just as fundamental, and this is possible thanks to the potential models involving spherical harmonics of a very high degree.

A radical change came about in the year 2000. Until then, satellites were in relatively high orbits, e.g., 5,900 km for LAGEOS, 800 km for Starlette,<sup>23</sup> to minimise any atmospheric friction. But from this date, drag compensation systems have made it possible to maintain satellites in relatively low orbits that are all the more sensitive to gravity anomalies.

The satellite CHAMP (Challenging Microsatellite Payload for geophysical research and applications) can determine the geoid to an accuracy of 10 cm (and 0.5 mGal for gravity). This improvement by a factor of 10 over previous missions is largely due to its low orbit (450 km), continuous GPS monitoring of the orbit, and a highly sensitive onboard accelerometer.

The GRACE mission (Gravity Recovery And Climate Experiment) comprises two twin satellites GRACE-A and B, which follow one another around<sup>24</sup> on the same orbit, separated by a distance of 200 km. The low orbit (480 km) and accurate measurement of the distance between GRACE-A and B, to within a few micrometres, has led to even better results: the geoid is known to within 1 cm on a spatial scale of 200 km (see Fig. 3.6). This is so accurate that we can now produce monthly maps of the geoid and monitor the evolution of large water masses, such as the major river basins.

<sup>23</sup>The pleasant name Starlette is a nice example of a contorted acronym: *Satellite de Taille Adaptée avec Réflecteurs Laser pour les Etudes de la Terre*.

<sup>24</sup>Whence the nickname of Tom and Jerry given by the mission team.



FIG. 3.7 : *Artist's view of the satellite GOCE. The shape is designed to offer minimal resistance to atmospheric friction. The image shows the ions ejected by the drag compensation system. Credit: ESA.*

The satellite<sup>25</sup> GOCE (Gravity field and steady state Ocean Circulation Experiment) has improved our knowledge of the geoid still further, with a very low orbit (200 km) and a gradiometer comprising six accelerometers with an accuracy of  $10^{-12} \text{ m s}^{-2}$ . The satellite is equipped with an ion motor which counteracts the forces of atmospheric friction in real time. Thanks to thrusts of a few mN from its *drag compensation system*, the satellite is effectively in permanent free fall (Fig. 3.7).

Slightly further head, the LICODY project (Laser Interferometry for Core and Ocean Dynamics) plans to use laser ranging between satellites in a formation.

We may say that space geodesy has finally become a “dialectic” science in the sense that geopotential models are better known by localising satellites and studying their trajectories, and the position of the satellites is better determined by improved potential models.

### 3.5.3 Development of Geopotential Models

#### The Main Models

The first satellite data were integrated into existing models and, from 1970, certain models were established exclusively on the basis of space data. The SAO SE-1 model (Smithsonian Astrophysical Observatory-Standard Earth), considered to be the first satellite-only model, presented a degree 8 expansion of the geopotential in 1966. In 1973, the SE-3 model (degree 24) used the first laser ranging measurements to establish the distances to satellites. The NWL model (Naval Weapon Laboratory) was mainly based on satellites in the Transit series. There followed many other models, among which we shall focus

<sup>25</sup>In the space community, GOCE is generally pronounced “go-chay”.



on the US models GEM, JGM, OSU, EGM, and GGM, and the European models GRIM and EIGEN.

The GEM model (Goddard Earth Model) was established by NASA's Goddard Space Flight Center (GSFC) in the United States as a reaction to the classified US military models. The first model GEM-1 was published in 1972, expanding the potential to degree 12. The GEM-T2 model, published in 1990, exploited the data from 31 satellites. It gave a model with all coefficients up to degree 36, and some up to degree 50, and it also provided a very high order expansion for the tides.

The JGM model (Joint Gravity Model) was produced jointly by NASA and the University of Texas. In 1994, JGM-2 (degree 70) amended GEM-T3 (degree 50), itself successor to GEM-T2, with the first results from TOPEX/Poseidon, and JGM-3 integrated the data from other satellites such as LAGEOS-2.

The EGM model (Earth Gravity Model) is the result of a collaboration between GSFC-NASA, NIMA (National Imagery and Mapping Agency), and OSU (Ohio State University), which has established many models, from OSU68 to OSU91. In 1996 came EGM96S of degree 70, with data provided solely by satellites, and EGM96 of degree 360, adjoining geophysical data. They used data from 40 satellites, including satellite to satellite measurements, with the GPS constellations<sup>26</sup> and TDRSS. The latest model EGM2008 was based mainly on GRACE data to achieve an expansion up to degree 2190.

Since 2002, the GGM model (GRACE Gravity Model) has been developed by the University of Texas using only data from GRACE: accelerometer, attitude, and distance between the two satellites (K-band range-rate).

In Europe, the GRGS (*Groupe de Recherche en Géodésie Spatiale*) in France and the DGFI (*Deutsches Geodätisches Forschungsinstitut*) in Germany have worked jointly to produce the GRIM model (GR for GRGS and IM for the institute in Munich). The first model was GRIM1, published in 1975 (degree 10). In 2000, there followed the GRIM5-S1 and GRIM5-C1 models, the first based solely on satellite data<sup>27</sup> and the second using all data. The latter models were superseded by the EIGEN model (European Improved Gravity model of the Earth by New techniques),<sup>28</sup> produced by the GFZ-Postdam and the GRGS-Toulouse. In 2002, EIGEN-1S amended GRIM5-S1 with the data from CHAMP, supplemented by LAGEOS-1 and 2, Starlette, and Stella. Other models were to come, using data from the GRACE mission. In 2008,

<sup>26</sup>The satellites Navstar/GPS-35 and 36 (or USA-96, 100), launched in 1993 and 1994, are equipped with laser reflectors.

<sup>27</sup>The satellites used were Starlette, EGP (Ajisai), LAGEOS-1 and 2, Geosat, SPOT-2 and 3, ERS-1 and 2, Stella, Westpac-1 (WPLTN-1, West Pacific Laser Tracking Network), TOPEX/Poseidon, GFZ-1 (*GeoForschungsZentrum*), D1-C, D1-D, GEOS-3, Meteor-3-07, Nova-3, Etalon-1 and 2 (Kosmos-1989 and 2024), and PEOPLE.

<sup>28</sup>This is another acronym with subtle connotations, recalling the German word *Eigenwert* introduced into mathematics by Hilbert and transformed to "eigenvalue" in English. The English word corresponding to *eigen* is "own", from the Old English *āgen*.

there was the complete EIGEN-GL05C model of degree and order 360 (corresponding to a wavelength of  $1^\circ$ , or  $\lambda/2 = 55$  km). In 2011, the EIGEN-6 model incorporated data from GOCE and LAGEOS: EIGEN-6S model (degree 240) and EIGEN-6C model (degree 1420) with gravity data and altimetry data. In 2012, it was amended<sup>29</sup> to produce EIGEN-6C2 (degree 1949). The development of the European model is summarised in Table 3.4.

Naturally, current models take into account the tides and the atmosphere. They also take into consideration the time variations of the first spherical harmonic coefficients<sup>30</sup> which are due to isostatic adjustment, in a process called post-glacial rebound,<sup>31</sup> and other factors relating to climate change.

### Comparison of Geopotential Models

Geopotential models cannot be compared term by term beyond degree 5. Two models can have rather different terms and yet still have a very close final result: different weightings of the spherical harmonics can lead to very close results. Beyond degree 16, even the signs of the coefficients can change from one model to another, without there being any harmful effect on the restitution of the geoid and satellite tracking. This highlights a problem when truncating series: the coefficients of a model of degree 10 do not correspond to the coefficients of the first  $10^\circ$  in a model of degree 20.

As an example, Table 3.3 gives the coefficients  $C_{l0}^*$  for seven models mentioned above, in fact, coefficients of order 0 and degree  $l$  from 2 to 10. We

---

<sup>29</sup>EIGEN-6C2 is a combined global gravity field of a maximum degree/order 1949 which has been inferred from the combination of the following data:

1. Satellite data.
  - 25 years of LAGEOS (SLR) data from the time span January 1985 till December 2010.
  - 7.8 years of GRACE (GPS-SST and K-band range-rate) data from the time span March 2003 till December 2010.
  - 350 days of GOCE data (satellite gradiometry only) from the time span 1 Nov 2009 till 19 April 2011.
2. Surface data.
  - Global gravity anomaly data set which was obtained from altimetry over the oceans.
  - Geoid data over the oceans (from DTU).
  - Geoid heights over the continents generated from EGM2008.
 Document: GFZ-GRGS.

<sup>30</sup>As an example, here are the values from the EGM96 model. For the time variation:  $dC_{20}^*/dt = +1.162755 \times 10^{-11} \text{ year}^{-1}$ , or  $dJ_2/dt = \dot{J}_2 = -2.60 \times 10^{-11} \text{ year}^{-1}$ ,  $dC_{21}^*/dt = -0.337 \times 10^{-11} \text{ year}^{-1}$ , and  $dS_{21}^*/dt = +1.606 \times 10^{-11} \text{ year}^{-1}$ . This variation, particularly clear between 1985 (when measurements began) and 1995, is considered to be the signature of post-glacial rebound. From 1995 to 2013,  $J_2$  ceased to vary. Post-glacial rebound seems to have been compensated by the melting of ice and other effects due to global warming. The contribution of the tides is  $4.173 \times 10^{-9}$  for  $C_{20}^*$ .

<sup>31</sup>Since the melting of the polar ice caps, the ground level has been rising by several centimetres per year for the past few thousand years, whether it be in Canada, Scandinavia, or the Antarctic.

Year	Model	Contribution	$L$	$N$
1975	GRIM1		10	120
1976	GRIM2		23	575
1981	GRIM3		36	1,368
1991	GRIM4-C1		50	2,600
1995	GRIM4-C4		72	5,328
2000	GRIM5-C2		120	14,640
2002	EIGEN-1	CHAMP	120	14,640
2003	EIGEN-2	CHAMP	140	19,880
2007	EIGEN-4	GRACE	160	25,920
2008	EIGEN-5	GOCE	360	130,320
2011	EIGEN-6	GOCE	1,440	2,076,480
2012	EIGEN-6C2	GOCE	1,949	3,802,499

TABLE 3.4: Main stages in the establishment of the European models GRIM, then EIGEN, developed by the GRGS and the GFZ.  $L$  maximal degree,  $N$  number of unknowns processed to establish the model,  $N = L \times (L + 2)$ .

	Units	Whole no.	GEM	JGM	GRIM	EGM	EIGEN
$\mu$	$\text{km}^3 \text{s}^{-2}$	398,600	0.436	0.4415	0.4415	0.4415	0.4415
$R$	km	6,378	0.137	0.13630	0.13646	0.13630	0.13646
$1/f$	Dimensionless	298	0.257	0.25765	0.25765	0.25765	0.25765

TABLE 3.5: Comparison between the different models: GEM-T2, JGM-3, GRIM5, EGM96, EIGEN-CHAMP03S. Values of geocentric gravitational constant  $\mu = GM$ , equatorial radius  $R$ , and flattening ( $1/f$ ). The whole number part is the same for all these models, i.e., only the decimal changes.

recall that, for  $l = 0$ , the coefficient is equal to unity, and for  $l = 1$ , it is zero. All coefficients in the table are in units of  $10^{-6}$ .

In the case  $m = 0$ , the normalisation relation (3.22) becomes simply

$$C_{l0} = \sqrt{2l + 1} C_{l0}^* .$$

We then obtain the correspondence between Tables 3.3 and 3.2, e.g.,

$$J_2 = -\sqrt{5} C_{20}^* = \sqrt{5} \times 484.16511 \dots \times 10^{-6} = 1,082.62622 \dots \times 10^{-6} .$$

These coefficients  $C_{lm}$  are associated with values of  $\mu$ ,  $R$ , and  $f$  that are specific to each model (see Table 3.5).





FIG. 3.8 : *Preparation of LAGEOS-2. The satellite, of diameter 60 cm, is equipped with 426 reflectors (diameter 38.1 mm, depth 27.8 mm), made from cube corners whose  $90^\circ$  angles are formed to an accuracy of 0.5 arcsec. Credit: Agenzia Spaziale Italiana (ASI).*

### 3.5.4 Evaluation of the Geocentric Gravitational Constant

The geocentric gravitational constant  $\mu = GM$  plays a key role in space mechanics. It can be obtained to very high accuracy, well above what can be achieved for the universal constant of gravitation  $G$ .<sup>32</sup> The first values for  $\mu$  were given by Kepler’s third law applied to the lunar orbit. More and more precise values were obtained using the space probes Ranger, Mariner, and Venera, then satellites, preferably with high altitude, since lower satellites are subject to non-gravitational effects.

A breakthrough was made in the 1980s with the advent of the technique known as Lunar Laser Ranging (LLR), which consists in measuring the distance from the Earth to the Moon using a laser. At the present time,

---

<sup>32</sup>*Henry Cavendish* (1731–1810), the British physicist and chemist, was the first to obtain a precise value for  $G$ , which he published in 1798 in a famous paper entitled *Experiments to determine the density of the Earth*. He used a subtle method: instead of taking advantage of very large masses (like those who, at the time, sought to measure the deviation of a plumb line by a mountain), he used a torsion balance with a very fine thread, suspending two small metal weights (50 g). Bringing two large lead balls (30 kg) to a distance of 15 cm, he measured the torsion of the thread, using a mirror to create a “light lever”, and deduced  $G$  from the period of the motion ( $\sim 2$  h). He thereby calculated the density of the Earth and found  $d = 5.48$  (current value 5.52). This density is greater than that of the rocks in the Earth’s crust ( $\sim 2.7$ ), and Cavendish thus demonstrated that the Earth contained a very dense central part. The method was later refined by Charles Boys (1895) using a very fine quartz thread (2  $\mu\text{m}$ ) and still smaller masses (2.7 g, 7.5 kg at 15 cm), over a short period (3 min). This type of experiment is still used to measure  $G$ , but the relative accuracy does not exceed  $\delta G/G = 1.2 \times 10^{-4}$ . Other ways are now sought to improve accuracy. Current recommendations (CODATA 2010) give the value

$$G = (6.67384 \pm 0.00080) \times 10^{-11} \text{ m}^3 \text{ kg}^{-1} \text{ s}^{-2}.$$

Method	Year	$\mu$ ( $\text{km}^3 \text{s}^{-2}$ )	Error
Lunar orbit	1959	398,620.	$\pm 6$ .
Explorer-27	1965	398,602.	$\pm 4$ .
Ranger-6, 7, 8, 9	1966	398,601.0	$\pm 0.7$
Mariner-9	1971	398,601.2	$\pm 2.5$
Venera-8	1972	398,600.4	$\pm 1.0$
ATS-6 / GEOS-3	1979	398,600.40	$\pm 0.1$
Laser/Moon	1985	398,600.444	$\pm 0.010$
Laser/LAGEOS	1992	398,600.4415	$\pm 0.0008$
Laser/LAGEOS	2000	398,600.4415	$\pm 0.0002$

TABLE 3.6 : *Measured geocentric gravitational constant  $\mu = GM$  and estimated error. Historical evolution indicating method used and year.*

the most accurate measurements are obtained by laser ranging measurements made on the LAGEOS satellites<sup>33</sup> (see Fig. 3.8).

Table 3.6 shows the values obtained for  $\mu$ , together with error estimates, according to various methods (mentioning also the year). The relative accuracy in  $\mu$  is currently  $10^{-10}$ , compatible with an accuracy of centimetre order in the semi-major axis of the LAGEOS orbit.

## 3.6 Appendix: Terrestrial Reference Systems

### 3.6.1 Celestial Reference System

The International Celestial Reference System (ICRS) is an idealized barycentric coordinate system, with origin at the barycenter of the Solar System, to which celestial positions are referred. It has fixed axes and its time scale<sup>34</sup>

<sup>33</sup>LAGEOS-1 (NASA), launched 4 May 1976, and LAGEOS-2 (NASA-ASI, Italy), launched 22 October 1992, are almost identical satellites, of mass 410 kg and diameter 60 cm, each carrying 426 circular reflectors (422 fused silica glass and 4 germanium). They are often referred to as LAGEOS and LAGEOS-II, respectively. Characteristics of similar geodetic satellites: the Japanese satellite Ajisai, launched on 2 August 1986, mass 685 kg, diameter 2.15 m, 1,436 triangular fused silica reflectors; the Soviet satellites Etalon-1 and 2, launched on 10 January 1989 and on 31 May 1989, identical, mass 1,415 kg, diameter 1.29 m, 2,146 hexagonal reflectors (2,140 fused silica, 6 germanium).

<sup>34</sup>The International Time Bureau (*Bureau International de l'Heure*, or BIH) was set up in Paris at the beginning of the twentieth century (officially in 1912, but effectively in 1919) to centralise time determinations made around the world and hence to define a universal time scale. It is associated with the Paris Observatory. For these historical reasons, the official acronyms of the various time scales used by astronomers and physicists maintain the order of the words in the French name, e.g., TAI, TCB, etc., with the sole exception of UT. In 1988, the BIH founded the IERS (International Earth Rotation and Reference Systems Service) to monitor the parameters of the Earth's rotation, while the organisation in charge of International Atomic Time (*Temps Atomique International* TAI) was transferred to the

is Barycentric Coordinated Time (*Temps Coordonnée Barycentrique* TCB), which takes into account general relativistic effects.

The International Celestial Reference Frame (ICRF) is the realisation of the ICRS. The frame is materialised by the positions of hundreds of extragalactic quasars (quasi-stellar radiources), these being determined to very high accuracy, in fact better than 1 milli arcsec, using the VLBI technique explained below.

### 3.6.2 Terrestrial Reference System

In addition to the Earth's rotation, very slightly slowed down by the effect of the tides, two other motions need to be taken into account, due to the Sun–Moon system. One is *precession*, the axis of rotation tracing out a cone with semi-angle at the apex equal to the obliquity  $\varepsilon$ . This has a cycle of 25,800 years (see Fig. 6.7). The other is *nutation*, of amplitude  $17''$ , for which the main cycle is 18.6 years.

All these motions are very well understood and modelled, as can be seen from (8.49). But there is also an unpredictable movement of the polar axis (see Fig. 7.6). To model this, one must adopt a reference system that represents the Earth in its rotational movement. Since the Earth is a deformable solid, the axes of the system can be fixed by convention with the help of materialised points. Indeed, the surface is being continually deformed by the action of the tectonic plates, to the extent of a few centimetres a year, but also by seismic activity.

The International Terrestrial Reference System (ITRS) has its origin at the Earth's center of mass, including the oceans and the atmosphere. Its orientation is specified by the IERS. It is conventional at the epoqe 1984.0 but has since been guided by the condition of non-rotation of the Earth's crust: the relative angular momentum of the Earth's surface, calculated with positions and velocities expressed in the terrestrial system, is thus zero. The time scale is Geocentric Coordinated Time (*Temps Coordonnée Géocentrique* TCG).

The International Terrestrial Reference Frame (ITRF) is a realisation of the ITRS. It is defined jointly by astronomers and geodesists. For this Cartesian orthonormal system ( $O; x, y, z$ ):

- The origin  $O$  is chosen close to the Earth's center of mass, the value obtained by SLR and averaged over several years.
- The coordinates are scaled by VLBI and SLR.
- The orientation of the axes relative to the Earth's crust is fixed by convention. Its temporal variation is obtained by matching observed velocities

---

International Bureau of Weights and Measures (*Bureau International des Poids et Mesures* BIPM).

Method	SLR	VLBI	DORIS	GNSS
Celestial frame				
ICRF		***		
Terrestrial frame				
center of mass	***		*	*
Tectonic motion	**	***	**	***
Network density	*	*	**	***
Earth's rotation				
Length of day, UT1	*	***		*
Polar motion	**	**	*	***
Nutation		***		
Satellite orbitography				
MEO–GNSS	*			***
MEO–geodetic satellite	***			
LEO–environmental satellite	**		***	***
LEO–geodetic satellite	*			***

TABLE 3.7 : *Reference systems and techniques used in space geodesy. The contribution of the method is graded by asterisks: fairly important (\*), important (\*\*), very important or fundamental (\*\*\*)*. Abbreviations: for UT1, see Chap. 7; for MEO and LEO, see Chap. 9. Table with courtesy of F. Deleflie, D. Gambis, X. Collilieux.

to those obtained using a geophysical model of the motion of the tectonic plates which does not involve any overall rotation.

The frame is materialised by hundreds of stations (ITRF2008: 934 stations in 580 different sites). Their coordinates are determined by one or more of the following techniques:

- Very Long Baseline Interferometry (VLBI), since 1980.
- Satellite Laser Ranging (SLR), since 1983.
- Doppler Orbitography and Radiopositioning Integrated by Satellite (DORIS), since 1993.
- Static use of GPS, since 1994 (see Chap. 14).

We now outline each of these techniques, emphasising their relative importance in space geodesy (see also Table 3.7). Several stations bring together two, three, or even four (at three stations) of these techniques, and thus constitute genuine anchor points for the reference systems.

### Satellite Laser Ranging (SLR)

From a ground station,<sup>35</sup> laser pulses are emitted to a satellite equipped with reflectors (Fig. 3.8). A very small part of the emitted beam returns to the

<sup>35</sup>At the present time, there are 43 stations, almost all in the northern hemisphere.

detector at the ground station. The distance is then obtained to centimetre accuracy by measuring the time taken for the signal to return. In the beginnings of space geodesy, only dedicated satellites, such as LAGEOS-1, were equipped with reflectors (cube-corner mirrors). However, it was not long before a wide range of other satellites were equipped with suitable reflectors.<sup>36</sup>

The same technique<sup>37</sup> works with five reflectors set up on the Moon by the three US missions Apollo-11, 14, and 15 and the two unmanned Soviet missions Luna-17 and 21, and also with the LRO in orbit around the Moon.

### Very Long Baseline Interferometry (VLBI)

Very long baseline interferometry is an astronomical technique developed since 1980, although the first experiments date to 1967. The idea is to use two widely separated antennas to measure the time difference between the arrival of the same signal (in the centimetre wavelength range) from a quasar. Today there are around 40 VLBI stations on Earth. The resolution is proportional to the length of the baseline, i.e., the distance between the two antennas, so it is limited by the diameter of the Earth (of the order of a few thousand kilometres). However, the baseline can be made longer by using satellites in high orbits.

Earth-based VLBI gives highly accurate results, reaching the milli arcsec ( $1 \text{ mas} = 4.85 \times 10^{-9} \text{ rad}$ ), and a great many parameters can be fitted simultaneously. Given the positions of hundreds of extragalactic sources, one can determine the Earth's orientation in space, and hence also its rotation (UT1, polar motion, precession, nutation) viewed as a transformation between the celestial frame ICRF and the terrestrial frame ITRF.

### Doppler Orbitography and Radiopositioning Integrated by Satellite (DORIS)

The DORIS system was designed and developed by the French space agency, the CNES, in collaboration with the GRGS (*Groupe de Recherches en Géodésie Spatiale*) and the IGN (*Institut Géographique National*). Small energy-autonomous beacons are distributed uniformly around the planet, on

---

<sup>36</sup>The main satellites are as follows. Satellites for geodesy: LAGEOS-1 and 2, LARES, GFO, GFZ-1, Stella, Starlette, Wespac-1, Etalon-1 and 2, Ajisai, CHAMP, GRACE-A and B, GOCE; the Japanese satellite H2A-LRE in geosynchronous transfer orbit (GTO). Environmental and oceanographic satellites: TOPEX/Poseidon, Jason-1 and 2, ERS-1 and 2, Envisat, TerraSAR-X and TanDEM-X, ICESat, CryoSat-2, Meteor-2-21 (Fizeau), HY-2A. Navigation satellites: Navstar/GPS-35 and 36, the Japanese satellite QZS-1, practically all the Russian GLONASS satellites, the European satellites GIOVE-A and B and operational Galileo satellites; from Compass-M1, the Chinese satellites in the Compass-M series, Compass-I and Compass-G. Astronomical satellites: RadioAstron on a very high orbit.

<sup>37</sup>The ratio of the number of photons received to the number of photons emitted, called the *link budget*, goes as  $r^{-4}$ , where  $r$  is the distance. When the target is the Moon, this ratio is very small indeed, in fact, just a few photons over the whole night! Only two stations have taken data over a long period: the McDonald Observatory in Texas and the OCA in Grasse, France.

both continents and oceans. These emit a signal which is received by satellites equipped for this purpose. The system is coordinated by a master beacon at the CNES headquarters in Toulouse. The position of a satellite is determined to within a centimetre thanks to the network of stations used as reference points on the ground. Conversely, the system can be used to accurately relate given points to the ITRF. A dozen or so satellites in low Earth orbit (LEO) are equipped with the DORIS system.<sup>38</sup>

### Global Positioning System (GPS)

The whole of Chap. 14 will be devoted to the satellite navigation system (GNSS), commonly known as GPS. In the appendix on GPS and tectonic plates (see Sect. 14.10), we explain how the positions of static GPS receiving stations can be ascertained with millimetre accuracy. These stations contribute to maintaining the ITRF.

## 3.7 Appendix: Summary of Legendre Functions

### Legendre Polynomials

The generating function for the Legendre<sup>39</sup> polynomials is

$$\frac{1}{\sqrt{1-2tx+t^2}} = \sum_{n=0}^{\infty} P_n(x)t^n. \quad (3.43)$$

These polynomials, which are the coefficients in this power series in  $t$ , are defined for any  $n \geq 0$  by

$$P_n(x) = \frac{1}{2^n n!} \frac{d^n [(x^2 - 1)^n]}{dx^n}. \quad (3.44)$$

---

<sup>38</sup>The system has been or is still carried by the French satellites SPOT-2, 3, 4, and 5, Pléiades-1A and 1B, the French–Chinese HY-2, the French–US satellites TOPEX/Poseidon, Jason-1 and 2, the French-Indian SARAL, and the European satellites Envisat and CryoSat-2. It is also planned for the French–US Jason-3 and the European Sentinel-3-A.

<sup>39</sup>*Adrien Marie Legendre* (1752–1833) was a French mathematician. He introduced the polynomials which are now named after him in his *Recherches sur la figure des planètes* (1784). When put in charge of geodetic measurements (the distance between the Paris and Greenwich meridians) by the revolutionary government known as the *Convention*, he made significant contributions to spherical trigonometry. He obtained new results in number theory, and also in the study of elliptic functions, the beta and gamma functions, and the Euler integrals. His work *Eléments de Géométrie* was reprinted thirteen times between 1794 and 1827.

The first few Legendre polynomials are:

$$\begin{aligned}
 P_0(x) &= 1, & P_1(x) &= x, \\
 P_2(x) &= \frac{3x^2 - 1}{2}, & P_3(x) &= \frac{5x^3 - 3x}{2}, \\
 P_4(x) &= \frac{35x^4 - 30x^2 + 3}{8}, & P_5(x) &= \frac{63x^5 - 70x^3 + 15x}{8}, \\
 P_6(x) &= \frac{231x^6 - 315x^4 + 105x^2 - 5}{16}, & & \text{etc.}
 \end{aligned}$$

Considering only the zonal harmonics up to degree 6, the geopotential is given by (3.28) as

$$\begin{aligned}
 U(r, \psi) &= \frac{\mu}{r} \left[ 1 + \frac{J_2}{2} \left( \frac{R}{r} \right)^2 (1 - 3 \sin^2 \psi) + \frac{J_3}{2} \left( \frac{R}{r} \right)^3 (3 - 5 \sin^2 \psi) \sin \psi \right. \\
 &\quad - \frac{J_4}{8} \left( \frac{R}{r} \right)^4 (3 - 30 \sin^2 \psi + 35 \sin^4 \psi) \\
 &\quad - \frac{J_5}{8} \left( \frac{R}{r} \right)^5 (15 - 70 \sin^2 \psi + 63 \sin^4 \psi) \sin \psi \\
 &\quad \left. + \frac{J_6}{16} \left( \frac{R}{r} \right)^6 (5 - 105 \sin^2 \psi + 315 \sin^4 \psi - 231 \sin^6 \psi) \right].
 \end{aligned} \tag{3.45}$$

### Legendre Functions

The associated Legendre functions are defined in terms of the Legendre polynomials on the interval  $[-1, +1]$ , for all  $l \geq 0$  and for all  $0 \leq m \leq l$ , by

$$P_{lm}(x) = (1 - x^2)^{m/2} \frac{d^m P_l(x)}{dx^m}. \tag{3.46}$$

We have the relations

$$P_{l0}(x) = P_l(x), \quad P_{ll}(x) = \frac{(2l)!}{2^l l!} (1 - x^2)^{l/2},$$

and the first few associated Legendre functions are

$$\begin{aligned}
 P_{11}(x) &= \sqrt{1 - x^2}, \\
 P_{21}(x) &= 3x\sqrt{1 - x^2}, & P_{22}(x) &= 3(1 - x^2), \\
 P_{31}(x) &= \frac{3}{2}(5x^2 - 1)\sqrt{1 - x^2}, & P_{32}(x) &= 15x(1 - x^2), \\
 P_{33}(x) &= 15(1 - x^2)^{3/2}.
 \end{aligned}$$

# Chapter 4

## Keplerian Motion

### 4.1 Central Acceleration

#### 4.1.1 General Acceleration

##### Velocity and Acceleration

We consider a material point  $S$  in space, referred to an origin  $O$  and three fixed directions. The position vector, velocity, and acceleration of the point  $S$  are denoted by

$$\mathbf{r} = \mathbf{OS}, \quad \dot{\mathbf{r}} = \frac{d\mathbf{r}}{dt}, \quad \ddot{\mathbf{r}} = \frac{d^2\mathbf{r}}{dt^2}.$$

Consider the plane containing the position and velocity vectors. An orthonormal frame  $(O; \mathbf{i}, \mathbf{j})$  is defined in this plane, together with a polar coordinate basis  $(\mathbf{e}_r, \mathbf{e}_\theta)$ . Adjoining the unit vector along the  $Oz$  axis, we obtain the right-handed system

$$\mathbf{k} = \mathbf{i} \wedge \mathbf{j} = \mathbf{e}_r \wedge \mathbf{e}_\theta.$$

Let  $r$  be the length of the position vector, i.e.,  $r = \|\mathbf{r}\|$ , and  $\theta$  the angle between the  $\mathbf{i}$  axis and the position vector, i.e.,  $\theta = (\mathbf{i}, \mathbf{r})$ . The unit vectors  $\mathbf{e}_r$  and  $\mathbf{e}_\theta$  are defined by  $\mathbf{e}_r = \mathbf{r}/r$  and  $(\mathbf{e}_r, \mathbf{e}_\theta) = \pi/2$ . The angular speed and acceleration of the motion are denoted by  $\dot{\theta}$  and  $\ddot{\theta}$ .

In this plane coordinate system, the velocity and acceleration of the point  $S$  are obtained by successive derivatives of the expression for  $\mathbf{OS}$ . This gives

$$\mathbf{r} = r\mathbf{e}_r, \tag{4.1}$$

$$\dot{\mathbf{r}} = \dot{r}\mathbf{e}_r + r\dot{\theta}\mathbf{e}_\theta, \tag{4.2}$$

$$\ddot{\mathbf{r}} = (\ddot{r} - r\dot{\theta}^2)\mathbf{e}_r + \frac{1}{r}\frac{d}{dt}(r^2\dot{\theta})\mathbf{e}_\theta, \tag{4.3}$$

noting that  $r^2\ddot{\theta} + 2r\dot{r}\dot{\theta} = d(r^2\dot{\theta})/dt$ .



## Angular Momentum

The angular momentum per unit mass is defined by

$$\mathbf{C} = \mathbf{r} \wedge \dot{\mathbf{r}} . \quad (4.4)$$

Differentiating with respect to time, we obtain

$$\frac{d\mathbf{C}}{dt} = \dot{\mathbf{r}} \wedge \dot{\mathbf{r}} + \mathbf{r} \wedge \ddot{\mathbf{r}} = \mathbf{r} \wedge \ddot{\mathbf{r}} . \quad (4.5)$$

Moreover, using the definition and the relations (4.1) and (4.2), we obtain the expression

$$\mathbf{C} = r^2 \dot{\theta} \mathbf{k} . \quad (4.6)$$

### 4.1.2 Properties of Central Acceleration

Consider a material point  $S$  in space. Its motion is said to undergo central acceleration if there is some fixed point  $O$  such that, at each moment of time, the vector  $\mathbf{OS}$  and the acceleration vector are collinear. The motion of the point has central acceleration if and only if

$$\mathbf{r} \wedge \ddot{\mathbf{r}} = \mathbf{0} . \quad (4.7)$$

Inserting this defining relation in (4.5), we obtain

$$\frac{d\mathbf{C}}{dt} = \mathbf{0} , \quad (4.8)$$

which shows that, for this type of motion, the angular momentum is constant in time:

$$\mathbf{C} = \mathbf{r} \wedge \dot{\mathbf{r}} = \text{constant} . \quad (4.9)$$

If this constant is zero, the motion is in a straight line, since  $\mathbf{r}$  and  $\dot{\mathbf{r}}$  are collinear.

If the constant vector on the right-hand side of (4.9) is not zero, and this is the general case that we shall consider hereafter, the motion of the point is contained in the plane orthogonal to the constant vector. Let  $\mathcal{P}$  denote this plane.

The quantity  $C$  calculated from (4.6) is thus constant:

$$C = r^2 \dot{\theta} , \quad \text{with} \quad \mathbf{C} = C \mathbf{k} . \quad (4.10)$$

Note that  $\dot{\theta}$  cannot change sign during the motion.

### 4.1.3 Motion with Central Acceleration

#### Expressing the Acceleration

Setting

$$\ddot{\mathbf{r}} = \gamma \mathbf{e}_r, \quad \text{with } \gamma = f(r), \quad (4.11)$$

under the assumption that the acceleration is central, it follows that  $\gamma$  is the signed magnitude of this acceleration. Using the value for  $\ddot{\mathbf{r}}$  calculated in (4.3), we obtain the following two relations, one for each component:

$$\ddot{r} - r\dot{\theta}^2 = \gamma, \quad (4.12)$$

$$\frac{1}{r} \frac{d}{dt}(r^2\dot{\theta}) = 0. \quad (4.13)$$

The last relation shows once again that  $C$  is constant.

#### Areal Law

Let  $\mathcal{A}$  be the (magnitude of the) area swept out by the vector  $\mathbf{r}$ . The area element is the area of the triangle with base  $r d\theta$  and height  $r$ . Hence, we have  $d\mathcal{A} = (r/2)r d\theta$  and the areal speed (area swept out per unit time) is thus

$$\frac{d\mathcal{A}}{dt} = \frac{1}{2} r^2 \dot{\theta} = \frac{1}{2} C. \quad (4.14)$$

This is the areal law. It tells us that the area swept out is proportional to the time. Alternatively, equal areas are swept out in equal times (see Figs. 4.1 and 4.4).

#### Binet's Equations

Binet's equations give the velocity and acceleration as a function of the angle  $\theta$  and the auxiliary variable  $u$  defined by

$$u = \frac{1}{r}. \quad (4.15)$$

To find these relations, we eliminate the time  $t$  using (4.10), whence

$$\dot{\theta} = \frac{C}{r^2} = C u^2,$$

noting further that

$$r\dot{\theta} = C u, \quad r\dot{\theta}^2 = C^2 u^3.$$

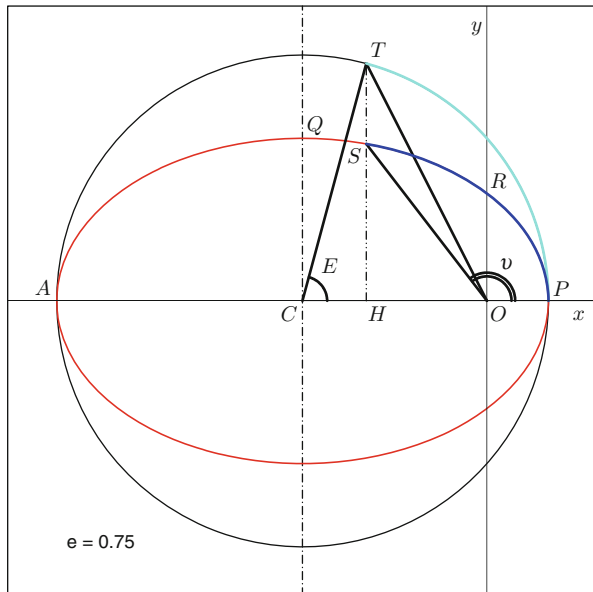


FIG. 4.1 : Elliptical trajectory. Ellipse and principal circle, indicating the notation for points and angles used to establish Kepler's equation geometrically.

Using the chain rule, we now have

$$\dot{r} = \frac{dr}{du} \frac{du}{d\theta} \frac{d\theta}{dt} = -\frac{\dot{\theta}}{u^2} \frac{du}{d\theta} = -C \frac{du}{d\theta} \quad (4.16)$$

and

$$\ddot{r} = \frac{d\dot{r}}{dt} = \left( \frac{d\dot{r}}{d\theta} \right) \dot{\theta} = \dot{\theta} \frac{d}{d\theta} \left( -C \frac{du}{d\theta} \right) = -C^2 u^2 \frac{d^2 u}{d\theta^2}. \quad (4.17)$$

Then from (4.2) and (4.3), we obtain the velocity and acceleration vectors relative to the basis  $(\mathbf{e}_r, \mathbf{e}_\theta)$ :

$$\dot{\mathbf{r}} = C \left( -\frac{du}{d\theta} \mathbf{e}_r + u \mathbf{e}_\theta \right), \quad (4.18)$$

$$\ddot{\mathbf{r}} = -C^2 u^2 \left( \frac{d^2 u}{d\theta^2} + u \right) \mathbf{e}_r. \quad (4.19)$$

Setting

$$V = \|\dot{\mathbf{r}}\|,$$

we obtain the two Binet equations from the last two equations. One refers to the velocity via its magnitude  $V$  and the other refers to the acceleration via the quantity  $\gamma$ :

$$V^2 = C^2 \left[ \left( \frac{du}{d\theta} \right)^2 + u^2 \right], \quad (4.20)$$

$$\gamma = -C^2 u^2 \left( \frac{d^2 u}{d\theta^2} + u \right). \quad (4.21)$$

## 4.2 Newtonian Acceleration

### 4.2.1 Equation for the Trajectory

A Newtonian acceleration is a central acceleration proportional to  $r^{-2}$ . The corresponding force is attractive.<sup>1</sup> The expression for the acceleration given in (4.11) thus becomes

$$\gamma = -\frac{\mu}{r^2}. \quad (4.22)$$

With the auxiliary variable  $u$ , we then have

$$\gamma = -\mu u^2. \quad (4.23)$$

This reveals the usefulness of the Binet equation for the acceleration (4.21) in the case of a Newtonian acceleration: comparing with (4.23), a factor of  $u^2$  cancels out. This leads to the equation

$$\frac{d^2 u}{d\theta^2} + u = \frac{\mu}{C^2}. \quad (4.24)$$

This is a second order linear differential equation with constant coefficients and the right-hand side is constant. It is easy to solve. The general solution is the sum of the general solution of the homogeneous equation, i.e., with the right-hand side set to zero, which introduces two integration constants, and a particular solution (just the right-hand side in this case):

$$u = A \cos(\theta - \theta_0) + \frac{\mu}{C^2}, \quad (4.25)$$

where  $A$  and  $\theta_0$  are the integration constants.

---

<sup>1</sup>The term ‘‘Coulombic’’ is usually reserved for electrostatic phenomena, where forces may be attractive or repulsive, while the word ‘‘Newtonian’’ refers to gravitational phenomena, where the forces are always attractive.

The expression for  $r$  is

$$r = \frac{p}{1 + e \cos(\theta - \theta_0)}, \quad (4.26)$$

where

$$p = \frac{C^2}{\mu} \quad (4.27)$$

and

$$e = Ap. \quad (4.28)$$

This is the equation for a conic section in polar coordinates with one focus at the origin  $O$ , parameter  $p$ , and eccentricity  $e$  [see (1.16)]. The quantities  $e$  and  $\theta_0$  are determined by the initial conditions. In order to study the relationship between these quantities and the initial conditions, that is, to investigate the main features of the trajectory, we use the Binet equation for the speed (4.20).

## 4.2.2 Types of Trajectory

### Eccentricity

Returning to the variable  $u$ , we now write

$$u = \frac{1 + e \cos(\theta - \theta_0)}{p}. \quad (4.29)$$

Differentiating this relation,

$$\frac{du}{d\theta} = -\frac{e}{p} \sin(\theta - \theta_0). \quad (4.30)$$

Substituting into (4.20), we have

$$e^2 + 2e \cos(\theta - \theta_0) + 1 = \frac{V^2}{C^2} p^2. \quad (4.31)$$

Equation (4.29) implies  $e \cos(\theta - \theta_0) = up - 1$ , and since  $p = C^2/\mu$ , we obtain

$$e^2 + 2 \left( u \frac{C^2}{\mu} - 1 \right) + 1 = \frac{V^2 C^2}{\mu^2}.$$

Returning to the variable  $r$ , the eccentricity is therefore given by

$$e^2 = 1 + \frac{2C^2}{\mu^2} \left( \frac{V^2}{2} - \frac{\mu}{r} \right). \quad (4.32)$$

Since  $e$ ,  $C$ , and  $\mu$  are constants, this equation shows the constancy of the quantity  $\mathcal{K}$  defined by

$$\mathcal{K} = \frac{1}{2}V^2 - \frac{\mu}{r} = \text{constant}. \quad (4.33)$$

At the end of the chapter, using the relation (4.111), we shall see that this quantity corresponds to the mechanical energy (per unit mass). For motion under a Newtonian acceleration,  $r$  and  $V$  vary in such a way that the relation (4.33) is always satisfied.

### Different Cases

We shall now investigate the quantities  $r$  et  $e$  defined by (4.26) and (4.32) (see Fig. 4.12). Depending on the value of  $\mathcal{K}$ , the eccentricity  $e$  can be greater than or less than unity. We see that the quantity

$$V_e = \sqrt{2\frac{\mu}{r}} \quad (4.34)$$

plays a specific role in this demarcation:

- If  $\mathcal{K} > 0$ , i.e.,  $V > V_e$ , then  $e > 1$ . We have a hyperbola with focus at the origin  $O$ . This time we have the branch which is concave with respect to the origin  $O$ , since the force is attractive.
- If  $\mathcal{K} = 0$ , i.e.,  $V = V_e$ , then  $e = 1$ . We have a parabola with focus at  $O$ .
- If  $\mathcal{K} < 0$ , i.e.,  $V < V_e$ , then  $e < 1$ . We now have an ellipse with one focus at  $O$ . In this case, there is a condition for the Eq. (4.32): the right-hand side cannot be negative. We must therefore have

$$V^2 - 2\frac{\mu}{r} \geq -\frac{\mu^2}{C^2} \quad \Longrightarrow \quad V^2 \geq 2\frac{\mu}{r} - \frac{\mu}{p},$$

whence the condition

$$V \geq V_s,$$

where

$$V_s = \sqrt{2\frac{\mu}{r} - \frac{\mu}{p}}. \quad (4.35)$$

The quantity  $V_s$  is the orbital insertion speed for putting a satellite into orbit at the distance  $r$ . We shall return to this case shortly. We shall also consider the special case of an ellipse with zero eccentricity, which is in fact a circle with center at  $O$ .

It is easy to understand the significance of the speed  $V_e$  defined above. When  $V \geq V_e$ , the point  $S$  describing a parabola or a branch of a hyperbola can go to infinity. On the other hand, when  $V < V_e$ , the point  $S$  remains forever

within a finite distance of  $O$  and the motion is periodic. This speed, which depends on  $r$ , is therefore known as the escape velocity at the distance  $r$ .

If the motion is to be periodic, the speed  $V$  must therefore satisfy the conditions

$$V_s \leq V < V_e . \quad (4.36)$$

The speed  $V$  of the body must be greater than  $V_s$  for it to be in orbit, but less than  $V_e$  for it to remain under the influence of the central gravitational attraction.<sup>2</sup>

Note that the nature of the trajectory does not depend on the orientation of the velocity vector, but only on its magnitude  $V$  at a point at distance  $r$  from the origin.

## 4.3 Trajectory and Period for Keplerian Motion

### 4.3.1 Definition of Keplerian Motion

Keplerian motion is the motion of a point mass in a central force field going as  $1/r^2$ , the center of the field being fixed. This field is a gravitational field created by another mass, assumed motionless. We consider only these two masses and make no attempt to include perturbations due to other bodies. In the present chapter, we shall study the motion of this material point  $S$  and it will suffice to consider that it is subject to a Newtonian acceleration, or, in terms of forces, that it experiences a central force of the form  $1/r^2$  in a Galilean frame.

Since the aim here is to study satellite trajectories, we shall hereafter consider only periodic trajectories, that is, elliptical trajectories with  $\mathcal{K} < 0$  or  $e < 1$ , unless otherwise specified.

### 4.3.2 Periodic Trajectories

#### Elliptical Trajectories

In the case of an elliptical trajectory, given the eccentricity in (4.32), we can write

$$1 - e^2 = -\frac{2C^2}{\mu^2}\mathcal{K}, \quad \text{with } \mathcal{K} < 0 .$$

---

<sup>2</sup>At the beginning of the space age, one finds the terms “first cosmic velocity”, “second cosmic velocity”, and so on, particular in the Soviet scientific literature. The third cosmic velocity is the one required to escape from the sphere of influence of the Solar System.

We also know that an ellipse is defined by its semi-major axis  $a$  and its eccentricity  $e$ . The parameter  $p$  is defined by  $p = a(1 - e^2)$ . Hence, by (4.27), we have

$$1 - e^2 = \frac{p}{a} = \frac{C^2}{\mu a}. \quad (4.37)$$

These relations imply

$$2\mathcal{K} = V^2 - \frac{2\mu}{r} = -\frac{\mu}{a}. \quad (4.38)$$

We may now deduce the expression for the speed  $V$  as a function of  $r$ :

$$V^2 = \mu \left( \frac{2}{r} - \frac{1}{a} \right). \quad (4.39)$$

We can check that the right-hand side is always positive since, in an ellipse,  $r$  is always less than  $2a$ .

To sum up, the equation for the elliptical trajectory can be written in polar coordinates in the form

$$r = r(\theta) = \frac{C^2}{\mu} \frac{1}{1 + e \cos(\theta - \theta_0)}, \quad (4.40)$$

where

$$e^2 = 1 - \frac{C^2}{\mu a}, \quad (4.41)$$

or alternatively,

$$r = r(\theta) = \frac{a(1 - e^2)}{1 + e \cos(\theta - \theta_0)}. \quad (4.42)$$

During the periodic motion of the point  $S$ , the distance  $r$  goes through a minimum and a maximum, denoted respectively by  $r_p$  and  $r_a$ <sup>3</sup>:

$$\begin{aligned} r_p &= r(\theta = \theta_0) = a(1 - e), \\ r_a &= r(\theta = \theta_0 + \pi) = a(1 + e). \end{aligned} \quad (4.43)$$

---

<sup>3</sup>The subscripts  $p$  and  $a$  stand for the perigee and the apogee, respectively, for motion around the Earth ( $\eta$   $\gamma$   $\eta$ ,  $\eta$   $\zeta$ ), or perihelion and aphelion, for motion around the Sun ( $\delta$   $\eta$   $\lambda$   $\omicron$   $\varsigma$ ,  $\omicron$   $\nu$ ). More generally, when the gravitational source is not specified, we speak of the periastron and apostron, or pericenter and apocenter. The prefixes “peri” and “apo” come from the adverbs  $\text{περί}$  and  $\text{ἀπό}$  meaning “above” and “far away”, respectively. The names perihelion and aphelion were invented by Kepler (1596) as an extension of the terms perigee and apogee used by Ptolemy.



The sum of these two lengths is obviously equal to the major axis of the ellipse, i.e.,  $r_p + r_a = 2a$ . The eccentricity can be expressed in the form

$$e = \frac{r_a - r_p}{r_a + r_p} = \frac{r_a}{a} - 1 = 1 - \frac{r_p}{a}. \quad (4.44)$$

Referring to (4.39), we see that the speed  $V$  goes through a maximum  $V_p$  for  $r = r_p$  and a minimum  $V_a$  for  $r = r_a$ , with respective values

$$V_p = \sqrt{\frac{\mu}{a}} \sqrt{\frac{1+e}{1-e}} = \sqrt{\frac{\mu}{p}} (1+e), \quad (4.45)$$

$$V_a = \sqrt{\frac{\mu}{a}} \sqrt{\frac{1-e}{1+e}} = \sqrt{\frac{\mu}{p}} (1-e). \quad (4.46)$$

We thus deduce the following relations between the speeds at the apsides<sup>4</sup>:

$$r_p V_p = r_a V_a = \sqrt{\frac{\mu}{p}} a (1 - e^2) = \sqrt{\mu p} = C.$$

We retrieve the angular momentum  $C$ , since, for these two extremal points on the ellipse, the velocity and the radial vector are orthogonal.

Note also that

$$\frac{V_p}{V_a} = \frac{r_a}{r_p} = \frac{1+e}{1-e}. \quad (4.47)$$

Using the eccentricity angle  $\epsilon$  defined by (1.27), the apsidal velocities can be written

$$V_p = \sqrt{\frac{\mu}{a}} \tan\left(\frac{\pi}{4} + \frac{\epsilon}{2}\right), \quad V_a = \sqrt{\frac{\mu}{a}} \tan\left(\frac{\pi}{4} - \frac{\epsilon}{2}\right). \quad (4.48)$$

The speed can be expressed in terms of the polar angle. From (4.31), we find

$$V^2 = \frac{\mu}{p} [1 + 2e \cos(\theta - \theta_0) + e^2] = \frac{\mu}{a} \frac{1 + 2e \cos(\theta - \theta_0) + e^2}{1 - e^2}. \quad (4.49)$$

**Example 4.1** Calculate the eccentricity of the orbit of an artificial Earth satellite with altitude 500 km at perigee and 40,000 km at apogee (Molniya orbit). Take  $R = 6,400$  km.

---

<sup>4</sup>The apsidal line is the line joining the perigee and the apogee. This line segment is the major axis of the ellipse. The perigee and apogee are the two apsides, also called the inferior apsis and superior apsis, respectively. This word comes from the Greek ἡ ἀψίς, ἴδιος, meaning “vault” or “celestial vault”, having lost the initial aspiration. The architectural term “apse”, which refers to the semicircular recess covered with a hemispherical vault, usually at the east end of a church, has the same origin.

► If  $h_p$  and  $h_a$  are the altitudes at perigee and apogee, then using the distances  $r_p$  and  $r_a$  defined by (4.43), we have

$$r_p = R + h_p, \quad r_a = R + h_a, \quad a = R + \frac{h_a + h_p}{2}.$$

With (4.44), we obtain the eccentricity

$$e = \frac{h_a - h_p}{2R + h_a + h_p}. \quad (4.50)$$

In the case of the Molniya orbit, we have

$$e = \frac{39,500}{12,800 + 40,500} \approx 0.75.$$

Moreover, (4.47) gives

$$\frac{V_a}{V_p} = \frac{1 - e}{1 + e} = 0.25/1.75 = 1/7.$$

With this type of orbit, the satellite is moving seven times slower at apogee than at perigee. ◀

### Special Case of Circular Trajectory

A circle is an ellipse with eccentricity  $e = 0$ . Equation (4.41) gives

$$\frac{C^2}{\mu} = a.$$

Substituting in (4.26), we obtain the expected relation for a circle, viz.,

$$r = \frac{C^2}{\mu} = a = p.$$

The speeds  $V_e$  and  $V_s$  defined by (4.34) and (4.35) become in this case

$$V_e = \sqrt{2\frac{\mu}{a}}, \quad V_s = \sqrt{\frac{\mu}{a}} = \frac{V_e}{\sqrt{2}}. \quad (4.51)$$

Moreover, the relation involving the constant  $\mathcal{K}$  gives

$$2\mathcal{K} = V^2 - \frac{2\mu}{a} = -\frac{\mu}{a},$$

whence

$$V = \sqrt{\frac{\mu}{a}} = \frac{C}{a}. \quad (4.52)$$

This shows that the magnitude  $V$  of the velocity is constant and equal to  $V_s$ . Circular motion is uniform.

Considering the value of  $\gamma$  given by (4.22), it can also be checked that we do retrieve the usual value for the acceleration in the case of a uniform circular motion:

$$\gamma = -\frac{\mu}{a^2} = -\frac{V^2}{a}.$$

### 4.3.3 Period and Mean Motion

#### Period

The period is the time  $T$  taken by the point  $S$  to describe the whole ellipse. Integrating (4.14) over one period, we obtain

$$\mathcal{A} = \frac{1}{2}CT.$$

In this case,  $\mathcal{A}$  represents the area of the ellipse, i.e.,  $\mathcal{A} = \pi ab$ , where  $b$  is the semi-minor axis of the ellipse. Recall further that  $b^2 = pa$ . Hence,

$$\mathcal{A} = \pi a \sqrt{pa} = \pi C \sqrt{\frac{a^3}{\mu}}.$$

The period is therefore

$$T = 2\pi \sqrt{\frac{a^3}{\mu}}. \quad (4.53)$$

This is called the period of revolution,<sup>5</sup> orbital period, or Keplerian period of the motion.<sup>6</sup> Note that, for an attractive body  $\mu$ , the Keplerian period depends only on the semi-major axis  $a$  and not on the eccentricity  $e$ .

---

<sup>5</sup>The word “revolution” comes from low Latin *revolutio, onis*, meaning “unfolding” or “return”, from the Latin verb *volvere*, meaning “roll”, with the prefix *re-*. Since the Middle Ages, it has come to mean the periodic return of a heavenly body to its point of departure. Copernicus used it in the title of his celebrated treatise. The transition to its present use, to refer to a radical or significant change of political, economic, or cultural regime, as exemplified by the French Revolution, came only much later. The scientific meaning thus predates the everyday use of the term. So when we see references to the “Copernican revolution”, e.g., Kant in 1787, we may say that we have come full circle.

<sup>6</sup>As we shall see later, when Keplerian motion is perturbed, we can define several periods relating to the actual motion, such as the nodal (or draconitic) period and the anomalistic period.

## Mean Motion

The corresponding angular speed  $n$ , called the mean motion, is defined as

$$n = \frac{2\pi}{T} = \sqrt{\frac{\mu}{a^3}}. \quad (4.54)$$

The mean motion is the angular speed (SI unit  $\text{rad s}^{-1}$ , radian per second) of a fictitious point in uniform circular motion at radius  $a$  and with the same period as a point in Keplerian motion on an orbit with semi-major axis  $a$ . With (4.53), the constant  $C$  in (4.14) can be expressed very simply as a function of  $n$  and the dimensions of the ellipse:

$$C = nab. \quad (4.55)$$

### 4.3.4 Relation Between Position and Time

The relations established above give us the trajectory in polar coordinates, i.e., the relation between  $r$  and  $\theta$ . They were obtained without reference to the time, since we started out from Binet's equations, which were themselves established by eliminating the time. In order to find an expression for the time  $t$  in terms of the polar coordinates, i.e., to determine the position of the point  $S$  at any time, we must go back to the constant in the areal law for motion with a central acceleration, as specified in (4.10). To obtain  $t$ , we integrate this relation:

$$dt = \frac{1}{C} r^2 d\theta. \quad (4.56)$$

By this integration, we obtain the time  $t$  as a function of the position of the point, as specified by  $r$  or  $\theta$ .

From a purely practical point of view, we usually require the inverse functional relation, i.e., the position as a function of the time  $t$ . There is no direct analytic solution and we must apply a special treatment. This is Kepler's problem. Here we discuss these points as follows:

- Determination of the time as a function of position in Sect. 4.4.
- Determination of the position as a function of time in Sect. 4.5.

## 4.4 Time as a Function of Position: The Three Anomalies

The time  $t$  is obtained using (4.56) and integrating  $r^2 d\theta$ . We consider two methods:

- In the first method, we eliminate  $r$ , expressing it as a function of  $\theta$ , i.e.,  $r = f(\theta)$ . We then obtain  $t$  from

$$t = \frac{1}{C} \int [f(\theta)]^2 d\theta .$$

- In the second approach, we eliminate  $\theta$ , first expressing  $d\theta$  in the form  $d\theta = g(r)dr$ , and then obtaining  $t$  from

$$t = \frac{1}{C} \int r^2 g(r) dr .$$

We shall also see how this last result can be obtained by a method based on the geometric properties of the ellipse.

#### 4.4.1 Expression for the Time and the Mean Anomaly $M$

In order to introduce the angles known as anomalies in a homogeneous way in the following,<sup>7</sup> we transform the time into an angle for any periodic trajectory with mean motion  $n$ . The required angle  $M$  varies linearly with time from  $M = 0$  for  $t = t_p$ , when the body is at perigee, to  $M = 2\pi$  for  $t = t_p + T$ , when the body next returns to perigee. The definition of this angle, called the mean anomaly, is therefore

$$M = n(t - t_p) . \quad (4.57)$$

#### 4.4.2 Expression $t = t(\theta)$ and the True Anomaly $v$

The starting point is (4.56), in which we replace  $r$  by its expression as a function of  $\theta$ , as given by (4.40):

$$dt = \frac{1}{C} \frac{p^2}{[1 + e \cos(\theta - \theta_0)]^2} d\theta .$$

---

<sup>7</sup>Kepler invented the term for these angles, from *anomalía*,  $\alpha$  in Latin. It originally comes from the Greek word ἡ ἀνωμαλία,  $\alpha\varsigma$ , which means “irregularity” (privative prefix  $\acute{\alpha}\nu$  and adjective  $\delta\mu\alpha\lambda\acute{o}\varsigma$ , meaning “self-similar” or “regular”). The idea behind this was to express the irregular behaviour of this angle in time (since the motion does not appear to be circular or regular). Kepler first used the term to indicate the position of Mars with respect to the Sun and he defined several anomalies. Among these were the three described in this chapter: the true anomaly (*anomalía coæquata vera*), the eccentric anomaly (*anomalía eccentrici*), and the mean anomaly (*anomalía media*). In his work *Astronomia Nova*, apart from the true anomaly, Kepler used the “artificial” anomaly (*anomalía coæquata fictitia*) and four other anomalies (*anomalía circularis* & *elliptica*, *anomalía distantaria*, *anomalía scrupularia*).

The minimal value of  $r$ , namely  $r = r_p$ , is obtained for  $\theta = \theta_0$  [see (4.43)], and it is convenient to measure angles from this origin. We thus make the change of variable

$$v = \theta - \theta_0 . \quad (4.58)$$

The angle  $v$  is called the true anomaly. We then calculate  $t = t(v)$  from

$$t = \frac{p^2}{C} \int \frac{dv}{(1 + e \cos v)^2} .$$

This type of function integrates as follows:

$$\begin{aligned} \mathcal{I} &= \int \frac{dv}{(1 + e \cos v)^2} = -\frac{e \sin v}{(1 - e^2)(1 + e \cos v)} + \frac{1}{(1 - e^2)} \int \frac{dv}{1 + e \cos v} , \\ \int \frac{dv}{1 + e \cos v} &= \frac{2}{\sqrt{1 - e^2}} \arctan \left( \sqrt{\frac{1 - e}{1 + e}} \tan \frac{v}{2} \right) . \end{aligned}$$

Using (4.37), we have

$$\frac{p^2}{C} = \sqrt{\frac{a^3}{\mu}} (1 - e^2)^{3/2} = \frac{(1 - e^2)^{3/2}}{n} ,$$

with the expression for the mean motion  $n$  given by (4.54).

Taking the time origin as  $t = t_p$  for  $r = r_p$  and  $v = 0$ , we now obtain

$$t - t_p = \frac{(1 - e^2)^{3/2}}{n} \mathcal{I} ,$$

which gives the time as a function of  $\theta$  via

$$n(t - t_p) = M = 2 \arctan \left( \sqrt{\frac{1 - e}{1 + e}} \tan \frac{v}{2} \right) - \frac{e \sqrt{1 - e^2} \sin v}{1 + e \cos v} . \quad (4.59)$$

We have thus expressed  $t$  as a function of the polar angle  $\theta$  or, which comes to the same,  $M$  as a function of  $v$ .

From this, we can write (4.42) in the form

$$r = r(v) = \frac{a(1 - e^2)}{1 + e \cos v} , \quad (4.60)$$

which gives the distance  $r$  as a function of the true anomaly.

For the speed, the expression (4.49) becomes

$$V^2 = \frac{\mu}{a} \frac{1 + 2e \cos v + e^2}{1 - e^2} . \quad (4.61)$$

### 4.4.3 Expression $t = t(r)$ and the Eccentric Anomaly $E$ Analytic Method for Obtaining Kepler's Equation

Instead of expressing  $d\theta$  directly as a function of  $r$ , we adopt a neighbouring approach, starting from (4.32). This relates  $V$  and  $r$  to the parameters of the ellipse and allows us to write

$$V^2 = \frac{2\mu}{r} - \frac{\mu^2}{C^2}(1 - e^2).$$

From the vector form (4.2) for the velocity, we have

$$V^2 = \dot{r}^2 + r^2\dot{\theta}^2 = \dot{r}^2 + \frac{C^2}{r^2},$$

where  $\theta$  has been eliminated using the areal law (4.14). This leads to

$$\dot{r}^2 = \left(\frac{dr}{dt}\right)^2 = -\frac{\mu^2}{C^2}(1 - e^2) + \frac{2\mu}{r} - \frac{C^2}{r^2},$$

and the differential equation

$$dt = \frac{r \, dr}{\sqrt{-\mu^2(1 - e^2)r^2/C^2 + 2\mu r - C^2}}.$$

Replacing  $C^2$  by  $\mu a(1 - e^2)$ , we obtain the following simplifications:

$$\begin{aligned} -\frac{\mu^2}{C^2}(1 - e^2)r^2 + 2\mu r - C^2 &= -\frac{\mu}{a}r^2 + 2\mu r - \mu a(1 - e^2) \\ &= \frac{\mu}{a}(-r^2 + 2ar - a^2 + a^2e^2) \\ &= \frac{\mu}{a}[a^2e^2 - (r - a)^2], \end{aligned}$$

whereupon

$$dt = \sqrt{\frac{a}{\mu}} \frac{r \, dr}{\sqrt{a^2e^2 - (r - a)^2}}. \quad (4.62)$$

To integrate this equation, it is convenient to introduce the auxiliary angle variable  $E$  such that  $a - r = ae \cos E$ , which can also be defined by

$$\cos E = \frac{1}{e} \left(1 - \frac{r}{a}\right). \quad (4.63)$$

This angle is called the eccentric anomaly.<sup>8</sup> It is illustrated in Fig. 4.1. Below we describe its geometric meaning in relation to the ellipse. Note that  $E = 0$  for  $r = r_p$  and  $E = \pi$  for  $r = r_a$  [see (4.43)].

---

<sup>8</sup>Eccentric means off-center. The center in question is not the center of the circle or the ellipse, but the focus of the ellipse, which is the center of attraction. In Chap. 1, this angle appears in the relation (1.29).

We now make the change of variable

$$r = a(1 - e \cos E), \quad (4.64)$$

so that  $dr = ae \sin E dE$ . As a function of  $E$ , (4.62) becomes

$$dt = \sqrt{\frac{a}{\mu}} a(1 - e \cos E) dE.$$

The integration is carried out taking the time origin at  $t = t_p$  for  $r = r_p$  and  $E = 0$ :

$$t - t_p = \sqrt{\frac{a^3}{\mu}} (E - e \sin E).$$

Bringing in the mean motion  $n$ , we obtain

$$n(t - t_p) = M = E - e \sin E. \quad (4.65)$$

This is known as Kepler's equation. We have thus expressed  $t$  as a function of  $r$ , or equivalently,  $M$  as a function of  $E$ .

### Geometric Method for Obtaining Kepler's Equation

We use the areal law and the fact that the ellipse is an affine transformation of the principal circle with expansion  $\sqrt{1 - e^2}$ , axis  $Ox$ , and direction  $Oy$ . Integrating the areal law (4.14) from  $t_p$  to  $t$ , we obtain

$$t - t_p = \frac{2}{C} \mathcal{A},$$

where the quantity  $\mathcal{A}$  is the area swept out between these two times, i.e., in the notation of Fig. 4.1, the area of the curvilinear triangle  $OPS$ . Let  $\mathcal{A}'$  be the area of the curvilinear triangle  $OPT$ , where  $T$  is the point giving  $S$  under the affine transformation. We thus have

$$\mathcal{A} = \sqrt{1 - e^2} \mathcal{A}'.$$

Replacing  $C$  by  $\sqrt{\mu a(1 - e^2)}$ , we now have

$$t - t_p = \frac{2}{\sqrt{\mu a}} \mathcal{A}'.$$

The area  $\mathcal{A}'$  is calculated to be

$$\begin{aligned} \mathcal{A}' &= \text{sector } CPT - \text{triangle } COT \\ &= \text{sector } \{\text{angle } E\} - \frac{1}{2} CO \times HT \\ &= \frac{1}{2} a^2 E - \frac{1}{2} (ae) \times (a \sin E) = \frac{1}{2} a^2 (E - e \sin E). \end{aligned}$$

This geometrical method yields Kepler's equation very quickly, with the expression for  $\mathcal{A}'$  and introducing the mean motion:

$$n(t - t_p) = M = E - e \sin E. \quad (4.66)$$



### Expressions Involving the Anomaly $E$

The eccentric anomaly  $E$  has no counterpart in physical reality. It is merely a mathematical tool that proves useful in calculations and often leads to simple expressions. For example, a few manipulations yield

$$\dot{r} = \frac{\sqrt{\mu a}}{r} e \sin E, \quad (4.67)$$

$$\mathbf{r} \cdot \dot{\mathbf{r}} = r \dot{r} = \sqrt{\mu a} e \sin E, \quad (4.68)$$

and

$$V^2 = \frac{\mu}{a} \frac{1 + e \cos E}{1 - e \cos E}. \quad (4.69)$$

#### 4.4.4 Relating the Anomalies

##### Relation Between the Anomalies $v$ and $E$

To establish the relations between  $v$  and  $E$  (see Fig. 4.1), the ellipse is equipped with a frame  $(Ox, Oy)$ . Let  $O$  be the principal focus, the center of the Newtonian field, and  $C$  the center of the ellipse. The major axis is  $AP$ , where  $P$  (perigee) is the point on the ellipse closest to  $O$  and  $A$  (apogee) the point furthest away. We choose the  $Ox$  axis along  $OP$  and the  $Oy$  axis at  $90^\circ$  to it in the anticlockwise direction. Let  $R$  be the intersection of  $Oy$  with the ellipse, and  $Q$  the intersection of the line parallel to  $Oy$  through  $C$  with the ellipse. We then have the following correspondence:

$$a = CP, \quad b = CQ, \quad p = OR, \quad ae = CO, \quad r_p = OP, \quad r_a = OA.$$

We also draw the circle with center  $C$  and radius  $CP$  which contains the ellipse and is tangent to it at  $P$  and  $A$ . This is the principal circle. Let  $S$  be an arbitrary point on the ellipse and  $H$  its projection onto  $Ox$ .

The true anomaly can be defined immediately as the polar angle

$$v = (\mathbf{Ox}, \mathbf{OS}).$$

The eccentric anomaly is obtained geometrically from its definition as

$$E = (\mathbf{Cx}, \mathbf{CT}),$$

where the point  $T$  is the intersection of the straight line  $HS$  with the principal circle. Indeed, according to the relation (4.63), we have  $\cos E = (a - r)/ae$ . Transforming  $(a - r)$  in such a way as to bring in  $v$ , i.e.,

$$a - r = a(1 - e^2) - r + ae^2 = r(1 + e \cos v) - r + ae^2 = e(r \cos v + ae),$$

we find

$$\cos E = \frac{r \cos v + ae}{a} = \frac{CH}{CT},$$

using the notation from Fig. 4.1. The angle  $E$  is indeed the angle  $C$  of the right-angled triangle  $HCT$ .

To obtain the relation between the angles  $v$  and  $E$ , we write down the coordinates of the point  $S$ , viz.,

$$x = r \cos v = a(\cos E - e), \quad (4.70)$$

$$y = r \sin v = a\sqrt{1 - e^2} \sin E, \quad (4.71)$$

whence

$$\sqrt{x^2 + y^2} = r = a(1 - e \cos E),$$

and deduce the relations between the true and eccentric anomalies. Note that  $v$  and  $E$  change sign together.

For  $v$  as a function of  $E$ ,

$$\cos v = \frac{\cos E - e}{1 - e \cos E}, \quad \sin v = \frac{\sqrt{1 - e^2} \sin E}{1 - e \cos E},$$

We calculate the quantities  $(1 + \cos v)$  and  $(1 - \cos v)$ , viz.,

$$1 + \cos v = \frac{(1 - e)(1 + \cos E)}{1 - e \cos E} \implies \cos^2 \frac{v}{2} = \frac{1 - e}{1 - e \cos E} \cos^2 \frac{E}{2},$$

$$1 - \cos v = \frac{(1 + e)(1 - \cos E)}{1 - e \cos E} \implies \sin^2 \frac{v}{2} = \frac{1 + e}{1 - e \cos E} \sin^2 \frac{E}{2},$$

to arrive at the relation

$$\tan \frac{v}{2} = \sqrt{\frac{1 + e}{1 - e}} \tan \frac{E}{2}. \quad (4.72)$$

For  $E$  as a function of  $v$ ,

$$\cos E = \frac{\cos v + e}{1 + e \cos v}, \quad \sin E = \frac{\sqrt{1 - e^2} \sin v}{1 + e \cos v},$$

$$\tan \frac{E}{2} = \sqrt{\frac{1 - e}{1 + e}} \tan \frac{v}{2}. \quad (4.73)$$

We can also express the difference  $(v - E)$  as a function of  $v$  or  $E$ :

$$\tan \frac{v - E}{2} = \frac{\beta \sin E}{1 - \beta \cos E} = \frac{\beta \sin v}{1 + \beta \cos v}, \quad (4.74)$$

where

$$\beta = \frac{e}{1 + \sqrt{1 - e^2}} = \frac{1 - \sqrt{1 - e^2}}{e}. \quad (4.75)$$

With the eccentricity angle  $\epsilon$  defined by (1.27), we have

$$\beta = \tan \frac{\epsilon}{2}, \quad (4.76)$$

$$\tan \frac{v}{2} = \tan \left( \frac{\pi}{4} + \frac{\epsilon}{2} \right) \tan \frac{E}{2}, \quad \tan \frac{E}{2} = \tan \left( \frac{\pi}{4} - \frac{\epsilon}{2} \right) \tan \frac{v}{2}.$$

### Differential Relations Between the Anomalies

From the definition of  $M$ , we have

$$\frac{dM}{dt} = n. \quad (4.77)$$

Equation (4.65) yields

$$n = \frac{dM}{dt} = (1 - e \cos E) \frac{dE}{dt} \quad (4.78)$$

and

$$\frac{dE}{dM} = \frac{1}{1 - e \cos E}. \quad (4.79)$$

The relation between  $dM$  and  $dv$  is deduced from the areal law. Equation (4.14) gives

$$\frac{d\theta}{dt} = \frac{C}{r^2} = \frac{na^2\sqrt{1 - e^2}}{r^2},$$

and since  $d\theta$  and  $dv$  are equivalent, we have

$$n = \frac{dM}{dt} = \frac{r^2}{a^2\sqrt{1 - e^2}} \frac{dv}{dt}, \quad (4.80)$$

and hence,

$$\frac{dv}{dM} = \frac{a^2}{r^2} \sqrt{1 - e^2}. \quad (4.81)$$

Using (4.64), (4.79), and (4.81), we have the following three useful relations:

$$\frac{dE}{dM} = \frac{a}{r}, \quad \frac{dv}{dM} = \frac{ab}{r^2}, \quad \frac{dv}{dE} = \frac{b}{r}. \quad (4.82)$$

## 4.5 Position as a Function of Time: Kepler's Problem

### 4.5.1 Methods for Solving Kepler's Problem

We have just seen how to express the time in terms of the three anomalies in an analytical way. The converse problem consists in expressing the true anomaly in terms of time. This is called Kepler's problem. It has no analytical solution.

At a given time  $t$ , defining the value  $M = M(t)$  of the mean anomaly, Kepler's equation becomes

$$E - e \sin E = M. \quad (4.83)$$

We wish to obtain  $E$  as a function of  $M$ , so that we may subsequently obtain  $v$ .

Since Kepler's time, dozens of methods<sup>9</sup> have been put forward to solve this transcendental equation in  $E$ . We shall present the following:

- An iterative numerical method.
- An overview of methods using series expansions and an approximate formula for small eccentricities.

We shall focus mainly on the first method, which is currently the most widely used. It can yield any required accuracy, and with today's computers these otherwise tedious calculations now take only a fraction of a microsecond.

### 4.5.2 Solution by Numerical Iteration

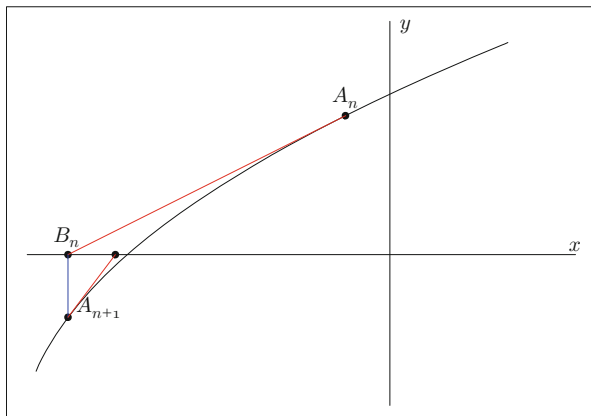
#### Newton–Raphson Method

The idea of the Newton–Raphson method, used here to solve Kepler's problem, is to approximate a curve near a point by its tangent at that point (first order Taylor expansion) and then to proceed by iteration. The equation of the curve is first transformed into the form  $f(x) = 0$ . We check that there is a solution and that it is unique.

We draw the tangent at a point  $A_n$  on the curve which has coordinates  $(x = x_n, y = f(x_n))$  (see Fig. 4.2). It cuts the  $x$  axis at a point  $B_n$  with

---

<sup>9</sup>In January 1900, the *Bulletin Astronomique* of the Paris Observatory provided a bibliography of 123 papers dealing with the solution of Kepler's problem, either analytically or graphically. Some of the great names of astronomy and mathematics appear on the list, including Kepler (1609), Newton (1687), Cassini (1719), Simpson (1740), Euler (1747), Lalande (*Astronomie*, 1764), Lagrange (*Sur le problème de Kepler*, 1769), Gauss (*Theoria motus*, 1809), Littrow (*Anomalix verax per mediam determinatio*, 1814), Delambre (1817), Bessel (*Über das Keplersche Problem*, 1818), Laplace (*Mémoire sur le développement de l'anomalie vraie*, 1823), Wallace (*Two elementary solutions of Kepler's problem*, 1835), Encke (*Auflösung des Keplerschen Gleichung*, 1850), Cauchy (1854), Lehmann (*Ueber eine definitive Lösung des Keplerschen Problems*, 1855, followed by many other purportedly definitive publications over several years), Le Verrier (1855), and Radau (1882).

FIG. 4.2 : *The Newton–Raphson iterative method.*

coordinates  $(x = x_{n+1}, y = 0)$ . From  $B_n$ , we find the point on the curve with the same abscissa as  $B_n$ , denoted by  $A_{n+1} = (x = x_{n+1}, y = f(x_{n+1}))$ , and then repeat the process until we obtain convergence.

The gradient of the straight line joining the points  $A_n$  and  $B_n$  is

$$f'(x_n) = \frac{y_n - 0}{x_n - x_{n+1}},$$

whence

$$x_{n+1} = x_n - \frac{f(x_n)}{f'(x_n)}. \quad (4.84)$$

### Iterative Solution

Consider Kepler's equation, written in the form

$$f(E) = E - e \sin E - M,$$

with  $E$  playing the role of  $x$ . The solution will be such that  $f(E) = 0$ . The derivative of  $f$  with respect to  $E$  is

$$f'(E) = 1 - e \cos E.$$

Note that, if  $M$  is equal to 0 or  $\pi$ , the solution is  $E = M$ . We first check that there is a solution and that it is unique. We thus consider  $E$  and  $M$  in the open interval  $(0, \pi)$  and we see that  $f(0) = -M$  and  $f(\pi) = \pi - M$ . There is therefore at least one solution, since for this continuous function, we have  $f(0) < 0$  and  $f(\pi) > 0$ . As the derivative is always positive,  $f'(E) > 0$  with  $e < 1$ , the function is strictly increasing and the solution is thus unique. We can apply the same argument in the interval  $(-\pi, 0)$ .

We therefore apply the iteration formula

$$E_{n+1} = E_n - \frac{E_n - e \sin E_n - M}{1 - e \cos E_n} . \quad (4.85)$$

We begin with an initial value  $E_0$ , to be defined. When we consider that the solution has been obtained to within the required accuracy, we set  $E = E_{n+1}$ . With the resulting solution  $E$ , we obtain  $v$  by (4.72), i.e.,

$$v = 2 \arctan \left( \sqrt{\frac{1+e}{1-e}} \tan \frac{E}{2} \right) . \quad (4.86)$$

### Convergence of the Iteration

The rate of convergence, i.e., the number  $N$  of iterations needed to obtain the result, depends on  $e$ ,  $M$ , and the chosen initial value  $E_0$ . It also depends on the required accuracy, which we denote by  $\mathcal{Q}_k$ , meaning that the selected angle is known with an error of less than  $10^{-k}$  degrees, or put another way, for  $E$  expressed in degrees, the first  $k$  decimal places are exact.

The number  $N$  can be expressed as a function, viz.,

$$N = N(e, M; E_0, \mathcal{Q}_k) .$$

The rate of convergence is no longer an issue today, due to the high speed of computer calculations. But in homage to the astronomers who, over four centuries, carried out calculations of this kind, we shall give here some indications of what is involved.

Classically, we set

$$E_0 = M ,$$

to start the iteration. In this case, convergence is rather fast, unless  $e > 0.9$  when the values of the mean anomaly are small, i.e.,  $|M| < 20^\circ$ . The rate of convergence can be significantly increased by starting with

$$E_0 = \begin{cases} M + e & \text{if } M \geq 0 , \\ M - e & \text{if } M \leq 0 , \end{cases}$$

which we may write as

$$E_0 = M + e \times \sigma(M) ,$$

where  $\sigma(M)$  represents the function sign  $M$ , equal to  $+1$  for  $M > 0$  and  $-1$  for  $M < 0$ . The angles  $E$  and  $M$  are given in radians and take values in the interval  $(-\pi, +\pi)$ .

Figure 4.3 illustrates these two cases, plotting

$$N = N(e, M; E_0 = M, \mathcal{Q}_6) , \quad N = N(e, M; E_0 = M + e \times \sigma(M), \mathcal{Q}_6) .$$

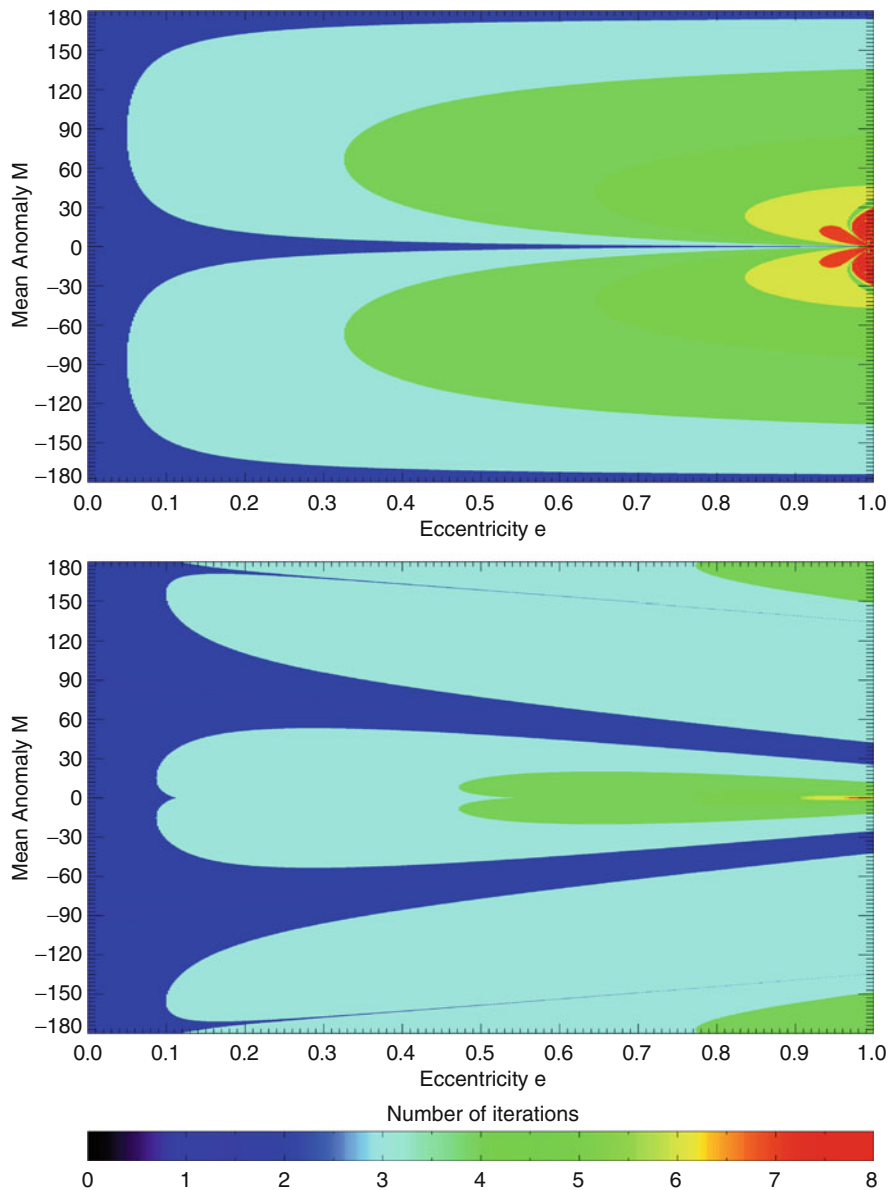


FIG. 4.3: Solving Kepler's problem. For a given value of the mean anomaly  $M$  and the eccentricity  $e$ , Kepler's problem is solved by the Newton–Raphson method. When the result is obtained to an accuracy of  $10^{-6}$  degrees, we indicate the number of iterations that were required and represent it on the graph with a colour. The (dimensionless) eccentricity  $e$  is indicated on the horizontal axis and the mean anomaly  $M$  (in degrees) on the vertical axis. Upper: Initial value  $E_0 = M$ . Lower: Initial value  $E_0 = M + e\sigma(M)$ , where  $\sigma(M)$  is the sign of  $M$ .

**Example 4.2** Calculate the position in polar coordinates, at time steps of 1 h, of an Earth-orbiting satellite with eccentricity  $e = 0.74$  and period  $T = 12$  h.

► This satellite has a Molniya orbit. For the mean anomaly, 1 h corresponds to  $360/T = 360/12 = 30^\circ$ . We thus solve Kepler's problem in detail for  $M = 30^\circ$ . The angles are converted into radians in the interval  $(-\pi, +\pi)$ . We use (4.85). The iteration begins with  $E_0 = M = \pi/6$ . We then calculate  $E_1$ :

$$E_1 = \frac{\pi}{6} - \frac{\pi/6 - 0.74 \sin(\pi/6) - \pi/6}{1 - 0.74 \cos(\pi/6)} = 1.55383,$$

and likewise  $E_2$ ,  $E_3$ , and so on:

$$E_2 = 1.55383 - \frac{1.55383 - 0.74 \sin(1.55383) - \pi/6}{1 - 0.74 \cos(1.55383)} = 1.25980,$$

$$E_3 = 1.25980 - \frac{1.25980 - 0.74 \sin(1.25980) - \pi/6}{1 - 0.74 \cos(1.25980)} = 1.21882,$$

$$E_4 = 1.21882 - \frac{1.21882 - 0.74 \sin(1.21882) - \pi/6}{1 - 0.74 \cos(1.21882)} = 1.21803,$$

$$E_5 = 1.21803 - \frac{1.21803 - 0.74 \sin(1.21803) - \pi/6}{1 - 0.74 \cos(1.21803)} = 1.21803.$$

We consider the result to be obtained after five iterations, given the desired accuracy, which is  $\mathcal{Q}_4$  here. Hence,

$$E = 1.21803.$$

Altering the first estimate, we can start the iteration with

$$E_0 = M + e = \pi/6 + 0.74 = 1.26360.$$

We then calculate

$$E_1 = 1.2180197, \quad E_2 = 1.21803, \quad E_3 = 1.21803.$$

The convergence is faster.

Having determined the eccentric anomaly to have the value  $E = 1.21803$  rad =  $69.7880^\circ$ , we obtain  $v$  using (4.86):

$$v = 2 \arctan \left( \sqrt{\frac{1.74}{0.26}} \tan \frac{69.7880}{2} \right) = 122.0062^\circ.$$



Figure 4.4 (upper) shows the values of  $v$  in degrees as obtained by interaction on  $E$ , for the required values of  $M$ . By the symmetry of the Kepler problem, it is not necessary to calculate the angles  $M$  in the range from  $-180^\circ$  to  $0^\circ$ . We merely replace  $M$  by  $-M$  and, in the results, replace  $E$  and  $v$  likewise by  $-E$  and  $-v$ . To determine the distance  $r$ , we first calculate the semi-major axis using (4.53), whence  $a = 26,609$  km. We calculate  $r = r(v)$  using (4.60) and the results are shown in Fig. 4.4 (upper). Clearly,  $r(-v) = r(v)$  (angles in degrees).

Note also that, if we wish to know when the satellite has reached a given value of the true anomaly, e.g.,  $90^\circ$ , we obtain the result directly, without solving Kepler's problem, by using (4.59) and setting  $v = \pi/2$  rad:

$$M = 2 \arctan \sqrt{\frac{0.76}{1.74}} - 0.74 \sqrt{1 - 0.74^2} = 0.73773 - 0.49773 ,$$

which gives  $M = 0.23000$  rad =  $13.751^\circ$  equivalent to  $13.751/30$  h = 28 min. The value of  $r$  at this time corresponds to the parameter  $p$ . In this case,

$$r = r(v = \pi/2) = a(1 - e^2) = p = 12,037 \text{ km} .$$

Referring to Fig. 4.1, the satellite  $S$  takes 28 min to go from the point  $P$ , the perigee ( $v = 0^\circ$ ), to the point  $R$  with true anomaly  $v = 90^\circ$ , and it takes 5 h 32 min to go from  $R$  to the apogee  $A$  ( $v = 180^\circ$ ).

**Note.** Here we have been considering a Molniya-type satellite, with a period of half a mean solar day (720 min). In reality, the period of such a satellite is half a sidereal day (718 min).

Figure 4.4 (lower) illustrates the results from this example. ◀

### 4.5.3 Other Methods of Solution

Here we outline the underlying idea of methods which transform the quantity  $E - M$  in a different way. When  $E$  is obtained from  $M$ , we calculate  $v = v(E)$ .

#### Bessel Functions

The function  $E - M = e \sin E$  is an odd periodic function of  $M$ . We expand it in a Fourier series, using the Bessel functions of the first kind  $J_k$ :

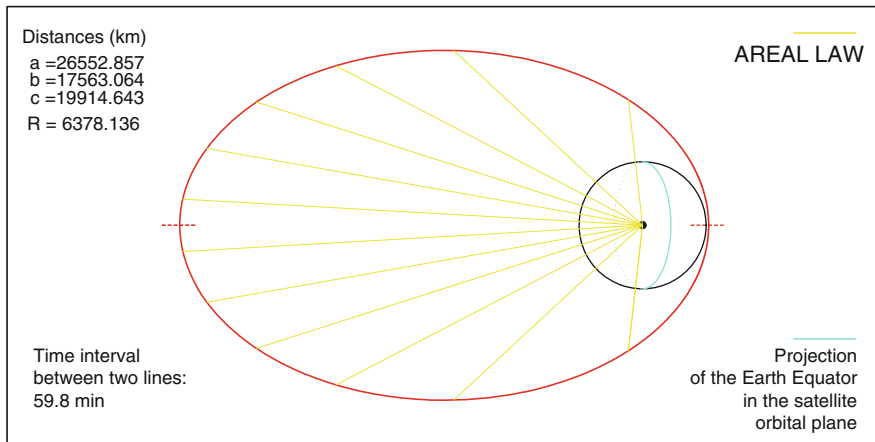
$$E - M = 2 \sum_{k=1}^{\infty} \frac{1}{k} J_k(ke) \sin kM . \quad (4.87)$$

$t$	$M$	$E_1$	$E_2$	$E_3$	$E_4, E_5$	$v$	$r$
0	0	00.000	00.000	00.000	00.000	00.000	6,918
1	30	89.028	72.181	69.833	69.788	122.006	19,806
2	60	118.283	102.775	101.550	101.542	144.969	30,548
3	90	132.399	125.001	124.811	124.811	157.156	37,850
4	120	146.802	144.587	144.576	144.576	165.924	42,655
5	150	162.920	162.646	162.646	162.646	173.248	45,403
6	180	180.000	180.000	180.000	180.000	180.000	46,299

**Molniya** ( Молния )

Orbit and central body  
in the orbital plane

$a = 26552.857$  km      Equiv. Altit. = 20174.7 km  
 $e = 0.750000$   
 CRITICAL Incl. =  $63.43^\circ$   
 Arg. Perigee =  $+270.00^\circ$   
 Period = 717.72 min



*Iξων*  
**MC • LMD**

FIG. 4.4: Upper: Iterative solution of Kepler's problem. Obtaining the true anomaly with initial estimate  $E_0 = M$ . The mean anomaly  $M$  is proportional to the time  $t$ , measured from the perigee. The different values  $E_i$  obtained by iteration are indicated, with convergence from  $E_4$  in this case. Finally, we obtain the true anomaly  $v$  and the distance from the focus  $r$  is in km. The time  $t$  is in hours, the angles  $M$ ,  $E$ , and  $v$  are in degrees, and the distance  $r$  is in km. Lower: Trajectory of a Molniya satellite in elliptical orbit with eccentricity  $e = 0.74$ . The period is 718 min (almost 12h). The position of the satellite at each hour is denoted by a straight line joining it to the center of attraction, i.e., the center of the Earth, which is the focus of the ellipse. This illustrates the areal law (Kepler's second law).

### Expansion in Powers of the Eccentricity

Starting with  $E - M = e \sin E$ , Lagrange wrote  $E - M$  in the form of a power series in the eccentricity:

$$E - M = \sum_{k=1}^{\infty} \frac{e^k}{k!} \frac{d^{k-1} \sin^k M}{dM^{k-1}} . \quad (4.88)$$

Laplace showed that the radius of convergence was  $e_0 = 0.66274\dots$ . This method is therefore unsuitable for eccentricities greater than this value. For small eccentricities, an expansion to order 3 in the eccentricity is given by (4.94).

### Approximate Result for Low Eccentricities

We express  $\cos M$  and  $\sin M$  using (4.83), going to first order in  $e$ . This amounts to writing

$$\cos(e \sin E) \approx 1 , \quad \sin(e \sin E) \approx e \sin E .$$

We thus obtain

$$\cos M = \cos(E - e \sin E) \approx \cos E + e \sin^2 E = e + (1 - e \cos E) \cos E ,$$

$$\sin M = \sin(E - e \sin E) \approx (1 - e \cos E) \sin E ,$$

which yields

$$\tan E \approx \frac{\sin M}{\cos M - e} . \quad (4.89)$$

## 4.6 Representation of Anomalies

### 4.6.1 Representation of Anomalies $v(M)$ and $E(M)$

During a period, up to a factor of  $n$ , the mean anomaly  $M$  thus represents the time elapsed since the passage at point  $P$ . We can plot graphs giving the evolution of  $v$  and  $E$  as a function of time, i.e., the functions  $v(M)$  and  $E(M)$ . On the graphs shown here,  $M$  varies over one period, from  $M = -\pi$  ( $S$  at  $A$ ) to  $M = +\pi$  ( $S$  at  $A$ ), passing through  $M = 0$  ( $S$  at  $P$ ) (see Fig. 4.1).

Figure 4.5 (upper) shows the function  $v(M)$  for various values of the eccentricity between  $e = 0.0$  and  $e = 0.9$ , at intervals of 0.1. The two angles are equal when  $e = 0.0$  (circular trajectory), while the deviation increases with  $e$ . When  $S$  is close to the periastron  $P$  ( $M = 0, v = 0$ ), ever bigger variations in  $v$  correspond to small variations in  $M$  (i.e., the time) as  $e$  increases. In contrast,

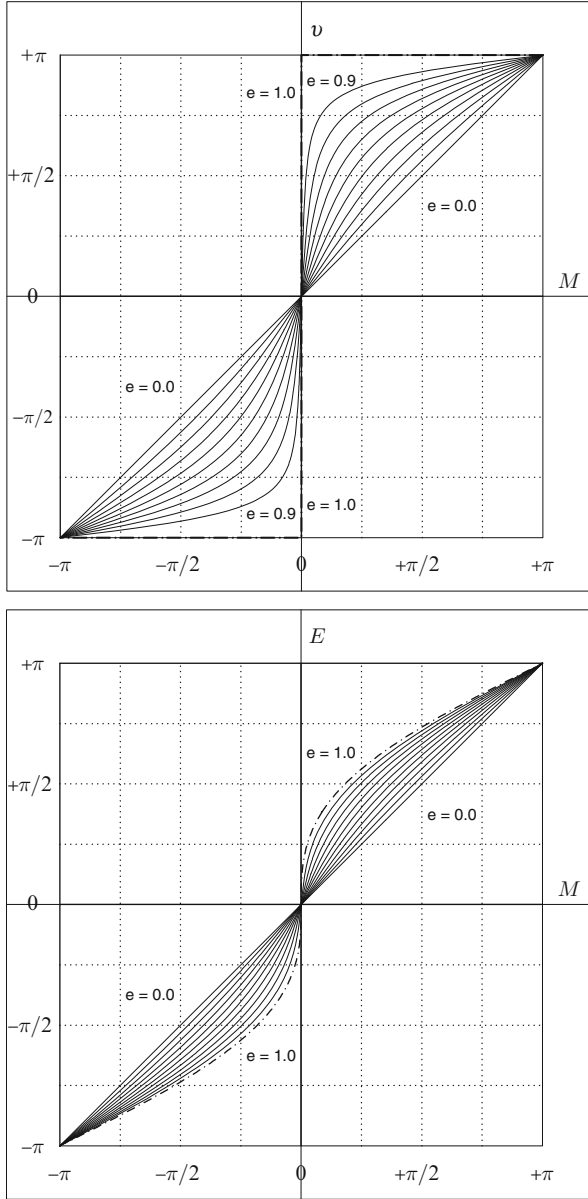


FIG. 4.5: Upper: Dependence  $v(M)$  of the true anomaly  $v$  on the mean anomaly  $M$  over a period, for 10 values of the eccentricity between  $e = 0.0$  and  $e = 0.9$ , at intervals of  $e = 0.1$ , together with the limiting value  $e = 1$ . Angles in radians. Lower: Dependence  $E(M)$  of the eccentric anomaly  $E$ , as in the upper graph.

when  $S$  is close to the apoastron  $A$  ( $|M| = \pi, |v| = \pi$ ), large variations in  $M$  correspond to small variations in  $v$ . This is of course an illustration of the areal law.

Figure 4.5 (lower) shows the function  $E(M)$  for various values of the eccentricity between  $e = 0.0$  and  $e = 0.9$ , at intervals of 0.1. As for the last function, the two angles are equal for  $e = 0.0$  and the deviation increases with  $e$ , although in a less marked way than for  $v(M)$ .

For all the figures in this Sect. 4.6, we consider the case  $e = 1.0$ . This is a limiting case, as the eccentricity of the ellipse tends to unity from below.<sup>10</sup>

## 4.6.2 Equation of Center

In Keplerian motion, it is useful to compare the true and mean anomalies. In astronomy, one defines the equation of center, denoted by  $E_C$ , as the difference between these two anomalies. This quantity<sup>11</sup> is an angle:

$$E_C = v - M . \quad (4.90)$$

We shall need this when studying the apparent motion of the Sun around the Earth or Mars.

The graph of the function  $(v - M)(M)$  is shown in Fig. 4.6 (upper), which should be compared with Fig. 4.5 (upper). The values of  $v$  corresponding to the maximum and minimum of  $(v - M)$  are symmetric with respect to the origin (the periastron).

**Example 4.3** Calculate the value and position of the extremum of the equation of center  $E_C$ .

► By symmetry, we consider  $E_C = v - M$  for  $M$  taking values between 0 and  $\pi$ . The maximum of  $E_C$  is given by  $dv = dM$ . From (4.81), we obtain the value  $r_m$  for which  $E_C$  is maximum, namely,  $r_m = \sqrt{ab}$ . Using (4.60), which gives  $r(a, e, v)$ , we have

$$r_m = \frac{a(1 - e^2)}{1 + e \cos v_m} = a (1 - e^2)^{1/4} ,$$

<sup>10</sup>For  $v(M)$ , the graph is discontinuous:  $v(\pi) = \pi \times \sigma(M)$  and  $v(0) = 0$ , denoting the sign of  $M$  by  $\sigma(M)$ . For  $E(M)$ , the representative curve is the reflection of  $M(E) = E - \sin E$  in the first bisector.

<sup>11</sup>The term “equation” taken from algebra was defined in its modern sense by Descartes in 1637. Prior to this, at least as early as 1250, the word was used in astronomy. It was specified and used by Kepler (*æquatio, nis*, in Latin) as “that variable quantity, determined by calculation, which must be added or subtracted from the mean motion to obtain the true motion”. This is how one should understand the name “equation of center”, but also “equation of time”.

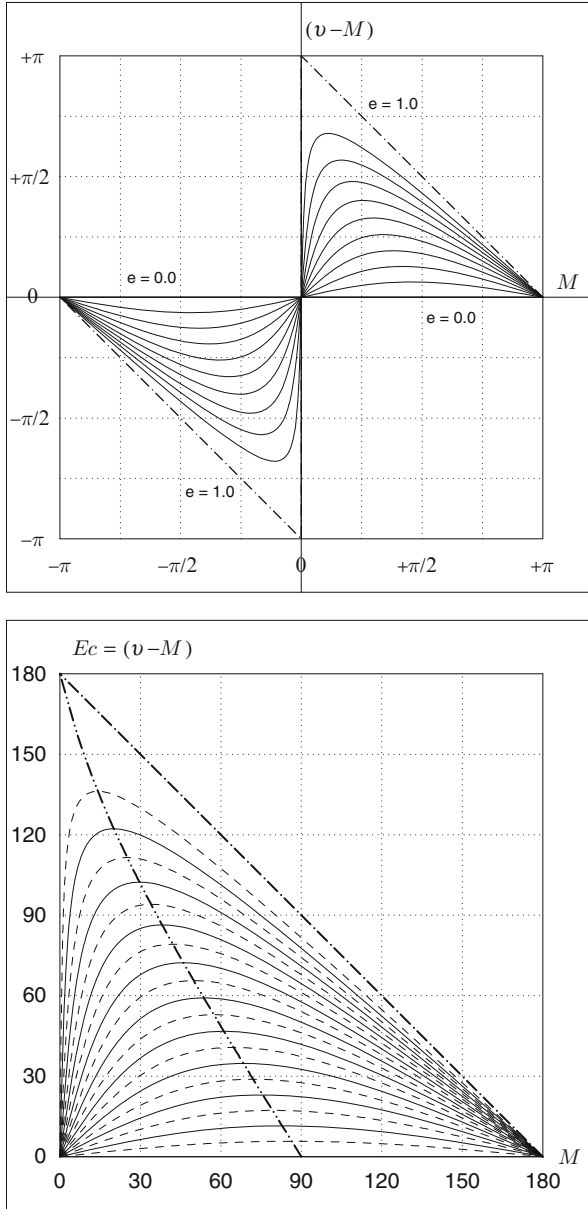


FIG. 4.6: Equation of center. Dependence  $(v - M)(M)$  of the difference between the true anomaly  $v$  and the mean anomaly  $M$  on  $M$  over one period. Upper: For ten values of the eccentricity, from  $e = 0.0$  to  $e = 0.9$ , at intervals of  $e = 0.1$ , together with the limiting value  $e = 1$ . Angles in radians. Lower: Magnification of upper graph, for values of  $e$  from 0.00 to 1.00, in steps of 0.05. The locus of the maximum of the function  $E_C$  as a function of  $e$  is shown by a dash-dotted line. Angles in degrees.

$e$	$M_m$ (rad)	$v_m$ (rad)	$E_{Cm}$ (rad)	$M_m$ (°)	$v_m$ (°)	$E_{Cm}$ (°)
0.0	1.5708	1.5708	0.0000	90.00	90.00	0.00
0.1	1.4457	1.6460	0.2002	82.83	94.31	11.47
0.2	1.3203	1.7221	0.4019	75.65	98.67	23.03
0.3	1.1940	1.8004	0.6065	68.41	103.16	34.75
0.4	1.0662	1.8822	0.8160	61.09	107.84	46.75
0.5	0.9364	1.9694	1.0330	53.65	112.84	59.19
0.6	0.8033	2.0647	1.2615	46.02	118.30	72.28
0.7	0.6650	2.1730	1.5080	38.10	124.50	86.40
0.8	0.5176	2.3037	1.7861	29.66	131.99	102.34
0.9	0.3503	2.4838	2.1335	20.07	142.31	122.24
1.0	0.0000	3.1416	3.1416	0.00	180.00	180.00
0.01671	1.5499	1.5833	0.0334	88.80	90.72	1.91
0.09341	1.4540	1.6410	0.1870	83.31	94.02	10.71
0.001144	1.5694	1.5717	0.0023	89.92	90.05	0.13
0.740000	0.6075	2.2217	1.6143	34.80	127.29	92.49

TABLE 4.1 : Position of the maximum of the equation of center  $E_{Cm}$  as a function of the eccentricity. Also given are the corresponding values of the mean anomaly  $M_m$  and the true anomaly  $v_m$ . Angles in radians (rad) and in degrees (°). (a) Eccentricities from 0.0 to 1.0, in steps of 0.1 (0.0 and 1.0 are limiting values). (b) Eccentricities of the heliocentric orbit of the Earth and Mars. (c) Eccentricities of SPOT-5 ( $e = 0.001144$ ) and Molniya ( $e = 0.74$ ).

where  $v_m$  is the value of the true anomaly corresponding to the maximum of  $E_C$ , whereupon

$$v_m = \arccos \left[ \frac{1}{e}(1 - e^2)^{3/4} - 1 \right]. \quad (4.91)$$

The angle  $v_m$  varies from  $\pi/2$  (for  $e = 0$ ) to  $\pi$  (for  $e = 1$ ). Using (4.59), we calculate  $M(v_m)$ , an angle varying from  $\pi/2$  (for  $e = 0$ ) to 0 (for  $e = 1$ ). The maximum of the equation of center  $E_{Cm}$ , viz.,

$$E_{Cm} = v_m - M(v_m), \quad (4.92)$$

varies from  $\pi/2$  (for  $e = 0$ ) to  $\pi$  (for  $e = 1$ ) (see Fig. 4.6 lower and Table 4.1).

For low eccentricities, we have

$$\cos v_m \approx -\frac{3}{4}e \quad \Longrightarrow \quad v_m = \frac{\pi}{2} + \frac{3}{4}e,$$

$$E_{Cm} = v_m - M_m = 2e \sin M \approx 2e \quad \Longrightarrow \quad M_m = \frac{\pi}{2} - \frac{5}{4}e.$$

The locus of the maxima is plotted in Fig. 4.6 (lower). ◀

### Low Eccentricities

From (4.72), we can expand  $v$  in the general case as a series in  $E$ , and from (4.88), if  $e$  is not too large, we can expand  $E$  as a series in  $M$ . To order 3 in  $e$ , we obtain successively:

$$v = E + \left( e + \frac{e^3}{4} \right) \sin E + \frac{e^2}{4} \sin 2E + \frac{e^3}{12} \sin 3E, \tag{4.93}$$

$$E = M + \left( e - \frac{e^3}{8} \right) \sin M + \frac{e^2}{2} \sin 2M + \frac{3e^3}{8} \sin 3M, \tag{4.94}$$

then  $v$  as a function of  $M$ , and finally the equation of center:

$$v - M = E_C = \left( 2e - \frac{e^3}{4} \right) \sin M + \frac{5e^2}{4} \sin 2M + \frac{13e^3}{12} \sin 3M. \tag{4.95}$$

To order one in  $e$ , we can cut off the above expansions or obtain the result directly using (4.74) for  $v - E$ , with  $\beta = e/2$  from (4.75) and (4.65) for  $E - M$ . Since the three angles (anomalies) are very close when  $e$  is small, we can write

$$v - E \approx e \sin E \approx e \sin M, \tag{4.96}$$

$$E - M = e \sin E \approx e \sin M, \tag{4.97}$$

$$E_C = v - M \approx 2e \sin M. \tag{4.98}$$

In the same way, the expansions of  $r/a$  and  $a/r$  were calculated by Lagrange. To order 3, we obtain

$$\frac{r}{a} = 1 + \frac{e^2}{2} - \left( e - \frac{3e^3}{8} \right) \cos M - \frac{e^2}{2} \cos 2M - \frac{3e^3}{8} \cos 3M, \tag{4.99}$$

$$\frac{a}{r} = 1 - \left( e - \frac{e^3}{8} \right) \cos M + e^2 \cos 2M + \frac{9e^3}{8} \cos 3M. \tag{4.100}$$

### 4.6.3 Summary of Anomalies

Let us sum up the results of the preceding sections. If we express the time  $t$ , represented by  $M$ , as a function of polar coordinates  $\theta$  and  $r$ , represented by  $v$  and  $E$ , respectively, we obtain the analytical relations  $M(v)$  and  $M(E)$ :

$$\begin{aligned} v &\longmapsto M = M(v), && \text{equation (4.59)}, \\ E &\longmapsto M = M(E), && \text{equation (4.65)}, \\ v = v(E) &\longleftrightarrow E = E(v) && \text{equations (4.72) and (4.73)}. \end{aligned}$$



If we express the polar angle  $\theta$ , represented by  $v$ , as a function of time  $t$ , itself represented by  $M$ , we must go through  $E$ , solving Kepler's problem by iteration:

$$\begin{aligned} M &\longmapsto E = E(M) && \text{iteration (4.85),} \\ E &\longmapsto v = v[E(M)] = v(M) && \text{equation (4.86).} \end{aligned}$$

When we study a particular trajectory, we generally consider a sequence of times  $t$  with a given separation, and at each time  $t_i, t_{i+1}, \dots$ , we solve Kepler's problem to obtain the true anomaly.

The three anomalies  $v$ ,  $E$ , and  $M$  do not play similar roles:

- $v(t)$  can be used to identify the position of the body on its orbit and to determine the radial vector  $r$  with the help of (4.26) or (4.60).
- $M(t)$  is in effect another way to represent time.
- $E(t)$  serves mainly to solve Kepler's problem, but it also arises in the Lagrange equations of the perturbed motion [see (6.34) and (6.35)].

**Example 4.4** Calculate the true anomaly for the planet Mars when the mean anomaly is  $M = 98.679^\circ$ . The eccentricity of the orbit of Mars around the Sun is  $e = 0.09341$ .

► We do the calculations using the various methods discussed above, the iterative method and the approximate methods, which are well suited to planetary motions, up to a certain level of accuracy, since the eccentricity is low.

**Iterative Method.** Angles are given in degrees, but we convert them to radians for the calculation, or change  $e$  to  $(180/\pi)e$  to keep the angles in degrees. Setting  $E_0 = M$ , we obtain in successive iterative steps using (4.85):

$$E_0 = 98.679, \quad E_1 = 103.896, \quad E_2 = 103.875, \quad E_3 = 103.875.$$

Two iterations achieve the required accuracy. We find  $v$  using (4.86):

$$E = E_3 = 103.875 \quad \Longrightarrow \quad v = 109.020.$$

**Approximate Formula (4.89).** We obtain  $\tan E = -4.04648$ , which corresponds to an angle of  $-76.119^\circ$ , whence

$$E = 180 - 76.119 = 103.881 \quad \Longrightarrow \quad v = 109.027.$$

**Series Expansion of  $E = E(M)$  Using (4.94).** To first order,

$$E = 98.679 + \frac{180}{\pi} 0.0934 \sin(98.679) = 103.969,$$

whence  $v = 109.112$ . To second order, we find  $E = 103.895$ , whence  $v = 109.039$ , and to third order,  $E = 103.873$  and  $v = 109.019$ .

Method	Reference	$E$	$v$	$v - v_0$
Iteration	(4.85)	103.875	109.020	0
Approximate formula	(4.89)	103.881	109.027	+0.007
First order expansion of $E$	(4.94)	103.969	109.112	-0.008
Second order expansion of $E$	(4.94)	103.895	109.039	+0.019
Third order expansion of $E$	(4.94)	103.873	109.019	-0.001
First order expansion of $v$	(4.95)	-	109.259	+0.239
Second order expansion of $v$	(4.95)	-	109.073	+0.053
Third order expansion of $v$	(4.95)	-	109.016	-0.004

TABLE 4.2: Kepler’s problem. Results using different methods. The exact value  $v_0$  is the one given by iteration. The angles  $E$ ,  $v$ , and  $v - v_0$  are in degrees. Case investigated here: eccentricity of orbit  $e = 0.09341$  (planet Mars),  $M = 98.679^\circ$ .

**Series Expansion of  $v = v(M)$  Using (4.95).** In this case, we no longer solve Kepler’s problem, since we obtain  $v$  directly from  $M$ . Naturally, this is only possible because we have an approximate formula. To first order,

$$v = 98.679 + 2 \frac{180}{\pi} 0.0934 \sin(98.679) = 109.259 .$$

To second order, we find  $v = 109.073$  and to third order,  $v = 109.016$ .

All these results are recorded in Table 4.2. The exact value of  $v$  is  $v_0$ , given by the iterative method. The discrepancy  $v - v_0$  is given in degrees. ◀

**Example 4.5** Calculate the average value of the radial vector  $r$  over one revolution for different choices of the integration angle.

► When a point describes a full revolution around an ellipse, we can calculate the average value  $\bar{r}_\alpha$  of its distance  $r$  from the focus of the ellipse. This will depend on the angle  $\alpha$  used to describe the motion:

$$\bar{r}_\alpha = \frac{1}{2\pi} \int_0^{2\pi} r(\alpha) d\alpha .$$

The angle  $\alpha$  can be one of the three anomalies  $v$ ,  $E$ , or  $M$ .

**True Anomaly  $v$ .** The radial vector  $r(v)$  is defined by (4.60). The primitive of  $(1 + e \cos v)^{-1}$  was calculated when we established (4.59). We thus find

$$\bar{r}_v = \frac{a(1 - e^2)}{2\pi} \int_0^{2\pi} \frac{dv}{1 + e \cos v} = \frac{a\sqrt{1 - e^2}}{\pi} \left[ \arctan \left( \sqrt{\frac{1 - e}{1 + e}} \tan \frac{v}{2} \right) \right]_0^{2\pi} .$$

Using (4.73), we obtain

$$\bar{r}_v = \frac{a\sqrt{1-e^2}}{\pi} \left[ \frac{E}{2} \right]_0^{2\pi} = a\sqrt{1-e^2} = b.$$

**Eccentric Anomaly  $E$ .** With  $r$  defined by (4.64), we write

$$\bar{r}_E = \frac{a}{2\pi} \int_0^{2\pi} (1 - e \cos E) dE = \frac{a}{2\pi} [E]_0^{2\pi} = a.$$

For  $e = 1$ , the limiting case,  $r_E/a = 1 - \cos E = 2 \sin^2(E/2)$ .

**Mean Anomaly  $M$ .** With  $r$  defined by (4.64), we use the relation (4.79) between  $dE$  and  $dM$  to obtain

$$\bar{r}_M = \frac{1}{2\pi} \int_0^{2\pi} r dM = \frac{a}{2\pi} \int_0^{2\pi} (1 - e \cos E)^2 dE.$$

Expanding, the integral of the term with period  $2\pi$  is zero and we find

$$\int_0^{2\pi} (1 - e \cos E)^2 dE = \int_0^{2\pi} (1 + e^2 \cos^2 E) dE = \left(1 + \frac{e^2}{2}\right) \int_0^{2\pi} dE,$$

whence

$$\bar{r}_M = a \left(1 + \frac{e^2}{2}\right).$$

The time average of  $r$  over one period is not equal to the semi-major axis. We recover the value of  $\bar{r}_M/a$  using (4.99).

**Summary.** With the reduced distance  $\eta = r/a$ , already defined above, we denote the average values by  $\bar{\eta}_\alpha$ :

$$\bar{\eta}_v = \sqrt{1-e^2}, \quad \bar{\eta}_E = 1, \quad \bar{\eta}_M = 1 + \frac{e^2}{2}.$$

The functions  $\eta_\alpha = r(\alpha)/a$  are shown for each anomaly in the upper parts of Figs. 4.7, 4.8, and 4.9. Graphs represent only half a revolution, given that the ellipse is symmetric in the apsidal axis. ◀

**Example 4.6** *Represent the speed  $V$  as a function of the relevant anomaly (true, eccentric, or mean).*

► We expressed the speed  $V(r)$  of a satellite in elliptical orbit, as given by (4.39), relative to the speed  $V_c$  of a satellite in a circular orbit with the same

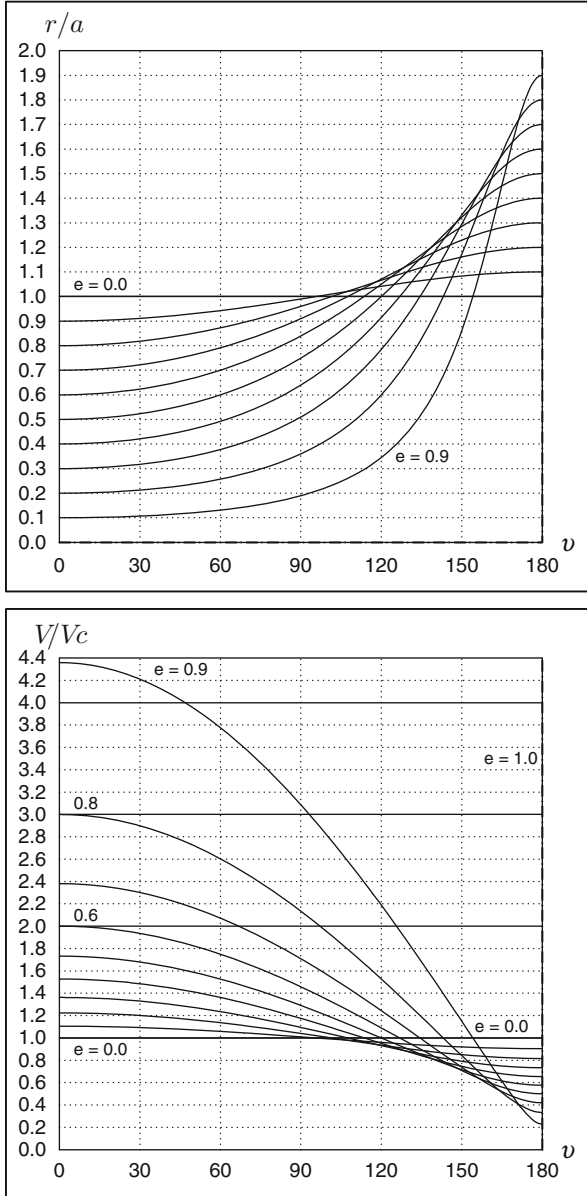


FIG. 4.7 : Upper: Reduced distance  $\eta = r/a$ . Lower: Speed  $V/Vc$ . Quantities are given as a function of the true anomaly  $v$  for various values of the eccentricity  $e$  from 0.0 to 1.0 in steps of 0.1. Angles in degrees.

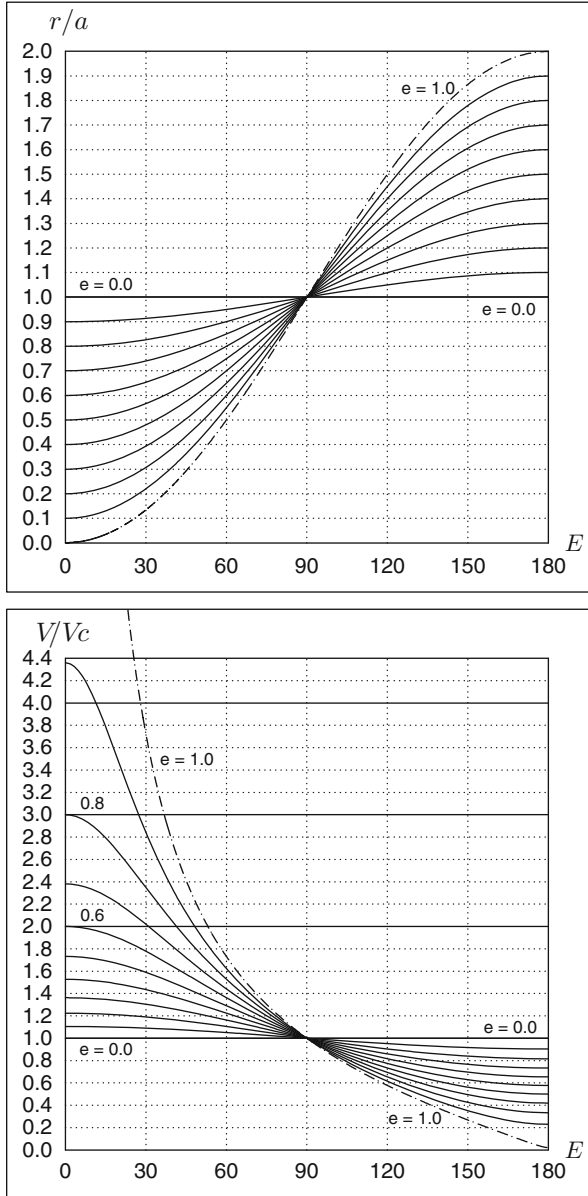


FIG. 4.8 : Upper: Reduced distance  $\eta = r/a$ . Lower: Speed  $V/V_c$ . Quantities are given as a function of the eccentric anomaly  $E$  for various values of the eccentricity  $e$  from 0.0 to 1.0 in steps of 0.1. Angles in degrees.

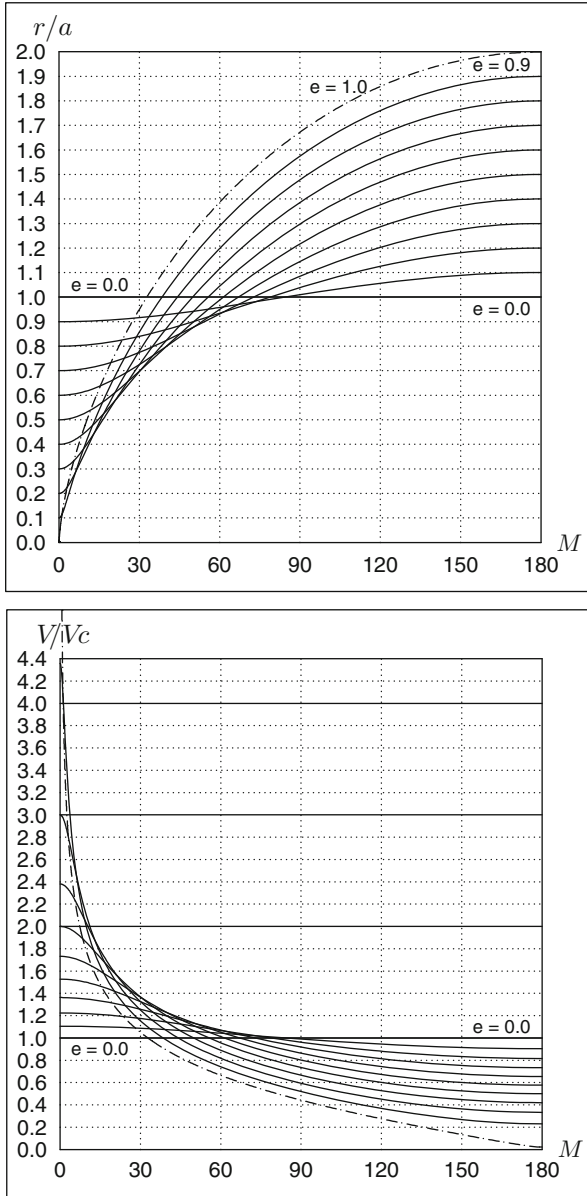


FIG. 4.9 : Upper: Reduced distance  $\eta = r/a$ . Lower: Speed  $V/V_c$ . Quantities are given as a function of the mean anomaly  $M$  for various values of the eccentricity  $e$  from 0.0 to 1.0 in steps of 0.1. Angles in degrees.

semi-major axis  $a$ , as given by (4.52). Using the reduced distance  $\eta$  defined by (2.38), we have

$$\frac{V}{V_c} = \sqrt{\frac{2}{\eta} - 1}, \quad \text{with} \quad V_c = \sqrt{\frac{\mu}{a}}. \quad (4.101)$$

Expressing  $r$  as a function of  $v$ , then of  $E$  and  $M$ , we obtain successively the dependence of the speed on the anomalies. The function  $V(v)$  is given by (4.61) and  $V(E)$  by (4.69). In the limiting case  $e = 1$ , the speed  $V(E)$  is given by

$$\left[ \frac{V(E)}{V_c} \right]^2 = \frac{1 + e \cos E}{1 - e \cos E} = \cot \frac{E}{2}.$$

The lower parts of Figs. 4.7, 4.8, and 4.9 show just half a revolution with the origin at the perigee, the other half revolution being symmetric, of course. At perigee (anomaly =  $0^\circ$ ,  $\eta = 1 - e$ ) and at apogee (anomaly =  $180^\circ$ ,  $\eta = 1 + e$ ), the values of the speed ( $V_p$  and  $V_a$ , respectively) are the same for each of the three graphs:

$$\frac{V_p}{V_c} = \sqrt{\frac{1+e}{1-e}}, \quad \frac{V_a}{V_c} = \sqrt{\frac{1-e}{1+e}}, \quad \frac{V_p}{V_a} = \frac{1+e}{1-e}.$$

For example, for  $e = 0.6$ ,  $(1+e)/(1-e) = 4$  and hence  $V_p/V_c = 2.0$ ,  $V_a/V_c = 0.5$ , and  $V_a/V_p = 4$ . We note that, since  $V_p V_a = V_c^2$ , the quantity  $V_c$  is the geometric mean of the two extremal speeds  $V_p$  and  $V_a$ . ◀

**Example 4.7** *Represent the angle between the velocity vector  $V$  and the radial vector as a function of the relevant anomaly (true, eccentric, or mean).*

► Writing the velocity  $\mathbf{V}$  in the form  $\mathbf{V} = V_r \mathbf{e}_r + V_\theta \mathbf{e}_\theta$ , the angle  $\alpha$  between  $\mathbf{V}$  and  $\mathbf{r}$  is given by  $\tan \alpha = V_\theta/V_r$ . Using (4.18) and (4.30), we obtain  $\alpha$  as a function of the polar angle  $\theta$ , represented here by the true anomaly  $v$ :

$$\alpha(v) = \arctan \frac{1 + e \cos v}{e \sin v}, \quad \frac{d\alpha}{dv} = -e \frac{e + \cos v}{1 + 2e \cos v + e^2}. \quad (4.102)$$

Figure 4.10 (upper) shows the graph of  $\alpha(v)$ . Calculating the derivative  $d\alpha/dv$ , we find that the minimum of each curve occurs at  $v = \arccos(-e)$ . For a circular trajectory ( $e = 0$ ),  $\alpha$  is obviously a right-angle. For an orbit infinitely close to a parabola,  $e = 1$ , we have  $\tan \alpha = \cot(v/2)$ , and therefore  $\alpha = (\pi/2) - (v/2)$ ,  $d\alpha/dv = -1/2$ .

The graph of  $\alpha(E)$  shown in Fig. 4.11 has axial symmetry, a consequence of the definition of  $E$ :

$$\alpha(E) = \arctan \frac{\sqrt{1-e^2}}{e \sin E}, \quad \frac{d\alpha}{dE} = -e \frac{\sqrt{1-e^2} \cos E}{1 - e^2 \cos^2 E}. \quad (4.103)$$

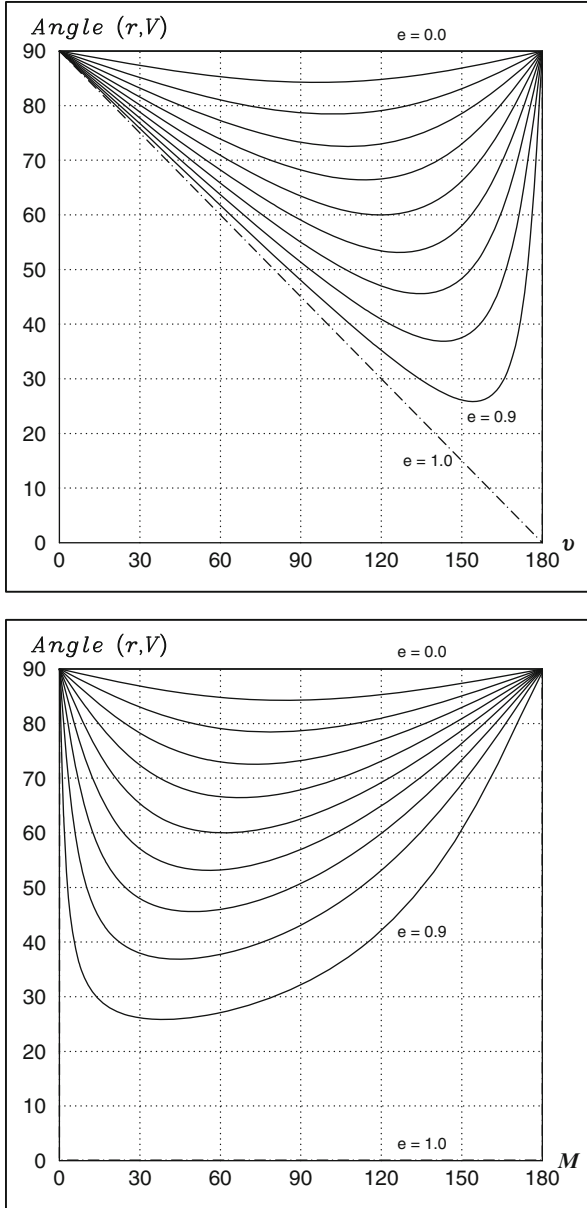


FIG. 4.10 : Angle  $\alpha$  between the velocity and the radial vector as a function of the true anomaly (upper) and the mean anomaly (lower). Graphs plotted for various values of the eccentricity  $e$  between 0.0 and 1.0 in steps of 0.1. Angles in degrees.

Figure 4.10 (lower) shows the graph of  $\alpha(M)$ . There is no analytic formula for  $\alpha(M)$  (see Sect. 4.5). ◀



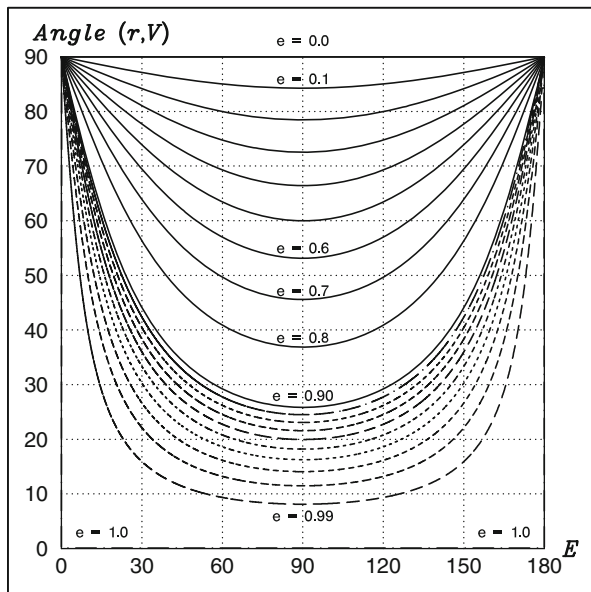


FIG. 4.11 : Angle  $\alpha$  between the velocity and the radial vector as a function of the eccentric anomaly  $E$ . Graphs plotted for various values of the eccentricity  $e$  between 0.0 and 1.0 in steps of 0.1 and from 0.90 to 1.00 in steps of 0.01. Angles in degrees.

## 4.7 First Integrals of the Motion

### 4.7.1 Conservation Laws

Starting from the expression for the Newtonian acceleration, we have obtained the equation of motion by two integrations, to go from  $\ddot{\mathbf{r}}$  to  $\dot{\mathbf{r}}$  to  $\mathbf{r}$ . Following this rather detailed solution, we shall now give a brief presentation of a more synthetic method. The motivation for this is that it brings out the quantities remaining constant throughout the motion. These values are obtained with just one integration, to go from  $\ddot{\mathbf{r}}$  to  $\dot{\mathbf{r}}$ . This is why they are referred to as first integrals of the motion. Starting from the equation of motion in the case of a Newtonian acceleration, viz.,

$$\ddot{\mathbf{r}} = -\frac{\mu}{r^2} \mathbf{e}_r, \quad (4.104)$$

we obtain the conservation of energy, angular momentum, and Laplace vector (which gives the equation of motion).

#### Conservation of Energy

We take the scalar product of both sides of (4.104) with the velocity vector  $\dot{\mathbf{r}}$ :

$$\ddot{\mathbf{r}} \cdot \dot{\mathbf{r}} = \frac{1}{2} \frac{d}{dt} (\dot{\mathbf{r}}^2) = \frac{1}{2} \frac{d}{dt} (\dot{r}^2) ,$$

$$-\frac{\mu}{r^2} \mathbf{e}_r \cdot \dot{\mathbf{r}} = -\frac{\mu}{r^2} \dot{r} = \frac{d}{dt} \left( \frac{\mu}{r} \right) .$$

Equation (4.104) thus gives

$$\frac{d}{dt} \left( \frac{1}{2} \dot{r}^2 - \frac{\mu}{r} \right) = 0 , \quad (4.105)$$

whence

$$\mathcal{K} = \frac{1}{2} \dot{r}^2 - \frac{\mu}{r} = \text{constant} . \quad (4.106)$$

This expresses conservation of energy. We recover (4.33) by setting  $V^2 = \dot{r}^2$ .

### Conservation of Angular Momentum

We take the vector product of each side of (4.104) with the radial vector  $\mathbf{r}$ . This yields

$$\mathbf{r} \wedge \ddot{\mathbf{r}} = -\frac{\mu}{r^2} \mathbf{r} \wedge \mathbf{e}_r = \mathbf{0} .$$

Using the derivative (4.5) of the definition (4.4), we obtain

$$\mathbf{C} = \mathbf{r} \wedge \dot{\mathbf{r}} = \text{constant} , \quad (4.107)$$

which expresses conservation of angular momentum. The motion is restricted to a plane. We recover the relation (4.9).

### Conservation of the Laplace Vector: Equation for the Trajectory

We consider the vector product of the acceleration and the angular momentum:

$$\ddot{\mathbf{r}} \wedge \mathbf{C} = -\frac{\mu}{r^2} \mathbf{e}_r \wedge r^2 \dot{\theta} \mathbf{k} = \mu \dot{\theta} \mathbf{e}_\theta = \mu \frac{d\mathbf{e}_r}{dt} .$$

Now, since  $\mathbf{C}$  is constant, we have

$$\frac{d}{dt} (\dot{\mathbf{r}} \wedge \mathbf{C}) = \ddot{\mathbf{r}} \wedge \mathbf{C} ,$$

whence

$$\frac{d}{dt} (\dot{\mathbf{r}} \wedge \mathbf{C}) = \frac{d}{dt} (\mu \mathbf{e}_r) . \quad (4.108)$$

Considering this relation, we define the vector  $\mathbf{A}$ , known as the Laplace vector (or Laplace–Runge–Lenz vector), which has the property of being a constant vector:

$$\mathbf{A} = \frac{\dot{\mathbf{r}} \wedge \mathbf{C}}{\mu} - \mathbf{e}_r = \text{constant} . \quad (4.109)$$

This vector  $\mathbf{A}$  is perpendicular to  $\mathbf{C}$ , since  $\dot{\mathbf{r}} \wedge \mathbf{C}$  and  $\mathbf{e}_r$  are both perpendicular to  $\mathbf{C}$ . It thus lies in the plane of motion. In order to evaluate  $\mathbf{A}$ , we calculate  $\dot{\mathbf{r}} \wedge \mathbf{C}$ :

$$\dot{\mathbf{r}} \wedge \mathbf{C} = \left( \dot{r} \mathbf{e}_r + r \dot{\theta} \mathbf{e}_\theta \right) \wedge C \mathbf{k} = C \left( r \dot{\theta} \mathbf{e}_r - \dot{r} \mathbf{e}_\theta \right) .$$

If we project  $\mathbf{A}$  onto  $\mathbf{e}_r$  and use the value of  $C$  given by (4.6), we have

$$\mathbf{A} \cdot \mathbf{e}_r = \left( \frac{C}{\mu} \frac{r^2 \dot{\theta}}{r} \mathbf{e}_r - \mathbf{e}_r \right) \cdot \mathbf{e}_r = \frac{1}{r} \frac{C^2}{\mu} - 1 .$$

We thus obtain the expression for  $r$ :

$$r = \frac{C^2}{\mu} \frac{1}{1 + \mathbf{A} \cdot \mathbf{e}_r} . \quad (4.110)$$

Let  $v$  be the angle between the radial vector and the fixed vector  $\mathbf{A}$ . Setting  $\mathbf{A} \cdot \mathbf{e}_r = \|\mathbf{A}\| \cos v$  and  $p = C^2/\mu$ , we find that the trajectory is an ellipse. Comparing formulas, we see that  $\|\mathbf{A}\|$  corresponds to the eccentricity. The distance  $r$  goes through a minimum when the vectors  $\mathbf{A}$  and  $\mathbf{e}_r$  are collinear (with  $v = 0$ ): the vector  $\mathbf{A}$  goes through the periastron and  $v$  therefore represents the true anomaly as defined earlier. Once the Laplace vector  $\mathbf{A}$  is known, we automatically have the eccentricity and the direction of the periastron.

**Note.** The conservation of these quantities is expressed by Noether's theorem.<sup>12</sup>

---

<sup>12</sup>*Emmy Noether* (1882–1935) was a German mathematician, considered as the founder of modern algebra (inventor of rings and ideals). Noether's theorem (1918) says that a conservation law is a consequence of the invariance of a physical law under a continuous transformation with one parameter. (This is proven using the Lagrangian formalism for the equations of classical mechanics.) As far as we are concerned here:

- Conservation of momentum results from the invariance of the laws of physics under translation, due to the homogeneity of space.
- Conservation of angular momentum results from the invariance of the laws of physics under rotation, due to the isotropy of space.
- Conservation of energy results from the invariance of the laws of physics under time translations, due to the uniformity of the flow of time.

### 4.7.2 Note on Energy

When we study the Keplerian motion of a satellite, its mass never enters our considerations.<sup>13</sup> This is why we have always spoken of acceleration rather than force. Everything we have said so far can be recast. For example, one could speak of a Newtonian force applied to a material point  $S$  of mass  $m$ . This would lead us to introduce the standard definition of energy. In the case of a Newtonian attraction, the force is

$$\mathbf{F} = -m \frac{\mu}{r^2} \mathbf{e}_r .$$

This corresponds to a potential energy  $\mathcal{U}$  (recalling that  $\mathbf{F} = -\mathbf{grad} \mathcal{U}$ , with the convention that  $\mathcal{U}$  vanishes for infinite  $r$ ),

$$\mathcal{U} = -m \frac{\mu}{r} .$$

The point  $S$ , moving at speed  $V$  has kinetic energy  $\mathcal{T}$  given by

$$\mathcal{T} = \frac{1}{2} m V^2 .$$

The mechanical energy  $\mathcal{E}$  is thus

$$\mathcal{E} = \mathcal{T} + \mathcal{U} = m \left( \frac{V^2}{2} - \frac{\mu}{r} \right) . \quad (4.111)$$

The angular momentum  $\mathbf{L}$  is by definition

$$\mathbf{L} = \mathbf{r} \wedge m \dot{\mathbf{r}} . \quad (4.112)$$

The quantities considered earlier are thus equivalent to those related to the energy:

$$\mathcal{K} = \frac{\mathcal{E}}{m} , \quad C = \frac{L}{m} .$$

Equation (4.33), which establishes that  $\mathcal{K}$  is constant, is thus equivalent to

$$\mathcal{E} = m\mathcal{K} = \text{constant} , \quad (4.113)$$

which expresses the conservation of mechanical energy  $\mathcal{E}$ .

For periodic motion, (4.38) yields

$$\mathcal{E} = -\frac{1}{2} m \frac{\mu}{a} , \quad (4.114)$$

which is negative, due to the convention  $\mathcal{U}(\infty) = 0$ . We see that  $a$  is related to  $\mathcal{E}/m$ , which shows that the period depends only on the mechanical energy per unit mass of the material point under consideration.

---

<sup>13</sup>In the study of perturbed motion, the mass of the body is relevant in certain specific instances, such as the study of air resistance in the upper atmosphere or radiation pressure.

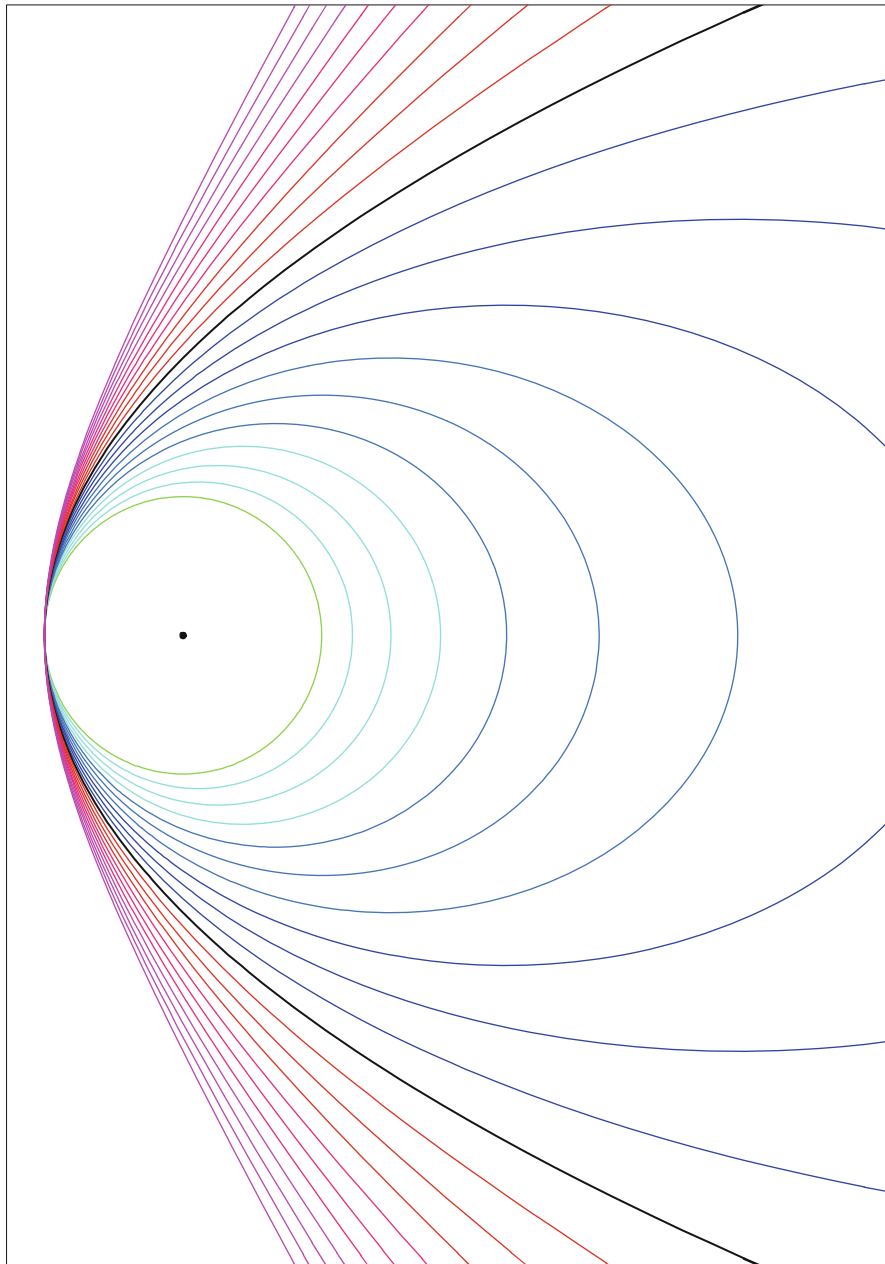


FIG. 4.12 : Trajectories and energy. The distance from the focus to the periastron is constant. The minimal energy  $-\mathcal{E}_0$  corresponds to the orbital insertion speed, and the trajectory is a circle. We then give the object an energy  $\mathcal{E} = -\mathcal{E}_0(1 - e)$ , where  $e$  is the eccentricity, given in steps of 0.1. As the energy increases, the elliptical trajectory moves further and further off center, until it becomes a parabola for  $e = 1$  (thick black curve). Then for  $e > 1$ , the trajectory is one concave branch of a hyperbola.

**Example 4.8** *Trajectories of various point objects in orbit around a pointlike center of attraction, with different energies, but having the same distance at periastron (perigee).*

► We consider a point of mass  $m$  in a circular orbit of radius  $r_0$ . It has energy

$$\mathcal{E} = -\mathcal{E}_0, \quad \text{with} \quad \mathcal{E}_0 = \frac{1}{2}m\frac{\mu}{r_0}.$$

If we increase the energy while fixing the distance at perigee (focus–perigee distance  $r_p = r_0$ ), the eccentricity increases:

$$r_p = a(1 - e) = r_0, \quad a = \frac{r_0}{1 - e}, \quad p = a(1 - e^2) = (1 + e)r_0,$$

and the energy is

$$\mathcal{E} = -\frac{1}{2}m\frac{\mu}{r_0}(1 - e) = -\mathcal{E}_0(1 - e).$$

The trajectories are shown in Fig. 4.12 when the eccentricity increases in steps of 0.10. For  $e = 0$ , with negative energy  $\mathcal{E} = -\mathcal{E}_0$ , the trajectory is a circle. It becomes an ellipse, ever further off center, as the energy increases, provided that  $e < 1$ . For  $e = 1$ , with energy  $\mathcal{E} = 0$ , the trajectory is a parabola. For  $e > 1$ , with energy  $\mathcal{E} > 0$ , the trajectory is a hyperbola (concave branch). When the trajectory is given in polar coordinates using (1.17) or (4.60),  $a$  is positive for the ellipses, infinite for the parabola, and negative for the hyperbolas. Sign conventions can be avoided by using the parameter  $p$  in the general equation for the conic sections, as in (1.16). ◀

## 4.8 Historical Note on Universal Attraction

### 4.8.1 Kepler’s Laws

Since ancient times, astronomy had been dominated by Ptolemy’s<sup>14</sup> geocentric system, but by the fifteenth century, the inadequacies of this system had become clear to several astronomers, for instance, in the universities of

---

<sup>14</sup>*Claudius Ptolemaios* (Κλαυδῖος Πτολεμαῖος), who lived roughly from 90 to 168 AD, was a Greek mathematician, astronomer, and geographer from Alexandria (Claudius is a Roman first name, while Ptolemaios is a Greek name ὁ πτολεμαῖος, ου, meaning warlike). He wrote a number of things, the best known being the *Geography* and the *Almagest*. In the *Geography* (which means literally “drawing of the Earth”), he situates hundreds of places, including towns, mountains, and others, with the correct latitude and somewhat overestimated longitudes. In the *Almagest* (a title attributed to it later by Arab astronomers, from *Al*, “the”, the definite article in Arabic, and *megistos*, the superlative of *mega*, in Greek, meaning “very big”), he presents the geocentric planetary system, called the Ptolemaic system. To obtain good agreement between observation and model, he has each planet (and in particular Mars) describe a circle called an epicycle, whose center moves around another circle, called the deferent, centered on the motionless Earth. He refined this model with the eccentric (shifted deferent), the equant point, and other modifications. The work of Ptolemy, the last astronomer of the ancient world, was transmitted to Europe by the Arabs, where it formed the foundation of astronomy in the Middle Ages and the Renaissance.

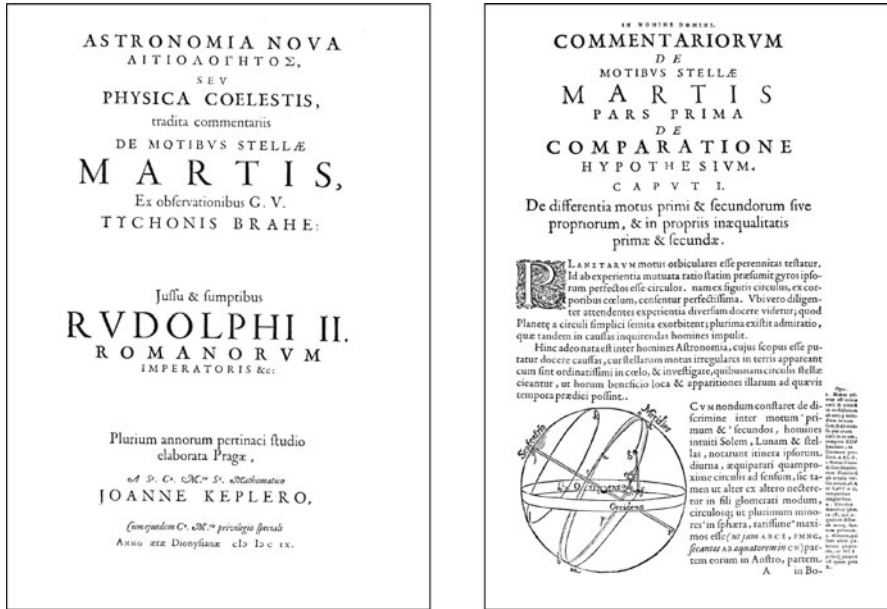


FIG. 4.13 : Kepler's *Astronomia Nova*, edited in Prague in 1609—MDCIX. Left: Title page. Right: First page.

Bologna or Padua. However, Copernicus<sup>15</sup> was the first to reject the geocentric system in favour of a heliocentric model.

<sup>15</sup> *Nicolaj Kopernik* (1473–1543), in Latin *Nicolaus Copernicus Torinensis*, was a Polish astronomer. Following his studies in Italy, Copernicus returned to Poland and devised a cosmological system which replaced the Earth by the Sun as the center of the Universe. This was the heliocentric, or Copernican system, in which the orbit of each planet is a sphere centered on the Sun. He completed his treatise *De Revolutionibus orbium cœlestium* around 1530. However, fearing the reaction of both the Catholic hierarchy and the newly born Lutheran movement, he held back the publication. The book was finally printed in Nuremberg in 1543, the year of his death, thanks to the determination of his pupil Rheticus. The editor Petreius demanded a preface, but we do not know whether the author gave his agreement. Written by the theologian Osiander, it warned the reader that the system there described was merely a way of looking at the problem that could help to carry out calculations, and that it in no way put in doubt the Bible.

In those days, the authorities had radical ways of dealing with anyone foolish enough to contest religious dogma or biblical truths. The doctor Michel Servet, of Spanish origin, was the first to carry out a scientific investigation of the blood circulation. As a result, he was arrested in 1553 in the Protestant republic of Geneva, condemned to death, and burnt at the stake under the eye of Calvin himself.

As it turned out, it was not until 1616 that *De Revolutionibus* was finally listed on the Index of the Holy Office. For decades, the book was unfavourably viewed by astronomers. Its message was too radically different, and on top of that, it did not provide good predictions. For the planet Mars, the positions given by Copernicus were less accurate than those given by Ptolemy's epicycles!

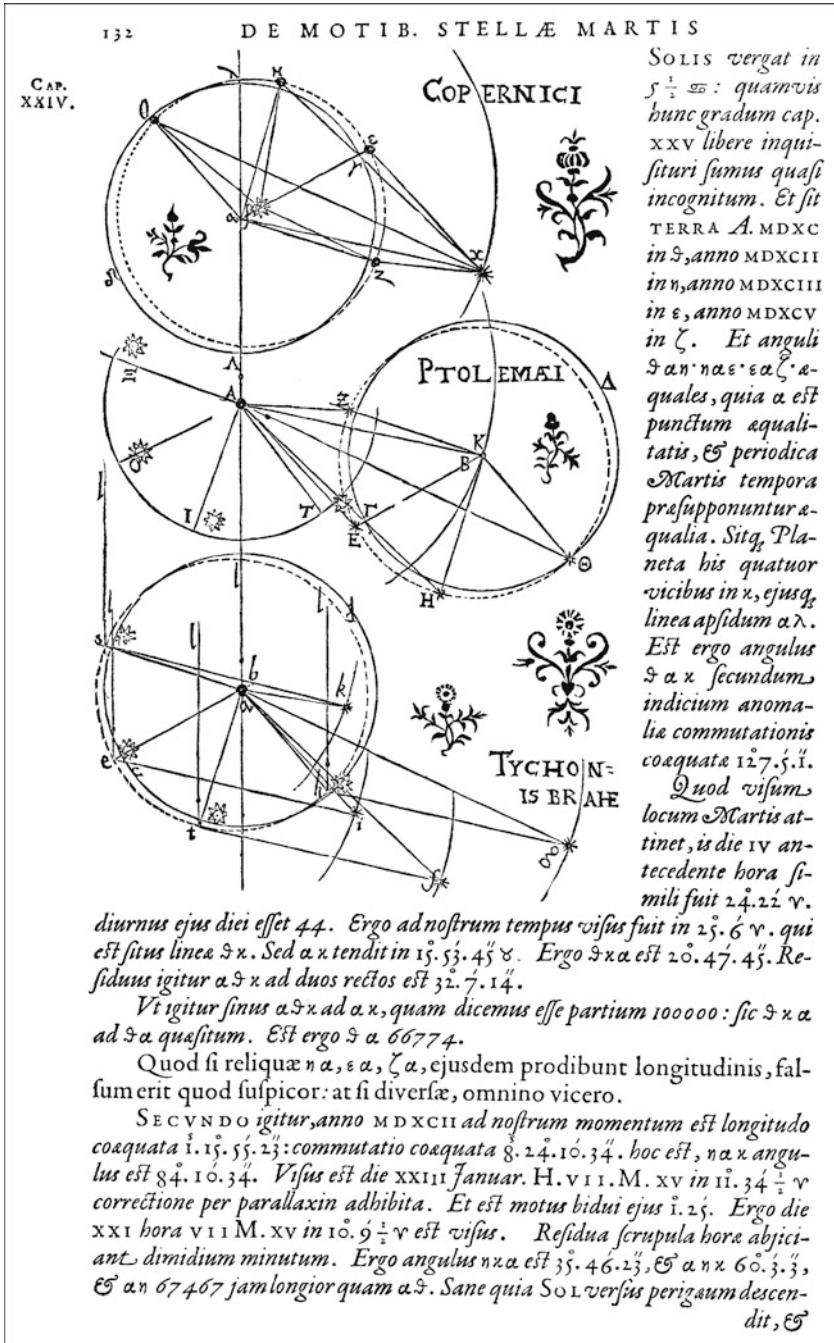


FIG. 4.14: Kepler's *Astronomia Nova*. Page 132, showing the three systems: Copernican (heliocentric), Ptolemaic (geocentric), and the hybrid system due to Tycho Brahe.



As can be seen from Figs. 4.13 and 4.14, Kepler favoured the new and “revolutionary” system. Using observations made by Tycho Brahe,<sup>16</sup> he explained the motion of the planets in the Solar System by the following three propositions (Kepler’s laws)<sup>17</sup>:

1. Law of ellipses. The trajectory of each planet lies in a plane (a) and it is an ellipse in which one focus is the Sun (b).

---

<sup>16</sup> *Tyge Brahe*, commonly known as Tycho Brahe, (1546–1601), was a Danish astronomer. He spent 20 years in his observatory in Uraniborg (“City of the Sky”), in Denmark, making very accurate astronomical measurements. He was the first to take into account the refraction of light. The accuracy of his observations was 1′ (1 arcmin, or 1/60 of a degree), while his contemporaries were not doing better than 10′. He measured the motion of the planet Mars, observing ten oppositions. His model of the Universe was a compromise between Ptolemy’s geocentric model and the heliocentric model of Copernicus. In 1597, he left for Bohemia where he worked with Kepler to set up the astronomical tables known as *Tabulae Rudolphinae*.

<sup>17</sup> The German astronomer *Johannes Kepler* (1571–1630), in Latin *Ioannes Keplerus*, published the first two laws in 1609, in *Astronomia Nova Aπιστολογητος seu Physica Caelestis*, and the third in 1619, in *Harmonices Mundi*. However, it would be wrong to think that the laws appear in a totally clear manner in these writings, as they would in today’s scientific papers. The mathematical terminology was heavy and the explanations hard to follow. There are even cases of one error of reasoning balancing out another.

The first of these two books is almost exclusively devoted to describing the orbit of Mars (whence the subtitle *Tradita comentariis de motibus stellæ Martis ex observationibus G. V. Tychonis Brahe*). The second law appears at the beginning of this work and the first at the end. Naturally, they concern only the elliptical trajectory of the planet Mars. The Greek word attached to the title *Astronomia Nova* is the substantive arising from the verb ἀπιστολογέω, meaning “to seek causes”. But although these works seem difficult to follow nowadays, they nevertheless attest to the extraordinary discoveries made by their author. To demonstrate the eccentricity of the orbit of Mars or the Earth required a great level of trust in Tycho Brahe’s observations, made with the naked eye, and a considerable degree of mathematical ability. Many other moral qualities were also involved. Courage and self-confidence were essential to take such a revolutionary theory to its logical conclusions in the face of universal opposition, in a climate of family problems and widespread religious hostility, as the wars of religion tore Europe apart. Perseverance was another quality we may safely attribute: in *Astronomia Nova*, following fifteen pages of close calculations, Kepler tells us that he had to repeat them seventy times in order to arrive at the result. In his own words: “If this method seems possible and tedious, take pity on me, for I undertook these calculations 70 times, and you should not be surprised to find that I have spent 5 years on the theory of Mars. There will no doubt be several subtle geometers, like Viète, who will say that the method is not geometric. But let them solve the problem themselves if they are not satisfied.” This can help us to understand the astonishing clause in the title of *Astronomia Nova* (see Fig. 4.14): *Plurimum annorum pertinaci studio elaborata Pragæ* (Written in Prague after several years of obstinate effort).

Kepler was deeply convinced that the cosmic and hence divine order had to be perfect, and had great difficulty renouncing the perfection of the circular orbit in favour of the ellipse, blemished as it was by the failings of the real world. Throughout his approach to science, Kepler was guided by this search for divine harmony. In his last work, this led to the musical harmony of the planets and the geometrical harmony of the regular polyhedra (Platonic solids) he fitted around the planetary orbits. In this context, Kepler wrote: “There are six planets because there are five regular polyhedra. I cannot begin to express my wonder before this discovery.”

2. Areal law. The areas swept out by the radial vector are proportional to the time it takes to sweep them out.
3. Harmonic law. The square of the period of revolution is proportional to the cube of the length of the major axis.

These correspond to our earlier equations in the following way:

$$\begin{aligned} \text{Law (1a)} &\iff \text{equation (4.8)}, \\ \text{Law (1b)} &\iff \text{equation (4.40)}, \\ \text{Law (2)} &\iff \text{equation (4.14)}, \\ \text{Law (3)} &\iff \text{equation (4.53)}. \end{aligned}$$

Note that laws (1a) and (2) apply in the case of central accelerations, and laws (1b) and (3) in the case of central accelerations with  $1/r^2$  dependence, i.e., Newtonian accelerations.

At the end of Chap. 15, in the historical note on Kepler and the planet Mars (see Sect. 15.11), we display certain passages from *Astronomia Nova* which attest to the accuracy and originality of Kepler's work. At the end of Chap. 16, in the historical note on Kepler and the Solar System (see Sect. 16.10), we include two tables of values from *Harmonices Mundi* which Kepler used to establish his third law.

## 4.8.2 Newton and the Law of Universal Attraction

While Kepler was the founder of celestial mechanics, it was Galileo<sup>18</sup> who laid the foundations for terrestrial mechanics, at the same period. But it

---

<sup>18</sup>Galileo Galilei (1564–1642) was an Italian physicist and astronomer. Founder of dynamics and the first genuine experimenter, he studied the free fall of bodies and parabolic motion. He propounded the principle of inertia, which corresponds to Newton's first law. Shortly after the invention of the refracting telescope, he began to use this instrument to observe the sky. In 1610, he discovered four moons in orbit around Jupiter, and it was this observation that persuaded him that the Earth and the other planets were in orbit around the Sun. The discovery of the crescent of Venus (impossible in a geocentric system) confirmed this idea and he communicated it to Kepler. Galileo recorded all his astronomical discoveries in *Sidereus Nuncius* (the Celestial Messenger).

An unflinching advocate of the Copernican system, Galileo was condemned for the first time by the Inquisition on 16 February 1616, under the papacy of Paul V. In 1632, he published *Dialogo sopra i due massimi sistemi del mondo, Tolemaico et Copernicano*. This was not written in Latin, but in the local vernacular or *volgare* of Italy or Tuscany. That, too, was revolutionary. In this work, he made his preferences perfectly clear and was condemned a second time for heresy on 22 June 1633, under the papacy of Urban VIII, who proclaimed: "The opinion that the Sun sits motionless at the center of the world is absurd, a false philosophy, and formally heretical, because it explicitly contradicts the Holy Scriptures." Only by getting down on his knees and abjuring did he avoid being burnt at the stake. But he was still imprisoned at the age of 70 and ended his days under house arrest.

At the end of the twentieth century, a Vatican commission was convened in 1981 under John Paul II to reconsider what had been done to Galileo. Its conclusions were announced on 31 October 1992: the Church recognised the errors of Galileo's judges but was unable to proclaim his vindication.

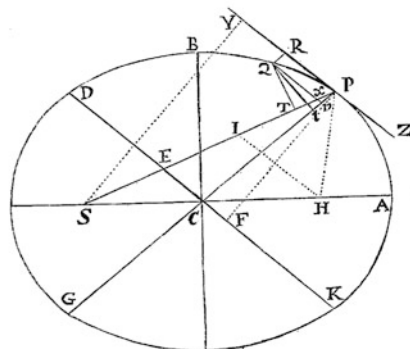
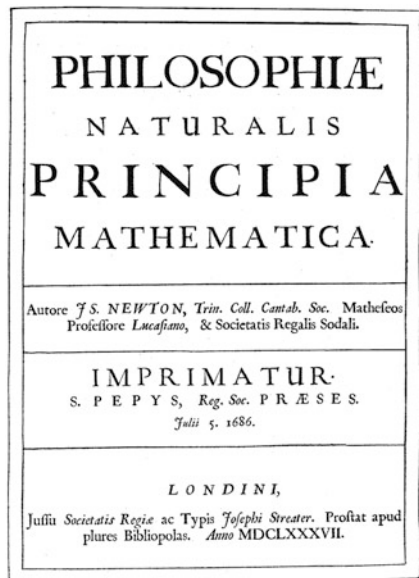


FIG. 4.15: *Newton's Principia*, published in London in 1687—MDCLXXXVII. Left: Title page. Right: Page 50, where Newton shows geometrically that, if the point  $P$ , subject to a force with center  $S$ , describes an ellipse with focus at  $S$ , then this force is inversely proportional to the square of the distance  $SP$ .

required the genius of Newton to synthesise these two aspects of the same phenomenon into a single idea: the universal law of attraction. Today, we show that an attraction of type  $1/r^2$  between the Sun and the planets leads to an elliptical trajectory for the planets. But historically, Newton had to piece together the rudiments of infinitesimal calculus (called the method of fluxions) and, starting from the elliptical trajectories discovered by Kepler, deduce that the forces at play had to have the  $1/r^2$  dependence, whereupon he could put forward his law of universal attraction (see Fig. 4.15).

Let us rewrite Newton's demonstration using the notation of modern mathematics. We begin, as he did, with the principle that the forces were central. We consider a material point, whose position is defined by a radial vector  $\mathbf{r}$  describing an ellipse. We can then write

$$u = \frac{1}{r} = \frac{1 + e \cos \theta}{a(1 - e^2)}, \quad (4.115)$$

from which we deduce

$$\frac{du}{d\theta} = -\frac{e \sin \theta}{a(1 - e^2)}, \quad \frac{d^2u}{d\theta^2} = -\frac{e \cos \theta}{a(1 - e^2)}.$$

Substituting this into Binet's equation (4.21), which we recall refers to central forces, we obtain

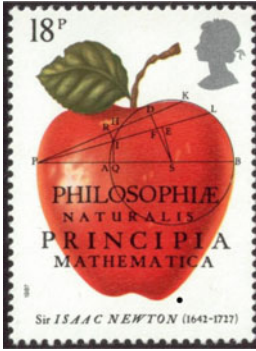


FIG. 4.16 : *British stamp commemorating Newton's work.*

$$\begin{aligned}\ddot{\mathbf{r}} &= -C^2 u^2 \left[ -\frac{e \cos \theta}{a(1-e^2)} + \frac{1+e \cos \theta}{a(1-e^2)} \right] \mathbf{e}_r \\ &= -C^2 u^2 \frac{1}{a(1-e^2)} \mathbf{e}_r = -\frac{C^2}{a(1-e^2)} \frac{1}{r^2} \mathbf{e}_r .\end{aligned}$$

Now  $C$  is given by  $\pi ab = CT/2$  (this is the areal law, which also refers to central forces), i.e.,

$$C = \frac{2\pi}{T} a^2 \sqrt{1-e^2} .$$

We can therefore deduce that

$$\ddot{\mathbf{r}} = -\frac{4\pi^2}{T^2} a^3 \frac{1}{r^2} \mathbf{e}_r , \quad (4.116)$$

whereby we obtain

$$\ddot{\mathbf{r}} = -\frac{\mu}{r^2} \mathbf{e}_r , \quad \text{with } \mu = \frac{4\pi^2}{T^2} a^3 .$$

Tycho Brahe's observations as interpreted by Kepler showed that this quantity  $\mu$  remains constant for all planets gravitating around the Sun. Newton thus deduced that it could be written in the form

$$\mu = GM_S ,$$

where  $M_S$  is the mass of the Sun and  $G$  is a universal constant.

Finally, the attractive force exerted by a body of mass  $M$  on a body of mass  $m$  (and conversely) could be written

$$\mathbf{F} = m\ddot{\mathbf{r}} = -G \frac{Mm}{r^2} \mathbf{e}_r . \quad (4.117)$$

This is indeed the law of universal attraction between two bodies of masses  $M$  and  $m$ , where  $G$  is the gravitational constant (Fig. 4.16).

# Chapter 5

## Satellite in Keplerian Orbit

From now on, we shall be mainly concerned with the periodic motion of a body, the artificial satellite,<sup>1</sup> in the gravitational field of the Earth.

### 5.1 Two-Body Problem

We consider two bodies  $A_1$  and  $A_2$ , with masses  $m_1$  and  $m_2$ , respectively, moving in a Galilean frame  $(O_0; x, y, z)$ . The system is isolated in the sense that each body feels only the attractive force of the other. This is the statement of the two-body problem. The aim is to determine the motion of the two bodies.

---

<sup>1</sup>In latin, *satelles*, *satellit*is was a bodyguard, soldier, assistant, or accomplice. The origins of the word are obscure. Some claim an Etruscan origin. The word *satellite* appears in French around 1265 to denote an armed man who carries out the orders of a commander, then in the form *satellite*, around 1500, to refer to a man depending in some way on another, or accompanying another. It was Kepler, in 1611, who gave it the modern meaning of “satellite” in the Latin term *satelles*, which he used to refer to the four satellites of Jupiter, recently discovered by Galileo with his refracting telescope. He wrote: *De quattuor Jovis satellibus erronibus*, that is, “Concerning the four wandering companions of Jupiter”. The term “artificial satellite” appeared around 1950.

In many languages, “satellite” is expressed by a word coming directly from the Latin term modernised by Kepler, as in the Latin and Anglo-Saxon languages. In others, it is the word for “moon” which is used, as in Arabic, *qamar šanā’i*, meaning “artificial moon”.

However, certain languages have kept to the first idea of *satelles*. In modern Greek, the satellite is still a bodyguard, since it is called *doryphoros*, ὁ δορυφόρος, ου, “armed with a spear”, built up from τὸ δόρυ, ατος, “spear”, and the suffix φορός, “which carries”. In Russian, *sputnik* is the travel companion (*put*, “way”). In Chinese, the satellite is called *wei xing*, “guardian star”, a word written with the two ideograms *wei*, “guard”, and *xing*, “star”. The same form is found in Japanese.

Taking an arbitrary origin  $O$ , Newton's second law takes the form

$$m_1 \frac{d^2 \mathbf{OA}_1}{dt^2} = -Gm_1 m_2 \frac{\mathbf{A}_1 \mathbf{A}_2}{\|\mathbf{A}_1 \mathbf{A}_2\|^3},$$

$$m_2 \frac{d^2 \mathbf{OA}_2}{dt^2} = -Gm_1 m_2 \frac{\mathbf{A}_2 \mathbf{A}_1}{\|\mathbf{A}_2 \mathbf{A}_1\|^3},$$

which yields the relation

$$m_1 \frac{d^2 \mathbf{OA}_1}{dt^2} + m_2 \frac{d^2 \mathbf{OA}_2}{dt^2} = 0. \quad (5.1)$$

The barycenter  $C$  of the two points  $A_1$  and  $A_2$  (also called the center of mass) is defined by

$$m_1 \mathbf{OA}_1 + m_2 \mathbf{OA}_2 = (m_1 + m_2) \mathbf{OC}.$$

We thus have

$$\frac{d^2 \mathbf{OC}}{dt^2} = 0 \quad \Longrightarrow \quad \mathbf{OC} = \mathbf{v}_0 t + \mathbf{u}_0,$$

where the vectors  $\mathbf{v}_0$  and  $\mathbf{u}_0$  are constant.

Since  $C$  is in uniform motion with respect to  $(O_0; x, y, z)$ , this shows that the frame  $(C; x, y, z)$  is Galilean. Using (5.1) and the expressions for the accelerations, we obtain

$$\frac{d^2 \mathbf{A}_1 \mathbf{A}_2}{dt^2} = -G(m_1 + m_2) \frac{\mathbf{A}_1 \mathbf{A}_2}{\|\mathbf{A}_1 \mathbf{A}_2\|^3}. \quad (5.2)$$

Taking the barycenter  $C$  of these two points as the origin, we thus have

$$\mathbf{r}_1 = \mathbf{CA}_1, \quad \mathbf{r}_2 = \mathbf{CA}_2, \quad \mathbf{r}_{12} = \mathbf{r}_2 - \mathbf{r}_1,$$

and from the definition of the barycenter,

$$m_1 \mathbf{r}_1 + m_2 \mathbf{r}_2 = \mathbf{0}.$$

Equation (5.2) gives the equation of motion:

$$\ddot{\mathbf{r}}_{12} = -G(m_1 + m_2) \frac{\mathbf{r}_{12}}{\|\mathbf{r}_{12}\|^3}, \quad (5.3)$$

as observed with respect to a Galilean frame of reference.

The motion of the points  $A_1$  and  $A_2$  can then be deduced from the motion of  $\mathbf{r}_{12}$  via the relations

$$\mathbf{r}_1 = -\frac{m_2}{m_1 + m_2} \mathbf{r}_{12}, \quad \mathbf{r}_2 = +\frac{m_1}{m_1 + m_2} \mathbf{r}_{12}.$$

As an example, for the motion of the Moon ( $A_2$ ) around the Earth ( $A_1$ ), we have  $m_1 = 81 m_2$ : the motion is studied relative to the barycenter of the Earth–Moon system.

For an artificial satellite ( $A_2$ ) around the Earth ( $A_1$ ),  $m_2$  is negligible in comparison with  $m_1$  and we have

$$\mathbf{r}_1 = \mathbf{0}, \quad \mathbf{r}_2 = \mathbf{r}_{12}.$$

In brief, the motion of an artificial satellite around the Earth will be treated as follows:

- To begin with, it will be considered as a two-body problem in which one body (the satellite) has negligible mass compared with the other. It will therefore be in Keplerian motion and the orbit it follows will be called the Keplerian orbit.
- In a second step, this motion will be considered to be perturbed. The real orbit which results will be called the perturbed orbit.

## 5.2 Orbital Elements

### 5.2.1 Specifying the Satellite Orbit in Space

#### Frame of Reference

The fundamental principle of mechanics known as the Galilean principle of relativity says that the properties of space and time are the same, and the laws of mechanics are identical, in all inertial frames of reference.

We consider a satellite in periodic motion around the Earth. Let us define the frame  $(O; x, y, z)$ . The origin  $O$  is the center of the Earth, which is taken to be a sphere  $\Sigma$ . The axis  $Oz$  is the axis joining the poles, oriented from the south to the north. The plane  $xOy$  is the equatorial plane of the Earth, denoted  $\mathcal{E}$ , which cuts the terrestrial sphere at the equator. The axis  $Ox$  is chosen arbitrarily to point towards a distant star or the vernal point. The axis  $Oy$  is deduced from the other two axes in such a way as to obtain a right-handed orthonormal frame. The frame associated with this coordinate system is considered to be Galilean and will be denoted by  $\mathfrak{R}$  (see Fig. 5.1).

The motion of the satellite is Keplerian, i.e., in  $\mathfrak{R}$ , the trajectory is a conic section, in this case an ellipse, with one focus at the center of attraction  $O$ , and lying in a plane  $\mathcal{P}$ . The trajectory of the satellite is called the orbit.<sup>2</sup> The plane  $\mathcal{P}$  is called the orbital plane. For Keplerian motion, one speaks of a Keplerian or Kepler orbit.

---

<sup>2</sup>From the old French *orbite*, first attested in 1314. It derives from the Latin *orbita*, *α*, meaning “mark left by a wheel”, then “closed curve described by a heavenly body”. The word made its appearance in astronomy in the seventeenth century, then in astronautics in around 1950 for artificial satellites.

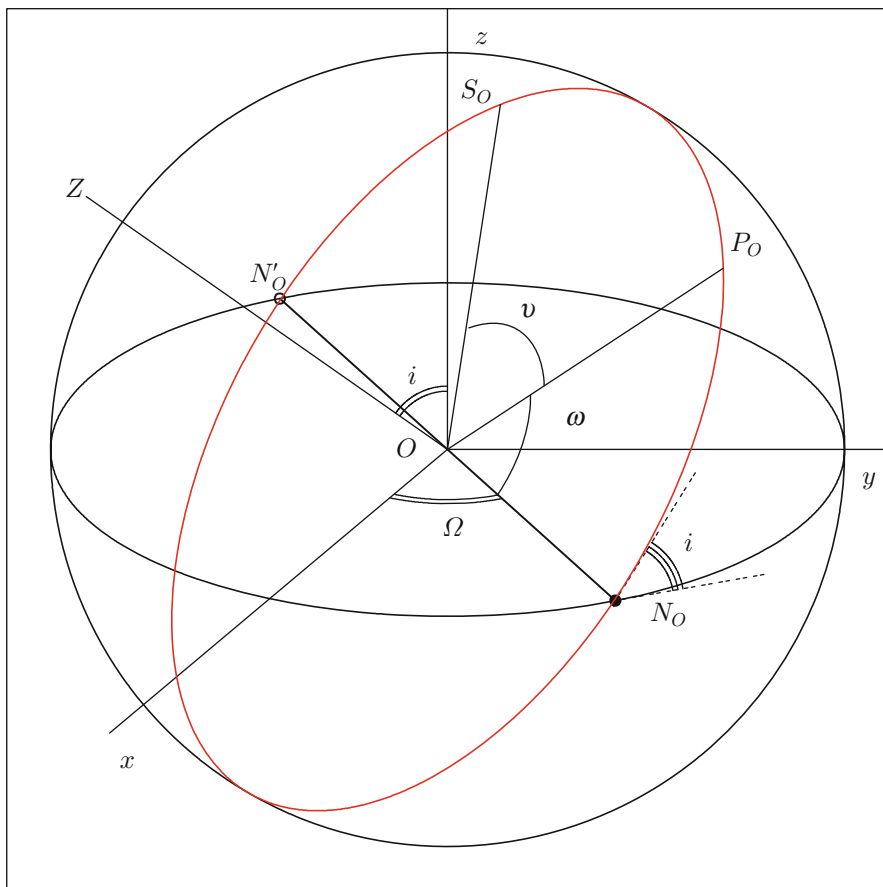
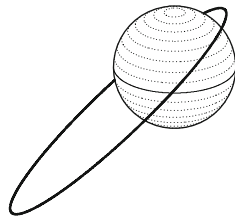


FIG. 5.1 : Ground track of the orbit in the Galilean frame. Projection of points on the ground track:  $S_0$  is the projection of the point  $S$  (satellite) and  $P_0$  is the projection of the perigee  $P$  onto the ground track.  $N_0$  and  $N'_0$  are the projections of the ascending node  $N$  and the descending node  $N'$  onto the ground track. The equatorial plane of the Earth is  $(xOy, N_0, N'_0)$ , normal to the polar axis  $Oz$ . The orbital plane is  $(O, P_0, S_0, N_0, N'_0)$ , normal to  $OZ$ . Four of the orbital elements are the right ascension  $\Omega$  of the ascending node, the inclination  $i$ , the argument of the perigee  $\omega$ , and the true anomaly  $v$ . The other two orbital elements specify the ellipse, viz., the semi-major axis  $a$  and the eccentricity  $e$ , not shown in the figure. Upper image: Orbit viewed in a Galilean frame.



In this Galilean frame, the orbital plane  $\mathcal{P}$  is fixed. Let  $OZ$  denote the straight line perpendicular to  $\mathcal{P}$  at  $O$ . The intersection of the planes  $\mathcal{P}$  and  $\mathcal{E}$  is a straight line through  $O$ , called the line of nodes. The two nodes are the points of intersection of the orbit and the terrestrial equatorial plane  $\mathcal{E}$ , with  $N$  the ascending node, where the satellite passes from the southern hemisphere to the northern hemisphere, and  $N'$  the descending node, where the satellite passes from the northern hemisphere to the southern hemisphere.

### Specifying a Point on an Orbit

In order to specify a point in Keplerian motion in space, the first step is to identify the orbit, and then the point on the orbit. We thus define successively:

- the location of the orbital plane in this frame,
- the position of the elliptical orbit in this plane,
- the characteristics of the ellipse,
- the position of the moving point, i.e., the satellite, on the orbit.

We shall find that six parameters are necessary and sufficient to determine the position of the satellite in  $\mathfrak{R}$ . Let us now go through each of these points.

**Locating the Orbital Plane in the Frame.** Two angles, those of the spherical coordinate system, fix  $\mathcal{P}$  relative to  $\mathcal{E}$ , given that  $\mathcal{P}$  contains  $O$ . These angles are an azimuthal angle and a height angle. The angle  $\Omega$  of the plane  $\mathcal{E}$ , which specifies the line of nodes (in the direction of the ascending node) relative to the zero axis, is called the right ascension of the ascending node:

$$\Omega = (\mathbf{Ox}, \mathbf{ON}) .$$

The angle  $i$  is the dihedral angle  $i = (\mathcal{E}, \mathcal{P})$  between the orbital and equatorial planes. This is called the inclination. It can also be defined in terms of the normals to the planes by

$$i = (\mathbf{Oz}, \mathbf{OZ}) .$$

All possible positions of  $\mathcal{P}$  relative to  $\mathcal{E}$  are obtained as  $\Omega$  varies over the interval  $[0, 2\pi)$  and  $i$  varies over  $[0, \pi)$ .

**Characterising the Ellipse.** Since its focus is at  $O$ , the center of attraction, the ellipse is characterised by two parameters, its semi-major axis  $a$  and its eccentricity  $e$ .

**Locating the Ellipse in the Orbital Plane.** The ellipse is specified in  $\mathcal{P}$  by choosing the position of a point, traditionally the perigee  $P$ , and then specifying the argument of the perigee  $\omega$ , which is the angle between the apsidal line and the line of nodes:

$$\omega = (\mathbf{ON}, \mathbf{OP}) .$$

**Locating the Satellite in Its Orbit.** A point  $S$  on the ellipse is perfectly determined by its polar angle, centered on  $O$ . This is the true anomaly  $v$ , already defined as

$$v = (\mathbf{OP}, \mathbf{OS}) .$$

The mean anomaly  $M$  is general preferred over  $v$ . In Chap. 4, we considered the bijective relation between these two variables [see (4.59)].

We can also use the angle  $\alpha$ , called the position on orbit or the argument of the latitude, or the nodal elongation, defined by

$$\alpha = \omega + v , \tag{5.4}$$

which specifies the position of  $S$  relative to the ascending node.

### 5.2.2 Keplerian Elements

The parameters discussed above define the orbit and the position of the satellite on the orbit. These parameters constitute the six orbital elements, also known as the Keplerian elements. They are generally presented in the following order:

$$a, e, i, \Omega, \omega, M .$$

The parameter  $a$  has dimensions of length, whilst the five others ( $e$  and the four angles) are dimensionless.

Six parameters, including at least one length, are necessary and sufficient to specify the motion of a point. The position of a point (3 position coordinates) and its velocity (the 3 velocity components) at a given time can provide the initial conditions required to integrate the equations of motion, thereby determining the position of a point on its trajectory (3 + 3 = 6 parameters).

Other sets than the Kepler elements can be used. We may also use those of Laplace, Delaunay, Hill, or others. Each is designed to meet different needs. The six Keplerian elements play a clear didactic role in the study of perturbed motion, because it is then easy to see which ones vary and which ones do not (see Table 5.1). These angles can be expressed in terms of the Euler angles (see the appendix to the chapter in Sect. 5.4).

In Chap. 8, and in particular in Sect. 8.4, we discuss the orbital elements that are used in practice to locate satellites to high levels of accuracy. We shall then establish the relation between these elements and the Keplerian elements discussed above.

### 5.2.3 Adapted Orbital Elements

In certain cases, the Keplerian elements do not provide a precise enough system of parameters. They are then combined in such a way as to provide

	Angle	Angle	Range	Plane	Euler angle
$\Omega$	R.A. of ascending node	$(Ox, ON_0)$	0–360	$\in \mathcal{E}$	Precession
$i$	Inclination	$(Oz, OZ)$	0–180	$(\mathcal{E}, \mathcal{P})$	Nutation
$\omega$	Argument of the perigee	$(ON_0, OP_0)$	0–360	$\in \mathcal{P}$	Proper rotation
$v$	True anomaly	$(OP_0, OS_0)$	0–360	$\in \mathcal{P}$	Proper rotation

TABLE 5.1 : Kepler elements (angles). The angles refer to Fig. 5.1. Ranges are given in degrees. R.A. = right ascension.

better adapted parameters. We shall now list the combinations used to get around the difficulties. No attempt has been made to give more than a simple inventory. These methods are used for a highly refined description of satellite motion (accurate positioning and station-keeping), which lie beyond the scope of the present book.

### Near-Circular Orbits

For eccentricities close to zero, the orbit is said to be near-circular. The perigee is then poorly defined, in the sense that small fluctuations in  $e$  lead to large variations in  $\omega$ . Moreover, in this case,  $v$  and  $M$  are very close. To specify the position of the satellite in its orbit, it is more convenient to take the origin at the ascending node, with  $\tilde{\alpha} = \omega + M$ , than at the perigee, with  $M$ . The Keplerian elements are then replaced by the following adapted parameters:

$$a, \quad e_x = e \cos \omega, \quad e_y = e \sin \omega, \quad i, \quad \Omega, \quad \tilde{\alpha} = \omega + M .$$

### Near-Equatorial Orbits

If the orbit lies almost in the equatorial plane, the ascending node is ill-defined. There may even be discontinuities in  $\Omega$  when the plane of the orbit crosses the equatorial plane: the ascending node becomes the descending node. In this case, it is preferable to use the following parameters:

$$a, \quad e, \quad \tilde{\omega} = \omega + \Omega, \quad h_x = 2 \sin \frac{i}{2} \cos \Omega, \quad h_y = 2 \sin \frac{i}{2} \sin \Omega, \quad M .$$

### Near-Circular Near-Equatorial Orbits

If the conditions of the last two cases are brought together simultaneously (as in the case of geostationary satellites), neither the line of nodes nor the apsidal line are clearly defined. We then use the angles  $\tilde{\omega} = \omega + \Omega$  and  $\tilde{\lambda} = \tilde{\omega} + M = \omega + \Omega + M$ . Suitable adapted parameters are as follows:

$$a, \quad e \cos \tilde{\omega}, \quad e \sin \tilde{\omega}, \quad 2 \sin \frac{i}{2} \cos \Omega, \quad 2 \sin \frac{i}{2} \sin \Omega, \quad \tilde{\lambda} .$$

### 5.3 Keplerian Period

Whatever the eccentricity of an elliptical orbit may be, the Keplerian period is given by (4.53). We denote this by  $T_0$  to distinguish it from periods defined for perturbed motion:

$$T_0 = 2\pi \sqrt{\frac{a^3}{\mu}} . \quad (5.5)$$

It is convenient to define the period  $T_{0(h=0)}$  of a fictitious satellite in circular orbit at ground level on a spherical Earth of radius  $R$ :

$$T_{0(h=0)} = 2\pi \sqrt{\frac{R^3}{\mu}} . \quad (5.6)$$

We also define the reduced (dimensionless) distance  $\eta = a/R$  of the satellite from the center of the Earth, as already given in (2.38). We may then express  $T_0$  in terms of  $a$ ,  $\eta$ , or  $h$ :

$$\frac{T_0(a)}{T_{0(h=0)}} = \left(\frac{a}{R}\right)^{3/2} , \quad (5.7)$$

$$T_0(\eta) = \eta^{3/2} T_{0(h=0)} . \quad (5.8)$$

Numerical calculation of the period of the satellite orbiting at ground level gives

$$T_{0(h=0)} = 5,069.34 \text{ s} = 84.4891 \text{ min} . \quad (5.9)$$

The maximal number of revolutions per day is therefore, for an Earth-orbiting satellite,

$$\nu_{0(h=0)} = 17.044 . \quad (5.10)$$

This notion of daily orbital frequency is further developed in Chap. 7.

Figure 5.2 can be used as a quick way to evaluate the period as a function of altitude. Several satellite appellations appear on the figure (LEO, MEO, GEO). These will be explained later.

For a near-circular orbit, we define the height  $h$  above a spherical Earth by

$$h = a - R , \quad R = R_e = \text{equatorial radius} .$$

Equation (5.8) becomes

$$T_0(h) = \left(1 + \frac{h}{R}\right)^{3/2} T_{0(h=0)} .$$

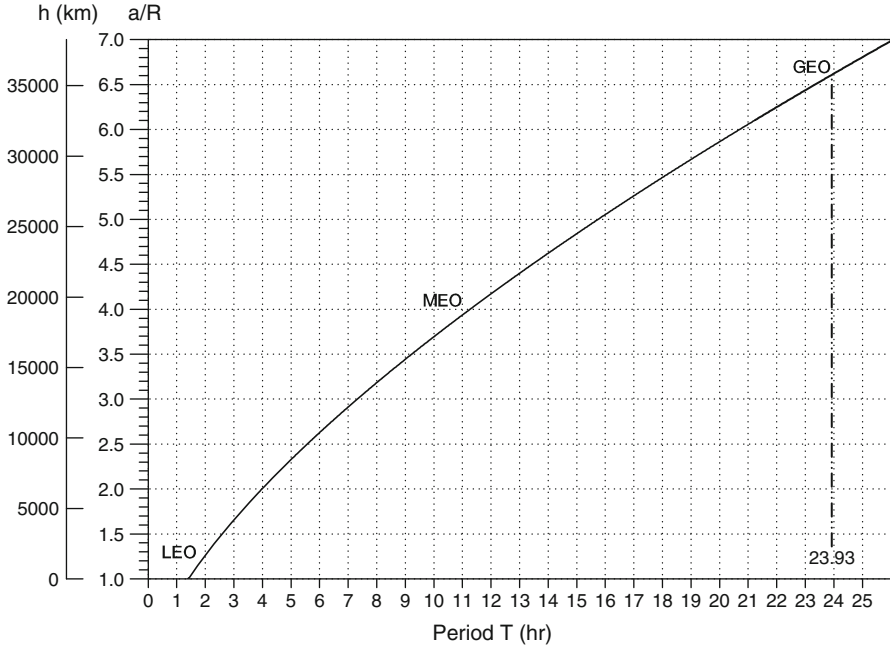


FIG. 5.2: Keplerian period of a satellite as a function of the semi-major axis  $a$  (and the altitude for a circular orbit). The abbreviations LEO, MEO, and GEO are explained below.

When  $h$  is much smaller than  $R$  (the case of low altitudes, i.e., LEO satellites), we have

$$T_0(h) \approx \left(1 + \frac{3h}{2R}\right) T_{0(h=0)} .$$

### Circular Motion

The upper graph in Fig. 5.3 shows the trajectory of a satellite with circular orbit (in its orbital plane) for various altitudes and over the same lapse of time, chosen here to be equal to  $T_{0(h=0)}$ , i.e., 84.5 min. The frame is the Galilean frame  $\mathfrak{R}$ . The satellite is moving in a direct or prograde orbit. The trajectory shown begins on the vertical axis, on which the values of  $\eta = a/R$  are indicated, and ends at a black dot. For  $\eta = 1.0$ , the trajectory makes a complete round trip, for  $\eta = 1.6$ , just half a revolution, and for  $\eta = 2.5$ , one quarter of a revolution (since  $1.6^{-3/2} \approx 1/2$  and  $2.5^{-3/2} \approx 1/4$ ).

Consider now the lower graph of Fig. 5.3, representing the Earth’s equatorial plane. On this graph, which extends the last one, we have also marked with a dot-dashed line the angle through which the Earth has rotated relative to  $\mathfrak{R}$  in 84.5 min. For  $\eta < 6.6$ , the satellite moves around faster than the

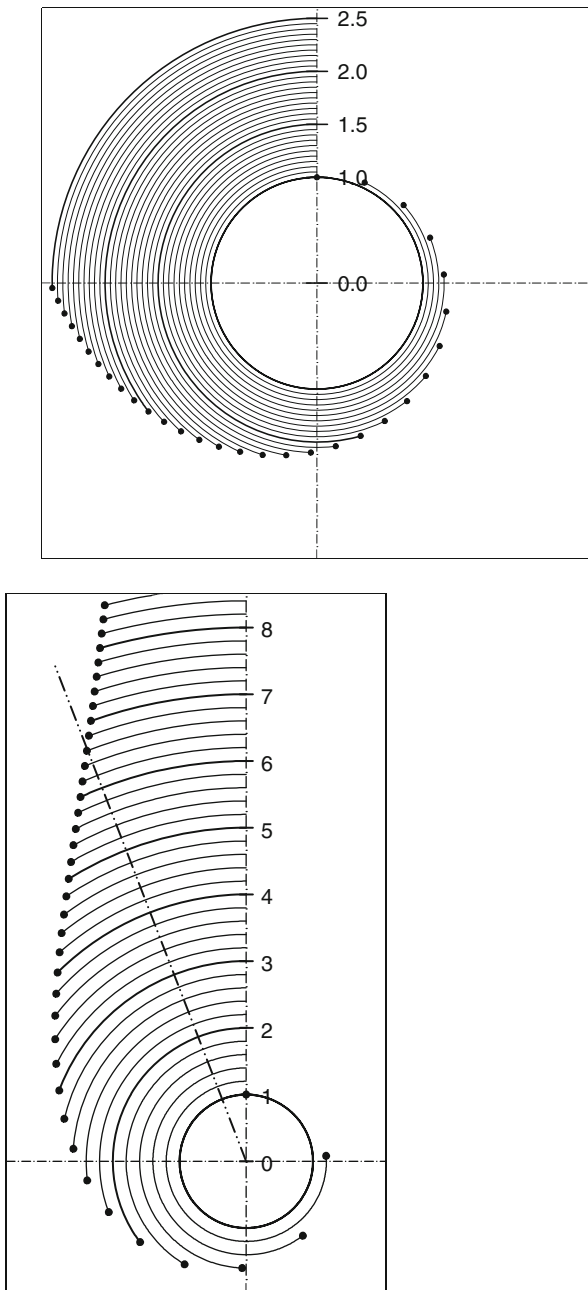


FIG. 5.3: *Spherical representation of the Earth and circular satellite trajectories as a function of the reduced distance  $\eta$ . Orbital plane. Galilean frame  $\mathcal{R}$ . Lapse of time represented: 84.5 min (Keplerian period of revolution of a fictitious satellite at ground level). Upper: Arbitrary orbital plane. Lower: Orbital plane coincident with the Earth's equatorial plane. View from a point situated on the Earth's axis, above the North Pole. The dot-dashed line indicates the angle of rotation of the Earth over 84.5 min in the frame  $\mathcal{R}$ .*

Earth, otherwise more slowly. For  $\eta = 6.6$ , an equatorial satellite revolves at the same angular speed as the Earth in the frame  $\mathfrak{R}$ . In a terrestrial frame  $\mathfrak{R}_T$  fixed with respect to the Earth, this satellite will appear to be motionless. It is said to be geostationary. We shall return to this case in Chap. 7.

## 5.4 Appendix: Rotation of a Solid—Euler and Cardan Angles

The rotation of a rigid solid can be defined as the transformation from one Cartesian frame to another. It can be shown that this transformation can be decomposed into three elementary rotations, in a well defined order, about the coordinate axes.

The three axes  $Ox$ ,  $Oy$ , and  $Oz$  are labelled 1, 2, and 3. The rotation  $\mathcal{R}$  decomposes into three successive rotations through angles  $\alpha_1$ ,  $\alpha_2$ , and  $\alpha_3$  :

- $\mathcal{R}_i(\alpha_1)$ : rotation through  $\alpha_1$  about axis  $i$ , with  $i = 1, 2$ , or  $3$ .
- $\mathcal{R}_j(\alpha_2)$ : rotation through  $\alpha_2$  about axis  $j$ , with  $j = 1, 2$ , or  $3$ , and  $j \neq i$ .
- $\mathcal{R}_k(\alpha_3)$ : rotation through  $\alpha_3$  about axis  $k$ , with  $k = 1, 2$ , or  $3$ ,  $k \neq j$ .

Using  $\circ$  to denote compositions of transformations, we thus have

$$\mathcal{R} = \mathcal{R}_k(\alpha_3) \circ \mathcal{R}_j(\alpha_2) \circ \mathcal{R}_i(\alpha_1) . \quad (5.11)$$

There are therefore  $3 \times 2 \times 2 = 12$  ways to carry out this composition. In practice, only two of these are actually used: the Euler<sup>3</sup> system (Fig. 5.4) and the Cardan<sup>4</sup> system (see Table 5.2).

---

<sup>3</sup>*Leonhard Euler* (1707–1783) was a prolific Swiss mathematician whose work ranged over all the mathematics of the day. He was the first to develop the idea of a function of a variable, usually denoted  $f(x)$ , applying it to exponential, logarithmic, and trigonometric functions in his *Introduction in analysis infinitorum* (1748). He introduced the notation  $e$ ,  $\pi$ , and  $i$ , and obtained the celebrated result

$$e^{i\pi} + 1 = 0 .$$

He also invented graph theory, applying it to solve (negatively) the problem of the seven bridges of Königsberg, and worked on convex polyhedra, showing that there are exactly five Platonic solids.

In mechanics, and in particular in his *Mechanica sive motus scientia analytica exposita* (1736), he analysed the motion of a material point using Euler angles and Euler variables. His clear expositions revolutionised algebra, geometry, and number theory.

In astronomy, he studied the mutual perturbations of Saturn and Jupiter in *Theoria motuum planetarium et cometarum* (1744), the precession of the equinoxes (1749), the restricted three-body problem, and the motion of the Moon (1772).

<sup>4</sup>*Gerolamo Cardano* (1501–1576), known in English as *Jerome Cardan*, was an Italian mathematician. He found a way of solving third order polynomial equations. He invented a mechanical device, the Cardan suspension, that could make a compass insensitive to a ship's motion. The names of the Cardan angles, roll, pitch, and yaw, are borrowed from naval vocabulary. Doctor, astrologer, and generally unusual character, Cardan is said to have stopped eating so that he could die on the day he had predicted using his horoscope!



FIG. 5.4 : Swiss stamp commemorating Leonhard Euler (1707–1783).

System	Axis $i$	Axis $j$	Axis $k$	$\alpha_1$	$\alpha_2$	$\alpha_3$
Euler	3 : $Oz$	1 : $Ox$	3 : $Oz$	Precession	Nutation	Proper rotation
Cardan	1 : $Ox$	2 : $Oy$	3 : $Oz$	Roll	Pitch	Yaw

TABLE 5.2 : Axes of rotation and names of the angles used to decompose rotations in the Euler system and the Cardan system (Euler angles and Cardan angles, respectively).

## Euler Angles

The sequence  $[3, 1, 3]$  characterises the Euler system. The decomposition is illustrated in Fig. 5.1:

- The first rotation  $\mathcal{R}_i(\alpha_1)$ , with  $i = 3$ , is made around the  $Oz$  axis to transform  $Ox$  to  $ON_0$ . The angle  $\alpha_1$  is the angle of precession,  $\alpha_1 = \Omega$ .
- The second rotation  $\mathcal{R}_j(\alpha_2)$ , with  $j = 1$ , is made around the  $Ox$  axis, now represented by  $ON_0$ , to transform  $Oz$  to  $OZ$ . The angle  $\alpha_2$  is the angle of nutation, the angle  $i$  between the two planes.
- The third rotation  $\mathcal{R}_k(\alpha_3)$ , with  $k = 3$ , is made around the  $Oz$  axis, now represented by  $OZ$ , to transform  $ON_0$  to  $OP_0$ . The angle  $\alpha_3$  is the angle of proper rotation,  $\alpha_3 = \omega$ .

For this system, the given rotation is uniquely defined by

$$0 \leq \alpha_1 < 2\pi, \quad 0 \leq \alpha_2 \leq \pi, \quad 0 \leq \alpha_3 < 2\pi.$$

Replacing  $P_0$  by  $S_0$  and hence  $\alpha_3 = \omega$  by  $\alpha_3 = \omega + v$ , we see that this decomposition is well suited to studying the orbital motion of a satellite. The rotation matrix corresponding to  $\mathcal{R}$  is obtained as the product of three simple matrices.

## Cardan Angles

When the satellite is no longer treated as a point, but rather as a complex technological object carrying emitting and receiving instruments, solar panels, and so on, it is also important to control its attitude, i.e., its orientation in the



space around its center of gravity. The Cardan system is then highly suited. It corresponds to the sequence [1, 2, 3].

The three Cardan angles are called roll, pitch, and yaw. They depend on the choice of axes relative to the line of sight from the Earth to the satellite. We shall return to these angles in Chap. 12, which discusses what can be viewed from the satellite.

**Note on Other Naming Systems.** In this book, we use the term Euler angles to distinguish from the Cardan angles. In the literature, the Euler angles are also known as the Tait–Bryan angles. In some references, the term Euler angles may refer to any set of three angles (denoted here by  $\alpha_1, \alpha_2, \alpha_3$ ) used to decompose rotations.

# Chapter 6

## Satellite in Real (Perturbed) Orbit

### 6.1 Perturbing Forces

#### 6.1.1 From Ideal to Real Orbits

Up to now, we have been discussing the Keplerian motion of an Earth-orbiting satellite: this satellite is pointlike and subject to the gravitational attraction of a pointlike Earth. It has a fixed orbit in a fixed plane, and this remains immutable relative to a Galilean frame. We have seen that the Earth's attraction reduces to the attraction due to a point mass, provided that the Earth can be treated as spherical, with a spherically symmetric mass distribution (conditions for applying Gauss' theorem).

But when we observe the motion of a satellite with sufficient accuracy, we find that it does not follow exactly this kind of Keplerian motion. The difference is only very slight over one revolution, but increases steadily as time goes by until it becomes easily discernible after a few days. One might say that the Keplerian orbit is gradually distorted.

The difference between the true motion and the ideal Keplerian motion results from two considerations, as we have already mentioned:

- The Earth is not exactly spherical and the mass distribution is not exactly spherically symmetric.
- The satellite feels other forces apart from the Earth's attraction, such as attractive forces due to other heavenly bodies and forces that can be globally categorised as frictional.

The effects of these perturbations will be the subject of this chapter.

### 6.1.2 Order of Magnitude of Perturbing Forces

The forces felt by a satellite in geocentric orbit are examined below as a function of the altitude of the satellite and summed up in Fig. 6.1. From a physical standpoint, it is useful to divide these forces into two categories, depending on whether or not they are conservative.

Conservative forces are ones that can be derived from a potential, e.g., gravitational forces such as the gravitational attraction of the Earth and attraction to other heavenly bodies. Non-conservative forces are forces that cannot be derived from a potential, i.e., dissipative forces involving energy loss. Apart from atmospheric drag, which falls off very rapidly with increasing altitude, the relevant forces here are due to radiation pressure.

It is important to assess the orders of magnitude of the various forces. For example, for a satellite at an altitude of 800 km in a near-circular orbit, taking the central attraction to be unity, the other attractive effects have the following much lower values:

- $10^{-3}$  for the perturbation due to the flattening of the Earth,
- $10^{-6}$  for perturbations due to other irregularities of the geoid,
- $10^{-7}$  for the attraction of the Moon,
- $10^{-8}$  for the attraction of the Sun.

The other forces, conservative or otherwise, generally never exceed order  $10^{-8}$ .

These are orders of magnitude, to which we shall return later on. However, we can already see that all these forces (except the main one) can be treated as perturbations. They are not dealt with together in one global treatment, but one by one, as quantities that remain small relative to the main force, which is the central Newtonian attraction.

The set of forces mentioned above can be written in terms of the accelerations:

$$\boldsymbol{\gamma} = \boldsymbol{\gamma}_{\text{CCC}} + \boldsymbol{\gamma}_{\text{CCN}} + \sum_i \boldsymbol{\gamma}_{\text{C}_i} + \sum_j \boldsymbol{\gamma}_{\text{D}_j}, \quad (6.1)$$

using the suffixes explained in Table 6.1. The leading term is  $\boldsymbol{\gamma}_{\text{CCC}}$ , compared with which all the others are very small. Naturally, we have the equivalence

$$\boldsymbol{\gamma}_{\text{CCC}} = \mathbf{g}(r) = -\frac{\mu}{r^2} \mathbf{e}_r, \quad (6.2)$$

where the vector field  $\mathbf{g}(r)$  represents the Newtonian gravitational field of the Earth, previously defined in (3.11).

### 6.1.3 Potential

To begin with, let us consider only those terms due to conservative forces so that we may use the idea of potential. We know that the potential  $U$  associated with a vector field  $\boldsymbol{\gamma}$  is given by

$$\boldsymbol{\gamma} = \mathbf{grad} U ,$$

and using the linearity properties of the gradient operator  $\mathbf{grad}$ , we have

$$U = U_{CCC} + U_{CCN} + \sum_i U_{Ci} . \quad (6.3)$$

The Earth's gravitational potential is

$$U_{CC} = U_{CCC} + U_{CCN} .$$

We calculated this in Chap. 3, obtaining the general form (3.28) and the truncated form (3.27), cutting off after degree 2.

The leading order term  $U_{CCC}$ , hereafter written  $U_0$ , corresponds to the “Keplerian” central attraction, viz.,

$$U_{CCC} = U_0 = \frac{\mu}{r} = \frac{GM}{r} . \quad (6.4)$$

### 6.1.4 Perturbations and Altitude of a Satellite

Let us now investigate the whole range of perturbative forces (accelerations) affecting a satellite  $S$  at distance  $r$  from the center  $O$  of the Earth. We may also express them in terms of  $h$ , the altitude of the satellite, given by  $h = r - R$ , where  $R$  is the equatorial radius of the Earth. Figure 6.1 shows the value of the acceleration  $\boldsymbol{\gamma}$  as a function of the reduced distance  $\eta = r/R$ , using a log–log scale:

- On the horizontal axis  $x = \log \eta$ , with minimal value  $x = 0$ , i.e.,  $r = R$  or  $h = 0$ , corresponding to ground level.
- On the vertical axis,  $y = \log \gamma_i$ , where  $\gamma_i$  is the acceleration under consideration.

The figure shows typical altitudes of three types of satellite (we shall discuss these types in more detail later):

- $h = 1,000$  km for satellites in low orbit (LEO),
- $h = 20,000$  km for positioning satellites (MEO),
- $h = 36,000$  km for geostationary satellites (GEO).

The figure shows the sensitivity of the different types of satellite to the various perturbing forces depending on their altitudes. The forces, divided into conservative and non-conservative (or dissipative), are summarised in Table 6.1.

#### Conservative Forces

The gravitational forces acting on the satellite come from the following sources:

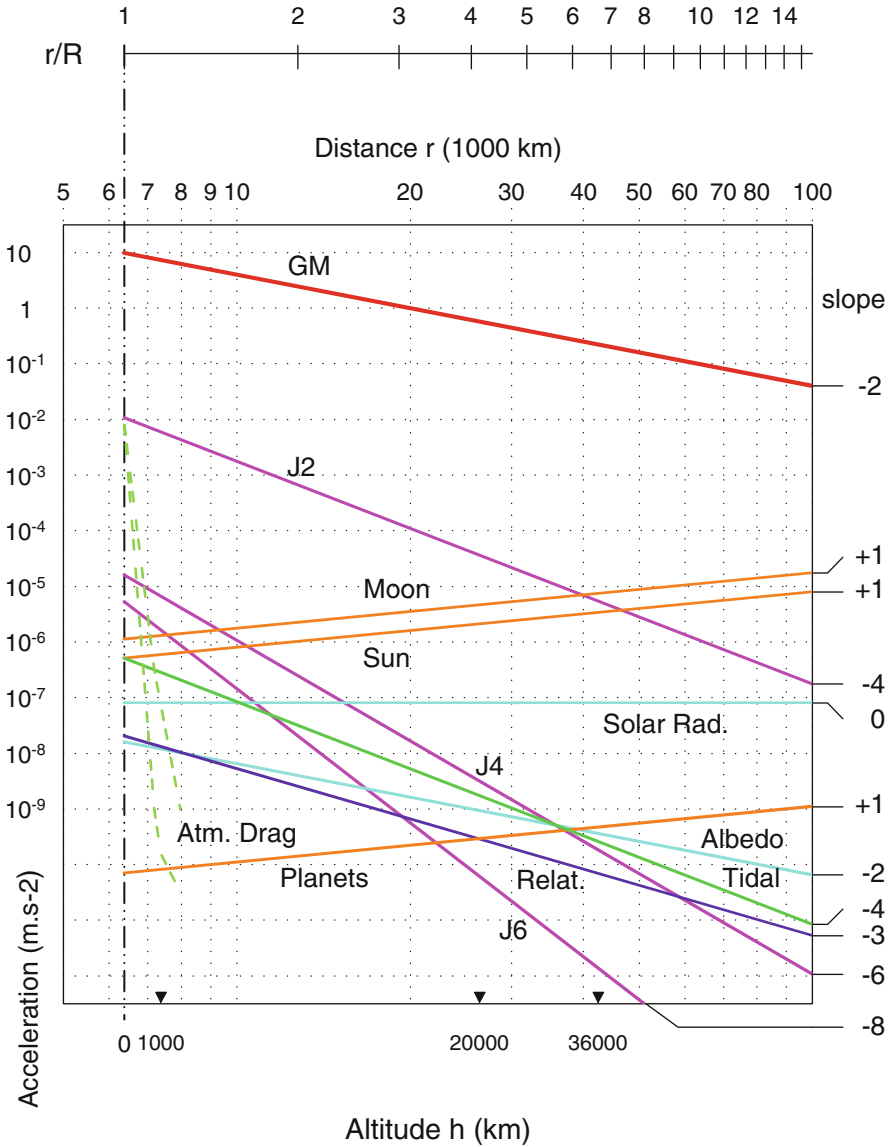


FIG. 6.1: Central acceleration and perturbative accelerations as a function of the distance  $r$  of the satellite from the center of the Earth, shown on a log-log scale. Over the ranges considered, the curves can be approximated as straight lines with slopes as noted. The altitudes of the three types of satellite have also been indicated in the order LEO, MEO, and GEO.

Symbol	Type of force	
C		Conservative forces
	CC	• Attraction of the Earth
	CCC	• ◦ Central term $\mu = GM$
	CCN	• ◦ Other terms than CCC
	CL	• Attraction of the Moon
	CS	• Attraction of the Sun
	CP	• Attraction by other planets
	CT	• Tidal effects (land, oceans)
CR	• Relativistic effects	
D		Dissipative forces
	DF	• Atmospheric drag
	DP	• Solar radiation pressure
	DA	• Albedo effect

TABLE 6.1 : List of forces that might affect a satellite.

**(a) Attraction by the Earth.** The central acceleration, denoted here by  $\gamma_{CCC}$ , is given by (6.2), viz.,

$$\gamma_{CCC}(r) = g(r) = \frac{\mu}{r^2} . \tag{6.5}$$

It is thus represented by a straight line of slope  $p = -2$  in a graph using a log–log scale, since we have  $y = \log(\mu/R^2) - 2x$ . The value at the origin ( $x = 0$ , i.e.,  $r = R$  or  $h = 0$ ) is

$$\gamma_{CCC}(R) = g(R) = g_0 = \frac{\mu}{R^2} , \tag{6.6}$$

with average numerical value

$$g_0 = 9.80 \text{ m s}^{-2} .$$

Concerning the  $J_2$  term, the potential  $U_{CCN.J_2}$  given by (3.27) goes as  $r^{-3}$ . The corresponding acceleration  $\gamma_{CCN.J_2}$  thus goes as  $r^{-4}$ , whence the slope  $p = -4$  of the straight line representing it on the log–log graph. As value at the origin ( $h = 0$ ), we have taken

$$\gamma_{CCN.J_2}(R) = g_0 J_2 ,$$

which is an average value over the latitudes frequented by the satellite.

The acceleration  $\gamma_{CCN.J_N}$  for the terms  $J_n$  with  $n > 2$  leads to an even steeper slope. We shall see below that only those terms  $J_n$  with even  $n$  have any long-term (secular) influence on the satellite. Equation (3.28) shows that the potential goes as  $r^{-(n+1)}$ , and the acceleration therefore as  $r^{-(n+2)}$ . The slope is  $p = -6$  for  $J_4$ ,  $p = -8$  for  $J_6$ , and so on. At the origin, the numerical values are

$$g_0 J_2 = 1.1 \times 10^{-2} \text{ m s}^{-2},$$

$$g_0 J_4 = 1.6 \times 10^{-5} \text{ m s}^{-2}, \quad g_0 J_6 = 5.3 \times 10^{-6} \text{ m s}^{-2},$$

where we have of course taken the absolute values of the terms  $J_n$ .

**(b) Attraction by the Sun and Moon.** We consider an attracting body (the Sun or Moon) and calculate its action on the satellite. As the Earth also feels an attraction from the same source, we must calculate the differential attraction felt by the satellite in a coordinate system fixed relative to the center of the Earth.

The differential attraction due to the Sun produces the acceleration  $\gamma_{\text{CS}}$  (calculated in Sect. 6.11 at the end of the chapter). Equation (6.151) yields

$$\gamma_{\text{CS}} = 2 \frac{\mu_{\text{S}}}{a_{\text{S}}^3} r, \quad (6.7)$$

where  $\mu_{\text{S}}$  is the heliocentric gravitational constant and  $a_{\text{S}}$  is the Earth–Sun distance, i.e., the semi-major axis of the Earth’s orbit around the Sun.

For the differential attraction due to the Moon, the acceleration  $\gamma_{\text{CL}}$  can be calculated to a first approximation by a similar argument:

$$\gamma_{\text{CL}} = 2 \frac{\mu_{\text{L}}}{a_{\text{L}}^3} r, \quad (6.8)$$

where  $\mu_{\text{L}}$  is the lunar gravitational constant and  $a_{\text{L}}$  is the Earth–Moon distance, i.e., the semi-major axis of the geocentric lunar orbit.

For the range of values represented here,  $\gamma_{\text{CS}}$  and  $\gamma_{\text{CL}}$  are proportional to  $r$ , so that their variation has slope  $p = +1$ . At the origin ( $h = 0$ ), numerical values are

$$\gamma_{\text{CS}}(R) = 2 \frac{\mu_{\text{S}}}{a_{\text{S}}^3} R = 0.5 \times 10^{-6} \text{ m s}^{-2}, \quad \gamma_{\text{CL}}(R) = 2 \frac{\mu_{\text{L}}}{a_{\text{L}}^3} R = 1.1 \times 10^{-6} \text{ m s}^{-2}.$$

The effect of the Moon is more than twice that of the Sun.<sup>1</sup>

**(c) Attraction by Other Planets.** This differential attraction causes a very small acceleration of the satellite, denoted  $\gamma_{\text{CP}}$ , also of slope  $p = +1$ . For each planet, the order of magnitude is given by

$$\gamma_{\text{CP}} = 2 \frac{\mu_{\text{P}}}{a_{\text{P}}^3} r, \quad (6.9)$$

---

<sup>1</sup>There is a trick for obtaining a relation between the two accelerations  $\gamma_{\text{CS}}(r)$  and  $\gamma_{\text{CL}}(r)$ . Their ratio is

$$\frac{\gamma_{\text{CL}}(r)}{\gamma_{\text{CS}}(r)} = \frac{\mu_{\text{L}}}{\mu_{\text{S}}} \left( \frac{a_{\text{S}}}{a_{\text{L}}} \right)^3.$$

where  $\mu_P$  is the gravitational attraction of the planet and  $a_P$  is the Earth–planet distance. Depending on the configuration of the planets, the maximal perturbative accelerations are

$$\gamma_{CP} \sim 10^{-10} \text{ m s}^{-2} \text{ due to Venus,} \quad \gamma_{CP} \sim 10^{-11} \text{ m s}^{-2} \text{ due to Jupiter.}$$

**(d) Tidal Effects.** The ocean tides are caused by the perturbing effects of the Sun and Moon. This idea was first put forward by Newton, then Bernoulli, and the theory was completed by Laplace and Kelvin. The phenomenon is familiar to us and easy to observe. It is less well known that this same perturbation also affects the Earth’s crust: twice a day, the Earth’s solid envelope rises and falls with an amplitude of around three decimeters (and six for the liquid envelope, i.e., the oceans).

Both ocean and land tides involve friction, so this phenomenon is not conservative. Indeed, this effect explains the gradual reduction of the Earth’s rotation. However, the effect of the tides on a satellite can be found using the fact that the relevant stresses derive from a potential. It can be shown that the interaction potential goes as  $r^{-3}$ , giving rise to an acceleration that goes as  $r^{-4}$ . For  $r = R$ , we have  $\gamma_{CT} \sim 5 \times 10^{-7} \text{ m s}^{-2}$ . The effect of the ocean tides is roughly one tenth of the effect of the land tides.

**(e) Relativistic Effects.** The speed  $V$  of a satellite never exceeds a few kilometers a second. This is very small compared with the speed of light  $c$  and a relativistic treatment is generally unnecessary. However, since the TOPEX/Poseidon mission, relativistic effects have been taken into account for altimetry and positioning (GPS-type) satellites. It can be shown that the correction amounts to considering a so-called relativistic acceleration, whose leading term is  $\gamma_{CR}$  given by

$$\gamma_{CR} = \frac{\mu}{r^2} \frac{3V^2}{c^2}. \quad (6.10)$$

---

Now we know from solar eclipses that the apparent diameters of the Sun and Earth are equal as viewed from the Earth. We thus have the relation

$$\frac{R_L}{a_L} = \frac{R_S}{a_S},$$

where  $R_L$  and  $R_S$  are the respective radii. Expressing the masses through the densities  $\rho_L$  and  $\rho_S$ , we obtain

$$\frac{\mu_L}{\mu_S} = \frac{\rho_L}{\rho_S} \left( \frac{R_L}{R_S} \right)^3,$$

whence, inserting the numerical values, we determine the value of the ratio as

$$\frac{\gamma_{CL}(r)}{\gamma_{CS}(r)} = \frac{\rho_L}{\rho_S} = \frac{3.3437}{1.4808} \approx 2.25.$$



For a circular orbit, with (4.52), we obtain

$$\gamma_{\text{CR}} = \frac{3\mu^2}{c^2} \frac{1}{r^3}, \quad (6.11)$$

giving a slope of  $p = -3$ .

At the origin ( $h = 0$ ), we have

$$\gamma_{\text{CR}}(R) = g_0 \frac{3\mu}{c^2 R} = 1.6 \times 10^{-8} \text{ m s}^{-2},$$

The main consequence of this is a secular effect on the argument of the perigee, namely that the perigee of the orbit moves around more quickly than classical calculations would suggest. Indeed the effect is known as the advance of the perigee or the precession of the perigee.<sup>2</sup> For planets in orbit around the Sun, we speak of the advance or the precession of the perihelion, a phenomenon first explained by Albert Einstein (see the historical note in Sect. 6.8.3 at the end of the chapter).

Calculations of this apsidal precession give a variation  $\Delta_1\omega$  in the argument of the perigee  $\omega$  for each revolution, where

$$\Delta_1\omega = \frac{6\pi\mu}{a(1-e^2)c^2}. \quad (6.12)$$

The subscript 1 indicates that the value corresponds to one revolution, while a subscript Y is used for the value obtained over 1 year. This value is very small (a fraction of an arcmin per year), whether the satellite is in near-circular or eccentric orbit:

- SPOT-5 ( $a = 7.20 \times 10^6$  m),  $\Delta_1\omega = 1.16 \times 10^{-8}$  rad,  $\Delta_Y\omega = 12''.4$ .
- TOPEX/Poseidon ( $a = 7.71 \times 10^6$  m),  $\Delta_1\omega = 1.08 \times 10^{-8}$  rad,  $\Delta_Y\omega = 10''.5$ .
- Navstar/GPS ( $a = 26.56 \times 10^6$  m),  $\Delta_1\omega = 3.15 \times 10^{-9}$  rad,  $\Delta_Y\omega = 0''.48$ .
- Molniya ( $a = 26.56 \times 10^6$  m,  $e = 0.74$ ),  $\Delta_1\omega = 6.89 \times 10^{-9}$  rad,  $\Delta_Y\omega = 1''.04$ .

The force bringing about the advance of the perigee should be considered as conservative, since the same effect can be obtained by including a small time-independent and hence conservative quadrupole moment going as  $r^{-3}$  in the gravitational force.

---

<sup>2</sup>According to the general theory of relativity, the Earth's gravitational field affects spacetime in the vicinity of the satellite, whose trajectory thus differs slightly from the one calculated using classical celestial mechanics. This action can be represented by a "relativistic acceleration". It can be shown that it decomposes into three terms: the Schwarzschild term, the geodetic precession, and the Lense-Thirring precession. The first is the greater of the three, providing the acceleration  $\gamma_{\text{CR}}$  discussed here. The other two are considered when we discuss the satellite GP-B in Chap. 7.

## Non-Conservative Forces

Non-gravitational perturbing forces are independent of the satellite mass  $M_s$ . The corresponding accelerations thus go as  $1/M_s$ . Along with the forces discussed below, one must include forces applied to the satellite (usually by gas jets) when modifying its trajectory. These are the non-conservative forces used to guide the satellite.

**(a) Atmospheric Drag.** For satellites in low orbit ( $h < 1,200$  km), friction with molecules of residual atmospheric gases can be quite significant. This effect depends on the shape of the satellite, and in particular the shape of its solar panels, but also on the state of the upper atmosphere, which is difficult to model theoretically, because it involves several factors, including solar activity. These effects are further discussed in an appendix at the end of the chapter (see Sect. 6.6). Atmospheric effects become very weak above  $h = 1,000$  km and fall off very quickly with altitude. Hence, they are very slight for TOPEX/Poseidon at an altitude of 1,300 km, and non-existent for LAGEOS at 6,000 km.

**(b) Radiation Pressure.** Solar radiation pressure goes as  $a_S^{-2}$ , and so is independent of  $r$  (since  $r \ll a_S$ ). The actual consequences of this radiation pressure on the satellite depend on its shape, coating materials, and configuration.<sup>3</sup> These go to zero when the satellite passes into the Earth's shadow with respect to the Sun. The corresponding perturbative acceleration is evaluated to be

$$\gamma_{DP}(r) = \gamma_{DP} = \text{constant} \sim 10^{-7} \text{ m s}^{-2}.$$

**(c) Albedo Effect.** The effects of scattered radiation, i.e., visible (short wavelength) radiation scattered by the Earth, known as the albedo effect, and infrared (long wavelength) radiation emitted by the Earth, depend on the region overflown and the altitude. These effects can be considered to go as  $r^{-2}$ .

## 6.2 Perturbative Methods: Presentation

### 6.2.1 Orbit Propagation: Numerical and Analytical Methods

In this chapter, we have been concerned so far with perturbations which represent the difference between the Newtonian potential and the true poten-

---

<sup>3</sup>This perturbative effect was quite large for the first balloon satellites, such as Echo-1, launched in 1960, Echo-2 in 1964, and PAGEOS in 1966. These very light satellites, comprising an aluminised mylar envelope just 13  $\mu\text{m}$  thick, blown up after the launch, had a diameter of 30–40 m.

tial. We shall now see how this difference of potential can lead to a deviation in the satellite motion. The term “orbit determination” refers to any method for establishing the trajectory of a satellite given its force field and initial position.

Such methods are classified according to whether integration of the equation of motion is numerical or analytic. The first method provides series of numbers. It is efficient but not particularly intuitive. The second expresses modifications of the motion in a clear and pictorial way, e.g., one could say whether the eccentricity increases, or the orbit begins to precess, and so on.

Another contrast is that the numerical method is long-winded but highly accurate, while the analytic method is faster but does not always achieve the same accuracy. When dealing with an orbital rendezvous, or trying to avoid collisions between satellites, the first method prevails, while the analytical method is quite adequate for standard orbitography. The *Ixion* software and all the programs discussed in this book are based upon the analytical method. We shall outline the basic principles underlying each method. However, we shall only go into the details of the analytical method, using the Lagrangian approach.

When the satellite is subjected to the sum of the Newtonian central acceleration and a perturbative acceleration, since we take the perturbation to be small, we may assume that the trajectory will remain rather close to the conic section:

$$\ddot{\mathbf{r}} = \mathbf{grad} U_0 + \gamma_P, \quad U_0 = \frac{\mu}{r}. \quad (6.13)$$

Here  $\gamma_P$  is the perturbation term, assumed much smaller than the main term, i.e.,

$$\gamma_P \ll \frac{\mu}{r^2}.$$

We shall only consider perturbative accelerations deriving from a potential, in which case we have

$$\gamma_P = \mathbf{grad} \mathcal{R},$$

with  $\mathcal{R}$  the perturbing potential. The satellite is thus affected by the potential

$$U = U_0 + \mathcal{R}. \quad (6.14)$$

## Numerical Method

The relevant system of equations is:

$$\begin{cases} \ddot{\mathbf{r}} = -\mu \frac{\mathbf{r}}{r^3} + \gamma_P, \\ \mathbf{r}(t=0) = \mathbf{r}_0, \quad \dot{\mathbf{r}}(t=0) = \dot{\mathbf{r}}_0. \end{cases} \quad (6.15)$$

These are integrated by successive construction of the orbital elements. The so-called  $k$ -step method determines the elements at times  $t = t_{n+1}$  using the  $k$  elements obtained previously. For example, when  $k = 1$ , the integration between times  $t = t_0$  and  $t = t_N$  is done in one step  $h = (t_N - t_0)/N$ . At time  $t_{n+1}$ , each Cartesian coordinate  $y$  is expressed in terms of the value of  $y$  at time  $t_n$ :

$$y(t_{n+1}) = y(t_n + h) = y(t_n) + h\Phi.$$

With the Euler method,  $\Phi$  is the derivative  $y'(t_n)$ . Better suited and more elaborate methods have been developed:

- Purely mathematical approaches, such as Runge–Kutta integration, introduced at the end of the nineteenth century, where the function  $\Phi$ , in its most standard form, is just a fourth order Taylor expansion.
- Methods developed by astronomers to determine the motions of planets and other heavenly bodies, e.g., Adams–Bashforth or Adams–Moulton, known as multistep methods.
- Approaches designed specifically for artificial satellites since 1957, such as the Cowell method.

### Analytical Method

We showed previously that Keplerian motion of a satellite is specified by six orbital elements, the Keplerian elements. It can be shown that there is a bijective correspondence  $\mathcal{B}$  between the six elements and the six Cartesian components of the vectors  $\mathbf{r}$  and  $\dot{\mathbf{r}}$  in a Galilean frame  $\mathfrak{R}$ :

$$\left\{ x(t), y(t), z(t), \dot{x}(t), \dot{y}(t), \dot{z}(t) \right\} \xrightarrow{\mathcal{B}} \left\{ a(t), e(t), i(t), \Omega(t), \omega(t), M(t) \right\}.$$

In Keplerian motion, the five parameters  $(a, e, i, \Omega, \omega)$  fixing the position of the orbit remain constant, while  $M$  varies linearly, i.e.,  $M = n(t - t_p)$ , where  $t_p$  is the time of perigee passage. For perturbed motion, investigation of the transformation  $\mathcal{B}$  shows that (6.13) is equivalent to the 6 relations:

$$\begin{cases} \dot{a} = g_1, & \dot{e} = g_2, & \dot{i} = g_3, \\ \dot{\Omega} = g_4, & \dot{\omega} = g_5, & \dot{M} - n_0 = g_6, \end{cases} \quad (6.16)$$

where  $n_0 = \sqrt{\mu/a_0^3}$  and  $a_0$  is for the time being the value of  $a$  without perturbation. The terms  $g_i$  are small.

A standard approach is to use an iterative method at this point. The time-varying parameters are called osculating orbital elements. They are the parameters of the Keplerian orbit that the satellite would follow if the perturbations were to suddenly vanish at the given instant. These osculating elements<sup>4</sup> provide a better way of describing the deformation of the orbit than

---

<sup>4</sup>The word “osculating” does not mean the same thing here as in geometry. In the purely geometrical context, two curves are said to be osculating if their two centers of curvature

the values of the position and velocity. As an example, this method allows one to establish the critical inclination of the orbit, as we shall see later.

The perturbation method consists in solving the six equations above, known as Lagrange's equations (see Fig. 6.2).<sup>5</sup>

## 6.2.2 Basic Principles

The actual motion is obtained by calculating the small variations around the first integrals of the unperturbed motion. For a perturbative acceleration field deriving from a potential, (6.13) and (6.14) give the equation of motion as

$$\ddot{\mathbf{r}} = \mathbf{grad} U, \quad U = U_0 + \mathcal{R}. \quad (6.17)$$

Transcribing this for each Cartesian component of  $\mathbf{r}$ , we have

$$\frac{d^2x}{dt^2} = \frac{\partial U}{\partial x}, \quad \frac{d^2y}{dt^2} = \frac{\partial U}{\partial y}, \quad \frac{d^2z}{dt^2} = \frac{\partial U}{\partial z}.$$

We now write down the results for  $x$ . The first of the above equations yields

$$\dot{x} = \frac{dx}{dt}, \quad (6.18)$$

$$\frac{d\dot{x}}{dt} = \frac{\partial U}{\partial x}. \quad (6.19)$$

Bringing in the 6 Keplerian orbital elements (or any 6 suitably chosen variables), we obtain  $\dot{x}$  as a sum of 6 terms, and hence  $\ddot{x}$  as a sum of 36 terms.

coincide for some point of contact between them. In the present context, in the investigation of trajectories in space, the osculating ellipse defined by the osculating orbital elements is tangent to the actual trajectory, since the velocity vector is the same, but it does not have exactly the same radius of curvature, since the accelerations are different. The term was originally invented by geometers in 1752 and then slightly deflected from its geometrical meaning by the needs of astronomy. The etymology of the word attests to this corruption. Indeed, it comes from the Latin *osculatio*, the noun from the verb *osculare*, meaning “to kiss”. This in turn derives from *osculum*, “little mouth”, a diminutive form of *os*, *oris*, which is the standard term for “mouth”. The idea which therefore underpins this term is therefore one of extended and continued contact.

<sup>5</sup>Joseph Louis de Lagrange (1736–1813) was a French mathematician. He applied his analytical theories to the motion of the Moon and the periodic variation of the major axes of the planets, published in *Théorie de la libration de la Lune et autres phénomènes qui dépendent de la figure non sphérique de cette planète* (1763), and he also invented the notion of gravitational potential in 1772. All these ideas were brought together in his magnum opus *Mécanique analytique* (1788). He invented the theory of perturbations to study the motion of the heavenly bodies, published in *Sur la théorie des variations des éléments des planètes* (1808). He also continued Euler's work, devising a final version of the method known as variation of constants, published in *Sur la théorie générale de la variation des constantes arbitraires dans tous les problèmes de mécanique* (1810). His name is still associated with the equations and mathematical tools used in these theories.

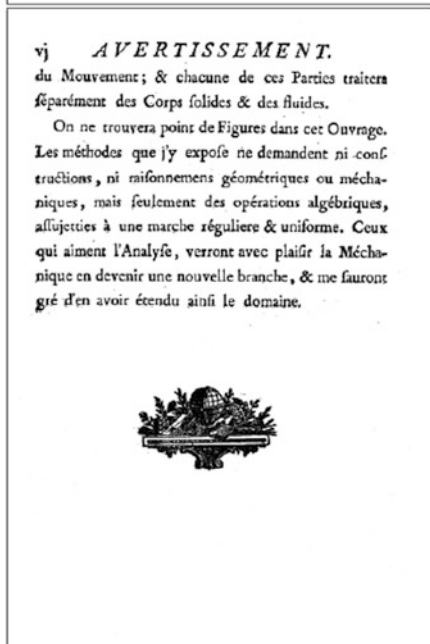
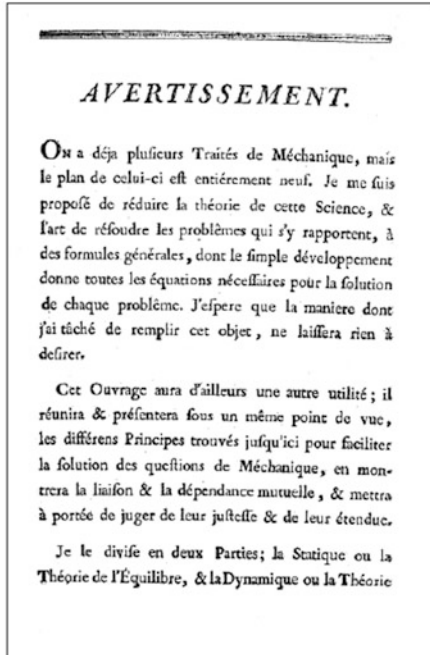
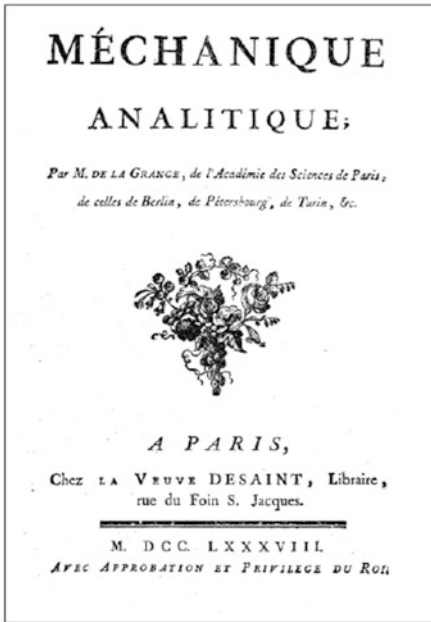


FIG. 6.2 : Mécanique analytique by J.L. Lagrange, published in Paris in 1788 (MDC-CLXXXVIII). Left: Title page. Right: Warning to the reader. The author explains his highly novel approach, in which mechanics becomes a branch of analysis. And just to demonstrate the abstract nature of the treatise, he adds: “the reader will find no figures in this work.”

The perturbation method solves the differential equations by the method known as variation of constants. The choice of certain variables, called canonical variables, allows us to obtain Lagrange's equations in a very simple form, the canonical form, as the relations (6.60). Several sets of six variables offer this possibility, such as the Delaunay variables, the Poincaré variables, or the Whittaker (or Hill) variables.

More will be said about the Delaunay variables later, but for the moment, let us not enter into the details of these powerful mathematical theories, developed principally to calculate planetary orbits, and to which we now attach the names of Euler, Lagrange, Laplace, Gauss, and Poincaré.

### 6.2.3 Lagrange Brackets

We denote the Cartesian coordinates by  $\xi_i$ , with  $i = 1, 2, 3$ :

$$\xi_1 = x, \quad \xi_2 = y, \quad \xi_3 = z.$$

The equation of motion (6.17) is

$$\ddot{\xi}_i = \frac{\partial U}{\partial \xi_i}. \quad (6.20)$$

The Keplerian orbital elements are denoted by  $S_j$ , with  $j = 1, 2, 3, 4, 5, 6$ :

$$S_1 = a, \quad S_2 = e, \quad S_3 = i, \quad S_4 = \Omega, \quad S_5 = \omega, \quad S_6 = \Theta.$$

The element  $S_6$  is the initial mean anomaly. It is introduced here instead of  $M$  in order to have  $\dot{M} - n$  appear directly in (6.16). We have the very simple relation

$$\Theta = M - nt = -nt_p, \quad (6.21)$$

where  $t_p$  is the time of passage at perigee. Equations (6.18) and (6.19) then become

$$\sum_{j=1}^6 \frac{\partial \xi_i}{\partial S_j} \frac{dS_j}{dt} = \dot{\xi}_i, \quad i = 1, 2, 3, \quad (6.22)$$

$$\sum_{j=1}^6 \frac{\partial \dot{\xi}_i}{\partial S_j} \frac{dS_j}{dt} = \frac{\partial U}{\partial \xi_i}, \quad i = 1, 2, 3. \quad (6.23)$$

Multiplying the three equations (6.22) by  $-\partial \dot{\xi}_i / \partial S_k$  and the three equations (6.23) by  $\partial \xi_i / \partial S_k$  and adding, we obtain the system

$$\sum_{i=1}^3 \sum_{j=1}^6 \left( -\frac{\partial \dot{\xi}_i}{\partial S_k} \frac{\partial \xi_i}{\partial S_j} + \frac{\partial \xi_i}{\partial S_k} \frac{\partial \dot{\xi}_i}{\partial S_j} \right) \frac{dS_j}{dt} = \sum_{i=1}^3 \left( -\frac{\partial \dot{\xi}_i}{\partial S_k} \dot{\xi}_i + \frac{\partial \xi_i}{\partial S_k} \frac{\partial U}{\partial \xi_i} \right), \quad (6.24)$$

for  $k = 1, 2, 3, 4, 5, 6$ . This system is equivalent to (6.13), which represent the problem we are trying to solve. Let us examine the two sides of the equality.

Regarding the left-hand side, we use the following notation. We set

$$[S_k; S_j] = \sum_{i=1}^3 \left( \frac{\partial \xi_i}{\partial S_k} \frac{\partial \dot{\xi}_i}{\partial S_j} - \frac{\partial \dot{\xi}_i}{\partial S_k} \frac{\partial \xi_i}{\partial S_j} \right). \tag{6.25}$$

The notation  $[S_k; S_j]$  is the Lagrange bracket. We thus have 36 Lagrange brackets.

The right-hand side comprises two terms. The first can be written

$$-\sum_{i=1}^3 \frac{\partial \dot{\xi}_i}{\partial S_k} \dot{\xi}_i = -\frac{1}{2} \sum_{i=1}^3 \frac{\partial \dot{\xi}_i^2}{\partial S_k} = -\frac{1}{2} \frac{\partial}{\partial S_k} \sum_{i=1}^3 \dot{\xi}_i^2.$$

At this point, the quantity  $T$  appears, with the dimensions of a potential and representing the kinetic energy per unit mass:

$$T = \frac{1}{2} \sum_{i=1}^3 \dot{\xi}_i^2 = \frac{1}{2} V^2, \tag{6.26}$$

where  $V$  is the magnitude of the velocity at the given point. The first term can then be written in the form

$$-\frac{\partial T}{\partial S_k}.$$
(6.27)

The second term transforms to

$$\sum_{i=1}^3 \frac{\partial U}{\partial \xi_i} \frac{\partial \xi_i}{\partial S_k} = \frac{\partial U}{\partial S_k}.$$
(6.28)

If we set

$$F = U - T, \tag{6.29}$$

the system (6.24), and hence also (6.13), is equivalent to

$$\sum_{j=1}^6 [S_k; S_j] \frac{dS_j}{dt} = \frac{\partial F}{\partial S_k}, \quad k = 1, 2, 3, 4, 5, 6. \tag{6.30}$$

This quantity  $F$  has dimensions of energy per unit mass. It is sometimes called the force function or the Hamiltonian function, since it is equal to minus the Hamiltonian (see Sect. 4.7).<sup>6</sup>

---

<sup>6</sup>If we compare the Eqs. (4.111) and (6.29) giving the energy, we note that, with the notation used here and  $m$  for the mass of the satellite, we have



## 6.2.4 Properties of the Lagrange Bracket

### Antisymmetry

From the definition (6.25), it is clear by inspection that

$$[S_k; S_k] = 0, \quad [S_k; S_j] = -[S_j; S_k].$$

We deduce that, of the 36 brackets, 6 are zero and among the 30 remaining which may not be zero, only 15 need be calculated.

### Constancy of Lagrange Bracket in Time

The Lagrange bracket is defined by (6.25) as the sum of three terms. To calculate the time derivative of a Lagrange bracket, we begin with just one element of the sum, the  $i$ th element. This gives

$$\begin{aligned} \frac{d}{dt} ([S_k; S_j]_i) &= \frac{d}{dt} \left( \frac{\partial \xi_i}{\partial S_k} \frac{\partial \dot{\xi}_i}{\partial S_j} - \frac{\partial \dot{\xi}_i}{\partial S_k} \frac{\partial \xi_i}{\partial S_j} \right) \\ &= \frac{\partial \dot{\xi}_i}{\partial S_k} \frac{\partial \dot{\xi}_i}{\partial S_j} + \frac{\partial \xi_i}{\partial S_k} \frac{\partial \ddot{\xi}_i}{\partial S_j} - \frac{\partial \ddot{\xi}_i}{\partial S_k} \frac{\partial \xi_i}{\partial S_j} - \frac{\partial \dot{\xi}_i}{\partial S_k} \frac{\partial \dot{\xi}_i}{\partial S_j} \\ &= \frac{\partial \xi_i}{\partial S_k} \frac{\partial \ddot{\xi}_i}{\partial S_j} - \frac{\partial \ddot{\xi}_i}{\partial S_k} \frac{\partial \xi_i}{\partial S_j}. \end{aligned} \quad (6.31)$$

To obtain a more symmetrical form that will allow some simplification later on, it is useful to add and subtract the expression

$$\dot{\xi}_i \frac{\partial^2 \xi_i}{\partial S_k \partial S_j} + \ddot{\xi}_i \frac{\partial^2 \xi_i}{\partial S_k \partial S_j}. \quad (6.32)$$

We then obtain

$$\begin{aligned} \frac{d}{dt} ([S_k; S_j]_i) &= \frac{\partial}{\partial S_k} \left( \dot{\xi}_i \frac{\partial \dot{\xi}_i}{\partial S_j} - \ddot{\xi}_i \frac{\partial \xi_i}{\partial S_j} \right) - \frac{\partial}{\partial S_j} \left( \dot{\xi}_i \frac{\partial \dot{\xi}_i}{\partial S_k} - \ddot{\xi}_i \frac{\partial \xi_i}{\partial S_k} \right) \\ &= \frac{\partial}{\partial S_k} \left( \dot{\xi}_i \frac{\partial \dot{\xi}_i}{\partial S_j} - \frac{\partial U}{\partial \xi_i} \frac{\partial \xi_i}{\partial S_j} \right) - \frac{\partial}{\partial S_j} \left( \dot{\xi}_i \frac{\partial \dot{\xi}_i}{\partial S_k} - \frac{\partial U}{\partial \xi_i} \frac{\partial \xi_i}{\partial S_k} \right), \end{aligned}$$

---


$$U = -mU, \quad \mathcal{T} = +mT, \quad \mathcal{E} = \mathcal{T} + U = -m(U - T) = -mF$$

$$\implies -\mathcal{E}/m = F = U - T.$$

When studying orbits and space trajectories, it is preferable to use accelerations rather than forces, and the potential  $U$  rather than the potential energy  $-U$ , since the mass of the satellite is irrelevant to these calculations (except in the case of atmospheric drag and radiation pressure effects). Moreover, we have seen that the energy  $\mathcal{E}$  is negative for periodic motion. The convention for  $F$  means that this quantity has positive values.

where the last equality is obtained using the fundamental relation (6.20). We now sum over the three values of  $i$ , taking the partial derivatives with respect to  $S_j$  and  $S_k$  outside the sum and using the relations (6.26) for  $T$ , (6.28) for the derivative of  $T$ , and (6.29) for  $F$ , to obtain

$$\begin{aligned} \frac{d}{dt}[S_k; S_j] &= \frac{\partial}{\partial S_k} \left[ \sum_{i=1}^3 \left( \dot{\xi}_i \frac{\partial \dot{\xi}_i}{\partial S_j} - \frac{\partial U}{\partial \xi_i} \frac{\partial \xi_i}{\partial S_j} \right) \right] \\ &\quad - \frac{\partial}{\partial S_j} \left[ \sum_{i=1}^3 \left( \dot{\xi}_i \frac{\partial \dot{\xi}_i}{\partial S_k} - \frac{\partial U}{\partial \xi_i} \frac{\partial \xi_i}{\partial S_k} \right) \right] \\ &= \frac{\partial}{\partial S_k} \left( \frac{\partial T}{\partial S_j} - \frac{\partial U}{\partial S_j} \right) - \frac{\partial}{\partial S_j} \left( \frac{\partial T}{\partial S_k} - \frac{\partial U}{\partial S_k} \right) \\ &= \frac{\partial^2 F}{\partial S_k \partial S_j} - \frac{\partial^2 F}{\partial S_j \partial S_k} \\ &= 0. \end{aligned}$$

The equation

$$\frac{d}{dt}[S_k; S_j] = 0 \tag{6.33}$$

shows finally that the expression  $[S_k; S_j]$  is constant in time. The value of the bracket can of course change in time if one or more of the orbital parameters are time dependent. However, during one revolution, we may consider the parameters  $S_i$  to be constant and  $[S_k; S_j]$  thus remains constant too. This means that, in order to obtain its value, we can do so at a single point on the orbit.

## 6.3 Perturbative Method: Solution

### 6.3.1 Calculating the Coordinates

#### Coordinates in the Orbital Plane

To calculate the factors  $\partial \dot{\xi}_i / \partial S_k$  and  $\partial \xi_i / \partial S_j$  in the Lagrange brackets, we express the Cartesian coordinates in terms of the parameters. To do so, we write the position of the satellite in a right-handed orthonormal frame  $(O; X, Y, Z)$  fixed relative to the plane  $\mathcal{P}$  of the orbit, where  $O$  is the center of attraction, i.e., the center of the Earth. The plane  $\mathcal{P}$  contains  $OX$  and  $OY$ , while  $OX$  passes through the perigee  $P$  and  $OZ$  is perpendicular to  $\mathcal{P}$  and lies in the direction of the angular momentum  $\mathbf{C}$  of the satellite. In this frame, we may write the components  $X, Y, Z$ , of the radial vector using (4.70) and (4.71):

$$\begin{aligned} X &= r \cos v = a(\cos E - e) , \\ Y &= r \sin v = a\sqrt{1 - e^2} \sin E , \\ Z &= 0 . \end{aligned}$$

We recall that the eccentric anomaly  $E$  arising in these formulas is related to the mean anomaly  $M$ , used as orbital element, by Kepler's equation (4.65). Differentiating with respect to time, we obtain

$$(1 - e \cos E) \frac{de}{dt} = n = \sqrt{\frac{\mu}{a^3}} ,$$

and the speeds are

$$\begin{aligned} \dot{X} &= -\sqrt{\frac{\mu}{a}} \frac{\sin E}{1 - e \cos E} , \\ \dot{Y} &= \sqrt{\frac{\mu}{a}} \sqrt{1 - e^2} \frac{\cos E}{1 - e \cos E} , \\ \dot{Z} &= 0 . \end{aligned}$$

### Coordinates in the Equatorial Plane

To transform from this frame to one identified with the frame  $\mathfrak{R}$ , viz., the frame  $(O; x, y, z)$  fixed relative to the equatorial plane  $\mathcal{E}$ , where  $Oz$  lies along the polar axis, we must carry out three rotations, as specified by the Euler angles  $\alpha_1 = \Omega$ ,  $\alpha_2 = i$ ,  $\alpha_3 = \omega$  discussed in Chap. 5 (see Fig. 5.1). The desired coordinates  $x, y, z$  and  $\dot{x}, \dot{y}, \dot{z}$  are deduced from  $X, Y, Z$  and  $\dot{X}, \dot{Y}, \dot{Z}$  by the product of three transformation matrices. The detailed calculation of these three matrices and their product is carried out later, when we calculate the ground track of the satellite. The transformation matrix  $\mathbf{P}$  is given by (8.8).

For the angles used here, we obtain the  $3 \times 3$  matrix

$$\mathbf{P} = \begin{pmatrix} \cos \Omega \cos \omega & -\cos \Omega \sin \omega & \sin \Omega \sin i \\ -\sin \Omega \sin \omega \cos i & -\sin \Omega \cos \omega \cos i & \\ \sin \Omega \cos \omega & -\sin \Omega \sin \omega & -\cos \Omega \sin i \\ +\cos \Omega \sin \omega \cos i & +\cos \Omega \cos \omega \cos i & \\ \sin \omega \sin i & \cos \omega \sin i & \cos i \end{pmatrix} .$$

The quantities  $X, Y, Z, \dot{X}, \dot{Y}, \dot{Z}$  depend only on the three orbital elements  $a$ ,  $e$ , and  $E$  (and  $E$  will subsequently be replaced by  $M$ ). The entries of the matrix  $\mathbf{P}$  depend only on the three other elements  $\Omega$ ,  $i$ , and  $\omega$ . The quantities  $x, y, z, \dot{x}, \dot{y}, \dot{z}$  depend on the six orbital elements:

$$\begin{pmatrix} x \\ y \\ z \end{pmatrix} = \mathbf{P}(\Omega, i, \omega) \begin{pmatrix} X(a, e, E) \\ Y(a, e, E) \\ 0 \end{pmatrix} , \quad (6.34)$$

$$\begin{pmatrix} \dot{x} \\ \dot{y} \\ \dot{z} \end{pmatrix} = P(\Omega, i, \omega) \begin{pmatrix} \dot{X}(a, e, E) \\ \dot{Y}(a, e, E) \\ 0 \end{pmatrix}. \tag{6.35}$$

Denoting the coordinates  $x, y, z$  by  $\xi_i$ , as discussed above, and  $\dot{x}, \dot{y}, \dot{z}$  by  $\dot{\xi}_i$ , we have

$$\xi_i = P_{i1}X + P_{i2}Y, \quad \dot{\xi}_i = P_{i1}\dot{X} + P_{i2}\dot{Y}, \quad i = 1, 2, 3,$$

where  $P_{ij}$  is the entry on row  $i$  and column  $j$  of the matrix  $P$ .

### Calculating Derivatives with Respect to Orbital Elements

Differentiating the three values of  $\xi_i$  specified above with respect to the orbital elements yields:

$$\begin{aligned} \frac{\partial \xi_i}{\partial S_k} &= \frac{\partial P_{i1}}{\partial S_k} X + \frac{\partial P_{i2}}{\partial S_k} Y && \text{if } S_k = \Omega, i, \omega, \\ \frac{\partial \xi_i}{\partial S_k} &= P_{i1} \frac{\partial X}{\partial S_k} + P_{i2} \frac{\partial Y}{\partial S_k} && \text{if } S_k = a, e, E, \end{aligned}$$

with analogous results for  $\dot{\xi}_i$ :

$$\begin{aligned} \frac{\partial \dot{\xi}_i}{\partial S_k} &= \frac{\partial P_{i1}}{\partial S_k} \dot{X} + \frac{\partial P_{i2}}{\partial S_k} \dot{Y} && \text{if } S_k = \Omega, i, \omega, \\ \frac{\partial \dot{\xi}_i}{\partial S_k} &= P_{i1} \frac{\partial \dot{X}}{\partial S_k} + P_{i2} \frac{\partial \dot{Y}}{\partial S_k} && \text{if } S_k = a, e, E. \end{aligned}$$

- We calculate the derivatives of  $X, Y, \dot{X}, \dot{Y}$  with respect to  $S_k$ , then take their value at some arbitrary point on the orbit. Naturally, we choose the perigee, where  $v = E = M = 0$ , since this point allows the greatest simplification. The relation between  $dE$  and  $dM$ , which follows from (4.79), has already been noted above. Calculation of  $\partial X / \partial S_k$  yields

$$\frac{\partial X}{\partial a} = \cos E - e, \quad \frac{\partial X}{\partial e} = -a, \quad \frac{\partial X}{\partial M} = -a \sin E \frac{1}{1 - \cos E},$$

and the values of these quantities at perigee are

$$\frac{\partial X}{\partial a} = 1 - e, \quad \frac{\partial X}{\partial e} = -a, \quad \frac{\partial X}{\partial M} = 0.$$

Likewise for the other coordinates, differentiating and evaluating at perigee, we obtain

$$\frac{\partial Y}{\partial a} = 0, \quad \frac{\partial Y}{\partial e} = 0, \quad \frac{\partial Y}{\partial M} = a \sqrt{\frac{1+e}{1-e}},$$

$$\frac{\partial \dot{X}}{\partial a} = 0, \quad \frac{\partial \dot{X}}{\partial e} = 0, \quad \frac{\partial \dot{X}}{\partial M} = -\frac{na}{(1-e)^2},$$

$$\frac{\partial \dot{Y}}{\partial a} = -\frac{n}{2} \sqrt{\frac{1+e}{1-e}}, \quad \frac{\partial \dot{Y}}{\partial e} = \frac{na}{(1-e)^{3/2}}, \quad \frac{\partial \dot{Y}}{\partial M} = 0.$$

- The differentiation of  $P_{ij}$  with respect to  $S_k$  is done in the standard manner, with no possible simplification.

### 6.3.2 Calculating the Lagrange Brackets

#### Calculating $[a; M]$

Here we calculate the Lagrange bracket  $[a; M]$ . According to the definition (6.25), this is

$$[a; M] = \sum_{i=1}^3 \left( -\frac{\partial \dot{\xi}_i}{\partial a} \frac{\partial \xi_i}{\partial M} + \frac{\partial \xi_i}{\partial a} \frac{\partial \dot{\xi}_i}{\partial M} \right).$$

With the previous results, we have

$$\begin{aligned} \frac{\partial \xi_i}{\partial a} &= P_{i1} \frac{\partial X}{\partial a} + P_{i2} \frac{\partial Y}{\partial a} = P_{i1}(1-e), \\ \frac{\partial \dot{\xi}_i}{\partial a} &= P_{i1} \frac{\partial \dot{X}}{\partial a} + P_{i2} \frac{\partial \dot{Y}}{\partial a} = -P_{i2} \frac{n}{2} \sqrt{\frac{1+e}{1-e}}, \\ \frac{\partial \xi_i}{\partial M} &= P_{i1} \frac{\partial X}{\partial M} + P_{i2} \frac{\partial Y}{\partial M} = P_{i2} a \sqrt{\frac{1+e}{1-e}}, \\ \frac{\partial \dot{\xi}_i}{\partial M} &= P_{i1} \frac{\partial \dot{X}}{\partial M} + P_{i2} \frac{\partial \dot{Y}}{\partial M} = -P_{i1} \frac{na}{(1-e)^2}, \end{aligned}$$

and we obtain

$$[a; M] = \frac{na}{1-e} \sum_{i=1}^3 \left( -P_{i1}^2 + \frac{1+e}{2} P_{i2}^2 \right).$$

The matrix  $P$  is such that, for all  $j$ , we have

$$\sum_{i=1}^3 P_{ij}^2 = 1,$$

whence, finally,

$$[a; M] = \frac{na}{1-e} \left( -1 + \frac{1+e}{2} \right) = -\frac{na}{2}.$$

### Values of the Lagrange Brackets

The other brackets are calculated in like manner. Of the 15 to be evaluated, as noted earlier, calculation reveals that 9 of them are zero. The 6 nonzero brackets are as follows:

$$[a; \Omega] = -[\Omega; a] = -\frac{na}{2} \sqrt{1 - e^2} \cos i , \tag{6.36}$$

$$[a; \omega] = -[\omega; a] = -\frac{na}{2} \sqrt{1 - e^2} , \tag{6.37}$$

$$[a; M] = -[M; a] = -\frac{na}{2} , \tag{6.38}$$

$$[e; \Omega] = -[\Omega; e] = +na^2 \frac{e}{\sqrt{1 - e^2}} \cos i , \tag{6.39}$$

$$[e; \omega] = -[\omega; e] = +na^2 \frac{e}{\sqrt{1 - e^2}} , \tag{6.40}$$

$$[i; \Omega] = -[\Omega; i] = +na^2 \sqrt{1 - e^2} \sin i . \tag{6.41}$$

### 6.3.3 Lagrange Equations

#### Obtaining the Lagrange Equations

We can now rewrite (6.30), expressing the partial derivatives of  $F$  in terms of the nonzero Lagrange brackets, whence the six quantities  $\partial F / \partial S_k$ , with  $k = 1, \dots, 6$  are given by

$$\frac{\partial F}{\partial a} = +[a; \Omega] \dot{\Omega} + [a; \omega] \dot{\omega} + [a; M] \dot{M} , \tag{6.42}$$

$$\frac{\partial F}{\partial e} = +[e; \Omega] \dot{\Omega} + [e; \omega] \dot{\omega} , \tag{6.43}$$

$$\frac{\partial F}{\partial i} = +[i; \Omega] \dot{\Omega} , \tag{6.44}$$

$$\frac{\partial F}{\partial \Omega} = -[a; \Omega] \dot{a} - [e; \Omega] \dot{e} - [i; \Omega] \dot{i} , \tag{6.45}$$

$$\frac{\partial F}{\partial \omega} = -[a; \omega] \dot{a} - [e; \omega] \dot{e} , \tag{6.46}$$

$$\frac{\partial F}{\partial M} = -[a; M] \dot{a} . \tag{6.47}$$

Looking at the structure of the two sets of equations above, we understand why it was worth treating the parameters in the given order  $a, e, i, \Omega, \omega, M$ .

We solve the linear system of six Eqs. (6.42)–(6.47) and insert the expressions for the Lagrange brackets. This results in a matrix equation which yields the time derivatives of the orbital elements in terms of the partial derivatives of the function  $F$  with respect to the orbital elements:

$$\begin{pmatrix} da/dt \\ de/dt \\ di/dt \\ d\Omega/dt \\ d\omega/dt \\ dM/dt \end{pmatrix} = L_0 \begin{pmatrix} \partial F/\partial a \\ \partial F/\partial e \\ \partial F/\partial i \\ \partial F/\partial \Omega \\ \partial F/\partial \omega \\ \partial F/\partial M \end{pmatrix}. \quad (6.48)$$

The matrix  $L_0$  is denoted by  $L$  in Table 6.2, and we shall see below that these two matrices are one and the same.

We note two important properties of  $L_0$ :

- It is antisymmetric.
- It depends only on the three elements  $a, e, i$ , i.e.,  $L_0 = L_0(a, e, i)$ .

We obtain the following values for each of the orbital elements, with the abbreviations  $\sigma$ ,  $\tau$ , and  $\bar{\tau}$  as defined in Table 6.2:

$$\frac{da}{dt} = \frac{1}{na} \left( 2 \frac{\partial F}{\partial M} \right), \quad (6.49)$$

$$\frac{de}{dt} = \frac{1}{na^2} \tau \left( -\bar{\tau} \frac{\partial F}{\partial \omega} + \frac{\partial F}{\partial M} \right), \quad (6.50)$$

$$\frac{di}{dt} = \frac{1}{na^2} \sigma \bar{\tau} \left( -\frac{\partial F}{\partial \Omega} + \cos i \frac{\partial F}{\partial \omega} \right), \quad (6.51)$$

$$\frac{d\Omega}{dt} = \frac{1}{na^2} \sigma \bar{\tau} \left( \frac{\partial F}{\partial i} \right), \quad (6.52)$$

$$\frac{d\omega}{dt} = \frac{1}{na^2} \bar{\tau} \left( \tau \frac{\partial F}{\partial e} - \sigma \cos i \frac{\partial F}{\partial i} \right), \quad (6.53)$$

$$\frac{dM}{dt} = \frac{1}{na^2} \left( -2a \frac{\partial F}{\partial a} - \tau \frac{\partial F}{\partial e} \right). \quad (6.54)$$

This system of equations constitutes the full set of Lagrange equations expressed in terms of  $F$ .

### Introducing the Perturbative Potential

Rather than use the function  $F$ , we bring in the perturbative potential  $\mathcal{R}$ , defined by (6.14). With the expressions for  $U$  and  $T$ , (6.29) becomes

$$F = \frac{\mu}{r} + \mathcal{R} - \frac{V^2}{2} = \frac{\mu}{2a} + \mathcal{R}, \quad (6.55)$$

because we can apply (4.38), obtained for a periodic orbit, to the osculating elements of the orbit.

The perturbing potential  $\mathcal{R}$  thus replaces  $F$  in the partial derivatives of the above system with

$$\frac{\partial F}{\partial S_j} = \frac{\partial \mathcal{R}}{\partial S_j}, \quad \text{for } S_j = e, i, \Omega, \omega, M,$$

$$\begin{aligned}
\frac{da}{dt} &= \frac{1}{na} \left( 2 \frac{\partial \mathcal{R}}{\partial M} \right) \\
\frac{de}{dt} &= \frac{1}{na^2} \frac{1-e^2}{e} \left( -\frac{1}{\sqrt{1-e^2}} \frac{\partial \mathcal{R}}{\partial \omega} + \frac{\partial \mathcal{R}}{\partial M} \right) \\
\frac{di}{dt} &= \frac{1}{na^2 \sqrt{1-e^2} \sin i} \left( -\frac{\partial \mathcal{R}}{\partial \Omega} + \cos i \frac{\partial \mathcal{R}}{\partial \omega} \right) \\
\frac{d\Omega}{dt} &= \frac{1}{na^2 \sqrt{1-e^2} \sin i} \left( \frac{\partial \mathcal{R}}{\partial i} \right) \\
\frac{d\omega}{dt} &= \frac{1}{na^2 \sqrt{1-e^2}} \left( \frac{1-e^2}{e} \frac{\partial \mathcal{R}}{\partial e} - \frac{\cos i}{\sin i} \frac{\partial \mathcal{R}}{\partial i} \right) \\
\frac{dM}{dt} - n &= \frac{1}{na^2} \left( -2a \frac{\partial \mathcal{R}}{\partial a} - \frac{1-e^2}{e} \frac{\partial \mathcal{R}}{\partial e} \right)
\end{aligned}$$

In matrix form:

$$\begin{pmatrix} da/dt \\ de/dt \\ di/dt \\ d\Omega/dt \\ d\omega/dt \\ dM/dt - n \end{pmatrix} = \mathbf{L} \begin{pmatrix} \partial \mathcal{R} / \partial a \\ \partial \mathcal{R} / \partial e \\ \partial \mathcal{R} / \partial i \\ \partial \mathcal{R} / \partial \Omega \\ \partial \mathcal{R} / \partial \omega \\ \partial \mathcal{R} / \partial M \end{pmatrix}$$

$$\mathbf{L} = \frac{1}{na^2} \begin{pmatrix} 0 & 0 & 0 & 0 & 0 & +2a \\ 0 & 0 & 0 & 0 & -\tau\bar{\tau} & +\tau \\ 0 & 0 & 0 & -\sigma\bar{\tau} & +\sigma\bar{\tau} \cos i & 0 \\ 0 & 0 & +\sigma\tau & 0 & 0 & 0 \\ 0 & +\tau\bar{\tau} & -\sigma\bar{\tau} \cos i & 0 & 0 & 0 \\ -2a & -\tau & 0 & 0 & 0 & 0 \end{pmatrix}$$

$$\sigma = \frac{1}{\sin i}, \quad \tau = \frac{1-e^2}{e}, \quad \bar{\tau} = \frac{1}{\sqrt{1-e^2}}$$

TABLE 6.2: Lagrange equations for the six orbital elements as a function of the perturbing potential  $\mathcal{R}$ .

and

$$\frac{\partial F}{\partial a} = -\frac{\mu}{2a^2} + \frac{\partial \mathcal{R}}{\partial a} = -\frac{n^2 a}{2} + \frac{\partial \mathcal{R}}{\partial a}, \quad \text{for } S_j = a.$$

In the above Lagrange system of equations, we can thus replace  $\partial F / \partial S_j$  by  $\partial \mathcal{R} / \partial S_j$  in the first five equations. The last equation, viz., (6.54), becomes

$$\frac{dM}{dt} = n - \frac{2}{na} \frac{\partial \mathcal{R}}{\partial a} - \frac{1}{na^2} \frac{1-e^2}{e} \frac{\partial \mathcal{R}}{\partial e}.$$



## Lagrange Equations in Terms of the Perturbative Potential

We can now write the equations for the time dependence of the orbital elements in terms of the perturbing potential  $\mathcal{R}$ . The results are shown in Table 6.2. This system of equations constitutes the full set of Lagrange's equations, which correspond, by successive equivalences, to the original equation given in (6.13), i.e., the equation of motion. This can be written in matrix form using the matrix  $\mathbf{L}$ , equivalent to  $\mathbf{L}_0$  defined above by (6.48). It corresponds to the initial system of equations (6.17) or (6.20), in which we have substituted  $M$  for  $\Theta$ :

$$M - nt = \Theta, \quad \frac{\partial \mathcal{R}}{\partial M} = \frac{\partial \mathcal{R}}{\partial \Theta}.$$

To conclude this section, we have shown that, when the perturbative acceleration field derives from a potential, the satellite motion is defined by Lagrange's equations. We check that, if  $\mathcal{R} = 0$ , we recover the solution of the two-body problem, i.e., Kepler's solution in which  $a, e, i, \Omega, \omega$  are constant and the mean anomaly is given by  $M = n(t - t_p)$ , corresponding to  $\Theta$  constant. In the general iterative case, we treat  $\mathcal{R}$  as expressed in terms of the new variables.

### 6.3.4 Metric and Angular Orbital Elements

The matrix  $\mathbf{L}$  clearly brings out the separation of the orbital elements into two groups: on the one hand  $a, e, i$ , and on the other,  $\Omega, \omega, M$ . Indeed we see that, in Lagrange's equations, the time derivatives of  $a, e, i$  involve only the partial derivatives of  $\mathcal{R}$  with respect to  $\Omega, \omega, M$ , and conversely. This can be expressed in a global manner as follows:

$$\begin{aligned} \left\{ \frac{da}{dt}, \frac{de}{dt}, \frac{di}{dt} \right\} &= f_1 \left( a, e, i; \frac{\partial \mathcal{R}}{\partial \Omega}, \frac{\partial \mathcal{R}}{\partial \omega}, \frac{\partial \mathcal{R}}{\partial M} \right), \\ \left\{ \frac{d\Omega}{dt}, \frac{d\omega}{dt}, \frac{dM}{dt} \right\} &= f_2 \left( a, e, i; \frac{\partial \mathcal{R}}{\partial a}, \frac{\partial \mathcal{R}}{\partial e}, \frac{\partial \mathcal{R}}{\partial i} \right), \end{aligned}$$

where  $f_1$  and  $f_2$  are functions of  $a, e, i$  and the partial derivatives mentioned.

The parameters  $(a, e, i)$  are called metric orbital elements,<sup>7</sup> or more briefly, metric elements, while the parameters  $\Omega, \omega, M$  are called angular (or angle) elements.

---

<sup>7</sup>This term serves to distinguish the two groups of orbital elements. However, the term "metric" is open to discussion. If it refers to the notion of length, only the quantity  $a$  is actually a length. If it is intended to contrast with the notion of angle, the inclination is actually an angle. Here, when the word "metric" is attributed to  $e$  and  $i$ , it indicates that these two elements behave mathematically like  $a$ . The Delaunay variables discussed later avoid this ambiguity, since variables in the same group have the same physical dimensions.

If  $p_i$  denote the metric elements and  $q_i$  the angular elements, the last two relations can be written in the form

$$\dot{p}_i = f_1 \left( p_i; \frac{\partial \mathcal{R}}{\partial q_i} \right), \quad \dot{q}_i = f_2 \left( p_i; \frac{\partial \mathcal{R}}{\partial p_i} \right). \tag{6.56}$$

**Note.** The quantity  $na^2\sqrt{1 - e^2}$  arises three times in the denominator of the expressions in the system of equations presented in Table 6.2. Returning to the Keplerian orbit relations for the osculating elements, (4.27) becomes

$$C^2 = \mu p = \mu a(1 - e^2) = n^2 a^4 (1 - e^2),$$

and we thus see that the quantity in question is the magnitude of the angular momentum of the satellite, denoted by  $C$ :

$$C = na^2\sqrt{1 - e^2} = nab. \tag{6.57}$$

### 6.3.5 Poorly Defined Parameters

There are two situations, already discussed in the context of orbital elements in Chap. 5, which can raise difficulties for the definition of certain parameters: the case  $e = 0$  and the case  $i = 0$ :

- The eccentricity  $e$  occurs in the denominator of the expressions for  $\dot{e}$ ,  $\dot{\omega}$ , and  $\dot{M}$  in Lagrange’s equations (see Table 6.2). If  $e$  is zero, these quantities are not defined. This is to be expected since, as we have seen, the perigee is not then defined, and this means that  $\omega$  and  $M$  cannot be either.
- The inclination  $i$  occurs in the denominator of  $\dot{i}$ ,  $\dot{\Omega}$ , and  $\dot{\omega}$ . If  $i$  is zero, these quantities are not defined. This is also to be expected since, as the ascending node is not defined,  $\Omega$  and  $\omega$  cannot be either.

In these two cases, one solution is to drop the “standard” orbital elements and replace them by others, obtained by suitably chosen combinations of those. However, we shall see later that, when the perturbing potential is limited to the  $J_{2n}$  term of the geopotential, the function  $\mathcal{R}$  is such as to remove the indeterminacy when  $e = 0$  or  $i = 0$ . For example, with regard to the indeterminacy that arises in  $\dot{\Omega}$ , we shall see that  $\mathcal{R}$  is a function of  $\sin^2 i$ . Its derivative with respect to  $i$  yields a term in  $\sin i \cos i$  which cancels the term in  $\sin i$  in the denominator of  $\dot{\Omega}$ . In this case, the quantity  $\dot{\Omega}$  is perfectly well defined for  $i = 0$ .

With this type of perturbative potential, we shall find that all the angular speeds  $\dot{\Omega}$ ,  $\dot{\omega}$ ,  $\dot{M}$  are well defined for  $e = 0$  or  $i = 0$  (or  $e = 0$  and  $i = 0$ ), even if the zero point of the angles is not.

### 6.3.6 Delaunay Elements

The form of the matrix  $L$  given in Table 6.2, together with the symmetries and similarities in the Lagrange brackets, suggest making a change of

variables to obtain an even simpler formulation of the results and to group the elements into two homogeneous sets. These elements are known as the Delaunay elements.<sup>8</sup> These variables are written as follows, clearly separating the elements  $L, G, H$ , which have the dimensions of angular momentum per unit mass (action variables) and the associated angular elements  $l, g, h$ , which are dimensionless (angle variables):

$$\begin{cases} L = \sqrt{\mu a}, & G = L\sqrt{1-e^2}, & H = G \cos i, \\ l = M, & g = \omega, & h = \Omega. \end{cases} \quad (6.58)$$

The Lagrange equations can now be written in a very simple form, called the Delaunay equations:

$$\begin{cases} \frac{dL}{dt} = \frac{\partial F}{\partial l}, & \frac{dG}{dt} = \frac{\partial F}{\partial g}, & \frac{dH}{dt} = \frac{\partial F}{\partial h}, \\ \frac{dl}{dt} = -\frac{\partial F}{\partial L}, & \frac{dg}{dt} = -\frac{\partial F}{\partial G}, & \frac{dh}{dt} = -\frac{\partial F}{\partial H}, \end{cases} \quad (6.59)$$

where

$$F = \frac{\mu^2}{2L^2} + \mathcal{R}.$$

In canonical form, the equations are even simpler than in (6.56):

$$\dot{p}_i = \frac{\partial F}{\partial q_i}, \quad \dot{q}_i = -\frac{\partial F}{\partial p_i}, \quad (6.60)$$

where the  $p_i$  are the action variables and the  $q_i$  the associated angle variables.

According to (6.57),  $G$  is the angular momentum  $C$  and  $H$  is its projection onto the polar axis  $Oz$ :

$$H = C \cos i = C_z. \quad (6.61)$$

We shall not use the Delaunay variables in what follows (except for  $H$  a little later). They are given here as an example of a homogeneous notation, in the

---

<sup>8</sup> Charles Delaunay (1816–1872) was a French astronomer and author of many works, including a very detailed study of the motion of the Moon. He detected a slight disagreement between his predictions and observational results. Le Verrier claimed that the error lay in Delaunay's formulas, but the latter replied that the disagreements were the result of unknown causes. In 1865, Delaunay put forward the hypothesis that the discrepancy was due to a very gradual slowing down of the Earth's rotation, caused by friction due to the tides. This is indeed the accepted theory today. Delaunay's method is no longer used to study the motion of the Moon, but it is still current practice for the moons of other planets.

It is worth making a few remarks about his magnum opus, *Théorie du mouvement de la Lune* (1867). The perturbation function  $\mathcal{R}$  is given in the form of an equation with 1967 terms, occupying 21 pages. As the author notes, it remains only to integrate  $\mathcal{R}$  to obtain the coordinates of the Moon as a function of time, using the Delaunay elements. That takes up the following 860 pages. (One must see it to believe it!)

sense of physical dimensions, leading to canonical equations. The Hamiltonian method due to Von Zeipel and Brouwer<sup>9</sup> involves integrating Lagrange's equations using the Delaunay variables.

## 6.4 Perturbative Method: Results for the Geopotential up to $J_2$

In order to achieve what we set out to, that is, to find the time derivatives of the six orbital elements, we must apply Lagrange's equations. We must therefore feed in the value of the perturbative potential  $\mathcal{R}$ . We shall consider here the perturbation due to the geopotential. We shall not tackle the other gravitational potentials, such as the lunisolar attraction potential, treated here as negligible.

As far as the geopotential is concerned, we shall proceed in stages, initially considering the first zonal harmonic (see Sect. 6.4.1), corresponding to the term in  $J_2$ , then all the zonal harmonics up to the term in  $J_n$  (see Sect. 6.5.1), and finally the general case, including all the zonal, sectorial, and tesseral harmonics (see Sect. 6.5.2).

### 6.4.1 Expression for the Perturbative Potential up to $J_2$

We expand the potential to second degree. Then using (3.27) and putting  $U = U_0 + \mathcal{R}$ , we find the following value for  $\mathcal{R}$ :

$$\mathcal{R} = -\frac{\mu R^2}{r^3} J_2 \frac{3 \sin^2 \psi - 1}{2}. \quad (6.62)$$

To integrate this over a period, we first find  $r$  and  $\psi$ .

#### Expressions for $r$ and $\psi$

The distance  $r$  can be expressed as a function of  $a$ ,  $e$ , and  $v$ , as we have seen. Equation (4.60) gives

$$r = \frac{a(1 - e^2)}{1 + e \cos v}. \quad (6.63)$$

The angle  $\psi$  is the geocentric latitude of the satellite. To find an expression for  $\psi$ , we consider the following points, as shown in Fig. 6.3: the projection  $N$  of the ascending node, the projection  $S_0$  of the satellite, and the point  $Q$  where the meridian through  $S_0$  intersects the equator, i.e., the intersection of the half-plane  $S_0Oz$  with the equatorial circle. In the spherical triangle  $NS_0Q$ ,

---

<sup>9</sup>This method was developed by Von Zeipel in 1916 to study asteroids, and it was taken up again by Brouwer in 1959 for application to artificial satellites.

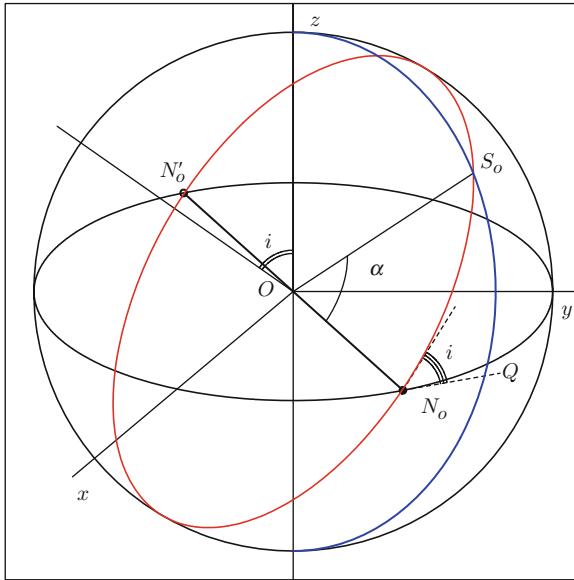


FIG. 6.3 : *Subsatellite point  $S_0$ , specified by the position on orbit  $\alpha$ , angle measured from the ascending node.*

which has a right-angle at  $Q$ , the angle  $N$  is the dihedral angle  $(\mathcal{E}, \mathcal{P})$ , i.e., the inclination  $i$ . The known sides of the triangle (arcs of a great circle) are

$$\widehat{QS_0} = \psi, \quad \widehat{NS_0} = \alpha.$$

Along with (ST VIII), the sine rule (see Sect. 6.13) gives

$$\frac{1}{\sin \alpha} = \frac{\sin i}{\sin \psi}. \quad (6.64)$$

Now, with  $\alpha = \omega + v$  (since  $\alpha$  is the position on orbit), this leads to

$$\sin \psi = \sin i \sin(\omega + v). \quad (6.65)$$

### Expression for $\mathcal{R}$

It thus turns out that  $\mathcal{R}$  is a function of constant quantities ( $a, e, i, \omega$  are considered to be constant over one revolution) and  $v$ . It thus varies periodically, with the same period  $T = 2\pi/n$  as the Keplerian motion. We note that  $\mathcal{R}$  does not depend on  $\Omega$ . This was to be expected insofar as the only perturbation we are considering arises from the replacement of the sphere by an ellipsoid of revolution. In this situation, the terrestrial longitude is irrelevant. The position of the ascending node, and hence the value of  $\Omega$ , is of no consequence, and we have

$$\frac{\partial \mathcal{R}}{\partial \Omega} = 0. \quad (6.66)$$

### Integrating $\mathcal{R}$ over a Period

We calculate  $\langle \mathcal{R} \rangle$ , the average value of  $\mathcal{R}$  over one period  $T$ , by integrating with respect to time, i.e., with respect to the mean anomaly  $M$ :

$$\langle \mathcal{R} \rangle = \frac{1}{T} \int_0^T \mathcal{R} dt = \frac{1}{2\pi} \int_0^{2\pi} \mathcal{R} dM .$$

We first express  $dM$  as a function of  $dv$ . This relation is given by (4.81), which we obtained by applying the areal law:

$$dM = \frac{r^2}{a^2 \sqrt{1-e^2}} dv .$$

Using the variables  $r$ ,  $\psi$ , and  $v$ , and as the bounds of integration are the same for  $v$  and  $M$ , we obtain

$$2\pi \langle \mathcal{R} \rangle = -\frac{\mu R^2 J_2}{2a^2(1-e^2)^{1/2}} \int_0^{2\pi} \frac{3 \sin^2 \psi - 1}{r} dv .$$

Using (6.63) and (6.65), this yields

$$2\pi \langle \mathcal{R} \rangle = -\frac{\mu R^2 J_2}{2a^3(1-e^2)^{3/2}} \mathcal{I} ,$$

where

$$\mathcal{I} = \int_0^{2\pi} \left\{ \frac{3 \sin^2 i}{2} [1 - \cos 2(v + \omega)] - 1 \right\} (1 + e \cos v) dv .$$

Expanding the terms in this expression, we see that integration of the terms periodic in  $v$  over the interval  $[0, 2\pi]$  will give zero, e.g.,

$$\int_0^{2\pi} \cos v \cos 2(\omega + v) dv = \frac{1}{6} \int_0^{2\pi} [\sin(3v + 2\omega) + 3 \sin(v + 2\omega)] dv = 0 .$$

The only nonzero contribution comes from the constant terms, independent of  $v$ , which yields

$$\int_0^{2\pi} \left( \frac{3 \sin^2 i}{2} - 1 \right) dv = 2\pi \left( \frac{3 \sin^2 i}{2} - 1 \right) .$$

The average value of the potential is thus, up to degree 2,

$$\langle \mathcal{R}_2 \rangle = \langle \mathcal{R} \rangle = -\frac{1}{4} \frac{\mu R^2}{a^3(1-e^2)^{3/2}} J_2 (3 \sin^2 i - 2) . \quad (6.67)$$

## Periodic and Secular Variations

The integration of  $\mathcal{R}$  over one period shows that we can decompose this quantity into two parts:

$$\mathcal{R}(v) = \mathcal{R}_s + \mathcal{R}_p(v), \quad (6.68)$$

where the constant  $\mathcal{R}_s = \langle \mathcal{R} \rangle$  represents the average value and the periodic part  $\mathcal{R}_p$  averages to zero over one period. The only part of the potential having a long-term effect (over times longer than the period  $T$ ) is therefore  $\mathcal{R}_s$ . These variations, slow but proportional to the time, are called secular<sup>10</sup> variations (in contrast to  $\mathcal{R}_p$ , which causes only periodic effects).

The secular variations of the elements are obtained by differentiating this part  $\mathcal{R}_s$  of the perturbative potential  $\mathcal{R}$ . Equation (6.67) shows that  $\mathcal{R}_s = \langle \mathcal{R} \rangle$  can be expressed entirely in terms of the metric elements:

$$\mathcal{R}_s = \mathcal{R}_s(a, e, i).$$

### 6.4.2 Variation of the Orbital Elements

#### Calculating the Variation of the Orbital Elements

We can at last apply Lagrange's equations. Referring to the six equations in Table 6.2, we replace the perturbing potential  $\mathcal{R}$  by its secular part  $\mathcal{R}_s$ . The time derivatives  $da/dt$ ,  $de/dt$ , and  $di/dt$  of the metric elements obtained by differentiating with respect to the angle elements are therefore all zero. Consequently, the parameters  $a$ ,  $e$ ,  $i$  remain constant in time.

On the other hand, we see that the time derivatives of the angle elements  $d\Omega/dt$ ,  $d\omega/dt$ ,  $dM/dt$ , obtained by differentiating with respect to the metric elements, are nonzero. The partial derivatives of  $\mathcal{R}_s$  expressed in (6.67) yield

$$\frac{\partial \mathcal{R}_s}{\partial a} = -\frac{3}{a} \mathcal{R}_s, \quad \frac{\partial \mathcal{R}_s}{\partial e} = \frac{3e}{1-e^2} \mathcal{R}_s, \quad \frac{\partial \mathcal{R}_s}{\partial i} = \frac{6 \sin i \cos i}{3 \sin^2 i - 2} \mathcal{R}_s. \quad (6.69)$$

We replace  $\mu$  by  $n^2 a^3$  to obtain the final result:

$$\dot{a} = 0, \quad (6.70)$$

$$\dot{e} = 0, \quad (6.71)$$

$$\dot{i} = 0, \quad (6.72)$$

$$\dot{\Omega} = -\frac{3}{2(1-e^2)^2} n J_2 \left( \frac{R}{a} \right)^2 \cos i, \quad (6.73)$$

---

<sup>10</sup>The word "secular" comes from the Latin *sæculum*, meaning "century", "occurring every hundred years". In the sixteenth century, the term was taken up in astronomy to indicate an effect that would take centuries to become noticeable.

$$\dot{\omega} = \frac{3}{4(1-e^2)^2} n J_2 \left( \frac{R}{a} \right)^2 (5 \cos^2 i - 1) , \quad (6.74)$$

$$\dot{M} - n = \Delta n = \frac{3}{4(1-e^2)^{3/2}} n J_2 \left( \frac{R}{a} \right)^2 (3 \cos^2 i - 1) . \quad (6.75)$$

As a function of time  $t$ , and starting from the origin  $t = 0$ , the orbital elements are thus

$$a(t) = a_0 , \quad e(t) = e_0 , \quad i(t) = i_0 , \quad (6.76)$$

$$\Omega(t) = \Omega_0 + \dot{\Omega}t , \quad \omega(t) = \omega_0 + \dot{\omega}t , \quad (6.77)$$

$$M(t) = M_0 + nt + (\Delta n)t . \quad (6.78)$$

This system of equations represents the solution of the equation of motion (6.13) as a function of the orbital elements.

### Remarks Concerning the Variation of the Orbital Elements

To sum up, if we compare the actual trajectory of the satellite (perturbed by the action of the  $J_2$  term of the geopotential) with the Keplerian trajectory, we observe the following points:

1. The semi-major axis  $a$  of the orbit remains constant.
2. The eccentricity  $e$  of the orbit remains constant.
3. The inclination  $i$  of the orbit with respect to the equatorial plane is constant.
4. The orbital plane rotates uniformly about the polar axis with a constant angular speed  $\dot{\Omega}$ . This motion is known as precession of the orbit or nodal precession.<sup>11</sup> When we speak of precession without further specification, we are generally referring to this motion. According to (6.73), it can occur either in the prograde or the retrograde direction, depending on the inclination of the satellite orbit:

$$\text{prograde } \dot{\Omega} \geq 0 \iff \cos i \leq 0 \iff i^\circ \notin \mathcal{D}_1 ,$$

$$\text{retrograde } \dot{\Omega} \leq 0 \iff \cos i \geq 0 \iff i^\circ \in \mathcal{D}_1 ,$$

where  $\mathcal{D}_1 = [0.00, 90.00]$  in degrees of arc.

---

<sup>11</sup>The word “nodal” means that the motion concerns the line of nodes, i.e., the line joining the ascending and descending nodes. This straight line is the intersection of the equatorial plane with the orbital plane, as introduced in Chap. 5. The word “apsidal”, used in a moment, means that the motion concerns the line of apsides, i.e., the line joining the perigee and the apogee, as discussed in Chap. 4.



5. The perigee, and hence the whole orbit, rotate uniformly in the plane of the orbit with constant angular speed  $\dot{\omega}$ . This motion is called apsidal precession. According to (6.74), it can occur in the prograde or retrograde direction, depending on the inclination of the satellite orbit:

$$\text{prograde } \dot{\omega} \geq 0 \iff \sin^2 i \leq \frac{4}{5} \iff i^\circ \notin \mathcal{D}_2 ,$$

$$\text{retrograde } \dot{\omega} \leq 0 \iff \sin^2 i \geq \frac{4}{5} \iff i^\circ \in \mathcal{D}_2 ,$$

where  $\mathcal{D}_2 = [63.43, 116.57]$  in degrees of arc. We define the critical inclination by

$$i_C = \arcsin\left(\frac{2}{\sqrt{5}}\right) . \quad (6.79)$$

For the two values, the angle  $i_C$  and its supplement, the rate of apsidal precession  $\dot{\omega}$  is zero:

$$\dot{\omega} = 0 \iff \begin{cases} i = i_C = 63.43^\circ , \\ i = 180^\circ - i_C = 116.57^\circ . \end{cases} \quad (6.80)$$

The value of the critical inclination is independent of  $a$  and  $e$ . It is important for certain satellites in highly elliptical orbit, because one seeks to avoid apsidal precession: as we shall see, in the case of Molniya-type communications satellites, the position of the apogee remains fixed on the orbit.

When  $\dot{\omega}$  is calculated using an expansion going beyond the  $J_2$  term, the value obtained for  $i_C$  depends very slightly on  $a$  and  $e$ . It differs by a few hundredths of a degree from the value given by (6.79) (see Example 7.1).

6. The (true) mean motion of the satellite is not the same as it would have been if there were no flattening. According to (6.75), it may be faster or slower depending on the inclination of the satellite:

$$\text{faster } \Delta n \geq 0 \implies \sin^2 i \leq \frac{2}{3} \implies i^\circ \notin \mathcal{D}_3 ,$$

$$\text{slower } \Delta n \leq 0 \implies \sin^2 i \geq \frac{2}{3} \implies i^\circ \in \mathcal{D}_3 ,$$

where  $\mathcal{D}_3 = [54.74, 125.26]$ . Below we define the various periods associated with the motion.

Example calculations are given in the following chapters. Figures 7.1, 7.3, and 7.4 show dependence of the quantities  $\dot{\Omega}$ ,  $\dot{\omega}$ , and  $\Delta n$ , respectively, on the inclination.

**Note.** The signs of the three quantities  $\dot{\Omega}$ ,  $\dot{\omega}$ , and  $\dot{M} - n$  relating to the angle elements depend only on the inclination  $i$ .

## 6.5 Perturbative Method: Results for General Case

### 6.5.1 Geopotential up to $J_n$

#### Remark Concerning Zonal Harmonics

There is an interesting point when we assume that the Earth has an axial symmetry, as we shall see below. In this case, the geopotential involves only zonal harmonics (i.e., the expansion involves only the  $J_n$  terms and not the sectorial or tesseral harmonics), whose contribution to the full potential is by far the greatest, as we have seen. The perturbative acceleration  $\gamma_P$  defined by (6.15) then lies in the plane containing the satellite and the polar axis. It can thus be decomposed as

$$\gamma_P = \gamma_1 \mathbf{e}_r + \gamma_2 \mathbf{e}_z, \quad (6.81)$$

where the unit vector along  $\mathbf{OS}$  is denoted by  $\mathbf{e}_r$ , and the unit vector along the polar axis  $\mathbf{Oz}$  by  $\mathbf{e}_z$ . Using (4.5), the time derivative of the angular momentum  $\mathbf{C}$  is

$$\begin{aligned} \frac{d\mathbf{C}}{dt} &= \mathbf{r} \wedge \ddot{\mathbf{r}} = r \mathbf{e}_r \wedge \left[ \left( -\frac{\mu}{r^2} + \gamma_1 \right) \mathbf{e}_r + \gamma_2 \mathbf{e}_z \right] \\ &= r \gamma_2 (\mathbf{e}_r \wedge \mathbf{e}_z), \end{aligned}$$

which is perpendicular to  $\mathbf{e}_z$ . If  $C_z$  is the projection of  $\mathbf{C}$  onto the polar axis, we thus have

$$\frac{dC_z}{dt} = \frac{d\mathbf{C}}{dt} \cdot \mathbf{e}_z = 0.$$

We saw earlier, in (6.61), that  $C_z$  corresponds to the Delaunay variable  $H$ , which gives here

$$\frac{dH}{dt} = \frac{dC_z}{dt} = 0.$$

We deduce the following property:

$$H = \sqrt{\mu a(1 - e^2)} \cos i = \sqrt{\mu p} \cos i = \text{constant}. \quad (6.82)$$

This relation is a very general feature of orbits perturbed by zonal terms with the same axis. We note the following formula, obtained by differentiating (6.82):

$$\frac{1}{2a} da = \frac{e}{1 - e^2} de + \tan i di. \quad (6.83)$$

As  $H$  is the metric element associated with the angle element  $h = \Omega$ , it follows from (6.59) that

$$\frac{dH}{dt} = \frac{\partial F}{\partial \Omega} = 0, \quad (6.84)$$

which shows that the function  $F$  does not depend on  $\Omega$ . We may then recover the result noted earlier: if the geopotential does not involve the longitude, that is, if it only involves the zonal harmonics, then  $\mathcal{R}$  (or  $F$ ) is independent of  $\Omega$ , as can be seen in the relation (6.66).

### Calculating the Perturbative Potential $\mathcal{R}$

We now consider the Earth as a body with axial symmetry. The potential  $U$  involves only the terms  $J_n$ . The full formula (3.28) reduces to

$$U(r, \psi) = \frac{\mu}{r} \left[ 1 - \sum_{n=2}^{\infty} \left( \frac{R}{r} \right)^n J_n P_n(\sin \psi) \right]. \quad (6.85)$$

The perturbative potential  $\mathcal{R}$  is obtained as the difference between  $U$  and  $U_0$ . This then replaces the value given by (6.62).

**(a) Third Degree Expansion.** We begin our calculation of  $\mathcal{R}$  by expanding up to third degree, thereby bringing in the Legendre polynomials  $P_2(\sin \psi)$  and  $P_3(\sin \psi)$ . We obtain

$$\mathcal{R} = -\frac{\mu}{r} \left[ J_2 \left( \frac{R}{r} \right)^2 \frac{3 \sin^2 \psi - 1}{2} + J_3 \left( \frac{R}{r} \right)^3 \frac{5 \sin^2 \psi - 3}{2} \sin \psi \right]. \quad (6.86)$$

Written in simplified form (with  $\mathcal{R}_n$  for degree  $n$ ),

$$\mathcal{R} = \mathcal{R}_2 + \mathcal{R}_3,$$

where  $\mathcal{R}_2$  corresponds to the sum  $\mathcal{R}_s + \mathcal{R}_p$  given in (6.68).

As before for  $\mathcal{R} = \mathcal{R}_2$ , we calculate the average value  $\langle \mathcal{R}_3 \rangle$  of  $\mathcal{R}_3$  over a period:

$$2\pi \langle \mathcal{R}_3 \rangle = \int_0^{2\pi} \mathcal{R}_3 dM = -\frac{\mu R^3 J_3}{2a^2(1-e^2)^{1/2}} \int_0^{2\pi} \frac{5 \sin^2 \psi - 3}{r^2} \sin \psi dv,$$

using (4.81). Further, with the help of (6.63) and (6.65), we obtain

$$2\pi \langle \mathcal{R}_3 \rangle = -\frac{\mu R^3 J_3}{2a^4(1-e^2)^{5/2}} \sin i \mathcal{J},$$

where

$$\mathcal{J} = \int_0^{2\pi} [5 \sin^2 i \sin^2(\omega + v) - 3] (1 + e \cos v)^2 \sin(\omega + v) dv.$$

This integration is tedious to carry out “by hand”. With a clever decomposition, one can use tables giving the values of definite integrals (from 0 to  $2\pi$ ). These tables, like those of F. Tisserand, avoid the need to recalculate integrals. They have been established over the centuries by astronomers. The simplest thing today is to use a suitable computer software. We thus obtain

$$\mathcal{J} = 2\pi \frac{3e}{4} (5 \sin^2 i - 4) \sin \omega ,$$

whence the expression for  $\langle \mathcal{R}_3 \rangle$  is

$$\langle \mathcal{R}_3 \rangle = \frac{3}{8} \frac{\mu R^3 e}{a^4 (1 - e^2)^{5/2}} J_3 (-5 \sin^2 i + 4) \sin i \sin \omega . \quad (6.87)$$

This term  $\mathcal{R}_3(a, e, i, \omega)$  will lead to long-period variations because it depends on the angle element  $\omega$  in addition to the metric elements. It can be written in the form

$$\langle \mathcal{R}_3 \rangle (a, e, i, \omega) = \langle \mathcal{R}'_3 \rangle (a, e, i) \sin \omega .$$

However, it will not produce secular variations, because if we integrate its value over a round trip of the perigee during its apsidal revolution, the result will be zero:

$$\begin{aligned} 2\pi \langle \langle \mathcal{R}_3 \rangle \rangle &= \int_0^{2\pi} \langle \mathcal{R}_3 \rangle (a, e, i, \omega) d\omega \\ &= \langle \mathcal{R}'_3 \rangle (a, e, i) \int_0^{2\pi} \sin \omega d\omega = 0 . \end{aligned} \quad (6.88)$$

Looking at the successive integrations, we note that  $\langle \langle \mathcal{R}_3 \rangle \rangle$  is equal to 0, because  $\sin \psi$  is a factor in  $\mathcal{R}_3$ , and that in turn because  $x = \sin \psi$  is a factor in the Legendre polynomial  $P_3(x)$ .

Referring to the appendix on Legendre functions in Sect. 3.7, we see that the variable  $x$  is a factor in the expressions for all odd degree polynomials. We deduce, therefore, that the terms  $J_n$  with odd  $n$  make no contribution to the secular variation of the orbital elements:

$$\langle \langle \mathcal{R}_n \rangle \rangle = 0 \quad \text{for odd } n \quad \iff \quad \text{no secular variation} . \quad (6.89)$$

**(b) Fourth Degree Expansion.** For degree 4, we use the Legendre polynomial  $P_4(\sin \psi)$  and proceed as before. This leads to

$$\langle \mathcal{R}_4 \rangle = \frac{1}{64} \frac{\mu R^4 e}{a^5 (1 - e^2)^{7/2}} J_4 (-105 \sin^4 i + 120 \sin^2 i - 24) . \quad (6.90)$$

Like  $\mathcal{R}_2$ , the term  $\mathcal{R}_4$  will produce secular variations for the three angle elements  $\Omega$ ,  $\omega$ , and  $M - nt$ . Here, these variations will be proportional to  $J_4$ .

If we consider secular variations beyond degree 2, we can no longer neglect the fact that the mean motion  $n$ , which enters into the expressions for  $\Omega$ ,  $\dot{\omega}$ , and  $\dot{M} - n$ , has a secular variation proportional to  $J_2$ . There will thus be a term in  $J_2^2$  in addition to the terms in  $J_4$ ,  $J_6$ , etc. Note that, if  $J_2$  is of order  $10^{-3}$ , the terms  $J_4$ ,  $J_6$ , etc., are of order  $10^{-6}$ , as is  $J_2^2$  [see (7.15)–(7.17) and Table 7.1].

### Periodic and Secular Variations

From (6.85), we obtain  $\mathcal{R}$  as a function of five orbital parameters (since  $\Omega$  does not occur):

$$\mathcal{R} = \mathcal{R}(a, e, i, \omega, M).$$

The potential  $\mathcal{R}$  decomposes into a sum of terms  $\mathcal{R}_n$ , one for each term  $J_n$ . We consider Lagrange's equations as given in Table 6.2. It can be shown that:

- If a term  $\mathcal{R}_n$  depends on neither  $M$  nor  $\omega$ , it causes a variation in the relevant orbital element which is proportional to the time, i.e., a secular variation.
- If a term  $\mathcal{R}_n$  depends on  $\omega$ , but not on  $M$ , there will be a variation whose period will be of the order of the apsidal precession, i.e., a long-period periodic variation.
- If a term  $\mathcal{R}_n$  depends on both  $\omega$  and  $M$ , there will be a variation whose period will be of the order of the Keplerian period, i.e., a short-period periodic variation.

To sum up, periodic variations are divided into short-period variations, corresponding to the period of  $M$ , and long-period variations, occurring over several tens of days ( $\sim 1,000T$ ), corresponding to the apsidal period of  $\omega$ . The latter are mainly due to the influence of the  $J_3$  term which affects especially  $e$  and the angle elements. There is no long-period perturbation of the semi-major axis  $a$ . This result is known as the invariability of the major axis, and it applies to many types of motion in astronomy (see Sect. 6.9).

Secular variations are variations proportional to time. Naturally, it is this kind of variation that deviates the satellite from its Keplerian orbit. We have seen that the  $J_2$  term causes secular deviations in the three angle elements, while having no effect on the metric elements. The other zonal harmonics, although only the even ones, i.e.,  $J_4, J_6, \dots, J_{2p}, \dots$ , also contribute to secular deviations (see Table 7.1). Figure 6.4 shows in a schematic way all the periodic and secular variations of the orbital elements.

**Example 6.1** Calculate the effect of perturbations when the geopotential is expanded up to the term in  $J_3$ . Long-period variations.

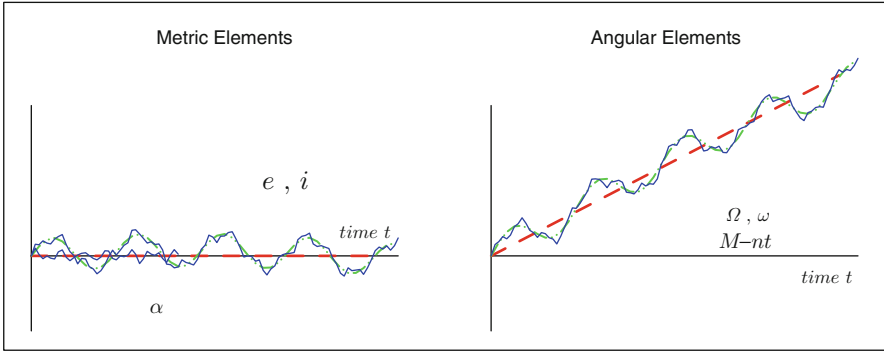


FIG. 6.4: Schematic view of the temporal variation of the orbital elements. Short-period variations are shown with a continuous curve and long-period variations with a dot-dashed curve. Secular variations are shown with a dashed line. The amplitudes of the periodic variations have been greatly exaggerated for visibility.

► The potential  $\mathcal{R}$  is given by (6.86). We have just seen that it can be written in the form

$$\mathcal{R} = (\mathcal{R}_s + \mathcal{R}_p) + \mathcal{R}_3 ,$$

if the expansion is cut off at degree 3. The term  $\mathcal{R}_s(a, e, i)$  is given by (6.67). The term  $\mathcal{R}_p(a, e, i, \omega, M)$  leads to short-period variations which we shall not discuss here. The term  $\mathcal{R}_3$  is given by (6.87). This term  $\mathcal{R}_3(a, e, i, \omega)$  will produce long-period variations which we shall now calculate.

Since  $\partial\mathcal{R}_3/\partial M = 0$  and  $\partial\mathcal{R}_3/\partial\Omega = 0$ , the equations for the metric elements, the first three Lagrange equations (see Table 6.2), become

$$\frac{da}{dt} = 0 , \quad \frac{de}{dt} = -\frac{1}{na^2} \frac{\sqrt{1-e^2}}{e} \frac{\partial\mathcal{R}_3}{\partial\omega} , \quad \frac{di}{dt} = \frac{1}{na^2} \frac{1}{\sqrt{1-e^2}} \frac{\cos i}{\sin i} \frac{\partial\mathcal{R}_3}{\partial\omega} .$$

This implies

$$\frac{de}{di} = -\frac{1-e^2}{e} \tan i , \quad (6.91)$$

which is equivalent to (6.83) when  $a$  is constant (and this is almost always the case for the kinds of motion occurring in astronomy). To calculate the variation arising in  $i$  as a result of  $\mathcal{R}_3$ , we start with  $di/dt$  above, differentiate  $\mathcal{R}_3$  with respect to  $\omega$ , and replace  $\mu$  by  $n^2a^3$ . This gives

$$\frac{di}{dt} = \frac{3e}{2(1-e^2)^3} nJ_3 \left(\frac{R}{a}\right)^3 \left(1 - \frac{5}{4} \sin^2 i\right) \cos i \cos \omega . \quad (6.92)$$

To find the long-period variation in  $i$  due to the zonal harmonic  $J_3$ , we rewrite  $di/d\omega$ , with the value for  $\dot{\omega}$  calculated using (6.74):

$$\frac{di}{d\omega} = \frac{di}{dt} \frac{dt}{d\omega} = \frac{1}{\dot{\omega}} \frac{di}{dt} = \frac{1}{2} \frac{e}{1-e^2} \frac{J_3}{J_2} \left( \frac{R}{a} \right) \cos i \cos \omega .$$

The required quantity is thus

$$\Delta_{\text{LP}_3} i = \frac{1}{2} \frac{e}{1-e^2} \frac{J_3}{J_2} \left( \frac{R}{a} \right) \cos i \sin \omega , \quad (6.93)$$

where the subscript  $\text{LP}_3$  indicates that this is a long-period effect due to the zonal harmonic  $J_3$ . To obtain the corresponding variation in  $e$ , we use (6.91), taking  $\Delta_{\text{LP}_3} e / \Delta_{\text{LP}_3} i$  for  $de/di$ :

$$\Delta_{\text{LP}_3} e = -\frac{1}{2} \frac{J_3}{J_2} \left( \frac{R}{a} \right) \sin i \sin \omega . \quad (6.94)$$

Conversely, one can determine the value of  $J_3$  by measuring the values of  $\Delta_{\text{LP}_3} i$  and  $\Delta_{\text{LP}_3} e$  (see the historical note in Sect. 6.7).

**Important Note.** For near-circular orbits ( $e \sim 10^{-3}$ ), we find that, with (6.93) and (6.93), or directly from (6.91), we have

$$\Delta_{\text{LP}_3} i \approx -\frac{e}{\tan i} \Delta_{\text{LP}_3} e . \quad (6.95)$$

Owing to the factor  $e$ , the variation  $\Delta_{\text{LP}_3} i$  of the inclination is negligible compared with the variation of the eccentricity  $\Delta_{\text{LP}_3} e$  (except for equatorial orbits). ◀

**Example 6.2** Calculate the variation of the orbital elements over one revolution.

► Recall that  $p$  is the semi-latus rectum of the ellipse, with  $p = a(1 - e^2)$ . These variations carry the subscript 1 to indicate that they refer to the value obtained over one revolution. The variations, be they secular or long-period, are sufficiently slow to be able to avoid integrating over the time  $t$ . Indeed, it suffices to multiply the derivative with respect to  $t$  of the relevant quantity by  $T = 2\pi/n$ .

For the angle elements, the periodic variations are negligible compared with secular variations. However, these periodic variations are “visible” for the metric elements, where there are no secular variations.

For the angle variables, we write  $\Delta_1 \Omega = \dot{\Omega} T$  and  $\Delta_1 \omega = \dot{\omega} T$ , where the angles are of course given in radians. To first order, we take for  $\dot{\Omega}$  and  $\dot{\omega}$  the

values given by (6.73) and (6.74), respectively, as a function of  $J_2$  alone, when expanding the geopotential:

$$\Delta_1 \Omega = -3\pi J_2 \left(\frac{R}{p}\right)^2 \cos i, \quad (6.96)$$

$$\Delta_1 \omega = +3\pi J_2 \left(\frac{R}{p}\right)^2 2 \left(1 - \frac{5}{4} \sin^2 i\right). \quad (6.97)$$

For the metric variables, the case for  $a$  can be dealt with immediately, since we may consider that  $\dot{a}$  is zero (invariability of the major axis). Concerning the expressions for  $\dot{e}$  and  $\dot{i}$ , we use (6.92) and (6.91). We consider only the first term (the  $J_3$  term) of the expansion. For the variations over one period, we then obtain

$$\Delta_1 a \approx 0, \quad (6.98)$$

$$\Delta_1 e = -3\pi J_3 \left(\frac{R}{p}\right)^3 (1 - e^2) \left(1 - \frac{5}{4} \sin^2 i\right) \sin i \cos \omega, \quad (6.99)$$

$$\Delta_1 i = +3\pi J_3 \left(\frac{R}{p}\right)^3 e \left(1 - \frac{5}{4} \sin^2 i\right) \cos i \cos \omega. \quad (6.100)$$

The critical inclination plays an important role for  $\Delta_1 \omega$ ,  $\Delta_1 e$ , and  $\Delta_1 i$ . ◀

## 6.5.2 Full Geopotential

When we consider the geopotential  $U(r, \lambda, \psi)$  given by (3.17), it is extremely difficult to calculate the effects of the perturbative potential  $\mathcal{R}$ . However, let us just mention the existence of orbital resonance phenomena: the influence of certain tesseral coefficients  $C_{lm}$  and  $S_{lm}$ , defined by (3.20) and (3.21), can, for one specific orbit, significantly exceed the effects of coefficients with higher or lower order and degree. For these values, the periodic perturbations have relatively large amplitude. W. Kaula has developed a formalism which predicts the resonances associated with these specific orbits.

This resonance phenomenon is particularly important for recurrent satellites with a 1-day recurrence cycle, i.e., effecting a whole number  $\nu$  of revolutions per day. Tesseral harmonics with order a multiple of  $\nu$  must be taken into account in orbital extrapolations, i.e., precise determination of satellite position at a given time from its osculating elements. Particularly important are the following:



Source of perturbation	Secular variation			Periodic variation	
	Large	Small	Indirect	Moderate	Small
Earth's gravity	$\Omega, \omega$	–	–	$e$	$i, \Omega, \omega$
Atmosphere	$a, e$	$i$	$\Omega, \omega$	–	$\Omega, \omega$
Lunisolar gravity	–	–	–	–	$a, e, i, \Omega, \omega$

TABLE 6.3 : Sources of perturbation and the effect (secular or periodic variation) induced on the five orbital elements  $a, e, i, \Omega,$  and  $\omega$ , for a satellite in low-Earth orbit, according to the King-Hele theory.

- For satellites of medium altitude which do two revolutions per day (whence  $\nu = 2$ ), harmonics of order 2, 4, 6, . . . , whether the orbit is circular, as for Navstar/GPS, or highly elliptic, as for Molniya.<sup>12</sup>
- For geosynchronous satellites,<sup>13</sup> harmonics of order 1, 2, 3, . . . .

More generally, this phenomenon affects all recurrent satellites, where  $\nu$  is a rational number, i.e., after a certain number of days, the satellite ground track is repeated (see the further discussion below). For example, for the satellites SPOT-1 to -5, where  $\nu = 14 + 5/26$ , there is a resonance for the tesseral terms of orders 15 and 29.

### 6.5.3 Other Perturbative Forces Deriving from a Potential

The non-terrestrial gravitational potential is due almost entirely to the lunisolar potential. The elements  $a$  and  $e$  are not affected by secular variations. The various orbital elements undergo slight variations with long period. For certain orbits, we observe a very slight secular drift in  $\Omega$ . These results are summarised in Table 6.3, for a low-orbiting satellite.

### 6.5.4 Perturbative Forces not Derived from a Potential

Atmospheric drag has ever greater effect as the satellite orbit becomes lower. It can be shown that  $e$  tends to decrease (drag is greater at the perigee than at the apogee, and this has the effect of making the orbit more circular). Furthermore,  $a$  decreases (one would expect friction to make the satellite fall toward the Earth). The other elements are not significantly affected, at least

<sup>12</sup>For Molniya, the tesseral harmonic coefficients with the most effect are  $C_{22}, C_{32}, C_{52}, C_{44}, C_{54}, C_{64}, C_{66}, C_{76}, C_{86}, C_{98}$ , and the corresponding  $S_{lm}$ .

<sup>13</sup>For a geostationary satellite, resonance periods of 24 h and 48 h are associated with tesseral harmonics of order 1 ( $C_{31}, C_{41}$ , and the corresponding  $S_{11}$ ), and resonance periods of 12, 24, 36, and 48 h are associated with those of order 2 ( $C_{22}, C_{32}, C_{42}$ , and the corresponding  $S_{12}$ ).

not directly. However, the changes in  $a$  and  $e$ , which may be considered proportional to the time  $t$  (secular variation), induce changes in the angle parameters which rapidly dominate over periodic variations because they are proportional to  $t^2$  (for variations going as  $t^2$ , see also the drift in local time and Example 10.7 in Chap. 10). Forces induced by (solar and terrestrial) radiation pressure also affect the variation of the orbital elements (see Table 6.3). The effect of atmospheric drag on  $a$  is treated in the appendix in Sect. 6.6.

When the perturbing acceleration  $\gamma_P$  does not derive from a potential, we use a coordinate system moving with the orbit and decompose the vector relative to this. This gives a system of equations called Gauss' equations. We shall not discuss this method further.

### 6.5.5 Different Definitions of the Period

The three angles associated with Keplerian motion, the anomalies  $v$ ,  $E$ , and  $M$ , increase by  $2\pi$  when the time increases by  $2\pi/n$ , where  $n$  is the mean motion. As can be seen from (4.65) and (4.57), the origin from which these angles are measured is taken at the time  $t = t_p$  when the satellite passes the perigee. The time lapse between two successive passages at perigee is called the anomalistic period.<sup>14</sup> It is therefore the anomalistic period  $T_a$  which is obtained with the mean motion  $n$ , and this differs from the period  $T_0$  obtained with the Keplerian mean motion  $n_0$ . We have the definition

$$nT_a = n_0T_0 . \quad (6.101)$$

With  $n = n_0 + \Delta n$ , calculated using (6.75), we obtain

$$T_a = \left(1 - \frac{\Delta n}{n}\right) T_0 . \quad (6.102)$$

We would also like to know the time interval between two passages at the ascending node (or the descending node). This is the nodal period or draconitic<sup>15</sup> period  $T_d$ . This differs from  $T_a$  because the perigee moves through apsidal precession. It should be noted that this happens *even in the case of a circular orbit*, since  $\dot{\omega}$  does not vanish when  $e$  is zero. We have the relation

$$n_d T_d = n T_a , \quad (6.103)$$

<sup>14</sup>The adjective “anomalistic” derives from the word “anomaly”, since the three anomalies are all zero (modulo  $2\pi$ ) at the perigee.

<sup>15</sup>The adjective “draconitic” was originally used for the draconitic period or month, which refers to the passage of the Moon at its ascending node. The word comes from the Greek  $\delta\rho\acute{\alpha}\kappa\omega\nu$ ,  $\omicron\nu\tau\omicron\varsigma$ , meaning “dragon” (literally, “which stares”). Eclipses only occur when the Moon passes through a node of its orbit. In ancient times, the Greeks thought that, during an eclipse, the moon was swallowed up by a dragon, hiding near the nodes of the lunar orbit.

where  $n_d$  is the mean motion when the ascending node is taken as origin. Composing the two motions, we have

$$n_d = n + \dot{\omega}, \quad (6.104)$$

yielding one period in terms of the other:

$$T_d = \frac{1}{1 + \dot{\omega}/n} T_a, \quad (6.105)$$

$$T_a = \left(1 + \frac{\dot{\omega}}{n}\right) T_d. \quad (6.106)$$

The draconitic period  $T_d$  is given in terms of the Keplerian period  $T_0$  by

$$T_d = \frac{1 - \Delta n/n}{1 + \dot{\omega}/n} T_0, \quad (6.107)$$

or, to a first approximation,

$$T_d \approx \left(1 - \frac{\dot{\omega} + \Delta n}{n}\right) T_0 \quad (6.108)$$

With this approximation and for a circular orbit, i.e.,  $e = 0$  in (6.74) and (6.75), we obtain

$$T_d \approx \left[1 - \frac{3}{2} J_2 \left(\frac{R}{a}\right)^2 (4 \cos^2 i - 1)\right] T_0. \quad (6.109)$$

For  $i = 60^\circ$  and  $i = 120^\circ$ , we note that the draconitic period  $T_d$  is equal to the Keplerian period  $T_0$ .

In brief, the period  $T_a$  is mainly used to calculate the semi-major axis of the orbit. For everything relating to the motion of the satellite in a frame fixed relative to the Earth, it is the draconitic period  $T_d$  which comes into play. For Keplerian motion, there is no need to make these distinctions between periods, since they obviously coincide in this case.

## 6.6 Appendix: Atmospheric Drag

### 6.6.1 Description of the Earth's Atmosphere

The Earth's atmosphere can be divided up according to physical criteria into zones determined by altitude and called spheres.

If we use the criterion of vertical temperature gradient, then starting at ground level, we encounter the troposphere and the stratosphere in roughly the first 50 km, the mesosphere up to 100 km, then the thermosphere and the exosphere. The lower regions, below 200 km, are of no relevance to satellites

except for questions of signal transmission, something we shall return to when we discuss navigation satellites (GPS) in Chap. 14.

If the criterion is the relative proportions of the majority chemical constituents, we distinguish the homosphere and the heterosphere, the transition being located at around 100 km altitude. In the homosphere, thanks to mixing effects, the atmosphere remains homogeneous with regard to its chemical components (at least those that are not subject to photochemical reactions), and this whatever the pressure. The air we breathe on the coast or at the top of a mountain is also composed of 78 % nitrogen  $N_2$ , 21 % oxygen  $O_2$ , and 1 % argon Ar. But above 100 km altitude, owing to the rarefaction of the air and the high temperature (a high level of molecular agitation with a large mean free path for the particles), the relative proportions of the constituents changes completely and becomes mass dependent. Between 160 and 600 km, the predominant gas is monatomic oxygen O, and beyond that, one finds a predominance of the lighter atoms, i.e., helium He (dominant up to 2,000 km) and hydrogen H.

When we are interested in satellite motions, the crucial altitude range is 200–1,200 km. It soon becomes catastrophic for a satellite to pass at altitudes below 200 km, and above 1,200 km, the effects of atmospheric drag can be neglected, even over long periods, although other dissipative phenomena then become important, e.g., solar radiation pressure.

### 6.6.2 Density of the Atmosphere

When investigating atmospheric drag, the fundamental quantity we need to know is the mass per unit volume of the air. Generally known as the atmospheric density, it is denoted by  $\rho$  and expressed in units of  $\text{kg m}^{-3}$  (although strictly speaking the density is not a mass per unit volume).

It is easy to calculate the altitude dependence of the density if we assume that the atmosphere is at rest and isothermal, using the laws of thermodynamics. The result is an exponential function:

$$\rho(h) = \rho_0 e^{-h/H}, \quad (6.110)$$

where  $\rho_0$  is the density at the reference altitude  $z_0$  and  $h = z - z_0$  represents the difference in altitude. The quantity  $H$ , with units of length, is the scale factor, given by standard calculation as

$$H = \frac{\mathfrak{R}T}{\overline{M}g}, \quad (6.111)$$

with  $\mathfrak{R} = 8.31$  (SI units) the perfect gas constant,  $T$  the temperature (K),  $\overline{M}$  the mean molar mass (kg) of the components, and  $g$  the acceleration due to gravity ( $\text{m s}^{-2}$ ).

At sea level, at a temperature of  $15^\circ\text{C}$  and a pressure of  $1,013\text{hPa}$ , we have

$$T = 273 + 15 = 288 \text{ K}, \quad \bar{M} = \frac{4}{5} \times 28 + \frac{1}{5} \times 32 \approx 29 \text{ g}.$$

The value of  $\rho$  is thus

$$\rho_0 = \frac{29}{22.4} \times \frac{273}{288} = 1.23 \text{ kg m}^{-3}.$$

Calculating the scale factor, we find that

$$H = \frac{8.31 \times 288}{29 \times 10^{-3} \times 9.81} = 8413 \text{ m}, \quad \text{or } H \approx 8.4 \text{ km}.$$

At an altitude of about  $8\text{ km}$ , the density is divided by a factor of  $e$ , the Euler number, as compared with its value at sea level, whence it is equal to  $\rho = 0.44 \text{ kg m}^{-3}$ .

Even though the actual atmosphere may differ to some extent from the above idealisation and the conditions assumed in establishing (6.110), the formula for  $\rho(h)$  is nevertheless applicable in most cases, as experience shows.

At a given altitude in the relevant altitude range for our present purposes, viz.,  $200\text{--}1,200\text{ km}$ , the atmospheric density depends sensitively on the level of solar activity, whence its variations are driven by several cycles with different periods:

- An 11 year cycle which has been known for a long time, as revealed by observation of sunspots (since 1749). Rather than simply counting spots, a more objective criterion has been used since 1947, with the measurement, known as  $F_{10.7}$ , of the Sun's emission of the  $10.7\text{ cm}$  radio wave. Over the past 50 years, maxima have occurred in the years 1968, 1980, 1991, 2002, and 2013.
- An annual cycle, related to seasonal effects.
- A 27 day cycle related to the synodic period of rotation of the Sun about its own axis.
- A daily cycle, with a maximum for  $\rho$  at around  $15\text{ h}$  local time ( $\tau_{\text{LMT}}$ ) and a minimum  $12\text{ h}$  later.

In addition, the atmospheric density also depends on the latitude of the observation point.

### 6.6.3 Models of the Atmosphere

In the face of such complexity, it was only logical to set up models of the atmosphere. The first date back to the 1960s and 1970s, developed by Jacchia (J65, J71, etc.) in the USA, and Hedin and Barlier (DTM78) in Europe. Current models, such as JB2006, DTM2007, MSIS-90, NRLMSIS, and

$h$ (km)	$\rho$ (kg m <sup>-3</sup> )						$H$ (km)			
	Minimal			Maximal			Minimal		Maximal	
	N	D		N	D		N	D	N	D
100	9.8	9.8	10 <sup>-9</sup>	9.8	9.8	10 <sup>-9</sup>	6	6	6	6
200	1.8	2.1	10 <sup>-10</sup>	3.2	3.7	10 <sup>-10</sup>	33	38	43	49
300	0.5	1.1	10 <sup>-11</sup>	2.6	4.7	10 <sup>-11</sup>	45	53	57	68
400	0.5	1.6	10 <sup>-12</sup>	5.0	12.0	10 <sup>-12</sup>	53	61	70	80
500	0.4	2.0	10 <sup>-13</sup>	8.5	31.0	10 <sup>-13</sup>	60	67	75	89
600	1.0	3.9	10 <sup>-14</sup>	20.	100.	10 <sup>-14</sup>	76	76	82	96
700	0.4	1.0	10 <sup>-14</sup>	5.	31.	10 <sup>-14</sup>	134	96	93	105
800	2.4	4.3	10 <sup>-15</sup>	17.	110.	10 <sup>-15</sup>	213	139	114	116
900	1.6	2.4	10 <sup>-15</sup>	7.	43.	10 <sup>-15</sup>	325	215	153	134
1,000	9.6	17.0	10 <sup>-16</sup>	42.	200.	10 <sup>-16</sup>	418	309	217	165

TABLE 6.4: Atmospheric density represented by the mass per unit volume  $\rho$  as a function of the altitude  $h$ , for years of minimal and maximal solar activity, and during the night (N) or the day (D). The scale factor  $H$  is also given. Values are averaged over latitudes and seasons. Model MSIS-90.

others, direct descendants of the pioneers, naturally reflect the exponential improvement in computer calculation capacity.

Without going into the details, we can now obtain the atmospheric density as a function of altitude  $h$ , local time  $\tau_{\text{LMT}}$ , the day of the year  $D$ , and the latitude  $\psi$ :

$$\rho_i(h, \tau_{\text{LMT}}, D, \psi), \quad i = 1, 2, \dots, n, \tag{6.112}$$

where the index  $i$  indicates the level of solar activity ( $i = 1$  for a year of minimal activity,  $i = 2$  maximal,  $i = 3$  average, and so on). Table 6.4 gives an idea of the kind of values one finds for  $\rho$ .

### 6.6.4 Calculation of Atmospheric Drag: The Notion of $\Delta V$

We consider a satellite in Earth orbit, denoting its speed in the Galilean frame  $\mathfrak{R}$  by  $V$  and its speed relative to the atmosphere by  $V_\alpha$ . If the atmosphere is at rest and without wind,  $V_\alpha$  is equal to  $V'$ , the speed relative to the terrestrial frame  $\mathfrak{R}_T$ .

Let  $S$  be the cross-sectional area of the satellite in the direction normal to its displacement. In a time  $dt$ , the mass  $dm$  of air of mass per unit volume  $\rho$  encountered by the satellite is

$$dm = \rho S V_\alpha dt. \tag{6.113}$$

The corresponding momentum  $dp$  is

$$dp = V_\alpha dm = \rho S V_\alpha^2 dt, \quad (6.114)$$

and the force of friction  $F$  is therefore

$$F = \frac{dp}{dt} = \rho S V_\alpha^2.$$

To take into account the nature of the impacts of the air molecules on the satellite surface, we multiply  $F$  by a coefficient<sup>16</sup>  $C_d/2$ , whence

$$F = \frac{1}{2} C_d \rho S V_\alpha^2. \quad (6.115)$$

The dimensionless friction coefficient  $C_d$  varies from 1.5 to 3.0, depending on the shape of the satellite. It can be shown that it is equal to 2 for a sphere.

The friction force  $F$ , given vectorially by

$$\mathbf{F} = -F \frac{\mathbf{V}_\alpha}{V_\alpha}, \quad (6.116)$$

has the effect of slowing down the satellite of mass  $M_s$ . Applying the fundamental law of dynamics, we have

$$d\mathbf{V} = \frac{\mathbf{F}}{M_s} dt, \quad dV = -\frac{1}{2} C_d \frac{S}{M_s} \rho V_\alpha^2 dt. \quad (6.117)$$

We set

$$B = C_d \frac{S}{M_s}. \quad (6.118)$$

The coefficient  $B$ , known as the ballistic coefficient, has units of  $\text{m}^2 \text{kg}^{-1}$ . It characterises the satellite with respect to drag.<sup>17</sup> The larger the value of  $B$ , the greater the drag effect will be. For example, for a “standard” satellite with  $M_s = 500 \text{ kg}$ ,  $S = 10 \text{ m}^2$ ,  $C_d = 2.3$ , we have  $B = 0.046 \text{ m}^2 \text{kg}^{-1}$  and  $1/B = 21.7 \text{ kg m}^{-2}$ .

In the space technology community, it is standard practice to denote the (magnitude of the) change in the velocity over a finite time  $T$  by  $\Delta V$  (pronounced Delta V):

$$\Delta V = \frac{1}{2} B \int_0^T \rho V_\alpha^2 dt. \quad (6.119)$$

If  $\Delta V$  is calculated over one revolution, this is written  $\Delta_1 V$ .

<sup>16</sup>It is amusing to note that the factor of 1/2 in front of  $C_d$  has no better justification than to make this formula (6.115) look like other formulas of this kind, such as the formula for the kinetic energy, where the factor of 1/2 has a mathematical origin.

<sup>17</sup>To minimise these effects, the passive satellite Starlette (without its own energy supply) is designed as a sphere coated with 60 laser reflectors. It has a uranium core of density 18.7. The mass of the satellite is 47 kg and its diameter 48 cm. With  $C_d = 2$ , we have  $B = 7.70 \times 10^{-3}$  and  $1/B = 130 \text{ kg m}^{-2}$ .

### Simplified Case

Let us calculate the value of  $\Delta V$  and the change over one revolution of the semi-major axis  $a$  and the period  $T$  for a satellite in circular orbit. We assume that the atmospheric density is constant over one revolution and equal to  $\rho_0$ . We identify  $V_\alpha$  with  $V$  and consider the Keplerian case, taking the Earth to be spherical. Since  $2\pi a = VT$ , we thus find

$$\Delta_1 V = \pi B \rho_0 a V . \tag{6.120}$$

Differentiating  $V = \sqrt{\mu/a}$ , we have  $da/a = -2\pi B \rho_0 a$ , whereupon

$$\Delta_1 a = -2\pi B \rho_0 a^2 . \tag{6.121}$$

Likewise for the period, with  $dT/T = (3/2)da/a$ , we have

$$\Delta_1 T = -6\pi^2 B \rho_0 \frac{a^2}{V} . \tag{6.122}$$

**Example 6.3** Calculate the daily drop in altitude for a SPOT-type satellite.

► For a SPOT-type satellite, with  $B = 0.046$  and  $a = 7,200$  km, and which makes about 14 revolutions per day, application of (6.121) yields

$$\Delta_D a = 14\Delta_1 a = -2 \times 10^{-14} \rho ,$$

where  $\Delta_D$  is the change in  $a$  over 1 day. We may thus estimate the drop in altitude each day using the values for  $\rho$  at 800 km altitude:

Solar activity		
Calm	$\rho = 3 \times 10^{-15}$	$\Delta_D a = -0.6$ m
Average	$\rho = 1 \times 10^{-14}$	$\Delta_D a = -2.0$ m
High	$\rho = 5 \times 10^{-14}$	$\Delta_D a = -10$ m
Very high	$\rho = 1.5 \times 10^{-13}$	$\Delta_D a = -30$ m

These results give an indication of the orders of magnitude involved here. ◀

### Improvements in Atmospheric Models

The satellites CHAMP, GRACE-A and -B, and GOCE are equipped with highly sensitive 3-axis accelerometers which measure the acceleration  $\mathbf{a}_d$  and can be used to pilot drag compensation forces. According to (6.115) and (6.116),

$$\mathbf{a}_d = -\frac{1}{2} B \rho V_\alpha^2 \frac{\mathbf{V}_\alpha}{V_\alpha} . \tag{6.123}$$



The values of  $\mathbf{a}_d$ ,  $B$ , and  $V_\alpha$  are known, and we thus obtain the value of  $\rho$  at all times along the trajectory. The sensitivity of the accelerometers is constantly being improved as can be seen from the values  $10^{-9} \text{ m s}^{-2}$  for CHAMP,  $10^{-10}$  for GRACE, and  $10^{-12}$  for GOCE.

### 6.6.5 Effect of Drag on the Orbit

Analytical models of orbit propagation use similar methods to those presented here. With the software *Ixion*, assuming that the satellite characteristics are well defined, we calculate the position of the satellite, its geodetic altitude, and its velocity relative to the Earth at each instant of time, in adjustable steps of a few seconds. If the atmospheric model provides the wind velocity, we calculate the vector  $\mathbf{V}_\alpha$ , otherwise  $\mathbf{V}'$ . With  $\rho$  given at the relevant altitude, place, and time, we calculate the frictional force  $\mathbf{F}$  using (6.115) for each integration step.

Going back to the equations of motion with this force  $F$ , we use the King-Hele theory to calculate  $\dot{a}$  and  $\dot{e}$ , the time derivatives of the semi-major axis  $a$  and the eccentricity  $e$ . Calculation of the other parameters is complex. The change in  $i$  is very small, and the periodic variations in  $\Omega$  and  $\omega$  are swamped by their secular variations. The software continuously tracks the modified trajectory. Or if the satellite is being held to a given trajectory, we deduce the quantity  $\Delta V$  needed to do this.

### 6.6.6 Simplified Calculations for an Eccentric Orbit: Air Braking

The quantity  $\Delta V$  is very important in space engineering, and in particular for mission control. While atmospheric drag leads to a certain value of  $\Delta V$ , conversely, a certain amount of  $\Delta V$  can be used to compensate for drag or to carry out maneuvers to change the orbit. For those in charge of the technical aspects, the cumulated value of  $\Delta V$  over the whole mission can be directly translated into an amount of fuel.

While  $\Delta V$  is tedious to calculate either analytically or numerically, the following method provides a simple way to estimate it over one period in the case of elliptical orbits. The basic idea is that almost all the drag occurs near the perigee, owing to the exponential decrease in  $\rho$  with altitude, as attested by (6.110). During this relatively brief lapse of time, the speed  $V$  of the satellite can be treated as constant, equal to  $V_p$ , the speed at perigee.<sup>18</sup>

---

<sup>18</sup>For example, for a Molniya satellite,  $h_p = 200 \text{ km}$ ,  $e = 0.75$ ,  $a = 26,313 \text{ km}$ ,  $T = 708 \text{ min}$ , with a perigee passage at  $h = 200 \text{ km}$ ,  $\eta = 1.031$ , at time  $t = 0$ , the passage at altitude  $h = 600 \text{ km}$ ,  $\eta = 1.091$ , occurs at time  $t = 346 \text{ s}$ . The satellite has thus spent  $2 \times 346 = 692 \text{ s} = 11.5 \text{ min}$  in atmospheric layers between 200 and 600 km, which represents  $11.5/708 = 0.016$ , or 1.6% of the time of one revolution. The relative difference in the speed of the satellite between the two points is

Here we take the planet to be spherical and neglect its rotational speed and also the wind speed compared with the speed of the satellite near perigee. With (4.45), we thus find

$$V_\alpha = V = V_p = \sqrt{\frac{\mu}{a}} \sqrt{\frac{1+e}{1-e}}.$$

We also make the highly reasonable assumption that  $a$  and  $e$  do not change over one revolution.

We denote the altitude of the satellite by  $z$  and its altitude at perigee by  $z_p$ . We also denote the value of  $\rho$  at perigee by  $\rho_p$  and the scale factor at this altitude by  $H$ . Over one period of length  $T$ , the value  $\Delta_1 V$  of  $\Delta V$  is then given by

$$\Delta_1 V = \frac{1}{2} B \int_0^T \rho V^2 dt = \frac{1}{2} B \rho_p \frac{\mu}{a} \frac{1+e}{1-e} \int_{-T/2}^{+T/2} \exp\left(-\frac{z-z_p}{H}\right) dt. \quad (6.124)$$

Using the eccentric anomaly  $E$ , we obtain the relations

$$r = a(1 - e \cos E), \quad r_p = a(1 - e), \quad z - z_p = r - r_p = ae(1 - \cos E).$$

The lapse of time over which drag is effective is very short and centered on the passage at perigee. In this case, the anomalies  $M$  and  $E$  are much smaller than 1. We may thus write

$$1 - \cos E \approx \frac{E^2}{2}, \quad M = E - e \sin E \approx E(1 - e).$$

This gives  $E$  as a function of  $M$  and hence  $z - z_p$  as a function of time:

$$E = \frac{M}{1 - e} = \sqrt{\frac{\mu}{a^3}} \frac{1}{1 - e} t, \quad (6.125)$$

$$z - z_p = ae \frac{E^2}{2} = \frac{1}{2} \mu \frac{e}{a^2(1 - e)^2} t^2, \quad (6.126)$$

$$\frac{z - z_p}{H} = \frac{1}{2} \frac{\mu e}{H r_p^2} t^2. \quad (6.127)$$

First we note that the integral of a Gaussian is

$$\int_{-\infty}^{+\infty} \exp(-\alpha x^2) dx = \sqrt{\frac{\pi}{\alpha}}.$$

During a revolution of period  $T$  occurring between  $t = -T/2$  and  $t = +T/2$ , drag is only really operative near  $t = 0$ . It is neither here nor there

---


$$-\frac{dV}{V} = (2 - \eta)^{-1} \frac{dr}{r} \approx (1 + e)^{-1} \frac{dh}{r} = 0.033,$$

or 3.3%, and we thus justify treating the speed as constant. The ratio of the atmospheric densities between 600 and 200 km altitude is  $10^{-4}$ .

whether a friction-related quantity is integrated over one period, in the range  $[-T/2, +T/2]$ , or over the range  $(-\infty, +\infty)$ . We thus have

$$\begin{aligned} \int_{-T/2}^{+T/2} \exp\left(-\frac{z-z_p}{H}\right) dt &= \int_{-\infty}^{+\infty} \exp\left(-\frac{1}{2} \frac{\mu e}{H r_p^2} t^2\right) dt \\ &= \sqrt{\frac{2\pi H}{\mu e}} r_p, \end{aligned} \quad (6.128)$$

and finally,

$$\Delta_1 V = \sqrt{\frac{\pi}{2}} B \rho_p \sqrt{\mu} \frac{1+e}{\sqrt{e}} \sqrt{H}. \quad (6.129)$$

This is a remarkably simple formula, because it only involves the geometry of the ellipse (through  $e$ ), the scale factor  $H$ , and the mass per unit volume  $\rho_p$  of the atmosphere at perigee. The semi-major axis  $a$ , which enters indirectly through the period  $T$ , and the altitude at perigee, which determines  $\rho_p$ , do not appear explicitly.

The result can be applied as long as the effective drag time near the passage at perigee is small compared with the whole period. This effective drag time  $\Delta t_{\text{eff}}$  is defined by

$$\rho_p \Delta t_{\text{eff}} = \int_{-T/2}^{+T/2} \rho dt. \quad (6.130)$$

With the assumptions made above, calculation leads to

$$\frac{\Delta t_{\text{eff}}}{T} = \sqrt{\frac{H}{2\pi a}} \frac{1-e}{\sqrt{e}}. \quad (6.131)$$

If we set the condition  $\Delta t_{\text{eff}}/T < 0.1$ , with  $H = 50$  km,  $a = 26,500$  km, we obtain the constraint

$$e > 0.03 \quad \Longleftrightarrow \quad (6.129) \text{ is applicable.}$$

This formula is particularly useful for the study of atmospheric braking, a technique for circularising orbits, although more often used on Mars than on the Earth.<sup>19</sup> Indeed, it is with Mars missions in mind that we have set out the above theory. We have compared the resulting values of  $\Delta_1 V$  with those obtained by stepwise numerical integrations using an atmospheric model (MCD-LMD). The error never exceeds 5%.

---

<sup>19</sup>For Earth-orbiting satellites, this method is considered for transforming GTO orbits into LEO orbits, in the case of passenger satellites (which thus have little fuel autonomy) launched with a GEO mission.

## 6.7 Historical Note: First Determinations of the Harmonics $J_n$

It was by monitoring the first satellites (mainly visually, using dedicated telescopes) that astronomers were able to calculate the first coefficients of the zonal spherical harmonics, having first determined the exact orbits. Let us give a brief account of these developments. US astronomers used the Baker–Nunn camera, named after its two inventors (see Fig. 6.5).

### 6.7.1 First Satellite Determination of $J_2$

The “beep-beep” sound emitted by Sputnik-1 came as a surprise to the world. Before the scientific community could react, 1957 $\alpha$  (the name attributed to the satellite with the classification of the day, abandoned since 1 January 1963) had already burnt up in the Earth’s atmosphere.

Measurements only began with Sputnik-2 (1957 $\beta$ ). With 33 visual observations made in the skies of Czechoslovakia between 7 December 1957 and 21 March 1958, the astronomer E. Buchar succeeded in determining the motion of the ascending node of the orbit:

$$\dot{\Omega} = -2.9007 \pm 0.0046 \quad \text{degrees per day .}$$

The metric elements of the satellite were determined to be as follows:

$$a/R = 1.1127 , \quad e = 0.0731 , \quad i = 65.29^\circ .$$

The period and mean motion are also known:

$$T = 99.2 \text{ min} , \quad n = 1.0556 \times 10^{-3} \text{ rad s}^{-1} .$$



FIG. 6.5 : *Baker–Nunn satellite tracking camera telescope. Installation at the Smithsonian Astrophysical Observatory (SAO) at the Woomera base in Australia in January 1958. Credit: NASA, Woomera Space Center.*

Using (6.73), we deduce the value of  $J_2$  to be

$$J_2 = 2.9007/2675.0 = 1.0844 \times 10^{-3} .$$

The flattening  $f$  can be obtained from (3.33), the first of Clairaut's equations:

$$f = \frac{3J_2 + m_a}{2} , \quad (6.132)$$

where  $m_a$  is defined by (3.34) and has known value. Buchar thus obtained

$$\frac{1}{f} = 297.7 \pm 0.3 .$$

Shortly afterwards, refining the results from Sputnik-2, D. King-Hele obtained

$$\frac{1}{f} = 298.1 \pm 0.1 .$$

Estimates of  $1/f$  have barely changed since then, whereas they varied between 293 and 300 prior to 1958 (see Table 2.1).

### 6.7.2 First Satellite Determination of $J_3$

While  $J_2$  is determined from the secular variation of  $\Omega$ , the coefficient  $J_3$  is related to the long-period variation of  $e$ . The first determination of  $J_3$  was made by J.A. O'Keefe from observations of the orbit of Vanguard-1 (1958 $\beta_2$ ). The eccentricity  $e$  varied sinusoidally with a period of about 80 days, corresponding to the cycle of the apsidal line, with duration  $2\pi/\dot{\omega}$  and amplitude  $\Delta e$  given by

$$\Delta e = (42 \pm 3) \times 10^{-5} .$$

At the beginning of the mission, the orbital characteristics were

$$h_p = 654 \text{ km}, \quad h_a = 3,969 \text{ km}, \quad a = 8,681 \text{ km}, \quad e = 0.1090 ,$$

$$i = 34.25^\circ, \quad T = 134.2 \text{ min} .$$

The motion of the perigee is found from  $\dot{\omega} = 4.40^\circ$  per day, implying a cycle of 82 days.

The amplitude of the variation in  $e$  is  $|\Delta_{LP_3} e|$  when we insert  $\omega = 90^\circ$  in (6.94). With  $\Delta_{LP_3} e = \Delta e = 42 \times 10^{-5}$ , we obtain

$$J_3 = -2J_2 \left( \frac{a}{R} \right) \frac{1}{\sin i} \Delta_{LP_3} e = -4.8424 J_2 \Delta_{LP_3} e \approx -2.2 \times 10^{-6} .$$

This is close to  $J_3 = -2.54 \times 10^{-6}$ , the value given in Table 3.2.

### 6.7.3 First Determinations of $J_n$ up to $J_{14}$

In 1963, Y. Kozai used observations of the nine US satellites<sup>20</sup> launched between 1959 and 1962 to determine the first 14 coefficients of the zonal harmonics  $J_n$ . To do this, he neglected short-period variations and assumed that all the long-period variations were modulated by the motion of the perigee, i.e., that they varied as  $\omega$ .

Regarding the metric elements, (6.76) implies

$$e = e_0 + A_e \sin \omega, \quad i = i_0 + A_i \sin \omega, \quad (6.133)$$

where  $A_e$  and  $A_i$  are coefficients depending solely on the metric elements  $a$ ,  $e$ ,  $i$  and the zonal harmonics  $J_n$ , which may therefore be treated as constant over several revolutions. Restricting to order 3,  $A_e \sin \omega$  and  $A_i \sin \omega$  are given by (6.94) and (6.93), respectively.

Regarding the angle elements, starting from (6.77), he added the periodic variation to the secular variation to obtain

$$\Omega = \Omega_0 + \dot{\Omega}t + A_\Omega \cos \omega, \quad (6.134)$$

$$\omega = \omega_0 + \dot{\omega}t + A_\omega \cos \omega. \quad (6.135)$$

Given the theoretical dependence of the coefficients  $A_e$ ,  $A_i$ ,  $A_\Omega$ , and  $A_\omega$  on the first 14  $J_n$ , these observations provided dozens of equations that could be solved numerically.

## 6.8 Historical Note: Success in Calculating Perturbations

Two astronomers, Clairaut in the eighteenth century and Le Verrier in the nineteenth, were particularly successful in calculating perturbations, while Einstein solved the “mystery” of the advance of the perihelion of the planet Mercury in the twentieth century.

### 6.8.1 The Delayed Return of Halley’s Comet

In 1705, in *Cometographia*, the astronomer Halley<sup>21</sup> described the orbits of 24 comets. Applying the new theory by Newton, he calculated their orbital

---

<sup>20</sup>These satellites had orbits with a wide range of inclinations, from 28° to 95°. They were, in chronological order: 1959 $\alpha$  (Vanguard-2), 1959 $\eta$  (Vanguard-3), 1960 $\iota_2$  (rocket which launched Echo-1), 1961 $\nu$  (Explorer-12), 1961 $o$  (Transit-4A), 1961 $\alpha\delta_1$  (Midas-4), 1962 $\alpha\epsilon$  (Discoverer-34), 1962 $\beta\mu$  (ANNA-1B), 1962 $\beta\nu$  (Relay-1). All these orbits were determined by tracking them with Baker–Nunn cameras.

<sup>21</sup>*Edmund Halley* (1656–1742) was a British astronomer. Although he is remembered for his discovery of the periodicity of a comet, Halley was an all-round scientist. He visited Saint Helena to draw up the first map of the southern skies. During his travels on the ocean, he

elements and asserted that several comets with the same elements were in fact one and the same comet, having a period of 76 years. After a passage in 1682, he predicted a further passage in 1758, and the comet was later named after him.

As the time of the predicted return drew close, the whole astronomical community was on tenterhooks. In 1757, the astronomer mathematician Clairaut suggested that Jupiter might significantly perturb the comet. He wanted to calculate the effects<sup>22</sup> before the date announced, and hence acquired the services of two young astronomers, Jérôme Lalande<sup>23</sup> and Nicole-Reine Lepaute, recognised for their calculational skills. After exhausting work “against the clock”, they concluded that, as a result of Jupiter and Saturn’s gravitational perturbations, the comet would not reach its perihelion in November 1758, as the now deceased Halley had predicted, but rather in April 1759 (with an error of 1 month). In the end, the comet returned to perigee on 13 March 1759.

These calculations, which Clairaut presented in *Théorie du mouvement des comètes* (1760), convincingly confirmed Newton’s theory. It should be noted that Lagrange only published his theory of perturbations some 28 years later.

## 6.8.2 The Discovery of Neptune by Le Verrier

The most spectacular application of the theory of perturbations was the discovery of a new planet, Neptune, by Le Verrier.<sup>24</sup> The planet Uranus had been discovered in 1781 by Herschel. In 1844, Le Verrier studied its orbit (over an arc of 270°: it had a period of 84 years, and had been discovered

---

produced a detailed chart of the magnetic declination, measured the period of a pendulum at different latitudes, investigated ocean currents, and studied the distribution of winds to produce a forerunner of the weather chart. Halley also translated several books of geometry by Apollonius of Perga from Arabic, the original Greek versions having been lost.

<sup>22</sup> “Even if Clairaut had wished to follow Halley’s example in assuming that one might neglect the effects of Jupiter on the comet during the years when these bodies were widely removed from one another, it did not take him long to understand that such a position was untenable. Indeed, the first calculations showed that, even when the comet is far from Jupiter, its orbit is nevertheless disturbed, especially by the action of Jupiter on the Sun; for by displacing the Sun by a small amount, Jupiter gives the orbit of the planet a different focus. Clairaut determined all these effects with great elegance.” Pierre Brunet, *La vie et l’œuvre de Clairaut*, 1952.

<sup>23</sup> *Joseph Jérôme Lefrançois de Lalande*, or *Jérôme Lalande* for short (1732–1807), was a French astronomer. He was spotted very early on for the accuracy of his observations, e.g., his measurement of the parallax of the Moon (1751), and the parallax of the Sun during the transit of Venus in 1761 and 1769. He also studied the rotation of the Sun and the shape of the Earth. He was famous in his own time, perhaps even the first high profile astronomer, noted for his skills as a teacher and populariser of science. And he was also an outspoken atheist, declaring: “We know nothing. We believe in miracles and witchcraft, we are afraid of thunder and spiders, and all we think to do is believe in God.”

<sup>24</sup> *Urbain Le Verrier* (1811–1877) was a French astronomer who remains famous for his mathematical discovery of the planet Neptune. He subsequently devoted himself to the theory of the Solar System and the calculation of ephemerides. See also the note on Delaunay.

only 63 years earlier<sup>25</sup>) and detected a slight disagreement in the calculations. He deduced that the perturbation due to a more distant and as yet unknown planet must be added to the effects produced by the known planets.

He thus set out to do the perturbation calculations under the following hypotheses concerning the “disturbing” planet:

- It moves in the plane of the ecliptic.
- The semi-major axis of its orbit is given by the so-called Titius–Bode law (with  $n = 7$ , we have  $a = 38.8$  a.u.).

The other orbital elements and the mass were treated as unknown quantities. Their values were obtained by solving a system of 33 equations, each corresponding to one observation.

In August 1846, he announced that he had located the planet, specifying  $a = 36.15$  a.u.,  $e = 0.108$ , and distance from the Sun = 33.06 a.u. (for the Titius–Bode theory and the orbital elements of Neptune, see Chap. 16). He provided accurate coordinates and, on 23 September 1846, the German astronomer Galle claimed to have identified a new planet at precisely the point indicated, using his telescope at the Berlin observatory.<sup>26</sup> It was named Neptune soon afterwards.

Le Verrier’s success<sup>27</sup> drew astronomy, and science in general, into the limelight. Arago recorded these events with the famous remark: “M. Le Verrier found a new planet at the nib of his pen.” But even Le Verrier was unable to explain the advance of the perihelion of Mercury with the theory of perturbations, as we shall see below.

### 6.8.3 Advance of the Perihelion of Mercury

In 1859, Le Verrier studied the effects of perturbations on the planet Mercury using observations made since 1697 (mainly 397 meridian observations made at the Paris observatory between 1801 and 1842). Mercury’s orbit is

---

On 14 November 1854, a hurricane destroyed part of the French and allied navies in the Crimean war. Le Verrier realised that this storm had crossed Europe from west to east and set up the first network of weather stations in 1855.

<sup>25</sup>In fact, Le Verrier also used observations made earlier, for astronomers had realised that the planet Uranus had already been spotted in the sky as early as 1690, and taken for a star. For his calculations, he used 7 observations made prior to 1781 and 26 made afterwards.

<sup>26</sup>Tisserand devoted the whole of Chap. XXIII in Vol. 1 of his *Mécanique céleste* to the discovery of Neptune by Le Verrier, ending with the declaration: “M. Galle observed the planet at just 52’ from the assigned position.” Note that, on 2 July 2011, Neptune had completed a full revolution, i.e., 60,182 days after 23 September 1846, whence the planet was then located at precisely the position where Galle had first observed it.

<sup>27</sup>The astronomer J.C. Adams claimed to have obtained the same results simultaneously. However, this was never clearly confirmed. The whole episode seems to be yet another story of rivalry between British and French scientists.



Planet	Perturbation
Venus	277.8
Earth	90.0
Mars	2.5
Jupiter	153.6
Saturn	7.3
Other	0.2
Total	531.4

Category	Perturbation
Planets	531.4
Equinoxes	5,025.6
Total	5,557.0
Observed	5,599.7
Difference	42.7

TABLE 6.5 : Causes of the precession of the perihelion of Mercury and values of the perturbations in seconds of arc per century.

highly eccentric, with  $e = 0.2056$ . Newtonian mechanics can predict the motion of its perihelion (apsidal precession) due to the perturbing effects of the other planets. By taking into account all these planetary perturbations, Le Verrier arrived at a value of  $531''$  per century. But measurements gave  $574''$ , leaving a discrepancy of  $43''$ . The US astronomer Simon Newcomb obtained the same results in 1882.

To fully appreciate the accuracy of the measurements at the time (see Table 6.5), it is instructive to compare these  $43''$  with the precession of the equinoxes of the Earth, which is some  $5,026''$  per tropical century (for the value measured from Earth is the sum of all these effects).

In 1889, F. Tisserand ended his monumental work *Traité de Mécanique Céleste* with the statement that the advance of the perihelion of Mercury was the greatest enigma of the day. He refuted all other explanations that had been put forward:

- Le Verrier had tried to explain the discrepancy by the presence of a hypothetical planet between Mercury and the Sun. A name had already been found for it: Vulcan.
- Newcomb thought the disagreement might be due to the non-sphericity of the Sun.
- Hall had even called the laws of gravity into question, suggesting an attractive force going rather as  $r^{-2.000000151}$ .

One sees the extent to which this unexplained discrepancy was an enigma to the most brilliant astronomers. F. Tisserand concludes with the words:

One might think that the attractions between celestial bodies could only be transmitted over distance through the mediation of some kind of medium. But as yet we know nothing of these modes of transmission.

It was Einstein<sup>28</sup> who, in 1916, came up with the explanation, applying his new theory of general relativity. Expressing the equation of motion in this context (the geodesic equation for planetary trajectories, as determined by the Schwarzschild metric), the classical equation (4.24) is replaced by

$$\frac{d^2u}{d\theta^2} + u = \frac{\mu}{C^2} + \frac{3\mu}{c^2}u^2, \quad (6.136)$$

where  $C$  is the angular momentum per unit mass and  $c$  is the speed of light. Equation (6.136) is a differential equation for the Binet variable  $u$ , but it has no analytic solution. However, we know that the desired solution for  $u$  is very close to  $u_0$ , the solution of (4.24). We may thus replace  $u$  by  $u_0$  in the extra term in (6.136). Considering small values for the eccentricity of the orbit, we write

$$u = \frac{\mu}{C^2} [1 + e \cos(\theta - \theta_0)], \quad u^2 \approx \frac{\mu^2}{C^4} [1 + 2e \cos(\theta - \theta_0)],$$

whence (6.136) becomes

$$\frac{d^2u}{d\theta^2} + u = \frac{\mu}{C^2} \left\{ 1 + \varepsilon [1 + 2e \cos(\theta - \theta_0)] \right\}, \quad (6.137)$$

with the dimensionless number  $\varepsilon$  defined by

$$\varepsilon = 3 \left( \frac{\mu}{cC} \right)^2, \quad \varepsilon \ll 1. \quad (6.138)$$

We seek  $u$  in the form

$$u = \frac{\mu}{C^2} \left\{ 1 + e \cos[(1 - \varepsilon)\theta - \theta_0] \right\}, \quad (6.139)$$

and then check that it does indeed solve (6.137). The desired trajectory is thus given by

$$r(\theta) = \frac{a(1 - e^2)}{1 + e \cos[(1 - \varepsilon)\theta - \theta_0]}, \quad (6.140)$$

where  $r = 1/u$ . This should be compared with (4.42).

---

<sup>28</sup> *Albert Einstein* (1879–1955) was a German (then Swiss, then American) physicist. He entered upon the academic scene with brilliance in 1905, his *annus mirabilis*, with three fundamental, and indeed revolutionary, publications: Brownian motion (the size of molecules), the photoelectric effect (the particle nature of light), and the special theory of relativity (modification of Newtonian mechanics and the equivalence of matter and energy). The three papers appeared in *Annalen der Physik*, which was edited at the time by Max Planck. From 1915, he developed his theory of gravity and the general theory of relativity. The field equations are differential equations which describe the behaviour of the gravitational field, represented by the spacetime metric, in terms of the distribution of matter and energy. Euclidean space must be replaced by a Riemannian space that is “curved” by the masses located within it. Einstein’s theories form the basis of modern physics.

Two successive passages at perihelion determine the polar angles  $\theta_1$  and  $\theta_2$ . We thus have

$$\Delta\theta = \theta_2 - \theta_1 = \frac{2\pi}{1 - \varepsilon} \approx 2\pi(1 + \varepsilon) = 2\pi\varepsilon [2\pi].$$

With (4.27), we have  $\varepsilon = 3\mu/c^2p$  and hence,

$$\Delta\theta = \frac{6\pi\mu}{a(1 - e^2)c^2}, \quad (6.141)$$

which is denoted by  $\Delta_1\omega$  in (6.12).

For Mercury,<sup>29</sup> we obtain

$$\Delta_1\omega = 5.0344 \times 10^{-7} \text{ rad.}$$

Since Mercury completes 414.2 revolutions per century, we have finally

$$\Delta\omega = 414.2\Delta_1\omega = 2.0853 \times 10^{-7} \text{ rad} = 43''.$$

Current measurements give the discrepancy as

$$\Delta\omega = 42.980 \pm 0.002 \text{ arcsec.}$$

## 6.9 Astronomical Note: Perturbations and the Solar System

### 6.9.1 Stability of the Solar System

#### Invariability of the Semi-Major Axes of the Planetary Orbits

Applying the newly established universal law of gravitation in 1687, Newton observed that each planet whose orbit was determined by the Sun's attraction would necessarily attract every other planet, even though these attractions might be very weak. He noted that, with so many perturbations around, irregularities will be "apt to increase, till this System wants a Reformation". He clearly felt that some divine intervention would be required from time to time to put things straight once more.

With the help of observations made by the Chaldeans in the second century BC and transmitted by Ptolemy, Halley calculated that Jupiter was moving closer to the Sun, while Saturn was moving away. In 1752, Euler, and in 1774,

---

<sup>29</sup>The advance of the perihelion also occurs for other planets, but it is all the weaker as the planet is more remote from the Sun (whence it moves less quickly in a Copernican frame). For example, we observe  $8''.63$  per century for Venus,  $3''.84$  for the Earth, and  $1''.35$  for Mars. For the Moon, in its motion relative to the Earth, it is  $2''$  per century. All these values can be calculated using (6.12).

Lagrange also tackled this problem. Their results were contradictory, and in fact both their calculations were erroneous, but they nevertheless marked the beginnings of perturbative investigations.

Laplace<sup>30</sup> returned to these calculations in 1776. He showed that the semi-major axis of each orbit was constant:  $a$  has no secular term, at least not in the first order expansion of the perturbations. He deduced that the Solar System would be stable for a million years. He calculated that the quasi-resonance 5:2 between the mean motions of Jupiter and Saturn would cause an oscillation of the longitude of Saturn by  $46'50''$ , with a period of 900 years, and thus recovered the values given by Halley. For Laplace, this stability of the major axes was a definitive confirmation of Newton's laws (Fig. 6.6).

In 1890, Poisson showed that  $a$  does not have a second order secular term either.

### Stability of the Solar System

In 1856, Le Verrier considered that, if Laplace's results were to remain valid over very long times, it would be necessary to consider higher order expansions. However, Poincaré<sup>31</sup> understood that the method suggested by Le Verrier was not correct. In his thesis presented in 1879, he showed that the terms of the series expansions used in the perturbative method do not

---

<sup>30</sup> *Pierre Simon de Laplace* (1749–1827) was a French mathematician, astronomer, and physicist. Noting that all the observable bodies in the Solar System rotate in the same direction (he included the 29 revolutions or rotations of planets and moons, and even the rotation of the Sun itself), and taking the cue from Herschel's observations of the nebulas, he devised a first cosmogonic system in *Exposition du système du Monde* (first edition in 1796 and fifth in 1824). According to this view, the Solar System and all other objects in the universe were produced by the condensation of a primordial nebula, the preferred hypothesis even today. During cooling, the rotation of this nebula would have generated a succession of rings in the same plane (the ecliptic), and these would have given birth to the planets and their moons, with the central nucleus becoming the Sun. In his *Mécanique céleste* (first edition in 1798 and sixth in 1825), he revisited all the theories elaborated since Newton. Victor Hugo had this to say (V. Hugo, *Choses vues*, 1887):

M. Arago had a favourite anecdote. When Laplace published his *Mécanique céleste*, he would say, the Emperor Napoleon summoned him. The emperor was furious.

— What, he cried when he saw Laplace, you make a whole system of the world, you list the laws of all creation, and yet in your book you speak not once of the existence of God!

— Sire, replied Laplace, I had no need of that hypothesis.

In the two centuries from Kepler to Laplace, the relationship between astronomers and the divine order had changed considerably. Laplace also established fundamental results in mathematics (harmonic functions, differential equations, probabilities) and in physics (electromagnetism, thermodynamics).

<sup>31</sup> *Henri Poincaré* (1854–1912) was a French mathematician. He studied the changes of variables that preserve the canonical form of the equations of mechanics (with the Jacobi formulation). He thus arrived at quite novel results in *Sur le problème à trois corps et les équations de la dynamique* (1889). He further developed this work in *Les méthodes nouvelles de la mécanique céleste* (1899).

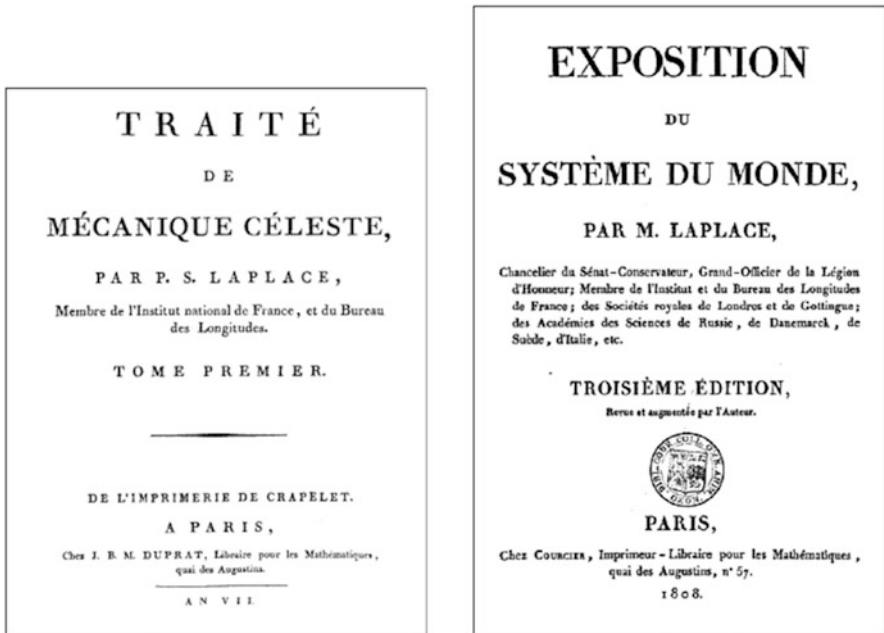


FIG. 6.6 : Laplace's two fundamental works on astronomy.

converge over the time lapse under consideration. For a dynamical system involving three or more bodies, he showed that the solution depends strongly on the initial conditions—in modern terms it is chaotic (chaos theory). Then around 1960, the problem was investigated in the light of the Kolmogorov–Arnold–Moser (KAM) theory.

Since 1990, J. Laskar at the Paris observatory has been using methods adapted to the increasing performance of computer calculations. For his numerical simulations, he considers initial conditions<sup>32</sup> that differ very slightly from one another. In his last report (2010), he showed that in 99 % of cases the Solar System will remain stable for 5 billion years (5 Gyr), i.e., without collisions. In 1 % of cases, there is some form of instability: through its increased eccentricity, Mercury collides with the Sun or Venus and thereby destabilises the orbits of all the inner planets (as far out as Mars).

The Solar System had a major period of instability just after its formation, during about the first billion years, no doubt due to the migrations of the giant planets. Then, once the eight major planets were in place, it became practically stable.

<sup>32</sup>Initial conditions refer to the positions of the bodies making up the Solar System at the present time. J. Laskar has considered 2,500 very similar sets of conditions. He has shown that the error in the position is multiplied by a factor of 10 every 10 million years (10 Myr). For example, an error of 15 m becomes an uncertainty of 1,500 km after 50 Myr and 1 a.u. (astronomical unit) after 100 Myr.

### 6.9.2 Precession of the Equinoxes

A simplified model of the terrestrial ellipsoid is given by a sphere with an equatorial bulge. The mass of this bulge, uniformly distributed around the equator, is such that the moments of inertia  $I_x$  with respect to an equatorial diameter and  $I_z$  with respect to the polar axis are the same as for the ellipsoid. This is a standard method for calculating the precession of the equinoxes.

If the Earth were a sphere composed of homogeneous concentric layers, the gravitational effect exerted by the bodies of the Solar System, and in particular the Moon and Sun, would reduce to a force through its center. The Earth's motion would then be a uniform motion around a fixed axis. The equatorial plane would be fixed relative to the plane of the ecliptic. The straight line at the intersection of these two planes, the line of nodes (called here the line of the equinoxes), would thus be fixed with respect to a Copernican frame.

Let us consider the bulging Earth model. As the precessional motion here is very slow compared with the Moon's revolutions, or the apparent revolutions of the Sun around the Earth, we may replace the Moon and the Sun by an equivalent mass distribution along their orbits, considered as circular, in the plane of the ecliptic (which is an approximation for the Moon). This is Gauss' method.<sup>33</sup> It can be shown (using Lagrange and Poisson's theory of motion with the gyroscopic approximation) that the moment of the gravitational forces exerted by the mass of the Sun and Moon on this equatorial bulge causes a motion of the Earth's axis of rotation, whilst the angle between the equatorial and ecliptic planes remains fixed. This angle  $\varepsilon$  is the obliquity. The line of nodes moves in the retrograde direction (opposite to the direction of the Earth's rotation). This motion, known as the precession of the equinoxes, is very slow on the human time scale: one round trip every 25,800 year, or  $50''.29$  per year, with the Moon contributing  $34''$  and the Sun  $16''$ . The angular momentum and hence the rate of precession is proportional to the difference  $I_x - I_z$  between the moments of inertia, related to the  $J_2$  term. The rate of precession is also proportional to  $\cos \varepsilon$ .

The precession of the equinoxes has been known since ancient times, thanks to Hipparchos.<sup>34</sup>

---

<sup>33</sup>In 1818, Gauss published a monograph on the secular perturbations of a planet's motion when it is affected by another planet. The method consists in replacing the perturbing body by a torus, distributing the matter of the body along its trajectory.

<sup>34</sup>*Hipparchos of Nicaea* (second century BC), ὁ Ἱππάρχος, οὐ, was a Greek astronomer. By his observations made in Rhodes, he was the first astronomer to make truly accurate measurements of the positions of the stars, specifying their positions on the celestial sphere using meridians and parallels. He introduced into Greece the Babylonian idea of dividing the circle into degrees, minutes, and seconds. He may be considered as the inventor of trigonometry. He invented the stereographic projection. He discovered the precession of the equinoxes by comparing his measurements of stellar positions with those made by Timocharis a century and a half earlier, and also with those made much earlier by the Babylonians. The works of Hipparchos did not reach us directly, but were mentioned by the geographer Strabo and the astronomer Ptolemy.

## Precession of the Line of Nodes of a Satellite

With the same type of argument, one can calculate approximately the precessional motion of the circular orbit of a satellite. Consider a satellite in circular orbit around the Earth with its equatorial bulge. We distribute the mass of the satellite uniformly around its trajectory (the rate of precession is roughly one ten thousandth of the orbital angular speed of the satellite) and calculate the moment of the gravitational forces between these two rings. We then show that the orbit undergoes a precessional motion in which the angle between the orbital plane of the satellite and the equatorial plane of the Earth (the inclination  $i$  of the satellite) remains constant. We calculate the moment of the gravitational forces, then the rate of precession  $\dot{\Omega}$ , which is proportional to  $I_x - I_z$ , hence to  $J_2$  and  $\cos i$ .

### 6.9.3 The Earth as a Satellite

#### Orbital Elements of the Earth

One can use the analogy between an artificial satellite in orbit around the Earth and the Earth viewed as a satellite of the Sun. But let us first note a basic difference between the two problems:

- The artificial satellite is considered as a point with respect to the Earth and its Keplerian motion is mainly perturbed by the flattening of the attracting body (via the  $J_2$  term of the Earth).
- As a satellite of the Sun, the Earth cannot be treated as a point, but must be considered as a rotating solid, whose polar axis of rotation defines the equatorial plane, and whose non-spherical nature (the  $J_2$  term of the Earth) induces perturbations. The Sun is spherical.<sup>35</sup> To these perturbations, one must add those due to the Moon.

The Keplerian orbital elements of the Earth are as follows:

- $a$  is the semi-major axis of the Earth's orbit,  $a_S = 1$  astronomical unit.
- $e$  is the eccentricity of the orbit,  $e = 0.0167$ .
- $i$  is represented here by the obliquity  $\varepsilon$ , the angle between the plane of the ecliptic (orbital plane of the Earth) and the equatorial plane of the Earth.
- $\Omega$  is the angle between the line of nodes (the line of the equinoxes, direction of the vernal point) and an arbitrary origin, fixed relative to the stars.
- $\omega$  is the angle between the direction of the vernal point and the perihelion (at the present time, the Earth passes through the vernal point on 21 March and the perihelion on 3 January, dates of the Gregorian calendar, accurate to within 1 day).
- The effect on  $M - nt$  is not considered here.

---

<sup>35</sup>Current theories give the Sun's  $J_2$  value at about  $2 \times 10^{-7}$ .

## Variations of the Orbital Elements

Perturbations affect these elements as shown schematically in Fig. 6.4. Short-period variations are neglected:

**Metric Elements.** For these elements, there is no secular variation:

- Invariability of the semi-major axis  $a$  (stability of the major axes, studied by Laplace, Poisson, Poincaré, as discussed above).
- Long-period variation for  $e$  and  $\varepsilon$ .  $e$  varies between 0.005 and 0.050, with a period of 1,00,000 year and  $\varepsilon$  varies between  $22^\circ$  and  $25^\circ$ , with a period of 40,000 year.

**Angle Elements.** For these elements, there are secular variations for  $\Omega$  and  $\omega$ .  $\Omega$  has a retrograde cycle<sup>36</sup> of 25,800 year, or  $\dot{\Omega} = -50''.29$  per year, called precession of the equinoxes.  $\omega$  has a prograde cycle of 110,000 years, or  $\dot{\omega} = 11''.06$  per year.

These variations are shown schematically in Fig. 6.7 (upper) for each orbital element, noting the value of the period or cycle as appropriate. Time is shown on the horizontal axis in units of kiloyears (1 kyr =  $10^3$  year). The zero time is chosen arbitrarily at the moment when each element has its average value.

## Milankovitch Paleoclimatology Theory

The Milankovitch theory considers the combination of these periods (100 and 40 kyr) and cycles (26 and 110 kyr) in order to explain the succession of hot and cold periods (ice ages) of the Earth's past climate. Taken up in 1980 by A. Berger, this theory obtained a striking experimental confirmation with the analysis of air bubbles trapped in the Greenland and Antarctic ice over a period of 8,00,000 year in samples taken to a depth of 3,260 m.

In the Milankovitch theory, the main variable is the climate parameter  $P$  defined by

$$P = e \sin \omega_0 , \quad (6.142)$$

where  $\omega_0$  is the position of the perigee relative to the spring equinox (ascending node or vernal point):

$$\omega_0 = \omega - \Omega . \quad (6.143)$$

Note that the two angles  $\omega$  and  $\Omega$  are defined in different planes making an angle  $i = \varepsilon$  (the obliquity) to one another. Their difference  $\omega_0$ , called the

---

<sup>36</sup>A cycle is the length of time at the end of which the relevant point on the orbit (the vernal point or the perigee) returns to the same position relative to a Copernican frame. The cycle relates to a secular variation. For long- or short-period variations, we speak of the period.



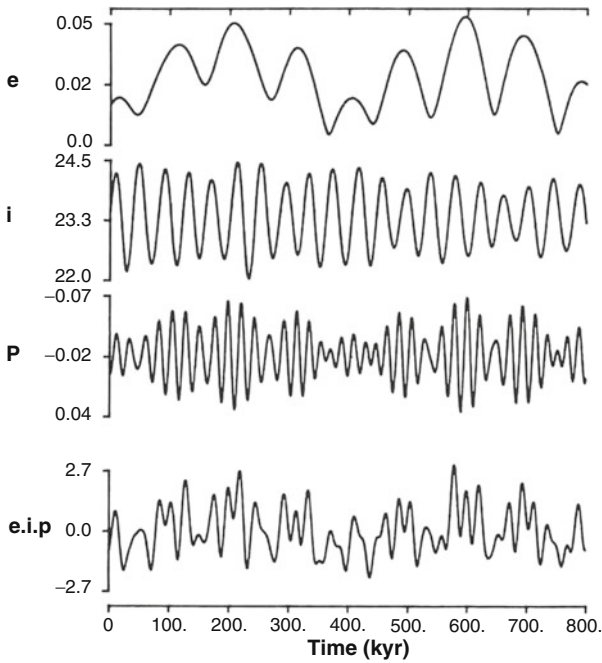
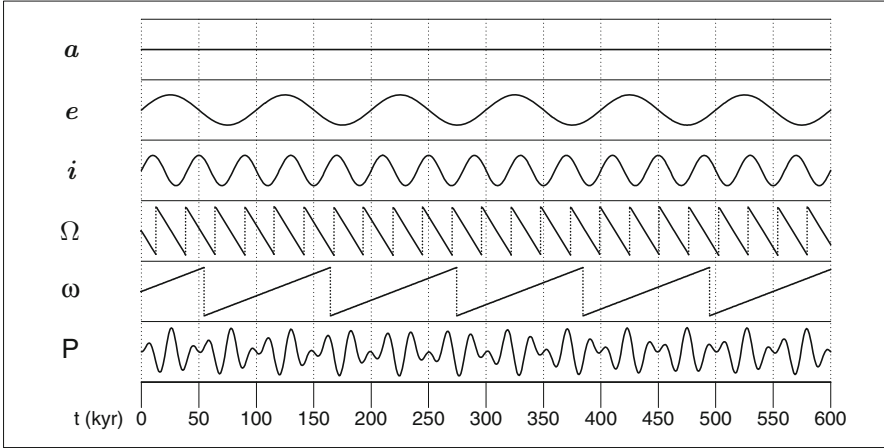


FIG. 6.7: *Milankovitch paleoclimatology theory*. Upper: *Highly simplified diagram showing the variations of the Earth's orbital elements over time  $t$  (in kiloyears):  $a$  (no variation),  $e$  and  $i$  (periodic variation),  $\Omega$  and  $\omega$  (secular variation).  $P$  is the climate parameter. Each element is taken to have its average value at time 0.* Lower: *Values obtained by accurate astronomical calculations. Variations of the metric elements  $e$  (eccentricity) and  $i$  (inclination), variation of  $P$  (climate parameter), and combination of the three variations. Horizontal axis: Time before present (kyr).* Credit: T.J. Crowley and G.R. North.

climatic precession, is the significant element when considering the behaviour of the climate.

The rate of climatic precession  $\dot{\omega}_0$  is thus given by the algebraic difference between the two rates of secular variation  $\dot{\Omega}$  and  $\dot{\omega}$ :

$$\dot{\omega}_0 = \dot{\omega} - \dot{\Omega} = 11''.06 + 50''.29 = 1'1''.35 \text{ per year}, \quad (6.144)$$

which corresponds to a cycle of 21 kyr. Figure 6.7 (lower) shows the accurately calculated variations in  $e$ ,  $i$ , and the parameter  $P$ .

## 6.10 Appendix: Astronomical Constants

### 6.10.1 Systems of Units

#### International System of Units (SI)

The international system of units, known as SI units, is built upon the following base units for seven physical quantities: length (meter, m), mass (kilogram, kg), time (second, s), electric current (ampere, A), thermodynamic temperature (kelvin, K), quantity of matter (mole, mol), and luminous intensity (candela, cd). Here we list the definition and year of application of the unit for each of the first three quantities (the only ones relevant to celestial mechanics):

- The unit of length, the meter, is the distance travelled by light in vacuum<sup>37</sup> during a time lapse of  $1/299,792,458$  s (1983).
- The unit of mass, the kilogram, is the mass of the International Prototype Kilogram, made from a platinum–iridium alloy and stored at the International Bureau of Weights and Measures (Bureau International des Poids et Mesures BIPM) in Paris (1889, 1901).
- The unit of time, the second, is defined as the duration of 9,192,631,770 periods of the radiation corresponding to the transition between the two hyperfine levels of the ground state of the caesium 133 atom (1967).

#### Astronomical System of Units

The base units of the astronomical system, as recommended by the International Astronomical Union (IAU), are as follows:

- The unit of length is the astronomical unit (a.u.), a conventional unit of length equal to exactly 149,597,870,700 m. This value has been chosen to be consistent with that in the IAU System of astronomical constants in use since 2009. This definition has to be used with all time scales such as TCB,

---

<sup>37</sup>Time can now be measured much more accurately than length. For this reason, it was decided to define the unit of length on the basis of a time measurement. The speed of light is thus given now as a definite value, with zero error by definition.

TDB, TCG, TT, etc. The unique symbol to be used for the astronomical unit is a.u. (IAU 2012 resolution B2).<sup>38</sup>

- The unit of mass is the mass of the Sun  $M_{\text{S}}$ .
- The unit of time is the day (d).

The correspondence between these and SI units is as follows:

$$1 \text{ a.u.} = 1.495978707 \times 10^{11} \text{ m},$$

$$1 M_{\text{S}} = 1.9889 \times 10^{30} \text{ kg},$$

$$1 \text{ d} = 86,400 \text{ s}.$$

Auxiliary time units are the Julian year, equal to 365.25 days, and the Julian century, equal to 36,525 days. The length of the year or century is not related to the Gregorian calendar. The length of the day is not related to the rotation of the Earth, which is not strictly uniform.

## 6.10.2 Astronomical Constants

Table 6.6 lists the IAU 2009 constants, including changes to the astronomical unit made in IAU 2012. We have only mentioned constants used in this book.

**Note.** For some of these constants relating to geodesy, such as  $R_{\text{e}}$ ,  $J_2$ , or  $\mu$ , there is a very slight difference between these values and the ones used in the geopotential models.

## 6.10.3 Time Scales

### Definitions of Time Scales

The following is taken from the Standards of Fundamental Astronomy (SOFA) document on time scales, published by the IAU. Several time scales play an important role in astronomy<sup>39</sup>:

- TAI (International Atomic Time): the official timekeeping standard.
- UTC (Coordinated Universal Time): the basis of civil time.
- UT1 (Universal Time): based on Earth rotation.
- TT (Terrestrial Time): used for Solar System ephemeris look-up.

---

<sup>38</sup>The old definition of the astronomical unit was that length for which the Gaussian gravitational constant  $k$  takes the value of 0.017,202,098,95 when the units of measurements are the astronomical unit of length, mass, and time. The dimensions of  $k^2$  are those of the constant of gravitation  $G$ , i.e.,  $\text{L}^3\text{M}^{-1}\text{T}^{-2}$ . Equivalently, it is the radius of an unperturbed circular Newtonian orbit about the Sun of a particle having infinitesimal mass, moving with an angular frequency of 0.017,202,098,95 radians per day.

<sup>39</sup>For the notation and abbreviations, see the appendix in Sect. 3.6.

Quantity	Value	Uncertainty	Unit
Natural defining constants			
Speed of light ( $c$ )	$2.99792458 \times 10^8$	Defined	$\text{m s}^{-1}$
Auxiliary defining constants			
Astronomical unit (a.u.)	149,597,870,700	Defined	m
$1 - \text{dTT}/\text{dTTCG}$ ( $L_G$ )	$6.969290134 \times 10^{-10}$	Defined	–
$1 - \text{dTDB}/\text{dTTCB}$ ( $L_B$ )	$1.550519768 \times 10^{-8}$	Defined	–
ERA at J2000.0 ( $\vartheta_0$ )	0.7790572732640	Defined	Rev
Rate of advance ERA	1.00273781191135448	Defined	$\text{Rev d}^{-1}$
Natural measurable constants			
Cst. of gravitation ( $G$ )	$6.67428 \times 10^{-11}$	$6.7 \times 10^{-15}$	$\text{m}^3 \text{kg}^{-1} \text{s}^{-2}$
Body constants			
Helioc. grav. cst. ( $GM_S$ )			
• [TCB-compatible]	$1.32712442099 \times 10^{20}$	$1.0 \times 10^{10}$	$\text{m}^3 \text{s}^{-2}$
• [TDB-compatible]	$1.32712440041 \times 10^{20}$	$1.0 \times 10^{10}$	$\text{m}^3 \text{s}^{-2}$
E. equator. radius ( $R_e$ )			
• [TT-compatible]	6,378,136.6	0.1	m
Dynamical form ( $J_2$ )	$1.0826359 \times 10^{-3}$	$1 \times 10^{-10}$	–
Geoc. grav. cst. ( $GM$ )			
• [TT-compatible]	$3.986004415 \times 10^{14}$	$8 \times 10^5$	$\text{m}^3 \text{s}^{-2}$
Potential of the geoid	$6.26368560 \times 10^7$	$5 \times 10^{-1}$	$\text{m}^2 \text{s}^{-2}$
E. ang. velocity ( $\varpi$ )			
• [TT-compatible]	$7.292115 \times 10^{-5}$	–	$\text{rad s}^{-1}$
Initial values			
Obliquity of the ecliptic at J2000.0 ( $\varepsilon_{\text{J2000}}$ )	$8.4381406 \times 10^4$ $= 23^\circ 26' 21''.406$	$1 \times 10^{-3}$ 0.001''	" –

TABLE 6.6 : IAU 2009 system of astronomical constants. The table lists the name of the quantity, the value in SI units (unless stated otherwise), and the uncertainty, which is given in the same units as the value. Abbreviations: ERA: Earth rotation angle; helioc., geoc. grav. cst.: heliocentric, geocentric gravitational constant;  $\varpi$ : nominal mean angular velocity of Earth. Note: for the rate of advance of ERA,  $\text{d}\vartheta/\text{d}UT1$ , the unit is revolution per UT1-day.

- TCG (Geocentric Coordinate Time): used for calculations centered on the Earth in space.
- TCB (Barycentric Coordinate Time): used for calculations beyond Earth orbit.
- TDB (Barycentric Dynamical Time): a scaled form of TCB that keeps in step with TT on average.

**Atomic Time: TAI.** TAI is a laboratory time scale, independent of astronomical phenomena. It is realized through a changing population of about 200 high-precision atomic clocks.

**Solar Time: UT1 and UTC.** UT1 is defined through its relationship with the Earth rotation angle (the modern equivalent of mean solar time). Because the Earth's rotation rate is slightly irregular, for geophysical reasons, and is gradually decreasing, the UT1 second is not precisely matched to the SI second. In fundamental physics, the TAI second is used, but to point a telescope, UT1 is used. UTC is a compromise between the demands of precise timekeeping and the desire to maintain the current relationship between civil time and daylight.

The origin of TAI is taken equal to UT1 on 1 January 1958. As a clock, the Earth has got behind the accumulated atomic time by some 35 s (as of 2013). When TAI was adopted, it was decided that the unit of time of the UTC scale would be the TAI second, but that UTC should not be allowed to drift away indefinitely from the time determined by the Earth's rotation. It was thus decided that, while running with the TAI second, UTC should be shifted by 1 s whenever necessary, in such a way that its difference from UT1 should never exceed 0.9 s:

$$\text{TAI} - \text{UTC} = n \text{ seconds}, \quad n \text{ integer}, \quad (6.145)$$

$$\text{UT1} - \text{UTC} \leq 0.9 \text{ s}.$$

**Dynamical Time Scales: TT, TCG, TCB, and TDB.** Terrestrial time (TT) is the time scale used for geocentric ephemerides. Its unit of time is the SI second on the geoid, and TT can thus be deduced from TAI by a simple fixed time shift:

$$\text{TT} = \text{TAI} + 32.184 \text{ s}. \quad (6.146)$$

Relativity theory and today's observational accuracy require a distinction to be made between the dynamical time scales: coordinate time scale (of 4D spacetime) and proper time scale.

Geocentric coordinate time (TCG), related to the center of the Earth, differs from terrestrial time (TT) by a secular term:

$$\text{TCG} - \text{TT} = L_G(J - 2443144.5) \times 86,400 \text{ s}, \quad (6.147)$$

where  $J$  is the Julian day (JD). 1 January 1977, 0 h, corresponds to  $\text{JD} = 2,443,144.5$ . The coefficient  $L_G$  is defined in Table 6.6. The value of this term, which represents the influence of the geopotential and the daily rotation of the Earth on the flow of time, is evaluated in Chap. 14 (see the appendix in Sect. 14.11). This secular variation leads to a drift of 2.2 s per century.

The barycentric time scales TCB and TDB are not relevant to this book.

## Historical Note on Time Scales

Prior to 1960, the definition of the second was based on the Earth's rotation: one mean solar day was equal to 86,400 s. The time scale was Universal Time (UT). Between 1960 and 1967, to get around the fact that there were irregularities in the Earth's rotation, the orbital motion of the Earth was chosen to define the second, which thus became a fraction of the tropical year 1900. This time scale was Ephemeris Time (ET).

The year 1967 was historically important in this respect, because it was at this point that the definition of time left the field of astronomy to be taken over by the world of physics. The second was defined as the period of a certain type of radiation emitted by the caesium 133 atom.

## 6.11 Appendix: Gravitational Sphere of Influence

### 6.11.1 Attraction of the Sun and Earth

It is easy to understand why a low-orbiting satellite should feel only the Earth's attraction, since the Sun's attraction is extremely weak. But one must ask how far out one may continue to ignore the influence of this third body. In the following, we shall define the radius of the sphere beyond which we may consider that a satellite of the Earth escapes to become a satellite of the Sun. The idea of the sphere of gravitational influence was developed by the astronomer F. Tisserand.<sup>40</sup>

Consider three points  $A$  (Sun),  $B$  (Earth),  $C$  (satellite). The gravitational constant is  $\mu_S$  for the Sun and  $\mu$  for the Earth. Consider the special case when  $C$  lies between  $A$  and  $B$ , with the three bodies forming a straight line. We set

$$r = CB, \quad \text{satellite–Earth distance,}$$

$$a_S = AB, \quad \text{Sun–Earth distance,}$$

$$a_S - r = CA, \quad \text{satellite–Sun distance.}$$

Consider now the reduced (dimensionless) variables  $k$  and  $x$  defined by

$$k = \frac{\mu_S}{\mu}, \quad x = \frac{r}{a_S}. \quad (6.148)$$

Note that  $k \gg 1$  and  $x \ll 1$ . For the values of the astronomical quantities, see the appendix in Sect. 6.10 and Table 6.6.

---

<sup>40</sup>*Félix François Tisserand* (1845–1896) was a French astronomer. He continued Delaunay's work on the motion of the Moon and contributed to the *Catalogue photographique de la carte du ciel*. He then published his *Traité de mécanique céleste*, in four volumes (1889–1896), in the spirit of Laplace's work. See also the historical note on the advance of the perihelion of Mercury.

### Satellite Close to Earth

The main acceleration here is the central acceleration  $\gamma_{CC}$ , which we shall write  $\gamma_{T_0}$ , due to the Earth (Keplerian motion):

$$\gamma_{T_0} = \frac{\mu}{r^2}. \quad (6.149)$$

The perturbing acceleration for the satellite is the differential attraction  $\gamma_{CS}$ , here denoted by  $\gamma_{T_1}$ , due to the Sun:

$$\gamma_{T_1} = \frac{\mu_S}{(a_S - r)^2} - \frac{\mu_S}{a_S^2}. \quad (6.150)$$

In the expression for  $\gamma_{T_1}$ , the first term refers to the satellite and the second to the Earth (since the Sun acts on the satellite and on the Earth). Since  $r$  is small compared with  $a_S$ , we obtain

$$\gamma_{T_1} \approx \frac{\mu_S}{a_S^2} \left[ \left( 1 + \frac{r}{a_S} \right)^2 - 1 \right] \approx 2 \frac{\mu_S}{a_S^3} r. \quad (6.151)$$

The ratio of the accelerations is

$$Q_T = \frac{\gamma_{T_1}}{\gamma_{T_0}} = 2 \frac{\mu_S}{\mu} \left( \frac{r}{a_S} \right)^3 = 2kx^3. \quad (6.152)$$

**Note.** By bringing in the expression for the periods, we obtain

$$Q_T = 2 \frac{\mu_S/a_S^3}{\mu/r^3} = 2 \left( \frac{T_0}{T_S} \right)^2, \quad (6.153)$$

where  $T_0$  is the Keplerian period of the satellite around the Earth and  $T_S$  is the period of revolution of the Earth around the Sun, i.e.,  $T_S = 1$  y.

### Satellite Far from the Earth

If a satellite is very far from Earth, so that it is in fact a space probe, the Earth's attraction becomes very small compared with the Sun's. The central acceleration due to the Sun can be written

$$\gamma_{S_0} = \frac{\mu_S}{(a_S - r)^2} \approx \frac{\mu_S}{a_S^2}, \quad (6.154)$$

for even in this case,  $r$  is small compared with  $a_S$ . The perturbing acceleration for the satellite is the differential attraction due to the Earth, viz.,

$$\gamma_{S_1} = \frac{\mu}{r^2} - \frac{\mu}{a_S^2} \approx \frac{\mu}{r^2}. \quad (6.155)$$

The ratio of the accelerations is

$$Q_S = \frac{\gamma_{S_1}}{\gamma_{S_0}} = \frac{\mu}{\mu_S} \left( \frac{a_S}{r} \right)^2 = \frac{1}{kx^2}. \quad (6.156)$$

## 6.11.2 Determining the Sphere of Influence

### Sphere of Influence as Defined by Tisserand

The Earth's sphere of influence  $\Sigma$  is a sphere centered on the Earth with radius  $\rho_\Sigma$  defined by the point on the straight line joining the Sun and Earth such that  $Q_T = Q_S$ . This gives

$$2k^2 x^5 = 1, \quad (6.157)$$

or<sup>41</sup>

$$\rho_\Sigma = 2^{-1/5} \left( \frac{\mu}{\mu_S} \right)^{2/5} a_S. \quad (6.158)$$

For the Earth, one finds

$$\rho_\Sigma = 5.4 \times 10^{-3} a_S = 0.81 \times 10^6 \text{ km}, \quad \frac{\rho_\Sigma}{R} = 126,$$

using the numerical values of the astronomical quantities  $\mu_S$ , the heliocentric gravitational constant, and  $a_S$ , the astronomical unit. It is thus possible to treat  $r$  as small compared with  $a_S$ .

At the end of the book, we will apply this notion to other planets or celestial bodies than the Earth. For the planets of the Solar System, the values of  $\rho_\Sigma$  are given in Table 16.2b.

### Sphere of Influence: Simplified Definition

Another definition of the sphere of influence, denoted by  $\Sigma_0$ , adopts the condition  $Q_T = 1$ , which corresponds to

$$2kx^3 = 1. \quad (6.159)$$

---

<sup>41</sup>This demonstration is schematic insofar as we are considering the case of three bodies lying along a straight line. The full proof due to Tisserand shows that the surface we seek here is given by

$$\rho_\Sigma = \rho_\Sigma(\theta) = \left[ \left( \frac{\mu}{\mu_S} \right)^2 \frac{1}{\sqrt{1 + 3 \cos^2 \theta}} \right]^{1/5} a_S,$$

where the polar axis is the straight line Earth–Sun with origin at the center of the Earth. When  $\theta = 0$ , we retrieve (6.158). This surface of revolution around the polar axis differs only slightly from a sphere, since the polar radius varies by a factor of 1 to 0.87 ( $= 2^{-1/5}$ ). Tisserand's calculations were made to study the trajectories of comets in the vicinity of Jupiter: "If we write down the condition for equality of the attractive ratios, we obtain the equation of a surface for all the points of which it makes no difference whether we consider the heliocentric motion disturbed by the action of Jupiter, or the jovicentric motion disturbed by the action of the Sun." (*Traité de mécanique céleste*, Vol. IV). The equality of the ratios he is referring to is just  $Q_T = Q_S$ . The process had already been suggested by D'Alembert, Laplace, and Le Verrier. Laplace used the term sphere of activity.



We then have

$$\rho_{\Sigma_0} = 2^{-1/3} \left( \frac{\mu}{\mu_S} \right)^{1/3} a_S, \quad (6.160)$$

and for the Earth

$$\rho_{\Sigma_0} = 11.4 \times 10^{-3} a_S = 1.71 \times 10^6 \text{ km}, \quad \frac{\rho_{\Sigma_0}}{R} = 269.$$

If we use (6.153), the condition  $Q_T = 1$  imposes a limiting value for the period  $T_0$  equal to

$$T_0 = T_S / \sqrt{2} = 258 \text{ d}.$$

If the period of the satellite exceeds 258 days, this satellite will escape from the Earth's attraction. Note that  $\rho_{\Sigma_0}$  is roughly twice  $\rho_{\Sigma}$ . For further discussion of these two values, see the appendix on Lagrange points below.

## 6.12 Appendix: Lagrange Points

### 6.12.1 Restricted Three-Body Problem

The Lagrange points arise in the context of the restricted three-body problem, in which one of the bodies (here, the satellite) has negligible mass compared with the two others. The two “massive” bodies  $A$  and  $B$  revolve around their center of mass  $O$  (two-body problem) with constant angular speed  $\dot{\theta}$ . A third, much lighter body  $C$  feels the gravitational attraction of  $A$  and  $B$ .

Lagrange showed that there are five special positions in space at which the body  $C$  rotates about  $O$  with the same angular speed  $\dot{\theta}$ . In this situation, the point  $C$  is stationary in a Sun–Earth frame. The five points, traditionally denoted by  $L_1$  to  $L_5$ , are known as the Lagrange points or libration points<sup>42</sup> (see Fig. 6.8).

### 6.12.2 Simplified Study of Points $L_1$ and $L_2$

We shall now find in a schematic manner the position of the first two Lagrange points when  $B$  has much smaller mass than  $A$ , as is usually the case. These equilibrium points are unstable. We use the notation of Sect. 6.11. The center of mass is at  $A$ , and the body  $B$  revolves around  $A$  in a circular

---

<sup>42</sup>The word “libration” comes from the Latin *libratio*, which itself comes from *libra*, meaning “balance”. The Moon’s libration is a complex nodding motion around the central position, composed of a physical and a geometric libration (in longitude and in latitude). It is through this motion that we are able to see 59% of the Moon’s surface from Earth, instead of just a half. This term, generally applied to the case of lunar libration (also studied by Lagrange), is also used to refer to the five Lagrange points.

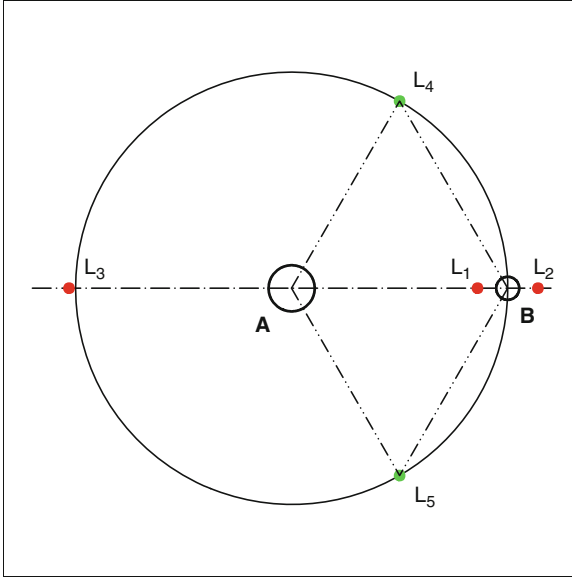


FIG. 6.8 : Schematic illustration of the five Lagrange points. The five points lie in the orbital plane of  $B$  around  $A$ . The mass of  $B$  is considered to be small compared with the mass of  $A$ .

orbit with constant angular speed  $\dot{\theta}$ . According to Kepler’s third law applied to body  $B$ , we have

$$\mu_S = \dot{\theta}^2 a_S^3 . \tag{6.161}$$

Consider a satellite  $C$  at  $L_i$ , close to  $B$ , on the straight line  $AB$ . The point  $L_1$  lies between  $A$  and  $B$ , with  $L_2$  outside. The distance from  $C$  to  $A$  is thus  $a_S + \varepsilon r$ , with  $\varepsilon = -1$  for  $L_1$  and  $\varepsilon = +1$  for  $L_2$ . For each point  $L_1$  and  $L_2$ , we express the fact that the resultant of the attractive accelerations is equal to the radial acceleration. Note that the angular speed<sup>43</sup> of  $L_1$  and  $L_2$  is  $\dot{\theta}$ . Projecting onto the  $AB$  axis and using the notation  $\varepsilon$ , we obtain

$$\frac{\mu_S}{(a_S + \varepsilon r)^2} + \varepsilon \frac{\mu}{r^2} = (a_S + \varepsilon r) \dot{\theta}^2 . \tag{6.162}$$

Dividing the left- and right-hand sides of (6.162) and (6.161) and using the reduced variables defined in (6.148), we find

$$\frac{1}{(1 + \varepsilon x)^2} + \varepsilon \frac{1}{kx^2} = 1 + \varepsilon x . \tag{6.163}$$

<sup>43</sup>If the bodies placed at  $L_1$  and  $L_2$  were in Keplerian orbit, the angular speeds would be different, since the two distances from the attractor  $A$  are different. They are not in this type of orbit because this is not a two-body problem, but a (restricted) three-body problem.

We can expand  $(1 + \varepsilon x)^2$  to first order in  $x$  since  $x \ll 1$ , whereupon

$$3\varepsilon x \approx \varepsilon \frac{1}{kx^2} .$$

Cancelling out  $\varepsilon$ , we find that  $x$  has the same value in both cases. In fact, it solves

$$3kx^3 = 1 . \quad (6.164)$$

For the distances  $\rho_{L_i}$ , we now have

$$BL_1 = BL_2 = \rho_{L_i} = \left( \frac{1}{3} \frac{\mu}{\mu_S} \right)^{1/3} a_S . \quad (6.165)$$

**Example 6.4** Calculate the positions of the Lagrange points  $L_1$  and  $L_2$  for various astronomical systems.

► For the Sun–Earth system, where  $k = 3.329 \times 10^5$ , or  $3k \approx 10^6$ , we have

$$\text{distance from center of Earth to } L_{1,2} : \quad \rho_{L_i} = 10^{-2} a_S \approx 1.5 \times 10^6 \text{ km} .$$

For the Earth–Moon system, where  $k = 81.3$ , replacing  $a_S$  by  $a_L$ , the mean radius of the lunar orbit, we find

$$\begin{aligned} \text{distance from center of Moon to } L_{1,2} : \quad \rho_{L_i} &= (243.9)^{-1/3} a_L = 0.16 a_L \\ &\approx 6. \times 10^4 \text{ km} . \end{aligned}$$

For the system consisting of Mars and its moon Phobos, where  $k = 5.05 \times 10^7$  and  $a_L = 9.38 \times 10^3$  km, we obtain

$$\text{distance from center of Phobos to } L_{1,2} : \quad \rho_{L_i} = 1.88 \times 10^{-3} a_L \approx 17.6 \text{ km} .$$

As the subplanetary equatorial radius of Phobos is 13.4 km, the points  $L_1$  and  $L_2$  are only 4.2 km from the surface of Phobos. ◀

### 6.12.3 Lagrange Points and Sphere of Influence

Let us compare the radii of the spheres of influence centered on the Earth with the distance from the Earth to the Lagrange points  $L_1$  and  $L_2$ . We use the reduced distances  $x$ , denoted by  $x_1$  and  $x_0$  for the spheres of influence (with either Tisserand's definition or the simplified definition) and  $x_L$  for the Lagrange points. We recall the three relations:

$$2k^2 x_1^5 = 1 , \quad 2kx_0^3 = 1 , \quad 3kx_L^3 = 1 .$$

Writing  $x_1$  and  $x_0$  in terms of  $x_L$ ,

$$x_0 = 1.14x_L, \quad x_1 = 1.35x_L^{6/5}, \quad \text{for the Earth } x_1 = 0.54x_L.$$

The Lagrange point cannot lie within the sphere of influence, i.e., the region of space where the Earth's attraction dominates. We may thus consider that the simplified definition, giving  $\rho_{\Sigma_0}$ , is in fact a little too simple. Here is an illustration.

In Fig. 6.1, we have plotted the various accelerations as a function of the distance from the center of the Earth. When the straight lines representing the central attraction, denoted by  $GM$ , and the differential attraction due to the Sun, denoted by  $\text{Sun}$ , intersect one another (actually off the graph), we have equality between the quantities given in (6.5) and (6.7), and this amounts to writing down the relation (6.159). This point of intersection (for  $r/R = 269$ ) can be used to obtain the radius  $\rho_{\Sigma_0}$ . In fact, for these values of  $r/R$ , it is no long possible to approximate  $\gamma_{CS}$  by a straight line. The true point of intersection between the two curves corresponds to the value calculated for  $\rho_{\Sigma}$  using Tisserand's definition. We mentioned the simplified method here because this is the one usually presented in the literature.

### 6.12.4 The Five Lagrange Points

A complete analysis to find the five points and the equilibrium conditions is much more involved and goes beyond the scope of this book. The classic method consists in writing the equations in a frame rotating about  $O$ . This produces two equations: one involves the first three points, and the other the last two. The position of the points is shown schematically in Fig. 6.8 (where  $O$  coincides with  $A$ ).

- Points  $L_1$ ,  $L_2$ , and  $L_3$  lie on the straight line  $AB$ . Let  $\alpha$  be the reduced mass and  $X$  the reduced distance defined by

$$\alpha = \frac{\mu}{\mu + \mu_S} = \frac{1}{1 + k}, \quad X = \frac{AL_i}{AB}. \quad (6.166)$$

We obtain the three possible values of  $X$ . Taking  $\alpha \approx 1/k$ , the first two, for  $L_1$  and  $L_2$ , are as calculated above, viz.,  $X = [1 \pm (\alpha/3)^{1/3}]$ . The third, for  $L_3$ , is  $X = -[1 + (5/12)\alpha]$ . These three equilibrium points are unstable.

- Points  $L_4$  and  $L_5$  can be shown to lie in the orbital plane of  $B$  around  $A$ , in such a way that triangles  $ABL_4$  and  $ABL_5$  are equilateral. The positions of  $L_4$  and  $L_5$  do not depend on the masses of the bodies  $A$  and  $B$ . It can also be shown that these positions are stable, provided that the mass of  $A$

$L_i$	$L_1$ (unstable)	$L_2$ (unstable)	$L_3$ (unstable)	$L_4$ (stable)	$L_5$ (stable)
$u_X$	$1 - \left(\frac{\alpha}{3}\right)^{1/3}$	$1 + \left(\frac{\alpha}{3}\right)^{1/3}$	$-\left(1 + \frac{5}{12}\alpha\right)$	$\frac{1}{2}$	$\frac{1}{2}$
$u_Y$	0	0	0	$\frac{\sqrt{3}}{2}$	$-\frac{\sqrt{3}}{2}$

TABLE 6.7: *Coordinates of the five Lagrange points of the A–B system in a frame moving with the straight line AB and with origin at A:  $u_X$  on the axis AB,  $u_Y$  in the direction perpendicular in the right-hand sense. Reduced distances with unit AB = 1. Reduced mass  $\alpha$  with  $\alpha \ll 1$ .*

is big enough compared with the mass of  $B$ , i.e., at least 25 times greater.<sup>44</sup>  $L_4$  and  $L_5$  are distinguished by the convention that  $L_4$  is the point that precedes  $B$  in its revolution, while  $L_5$  is the point following it.

The coordinates of the five Lagrange points are summarised in Table 6.7, while Table 6.8 indicates the positions of the Lagrange points for the Sun–Earth and Earth–Moon systems. Note that, for the latter system, exact calculation of  $x$  gives 0.15 and 0.17 for  $BL_i$ , whereas the approximate calculation in Example 6.4 gave 0.16 for both.

### 6.12.5 Lagrange Points in Astronomy

Lagrange’s theory was brilliantly confirmed in the field of planetary astronomy with the discovery of asteroids at the stable points  $L_4$  and  $L_5$  of the Sun–Jupiter system. The first, 588 Achilles, was discovered at  $L_4$  in 1906. This was followed by 617 Patroclus at  $L_5$ , and 624 Hector and 659 Nestor at  $L_4$ . Several hundred asteroids are now known at the two stable points<sup>45</sup> of this system, as illustrated in Fig. 6.9. The asteroids at  $L_4$  are called Greeks, while those at  $L_5$  are the Trojans. The current trend is to use the term Trojans<sup>46</sup>

<sup>44</sup>The exact calculation gives

$$k > k_0, \quad \text{with} \quad k_0 = \frac{25}{2} \left[ 1 + \sqrt{1 - \left(\frac{2}{25}\right)^2} \right] = 24.96.$$

The numerical value of  $k_0$  is called the Routh value. For the planets in the Solar System, this condition always holds by a large margin as far as the Sun is concerned. For the Earth–Moon system, it also holds, since  $k = 81$  in this case. The only known exception in the Solar System is provided by the Pluton–Charon system.

<sup>45</sup>The libration of these asteroids is  $14^\circ$  on average. It cannot exceed  $30^\circ$ .

<sup>46</sup>The duality between Greeks and Trojans is intended to illustrate the unending pursuit, immortalising the *Iliad* in the skies. However, there seems to have been some misunderstanding of Homer’s tale, for we find Patroclus with the Trojans and Hector with the Greeks, enough to make Achilles writhe on his funeral pyre!

$A$ – $B$ system	$L_1$	$L_2$	$L_3$	$L_4, L_5$
Sun–Earth				
$AL_i$ $X$	0.990	1.010	0.999	1.000
$BL_i$ $x$	0.00997	0.010	1.999	1.000
$AL_i$ $10^6$ km	148.10	151.10	149.4	149.6
$BL_i$ $10^6$ km	1.49	1.50	299.0	149.6
$BL_i$ $R$	234	236		
Earth–Moon				
$AL_i$ $X$	0.85	1.17	0.99	1.00
$BL_i$ $x$	0.15	0.17	1.99	1.00
$AL_i$ $10^3$ km	326.7	449.7	380.6	384.4
$AL_i$ $R$	51	71	60	60
$BL_i$ $10^3$ km	57.7	65.3	765.0	384.4

TABLE 6.8 : Distances of bodies  $A$  and  $B$  from the Lagrange points  $L_i$  ( $i = 1, \dots, 5$ ). Distances are given in reduced units  $X$  and  $x$  (dimensionless), in km, and in units of  $R$  (Earth radius).

for the asteroids in both groups and to extend the term to other systems. The Sun–Mars also provides examples of Trojan asteroids (discovered since 1990).

In 1980, several new moons of Saturn were discovered at the Lagrange points of the Saturn–Dione and Saturn–Tethys systems. These are known as the Lagrangian moons. They librate around the stable positions  $L_4$  and  $L_5$ .

### 6.12.6 Artificial Satellites at Lagrange Points

Since 1978, several artificial satellites have been placed at the point  $L_1$  of the Sun–Earth system (see Table 6.9). When the satellite arrives in the vicinity of the point  $L_1$ , about 1.5 million kilometers from Earth, it is placed in orbit around  $L_1$ , since this is an unstable position. It then describes a halo orbit, also denoted by L1LO, the  $L_1$  Lissajous orbit, since the trajectory looks like a Lissajous curve.

The first satellite to be placed in a halo orbit about the  $L_1$  point was ISEE-3 (Explorer-59), between 1978 and 1982. It was followed by Wind, SOHO, ACE, and Genesis, all of which carried out astronomical missions.

The view of the Sun is of course exceptional from  $L_1$  (a property put to good use by the satellite SOHO), and the solar wind can be collected well upstream of the Earth (satellite Wind). But the point  $L_1$  has another advantage: if one observes the Earth from this point, one always sees daylight! The satellite Triana was designed to exploit this in the guise of an unremitting environmental watchdog, and has been reactivated under the name of DSCOVR.

The L1LO orbit lies roughly in a plane tilted with respect to the ecliptic and has elliptical shape. It measures several hundred thousand kilometres

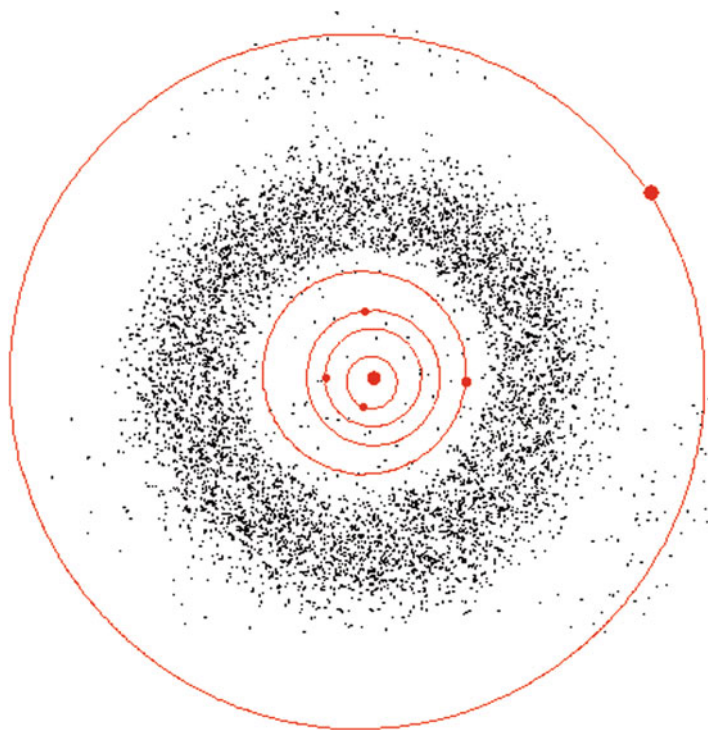


FIG. 6.9: Representation of the 7,722 currently known asteroids (dots) and planets (disks) by their projection onto the plane of the ecliptic on 1 January 2000. Moving out from the Sun at the center: orbits of Mercury, Venus, Earth, Mars, and Jupiter. The Main Belt lies between the orbits of Mars and Jupiter, but it is easy to make out the accumulation of Trojan asteroids on the orbit of Jupiter, close to the points  $L_4$  and  $L_5$  of the Sun–Jupiter system. Credit: SMCS, University of St Andrews.

across and the period of motion of the satellite around the Lagrange point is very long: 211 days for Wind, 180 days for SOHO, 179 days for Genesis. Since the Earth–satellite axis does not lie in the plane of the ecliptic, data transmission is not too seriously perturbed by electromagnetic or particle emissions from the Sun.

The point  $L_2$  of the Sun–Earth system was visited for the first time by the probe WMAP, and joined in 2009 by Planck and Herschel. Many other missions are destined for a halo orbit around this point (an L2LO orbit). These include the successors of Hipparcos and Hubble, namely GAIA and JWST, respectively, and longer term projects such as Eddington and Darwin.

For instruments cooled by liquid helium, for observation of the diffuse cosmic background (WMAP, Planck) or infrared emissions (Herschel, JWST), the position at the  $L_2$  point ensures observation in the direction away from the Sun will never be polluted by the view of the Earth.

Date	$L_1$	$L_2$	Probe
1978	●		ISEE-3
1994	●		Wind
1995	●		SOHO
1997	●		ACE
2001		●	WMAP
2001	●	○	Genesis
2009		●	Planck
2009		●	Herschel

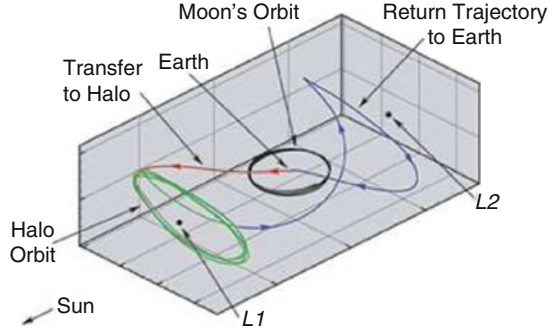


TABLE 6.9: *List of space vessels sent to Lagrange points, with launch date. Right: Genesis probe: mission trajectory to  $L_1$  and return to Earth with an orbital detour (loop-the-loop trajectory) to  $L_2$ . Credit: Shane Ross, NASA, JPL.*

The stable points were to be occupied by a US stereographic solar observation project, with satellites STEREO-Ahead and STEREO-Behind at  $L_4$  and  $L_5$ , respectively. The names can be understood by referring to Fig. 6.8 and noting that the motion of the Earth around the Sun occurs in the anti-clockwise direction in that view. However, this orbit had to be abandoned and the two satellites, with the same names, have been placed in a heliocentric orbit ahead of and behind the Earth's position. The Japanese project L5-Mission is planned for  $L_5$ .

Concerning the  $L_3$  point of the Sun–Earth system, it is not obvious what kind of project might be located there, except possibly a movie of the type Planet X.

## 6.13 Appendix: Spherical Trigonometry

### 6.13.1 Gauss' Relations

A spherical triangle is a triangle on a sphere of unit radius, whose sides are arcs of great circles (or angles at the center). The angles of the triangle are defined at each vertex in the tangent plane to the sphere (i.e., they are dihedral angles). The angles are usually denoted by  $A, B, C$  and the opposite sides by  $a, b, c$ , as shown in Fig. 6.10. It can be shown that a spherical triangle is determined by specifying three elements. A fourth element can be calculated from the three known elements. We then have  $(6 \times 5)/2 = 15$  relations.

These trigonometric relations are easily obtained by considering the following change of frame. Consider three points  $A, B, C$  on a sphere, forming a (non-flat) spherical triangle. We consider two orthonormal frames  $\mathfrak{R}_1$  and  $\mathfrak{R}'_1$  such that

$$\mathfrak{R}_1(O; i, j, k), \quad \mathfrak{R}'_1(O; i', j', k'), \quad i = OA, \quad i' = OB,$$

and such that  $k$  and  $k'$  coincide. We then have  $(i, i') = c$ .



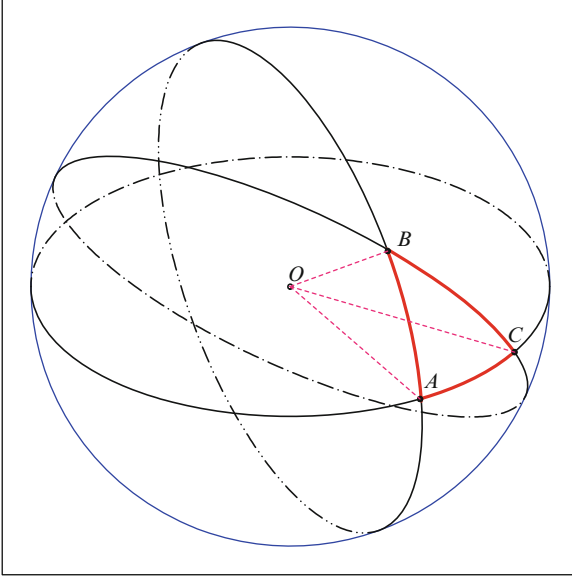


FIG. 6.10 : Spherical triangle  $ABC$  on a sphere with center  $O$  and unit radius. The angles  $A, B, C$  are dihedral angles. The corresponding sides  $a, b, c$  are arcs of great circles defined by  $a = BC, b = CA, c = AB$ .

The frame  $\mathcal{R}'_1$  is thus obtained from  $\mathcal{R}_1$  by rotating through an angle  $c$  about  $\mathbf{k}$ . In each of the two frames  $\mathcal{R}_1$  and  $\mathcal{R}'_1$ ,  $\mathbf{OC}$  can be written in Cartesian coordinates

$$\mathbf{OC} = \begin{pmatrix} \cos b \\ \sin b \cos A \\ \sin b \sin A \end{pmatrix}, \quad \mathbf{OC} = \begin{pmatrix} \cos a \\ -\sin a \cos B \\ \sin a \sin B \end{pmatrix}. \quad (6.167)$$

Using the matrix for the rotation through angle  $c$  about  $\mathbf{k}$ , we thus obtain

$$\begin{pmatrix} \cos a \\ -\sin a \cos B \\ \sin a \sin B \end{pmatrix} = \begin{pmatrix} \cos c & \sin c & 0 \\ -\sin c & \cos c & 0 \\ 0 & 0 & 1 \end{pmatrix} \times \begin{pmatrix} \cos b \\ \sin b \cos A \\ \sin b \sin A \end{pmatrix}. \quad (6.168)$$

We thus obtain the three relations known as Gauss' relations:

$$\cos a = \cos b \cos c + \sin b \sin c \cos A, \quad (6.169)$$

$$\sin a \cos B = \cos b \sin c - \sin b \cos c \cos A, \quad (6.170)$$

$$\sin a \sin B = \sin b \sin A. \quad (6.171)$$

### 6.13.2 Fifteen Relations for the Spherical Triangle

These three equations lead us to the 15 required relations, which are generally grouped as follows. The relations are numbered with Roman numerals from I to XV and the annotation ST, which stands for “spherical trigonometry”.

- Fundamental relations. These are deduced from (6.169) by cyclic permutations. They relate three sides and an angle:

$$\cos a = \cos b \cos c + \sin b \sin c \cos A, \quad (\text{ST I})$$

$$\cos b = \cos c \cos a + \sin c \sin a \cos B, \quad (\text{ST II})$$

$$\cos c = \cos a \cos b + \sin a \sin b \cos C. \quad (\text{ST III})$$

As a corollary, we obtain formulas relating three angles and one side:

$$\cos A = -\cos B \cos C + \sin B \sin C \cos a, \quad (\text{ST IV})$$

$$\cos B = -\cos C \cos A + \sin C \sin A \cos b, \quad (\text{ST V})$$

$$\cos C = -\cos A \cos B + \sin A \sin B \cos c. \quad (\text{ST VI})$$

- Sine formulas. These are deduced from (6.171). These three formulas relate two angles and the opposite sides:

$$\frac{\sin a}{\sin A} = \frac{\sin b}{\sin B} = \frac{\sin c}{\sin C}, \quad (\text{ST VII})$$

$$\frac{\sin a}{\sin A} = \frac{\sin b}{\sin B} = \frac{\sin c}{\sin C}, \quad (\text{ST VIII})$$

$$\frac{\sin a}{\sin A} = \frac{\sin b}{\sin B} = \frac{\sin c}{\sin C}, \quad (\text{ST IX})$$

- Cotangent formulas. These are deduced from (6.170), which involves five elements, and the two other Gauss relations. These formulas relate four consecutive elements of the triangle:

$$\cot a \sin b = \cos b \cos C + \sin C \cot A, \quad (\text{ST X})$$

$$\cot b \sin a = \cos a \cos C + \sin C \cot B. \quad (\text{ST XI})$$

The second of these follows from the first by fixing the angle  $C$  and permuting  $a$  and  $b$ ,  $A$  and  $B$ . By cyclic permutation, we now obtain

$$\cot b \sin c = \cos c \cos A + \sin A \cot B, \quad (\text{ST XII})$$

$$\cot c \sin b = \cos b \cos A + \sin A \cot C, \quad (\text{ST XIII})$$

$$\cot c \sin a = \cos a \cos B + \sin B \cot C, \quad (\text{ST XIV})$$

$$\cot a \sin c = \cos c \cos B + \sin B \cot A. \quad (\text{ST XV})$$

We thus obtain  $6 + 3 + 6 = 15$  relations. In the case of a right-angled spherical triangle, where one of the three angles is a right-angle, the above formulas reduce immediately to  $(5 \times 4)/2 = 10$  relations.

**Example 6.5** Calculate the distance  $D$  between two points  $M(\lambda, \varphi)$  and  $M'(\lambda', \varphi')$  on the Earth, specified by their longitude and latitude.

► To apply spherical trigonometry here, we treat the Earth as spherical. The latitude  $\varphi$  thus represents just as well the geographical, geodetic, or geocentric latitude. Consider the spherical triangle  $NMM'$ , where  $N$  represents the North Pole. If  $N$  corresponds to  $A$ ,  $M$  to  $B$ , and  $M'$  to  $C$ , the angle  $A$  and sides  $b$  and  $c$  can be written as follows in terms of the geographical data:

$$A = \lambda - \lambda', \quad c = \frac{\pi}{2} - \varphi, \quad b = \frac{\pi}{2} - \varphi'.$$

The required distance is then  $a$ , the length of the arc of great circle  $MM'$ . The first Gauss relation (6.169) or (ST 1) then gives

$$\cos a = \sin \varphi \sin \varphi' + \cos \varphi \cos \varphi' \cos(\lambda - \lambda'). \quad (6.172)$$

The required distance is  $D = Ra$ , if we consider the Earth as spherical with radius  $R$  and express  $a$  in radians. Note that, in this situation, we can obtain the result by writing the scalar product  $\mathbf{OM} \cdot \mathbf{OM}'$ .

Application: Calculate the distance from Paris to New York.

The geographical coordinates of Paris and New York are (48°50'N; 2°20'E) and (40°42'N; 74°00'W), respectively, which gives, for the points  $M$  and  $M'$ ,

$$\varphi = +48.87, \quad \lambda = +2.33, \quad \varphi' = +40.70, \quad \lambda' = -74.00.$$

The calculation yields

$$a = 0.91597 \text{ rad} = 52.48^\circ.$$

We thus obtain the distance directly in nautical miles (1 nautical mile is equivalent to 1' arcsec on the Earth's surface), viz.,

$$D = 52.48 \times 60 = 3149 \text{ nautical miles},$$

or in kilometers, if we introduce the Earth's radius, viz.,

$$D = 0.91597 \times R = 5842 \text{ km}.$$

The curve (arc of a great circle) joining two points on the surface of the Earth is said to be orthodromic.

**Note.** When two points are very close, it is better to transform the relation giving  $\cos a$ , using the half-angles to bring in the differences between the latitudes and the longitudes:

$$\sin^2 \frac{a}{2} = \sin^2 \frac{\varphi - \varphi'}{2} + \cos \varphi \cos \varphi' \sin^2 \frac{\lambda - \lambda'}{2}. \quad (6.173)$$

This formula is valid if  $a \in [0, \pi)$ . ◀

# Chapter 7

## Motion of Orbit, Earth and Sun

In the last chapter, we calculated the motion of the orbital plane of a satellite with respect to a Galilean frame, via the rate of nodal precession, and the motion of the orbit in this plane. At the beginning of this chapter, we shall review the way the Earth moves with respect to a Galilean frame. By composing the two motions, we will then be able to follow the motion of the satellite relative to the Earth, which was indeed our original aim.

We shall then study the apparent motion of the Sun relative to the Earth, so that we may subsequently study the cycles of the satellite in relation to the Sun. The aim here will ultimately be to specify the geometry of the satellite, its target, and the Sun: we consider a point on the Earth's surface and determine how this point is seen by the satellite and under what conditions of solar illumination.

In the last two sections, we examine two types of satellite orbit for which two of the quantities studied here play a key role. These quantities are the mean motion  $n$  and the nodal precession rate  $\dot{\Omega}$ . We shall find that they can take certain values of particular importance for the satellite. The first quantity  $n$  determines the geosynchronous orbits, and the second  $\dot{\Omega}$  the Sun-synchronous orbits.

### 7.1 Motion of the Orbit

#### 7.1.1 Secular Variations: Simplified Case

We reconsider here the equations giving the secular variations of the orbital elements for a circular orbit, in the context of a simplified geopotential (expansion up to degree 2). We then treat the general case.

Note that, for an orbit with eccentricity  $e$ , the formulas for the precession rates  $\dot{\Omega}$  and  $\dot{\omega}$  contain a multiplicative factor of  $(1 - e^2)^{-2}$  as compared with the expressions for the circular orbit. For low eccentricities, this factor is approximately  $1 + 2e^2$ , which remains very close to 1.

### Secular Variation of Orbital Elements

Keeping only the  $J_2$  term in the relative perturbation of the geopotential, we showed in Chap. 6 that the metric elements remained constant, whilst the angle elements underwent secular variations. Using (6.73) through (6.75), we obtain the values of  $\dot{\Omega}$ ,  $\dot{\omega}$ , and  $\dot{M}$  as a function of the metric elements and the mean motion  $n = \sqrt{\mu/a^3}$ :

$$\frac{\dot{\Omega}}{n} = -\frac{3}{2}J_2 \left(\frac{R}{a}\right)^2 \cos i, \quad (7.1)$$

$$\frac{\dot{\omega}}{n} = \frac{3}{4}J_2 \left(\frac{R}{a}\right)^2 (5 \cos^2 i - 1), \quad (7.2)$$

$$\frac{\dot{M} - n}{n} = \frac{\Delta n}{n} = \frac{3}{4}J_2 \left(\frac{R}{a}\right)^2 (3 \cos^2 i - 1). \quad (7.3)$$

The secular variation of the orbital element  $\Omega$  will play a key role when we come to study the trajectory of the satellite, as will the secular variations of the elements  $\omega$  and  $M$  when we calculate the period of the motion.

Concerning the parameter  $\omega$ , the secular variation  $\dot{\omega}$  is perfectly well defined by (6.74) when  $e = 0$ . However, the position of the perigee, determined by  $\omega$ , is not defined for a perfectly circular orbit (with  $e = 0$ ), and it is poorly defined in the case of a near-circular orbit. Concerning the parameter  $M$ , whose secular variation  $\dot{M} - n_0$  is perfectly well defined by (6.75) for  $e = 0$ , we encounter the same problem in defining an origin, for both circular and near-circular orbits. In these cases, we generally choose the ascending node as origin (see Sect. 5.2.3 on adapted orbital elements).

### Nodal Precession Rate

Using (7.1) and expressing the mean (Keplerian) motion, the nodal precession rate can be written

$$\dot{\Omega} = -\frac{3}{2}J_2 \sqrt{\frac{\mu}{R^3}} \left(\frac{R}{a}\right)^{7/2} \cos i, \quad (7.4)$$

and this can in turn be set in the form

$$\dot{\Omega}(a, i) = -K_0 \left(\frac{R}{a}\right)^{7/2} \cos i, \quad (7.5)$$

or again, using the reduced distance  $\eta$  defined earlier,

$$\dot{\Omega} = -K_0 \eta^{-7/2} \cos i, \quad (7.6)$$

with

$$K_0 = \frac{3}{2} J_2 \sqrt{\frac{\mu}{R^3}}. \quad (7.7)$$

We can also write  $K_0$  in the following form, using (5.5) and (5.6):

$$K_0 = \frac{3\pi}{T_{0(h=0)}} J_2, \quad (7.8)$$

or again, using (3.5) and denoting the average mass of the planet per unit volume by  $\rho_o$ ,

$$K_0 = \sqrt{3\pi\mathcal{G}} J_2 \sqrt{\rho_o}. \quad (7.9)$$

Concerning the units of the angular velocity, apart from radians per second (SI units), the units degrees per day and revolutions per year are also found in the literature. With these three units,  $K_0$  is expressed as follows:

$$K_0 = 2.012788 \times 10^{-6} \text{ rad s}^{-1}, \quad (7.10)$$

$$K_0 = 9.964014^\circ \text{d}^{-1}, \quad (7.11)$$

$$K_0 = 10.10949 \text{ rev year}^{-1}. \quad (7.12)$$

The function  $\dot{\Omega}(a, i)$  has been plotted in two different ways in Fig. 7.1:

- The upper panel shows  $\dot{\Omega}$  as a function of the semi-major axis  $a$  for different values of the inclination  $i$ .
- The lower panel shows  $\dot{\Omega}$  as a function of the inclination  $i$  for various values of the ratio  $a/R$ .

The altitude thus varies from  $h = 0$  for  $a/R = 1$  to  $h = R = R_e = 6,378 \text{ km}$  for  $a/R = 2$ , in steps of  $0.1R = 637.8 \text{ km}$ . Values of  $\dot{\Omega}$  are given in degrees per day.

These graphs are combined in the upper part of Fig. 7.2. We plot curves of fixed nodal precession rate  $\dot{\Omega}$  (nodal isoprecession curves) as a function of the inclination  $i$  and the altitude  $h$  (or  $a/R$ ). From these graphs, it is clear that, when  $h$  increases for a given inclination,  $\dot{\Omega}$  decreases. The further the satellite moves from the center of the Earth, the less it is affected by irregularities in the geopotential. We also see that, in the case of prograde orbits,  $\dot{\Omega}$  is negative, i.e., precession is retrograde, whereas in the case of retrograde orbits,  $\dot{\Omega}$  is positive. For a strictly polar orbit,  $\dot{\Omega}$  is always zero, at all altitudes.

The maximal value of  $|\dot{\Omega}|$  is obtained for  $i = 0^\circ$  or  $i = 180^\circ$ , with  $h = 0$ , and it is equal to  $K_0 = 9.96^\circ/\text{day}$ , or almost  $10^\circ$  per day. The value of  $\dot{\Omega}$ ,

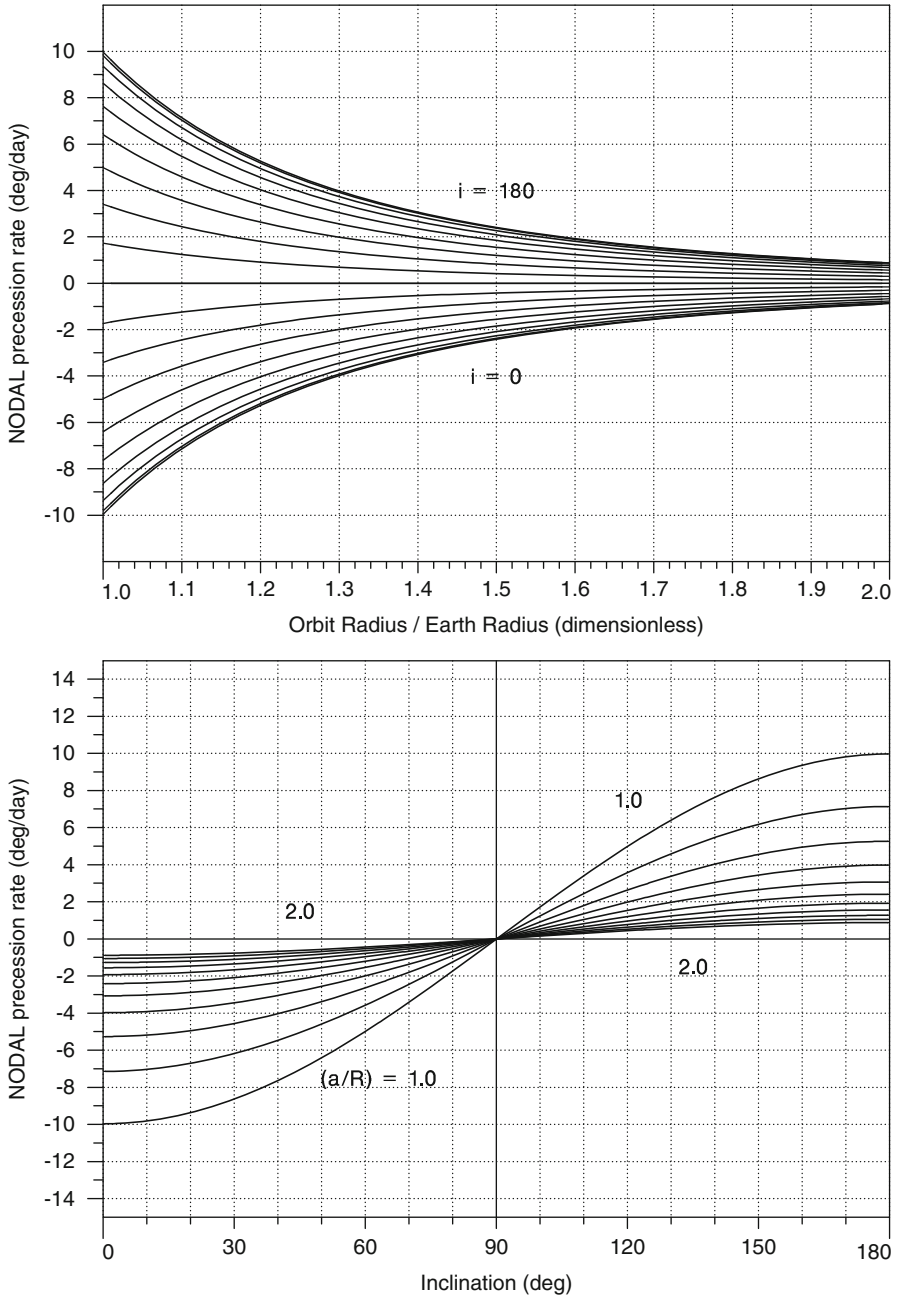


FIG. 7.1 : Nodal precession rate  $\dot{\Omega}(a, i)$  (in degree/day) for a circular or near-circular orbit. Upper: Dependence on the ratio  $\eta = a/R$  for various values of the inclination between  $i = 0^\circ$  and  $i = 180^\circ$ , in steps of  $10^\circ$ . Lower: Dependence on the inclination  $i$  for various values of the ratio  $\eta = a/R$  between  $\eta = 1.0$  and  $\eta = 2.0$ , in steps of  $0.1$ .

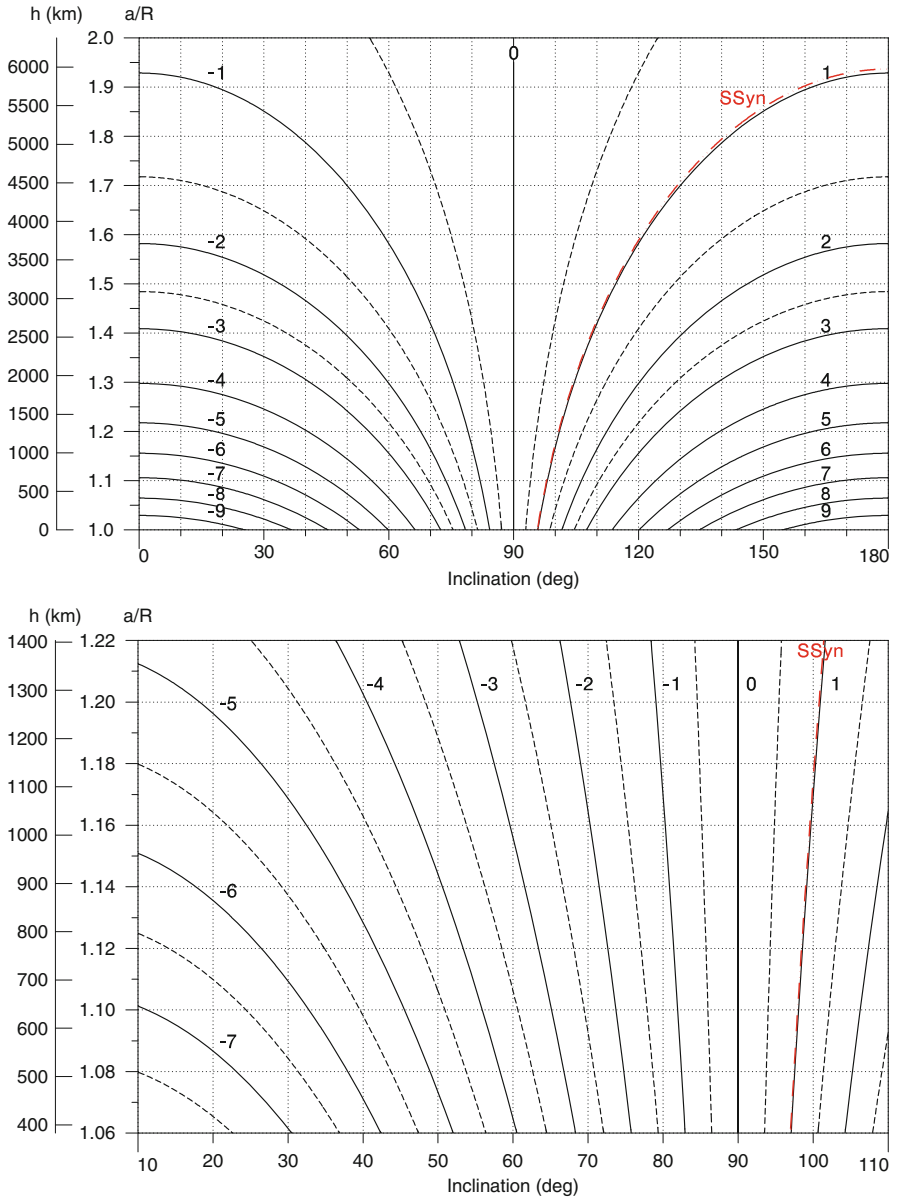


FIG. 7.2: Curves of given nodal precession rate in the graph giving the altitude  $h$  as a function of the inclination  $i$  for a circular or near-circular orbit. The nodal precession rate  $\dot{\Omega}$  is specified in degree/day. Upper: Altitude  $h$  between 0 and  $R$  for all inclinations. Lower: Usual range of operation of LEO satellites.



close to 1, and denoted by  $\text{SSyn}$  on the two graphs of Fig. 7.2, is relevant for the so-called Sun-synchronous satellites, which we shall discuss at the end of this chapter. (In this case,  $\dot{\Omega} = 0.986^\circ/\text{day}$ .)

Figure 7.2 (lower) enlarges the part of the graph relevant to satellites placed in low orbit, as we shall see shortly. For example, the satellite Meteor-3-07 has  $h \approx 1,200$  km and  $i \approx 83^\circ$ , for which we find the value  $\dot{\Omega} = -0.71^\circ/\text{day}$  on the graph. For Lageos-1, with  $h \approx 5,890$  km and  $i \approx 110^\circ$ , we find  $\dot{\Omega} = +0.34^\circ/\text{day}$ .

### Apsidal Precession Rate

The apsidal precession rate defined by (7.2) can also be expressed in terms of the constant  $K_0$  given by (7.7):

$$\dot{\omega} = \frac{1}{2}K_0 \left(\frac{R}{a}\right)^{7/2} (5 \cos^2 i - 1). \quad (7.13)$$

This is zero at the critical inclination defined in Chap. 6.

Figure 7.3 is a graph of  $\dot{\omega}(a, i)$  as a function of the inclination  $i$  for various values of the ratio  $a/R$ . The value of  $\dot{\omega}$  is given with the same units and the same scale as  $\dot{\Omega}$ . The two values of the critical inclination appear quite clearly on the graph at  $63.4^\circ$  and  $116.6^\circ$ . Example 7.1 illustrates this question further.

### Variation of the Mean Motion

Like the precession rates, the variation of the mean motion defined by (7.3) can be expressed in terms of  $K_0$ :

$$\Delta n = \frac{1}{2}K_0 \left(\frac{R}{a}\right)^{7/2} (3 \cos^2 i - 1). \quad (7.14)$$

Figure 7.4 graphs the variation  $\Delta n$  of the mean motion as a function of the inclination  $i$  for various values of the ratio  $\eta = a/R$ . We observe that, for  $i$  between  $57.7^\circ$  and  $125.3^\circ$ , the true motion is slower than the motion relative to a spherical Earth.

## 7.1.2 Secular Variations up to Degree 4

If we consider an elliptical orbit and the expansion of the geopotential to a high degree, the expressions for the variations of the orbital elements become extremely complex. We shall not be concerned here with the periodic variations, affecting all the orbital elements. The secular variations concern only the angle elements and we have shown that only the even zonal harmonics  $J_{2n}$  are involved.

Table 7.1 gives expressions for these secular variations in terms of  $a$ ,  $e$ , and  $i$ , up to degree 4 in  $R/p$ . As well as the terms of degree 2 for  $J_2$ , there

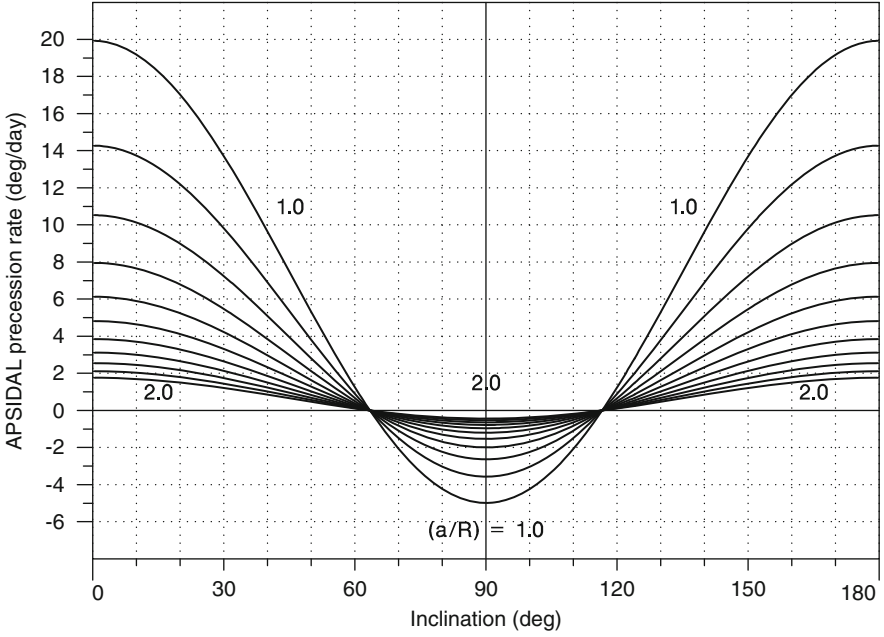


FIG. 7.3 : Apstial precession rate  $\dot{\omega}(a, i)$  (in degrees per day) for a circular or near-circular orbit as a function of the inclination  $i$  for various values of the ratio  $\eta = a/R$  between  $\eta = 1.0$  and  $\eta = 2.0$ , in steps of 0.1.

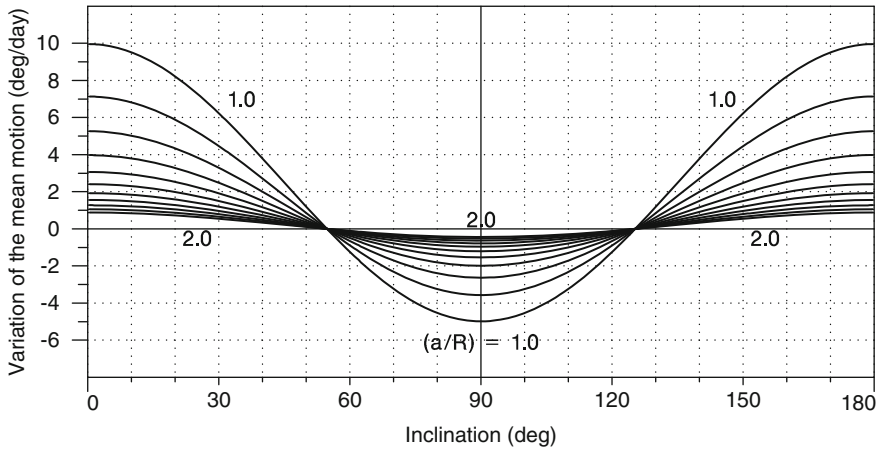


FIG. 7.4 : Variation of the mean motion  $\Delta n(a, i)$  (in degrees per day) for a circular or near-circular orbit as a function of the inclination  $i$  for various values of the ratio  $\eta = a/R$  from  $\eta = 1.0$  to  $\eta = 2.0$ , in steps of 0.1.

are two terms of degree 4, one for  $J_4$  and one for  $J_2^2$ . These quantities are expressed in terms of their quotient by  $n$ , the mean motion. In each case, one thus obtains a ratio of angular speeds, which is a dimensionless quantity.

The expressions for  $\dot{\Omega}$  and  $\dot{\omega}$  in (7.15) and (7.16), respectively, were obtained from J. Kovalevsky's analytical theory of satellite motion in [5], while the expression for  $\Delta n$  in (7.17) was derived using the theory of P.E. Koskela et al. in [18]. These results are also presented in a slightly different way in other books on space mechanics, such as [22, 28].

### 7.1.3 Secular Variations up to Degree $n$

In the literature, one can find analytic expressions for the secular variations up to order (see, e.g., [5]). These are complex, as one would imagine. The contribution of the terms in  $J_2^2$ ,  $J_4$ , and  $J_6$  for the variations  $\dot{\Omega}$  and  $\dot{\omega}$  are shown in Fig. 7.5. Roughly speaking, they represent one or two hundredths of the contributions due to  $J_2$ .

### 7.1.4 Removing Precessional Motion

By a clever choice of orbital parameters, secular variations can be cancelled out. In this way, precessional effects can be removed, which may be useful for certain missions.

#### Cancelling Nodal Precession

Some satellites have an inclination of  $90^\circ$  to within a few tenths of a degree. They are said to be strictly polar, or on a strictly polar orbit. Equation (7.15) shows that the rate of nodal precession is then zero, since the term  $\cos i$  is a factor in all the  $J_n$  terms.

The orbit of the satellite thus remains fixed<sup>1</sup> in  $\mathfrak{R}$ , making a constant angle with a fixed direction in space (the direction of the vernal point  $\gamma$ ). This orbit is sometimes called an inertial orbit. Strictly polar orbits are generally used by satellites studying remote regions of the Earth environment<sup>2</sup> and by military and geodetic satellites (the US Navy's Transit system, which was the first operational navigation system). The satellite CoRoT, designed for detection

---

<sup>1</sup>Over a few years, there is a slight precessional motion for these orbits, but less than a degree per year. This is due to other perturbations, such as the attraction of the Moon or Sun, radiation pressure, and so on.

<sup>2</sup>To study the magnetosphere, NASA launched two satellites on 3 August 1981 in a single launch: Dynamics Explorer-1 and -2 (Explorer-62 and -64, also called DE-A and DE-B), the first in a high-altitude orbit ( $h_p = 468$  km,  $h_a = 23,322$  km), the second in a low-altitude orbit ( $h_p = 304$  km,  $h_a = 1,002$  km). To ensure that they can make joint observations of the same phenomena, it was essential that they move in the same orbital plane, and this was only possible by choosing a polar plane,  $i = 90^\circ$ , since otherwise nodal precession would have been different for DE-A and DE-B.

$$\begin{aligned}
\frac{\dot{\Omega}}{n} &= J_2 \left(\frac{R}{p}\right)^2 \cos i \left(-\frac{3}{2}\right) \\
&+ J_2^2 \left(\frac{R}{p}\right)^4 \cos i \left[ \left(-\frac{45}{8} + \frac{3}{4}e^2 + \frac{9}{32}e^4\right) + \left(\frac{57}{8} - \frac{69}{32}e^2 - \frac{27}{64}e^4\right) s^2 \right] \\
&+ J_4 \left(\frac{R}{p}\right)^4 \cos i \left(\frac{15}{4} - \frac{105}{16}s^2\right) \left(1 + \frac{3}{2}e^2\right)
\end{aligned} \tag{7.15}$$

$$\begin{aligned}
\frac{\dot{\omega}}{n} &= J_2 \left(\frac{R}{p}\right)^2 \left(3 - \frac{15}{4}s^2\right) \\
&+ J_2^2 \left(\frac{R}{p}\right)^4 \left[ \left(\frac{27}{2} - \frac{15}{16}e^2 - \frac{9}{16}e^4\right) \right. \\
&\quad \left. + \left(-\frac{507}{16} + \frac{171}{32}e^2 + \frac{99}{64}e^4\right) s^2 \right. \\
&\quad \left. + \left(\frac{1185}{64} - \frac{675}{128}e^2 - \frac{135}{128}e^4\right) s^4 \right] \\
&+ J_4 \left(\frac{R}{p}\right)^4 \left[ \left(-\frac{3}{8} + \frac{15}{8}s^2 - \frac{105}{64}s^4\right) \left(10 + \frac{15}{2}e^2\right) \right. \\
&\quad \left. + \left(-\frac{15}{4} + \frac{165}{16}s^2 - \frac{105}{16}s^4\right) \left(1 + \frac{3}{2}e^2\right) \right]
\end{aligned} \tag{7.16}$$

$$\begin{aligned}
\frac{\Delta n}{n} &= \frac{\dot{M} - n}{n} = J_2 \left(\frac{R}{p}\right)^2 e' \frac{3}{4} (2 - 3s^2) \\
&\times \left\{ 1 + J_2 \left(\frac{R}{p}\right)^2 \frac{1}{8} \left[ 10 + 5e^2 + 8e' - \left(\frac{65}{6} - \frac{25}{12}e^2 + 12e'\right) s^2 \right] \right\} \\
&- J_2^2 \left(\frac{R}{p}\right)^4 e' \frac{5}{64} (2 - e^2) s^2 \\
&- J_4 \left(\frac{R}{p}\right)^4 e' \frac{45}{128} e^2 (8 - 40s^2 + 35s^4)
\end{aligned} \tag{7.17}$$

TABLE 7.1 : *Secular variations of the angle elements with expansion of the gravitational potential up to order 4. The semi-latus rectum  $p$  and the mean motion  $n$  are given by  $p = a(1 - e^2)$  and  $n = \sqrt{\mu/a^3}$ . Abbreviations:  $s = \sin i$ ,  $e' = \sqrt{1 - e^2}$ . Referring to Table 6.2, we have  $s = 1/\sigma$  and  $e' = 1/\bar{\tau}$ .*

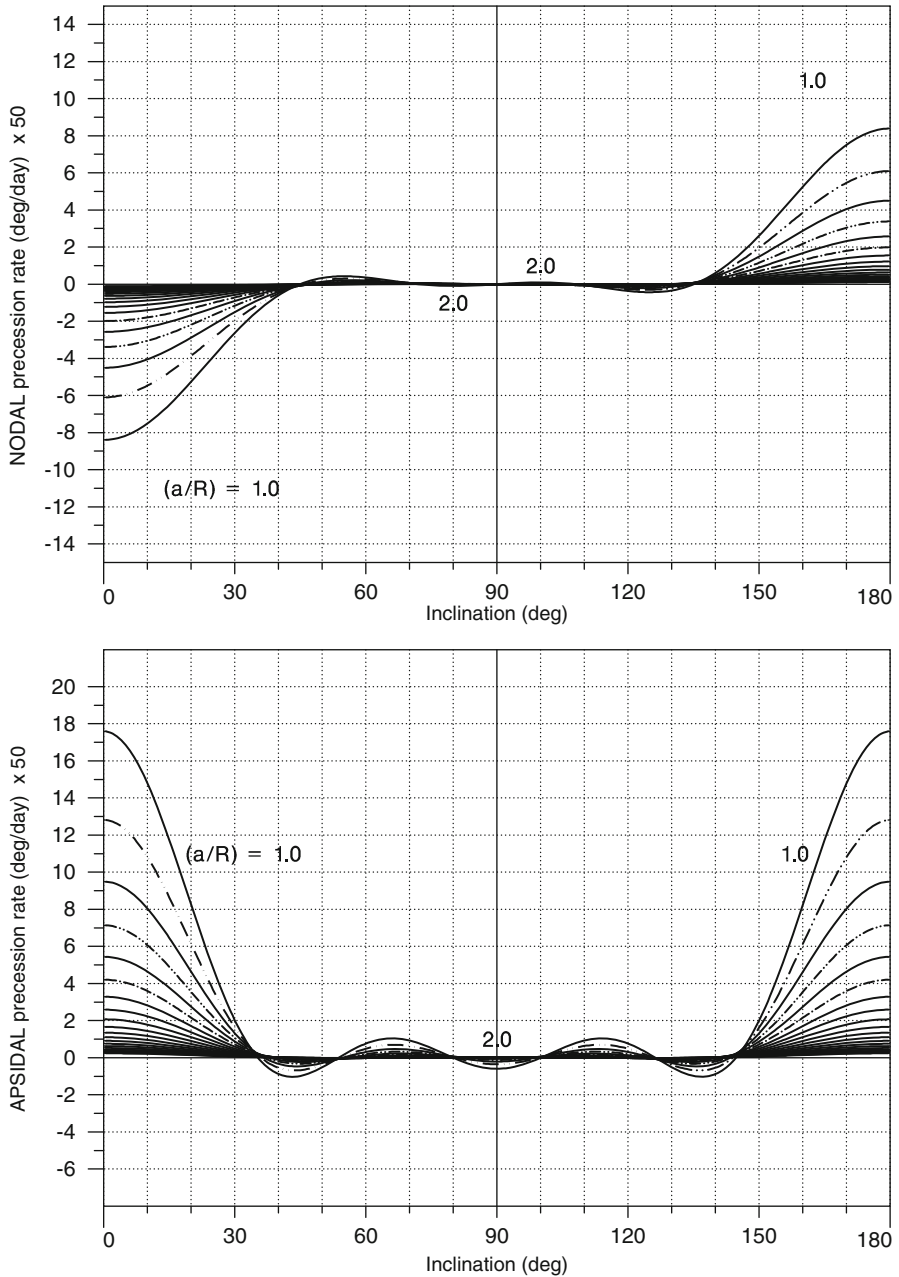


FIG. 7.5: Degree 6 expansion of the geopotential. Contributions of the terms in  $J_2^2$ ,  $J_4$ , and  $J_6$ . Upper: Contributions to the nodal precession rate. Lower: Contributions to the apsidal precession rate. For a circular or near-circular orbit as a function of  $i$  for various values of the ratio  $\eta = a/R$  between  $\eta = 1.0$  and  $\eta = 2.0$ , in steps of 0.1. Dotted lines:  $\eta = 1.05, 1.15, 1.25$ . Note the scale on the vertical axis.

of exoplanets and asteroseismology, is in an inertial orbit<sup>3</sup> with an inclination of  $i = 89.92^\circ$ .

The Gravity Probe Relativity Mission is testing Einstein's general theory of relativity. To do this, the satellite Gravity Probe B (GP-B) must have a polar inclination.<sup>4</sup>

Apart from the cases mentioned above, few space missions need to remove nodal precession altogether. However, it is common practice to select some specific nonzero value of  $\dot{\Omega}$  in the case of Sun-synchronous satellites, as we shall see later.

### Cancelling Apsidal Precession

When the secular apsidal variation vanishes, the argument of the perigee  $\omega$  remains constant. The fixed position of the perigee on an orbit, especially a highly eccentric orbit, may be a decisive factor. It is easy to solve

$$\dot{\omega}(a, e, i; J_n) = 0, \quad (7.18)$$

with  $\dot{\omega}$  defined by (7.16), if we restrict to order 2. For an expansion of  $\dot{\omega}$  cut off at  $J_2$ , (7.18) reduces to  $5 \cos^2 i = 1$  and the solution is given by (6.79). The inclination is equal to the critical inclination. This value  $i_C$  does not depend on any orbital parameter, even those of the given planet.

To higher order, solution is more involved, but it is straightforward to obtain results using numerical methods, given that the value of  $i$  is very close to the one specified by (6.79). The solution  $i$  depends very slightly on  $a$  and  $e$ , together with the coefficients  $J_n$ .

**Note.** In this book, when we mention a critical inclination in the various representations of the satellite ground tracks, we shall always be referring to the inclination calculated up to order 4 for  $\dot{\omega}$ .

**Example 7.1** Calculate the critical inclination for Molniya-type satellites.

► The characteristics of Molniya-3-50 on 10 April 2013 were:

$$a = 26,556.863 \text{ km}, \quad e = 0.7059346, \quad i = 64.3690^\circ, \quad \omega = 257.638^\circ.$$

---

<sup>3</sup>This orbit, free of nodal precession, remains fixed in a Galilean frame and the satellite views in a direction orthogonal to the orbital plane. In fact, it views the same region continually for a period of 180 days, then turns round to view in the opposite direction, thus avoiding the Sun. The two regions viewed are at the intersection of the galactic plane and the celestial equator.

<sup>4</sup>The satellite is equipped with gyroscopes and the aim is to measure effects predicted by general relativity: the geodesic effect (6,606 milliarcsec per year, or  $1.8 \times 10^{-3}$  degree/year) and the Lense–Thirring effect, or frame dragging (39 mas/year, or  $1.1 \times 10^{-5}$  degree/year). These two effects are maximally decoupled when the axis of rotation of the satellite on its orbit is orthogonal to the axis of rotation of the Earth, i.e.,  $i = 90^\circ$ .

To order 2, the solution is given by (6.79), given that this satellite has a prograde orbit ( $i < 90^\circ$ ):

$$i_C = 63.4349^\circ = i_C(J_2) .$$

With (7.16) and expanding  $\dot{\omega}$  up to  $J_4$ , the elements  $a$  and  $e$  come in. We obtain

$$i_C = 63.4246^\circ = i_C(J_4) .$$

This changes little if we expand beyond  $J_4$ . Note that

$$i_C(J_2) - i_C(J_4) = 0.0103^\circ \approx 0.01^\circ .$$

The inclination of this satellite, here  $i = 64.3690^\circ$ , is only  $0.06^\circ$  from the critical inclination  $i_C$ . This difference could be 1 or  $2^\circ$  without there being significant consequences. ◀

## Cancelling the Variation in the Mean Motion

Two values of the inclination, namely  $54.7^\circ$  and  $125.3^\circ$ , lead to a zero value for  $\Delta n$ , defined by (6.75), as discussed in Chap. 6. To our knowledge, this constraint has never been imposed for a space mission. However, it should be noted that the Navstar/GPS (Block II) satellites have an inclination of  $i = 55^\circ$  which leads to an almost zero value for  $\Delta n$ . The mean motion of these satellites is the same as if the Earth were spherical.

### 7.1.5 Effective Calculation of Period and Altitude

We shall now give two examples of calculations involving the relation between the period of a satellite and its altitude. In the first, we calculate the period of a satellite of known altitude, and in the second, the converse (and more difficult) problem, that is, we determine the altitude of a satellite of known period. Other examples of this type will be discussed in Chap. 11 (where the period will be defined by the recurrence condition).

When we speak of the altitude of a satellite in this context, we are in fact referring to the difference between the semi-major axis  $a$  of the orbit and the equatorial radius of the Earth, i.e.,  $h = a - R$ . The quantity  $h$  is usually used to describe the satellite, but it is the quantity  $a$  that is used in orbital calculations.

**Example 7.2** Calculate the period of the satellite TRMM in near-circular orbit at an altitude of 402 km, and with inclination  $35^\circ$ .

► For this satellite, on 10 April 2013, the orbital elements were as follows:

$$a = 6,780.345 \text{ km (or } h = 402.2 \text{ km)}, \quad i = 34.9580^\circ, \quad e = 5.5 \times 10^{-5} .$$

We may thus consider the orbit to be circular. We begin by calculating the Keplerian mean motion for  $a$ , viz.,

$$n_0 = \left[ \frac{3.98600436 \times 10^{14}}{(6.780345 \times 10^6)^3} \right]^{1/2} = 1.130813 \times 10^{-3} \text{ rad s}^{-1},$$

which gives the Keplerian period as

$$T_0 = \frac{2\pi}{n_0} = 5,556.34 \text{ s} = 92.606 \text{ min}.$$

Expressing the numerical factor, the relative  $\Delta n/n_0$  is then found to be

$$\frac{\Delta n}{n} = 8.119701 \times 10^{-4} \eta^{-2} (3 \cos^2 i - 1). \quad (7.19)$$

In this case, we obtain

$$\frac{\Delta n}{n_0} = 8.1197 \times 10^{-4} \left( \frac{6.378137 \times 10^6}{6.780348 \times 10^6} \right)^2 [3(0.81950)^2 - 1] = 7.291 \times 10^{-4}.$$

Using the more complex relation (7.17), we obtain  $7.299 \times 10^{-4}$ , which gives the true mean motion as

$$n = n_0 + \Delta n = 1.133562 \times 10^{-3} \text{ rad s}^{-1}.$$

The actual motion is thus faster than the Keplerian motion ( $\Delta n > 0$ , since we have  $i < 57.7^\circ$ ). The anomalistic period  $T_a$  is obtained from (6.102) as

$$T_a = \frac{92.606}{1 + 7.299 \times 10^{-4}} = 92.538 \text{ min}.$$

We now calculate the apsidal precession rate  $\dot{\omega}$ . Using (7.2) or (7.13), we have  $\dot{\omega}/n = 1.694 \times 10^{-4}$ , and using the more complex relation (7.16),  $\dot{\omega}/n = 1.699 \times 10^{-4}$ . The draconitic period  $T_d$  is found from (6.107) or (6.108) to be

$$T_d = 92.381 \text{ min}.$$

Note that the apsidal precession  $\dot{\omega}$  is positive, since  $i < 63.4^\circ$ , and that it is quite significant, with a value of  $\dot{\omega} = 9.51^\circ$  per day.

Finally, we have

$$T_d < T_a < T_0,$$

with a time difference in seconds of

$$T_a - T_d = 9.44 \text{ s}, \quad T_a - T_0 = -4.05 \text{ s}, \quad T_d - T_0 = -13.49 \text{ s}.$$

The satellite TRMM (Tropical Rainfall Measurement Mission) is a Japanese project in collaboration with NASA. It has a low inclination so as to cover the intertropical region and flies at low altitude to improve the efficiency of its radar instrumentation. From its launch in November 1997 until August 2001, it flew at an altitude of 350 km. Subsequently, in order to extend its lifetime (by reducing atmospheric drag), it was raised to an altitude of 402 km. ◀



**Example 7.3** Calculate the altitude of satellite Meteor-3-07, in near-circular orbit with draconitic period 109.421 min and inclination  $82.56^\circ$ .

- It is more difficult to calculate the altitude from the period than vice versa, as in Example 7.2. We proceed by iteration. Secular variations are calculated using relations up to degree 4.
- We begin by calculating  $a_0$ , the value of  $a$  corresponding to the Keplerian motion with the given period. The value of  $T_d$  is given by the satellite orbit bulletin as  $T_d = 109.421425$  min. In a first step, we thus set  $T_0 = T_d = 6,565.2856$  s. The calculation gives

$$a_0^3 = \frac{\mu}{4\pi^2} T_0^2 = \frac{3.98600436 \times 10^{14}}{4\pi^2} (6.5652856)^2 \times 10^6,$$

whence

$$a_0 = 7,578.129 \text{ km}.$$

With this value for  $a_0$ , the inclination  $i$  and  $n_0 = 2\pi/T_0$ , we can calculate  $\Delta n$  and  $\dot{\omega}$ . We find

$$\frac{\Delta n}{n_0} = -5.469 \times 10^{-4}, \quad \frac{\dot{\omega}}{n_0} = -5.267 \times 10^{-4}.$$

The true motion here is slower than the Keplerian motion ( $\Delta n < 0$ ), so that  $T_a > T_0$ , and the perigee revolves in the retrograde direction ( $\dot{\omega} < 0$ ), so that  $T_a < T_d$ . We thus have

$$T_d > T_a > T_0.$$

- Considering the approximate formula (6.108), we see that this value  $a_0$  for the orbital radius corresponds to the Keplerian period  $T_0$  and a draconitic period  $T_d$  given by

$$T_d = \left(1 + \frac{\Delta T}{T_0}\right) T_0.$$

with

$$\Delta T = T_d - T_0, \quad \frac{\Delta T}{T_0} \approx -\frac{\dot{\omega} + \Delta n}{n_0}.$$

Since the fractional differences are much smaller than unity, this yields

$$T_0 \approx \left(1 - \frac{\Delta T}{T_d}\right) T_d.$$

As the value of  $T_d$  is known, we obtain  $T_0$  from  $T_0 = T_d - \Delta T$ . Now for this value of  $T_0$ , there corresponds an orbit of radius  $a_1$ , obtained from  $a_0$  by  $a_1 = a_0 + \Delta a$ . The differential relation between  $a$  and  $T$  is

$$\frac{dT}{T} = \frac{3 da}{2 a} .$$

Going to finite increments,  $da$  corresponds to  $a_1 - a_0 = \Delta a$  and  $dT$  corresponds to  $T_0 - T_d = -\Delta T$ . We obtain

$$\Delta a = \frac{2 \dot{\omega} + \Delta n}{3 n_0} a_0 = -\frac{2}{3} 1.0735 \times 10^{-3} \times 7,578.129 = -5.423 \text{ km} .$$

We thus find

$$a_1 = 7,572.706 \text{ km} .$$

- The iteration continues in this way, using (6.107), and the results converge very rapidly to give

$$a = 7,572.704 \text{ km} ,$$

which corresponds to an equivalent altitude  $h = a - R = 1,194.6 \text{ km}$ .

For the values of the periods, we obtain

$$T_d = 109.421 \text{ min} , \quad T_a = 109.364 \text{ min} , \quad T_0 = 109.304 \text{ min} .$$

This shows how important it is to distinguish the various periods. The differences found here provide clear evidence for this:  $T_d - T_a = 3.46 \text{ s}$  and  $T_d - T_0 = 7.04 \text{ s}$ .

With the values obtained, we can calculate the nodal precession rate to be

$$\dot{\Omega} = -1.429 \times 10^{-7} \text{ rad s}^{-1} = 0.71^\circ/\text{day} ,$$

but this is not needed in the calculation of the period. ◀

## 7.2 Motion of the Earth

The motions of the Earth relative to a Galilean frame  $\mathfrak{R}$  fixed relative to the Sun can be broken down into three components:

- the revolution of the Earth axis about the Sun, with its yearly period.
- the rotation of the Earth about this axis, with daily period.
- the motion of the poles, which is a tiny movement of the Earth relative to its axis of rotation.

## 7.2.1 Motion of the Earth About the Sun

### Earth Revolutions

The angular speed with which the Earth axis moves around the Sun is denoted by  $\dot{\Omega}_S$ . (This is used by analogy with the rate of precession  $\dot{\Omega}$  of the longitude of the ascending node, but we add a subscript S to indicate the Sun.) It has the value

$$\dot{\Omega}_S = 1.99099299 \times 10^{-7} \text{ rad s}^{-1}, \quad (7.20)$$

which corresponds to

$$\dot{\Omega}_S = 0.9856^\circ/\text{day}. \quad (7.21)$$

### Definitions of the Year

The Earth takes 1 year to cover its elliptical orbit around the Sun. This is the period of revolution. There are several definitions of the year:

- **Sidereal Year.** This is the duration of the Earth's orbit about the Sun referred to a fixed (Copernican frame). It is equal to 365 days 6 h 9 min 9.76 s.
- **Tropical Year.** This is the duration of the Earth's orbit about the Sun referred to a moving average frame. In fact, it is the time elapsed between two consecutive transits of the Sun through the vernal equinox (the spring equinox). It is equal to 365 days 5 h 48 min 45.25 s.

The tropical year determines the recurrence of the seasons.<sup>5</sup> The tropical year is 20 min shorter than the sidereal year. This difference is due to the

---

<sup>5</sup>The civil year aims to be as close as possible to the tropical year. The Julian (civil) year, introduced in 45 BC under the auspices of Julius Caesar, with one leap year every four years, has an average duration of

$$N_{\text{civ(j)}} = 365 + 1/4 = 365.25 \text{ d}.$$

It thus differs from the tropical year by 0.78 days per century. In 325 AD, the Council of Nicaea specified how to calculate the date of Easter given the date of the spring equinox, which was 21 March at this time (it had been 25 March at the time of Caesar). In 1582, the discrepancy was therefore

$$0.78(1582 - 325)/100 = 9.8 \approx 10 \text{ d},$$

and the equinox occurred on 11 March (Easter being calculated from 21 March). To bring the vernal equinox back to 21 March and keep it there, (a) 10 days had to be removed from the calendar and (b) the average length of the civil year had to be slightly modified. This is what was decreed by Pope Gregory XIII in the papal bull known as *Inter gravissimas* (*Inter gravissimas pastoralis officii nostri curas . . .*, “among the most noble tasks of our pastoral ministry . . .”), which gave the Gregorian calendar: (a) the day following Thursday 4 October will be Friday 15 October 1582; (b) 3 days will be suppressed every 400 years (years that are multiples of 100, but not 400, will not be leap years). The Gregorian (civil) year thus has an average duration of

retrograde motion of the vernal equinox, known as the precession of the equinoxes (see Chap. 6).

- **Anomalistic Year.** This is the time elapsed between two transits at perihelion. It is equal to 365 days 6 h 13 m 53 s. It is used in calculations relating to the Keplerian motion of the Earth around the Sun.<sup>6</sup>

The durations of these years, denoted by  $N_{\text{sid}}$ ,  $N_{\text{tro}}$ , and  $N_{\text{ano}}$ , are given in decimal days by:

$$N_{\text{sid}} = 365.256363004 \text{ d} , \quad (7.22)$$

$$N_{\text{tro}} = 365.242190402 \text{ d} , \quad (7.23)$$

$$N_{\text{ano}} = 365.259641 \text{ d} . \quad (7.24)$$

## 7.2.2 Motion of the Earth About the Polar Axis

### Earth Rotational Motion

Let  $\dot{\Omega}_{\text{T}}$  be the angular speed of the Earth in its rotation about its own axis (using  $\dot{\Omega}$  because this is the angular speed of the longitude  $\Omega$  of the ascending node, and we affix the subscript T to indicate “terrestrial”). It has the value

$$\dot{\Omega}_{\text{T}} = 7.29211467 \times 10^{-5} \text{ rad s}^{-1} , \quad (7.25)$$

which corresponds to

$$\dot{\Omega}_{\text{T}} = 360.985559^\circ/\text{day} . \quad (7.26)$$

### Definitions of the Day

- **Astronomical Day.** As we saw earlier, the astronomical definition of the day is

$$1 \text{ d} = 86,400 \text{ s} .$$

- **Mean Day.** The mean day  $D_{\text{M}}$  is the time lapse, averaged over one year, between two meridian transits in the direction of the Sun, i.e., between two consecutive noons.<sup>7</sup>

---


$$N_{\text{civ}(g)} = 365 + 1/4 - 1/100 + 1/400 = 365.2425 \text{ d} .$$

It differs from the tropical year by only 0.3 days per millennium. The Julian year was defined by  $N_{\text{jul}} = N_{\text{civ}(j)}$  in Sect. 6.10.

<sup>6</sup>If we compare these definitions of the year with the definitions of the different periods of a satellite discussed in Chap. 6, the anomalistic year corresponds to the anomalistic period  $T_{\text{a}}$ , while the tropical year corresponds to the nodal or draconitic period  $T_{\text{d}}$ . The draconitic year is defined in terms of the lunar motion.

<sup>7</sup>The word “meridian” comes from the Latin adjective *meridianus*, meaning “relating to noon”, derived from *meridies*, *ei*, or “noon”. This noun is constructed from the locative form *\*mediei die*, “in the middle of the day”. The remainder *d - d* transformed to *r - d* by a well-known linguistic process known as dissimilation.

In practice, we have  $D_M = 1$  d. The mean day  $D_M$  was no longer used to define the second when it was demonstrated that the Earth's rotation was slowing down, which has consequences for the difference  $\text{TAI} - \text{UT1}$ .

- **Sidereal Day.** The sidereal day  $D_{\text{sid}}$  is the interval of time between two meridian transits in the direction of the vernal point<sup>8</sup>:

$$D_{\text{sid}} = D_M - 3 \text{ m } 55.9 \text{ s} . \quad (7.27)$$

The rate of rotation of the Earth is

$$\dot{\Omega}_T = 1.002737909350795 \text{ revolutions per sidereal day} . \quad (7.28)$$

This is the value used in the present book.

By taking into account the (very small) variations in the Earth's rotation, the ratio  $\alpha$  between the universal and sidereal time intervals is given by

$$\alpha = \dot{\Omega}_T + 5.9006 \times 10^{-11} T_u - 5.9 \times 10^{-15} T_u^2 , \quad (7.29)$$

where  $T_u$ , the time elapsed in a Julian century, is obtained by  $T_u = d_u/36,525$ , with  $d_u$  the number of days elapsed since 1 January 2000, at 12 h.

- **Stellar Day.** The stellar day is the time interval between two meridian transits in the direction of a fixed star.

The rate of rotation per stellar day is the quantity denoted by “rate of advance of ERA” in Table 6.6:

$$\dot{\Omega}_{\text{Tstell}} = 1.00273781191135448 \text{ revolutions per stellar day} . \quad (7.30)$$

## Angular Frequencies of the Motions

The duration of the tropical year in seconds can be written

$$N_{\text{tro}} = N'_{\text{yr}} \times D_M , \quad (7.31)$$

---

<sup>8</sup>The sidereal day is the time taken by the Earth, in its daily rotation, to return to a given direction which is not exactly fixed, since it follows the precessional motion of the equinoxes. The duration of the sidereal day is therefore

$$D_M \times \frac{N_{\text{tro}}}{N_{\text{tro}} + 1} = 86,164.09053083288 \text{ s} ,$$

or 23 h 56 min 04.0905 s. The duration of the stellar day is

$$D_M \times \frac{N_{\text{sid}}}{N_{\text{sid}} + 1} = 86,164.098903691 \text{ s} ,$$

or 23 h 56 min 04.0989 s. We thus see that the sidereal day is related to the tropical year and the stellar day to the sidereal year.

where  $N'_{\text{yr}}$  is the number of days in the tropical year and  $D_M$  is 86,400 s. The angular frequencies can then be expressed in radians per second in terms of the duration of the tropical year:

$$\dot{\Omega}_S = \frac{2\pi}{D_M} N'_{\text{yr}}, \quad \dot{\Omega}_T = \frac{2\pi}{D_M} \frac{N'_{\text{yr}} + 1}{N'_{\text{yr}}}. \quad (7.32)$$

This implies the following relation between the angular frequencies of these two motions of the Earth:

$$\dot{\Omega}_T - \dot{\Omega}_S = \frac{2\pi}{D_M}. \quad (7.33)$$

In degrees per day, this becomes

$$\dot{\Omega}_T - \dot{\Omega}_S = 360^\circ/\text{day}.$$

### 7.2.3 Motion of the Poles

If we represent on a map the successive positions of the virtual point where the Earth's axis of rotation cuts the ground surface, we obtain the polhody.<sup>9</sup> This indicates the instantaneous pole. It manifests the motion of the Earth's crust relative to the axis of rotation.

This motion was discovered through astronomical observations, mainly those of very long baseline interferometry (VLBI). Specific satellites, such as LAGEOS and those, like SPOT, equipped with the DORIS system, are now contributing, as we have seen in the discussion of terrestrial reference systems in Sect. 3.6.

Polar motion has two main components:

- A roughly circular oscillation with a cyclically varying diameter and a period of 14 months (435 days), discovered by Chandler in 1885.
- A slow and unpredictable drift of the average position of the pole.

In Fig. 7.6, the first component is represented by a dashed spiral for the period 2001–2006. The erratic displacements of the average position of the pole, or the mean pole, are represented by a continuous curve for the period 1900–2000. The unit is the second of arc, which corresponds to  $1852/60 \approx 31$  m at the surface of the Earth.

The diameter of the polhody on the Chandler cycle can reach  $0.5''$ , or about 15 m. With the advent of the GPS and the possibility of measuring

---

<sup>9</sup>The word *polhodie* was coined by the French mathematician L. Poinso in 1851 from the Greek  $\acute{\omicron}$   $\pi\acute{\omicron}\lambda\omicron\varsigma$ ,  $\omicron\upsilon$ , meaning “pivot” and  $\eta$   $\acute{\omicron}\delta\acute{\omicron}\varsigma$ ,  $\omicron\upsilon$ , meaning “way”. In principle, a Greek word like *hodos* only retains its initial aspiration (rough breathing) when it combines with the previous letter to form an aspirated letter, e.g., in the words “anode” and “cathode”. One should write “polode”.

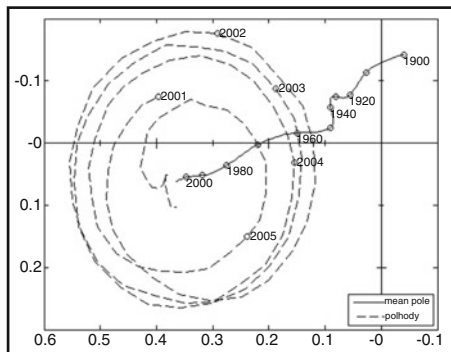


FIG. 7.6 : *Displacement of the mean pole (continuous curve) between 1900 and 2000. Detail of the polhody (dashed curve) between 2001 and 2006. Units: 1 arcsec (or 31 m). Vertical axis: along the zero meridian, pointing down towards Greenwich. Horizontal axis: along the meridian orthogonal to the zero meridian, pointing left toward the point on the equator at  $90^\circ$  W. Credit: IERS Earth Orientation Centre.*

positions to within a meter, it has naturally become essential to take the polar motion into account. However, in the present book, we shall not look further into this issue.

## 7.2.4 Motion of the Orbit and Earth

Later, we shall often need to compare the motion of a satellite, mainly characterised by the two angular speeds  $n$  (mean motion) and  $\dot{\Omega}$  (nodal precession rate), with the two motions of the Earth discussed above.

### Daily Orbital Frequency $\nu$

We denote the daily orbital frequency of the satellite by  $\nu$ . Strictly speaking, it is not a frequency, but rather a (dimensionless) number, representing as it does the number of round trips per day, counted from the ascending node. This quantity is related to the draconitic (nodal) period by

$$\nu = \nu_d = \frac{D_M}{T_d} . \quad (7.34)$$

With (7.33) and the definition of  $n_d$  in (6.103), we obtain

$$\nu = \frac{n_d}{\dot{\Omega}_T - \dot{\Omega}_S} . \quad (7.35)$$

We use the symbol  $P$  for the (dimensionless) number representing the nodal precession in round trips per year.<sup>10</sup> We have

$$\dot{\Omega} = \frac{2\pi}{D_M} \frac{P}{N'_{\text{yr}}} . \quad (7.36)$$

We thus obtain the following relations in terms of  $P$ :

$$\dot{\Omega}_T - \dot{\Omega} = \frac{2\pi}{D_M} \left( 1 + \frac{1-P}{N'_{\text{yr}}} \right) , \quad (7.37)$$

$$\dot{\Omega}_S - \dot{\Omega} = \frac{2\pi}{D_M} \frac{1-P}{N'_{\text{yr}}} . \quad (7.38)$$

We shall also need to compare  $\dot{\Omega}_T - \dot{\Omega}$  with  $n_d$ . We have

$$\frac{\dot{\Omega}_T - \dot{\Omega}}{n_d} = \frac{1}{\nu} \left( 1 + \frac{1-P}{N'_{\text{yr}}} \right) . \quad (7.39)$$

The following two expressions for the quantity  $P$  are particularly useful:

$$P = \frac{D_M}{2\pi} N'_{\text{yr}} \dot{\Omega} , \quad (7.40)$$

$$P = \frac{\dot{\Omega}}{\dot{\Omega}_S} . \quad (7.41)$$

The last relation merely reformulates the definition of  $P$ .

We also define the frequency  $\nu_a$ , which is the number of revolutions made by the satellite every day, counted from the perigee. It is related to the anomalistic period by

$$\nu_a = \frac{D_M}{T_a} . \quad (7.42)$$

This is the quantity published by space organisations like NORAD to calculate the orbital elements.

### Daily Recurrence Frequency $\kappa$

We use  $\kappa$  to denote the daily recurrence frequency. This dimensionless quantity, which will be important in the study of recurrent orbits in Chap. 11, is defined by

$$\kappa = \frac{n_d}{\dot{\Omega}_T - \dot{\Omega}} . \quad (7.43)$$

It is related to the daily orbital frequency  $\nu$  by

$$\frac{\nu}{\kappa} = \frac{\dot{\Omega}_T - \dot{\Omega}}{\dot{\Omega}_T - \dot{\Omega}_S} = 1 + \frac{1-P}{N'_{\text{yr}}} . \quad (7.44)$$

---

<sup>10</sup>This quantity is perhaps more meaningful than  $\dot{\Omega}$  expressed in radians per second. To avoid any confusion over units, we have used  $P$  for this quantity, expressed in round trips per year, whereas other quantities will be expressed in SI units, unless otherwise stated. The quantities  $P$  and  $\nu$ , like  $\nu_a$  and  $\kappa$  a little later on in our discussion, are ratios of angular frequencies, so they are indeed dimensionless numbers.



## 7.3 Apparent Motion of the Sun

The aim in studying the apparent motion of the Sun around the Earth is to represent the direction of the Sun and to understand different notions of solar time, viz., apparent (or true) and mean solar time.

### 7.3.1 Celestial Sphere and Coordinates

On the celestial sphere,<sup>11</sup> illustrated in Fig. 7.7, the equator and the ecliptic (the Sun's trajectory) intersect at two points. The point corresponding to the direction of the Sun when its declination crosses zero from below is the vernal point, traditionally denoted by  $\gamma$ . It corresponds to the spring equinox.<sup>12</sup> The dihedral angle between these two planes, known as the obliquity, is equal to  $\varepsilon = 23^\circ 26' 21'' = 23.44^\circ$ .

The direction of the Sun can be defined as follows, in two coordinate systems with origin at the center of the Earth.

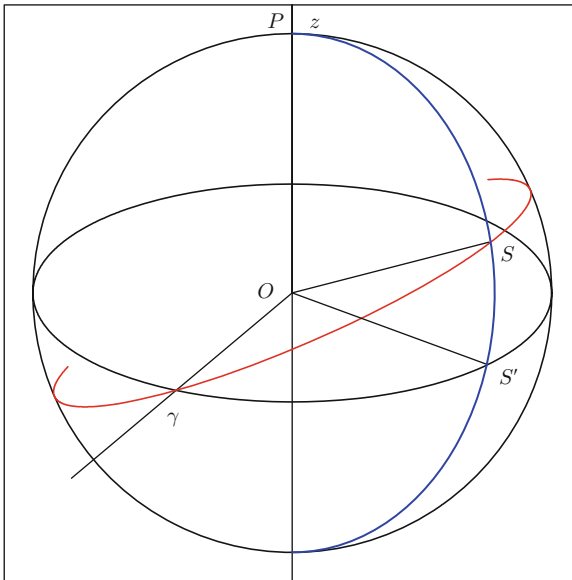


FIG. 7.7: *Celestial sphere, with vernal equinox ( $\gamma$ ), the Sun ( $S$ ), the equatorial plane  $O\gamma S'$ , the ecliptic  $O\gamma S$ , the celestial north pole  $P$ , and the meridian  $PSS'$ . In the spherical triangle  $\gamma SS'$ , the arc  $\gamma S$  represents the celestial longitude  $l$ , the arc  $\gamma S'$  the right ascension  $\alpha$ , and the arc  $SS'$  the declination  $\delta$ . The angle at  $\gamma$  is the obliquity  $\varepsilon$  and the angle at  $S'$  is a right-angle.*

<sup>11</sup>One commonly represents directions in space by means of points on a sphere with arbitrary center and radius, called the celestial sphere. With any particular direction, one associates the point of intersection of the celestial sphere and the straight line in that direction with origin at the center of the sphere.

<sup>12</sup>The word “vernal” comes from the Latin *vernalis*, the adjective derived from *ver*, *veris*, meaning “spring”.

**(a) Ecliptic Coordinates.** The reference plane is the plane of the Sun's apparent trajectory during its annual revolution, known as the plane of the ecliptic, or just the ecliptic. The origin of these coordinates is taken at the vernal equinox. The angle of azimuth gives the Sun's longitude  $l$ , also called the celestial longitude or ecliptic longitude. The height angle gives the Sun's latitude  $b$ , called the celestial latitude or ecliptic latitude. By definition,  $b = 0$  corresponds to the ecliptic itself.

**(b) Celestial Coordinates.** The plane of reference is the Earth's equatorial plane. The coordinate origin is taken at the vernal equinox. The angle of azimuth is the right ascension  $\alpha$ , the dihedral angle between the meridians in the direction of the Sun and the direction of the vernal equinox. The height angle is the declination  $\delta$ , which is the angle between the direction of the Sun and the reference plane. By definition, the right ascension is related to the hour angle  $H$  and the apparent solar time defined below. Concerning the declination, it varies during the year in an almost sinusoidal manner, between the bounds  $\delta = \varepsilon$  at the summer solstice and  $\delta = -\varepsilon$  at the winter solstice. The values  $\delta = 0$  are attained at the equinoxes. We shall return to this point below (see Fig. 7.10).

### 7.3.2 Hour Angle

We consider an arbitrary point on the Earth (apart from the poles), defined by its geocentric coordinates  $(\lambda, \psi)$  in  $\mathfrak{R}_T$ . The meridian plane through this location, denoted by  $\mathcal{M}$ , is the half-plane containing the polar axis and this point. At a given time, we define the meridian plane of the Sun's direction, denoted by  $\mathcal{S}$ , as the half-plane containing the polar axis and this direction, with longitude  $\lambda_S$ . The dihedral angle between these two half-planes is called the hour angle, denoted by  $H$ :

$$H = \text{dihedral angle}(\mathcal{M}, \mathcal{S}) = \lambda - \lambda_S . \quad (7.45)$$

The angle  $H$  is measured in the retrograde sense. This convention can be explained as follows. The idea is that the variations in  $H$  and the time should occur in the same sense during the day, so that  $H$  is negative in the morning, zero at midday, and positive in the evening.

The hour angle (which is in fact an azimuthal angle) can be defined for an arbitrary direction. When it is defined specifically for the direction of the Sun, as here, it is also called the apparent (or true) solar time. The hour angle and the apparent solar time are angles, generally given in degrees or hours, where 1 h corresponds to  $15^\circ$ , since 24 h corresponds to  $360^\circ$ .

### 7.3.3 Equation of Time

The apparent solar time defined by the apparent motion of the Sun is a "natural" idea. It is the time given by a sundial. But this motion does not

have the regularity required to form the basis for a time scale. It would be regular, or uniform, if the Earth's orbit were circular and if its plane contained the Earth's equatorial plane.

### Equation of Center

We consider the position of the Sun as defined by ecliptic coordinates. The Sun's trajectory relative to the Earth is not circular, but elliptical. The celestial longitude  $l$  does not therefore vary in a uniform manner, but corresponds to the true anomaly  $v$ , with a different origin. Indeed,

$$l = v - v_\gamma , \quad (7.46)$$

taking the origin of  $v$  at the perigee, which corresponds on average to 3 January, and the origin of  $l$  at the vernal equinox, which corresponds on average to 21 March. The true anomaly<sup>13</sup> of the vernal equinox is

$$v_\gamma = 77^\circ . \quad (7.47)$$

The regular motion is characterised by the mean anomaly  $M$ , proportional to the time elapsed since the passage at perigee. The difference, induced by the nonzero eccentricity, between the elliptical and the uniform motions is characterised by  $l - M$  or  $v - M$ , which are equal in value up to a constant. We set

$$E_C = v - M , \quad (7.48)$$

a quantity known as the equation of center, already mentioned in Chap. 4, where it was defined by (4.90) in the discussion of Keplerian motion.

When  $e$  is small, as happens for the Earth orbit ( $e = 0.0167$ ), we have seen that this quantity is given by (4.98), viz.,

$$E_C \approx 2e \sin M . \quad (7.49)$$

The function  $E_C$  is sinusoidal, with period one year and maximum  $E_{C_m}$  given by

$$E_{C_m} = 2e = 0.0334 \text{ rad} .$$

Its graph is shown by the dashed curve in Fig. 7.8. It is zero twice a year, at the perigee (3 January) and at the apogee (5 July). It reaches its maximum on 3 April and its minimum on 5 October.

---

<sup>13</sup>Keplerian elements with respect to the mean ecliptic and equinox of J2000.0, for Earth-Moon Barycentre [JPL-DE405]:  $\Omega = 0$ ,  $\omega = 102.93768 - 180 = -77.06232$ ,  $v_\gamma = -\omega \approx 77^\circ$ .

### Reduction to the Equator

We now consider the Sun's position as defined by celestial equatorial coordinates. The equatorial plane makes an angle  $\varepsilon$  with the ecliptic, as defined above. It follows that the right ascension  $\alpha$  does not vary uniformly with the longitude  $l$ .

The celestial sphere is represented in Fig. 7.7, where  $O$  is the center of the Earth,  $P$  the celestial north pole,  $\gamma$  the vernal equinox,  $S$  the position of the Sun, and  $S'$  the intersection of the meridian half-plane of  $S$  with the celestial equator. Concerning the spherical triangle  $\gamma S S'$ , the angles and sides (arcs) are:

$$\begin{aligned} \text{angle } \gamma &= \varepsilon, & \text{angle } S' &= \pi/2, \\ \widehat{\gamma S} &= l, & \widehat{\gamma S'} &= \alpha, & \widehat{S S'} &= \delta. \end{aligned}$$

We would like to express  $\alpha$  as a function of  $\varepsilon$  and  $l$ . Using (ST XIII), we obtain

$$\cot l \sin \alpha = \cos \alpha \cos \varepsilon, \quad \text{hence} \quad \sin \alpha \cos l = \cos \alpha \sin l \cos \varepsilon.$$

Expressing  $\cos \varepsilon$  in terms of the tangent of the half-angle, this implies that

$$\sin \alpha \cos l \left(1 + \tan^2 \frac{\varepsilon}{2}\right) = \cos \alpha \sin l \left(1 - \tan^2 \frac{\varepsilon}{2}\right),$$

whence

$$\sin(\alpha - l) = -\tan^2 \frac{\varepsilon}{2} \sin(\alpha + l). \tag{7.50}$$

The proximity of  $\alpha$  and  $l$  is thus expressed in terms of the obliquity  $\varepsilon$ , and we may write

$$\alpha \approx l - \tan^2 \frac{\varepsilon}{2} \sin 2l. \tag{7.51}$$

The reduction to the equator is defined as

$$E_R = \alpha - l. \tag{7.52}$$

This characterises the discrepancy, introduced by the obliquity, between the true motion and uniform motion.

In the argument of the sine function, we may put  $l \approx M - v_\gamma$ , which yields

$$E_R \approx -\tan^2 \frac{\varepsilon}{2} \sin 2(M - v_\gamma). \tag{7.53}$$

This function  $E_R$  is sinusoidal, with biannual period, and has a maximum  $E_{R_m}$  given by

$$E_{R_m} = \tan^2 \frac{\varepsilon}{2} = 0.0431 \text{ rad}.$$

It goes to zero four times a year, at the two equinoxes (21 March and 23 September) and at the two solstices (21 June and 22 December). Its graph is shown by the dash-dotted curve in Fig. 7.8.

## Equation of Time

Consider the apparent motion of the Sun relative to the Earth. Its position is defined by the right ascension  $\alpha$ . The position that it would have in a uniform motion of the same period is defined by the mean anomaly  $M$ . Taking the same origin, viz., the vernal equinox, we must therefore compare  $\alpha$ , which characterises the apparent solar time, with  $M - v_\gamma$ , which characterises the mean solar time. The difference between these two angles is called the equation of time  $E_T$ :

$$E_T = \alpha - (M - v_\gamma) = \alpha - l + l - M + v_\gamma = (\alpha - l) + (v - M) .$$

This shows that the equation of time is the sum of the two quantities  $E_C$  and  $E_R$  defined above:

$$E_T = E_C + E_R . \quad (7.54)$$

It thus has the value

$$E_T = 2e \sin M - \tan^2 \frac{\varepsilon}{2} \sin 2(M - v_\gamma) . \quad (7.55)$$

Recall that  $M = n(t - t_p)$ , with  $n = 2\pi/T$ , where  $T$  is equal to one year (strictly speaking, one anomalistic year). The mean value of  $E_T$  over the year is zero by definition.

To the accuracy required here, it is convenient to consider the period equal to one civil year of 365 days and to characterise  $M$  by the day  $D$  of the year, taking the beginning of the year as zero point, i.e.,  $D = 1$  for 1 January,  $D = 2$  for 2 January, ...,  $D = 365$  for 31 December. Then, with the passage at perigee for  $D = 3$ , and noting that  $78 \approx 77 \times 365/360$ , we have

$$M = \frac{360}{365}(D - 3) , \quad v_\gamma = 77 \quad (7.56)$$

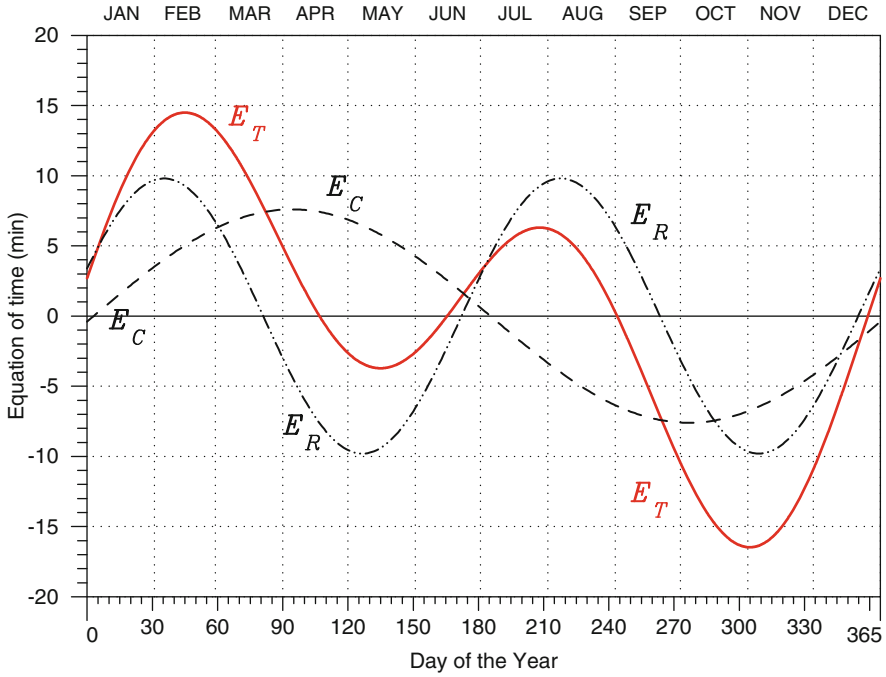
$$M - v_\gamma = \frac{360}{365}(D - 3) - 77 = \frac{360[(D - 3) - 78]}{365} = \frac{360}{365}(D - 81) . \quad (7.57)$$

To express  $E_T$  in time units, we convert radians to minutes of time. In one trip round the orbit, the right ascension changes by 24 h, so  $2\pi$  rad is equivalent to 1,440 min. Finally, expressing the arguments of the sine function in degrees, we obtain

$$E_T(D)[\text{min}] = 7.64 \sin \left[ \frac{360}{365}(D - 3) \right] - 9.87 \sin \left[ \frac{720}{365}(D - 81) \right] . \quad (7.58)$$

With this simplified formula, which is quite adequate for most situations, we observe that the two effects decouple in  $E_T$ . The eccentricity affects  $E_C$  and the obliquity affects  $E_R$ . This is due to the fact that the quantities  $e$  and  $\tan^2(\varepsilon/2)$  are much smaller than unity. Extremely detailed and precise expressions for  $E_T$  can be found in the astronomical literature.

Figure 7.8 shows a graph of  $E_T$  calculated using (7.58), noting the maxima, minima, and zeros. In particular, we see that the equation of time varies with an amplitude of one quarter of an hour and goes to zero four times a year.



Day $D$	Day+month	$E_T$ [min]
45	14 Feb	+14.30
107	17 Apr	0
135	15 May	-3.60
166	15 Jun	0
207	26 Jul	+6.37
244	01 Sep	0
305	01 Nov	-16.43
359	25 Dec	0

FIG. 7.8: Graph of the equation of time as a function of the day of the year  $D$ . The equation of time  $E_T$  is the sum of the equation of center  $E_C$  and the reduction to the equator  $E_R$ . All these quantities are expressed in minutes. The table shows the maxima, minima, and zeros of  $E_T$  with corresponding dates. These dates may vary by one or two days on either side, depending on the year.

**Note.** The sign convention in the definition of  $E_T$  sometimes changes, depending on the field of study, as does the convention for geographical longitudes. One must therefore exercise some caution over the sign used for calculations.

### 7.3.4 Solar Time

#### Universal Time and Mean Solar Time

Universal time UT, or more exactly UT1 (see Chap. 6), is related to the Earth's rotation. At an arbitrary location with longitude  $\lambda$ , we define the local mean solar time LMT by

$$\text{LMT} = \text{UT} + \frac{\lambda}{15} \quad (\lambda \text{ in degree, time in hour}), \quad (7.59)$$

with the convention for the longitudes ( $-W/+E$ ) already mentioned. UT is thus the mean solar time at the Greenwich meridian,<sup>14</sup> i.e., the zero meridian.

#### Mean Solar Time and Apparent Solar Time

With the above calculations,<sup>15</sup> we see that the equation of time, the sum of  $E_C$  and  $E_R$ , is the amount (see Fig. 7.9) by which the local mean solar time (LMT) exceeds the local apparent solar time (LAT):

$$E_T = \text{LMT} - \text{LAT}. \quad (7.60)$$

The civil time at a given location is the mean solar time at this location increased by 12 h. Throughout the rest of this book, the solar times we refer to will be civil times. Noting the value at noon, we have the relation

$$H = 0 \iff \text{LAT} = 12 \text{ h}, \quad \text{LMT} = 12 \text{ h} + E_T.$$

In the following,  $t$  will denote the time in UT and  $\tau$  the corresponding time in LMT. At a place with longitude  $\lambda$ , we then have

$$\tau(t, \lambda) = \tau = t + \frac{\lambda}{15}. \quad (7.61)$$

Time on the LMT scale is also called local time, while time on the LAT scale is called solar time.

**Example 7.4** *The Russian satellite Resurs-O1-4 was launched on 10 July 1998, at 06:30 UT from the Baikonur base in Kazakhstan. Calculate the time on the LMT and LAT time scales at this location and time.*

► The geographical coordinates of the Baikonur space center are  $68^\circ 16'$  E;  $45^\circ 38'$  N. Hence, for the longitude  $\lambda = +68.27^\circ$ , and the local mean time is

$$\text{LMT} + 68.27/15 = \text{UT} + 4.551 = 06 \text{ h } 30 \text{ min} + 4 \text{ h } 33 \text{ min} = 11 \text{ h } 03 \text{ min}.$$

<sup>14</sup>The old name of Greenwich Mean Time (GMT) is judged inappropriate by astronomers and has been out of use for several decades. It should be avoided, even though it still turns up in certain contexts.

<sup>15</sup>To these irregularities in the apparent solar time correspond variations in the length of the apparent solar day, i.e., the time elapsed between two consecutive solar noons. This varies between 23 h 59 min 39 s and 24 h 00 min 30 s.

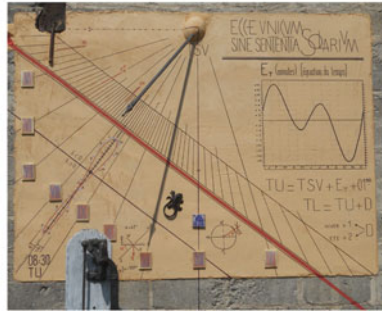
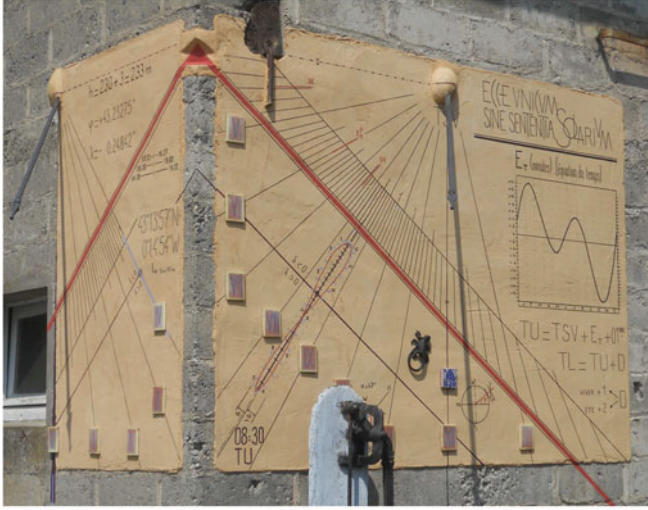


FIG. 7.9: The equation of time specifies the difference between the time we read on a sundial ( $LAT$ ) and the time we read on our watch (effectively  $LMT$ ). The author's own sundial in Angaïs (Pyrénées-Atlantiques, France). Photos: M. C.

The date enters the equation of time:  $E_T(D = 191) = 5.2$  min. We thus obtain the apparent solar time as

$$LAT = LMT - E_T = 11 \text{ h } 03 \text{ min} - 0 \text{ h } 05 \text{ min} = 10 \text{ h } 58 \text{ min} .$$

In conclusion, at Baikonur, the time 06:30 UT corresponds to 11:03 LMT and 10:58 LAT. ◀

### 7.3.5 Declination

The solar declination is very simply expressed as a function of the Sun's celestial longitude  $l$  and the obliquity  $\varepsilon$ . Considering the right-angled spherical



triangle shown in Fig. 7.7 and using the values of the angles given in the figure caption or the section describing the reduction to the equator, we may use the sine rule (ST VIII) from spherical trigonometry to show that

$$\sin \delta = \sin l \sin \varepsilon . \quad (7.62)$$

Clearly, we obtain the declination  $\delta$  in terms of the date (via the mean anomaly  $M$ ). Using the equation of center, we have from (7.46), (7.47), and (7.49),

$$l = v - v_\gamma = M + 2e \sin M - v_\gamma = (M - v_\gamma) + 2e \sin M . \quad (7.63)$$

We use the day of the year  $D$  ( $D = 1$  to  $D = 365$ ). With (7.56) and (7.57), we have seen how  $M$  and  $M - v_\gamma$  are related to  $D$ . For angles expressed in degrees, as is usual, we must give the eccentricity  $e$  in degrees, multiplying it by the coefficient of conversion from radians to degrees:

$$e = 0.0167 \times 180/\pi = 0.96^\circ .$$

This gives

$$\sin \delta = \sin \varepsilon \sin \left[ \frac{360}{365}(D - 81) + 1.92 \sin \frac{360}{365}(D - 3) \right] , \quad (7.64)$$

or putting in the numerical value of the obliquity,

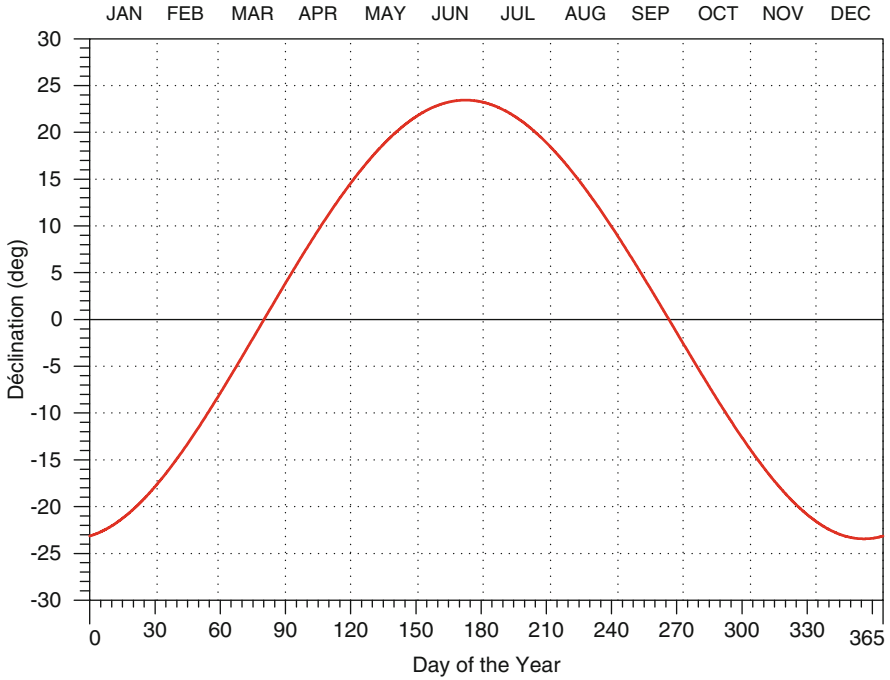
$$\delta(D) = \arcsin \left\{ 0.39795 \sin \left[ \frac{360}{365}(D - 81) + 1.92 \sin \frac{360}{365}(D - 3) \right] \right\} . \quad (7.65)$$

We recall that the value from (7.49) is approximate (although a very good approximation here). Equation (7.65) gives the declination to within  $0.2^\circ$ , which is quite adequate when studying solar angles, with dates defined in a whole number of days. (The apparent diameter of the Sun is  $0.5^\circ$ , and the variation of  $\delta$  is  $0.4^\circ$  a day near the equinoxes.)

The variation of the declination with date is shown in Fig. 7.10. The significant dates are indicated. Note that the lengths of the seasons, as defined by  $90^\circ$  intervals of solar longitude, are unequal. The passage at perigee (3 January) is, in our century, close to the winter solstice (22 December), and the seasons close to these dates (autumn and winter) are shorter than the seasons near the passage at apogee. This is just an example of Kepler's second law, the areal law.

### 7.3.6 Julian Day, Julian Date

In order to calculate the time difference between two given dates, or to identify a particular date in history without ambiguity, we use the Julian day. The days are counted one after the next, without bringing in reference



Day $D$	Day+month	$\delta$ [deg]	$\delta$	Beginning of season	Length of season
21	21 Jan	-20.00			89
54	23 Feb	-10.00			
80	21 Mar	0.00	$\delta = 0$	Spring equinox	
106	16 Apr	+10.00			93
141	21 May	+20.00			
173	22 Jun	+23.44	$\delta = +\varepsilon$	Summer solstice	
205	24 Jul	+20.00			93
240	28 Aug	+10.00			
266	23 Sep	0.00	$\delta = 0$	Autumn equinox	
293	20 Oct	-10.00			90
326	22 Nov	-20.00			
356	22 Dec	-23.44	$\delta = -\varepsilon$	Winter solstice	

FIG. 7.10 : Solar declination  $\delta$  as a function of the day  $D$ . The table shows key values of  $\delta$  with the corresponding value of  $D$ . The obliquity of the Earth is  $\varepsilon = 23.44^\circ$ . Lengths of seasons are given in days.

to month or year, and without discontinuity when a change is made in the calendar. The zero point is taken in a sufficiently remote past to incorporate historical events.<sup>16</sup>

The Julian date (JD) corresponds to the Julian day increased by the fraction of the day as counted from 12 h. On 1 January 2000, we then have the following correspondence between the date of the Gregorian calendar and the Julian date:

$$2000-01-01 \quad 12:00:00 \quad \iff \quad \text{JD} = 2,451,545.0 . \quad (7.66)$$

We shall use this notion of Julian date for the NORAD orbital elements in Chap. 8, and for calculations relating to the orbit of Mars in Chap. 16.

One can also use the modified Julian date (MJD), obtained from the Julian date as follows<sup>17</sup>:

$$\text{MJD} = \text{JD} - 2,400,000.5 . \quad (7.67)$$

## 7.4 Geosynchronicity

### 7.4.1 Definition

We consider the Earth's rotation and the rotation of a satellite  $S$  in the Galilean frame  $\mathfrak{R}$ . The satellite is said to be geosynchronous if its motion

---

<sup>16</sup> *Joseph Juste Scaliger* (1540–1609), the French scholar, proposed a new chronology in his *De emendatione temporum* (On the correction of time) in 1583. His idea was to produce a continuous count of the years in such a way as to cover all the great civilisations. He called this the Julian system, by analogy with the Julian calendar (introduced by Julius Caesar). The Julian numbering system, quoted by Kepler, was used by astronomers from 1860. They then added the idea of Julian day and Julian date. Scaliger considered the cycles involved in calculating the date of Easter, which was a major concern for astronomers in the Christian world:

- The solar cycle (or dominical cycle) of 28 years (7 times 4, with 7 being the number of days in the week, and there being one leap year every 4 years).
- The lunar cycle (the golden number, or the Metonic cycle) of 19 years (235 lunations in 19 years).
- The cycle of indiction, of 15 years (a number of historical rather than astronomical significance).

To each year there corresponds a set of three numbers, one for each cycle. Every  $28 \times 19 \times 15 = 7,980$  year, the years return to the same values for the three cycles (28, 19, and 15 being coprime). Scaliger chose as origin the year when the numbers of the cycles were all equal to 1. In an imaginary Gregorian calendar, this corresponds to the date Monday 1 January –4712, 12 h. This year (4713 BC) is a leap year.

<sup>17</sup> A total of 2,400,000 days are removed from the Julian date, giving an origin on 17 November 1858, and the origin is taken at midnight rather than at midday.

around the Earth and the rotation of the Earth about its axis have the same angular frequency, i.e., if the mean motion  $n$  of the satellite is equal to  $\dot{\Omega}_T$ , i.e.,

$$\text{geosynchronous satellite} \iff n = \dot{\Omega}_T . \quad (7.68)$$

This condition can be met by a satellite whose orbital elements  $e$  and  $i$  are nonzero. However, in practice, what one usually seeks in a geosynchronous motion is that the projection  $S_0$  of the satellite position on the Earth's surface should be immobile (in the frame  $\mathfrak{R}_T$ ). The satellite is then said to be geostationary and this point  $S_0$  is called the subsatellite point of the geostationary satellite.

To achieve this, the vectors representing the Earth's rotation and the satellite's rotation should be equal. Concerning their directions, they must therefore be collinear. As the Earth's rotation vector lies along the polar axis  $\mathbf{Oz}$ , the same must also be true for the rotation vector of  $S$ . Since the orbit of  $S$  is planar and this plane must contain the center of attraction  $O$ , the center of the Earth, it must lie in the equatorial plane (whence  $i = 0$ ). The magnitudes of these vectors are equal since the satellite is geosynchronous. As the value of  $\dot{\Omega}_T$  is constant, the motion of  $S$  must be uniform, whereupon the subsatellite point will be stationary. The orbit of  $S$  must therefore be circular, i.e., with constant altitude:

$$\text{geostationary satellite} \iff \begin{cases} n = \dot{\Omega}_T , \\ i = 0 , \\ h = \text{constant} . \end{cases} \quad (7.69)$$

A geostationary satellite is thus geosynchronous.<sup>18</sup> The converse is not always true, e.g., Tundra-type orbit. Its position is determined by the longitude of the subsatellite point, called the parking longitude of the geostationary satellite.

## 7.4.2 Calculating the Orbit

To calculate the radius of the circular orbit of  $S$ , we begin by considering the value of the Keplerian mean motion. Setting  $n_0 = \dot{\Omega}_T$ , we obtain

$$a_0^3 = \frac{\mu}{\dot{\Omega}_T^2} = 7.4960128 \times 10^{22} ,$$

$$a_0 = 42,164.159 \text{ km} , \quad h_0 = 35,786 \text{ km} .$$

---

<sup>18</sup>In  $\mathfrak{R}$ , the satellite is synchronous, whilst in  $\mathfrak{R}_T$ , it is stationary. The word *geosynchronous*, meaning "synchronised with the Earth", takes its origins from the Greek roots and is more satisfying than the word "geostationary", which is a Greek-Latin hybrid.

Using the iterative method to obtain the altitude from the period, as illustrated in Example 7.3, we obtain

$$a_1 = 42,164.199 \text{ km}, \quad h_1 = 35,786 \text{ km}.$$

At this altitude, as can be seen from Fig. 6.1, the main perturbation no longer comes from the  $J_2$  term in the geopotential, but from the lunisolar potential. Iterative calculations like those considered previously are no longer suited to the problem. By studying the various perturbations (indeed, rather weak compared with the leading term), one can extract the precise value of the orbital radius, which we shall indicate here with a subscript GS to denote geostationary:

$$a_{\text{GS}} = 42,165.785 \text{ km}, \quad h_{\text{GS}} = 35,788 \text{ km}, \quad (7.70)$$

or as a function of the Earth's equatorial radius  $R$ :

$$a_{\text{GS}} = 6.611R, \quad h_{\text{GS}} = 5.611R. \quad (7.71)$$

In terms of the reduced distance  $\eta$ , we have

$$\eta_{\text{GS}} = \frac{a_{\text{GS}}}{R} = 6.611. \quad (7.72)$$

### 7.4.3 Geostationary Satellites

It is easy to grasp the importance of the geostationary satellite. The point is that it always “views” the same regions, and with the same geometry (as we shall see in Chap. 14). For communications satellites and Earth-observation satellites, these are crucial points. For example, such a position allows a weather satellite to make a “film” in real time, with one image every 15 min, showing the development of cloud formations.

It is just as easy to see the drawbacks of this kind of orbit. A geostationary satellite cannot view the whole of the Earth's surface, either in longitude (which explains why one must arrange several of them at different longitudes), or in latitude (regions above  $55^\circ$  are difficult to attain in this way). Moreover, one is forced to view from a great distance.

#### Historical Note on Geosynchronous Satellites

Geosynchronous orbits have been a target since the beginnings of the space age, starting with the US satellite series called Syncom (Synchronous Communications Satellite), experimental communications satellites<sup>19</sup> (mass 39 kg). The first, Syncom-1,  $i = 33.3^\circ$ , was lost at launch. The next, Syncom-2,

---

<sup>19</sup>Launch dates: Syncom-1 on 14 February 1961, Syncom-2 on 26 July 1963, and Syncom-3 on 19 August 1964.

$i = 32.8^\circ$ , was the first geosynchronous satellite. It provided the first telephone link between the Bight of Benin and the United States, on 31 July 1963 (see the upper panel of Fig. 9.16). Syncom-3 can be considered as the first geostationary satellite, since its inclination was  $i = 0.1^\circ$ . It is thanks to this satellite that the Tokyo Olympic Games of 1964 could be followed live in the United States.

Satellites in the subsequent ATS series (Applications Technology Satellite) were already much bigger (mass 930 kg for ATS-6).<sup>20</sup> The Intelsat series (International Telecommunications Satellite Organisation) was the first family of commercial communications satellites.<sup>21</sup>

The first images from geostationary satellites were those taken by ATS-1 and ATS-3, but the first meteorological satellites on this orbit belonged to the SMS series (Synchronous Meteorological Satellite), launched in 1974 and 1975, SMS-1 with  $i = 15.5^\circ$  and SMS-2 with  $i = 12.0^\circ$ . They were followed by the GOES series, from GOES-1 (SMS-3 operational) at  $i = 12.4^\circ$  to GOES-7 at  $i = 1.2^\circ$ . For the GOES-Next series, starting with GOES-8, orbits were equatorial, with  $i \approx 0.2^\circ$ .

The first Soviet geostationary satellite was placed in orbit much later, such satellites being of little use to a country like Russia. This was Kosmos-637, launched on 26 March 1974 with  $i = 14.5^\circ$ . Shortly afterwards, the French–German communications satellite *Symphonie-1* was launched, on 19 December 1974, with  $i = 14.9^\circ$ . The first satellite of the European organisation ESA was METEOSAT-1, launched in 1977 with  $i = 11.9^\circ$ . Since 1990, these meteorological satellites have been placed on near-equatorial ( $i < 1.5^\circ$ ), near-circular ( $e \sim 2 \times 10^{-4}$ ) orbits.

On 1 January 2010, there were more than a 1,000 satellites on near-geostationary geosynchronous orbits (in fact, 1,186 objects measuring more than 1 m across), including 381 in operation, and among them, 239 for communications and 16 for meteorology.

Regarding the problem of solar eclipse faced by geostationary satellites, see Chap. 10.

---

<sup>20</sup> Apart from two failures, for ATS-2 and -4, all the satellites were placed on slightly inclined orbits. Launch dates: ATS-1 on 7 December 1966,  $i = 14.5^\circ$ , remained operational for 18 years, until April 1985, ATS-3 on 5 November 1967,  $i = 14.5^\circ$ , ATS-5 on 12 August 1969,  $i = 14.5^\circ$ , and ATS-6 on 30 May 1974,  $i = 13.1^\circ$ .

<sup>21</sup> The first in the series was Intelsat-1 F-1, also known as *Early Bird*, launched on 6 April 1965,  $i = 14.7^\circ$  (stationed over the Atlantic to establish “fixed” telephone links between Europe and the United States). Since then the Intelsat satellites have been launched on a regular basis and placed over the Atlantic, Indian, and Pacific oceans. An intergovernmental consortium set up in 1964, Intelsat became a private company in 2001. After taking over PanAmSat in 2006, Intelsat has 55 satellites in operation at the time of writing (2013).

### 7.4.4 Drift of the Geostationary Orbit

The geostationary satellite undergoes the effects of various perturbations, causing it to drift from its course as time goes by. In other words, the subsatellite point  $S_0$  is no longer exactly the assigned reference point. There are two kinds of drift: longitudinal drift and latitudinal drift.

#### Longitudinal Drift

For meteorological satellites, the longitudinal drift of  $S_0$  can be compensated, if it is not too great, by correcting the transmitted image. A very slight variation in  $a$  causes this shift and the satellite is then no longer geosynchronous. If  $a$  increases, the period also increases and the mean motion decreases. Hence, the satellite rotates less quickly than the Earth in  $\mathfrak{R}$ , whence the subsatellite point  $S_0$  moves westward in  $\mathfrak{R}_T$ . Likewise, if  $a$  decreases,  $S_0$  moves eastward. This phenomenon is shown schematically in Fig. 7.11 (see also the lower panel of Fig. 5.3).

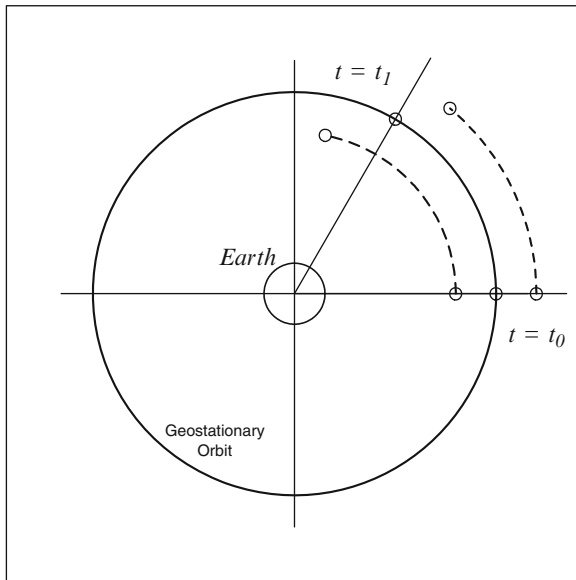


FIG. 7.11 : Orbit of a geostationary satellite and two other satellites at higher and lower altitudes than those required by geosynchronicity. At time  $t = t_0$ , the three satellites have the same subsatellite point. At time  $t = t_1$ , the subsatellite point of the lowest satellite has slipped eastward, while that of the highest satellite has slipped westward, relative to the subsatellite point of the geostationary satellite. The diagram shows the Earth viewed from a point located high above the North Pole in the Galilean frame  $\mathfrak{R}$ .

We shall calculate the displacement  $\Delta_1 l$  of the subsatellite point over one day for a variation  $\Delta a$  in the orbital radius (or altitude). In  $\mathfrak{R}$ , the subsatellite point of a geostationary satellite moves a distance  $l$  between times  $t_0$  and  $t_1$ , where

$$l = R\dot{\Omega}_T(t_1 - t_0).$$

In  $\mathfrak{R}$ , the subsatellite point of a satellite with mean motion  $n$  moves through a distance  $l'$  in the same time, where

$$l' = Rn(t_1 - t_0).$$

The difference measures the deviation in  $\mathfrak{R}$ , or in  $\mathfrak{R}_T$ , which is the drift we seek here:

$$l' - l = R(n - \dot{\Omega}_T)(t_1 - t_0).$$

If the second satellite is close to the geostationary orbit, with  $a = a_{\text{GS}} + \Delta a$  and  $n = \dot{\Omega}_T + \Delta n$ , we have the relation

$$\frac{dn}{n} = -\frac{3}{2} \frac{da}{a} \implies \frac{\Delta n}{\dot{\Omega}_T} \approx -\frac{3}{2} \frac{\Delta a}{a_{\text{GS}}},$$

and setting  $\Delta l = l' - l$ , we have

$$\Delta l = R\Delta n(t_1 - t_0) = -\frac{3}{2} \Delta a \frac{R}{a_{\text{GS}}} \dot{\Omega}_T(t_1 - t_0).$$

The value  $\eta_{\text{GS}} = a_{\text{GS}}/R$  is determined by (7.72) for a geostationary satellite.

If we consider a time interval of exactly one day,  $t_1 - t_0 = D_M$ , we may express  $\dot{\Omega}_T D_M$  using (7.32). This gives  $\Delta_1 l$  (the subscript 1 indicates that we are considering a time interval of 1 day), the displacement of the subsatellite point over one day:

$$\Delta_1 l = -\frac{3}{2} \frac{1}{6.611} 2\pi \frac{366.25}{365.25} \Delta a = -1.4295 \Delta a \quad (\text{per day}). \quad (7.73)$$

The sign here is valid if we apply the usual conventions concerning the longitudes for  $\Delta l$ , i.e., negative for west and positive for east ( $-W/+E$ ).

We now apply this to two examples. In the first, we calculate the drift of a satellite that is not exactly at the required altitude, and in the second, we show how one may take advantage of this drift to modify the position of the satellite.

**Example 7.5** Calculate the longitudinal drift over one week of the subsatellite point of a geostationary satellite whose altitude has increased by 100 m.

► With  $\Delta a = \Delta h = 100$  m, (7.73) gives  $\Delta l = -143$  m/day. The position of the subsatellite point on the ground thus moves 1.0 km westward in one week. ◀



**Example 7.6** *As part of the INDOEX project (Indian Ocean Experiment), the European organisation of meteorological satellites EUMETSAT decided to move the satellite METEOSAT-5 from its standby position ( $10^\circ W$ ) to a new position above the Indian ocean ( $63^\circ E$ ). The method used consisted in shifting the satellite to a lower orbit, whereupon it would drift eastward. Indeed, leaving its initial geostationary position on 14 January 1998, it arrived at its new geostationary position on 19 May 1998. Calculate how much the radius of the orbit was adjusted to make this transfer.*

► The departure and arrival dates were  $D = 14$  and  $D = 139$ , respectively, separated by 125 days. Since it takes 12 h to go from one orbit to the other, we consider that the transfer took 124 days. The distance between the two positions is  $73^\circ$ . The satellite therefore had to move through  $73/124 = 0.589^\circ$  per day relative to the Earth, which corresponds to 65.53 km per day on the ground track. Since the shift was eastward, we thus have  $\Delta l = 65.53$  km/day. Applying (7.73), we find

$$\Delta a = -\frac{\Delta l}{1.4295} = -45.84 \text{ km}.$$

The satellite was therefore placed on an orbit 46 km lower. Note that only the two maneuvers at the beginning and the end required energy input, while the trip itself cost nothing.<sup>22</sup> ◀

## Latitudinal Drift

Latitudinal variations of  $S_0$  (in which  $S$  therefore moves slightly outside the equatorial plane under the action of gravitational forces of the Moon and Sun) show up through a distortion of the ground track. The orbit is slightly tilted with respect to the equatorial plane ( $i \neq 0$ ). During the day, the subsatellite point is not fixed but varies between latitudes  $\psi = +i$  and  $\psi = -i$ . If the orbit remains circular, the intersection of the straight line  $OS$  (joining the center of the Earth  $O$  to the satellite  $S$ ) with the horizontal equatorial plane of the node of the orbit traces out a figure of 8, as can be seen in Fig. 9.16 (upper). This is *not* a Bernoulli lemniscate (see Example 8.4).

### 7.4.5 Stationkeeping

The art of maintaining geostationary satellites in position has been the subject of considerable scientific effort. On the one hand, the problem requires

---

<sup>22</sup>The speed of the transfer does have an energy cost. The faster one needs to go, the lower the transfer orbit should be. For each transfer maneuver of METEOSAT-5 in the above example, which required two burns, one on the starting orbit and one on the final orbit, EUMETSAT indicate that 300 g of fuel were burnt. The satellite was carrying 6 kg of propellant before the move.

specially adapted tools, for the geostationary orbit is highly specific, with  $e = 0$  and  $i = 0$ , whence the angles  $\Omega$  and  $\omega$  are undetermined. On the other hand, the economic stakes are significant. The satellites on these orbits are very costly and may represent huge profits, so there is no question of allowing them to drift out of orbit.

Stationkeeping involves repositioning a satellite within its “window” after a certain time. (A typical window would constitute about  $1^\circ$  in the east–west direction, and  $-0.1^\circ$  to  $+0.1^\circ$  in the north–south direction.) Stationkeeping operations require maneuvers in which fuel is burnt, and this necessarily puts a limit on the lifetime of the satellite. North–south control represents the greater part of the fuel consumption involved in stationkeeping.<sup>23</sup>

The orbit of a geosynchronous satellite evolves as time goes by:

- The semi-major axis  $a$  evolves under the effect of tesseral terms in the geopotential.
- The eccentricity  $e$  (since the distorted orbit is no longer circular) changes under the influence of solar radiation and the lunisolar attraction.
- The inclination  $i$  is affected mainly by the Sun and Moon, since the plane of the ecliptic in which the Sun appears to move is tilted at  $23^\circ$  to the plane of the satellite orbit (the Earth’s equatorial plane), and the plane of the lunar orbit also lies in the plane of the ecliptic, to within  $5^\circ$ .

We now give closer examination to the evolution of  $a$ .

### Longitudinal Acceleration

If a geostationary satellite is left to evolve without further intervention, it will tend to move toward points of specific longitude on the Earth’s equator, depending on where it started out. This effect is largely a manifestation of the tesseral harmonic  $P_{22}$ . The terms  $C_{22}$  and  $S_{22}$  are nonzero, whereas they are taken as zero in any model with cylindrical symmetry [see (3.24)]. We shall calculate this drift by ascertaining its longitudinal acceleration, first by expanding the geopotential to second order, then going to third order.

**(a) Second Order Expansion of the Geopotential.** We return to (3.23), in which we set  $C_{11} = 0$  and  $S_{11} = 0$ . (As we have seen, this comes from the fact that the coordinate origin is chosen at the center of mass.) Introducing the Legendre functions and polynomials, we obtain

---

<sup>23</sup>For the satellite TDF-1, north–south control represents 95% of its consumption. Launched in 1988, this satellite was held in position throughout its period of use. It was then placed in a graveyard orbit, where it was allowed to drift.

$$\begin{aligned}
 U(r, \lambda, \psi) = \frac{\mu}{r} \left\{ 1 + \left( \frac{R}{r} \right)^2 \left[ C_{20} \frac{3 \sin^2 \psi - 1}{2} \right. \right. \\
 + (C_{21} \cos \lambda + S_{21} \sin \lambda) 3 \sin \psi \cos \psi \\
 \left. \left. + (C_{22} \cos 2\lambda + S_{22} \sin 2\lambda) 3 \cos^2 \psi \right] \right\}. \quad (7.74)
 \end{aligned}$$

For a satellite in equatorial orbit, i.e., with  $\psi = 0$ , and replacing  $-C_{20}$  by  $J_2$ , as we have seen in (3.26), the potential is

$$U(r, \lambda, 0) = \frac{\mu}{r} \left\{ 1 + \left( \frac{R}{r} \right)^2 \left[ \frac{J_2}{2} + 3(C_{22} \cos 2\lambda + S_{22} \sin 2\lambda) \right] \right\}, \quad (7.75)$$

which can be written in the form

$$U(r, \lambda, 0) = U_0 + \mathcal{R}(r, \lambda, 0). \quad (7.76)$$

With  $U = U_0 = \mu/r$ , we obtain the radius  $r = a_0$  of the Keplerian geostationary orbit.

Considering

$$U = \frac{\mu}{r} \left[ 1 + \left( \frac{R}{r} \right)^2 \frac{J_2}{2} \right],$$

we obtain the value  $a_1$  calculated previously, which we denote here by  $a$ . It is thus the perturbing potential  $\mathcal{R}'$  given by

$$\mathcal{R}'(a, \lambda) = 3 \frac{\mu}{a} \left( \frac{R}{a} \right)^2 (C_{22} \cos 2\lambda + S_{22} \sin 2\lambda) \quad (7.77)$$

that causes the drift in longitude. We set

$$J_{22} = \sqrt{C_{22}^2 + S_{22}^2} = \sqrt{\frac{5}{12}} \sqrt{C_{22}^{*2} + S_{22}^{*2}}, \quad (7.78)$$

and introduce the quantity  $\lambda_{22}$  such that

$$C_{22} = J_{22} \cos 2\lambda_{22}, \quad S_{22} = J_{22} \sin 2\lambda_{22},$$

whereupon the potential  $\mathcal{R}'$  can be written

$$\mathcal{R}'(a, \lambda) = 3 \frac{\mu}{a} \left( \frac{R}{a} \right)^2 J_{22} \cos 2(\lambda - \lambda_{22}). \quad (7.79)$$

This longitude  $\lambda_{22}$  is thus simply obtained from  $C_{22}$  and  $S_{22}$ , coefficients which account for the fact that the equipotential line at the equator is not a circle but an ellipse:

$$\lambda_{22} = \frac{1}{2} \arctan \frac{S_{22}}{C_{22}} = \frac{1}{2} \arctan \frac{S_{22}^*}{C_{22}^*}. \quad (7.80)$$

For the Earth (the EGM2008 or EIGEN models give the same values), we have

$$J_{22} = 1.8156 \times 10^{-6}, \quad \lambda_{22} = -14.93^\circ.$$

The Lagrange equations (see Table 6.2) give the time dependence of  $a$  under the effects of the perturbation:

$$\frac{da}{dt} = \frac{1}{na} \left( 2 \frac{\partial \mathcal{R}}{\partial M} \right). \quad (7.81)$$

In a uniform circular motion (as is the case, to first order, for a geostationary satellite), the mean anomaly  $M$  and the longitude  $\lambda$  are equal up to an additive constant and we thus have

$$\frac{d\lambda}{dt} = \frac{dM}{dt} = n, \quad (7.82)$$

which is just the mean motion. With the values for  $\mathcal{R}$  and  $\mathcal{R}'$  obtained above, we can write

$$\frac{\partial \mathcal{R}}{\partial M} = \frac{\partial \mathcal{R}}{\partial \lambda} = \frac{\partial \mathcal{R}'}{\partial \lambda} = -6 \frac{\mu}{a} \left( \frac{R}{a} \right)^2 J_{22} \sin 2(\lambda - \lambda_{22}). \quad (7.83)$$

With Kepler's third law, we obtain

$$2 \frac{dn}{n} = -3 \frac{da}{a},$$

and thus

$$\frac{dn}{dt} = -\frac{3}{2} \frac{n}{a} \frac{da}{dt}, \quad (7.84)$$

whence we may calculate the longitudinal acceleration:

$$\frac{d^2 \lambda}{dt^2} = -\frac{3}{2} \frac{n}{a} \frac{da}{dt} = -\frac{3}{a^2} \frac{\partial \mathcal{R}'}{\partial \lambda} = 18 \frac{\mu}{a^3} \left( \frac{R}{a} \right)^2 J_{22} \sin 2(\lambda - \lambda_{22}).$$

Therefore, with  $\mu/a^3 = n^2 = \dot{\Omega}_T^2$  and the reduced distance  $\eta_{GS}$ , we have

$$\ddot{\lambda} = 18 \left( \frac{\dot{\Omega}_T}{\eta_{GS}} \right)^2 J_{22} \sin 2(\lambda - \lambda_{22}). \quad (7.85)$$

The numerical values for the Earth give

$$\ddot{\lambda} = \mathcal{A} \sin 2(\lambda - \lambda_{22}) , \quad (7.86)$$

with

$$\frac{\dot{\Omega}_{\text{T}}}{\eta_{\text{GS}}} = \frac{7.292 \times 10^{-5}}{6.611} = 1.1030 \times 10^{-5} \text{ rad s}^{-1} ,$$

$$\begin{aligned} \mathcal{A} &= 18 \left( \frac{\dot{\Omega}_{\text{T}}}{\eta_{\text{GS}}} \right)^2 J_{22} = 18 \times 1.2166 \times 10^{-10} \times 1.8154 \times 10^{-6} \\ &= 3.9756 \times 10^{-15} \text{ rad s}^{-2} , \end{aligned} \quad (7.87)$$

and

$$\mathcal{A} = 3.9756 \times 10^{-15} \times (180/\pi) \times (86,400)^2 = 1.701 \times 10^{-3} \text{ deg day}^{-2} , \quad (7.88)$$

for the coefficient  $\mathcal{A}$  in (degrees/day) per day.

**(b) Third Order Expansion of the Geopotential.** If we write the potential  $U(r, \lambda, \psi)$  to order 3, (3.17) tells us to include terms involving the Legendre functions  $P_{3m}$ . For  $\psi = 0$ ,

$$P_{30} = 0 , \quad P_{31} = -\frac{3}{2} , \quad P_{32} = 0 , \quad P_{33} = 15 .$$

As before, we define

$$J_{31} = \sqrt{C_{31}^2 + S_{31}^2} = \sqrt{\frac{7}{6}} \sqrt{C_{31}^{*2} + S_{31}^{*2}} , \quad (7.89)$$

$$J_{33} = \sqrt{C_{33}^2 + S_{33}^2} = \sqrt{\frac{7}{360}} \sqrt{C_{33}^{*2} + S_{33}^{*2}} , \quad (7.90)$$

$$\lambda_{31} = \arctan \frac{S_{31}^*}{C_{31}^*} , \quad \lambda_{33} = \frac{1}{3} \arctan \frac{S_{33}^*}{C_{33}^*} . \quad (7.91)$$

For the Earth (the EGM2008 or EIGEN model), we have

$$J_{31} = 2.2095 \times 10^{-6} , \quad \lambda_{31} = 6.97^\circ ,$$

$$J_{33} = 0.2214 \times 10^{-6} , \quad \lambda_{33} = 20.99^\circ .$$

With the calculation of  $\partial\mathcal{R}'/\partial\lambda$  and the same procedure as before, we obtain

$$\ddot{\lambda} = 3 \left( \frac{\dot{\Omega}_{\text{T}}}{\eta_{\text{GS}}} \right)^2 \left\{ 6J_{22} \sin 2(\lambda - \lambda_{22}) + \frac{1}{\eta_{\text{GS}}} \left[ -\frac{3}{2}J_{31} \sin(\lambda - \lambda_{31}) + 45J_{33} \sin 3(\lambda - \lambda_{33}) \right] \right\}. \tag{7.92}$$

Bringing in the coefficient  $\mathcal{A}$  defined above by (7.86), we have

$$\ddot{\lambda} = \mathcal{A} \left\{ \sin 2(\lambda - \lambda_{22}) + \frac{1}{4\eta_{\text{GS}}J_{22}} \left[ -J_{31} \sin(\lambda - \lambda_{31}) + 30J_{33} \sin 3(\lambda - \lambda_{33}) \right] \right\}. \tag{7.93}$$

For the Earth, numerical calculation gives

$$\ddot{\lambda} = \mathcal{A} \left[ \sin 2(\lambda - \lambda_{22}) - 0.0460 \sin(\lambda - \lambda_{31}) + 0.1383 \sin 3(\lambda - \lambda_{33}) \right]. \tag{7.94}$$

The graph of  $\ddot{\lambda}(\lambda)$  in Fig. 7.12 gives the dependence of the longitudinal acceleration  $\ddot{\lambda}$  on the longitude  $\lambda$ . Since longitudes are counted positively toward the east, we thus have

$$\ddot{\lambda} > 0 \implies \text{eastward displacement}, \quad \ddot{\lambda} < 0 \implies \text{westward displacement}.$$

The solutions of  $\ddot{\lambda} = 0$  are four longitudes shown on the graph where  $\ddot{\lambda}(\lambda)$  intersects the horizontal axis. The two stable points are on the decreasing portions of the curves, and the unstable points on the increasing portions:

$$\text{stable points: } \lambda = 75.059^\circ = 75^\circ 04' \text{E}, \quad \lambda = 255.089^\circ = 104^\circ 59' \text{W},$$

$$\text{unstable points: } \lambda = 162.098^\circ = 162^\circ 06' \text{E}, \quad \lambda = 348.577^\circ = 11^\circ 25' \text{W}.$$

The values are indicated on Fig. 7.12.

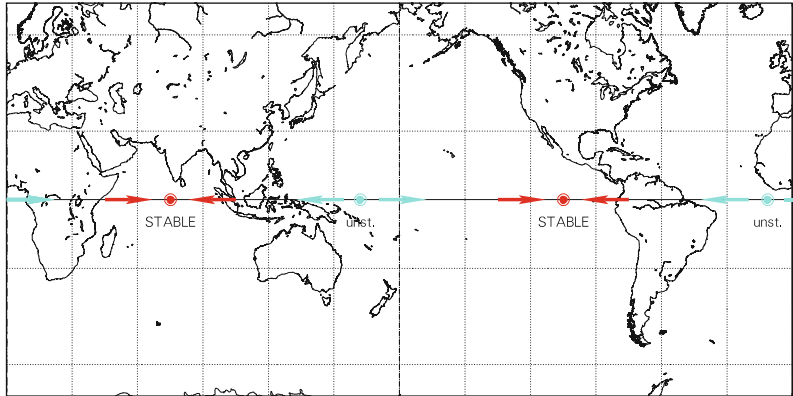
Looking at the map of anomalies of the geoid in Fig. 3.5, we observe that the stable point  $\lambda = 75^\circ \text{E}$  corresponds to the longitude of the potential trough located south of India. The two unstable points correspond to the latitudes of the peaks, one located in Papua New Guinea at  $\lambda = 162^\circ \text{E}$ , and the other in Iceland at  $\lambda = 11^\circ \text{W}$ .

Equation (7.94) shows that it is the degree 2 harmonic that contributes most. The four longitudes obtained solely from  $\lambda_{22}$ , viz.,

$$\lambda = \lambda_{22} + k90^\circ, \quad k = 1, 2, 3, 4,$$

Projection: Mercator      Project. centre: 0.0 ° ; 180.0 ° W  
 Property: Conformal      Aspect: Direct  
 ⊕ T.:Cylindrical - Graticule: 30°    \$5.3\{ [+90.0/ +0.0/ +90.0] [-]

Ίξιων  
**MC \* LMD**  
 ΑΤΛΑΣ



**GEOSTATIONARY**      a<sub>GS</sub> = 42165.785 km      Gravitat. Model: EGM2008  
 Longitudinal Acceleration      Inclination = 0.00°  
 Stable Point ... 75.1 ° E  
 Stable Point ... 104.9 ° W

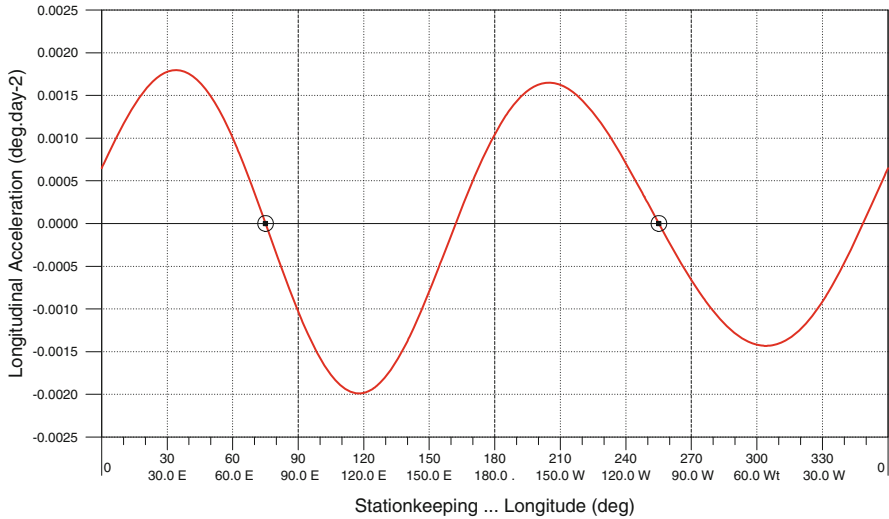


FIG. 7.12 : Dependence of the longitudinal acceleration of a geostationary satellite on the longitude. Points with zero acceleration are equilibrium points, viz.,  $\lambda = 75.1^\circ E$  and  $\lambda = 104.9^\circ W$  for the stable points (circles) and  $\lambda = 162.1^\circ E$  and  $\lambda = 11.4^\circ W$  for the unstable points. In the case presented here, the geostationary satellite is only affected by orbital perturbations due to the geopotential (EGM2008 model). Upper: Map showing positions of stable and unstable points.

that is,  $75^\circ$ ,  $165^\circ$ ,  $255^\circ$ , and  $345^\circ$ , are very close to the four longitudes obtained using (7.94) and going to order 3. The contributions from the other terms become negligible from order 4, since a further multiplicative factor of  $1/\eta_{GS}$ , or 0.15, comes in for each new order.

**Example 7.7** *Describe the longitudinal drift of a geostationary satellite located over the Greenwich meridian.*

► A satellite stationed at longitude  $\lambda = 0^\circ$  is subject to an acceleration  $\ddot{\lambda}(0^\circ) = 0.737 \times 10^{-3} \text{ deg day}^{-2}$ . This positive value indicates an eastward displacement, and  $\ddot{\lambda}$  increases to  $\ddot{\lambda}(34^\circ) = 1.885 \times 10^{-3} \text{ deg day}^{-2}$ . The satellite continues to drift eastward to  $\lambda = 75.082^\circ$ , a longitude at which  $\ddot{\lambda} = 0$ . From this time on, if it moves slightly eastward or westward, it will be brought back to the stable equilibrium point. ◀

**Example 7.8** *Maintaining the Chinese geostationary positioning satellite Beidou-1A in place.*

► The Chinese positioning system uses two geostationary satellites, Beidou-1A and -1B. Their positions must be very accurately known (see Chap. 14). The effective stationing longitude  $\lambda_S$  of each satellite must remain very close to the nominal longitude  $\lambda_{S0}$ , to within a very tight margin:

$$\lambda_S = \lambda_{S0} \pm 0.1^\circ .$$

For the satellite Beidou-1A, the values of  $\lambda_S$  are noted in Fig. 7.13 as a function of time over a period of two and half years. For the reference value  $\lambda_{S0} = 139.95^\circ\text{E}$ , Fig. 7.12 indicates  $\ddot{\lambda} = -1.5 \times 10^{-3} \text{ deg day}^{-2}$ . This negative acceleration, i.e.,  $d^2\lambda/dt^2 < 0$ , tells us that the satellite tends to move westward toward the stable point  $75^\circ\text{E}$ . When it approaches the longitude  $139.85^\circ$ , its engines are started so as to reduce the altitude of the satellite. This causes it to slip eastward to  $140.05^\circ$  or  $140.10^\circ$ . Such maneuvers are carried out every month or so. The satellite is then brought westward with an acceleration  $\ddot{\lambda}$ , giving the function  $\lambda_S(t)$  a parabolic shape. ◀

### 7.4.6 Geosynchronous Satellites with Highly Eccentric Orbits

Countries like Russia and Canada, situated as they are at high latitudes, have little use for geostationary satellites, which are equatorial. As we shall see shortly, the choice of an orbit that is both inclined and elliptical (to take advantage of the areal law), can be favourable for northerly regions. In order to



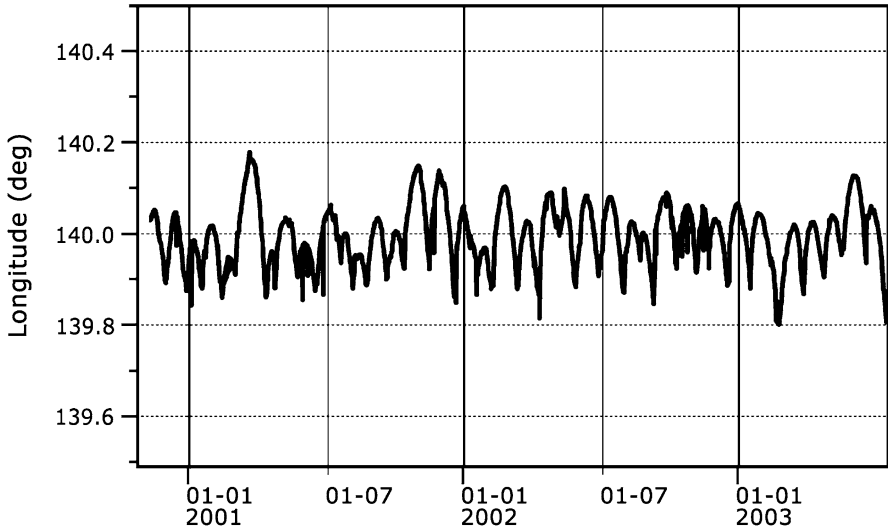


FIG. 7.13 : Actual stationing longitude of the satellite Beidou-1A as a function of time over a period of 33 months, from 1 October 2000 to 1 August 2003. Credit: China Academy of Space and Technology (CAST).

reduce apsidal precession to a minimum, the critical inclination  $i = i_C = 63.4^\circ$  is essential. The period can be fixed at one (sidereal) day so as to obtain a geosynchronous satellite.

The Tundra-type orbit was studied by both Russia and Canada and the idea taken up again by the European Space Agency (ESA) for its Archimedes project. Two different orbits are planned: Tundra (or Tundra 2) and Supertundra (or Tundra 1), with the value  $a = 42,163$  km almost independent of the eccentricity and very close to  $a_{GS}$  as given by (7.70). Since the values of the inclination and period are determined, we have:

- For Tundra,  $e = 0.2668$ ,  $h_p = 24,536$  km,  $h_a = 47,034$  km.
- For Supertundra,  $e = 0.4230$ ,  $h_p = 17,950$  km,  $h_a = 53,620$  km.

The visibility time, over which the satellite is visible under acceptable geometrical conditions for the relevant regions (see Chap. 13), is 8 h for the first of these orbits and 12 h for the second, once the position of the apogee has been correctly established. This means that three and two satellites are needed, respectively, to achieve permanent coverage. Under such conditions, we may say that we have obtained the equivalent of one geostationary satellite but at high latitude.

The Tundra orbit has been used successfully since 2000 by the SD-Radio constellation of US communications satellites.<sup>24</sup>

<sup>24</sup>The three satellites Sirius-1, -2, and -3 (also called SD-Radio-1, -2, and -3), launched from Kazakhstan on 30 June, 5 September, and 30 November 2000, are on a geosynchronous

## 7.5 Sun-Synchronicity

### 7.5.1 Definition

The orbital plane  $\mathcal{P}$  of the satellite rotates in  $\mathfrak{R}$ , about the polar axis, at a rate  $\dot{\Omega}$ , which characterises the angular speed of the vector  $\mathbf{ON}$  in the plane  $\mathcal{E}$ , where  $O$  is the center of the Earth and  $N$  the ascending node, as shown in Fig. 5.1.

We seek a type of orbit in which the passage at the ascending node always occurs at the same solar time. We thus require  $\mathbf{ON}$  to make a constant angle with the direction of the Sun, since the hour angle (and hence the local mean time) is the dihedral angle between the meridian plane of the relevant point (here  $N$ ) and the plane containing the polar axis and the Sun. For this to happen, the nodal precession rate  $\dot{\Omega}$  must equal the angular speed of the Earth's motion around the Sun. Such a satellite is said to be Sun-synchronous or heliosynchronous:

$$\text{Sun-synchronous satellite} \iff \dot{\Omega} = \dot{\Omega}_{\text{S}} . \quad (7.95)$$

A satellite with an elliptical orbit can be Sun-synchronous, in which case the nodal precession rate is given in the form  $\dot{\Omega} = \dot{\Omega}(a, e, i)$ . We shall return to this case below, with the example of the satellite Ellipso Borealis. However, in most cases, and in particular for Earth-observation satellites,<sup>25</sup> only circular and near-circular orbits are used, so that  $\dot{\Omega} = \dot{\Omega}(a, i)$ .

The ground track of a Sun-synchronous satellite always crosses a given latitude at the same time (local mean time), which is not the crossing time of the ascending node, and which becomes ever further away from it as one moves away from the equator.

If  $P$  is the nodal precession rate in round trips per year, the condition for Sun-synchronicity can clearly be written

$$P = 1 . \quad (7.96)$$

### 7.5.2 Constant of Sun-Synchronicity

The condition (7.95) and the values of  $K_0$  and  $\dot{\Omega}_{\text{S}}$  defined by (7.5) and (7.20) lead us to define a quantity  $k_{\text{h}}$  by

---

orbit:  $e = 0.2700$ ,  $h_{\text{p}} = 24,400$  km,  $h_{\text{a}} = 47,170$  km. They are operational for North America between longitudes  $60^{\circ}\text{W}$  and  $140^{\circ}\text{W}$ , and broadcast paying music programmes for car radios. Between 2001 and 2006, this music-loving private operator sent the four satellites Rock and Roll, then Rythm and Blues, into geostationary orbit.

<sup>25</sup>Satellites devoted to magnetospheric studies are often placed in elliptical Sun-synchronous orbits. Examples are MagSat, Ørsted, or the two German satellites Aeos-1 and -2. One should also mention those satellites whose orbits, originally intended to be circular, have become elliptical owing to launch errors, e.g., Nimbus-1, mentioned below.

$$k_h = \frac{K_0}{\dot{\Omega}_S}, \quad (7.97)$$

which yields

$$k_h = \sqrt{\frac{3}{4\pi}} J_2 \sqrt{\frac{\mu}{R^3}} T_{\text{sid}}. \quad (7.98)$$

This dimensionless constant  $k_h$ , which we shall call the constant of Sun-synchronicity, plays a very important role in the study of satellites. It depends only on:

- Characteristics of the planet playing host to the satellite, such as the mass (via  $\mu$ ), radius ( $R$ ) (in fact the mass per unit volume  $\rho_o$ ), and the flattening (the ellipticity factor  $J_2$  of the potential).
- The motion of the planet around the Sun, determining the sidereal year  $T_{\text{sid}}$ .

It can also be expressed in terms of the Keplerian period of the satellite at altitude 0, where it clearly appears as a ratio of periods:

$$k_h = \frac{3}{2} \frac{T_{\text{sid}}}{T_{0(h=0)}} J_2, \quad (7.99)$$

or again, using the notation of (7.9),

$$k_h = \frac{3\mathcal{G}}{4\pi} J_2 \sqrt{\rho_o} T_{\text{sid}}. \quad (7.100)$$

This constant arises when considering the conditions for Sun-synchronicity, but also more generally, in all aspects of the motion of the satellite orbit relative to its host planet and the Sun.

For the Earth, it has the value

$$k_h = 10.10949. \quad (7.101)$$

This value of the constant,  $k_h \approx 10.11$ , means that, for a satellite of altitude  $h = 0$  and inclination  $i = 0$ , the nodal precession rate is 10.11 times greater than the angular speed of the Earth's axis in its motion around the Sun (absolute value).

### 7.5.3 Calculating the Orbit: Circular Case

#### Sun-Synchronous Inclination

Equations (7.4)–(7.7), together with (7.95) and (7.97) give

$$\dot{\Omega}(a, i) = \dot{\Omega}_S \iff -\frac{1}{\cos i} \left(\frac{a}{R}\right)^{7/2} = k_h. \quad (7.102)$$

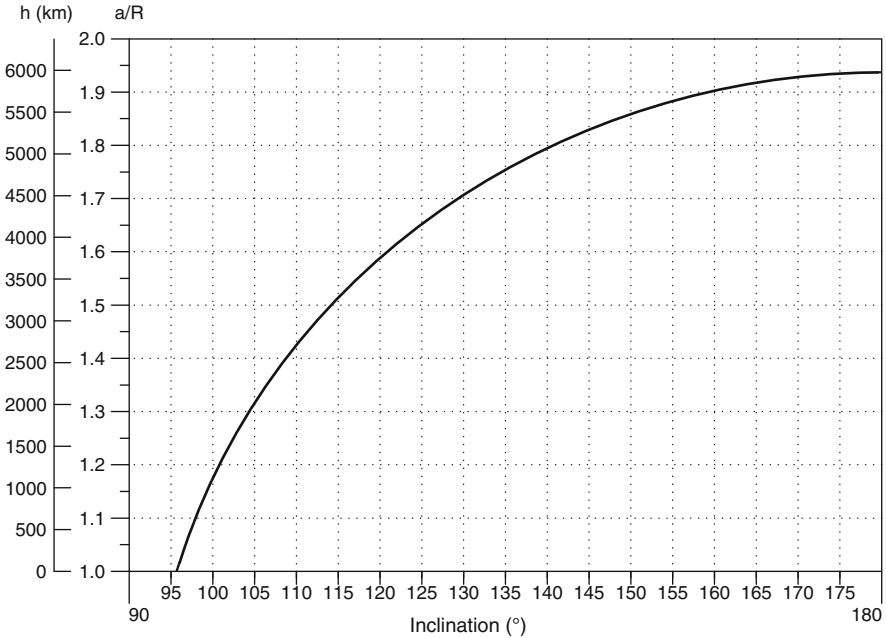


FIG. 7.14 : Satellite altitude as a function of angle of inclination for Sun-synchronous satellites with circular orbit. The whole range of possible values is shown.

Introducing the reduced distance  $\eta = a/R$ , we obtain a very simple expression for the Sun-synchronicity condition:

$$\eta^{7/2} = -k_h \cos i . \tag{7.103}$$

This gives  $\eta$  as a function of  $i$ :

$$\eta = (-k_h \cos i)^{2/7} \tag{7.104}$$

or  $i$  as a function of  $\eta$ :

$$i = \arccos \left( -\frac{\eta^{7/2}}{k_h} \right) . \tag{7.105}$$

We thus see that:

- The quantities  $i$  and  $a$  are related, so that, if we choose one, the other is thereby fixed.
- The value of  $\cos i$  must be negative for this equality to hold, which shows that a Sun-synchronous orbit is necessarily retrograde.

Figure 7.14 shows the curve of  $\eta$  (or  $a$ , or  $h$ ) as a function of  $i$ . In general, the quantity  $a$  is chosen and the value of  $i$  is then deduced from (7.105), in

which case it is called the inclination of the Sun-synchronous orbit, or more elliptically, the Sun-synchronous inclination. In this case, we may attach<sup>26</sup> the subscript HS to  $i$ , writing  $i_{\text{HS}} = i_{\text{HS}}(a) = i(a)$ .

### Bounds on $i$ and $h$ for a Sun-Synchronous Satellite

The minimum value of  $i_{\text{HS}}$ , written  $i_{\text{HS min}}$  or  $i_{\text{m}}$ , is obtained for  $h = 0$ , i.e., for a fictitious satellite revolving at ground level. With  $\eta = 1$ , we have

$$i_{\text{HS min}} = i_{\text{m}} = \arccos\left(-\frac{1}{k_{\text{h}}}\right) = \arccos(-0.0989) = 95.7^\circ. \quad (7.106)$$

The maximum value of  $h$ , written  $h_{\text{HS max}}$ , is obtained for  $i = 180^\circ$ :

$$\eta_{\text{HS max}} = (k_{\text{h}})^{2/7} = 1.9367, \quad (7.107)$$

$$a_{\text{HS max}} = 12,331 \text{ km}, \quad h_{\text{HS max}} = 5,964 \text{ km}. \quad (7.108)$$

It is therefore impossible to have a Sun-synchronous satellite (in near-circular orbit) at inclination lower than  $96^\circ$ , or altitude above about 6,000 km.

### Calculations for a Standard Sun-Synchronous Satellite

Most Sun-synchronous satellites currently operating have altitude around 800 km (between 700 and 900 km for remote sensing, and lower for reconnaissance missions). Figure 7.14 shows that, at these altitudes, the relation between  $i_{\text{HS}}$  and  $h$  is almost linear.

Let us now examine the variation of  $i$  near the central value for the range of altitudes mentioned here, i.e.,  $h_1 = 800$  km. The inclination corresponding to this altitude  $h_1$  is  $i_1 = i_{\text{HS}_1} = 98.60^\circ$ . Differentiating (7.103), we obtain

$$\frac{7}{2} \frac{da}{a} = -\tan i \, di.$$

Taking  $i$  near  $i_{\text{HS}_1}$  and  $a$  near  $R + h_1$ , we have the following relation between finite increments  $\Delta i_{\text{HS}}$  (in degrees) and  $\Delta h$  or  $\Delta a$  (in kilometers):

$$\Delta i_{\text{HS}} = 4.17 \times 10^{-3} \Delta h. \quad (7.109)$$

### Calculating the Orbit with Expansion up to $J_n$

Up to now, we have obtained results using (7.102), the basic relation for Sun-synchronicity, with the value of  $\dot{\Omega}$  limited to the  $J_2$  term. This therefore corresponds to the relation

---

<sup>26</sup>Here we use HS as subscript for Sun-synchronous. It refers to the occasionally heard “heliosynchronous”, a word made up only of Greek roots, hence more satisfying from a linguistic standpoint.

$$\dot{\Omega} = \dot{\Omega}_S, \quad \text{with} \quad \frac{\dot{\Omega}}{n} = J_2 A_2 \cos i \quad \text{and} \quad A_2 = \left(\frac{R}{p}\right)^2 \left(-\frac{3}{2}\right). \quad (7.110)$$

When we use an expansion up to degree  $l$  for  $\dot{\Omega}$ , where  $l$  is even and we set  $l = 2m$ , this becomes

$$\dot{\Omega} = \dot{\Omega}_S, \quad \text{with} \quad \frac{\dot{\Omega}}{n} = \left[ J_2 A_2 + J_2^2 B_2(i) + \sum_{j=2}^m J_{2j} A_{2j}(i) \right] \cos i, \quad (7.111)$$

where

$$A_{2j}(i) = \left(\frac{R}{p}\right)^{2j} \sum_{k=0}^{j-1} q_{2k}^{(j)} \sin^{2k} i, \quad B_2(i) = \left(\frac{R}{p}\right)^4 (q'_0 + q'_2 \sin^2 i),$$

and the coefficients  $q_{2k}^{(j)}$  and  $q'_{2k}$  involve numerical terms and the value of the eccentricity  $e$ .

If we solve (7.111) for the inclination  $i_{\text{HS}}$ , we obtain an equation of degree  $l - 1$  in  $\cos i$ . This equation is in fact easy to solve because the terms  $J_2^2$  and  $J_l$  do not exceed  $10^{-3} J_2$ . We begin by calculating  $i$  in the case when only  $J_2$  is considered, using (7.102) or (7.110). Inserting this value in (7.111), and after several iterations, we obtain the required value. The correction is very small. For  $h = 800$  km, we have  $i_{\text{HS}}(J_4) = 98.628^\circ$  and  $i_{\text{HS}}(J_2) = 98.603^\circ$ , i.e., a difference of  $0.025^\circ$ .

**Note.** The value of the Sun-synchronous inclination  $i_{\text{HS}}$  is indicated in all figures in this book showing the ground tracks of Sun-synchronous satellites. Obtained using the expansion to order  $J_4$ , they differ by a few hundredths of a degree from the value obtained directly by (7.105).

**Example 7.9** Calculate the inclination of the Landsat satellites.

► The US programme Landsat was the first civilian programme for observation of Earth resources (NASA). These satellites are in circular Sun-synchronous orbit. The first three (Landsat-1 to -3) were at an altitude of 908 km, but for the following, Landsat-4 to -8, the altitude was lowered to 700 km:

- Landsat-3:  $a = 7,285.799$  km,  $\eta = a/R = 1.142308$ ,

$$\cos i = -\eta^{7/2}/k_h = -1.593095/10.10949 = -0.15758,$$

$$i = \arccos(-0.15758) = 99.07^\circ.$$

Expanding the geopotential to order 4, we obtain  $i = 99.09^\circ$ .

- Landsat-8:  $a = 7,077.738$  km,  $\eta = a/R = 1.109687$ ,

$$\cos i = -\eta^{7/2}/k_h = -1.439469/10.10949 = -0.14245 ,$$

$$i = \arccos(-0.14245) = 98.19^\circ .$$

Expanding the geopotential to order 4, we obtain  $i = 98.21^\circ$ .

A difference of altitude  $\Delta h = 908 - 700 = 208$  km leads to a change in the angle equal to  $\Delta i_{\text{HS}} = 99.09 - 98.21 = 0.88^\circ$ . This value can also be obtained using (7.109):

$$\Delta i_{\text{HS}} = 4.17 \times 10^{-3} \times 208 = 0.88^\circ . \quad \blacktriangleleft$$

## 7.5.4 Calculating the Orbit: Elliptical Case

### Sun-Synchronous Inclination

To examine the case of an orbit with eccentricity  $e$ , we use (6.73) or (7.15) to order 2. This yields

$$\eta = \left[ -\frac{k_h}{(1-e^2)^2} \cos i \right]^{2/7} . \quad (7.112)$$

In general,  $a$  and  $e$  are chosen and we obtain the inclination  $i$  from

$$i = \arccos \left[ -\frac{\eta^{7/2}}{k_h} (1-e^2)^2 \right] . \quad (7.113)$$

It is important to note that not all values of  $e$  are possible.

Consider for instance a circular orbit of altitude  $h = 640$  km, or  $\eta = 1.1$ . If we increase the eccentricity  $e$  of this orbit, while keeping the same semi-major axis  $a$ , we obtain a maximal value  $h_a = 1,280$  km for the altitude at apogee, corresponding to  $h_p = 0$  km for the altitude at perigee. It is easy to see that one could not go below this value for  $h_p$ ! The eccentricity thus has a maximal value  $e_1$ , which depends on  $a$  (and the radius  $R$  of the planet). In this example,  $e_1 = 0.09$ .

Quite generally, putting  $h_p = 0$ , we have

$$a_1(1 - e_1) = R ,$$

or

$$\eta_1 = \frac{1}{1 - e_1} , \quad \text{whence } e_1 = 1 - \frac{1}{\eta_1} , \quad (7.114)$$

where  $a_1$  and  $\eta_1 = a_1/R$  are the values corresponding to  $e_1$ .

Figure 7.15 shows the relation between  $\eta$  and  $i$  for several values of  $e$  within the range of possible values. Since  $\dot{\Omega}$  varies for Sun-synchronous satellites in the same direction as  $e$ , the angle  $i$  decreases when  $e$  increases, for a given value of  $a$ .

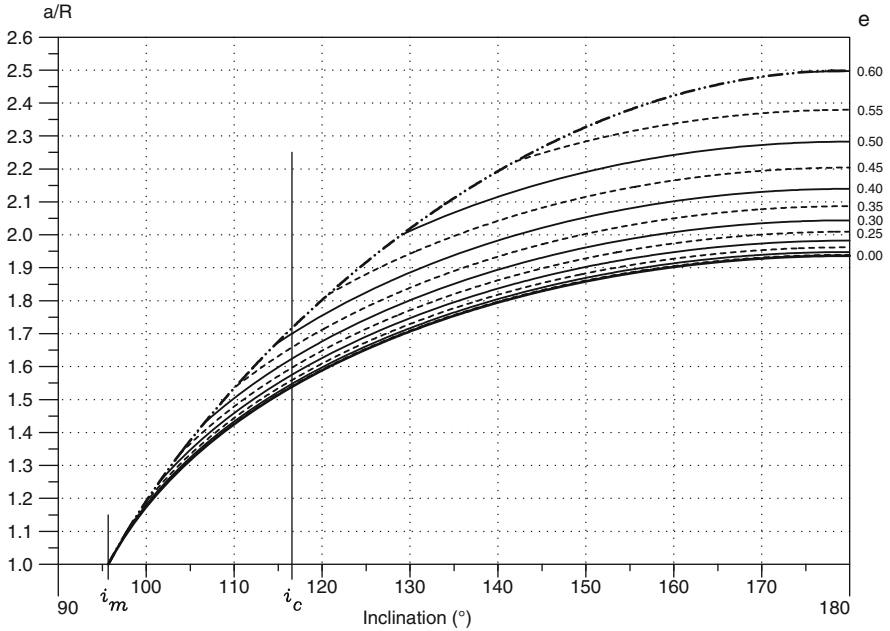


FIG. 7.15 : Reduced distance  $\eta = a/R$  as a function of the inclination  $i$  for Sun-synchronous satellites with elliptical orbit for various values of the eccentricity  $e$ . The whole range of possible values is shown. The specific values  $i_m$  and  $i_c$  are indicated (see text).

**Bounds on  $i$ ,  $a$ , and  $e$  for a Sun-Synchronous Satellite**

The inclination  $i$  varies between  $i_{HS\min} = 95.7^\circ$ , obtained from (7.106), to  $180^\circ$ . For a given inclination,  $\eta$  varies between  $\eta_0$ , given by (7.112) with  $e = 0$ , and  $\eta_1$ , given by this same equation when  $e$  takes the value  $e_1$ . Since  $e_1$  and  $\eta_1$  are related by (7.114), we obtain

$$-\frac{1}{k_h} \eta^{3/2} \left( 2 - \frac{1}{\eta} \right)^2 = \cos i, \tag{7.115}$$

and  $\eta_1$  is the solution of this equation, provided that the term on the left is less than or equal to 1.

For  $i = 180^\circ$ ,  $\eta$  varies between  $\eta_0 = 1.9367$  for  $e = 0$  to  $\eta_1 = 2.4988$  for  $e_1 = 0.5998$  (see Fig. 7.15, where the latter value has been taken as 0.60).

**Sun-Synchronous Satellites in Highly Eccentric Orbit**

In the vast majority of cases, Sun-synchronous orbits are near-circular, since they are used for Earth observation missions which require the altitude to remain as close to constant as possible. However, there are some planned elliptical orbits in the field of communications.



For a highly eccentric orbit, the Sun-synchronicity condition also depends on a further constraint. Indeed, to ensure that the perigee does not drift on the orbit, the inclination must be chosen at its critical value, as given by (6.79). It is essential that this value be greater than  $90^\circ$ , or  $i = 116.6^\circ$ . The orbit of Ellipso Borealis exemplifies this.

**Example 7.10** *Notes on the orbit of satellites in the Ellipso Borealis constellation.*

► The satellite Ellipso Borealis has inclination  $i = 116.6^\circ$  in order to cancel apsidal precession. As the inclination is fixed, we thus select  $a$  and  $e$  as appropriate for a Sun-synchronous orbit. The critical inclination  $i_C$  is indicated in Fig. 7.15. If we solve (7.112) for  $\eta_0$  and (7.115) for  $\eta_1$ , we obtain

$$\eta_0 = 1.5389 \quad \text{for } e = 0 ,$$

$$\eta_1 = 1.7169 \quad \text{for } e = e_1 = 1 - 1/\eta_1 = 0.4174 .$$

The semi-major axis thus lies between  $a_0 = 9,815.4\text{ km}$  and  $a_1 = 10,951.1\text{ km}$ . For other reasons relating to the period and also the question of recurrence, the semi-major axis is taken equal to  $a = 10,559.2\text{ km}$ , which corresponds to an eccentricity of  $e = 0.3463$  (see Table 11.7). The altitudes at the perigee and apogee are  $h_p = 524\text{ km}$  and  $h_a = 7,838\text{ km}$ , respectively. This configuration of critical inclination, Sun-synchronicity, and recurrence is rather novel and particularly interesting from the point of view of orbitography. ◀

## 7.5.5 Sun-Synchronous Satellites

Sun-synchronicity makes judicious use of the nodal precession of the satellite orbit. It is a fundamental advantage in space-based observation to be able to guarantee the passage of a satellite at constant local time for a given latitude, hence in lighting conditions such that the solar zenithal angle varies annually over a well defined (and rather narrow) range.

### Historical Note on Sun-Synchronous Satellites

The first recorded Sun-synchronous satellite was SAMOS-2 (Satellite and Missile Observation System), a US military photographic reconnaissance satellite, launched on 31 January 1961, with  $h_p = 474\text{ km}$ ,  $h_a = 557\text{ km}$ , and  $i = 97.4^\circ$ .

The first civilian arena to be interested in Sun-synchronous orbits was meteorology. The satellite Nimbus-1 was launched on 28 August 1964. As the launch was not entirely successful, it ended up on an eccentric, although

nevertheless Sun-synchronous orbit, with  $h_p = 429$  km,  $h_a = 937$  km. It was followed by TIROS-9 and TIROS-10 (Television and Infra Red Observation Satellite), launched in 1965 into an eccentric orbit for the former and a near-circular orbit with  $h \approx 760$  km,  $i = 98.8^\circ$ , for the latter. All US meteorological satellites were subsequently placed in Sun-synchronous orbits: Nimbus, ESSA, and NOAA on the civilian side, and DMSP for the military.

In contrast, the Soviet Union sent up dozens of meteorological satellites, at a rate of three or four per year, as part of the series Meteor-1, -2, and -3, for which they opted for a prograde non-Sun-synchronous near-polar orbit. Only the last four of the Meteor-1 series were Sun-synchronous, launched between 1977 and 1981, with  $h \approx 600$  km,  $i = 97.7^\circ$ . However, these satellites in the Meteor-P series (Meteor-Priroda, where *priroda* means “nature” in Russian), adaptations of the meteorological satellites, were more generally destined for the study of the environment and remote sensing.

Indeed, remote-sensing applications have an even greater interest in Sun-synchronous orbits than does meteorology. The first programme in this field was American, with the Landsat programme, which began in 1972 and launched all its satellites into Sun-synchronous orbit. Corresponding programmes, such as the French SPOT, the European ERS, the Indian IRS, and the Russian Resurs-O, were all based on Sun-synchronous satellites, like the environmental missions, e.g., EOS, Envisat, ADEOS, and the many programmes implemented since 2000, e.g., Ikonos, then GeoEye, QuickBird, then WorldView, to provide images with resolution of the order of a meter or half a meter on a commercial basis.

Military reconnaissance satellites are also to be found in the latter category, and they are of course Sun-synchronous, like the French Hélios satellites, if they are intended to operate over long periods. At the beginning of the space age, military reconnaissance missions were very short, from a few days to about a week, for most Soviet satellites and some US satellites. In this case, the idea of a Sun-synchronous orbit would be meaningless. Indeed, any orbit is Sun-synchronous as long as nodal precession has not had sufficient time to become noticeable. Furthermore, near-polar orbits are not necessarily convenient for overflying “sensitive” regions.

### 7.5.6 Orbit Maintenance

As for any satellite, the orbit of a Sun-synchronous satellite will tend to drift as time goes by, leading to slight modifications in the orbital elements. The two main perturbative effects are the lunisolar attraction and atmospheric drag. The first of these causes a slight variation in the satellite inclination, while the second causes braking and hence a reduction in altitude, as seen in Example 6.3.

In the case of Sun-synchronous satellites, it is of particular importance to achieve a constant crossing time at the ascending node (in local time or LMT). If, like the SPOT, Landsat, ERS, and ADEOS satellites, the Sun-synchronous

satellite is recurrent, in the sense that its ground track must repeat exactly the same locus after a certain number of revolutions (see Chap. 11), it is even more important to maintain the orbit.

Consider the example of the SPOT satellites, for which the passage at the descending node is fixed at  $\tau_{\text{DN}} = 10:30 \pm 0:10$ . To respect the recurrence condition, which requires the ground track to pass within 3 km of the equator, altitude corrections are necessary. These maneuvers take place every 2–8 weeks depending on the level of solar activity. Every 18 months or so, the inclination is reset. Such frequent maneuvers mean that the crossing time at the descending node is in fact  $\tau_{\text{DN}} = 10:30 \pm 0:02$  (the maximal discrepancy of 2 min being well below the variation in the equation of time).

Certain Sun-synchronous satellites are no longer maintained in orbit (by necessity or by choice), and the local crossing time at the ascending node drifts in consequence (see Fig. 10.15). We shall return to this point in Chap. 10 when we study the crossing times of Sun-synchronous satellites.

# Chapter 8

## Ground Track of a Satellite

### 8.1 Position of Satellite on Its Orbit

Let  $\mathfrak{R}(O; x, y, z)$  be the Galilean reference frame already defined. The satellite  $S$  is in an elliptical orbit around the center of attraction  $O$ . The orbital plane  $\mathcal{P}$  makes a constant angle  $i$  with the equatorial plane  $\mathcal{E}$ . However, although the plane  $\mathcal{P}$  is considered as fixed relative to  $\mathfrak{R}$  in the Keplerian motion, in a real (perturbed) motion, it will in fact rotate about the polar axis. This is precessional motion,<sup>1</sup> occurring with angular speed  $\dot{\Omega}$ , as calculated in the last two chapters. A schematic representation of this motion is given in Fig. 8.1. We shall describe the position of  $S$  in  $\mathfrak{R}$  using the Euler angles.

#### 8.1.1 Using Euler Angles to Describe Satellite Motion

The three Euler angles<sup>2</sup>  $\alpha_1$ ,  $\alpha_2$ , and  $\alpha_3$ , were introduced in Chap. 5 to specify the orbit and its perigee in space (see in particular the appendix in Sect. 5.4). In the present case, we wish to specify  $S$ . We have already established the correspondence between the Euler angles and the orbital elements (see Fig. 5.1 and Table 5.1):

---

<sup>1</sup>The word “precession”, meaning “the action of preceding”, was coined by Copernicus around 1530 (*præcessio, nis* in Latin) to speak about the precession of the equinoxes, i.e., the retrograde motion of the equinoctial points. This term was then taken up in mechanics to describe the corresponding Euler angle. In the motion of the satellite orbital plane, the word “precession” clearly refers to a motion that may actually be prograde, as well as retrograde.

<sup>2</sup>The three Euler angles are traditionally denoted by  $\psi$ ,  $\theta$ ,  $\varphi$ , or by  $\varphi$ ,  $\theta$ ,  $\psi$ , in those orders. To avoid confusion with the latitudes denoted by  $\psi$  and  $\varphi$  elsewhere in the book, we have chosen to use the notation  $\alpha_i$ ,  $i = 1, 2, 3$ .

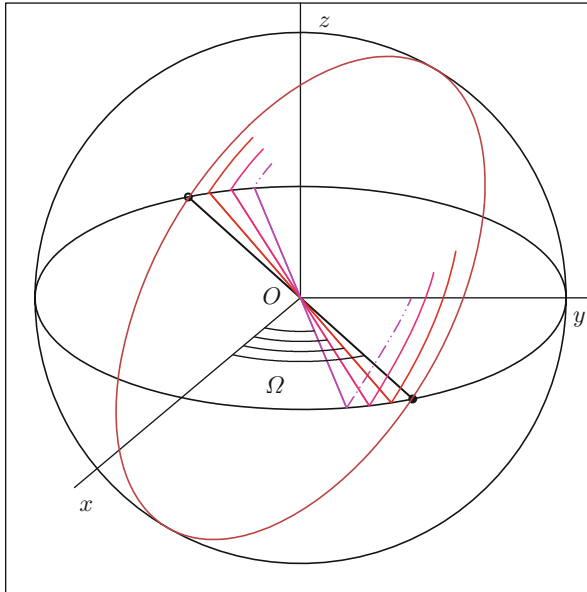


FIG. 8.1 : *Precessional motion of the orbit in the frame  $\mathfrak{R}$ . The orbital plane rotates about the polar axis, maintaining a fixed inclination relative to the equatorial plane ( $xOy$ ). Its projection onto the equatorial plane can be used to measure  $\Omega$ , the longitude of the ascending node, whose variation is given by  $\dot{\Omega}$ . If the satellite has a prograde orbit (as here, where the ascending node has been indicated by a small black circle, the descending node by a small white circle, and the latest ground track by a dash-dotted curve), the precessional motion is retrograde, i.e.,  $\dot{\Omega} < 0$ .*

$$\alpha_1 = \Omega , \quad (8.1)$$

$$\alpha_2 = i , \quad (8.2)$$

$$\alpha_3 = \omega + v . \quad (8.3)$$

Although they are fixed for the Keplerian orbit, the angles  $\Omega$ ,  $\omega$ , and  $M - nt$  vary in time and the inclination  $i$  remains constant for a real orbit (if we consider only secular variations).

The distance from  $S$  to the center of attraction  $O$  is given by (4.60), expressed in terms of the true anomaly  $v$ :

$$r = \frac{a(1 - e^2)}{1 + e \cos v} . \quad (8.4)$$

Since this distance is specified, the position of  $S$  is determined by composing the following three rotations, shown schematically in Fig. 8.2 and described below. The ascending node is denoted by  $N$ .

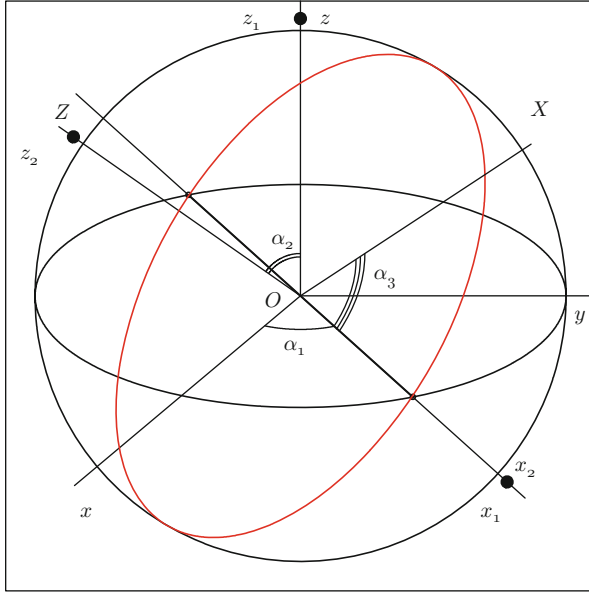


FIG. 8.2: The three rotations taking a given point on a sphere to another arbitrary point, using the three Euler angles. Black circles indicate the three axes of rotation:  $Oz = Oz_1$  for  $[P_1]$ ,  $Ox_1 = Ox_2$  for  $[P_2]$ ,  $Oz_2 = OZ$  for  $[P_3]$ .

- Precessional motion in  $\mathcal{E}$ , taking the straight line  $Ox$  onto the straight line  $ON (= Ox_1)$ :  
 $\implies P_1$  : rotation through angle  $(Ox, Ox_1) = \alpha_1$  about axis  $Oz$  .
- Rotation of  $\mathcal{E}$  onto  $\mathcal{P}$  about the line of nodes:  
 $\implies P_2$  : rotation through angle  $(Oz_1, Oz_2) = \alpha_2$  about axis  $Ox_1$  .
- Rotation in  $\mathcal{P}$  which takes the straight line  $ON (= Ox_1 = Ox_2)$  onto the straight line  $OS$  (or  $OX$ ):  
 $\implies P_3$  : rotation through angle  $(Ox_2, OX) = \alpha_3$  about  $Oz_2 = OZ$  .

Note that, in the case of the Euler angles, this decomposition is one-to-one with the following domains:

$$\alpha_1 \in [0, 2\pi) , \quad \alpha_2 \in [0, \pi] , \quad \alpha_3 \in [0, 2\pi) .$$

The axes and angles of rotation are summarised here:

$$\begin{aligned} (Ox, Oy, Oz) &\xrightarrow{P_1} (Ox_1, Oy_1, Oz_1 = Oz) , \\ (Ox_1, Oy_1, Oz_1) &\xrightarrow{P_2} (Ox_2 = Ox_1, Oy_2, Oz_2) , \\ (Ox_2, Oy_2, Oz_2) &\xrightarrow{P_3} (OX, OY, OZ = Oz_2) . \end{aligned}$$

We then deduce the three rotation matrices:

$$P_1 = \begin{pmatrix} \cos \alpha_1 & -\sin \alpha_1 & 0 \\ \sin \alpha_1 & \cos \alpha_1 & 0 \\ 0 & 0 & 1 \end{pmatrix}, \quad (8.5)$$

$$P_2 = \begin{pmatrix} 1 & 0 & 0 \\ 0 & \cos \alpha_2 & -\sin \alpha_2 \\ 0 & \sin \alpha_2 & \cos \alpha_2 \end{pmatrix}, \quad (8.6)$$

$$P_3 = \begin{pmatrix} \cos \alpha_3 & -\sin \alpha_3 & 0 \\ \sin \alpha_3 & \cos \alpha_3 & 0 \\ 0 & 0 & 1 \end{pmatrix}. \quad (8.7)$$

The matrix product of these three matrices gives the matrix  $P$ , calculated below.

### 8.1.2 Position of Satellite in Cartesian Coordinates

Without loss of generality, we consider that  $N$  is on the axis  $Ox$  at zero time. Its coordinates are thus  $(r, 0, 0)$ . The coordinates of  $S(X, Y, Z)$  are obtained from those of  $N(x, y, z)$  by applying  $P$ :

$$\begin{pmatrix} X \\ Y \\ Z \end{pmatrix} = P \begin{pmatrix} x \\ y \\ z \end{pmatrix} = P \begin{pmatrix} r \\ 0 \\ 0 \end{pmatrix}.$$

We see that only the first column of the matrix  $P$  will be required for this calculation. We thus calculate the matrix product  $P = P_1 P_2 P_3$ , writing it in the form

$$P = \begin{pmatrix} \cos \alpha_1 \cos \alpha_3 - \sin \alpha_1 \sin \alpha_3 \cos \alpha_2 & P_{12} & P_{13} \\ \sin \alpha_1 \cos \alpha_3 + \cos \alpha_1 \sin \alpha_3 \cos \alpha_2 & P_{22} & P_{23} \\ \sin \alpha_3 \sin \alpha_2 & P_{32} & P_{33} \end{pmatrix}, \quad (8.8)$$

which gives

$$\begin{pmatrix} X \\ Y \\ Z \end{pmatrix} = r \begin{pmatrix} \cos \alpha_1 \cos \alpha_3 - \sin \alpha_1 \sin \alpha_3 \cos \alpha_2 \\ \sin \alpha_1 \cos \alpha_3 + \cos \alpha_1 \sin \alpha_3 \cos \alpha_2 \\ \sin \alpha_3 \sin \alpha_2 \end{pmatrix}. \quad (8.9)$$

Using the orbital elements given by (8.1) through (8.4), we obtain

$$\begin{pmatrix} X \\ Y \\ Z \end{pmatrix} = \frac{a(1-e^2)}{1+e \cos v} \begin{pmatrix} \cos \Omega \cos(\omega+v) - \sin \Omega \sin(\omega+v) \cos i \\ \sin \Omega \cos(\omega+v) + \cos \Omega \sin(\omega+v) \cos i \\ \sin(\omega+v) \sin i \end{pmatrix}. \quad (8.10)$$

### 8.1.3 Position of Satellite in Spherical Coordinates

We consider a spherical coordinate system in the Galilean frame  $\mathfrak{R}$ . The plane of reference is the equatorial plane  $xOy$  of the Earth, while  $Oz$  is the polar axis and the position of  $Ox$  is fixed in space. The point  $S$  can be specified in  $\mathfrak{R}$  by its spherical coordinates, namely, the distance  $r = \|\mathbf{OS}\|$ , the longitude  $\lambda$ , and the geocentric latitude  $\psi$ , measured with the usual convention following from the right-handed trigonometric system. The longitude of  $Ox$  (position of  $N$  at zero time) is denoted by  $\lambda_0$ . Hence,

$$\begin{pmatrix} X \\ Y \\ Z \end{pmatrix} = r \begin{pmatrix} \cos \psi \cos(\lambda - \lambda_0) \\ \cos \psi \sin(\lambda - \lambda_0) \\ \sin \psi \end{pmatrix}. \tag{8.11}$$

We thus obtain the position of  $S(\lambda, \psi)$  as a function of time and the other orbital parameters:

$$\psi = \arcsin [\sin(\omega + v) \sin i], \tag{8.12}$$

$$\lambda = \lambda_0 + \arccos \frac{\cos \Omega \cos(\omega + v) - \sin \Omega \sin(\omega + v) \cos i}{\cos \psi}, \tag{8.13}$$

$$(\lambda - \lambda_0) \text{ from the sign of } [\sin \Omega \cos(\omega + v) + \cos \Omega \sin(\omega + v) \cos i], \tag{8.14}$$

with

$$\lambda - \lambda_0 \in (-\pi, +\pi).$$

If  $|\psi| = \pi/2$ , then  $\lambda$  is not determined (and its determination would be pointless).

These equations (8.12)–(8.14) can be written more concisely if the Cartesian coordinates  $X$ ,  $Y$ , and  $Z$  have already been calculated:

$$\psi = \arcsin \frac{Z}{r}, \tag{8.15}$$

$$\lambda = \lambda_0 + \arccos \frac{X}{r \cos \psi}, \quad \lambda - \lambda_0 \text{ from the sign of } Y. \tag{8.16}$$

## 8.2 Ground Track of Satellite

### 8.2.1 Equation for Ground Track

In most practical cases, one needs to know the position of the satellite relative to the Earth. One must therefore represent  $S$  in the frame  $\mathfrak{R}_T$ , whose



axes in the equatorial frame rotate with the Earth. The transformation from this frame to the Galilean frame  $\mathfrak{R}$  is obtained by a simple rotation about the polar axis  $Oz$  with angular speed  $-\dot{\Omega}_T$ , since  $\mathfrak{R}_T$  rotates in  $\mathfrak{R}$  with angular speed  $\dot{\Omega}_T$ . Bear in mind that these calculations are carried out in the Galilean frame  $\mathfrak{R}$ , but the results may be expressed in any frame that suits us.

With the above definition of  $\lambda_0$ , the equations giving the position of  $S$  are the same in  $\mathfrak{R}_T$  as in  $\mathfrak{R}$ , provided that we replace the value of  $\alpha_1$  in (8.1) by

$$\alpha_1 = \lambda_0 + (\dot{\Omega} - \dot{\Omega}_T)(t - t_{AN}), \quad (8.17)$$

where the time origin, taken as the time of passage at the ascending node  $N$ , is denoted by  $t = t_{AN}$ .

The ground track  $T$  of the satellite is defined as the intersection of the straight line segment  $OS$  with the Earth's surface, as we have seen in Sect. 2.2.1, when discussing the geocentric ground track and the nadir. The position of  $T$  is given in spherical coordinates: the longitude  $\lambda$  and the geocentric latitude  $\psi$  are the same as for  $S$  in  $\mathfrak{R}_T$ , and the distance  $\|OT\|$  is  $R_\psi$ , defined by (1.38). The geodetic (or geographic) ground track is obtained by calculating the geodetic latitude  $\varphi_T$  from the geocentric latitude  $\psi$  using (2.4).

In order to obtain the successive positions of the nadir, one must calculate the geodetic latitude of the nadir  $\varphi$ , which requires knowing the altitude of the satellite and using one of the methods discussed in Sect. 2.2.1. It is the geodetic projection of the nadir that corresponds strictly to the subsatellite point.

For a given position of the satellite, the values  $\psi$ ,  $\varphi_T$ , and  $\varphi$  differ very slightly, as shown in Example 2.2. Depending on the accuracy required, charts of the ground track are set up using  $\psi$ , the simplest solution, or using  $\varphi$ , to get a rigorously accurate result. Ground tracks generated by *Ixion* are geodetic ground tracks of the nadir.

## 8.2.2 Maximum Attained Latitude

The intersection of the orbital plane  $\mathcal{P}$ , passing through the center of the Earth, and the equatorial plane  $\mathcal{E}$ , considered as a plane of symmetry of the planet, defines a maximal geocentric latitude  $\psi_m$  symmetrically in both the northern and the southern hemisphere. The range over which the ground track can vary is

$$\psi \in [-\psi_m; +\psi_m].$$

This angle  $\psi_m$  is equal to the inclination  $i$ , the dihedral angle between  $\mathcal{P}$  and  $\mathcal{E}$ , when  $i$  is acute, and its supplement if  $i$  is obtuse. We thus have the relations

$$\begin{cases} 0^\circ \leq i \leq 90^\circ \text{ (prograde)} \implies \psi_m = i, \\ 90^\circ \leq i \leq 180^\circ \text{ (retrograde)} \implies \psi_m = 180^\circ - i. \end{cases} \quad (8.18)$$

Expressing  $Z$  with the help of (8.10) and (8.11), we find that, when  $\sin(\omega + v)$  reaches an extremum, we have  $\sin \psi_m = \pm \sin i$ . Using  $\psi_m$ , we can calculate the maximal geodesic latitude  $\varphi_m$  of the nadir, observing that  $\varphi_m$  is always slightly greater than  $\psi_m$ .

**Example 8.1** *Calculate the maximal latitudes attained by Jason-2 and ICE-Sat.*

► The ocean topography satellite Jason-2 has a near-circular orbit at altitude  $h = 1,336$  km, with inclination  $i = 66.040^\circ$ . The maximal geocentric latitude of the ground track is thus

$$\psi_m = i = 66.040^\circ .$$

This latitude corresponds to the geodetic latitude  $66.183^\circ$ . To calculate the latitude of the nadir, we use (2.36) to order 1 in  $f$ :

$$\delta\varphi = \varphi - \psi = \frac{f}{\eta} \sin 2\psi ,$$

whence, with  $f = 1/298.3$  and  $\eta = 1 + h/R_e = 1.2095$ ,

$$\delta\varphi = (298.3 \times 1.2095)^{-1} \sin(2\psi_m) = 2.0571 \text{ mrad} = 0.118^\circ ,$$

and

$$\varphi_m = 66.158^\circ .$$

The iterative calculation using the algorithm in Table 2.4 gives the same result. This difference  $\delta\varphi$  between the two latitudes corresponds to 13.1 km on the ground.

The altimetry satellite ICESat is equipped with a laser that points to the nadir. It is in near-circular orbit at altitude  $h = 592$  km, and with inclination  $i = 94.003^\circ$ . The maximal geocentric latitude of the ground track is thus

$$\psi_m = 180^\circ - i = 85.997^\circ .$$

This latitude corresponds to the geodetic latitude  $86.024^\circ$ . Proceeding as before, with  $\eta = 1.0928$ , we obtain  $\varphi_m = 86.021^\circ$ , or a difference of  $\delta\varphi = 0.024^\circ$ , corresponding to 2.7 km on the ground. See also Example 2.2. ◀

## 8.3 Ground Track of Satellite in Circular Orbit

Circular or near-circular orbits are very common. We now discuss some notions developed specifically for these orbits, such as the equatorial shift or the apparent inclination.

### 8.3.1 Equation for Satellite Ground Track

When the orbit is circular, the motion is uniform with angular frequency  $n$ , the mean motion. Using the notation introduced above, the value of  $\alpha_3$  in (8.3) can be replaced by

$$\alpha_3 = n(t - t_{AN}) . \quad (8.19)$$

We thus obtain the equation for the ground track as a function the time  $t$ .

#### Sun-Synchronous Satellites

For Sun-synchronous satellites, the angle  $\alpha_1$  takes a specific value since we have  $\dot{\Omega} = \dot{\Omega}_S$ . We have seen that the two angular frequencies characterising the Earth's (annual and daily) motion are related by (7.33). According to (8.17), we thus have

$$\frac{d\alpha_1}{dt} = \dot{\alpha}_1 = \dot{\Omega}_S - \dot{\Omega}_T = -\frac{2\pi}{D_M} . \quad (8.20)$$

Using the daily orbital frequency as given by (7.35), we obtain, for Sun-synchronous satellites, the very simple relation

$$\dot{\alpha}_1 = -\frac{n}{\nu} . \quad (8.21)$$

We shall see the very important consequences of this relation in the following chapters, in particular when studying the crossing time of the satellite and the question of recurrent orbits.

### 8.3.2 Equatorial Shift

The difference in longitude between two consecutive ascending nodes  $\lambda_1$  and  $\lambda_2$ , separated by one revolution, is called the equatorial shift, denoted by  $\Delta\lambda_E$ :

$$\Delta\lambda_E = \lambda_2 - \lambda_1 . \quad (8.22)$$

#### Rough Calculation

It is sometimes sufficient to carry out a quick calculation of the equatorial shift, which is then denoted by  $\Delta_0\lambda_E$ . Indeed, to a first approximation we may say that, during one revolution of period  $T$  (and we may take the Keplerian period here), the orbit of the satellite will not have moved relative to  $\mathfrak{R}$ , while the Earth makes one complete turn every day, i.e., it rotates through  $15^\circ$  per hour, or  $1^\circ$  every 4 min relative to this same frame. In this context, we do not bother with the precession of the orbit, or the Earth's motion relative to the Sun over the time taken for the satellite to complete one revolution. This amounts to using the approximate relations  $\dot{\alpha}_1 \approx -\dot{\Omega}_T$  and  $\dot{\Omega}_T \approx 2\pi/D_M$ .

We have the simplified relation

$$\Delta_0 \lambda_E [\text{deg}] = -\frac{T [\text{min}]}{4}, \quad (8.23)$$

where the minus sign indicates a shift westwards.

### Exact Calculation

During one revolution lasting  $T = T_d$ , the orbital plane will have rotated through an angle  $\alpha_1$  with respect to  $\mathfrak{R}_T$ . The exact value of the equatorial shift, as given by (8.17) with  $t - t_{AN} = T$ , is therefore

$$\Delta \lambda_E = \alpha_1 T = -(\dot{\Omega}_T - \dot{\Omega})T = -\frac{2\pi}{\kappa}. \quad (8.24)$$

We note the following points, which follow from (8.24):

- The equatorial shift is always negative, since  $\dot{\Omega}_T$  is greater than  $\dot{\Omega}$ . The shift is westward for a satellite below the geosynchronous orbit.
- For satellites in Sun-synchronous orbit, we obtained the specific value of  $\alpha_1$ , according to (8.20). Over one nodal period  $T$ , we have

$$\Delta \lambda_E = \alpha_1 T = -\frac{2\pi}{D_M} T = -\frac{2\pi}{\nu}. \quad (8.25)$$

Writing the angles in degrees and the time in minutes, we obtain (8.23). For a Sun-synchronous satellite, the approximate formula is identical to the exact one. This is because the two approximations we made in the rough calculation (neglecting precession and the annual motion of the Earth) exactly balance for this type of satellite.

- For satellites in geosynchronous orbit,  $T = 2\pi/\dot{\Omega}_T$  and  $\dot{\Omega}$  is negligible. (In any case, it is not the leading term in the perturbation treatment for this type of satellite.) We thus have

$$\Delta \lambda_E = -\dot{\Omega}_T T = -2\pi = 0 \pmod{2\pi}, \quad (8.26)$$

where the notation  $\pmod{2\pi}$  indicates that we calculate modulo  $2\pi$ . There is no equatorial shift for such a satellite. The projection of two consecutive ascending nodes does not move on the Earth. (If the satellite is geostationary, it is difficult even to speak of an ascending node.)

We use  $D_E$  to denote the equatorial shift expressed in units of length (usually km), whence

$$D_E = R \Delta \lambda_E = -\frac{2\pi R}{\kappa}, \quad (8.27)$$

where  $R$  is the equatorial radius of the planet. The sign corresponds to the west-to-east convention for longitudes.

**Example 8.2** Calculate the equatorial shift for the satellite Meteor-3-07.

► The characteristics of the orbit of this satellite are given in Example 7.3. For the quick calculation, we use (8.23) with  $T = 109.4$  min. Then,

$$\Delta_0 \lambda_E = -109.4/4 = -27.35^\circ, \quad D_E = -3,045 \text{ km}.$$

For the exact calculation, with the values already given, viz.,

$$\begin{aligned} \dot{\Omega}_T &= 729.212 \times 10^{-7} \text{ rad s}^{-1}, \\ \dot{\Omega} &= -1.429 \times 10^{-7} \text{ rad s}^{-1}, \\ \dot{\Omega}_T - \dot{\Omega} &= 730.641 \times 10^{-7} \text{ rad s}^{-1}, \end{aligned}$$

and  $T = 6,565.28$  s, we obtain

$$\Delta \lambda_E = -0.4797 \text{ rad} = -27.48^\circ, \quad D_E = -3,059.51 \text{ km}.$$

The equatorial shift of the satellite Meteor-3-07 is thus 3,059.5 km westward (see Fig. 8.3). ◀

### 8.3.3 Apparent Inclination

#### Definition and Calculation of Apparent Inclination

The apparent inclination is the angle between the ground track and the equator. This angle  $i'$  differs from the angle  $i$  representing the inclination, which is the inclination of the orbital plane of the satellite with respect to the equatorial plane. This happens because  $i$  is measured in  $\mathfrak{R}$ , whereas  $i'$  is measured in  $\mathfrak{R}_T$ .

To calculate  $i'$ , we consider in  $\mathfrak{R}_T$  the tangent plane to the Earth at  $N_0$ , the point on the Earth's surface corresponding to the ascending node, using the orthogonal unit vectors  $\mathbf{e}_\lambda$ , tangent to the equator, and  $\mathbf{e}_\psi$ , tangent to the meridian through  $N_0$ . In the Galilean frame  $\mathfrak{R}$ , let  $\mathbf{V}_a$  be the absolute velocity (given by the angular velocity) of the satellite at the instant when it crosses the equator and let  $\mathbf{V}_f$  be the frame velocity of the point  $N_0$ . For  $\mathbf{V}_a$ , one must take into account the rate of nodal precession of the orbital plane, while  $\mathbf{V}_f$  is simply the rotational velocity of the Earth:

$$\mathbf{V}_a = \begin{pmatrix} n \cos i + \dot{\Omega} \\ n \sin i \end{pmatrix}, \quad \mathbf{V}_f = \begin{pmatrix} \dot{\Omega}_T \\ 0 \end{pmatrix}.$$

By the usual rule for composing velocities, we obtain the relative velocity  $\mathbf{V}_r$  of the satellite in the terrestrial frame  $\mathfrak{R}_T$  as

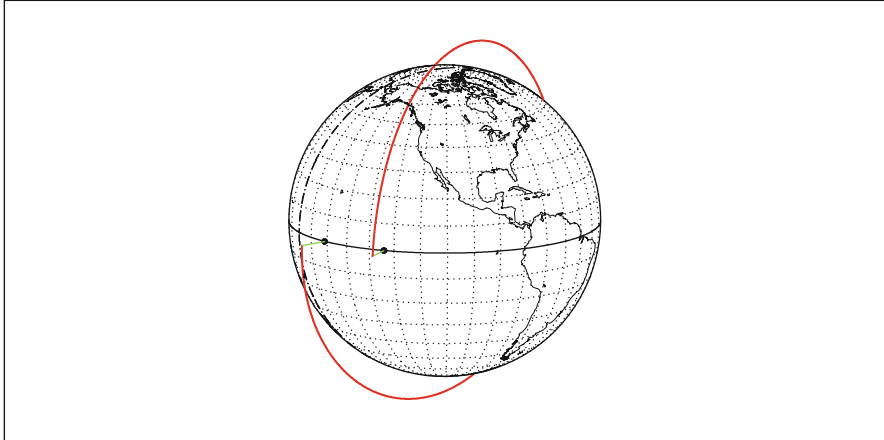
$$\mathbf{V}_r = \mathbf{V}_a - \mathbf{V}_f = \begin{pmatrix} n \cos i + \dot{\Omega} - \dot{\Omega}_T \\ n \sin i \end{pmatrix}.$$

**Meteor-3-07** < **Mereop** >

Orbit - ref.: Earth

Altitude = 1194.6 km                      a = 7572.702 km  
 Inclination = 82.56 °  
 Period = 109.42 min    \* rev/day = 13.16  
 Equat. orbital shift = 3059.5 km ( 27.5 °)

>>>> Time span shown: 109.4 min = 0.08 day



Projection: Orthographic    Project. centre: 12.0 ° N; 111.0 ° W    Asc. Node: -133.95 ° [07:43 UTC]    *Ιξίων*  
 Property: none    Aspect: Oblique    Max. attained latit. = 82.6 °    **MC ★ LMD**  
 ⊕ T.:Azimuthal - Graticule: 10° {4.2} [-90.0/ +78.0/-159.0] [-] EIGEN6C2    *Ατλας*

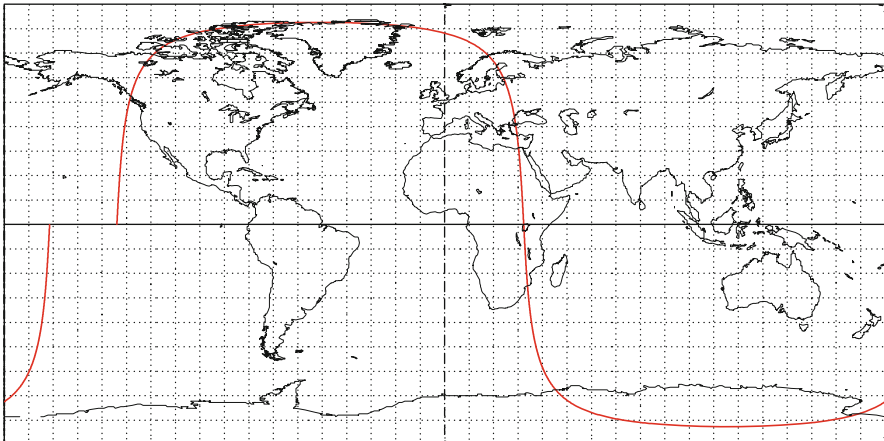
**Meteor-3-07** < **Mereop** >

Orbit - Ground track

Altitude = 1194.6 km                      a = 7572.702 km  
 Inclination = 82.56 °  
 Period = 109.42 min    \* rev/day = 13.16  
 Equat. orbital shift = 3059.5 km ( 27.5 °)

Recurrence = [13; +7; 71] 930

>>>> Time span shown: 109.4 min = 0.08 day



Proj.: Plate-carrée    Project. centre: 0.0 ° ; 0.0 °    Asc. Node: -133.95 ° [07:43 UTC]    *Ιξίων*  
 Property: none    Aspect: Direct    App. inclin. = 86.93 °    **MC ★ LMD**  
 ⊕ T.:Cylindrical - Graticule: 10° {4.2} [+0.0/ +0.0/ +0.0] [-] EIGEN6C2    *Ατλας*

FIG. 8.3 : Orbit and ground track of the satellite Meteor-3-07 over one revolution. The distance between the two successive ascending nodes is the equatorial shift.

The apparent inclination is then given by

$$\tan i' = \frac{n \sin i}{n \cos i - (\dot{\Omega}_T - \dot{\Omega})}. \quad (8.28)$$

In terms of the daily recurrence frequency  $\kappa$  defined by (7.43), we may write

$$\tan i' = \frac{\sin i}{\cos i - 1/\kappa}. \quad (8.29)$$

Expanding  $\tan(i' - i)$ , we obtain

$$\delta i = i' - i = \arctan \frac{\sin i}{\kappa - \cos i}. \quad (8.30)$$

Note that we always have  $i' \geq i$ .

For a Sun-synchronous satellite, we may replace  $\kappa$  by  $\nu$ , since according to (7.44), these two daily frequencies are equal.

For a satellite in a non-circular elliptical orbit, this calculation is of course possible, but  $n$  must be replaced by the instantaneous angular velocity of the satellite at  $N_0$ . Since this depends on the position of the perigee and the eccentricity, there is no simple general expression for  $i'$ .

**Example 8.3** Calculate the apparent inclination for the LEO satellite Terra and for an MEO Navstar satellite in the GPS constellation.

► The satellite Terra has a near-circular Sun-synchronous orbit with inclination  $i = 98.21^\circ$  and nodal period  $T_d = 98.884$  min. We calculate  $1/\nu$  from  $T_d$ , with the result

$$1/\nu = T_d/1440 = 0.06867.$$

We can then apply (8.29) directly since, in the Sun-synchronous case,  $\kappa = \nu$ , so

$$\tan i' = \frac{\sin 98.21}{\cos 98.21 - 0.06867} = -\frac{0.98975}{0.21147} = -4.68030,$$

and hence,

$$i' = 102.06^\circ, \quad i' - i = 3.85^\circ.$$

This inclination  $i'$  can be measured on images taken by Terra, as can be seen in Figs. 9.25 and 9.26.

The characteristics of Navstar/GPS are  $a = 26,560$  km and  $i = 55.00^\circ$ . The period is  $T_d = 717.978$  (half a sidereal day). We find  $\kappa$  by calculating the nodal precession rate:

$$\dot{\Omega} = -0.03878 \text{ deg/day}, \quad \nu = 2.0056, \quad \kappa = 2.0000,$$

$$\tan i' = \frac{\sin 55.00}{\cos 55.00 - 0.5000} = -\frac{0.81915}{0.07358} = 11.13335,$$

and hence,

$$i' = 84.87^\circ, \quad i' - i = 29.87^\circ.$$

At the equator, the ground track of the satellite is very close to the meridian of the ascending node (in fact, within  $5^\circ$ ), see Fig 14.6. ◀

**Example 8.4** Calculate the apparent inclination for the ground track of a geosynchronous satellite in circular orbit.

► For a geosynchronous satellite, we have  $\dot{\Omega}_T/n = 1$  and the term  $\dot{\Omega}$  is negligible. Equation (8.28) becomes

$$\tan i' = \frac{\sin i}{\cos i - 1} = -\frac{\cos(i/2)}{\sin(i/2)} = \tan\left(\frac{\pi}{2} + \frac{i}{2}\right),$$

whence

$$i' = 90^\circ + \frac{i}{2}, \quad i' - i = 90^\circ - \frac{i}{2}.$$

When  $i$  is very small, e.g.,  $i = 1^\circ$ , we have  $i' = 90.5^\circ$ : the ground track is not a point but a small line segment almost perpendicular to the equator, between latitudes  $1^\circ\text{N}$  and  $1^\circ\text{S}$ , which transforms into a figure of 8 (see Example 8.5) when  $i$  increases, growing larger with  $i$ .

The first operational geosynchronous satellite, Syncom-2, had inclination  $32.8^\circ$ . Its ground track made an angle of  $106.4^\circ$  with the equator, or an angle of  $16.4^\circ$  with the nodal meridian, as can be seen from the upper part of Fig. 9.16. ◀

**Example 8.5** Calculate the coordinates of the ground track of a geosynchronous satellite in circular orbit.

► For such a satellite, the ground track can be relatively simple expressed. The orbital characteristics are

$$r = a = a_{GS}, \quad e = 0, \quad v = M = nt, \quad n = \dot{\Omega}_T, \quad \dot{\Omega} \approx 0.$$



Furthermore, we choose  $\lambda_0 = 0$  and  $\omega = 0$ . The Euler angles thus have the values

$$\alpha_1 = \dot{\Omega}_T t = -nt, \quad \alpha_2 = i, \quad \alpha_3 = \omega + v = M = nt.$$

With (8.8) and (8.10) and setting  $C = \cos i$ , we obtain the coordinates of the ground track:

$$\begin{pmatrix} X \\ Y \\ Z \end{pmatrix} = R \begin{pmatrix} (1 - C) \cos^2 nt + C \\ -(1 - C) \sin nt \cos nt \\ \sqrt{1 - C^2} \sin nt \end{pmatrix}. \quad (8.31)$$

We obtain the geocentric coordinates, i.e., the longitude  $\lambda$  and the latitude  $\psi$ , using (8.15) and (8.16). Figure 8.4 (upper) shows the ground tracks for various values of the inclination.

**Note.** It is often claimed in the literature that the figure of 8 trajectory of inclined geostationary satellites is a Bernoulli lemniscate. Let us ignore the fact that the lemniscate is a plane curve, unlike the trajectory or its ground track. We can write down the projection of the trajectory on a plane perpendicular to the Earth radius passing through the ascending node with longitude  $\lambda_0$ . For the Cartesian coordinates of the ground track, we use  $x_1$  for the (abscissa) coordinate in the equatorial plane and  $y_1$  for the (ordinate) coordinate along the polar axis. Setting  $\theta = nt$  and  $R = 1$  and using (8.31), we see that  $x_1$  corresponds to  $Y$  and  $y_1$  to  $Z$ . We then obtain

$$\begin{cases} x_1 = -(1 - C) \sin \theta \cos \theta, \\ y_1 = \sqrt{1 - C^2} \sin \theta. \end{cases} \quad (8.32)$$

After normalisation, the parametric equation for the lemniscate is

$$\begin{cases} x_2 = -(1 - C) \frac{\sin \theta \cos \theta}{1 + \cos^2 \theta}, \\ y_2 = \sqrt{1 - C^2} \frac{\sin \theta}{1 + \cos^2 \theta}. \end{cases} \quad (8.33)$$

Equations (8.32) and (8.33) are different, but in both cases, the derivatives at the origin (which give the apparent inclination) are in fact the same:

$$\tan i' = \left. \frac{dy}{dx} \right|_0 = -\frac{\cos(i/2)}{\sin(i/2)} = \tan \left( \frac{\pi}{2} + \frac{i}{2} \right) \implies i' - i = 90^\circ - \frac{i}{2}.$$

As can be seen quite clearly in Fig. 8.4 (lower), the projection of the ground track is not a lemniscate. The two curves differ, but the tangents at the origin are the same. ◀

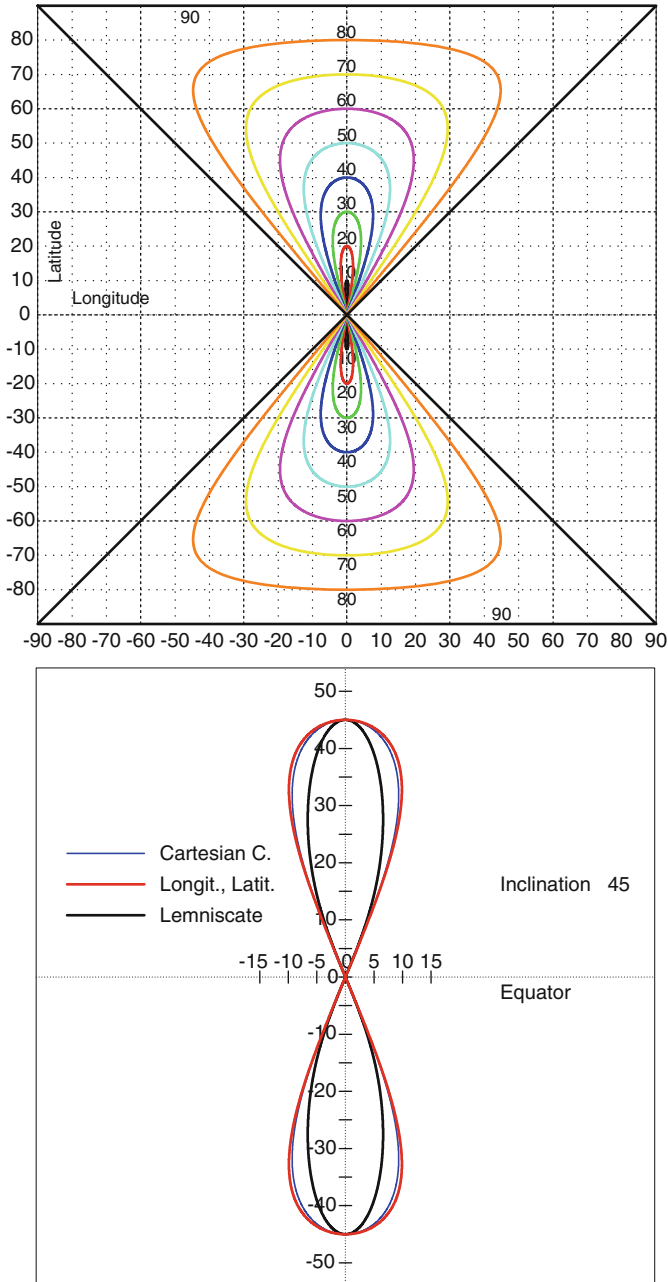


FIG. 8.4: Ground track of a geosynchronous satellite in circular orbit. Upper: for different inclinations in steps of  $10^\circ$  from  $0^\circ$  to  $90^\circ$ . Lower: for an inclination of  $45^\circ$ . Projection of the ground track in Cartesian coordinates, obtained from (8.32), in geocentric coordinates (longitude, latitude), obtained from (8.31), and the normalised lemniscate, obtained from (8.33).

### 8.3.4 Angle Between Ground Track and a Meridian

We calculate the angle between the satellite ground track and a meridian for an arbitrary point on the ground track. The calculation of the angle between the ground track and a line of latitude gives a generalisation of the apparent inclination. However, in practice, it is more useful to know the angle between the ground track and the north–south direction.

In the frame  $\mathfrak{R}$ , the satellite orbit cuts the meridian at an angle  $j$ . Referring to Fig. 10.15,  $P$  is the subsatellite point (with latitude  $\psi$ ),  $N$  is the point on the ground track corresponding to the ascending node (the dihedral angle at  $N$  gives the inclination  $i$ ), and  $PQ$  is the meridian through  $P$ , where  $Q$  is on the equator. The dihedral angle at  $P$ , in the spherical triangle  $PQN$ , is the angle  $j$  that we wish to determine. Using the relation (ST V), we obtain

$$\sin j = \frac{\cos i}{\cos \psi}. \quad (8.34)$$

To calculate  $j'$ , we consider in  $\mathfrak{R}_T$  the plane tangent to the sphere of radius  $R$  at the relevant point, with latitude  $\psi$ , and orthogonal unit vectors  $\mathbf{e}_\lambda$  and  $\mathbf{e}_\psi$  as already defined. As in the calculation of the apparent inclination, we write

$$\mathbf{V}_a = \begin{pmatrix} n \sin j + \dot{\Omega} \cos \psi \\ n \cos j \end{pmatrix}, \quad \mathbf{V}_f = \begin{pmatrix} \dot{\Omega}_T \cos \psi \\ 0 \end{pmatrix},$$

$$\mathbf{V}_r = \mathbf{V}_a - \mathbf{V}_f = \begin{pmatrix} n \sin j - (\dot{\Omega}_T - \dot{\Omega}) \cos \psi \\ n \cos j \end{pmatrix}.$$

It follows that

$$\tan j' = \frac{\sin j - (1/\kappa) \cos \psi}{\cos j}, \quad (8.35)$$

and expressing  $j$  with the help of (8.34),

$$\tan j' = \frac{\cos i - (1/\kappa) \cos^2 \psi}{\sqrt{\cos^2 \psi - \cos^2 i}}. \quad (8.36)$$

We obtain the adjustment angle  $\delta j$  as a function of  $i$  and  $\psi$ , viz.,

$$\delta j = j' - j = \arctan \frac{\sqrt{\cos^2 \psi - \cos^2 i}}{\kappa - \cos i}. \quad (8.37)$$

This can be compared with (8.30) by setting  $\psi = 0$ . The adjustment angle  $\delta j$  is maximal at the equator. When the maximal geocentric latitude is reached, it can be checked that the ground track is normal to the meridian. For a Sun-synchronous satellite,  $\kappa$  can be replaced by  $\nu$ .

Example 12.7 gives a direct application and a concrete illustration of the calculation of  $\delta j$  using (8.37).

### 8.3.5 Velocity of a Satellite and Its Ground Track

The satellite velocity can be calculated very accurately with the equations of motion discussed earlier. Here we calculate the velocity of the satellite and its ground track to a good level of accuracy, treating circular Keplerian motion. This section could therefore have appeared in Chap. 5, but we preferred to discuss these issues here, after dealing with the Earth's rotation, defining the notion of ground track, and describing the various kinds of satellites, especially, geosynchronous satellites.

#### Definitions of the Different Velocities

The velocities of the satellite  $S$  and its ground track  $S_0$  in  $\mathfrak{R}$  can be simply expressed in terms of the mean motion  $n$ :

$$\mathbf{V} = \frac{d\mathbf{OS}}{dt}, \quad V = an = \sqrt{\frac{\mu}{a}}, \quad (8.38)$$

$$\mathbf{V}_0 = \frac{d\mathbf{OS}_0}{dt}, \quad V_0 = Rn = \frac{R}{a}V = \frac{R}{a}\sqrt{\frac{\mu}{a}}. \quad (8.39)$$

In the terrestrial frame  $\mathfrak{R}_T$ , we consider a point on the Earth's surface, e.g.,  $S_0$ , and the right-handed triad of unit vectors associated with spherical coordinates, viz.,  $(\mathbf{e}_r, \mathbf{e}_\lambda, \mathbf{e}_\psi)$ . In the plane  $(\mathbf{e}_\lambda, \mathbf{e}_\psi)$  tangent to the Earth (the local horizontal plane), the vector  $\mathbf{e}_\lambda$  lies along a line of latitude and the vector  $\mathbf{e}_\psi$  along a meridian. In this frame, the velocity  $\mathbf{w}$  of the ground track is

$$\mathbf{w} = \mathbf{V}_0 - R\dot{\Omega}_T \cos \psi \mathbf{e}_\lambda.$$

If  $\mathbf{e}_u$  is the unit vector along  $\mathbf{V}_0$ , we obtain an expression for  $\mathbf{w}$ , which can be called the relative velocity of the ground track or the velocity of the ground track relative to the ground:

$$\mathbf{w} = R(n \mathbf{e}_u - \dot{\Omega}_T \cos \psi \mathbf{e}_\lambda). \quad (8.40)$$

#### Velocity at the Equator

In order to compare the values obtained for different satellites, we consider the relative velocity  $\mathbf{w}$  at the ascending (or descending) node, i.e., at the equator, where we shall denote it by  $\mathbf{w}_E$ :

$$\frac{\mathbf{w}_E}{R} = n \mathbf{e}_u - \dot{\Omega}_T \mathbf{e}_\lambda.$$

This can be expressed in terms of the inclination  $i$  of the satellite:

$$\frac{\mathbf{w}_E}{R} = (n \cos i - \dot{\Omega}_T) \mathbf{e}_\lambda + n \sin i \mathbf{e}_\psi. \quad (8.41)$$

If  $w_E$  is the magnitude of  $\mathbf{w}_E$  taken in the direction of motion, we obtain the following results for the three values  $i = 0^\circ$ ,  $90^\circ$ , and  $180^\circ$  of the inclination:

$$\frac{w_E}{R} = \begin{cases} n - \dot{\Omega}_T, & i = 0^\circ, \\ \sqrt{n^2 + \dot{\Omega}_T^2}, & i = 90^\circ, \\ n + \dot{\Omega}_T, & i = 180^\circ. \end{cases} \quad (8.42)$$

Table 8.1 shows, for various satellites, the velocities  $V$  and  $V_0$  of the satellite and its ground track in  $\mathfrak{R}$ , and the relative velocity  $w_E$  of the ground track in  $\mathfrak{R}_T$  for these three values of  $i$ . These results are shown for all altitudes between 0 and 1,600 km, in steps of 100 km, then for several altitudes typical of certain kinds of mission.

The maximal velocity of the ground track relative to the ground is  $8.4 \text{ km s}^{-1}$ , obtained for a retrograde satellite at ground level. More realistically, the velocity of the ground track at the equator for an operational Sun-synchronous satellite is  $6.6 \text{ km s}^{-1}$ . For a geosynchronous satellite with  $i = 0$ , hence geostationary, we find  $w_E = w_E(i = 0) = 0.00$ .

Regarding the last satellite in Table 8.1, it is not an artificial satellite, but a simplified model of the Moon (circular Keplerian orbit), at a distance of 380,000 km, and with a period of about 27 days. Note that, in  $\mathfrak{R}$ , the sidereal period is 27.32 days. In  $\mathfrak{R}_T$ , the period that takes into account the motion of the Earth is 29.53 days, or one lunar month.<sup>3</sup> This period, known as the synodic period, is explained below.

### Synodic Period

The idea of synodic period<sup>4</sup> is often used to speak about both satellites and planets. Consider two bodies in the same Galilean frame, moving uniformly with angular speeds (mean motions)  $n$  and  $n_1$ . The motion of the first relative to the second is a (relative) motion of angular speed  $n'$  given by

$$n' = n - n_1. \quad (8.43)$$

In terms of periods, this means that

$$\frac{1}{T'} = \frac{1}{T} - \frac{1}{T_1}, \quad (8.44)$$

<sup>3</sup>It is no accident that the word “month” is so similar to “Moon”, and the same is true of these words in German and related languages. The Indo-European root *\*men*, *\*mes* refers to the Moon, lunation (lunar month), and measurement or mensuration (of time). Many languages in this family still use similar terms, but this is not the case in Greek or Latin. These two languages called the Moon “the bright one” ( $\eta$   $\sigma\epsilon\lambda\eta\gamma\eta$ ,  $\eta\varsigma$ ; *luna*,  $\alpha$ ), which gives the present French name “Lune”. See also the note on Chandrasekhar.

<sup>4</sup>The noun  $\eta$   $\sigma\acute{\upsilon}\nu\omicron\delta\omicron\varsigma$ ,  $\omicron\upsilon$ , “synod”, is made up of  $\sigma\acute{\upsilon}\nu$ , meaning “with” or “together”, and  $\eta$   $\delta\acute{\omicron}\delta\omicron\varsigma$ ,  $\omicron\upsilon$ , meaning “path” or “journey”. In Ancient Greek, it already had the double meaning of “meeting” and “conjunction of heavenly bodies”, both of which illustrate the idea of “things happening at the same time”.

$h$ (km)	$a$ (km)	$\nu$ (rev/d)	$T_0$ d h m	$V$	$V_0$	$w_E$ 0	$w_E$ 90	$w_E$ 180	$\mathcal{T}$
0	6,378	17.04	1h24	7.91	7.91	7.44	7.92	8.37	g
100	6,478	16.65	1h26	7.84	7.72	7.26	7.74	8.19	R
200	6,578	16.27	1h28	7.78	7.55	7.08	7.56	8.01	R
300	6,678	15.91	1h31	7.73	7.38	6.91	7.39	7.84	S
400	6,778	15.56	1h33	7.67	7.22	6.75	7.23	7.68	S
500	6,878	15.22	1h35	7.61	7.06	6.60	7.07	7.52	O
600	6,978	14.89	1h37	7.56	6.91	6.44	6.92	7.37	O
700	7,078	14.58	1h39	7.50	6.76	6.30	6.78	7.23	O
800	7,178	14.28	1h41	7.45	6.62	6.16	6.64	7.09	O
900	7,278	13.98	1h43	7.40	6.49	6.02	6.50	6.95	O
1,000	7,378	13.70	1h45	7.35	6.35	5.89	6.37	6.82	O
1,100	7,478	13.42	1h47	7.30	6.23	5.76	6.24	6.69	O
1,200	7,578	13.16	1h49	7.25	6.10	5.64	6.12	6.57	O
1,300	7,678	12.90	1h52	7.21	5.99	5.52	6.00	6.45	O
1,400	7,778	12.66	1h54	7.16	5.87	5.41	5.89	6.33	O
1,500	7,878	12.42	1h56	7.11	5.76	5.29	5.78	6.22	
1,600	7,978	12.18	1h58	7.07	5.65	5.19	5.67	6.11	
2,000	8,378	11.32	2h07	6.90	5.25	4.79	5.27	5.71	
3,000	9,378	9.56	2h31	6.52	4.43	3.97	4.46	4.90	
4,000	10,378	8.21	2h55	6.20	3.81	3.34	3.84	4.27	
5,000	11,378	7.15	3h21	5.92	3.32	2.85	3.35	3.78	G
6,000	12,378	6.30	3h48	5.67	2.92	2.46	2.96	3.39	G
10,390	16,768	4.00	6h00	4.88	1.85	1.39	1.91		I
20,183	26,561	2.01	11h58	3.87	0.93	0.47	1.04		P
35,786	42,164	1.00	23h56	3.07	0.47	0.00			C
110,000	116,378	0.22	4d13h45	1.85	0.10	-0.36	0.47		V
376,805	383,183	0.04	27d07h43	1.02	0.02				M

TABLE 8.1 : *Velocity of the satellite and its ground track and relative velocity for various satellites in circular (Keplerian) orbit. For each satellite, we give the altitude  $h$  (in km) and the length of the semi-major axis  $a$ , or the distance from the center of the Earth (in km), the daily frequency  $\nu$  (in revolutions per day), the Keplerian period  $T_0$  (in hours and minutes), and the velocities  $V$ ,  $V_0$ ,  $w_E$  defined in the text for the three values  $0^\circ$ ,  $90^\circ$ , and  $180^\circ$  of the angle  $i$  (in  $\text{km s}^{-1}$ ). Abbreviations indicate the type  $\mathcal{T}$  of the given satellite: g (ground level), R (intelligence, reconnaissance), S (space shuttle, manned flights, and Earth observation), O (Earth observation, LEO), G (geodesy), I (communications, ICO type orbit, between LEO and MEO), P (positioning by GPS, MEO), C (geostationary, GEO), V (Vela type), M (Moon). If there is no symbol in this column, this indicates that the orbit is not used.*

where  $T'$  is the synodic period. A negative value of the period  $T'$  indicates that the motion has period  $|T'|$ , but in the opposite direction.

For the Moon in its motion about the Earth, which is itself revolving about the Sun ( $T_1 = N_{\text{sid}}$ ), we have

$$\frac{1}{T'} = \frac{1}{27.32} - \frac{1}{365.25} \quad \Longrightarrow \quad T' = 29.53 \text{ d} .$$

For a geostationary satellite, for which  $T = T_1 = 1 D_{\text{sid}}$  (sidereal day), the synodic period is considered to be infinite. For a GPS satellite,  $T = 0.5 D_{\text{sid}}$  and  $T_1 = 1 D_{\text{sid}}$ , whence  $T' = 1 D_{\text{sid}}$ , which shows that the satellite only crosses a given meridian once a day.

### 8.3.6 Eliminating Time from the Ground Track Equation

For a circular orbit, we can express the longitude  $\lambda$  as a function of the geocentric latitude  $\psi$ , with the help of the inclination  $i$  and the frequency  $\kappa$ , but without bringing in the time  $t$  (elimination of time). At the time  $t_{\text{AN}}$ , the geocentric ground track of the satellite crosses the equator at  $A$ , the point on the surface corresponding to the ascending node, taken as origin. At time  $t$ , the ground track is at  $S$ . In the Galilean frame  $\mathfrak{R}$  (defined by the Earth's equatorial plane and the polar axis  $Oz$ , keeping the axis  $OA$  fixed), the length of the arc  $AS$  (arc of a great circle) represents the position on orbit  $\alpha$ :

$$\alpha = \widehat{AS} = n_{\text{d}}(t - t_{\text{AN}}) , \quad (8.45)$$

where  $n_{\text{d}}$  is the mean motion relating to the nodal period  $T_{\text{d}}$ .

The longitude  $\lambda_{\text{G}}$  of the satellite in this same frame  $\mathfrak{R}$  is given by the arc  $AS'$ , where  $S'$  is the intersection of the meridian  $PS$  with the equator (see Fig. 8.5):

$$\lambda_{\text{G}} = \widehat{AS}' .$$

Relative to a terrestrial frame  $\mathfrak{R}_{\text{T}}$ , the longitude  $\lambda_{\text{T}}$  is

$$\lambda_{\text{T}} = \lambda_{\text{G}} - (\dot{\Omega}_{\text{T}} - \dot{\Omega})(t - t_{\text{AN}}) .$$

Using the recurrence frequency  $\kappa$ , we obtain

$$\lambda_{\text{T}} = \lambda_{\text{G}} - \frac{n_{\text{d}}}{\kappa}(t - t_{\text{AN}}) ,$$

whence we may eliminate the time using (8.45), to give

$$\lambda_{\text{T}} = \lambda_{\text{G}} - \frac{\alpha}{\kappa} .$$

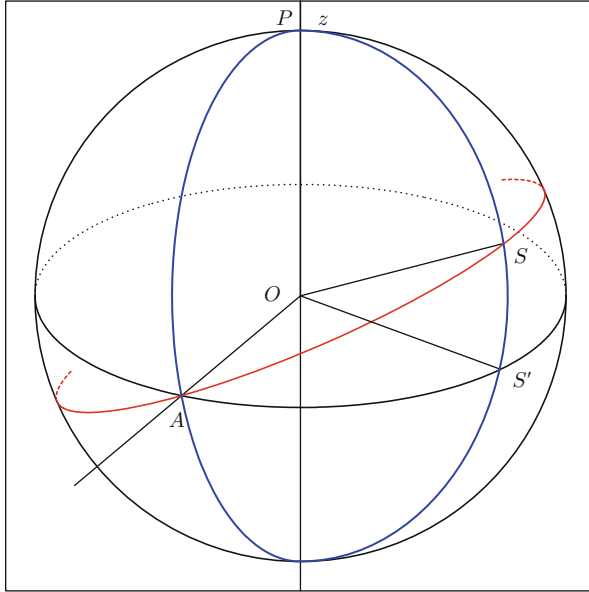


FIG. 8.5 : Ground track of the orbit in a Galilean frame. Investigation of the relation in spherical geometry between the latitude and longitude for a point  $S$  on the ground track. The ascending node is at  $A$ . In the spherical triangle  $ASS'$ , the arc  $AS'$  represents the longitude and the arc  $S'S$  the latitude. The angle  $A$  is the inclination and the angle  $S'$  is a right-angle.  $P$  is the pole.

In the spherical triangle  $ASS'$ , we know the following angles and sides (arcs):

$$\text{angle } A = i, \quad \text{angle } S' = \pi/2,$$

$$a = \widehat{SS'} = \psi, \quad s = \widehat{AS'} = \lambda_G, \quad s' = \widehat{AS} = \alpha,$$

$$\text{(ST X)} \implies \sin \lambda_G = \frac{\tan \psi}{\tan i}, \quad \text{(ST VIII)} \implies \sin \alpha = \frac{\sin \psi}{\sin i}.$$

We thus obtain an expression for the longitude:

$$\lambda_T = \arcsin \frac{\tan \psi}{\tan i} - \frac{1}{\kappa} \arcsin \frac{\sin \psi}{\sin i}. \quad (8.46)$$

Taking the Greenwich meridian as zero longitude rather than  $A$ , we have

$$\lambda_T = \lambda - \lambda_{AN},$$

where  $\lambda$  and  $\lambda_{AN}$  are the longitudes of  $S$  and  $A$ , respectively.

Finally, we obtain the longitude  $\lambda$  of the satellite in circular orbit:

$$\lambda = \lambda_{AN} + \arcsin \frac{\tan \psi}{\tan i} - \frac{1}{\kappa} \arcsin \frac{\sin \psi}{\sin i}. \quad (8.47)$$



## Angle Between the Ground Track and a Meridian

We can obtain an expression for  $\tan j'$  analytically. This gives the angle between the ground track and the meridian, via (8.35). Using (8.47), which gives the longitude  $\lambda$  in terms of the latitude  $\psi$ , we take the derivative

$$\begin{aligned} \frac{d\lambda}{d\psi} &= \frac{1}{\sqrt{\tan^2 i - \tan^2 \psi}} \frac{1}{\cos^2 \psi} - \frac{1}{\kappa} \frac{1}{\sqrt{\sin^2 i - \sin^2 \psi}} \cos \psi \\ &= \frac{1}{\cos \psi} \frac{\cos i - (1/\kappa) \cos^2 \psi}{\sqrt{\sin^2 i - \sin^2 \psi}}. \end{aligned}$$

For an increment  $dY = R d\psi$  along the meridian, there corresponds an increment  $dX = R \cos \psi d\lambda$  along a parallel. Hence,

$$\frac{dX}{dY} = \cos \psi \frac{d\lambda}{d\psi} = \frac{\cos i - (1/\kappa) \cos^2 \psi}{\sqrt{\cos^2 \psi - \cos^2 i}}, \quad (8.48)$$

and this quantity corresponds to  $\tan j' = dX/dY$  as given by (8.36).

## 8.4 Appendix: NORAD Orbital Elements

### 8.4.1 NORAD: The Organisation

The North American Aerospace Defence Command (NORAD) is a joint organisation between the US and Canada to monitor North American air space. The headquarters are at the Peterson airforce base in Colorado, USA. It was founded in 1957, during the Cold War. The United States was concerned about the possibility of missiles launched from the USSR, which would have arrived from the north.

NORAD operates dozens of radars, with which it can detect any object measuring more than a meter across in space, and 10 cm up to an altitude of 8,000 km. All satellites are detected and identified by these radars. Their motion is calculated using propagation models (orbitography software), then adjusted by further radar measurements. The orbital elements are coded in two-line elements (TLE), discussed below. For “unclassified” satellites, these results, be they radar measurements or calculations, are broadcast several times a day (one to three times).

American intelligence satellites, or more generally, any US satellite considered to have a “sensitive” mission, are excluded from the broadcasts, but the French military satellites Hélios and Essaim were not. Hence, with the assistance of an orbitography software like *Ixion*, it was easy to determine which of these satellites were maintained on the correct orbit and which were drifting. Dissatisfied with this attitude, the French Defence Ministry set up the system known as GRAVES (*Grand réseau adapté à la veille spatiale*), which went

into operation in 2005, and which can detect any satellite overflying France. Almost thirty NORAD “classified” satellites were thereby brought to light.

Thanks to GRAVES, Paris was able to negotiate with Washington: “We agree to show discretion with regard to certain of your satellites, provided that you stop broadcasting data concerning our more ‘sensitive’ satellites.” The move paid off in the end, since from 8 December 2009, just before the launch of Hélios-2B, the satellites Hélios and Essaim were taken off the NORAD TLE listing.

### 8.4.2 Two-Line Element (TLE) Set Format

NORAD detects objects in orbit and provides their orbital elements in the form of two lines of 69 characters (numbers, letters, signs, and spaces). These data comprise the NORAD two-line element set format, abbreviated to TLE and accessible by Internet. For each satellite, the data appear in the following form:

```

AAAAAAAAAAAAAAAAAAAAAAAA
1 NNNNNU NNNNAAA NNNNN.NNNNNNNN +.NNNNNNNN +NNNNN-N +NNNNN-N N NNNNN
2 NNNNN NNN.NNNN NNN.NNNN NNNNNNNN NNN.NNNN NNN.NNNN NN.NNNNNNNNNNNNNN
    
```

Line 0 names the orbiting object (satellite, or rocket element) in 24 characters. The standard TLE comprises lines 1 and 2, in a format used by NORAD and NASA. Line 1 gives the date and information concerning atmospheric drag. The orbital elements are in line 2. The exact description of this format is shown in Table 8.2.

### 8.4.3 Decoding the TLE

The correspondence between the six classic Keplerian elements discussed in Chap. 5 and the six NORAD elements is immediate for the metric elements  $i$  and  $e$  and the angle elements  $\Omega$ ,  $\omega$ , and  $M$ . The semi-major axis  $a$  is obtained from the mean motion  $n$ .

In order to use these orbital elements in a practical context, two of them require preliminary calculations:

- As we have just seen, the semi-major axis  $a$  is not given directly by the NORAD elements. The number of revolutions per day gives the anomalistic period  $T_a$  (because the period, in this orbital study, is defined as the time elapsed between two successive transits at perigee). We obtain the value of  $a$  by an iterative method like the one used in Example 7.3.
- The angle  $\Omega$ , the right ascension of the ascending node, is measured in a Galilean frame from the direction of the vernal equinox. But in practice, one needs to know  $\lambda_0$ , the longitude of the ascending node of the orbit, i.e., the angular elongation of this point in a terrestrial frame, measured from the Greenwich meridian. With the usual notation, we can say that  $\Omega$  is measured in  $\mathfrak{R}$ , and  $\lambda_0$  in  $\mathfrak{R}_T$ .

---

Line	Column	Description
1	01	Line number of element data
1	03–07	Satellite number
1	08	Classification (U=unclassified)
1	10–11	International designator (last two digits of launch year)
1	12–14	International designator (launch number of the year)
1	15–17	International designator (piece of the launch)
1	19–20	Epoch year (last two digits of year)
1	21–32	Epoch (day of the year and fractional portion of the day)
1	34–43	First time derivative of mean motion
1	45–52	Second time derivative of mean motion (decimal point assumed)
1	54–61	Drag term (decimal point assumed), B* model
1	63	Ephemeris type
1	65–68	Element number
1	69	Checksum (modulo 10)
2	01	Line number of element data
2	03–07	Satellite number
2	09–16	$i$ Inclination (degrees)
2	18–25	$\Omega$ Right ascension of the ascending node (degrees)
2	27–33	$e$ Eccentricity (decimal point assumed)
2	35–42	$\omega$ Argument of perigee (degrees)
2	44–51	$M$ Mean anomaly (degrees)
2	53–63	$n$ Mean motion (revolutions per day)
2	64–68	Revolution number at epoch
2	69	Checksum (modulo 10)

---

TABLE 8.2: *Description of the NORAD two-line element. Credit: NORAD.*

We first calculate the angle  $\Omega_{G00}$  between the Greenwich meridian and the vernal equinox at 0h UT on the relevant day. This angle corresponds to the mean sidereal time GMST (Greenwich Mean Sidereal Time) at 0h, written  $q_{G00}$  and measured in seconds. It is obtained from the relation<sup>5</sup>

$$q_{G00} = 24110.54841 + 8640184.812866T_u + 9.3104 \times 10^{-2}T_u^2 - 6.2 \times 10^{-6}T_u^3, \quad (8.49)$$

---

<sup>5</sup>The expression for  $q_{G00}$  contains four terms:

- The first gives the position of the Greenwich meridian at the date taken as origin, viz., J2000.0.
- In the second, the coefficient of  $T_u$  is equal to the number of seconds in one day (86,400) multiplied by the number of days in one Julian century (36,525), divided by the number of days in the tropical year ( $N_{\text{tro}} = 365.2421897$ ).
- The third is related to nutation.
- The fourth accounts for the precession of the equinoxes.

where  $T_u$ , the time in Julian centuries, is defined by  $T_u = d_u/36525$ , with  $d_u$  the number of days elapsed since 1 January 2000 at 12h (chosen date origin, called J2000.0, corresponding to the Julian date JD 2451545.0).

If  $\Delta D$  is the fraction of the day elapsed since 0h (given in line 1 of the TLE), we can calculate the sidereal time (GMST) at the relevant time  $t$  (UT):

$$q_{Gt} = q_{G00} + 86400\dot{\Omega}_T\Delta D \pmod{86400}, \tag{8.50}$$

where  $\dot{\Omega}_T$  is the angular speed of rotation of the Earth in rev/day, as given by (7.28). It is not really necessary to use (7.29). With the equivalence between days and revolutions (1 day is  $360^\circ$ ), we can obtain  $\Omega_{Gt}$  in degrees from  $q_G$  in seconds:

$$\Omega_{Gt} = \frac{q_{Gt}}{240}, \tag{8.51}$$

which is the angle between the Greenwich meridian and the vernal equinox at the relevant UT time.

The positions of the ascending node and the Greenwich meridian, denoted  $\Omega$  and  $\Omega_{Gt}$ , respectively, are measured from the same origin at the same time. We thus obtain the longitude  $\lambda_0$  of the ascending node in a terrestrial frame:

$$\lambda_0 = \Omega - \Omega_{Gt}. \tag{8.52}$$

With  $\omega$  and  $v$  (obtained from  $M$  and  $e$ ), we can calculate the crossing time of the satellite at the ascending node and its position  $\lambda_{AN}$  (taking into account the precession of the orbit over this time interval). The longitude and the UT time thus give the LMT crossing time at the ascending node.

**Example 8.6** Calculate the orbital elements of the ICESat satellite from the NORAD elements.

► During the first few months of its mission, the satellite ICESat followed a so-called calibration orbit. Its ground track had to repeat every 8 days (we return to the question of recurrence in Chap. 11). The NORAD elements for the given day during this calibration phase, were as follows:

```
ICESAT
1 27642U 03002A 03175.25018279 .00000722 00000-0 75456-4 0 1631
2 27642 94.0031 263.4514 0002250 85.5696 274.5785 14.90462832 24163
```

We obtain the date from

$$03175.25018279: \text{year} = 03, \text{day} = 175, \text{hour} = 0.25018279 \times 24.$$

giving 24 June 2003 at 06:00:15.79 UTC. Just for information, this was revolution number 2416, counting from the satellite's first passage at perigee. The following elements are obtained immediately:

$$n = 14.90462832 \text{ rev/day}, \quad e = 0.0002250, \quad i = 94.0031^\circ,$$

$$\Omega = 263.4514^\circ, \quad \omega = 85.5696^\circ, \quad M = 274.5785^\circ.$$

With the mean anomaly  $M$ , we can calculate the eccentric and true anomalies, very close to  $M$  since the eccentricity is extremely small:  $E = 274.566^\circ$  and  $v = 274.553^\circ$ . With  $n$ , we find the anomalistic period

$$T_a [\text{min}] = 1440/n, \quad \text{whence } T_a = 96.61428 \text{ min}.$$

We can calculate the position on orbit  $\alpha = \omega + v$ :

$$\alpha = 85.569 + 274.553 = 360.122 = 0.122 \pmod{360}.$$

The position of the satellite at the initial time is not therefore the ascending node, but rather a point located slightly above the equator, in the northern hemisphere. We can calculate the difference between the initial time and the ascending node crossing time, first in mean anomaly, then in time:

$$\Delta M = M - M(v = -\omega) = 274.579 - 274.457 = 0.122,$$

$$\Delta t = \frac{0.122}{360} \times T_a = 1.971 \text{ s}.$$

To begin with, we set  $T_0 = T_a$ , and with this Keplerian period, we obtain the value of the semi-major axis of the Keplerian orbit:  $a_0 = 6,974.6 \text{ km}$ . We calculate the secular variation related to the mean motion,  $\Delta n/n = -0.6695 \times 10^{-3}$ , then recalculate  $a$ . After several iterations, this yields  $a = 6,971.515 \text{ km}$  or an altitude of  $h = a - R = 593 \text{ km}$ . With the values of  $a$  and  $i$ , we can calculate the precession rates and periods. This yields:

nodal precession	$\dot{\Omega} = +0.5079^\circ/\text{day},$
apsidal precession	$\dot{\omega} = -3.5508^\circ/\text{day},$
anomalistic period	$T_a = 96.61428 \text{ min (check)},$
draconitic period	$T_d = 96.67818 \text{ min}.$

To calculate the longitude of the orbital plane at the initial time, we determine the Julian date of the relevant time, namely JD 2452814.75018279, which gives

$$d_u = \text{JD} - \text{J2000.0} = 1269.75018279, \quad T_u = d_u/36525.$$

Using (8.49),

$$q_{G00} = 65217.588 \pmod{86400},$$

and then with  $\Delta D = 0.25018279$ , we obtain

$$\begin{aligned} q_{Gt} &= q_{G00} + 86400 \times 1.00273790934 \times 0.25018279 \\ &= q_{G00} + 21674.993 = 86892.581 = 492.581 \pmod{86400}. \end{aligned}$$

If  $q_{Gt}$  is in seconds, then  $\Omega_{Gt}$  is in degrees:

$$\Omega_{Gt} = 492.581/240 = 2.052.$$

With (8.52), we thus have

$$\lambda_0 = 263.451 - 2.052 = 261.399.$$

We can calculate the displacement  $\Delta\lambda = \lambda_0 - \lambda_{AN}$  of the orbital plane in the terrestrial plane, taking into account nodal precession during the time  $\Delta t$ . The quantity  $\Delta\lambda$  is very small here, viz.,  $\Delta\lambda = -0.008$ . We thus obtain  $\lambda_{AN}$ , the longitude of the transit at the ascending node:

$$\lambda_{AN} = \lambda_0 - \Delta\lambda = 261.399 + 0.008 = 261.407.$$

For a transit at the ascending node at longitude  $261.407^\circ$ , i.e.,  $98.593^\circ$  W, the time 06:00:14 UT corresponds to 23:25:52 LMT.

These elements suffice to represent the ground track of the ICESat satellite over 8 days. During this time, the satellite should pass through the vertical at the calibration site in White Sands (Arizona, USA). Figure 8.6 shows that this constraint was respected. ◀

#### 8.4.4 Conditions of Use

In order to exploit NORAD data in the form of the TLE, one must use an orbitography software to get from  $n$  to  $a$ . If we then insert the six orbital elements for the given day  $D$  into the program, we can obtain very accurate results concerning the position of the satellite (to within 100 m) over a period of 1 or 2 weeks before and after  $D$ .

For satellites that must be held on orbit over long periods (several months), and if up-to-date NORAD data is not available, it is better to use the nominal orbital elements rather than obsolete TLE data. Indeed, recurrent Sun-synchronous satellites such as SPOT, or non-Sun-synchronous satellites like those in the A-train, such as Jason, are repositioned on their reference orbit several times a month. NORAD TLE data is not well suited to very high precision operations, such as orbital docking maneuvers.

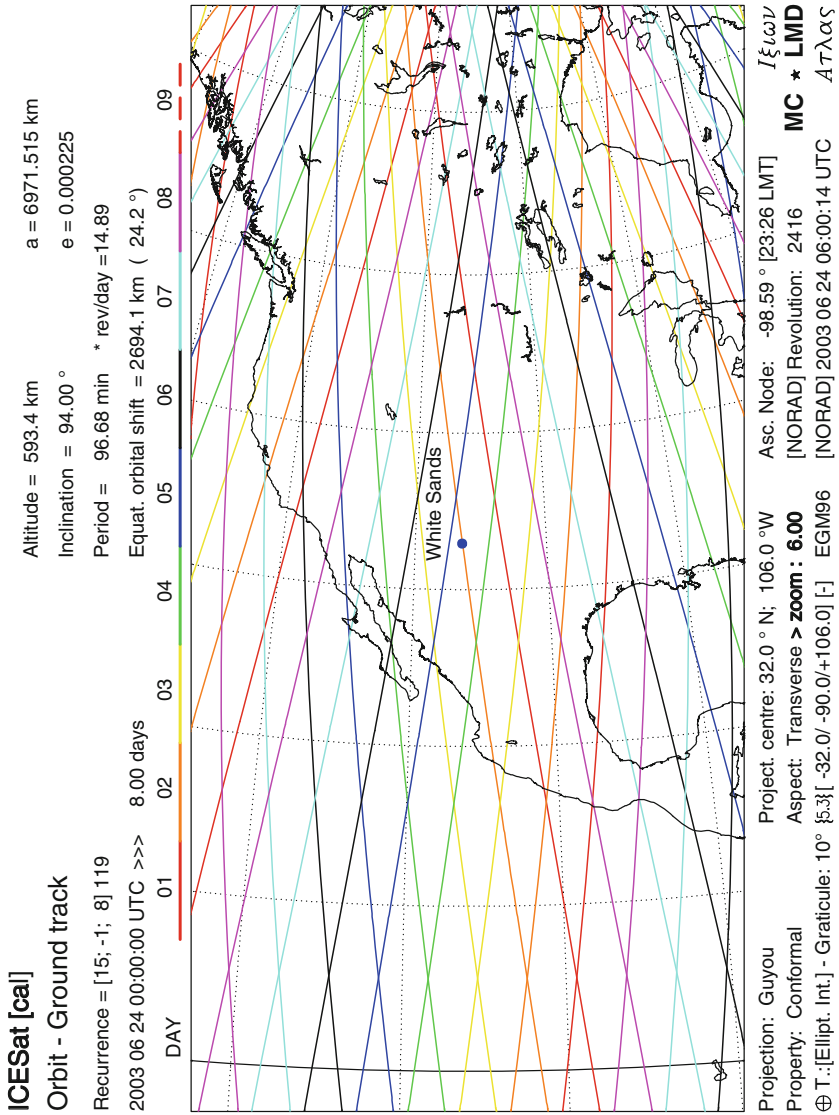


FIG. 8.6 : Transit of the ICESat satellite through the vertical of the calibration site at White Sands (Arizona, USA). Calibration phase.

## 8.5 Appendix: Cartographic Projections

### 8.5.1 Definitions and Properties

A cartographic projection is a transformation mapping a point of the sphere (or an ellipsoid), specified by its spherical coordinates  $\lambda$ ,  $\varphi$  (longitude, latitude), in a bijective manner onto its coordinates  $x$ ,  $y$  on the map:

$$\text{cartographic projection } f = \{f_1, f_2\} \quad \begin{cases} x = f_1(\lambda, \varphi), \\ y = f_2(\lambda, \varphi). \end{cases}$$

There exist infinitely many such projections.

The main problem to be solved by a cartographic projection can be put succinctly as follows: the sphere is not developable. This means that the surface of a sphere cannot be mapped onto a plane without distorting or tearing it.<sup>6</sup> Theoretical study of this question was carried out contemporaneously by Lambert<sup>7</sup> in 1772, Euler in 1777, and Lagrange in 1779. It was definitively solved by Gauss in (1822), who studied the conditions under which an arbitrary surface could be mapped onto another arbitrary surface.

A cartographic projection can have (exclusively) one or other of the following two properties:

- Angles are conserved, and the projection is said to be conformal.
- Areas are conserved, and the projection is said to be equal-area.

It may be that it has neither of these properties,<sup>8</sup> but it can never have both. In fact, the map can conserve the angles or the area of a figure, but it can never conserve the perimeter. No map can conserve distances in all directions. In other words, no projection can have constant scale over the whole field of projection.

In a conformal projection, the parallels and the meridians on the map intersect at right-angles, since the same is true on the sphere, where they form two sets of orthogonal curves. In an equal-area projection, a country twice as

---

<sup>6</sup>Unlike the sphere, a cylinder is developable. If the body of a big cat could be assimilated to a cylinder, one could understand how the tiger might change into a bedside rug without deformation.

<sup>7</sup>*Jean Henri Lambert* (1728–1777) was a Swiss and German astronomer, mathematician, and physicist, with French ancestry. In astronomy, he calculated the trajectories of comets and understood that the Milky Way was just a modest galaxy in the Universe. In physics, he discovered the fundamental law of photometry. In his many mathematical works, among which he demonstrated the irrationality of  $\pi$  (1766), he attributed great importance to problems of perspective and cartographic projections. He defined a great many projections, several of which bear his name today. The best known is the conformal conical projection, used in France for the map of France since 1922 and the cadastral survey since 1938.

<sup>8</sup>The older literature is full of different adjectives describing these properties, e.g., auto-gonal and orthomorphich for conformal, and authalic, homolographic, equiareal, and equivalent for equal-area, while an aphyllactic projection is one that is neither equal-area nor conformal. Such terms have now fallen into disuse.



big as another is represented on the map by an area twice as big. When the whole Earth is represented, it can be considered as spherical since projecting the terrestrial sphere or ellipsoid onto a plane leads to quite imperceptible differences in the resulting maps, whatever projection may be used. The same is not true for accurate regional maps, however.

### 8.5.2 Classifying Projections by Type or Aspect

Projections can be classified by type or by aspect. The type tells us how the sphere appears when projected onto the map, i.e., cylindrical, conical, azimuthal, and so on. We use the word “appears” because a cartographic projection is not usually (and the exceptions are very rare) a projection in the sense of an intersection between a straight line and a plane. For example, the Mercator projection is said to be cylindrical, but it is not the “projection” of this sphere from its center onto a cylinder that is tangent to it at the equator (as one often reads).

The aspect of a projection can be direct (or normal), transverse, or oblique. For example, for a stereographic projection (of azimuthal type) with direct aspect (also called polar in this case), the point of contact of the plane of projection with the sphere occurs at the pole, while it occurs on the equator for a transverse projection (also called equatorial in this case). For an arbitrary point of contact, the projection is said to be oblique.

The computer software *Atlas* which we have devised is coupled with the orbitography part of our program *Ixion*. Any satellite ground track can thus be mapped out with the chosen projection. In each representation, every effort is made to apply the most suitable cartographic projection. On all the maps presented here, plotted using *Atlas*, we indicate the main features of the projection: name, properties, type, and aspect. Also given in the key are the coordinates (longitude and latitude) of the center of the map, together with the three Euler angles which define the rotation of the globe for the projection from the standard initial position.

The projections used in the present book can be grouped as follows:

- *Conformal Projections*. Angles are conserved here. In particular, the angle between the ground track (of the satellite or its swath) and the given meridian is conserved. The main projections here are:
  - The Mercator projection.
  - The stereographic projection.
  - The projections due to Guyou, Adams, and Peirce, based on elliptic integrals of the first kind.
- *Equal-Area Projections*. These projections are used when it is important to respect surface areas. The main projections used in this book are:
  - The Behrmann projection (dilated Lambert equal-area cylindrical projection) and the Lorgna projection.

- The Mollweide and Sanson projections.
- The Craster parabolic, Boggs eumorphic, or Goode homolosine projections, often in interrupted form.
- The Hammer–Aitoff and Hammer–Wagner projections.
- *Perspective Projections.* Although they have no special properties, these projections are rather visual, representing the planet as if it were seen from space, viewed from various distances. The main projections used are:
  - The perspective view projection, where the viewing point is at a finite distance (expressed as a number of planetary radii).
  - The orthographic projection, where the viewing point is at infinity. This is the projection used to represent, not the ground track, but the orbit of the satellite in 3D, in such a way as to make the altitude apparent.
  - The Armadillo projection, due to Raisz, which represents the sphere in a rather picturesque manner, projected on a torus.
- *Specific Projections.* In 1977, the American cartographer John P. Snyder (1926–1997) invented a specific projection to represent satellite ground tracks for the satellite ERTS-1 (Landsat-1) and the following satellites in the Landsat programme. This satellite-tracking projection keeps the meridians regularly spaced and modifies the spacing of the parallels in such a way that the satellite ground track is a straight line. We have adapted this to any type of satellite. We shall return to this in more detail below.
- *Archaic Projection.* The so-called *plate-carrée* projection is very frequently (if not exclusively) used in books and documents concerned with satellite ground tracks. It represents longitudes and latitudes linearly along the abscissa and ordinate, respectively. This projection is somewhat simple-minded (amounting to  $x = \lambda$ ,  $y = \varphi$ ), even primitive (it was fashionable ... in the Middle Ages). It has no particular properties, being neither conformal nor equal-area, and its only mathematical value is its simplicity. This is no longer an argument with the advent of computer programming. It has not been used here, except for the first map (see Fig. 8.3) at the beginning of the chapter (not wishing to upset habits too early on).

### 8.5.3 Description of Three Projections

Here we give brief descriptions of two of the best known conformal projections, the stereographic projection and the Mercator projection. We also present the Snyder projection, which is specific to satellites. In all three cases, the Earth is treated as spherical with radius  $R = 1$ , and the latitude  $\psi$  is the geocentric latitude.

## Mercator Projection

In its direct aspect, a cylindrical projection can be written in the form

$$\begin{cases} x = \lambda, \\ y = f(\psi). \end{cases} \quad (8.53)$$

Meridians are represented by equidistant lines, perpendicular to the equator. Parallels are straight lines parallel with the equator, hence perpendicular to the meridians, and whose positions on the map depend only on the latitude.

For such a projection to be conformal, the function  $f(\psi)$  has to be suitably chosen. For a cylindrical projection, this function is unique. It is traditionally denoted by  $\mathcal{L}(\psi)$ . The spacing between parallels is greater as one moves away from the equator. If two meridians are separated by  $\Delta\lambda$  in longitude, their separation on the globe is  $R\Delta\lambda \cos \psi$  at latitude  $\psi$ , going from  $R\Delta\lambda$  at the equator to 0 at the poles.

Since the cylindrical projection maintains constant separations between the meridians on the map, the parallels must be separated by an amount proportional to the integral of  $1/\cos \psi$ . The reciprocal of  $\cos \psi$  is sometimes denoted by  $\sec \psi$ , abbreviation for the trigonometric function secant. The function  $\mathcal{L}(\psi)$  is obtained from

$$\mathcal{L}(\psi) = \int_0^{\psi} \frac{du}{\cos u}. \quad (8.54)$$

This integral defines the unique conformal cylindrical projection, known as the Mercator projection:

$$\begin{cases} x = \lambda, \\ y = \ln \tan \left( \frac{\pi}{4} + \frac{\psi}{2} \right), \end{cases} \quad (8.55)$$

which brings in the natural or Napierian logarithm of the tangent.

In its direct equatorial form, this projection is rarely used beyond  $60^\circ$ . The poles are pushed to infinity.<sup>9</sup> In its transverse form, the Mercator projection is called the Gauss projection, or the Universal Transverse Mercator (UTM).

---

<sup>9</sup>Certain cylindrical projections, such as the Arden–Close or Miller projections, are intended to “improve” Mercator, representing the poles by means of mathematical tricks. However, they thereby stray from the basic motivation for the Mercator projection, namely, the property of being conformal.

The first direct conformal cylindrical map of the world was established in 1569 by Mercator<sup>10</sup> for the purposes of navigation (*ad usum navigantium*). It proved extremely useful to mariners.<sup>11</sup>

Mercator never explained his method. We now know that he carried out the integration of the secant by hand, as it were, taking steps of the order of one degree. He did not know about logarithms, a theory established only in 1614 by John Napier (or Neper), whence the name Napierian logarithm. The Mercator projection was formulated mathematically in 1599 by Edward Wright.



FIG. 8.7 : *Frontispiece of the 1595 edition of the Mercator Atlas.*

<sup>10</sup> *Gerardus Mercator* (1512–1594) was a Flemish mathematician and geographer. (At this time, university members commonly Latinised their names. In this case, Gerhard Kremer changed his name to Gerardus Mercator, since *mercator* means “merchant” in Latin, just as *kremer* does in Flemish.) He made globes, maps, and astronomical instruments for Charles Quint. Realising that accurate maps were not only useful for navigation but had strategic and commercial importance, he established the first conformal cylindrical projection and thereby founded modern mathematical cartography. His main work was the *Atlas sive cosmographicæ meditationes de fabrica mundi et fabricati figura*, a huge collection of maps, not all of which use the Mercator projection. The *Atlas* was expanded and re-edited many times. After his death, his son Rumold, then the geographer Jodocus Hondius, continued this work of cartography and edition. For his first collection of maps in 1583, Mercator chose the name “Atlas” and illustrated the frontispiece of the work with the picture in Fig. 8.7 of the Greek god Atlas, who holds up the sky and observes the Earth from above. Later, the word “atlas” would become the standard name for this type of geographical work.

<sup>11</sup> One first determines the shortest path between two points (orthodromy). This is then plotted on the Mercator map and approximated by a succession of straight-line segments (loxodromy). The Mercator map indicates the course to follow and hold, since the projection is conformal.

By the end of the twentieth century, several commentators (not cartographers) had asserted that the Mercator projection was politically incorrect.<sup>12</sup> So here is an unexpected property of the logarithm!

### Snyder Projection

The Snyder projection is a projection of cylindrical type, with longitudes regularly spaced on the map. In order to represent the ground tracks by straight-line segments, the latitude and longitude must be linearly related over a given revolution. Using the relation (8.47), we obtain

$$\begin{cases} x = \lambda - \lambda_{AN}, \\ y = \arcsin \frac{\tan \psi}{\tan i} - \frac{1}{\kappa} \arcsin \frac{\sin \psi}{\sin i}, \end{cases} \quad (8.56)$$

where  $x$  and  $y$  are Cartesian coordinates on the map and  $\lambda_{AN}$  is the longitude of the initial ascending node. The latitudes are thus “dilated” as one moves away from the equator. The projection is shown in Figs. 8.8 and 8.9, with different dilations for the latitudes.

This projection only applies to circular orbits and necessarily uses geocentric latitudes.

### Stereographic Projection

The stereographic projection<sup>13</sup> has been the subject of considerable coverage in the literature, in proportion with the extent and variety of its geometrical properties. Here we shall explain how it works with a very simple example drawn from the field of cartography.

---

<sup>12</sup>We exemplify with two extracts to this effect:

Any projection inevitably distorts, none is completely innocent. The classic projection in our old school atlas is the Mercator projection, based on a factitious graticule which plots not only the “parallels” but also the meridians as parallel straight lines. The polar regions are stretched out of all proportion, while the “temperate” (= white) regions occupy a much greater space than their actual area would justify. The equator is pushed right down to the bottom of the map, which gives a completely false impression of the ratio of land to sea.

Jean Chesneau, *L'état du Monde 1982. Annuaire économique et géopolitique mondial*, François Maspero éd., Paris 1982.

The distortions of Mercator's map did not seem strange to Europeans in the sixteenth century, an era of expanding colonial empires. Yet today, although European colonialism belongs largely to the past, Mercator's sixteenth-century map still retains much of its grip.

United Nations Development Programme. *Maps and Map-Makers*, UNESCO Courier, June 1991.

<sup>13</sup>This adjective comes from the Greek στερεός, meaning solid, and γράφειν, meaning to engrave or write. Ptolemy reports that the stereographic projection was established by Hipparchos of Nicaea.

**Landsat-8****Orbit - Ground track**

Recurrence = [15; -7; 16] 233

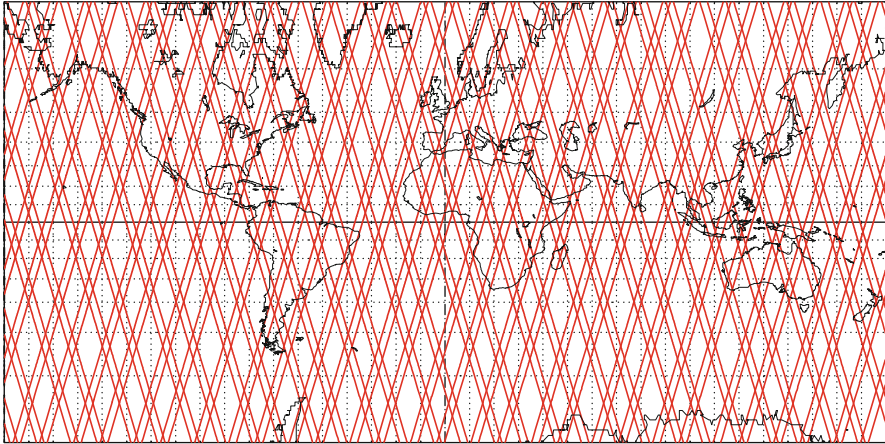
&gt;&gt;&gt;&gt; Time span shown: 5760.0 min = 4.00 days

Altitude = 699.6 km      a = 7077.736 km

Inclin./SUN-SYNCHRON.= 98.21 °

Period = 98.88 min \* rev/day = 14.56

Equat. orbital shift = 2751.9 km ( 24.7 °)



Proj.: Snyder-Satel.Track/55°    Project centre: 0.0 ° ; 0.0 °    Asc. Node: 103.02 ° [22:15 LMT]

Property: none [Geoc.L]    Aspect: Direct

App. inclin. = 102.06 °

⊕ T.:Cylindrical - Graticule: 10° [4.2] [ +0.0/ +0.0/ +0.0] [-] EIGEN6C2

Ιξίων

MC \* LMD

Ατλας

**Jason-2 / OSTM****Orbit - Ground track**

Recurrence = [13; -3; 10] 127

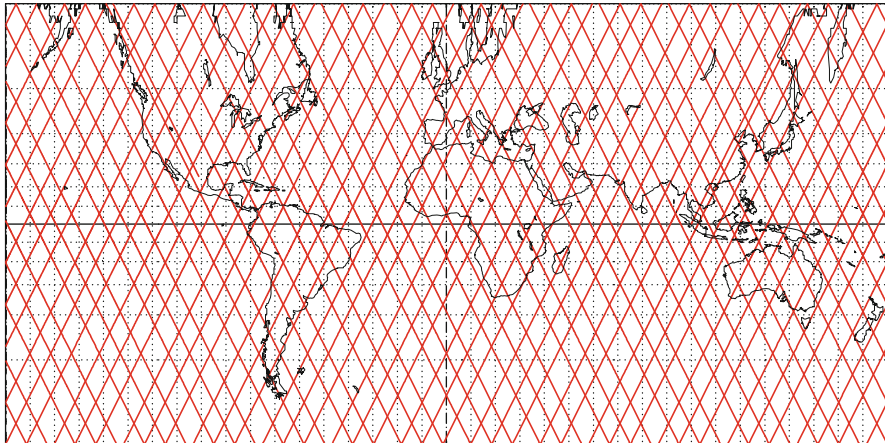
&gt;&gt;&gt;&gt; Time span shown: 4320.0 min = 3.00 days

Altitude = 1336.3 km      a = 7714.433 km

Inclination = 66.04 °

Period = 112.43 min \* rev/day = 12.81

Equat. orbital shift = 3155.5 km ( 28.3 °)



Proj.: Snyder-Satel.Track/35°    Project centre: 0.0 ° ; 0.0 °    Asc. Node: 99.92 ° [00:00 LMT]

Property: none [Geoc.L]    Aspect: Direct

App. inclin. = 70.29 °

⊕ T.:Cylindrical - Graticule: 10° [4.2] [ +0.0/ +0.0/ +0.0] [-] EIGEN6C2

Ιξίων

MC \* LMD

Ατλας

FIG. 8.8 : Ground tracks of two satellite orbits. Upper: Landsat-8 (Sun-synchronous orbit). Lower: Jason-2 (prograde orbit). Snyder projection with different standard parallels. Upper: 55°. Lower: 35°.

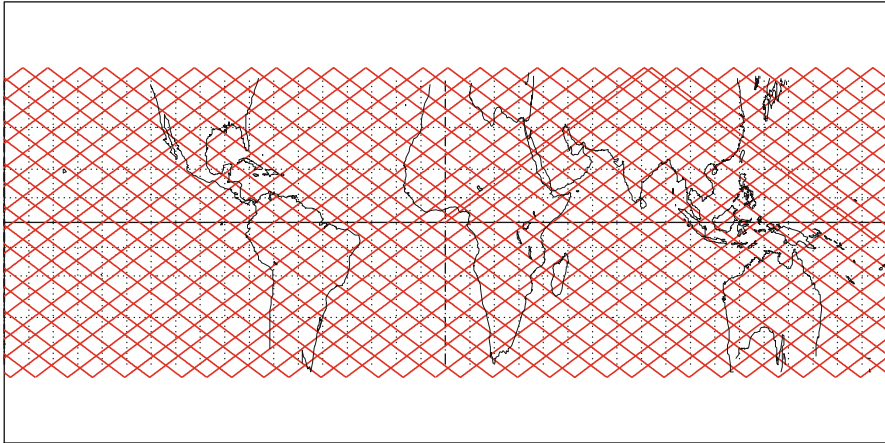


**TRMM [1] < 降雨 >**

Orbit - Ground track

>>>> Time span shown: 2880.0 min = 2.00 days

Altitude = 350.1 km                      a = 6728.216 km  
 Inclination = 34.99 °  
 Period = 91.31 min \* rev/day = 15.77  
 Equat. orbital shift = 2596.2 km ( 23.3 °)



Proj.: Snyder-Satel.Track/ 5°    Project. centre: 0.0 ° ; 0.0 °    Asc. Node: 0.00 °    *Ιξίων*  
 Property: none [Geoc.L]    Aspect: Direct    App. inclin. = 37.24 °    **MC ★ LMD**  
 ⊕ T.:Cylindrical - Graticule: 10° [4.2] [ +0.0/ +0.0/ +0.0] [-] EIGEN6C2    *Ατλας*

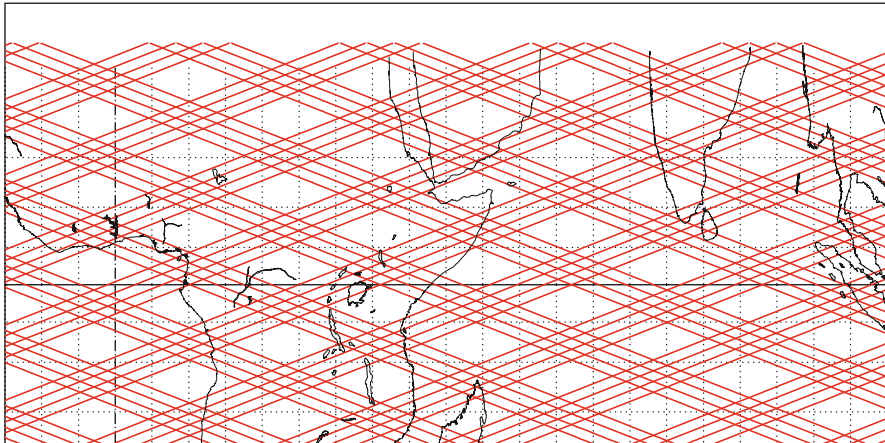
**Megha-Tropiques**

Orbit - Ground track

Recurrence = [14; -1; 7] 97

>>>> Time span shown: 5760.0 min = 4.00 days

Altitude = 865.5 km                      a = 7243.677 km  
 Inclination = 20.00 °  
 Period = 101.93 min \* rev/day = 14.13  
 Equat. orbital shift = 2892.0 km ( 26.0 °)



Proj.: Snyder-Satel.Track/ 0°    PC: 0.0 ° ; 0.0 ° /ZC: 8.0 ° N; 45.0 ° E    Asc. Node: 114.02 ° [08:22 LMT]    *Ιξίων*  
 Property: none [Geoc.L]    Aspect: Direct > **zoom : 3.00**    App. inclin. = 21.52 °    **MC ★ LMD**  
 ⊕ T.:Cylindrical - Graticule: 5° [5.3] [ +90.0/ +0.0/ -90.0] [-] EIGEN6C2    *Ατλας*

FIG. 8.9 : Ground tracks of two satellites in prograde orbits. Upper: TRMM. Lower: Megha-Tropiques, with zoom. Snyder projection with different standard parallels. Upper: 5°. Lower: 0°.

Consider a sphere (the Earth) with center  $O$ , equatorial plane, and two poles. Choose a particular point  $A$ , called the pole of projection, the South Pole in this application. Draw the straight line joining a point  $P$  of the sphere to the pole  $A$ . The intersection of the straight line with the equatorial plane defines a point  $M$  which is the image of  $P$  in the stereographic projection with pole  $A$ .

This transformation projects the whole sphere, excepting the point  $A$ , onto the equatorial plane. The whole northern hemisphere lies within the equatorial circle, while the whole southern hemisphere lies outside it. In cartography, two projections are preferred, with each map being bounded by the equator, and changing the pole when we change hemisphere. Clearly, any other point on the sphere could be chosen as the pole. By taking the pole of projection on the equator, one obtains maps with an equatorial aspect (see Fig. 8.10). It can be shown that this projection is conformal. A circle on the sphere is mapped to a circle on the plane (unless the circle passes through the pole of projection, when one obtains a straight line).

A point  $P$  on the sphere is specified by its longitude  $\lambda$  and its geocentric latitude  $\psi$ . In the case discussed above, with the point  $A$  at the South Pole, the angle at the center  $(\mathbf{AO}, \mathbf{OP})$  represents the colatitude of the point  $P$ , and it is twice the inscribed angle  $(\mathbf{AO}, \mathbf{AP})$ :

$$(\mathbf{AO}, \mathbf{OP}) = \frac{\pi}{2} - \psi, \quad (\mathbf{AO}, \mathbf{AP}) = \frac{\pi}{4} - \frac{\psi}{2}.$$

On the equatorial plane, the point  $P$  projects to  $M$  with the same azimuthal angle  $\lambda$ . The polar coordinates  $(r, \theta)$  of  $M$  are

$$\begin{cases} \theta = \lambda, \\ r = \tan\left(\frac{\pi}{4} - \frac{\psi}{2}\right). \end{cases}$$

Projecting on the  $(x, y)$  axes, we obtain the equation for the azimuthal stereographic projection:

$$\begin{cases} x = r \cos \lambda, \\ y = r \sin \lambda. \end{cases} \quad (8.57)$$





**Landsat-8**

**Orbit - Ground track**

Recurrence = [15; -7; 16] 233

>>>> Time span shown: 720.0 min = 0.50 day

Altitude = 699.6 km

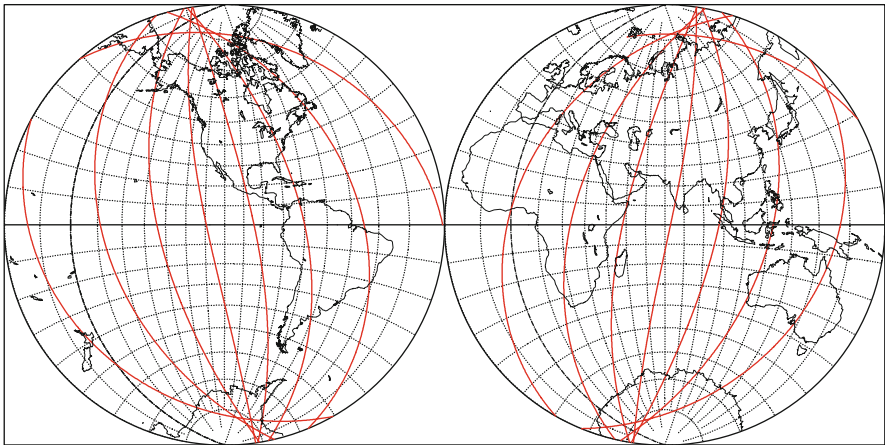
a = 7077.736 km

Incl. / SUN-S. = 98.21 °

e = 0.000179

Period = 98.88 min \* rev/day = 14.56

Equat. orbital shift = 2751.9 km ( 24.7 °)



Projection: Stereographic

Pr. centre (r.): 0.0 ° ; 69.9 °E

Asc. Node: -20.58 ° [22:15 LMT]

Property: Conformal

Aspect: Equatorial

Ιξίων

MC \* LMD

⊕ T.: Azimuthal - Graticule: 10° [4.2] [-90.0/ +90.0/ +20.1] [-] EIGEN6C2

Ατλας

FIG. 8.10 : Stereographic projection. Upper: map of the world taken from the Mercator Atlas, 1587. Lower: ground track of the orbit of Landsat-8, over half a day.

# Chapter 9

## Orbit and Mission

### 9.1 Classifying Orbit Types

Satellite orbits can be classified according to various criteria: the inclination, the altitude, the eccentricity, or various properties.

#### Classification by Inclination

We have seen that the angle of inclination  $i$  of the orbit (angle of nutation  $\alpha_2$  for the Euler angles) is defined to lie between  $0^\circ$  and  $180^\circ$ . If  $i$  is less than  $90^\circ$ , the orbit is prograde, whereas if  $i$  is greater than  $90^\circ$ , it is retrograde. When  $i = 90^\circ$ , the orbit is polar. One may say strictly polar, because when  $i$  lies between  $80^\circ$  and  $100^\circ$ , one often describes it as a polar orbit, whereas near-polar would be more appropriate.

If  $i = 0^\circ$  (or  $i = 180^\circ$ , although this has never happened), the orbit is equatorial, and for  $i$  less than  $10^\circ$ , it is near-equatorial.

#### Classification by Altitude

Satellites in near-circular orbit are classified according to their mean altitude. We speak of a low Earth orbit (LEO) when the satellite flies at an altitude below 1,500 km, a medium Earth orbit (MEO) for GPS satellites at an altitude of around 20,000 km, and a geostationary Earth orbit (GEO) (also sometimes called the Clarke orbit) for geostationary satellites at an altitude of 36,000 km. We shall often use these abbreviations, which are concise and

consistent.<sup>1</sup> Almost all satellites in orbits with low eccentricity fall into one of these three categories. (For example, it is very rare to find a satellite at an altitude of 8,000 km.)

For highly elliptical orbits,<sup>2</sup> such as the Molniya or Tundra orbits, we use the abbreviation HEO (highly eccentric orbit). The name GTO (geostationary transfer orbit) is usually a temporary one, because the satellite has been placed on this highly eccentric orbit for transfer towards a GEO orbit. Some satellites can be found in such orbits, some deliberately placed there, others because the apogee thrust used to make the orbit circular has been unsuccessful. Finally, if a satellite has not been correctly placed in orbit, it is sometimes given the title FTO (failed transfer orbit)!

The orbits L1LO and L2LO refer to halo orbits around the Lagrange points, which were discussed in Sect. 6.12.

### **Orbit and Revolution**

Since all scientific enterprise is based on a precise use of language, one must mention a very common error which consists in saying “orbit” instead of “revolution” or “round trip”, an error which occurs in English, French, and very likely other languages too. For example, we may read: the satellite Terra during orbit 7778. . . . This confusion is unjustified, and indeed, it is never encountered in astronomy: one never says that the Moon makes one orbit around the Earth every month.

## **9.2 Classifying Satellites by Mission**

Our classification of satellites according to mission, which is of course rather arbitrary, aims to illustrate the various types of orbit. We begin with satellites designed for geophysics and Earth observation, then for navigation and communications, astronomy, technological development, and others that elude straightforward classification. We shall touch briefly upon military satellites and their specific missions, and satellites carrying humans.

The mission of a satellite often covers a range of different areas, e.g., an oceanographic satellite may also take part in a geodesy mission or a mission to develop altimetric techniques, and there has always been a large dose of ideology in satellite missions, especially at the beginning of the space age. More will be said about this below.

---

<sup>1</sup>When we are referring to the satellite as LEO rather than the orbit, we understand of course that we mean a low-Earth orbiting satellite. One does occasionally find the term GEO meaning geosynchronous Earth orbit, as opposed to GSO for geostationary orbit. In addition, and somewhat unnecessarily, one finds the term IGSO meaning inclined geosynchronous orbit for geosynchronous orbits that are tilted and therefore not geostationary.

<sup>2</sup>For Molniya-type orbits, the term THEO (12 h eccentric orbit) is sometimes used. For very high orbits, like the orbit of Geotail, we use the term VHO (very high orbit).

With regard to military (or partly military) satellites, the nomenclature is often somewhat vague (even confused). From 1984, the United States called some of its satellites USA followed by a number specifying order of launch. Previously, these satellites had been called OPS followed by a four-figure number, without chronological ordering. Between 1964 and 1984, more than 400 OPS satellites were launched.<sup>3</sup> The USSR, then Russia, also created confusion with its Kosmos satellites: this name (from the Russian word КОСМОС, originating itself from the Greek word ὁ κόσμος, οὐ, meaning “order” or “well-ordered”, hence “universe”) groups a whole multitude<sup>4</sup> of satellites (not always military), on every kind of orbit and for every available type of mission. The People’s Republic of China did likewise with the appellation DFH (Dong Fang Hong, where *dong fang* means “Orient” and *hong* means “red”), which covers the great majority of Chinese satellites. Without doing anything to simplify the situation, these satellites are also recorded by Western organisations under the appellation PRC (People’s Republic of China), with a different numbering system.

In the Japanese tradition, every satellite gets two names, the first, in English (a name or acronym), and the second in Japanese, provided that the launch is successful, e.g., the satellite GOSat became Ibuki. This tradition (or should one say superstition?) is also to be found with the US organisation NOAA: it attributes a letter to the satellite, and this letter becomes a number after the launch. The satellite NOAA-N became NOAA-18, while NOAA-B, the second in the series, does not appear in the numbering system, because it was not inserted into the correct orbit.<sup>5</sup>

Satellites placed in orbit by the US Space Shuttle are indicated as follows: launched by STS-(number). An unspecified member of a satellite series is denoted by *-n*, e.g., Molniya-*n*.

Launch dates are noted up to 1 July 2013.

### 9.2.1 The First Satellites

Convinced of their supremacy in space, the United States spent the 1950s engaged in fierce internal competition over who would be first to put an arti-

---

<sup>3</sup>In fact, 418 satellites were launched, from OPS/3367 on 19 January 1964 to OPS/8424 on 17 April 1984.

<sup>4</sup>The launch dates were as follows: Kosmos-1 (or Sputnik-11) on 16 March 1962, Kosmos-1001 on 4 April 1978, and Kosmos-2001 on 14 February 1989. The launch rate then subsided somewhat. We give here the last Kosmos launched in the given year: Kosmos-2054 (1989), Kosmos-2120 (1990), Kosmos-2174 (1991), Kosmos-2229 (1992), Kosmos-2267 (1993), Kosmos-2305 (1994), Kosmos-2325 (1995), Kosmos-2336 (1996), Kosmos-2348 (1997), Kosmos-2364 (1998), Kosmos-2368 (1999), Kosmos-2376 (2000), Kosmos-2386 (2001), Kosmos-2396 (2002), Kosmos-2404 (2003), Kosmos-2412 (2004), Kosmos-2417 (2005), Kosmos-2424 (2006), Kosmos-2436 (2007), Kosmos-2448 (2008), Kosmos-2458 (2009), Kosmos-2469 (2010), Kosmos-2478 (2011), Kosmos-2481 (2012). Since 2000, the Glonass satellites half made up half of the Kosmos series.

<sup>5</sup>Note that, of the first 20 NOAA launches, 19 have been successful.



FIG. 9.1 : Stamps celebrating Soviet supremacy in space.



FIG. 9.2 : Technician preparing the satellite Sputnik-1. The satellite comprised a metallic sphere with four antennas. The sphere (diameter 58 cm) contained an emitter and a battery. Total mass 84 kg. Credit: Academy of Sciences of the Union of Soviet Socialist Republics.

ficial satellite into orbit. The two parties were the US Navy with its Vanguard project and the US Army with the Orbiter project. But from 1955, the former, with its powerful and effective Naval Research Laboratory (NRL), was sole leader in the “race into space”, as they prepared to launch the tiny device nicknamed *the grapefruit satellite* (1.5 kg). Then on 4 October 1957, the USSR shook the world with Sputnik-1, a satellite weighing in at 84 kg (see Figs. 9.1 and 9.2).

The US government, which was to take a second uppercut on 3 November with the successful appearance of Sputnik-2 on the scene, this time weighing in at 508 kg (including a dog), was quick to react. The US army launched the Explorer programme in collaboration with the Jet Propulsion Laboratory/California Institute of Technology (JPL/Caltech). On 31 January 1958, Explorer-1 (14 kg) was successfully launched (see Fig. 9.3). After several failed launches, Vanguard-1 was placed in orbit on 17 March 1958. The US government put a stop to this dual development by founding the National Aeronautics and Space Administration (NASA) on 1 October 1958.

For any country, the act of placing its first satellite in orbit with its own rocket system carries a significant ideological connotation. There is no need to



FIG. 9.3 : *The three mission leaders for Explorer-1: W.H. Pickering (director of JPL/satellite), J. Van Allen (instrument), and W. von Braun (rocket) (left to right), lifting a scale model of the satellite following its successful launch on 31 January 1958. The satellite, weighing 14 kg, became the first US satellite in orbit. Thanks to its on-board equipment, it discovered the radiation belts surrounding the Earth, known today as the Van Allen belts. Credit: NASA.*

ask more of one's inaugural satellite than a distant "bip bip", even if, thanks to Explorer-1, Van Allen managed to identify the radiation belts around the Earth that now carry his name. The symbolic message was also military during the Cold War: if we can launch a satellite, we can also launch a nuclear warhead!

After the two superpowers, as they were considered at the time, de Gaulle's France launched its own satellite A-1 (known as Astérix) on 26 November 1965. Then followed the two main Asian nations, Japan with Ohsumi and China with DFH-1. In 1971, the United Kingdom, with X-3 (known as Prospero) also showed that it had the knowhow. Other firsts occurred on a more strained geopolitical stage. One could mention India with Rohini (or RS-1) and Israel with Ofeq-1 in 1980, and when Iran launched Omid-1 (meaning "hope" in Farsi) in 2009, using an Iranian rocket, the ideological aim was clearly stated in a presidential announcement.<sup>6</sup>

In 2012, NORAD confirmed that North Korea had placed the satellite Kwangmyongsong-3-2 ("star of hope") in orbit using a local launch system.

<sup>6</sup>In the dramatic words of President Mahmoud Ahmadinejad: "Iran's presence in space, with the aim of expanding monotheism, peace, and justice, has now been officially recorded in history." Islamic Republic News Agency (IRNA), Tehran, 3 February 2009.



## 9.2.2 Satellites for Geodesy

We have already mentioned these satellites in Chap. 3, where we gave a complete list of the satellites used for the geopotential models JGM, EGM, GRIM, and EIGEN.

The satellite Sputnik-2 can be considered as a geodesy satellite. In the beginnings of space-based geodesy, many satellites were placed above the LEO altitude in order to reduce atmospheric drag. Examples are PAGEOS, launched in 1966, between 3,000 and 5,200 km, with  $i = 84.4^\circ$ , and the two LAGEOS (Laser Geodynamics Satellite), in high circular orbits with  $h = 5,900$  km and inclinations  $i = 109.8^\circ$  for LAGEOS-1 and  $i = 52.6^\circ$  for LAGEOS-2. The ground tracks of LAGEOS-1 and LAGEOS-2 are shown in Fig. 9.4.

The satellites SECOR-7, -8, and -9 at 3,700 km altitude and the Soviet satellites Etalon-1 and -2 (Kosmos-1989 and -2024), launched in 1989 with Glonass, are in a circular MEO orbit with  $h = 19,130$  km and  $i = 64.8^\circ$ . Others are at altitudes between 1,000 and 1,500 km: the fifteen Soviet Geo-1K satellites, such as Kosmos-2226, the French Starlette satellite, and the US pioneer ANNA-1B, launched in 1962,  $h = 1,120$  km,  $i = 50.1^\circ$ . Also in this category is the Japanese satellite EGP (Ajisai), whose ground track is shown in Fig. 9.5 (lower). The Japanese satellite LRE (Laser Ranging Experiment), launched into an eccentric orbit in 2001, with  $h_p = 271$  km,  $h_a = 36,214$  km,  $i = 28^\circ$ , is equipped with 126 laser reflectors.

There are some Sun-synchronous satellites between 800 and 1,000 km, such as TOPO-1 and those launched after 1993, Stella and Westpac-1 (Sun-synchronous because they are microsattellites that were themselves launched with Sun-synchronous satellites). Since then, geodesy satellites have been placed in lower orbits. An example is GFZ-1 (*Geo Forschungs Zentrum*), launched in 1995, with  $h = 380$  km and  $i = 51.6^\circ$ .

Our knowledge of the geopotential has become so precise that a whole new generation of geodesy satellites<sup>7</sup> has been put in operation since 2000. They carry ultra-sensitive accelerometers. Their altitudes must be as low as possible for better detection of gravitational anomalies, while a continuous thrust compensates for the higher level of atmospheric drag,<sup>8</sup> as we have seen in Chap. 3 for the satellites CHAMP, GRACE, and GOCE (see Figs. 3.6 and 3.7).

The Italian satellite LARES (Laser Relativity Satellite, also known as LAGEOS-3, see Fig. 9.5 upper),<sup>9</sup> with  $h = 1,442$  km and  $i = 69.49^\circ$ , works

<sup>7</sup>Launch dates: CHAMP on 15 June 2000, GRACE-A and -B on 17 March 2002, and GOCE on 17 March 2009.

<sup>8</sup>At this altitude, and for GOCE with mass 800 kg, the acceleration due to atmospheric friction is  $1.5 \times 10^{-5} \text{ m s}^{-2}$ , whereas the acceleration due to radiation pressure is a mere  $6.1 \times 10^{-8} \text{ m s}^{-2}$ . This can be compared with  $6.0 \times 10^{-8}$  and  $3.7 \times 10^{-8}$  for  $\mu$ SCOPE, a 120 kg satellite planned for circular orbit at an altitude of 700 km.

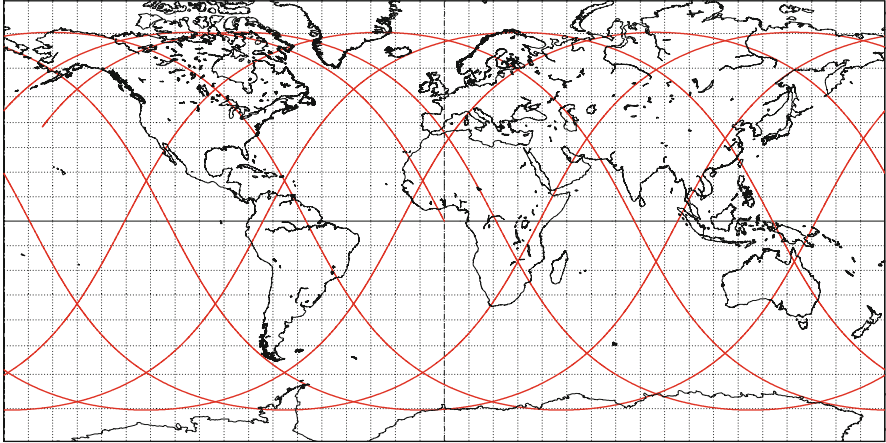
<sup>9</sup>Launch dates: LAGEOS-1 on 4 May 1976, LAGEOS-2 on 23 October 1992 (by STS-52), LARES on 13 February 2012.

**LAGEOS-1**

## Orbit - Ground track

&gt;&gt;&gt;&gt; Time span shown: 1440.0 min = 1.00 day

Altitude = 5891.9 km                      a = 12270.012 km  
 Inclination = 109.81 °  
 Period = 225.49 min    \* rev/day = 6.39  
 Equat. orbital shift = 6286.6 km ( 56.5 °)



Projection: Arden-Close

Project. centre: 0.0 ° ; 0.0 °

Asc. Node: 0.00 °

Ιξίων

Property: none

Aspect: Direct

App. inclin. = 117.79 °

MC \* LMD

⊕ T.:Cylindrical - Graticule: 10° {5.3[ +0.0/ +0.0/ +0.0] [-] EGM2008

Ατλας

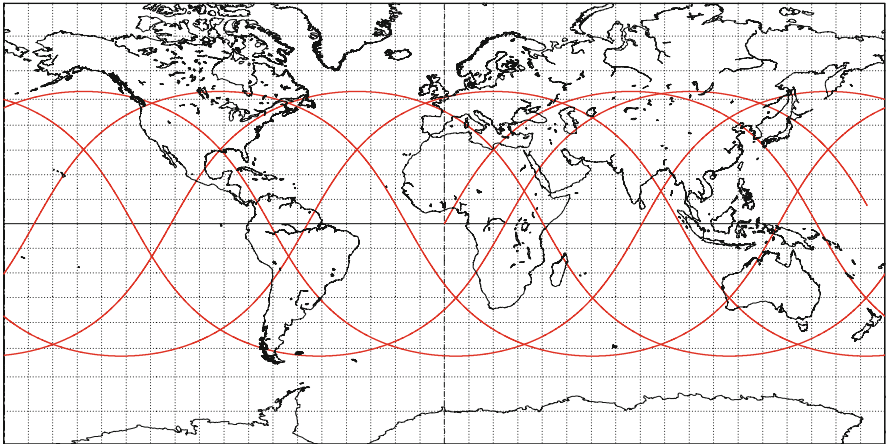
**LAGEOS-2**

## Orbit - Ground track

Recurrence = [ 6;+65;146] 941

&gt;&gt;&gt;&gt; Time span shown: 1440.0 min = 1.00 day

Altitude = 5783.9 km                      a = 12162.067 km  
 Inclination = 52.64 °  
 Period = 222.42 min    \* rev/day = 6.47  
 Equat. orbital shift = 6217.8 km ( 55.9 °)



Projection: Arden-Close

Project. centre: 0.0 ° ; 0.0 °

Asc. Node: 0.00 °

Ιξίων

Property: none

Aspect: Direct

App. inclin. = 60.40 °

MC \* LMD

⊕ T.:Cylindrical - Graticule: 10° {5.3[ +0.0/ +0.0/ +0.0] [-] EGM2008

Ατλας

FIG. 9.4 : LAGEOS geodesy satellites. Ground tracks of the orbits over 1 day. Upper: Retrograde for LAGEOS-1. Lower: Prograde for LAGEOS-2. The satellites have the same altitude.

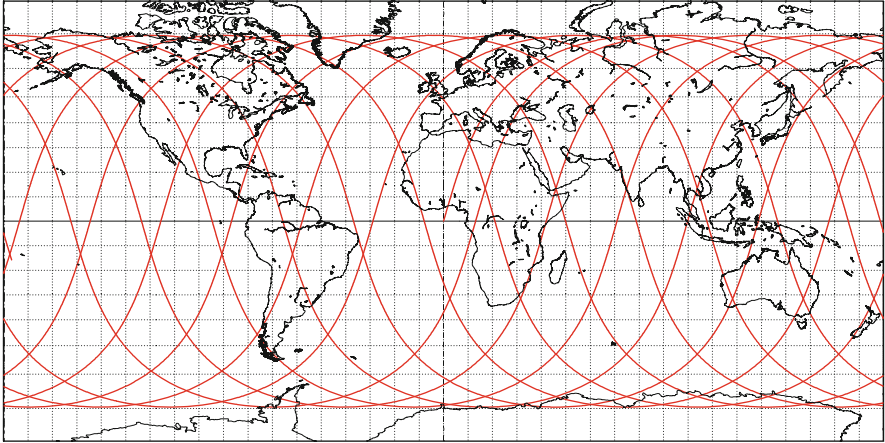


**LARES**

**Orbit - Ground track**

>>>> Time span shown: 1440.0 min = 1.00 day

Altitude = 1442.2 km                      a = 7820.301 km  
 Inclination = 69.49 °  
 Period = 114.77 min \* rev/day =12.55  
 Equat. orbital shift = 3218.0 km ( 28.9 °)



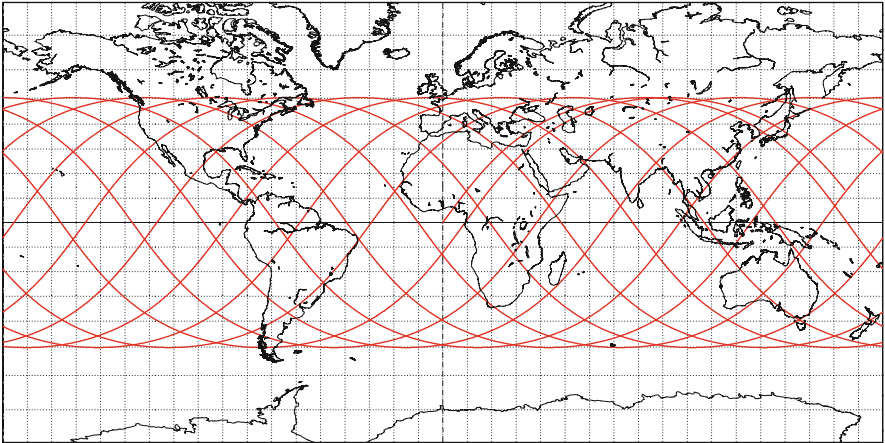
Projection: Arden-Close      Project. centre: 0.0 ° ; 0.0 °      Asc. Node: 0.00 °      *Ιξίων*  
 Property: none              Aspect: Direct              App. inclin. = 73.91 °      MC \* LMD  
 ⊕ T.:Cylindrical - Graticule: 10° §.3[ +0.0/ +0.0/ +0.0] [-] EGM2008      *Ατλας*

**EGP - Ajisai** ( *あじさい* )

**Orbit - Ground track**

>>>> Time span shown: 1440.0 min = 1.00 day

Altitude = 1488.5 km                      a = 7866.608 km  
 Inclination = 50.01 °  
 Period = 115.65 min \* rev/day =12.45  
 Equat. orbital shift = 3254.8 km ( 29.2 °)



Projection: Arden-Close      Project. centre: 0.0 ° ; 0.0 °      Asc. Node: 0.00 °      *Ιξίων*  
 Property: none              Aspect: Direct              App. inclin. = 53.77 °      MC \* LMD  
 ⊕ T.:Cylindrical - Graticule: 10° §.3[ +0.0/ +0.0/ +0.0] [-] EGM2008      *Ατλας*

FIG. 9.5 : Geodesy satellites. Upper: LARES (LAGEOS-3). Lower: EGP (Ajisai). Ground tracks of orbits over 1 day.

in collaboration with the two LAGEOS and the two GRACE satellites to improve gravitational models and our understanding of the effects predicted by general relativity, such as the Lense–Thirring effect.

**Example 9.1** Calculate the relative positions of the two geodesy satellites GRACE-A and -B.

► We use the NORAD data for two neighbouring transits on 31 December 2004, around 17:09 UT:

GRACE-A

```
1 27391U 02012A 04366.71456748 .00002198 00000-0 71465-4 0 8703
2 27391 89.0239 219.2934 0015306 313.4780 46.5231 15.31315612155826
```

GRACE-B

```
1 27392U 02012B 04366.71492843 .00002319 00000-0 75411-4 0 8597
2 27392 89.0243 219.2966 0016587 315.5508 44.4470 15.31314968155825
```

We can calculate the semi-major axis  $a$  for each orbit. The metric orbital elements are:

- GRACE-A:  $a = 6,846.810$  km, or  $h = 468.7$  km,  $e = 0.0015306$ ,  $i = 89.0239^\circ$ .
- GRACE-B:  $a = 6,846.811$  km, or  $h = 468.7$  km,  $e = 0.0016587$ ,  $i = 89.0243^\circ$ .

The NORAD times  $t_{0A}$  and  $t_{0B}$  deduced from the TLE are:

- $t_{0A} = 17:08:58.630$  UT for GRACE-A.
- $t_{0B} = 17:09:29.816$  UT for GRACE-B.

With  $\omega$  and  $v$  (deduced from  $M$  and  $e$ ), we calculate the ascending node crossing times  $t_A$  and  $t_B$  of the satellites (see Example 8.6):

- $t_A = 17:08:56.620$  UT for GRACE-A.
- $t_B = 17:09:27.767$  UT for GRACE-B.

In the Galilean frame, the difference between the longitudes of the ascending node is obtained directly from the TLE (the nodal precession over 2 s, the time elapsed between  $t_{0A}$  and  $t_A$ , is negligible):

- $\Delta\Omega = \Omega_B - \Omega_A = 219.2966^\circ - 219.2934^\circ = 0.0032^\circ$ .

The two orbits are practically identical ( $\Delta a = 1$  m) and lie in the same plane ( $\Delta\Omega = 11$  arcsec). The two satellites thus follow one another around this common orbit. The time difference is

- $\Delta t = t_B - t_A = 31.147$  s.

However, in the terrestrial frame, the ground tracks are distinct and “parallel”. For the longitude of the ascending node, calculation gives

- $\lambda_A = 221.5933^\circ$  for GRACE-A and  $\lambda_B = 221.4663^\circ$  for GRACE-B.

The difference in longitude is therefore

- $\Delta\lambda = \lambda_B - \lambda_A = -0.1270^\circ$ .

This corresponds to 14 km on the equator. It also corresponds to the following interval of time for the Earth’s rotation in the Galilean frame:

- $\Delta_{t\lambda} = -\Delta\lambda/\dot{\Omega}_T = 30.381 \text{ s}$ .

If we transform the angular increment  $\Delta\Omega$  into time using

$$\Delta_{t\Omega} = -\Delta\Omega/\dot{\Omega}_T = 0.766 \text{ s},$$

we obtain finally,

- $\Delta_{t\lambda} + \Delta_{t\Omega} = 30.381 + 0.766 = 31.147 \text{ s}$ .

This is the value found above for  $\Delta t$ .

In order to establish the local crossing time at the ascending node, we calculate the time in LMT:

- $\tau_A = 7.92195$  and  $\tau_B = 7.92214$ .

This is almost the same time for the two satellites:

- $\tau_A = 07:55:19$  and  $\tau_B = 07:55:20$ .

The difference is just  $\Delta_{t\Omega}$ . At the equator, the speed of the two satellites is 7.630 km/s and the speed of the ground track is 7.108 km/s. The difference between the two GRACE satellites is thus 237.9 km in space and 221.7 km for the ground tracks.

Figure 9.7 illustrates the above calculations. ◀

## 9.2.3 Earth Environment Satellites

### Terrestrial Magnetic Field and Its Manifestations

To study the Earth’s magnetic field, two satellites are in Sun-synchronous LEO, but elliptical orbit, namely the American MagSat (Magnetic field Satellite, AEM-3, Explorer-61), launched in 1979, with  $h_p = 352 \text{ km}$ ,  $h_a = 561 \text{ km}$ , and  $i = 96.8^\circ$ , and the Danish Ørsted, launched in 1999, with  $h_p = 450 \text{ km}$ ,  $h_a = 850 \text{ km}$ , and  $i = 96.5^\circ$ .

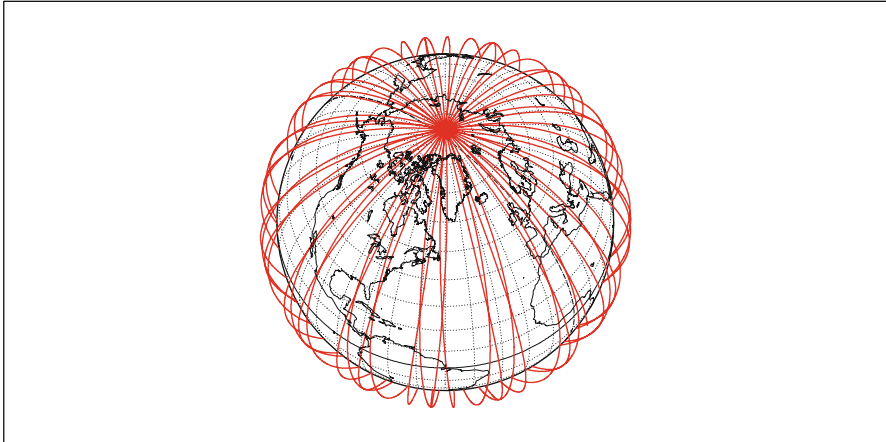
To study the radiation belts, the Chinese satellite SJ-5 (Shi Jian-5, DFH-47, where *shi jian* means “achievement”), launched in 1999 at the same time as FY-1C (DFH-46), is in a circular Sun-synchronous orbit with  $h = 855 \text{ km}$ . The military aspects of this study have been entrusted to the six satellites

**GP-B**

Orbit - ref.: Earth

>>>> Time span shown: 2880.0 min = 2.00 days

Altitude = 650.0 km                      a = 7028.136 km  
 Inclination = 90.00 °  
 Period = 97.86 min    \* rev/day =14.72  
 Equat. orbital shift = 2730.9 km ( 24.5 °)



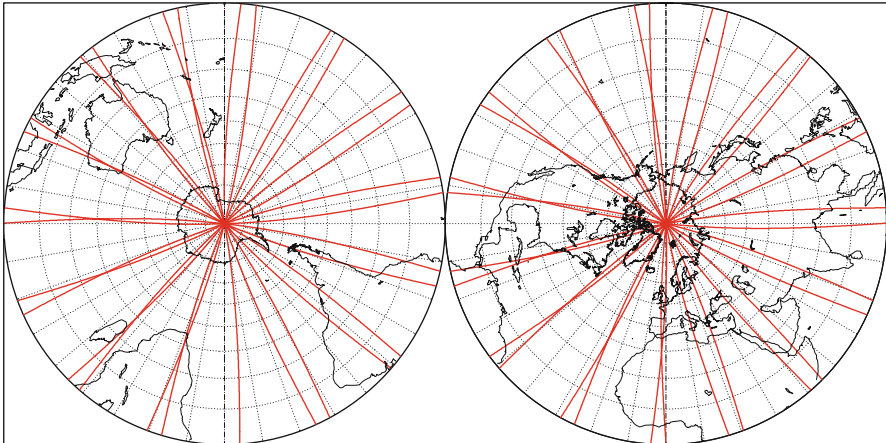
Projection: Orthographic    Project. centre: 60.0 ° N; 50.0 ° W    Asc. Node: 0.00 °                      *Ιξίων*  
 Property: none                      Aspect: Oblique                      MC ★ LMD  
 ⊕ T.:Azimuthal - Graticule: 10°    [-90.0/+30.0/+140.0] [-]    EGM2008                      *Ατλας*

**GP-B**

Orbit - Ground track

>>>> Time span shown: 1440.0 min = 1.00 day

Altitude = 650.0 km                      a = 7028.136 km  
 Inclination = 90.00 °  
 Period = 97.86 min    \* rev/day =14.72  
 Equat. orbital shift = 2730.9 km ( 24.5 °)



Projection: Stereographic    Pr. centre (r.): 90.0 ° N; 0.0 °                      Asc. Node: 0.00 °                      *Ιξίων*  
 Property: Conformal                      Aspect: Direct                      App. inclin. = 93.90 °                      MC ★ LMD  
 ⊕ T.:Azimuthal - Graticule: 10°    [+0.0/+0.0/+0.0] [-]    EGM2008                      *Ατλας*

FIG. 9.6 : Satellite GP-B with polar inclination. Upper: Orbit over 2 days. Lower: Ground track over 1 day.

**GRACE-A**

Orbit - Ground track

Recurrence ~ [15;+38;149]2273

2004 12 31 17:08:57 UTC >>> 1440.0 min = 1.00 day

Altitude = 468.7 km

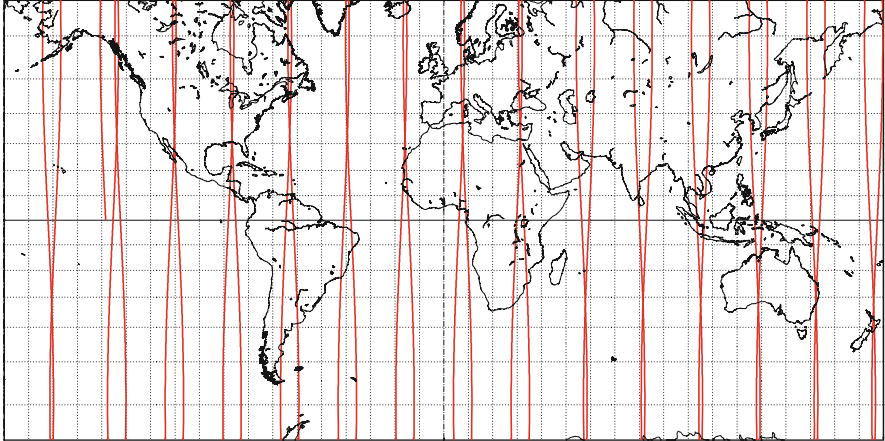
Inclination = 89.02 °

Period = 94.10 min \* rev/day=15.30

Equat. orbital shift = 2627.0 km ( 23.6 °)

a = 6846.809 km

e = 0.001531



Projection: Mercator

Project. centre: 0.0 ° ; 0.0 °

Asc. Node: -138.41 ° [07:55 LMT]

Ιξίων

Property: Conformal

Aspect: Direct

[NORAD] Revolution: 15582

MC ★ LMD

⊕ T.:Cylindrical - Graticule: 10° [5.3] [+0.0/ +0.0/ +0.0] [-] EGM96

[NORAD] 2004 12 31 17:08:57 UTC

Ατλας

**GRACE-B**

Orbit - Ground track

Recurrence = [15;+38;149]2273

2004 12 31 17:09:28 UTC >>> 720.0 min = 0.50 day

Altitude = 468.7 km

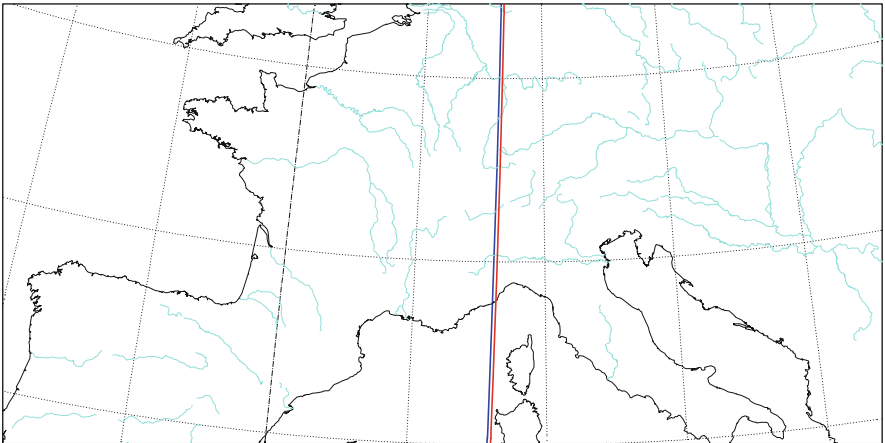
Inclination = 89.02 °

Period = 94.10 min \* rev/day=15.30

Equat. orbital shift = 2627.0 km ( 23.6 °)

a = 6846.811 km

e = 0.001659



Proj.: UTM / Zone 32

PC: 0.0 ° ; 9.0 °E /ZC: 46.0 ° N; 6.0 ° E

Asc. Node: -138.53 ° [07:55 LMT]

Ιξίων

Property: Conformal

Aspect: Direct > zoom : 15.00

[NORAD] Revolution: 15582

MC ★ LMD

⊕ T.:Cylindrical - Graticule: 5° [5.3] [+0.0/ -90.0/ -9.0] [+90] EGM96

[NORAD] 2004 12 31 17:09:28 UTC

Ατλας

FIG. 9.7 : GRACE satellites. Upper: Orbital ground track of GRACE-A over 1 day. Lower: Orbital ground track of GRACE-B (zoom) for one passage, superposing the ground track of GRACE-A, slightly to the east ( $\Delta\lambda = \lambda_B - \lambda_A = -0.1271^\circ$ ).

Shi Jian-6, launched in pairs every 2 years (SJ-6A and -6B in 2004, SJ-6C and -6D in 2006, and SJ-6E and -6F in 2008, also called DFH-60 and -61, -70 and -71, and -80 and -81, in the same order). On a Sun-synchronous orbit at  $h = 600$  km, they follow each other at an interval of 1 min.

In near-polar LEO orbit, between 800 and 1,000 km, are the even-numbered OGO satellites (Orbiting Geophysical Observatory), OGO-2, -4, and -6, known as POGO (Polar OGO), launched between 1965 and 1969, the Swedish satellites Astrid-1 and -2, launched in 1995 and 1998, and the strictly polar satellite Polar BEAR (Beacon Experiments and Auroral Research).

### Magnetosphere and Heliosphere

To study the magnetosphere, that is, the zone of interaction between particles excited by the solar wind and the Earth's magnetic field, satellite orbits have to be very high and highly elliptical. The first US satellite to be placed in orbit, Explorer-1, with  $h_p = 347$  km,  $h_a = 1,859$  km, and  $i = 33.2^\circ$ , already had some of these features. As we have seen, it discovered two radiation belts around the Earth, since referred to as the Van Allen belts. This radiation was studied by the Soviet Elektron programme, for which four satellites were launched in two pairs in 1964: Elektron-1 with -2 and Elektron-3 with -4. They all followed eccentric orbits, with inclination  $i \approx 61^\circ$ , and with  $h_a \sim 6,500$  km for the odd numbers,  $h_a \sim 65,000$  km for the even numbers.

Magnetospheric studies continued with a great many satellites launched between 1964 and 1968, such as the odd-numbered OGO satellites, OGO-1, -3, and -5, referred to as EOGO (Eccentric OGO), Explorer-34 (IMP-F or IMP-5, Interplanetary Monitoring Platform), launched in 1967 with  $h_p = 242$  km,  $h_a = 214,400$  km,  $i = 67.1^\circ$ , or Explorer-50 (IMP-J or IMP-8), launched into a very high orbit in 1973 with variable inclination between  $32^\circ$  and  $55^\circ$  (and after 30 years, this satellite is still operational). The justification for the polar orbits of Dynamics Explorer-1 and -2 was explained in Chap. 7.

For the experiment ISEE (International Sun–Earth Explorer), the two satellites ISEE-1 and -2 were launched in 1977 into highly eccentric orbits, with  $h_p \approx 400$  km,  $h_a \approx 138,000$  km,  $i = 12.7^\circ$  and  $13.5^\circ$ . Then in 1978, ISEE-3 was the first satellite to be placed in a halo orbit<sup>10</sup> around the Lagrange point  $L_1$ , an orbit known as L1LO (see the appendix on the Lagrange points in Sect. 6.12). The satellite Wind, launched in 1994, was also placed in an L1LO orbit around the point  $L_1$ , where it remained from May 1997 until April 1998. From this location, it was able to observe the solar wind before it became perturbed by the Earth's magnetosphere. It was subsequently placed

---

<sup>10</sup>When it had accomplished its mission, the satellite was withdrawn from the point  $L_1$  in June 1982. Using a lunar flyby as a gravity-assist maneuver, it was removed from the Earth's gravitational attraction and sent into heliocentric orbit for the ICE mission (International Cometary Explorer), in an encounter with a comet (perihelion 0.93 a.u., aphelion 1.03 a.u., inclination  $0.1^\circ$ , period 355 day).

**Van Allen Pr.-A (RBSP-A)**

Orbit - ref.: Earth

Recurrence = [ 3;-54;161] 429

2012 09 27 10:44:36 UTC &gt;&gt;&gt; 10.00 days

Equiv. altit. = 15559.4 km

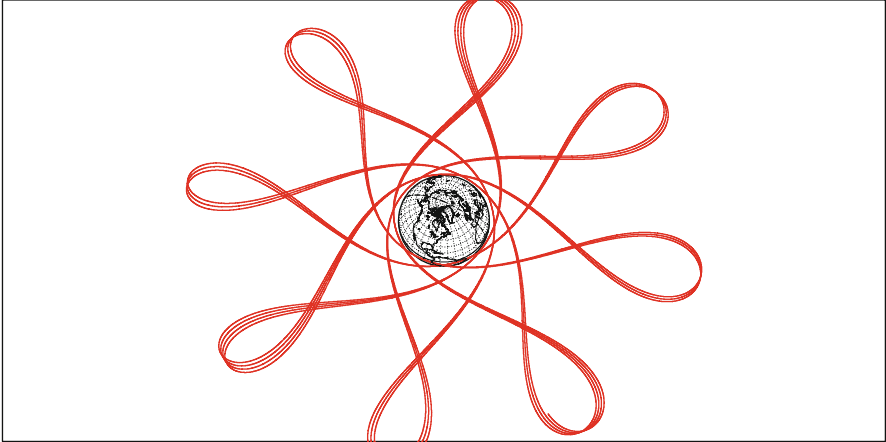
a = 21937.541 km

Inclination = 9.95 °

e = 0.682033

Period = 538.26 min \* rev/day = 2.68

h\_a = 30522 km; h\_p = 597 km; arg. perigee: +24.96 °



Projection: Orthographic

Project. centre: 65.0 ° N; 65.0 ° W

[NORAD] 2012 09 27 10:44:36 UTC//R= 75 *Ιξων*

Property: none

Aspect: Oblique

Asc. Node: 101.29 ° [17:30 LMT] MC ★ LMD

⊕ T.:Azimuthal - Graticule: 10°

[4.2] [-90.0/ +25.0/+155.0] [-] EGM2008

Apogee : 12.05 °

*Ατλας***Van Allen Pr.-B (RBSP-B)**

Orbit - ref.: Earth

2012 10 01 00:00:00 UTC &gt;&gt;&gt; 15.00 days

Equiv. altit. = 15639.0 km

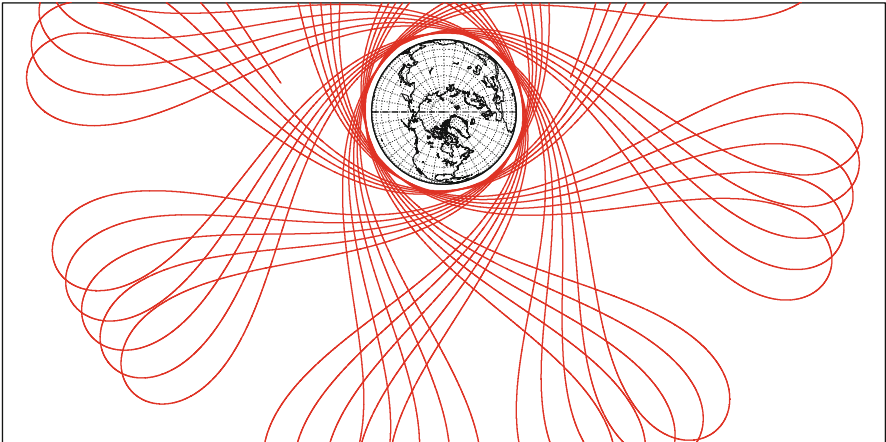
a = 22017.152 km

Inclination = 9.94 °

e = 0.682736

Period = 541.20 min \* rev/day = 2.66

h\_a = 30671 km; h\_p = 607 km; arg. perigee: +24.91 °



Projection: Orthographic

Project. centre: 90.0 ° N; 90.0 ° W

[NORAD] 2012 09 27 14:12:03 UTC//R= 75 *Ιξων*

Property: none

Aspect: Direct

Asc. Node: 49.37 ° [17:30 LMT] MC ★ LMD

⊕ T.:Azimuthal - Graticule: 10°

[4.2] [-90.0/ +0.0/-180.0] [-] EGM2008

Apogee : -39.55 °

*Ατλας*

FIG. 9.8: In a terrestrial frame, orbits of Van Allen Probe-A and -B, investigating the Van Allen radiation belts. Upper: Probe-A over 10 days. Lower: Probe-B over 15 days.

**STRV-1B**

Orbit - ref.: Earth

Recurrence = [ 3;-12;161] 471

2010 05 26 06:29:17 UTC &gt;&gt;&gt; 5.00 days

Equiv. altit. = 14233.5 km

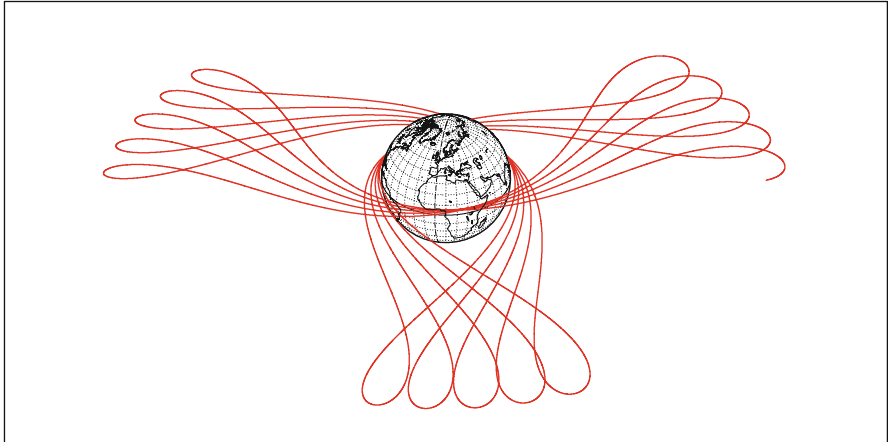
a = 20611.604 km

Inclination = 7.15 °

e = 0.679397

Period = 490.12 min \* Revol./d.= 2.94

h\_a = 28237 km ; h\_p = 230 km ; arg. perigee : +55.73 °



Projection : Orthographic

Centre Project.: 35.0 ° N ; 10.0 ° E

[NORAD] 2010 05 26 06:29:17 UTC / R: 15170 *Ιξίων*

Property : (none)

Aspect : Oblique

Asc. Node : -138.69 ° [21:15 LMT] **MC \* LMD**

⊕ T.:Azimutal - Graticule: 10°

§4.2[-90.0/ +55.0/ +80.0] [-] EGM96

Apogee : 155.21 °

*Ατλας***STRV-1C**

Orbit - ref.: Earth

Recurrence = [ 2; +2; 69] 140

2010 02 15 08:33:45 UTC &gt;&gt;&gt; 5.00 days

Equiv. altit. = 19934.7 km

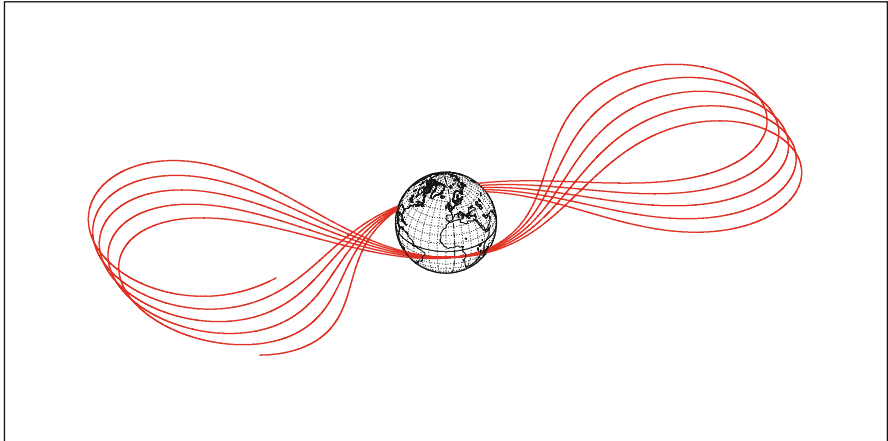
a = 26312.871 km

Inclination = 6.02 °

e = 0.734470

Period = 707.12 min \* Revol./d.= 2.04

h\_a = 39261 km ; h\_p = 609 km ; arg. perigee : +226.14 °



Projection : Orthographic

Centre Project.: 35.0 ° N ; 10.0 ° W

[NORAD] 2010 02 15 08:33:45 UTC / R: 6877 *Ιξίων*

Property : (none)

Aspect : Oblique

Asc. Node : -70.41 ° [03:52 TSM] **MC \* LMD**

⊕ T.:Azimutal - Graticule: 10°

§4.2[-90.0/ +55.0/+100.0] [-] EGM96

Apogee : 88.21 °

*Ατλας*

FIG. 9.9: In a terrestrial frame, GTO orbits of the experimental satellites STRV over 5 days. Upper: STRV-1B, about three revolutions per day. Lower: STRV-1C, about two revolutions per day.



on a highly complex orbit known as a petal orbit<sup>11</sup> from November 1998 to April 1999. The satellite ACE (Advanced Composition Explorer, Explorer-71), launched in 1997, is also in an L1LO orbit.

We should also mention the highly eccentric orbits of the following satellites: Interkosmos-24, a Soviet satellite launched in 1989,  $h_p = 511$  km,  $h_a = 2,950$  km,  $i = 82.6^\circ$ , with Magion-2 (see Fig. 9.11); Geotail (or GTL, Geomagnetic Tail Laboratory), a Japanese satellite launched in 1992,  $h_p = 41,360$  km,  $h_a = 508,500$  km,  $i = 22.4^\circ$ ; Polar, launched in 1996, on an orbit with variable parameters,<sup>12</sup>  $a \sim 60,000$  km,  $e \approx 0.7$ ,  $i \sim 80^\circ$ ; FAST (Fast Auroral Snapshot Explorer, SMEX-2, Explorer-70), launched in 1996,  $h_p = 353$  km,  $h_a = 4,163$  km,  $i = 83.0^\circ$ , (see Fig. 9.10 upper); Equator-S, launched in 1997,  $h_p = 496$  km,  $h_a = 67,230$  km,  $i = 7.0^\circ$  (orbit obtained by transfer via a GTO orbit); IMAGE (Imager for Magnetopause-to-Aurora Global Exploration, MIDEX-1, Explorer-78), launched in 2000, on a polar orbit with  $h_p \approx 1,000$  km and  $h_a$  of the order of seven Earth radii.

To study the Van Allen radiation belts, NASA placed the two satellites RBSP-A and -B (Radiation Belt Storm Probe) on a GTO orbit in 2012. They were later renamed the Van Allen Probes (see Fig. 9.8). With  $h_p \approx 550$  km and  $h_a \approx 31,100$  km ( $a = 21,980$  km,  $e = 0.682$ ), these twin satellites have a period of  $T = 540$  min, or 9 h, and make frequent crossings of the belt under investigation (see also the STRV satellites discussed under technological satellites and shown in Fig. 9.9).

The Russian Interball experiment is based on Interball Tail (or Interball-S2-X, Interbol-1, Prognoz-11), launched in 1995 on a highly elliptical orbit with period  $T = 91$  h, and Interball Aurora (or Interball-S2-A, Interbol-2, Prognoz-12), launched in 1996 on a Molniya orbit. In each case, the Czech satellites Magion (Magnetosphere–Ionosphere), Magion-4 then Magion-5, were launched jointly with an Interball satellite. The orbit of the forthcoming Interbol-3 is planned for  $h_a = 400,000$  km. We also mention the Chinese satellite KF1-SJ-4 (Shi Jian-4, DFH-38), launched in 1994 on a GTO orbit with  $i = 28.6^\circ$ .

To study the magnetosphere and phenomena related to the aurora borealis, between 1978 and 1989, Japan sent four satellites EXOS (Exospheric Observations) into alternately low and high eccentric orbits, with  $i = 69^\circ$  for

---

<sup>11</sup>The satellite left the point  $L_1$  in the Earthward direction, roughly in the plane of the lunar orbit, before moving into the petal orbit. In this configuration, the satellite moves alternately behind the Earth and the Moon. In this plane and in a frame moving with the Earth, the trajectory sketches out a daisy with the Earth at the center. The tips of the petals represent the different positions of the Moon in its rotation about the Earth. It has period 17.5 day and the radius of the ellipse is  $r_p \approx 6R$  to  $10R$ ,  $r_a \approx 80R$  (where the Earth–Moon distance is approximately  $60R$ ).

<sup>12</sup>This satellite, the Polar Plasma Laboratory, is part of the GGS mission (Global Geospace Science) with Wind and Geotail, and this is itself just one component of the ISTP programme (International Solar Terrestrial Physics), which includes the European missions SOHO and Cluster and the Russian mission Interball.

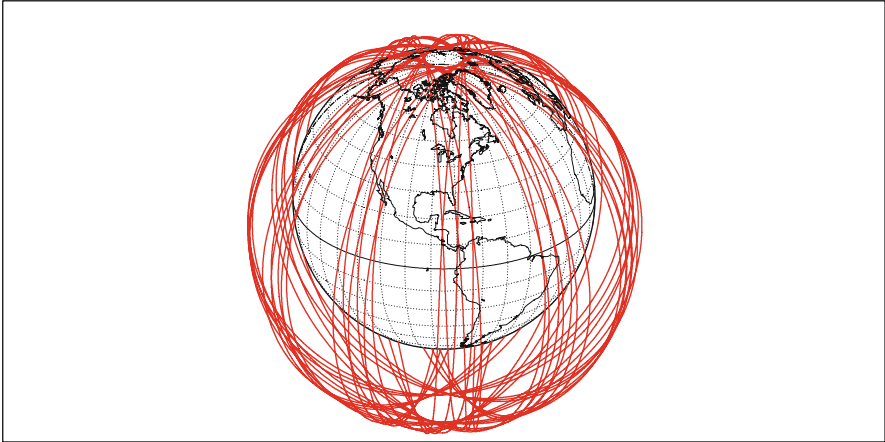
**FAST**

Orbit - ref.: Earth

Recurrence = [11;+11; 71] 792

2004 11 17 22:35:40 UTC >>> 4320.0 min = 3.00 days

Equiv. altit. = 2054.5 km      a = 8432.587 km  
 Inclination = 82.97 °      e = 0.202505  
 Period = 128.56 min \* rev/day = 11.20  
 h\_a = 3783 km; h\_p = 368 km; arg. perigee: +95.00 °



Projection: Orthographic      Project. centre: 28.0 ° N; 85.0 ° W      [NORAD] 2004 11 17 22:35:40 UTC//R= 33065 *Ιξίων*  
 Property: none      Aspect: Oblique      Asc. Node: 139.63 ° [07:54 LMT]      MC ★ LMD  
 ⊕ T.:Azimuthal - Graticule: 10°      {4.2}[-90.0/+62.0/+175.0] [-] EGM2008      Apogee : -85.12 °      Ατλας

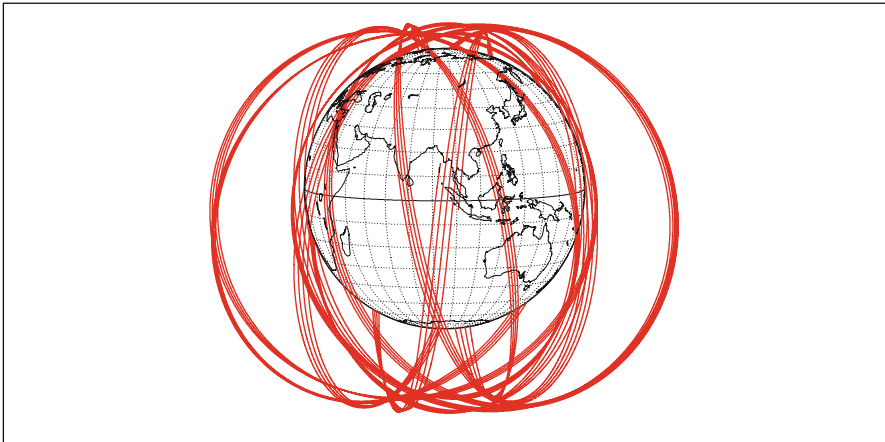
**Akebono (EXOS-D) 〈 あけぼの 〉**

Orbit - ref.: Earth

Recurrence = [10; -5;131]1305

2009 11 05 01:11:11 UTC >>> 5760.0 min = 4.00 days

Equiv. altit. = 2710.5 km      a = 9088.656 km  
 Inclination = 75.07 °      e = 0.269151  
 Period = 143.81 min \* rev/day = 10.01  
 h\_a = 5162 km; h\_p = 270 km; arg. perigee: +149.24 °



Projection: Orthographic      Project. centre: 5.0 ° N; 95.0 ° E      [NORAD] 2009 11 05 01:11:11 UTC//R= 60955 *Ιξίων*  
 Property: none      Aspect: Oblique      Asc. Node: 98.28 ° [07:44 LMT]      MC ★ LMD  
 ⊕ T.:Azimuthal - Graticule: 10°      {4.2}[-90.0/+85.0/ -5.0] [-] EGM2008      Apogee : -85.46 °      Ατλας

FIG. 9.10 : Ground tracks of elliptical orbits over 3 days. Upper: FAST. Lower: Akebono (EXOS-D).

EXOS-A (Kyokko, meaning “aurora”),  $i = 31^\circ$  for EXOS-B (Jikiken, meaning “magnetosphere”), and  $i = 75^\circ$  for EXOS-C (Ohzora, meaning “sky”) and EXOS-D (Akebono, meaning “dawn”) (see Fig. 9.10 lower).

The European experiment Cluster-2 comprises four satellites in formation.<sup>13</sup> They have a very high orbit, with  $h_p = 17,200$  km,  $h_a = 120,600$  km,  $i = 65^\circ$ ,  $T = 57$  h. The Double Star programme comprises two Chinese satellites carrying European instruments similar to those designed for Cluster, in eccentric orbits,<sup>14</sup> with perigee at 600 km altitude. The first, DSP-1,  $h_a = 79,000$  km, is in an equatorial orbit, and the second, DSP-2,  $h_a = 39,000$  km, is in a polar orbit.

The satellite IBEX (Interstellar Boundary Explorer, SMEX-10, Explorer-91) is on a very high near-equatorial orbit with a period of 7.6 days.<sup>15</sup>

China is pursuing its efforts in this field with the Kua Fu mission: they have placed one satellite, Kua Fu-A, at the Lagrange point  $L_1$ , and two satellites, Kua Fu-B1 and -B2, in polar LEO orbit.

The five satellites of the US mission THEMIS (Time History of Events and Macroscale Interactions during Substorms, MIDEX-5)<sup>16</sup> were launched together on 17 February 2007. The aim is to unambiguously determine<sup>17</sup> the regions where magnetic substorms are triggered and study the reconnection modes of the magnetic tail. There are five phases to the mission. (a)—First Phase. The five satellites are on the same orbit:  $h_p = 470$  km,  $h_a = 87,333$  km (or  $15.4R$ , where  $R$  is the Earth radius),  $i = 16.0^\circ$ . (b)—Dawn Phase. The apogee  $h_a$  of each satellite is modified:  $30R$  for THEMIS-1,  $20R$  for THEMIS-2,  $12R$  for THEMIS-3 and -4,  $10R$  for THEMIS-5. At the apogee, the satellites are situated above places where it is dawn on Earth. (c)—Tail Phase. The orbits remain unchanged, but owing to the motion of the Earth about the Sun, the satellites reach apogee at midnight. (d)—Dusk Phase. The satellites reach apogee at dusk. (e)—Final Phase. The apogee lies Sunward, with passage at noon.

<sup>13</sup>These satellites, Rumba, Salsa, Samba, and Tango, fly a few hundred kilometers apart. They were launched in two stages, on 16 June and 19 August 2000, to avoid repetition of the disaster when Cluster was launched together on 4 June 1996.

<sup>14</sup>DSP-1 (also called Tan Ce-1, meaning Explorer-1 in Chinese, or TC-1),  $a = 46,148.1$  km,  $e = 0.8494$ ,  $i = 28.5^\circ$ , launched on 29 December 2003. DSP-2 (Tan Ce-2 or TC-2),  $a = 26,228.1$  km,  $e = 0.7301$ ,  $i = 90^\circ$ , launched on 26 July 2004.

<sup>15</sup>Launch date 19 October 2008 and orbital characteristics  $h_p = 1.5R$ ,  $h_a = 47.8R$ ,  $a = 163,000$  km,  $e = 0.9025$ ,  $i = 10.993^\circ$ ,  $T = 183$  h.

<sup>16</sup>This is one of the Explorer missions. The satellites are also called Explorer-85, -86, -87, -88, and -89. In the MIDEX-5 framework, they are referred to as MIDEX-5A to -5E.

<sup>17</sup>It was the idea of a clear and objective determination that led to the name of this mission, THEMIS, from the Greek goddess of justice  $\eta \Theta\acute{\epsilon}\mu\iota\varsigma, \iota\tau\omicron\varsigma$ , or Themis. She sits at the deliberations of gods and men and in each instance preserves the equity of their decisions.

For such satellites, precessional motions are very slow<sup>18</sup> and each orbit thus remains practically fixed relative to a Galilean frame. At the end of 1 year, the mission was extended. The values  $h_p = 470$  km and  $i = 16.0^\circ$  were maintained throughout the whole mission.

The US project MMS (Magnetospheric Multiscale) plans to operate four satellites in formation, at the vertices of a tetrahedron. The inclination of the orbit is  $i = 28.5^\circ$  and the perigee remains constant at  $r_p = 1.2R$ . Concerning the apogee,  $r_a = 12.83R$  ( $T = 1.09$  day) in phase 1, then goes to  $r_a = 25.0R$  ( $T = 2.78$  day) in phase 2. The European project Cross-Scale will use a flotilla of seven satellites on an orbit with  $r_p = 10R$ ,  $r_a = 25R$ ,  $i = 14^\circ$ , and  $\omega = 205^\circ$ , giving a period of  $T = 4.3$  day.

## Ionosphere

To study the ionosphere,<sup>19</sup> there are the US satellites UARS (Upper Atmosphere Research Satellite),  $h = 570$  km,  $i = 56.9^\circ$ , and TIMED (Thermo-Iono-Mesosphere Energetics and Dynamics),  $h = 625$  km,  $i = 74.0^\circ$ . In addition, there is the Taiwanese satellite Rocsat-1 (Republic of China Satellite), with a slightly inclined orbit,  $h = 630$  km,  $i = 35^\circ$  (for an oceanographic mission) and many Interkosmos, such as Interkosmos-12, several Kosmos, such as Kosmos-196, and the Chinese satellites Atmosphere-1 and -2 (DFH-31 and -32), which are Sun-synchronous with  $h = 800$  km and  $h = 610$  km. The satellite SAMPEX (Solar Anomalous and Magnetospheric Particle Explorer, SMEX-1, Explorer-68) is near-polar, with  $h_p = 506$  km,  $h_a = 670$  km, and  $i = 81.7^\circ$  (Fig. 9.11).

## 9.2.4 Satellites for Meteorology and Climate Study

### Meteorology and the Study of the Atmosphere

The possibility of observation from space aroused the interest of meteorologists from an early stage. It was their dream to know the global state of the atmosphere in a single glance! In order to do so, the orbits used have always been Sun-synchronous LEO orbits (see Fig. 9.12) or GEO orbits (see Fig. 9.13), apart from the first satellites and the Meteor satellites.

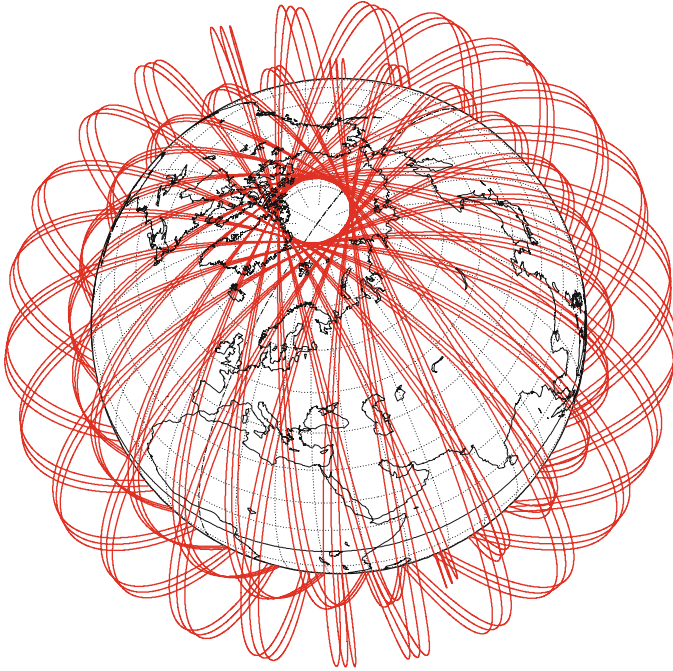
#### *LEO Meteorological Satellites*

In the case of NASA's NIMBUS programme,<sup>20</sup> the seven satellites were Sun-synchronous, from Nimbus-1 to Nimbus-6, on a fairly high LEO orbit

<sup>18</sup>For the satellites in Phase 1, the nodal precession rate is  $\dot{\Omega} = 0.10$  round/year, the apsidal precession rate is  $\dot{\omega} = 0.20$  round/year.

<sup>19</sup>Launch dates: UARS on 12 September 1991 (STS-48); TIMED on 7 December 2001 (with Jason-1 but in a different orbit); Rocsat-1 on 27 January 1999; Interkosmos-12 on 30 October 1974; Atmosphere-1 and -2 (DFH-31 and -32) on 3 September 1990; SAMPEX on 3 July 1992.

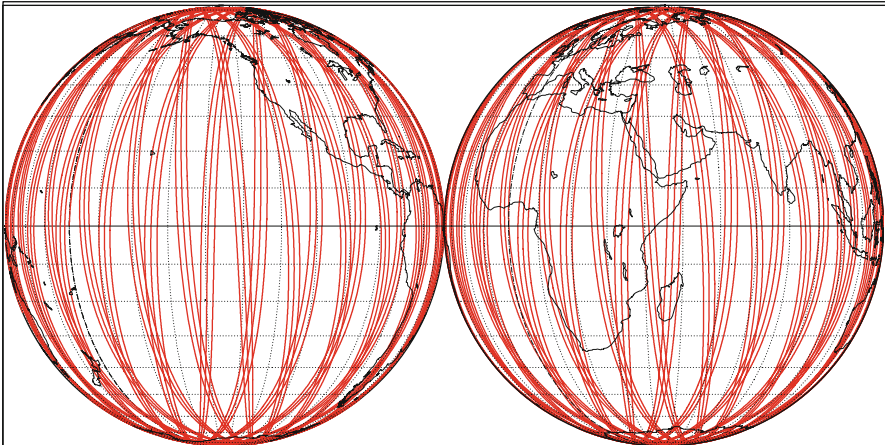
<sup>20</sup>Launch dates: Nimbus-1 on 28 August 1964; Nimbus-2 on 15 May 1966, Nimbus-3 on 14 April 1969; Nimbus-4 on 8 April 1970; Nimbus-5 on 11 December 1972; Nimbus-6 on 12 June 1975; Nimbus-7 on 24 October 1978.



**Interkosmos-24** ( **ИнтерКосмос** )  
 Elliptical orbit - Gr. track

>>>> Time span shown: 6.00 days

Equiv. altit. = 1447.3 km      a = 7825.471 km  
 Inclination = 82.59 °      e = 0.121592  
 Period = 114.94 min \* rev/day = 12.53  
 h\_a = 2399 km; h\_p = 496 km; arg. perigee: +156.46 °



Projection: Orthographic	Pr. centre (r.): 0.0 ° ; 45.0 °E	Longitude / Initialisation:	<i>Ιξίων</i>
Property: none	Aspect: Equatorial	Asc. Node: -180.00 ° [00:00 LMT]	MC * LMD
⊕ T.: Azimuthal - Graticule: 10°	⌘.2⌘ [-90.0/ +90.0/ +45.0] [-] EGM2008	Apogee : -0.85 °	<i>Ατλας</i>

FIG. 9.11 : Orbit and ground track of the satellite *Interkosmos-24* over 6 days. The representation clearly indicates the position of the perigee, whereas the representation of the ground track does not.





with  $h = 1,100$  km and  $i = 99.9^\circ$ , while Nimbus-7 followed a slightly lower orbit with  $h = 950$  km and  $i = 99.1^\circ$ .

The programme run by what is known today as the National Oceanic and Atmospheric Administration (NOAA), the American meteorological office, can be divided into five series: TIROS (Television and Infra Red Observation Satellite), TOS (TIROS Operational System), ITOS (Improved TOS), TIROS-N and ATN (Advanced TIROS-N). The first comprises 12 satellites and began on 1 April 1960 with the launch of the first meteorological satellite,<sup>21</sup> TIROS-1. Up to TIROS-8, launched in 1963, the orbits were similar, with  $h \approx 680$  km and  $i$  between  $48^\circ$  and  $58^\circ$ . Subsequently, all further satellites were Sun-synchronous: TIROS-9 and -10, launched in 1964, and ESSA-1 and 2 (Environmental Science Service Administration), launched in 1966. The TOS series comprised seven satellites, from ESSA-3 to ESSA-9, launched from 1966 to 1969, on the orbit  $h = 1,450$  km,  $i = 102^\circ$ . The ITOS series used exactly the same orbit for six satellites, ITOS-1, NOAA-1, -2, -3, -4, -5, launched from 1970 to 1976. The last two series<sup>22</sup> adopted a lower orbit:  $h = 800$  km,  $i = i_{\text{HS}} = 98.8^\circ$  for TIROS-N, with the satellites TIROS-N and NOAA-6 and -7; and  $h$  from 820 to 860 km,  $i = i_{\text{HS}}$  for ATN, with the satellites NOAA-8 to -18.

The POES programme (Polar-orbiting Operational Environmental Satellites) concerns the two last series. Its planned successor was the NPOESS programme (National POES System), a joint project by several US institutions, namely the NOAA, NASA, and the Department of Defense (DoD, which runs the DMSP series), known as “Three Agencies, One Mission”, coordinated by the satellite NPP (NPOESS Preparatory Project)<sup>23</sup> at altitude  $h = 824$  km. The six NPOESS satellites, from NPOESS-1 to -6, were planned to follow almost the same orbit as NPP, at  $h = 828$  km.

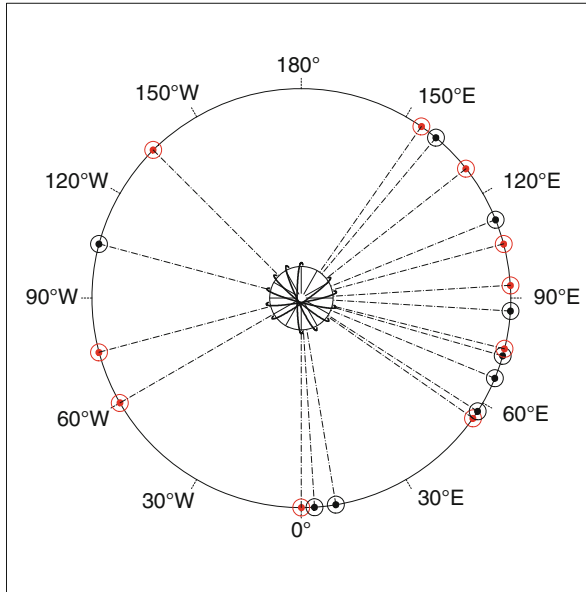
In February 2010, the US government reconsidered the various contributions of the NOAA, NASA, and the DoD and replaced NPOESS by JPSS (Joint Polar Satellite System). This new programme was based on a close collaboration with the European organisation EUMETSAT and its MetOp

---

<sup>21</sup>The three US satellites launched in 1959 had provided useful meteorological data. These were Vanguard-2, Explorer-6 (first photograph of the Earth), and Explorer-7 (first data concerning the Earth radiation budget). However, the first satellite devoted entirely to meteorology was TIROS-1.

<sup>22</sup>Launch dates: TIROS-N on 13 October 1978; NOAA-6 on 27 June 1979; NOAA-7 on 23 June 1981; NOAA-8 on 28 March 1983; NOAA-9 on 12 December 1984; NOAA-10 on 17 December 1986; NOAA-11 on 24 September 1988; NOAA-12 on 14 May 1991; NOAA-13 on 9 August 1993, only operated for a few days; NOAA-14 on 30 December 1994; NOAA-15 on 13 May 1998; NOAA-16 on 21 September 2000; NOAA-17 on 24 June 2002; NOAA-18 on 20 May 2005; NOAA-19 on 6 February 2009.

<sup>23</sup>Launch date: NPP on 28 October 2011. The National Polar-orbiting Operational Environmental Satellite System Preparatory Project (NPP) was renamed National Polar-orbiting Partnership (NPP), and then, in January 2012, Suomi-NPP, after the American engineer Verner E. Suomi, considered to be the father of satellite meteorology (he built the first radiometer, aboard Explorer-7).



Location $\lambda_s$	Operator	Satellite (series)	Satellite in orbit	Type
0.0° –	EUMETSAT	METEOSAT	METEOSAT-10	MO
3.6°E	EUMETSAT	METEOSAT	METEOSAT-8	SO
9.5°E	EUMETSAT	METEOSAT	METEOSAT-9	SB
55.0°E	India	METSAT	INSAT-3E	MO
57.3°E	EUMETSAT	METEOSAT	METEOSAT-7	SO
74.0°E	India	METSAT	Kalpana-1	SO
76.0°E	Russia	GOMS	Elektro-1	MO
86.5°E	China	Feng Yun-2	FY-2D	SO
93.5°E	India	INSAT	INSAT-3A	MO
105.0°E	China	Feng Yun-2	FY-2E	MO
112.0°E	China	Feng Yun-2	FY-2F	SB
128.2°E	South Korea	COMS	COMS-1	MO
140.0°E	Japan	MTSAT	MTSAT-1R	SO
145.0°E	Japan	MTSAT	MTSAT-2	MO
135.0°W	US/NOAA	GOES-W	GOES-15	MO
105.0°W	US/NOAA	GOES	GOES-14	B
75.0°W	US/NOAA	GOES-E	GOES-13	MO
60.0°W	US/NOAA	GOES	GOES-12	MO

FIG. 9.13 : Meteorological geostationary satellites, with parking positions, as of 1 July 2013. Status of satellite: MO (main operational), SO (secondary operational), B (back-up), SB (on standby). The geostationary orbit and the Earth are drawn on the same scale. Orbits of Sun-synchronous satellites at altitude 800 km are also plotted on the same scale. The viewpoint is located very high up on the polar axis, above the North Pole.



satellite. However, in 2011, the DoD decided to carry out its own programme, DWSS (Defense Weather Satellite System). To be continued (see the appendix in Sect. 9.3).

The military satellites DMSP (Defense Meteorological Satellite Program) supply some data to the civilian sector. They are all Sun-synchronous, often following slightly elliptical orbits, with  $h$  between 750 and 850 km,  $i = i_{\text{HS}}$  from  $98.6^\circ$  to  $99.2^\circ$ . There were thirteen satellites launched from 1965 to 1969 for the first block (Block 4), from DMSP-4A F-1 (OPS/6026) to DMSP-4A F-13 (also called DMSP-4B F-3, or OPS/1127). The second block (Block 5) began in 1970 with DMSP-5A F-1 (OPS/0054) and is still running,<sup>24</sup> with the extension Block 5D3.

Soviet then Russian meteorological satellites<sup>25</sup> were not Sun-synchronous until 2001. They fall into three Meteor series, with near-polar LEO orbits. The first two series involved 48 satellites: Meteor-1, from Meteor-1-01 in 1969 to Meteor-1-27 in 1977, with  $h = 870$  km,  $i = 81.2^\circ$ ; Meteor-2, from Meteor-2-01 in 1975 to Meteor-2-21 in 1993, with  $h = 940$  km,  $i = 82.5^\circ$ . The third series involved six satellites in slightly higher orbits, with  $h = 1,200$  km,  $i = 82.6^\circ$ . The new generation, known as Meteor-M, are Sun-synchronous. The first of the series is Meteor-M-1,  $h = 816$  km,  $i = i_{\text{HS}} = 98.8^\circ$ ,  $\tau_{\text{AN}} = 21:30$ .

The Chinese satellites<sup>26</sup> in the FY-*odd* series (FY-1 and FY-3, where FY stands for Feng Yun, and *feng yun* means “wind and cloud”) are Sun-synchronous with  $h = 858$  km for FY-1 and  $h = 808$  km for FY-3.

The European MetOp satellites<sup>27</sup> (Meteorological Operational satellites) are of course Sun-synchronous, at an average altitude of  $h = 830$  km.

The Rocsat-3/COSMIC mission (Constellation Observing System for Meteorology, Ionosphere and Climate), renamed<sup>28</sup> FormoSat, is a collaboration between Taiwan and the USA. It comprises a constellation of microsattellites

<sup>24</sup>Launch dates: DMSP-5D2 F-8 (also called USA-26) on 20 June 1987; DMSP-5D2 F-9 (USA-29) on 3 February 1988; DMSP-5D2 F-10 (USA-68) on 1 December 1990; DMSP-5D2 F-11 (USA-73) on 28 November 1991; DMSP-5D2 F-12 (USA-106) on 29 August 1994; DMSP-5D2 F-13 (USA-109) on 24 March 1995; DMSP-5D2 F-14 (USA-131) on 4 April 1997; DMSP-5D3 F-15 (USA-147) on 12 December 1999; DMSP-5D3 F-16 (USA-172) on 18 October 2003; DMSP-5D3 F-17 (USA-191) on 4 November 2006; DMSP-5D3 F-18 (USA-210) on 18 October 2009. The DMSP series should contain two more satellites, F-19 (for 2014) and F-20 (for 2020). This should be followed by the first satellites of DWSS, viz., F-1 and F-2.

<sup>25</sup>Launch dates: Meteor-3-01 on 24 October 1985; Meteor-3-03 on 26 July 1988; Meteor-3-04 on 25 October 1989; Meteor-3-05 on 24 April 1991; Meteor-3-06 on 15 August 1991; Meteor-3-07 on 25 January 1994; Meteor-M-1 on 17 September 2009.

<sup>26</sup>Launch dates: FY-1A (DFH-24) on 6 September 1988; FY-1B (DFH-30) on 3 September 1990; FY-1C (DFH-46) on 10 May 1999; FY-1D (DFH-53) on 15 May 2002; FY-3A on 27 May 2008; FY-3B on 4 November 2010.

<sup>27</sup>Launch dates: MetOp-A on 19 October 2006; MetOp-B on 17 September 2012. MetOp-C is planned for 2017. After 2020, the following series is planned: EPS-SG (European Polar Satellite—Second Generation), with the satellites EPS-SG-A and -B.

<sup>28</sup>The Rocsat satellites (Republic of China Satellites) changed name in 2005 to become FormoSat, recalling the old name for the island of Taiwan, viz., Formosa or *Ilha Formosa* in Portugues.

flying at  $h = 800$  km with inclination  $i = 72^\circ$ , there being three planes containing two satellites each. Launched in 2006, the six satellites, from FormoSat-3A to FormoSat-3F, monitor the water vapour and other components of the atmosphere by radio-occultation of the GPS signal.

### *GEO Meteorological Satellites*

The geostationary programme has been very widely developed for the purposes of operational meteorology. In order to avoid large distortions due to the viewing angle, the various meteorological institutions have sought to distribute their satellites as harmoniously as possible around the geostationary orbit, under the coordination of the World Meteorological Organisation (WMO), see Fig. 9.14.

In the United States, these satellites are placed alternately on the longitudes of the east and west coasts. This approach was already in use for the SMS satellites (SMS-1 with  $\lambda_S = 75^\circ\text{W}$ ; SMS-2 with  $\lambda_S = 115^\circ\text{W}$ ) and was continued with the GOES series<sup>29</sup> (Geostationary Operational Environmental Satellite) and GOES-Next, the satellites begin designated GOES-East or GOES-West in the obvious way. The satellite GIFTS (Geosynchronous Imaging Fourier Transform Spectrometer, or EO-3 NMP, a joint project of NASA, the NOAA, and the US Navy) will be placed over the Indian ocean.

For Europe, the geostationary programme is run by EUMETSAT with the METEOSAT satellites. The various operational METEOSAT satellites<sup>30</sup> have all been placed at longitude  $\lambda_S = 0^\circ$ . Some of them can be reserved, or loaned (like METEOSAT-3 to replace GOES-E from February 1993 to May 1995), or sent on missions (like METEOSAT-5 for the INDOEX experiment, Example 7.6).

---

<sup>29</sup>Launch dates: SMS-1 on 17 May 1974; SMS-2 on 6 February 1975; GOES-1 (SMS-3) on 16 October 1975; GOES-2 on 16 June 1977; GOES-3 on 16 June 1978; GOES-4 on 9 September 1980; GOES-5 on 22 May 1981; GOES-6 on 28 April 1983; GOES-7 on 26 February 1987; GOES-8 on 13 April 1994; GOES-9 on 23 May 1995; GOES-10 on 25 April 1997; GOES-11 on 3 May 2000; GOES-12 on 23 July 2001; GOES-13 on 24 May 2006; GOES-14 on 27 June 2009; GOES-15 on 4 March 2010.

<sup>30</sup>Launch dates: METEOSAT-1 on 23 November 1977; METEOSAT-2 on 19 June 1981; METEOSAT-3 on 15 June 1988; METEOSAT-4 on 6 March 1989; METEOSAT-5 on 2 March 1991; METEOSAT-6 on 20 November 1993; METEOSAT-7 on 2 September 1997; METEOSAT-8 (MGS-1) on 28 August 2002; METEOSAT-9 (MGS-2) on 21 December 2005; METEOSAT-10 (MGS-3) on 5 July 2012. The MSG satellites (METEOSAT Second Generation) are renamed METEOSAT when they become operational. The satellite MSG-4 is planned for 2014. The new series known as MTG (METEOSAT Third Generation) is the third generation of the METEOSAT programme, planned to run for 20 years from 2018. It differs significantly from the first two generations, since the satellites will no longer spin permanently about their axis at 100 rev/min, but will have three-axis stabilisation. This allows the possibility of atmospheric sounding. The MTG programme comprises six satellites weighing 3 tonnes each: four MTG-I (imagers) and two MTG-S (sounders).

Although Russia generally prefers Molniya orbits to equatorial orbits, it nevertheless launched the GOMS programme (Geostationary Operational Meteorological Satellite) of geostationary satellites.<sup>31</sup>

For India, the INSAT series (Indian Satellite) contains satellites for the purposes of meteorology<sup>32</sup> and communications.

China has launched satellites<sup>33</sup> in the FY-*even* series (Feng Yun-2 and, from 2014, Feng Yun-4, not to be confused with the FY-*odd* series of LEO satellites already mentioned, viz., FY-1 and FY-3) since 1997.

Since 1977, Japan has been launching its geostationary GMS satellites<sup>34</sup> (Geostationary Meteorological Satellite), followed by MTSAT (Multi-functional Transport Satellite). This programme is also called Himawari (*himawari* means “sunflower”).

South Korea also takes part in the WMO programme with COMS-1 (Communication, Ocean, Meteorological Satellite).<sup>35</sup>

Figure 9.13 shows the (official) positions of the operational satellites as of 1 July 2013. In this distribution, one observes a large “hole” above the Pacific, and very closely spaced satellites at Asian longitudes. China and India prefer to control their own data.

#### *Satellites for Atmospheric Studies*

Satellites devoted to atmospheric research fly in low orbits,<sup>36</sup> like the two AEM satellites (Application Explorer Mission), HCMM (Heat Capacity Mapping Mission, or AEM-1) with  $h = 600$  km,  $i = i_{\text{HS}}$ , and SAGE (Stratospheric Aerosols and Gas Experiment, or AEM-2) with  $h = 600$  km,  $i = 55^\circ$ , or AIM (Aeronomy of Ice in the Mesosphere) with  $h = 580$  km,  $i = i_{\text{HS}} = 97.8^\circ$ , or

<sup>31</sup>Launch date: GOMS-1 on 31 October 1994. This series is also called Elektro and the satellite thus carries the names Elektro-1 or GOMS-Elektro-1 as well as GOMS-1.

<sup>32</sup>Launch dates: INSAT-1A on 10 April 1982; INSAT-1B on 30 August 1983 (launched by STS-8); INSAT-1C on 21 July 1988; INSAT-1D on 12 June 1990; INSAT-2A on 10 July 1992; INSAT-2B on 23 July 1993; INSAT-2E on 3 April 1999; METSAT-1 (Kalpana-1) on 12 September 2002; INSAT-3A on 9 April 2003; INSAT-3E on 27 September 2003. The METSAT satellites are called Kalpana in homage to Kalpana Chawla, the Indian astronaut lost in the explosion of Columbia, STS-107, on 1 February 2003. The word *kalpana* means “imagination” in Sanskrit and is a female first name.

<sup>33</sup>Launch dates: FY-2A (DFH-45) on 10 June 1997; FY-2B (DFH-49) on 25 June 2000; FY-2C on 19 October 2004; FY-2D on 8 December 2006; FY-2E on 23 December 2008.

<sup>34</sup>Launch dates: GMS-1 on 14 July 1977; GMS-2 on 10 August 1981; GMS-3 on 2 August 1984; GMS-4 on 5 September 1989; GMS-5 on 18 March 1995; MTSAT-1R (Himawari-6) on 26 February 2005 (to replace MTSAT-1, destroyed at launch on 15 November 1999); MTSAT-2 (Himawari-7) on 18 February 2006.

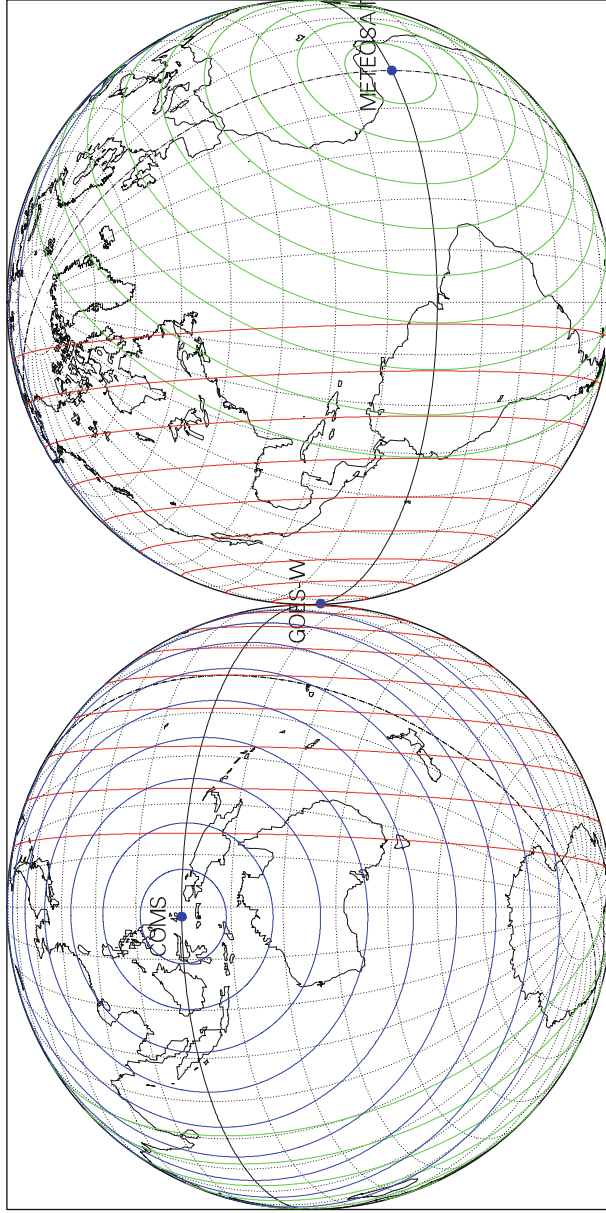
<sup>35</sup>Launch date: COMS-1 on 27 June 2010. COMS-1 is also called Chollian (from the Korean *Chun-Li-An*), which means “seen from a thousand *li*”, where the *li* is the Chinese and Korean unit of distance.

<sup>36</sup>Launch dates: HCMM (AEM-1, Explorer-58) on 26 April 1978; TOMS-EP on 2 July 1996; Odin on 20 February 2001; QuikTOMS on 21 September 2001, failed; SAGE (AEM-2, Explorer-60) on 18 February 1979; SciSat-1 on 13 August 2003; AIM (SMEX-9, Explorer-90) on 25 April 2007.

**Three Geostationary Satellites**

Altitude = 35787.6 km      a<sub>GS</sub> = 42165.785 km  
 Inclination = 0.00 °      Park. = 123°E, 135°W, 0°  
 Period = 1435.91 min      \* rev/day = 1.00  
 Equat. orbital shift = 40072.1 km

COMS, GOES-W, METEOSAT  
 [GEO Meteorological Satellites]



Projection: Orthographic      Pr. centre (r.): 25.0 ° N; 50.0 ° W      Iξωων  
 Property: none      Aspect: Oblique      MC ★ LMD  
 ⊕ T.:Azimuthal - Graticule: 10°      [-90.0/+140.0] [-]      EGM2008      ΑΤΛαα

FIG. 9.14 : Coverage of the Earth by three geostationary satellites.

the Swedish atmospheric and astrophysics satellite Odin with  $h = 622$  km,  $i = i_{\text{HS}}$ , and the Canadian satellite SciSat-1 with  $h = 650$  km,  $i = 73.9^\circ$ .

Satellites for ozone studies are Sun-synchronous: TOMS-EP (Total Ozone Mapping Spectrometer and Earth Probe),  $h = 750$  km, was Sun-synchronous and its successor<sup>37</sup> QuikTOMS should have been. Satellites studying the composition of the atmosphere, like ACE-A and ACE-B (Aerosol–Cloud–Ecosystem) and GACM (Global Atmospheric Composition Mission) will also be Sun-synchronous.

### Satellites for Climate and Climate-Change Studies

Climate change is very difficult to assess from in situ measurements, which are necessarily incomplete and sometimes inaccurate or biased. Only numerical models can teach us about the evolution of the climate over periods in excess of 10 years.

In order to run general circulation models for the atmosphere and ocean which simulate the climate, a whole range of climate parameters must be ascertained as accurately as possible. Among these, one could mention the type of cloud and the amount of water or ice it contains, the distribution of aerosols (dust and fine particles suspended in the air), the energy budget (incident radiation reflected and emitted, from the ultraviolet to the far infrared), wind speed and ocean currents, the roughness of the ground and development of vegetation, the thickness of the ice sheets, amounts of greenhouse gases, and the temperature of the ground and the sea surface. Only satellites<sup>38</sup> can determine such parameters, which can then be integrated into computer programs to “constrain” the model. These “space sentinels” thus play a fundamental and determining role in the business of climate study. Here we review the various aspects that come under investigation.

At the very beginning of the space age, several satellites were equipped with instruments for studying the Earth’s radiation budget. However, the first satellite dedicated entirely to this mission was ERBS (Earth Radiation Budget Satellite), launched by the Space Shuttle, with  $h = 600$  km,  $i = 57^\circ$ . In this field, important progress should be made with the ESA-JAXA mission known as EarthCARE (Earth Clouds, Aerosols and Radiation Explorer), with a low Sun-synchronous orbit,  $h = 394$  km,  $i = i_{\text{HS}} = 97.0^\circ$ .

Likewise, regarding rain measurements, several dedicated instruments have flown aboard various satellites, such as the DMSPP, but the first mission entirely devoted to this issue was the US–Japanese satellite TRMM (Tropical Rainfall Measurement Mission). Its low altitude,  $h = 350$  km, is essential since it carries a radar designed to detect water droplets. Its inclination of  $i = 35^\circ$  means that it obtains effective coverage of tropical regions (and Japan) (see Fig. 9.15 lower). Figure 9.19 shows a TRMM image of Hurricane Katrina.

<sup>37</sup>Depending how fast one writes it! The NASA satellites QuikTOMS and QuikScat are spelt like this, whereas those of DigitalGlobe are written QuickBird.

<sup>38</sup>Launch dates: ERBS on 5 October 1984 by STS-13 (STS-41-G); TRMM on 28 November 1997, see Example 7.2; SMOS on 2 November 2009; GOSat (Ibuki) on 23 January 2009; Megha-Tropiques on 12 October 2011.

**Terra**

**Orbit - Ground track**

Recurrence = [15; -7; 16] 233

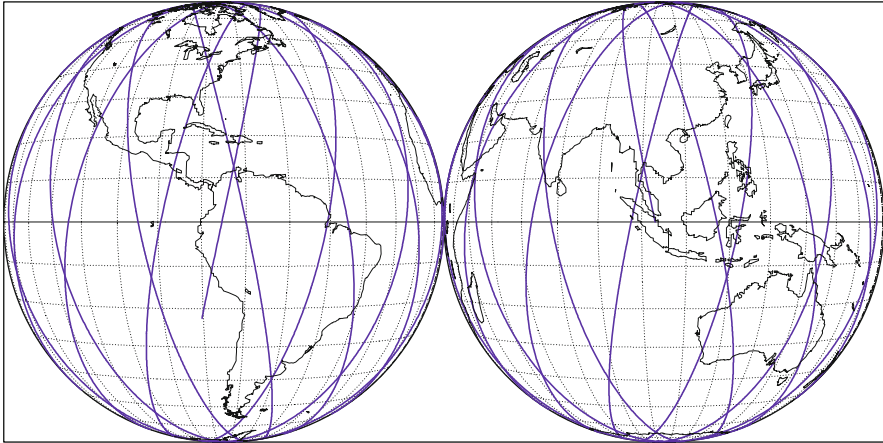
>>>> Time span shown: 1440.0 min = 1.00 day

Altitude = 699.6 km      a = 7077.736 km

Inclin./SUN-SYNCHRON.= 98.21 °

Period = 98.88 min \* rev/day=14.56

Equat. orbital shift = 2751.9 km ( 24.7 °)



Proj.: Perspect.V. h=5.61 R

Property: none

⊕ T.:Azimuthal - Graticule: 10°

Pr. centre (r.): 0.0 ° ; 105.0 °E

Aspect: Equatorial

⊘ 4.2 [-90.0/ +90.0/ -15.0] [-] EGM96

Asc. Node: 103.02 ° [22:30 LMT]

Ιξίωv  
MC \* LMD  
Ατλας

**TRMM [1] < 降雨 >**

**Orbit - Ground track**

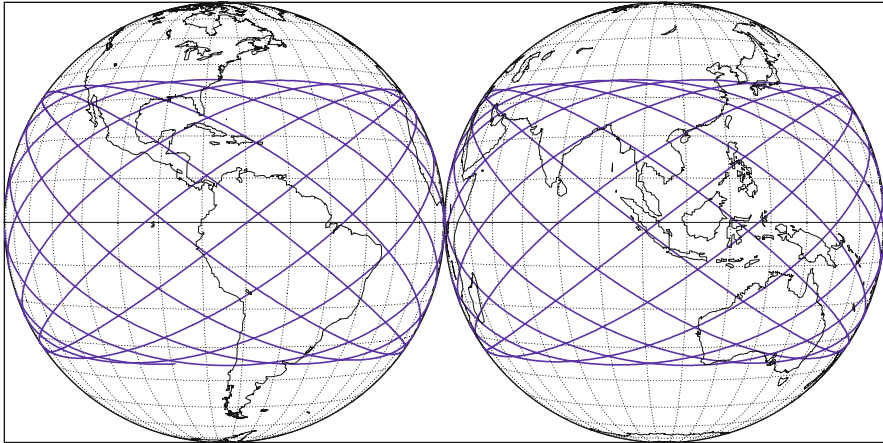
>>>> Time span shown: 1440.0 min = 1.00 day

Altitude = 350.1 km      a = 6728.216 km

Inclination = 34.99 °

Period = 91.31 min \* rev/day=15.77

Equat. orbital shift = 2596.2 km ( 23.3 °)



Proj.: Perspect.V. h=5.61 R

Property: none

⊕ T.:Azimuthal - Graticule: 10°

Pr. centre (r.): 0.0 ° ; 105.0 °E

Aspect: Equatorial

⊘ 4.2 [-90.0/ +90.0/ -15.0] [-] EGM96

Asc. Node: 0.00 °

Ιξίωv  
MC \* LMD  
Ατλας

FIG. 9.15 : Orbital ground tracks of Terra and TRMM over 1 day. Blue: View from a geostationary satellite with parking longitude 75° W (left) and 105° E (right).



**Syncom-2**

Orbit - Ground track

Recurrence = [ 1; +0; 1] 1

>>>> Time span shown: 1440.0 min = 1.00 day

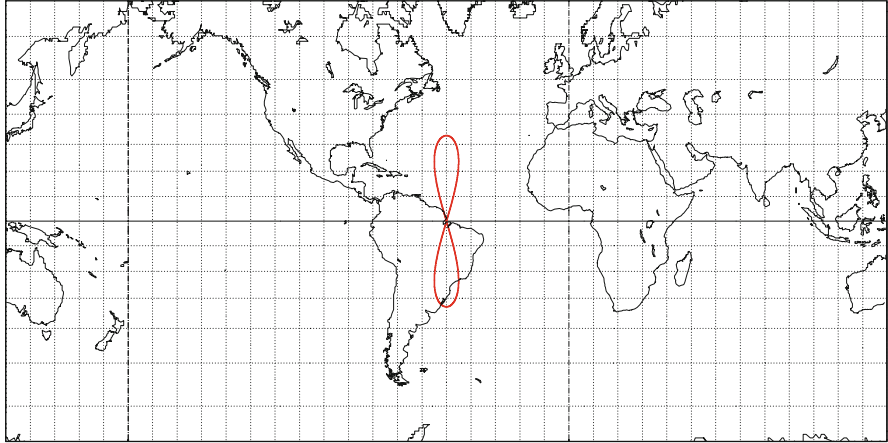
Altitude = 35787.6 km

a = 42165.785 km

Inclination = 32.80 °

Period = 1436.05 min \* rev/day = 1.00

Equat. orbital shift = 40075.8 km



Projection: Mercator

Project. centre: 0.0 ° ; 50.0 ° W

Asc. Node: -50.00 ° [00:00 LMT]

Property: Conformal

Aspect: Direct

App. inclin. = 106.40 °

⊕ T.:Cylindrical - Graticule: 10°

⌘.2⌘ [+90.0/ +0.0/ -40.0] [-] EGM2008

Ιξίων  
MC \* LMD  
Ατλας

**GTO / Ariane**

Elliptical orbit - Gr. track

>>>> Time span shown: 1250.0 min = 0.87 day

Equiv. altit. = 17993.5 km

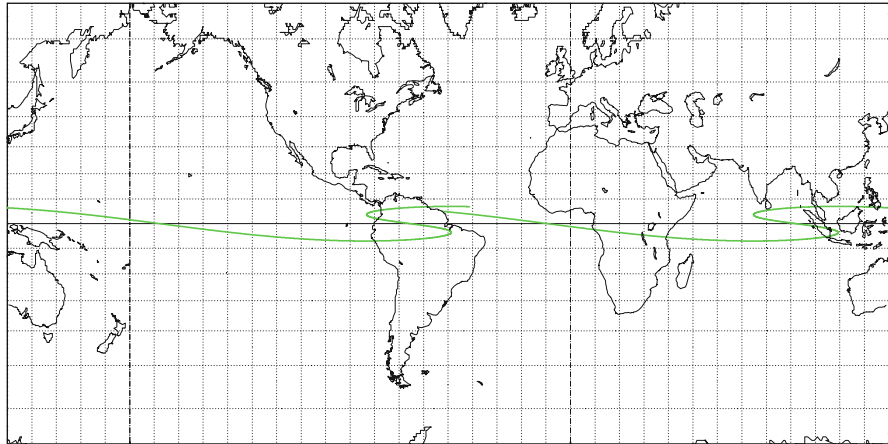
a = 24371.637 km

Inclination = 7.00 °

e = 0.730700

Period = 630.23 min \* rev/day = 2.28

h\_a = 35802 km; h\_p = 185 km; arg. perigee: +180.00 °



Projection: Mercator

Project. centre: 0.0 ° ; 50.0 ° W

Longitude / Initialisation:

Property: Conformal

Aspect: Direct

Asc. Node: -110.00 °

⊕ T.:Cylindrical - Graticule: 10°

⌘.2⌘ [+90.0/ +0.0/ -40.0] [-] GRIM5-C1

Apogee : 70.00 °

Ιξίων  
MC \* LMD  
Ατλας

FIG. 9.16 : Orbital ground tracks. Upper: The geosynchronous satellite Syncom-2. Lower: Transfer orbit with the Ariane launch vehicle launched from Kourou.

**Ofeq-5**

**Orbit - Ground track**

Recurrence - [16;-58;125]1942

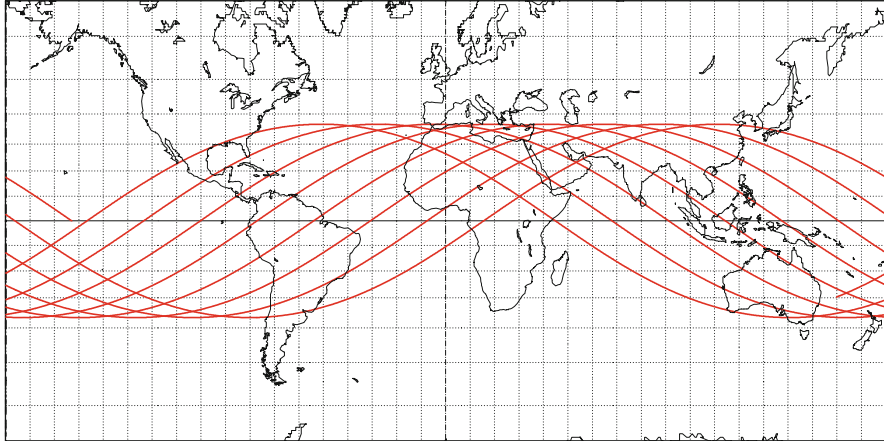
2005 11 27 21:37:55 UTC >>> 720.0 min = 0.50 day

Equiv. altit. = 482.9 km a = 6861.084 km

Inclination = 143.45 ° e = 0.000788

Period = 94.06 min \* rev/day=15.31

h\_a = 494 km; h\_p = 483 km; arg. perigee: +58.01 °



Projection: Mercator

Project. centre: 0.0 ° ; 0.0 °

Asc. Node: -152.90 ° [11:26 LMT]

Property: Conformal

Aspect: Direct

[NORAD] Revolution: 19574

Ιξίων  
MC ★ LMD

⊕ T.:Cylindrical - Graticule: 10°

{4.2}[ +0.0/ +0.0/ +0.0] [-] EGM2008

[NORAD] 2005 11 27 21:37:55 UTC

Ατλας

**Ofeq-7**

**Orbit - Ground track**

Recurrence = [15; +7; 16] 247

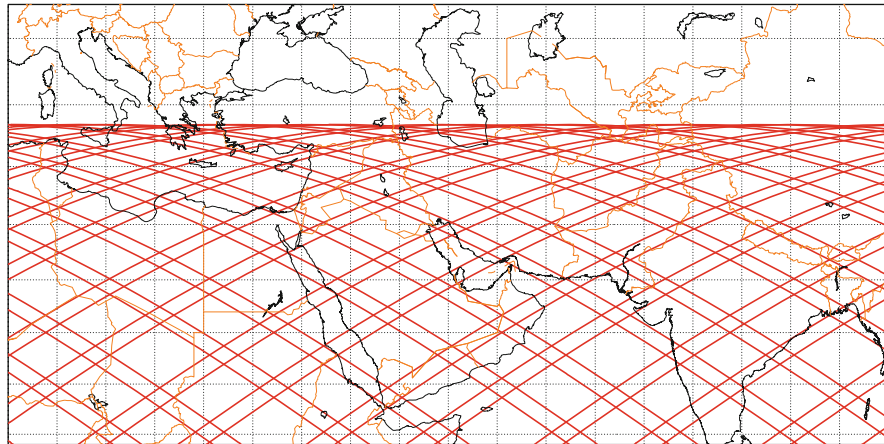
2009 12 11 01:53:27 UTC >>> 5760.0 min = 4.00 days

Equiv. altit. = 508.4 km a = 6886.555 km

Inclination = 141.75 ° e = 0.006889

Period = 94.60 min \* rev/day=15.22

h\_a = 560 km; h\_p = 465 km; arg. perigee: +135.66 °



Projection: Mercator

PC: 0.0 ° ; 0.0 ° /ZC: 30.0 ° N; 50.0 ° E

Asc. Node: -25.80 ° [00:10 LMT]

Property: Conformal

Aspect: Direct > zoom : 4.00

[NORAD] Revolution: 13934

Ιξίων  
MC ★ LMD

⊕ T.:Cylindrical - Graticule: 5°

{5.3}[ +90.0/ +0.0/ -90.0] [-] EGM2008

[NORAD] 2009 12 11 01:53:27 UTC

Ατλας

FIG. 9.17: Orbital ground tracks of Ofeq satellites, with retrograde orbits. Upper: Ofeq-5 over half a day. Lower: Ofeq-7 over 4 days, with zoom of the Middle East.





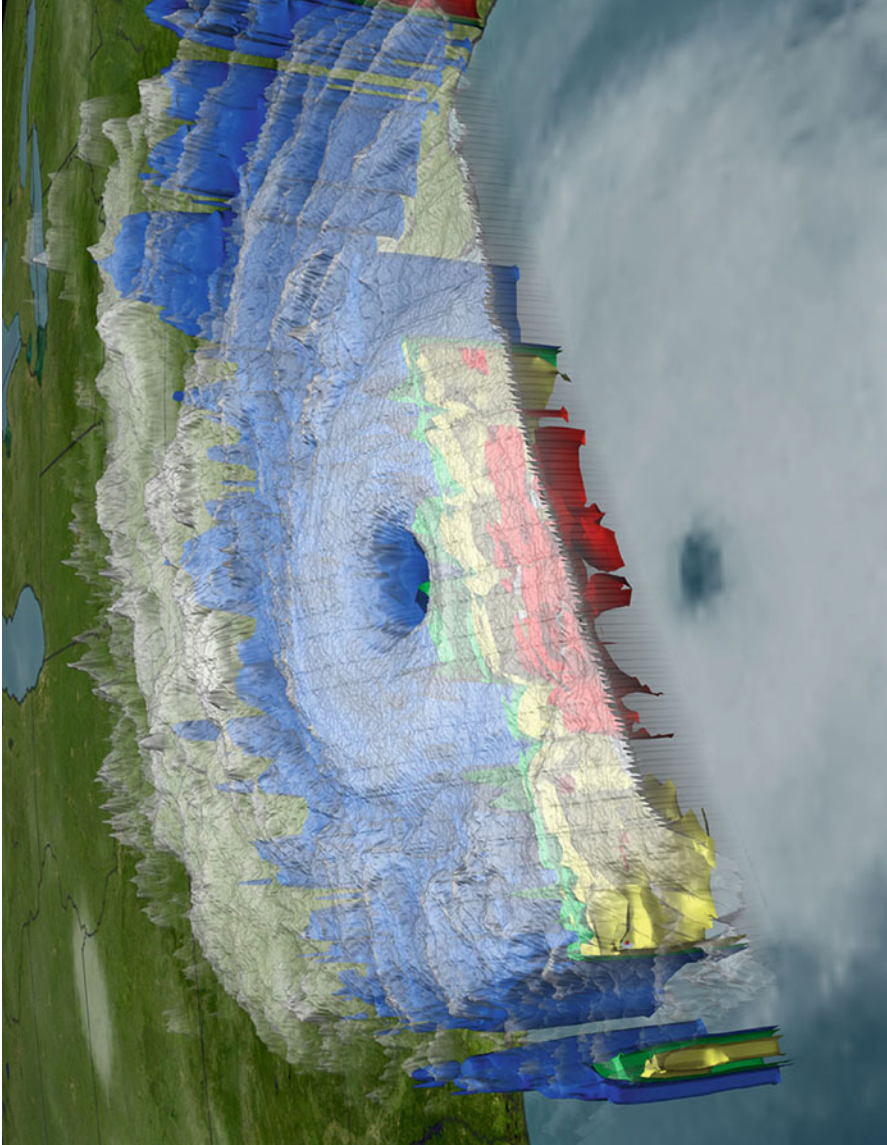


FIG. 9.19: Image of Hurricane Katrina on 28 August 2005 at 5:33 PM EDT (21:33 UTC) as seen by the TRMM satellite's PR (Precipitation Radar), VIRS (Visible Infrared Scanner), TMI (Tropical Microwave Imager), and the GOES-12 spacecraft. TRMM looks beneath the storm clouds to reveal the underlying rain structure.  $h$  is the precipitation per hour. Blue represents areas with  $h < 6$  mm, green areas with  $h < 12$  mm, yellow areas with  $h < 25$  mm, and red areas with  $h < 50$  mm. Credit: NASA/JAXA.

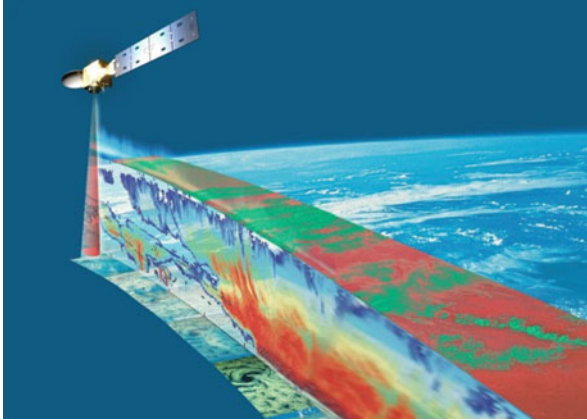


FIG. 9.20 : *EarthCARE (Earth Clouds, Aerosols and Radiation Explorer) is being implemented in cooperation with the Japanese Aerospace Exploration Agency (JAXA). The mission addresses the need for a better understanding of the interactions between cloud and radiative and aerosol processes that play a role in climate regulation. Credit: ESA–AOES Medialab.*



FIG. 9.21 : *SMOS satellite. This satellite comprises three arms which were deployed in space. They are inscribed in a circle of diameter 8 m. Artist's view. Credit: CNES.*

To study the water cycle in tropical regions, the French–Indian satellite Megha-Tropiques has gone into a slightly inclined orbit over the equator, with  $h = 866$  km and  $i = 20^\circ$  (see Fig. 9.18).

The joint project GPM (Global Precipitation Measurement) between the USA, Japan, and Europe continues and extends these rainfall missions. It comprises one primary satellite known as GPM-core, with  $h = 407$  km,  $i = 65^\circ$ , a satellite with lower inclination known as GPM-LIO (GPM Low Inclination Orbit), with  $h = 637$  km,  $i = 40^\circ$ , and a constellation of 6 to 8 Sun-synchronous satellites.

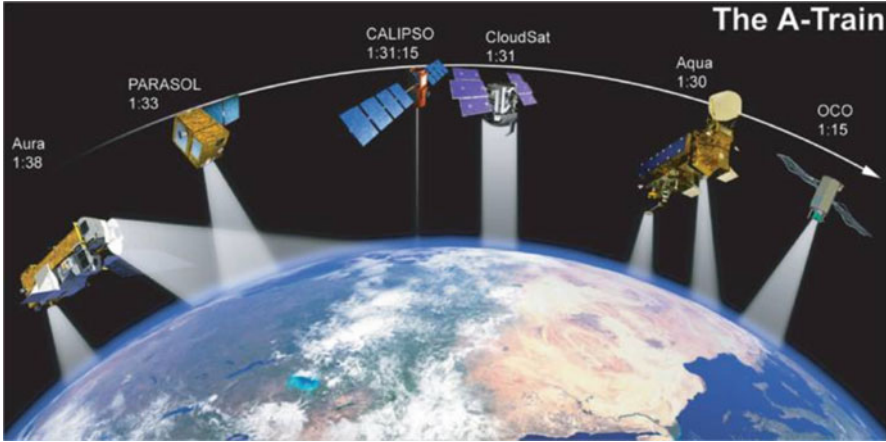


FIG. 9.22 : *A-Train*: a group of satellites following the same orbit. The crossing time at the equator is noted for each satellite (see Chap. 10). The launch of OCO failed. Credit: NASA.

The European satellite SMOS (Soil Moisture and Ocean Salinity) is mapping ocean salinity and ground humidity over the whole planet from its Sun-synchronous orbit with  $h = 757$  km,  $i = i_{\text{HS}} = 98.4^\circ$ . This multi-instrument satellite has three arms carrying a total of 69 small antennas. Using interferometry technology, the instrument picks up the very weak microwave signal emitted by the surface. This method of observation was developed for radioastronomy and it imposes the unusual configuration of the satellite (see Fig. 9.21), with three arms inscribed in a circle of diameter 8 m. The US–Argentinian satellite Aquarius/SAC-D (ESSP-6), with  $h = 651$  km and  $i = i_{\text{HS}}$ , is also measuring the salinity of the oceans.

Several of the satellites in the so-called A-Train (discussed further below) study aerosols and clouds (Parasol, Calispo, CloudSat), the chemistry of the atmosphere (Aura), and so on (see Fig. 9.22).

The Japanese satellite GOSat (Greenhouse Gases Observing Satellite, renamed Ibuki, which means “breath” in Japanese), with  $h = 666$  km,  $i = i_{\text{HS}}$ , is the first to detect the concentration of  $\text{CO}_2$  (carbon dioxide) in the atmosphere. The US satellite OCO-2 (Orbiting Carbon Observatory) will pursue a similar mission in the A-Train. The French–German project MERLIN (Methane Remote Sensing Lidar Mission), on a lower orbit, with  $h = 506$  km,  $i = i_{\text{HS}}$ , should measure the amount of methane present in the atmosphere (since methane is a major contributor to the greenhouse effect).

### Earth Resources, Remote-Sensing, and Environment

This category contains satellites carrying instruments whose resolution at ground level is between 50 and 5 m. These satellites are all LEO and, apart from those in the Resurs-F series and a few special cases, they are all Sun-synchronous. Recurrent and frozen orbits are required for these satellites.



The first programme, Landsat, dates from 1972, and its first three satellites had the same orbit characteristics, namely,  $h = 910$  km and  $i = i_{\text{HS}} = 99.1^\circ$ . From Landsat-4, the altitude was reduced to  $h = 700$  km,  $i = i_{\text{HS}} = 98.2^\circ$ , and this orbit has since been used, not only for all the Landsat satellites,<sup>39</sup> but also by other NASA satellites, such as EO-1 (Earth Observing) and the satellites of the EOS programme (Earth Observation Satellite).

These satellites are divided into EOS Morning (EOS-AM, where AM stands for *ante meridiem*) and EOS Afternoon (EOS-PM, where PM stands for *post meridiem*), named according to their crossing time at the equator. In the first group is the satellite Terra (EOS-AM-1) [see Fig. 9.15 (upper) for the ground track of the orbit and Figs. 9.24, 9.25, and 9.26 for images taken by its onboard instruments MODIS and MISR], and in the second are all the satellites of the A-Train (or Afternoon Train, see Fig. 9.22). This train of satellites provides a novel synergy for atmospheric studies, since the same scene can be observed simultaneously at a few minutes' interval by very different instruments, e.g., spectrometer, radar, or lidar. Although launched at widely spaced dates, up to five satellites have flown in formation on this same orbit: Aqua (EOS-PM-1), CloudSat and Calipso,<sup>40</sup> Parosol<sup>41</sup> and Aura (EOS-Chem-1). The satellite OCO (Orbiting Carbon Observatory, ESSP-5) failed to reach its orbit, as did Glory, which was supposed to take its place between Parosol and Aura, 2 years later. The time intervals are indicated in Fig. 9.22.

The satellite EO-1 (see Fig. 9.27) follows Landsat-7 at an interval of just 1 min (of time). In the following, we shall call this orbit, first used by Landsat-4, the Terra orbit. It can be defined to great accuracy by its recurrence (see Fig. 9.15 upper).

The satellite MTI (Multispectral Thermal Imager, or P97-3) is on a lower Sun-synchronous orbit, at  $h = 585$  km, for day and night observation, like

---

<sup>39</sup>Launch dates: ERTS-1 (Earth Resources Technology Satellite) on 23 July 1972, renamed Landsat-1 on 13 January 1975; Landsat-2 on 22 January 1975; Landsat-3 on 5 March 1978; Landsat-4 on 16 July 1982; Landsat-5 on 1 March 1985; Landsat-6 on 5 October 1993, launch failed; Landsat-7 on 15 April 1999; Terra (EOS-AM-1) on 18 December 1999; MTI on 12 March 2000; EO-1 and SAC-C on 21 November 2000; Aqua (EOS-PM-1) on 4 May 2002; CloudSat and Calipso on 28 April 2006; OCO on 24 February 2009, launch failed; Glory on 4 February 2011, launch failed; Landsat-8 on 11 February 2013.

<sup>40</sup>These two satellites, also called ESSP-4 and ESSP-3, respectively, are part of NASA's ESSP programme (Earth System Science Pathfinder), which also includes the two satellites, -A and -B, of the GRACE mission (ESSP-2), for geodesy, and VCL (Vegetation Canopy Lidar, ESSP-1, replaced by Glory), for environmental study. The satellites ESSP-5, -6, and -7 are also mentioned in this chapter. The US satellite ESSP-3 with French collaboration was originally called Picasso-Cena (Pathfinder Instruments for Cloud and Aerosol Spaceborne Observations—*Climatologie étendue des nuages et des aérosols*). However, the artist's family refused to allow free use of the name and it was renamed Calipso (Cloud Aerosol Lidar Infrared Pathfinder Satellite Observation), and not Calypso, doubtless to avoid legal proceedings with Homer's descendants.

<sup>41</sup>The French microsatellite Parosol (Polarization and Anisotropy of Reflectances for Atmospheric Science coupled with Observations from a Lidar) was launched as a passenger of Hélios-2A on 18 December 2004.



FIG. 9.23 : The German Aerospace Center (Deutsches Zentrum für Luft- und Raumfahrt DLR) and the space company Astrium have recently taken an important step forward in their mission to create a three-dimensional map of the world. On 14 October 2010, the radar satellite TanDEM-X transitioned to close formation flight with its “twin” TerraSAR-X. The two satellites are now flying together side-by-side, 350 m apart. Credit: DLR.

the two satellites planned for the NEMO project (Navy Earth Map Observation) at  $h = 606$  km, which will observe in hyperspectral mode, and SMAP (Soil Moisture Active Passive) at  $h = 670$  km, which will take the place of HYDROS (Hydrosphere State Mission, ESSP-7). The next 10 years should see many US environmental missions come into being on Sun-synchronous orbits, such as HypsIRI (Hyperspectral InfraRed Imager) at  $h = 624$  km, monitoring vegetation, ASCENDS (Active Sensing of CO<sub>2</sub> Emissions Over Nights, Days and Seasons) at  $h = 450$  km, observing carbon dioxide levels, and 3D-Winds (Three-Dimensional Tropospheric Winds) observing wind patterns using Doppler lidar and flying at  $h = 400$  km. The three CLARREO satellites (Climate Absolute Radiance and Refractivity Observatory) will be in a strictly polar orbit, i.e., with  $i = 90.0^\circ$ , at  $h = 750$  km, unless the project falls foul to budgetary restrictions.

The French programme of commercial remote-sensing has been carried out by the SPOT family of satellites<sup>42</sup> (*Satellites Pour l’Observation de la*

<sup>42</sup>Launch dates: SPOT-1 on 22 February 1986; SPOT-2 on 11 January 1990; SPOT-3 on 26 September 1993; SPOT-4 on 24 March 1998; SPOT-5 on 4 May 2002. These satellites, designed for 3 years’ operation, actually did much better than that. For instance, SPOT-2 was still working when taken out of orbit after more than 19 years of service. SPOT-6 was launched on 9 September 2012; Pléiades-1A on 17 December 2011; Pléiades-1B on 2 December 2012.

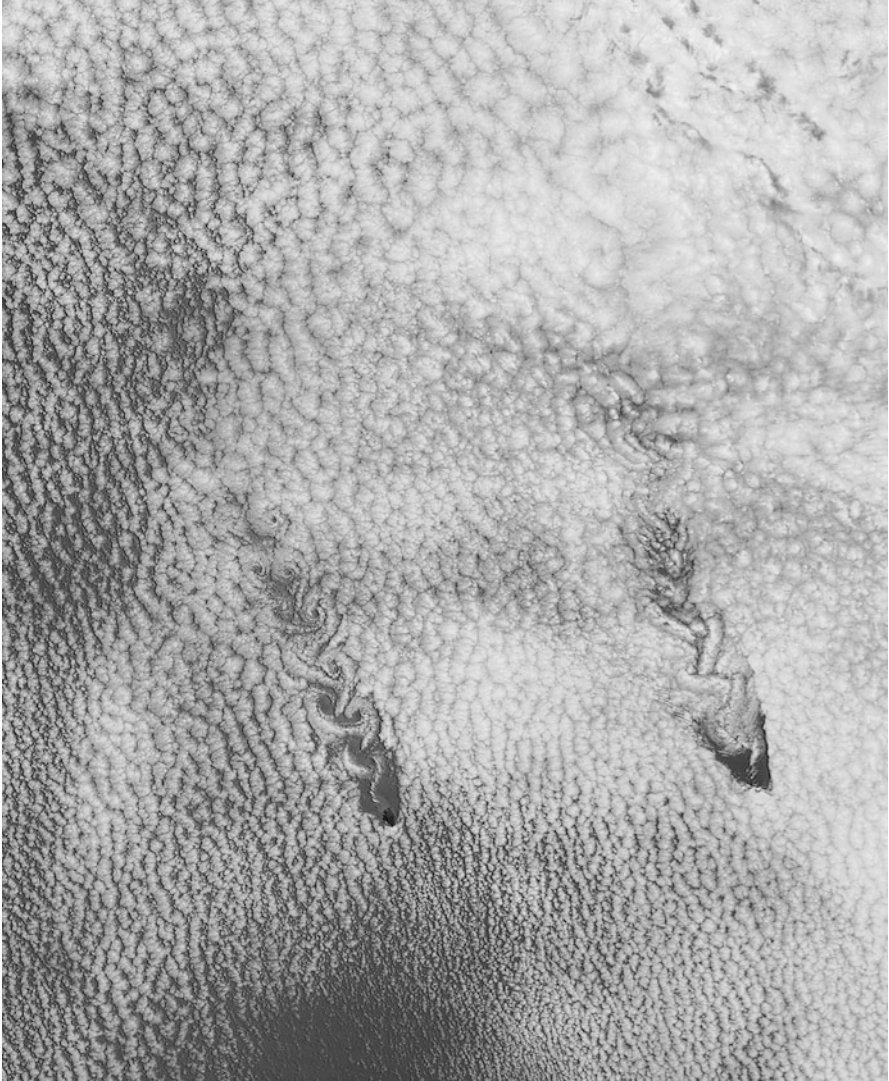


FIG. 9.24 : Image of vortices obtained by MODIS (Moderate Resolution Imaging Spectroradiometer) aboard the satellite Terra, in January 2013. These vortices (turbulence wake) form when clouds over the ocean are perturbed by a low altitude wind passing over an obstacle. The Juan Fernandez Islands are located roughly 800 km off the Chilean coast: Isla Alejandro Selkirk (left) and Isla Robinson Crusoe are volcanic islands situated along an east–west-trending submarine ridge. Each island boasts a tall summit: Isla Alejandro Selkirk reaches an altitude of 1,650 m above sea level, while Isla Robinson Crusoe reaches an altitude of 922 m. Credit (image and caption): NASA, Jeff Schmaltz, LANCE MODIS Rapid Response.



FIG. 9.25 : Brittany, Cornwall, the English Channel, and the Iroise sea. Image taken by the MISR instrument (Multi-angle Imaging SpectroRadiometer) aboard Terra. Revolution 7,778, 4 June 2001. The turquoise areas off the coast of Brittany reveal the intense efflorescence of phytoplankton (coccolithophores), whose shields made of tiny platelets (of the order of  $\mu\text{m}$ ) scatter solar light. At the top of the picture, the band of cirrus clouds is striped with aircraft trails. Credit (image and caption): NASA, GSFC, LaRC, JPL, MISR Team.

Terre), all precisely on the same orbit at  $h = 822\text{ km}$ , from SPOT-1 to -5. One can therefore speak of the SPOT orbit. The military also use images obtained by these satellites.<sup>43</sup> Indeed, the French army have their own SPOT-type satellites going under the name Hélios. The spatial resolution of SPOT satellites (5 m for SPOT-4, 2.5 m for SPOT-5) has been further improved

<sup>43</sup>In 1991, during the Gulf War (the operation known as Desert Storm), the US army used SPOT images, which were more practical with their 5 m resolution and 60 km panoramas than the much more detailed images procured by US intelligence satellites.



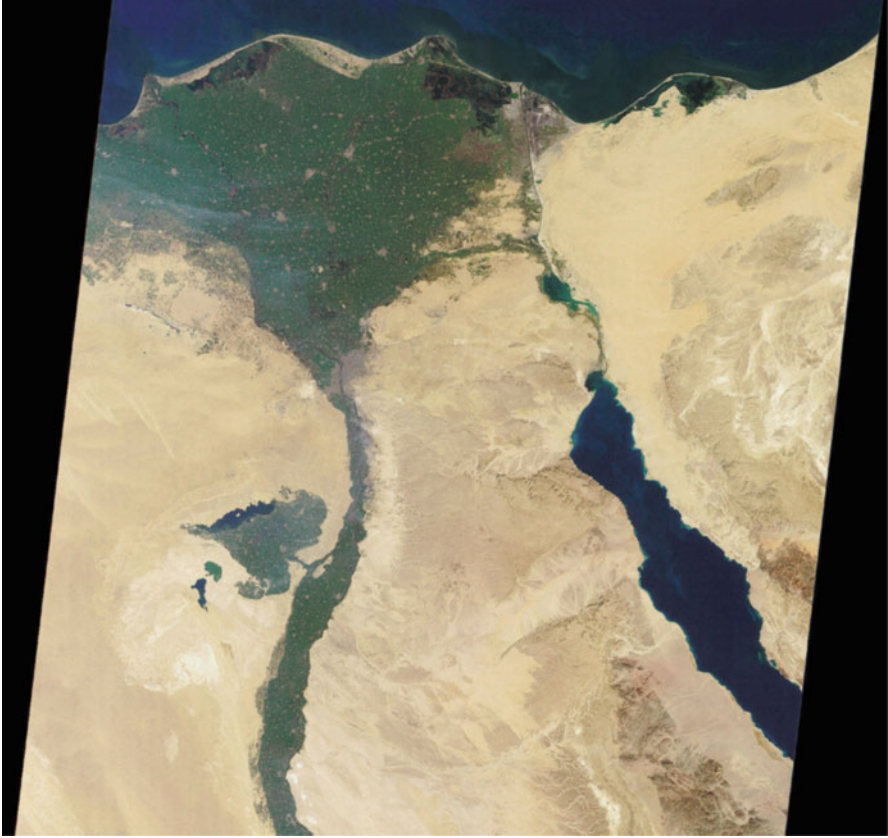


FIG. 9.26 : Nile valley, Egypt. Image taken by the MISR instrument aboard Terra. Revolution 5,956, 30 January 2001. The Nile crosses the Egyptian desert, accompanied by its strip of cultivated land. In the middle of the image, on the left bank, one can make out the Faiyum oasis. To the north beyond Cairo begins the delta. Between the Mediterranean and the Red Sea the Suez canal is visible, and on the other side of the Red Sea, the Sinai desert. Credit (image and caption): NASA, GSFC, LaRC, JPL, MISR Team.

(1 m) in the next generation of Pléiades-HR (Pléiades-1A and 1B), at a lower altitude, viz.,  $h = 695$  km, an orbit that is also used by SPOT-6.

In relation with Pléiades-HR, Italy is running the COSMO-SkyMed project (Constellation of Small Satellites for Mediterranean Basin Observation), a constellation<sup>44</sup> of four satellites equipped with radars and flying at  $h = 620$  km. The same orbit is planned for HypSEO (HyperSpectral Earth Observer). For extremely accurate and continually updated coverage of the Earth,

<sup>44</sup>Launch dates: COSMO-SkyMed-1 on 8 June 2007; COSMO-SkyMed-2 on 9 December 2007; COSMO-SkyMed-3 on 25 October 2008; COSMO-SkyMed-4 on 5 November 2010.

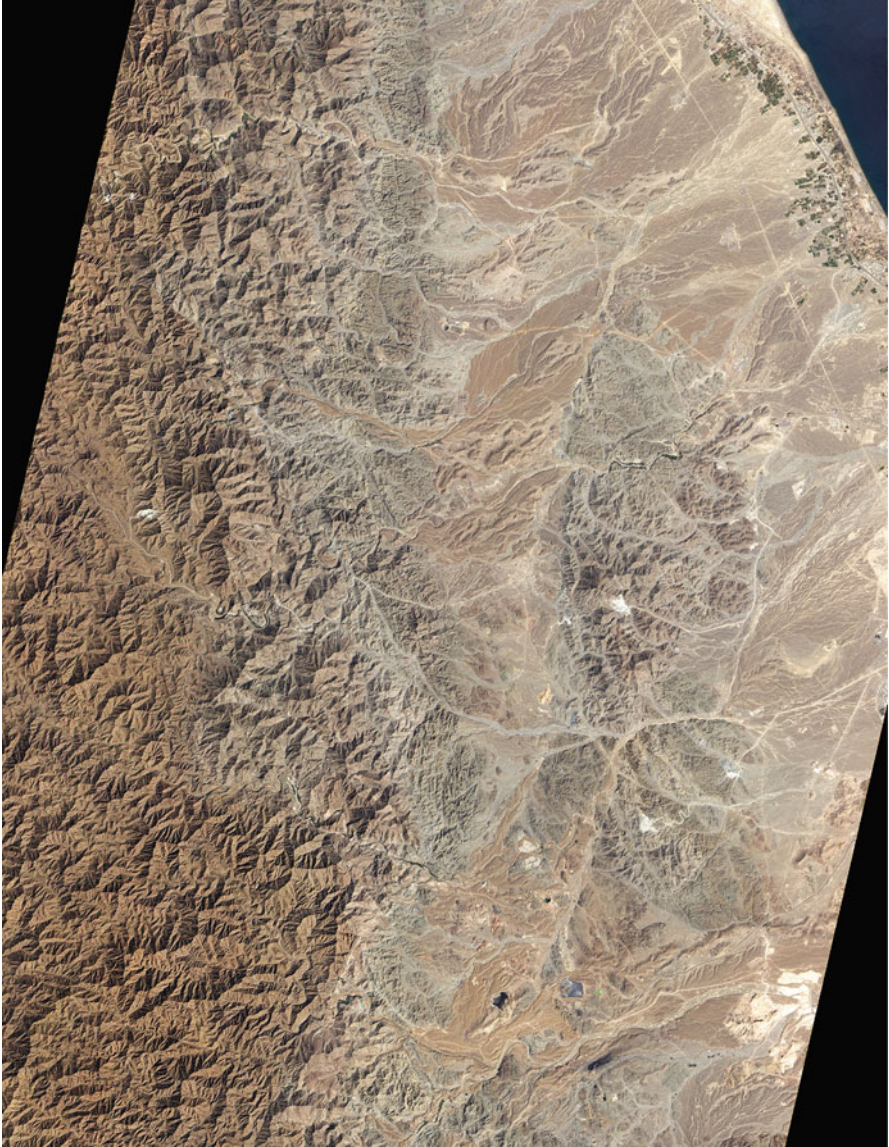


FIG. 9.27 : Oman, Arabic Peninsula. The mountains of north-eastern Oman are rugged, dry, and as much as 2,500 m above sea level. Yet millions of years ago, parts of these mountains were at the bottom of the sea. The Advanced Land Imager (ALI) on NASA's Earth Observing-1 (EO-1) satellite captured this natural-colour image of a portion of the Semail ophiolite on 6 March 2012. The image centers on Wadi Fizz, the site of some chromite deposits of interest to miners and manufacturers. Credit (image and caption): NASA, EO-1 team.

consideration is now being given to a constellation containing a very large number of satellites, like the e-Corce project (*e-Constellation d'observation récurrente cellulaire*).

The planned French–Israeli satellite VEN $\mu$ S (Vegetation and Environment monitoring a New Micro-Satellite) will be Sun-synchronous, at altitude  $h = 720$  km.

The German programme RapidEye<sup>45</sup> comprises a constellation of five satellites, RapidEye-1 to -5, with  $h = 600$  km,  $i = i_{HS}$ , and a resolution of 6.5 m. The ESA–German TerraSAR mission<sup>46</sup> comprises two satellites equipped with synthetic aperture radar (SAR). These are TerraSAR-X (in the X band),  $h = 505$  km, and Terra-SAR-L (in the L band),  $h = 620$  km. The satellite TanDEM-X (TerraSAR-X add-on for Digital Elevation Measurement) is on the same orbit as TerraSAR-X (see Fig. 9.23), in order to take images of the Earth in tandem.

Argentina is developing its SAOCOM programme (*Satélite Argentino de Observación con Microondas*), with the satellites SAOCOM-1A and -1B, rather similar to COSMO-SkyMed.

The Soviet then Russian programme began in 1979 with the series Resurs-F1 then -F2, using 6 tonne satellites in very low near-polar orbits, which operated for 14 days, then 30 days for the later version. Literally dozens were launched<sup>47</sup> in near-polar orbit,  $i = 82.3^\circ$ , with altitude  $h = 275$  km for Resurs-F1 and  $h = 240$  km for Resurs-F2. The satellites in the Resurs-O series<sup>48</sup> (*resurs* means “resource” in Russian) look more like other remote-sensing satellites: they are in Sun-synchronous orbit with  $h = 600$  km and  $i = 97.9^\circ$  for Resurs-O1-1 to -O1-3, and  $h = 820$  km and  $i = 98.8^\circ$  for Resurs-O1-4. The Resurs programme follows on from the Meteor-Priroda programme. The

<sup>45</sup>Joint launch of RapidEye-1, -2, -3, -4, and -5 on 29 August 2008. The satellites RapidEye-1 to -5 were subsequently attributed the Greek names Tachys (fast), Mati (eye), Choma (soil, terracing), Choros (space), and Trochia (orbit), respectively. Apart from *mati*, which is only a modern Greek word, the other names are both ancient and modern. For the evolving meaning of *trochia*, from “wheel rut” to “orbit”, see the earlier note on the word *orbita*.

<sup>46</sup>Launch dates: TerraSAR-X on 15 June 2007; TanDEM-X on 21 June 2010. The frequency bands for radar emission are traditionally denoted by letters: L (1–2 GHz), S (2–4 GHz), C (4–8 GHz), X (8–12 GHz), Ku (12–18 GHz), K (18–26.6 GHz), Ka (26.5–40 GHz). The wavelengths  $\lambda = c/\nu$  ( $\nu$  = frequency) corresponding to the centers of these bands are  $\lambda = 20$  cm for band L and  $\lambda = 3$  cm for band X. The choice of band depends on the phenomenon to be observed, and in particular the effect of the atmosphere on the emitted wave.

<sup>47</sup>The first 39 are recorded as Kosmos, from Kosmos-1127 in 1979 to Kosmos-1990 in 1989. There were 20 more under the name of Resurs-F, from Resurs-F-1 (type F1) in 1989 to Resurs-F-20 (type F2) in 1995, followed by the modified version, Resurs-F1M-1 in 1997 and Resurs-F1M-2 in 1999 (type F1M).

<sup>48</sup>Launch dates: Resurs-O1-1 (Kosmos-1689) on 3 October 1985; Resurs-O1-2 (Kosmos-1939) on 20 November 1988; Resurs-O1-3 on 4 November 1994; Resurs-O1-4 on 10 July 1998; Monitor-E on 26 August 2005; Resurs-DK-1 on 15 June 2006. The letters attached to the name Resurs are F for film, O for operational, and DK for Dmitry Kozlov, the father of the Yantar satellites.



new generation of satellites is represented by Monitor-E (E for experimental),  $h = 550$  km, resolution 8 m, and Resurs-DK-1,  $h_p = 356$  km,  $h_a = 585$  km,  $i = 69.9^\circ$ , resolution 1 m, modelled on the military satellites Yantar.

Satellites for general environmental monitoring are large, equipped with radar, flying at an altitude of  $h \approx 780$  km: for Canada, Radarsat-1 and -2; for Europe, ERS-1, -2 (European Remote Sensing Satellite) and Envisat (Environmental Satellite).<sup>49</sup>

The European Space Agency has many projects<sup>50</sup> in this area. The current trend is no longer to build very large satellites like Envisat (8.3 tonnes, 10 instruments), but to favour lighter missions.

In February 2008, the ESA and the European Union signed an agreement to officialise the Sentinel programme, spaceborne component of the GMES initiative (Global Monitoring for Environment and Security). The satellites are grouped into four families<sup>51</sup> each involving several satellites.

Large remote-sensing and environmental satellites weighing several tonnes require powerful launch vehicles which may be able to offer several piggy-back positions for very light passenger satellites. Such satellites, with various missions (although usually technological) also follow Sun-synchronous orbits very close to the orbit of the main satellite. These grouped launches<sup>52</sup> can

---

<sup>49</sup>Launch dates: Radarsat-1 on 4 November 1995; Radarsat-2 on 14 December 2007; ERS-1 on 17 July 1991; ERS-2 on 21 April 1995; Envisat on 1 March 2002.

<sup>50</sup>The satellite ADM (Atmospheric Dynamics Mission), renamed ADM-Aeolus, carries a lidar for wind study. In a more distant future, the ESA has selected three missions: the Sun-synchronous satellites ACE+ (Atmosphere and Climate Explorer), to study climate change, EGPM (European contribution to the Global Precipitation Monitoring mission), designed to study rainfall, and the constellation of three SWARM satellites for dynamical measurement of the magnetic field and its interaction with atmospheric processes (circular orbit,  $i = 86.8^\circ$  for all three, but at different altitudes, viz.,  $h = 450$  km for SWARM-A and -B, and  $h = 530$  km for SWARM-C).

<sup>51</sup>The Sentinel families are classified as follows:

- Sentinel-1, to develop a family of radar satellites to monitor the oceans and land masses, with Sentinel-1A, -1B, -1C.
- Sentinel-2, equipped with high-resolution optics in multispectral mode, with Sentinel-2A, -2B, -2C.
- Sentinel-3, equipped with medium resolution visible and IR optics and an altimetric radar, with Sentinel-3A, -3B, -3C. This mission is a direct descendant of the ERS, Envisat, T/P, and Jason missions.
- Sentinel-4 and -5, designed for atmospheric analysis, in GEO orbit for -4, with Sentinel-4A and -4B, and in LEO orbit for -5.

<sup>52</sup>Here are some examples of grouped launches where the main satellite is a large Sun-synchronous remote-sensing satellite. For the first three ERS-1, SPOT-3, and Hélios-2A, launched by Ariane, the passenger satellites were called ASAP (Ariane Structure for Auxiliary Payload). With ERS-1 (Europe): UoSAT-5 (or OSCAR-22) (GB), Orbcomm-X (USA), Tubsat-A (Germany), SARA (France). With SPOT-3 (France): Kitsat-2 (South Korea), PoSAT-1 (Portugal), Stella (France), HealthSat-2 (GB), ItamSat (Italy), EyeSat-1 (USA). With Hélios-2A (France): Parasol (France), Nanosat (Spain) and four French military satellites for electronic intelligence, Essaim-1 to 4. With Resurs-O1-4 (Russia): FaSat-1 (Chile), TMSat (Thailand), TechSat-1B (Israel), Westpac-1 (Australia), Safir-2 (Germany). With

provide an opportunity for countries with little experience in space to get their own satellite into orbit.

Countries occupying a very large territory use Sun-synchronous remote-sensing LEO satellites. For India, in its IRS programme<sup>53</sup> (Indian Remote Sensing), the first satellites, IRS-1A and -1B, are on a rather high orbit,  $h = 910$  km, while the rest, IRS-P2, -P3, -P6 (Resourcesat-1) and Resourcesat-2, are on a lower orbit,  $h = 817$  km. The 2.5 m resolution of the satellite Cartosat-1 (IRS-P5),  $h = 617$  km, has been improved to 1 m for the satellites Cartosat-2, -2A, and -2B,  $h = 630$  km. The next generation Cartosat-3 will have “military” resolution. The experimental satellite TES (Technology Experiment Satellite) was launched into a still lower orbit, with  $h = 565$  km. India is also developing a radar (SAR) satellite programme with RISat-1 (Radar Imaging Satellite) and RISat-2, with  $h = 608$  km and  $h = 550$  km, respectively.

China is developing several environmental programmes,<sup>54</sup> using exclusively Sun-synchronous satellites. Some of these are small, like Tan Suo-1, -2, and -3 (*tan suo* means “experimental” in Chinese),  $h = 608$  km, 703 km, and 581 km, respectively, Huan Jing-1A and -1B (*huan jing* means “environment”),  $h = 648$  km, and Chuang Xin-1-02 (“innovation”),  $h = 793$  km. Others are large satellites equipped with radar, for military as well as environmental purposes, in the Yao Gan series (RSS, *Remote Sensing Satellite, yao gan wei xing* means “remote-sensing satellite”, from *yao* meaning “far” and *gan* meaning “detection”). Regarding these satellites, Yao Gan-1, -2, -3, and -4 are around  $h = 640$  km, while Yao Gan-5 and -6 are at the lower altitude  $h = 480$  km, and Yao Gan-7 and -8 go back up to  $h = 660$  km, along with Yao Gan-10 and -11. The three satellites Yao Gan-9A, -9B, and -9C are in a non-Sun-synchronous orbit with  $h = 1,100$  km,  $i = 63.7^\circ$  for electronic intelligence

---

Meteor-3M-1 (Russia); Badr-B (Pakistan), Maroc-Tubsat (Morocco–Germany), Kompass and Reflektor (Russia). With Megha-Tropiques (India and France): VesselSat-1 (Luxembourg) and two Indian university satellites, SRMSAT and Jugnu.

<sup>53</sup>Launch dates: IRS-1A on 17 March 1988; IRS-1B on 29 August 1991; IRS-1C on 28 December 1995; IRS-1D on 4 June 1997; IRS-1E on 20 September 1993 (before IRS-1C), failed; IRS-P2 on 15 October 1994; IRS-P3 on 21 March 1996; TES on 22 October 2001; Resourcesat-1 (IRS-P6) on 17 October 2003; Cartosat-1 (IRS-P5) on 5 May 2005; Cartosat-2 (IRS-P7) on 10 January 2007; Cartosat-2A on 28 April 2008; Cartosat-2B on 12 July 2010; RISat-2 on 20 April 2009; Resourcesat-2 on 20 April 2011; RISat-1 on 26 April 2012 (after RISat-2).

<sup>54</sup>Launch dates: Tan Suo-1 (TS-1 or ExperimentalSat-1) on 18 April 2004; Tan Suo-2 (TS-2 or ExperimentalSat-2) on 18 November 2004; Tan Suo-3 (TS-3 ou ExperimentalSat-3) on 5 November 2008; Huan Jing-1A and -1B (HJ-1A and -1B, also called DFH-78 and -79) on 6 September 2008; Chuang Xin-1-02 (CX-1-02 or Innovation-1) on 5 November 2008; Yao Gan-1 (RSS-1 or JB5-1) on 26 April 2006; Yao Gan-2 (RSS-2 or JB6-1) on 25 May 2007; Yao Gan-3 (RSS-3 or JB5-2) on 11 November 2007; Yao Gan-4 (RSS-4 or JB6-2) on 1 December 2008; Yao Gan-5 (JB5-7) on 15 December 2008; Yao Gan-6 (JB8) on 22 April 2009; Yao Gan-7 (JB6-3) on 9 December 2009; Yao Gan-8 on 15 December 2009; Yao Gan-9A, -9B and -9C on 5 March 2010; Yao Gan-10 (JB5-3) on 9 August 2010; Yao Gan-11 (JB6-4) on 22 September 2010; Tian Hui-1 (TH-1, DFH-90) on 24 August 2010.

(ELINT). The Sun-synchronous satellite Tian Hui-1 at  $h = 500$  km takes stereographic images with 5 m resolution.

China and Brazil are working together on the CBERS programme<sup>55</sup> (China–Brazil Earth Resources Satellite), also known as Zi Yuan (“resources” in Chinese), with the satellites CBERS-1 and -2,  $h = 774$  km, and the following (ZY-1 series). China has also launched two satellites ZY-2 and -2B (ZY-2 series) in lower orbits, at  $h = 495$  km and  $h = 476$  km.

Taiwan has launched Rocsat-2, renamed FormoSat-2, in a novel Sun-synchronous orbit, about which we shall say more later on (see Chap. 11).

Australia is planning to launch its satellite ARIES-1 (Australian Resource Information and Environment Satellite).

The US private company Resource21 (21 indicates the twenty-first century) should launch five satellites, RS21-1 to RS21-5, at  $h = 700$  km, with a resolution of 10 m, as a follow-on to the Landsat heritage. This project seems to be on hold since 2003.

Japan has always attributed great importance to the environment in its space projects,<sup>56</sup> beginning with JERS-1 (Japan Earth Resource Satellite, or Fuyo-1, where *fuyo* means “purple rose” in Japanese),  $h = 568$  km, then the three large satellites ADEOS-1 and -2 (Advanced Earth Observing Satellite, also called Midori and Midori-2, where *midori* means “green”),  $h = 797$  km and  $h = 803$  km, and ALOS (Advanced Land Observation Satellite, or Daichi, “Earth”)  $h = 692$  km, all weighing around 4 tonnes. This programme was followed by the GCOM programme (Global Change Observing Mission), which has two parts, GCOM-W (Water) with two satellites,  $h = 700$  km, and GCOM-C (Carbon cycle) with two satellites,  $h = 798$  km. The Japanese satellite GCOM-W1 (Shizuku, “dewdrop”) has been inserted in the A-Train, between Aqua and OCO-2 (see Fig. 9.22).

Satellite-based environmental studies are now very varied. Among these we may mention the detection of forest fires, where onboard instruments have a ground resolution of about 100 m, as in the case of the Sun-synchronous German satellite BIRD (Bi-spectral InfraRed Detection),  $h = 575$  km. The projected Spanish satellite FuegoSat,  $h = 700$  km,  $i = 47.5^\circ$ , will be the precursor of a constellation of 12 satellites, FuegoFOC (Fire Observation Constellation). For surveillance of the Amazonian forest, Brazil is developing a project for two satellites, SSR-1 and -2 (*Satélite de Sensoriamento Remoto*), in strictly equatorial orbit with  $h = 900$  km,  $i = 0^\circ$ .

To study the polar ice caps and make precise measurements of variations in their thickness, a novel orbit (near-polar non-Sun-synchronous LEO) has

---

<sup>55</sup>Launch dates: CBERS-1 (ZY-1A, Zi Yuan-1A) on 14 October 1999; CBERS-2 (ZY-1B, Zi Yuan-1B) on 21 October 2003; CBERS-2B on 18 September 2007; ZY-2 (Zi Yuan-2, DFH-50, Jian Bing-3, JB-3) on 1 September 2000; ZY-2B (Zi Yuan-2B, DFH-55, Jian Bing-3B, JB-3B) on 27 October 2002; ZY-2C (Zi Yuan-2C, Jian Bing-3C, JB-3C) on 6 November 2004. The satellites ZY-2 use a CBERS platform (recorded as ZY-1 by China).

<sup>56</sup>Launch dates: JERS-1 on 11 February 1992; ADEOS-1 on 27 August 1996; ADEOS-2 on 14 December 2002; ALOS on 24 January 2006; GCOM-W1 on 18 May 2012.

been chosen for two missions,<sup>57</sup> one American and the other European: ICESat (Ice, Clouds, and Land Elevation, previously EOS-LAM),  $h = 600$  km,  $i = 94^\circ$ , and CryoSat (Cryosphere Satellite),  $h = 720$  km,  $i = 92^\circ$ . At these altitudes, the Sun-synchronous inclinations would be  $97.8^\circ$  and  $98.3^\circ$ . The US has an ambitious programme in this pressing field of investigation, with ICESat-2 on a similar orbit to ICESat and two other missions on Sun-synchronous orbits, DESDynI (Deformation, Ecosystem Structure and Dynamics of Ice) and SCLP (Snow and Cold Land Processes).

The British project DMC (Disaster Monitoring Constellation), with international cooperation, is currently underway.<sup>58</sup> It comprises a constellation of Sun-synchronous microsatellites with  $h = 686$  km.

We end this category of Earth-observation satellites with Triana,<sup>59</sup> a US mission with an unusual orbit for this kind of mission. After a 3.5 month journey, the satellite will be placed in a halo orbit around the Lagrange point  $L_1$  of the Earth–Sun system (orbit type L1LO, period 6 months). Its instruments will thus have a view of the Earth which is permanently illuminated, but from a very great distance (234 Earth radii, equivalent to four times the distance from the Earth to the Moon). The projected pixel size (resolution) is 8 km (1 arcsec). Due to the large dimensions of the halo orbit, it will be possible to observe alternately the North and South Poles of the Earth, focusing specifically on the stratospheric ozone. The project, dating to 1999, was first abandoned, then resumed<sup>60</sup> but without success under the name DSCO (Deep Space Climate Observatory) or DSCOVR. However, in 2012, it was taken up again and launch is planned for 2014.

## 9.2.5 Satellites for Remote-Sensing and Surveillance

### Commercial Remote-Sensing

Satellites in this category have a resolution of the order of 1 m in the visible frequency range (and a few meters if they carry out infrared observations), which was a level reserved for military satellites until 1994.

Set up in 1992, two US companies<sup>61</sup> share the main part of the market:

<sup>57</sup>Launch dates: ICESat on 13 January 2003; CryoSat on 8 October 2005, failed; CryoSat-2 on 8 April 2010.

<sup>58</sup>Launch dates: AlSat-1 (Algeria) on 28 November 2002; BilSat-1 (Turkey), NigeriaSat-1 (Nigeria) and BNSCSat (or UK-DMC) (GB) launched together on 27 September 2003; Beijing-1 (China) on 25 October 2005; UK-DMC2 (GB) and Deimos-1 (Spain) on 25 July 2009; AlSat-2A (Algeria) on 12 July 2010 (launched with Cartosat-2B).

<sup>59</sup>Rodrigo Triana was the first person among the sailors aboard Christopher Columbus' caravels to see the New World, in 1492.

<sup>60</sup>The project was supported by Al Gore while he was Vice President to Bill Clinton. However, when George W. Bush arrived on the scene, it was promptly shelved. And the attribution of the Nobel Peace Prize jointly to Al Gore and GIEC in 2007 was unable to give further impetus to this satellite project, sometimes referred to as GoreSat.

<sup>61</sup>They share several common features. Their trade marks are constructed by sticking two words together without a space, and they often change name. These successive changes

- GeoEye Inc., with a succession of satellites called OrbView (Orbimage), Ikonos, and GeoEye.
- DigitalGlobe, with a succession of satellites called EarlyBird/EarthWatch, QuickBird, and WorldView.

These satellites<sup>62</sup> are Sun-synchronous, crossing the ascending node at 10:30. The resolution<sup>63</sup> of their images is improving all the time. The first customers of these companies are the American agencies NASA and NIMA, or indeed Google for Google Maps.

We list the main satellites in chronological order, giving their resolution and altitude:

- Ikonos<sup>64</sup> (resolution 0.8 m/3 m),  $h = 680$  km.
- OrbView-3 (1 m/4 m),  $h = 451$  km.
- QuickBird-2 (0.6 m/2.5 m),  $h = 443$  km.
- WorldView-1 and -2 (0.5 m/2 m),  $h = 494$  km and  $h = 765$  km.
- GeoEye-1 (0.4 m/1.6 m),  $h = 679$  km.

Other countries are developing this field of accurate spaceborne cartography,<sup>65</sup> including France with Pléiades-HR (HR standing for high resolution), and Israel with EROS-A1 (resolution 1.9 m/5 m) and EROS-B (0.7 m/2.8 m), both at altitude  $h = 508$  km. With resolutions of the order of 2 m, countries new to the field of space technology are coming into their own, e.g., Thailand with THEOS (Thai Earth Observing System) (resolution 2 m/5 m), on a SPOT orbit at  $h = 822$  km, and the United Arab Emirates with DubaiSat-1 (2.5 m/5 m),  $h = 686$  km. With RazakSat (2.5 m/5 m),<sup>66</sup> Malaysia is making use of a near-equatorial orbit that is rarely exploited, with  $h = 685$  km,  $i = 9^\circ$ , sometimes referred to as NEO (near-equatorial orbit).

---

show up in the names of their satellites. The new European company set up jointly by EADS and private capital has followed this fashion, since it is called InfoTerra.

<sup>62</sup>Launch dates: OrbView-1 (Microlab-1) on 3 April 1995 (launched with Orbcomm-FM-1 and -2, non-Sun-synchronous); EarlyBird/EarthWatch-1 on 24 December 1997; Ikonos-1 on 27 April 1999, failed; Ikonos-2 on 24 September 1999; OrbView-4 (before OrbView-3) on 21 September 2001, failed; QuickBird-1 on 20 November 2000, failed; QuickBird-2 on 18 October 2001; OrbView-3 on 26 June 2003; WorldView-1 on 18 September 2007; GeoEye-1 on 6 September 2008; WorldView-2 on 8 October 2009.

<sup>63</sup>The resolution in panchromatic mode corresponds to black and white images, and in multispectral mode, to colour images, generally composed of blue, green, red, and near-infrared. The resolutions are indicated in the text by two lengths in meters: B&W resolution/colour resolution.

<sup>64</sup>The satellite Ikonos-1, lost at launch, was soon replaced by Ikonos-2, launched only 5 months later and renamed Ikonos to exorcise the failure of the first launch. The Greek noun  $\acute{o}$  εἰκῶν, ὄνοϛ means “image”. But why did they choose the genitive *ikonos*?

<sup>65</sup>Launch dates: EROS-A1 on 5 December 2000; EROS-B on 25 April 2006; THEOS on 1 October 2008; DubaiSat-1 on 29 July 2009.

<sup>66</sup>The satellite MACSat (Medium-sized Aperture Camera Satellite), launched on 4 July 2009, has been renamed Razaksat, after the Malaysian Prime Minister Abdul Razak, *Bapa Pembangunan Malaysia*, “the father of Malaysian development”.



## Military Remote-Sensing and Surveillance

For military applications, the main category of US surveillance satellites (or spy satellites, depending on one's point of view) carry the suggestive name Key Hole (KH). They fall into several series,<sup>67</sup> from KH-1 in 1959 to KH-13, currently operating. For the first few series up to KH-9 in 1986, the basic principle was always the same: a camera took photos, the film was placed in a capsule, and as astonishing as it may seem, the capsule was then thrown back to Earth. A parachute opened at an altitude of 20 km and, all being well, an aircraft equipped with a net intercepted the prize in flight (although it could also be picked up by ship in the ocean). Now that the first few series have been declassified, as they say in military circles, we may observe that the success rate was actually very low, with only two successful missions, Discoverer-14 and Discoverer-18, for the 27 satellites of the series KH-1 and -2 (satellites Discoverer-1 to -27). The subsequent series met with more success.

Concerning series KH-11 and -12, results are transmitted via SDS military satellites. It is claimed that images taken by the latest satellites have a resolution of 15 cm. However, this raises several questions regarding the influence of atmospheric turbulence, the problem of data accumulation, and so on. Satellites in the series KH-13 are KH-12 satellites made undetectable to radar and IR sensors, the so-called stealthy satellites, and those in the series 8X will apparently be gigantic telescope satellites called Monstersats, with centimeter resolution,<sup>68</sup> but in fact little is known for certain about these satellites.

Missions were very short for the first KH series, lasting only a few days, but then grew longer, to reach 19 days for KH-4B and 50 days with two capsules for KH-8. Orbits were generally low, with  $h$  between 200 and 400 km, near-polar (e.g., Discoverer-35,  $h = 260$  km,  $i = 82^\circ$ ) up to KH-3, then with lower inclination (e.g., KH-4A-14, or Orbis, OPS/3360,  $h_p = 117$  km,  $h_a = 329$  km,  $i = 70^\circ$ ) up to KH-6, and subsequently Sun-synchronous or very high inclination (e.g., KH-7-27,  $h_p = 139$  km,  $h_a = 375$  km,  $i = 117^\circ$ ) up to KH-11, where missions became much longer (which can justify the use of a Sun-synchronous orbit, as we have seen). The first eleven series involved a total of 262 satellites.

For KH-12, the satellites, at 20 tonnes, were sent up for long periods on Sun-synchronous elliptical orbits with  $h_p \approx 150$  km,  $h_a \approx 950$  km,  $i = i_{HS} \approx 98^\circ$ . Launches were regularly spaced: KH-12-1 (USA-86 in 1992), KH-12-2 (USA-116 in 1995), KH-12-3 (USA-129, NROL-2 in 1996), KH-12-4 (USA-

<sup>67</sup>These series have more or less officially certified code names, which become known after a certain time delay: Corona (KH-1 to -4), Argon (KH-5), Lanyard (KH-6), Gambit (KH-7, -8), Hexagon and Big Bird (KH-9), Dorian (KH-10, annul), Crystal Kennan (KH-11), Ikon and Improved Crystal (KH-12, also known as KH-11B). The name for the current series KH-13 is apparently Misty.

<sup>68</sup>Resolutions given by the US Air Force, which runs the programme: Series KH-1 (begun in 1959) 12 m; KH-2 (1960) 9 m; KH-3 (1961) 7.6 m; KH-4A (1963) 2.7 m; KH-6 (1963) 1.8 m; KH-8 (1966) 0.5 m. For KH-11 (1976) and KH-12 (1992) 0.15 m with a similar telescope to Hubble. For KH-13 0.10 m, 8X 0.05 m.

161, NROL-14 in 2001), KH-12-5 (USA-186, NROL-20 in 2005), KH-12-6 (USA-224, NROL-49 in 2011).

For KH-13, the series known as Misty, it seems that there have been two satellites on a near-circular orbit with  $h \sim 1,000\text{--}3,000$  km,  $i \approx 63^\circ$ : Misty-1 (USA-53 or AFP-731 launched by STS-36 in 1990) and Misty-2 (USA-144 or EIS-1 in 1999).

“All weather” military observation is carried out by the Lacrosse radar satellites, each with a mass of 20 tonnes. They have circular orbits with medium inclination: Lacrosse-1 (USA-34 or Onyx-1 launched by STS-27 in 1988),  $h = 440$  km,  $i = 57^\circ$ ; the four others, Lacrosse-2 (USA-69 or Onyx-2 in 1991), Lacrosse-3 (USA-133 or Onyx-3 in 1997), Lacrosse-4 (USA-152 or Onyx-4 in 2000), Lacrosse-5 (USA-182 or Onyx-5 in 2005),  $h \approx 680$  km with inclinations alternating between  $i = 68^\circ$  and  $i = 57^\circ$ .

The French programme<sup>69</sup> is based on the Hélios satellites<sup>70</sup> on Sun-synchronous orbits at  $h = 680$  km, and the German programme on the five SAR-Lupe radar satellites,<sup>71</sup> with  $h = 487$  km,  $i = i_{\text{HS}}$  (SAR stands for synthetic aperture radar and *lupe* means “magnifying glass” in German).

Soviet military surveillance was carried out by a multitude of Kosmos satellites. The first, in the Zenit series, had very low altitude,  $h \sim 150$  km, and characteristic inclinations of  $i = 63^\circ, 73^\circ, 82^\circ$ . Missions lasted a few days and the film was recovered with the satellite. The technique of recovering the capsule in flight appeared with satellites in the Yantar series (meaning “amber” in Russian) in 1975. The Arkon series is the equivalent of KH-12. Radar observation is carried out by the Almaz series (*almaz* meaning “diamond” in Russian, derived from the Arabic *al mās*, with the same meaning), 19 tonne satellites in low circular orbits,  $h = 300$  km,  $i = 72^\circ$ , with Kosmos-1870 (Almaz-T-2 or Resurs-R-2 launched in 1987) and Almaz-1 (Almaz-T-3 or Resurs-R-3 in 1991) and the Oblik series, the equivalent of Lacrosse.

Chinese military surveillance and remote-sensing satellites belong to the FSW-2 series (*Fanhui Shi Weixing*), such as FSW-2-3, launched in 1996,  $h = 125$  km,  $i = 63^\circ$ . They return to Earth after 2 weeks (as their name suggests: *fan hui shi* means “return” and *wei xing* means “satellite”). One should also mention the satellites Yao Gan-5 and -6 discussed above.

---

<sup>69</sup>Hélios, ὁ Ἥλιος, οὐ, is the Sun, a (non-Olympian) god of Greek mythology. He journeys across the sky during the day on a chariot drawn by four horses. Thanks to his dominating position and his perceptive gaze, as piercing as a ray of light, he sees everything that happens on Earth. It was by reference to these features, and with little modesty, that the French military named their reconnaissance programme. While it was very important in archaic times, the cult of the Sun lost its influence in classical times, and Hélios was often assimilated with Apollo.

<sup>70</sup>Launch dates: Hélios-1A : 7 July 1995; Hélios-1B : 3 December 1999; Hélios-2A : 18 December 2004; Hélios-2B : 18 December 2009.

<sup>71</sup>Launch dates: SAR-Lupe-1 on 19 December 2006; SAR-Lupe-2 on 2 July 2007; SAR-Lupe-3 on 1 November 2007; SAR-Lupe-4 on 27 March 2008; SAR-Lupe-5 on 22 July 2008.

Japan operates its optical or radar IGS satellites<sup>72</sup> (Intelligence Gathering Satellite) on low Sun-synchronous orbits, with  $h = 479$  km, mainly to provide early warning of attack by North Korea.

In parallel with the EROS programme, Israel has developed its military programme Ofeq (“horizon” in Hebrew), with satellites<sup>73</sup> on highly inclined elliptical orbits (see Fig. 9.17): Ofeq-5 ( $h_p = 370$  km,  $h_a = 750$  km,  $i = 143.5^\circ$ ), Ofeq-7 ( $h_p = 339$  km,  $h_a = 575$  km,  $i = 141.8^\circ$ ), Ofeq-9 ( $h_p = 343$  km,  $h_a = 588$  km,  $i = 141.8^\circ$ ).

With such inclinations, these satellites can cover latitudes below  $40^\circ$ . Although there is no precise information available about this programme, we may imagine two possible motivations for this kind of retrograde orbit. To begin with, a retrograde orbit increases the synodic frequency  $\nu'$  of the satellite (with a daily frequency of  $\nu \approx 15$ , we have  $\nu' \approx 16$  rather than  $\nu' \approx 14$  for a prograde orbit) and hence the viewing frequency. In addition, a westward launch from Israel, if it failed, would end up in the Mediterranean rather than in one of the neighbouring countries, a useful precaution in such a region.

A roughly equivalent orbit is used by TecSAR (also called Polaris), a radar satellite of the Israeli military programme with  $h_p = 405$  km,  $h_a = 580$  km,  $i = 41.03^\circ$ . This satellite, in a prograde orbit, was launched from India.

## 9.2.6 Oceanographic Satellites

The first oceanographic satellites had highly inclined orbits: GEOS-3 (Geodynamics Experimental Ocean Satellite),  $h = 847$  km,  $i = 115.0^\circ$ , and SeaSat,  $h = 780$  km,  $i = 108.1^\circ$ . The latter orbit was then used to within a few kilometers by Geosat and GFO-1 (Geosat Follow On).

The orbit of TOPEX/Poseidon is rather high, viz.,  $h = 1,330$  km, to avoid atmospheric drag as far as possible, and has a rather high inclination, viz.,  $i = 66^\circ$ , in order to overfly almost the whole expanse of the oceans.<sup>74</sup> To avoid any bias due to the influence of the Sun on the tides, it was essential that the orbit should not be Sun-synchronous. The satellites Jason-1, then Jason-2 (or OSTM, Ocean Surface Topography Mission), were placed on exactly the

---

<sup>72</sup>Launch dates: IGS-1A (IGS-Optical-1) and IGS-1B (IGS-Radar-1) on 28 March 2003; IGS-3A (IGS-Optical-2) on 11 September 2006; IGS-4V (IGS-E-Optical-3) and IGS-4B (IGS-Radar-2) on 24 February 2007; IGS-5A (IGS-Optical-3) on 28 November 2009; IGS-6A (IGS-Optical-4) on 22 September 2011; IGS-7A (IGS-Radar-3) on 12 December 2011; IGS-8A (IGS-Radar-4) and IGS-8B (IGS-Optical-5V) on 27 January 2013.

<sup>73</sup>Launch dates: Ofeq-1 on 19 September 1988; Ofeq-2 on 3 April 1990; Ofeq-3 on 5 April 1995; Ofeq-5 on 28 May 2002; Ofeq-7 on 10 June 2007; Ofeq-9 on 22 June 2010; TecSAR on 21 January 2008.

<sup>74</sup>Launch dates: GEOS-3 on 9 April 1975; Seasat on 28 June 1978; Geosat on 13 March 1985 (Geosat[GM] Geodetic Mission: April-Sept. 1986; Geosat [ERM] Exact Repeat Miss.: Nov. 1986–Jan. 1990); GFO-1 on 10 February 1998; TOPEX/Poseidon on 10 August 1992; Jason-1 on 7 December 2001; Jason-2 on 20 June 2008; SARAL on 25 February 2013.

same orbit<sup>75</sup> as TOPEX/Poseidon to ensure the continuity of the French–US mission, which will then be extended by Jason-3. The future US satellite SWOT (Surface Water and Ocean Topography), which is picking up from the WatER-HM project (Water Elevation Recovery and Hydrosphere Mapping), will be in a lower orbit, with  $h = 971$  km and a slightly different inclination  $i = 78^\circ$ , because it will also investigate water on the continental surfaces.

These altimetry satellites, together with the two Sun-synchronous European ERS satellites, have carried out accurate measurements of sea levels and their evolution, with very good results.<sup>76</sup> The orbit of the Indian–French satellite SARAL (Satellite with Argos and Altika) has the same characteristics as that of Envisat (but with different crossing times).

The satellites<sup>77</sup> in the Okean series, originally Soviet, then Russian–Ukrainian, then Russian (Ukraine having opted for the Sich series), are dedicated to study of the polar regions and oceans. The first satellites, Okean-O1-1 to -3, together with Sich-1, have altitude  $h \approx 650$  km and inclination  $i = 82.5^\circ$ , typical of many Meteor and hundreds of Kosmos satellites. The next in the series, Okean-O1-4 and Okean-O-1, have the same altitude, but on a Sun-synchronous orbit.

When their main mission is not altimetry, oceanographic satellites<sup>78</sup> are Sun-synchronous: the Japanese satellites MOS-1 and MOS-1B (Marine Observation Satellite, also called Momo and Momo-1B, where *momo* means “peach flower”),  $h = 908$  km; the Chinese Hai Yang satellites (*hai yang* means “ocean”) HY-1A and HY-1B,  $h = 798$  km, HY-2A,  $h = 960$  km; the Indian satellites Oceansat-1 (IRS-P4) and Oceansat-2,  $h = 720$  km; the US SeaStar (OrbView-2),  $h = 700$  km; the South Korean satellites Arirang-1, -2, and -3 (or KOMPSat-1, -2, and -3, Korea Multi-purpose Satellite)<sup>79</sup> to study the oceans and land masses,  $h = 690$  km. The Argentinian satellite SAC-D (*Satélite de*

<sup>75</sup>In September 2002, Topex/Poseidon was placed on a new orbit, half-way between its former paths (which had become those of Jason-1). “This tandem phase illustrates the scientific potential of an optimised constellation of altimetry satellites” (Aviso, CLS/CNES). The mission officially ended in January 2006. After the launch of Jason-2, Jason-1 was transferred to the former path of T/P, while Jason-2 took the place of Jason-1.

<sup>76</sup>Estimated measurement accuracy (averaged over a month): GEOS-3 25 cm; Seasat 5 cm; Geosat 4 cm; ERS-1 and -2 3 cm; TOPEX/Poseidon 2 cm; Jason-1 1 cm; Jason-2 1 cm.

<sup>77</sup>Launch dates: Okean-O1-1 on 5 July 1988; Okean-O1-2 on 28 February 1990; Okean-O1-3 (usually called Okean-3) on 4 June 1991; Okean-O1-4 on 11 October 1994; Sich-1 on 31 August 1995; Okean-O-1 (usually called Okean-O) on 17 July 1999.

<sup>78</sup>Launch dates: MOS-1 on 19 February 1987; MOS-1B on 7 February 1990; SeaStar on 1 August 1997; Oceansat-1 on 26 May 1999; HY-1A (Ocean-1 or DFH-54) on 12 May 2002 (with FY-1D); HY-1B on 11 April 2007; HY-2A on 15 August 2011; Oceansat-1 on 26 May 1999; Oceansat-2 on 23 September 2009; Arirang-1 (with ACRIMSAT) on 21 December 1999; Arirang-2 on 28 July 2006; Arirang-3 on 18 May 2012; QuikScat on 20 June 1999; Coriolis on 6 January 2003; SAC-D on 10 June 2011.

<sup>79</sup>The Koreans chose the name for their satellites in a most unusual way: *Arirang* is a popular Korean folk song which has become the unofficial national anthem.

*Aplicaciones Cientificas*),  $h = 651$  km, carries the American Aquarius instrument.<sup>80</sup>

Satellites equipped with a scatterometer to study the winds over the sea are also Sun-synchronous, e.g., QuikScat (Quick Scatterometer),  $h = 805$  km, and Coriolis<sup>81</sup> (also called WindSat or P98-2),  $h = 830$  km. The Chinese–French satellite CFOSAT (Chinese–French Oceanic Satellite) plans to use a lower orbit, with  $h = 514$  km.

## 9.2.7 Navigation Satellites

The first US navigation system was provided by the Transit satellites in strictly polar LEO orbit. They played a very important role at the inception of space geodesy.<sup>82</sup> Several of these satellites were equipped with nuclear generators.<sup>83</sup>

A comparable Soviet then Russian system was constructed using the Parus (military), Tsikada, and Nadezhda constellations of satellites in polar orbit, with  $h \approx 1,000$  km and  $i = 83^\circ$ .

Results of astonishing accuracy (positioning to within a few meters) are currently obtained with MEO satellite constellations. A whole chapter of this book is devoted to global satellite navigation systems, or positioning systems, commonly referred to as GPS (see Chap. 14).

---

<sup>80</sup>Aquarius was designed to fly aboard the US satellite of that name, but following a cooperation agreement with Argentina, the satellite became Aquarius/SAC-D, then SAC-D/Aquarius.

<sup>81</sup>*Gustave Gaspard Coriolis* (1792–1843) was a French mathematician and engineer. In his first work, *Du calcul de l'effet des machines* (1829), he introduced the ideas of work done by a force (force times displacement) and kinetic energy. In his paper *Sur le principe des forces vives dans le mouvement relatif des machines* (1831), he examined the various accelerations: absolute, relative, frame, and complementary. The latter subsequently became known as the Coriolis acceleration. This is today a basic feature in the study of geophysical fluids in motion, such as marine and atmospheric currents on the surface of the globe.

<sup>82</sup>In the geodesy literature, the satellites Transit-5B-1 and -5B-2 are referred to with the simplified notation VBN-1 and VBN-2.

<sup>83</sup>In 1961, Transit-4A was the first satellite equipped with a nuclear generator for its electricity supply, the so-called SNAP (System for Nuclear Auxiliary Power). These generators are now referred to by the acronym RTG (radioisotope thermoelectric generator). Other satellites in this series were equipped with RTG: Transit-4B in 1961, Transit-5B-1, -5B-2, and -5B-3 in 1963, and Triad-1 in 1972. The fuel was polonium-210 for the Transit-4 satellites, and plutonium-238 for the Transit-5 series. In the other US series, satellites with RTG (plutonium-238) were OPS/4682 (or Snapshot, a pun on SNAP), Nimbus-B (failed at launch), Nimbus-3 in an LEO orbit, and the two satellites LES-8 and -9 in GEO orbits. Concerning Soviet satellites equipped with RTG, it is known that there were accidents with Kosmos-954 and Kosmos-1402. Probes travelling far out into the Solar System are also equipped with nuclear generators. (Cassini is carrying 35 kg of plutonium-238, producing a power output of 750 W).

## 9.2.8 Communications Satellites

The principle of communication by relay is to send a signal, e.g., telephone, television, telecommunications, from a given point on the Earth to another by relaying it through a satellite which detects, amplifies, and retransmits it. A GEO satellite can of course do this, provided it is visible from the two points and in suitable conditions. For high latitudes, a group of HEO satellites can guarantee the link. With LEO satellites, the time for which the satellite is visible is rather short and a constellation is required. The reader is referred to Chap. 12 for further discussion of this point.

### GEO Telecommunications

Almost 300 satellites are currently operating in the necessarily one-dimensional geostationary orbit, and most of these are for communications.<sup>84</sup> These satellites have an average lifespan of about 12 years. Generally speaking, a country or group of countries sets up its satellite at the longitude of one of its meridians.<sup>85</sup>

A country like Indonesia can use a geostationary satellite to set up a telecommunications network between the hundreds of islands composing it, much more easily than using a network at ground level. Moreover, for many

---

<sup>84</sup>There are also around 15 weather satellites, some of which are dual purpose weather and communications, not forgetting the Chinese Beidou positioning satellites (see Chap. 14).

<sup>85</sup>As an example, we mention several operational satellites with their parking position in 2013. At the beginning of the twenty-first century, most European countries have abandoned their national satellites to join a European organisation. For instance, the Telecom satellites for France or DFS-Kopernikus for Germany have been absorbed into Eutelsat. Only Scandinavian countries like Norway and Sweden (owing to their remote position relative to geostationary coverage) and Spain (which also targets Latin America) have held onto their national satellites.

The first commercial satellite in this category, Anik-1 (Canada), was launched in 1972. We give one satellite per country or organisation, going round the geostationary orbit in the positive direction: Rascom-QAF-14 (African org.) 2.8°E; Sirius-4 [SES-Sirius-4] (Sweden) 4.8°E; Eutelsat-7A (Eutelsat org.) 7.0°E; Astra-1M (Astra org.) 19.2°E; Badr-6 (Arabsat org.) 26.0°E; PakSat-1 (Pakistan) 38.0°E; HellasSat-2 (Greece) 39.0°E; Türksat-3A (Turkey) 41.8°E; NigComSat-1R (Nigeria) 42.5°E; Azerspace-1 (Azerbaijan) 46.0°E; Yamal-202 (Russia) 49.0°E; YahSat-1B (United Arab Emirates) 52.5°E; INSAT-3E (India) 55.0°E; Intelsat-906 (Org. Intelsat) 64.1°E; Thaicom-5 (Thailand) 78.5°E; Esafi-1 (Tonga) 79.0°E; ChinaStar-1 (Macao/China) 87.5°E; SupremeSat-1 (Sri Lanka) 87.5°E; ST-3 (Singapore-Taiwan) 88.0°E; MeaSat-3 (Malaysia) 91.0°E; ChinaSat-9 (China) [Zhong Xing-9 or ZX-9] 99.2°E; AsiaSat-5 (Hong Kong/China) 100.5°E; KazSat-1 (Kazakhstan) 103.0°E; KoreaSat-5 [Mugunghwa-5] (South Korea) 113.0°E; Garuda-1 (Indonesia) 123.0°E; JCSat-12 [JCSat-RA] (Japan) 128.0°E; Vinasat-2 (Vietnam) 132.0°E; Agila-2 [Mabuhay-1] (Philippines) 146.0°E; Optus-D3 (Australia) 156.0°E; Galaxy-15 (PanAmSat org.) 133.0°W; DirectTV-8 (DirectTV org.) 100.8°W; BrazilSat-B4 (Brazil) 92.0°W; Nimiq-4 (Canada) 82.0°W; Venesat-1 [Simon-Bolivar-1] (Venezuela) 78.0°W; QuetzSat-1 (Mexico) 77.0°W; Nahuel-1 (Argentina) 71.8°W; Hispasat-1D (Spain) 30.0°W; Nilesat-201 (Egypt) 7.0°W; Amos-3 (Israel) 4.0°W; Thor-6 (Norway) 0.8°W.

countries, a geostationary communications satellite has an important symbolic value.<sup>86</sup>

The GEO communications satellites, which are becoming increasingly common, bigger, and more expensive,<sup>87</sup> currently represent the largest part of the commercial market for space activities.

GEO satellites for broadband Internet made their appearance in 2011 with Ka-Sat (parked at 9°E) and Via-Sat-1 (at 115°W).

GEO satellites are also widely used for military communications by satellites in the US series<sup>88</sup> LES, DSCS then WGS, the TDRS system, and the Milstar and AEHF series. Naturally, the same can be said of satellites in the

<sup>86</sup>The names chosen for these satellites serve to demonstrate this. The multiethnic country Indonesia, sometimes torn by internal conflict, chose the name Palapa, which means “unity” in Bahasa Indonesian, the official language. Developed countries in the New World seek the names of their satellites in the Amerindian languages, perhaps as a way of finding their roots. Canada named its satellites Anik and Nimiq, which means “brother” (for a sister) and “union” (or “bond that unites”) in Inuktitut (the Inuit or Eskimo language). Argentina uses the Araucanian word “Nahuel” (Araucan, Mapuche language), meaning “tiger”.

<sup>87</sup>The two satellites Westar-6 (Western Union Communications Satellite, US) and Palapa-B2 (Indonesia) were launched by STS-10 (STS-41-B) on 3 February 1984, but they never reached the geostationary orbit. The insurers, the new owners, paid for recovery and return of the satellites by the shuttle flight STS-14 (STS-51-A) on 16 November 1984. China bought Westar-6, and turned it into AsiaSat-1, launching the satellite itself on 7 April 1990. The other satellite became Palapa-B2R and was launched on 13 April 1990.

The adventures of AsiaSat did not end there. The satellite AsiaSat-3, launched by a Russian rocket on 24 December 1997, was placed on the wrong orbit, too highly inclined (a GTO orbit with  $i = 56^\circ$ ). After purchasing it, the new owner (Hughes) attempted a novel maneuver: the satellite was sent on two revolutions around the Moon ( $r_a = 488,000$  km,  $T = 15$  day, see the Luna-3 satellite). It then returned to a geostationary orbit and became HGS-1 (Hughes Global Services), before being renamed PAS-22. The replacement, AsiaSat-3S, was inserted into the wrong orbit on 21 March 1999:  $h_p \approx 10,000$  km,  $h_a = h_{GS}$ ,  $i = 13^\circ$ . Using its thrust motors, it was then moved into GEO orbit.

Another example of successful recovery, although less spectacular since it was carried out remotely while the satellite remained in GEO orbit, concerns the satellite Palapa-C1. Launched in 1996, it broke down in 1998. The manufacturer bought it back, repaired it under the name of HGS-3, then resold it to Turkey under the name of Anatolia-1, having displaced it in longitude. In 2002, Turkey sold it on to Pakistan, whence it became PakSat-1, but without changing place.

<sup>88</sup>US military GEO satellites are:

- LES (Lincoln Experimental Satellite in GEO orbit from LES-5 (launched in 1967) to LES-9 (in 1976).
- DSCS (Defense Satellite Communications System) and WGS (Wideband Global Satcom). Launched since 1971, their parking longitudes are over the Americas. In 2003, launch of DSCS-3A3 (USA-167) and DSCS-3B6 (USA-170); in 2007, WGS-1 (USA-195); in 2009, WGS-2 (USA-204) and WGS-3 (USA-211); in 2012, WGS-4 (USA-233).
- The TDRS satellites (Tracking and Data Relay Satellite) of the TDRSS series (TDRS System) are launched at intervals of 2–5 years. The first were launched by the US space shuttle, like TDRS-1 in 1983 (STS-6), or TDRS-2, lost in the explosion of Challenger in 1986, up to TDRS-7 in 1995 (STS-70). TDRS-8 was launched directly in 2000, as were TDRS-9 and -10 in 2002.
- The Milstar satellites (Military Strategic and Tactical Relay System), since 1994, then the AEHF satellites (Advanced Extreme High Frequency Satellite), like AEHF-



Soviet series Luch (with Kosmos-2054 and Luch-1, where *luch* means “light beam” in Russian) and Raduga (up to Raduga-32, where *raduga* means “rainbow”), and the Chinese satellites is the series STTW (with China-26).

The first high-speed data transmission by laser was carried out in November 2001 between the European GEO satellite Artemis, launched just before for this purpose, and the French LEO satellite SPOT-4. This prefigured transmissions between LEO satellites via a GEO satellite as intermediary. In December 2005, the first two-way link was made between Artemis and the Japanese satellite OICETS (Optical Inter-orbit Communications Engineering Test Satellite, renamed Kirari, meaning “glint, sparkle”), launched in August 2005 on an LEO orbit at  $h = 605$  km (see Fig. 9.36).

### HEO Telecommunications

The most commonly used HEO orbit is the one adopted by Soviet then Russian satellites, namely, the Molniya orbit,<sup>89</sup> since Kosmos-41 in 1964. The number of satellites launched in these orbits is staggering: 91 for Molniya-1, from Molniya-1-01 in 1965 to Molniya-1-91 in 1998, 17 for Molniya-2, from Molniya-2-01 in 1971 to Molniya-2-17 in 1977, and 53 for the current series Molniya-3, from Molniya-3-01 in 1974 to Molniya-3-53 in 2003.

The satellites in these three series have the same orbit, to within a few tens of kilometers<sup>90</sup>:  $h_p \approx 500$  km,  $h_a \approx 40,000$  km,  $i = 63^\circ$  (critical inclination). The period is 12 h (half a sidereal day):  $T = 717.7$  min,  $a = 26,553$  km,  $e$  between 0.72 and 0.75. The argument of the perigee is  $\omega = -90^\circ$ , which means that the perigee is located in the southern hemisphere, region of the Earth that the satellite overflies very quickly. On the other hand, at the apogee, the satellite is almost stationary for 9 h, when it is above Russia.

---

1 (USA-214) launched in 2010, are specialised in data transmission at ever higher rates. They are known to be in geostationary orbit, but apart from that, little else is known.

<sup>89</sup> *Molniya* means “lightning” in Russian. This refers to the fact that the satellite moves “as fast as lightning” at the perigee of its orbit. However, the main feature sought of this kind of satellite is to be slow at the apogee, when it overflies Russia! Now how do we say “snail” in Russian?

<sup>90</sup> As an example, here are the characteristics of several Molniya orbits with the launch date of the satellite, using the notation  $[h_p/h_a/i]$  (altitudes in kilometer, angles in degrees): Molniya-1-01 (23 April 1965) [538/39300/65.5]; Molniya-2-01 (25 November 1971) [516/39553/65.0]; Molniya-3-01 (21 March 1974) [250/40095/64.1]; Molniya-3-50 (8 July 1999) [464/39889/62.8]; Molniya-3-51 (20 July 2001) [407/40831/62.9]; Molniya-3-52 (25 October 2001) [615/40658/62.9]; Molniya-3-53 (19 June 2003) [637/39709/62.8].



**Молния** ( **МОЛНИЯ** )  
 Elliptical orbit - Gr. track

Recurrence = [ 2; +0; 1] 2

>>>> Time span shown: 1440.0 min = 1.00 day

TIME MARKER

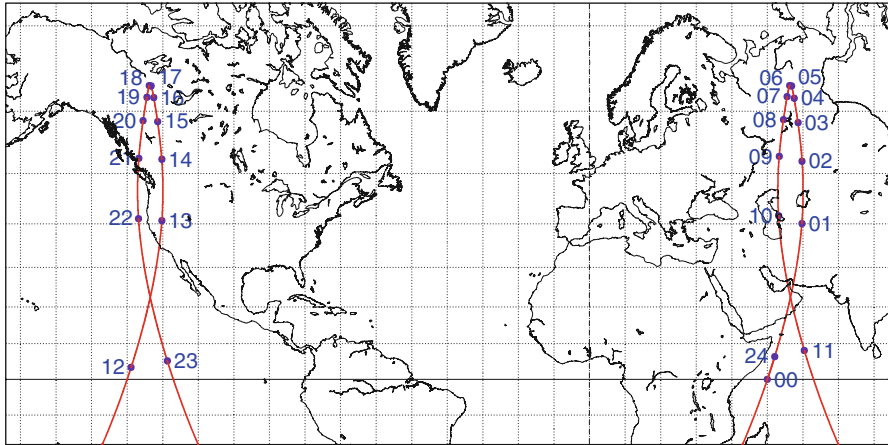
Equiv. altit. = 20174.7 km      a = 26552.865 km

CRITICAL Incln. = 63.41 °      e = 0.750000

Period = 717.72 min \* rev/day = 2.01

h\_a = 40089 km; h\_p = 260 km; arg. perigee = +270.00 °

Time marker: one point every 60.0 minutes



Projection: Mercator

Property: Conformal

⊕ T.:Cylindrical - Graticule: 10°

PC: 0.0 ° ; 0.0 ° /ZC: 40.0 ° N; 40.0 ° W

Aspect: Direct > zoom : 1.45

{5.3} [+90.0/ +0.0/ -90.0] [-] PZ-90

Longitude / Initialisation:

Asc. Node: 50.00 °

Apogee : 56.53 °

Ιξίων

MC ★ LMD

Ατλας

FIG. 9.28 : Ground track of the elliptical orbit of a Molniya satellite over 1 day. Time given in hours from 00 to 24, where 00 corresponds to the first ascending node, here at longitude 50° E. Times are given from 00 to 11 in the first revolution and from 12 to 23 in the second. Note that 24 appears slightly after 00. Indeed, the ground track is represented over 24 h, and the satellite, with period half a sidereal day, has then moved through slightly more than two revolutions in one mean day. The satellite is effective for Russian communications between the times denoted 01 and 10, i.e., for a period of 9 h.



This fundamental property is illustrated in Figs. 9.28 and 4.4 and Examples 4.1 and 4.2. The Molniya orbit and its ground track are shown in Figs. 9.29 and 9.30.

This orbit is at the critical inclination, which fixes the position of the perigee (and the apogee). Furthermore, the orbit is recurrent with a cycle of 1 day: the ground track passes through the same point every day. With three regularly spaced satellites on the same orbit, one almost achieves the equivalent of a geostationary satellite for the regions close to the ground track at apogee, each satellite being operational for 8 h. This is a judicious method for solving the problem of geosynchronicity at high latitudes.

The choice of a half-day period implies that one revolution in two is unusable for communications (since the apogee is once over Russia and once over Canada during the day). This allows a lower apogee than if the period were diurnal (as for Tundra or Supertundra).

The Russian communications satellites Meridian<sup>91</sup> (with a strong military component) are a modernised version of Molniya-3, also on the Molniya orbit. The US military satellites SDS (Space Defense System), from SDS-1 in 1976 to SDS-7 (USA-21) in 1987, follow Molniya orbits.

The Tundra and Supertundra orbits, shown in Fig. 9.31 and discussed in Chap. 7, are much less widely used. The constellation SD-Radio, which provides radio transmissions for American road users, is in a Tundra orbit. With its three satellites Sirius-1, -2, and -3, it constitutes the only operational examples of satellites in non-Molniya HEO orbit. The perigee of these two orbits is high, well above the Van Allen radiation belts. This is not so for the Molniya orbits, where satellites cross this belt on every revolution, an ordeal for electronic equipment. The planned orbit for the Sycomores satellites (*Système de Communications avec des Mobiles Reliés par Satellites*) is also a geosynchronous orbit, with  $a = 42,163.9$  km,  $e = 0.346$  (or  $h_p = 21,205$  km and  $h_a = 50,366$  km).

The following list of orbits concerns only those projects with some chance of realisation. Orbital and recurrence characteristics are given in Chap. 11.

The Loopus orbit,  $a = 30,000$  km,  $e = 0.6$  (see Fig. 9.33), lies outside the radiation belts. The period of the satellite is  $3/5$  of a day ( $T = 861.526$  min).

The US project VIRGO (or VirtualGeo, Virtual Geostationary) uses HEO orbits with a period of 8 h (exactly one third of a sidereal day), with  $a = 20,261$  km,  $e = 0.6458$ ,  $i = 63.4^\circ$  (see Fig. 9.32). As for Molniya, a VIRGO constellation effectively plays the role of a geostationary satellite.

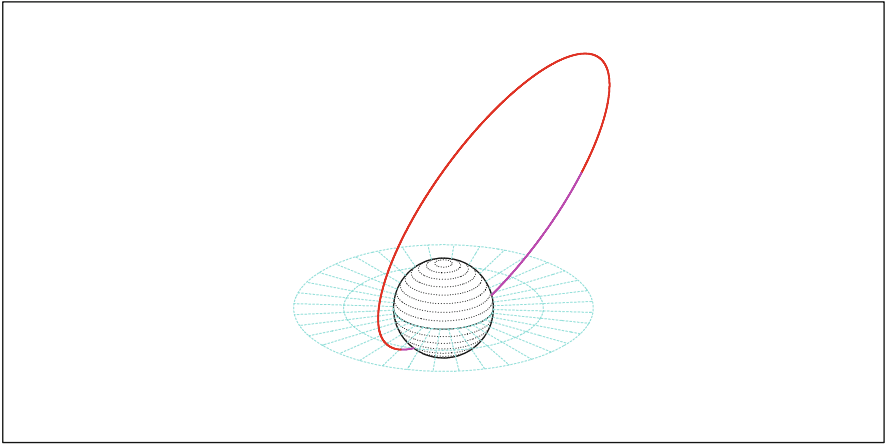
---

<sup>91</sup>Launch dates: Meridian-1 on 24 December 2006; Meridian-2 on 20 May 2009, launch failed; Meridian-3 on 11 February 2010; Meridian-4 on 4 May 2011; Meridian-5 on 23 December 2011, failed to reach orbit; Meridian-6 on 14 November 2012.

**Molniya** ( **Молния** )  
Orbit (Celestial ref.) [Galilean]

Equiv. altit. = 20174.7 km      a = 26552.857 km  
CRITICAL Incln. = 63.43 °      e = 0.750000  
Period = 717.72 min \* rev/day = 2.01  
h\_a = 40089 km; h\_p = 260 km; arg. perigee: +270.00 °

>>>> Time span shown: 1440.0 min = 1.00 day



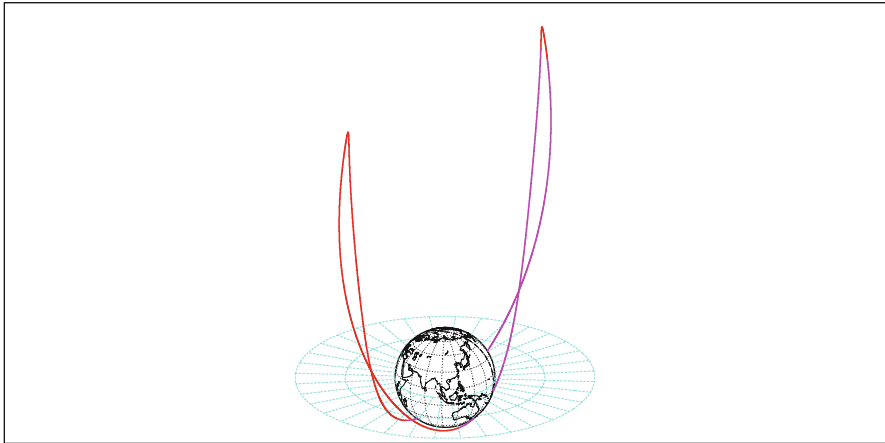
Projection: Orthographic      Project. centre: 25.0 ° N; 104.0 ° E      Longitude / Initialisation:      *Ιξίων*  
Property: none      Aspect: Oblique      Asc. Node: 60.71 °      MC ★ LMD  
⊕ T.:Azimuthal - Graticule: 10°      {-} [ -90.0/ +65.0/ -14.0] [-]      GRIM5-C1      *Ατλας*

**Molniya** ( **Молния** )  
Orbit - ref.: Earth

Equiv. altit. = 20174.7 km      a = 26552.857 km  
CRITICAL Incln. = 63.43 °      e = 0.750000  
Period = 717.72 min \* rev/day = 2.01  
h\_a = 40089 km; h\_p = 260 km; arg. perigee: +270.00 °

Recurrence = [ 2; +0; 1] 2

>>>> Time span shown: 1440.0 min = 1.00 day



Projection: Orthographic      Project. centre: 24.0 ° N; 104.0 ° E      Longitude / Initialisation:      *Ιξίων*  
Property: none      Aspect: Oblique      Asc. Node: 60.71 °      MC ★ LMD  
⊕ T.:Azimuthal - Graticule: 20°      {4.2} [ -90.0/ +66.0/ -14.0] [-]      GRIM5-C1      Apogee : 67.24 °      *Ατλας*

FIG. 9.29 : Representation of the HEO orbit of a Molniya satellite over 1 day. Upper: In a Galilean frame. Lower: In a terrestrial frame.

**Molniya** ( **Μολνιγια** )

Elliptical orbit - Gr. track

Recurrence = [ 2; +0; 1] 2

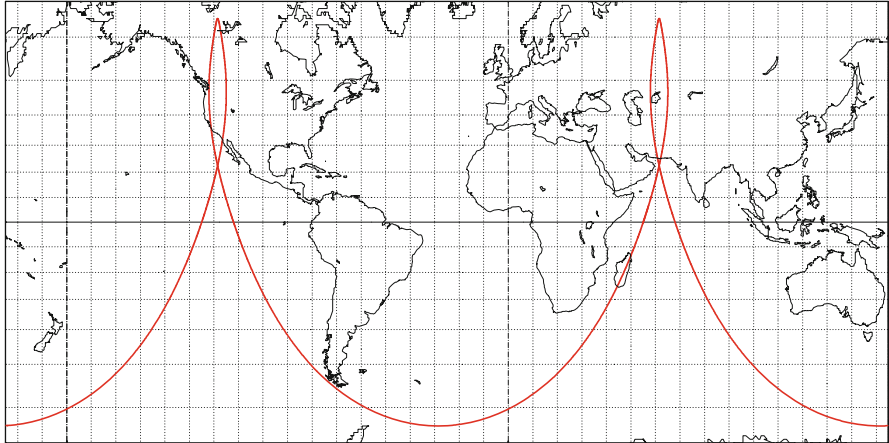
&gt;&gt;&gt;&gt; Time span shown: 1440.0 min = 1.00 day

Equiv. altit. = 20174.7 km      a = 26552.863 km

CRITICAL Incln. = 63.42 °      e = 0.750000

Period = 717.72 min      \* rev/day = 2.01

h\_a = 40089 km; h\_p = 260 km; arg. perigee: +270.00 °



Projection: Mercator

Property: Conformal

⊕ T.:Cylindrical - Graticule: 10°

Project. centre: 0.0 ° ; 25.0 ° W

Aspect: Direct

{4.2} [ +90.0/ +0.0/ -65.0] [-] GRIM5-C1

Longitude / Initialisation:

Asc. Node: 55.00 °

Apogee : 61.53 °

Ιξλων

MC \*LMD

Ατλας

**Molniya** ( **Μολνιγια** )

Elliptical orbit - Gr. track

Recurrence = [ 2; +0; 1] 2

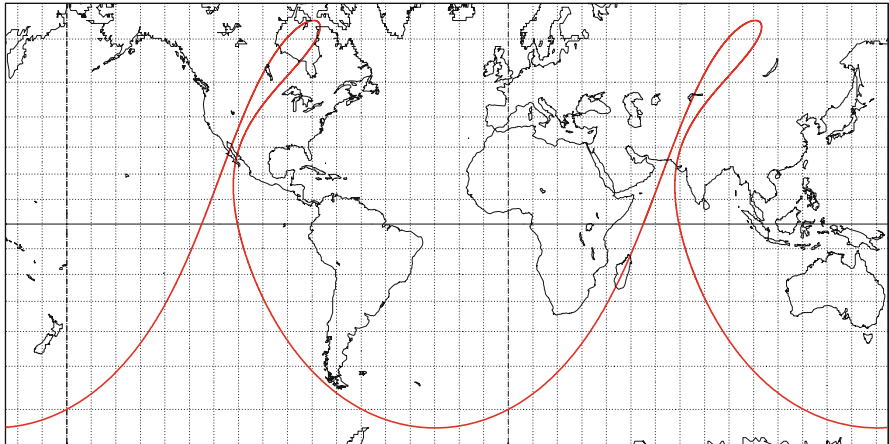
&gt;&gt;&gt;&gt; Time span shown: 1440.0 min = 1.00 day

Equiv. altit. = 20174.7 km      a = 26552.857 km

CRITICAL Incln. = 63.43 °      e = 0.750000

Period = 717.72 min      \* rev/day = 2.01

h\_a = 40089 km; h\_p = 260 km; arg. perigee: +290.00 °



Projection: Mercator

Property: Conformal

⊕ T.:Cylindrical - Graticule: 10°

Project. centre: 0.0 ° ; 25.0 ° W

Aspect: Direct

{4.2} [ +90.0/ +0.0/ -65.0] [-] GRIM5-C1

Longitude / Initialisation:

Asc. Node: 55.00 °

Apogee : 98.37 °

Ιξλων

MC \*LMD

Ατλας

FIG. 9.30 : Ground track of the HEO orbit of a Molniya satellite over 1 day, for two different positions of the perigee.

**Tundra**

Elliptical orbit - Gr. track

Recurrence = [ 1; +0; 1] 1

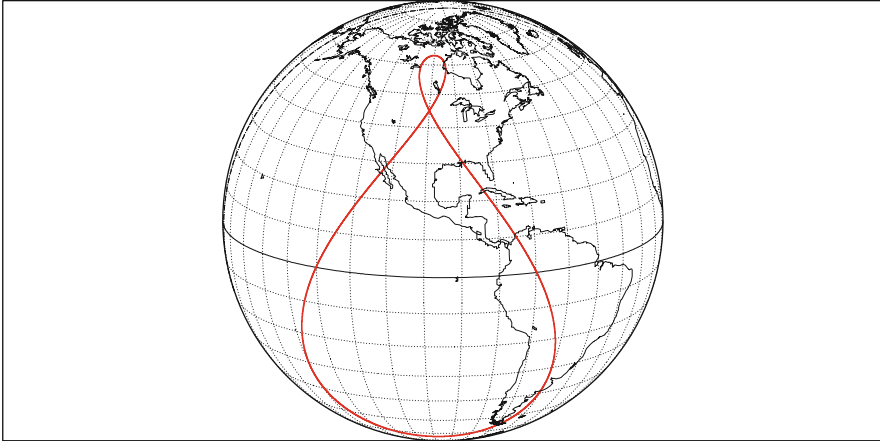
>>>> Time span shown: 1440.0 min = 1.00 day

Equiv. altit. = 35785.3 km      a = 42163.391 km

CRITICAL Incln. = 63.43 °      e = 0.266800

Period = 1436.04 min \* rev/day = 1.00

h\_a = 47034 km; h\_p = 24536 km; arg. perigee: +270.00 °



Projection: Orthographic

Property: none

⊕ T.:Azimuthal - Graticule: 10°

Project. centre: 15.0 ° N; 95.0 ° W

Aspect: Oblique

{4.2} [-90.0/ +75.0/-175.0] [-] EGM96

Longitude / Initialisation:

Asc. Node: -69.80 °

Apogee : -100.00 °

*Ιξίων*

MC \* LMD

*Ατλας*

**Supertundra**

Elliptical orbit - Gr. track

Recurrence = [ 1; +0; 1] 1

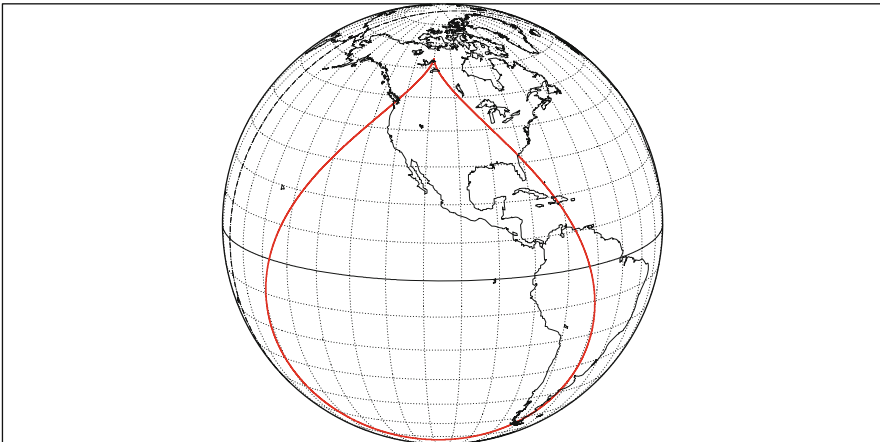
>>>> Time span shown: 1440.0 min = 1.00 day

Equiv. altit. = 35785.1 km      a = 42163.199 km

CRITICAL Incln. = 63.43 °      e = 0.423000

Period = 1436.03 min \* rev/day = 1.00

h\_a = 53620 km; h\_p = 17950 km; arg. perigee: +270.00 °



Projection: Orthographic

Property: none

⊕ T.:Azimuthal - Graticule: 10°

Project. centre: 15.0 ° N; 105.0 ° W

Aspect: Oblique

{4.2} [-90.0/ +75.0/-165.0] [-] EGM96

Longitude / Initialisation:

Asc. Node: -63.02 °

Apogee : -110.00 °

*Ιξίων*

MC \* LMD

*Ατλας*

FIG. 9.31 : Ground track of a satellite in a Tundra or Supertundra (HEO) orbit, over 1 day.

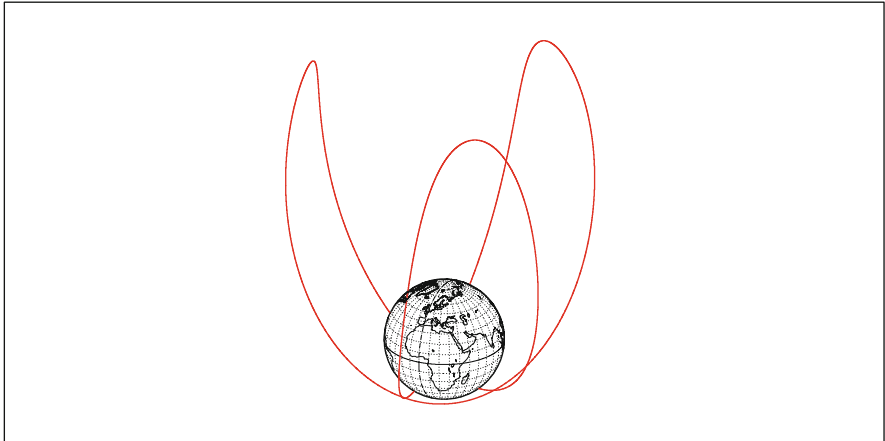
**VirtualGeo (VIRGO)**

Orbit - ref.: Earth

Recurrence = [ 3; +0; 1] 3

>>>> Time span shown: 1440.0 min = 1.00 day

Equiv. altit. = 13882.1 km      a = 20260.188 km  
 CRITICAL Incln. = 63.43 °      e = 0.660850  
 Period = 478.36 min \* rev/day = 3.01  
 h\_a = 27271 km; h\_p = 493 km; arg. perigee: +270.00 °



Projection: Orthographic	Project. centre: 25.0 ° N; 25.0 ° E	Longitude / Initialisation:	<i>Ιξίων</i>
Property: none	Aspect: Oblique	Asc. Node: 0.00 °	MC * LMD
⊕ T.:Azimuthal - Graticule: 10°	{4.2} [-90.0/ +65.0/ +65.0] [-] EGM96	Apogee : 36.78 °	<i>Ατλας</i>

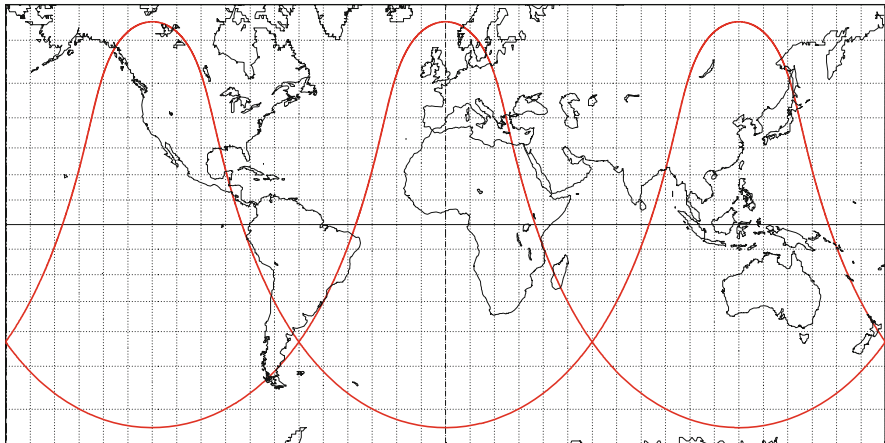
**VirtualGeo (VIRGO)**

Elliptical orbit - Gr. track

Recurrence = [ 3; +0; 1] 3

>>>> Time span shown: 1440.0 min = 1.00 day

Equiv. altit. = 13882.1 km      a = 20260.193 km  
 CRITICAL Incln. = 63.42 °      e = 0.660850  
 Period = 478.36 min \* rev/day = 3.01  
 h\_a = 27271 km; h\_p = 493 km; arg. perigee: +270.00 °



Projection: Mercator	Project. centre: 0.0 ° ; 0.0 °	Longitude / Initialisation:	<i>Ιξίων</i>
Property: Conformal	Aspect: Direct	Asc. Node: -36.78 °	MC * LMD
⊕ T.:Cylindrical - Graticule: 10°	{4.2} [+0.0/ +0.0/ +0.0] [-] EGM96	Apogee : 0.00 °	<i>Ατλας</i>

FIG. 9.32 : HEO orbit and ground track of a satellite in the VIRGO constellation, over 1 day.

**Loopus**

Orbit - ref.: Earth

Recurrence = [ 2; -1; 3] 5

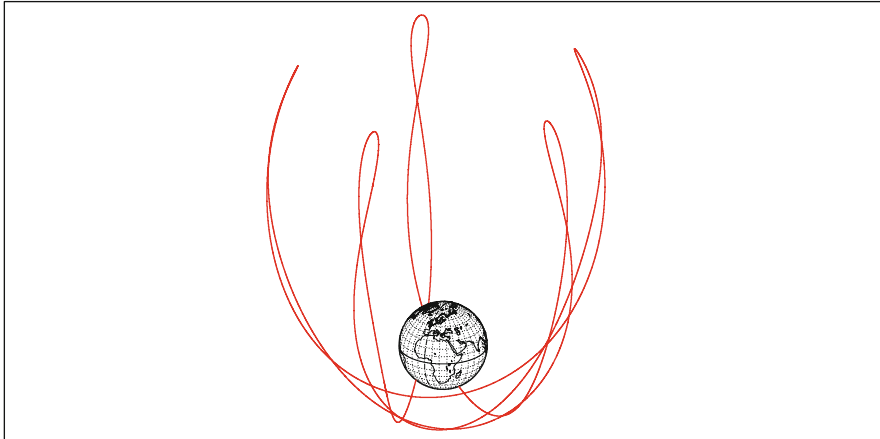
>>>> Time span shown: 4320.0 min = 3.00 days

Equiv. altit. = 23613.3 km      a = 29991.447 km

CRITICAL Incln. = 63.43 °      e = 0.600000

Period = 861.53 min \* rev/day = 1.67

h\_a = 41608 km; h\_p = 5618 km; arg. perigee: +270.00 °



Projection: Orthographic

Property: none

⊕ T.:Azimuthal - Graticule: 10°

Project. centre: 25.0 ° N; 25.0 ° E

Aspect: Oblique

{4.2} [ -90.0/ +65.0/ +65.0] [-] EGM96

Longitude / Initialisation:

Asc. Node: 0.00 °

Apogee : -2.61 °

Ιξίων

MC ★ LMD

Ατλας

**Loopus**

Elliptical orbit - Gr. track

Recurrence = [ 2; -1; 3] 5

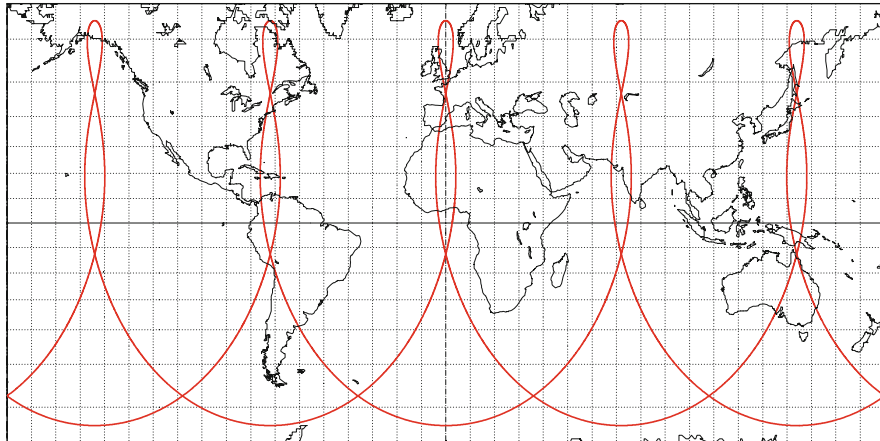
>>>> Time span shown: 4320.0 min = 3.00 days

Equiv. altit. = 23613.3 km      a = 29991.447 km

CRITICAL Incln. = 63.43 °      e = 0.600000

Period = 861.53 min \* rev/day = 1.67

h\_a = 41608 km; h\_p = 5618 km; arg. perigee: +270.00 °



Projection: Mercator

Property: Conformal

⊕ T.:Cylindrical - Graticule: 10°

Project. centre: 0.0 ° ; 0.0 °

Aspect: Direct

{4.2} [ +0.0/ +0.0/ +0.0] [-] EGM96

Longitude / Initialisation:

Asc. Node: 2.61 °

Apogee : 0.00 °

Ιξίων

MC ★ LMD

Ατλας

FIG. 9.33 : HEO orbit and ground track of a satellite in the Loopus constellation, over 3 days.

The COBRA project (Communications Orbiting Broadband Repeating Arrays), with the same orbital characteristics as VIRGO, makes judicious use of the argument of the perigee, which is not taken equal to  $270^\circ$ . With two orbits separated by  $40^\circ$  and the argument of the perigee  $\omega = 270^\circ \pm 38^\circ$ , we obtain a “teardrop” ground track (see Fig. 9.34).

The constellation project FLOWER uses a similar orbit to the last, with  $a = 22,883.8$  km,  $e = 0.65583$ .

The Ellipso Borealis orbit is highly original, as we have already seen: it is both Sun-synchronous and at the critical inclination. The relevant parameters are  $h_p = 633$  km,  $h_a = 7,605$  km,  $i = 116.6^\circ$ ,  $\omega = -90^\circ$ , and it has a period of 3 h ( $T = D_{\text{sid}}/8$ ) (see Fig. 10.7). The Ellipso project includes an HEO constellation, Borealis, containing ten satellites in two planes, together with a constellation, Concordia, of four (or perhaps 7) satellites in equatorial orbit with  $h = 8,050$  km and  $i = 0.0^\circ$  ( $T = J_{\text{sid}}/5$ ). The project has been shelved since 2003.

The project FLOWER CfTM (Constellation for Telemedicine) is in the same spirit as Ellipso Borealis, with parameters  $h_p = 3,094$  km,  $h_a = 9,709$  km,  $i = 116.6^\circ$ , and a period of 4 h.

### MEO Telecommunications

The JOCOS orbit (Juggler Orbit Constellation, since it gives the impression of juggling with the satellites), also known as the WEST orbit, is circular with  $h = 13,900$  km,  $i = 75^\circ$ , and period 8 h (one third of a sidereal day). The constellation project WEST (Wideband European Satellite Telecommunication) involves nine satellites on this MEO orbit, together with two GEO satellites (see Fig. 9.35).

Odyssey and ICO were to operate in a rarely occupied range of altitudes between MEO and LEO. The Odyssey project, abandoned in 2000, was a constellation containing three planes of four satellites,  $h = 10,354$  km,  $i = 50^\circ$ . The ICO constellation (Intermediate Circular Orbit), planned to have two planes of five satellites with  $h = 10,390$  km and  $i = 45^\circ$ , was replaced by a geostationary, ICO-G1, and a ground network.

### LEO Telecommunications

Communications using LEO satellites always require a constellation. For telephone communications, the advantage of LEO constellations is the very short response time: the journey time of the signal transiting via a GEO satellite is about 250 ms, and this quarter of a second is sometimes considered to be a nuisance. However, this is not a big enough advantage to ensure the



**COBRA**

Two orbits - ref.: Earth

Recurrence = [ 3; +0; 1] 3

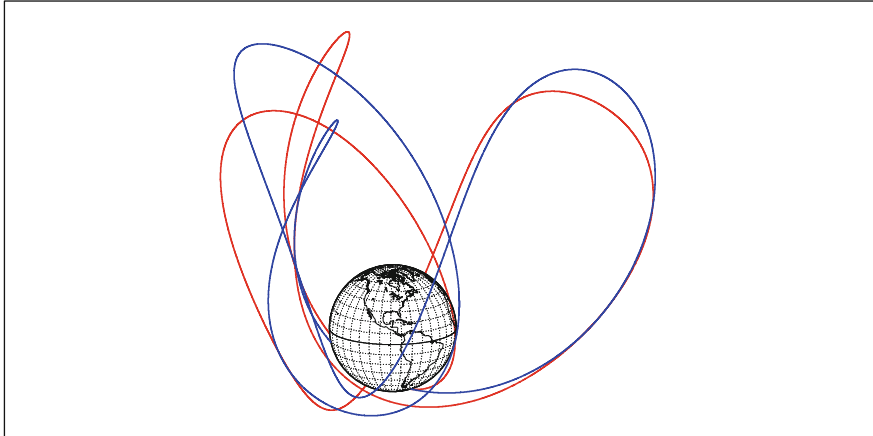
>>>> Time span shown: 1440.0 min = 1.00 day

Equiv. altit. = 13882.7 km      a = 20260.852 km

CRITICAL Incln. = 63.43 °      e = 0.645900

Period = 478.39 min \* rev/day = 3.01

h\_a = 26969 km; h\_p = 796 km; arg. per.: +232.0 ° / +308.0 °



Projection: Orthographic

Property: none

⊕ T.:Azimuthal - Graticule: 10°

Project. centre: 15.0 ° N; 88.0 ° W

Aspect: Oblique

{4.2} [ -90.0/ +75.0/+178.0] [-] EGM2008

Longitude / Initialisation:

Asc. Node: 0.0 ° / 40.0 °

Apogee: 166.6 ° / 133.4 °

*Ιξίων*

MC \* LMD

*Ατλας*

**COBRA**

Two elliptical orbits - Gr. track

Recurrence = [ 3; +0; 1] 3

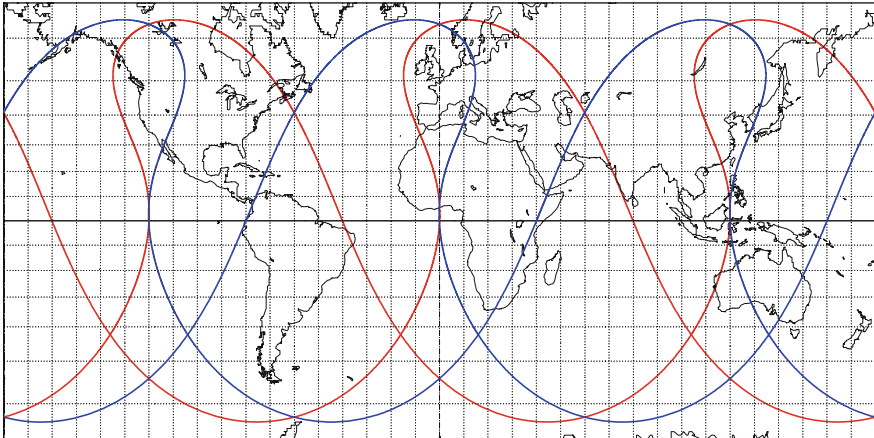
>>>> Time span shown: 1440.0 min = 1.00 day

Equiv. altit. = 13882.7 km      a = 20260.855 km

CRITICAL Incln. = 63.42 °      e = 0.645900

Period = 478.39 min \* rev/day = 3.01

h\_a = 26969 km; h\_p = 796 km; arg. per.: +232.0 ° / +308.0 °



Projection: Mercator

Property: Conformal

⊕ T.:Cylindrical - Graticule: 10°

Project. centre: 0.0 ° ; 0.0 °

Aspect: Direct

{4.2} [ +0.0/ +0.0/ +0.0] [-] EGM2008

Longitude / Initialisation:

Asc. Node: 0.0 ° / 40.0 °

Apogee: 166.6 ° / 133.4 °

*Ιξίων*

MC \* LMD

*Ατλας*

FIG. 9.34 : HEO orbits and ground tracks of two satellites in the COBRA constellation, over 1 day. Normal (red) curve for the first satellite, bold (blue) curve for the second.

**WEST-JOCOS**

Orbit - ref.: Earth

Recurrence = [ 3; +0; 1] 3

>>>> Time span shown: 1440.0 min = 1.00 day

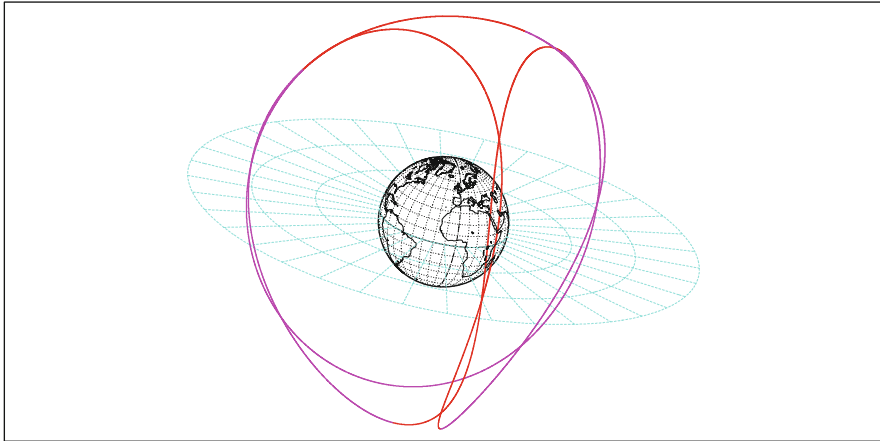
Altitude =13889.0 km

a =20267.139 km

Inclination = 75.00 °

Period = 478.63 min \* rev/day = 3.01

Equat. orbital shift =13358.3 km ( 120.0 °)



Projection: Orthographic

Project. centre: 20.0 ° N; 15.0 ° W

Asc. Node: 0.00 °

Property: none

Aspect: Oblique

Ιξίωv

MC \* LMD

⊕ T.:Azimuthal - Graticule: 10°

{4.2} [ -90.0/ +70.0/+105.0] [ -12] GRIM5-S1

Ατλας

**WEST-JOCOS**

Orbit - Ground track

Recurrence = [ 3; +0; 1] 3

>>>> Time span shown: 1440.0 min = 1.00 day

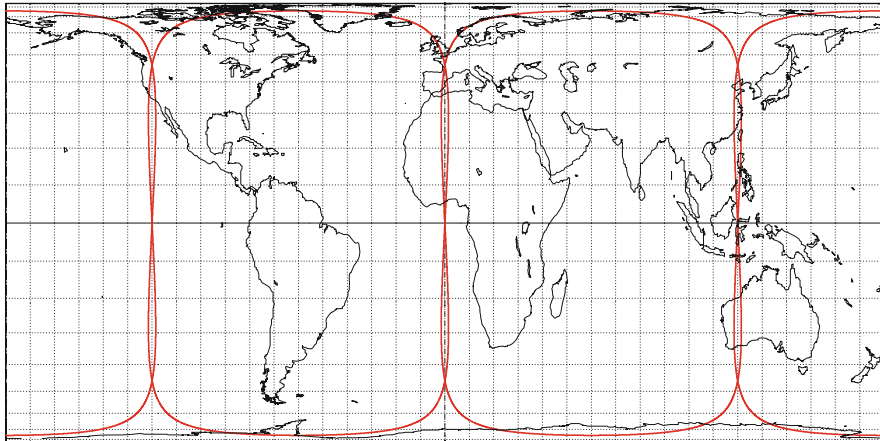
Altitude =13889.0 km

a =20267.139 km

Inclination = 75.00 °

Period = 478.63 min \* rev/day = 3.01

Equat. orbital shift =13358.3 km ( 120.0 °)



Projection: Behrmann

Project. centre: 0.0 ° ; 0.0 °

Asc. Node: 0.00 °

Property: Equal area

Aspect: Direct

App. inclin. = 94.41 °

Ιξίωv

MC \* LMD

⊕ T.:Cylindrical - Graticule: 10°

{4.2} [ +0.0/ +0.0/ +0.0] [-] GRIM5-S1

Ατλας

FIG. 9.35 : MEO orbit and ground track of a satellite in the JOCOS-WEST constellation, over 1 day.



FIG. 9.36 : Artist's view of the laser link between the Japanese satellite OICETS and the European satellite Artemis. Credit: JAXA.

success of a commercial venture. The difficulties encountered by Iridium<sup>92</sup> and GlobalStar clearly demonstrate this. The following satellite constellations are currently operating (or have failed):

- Orbcomm, 35 satellites (3 planes of 8),  $h = 810$  km,  $i = 45.0^\circ$ .
- Iridium, 88 satellites (6 planes of 11),  $h = 780$  km,  $i = 86.4^\circ$ .
- GlobalStar, 52 satellites (8 planes of 6),  $h = 1,410$  km,  $i = 52.0^\circ$ .
- GlobalStar NG, 52 satellites (8 planes of 6),  $h = 1,410$  km,  $i = 52.0^\circ$ .

---

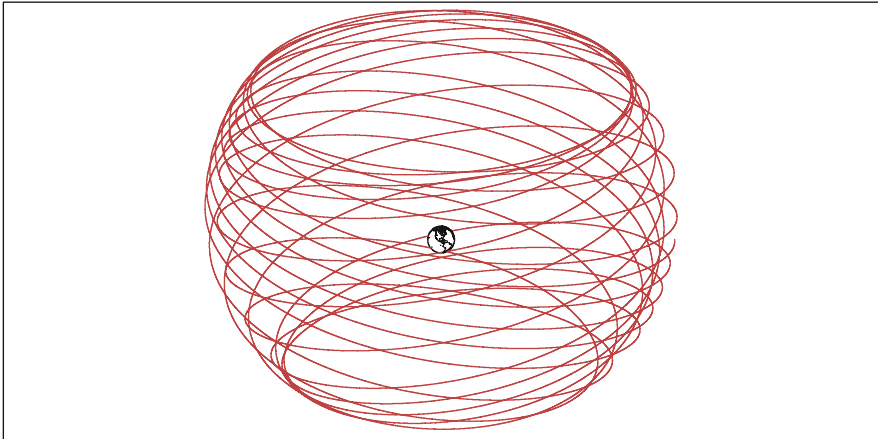
<sup>92</sup>Iridium, set up by Motorola, is a telephone and data transfer system for regions not covered by mobile phone networks. Faced with commercial failure, the first reaction in 2000 was to remove all the satellites from orbit. However, in the end, the system was taken over by the US Department of Defense. It is presently run by a private organisation supplying military and institutional customers for the main part. Originally, the constellation was to include 77 satellites, whence the name Iridium, which is the chemical element Ir with atomic number 77.

**Vela-4**

Orbit - ref.: Earth

>>> Time span shown: 30.00 days

Equiv. altit. = 103052 km      a = 109430.0 km  
 Inclination = 40.80 °      e = 0.100000  
 Period = 6004.28 min    \* rev/day = 0.24  
 h\_a = 113995 km; h\_p = 92109 km; arg. perigee: +255.00 °



Projection: Orthographic  
 Property: none  
 ⊕ T.:Azimuthal - Graticule:360°

Project. centre: 25.0 ° N; 90.0 ° W  
 Aspect: Oblique  
 {4.2} [-90.0/ +65.0/-180.0] [-] EGM2008

Longitude / Initialisation:  
 Asc. Node: 0.00 °  
 Apogee : -110.19 °

*Ιξίων*  
 MC ★ LMD  
 Ατλας

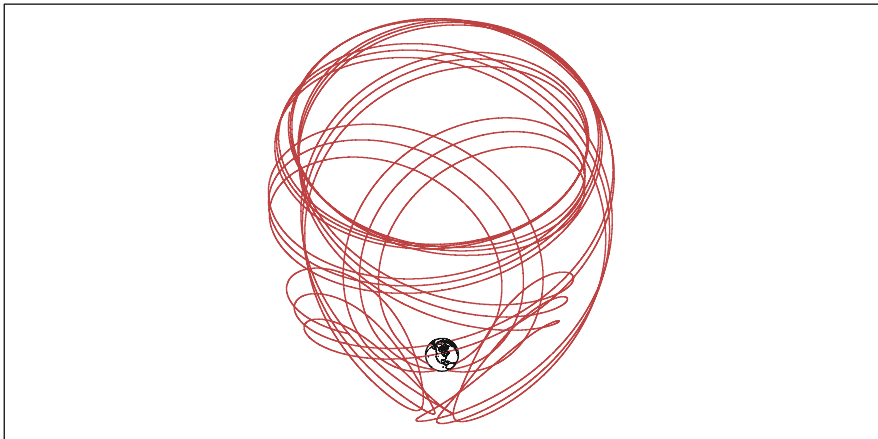
**Chandra (CXO)**

Orbit - ref.: Earth

Recurrence = [ 0;+23; 61] 23

2009 09 05 00:00:00 UTC >>> 23.00 days

Equiv. altit. = 74409.4 km      a = 80787.492 km  
 Inclination = 65.79 °      e = 0.767080  
 Period = 3808.75 min    \* rev/day = 0.38  
 h\_a = 136397 km; h\_p = 12457 km; arg. perigee: +275.57 °



Projection: Orthographic  
 Property: none  
 ⊕ T.:Azimuthal - Graticule:360°

Project. centre: 48.0 ° N; 95.0 ° W  
 Aspect: Oblique  
 {4.2} [-90.0/ +42.0/-175.0] [-] EGM2008

[NORAD] 2009 09 05 13:20:31 UTC//R= 531  
 Asc. Node: -118.70 ° [05:26 LMT]  
 Apogee : -105.29 °

*Ιξίων*  
 MC ★ LMD  
 Ατλας

FIG. 9.37 : Representation of orbits over long periods of time. Upper: Vela-4 satellite over 30 days. Lower: Chandra over 23 days.



Back-up satellites are included in the total number of satellites belonging to each constellation.<sup>93</sup> The Teledesic and SkyBridge projects have been shelved.<sup>94</sup>

The Russian system Gonets-D1 (*gonets* meaning “messenger”) is the commercial version of the military system Strela-3 (*strela* meaning “arrow”). It comprises<sup>95</sup> 48 satellites in 6 planes of 8, with  $h = 1,400$  km,  $i = 82.5^\circ$ .

## Passive Communication

We end this section with a quick glance at the “prehistory” of telecommunications, with the first attempts at transmission in passive mode. As their name would suggest, the satellites Echo-1 and -2 were launched as passive telecommunications relays. As one might imagine, the results were not very convincing and this experimental system was dropped. However, these two satellites were originally intended for space geodesy.

We should also mention another attempt to create a passive space communications system. The idea was to place a ring in orbit around the Earth to reflect radio waves. This was the US military experiment called Westford Needles.<sup>96</sup> The idea was to insert a package into orbit which, once opened, would

---

<sup>93</sup>Launch dates of the first and last satellites of each constellation:

(a) Orbcomm constellation (Machine to Machine Communications): Orbcomm-FM-1 and -FM-2 on 3 April 1995, launched with Microlab-1,  $h = 740$  km,  $i = 69.9^\circ$ ; Orbcomm-FM-3 and -FM-4 on 10 February 1998, launched with GFO-1,  $h = 830$  km,  $i = 108.0^\circ$ ; the other Orbcomm satellites were launched with  $i = 45.0^\circ$  in clusters of 8, starting with Orbcomm-FM-5 to -FM-12 on 23 December 1997 and ending with Orbcomm-FM-30 to -FM-36 on 4 December 1999, and supplemented by Orbcomm-FM-37 to -FM-41 on 19 June 2008.

(b) Iridium constellation: (beginning) Iridium-4 to -8 on 5 May 1997; (end of initial programme) Iridium-83 to -86 on 6 November 1998; (restart) Iridium-90 to -96 on 11 February 2002; Iridium-97 and -98 on 20 June 2002. The Iridium-Next constellation is planned for the same orbit.

(c) GlobalStar constellation: (beginning) GlobalStar-M001 to -M004 on 14 February 1998; (end) GlobalStar-M060 to -M064 on 8 February 2000; (supplement) GlobalStar-M065 to -M072 on 29 May and 20 October 2007, with  $h = 666$  km,  $i = 48.45^\circ$ .

(d) GlobalStar NG constellation (New Generation) or GlobalStar-2: (beginning) GlobalStar-M073 to -M078 on 19 October 2010; (current) GlobalStar-M093 to -M097 on 6 February 2013.

(e) Teledesic constellation: (demonstration satellite) Teledesic-1 on 26 February 1998.

<sup>94</sup>For Teledesic, the initial project, imagined by Microsoft in 1994, involved 840 active satellites (21 planes of 40), with altitude  $h = 700$  km. In 1997, the project was reduced to 288 satellites (12 planes of 24), with Sun-synchronous orbits at altitude  $h = 1,400$  km, then postponed indefinitely in 2002. Alcatel’s SkyBridge project for 80 satellites is no longer under consideration.

<sup>95</sup>To begin with, between 1992 and 2001, 12 satellites were sent up (6 planes of 2), Gonets-D1-1 to -12; then a further 36 satellites, but so far only one has been launched, namely Gonets-M-1, in 2005.

<sup>96</sup>First launched was the Westford-1 experiment on 21 October 1961, using the satellite Midas-4. This failed because the needles were not actually dispersed. The second experiment to be launched was Westford-2 on 9 May 1963, using the satellite Midas-7. This time the needles were coated with naphthalene and were regularly dispersed. These two satellites were in near-polar circular orbits at  $h = 3,600$  km.

distribute 480 million small copper needles (0.1 mm in diameter and 18 mm long, corresponding to half a wavelength at the frequency of 8 GHz used for transmission) along its trajectory. The experiment was severely criticised by astronomers who saw in this a source of optical and radio pollution. In the end, the needles constituted neither a reflector nor a pollutant.

## 9.2.9 Satellites for Astronomy and Astrophysics

### Astronomy and Astrometry

In most cases, astronomical missions are one-off experiments and the satellites are not systematically placed on the same orbits, as they might be for remote-sensing, for example. We shall discuss here several satellites for each region of the electromagnetic spectrum used in astronomy. Most of them are American and the remainder are mainly European.

NASA launched a programme of large orbiting observatories (Great Observatories Program), each in a specific region of the electromagnetic spectrum:

- For gamma rays ( $\gamma$  rays), the Gamma Ray Observer (GRO), renamed Compton.<sup>97</sup>
- For X rays, the Advanced X-ray Astrophysics Facility (AXAF), renamed Chandra.<sup>98</sup>
- In the visible part of the spectrum, the Hubble Space Telescope (HST), often simply called Hubble.<sup>99</sup>
- In the infrared region, the Space InfraRed Telescope Facility (SIRTF), renamed<sup>100</sup> the Spitzer Space Telescope (SST) or simply Spitzer, after its launch.

---

<sup>97</sup> *Arthur Holly Compton* (1892–1962) was an American physicist. His work on X rays led him to discover in 1923 the effect which now carries his name (interaction between matter and X rays). He also studied cosmic rays.

<sup>98</sup> *Subrahmanyan Chandrasekhar* (1910–1995) was an American astrophysicist of Indian birth. He carried out a great many theoretical studies on the internal structure of stars, publishing books that are often considered to be definitive on the subjects he treated, e.g., stellar evolution and white dwarfs, radiative transfer in stellar atmospheres (*Radiative Transfer*, 1950), hydrodynamics, black holes (*The Mathematical Theory of Black Holes*, 1983). The root “chand” means “Moon” or “bright” in Sanskrit.

<sup>99</sup> *Edwin Powell Hubble* (1889–1953) was an American astronomer. He produced a classification of extragalactic nebulae and, in 1928, established the law of spectral shifts, now known as the Hubble law, which says that the spectral shift of a galaxy (redshift) is proportional to its distance, thus confirming the hypothesis that the Universe is expanding. The constant of proportionality  $H_0$ , called the Hubble constant, is not precisely known and may even vary in time. It is measured in  $\text{km s}^{-1}$  per megaparsec. Its reciprocal, which has units of time, gives the age of the Universe to within an order of magnitude:  $1/H_0 \sim 10$  billion years.

<sup>100</sup> In honour of Lyman Spitzer Jr (1914–1957), the American astrophysicist who first suggested placing a large telescope in space.

These four missions were a considerable technological success. Each led to major scientific progress in its specific domain, see Figs. 9.39 and 9.40.

Concerning more modest missions, NASA's Explorer programme is well underway with three formats, depending on the budget: Medium Explorer (MIDEX), Small Explorer (SMEX), and University-class Explorer (UNEX).

In the following we outline this diversity of astronomical missions.

### *Cosmic Rays and Gamma Rays*

Gamma-ray astronomy began in 1961 with Explorer-11 (also called S-15),  $h_p = 480$  km,  $h_a = 1,460$  km,  $i = 29^\circ$ , which provided the first detection of gamma rays from space. This was followed by OSO-3 and OSO-7, both on the orbit  $h = 550$  km,  $i = 33^\circ$ , then Explorer-48 (SAS-2),  $h = 526$  km,  $i = 1^\circ$ , not forgetting the Vela satellites discussed further below.

In this field of investigation, orbits are generally low and not highly inclined, as for the HEAO satellites (High Energy Astrophysical Observatory), HEAO -1, -2 (renamed Einstein), and -3,  $h \approx 500$  km,  $i = 23^\circ$ ,  $23^\circ$ , and  $44^\circ$ , or the satellite HETE-2 (High Energy Transient Experiment, Explorer-79),  $h = 615$  km,  $i = 2^\circ$ .

The Compton satellite (CGRO), launched on 5 April 1991 by STS-37 with  $h = 450$  km,  $i = 28.5^\circ$ , had a mass of 15 tonnes, including 7 tonnes of instruments. Great precautions were taken when it was deliberately de-orbited on 3 June 2000. The US Swift satellites,<sup>101</sup>  $h = 595$  km,  $i = 20.6^\circ$  and Fermi,<sup>102</sup>  $h = 552$  km,  $i = 25.6^\circ$ , and also the Italian satellite Agile,  $h = 538$  km,  $i = 2.5^\circ$ , have very similar orbits.

The European satellite Integral (International Gamma-Ray Astrophysics Laboratory), launched on 17 October 2002, is on an HEO orbit with  $a = 87,699$  km,  $e = 0.8204$  (or  $h_p = 9,400$  km,  $h_a = 153,300$  km),  $i = 57^\circ$  to  $67^\circ$ , and a period  $T = 71.8$  h =  $3D_{\text{sid}}$ . Figure 9.38 shows how the representation of the orbit changes from a classic ellipse in  $\mathfrak{R}$  to an elegant closed curve in the form of a lasso in  $\mathfrak{R}_T$ .

### *X Rays*

Certain orbits are like those seen above, i.e., low, with  $h \approx 550$  km, and with low inclination:  $i = 53^\circ$  for ROSAT;  $i = 4^\circ$  for BeppoSAX (*Satellite per Astronomia a raggi X*);  $i = 23^\circ$  for XTE (X-ray Timing Explorer, Rossi, or RXTE, Explorer-69);  $i = 38^\circ$  for HESSI (High-Energy Solar Spectroscopic Imager, SMEX-6, or Explorer-81), renamed RHESSI (Reuven Ramaty HESSI);

<sup>101</sup>Launch dates: Swift (MIDEX-3 or Explorer-84), for detection of gamma-ray bursts (GRB), on 20 November 2004; GLAST (Gamma-ray Large Area Space Telescope), renamed Fermi or FGRST (Fermi Gamma-Ray Space Telescope) after the launch on 11 June 2008; Agile (*Astro-rivelatore Gamma a Immagini Leggero*) on 23 April 2007.

<sup>102</sup>*Enrico Fermi* (1901–1954) was an Italian physicist. At the beginning of his career, he developed the theory of quantum statistical mechanics, which explains the properties of electrons in metals (Fermi–Dirac statistics). In nuclear physics, he devised a theory of the weak interaction ( $\beta$ -decay and neutrinos). In 1939, he emigrated to the USA, where he built the first atomic pile and contributed to the development of the first atomic bomb. He also studied galaxies with Chandrasekhar.



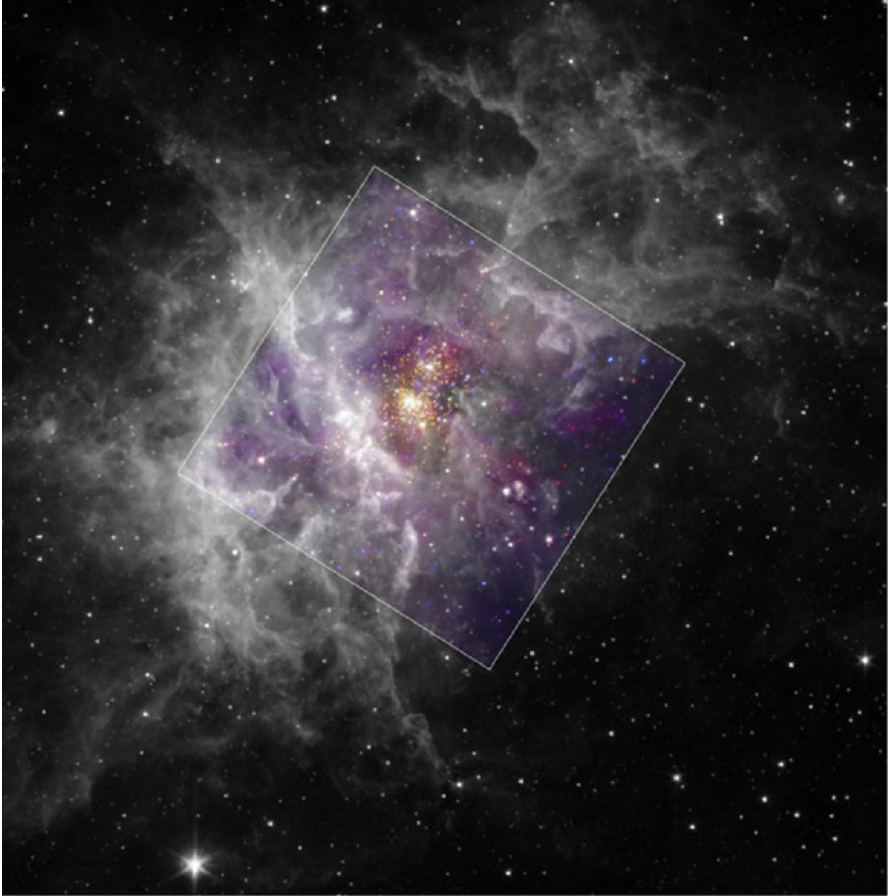


FIG. 9.39 : View made up from two images, one from Chandra and the other from Spitzer. The large format black and white photograph was obtained by the Spitzer space telescope in the infrared. It is completed in the center by a false colour photograph from the Chandra space telescope, which observes X-ray emissions. At the center is the Westerlund 2 cluster, surrounded by dust clouds forming a stellar nursery, with the name RCW 49 (20,000 light-years away in the constellation of Centaurus, southern hemisphere). Westerlund 2 is only 2 million years old and contains very bright and massive stars. The infrared signatures of protoplanetary disks can be identified in this star-forming region. Owing to the obscuring dust clouds, these stars cannot be observed by optical telescopes. The sides of the square Chandra image have length 50 light-years. Credit (images and caption): University of Liège, CXC, NASA (for Chandra) et University of Wisconsin, JPL, Caltech, NASA (for Spitzer).

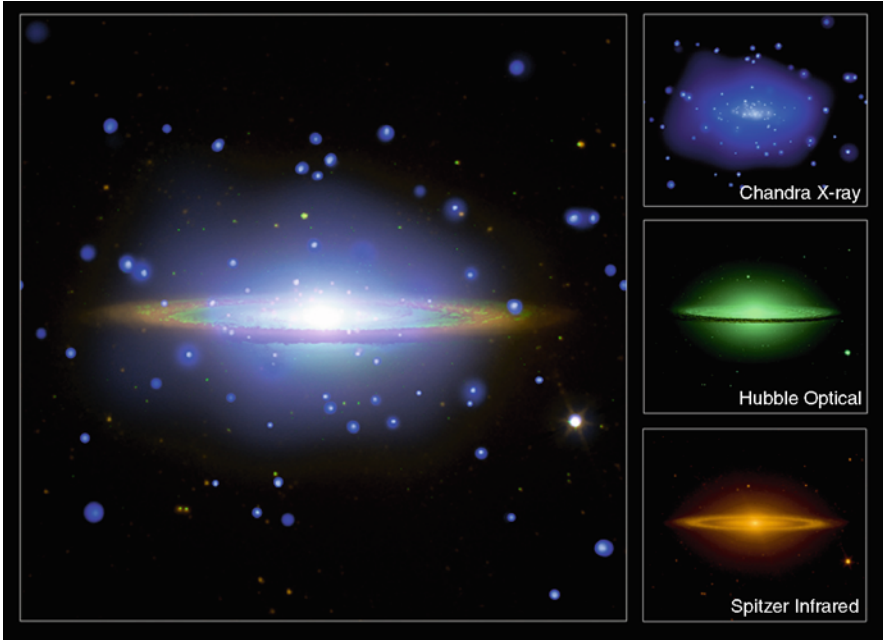


FIG. 9.40 : The Sombrero galaxy (M104) lies in the Virgo cluster, 28 million light-years from the Earth. It has a diameter of 50,000 light-years. The left-hand image is composed from the three images on the right: *Chandra* X-ray image showing a hot gas cloud resulting from supernova explosions at the center of the disk (in blue); *Hubble* visible image showing a spiral galaxy viewed edge on, with a dusty rim that blocks the light (in green); *Spitzer* image of this same rim, bright in the infrared (in red). Technical indications: Image size 8.4 arcmin. Coordinates (J2000.0) right ascension 12h 39min 59.4s, declination  $-11^{\circ} 37' 23''$ . Constellation Virgo. Observation on 31 May 2001. Credit (images and caption): (X ray) NASA, UMass., Q.D. Wang et al., (visible) NASA, STScI, AURA, Hubble Heritage, (IR) NASA, JPL, Caltech.

$i = 31.4^{\circ}$  for Suzaku (“vermillion bird” in Japanese, Astro-E2 before launch);  $i = 6^{\circ}$  for NuSTAR (Nuclear Spectroscopic Telescope Array, SMEX-11), see Fig. 9.41, and  $i = 28.5^{\circ}$  for the future GEMS (Gravity and Extreme Magnetism SMEX, SMEX-13).

The rest are very high and highly eccentric, as in the case of the Soviet satellites Astron and Granat, or the European satellite Exosat, launched in 1983, with  $a = 102,487$  km,  $e = 0.9344$ ,  $i = 72.5^{\circ}$ . In 1999, two large satellites, one American and the other European, used this type of orbit: Chandra (also called CXO, Chandra X-ray Observatory), launched on 23 July by STS-93 (see Fig. 9.37 lower), with  $h_p = 10,157$  km,  $h_a = 138,672$  km,  $i = 29.0^{\circ}$ ,  $T = 63.5$  h, and XMM (ESA’s X-ray Multi-Mirror Space Observatory, renamed XMM–Newton), launched on 10 December, with  $h_p = 7,417$  km,  $h_a = 113,678$  km,  $i = 38.8^{\circ}$ ,  $T = 47.9$  h.

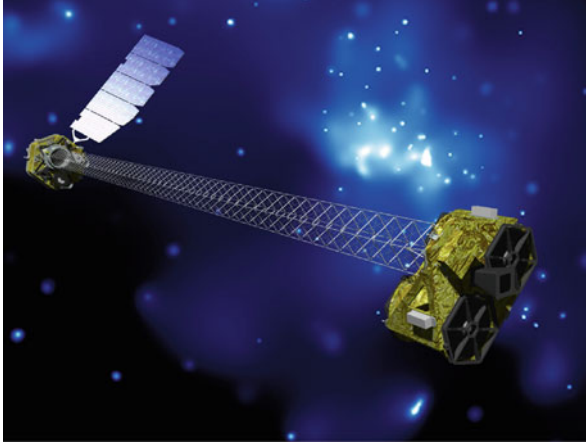


FIG. 9.41 : *The NuSTAR satellite, in low equatorial orbit ( $h = 627$  km,  $i = 6^\circ$ ). A 10 m deployable mast links the optics to the detectors in the focal plane (next to the solar panels). Artist's view. Credit: NASA.*

### *Ultraviolet (UV)*

These satellites use slightly inclined LEO orbits. The satellites OAO-1, -2, -3 (Orbiting Astronomical Observatory), launched between 1966 and 1972, followed orbits with  $h = 750$  km,  $i = 35^\circ$ ; OAO-3 was renamed Copernicus for the five hundredth anniversary of the birth of the famous astronomer.

Launched in 1978, IUE (International Ultraviolet Explorer, Explorer-57) operated for 18 years, instead of the planned 3 years, with a geosynchronous orbit ( $a = 42,166$  km,  $e = 0.2397$ ) inclined at  $i = 28.6^\circ$ . The US satellites EUVE (Extreme UV Explorer, Explorer-67),  $h = 515$  km,  $i = 28.4^\circ$ ; FUSE (Far UV Spectroscopic Explorer, MIDE-X-0, Explorer-77),  $h = 760$  km,  $i = 25.0^\circ$ ; GALEX (Galaxy Evolution Experiment, SMEX-7, Explorer-83),  $h = 690$  km,  $i = 28.0^\circ$  were launched in 1992, 1999, and 2003, respectively. The orbit of the Spanish satellite Minisat-01, launched in 1997,  $h = 570$  km, is also inclined at about  $30^\circ$  to the equator, since  $i = 151^\circ$  (which is the highest value yet put to use, to our knowledge).

### *Visible*

In the visible region of the electromagnetic spectrum, the two largest missions have been the European Hipparcos and the American Hubble (with ESA participation). Both have provided excellent results, despite a difficult start.

The Hipparcos satellite (High Precision Parallax Collecting Satellite), was devoted to astrometry, i.e., accurate measurement of stellar positions, and thus named in homage to the Greek astronomer (see the note on Hipparchos).<sup>103</sup> Launched on 8 August 1989, the satellite did not reach the planned

<sup>103</sup>The satellite determined the position, luminosity, and distance of 118,218 stars. The accuracy of the measurements (2 milliarcsec) was 100 times better than ground-based measurements of the day.

geostationary orbit but instead remained in the highly eccentric transfer orbit (GTO):  $h_p = 542 \text{ km}$ ,  $h_a = 35,840 \text{ km}$ ,  $i = 6.7^\circ$ . Rewriting the computer programs and redistributing the ground receiving stations, the mission was nevertheless carried successfully to completion.

The Hubble observatory was correctly launched by STS-31 on 24 April 1990. The problems began as soon as the first image came through, clearly showing that the telescope was shortsighted due to an inexcusable mirror defect.<sup>104</sup> The intention had always been to carry out maintenance via the Shuttle and this possibility was put to use primarily to correct the optics. The results did indeed come up to expectations and astronomy was revolutionised in the process.

In contrast, Hubble's successor must be beyond reproach from the moment of launch: NGST (New Generation Space Telescope), renamed<sup>105</sup> JWST (James Webb Space Telescope), should be placed at the Lagrange point  $L_2$  of the Sun–Earth system (see Sect. 6.12 on the Lagrange points), and it will be quite impossible to go out there and repair it! In addition to the visible region, JWST will also observe in the infrared and for this reason will be equipped with cryogenic systems.

The successor to Hipparcos, named GAIA (Global Astrometric Interferometer for Astrophysics, with reference to ῥ Γαῖα, ας, Gæe or Gaia, the personification of the Earth according to the Ancient Greeks) will also be placed there.<sup>106</sup> The main advantage of the halo orbit (L2LO) around the point  $L_2$  for stellar observation is that the Sun, the Earth, and the Moon are all located behind the line of sight of the telescope. The whole of the celestial sphere can then be observed as the year goes by, without blind spots. This region is also very stable as regards the thermal and particle environment.

The American planned astrometry mission is SIM Lite (formerly SIM, Space Interferometry Mission), on a heliocentric orbit that gradually moves away from the Earth, reaching a distance of some 95 million kilometers in 5 years.

---

<sup>104</sup>The main mirror of the Hubble Space Telescope was manufactured by the company Perkin-Elmer. It was only after launch that it was realised that the work had not been carried out correctly and that the telescope optics produced fuzzy images. The problem came from a faulty lens alignment, and the error was one millimeter, whereas the standard imposed for this project was a fraction of the visible wavelength, i.e., a hundred or so nanometers. Today, Perkin-Elmer has a highly diversified multinational activity but it has closed its department of astronomical optics.

<sup>105</sup>In honour of James E. Webb (1906–1992), NASA's second administrator, who directed the Apollo programme and was one of the instigators of the first interplanetary exploration.

<sup>106</sup>GAIA's mission is to observe and record a billion stars with an accuracy of  $10 \mu\text{arcsec}$ . For stars within 500 light-years, the distance will be known to within a few light-days.

### *Infrared (IR)*

The detection of IR radiation involves cooling the optical system and associated instrumentation in the satellites. The satellite ceases to function once its reserves of cryogenic fluid have been exhausted.

Many of these satellites have used Sun-synchronous orbits, such as IRAS (IR All-sky Survey),  $h = 890$  km, helium-cooled, launched in 1983, WIRE (Wide field IR Explorer, SMEX-5, Explorer-75),  $h = 560$  km, optics cooled by 3 kg of solid hydrogen, launched in 1999, Akari (Astro-F),  $h = 630$  km, with 170 L of liquid hydrogen for optics at 6 K, launched in 2006, WISE (Wide field IR Survey Explorer, Explorer-92, MIDEX-6, formerly NGSS),  $h = 525$  km, with a solid hydrogen supply that should last 10 months, launched in 2009.

The European satellite, ISO (Infrared Space Observatory), with American and Japanese participation, was equipped with a cryostat filled with superfluid helium. It operated between November 1995 and May 1998, on a highly eccentric orbit with a period of revolution of 1 day.<sup>107</sup> Its successor Herschel<sup>108</sup> (or HSO, Herschel Space Observatory), taking over from the FIRST project (Far IR and Submillimeter Telescope), launched on 14 May 2009 (jointly with Planck), was placed in orbit around the Lagrange point  $L_2$  for a period of 3 years.

The US satellite Spitzer, launched on 25 August 2003 under the name of SIRTf, is on a different orbit. It follows the Earth at a distance of 0.1 a.u. or 15 million kilometers. This heliocentric orbit, known as ETHO (Earth-trailing heliocentric orbit), maintains the satellite in an extremely cold environment, propitious for technological innovation.<sup>109</sup>

### *Microwave*

The US satellite COBE (Cosmic Background Explorer, Explorer-66) was launched in 1989 on a Sun-synchronous orbit at  $h = 880$  km,  $i = 99.0^\circ$ ,

<sup>107</sup>Orbital characteristics:  $h_p = 1,110$  km,  $h_a = 70,504$  km,  $i = 5.1^\circ$ ;  $a = 42,185$  km,  $e = 0.822$ ,  $T_d = 1,436$  min = 1 sidereal day. Cryostat: 2,200 L of superfluid helium. Temperatures of the various components: detector 2 K, optics 3–4 K, instruments 8 K.

<sup>108</sup>*William Herschel* (1738–1822) was a British astronomer of German origins. His life attests to an unusual intellectual development, revealing an exceptionally curious nature. He was led to mathematics by music, and from there moved on to astronomy. He made his own telescopes and they were the best of his day. He discovered Uranus in 1781, and then later, two of its moons, followed by two of the moons of Saturn. He demonstrated the displacement of the Solar System through the Galaxy and gave the coordinates of the apparent convergence point (the so-called apex) in 1783. In 1801, he discovered infrared radiation.

<sup>109</sup>In contrast to IRAS and ISO, however, Spitzer was designed with an innovative “warm-launch” cryogenic architecture. The observatory was launched at ambient temperature and radiatively (or passively) cooled in the deep recesses of space. Only the focal plane instruments and the liquid helium cryostat are enclosed in a vacuum shell containing liquid helium. This innovative launch architecture, combined with 360 L of liquid helium, yields an estimated mission lifetime of about 5 years. For the sake of comparison, IRAS used 520 L of cryogen during its 10 month mission (52 L per month as compared with 6).

and explored the millimeter radiation in space in order to study temperature fluctuations in the diffuse cosmological background via extremely precise measurements. (The temperature varies from 2.7249 to 2.7251 K, depending on the observed region.) This informs us about fluctuations in the matter density of the early universe.

Its successor WMAP (Wilkinson Microwave Anisotropy Probe, MIDE-X-2, Explorer-80), with angular resolution  $0.2^\circ$  compared with  $7^\circ$  for COBE, is placed<sup>110</sup> in an L2LO orbit.

The European satellite Planck,<sup>111</sup> launched with Herschel, is also placed at the point  $L_2$ . The Planck mission<sup>112</sup> is designed to study the origins of the Universe. Its instruments should map the anisotropy of the cosmic microwave background, equivalent to the radiation of a black body at 2.725 K, covering the whole celestial sphere with an angular resolution of the order of 5 arcsec (to be compared with  $7^\circ$  for COBE) and a temperature sensitivity of the order of  $2 \times 10^{-6}$ .

For the study of galactic molecular clouds, SWAS (Submillimeter Wave Astronomy Satellite, SMEX-3, Explorer-74), launched in 1998, is now on a low prograde orbit with  $h = 640$  km,  $i = 69.9^\circ$ .

### *Radio*

The first satellites to study radio sources were RAE-A and -B (Radio Astronomy Explorer, Explorer-38 and -49), launched in 1968 and 1973 on a highly inclined circular orbit with  $h = 5,850$  km and  $i = 120.9^\circ$ .

The observation of sources emitting in the radio region, i.e., wavelengths of the order of one meter or more, is not seriously affected by the Earth atmosphere, and sending instruments into orbit brings little improvement on this front. However, the point about putting satellites into orbit to study this frequency range is to construct as long a baseline as possible for the technique commonly known as VLBI (see Chap. 3).

---

<sup>110</sup>Launched on 30 June 2001, the MAP probe made four revolutions around the Earth on ever more eccentric orbits, reaching the vicinity of the Moon a month later. Using a lunar swing-by, it took another 2 months to arrive at the point  $L_2$  of the Sun–Earth system on 1 October 2001 and go into the halo orbit. MAP was renamed WMAP (or Wilkinson MAP) in February 2003, in honour of David T. Wilkinson of Princeton University, a world-famous cosmologist and MAP team member, who died in September 2002.

<sup>111</sup>*Max Planck* (1858–1947) was a German physicist. He studied blackbody radiation and found an expression for the blackbody spectrum as a function of temperature and frequency. This problem had stumped many physicists before him. Planck solved it in 1900 by introducing the idea of the energy quantum. The theory of these quanta then became the basis for much of modern physics.

<sup>112</sup>Two rather similar projects were originally proposed to the European Space Agency: COBRAS (Cosmic Background Radiation Anisotropy Satellite) and SAMBA (Satellite for Measurement of Background Anisotropies). They were combined into one under the title COBRAS/SAMBA. However, this pleasantly exotic but heavy and supremely redundant appellation was abandoned in favour of the short but enlightening name of Planck.



The Japanese are very active in this field. The satellite<sup>113</sup> Halca was the first in this category. It follows an HEO orbit with  $h_p = 569$  km,  $h_a = 21,415$  km, and  $i = 31.4^\circ$  (see Fig. 9.42 upper). Its successor will be Astro-G (or VSOP-2),  $h_p = 1,000$  km,  $h_a = 25,000$  km,  $i = 31^\circ$  (see Fig. 9.42 lower). The satellite comprises a dish 9 m in diameter to observe in the three frequency bands 8, 22, and 43 GHz. The last two of these, corresponding to wavelengths of 14 mm and 7 mm, require cryogenics.

The Russian satellite<sup>114</sup> Spektr-R (or RadioAstron) provides an even longer baseline, with  $h_p = 33,500$  km,  $h_a = 302,000$  km, and  $i = 72.4^\circ$  ( $a = 174,250$  km,  $e = 0.771$ ,  $T = 201$  h, or more than 8 days).

## Solar Astrophysics

Solar radiation is studied across the whole range of wavelengths. The Sun has been the subject of investigation since the very beginning of the Space Age, from 1962 to 1976, with LEO satellites at altitudes between 500 and 600 km, such as the eight observatories OSO-1 to -8 (Orbiting Solar Observatory),  $i = 33^\circ$ , and the three Explorers, IQSY (International Quiet Sun Year, Explorer-30), Solrad-9 and -10 (Solar Radiation,<sup>115</sup> Explorer-37 and -44),  $i \sim 55^\circ$ , or with slightly inclined HEO orbits, like the EPE programme (Energetic Particle Explorer), with EPE-A, -B, -C, and -D (Explorer-12, -14, -15, -26). The German satellites Helios-1 and -2 are in heliocentric orbits with perihelion 0.309 a.u., aphelion 0.985 a.u.,  $i = 0^\circ$ , in the plane of the ecliptic, and  $T = 190$  day.

Launched in 1980, the US satellite SMM (Solar Maximum Mission) was the first satellite to be repaired in flight by the Shuttle STS-11 (STS-41-C), in 1984. It operated until 1989 on the orbit  $h = 405$  km,  $i = 26.5^\circ$ .

Recent LEO satellites<sup>116</sup> are in Sun-synchronous orbits, like the US satellites TRACE (Transition Region and Coronal Explorer, SMEX-4, Explorer-73), with altitude  $h = 620$  km, ACRIMSAT (Active Cavity Radiometer Irradiance Monitor Satellite),  $h = 700$  km, or the IRIS project (Interface Region Imaging Spectrograph, SMEX-12),  $h = 636$  km, like the Japanese satellites Hinode (“sunrise”, Solar-B),  $h_p = 318$  km,  $h_a = 675$  km,  $i = i_{HS} = 98.3^\circ$ , and

<sup>113</sup>Launch date: Halca on 12 February 1997. Halca (Highly Advanced Laboratory for Communication and Astronomy), also called Muses-B or VSOP (VLBI Space Observatory Programme) was renamed Haruka (*haruka* means “remote”) after launch, in accordance with the Japanese tradition.

<sup>114</sup>Launched on 18 July 2011, it replaces the overambitious Russian project KRT-25 (with European participation), a 25 m radiotelescope, planned to follow a variable orbit. Over its 7 year lifespan, this orbit was to become more and more eccentric:  $h_p \approx 5,000$  km,  $h_a$  from 20,000 to 150,000 km,  $i = 63^\circ$ .

<sup>115</sup>It later transpired that the first Solrad missions, from Solrad-1 to -7B, between 1960 and 1965, were primarily spy satellites (ELINT). To give the Solrad programme a more scientific countenance, it was also referred to as GREB (Galactic Radiation Experimental Background) or GRAB (Galactic Radiation And Background).

<sup>116</sup>Launch dates: TRACE on 1 April 1998; ACRIMSAT on 21 December 1999; Hinode on 20 September 2006; Picard on 15 June 2010.

**Halca** 〈はるか〉

Orbit - ref.: Earth

Recurrence = [ 4;-41;193] 731

&gt;&gt;&gt;&gt; Time span shown: 5.00 days

Equiv. altit. = 10965.5 km

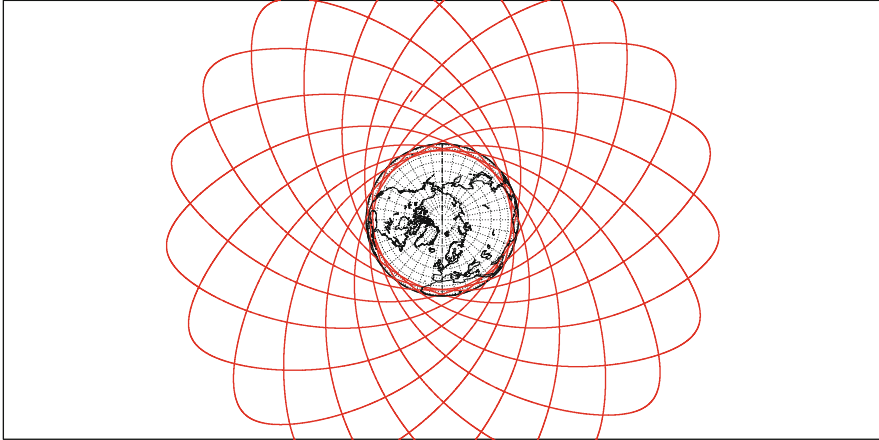
a = 17343.641 km

Inclination = 33.10 °

e = 0.600191

Period = 378.51 min \* rev/day = 3.80

h\_a = 21375 km; h\_p = 556 km; arg. perigee: +90.00 °



Projection: Orthographic

Property: none

⊕ T.:Azimuthal - Graticule: 10°

Project. centre: 90.0 ° N; 0.0 °

Aspect: Direct

{4.2} [ -90.0/ +0.0/ +90.0] [-] GRIM5-C1

Longitude / Initialisation:

Asc. Node: -166.80 °

Apogee : 143.89 °

Ιξίων

MC ★ LMD

Ατλας

**Astro-G**

Orbit - ref.: Earth

&gt;&gt;&gt;&gt; Time span shown: 5.00 days

Equiv. altit. = 13000.0 km

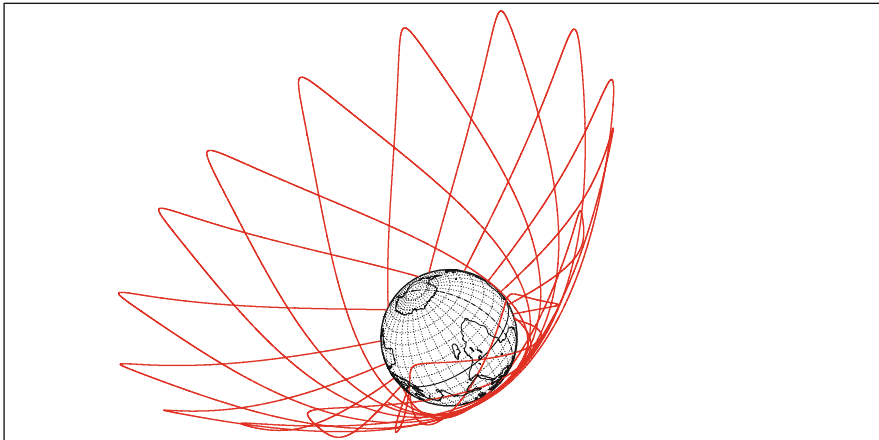
a = 19378.100 km

Inclination = 31.00 °

e = 0.619255

Period = 447.06 min \* rev/day = 3.22

h\_a = 25000 km; h\_p = 1000 km; arg. perigee: +90.00 °



Projection: Orthographic

Property: none

⊕ T.:Azimuthal - Graticule: 10°

Project. centre: 32.0 ° S; 45.0 ° E

Aspect: Oblique

{4.2} [ -90.0/+122.0/ +45.0] [-145] GRIM5-C1

Longitude / Initialisation:

Asc. Node: 0.00 °

Apogee : -41.40 °

Ιξίων

MC ★ LMD

Ατλας

FIG. 9.42 : Elliptical orbit of the two Japanese satellites for spaceborne VLBI, represented in a terrestrial frame. Upper: Halca (Haruka), Lower: Astro-G.



the French Picard (see the note on Picard),  $h = 725$  km. The Russian satellites are in prograde near-polar orbits with  $h = 520$  km,  $i = 82.5^\circ$ , with<sup>117</sup> Koronas-I, Koronas-F (AUOS-SM-KI and -KF), and Koronas-Foton.

With a different inclination, we find the Japanese satellite Solar-A (or Yokkoh, “Sun”), launched in 1991,  $h_p = 526$  km,  $h_a = 795$  km,  $i = 31.3^\circ$ , and the US satellite SORCE (Solar Radiation and Climate Experiment), launched in 2003 on the orbit  $h = 641$  km,  $i = 40.0^\circ$ .

Two large projects have inspired a collaboration between the ESA and NASA in this area: Ulysses and SOHO. The Ulysses probe, launched on 6 October 1990 by STS-41, set off first in the direction of Jupiter, to use it for a gravity-assist maneuver and thereby leave the plane of the ecliptic. On 1 November 1994, it overflew the south pole of the Sun, and on 1 October 1995, the north pole. The satellite SOHO (Solar and Heliospheric Observatory), launched on 2 December 1995, went to Lagrange point  $L_1$  to acquire a halo orbit. As well as its considerable contribution to our understanding of the Sun, it also discovered a great many comets.

Several missions should use the stable Lagrange points. Japan is planning its L5-Mission, which should monitor the Sun in order to provide a sort of space weather forecast, the aim being to improve the safety of space activities. The US mission called STEREO (Solar–Terrestrial Relation Observatory) intended to place its two satellites at the Lagrange points  $L_4$  and  $L_5$ , with STEREO-Ahead at  $L_4$  and STEREO-Behind at  $L_5$ , in order to carry out a kind of 3D observation of the Sun. Finally, this option was dropped and replaced by a heliocentric orbit with periods of  $365 \pm 20$  days. Launched on 26 October 2006, STEREO-A precedes the Earth (Ahead) with a period of 345 day, while STEREO-B follows (Behind) with a period of 385 day.

The US satellite SDO (Solar Dynamics Observatory), launched in 2010, follows a geosynchronous orbit with an inclination of  $i = 28.5^\circ$  and with ground track crossover at longitude  $\lambda_S = 110^\circ\text{E}$ .

Two further solar missions in the pipeline, Solar Orbiter for the ESA and Solar Probe Plus for NASA, should be in heliocentric orbits like Ulysses. Solar Orbiter will have variable apsides, with  $r_p$  varying from 0.23 to 0.29 a.u. (astronomical units) and  $r_a$  varying from 0.75 to 1.20 a.u., and with inclination (relative to the ecliptic)  $i = 25^\circ$  going to  $i = 34^\circ$  at the end of the mission, following several Venus flybys. Solar Probe Plus (also written Solar Probe +), following 7 Venus flybys between 2015 and 2021, will come very close to the

---

<sup>117</sup>Launch dates: Koronas-I on 2 March 1994; Koronas-F on 13 July 2001; Koronas-Foton on 30 January 2009. The letters I and F stand for Izmiran and Firas, the names of those who first conceived of these projects. Koronas-Foton is also called CORONAS-Photon (Complex Orbital Observations Near-Earth of Activity of the Sun), with the obvious allusion to the solar corona.

Sun, with  $r_p$  varying from 0.16 a.u. or  $35R_S$  (solar radii) to 0.04 a.u. or  $9.5R_S$ . At this point, it will be moving at 200 km/s (or 725,000 km/h) and its surface temperature will be 2000°C.

### Stellar Seismology and the Search for Exoplanets

Two satellites,<sup>118</sup> each carrying a small telescope, have been designed to study the seismology of stars. The Canadian satellite MOST (Microvariability and Oscillations of Stars, jokingly nicknamed the Humble Space Telescope by its developers), is in a Sun-synchronous orbit with  $h = 625$  km,  $i_{HS} = 98.7^\circ$ . The French satellite CoRoT (*Convection, Rotation et Transits planétaires*) is looking for planets in orbit around stars other than the Sun by detecting the transit (when the planet passes in front of its star and thereby diminishes its luminosity), as well as studying stellar seismology. It has a circular, strictly polar orbit with  $h = 897$  km (see Chap. 7).

The European project Eddington,<sup>119</sup> which would study the internal structure of stars and seek to detect extra-solar planets, should have been placed at the Lagrange point  $L_2$  on an L2LO orbit. However, in November 2003, the ESA postponed the mission indefinitely. Another project, a forerunner of Eddington and since abandoned, would have sent the satellite STARS to the Lagrange point  $L_5$  of the Earth–Moon system.

The ESA has two concurrent projects with satellites at the point  $L_2$ : PLATO (Planetary Transits and Oscillations of stars), which is an improved CoRoT, and EChO (Exoplanet Characterisation Observatory), which would analyse the atmospheres of transiting planets by spectroscopy (already known planets).

The European mission Darwin<sup>120</sup> will be devoted to astrobiology (also known as exobiology, to remove all possible confusion with “astrology”), but

<sup>118</sup> Launch dates: MOST on 30 June 2003; CoRoT on 27 December 2006.

<sup>119</sup> Arthur Stanley Eddington (1882–1944) was a British astronomer and physicist. He did much to promote the theory of relativity (see the note on Einstein), through the publication of his book *Space, Time and Gravitation* first published in 1920 but still being reprinted. He also laid the foundations for a new discipline, stellar dynamics, with *The Internal Constitution of the Stars* (1926), in which he shows that a star is subject to two opposing effects: it tends to contract under the effect of gravity, while the release of energy tends to push it apart.

<sup>120</sup> Charles Darwin (1809–1882) was an English naturalist. From 1831 to 1836, he took part in an expedition to South America (and in particular to the Galapagos islands) and Oceania aboard the HMS Beagle. As a geologist and botanist, he elaborated his theory of evolution on the basis of notes taken and collections brought back from this expedition. He concluded that the variability of the species is due to the effects of their environment and to sudden variations. These variations are only favoured by natural selection if they give the individual organism an advantage in its struggle for survival (subsistence and reproduction). His famous book *The Origin of Species* was published in 1859. Darwin’s theory, supported and developed by a great many intellectuals, was attacked without scientific argument by the conservative-minded and religious classes. Here was another problem of divine order!

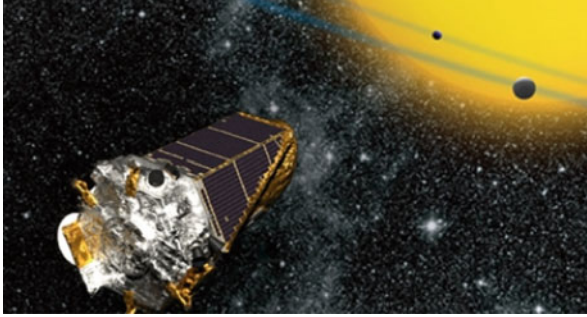


FIG. 9.43 : *Kepler*: NASA's first mission capable of finding Earth-size and smaller planets around other stars, by the transit method of detecting extrasolar planets. The *Kepler* instrument is a specially designed 0.95-meter diameter telescope (photometer). It has a very large field of view for an astronomical telescope (105 square degrees). Artist's view. Credit (image and caption): NASA.

it is a long-term project. The Darwin “flotilla”<sup>121</sup> will also be in an L2LO orbit.

The US satellite *Kepler*, launched on 7 March 2009, is in a heliocentric orbit with  $a = 1.01319$  a.u.,  $e = 0.03188$  and a period of  $T = 372.5$  day. In January 2013, the mission had located 2,740 candidate planets among which around 60 have now been confirmed as exoplanets (see Figs. 9.43 and 16.45).

For an even finer search for exoplanets, the mission TPF (Terrestrial Planet Finder), comprising a flotilla of satellites, is under study. Four telescopes in orbit, grouped at a distance of about a kilometer from a central satellite, thereby constitute a gigantic interferometer.

## Space Exploration

Probes sent out to observe other planets in the Solar System or their moons will be studied in Chaps. 15 and 16, together with comets and satellites in orbit around these celestial bodies.

---

<sup>121</sup>The Darwin flotilla comprises six satellites in formation. They lie strictly in the same plane and each is equipped with a telescope in such a way as to form an infrared interferometer. One master satellite, a short distance from the others, oversees the satellite positions and provides the link with the Earth. The aim is to detect planets orbiting other stars and to spy out possible signatures of life beyond our own Solar System.

### 9.2.10 Satellites for Fundamental Physics

The satellite Gravity Probe-B (GP-B), launched<sup>122</sup> on 19 April 2004, has a strictly polar LEO orbit, already mentioned in this chapter (see Fig. 9.6). The aim of the mission is to measure, using gyroscopes, the extent to which space and time are distorted by the presence of the Earth, within the framework of the general theory of relativity.

The mission STE-QUEST (Space-Time Explorer and Quantum Equivalence Principle Space Test), an ESA project, would investigate gravitational redshift predictions of general relativity, including the gravitational redshifts of the Earth and Sun, and carry out tests of the weak equivalence principle and the universal propagation of matter waves. Ultra-precise clocks would be carried on an elliptical orbit by the satellite (variation of the gravitational field for altitudes varying between 1,000 and 50,000 km). The orbit would be recurrent, overflying dedicated ground stations (Boulder, Torino and Tokyo). These novel orbits are shown in Figs. 9.44 and 9.45.

Two missions are being planned to provide experimental corroboration of the equivalence principle.<sup>123</sup> The French project  $\mu$ SCOPE (*Micro-Satellite à Compensation de traînée pour l'Observation du Principe d'Équivalence*), or Microscope, is designed to check the universality of free fall. The satellite will have a circular, Sun-synchronous LEO orbit at  $h \sim 700$  km. Drag effects on the satellite will be compensated by electric thrusters to ensure that the two test masses carried aboard undergo perfect free-fall conditions over thousands of kilometers (rather than just a few tens of meters, and without compensation for air resistance, if one drops the objects from the leaning tower of Pisa). The US satellite STEP (Satellite Test of the Equivalence Principle) will be

---

<sup>122</sup>The inception of this mission dates back to the beginnings of the space age. In 1959, physicists at Stanford university suggested this experiment and it was accepted by NASA in 1961. However, checking general relativity was not such an urgent matter as the race to the Moon, and it was put on hold. Then there came other priorities in the form of the planetary missions and the Space Shuttle.

The preliminary experiment GP-A took place in June 1976. It consisted in sending a clock (a hydrogen maser) into space in a suborbital flight at an altitude of 10,000 km. It succeeded in measuring a clock difference that bore out the predictions of Einstein's theory. During this time, dozens of theses were written at Stanford on this subject, but GP-B was still being put off! Finally, in 1995, the mission was rescheduled with a more definite timetable. Launched in 2004, the first certified results arrived in 2007, confirming the theory.

<sup>123</sup>The equivalence principle postulated by Einstein is based on the observation that all bodies, independently of their mass, have the same acceleration in a gravitational field for identical initial conditions. This is the universal principle of free fall: the passive gravitational mass of a body ( $m = m_g$  in the expression for the gravitational force, involving  $G$ ) is equal to the inertial mass ( $m = m_i$  in Newton's second law):

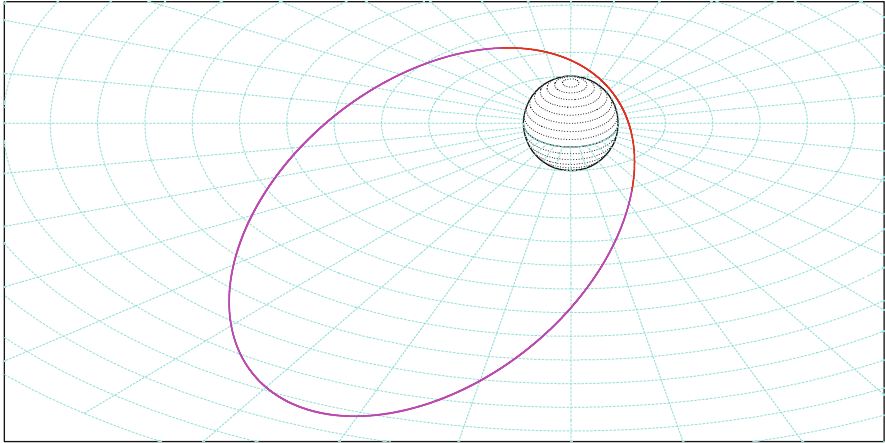
$$F = GMm_g/r^2, \quad F = m_i a.$$

**STE-QUEST**

Orbit (Celestial ref.) [Galilean]

>>>> Time span shown: 2880.0 min = 2.00 days

Equiv. altit. = 25791.1 km      a = 32169.238 km  
 Inclination = 72.07°      e = 0.773000  
 Period = 957.20 min \* rev/day = 1.50  
 h\_a = 50658 km; h\_p = 924 km; arg. perigee: +43.55°



Projection: Orthographic      Project. centre: 30.0° N; 80.0° W      Longitude / Initialisation:      *Ιξίων*  
 Property: none      Aspect: Oblique      Asc. Node: -3.00°      MC \* LMD  
 ⊕ T.: Azimuthal - Graticule: 10° {-} [-90.0/ +60.0/+170.0] [-] EGM2008      *Ατλας*

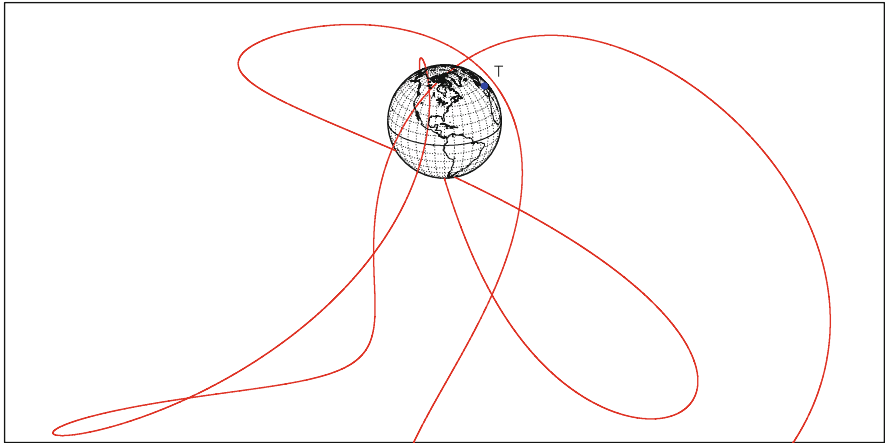
**STE-QUEST**

Orbit - ref.: Earth

Recurrence = [ 2; -1; 2] 3

>>>> Time span shown: 2880.0 min = 2.00 days

Equiv. altit. = 25791.1 km      a = 32169.238 km  
 Inclination = 72.07°      e = 0.773000  
 Period = 957.20 min \* rev/day = 1.50  
 h\_a = 50658 km; h\_p = 924 km; arg. perigee: +43.55°



Projection: Orthographic      Project. centre: 25.0° N; 80.0° W      Longitude / Initialisation:      *Ιξίων*  
 Property: none      Aspect: Oblique      Asc. Node: -3.00°      MC \* LMD  
 ⊕ T.: Azimuthal - Graticule: 10° {-} [-90.0/ +65.0/+170.0] [-] EGM2008      Apogee : -49.29°      *Ατλας*

FIG. 9.44 : Elliptical orbit of STE-QUEST. Upper: Galilean frame. Lower: Terrestrial frame. Perigee above Torino (T).

**STE-QUEST**

Elliptical orbit - Gr. track

Recurrence = [ 2; -1; 2] 3

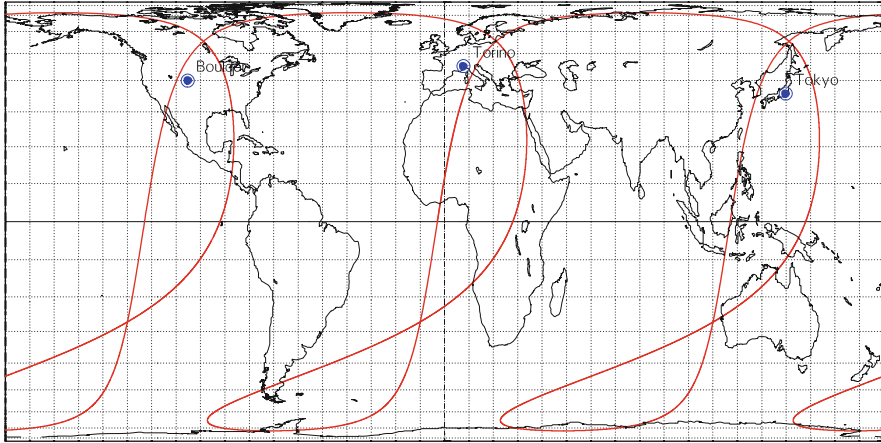
>>>> Time span shown: 2880.0 min = 2.00 days

Equiv. altit. = 25791.1 km      a = 32169.238 km

Inclination = 72.07 °      e = 0.773000

Period = 957.20 min \* rev/day = 1.50

h\_a = 50658 km; h\_p = 924 km; arg. perigee: +43.55 °



Projection: Behrmann

Project. centre: 0.0 ° ; 0.0 °

Longitude / Initialisation:

Ιξίων

Property: Equal area

Aspect: Direct

Asc. Node: -3.00 °

MC \* LMD

⊕ T.:Cylindrical - Graticule: 10°

{4.2} [+90.0/ +0.0/ -90.0] [-] EGM2008

Apogee : -49.29 °

Ατλας

**STE-QUEST**

Gr.tr. ( H < 5000 km) H: geodetic altitude

Recurrence = [ 2; -1; 2] 3

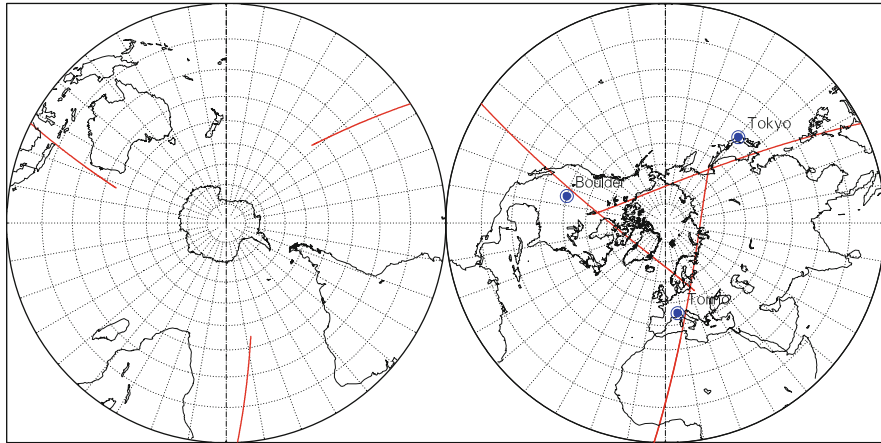
>>>> Time span shown: 2880.0 min = 2.00 days

Equiv. altit. = 25791.1 km      a = 32169.238 km

Inclination = 72.07 °      e = 0.773000

Period = 957.20 min \* rev/day = 1.50

h\_a = 50658 km; h\_p = 924 km; arg. perigee: +43.55 °



Projection: Stereographic

Pr. centre (r.): 90.0 ° N; 0.0 °

Longitude / Initialisation:

Ιξίων

Property: Conformal

Aspect: Direct

Asc. Node: -3.00 °

MC \* LMD

⊕ T.:Azimuthal - Graticule: 10°

{4.2} [-90.0/ +0.0/ +90.0] [-] EGM2008

Apogee : -49.29 °

Ατλας

FIG. 9.45 : Representation of the elliptical orbit of the satellite STE-QUEST in a terrestrial frame, showing the three receiving stations. Upper: Ground track. Lower: Ground track of the orbit at an altitude below 5,000 km.

much bigger, with cooled instruments to increase measurement accuracy.<sup>124</sup> It will also follow a circular, Sun-synchronous LEO orbit, at  $h = 550$  km. The European project GAUGE (General relativity and Unification of Gravity Explorer) is planned for the same type of orbit.

The joint ESA–NASA project LISA (Laser Interferometer Space Antenna) will attempt to detect gravitational waves using three satellites in formation on a heliocentric orbit.<sup>125</sup>

### 9.2.11 Technological Satellites

This is the category of satellites whose mission it is to assist in various kinds of technological development. The very first satellites fit well in this class. Technological satellites are used to test instruments, orbital maneuvers, communication techniques, and reentry methods. They are also used to test the design of electric or ion propulsion motors.

The satellite DODGE (Department Of Defense Gravity Experiment),  $h = 33,400$  km,  $i = 12^\circ$ , was sent into space in 1967 to further the development of geostationary satellites, although the first of these had already been launched some years previously. A camera aboard this satellite took the very first colour pictures of the Earth's disk.

The military satellite ARGOS (Advanced Research Global Observation Satellite, or P91-1) was launched into a Sun-synchronous LEO orbit in 1999 to test electric propulsion systems and detect X rays.

To study the effect of radiation on various types of equipment, several small technological satellites have been placed in highly elliptical orbits. These are in fact the geostationary transfer orbits (GTO) of the main satellites with which they were launched (see Fig. 9.16 lower). Such GTO orbits expose the satellites to an extremely testing environment, since they cross the Van Allen radiation belts on each revolution. With this mission, we find the British microsattelites STRV (Space Technology Research Vehicle), STRV-1A and -1B, launched in 1994 as passengers with Intelsat-702, and STRV-1C and -1D in 2000, passengers with PAS-1R (PanAmSat-1R), whose orbital elements, initially those of the GTO orbit, viz.,  $h_p = 300$  km,  $h_a = 36,000$  km,  $i = 7^\circ$ , subsequently evolved (see Fig. 9.9).

This category also covers calibration satellites, such as Radcal, with  $h \approx 800$  km,  $i = 89.5^\circ$ , for radar calibrations, Reflektor, launched with Meteor-3M-1, for laser calibrations, and the twelve nanosatellites (a few kilogram)

<sup>124</sup>The relation  $m_g/m_i = 1$  has been checked on Earth to an accuracy of  $10^{-12}$ . The  $\mu$ SCOPE experiment aims to achieve  $10^{-14}$  and STEP  $10^{-17}$ . Research on the STEP accelerometers began at Stanford university as early as 1971.

<sup>125</sup>The three satellites will be placed at the corners of an equilateral triangle with side 5 million kilometers. The center of the triangle will lie in the plane of the ecliptic, on the same heliocentric orbit as the Earth, but 20 days behind, i.e., 50 million kilometers away. The plane of the triangle will be slightly inclined to the plane of the ecliptic. The three satellites, linked by laser, will constitute a gigantic Michelson interferometer.



launched by STS-60 and -63, Oderacs-A to -F, and Oderacs-2A to -2F (Orbital Debris Radar Calibration Sphere), to calibrate spacecraft debris.

One type of experiment, called a tether experiment, involves connecting the satellite to a secondary body once it is already in orbit, using cables of different lengths. These cables may or may not be conducting. The first tests were carried out on the manned flights Gemini-11 and -12 (with a cable of 30 m). Also worth mentioning, launched into LEO orbit between 1993 and 1996, are the satellites SEDS-1 then -2 (Small Expendable Deployer System), with a cable 20 km long, and TiPS (Tether Physics and Survivability), with a 4 km cable. The orbit of the TiPS central satellite had the characteristics  $h = 1,022 \text{ km}$ ,  $i = 63.4^\circ$ ,  $e = 0.000$ .

In the United States, the universities carry out missions with small technological satellites, such as SNOE (Student Nitric Oxide Explorer, STEDI-1, Explorer-72) or TERRIERS (STEDI-2, Explorer-76). In Europe, this policy is mainly applied in the United Kingdom, with UoSAT (University of Surrey Satellites), and in Germany, with Tubsat (*Technische Universität Berlin Satellites*). These satellites, which can generally be subsumed under the heading of technological satellites, are almost always placed in Sun-synchronous orbits as passengers. The Russian remote-sensing satellites Kanopus-V-1 and -2 are modelled on UoSAT.

In this category, we may also include satellites with biology missions. The satellite Sputnik-2 carried a female dog by the name of Laika into space. Animals were sent in the Russian Bion satellites to study the effects of radiation. For example, in 1996, two monkeys flew in Bion-11,  $h = 300 \text{ km}$ ,  $i = 63^\circ$ , and in 2013, Bion-M1, the Zoo-spacecraft, carried a host of mice and newts,  $h = 575 \text{ km}$ ,  $i = 64.9^\circ$ . We may also mention the US LEO satellite OFO-1 (Orbital Frog Otolith), launched in 1970, occupied by two toads. The aim was to study their inner ear, seat of the vestibular organ (balance system). The Chinese satellite Shi Jian-8 (SJ-8, DFH-68), launched in 2006,  $h_p = 178 \text{ km}$ ,  $h_a = 428 \text{ km}$ ,  $i = 63.0^\circ$ , was subsequently recovered with its payload of plants and toadstools.

### 9.2.12 Satellites with Specific Military Missions

Many programmes have been developed by the military and civilian sectors, either jointly or in parallel, with similar areas of interest, such as remote-sensing, surveillance, and communications. However, certain programmes are specifically military, such as the detection of nuclear explosions. Here is a brief review.

#### Early Warning

These satellites are designed to detect enemy missiles as soon as possible during or after their launch. In the United States, the first programme was Midas (Missile Defense Alarm System), with near-polar LEO satellites,  $h \sim 3,000 \text{ km}$ , from Midas-3 in 1962 to Midas-12 in 1966. Satellites in the following



programme, IMEWS (Integrated Missile Early Warning Satellites), extended by DSP (Defense Support Program), have been geostationary,  $i \approx 0^\circ$ , from IMEWS-2 in 1971 to the current DSP missions. We know only that these are extremely heavy satellites carrying a multitude of sensors, mainly in the infrared. The last few launched were DSP-F-21 (USA-159) in 2001, DSP-F-22 (USA-176) in 2004, and DSP-F-23 (USA-197) in 2007.

The frequently modified NMD project (National Missile Defense) is based in the SBIRS satellites (Space Based IR System). As soon as a missile is fired, it is detected by SBIRS-High (a system<sup>126</sup> of four GEO satellites and two HEO satellites). The missile is then tracked by SBIRS-Low (a constellation of 24 satellites in six orbital planes). The first two SBIRS-Low satellites were launched together on a circular orbit with  $h = 1,350$  km and  $i = 58^\circ$  on 25 September 2009, under the names of STSS-1 and -2 (Space Tracking and Surveillance System, USA-208 and -209). The satellite NFIRE (Near Field Infrared Experiment), launched in 2007, is on a low, slightly inclined orbit, with  $h_p = 255$  km,  $h_a = 464$  km,  $i = 48.2^\circ$ .

The Soviet programme SPRN is equivalent to IMEWS, with a fleet of GEO satellites<sup>127</sup> from the Oko series (“eye”), either on a GEO orbit for Oko-US-KMO, or on an HEO orbit of Molniya type for Oko-US-K.

## Nuclear Surveillance

In August 1963, leaders from the USSR, the USA, and Great Britain met in Moscow to sign a treaty forbidding nuclear testing in the atmosphere. To enforce this resolution, the different world powers launched satellites that could detect explosions of this kind through the gamma-ray emissions they generate.

The US satellites Vela had novel circular orbits, at very high altitudes  $h \approx 110,000$  km, and inclinations varying between  $34^\circ$  and  $61^\circ$  (see Fig. 9.37 upper). They were launched in pairs, in diametrically opposed directions with respect to the center of the Earth, from Vela-1 and -2 in 1963 to Vela-11 and -12 in 1970, and remained operational until 1984. (“Vela” means “lookout” in Spanish. These satellites were also called Watchdogs or Vela Hotel.) They fulfilled a scientific mission that had not been planned at all at the outset: between 1969 and 1979, the satellites Vela-9 and -10 (OPS/6909 and OPS/6911) and Vela-11 and -12 (OPS/7033 and OPS/7044) mapped gamma-ray sources in space. Following the initial surprise and consternation (who was attacking whom?), it transpired that they had discovered what have since become known as gamma-ray bursts (GRB).

<sup>126</sup>SBIRS-GEO: SBIRS-GEO-1 (USA-230) launched on 7 May 2011; SBIRS-GEO-2 (USA-241) launched on 19 March 2013. SBIRS-HEO: see below, Trumpet-FO satellites.

<sup>127</sup>GEO orbit: 11 satellites from Oko-US-KMO-1 (Kosmos-1960) in 1988 to Oko-US-KMO-11 (Kosmos-2440) in 2008. HEO (Molniya) orbit: 83 satellites (86 launched, 3 failures) from Oko-US-K-1 (Kosmos-520) in 1972 to Oko-US-K-85 (Kosmos-2446) in 2008 and Oko-US-K-86 (Kosmos-2469) in 2010.

## Destruction of Satellites: Star Wars

It is of little interest in such a book as this to dwell upon satellite destruction programmes, like ASAT (Air-Launched Anti-Satellite Missile), FOBS (Fractional Orbital Bombardment System), or what is popularly referred to as “star wars”, i.e., the US programme SDI (Space Defense Initiative), since abandoned.

Most space nations have protested about (successful) satellite destruction tests, owing to the vast amount of debris they have generated.<sup>128</sup>

## Intelligence

Satellite interception of all kinds of electronic signal is considered to be of great importance by the military. This is SIGINT (signal intelligence), covering ELINT (electronic intelligence), the surveillance of communications, and IMINT (image intelligence), photographic surveillance. The US–British (and Commonwealth) project Echelon uses many ground stations and orbiting satellites.

The US SIGINT missions began with the GREB (or GRAB) and Ferret series<sup>129</sup> (starting in 1962 with Ferret-2), on LEO orbits. The whole range of orbit types was subsequently put to use for these activities. Each programme lasted for roughly a decade. At the present time, many of these satellites are launched on behalf of the NRO (United States National Reconnaissance Office).

We note the following programmes, from the second generation in the 1970s to the fifth in the 2000s:

- LEO: SSF (Subsatellite Ferrets), NOSS (Navy Ocean Surveillance Satellite), also known as White Cloud, and NOSS-Sub-sats (satellites in formation); satellites of the SBSS programme (Space-Based Space Surveillance), in Sun-synchronous orbits at  $h = 630$  km, current series<sup>130</sup> and satellites<sup>131</sup> of the NRO.

---

<sup>128</sup>On 11 January 2007, China carried out a test by launching a missile from the Xichang space center in the province of Sichuan. The target was the defunct weather satellite FY-1C, at an altitude of 853 km. Thousands of pieces of debris were thereby created and continued in orbit for months or years, depending on their dimensions. On 21 February 2008, the United States announced that their satellite USA-193 had been successfully intercepted at an altitude of 310 km by a missile launched by USS Lake Erie, anchored near Hawaii. Given the low altitude of this satellite, all the debris is considered to have burnt up in the atmosphere within 90 days.

<sup>129</sup>The word “ferret” comes from the French “furet”, which itself comes from Latin as a diminutive of *fur*, *furis*, meaning “thief”. The word “furtive” belongs to the group of words with this root, so it is perhaps well suited to a spy satellite.

<sup>130</sup>First launch: SBSS-1 (USA-216) on 21 September 2010. The motto of the SBSS mission, namely, *vidi, scio, patrocinator* (to see, to know, to protect), is clear enough. Its objective is to detect any object measuring more than one meter in orbit.

<sup>131</sup>Launch dates: NROL-66 (USA-225), also called RPP (Rapid Pathfinder Program) on 6 February 2011; NROL-34 (USA-229) on 15 April 2011. NROL means NRO launch.

- HEO: Jumpseat (from 1971 to 1983), Trumpet<sup>132</sup> (from 1994 to 1997), Prowler<sup>133</sup> (or Trumpet FO, currently operating).
- GEO: Canyon (from 1968 to 1977), Rhyolite/Aquacade (from 1970 to 1978), Chalet/Vortex (from 1978 to 1981), Magnum/Orion (from 1985 to 1989); Mercury<sup>134</sup> (from 1994 to 1998), Mentor or Advanced Orion (from 1995 to 2003), and Intruder<sup>135</sup> (currently operating).

Among the GEO satellites, one should distinguish those in a true geostationary orbit from those like Canyon and Chalet/Vortex that are in geosynchronous orbits,<sup>136</sup> but elliptical and inclined at about  $8^\circ$ , which makes it easier to locate the radars by triangulation.

There have been similar Soviet then Russian programmes, beginning in 1970 with Kosmos-389. The Tselina programme, in LEO orbit, is the equivalent of NOSS, with  $i = 82.6^\circ$  for the Tselina-D series and  $i = 71.0^\circ$  for the more recent Tselina-2 series.

### 9.2.13 Manned Satellites

We give here a few dates marking out the history of manned spaceflight, i.e., satellites in orbit with humans aboard: Vostok-1 (“Orient” in Russian), launched on 12 April 1961, for the first man in orbit (one revolution) and Apollo-11, launched on 16 July 1969, for the first steps on the Moon.

The idea of an orbital space station was first put into practice with the Soviet Salyut (“salvation”), from 1971 to 1986, followed by Mir (*mir* means both “world” and “peace” in Russian), from 1986 to 2000, on a near-circular orbit with  $h \sim 300$  km,  $i = 51.6^\circ$ . The USA used Skylab in 1973, on an equivalent orbit,  $h \sim 400$  km,  $i = 50.0^\circ$ . They then began to develop the

---

<sup>132</sup>The three satellites of the series Trumpet-1 (USA-103), Trumpet-2 (USA-112), and Trumpet-3 (USA-136) are in Molniya orbit with apogee over Russia. Their antennas have diameters of several tens of meters, and apparently between 100 and 150 m, for Trumpet-3. The data are gathered by the SDS satellites, also in Molniya orbit.

<sup>133</sup>Launch dates for the series Trumpet Follow-On: Trumpet-FO-1 (USA-184, NROL-22, SBIRS-HEO-1) on 28 June 2006; Trumpet-FO-2 (USA-200, NROL-28, SBIRS-HEO-2) on 13 March 2008.

<sup>134</sup>Mercury-1 (USA-105 or Jeroboam) and Mercury-2 (USA-118). This programme is sometimes called Mercury Advanced Vortex to distinguish it from the Mercury programme of manned flights.

<sup>135</sup>The three first satellites launched were Mentor-1 (USA-110) in 1995, Mentor-2 (USA-139, NROL-6) in 1998, and Mentor-3 (USA-171, NROL-19 or Homer) in 2003. These were followed by Mentor-4 (USA-202, NROL-26), the first of the Intruder series, also called IOSA (Integrated Overhead SIGINT Architecture, or Intruder-1), launched on 17 January 2009. According to *Aviation Week*, this is the largest, the most secret, and the most expensive US military satellite. Including the launch, it is said to have cost over two billion dollars. However, this record was soon beaten by the following, Mentor-5 (USA-223, NROL-32), launched on 11 November 2010.

<sup>136</sup>Geosynchronous orbit  $h_p = 30,500$  km,  $h_a = 41,000$  km,  $i = 7-9^\circ$ , for the seven Canyon satellites, from Canyon-1 (OPS/2222) in 1968 to Canyon-7 (OPS/9751) in 1977, and the six Vortex satellites, from Vortex-1 (OPS/9454 or Chalet-1) to Vortex-6 (USA-37 or Chalet-6).

ISS (International Space Station), from 1998, in collaboration with Russia and other nations. The orbit is circular, with  $h$  between 355 and 400 km and  $i = 51.6^\circ$ .

The space shuttle idea is based on the possibility of a reusable spacecraft, a satellite that becomes an aircraft in the landing stage. The five American Space Shuttles were Columbia (1981–2003), Challenger (1983–1986), Discovery (from 1984), Atlantis (from 1985), and Endeavour (from 1992). These flights are denoted by<sup>137</sup> STS (Space Transportation System). The STS programme ended<sup>138</sup> in 2011. All in all there were 135 shuttle flights, including 133 successes and 2 failures with Challenger STS-25 (STS-51-L) and Columbia STS-107.

The shuttle had two configurations: a payload of 24.4 tonnes for a low orbit,  $h = 204$  km,  $i = 28.5^\circ$ , and a payload of 12.5 tonnes for a higher orbit,  $h = 407$  km,  $i = 51.6^\circ$ . It was the latter configuration that was used for rendezvous with the ISS. For maintenance of Hubble, the shuttle went into a higher orbit. A great many satellites were placed in orbit by the shuttle. Once in orbit, the satellite left the cargo bay of the shuttle and moved to its destination under its own power (a nearby orbit, either geostationary or heliocentric).

### 9.2.14 Non-Scientific Satellites

The American organisation Celestrak, which records and classifies satellites into different categories, created a section entitled *Other* under the heading *Miscellaneous Satellites*. It is interesting to cast an eye over these unclassifiable objects.

For example, the sole aim of the Celestis satellites is to send the ashes of certain Earthlings into orbit.<sup>139</sup> Another remarkable oddity is the only

---

<sup>137</sup>From the first Columbia flight on 12 April 1981, STS-1, up to the end of 1983, with STS-9, flights were numbered sequentially, but from 1984, their number included the fiscal year, the point of launch, and a letter indicating the order for that year: STS-10 thus becomes STS-41-B. Following the Challenger disaster, STS-51-L, which was the 25th shuttle flight (STS-25), NASA decided to return to the system of numbering by scheduling order (which is not necessarily the same as launch order).

<sup>138</sup>Last flights in 2011 were Discovery (STS-133), Endeavour (STS-134), and Atlantis (STS-135).

<sup>139</sup>Other organisations classify these as burial satellites. Without wishing to carry out unnecessary advertising for the Celestis company, we may quote the following sales information: “Celestis offers to launch a symbolic portion of the cremated remains of the individuals into space”. Business is clearly booming: several satellites have been placed in orbit since 1997, not to mention a lunar impact with Lunar-01 (in fact, a capsule carried by Lunar Prospector) in 1998, following the same idea. There is a project to send such spacecraft into deep space and out of the Solar System. The first three satellites, Celestis-1 to -3, had very different orbits, because they were launched as passengers with much bigger missions. Of the following, Celestis-4 and Celestis-7, burnt up in space due to launch failure (grouped with OrbView-4 and QuikTOMS for the first, and Trailblazer for the second). So these were certainly the first examples of satellites in which the payload was in no way

Turkmen satellite TMC, which attests to the greatness of Turkmenistan and its president for life by its entirely passive presence.<sup>140</sup>

Other equally fascinating initiatives abound, but private financing is generally hesitant. Let us mention two projects that have not yet been completely finalised: KEO, which will remain in orbit for thousands of years (because at an altitude of 1,800 km or indeed in a GTO orbit) and will carry some items with which to remember mankind (blood, DNA, maps of the world, various messages and sundry other paraphernalia); and CiS (Cross in Space), a capsule containing a cross and the bible on microfilm.

### 9.3 Appendix: Delays in Scheduling Space Missions

There is an important issue that cannot be ignored when one considers space missions, namely, rescheduling and delayed launch. Such delays generally have no other consequence than shifting the mission back in time.<sup>141</sup> In some cases, however, it can lead to a change in the orbit, as we shall see with EarthCARE in Chap. 11. The reasons for delays are various (launch vehicles, instruments, etc.) and justifiable, but the consequences are there: missions never correspond to their original schedule! Space missions provide an excellent illustration of Hofstadter's law.<sup>142</sup> Space agencies maintain a certain artful vagueness when it comes to their schedules.

When a mission involves several satellites over a long period, governmental organisations have been known to make drastic changes. This is what happened in May 2010, when the US Congress decided to modify the NPOESS programme by transforming it into JPSS. Congress based its decision on a report by the United States Government Accountability Office (GAO), which shows the evolution of the cost forecast from 7.00 in August 2002 to 14.95 in June 2009, where the units are of course billions of dollars. This report clearly describes the planned launch date as a function of the date at which the forecast was made. The data is plotted in Fig. 9.46 for the three first satellites of the programme: NPP, C1, and C2 (the names of the satellites NPOESS-1 and

---

deteriorated by the explosion! Note that, between 2000 and 2007, these satellites were also given the names EarthView-01, -02, -03, and -04, respectively, which might cause some surprise in a remote-sensing bibliography.

<sup>140</sup>Launched with OICETS by a Russian rocket, TMC (Turkmenistan Memorial Capsule) encloses the country's flag and a book with the title *Rukhnama*, a historical and philosophical work written by Saparmurat Niyazov, president of Turkmenistan for life.

<sup>141</sup>For missions to other planets, Kepler's laws impose strict windows for launch dates. No delay was possible for Voyager-1 and -2, . . . , Cassini, and New Horizons. In the case of Rosetta, a delay of several months forced the ESA to change the target comet.

<sup>142</sup>The author of *Gödel, Escher, Bach: An Eternal Golden Braid* pronounced the following law which carries his name: "It always takes longer than you expect, even when you take into account Hofstadter's Law".

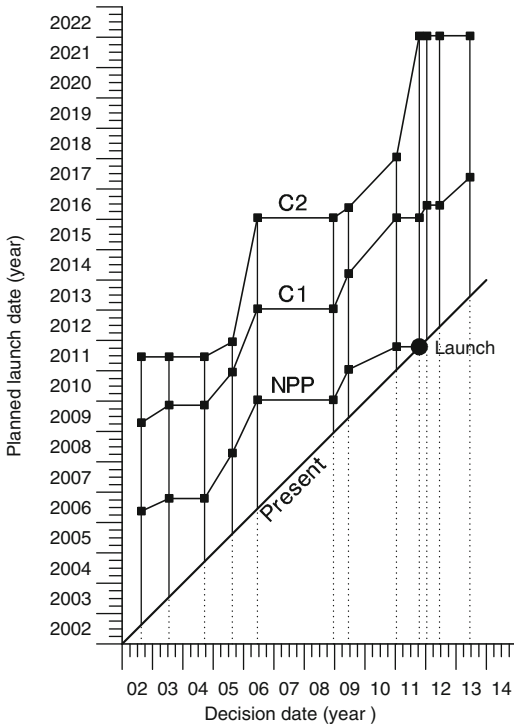


FIG. 9.46 : *Planned launch date against date decision was taken for the three first satellites of the new American meteorological programme JPSS (a joint project of NASA, the NOAA, and the DoD): NPP, JPSS-1 (denoted by C1), and JPSS-2 (denoted by C2). From a document published by the Government Accountability Office of the US Congress.*

-2 became JPSS-1 and -2, respectively, and are denoted by C1 and C2 in the report). It is extremely rare to be able to establish such a precise time chart on the basis of official documents.

Since the GAO report, things have become still more complicated! The military have decided to go it alone, leaving the JPSS to set up the DWSS. To be continued.

# Chapter 10

## Orbit Relative to the Sun: Crossing Times and Eclipse

We begin by studying the position of the orbital plane of an arbitrary satellite relative to the direction of the Sun, focusing on the notion of crossing time. We then turn more specifically to Sun-synchronous satellites for which this relative position provides the very definition of their orbit. We end the chapter with a more theoretical question, calculating the angle between the direction of the Sun and the plane of the orbit, and this will lead us to the study of solar eclipses, when the satellite is in the Earth's shadow.

### 10.1 Cycle with Respect to the Sun

#### 10.1.1 Crossing Time

At a given time, it is useful to know the local time on the ground track, i.e., the local mean time (LMT), deduced in a straightforward manner from the UT once the longitude of the place is given, using (7.59). The LMT on the ground track at this given time is called the crossing time or local crossing time. To obtain the local apparent time (LAT), one must know the day of the year to specify the equation of time  $E_T$ . In all matters involving the position of the Sun (elevation and azimuth) relative to a local frame, this is the time that should be used. The ground track of the satellite can be represented by giving the crossing time. We have chosen to represent the LMT in colour with the *Ixion* software.

For Sun-synchronous satellites like Suomi-NPP or SPOT-6, Figs. 10.2 and 10.4 show that the crossing time depends only on the latitude. For the HEO orbit of the satellite Ellipso Borealis, the stability of the crossing

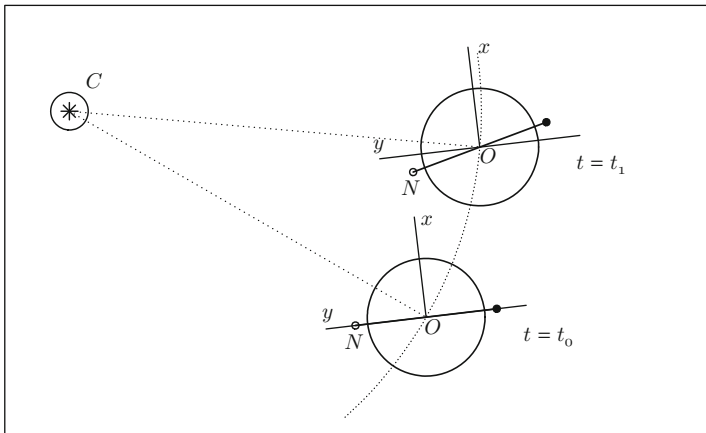


FIG. 10.1 : Position of the line of nodes in the geocentric frame  $\mathfrak{R}$  ( $O; x, y, z$ ) at two times  $t_0$  and  $t_1$ , where  $C$  is the center of the Sun,  $O$  is the center of the Earth, and  $Oxy$  lies in the equatorial plane. The ascending node is denoted by  $N$ .

time also shows up very clearly in Figs. 10.6 (lower) and 10.7. For non-Sun-synchronous satellites like Meteor-3-07 or Jason-2, the time difference shows up through a shift in the time from one revolution to the next, as can be seen from Figs. 10.3 and 10.5. For a low-inclination satellite such as Megha-Tropiques, we note certain specific configurations, illustrated by Figs. 10.10 and 10.11. If the ascending node crossing occurs at 06:00, the northern hemisphere will be viewed during the day, and the southern hemisphere during the night. After a few days, the crossing time at the equator will have changed. An example is given in Fig. 10.6 (upper) for the satellite Loopus in a highly eccentric orbit.

### 10.1.2 Calculating the Cycle $C_s$

We consider the orbit of the Earth around the Sun, treating it as circular, since in this calculation of the cycle, we identify LAT and LMT. In Fig. 10.1, the center of the Sun, and of the Earth's orbit, is denoted by  $C$ , while the center of the Earth is  $O$ . The ascending node of a satellite in orbit around the Earth is denoted by  $N$ . The dihedral angle between the meridian plane of the Earth containing  $N$  and the plane containing  $C$  gives  $H$ , the hour angle of the ascending node. This angle is represented in Fig. 10.1 by  $H = (\mathbf{OC}, \mathbf{ON})$ .

At time  $t = t_0$ , the hour angle of  $N$  is  $H(t_0) = H_0$ . At another time  $t = t_1$ , the plane of the satellite orbit will have changed due to the phenomenon of nodal precession by an angle  $\Omega$  relative to the frame  $\mathfrak{R}$ . The hour angle  $N$  is then given by

$$H(t_1) = H_1 = H_0 + \Omega - \alpha,$$



where  $\alpha$  is the angle through which the Sun–Earth direction has changed as the Earth moves on its orbit around the Sun, viz.,

$$\alpha = [\mathbf{CO}(t_0), \mathbf{CO}(t_1)] .$$

This angle  $\alpha$  is equal to the difference in ecliptic longitude  $l$  of the Sun at the two given times. Hence,

$$\Delta H = H_1 - H_0 = \Omega - \alpha ,$$

which represents the motion of the direction of the line of nodes with the direction of the Sun.

Setting  $\Delta t = t_1 - t_0$  for the time interval, the angles can be expressed in terms of the angular speeds:

$$\Omega = \dot{\Omega} \Delta t , \quad \alpha = \dot{\Omega}_S \Delta t ,$$

whence

$$\Delta H = (\dot{\Omega} - \dot{\Omega}_S) \Delta t . \tag{10.1}$$

The time interval  $\Delta t_S$  needed for the hour angle of the ascending node to vary by 24 h, or one round trip, is called the cycle relative to the Sun. Hence,

$$H(t + \Delta t_S) = H(t) \quad [\text{mod } 2\pi] ,$$

which implies that

$$\Delta t_S = \frac{2\pi}{\dot{\Omega} - \dot{\Omega}_S} .$$

Bringing in the nodal precession rate  $P$  in round trips per year as defined by (7.40) and (7.38),  $\Delta t_S$  becomes

$$\Delta t_S = -D_M \frac{N'_{yr}}{1 - P} .$$

The cycle relative to the Sun is usually given in days and we shall denote it by  $C_S$  ( $C$  for cycle and  $S$  for Sun). Since  $\Delta t_S$  is expressed in SI units, i.e., in seconds, we obtain  $C_S$  from the very simple expression

$$C_S = \frac{N_{tro}}{P - 1} . \tag{10.2}$$

The symbols  $N'_{yr}$  and  $N_{tro}$  are explained in Chap. 7.

The quantity  $P$  can be expressed in terms of the constant  $k_h$  defined by (7.98). This rate  $P$  is given by

$$P = -k_h \left( \frac{R}{a} \right)^{7/2} \cos i . \tag{10.3}$$

One can check that, for a Sun-synchronous satellite, one does indeed have  $P = 1$ .

In this way we obtain the cycle relative to the Sun as a function of the orbital characteristics, taking care to note the signs:

$$C_S = C_S(a, i) = -\frac{N_{\text{tro}}}{k_h(R/a)^{7/2} \cos i + 1}, \quad (10.4)$$

or with approximate numerical values ( $C_S$  in days),

$$C_S = -\frac{365.25}{10.11(R/a)^{7/2} \cos i + 1}. \quad (10.5)$$

The cycle relative to the Sun  $C_S = C_S(a, i)$ , is a very important characteristic of any satellite (Figs. 10.2, 10.3, 10.4, 10.5, 10.6, and 10.7).

### 10.1.3 Cycle $C_S$ and Orbital Characteristics

#### Cycle $C_S$ as a Function of Altitude and Inclination

The cycle  $C_S$  is a function of  $a$  and  $i$ . Figure 10.8 shows the variation  $C_S(i)$  for a fixed value of the altitude, viz.,  $h = 700$  km. The cycle  $C_S(i)$  is given in days, with the sign indicating the direction of rotation. We have also plotted the nodal precession rate  $P(i)$  in rev/yr, which is a sinusoidal curve, and  $P - 1$  which determines the vertical asymptote of  $C_S(i)$  by its intersection with the horizontal axis through the origin. This value of  $i$  corresponds to the inclination of the Sun-synchronous circular orbit for this altitude.

For the altitude represented here, typical of LEO satellites, we see that the cycle remains in the vicinity of 2 months ( $C_S \sim -60$  day) for inclinations below  $45^\circ$ . When  $i$  increases, the length of the cycle also increases. Above the Sun-synchronous inclination, the cycle decreases (but there are very few satellites in this configuration).

#### Specific Cases of the Cycle $C_S$

We note here certain specific values of the cycle  $C_S$  for different orbits:

- **Polar Satellites.** We see immediately from (10.4) or (10.5) that, if the satellite is strictly polar,  $C_S = -365.25$  day. The cycle is thus annual. One year goes by before we return to the same orbital configuration relative to the Sun, since the plane of the orbit does not rotate with respect to  $\mathfrak{R}$ . The negative value of  $C_S$  shows that the line of nodes moves in the retrograde direction relative to  $\mathfrak{R}_T$ .
- **Sun-Synchronous Satellites.** Equation (10.2) shows that, if  $\dot{\Omega} = \dot{\Omega}_S$ , the cycle is infinite. This happens for Sun-synchronous satellites and we may indeed treat  $C_S$  as infinite, since after a very great number of days, the angle  $H$  will not have changed. For Sun-synchronous satellites, the hour

angle of the ascending node, and hence the crossing time<sup>1</sup> of the satellite at the ascending node, is constant. For a given altitude, the cycle  $C_S$  is negative provided that  $i$  is less than the Sun-synchronous inclination given by (7.105). Beyond this value,  $C_S$  is positive.

- **Shortest Cycle.** The smallest value for the cycle is given by the minimum of  $|C_S(a, i)|$ . According to (10.5), it is obtained for  $i = 0$  and  $a = R$ , and the value is

$$|C_S|_{\min} = \frac{N_{\text{tro}}}{k_h + 1} = \frac{365.25}{11.11} = 32.9 \text{ day} . \tag{10.6}$$

The cycle relative to the Sun  $C_S$  can therefore never be less than 33 days.

### Nodal Precession and Cycle $C_S$

In order to visualise the nodal precession and bring out the significance of the cycle  $C_S$ , let us return to the graph in Fig. 10.1 and apply it to a few satellites in Example 10.2.

**Example 10.1** Calculate the cycle relative to the Sun for the satellites Meteor-3-07, Jason-2, ICESat, ERBS and UARS, and TRMM and Megha-Tropiques.

- These satellites have near-circular orbits. For Meteor-3-07, we have  $h = 1,194\text{km}$  and  $i = 82.56^\circ$ . Using (10.5), we obtain

$$\begin{aligned} C_S &= -\frac{365.25}{10.11 (6378/7572)^{7/2} \cos(82.56) + 1} = -\frac{365.25}{10.11 \times 0.5477 \times 0.1295 + 1} \\ &= -\frac{365.25}{0.7169 + 1} = -\frac{365.25}{1.7169} = -212.73 , \end{aligned}$$

which gives a cycle of 213 days (advance of crossing time).

For TOPEX/Poseidon, Jason-1 and -2, with  $h = 1,336\text{km}$  and  $i = 66.04^\circ$ , we obtain  $P = -2.107$ , which gives a cycle  $C_S = -117.47$ , or 117 days (advance of crossing time).

The satellite ICESat flies at low altitude,  $h = 592\text{km}$ , with inclination  $i = 94^\circ$  between the polar inclination, for which the cycle is 1 year ( $C_S = -365.25$ ), and the Sun-synchronous inclination  $i_{\text{HS}} = 97.8^\circ$  at this altitude, for which the cycle is infinite. The calculation gives  $P = 0.515$ , whence  $C_S = -752.7$ , which corresponds to a very long cycle, more than 2 years.

---

<sup>1</sup>The time related to the hour angle is LAT. A Sun-synchronous satellite crosses the ascending node at the same LMT. If there is no difference between LAT and LMT here, it is because we have used a simplified scenario for the Earth orbit. However, for the calculation of the cycle  $C_S$ , this could not be otherwise: we only want to know how many days it will be before the next crossing (to within a few minutes), whatever time of year it is. To treat an elliptical Earth orbit, we would have to specify the day we choose to begin the cycle.

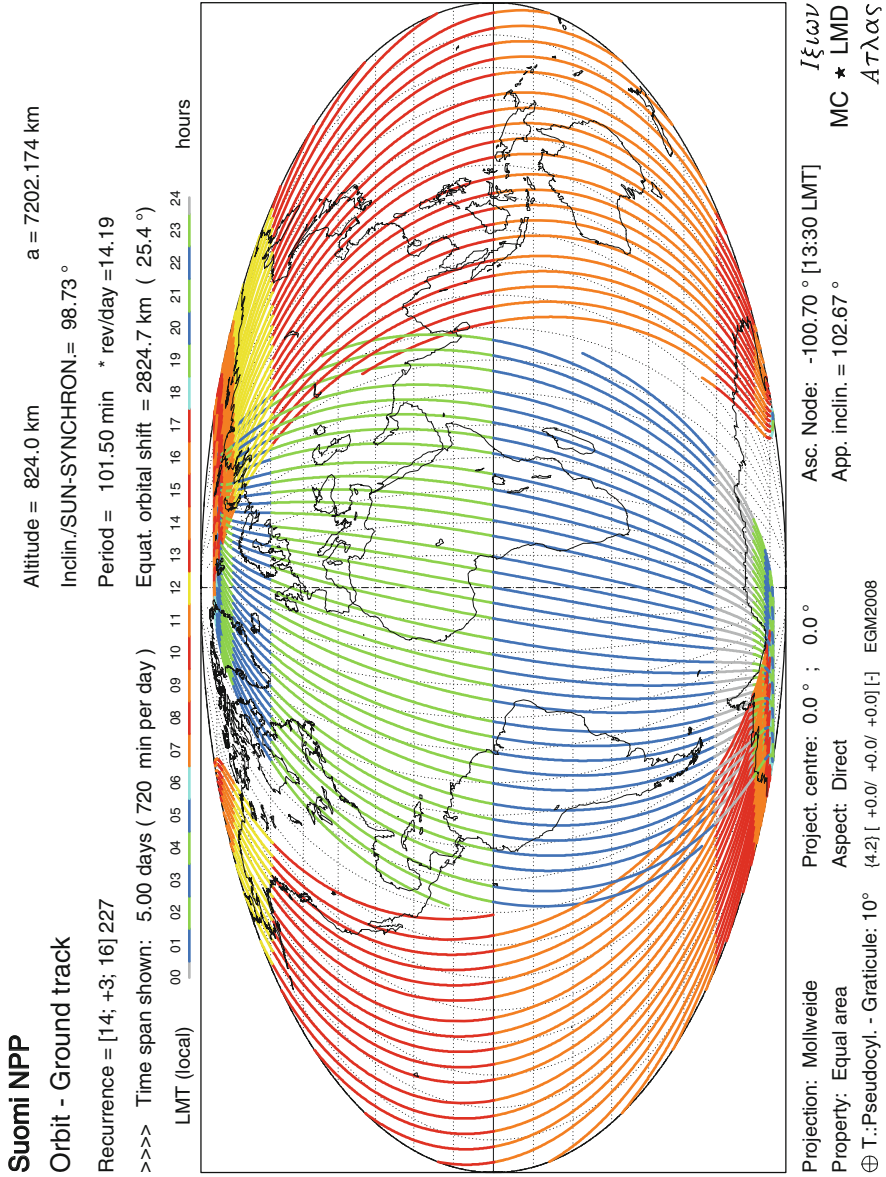


FIG. 10.2 : Ground track and crossing time for the Sun-synchronous satellite Suomi-NPP, over 5 days (12 consecutive hours per day).

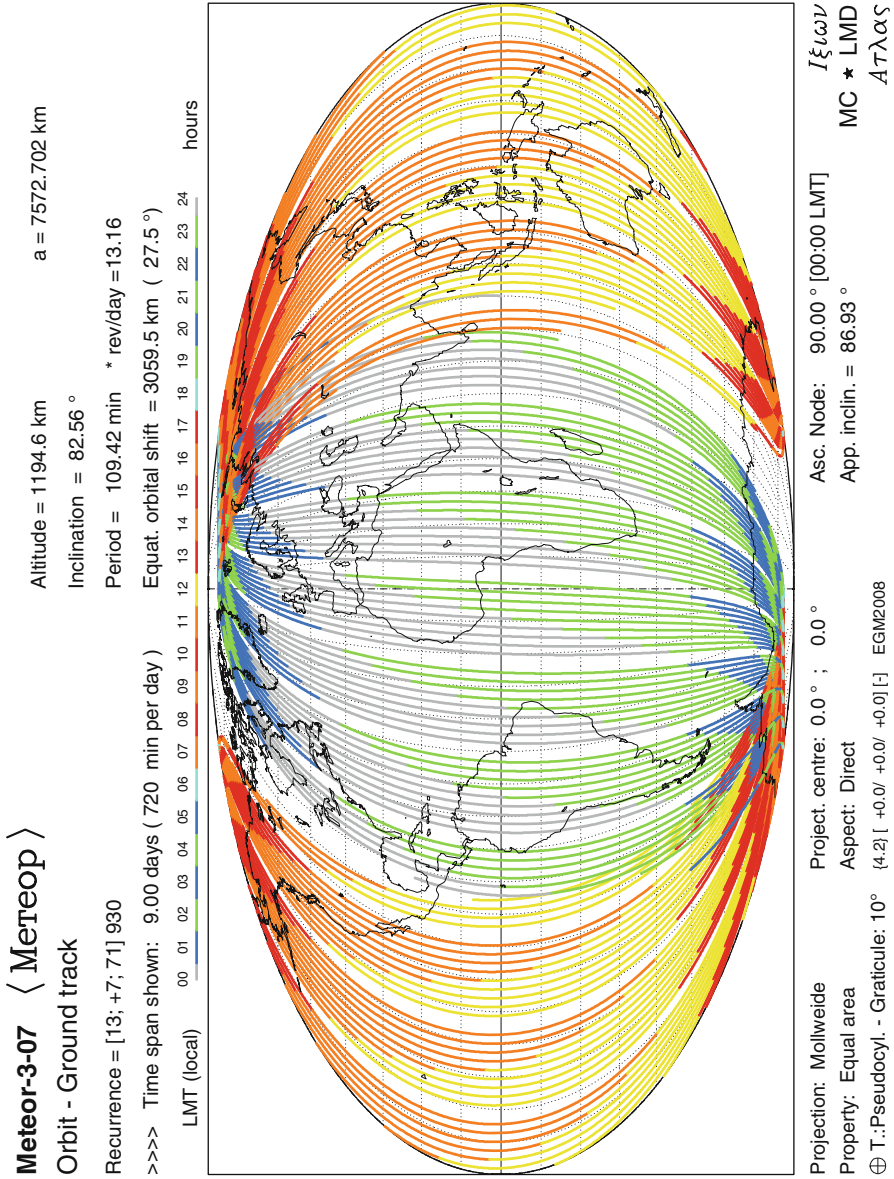


FIG. 10.3: Ground track and crossing time for the non-Sun-synchronous satellite Meteor-3-07, over 9 days (12 consecutive hours per day).

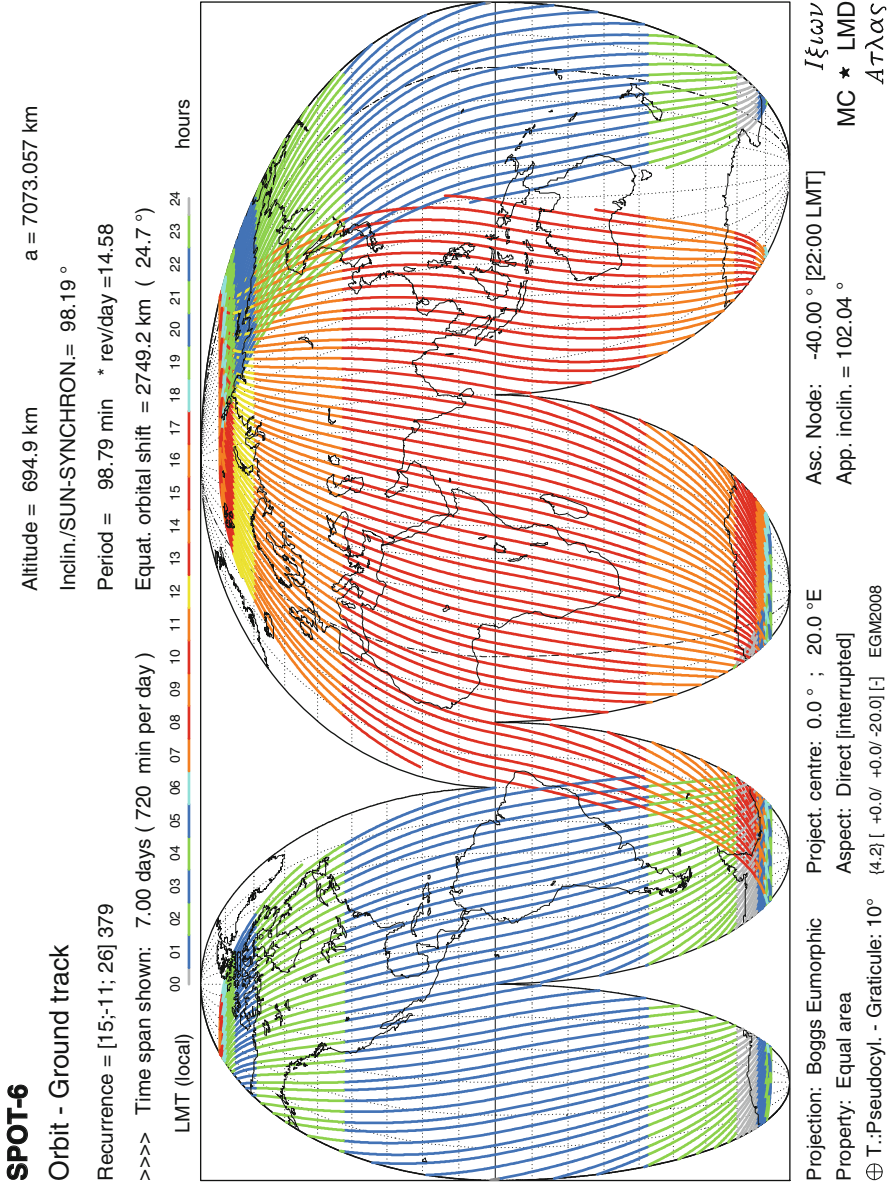


FIG. 10.4 : Ground track and crossing time for the Sun-synchronous satellite SPOT-6, over 7 days (12 consecutive hours per day).



**Jason-2 / OSTM**

**Orbit - Ground track**

Altitude = 1336.3 km a = 7714.434 km

Inclination = 66.04 °

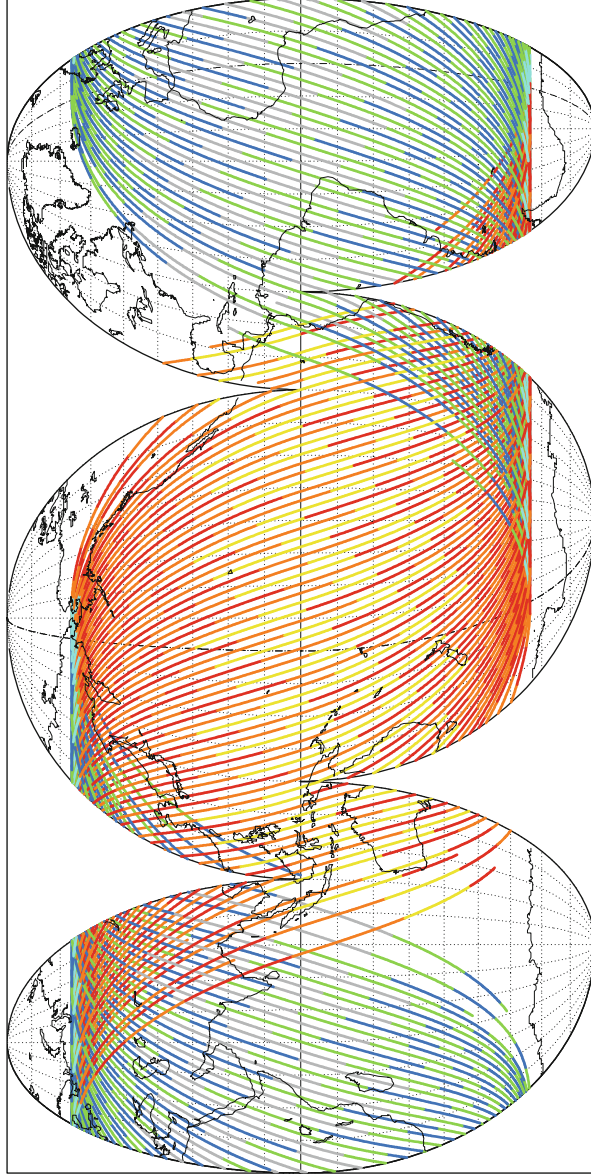
Recurrence = [13; -3; 10] 127

Period = 112.43 min \* rev/day = 12.81

Equat. orbital shift = 3155.5 km ( 28.3 °)

>>>> Time span shown: 10.00 days ( 720 min per day)

LMT (local) 00 01 02 03 04 05 06 07 08 09 10 11 12 13 14 15 16 17 18 19 20 21 22 23 24 hours



Projection: Boggs Eumorphic Project. centre: 0.0 ° ; 160.0 ° W  
 Property: Equal area Aspect: Direct [interrupted]  
 ⊕ T.:Pseudocyl. - Graticule: 10° {4.2} [ +0.0/ +0.0+160.0] [ EGM2008

Asc. Node: 111.26 ° [00:30 LMT]  
 App. inclin. = 70.29 °

$I \xi \zeta \omega \nu$   
 MC \* LMD  
 $A \tau \lambda \alpha \varsigma$

FIG. 10.5 : Ground track and crossing time for the non-Sun-synchronous satellite Jason-2, over 10 days (12 consecutive hours per day).

**Loopus**

Elliptical orbit - Gr. track

Recurrence = [ 2; -1; 3] 5

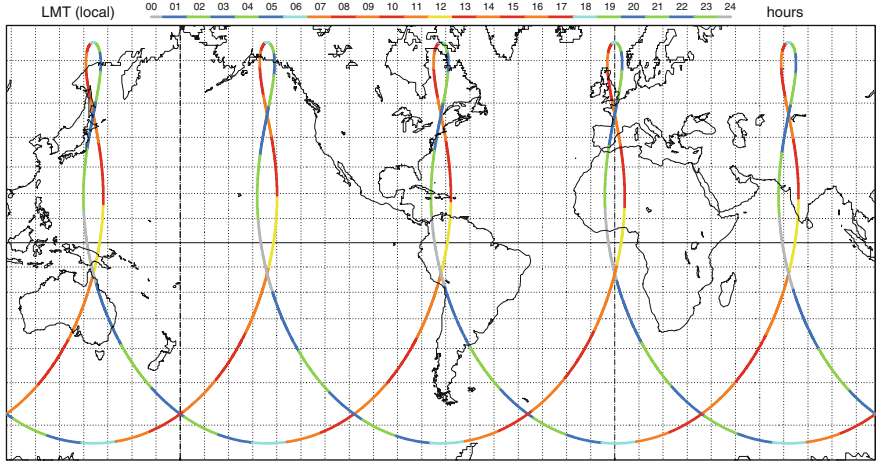
>>>> Time span shown: 4320.0 min = 3.00 days

Equiv. altit. = 23613.3 km      a = 29991.445 km

CRITICAL Incln. = 63.43 °      e = 0.600000

Period = 861.53 min \* rev/day = 1.67

h\_a = 41608 km; h\_p = 5618 km; arg. perigee: +270.00 °



Projection: Mercator

Property: Conformal

⊕ T.:Cylindrical - Graticule: 10°

Project. centre: 0.0 ° ; 72.0 ° W

Aspect: Direct

{4.2} [ +90.0/ +0.0/ -18.0] [-] EIGEN-C3

Longitude / Initialisation:

Asc. Node: 2.61 ° [12:00 LMT]

Apogee : 0.00 °

Ιξίων

MC ★ LMD

Ατλας

**Ellipso Borealis**

Orbit - ref.: Earth

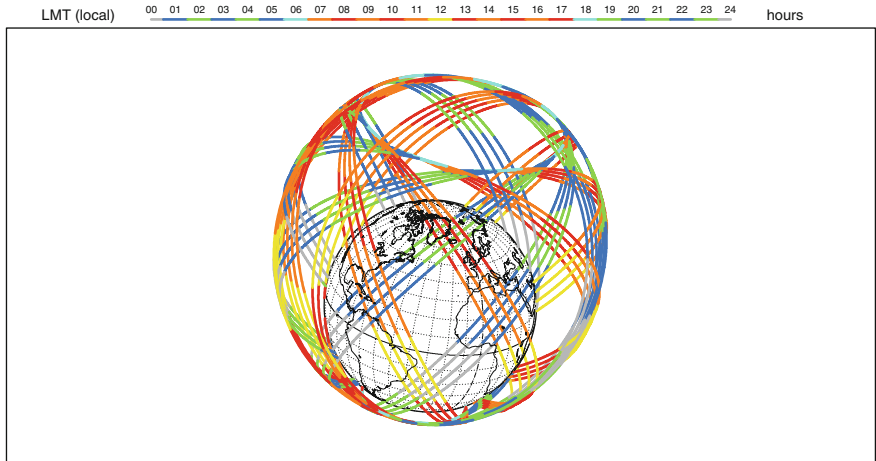
>>>> Time span shown: 5760.0 min = 4.00 days

Equiv. altit. = 4094.1 km      a = 10472.196 km

Incl/SUN-S.&CRIT. = 116.58 °      e = 0.326603

Period = 177.78 min \* rev/day = 8.10

h\_a = 7514 km; h\_p = 674 km; arg. perigee: +270.00 °



Projection: Orthographic

Property: none

⊕ T.:Azimuthal - Graticule: 10°

Project. centre: 26.0 ° N; 33.0 ° W

Aspect: Oblique

{4.2} [ -90.0/ +64.0/ +123.0] [-10] EGM2008

Longitude / Initialisation:

Asc. Node: -180.00 ° [12:00 LMT]

Apogee : 74.31 °

Ιξίων

MC ★ LMD

Ατλας

FIG. 10.6 : *Orbits and crossing times for two satellites in eccentric orbits with critical inclination. Upper: Loopus satellite project. Prograde and non-Sun-synchronous, over 3 days. Lower: Ellipso Borealis satellite project. Retrograde and Sun-synchronous, with  $\tau_{AN} = 12:00$ .*



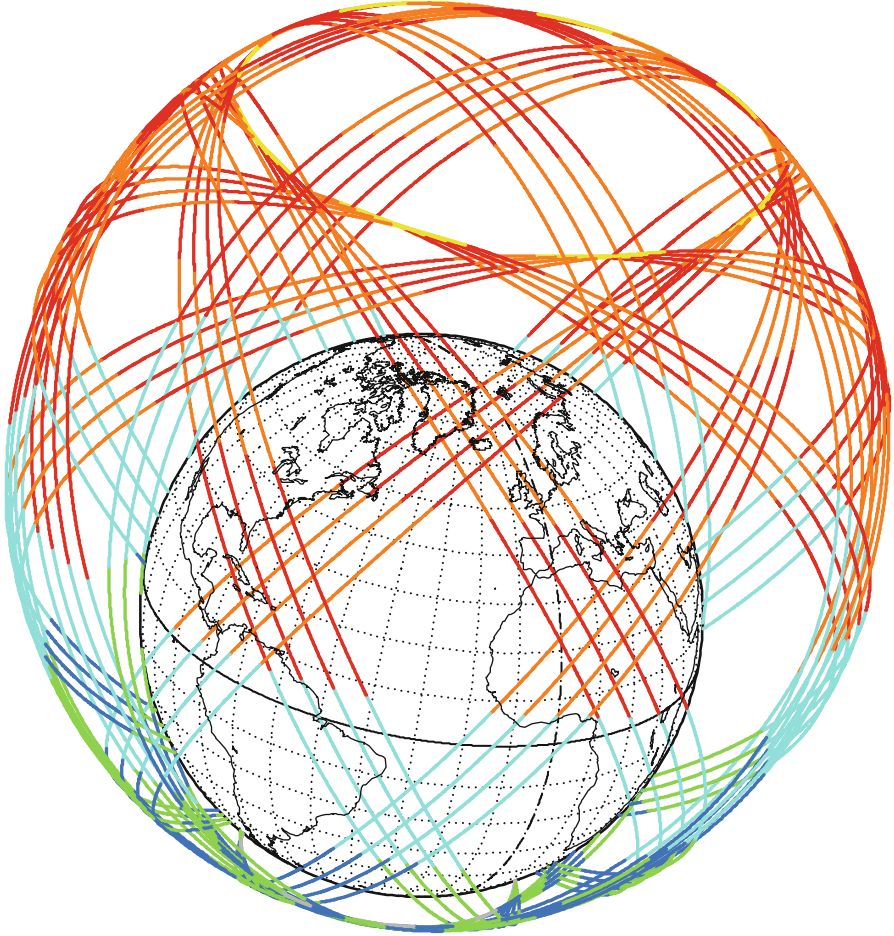


FIG. 10.7 : Orbit and crossing time for the Sun-synchronous satellite *Ellipso Borealis*, over 4 days. Same caption as for Fig. 10.6 (lower) except that the ascending node crossing time is  $\tau_{AN} = 18:00$  LMT.

The satellites ERBS and UARS, both launched by the Space Shuttle, have the same inclination and the same altitude to within a few kilometers. The calculation gives  $P = -3.986$ , whence  $C_S = -73.2$ , for ERBS, and  $P = -4.090$ , whence  $C_S = -72.0$ , for UARS. One often reads for these satellites that their cycle relative to the Sun is 36 days. There is thus confusion here between cycle and half-cycle. If on a given day the ascending node crossing occurs at noon, then 36 days later it is the descending node crossing that will occur at noon.

For low-inclination satellites on the equator, like TRMM and Megha-Tropiques, the cycle is short because the factor  $\cos i$  is close to unity. For

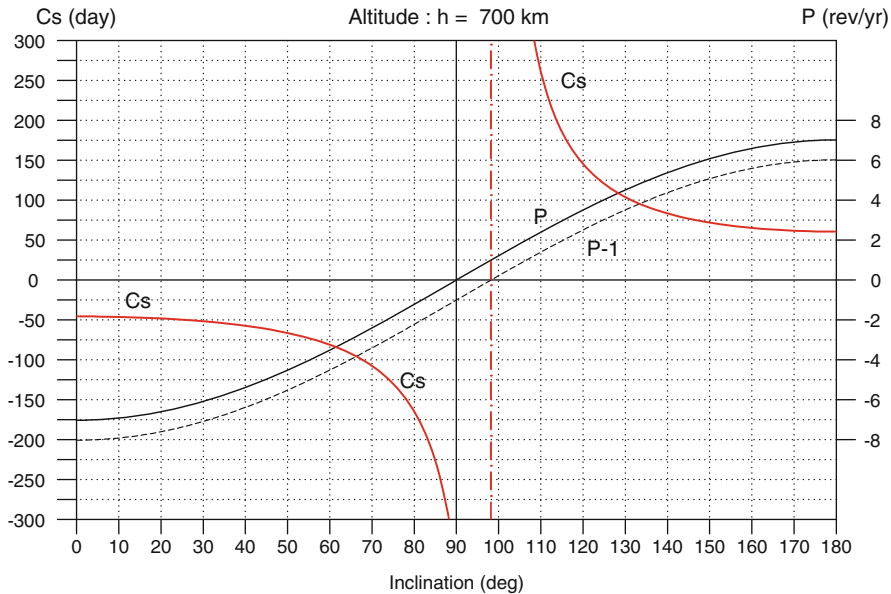


FIG. 10.8 : Variation of the cycle  $C_S$  relative to the Sun as a function of the inclination for a satellite at altitude  $h = 700 \text{ km}$ . The cycle  $C_S$  is given in days on the left ordinate, and the nodal precession rate  $P$  is given in rev/yr on the right ordinate.

TRMM,  $P = -6.894$ ,  $C_S = -46.3$  when  $h = 350 \text{ km}$ ,  $P = -6.710$ ,  $C_S = -47.4$  when  $h = 402 \text{ km}$ . For Megha-Tropiques,  $P = -6.115$ ,  $C_S = -51.3$ . For these satellites, the ascending node crossing moves forward half an hour every day. ◀

**Example 10.2** Visualising the cycle  $C_S$  for various satellites in prograde, polar, retrograde, and Sun-synchronous orbits.

► Figure 10.9 shows the position of the Earth on its orbit around the Sun and the position of the nodes (ascending in black, descending in white) of the satellite orbit. LMT and LAT are not distinguished on the graph.

For the two Sun-synchronous satellites, Radarsat-2 and Terra, it is clear that the shift of the orbital plane compensates the Earth's annual motion. For Radarsat-2, the normal to the orbit lies in the meridian plane passing through the Sun.

For a strictly polar satellite, the orbital plane is fixed in  $\mathfrak{R}$ . For the satellite CoRoT, which has this inertial orbit, stars are observed perpendicularly to the orbit, 6 months in one direction, and 6 months in the opposite direction, in such a way as to avoid viewing the Sun.

We may also consider several retrograde (negative) cycles, one very short for TRMM with its prograde orbit and one very long for LAGEOS-1 with its

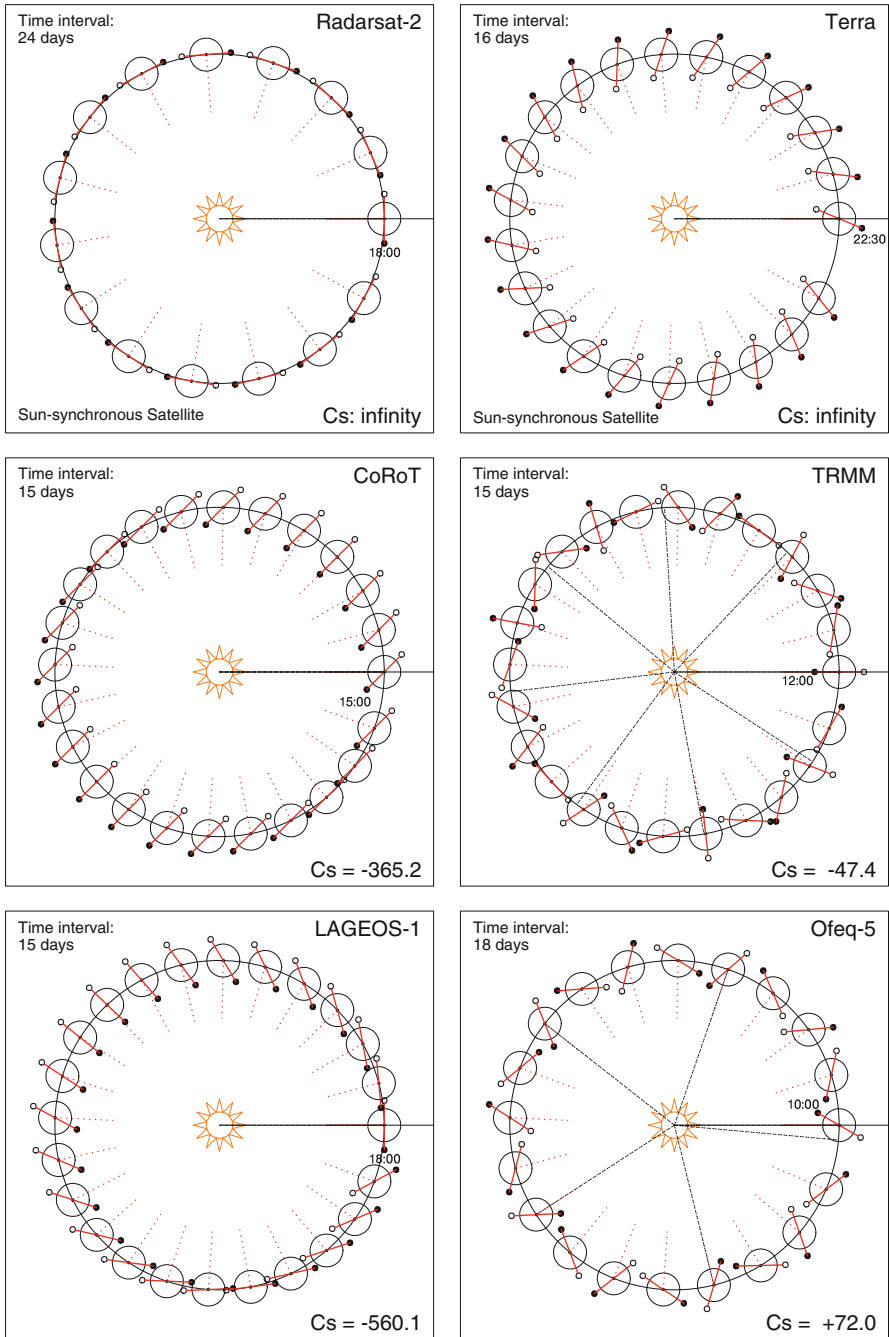


FIG. 10.9 : Cycle relative to the Sun for various satellites. The time given is the crossing time at the first ascending node.

**Megha-Tropiques**

Orbit - Ground track

Recurrence = [14; -1; 7] 97

>>>> Time span shown: 4320.0 min = 3.00 days

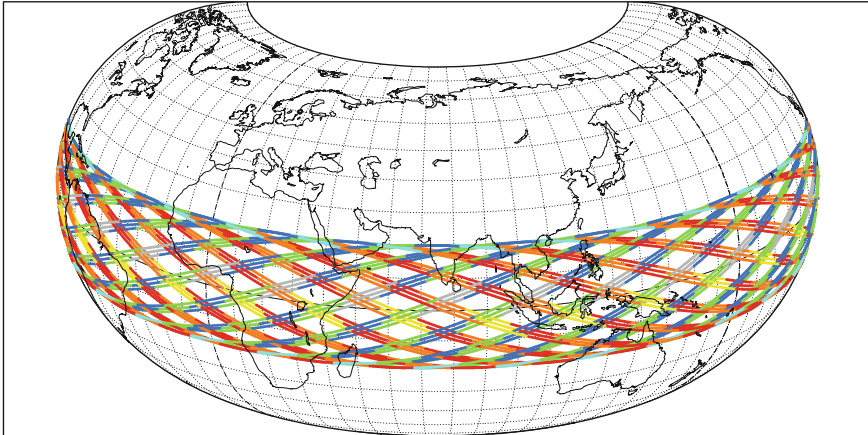
Altitude = 865.5 km      a = 7243.677 km

Inclination = 20.00 °

Period = 101.93 min \* rev/day=14.13

Equat. orbital shift = 2892.0 km ( 26.0 °)

LMT (local)      00 01 02 03 04 05 06 07 08 09 10 11 12 13 14 15 16 17 18 19 20 21 22 23 24      hours



Projection: Raisz Armadillo  
Property: none  
⊕ T.:(various) - Graticule: 10°

P.C.: 0.0 ° ; 75.0 °E / 28.1 °N; 75.0 °E  
Aspect: Direct  
{4.2} [+90.0/ +0.0/-165.0] [-] EIGEN6C2

Asc. Node: -105.00 ° [00:00 LMT]  
App. inclin. = 21.52 °

*Ιξίων*  
MC ★ LMD  
*Ατλας*

**Megha-Tropiques**

Orbit - Ground track

Recurrence = [14; -1; 7] 97

>>>> Time span shown: 4320.0 min = 3.00 days

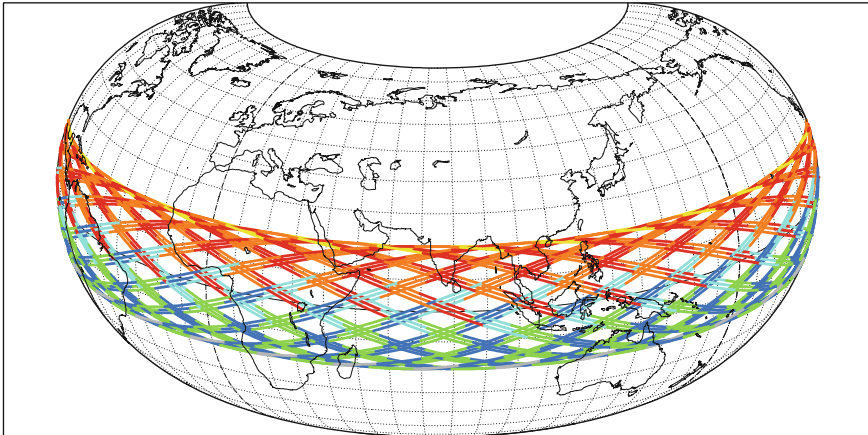
Altitude = 865.5 km      a = 7243.677 km

Inclination = 20.00 °

Period = 101.93 min \* rev/day=14.13

Equat. orbital shift = 2892.0 km ( 26.0 °)

LMT (local)      00 01 02 03 04 05 06 07 08 09 10 11 12 13 14 15 16 17 18 19 20 21 22 23 24      hours



Projection: Raisz Armadillo  
Property: none  
⊕ T.:(various) - Graticule: 10°

P.C.: 0.0 ° ; 75.0 °E / 28.1 °N; 75.0 °E  
Aspect: Direct  
{4.2} [+90.0/ +0.0/-165.0] [-] EIGEN6C2

Asc. Node: -105.00 ° [06:00 LMT]  
App. inclin. = 21.52 °

*Ιξίων*  
MC ★ LMD  
*Ατλας*

FIG. 10.10 : Ground track and crossing time for the non-Sun-synchronous satellite Megha-Tropiques, over 3 days. Ascending node crossing time 00:00 and 06:00 LMT.

**Megha-Tropiques**

Orbit - Ground track

Recurrence = [14; -1; 7] 97

>>>> Time span shown: 4320.0 min = 3.00 days

Altitude = 865.5 km

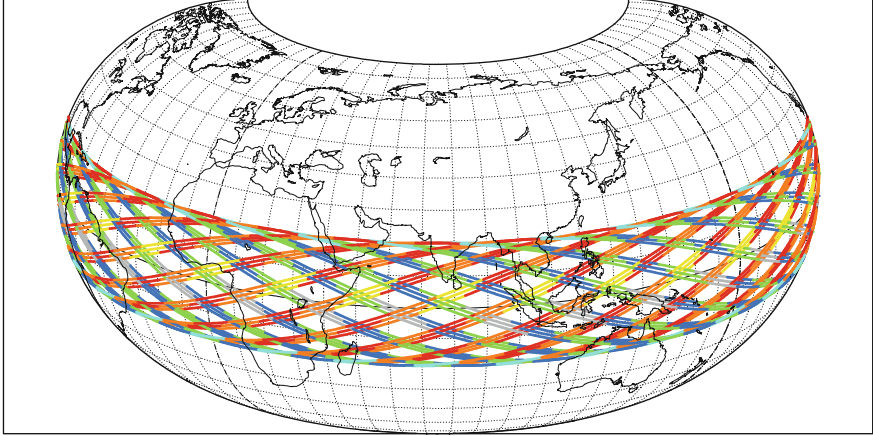
a = 7243.677 km

Inclination = 20.00 °

Period = 101.93 min \* rev/day=14.13

Equat. orbital shift = 2892.0 km ( 26.0 °)

LMT (local) 00 01 02 03 04 05 06 07 08 09 10 11 12 13 14 15 16 17 18 19 20 21 22 23 24 hours



Projection: Raisz Armadillo

P.C.: 0.0 ° ; 75.0 °E / 28.1 °N; 75.0 °E

Asc. Node: -105.00 ° [12:00 LMT]

Ιξίων

Property: none

Aspect: Direct

App. inclin. = 21.52 °

MC ★ LMD

⊕ T.:(various) - Graticule: 10°

{4.2} [+90.0/ +0.0/-165.0] [-] EIGEN6C2

Ατλας

**Megha-Tropiques**

Orbit - Ground track

Recurrence = [14; -1; 7] 97

>>>> Time span shown: 4320.0 min = 3.00 days

Altitude = 865.5 km

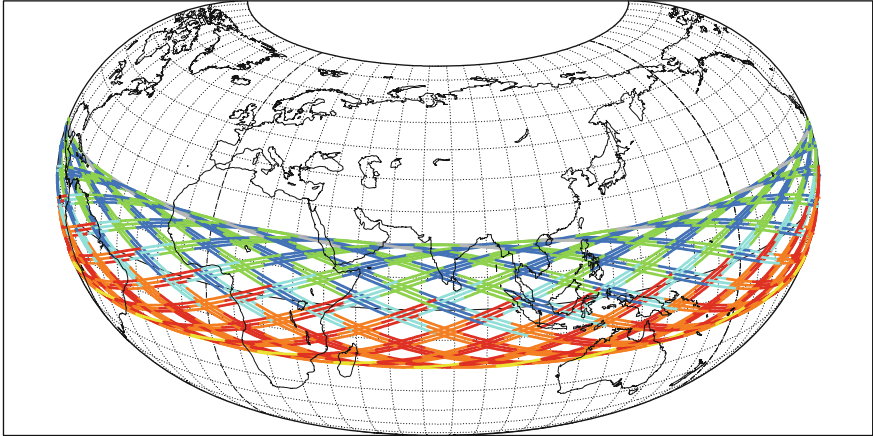
a = 7243.677 km

Inclination = 20.00 °

Period = 101.93 min \* rev/day=14.13

Equat. orbital shift = 2892.0 km ( 26.0 °)

LMT (local) 00 01 02 03 04 05 06 07 08 09 10 11 12 13 14 15 16 17 18 19 20 21 22 23 24 hours



Projection: Raisz Armadillo

P.C.: 0.0 ° ; 75.0 °E / 28.1 °N; 75.0 °E

Asc. Node: -105.00 ° [18:00 LMT]

Ιξίων

Property: none

Aspect: Direct

App. inclin. = 21.52 °

MC ★ LMD

⊕ T.:(various) - Graticule: 10°

{4.2} [+90.0/ +0.0/-165.0] [-] EIGEN6C2

Ατλας

FIG. 10.11 : Ground track and crossing time for the non-Sun-synchronous satellite Megha-Tropiques, over 3 days. Ascending node crossing time 12:00 and 18:00 LMT.

retrograde orbit ( $i = 110^\circ$ ,  $h = 5,892$  km). The satellite Ofeq-5 with retrograde elliptical LEO orbit ( $i = 143.5^\circ$ ) provides one of the rare examples of prograde precession. ◀

### 10.1.4 Cycle and Ascending Node Crossing Time

Knowing the initial conditions, it is a simple matter to obtain the crossing times at the ascending node at an arbitrary date, provided that we also know the cycle  $C_S$  relative to the Sun. Indeed, since the crossing time increases or decreases by 24 h every  $C_S$  days, it is easy to calculate the increase or decrease per day. Here is an example of this calculation (Figs. 10.10 and 10.11).

**Example 10.3** Calculate the dates during the year 1999 for which the LMT of the ascending node crossing is the same for the satellites TRMM and Resurs-O1-4.

► In order to study the Earth's radiation budget, TRMM and Resurs-O1-4 were equipped with the CERES and ScaRaB instruments, respectively. A joint measurement campaign was organised in January and February 1999. The aim was to compare the measurements obtained for the same region viewed by the two instruments at roughly the same times (with a leeway of  $\pm 15$  min). The Sun-synchronous satellite Resurs-O1-4 crosses the ascending node at 22:20 LMT. The initial conditions for TRMM are given by an ascending node crossing. For  $t_{AN}$  given in a notation indicating month day hr min s, we have

$$t_{AN} = 1999\ 01\ 21\ 20:43:47\ (\text{UT}), \lambda = +5.157^\circ .$$

We calculate the value of  $\tau_{AN}$ , the LMT crossing time, as

$$\tau_{AN} = t_{AN} + \frac{\lambda}{15} = 20:43:47 + 00:20:38 = 21:04:25 .$$

In Example 10.1, we found  $P = -6.894$ , which gives the cycle

$$C_S = -\frac{365.25}{7.894} = -46.29\ \text{day} .$$

We thus obtain the daily drift as

$$\frac{1440}{C_S} = -\frac{1440}{46.42} = -31.02\ \text{min} .$$

The difference between  $\tau_{AN} = 21:04$  on 21 January 1999 ( $D = 21$ ) and the chosen time of 22:20 is 76 min. The passage of TRMM at the chosen time

thus occurs with a shift of  $-76/31 = -2.45$  days, or 2 days earlier, i.e., on 19 January 1999 ( $D = 19$ ). The ascending node crossing time around 22:20 thus occurs on the days  $D_k$  given by

$$D_k = 19 + k|C_S|.$$

With  $D_0 = 19$  and  $k = 0, 1, 2, \dots, 7$ , we obtain all the dates required for the year 1999. If we need to know the dates of passage of TRMM at 22:20 at the descending node, we merely add a half-cycle to the values of  $D_k$ , which gives dates shifted by 23 days with respect to the first series. ◀

## 10.2 Crossing Time for a Sun-Synchronous Satellite

This section discusses Sun-synchronous Earth observation satellites in the broad sense. They are all in near-circular orbits.

### 10.2.1 Passage at a Given Latitude

The time in LMT at which a Sun-synchronous satellite crosses the ascending node is constant in time (provided that the orbit is suitably maintained, of course), because in the frame  $\mathfrak{R}$ , the nodal precession balances the motion of the Earth's axis about the Sun. This is the defining feature of Sun-synchronous orbits, as we shall see more clearly in the next example.

**Example 10.4** *Calculate the crossing time at two consecutive ascending nodes for a Sun-synchronous satellite.*

► Consider the first crossing at the ascending node at longitude  $\lambda_1$  and time  $t = t_0$  in UT. Let  $\tau_1$  be the corresponding LMT, so that, according to (7.61),

$$\tau_1 = t_0 + \frac{\lambda_1}{15},$$

with time in hours and longitudes in degrees.

The next passage (nodal period  $T$ ) will occur at longitude  $\lambda_2$  and at time  $t = t_0 + T$ . The corresponding LMT at the second crossing, denoted by  $\tau_2$ , is therefore

$$\tau_2 = t_0 + T + \frac{\lambda_2}{15}.$$



The longitude  $\lambda_2$  is obtained simply by considering the equatorial shift given by (8.25):

$$\lambda_2 = \lambda_1 + \Delta\lambda_E = \lambda_1 - 15T.$$

We thus have

$$\tau_2 = t_0 + T + \frac{\lambda_1 - 15T}{15} = t_0 + \frac{\lambda_1}{15} = \tau_1,$$

which shows that the LMT remains constant.

Since the mean motion is constant, the time taken to reach a given latitude from the equator will be the same for each revolution. We may thus say that, for a Sun-synchronous satellite:

- The LMT crossing time at a given latitude is constant.
- The LMT crossing time at a given meridian depends only on the latitude.



### Establishing the Relation Between $\psi$ and $\Delta\tau$

The relation between  $\tau$  (the LMT crossing time at the meridian) and  $\psi$  (the geocentric latitude) is found using the equations for the ground track and calculating the longitude corresponding to each latitude, whereupon the time can be found in LMT. However, there is a simpler way to obtain this relation from geometric considerations.

Consider the Earth in the geocentric pseudo-Galilean frame  $\mathfrak{R}$ , as shown in Fig. 10.12. At a given time, let  $A$  be the intersection of the meridian plane of the direction of the Sun with the Earth's equator. We consider the orbital plane of a Sun-synchronous satellite. Its ground track cuts the equator at  $N$ , the projection of the ascending node on the Earth's surface. This plane makes an angle  $i = i_{\text{HS}}$  with the equatorial plane. (This is indeed  $i$ , rather than the apparent inclination, since we are working in  $\mathfrak{R}$ .)

The angle  $H_{\text{AN}} = (\mathbf{OA}, \mathbf{ON})$  remains constant by the Sun-synchronicity condition, since  $H_{\text{AN}}$  measures the hour angle, and hence the time in LMT of the ascending node.

Consider a meridian defined by a point  $Q$  on the equator. The ground track of the orbit cuts this meridian at a point  $P$  of latitude  $\psi$ . The hour angle of  $P$  and of  $Q$  is  $H = (\mathbf{OA}, \mathbf{OQ})$ . We define

$$\Delta H = H - H_{\text{AN}} = (\mathbf{ON}, \mathbf{OQ}).$$

This angle thus measures the difference in hour angle between  $N$  and  $P$  (or  $Q$ ).

In the spherical triangle  $PQN$ , with a right-angle at  $Q$ , we know the side  $PQ$ ,  $(\mathbf{OQ}, \mathbf{OP}) = \psi$  and the angle  $N$ , representing the inclination of the orbital plane. We obtain  $\Delta H$  from the standard relation of spherical trigonometry, corresponding to the relation (ST XII), identifying  $PQN$  with  $CAB$ :



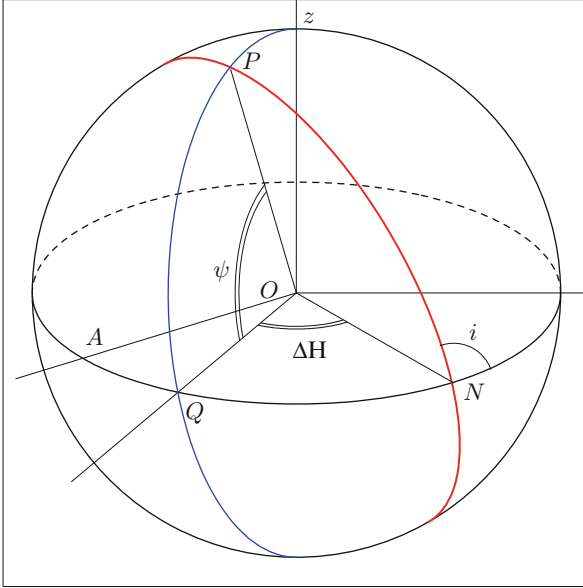


FIG. 10.12 : *Intersection of the ground track of a Sun-synchronous satellite orbit (ascending node  $N$ ) with a given meridian plane, defined by the point  $Q$  on the equator.*

$$\sin \Delta H = \frac{\tan \psi}{\tan i_{\text{HS}}} . \quad (10.7)$$

Naturally, this formula is valid whether the satellite orbit is prograde or retrograde. In the prograde case,  $\tan N$  and  $\sin \Delta H$  are positive. In the retrograde case, as here,  $\tan N = \tan(\pi - i_{\text{HS}})$  and  $\Delta H$  are negative.

Let  $\tau_{\text{AN}}$  and  $\tau$  be the local crossing times at the ascending node and  $P$ , respectively. Then,

$$\Delta \tau = \tau - \tau_{\text{AN}} = \frac{1}{K} \Delta H , \quad (10.8)$$

where  $K$  is a constant depending on the units, so that if time is in hours and angles are in degrees, then  $K = 15$  (since 1 h corresponds to 15 degrees).

We thus have the following relations between the latitude  $\psi$  and the difference in crossing times  $\Delta \tau$  :

$$\Delta \tau = \frac{1}{K} \arcsin \left( \frac{\tan \psi}{\tan i_{\text{HS}}} \right) , \quad (10.9)$$

or

$$\psi = \arctan \left( \tan i_{\text{HS}} \sin K \Delta \tau \right) . \quad (10.10)$$

This function  $\psi(\Delta t)$  is shown in Fig. 10.13.

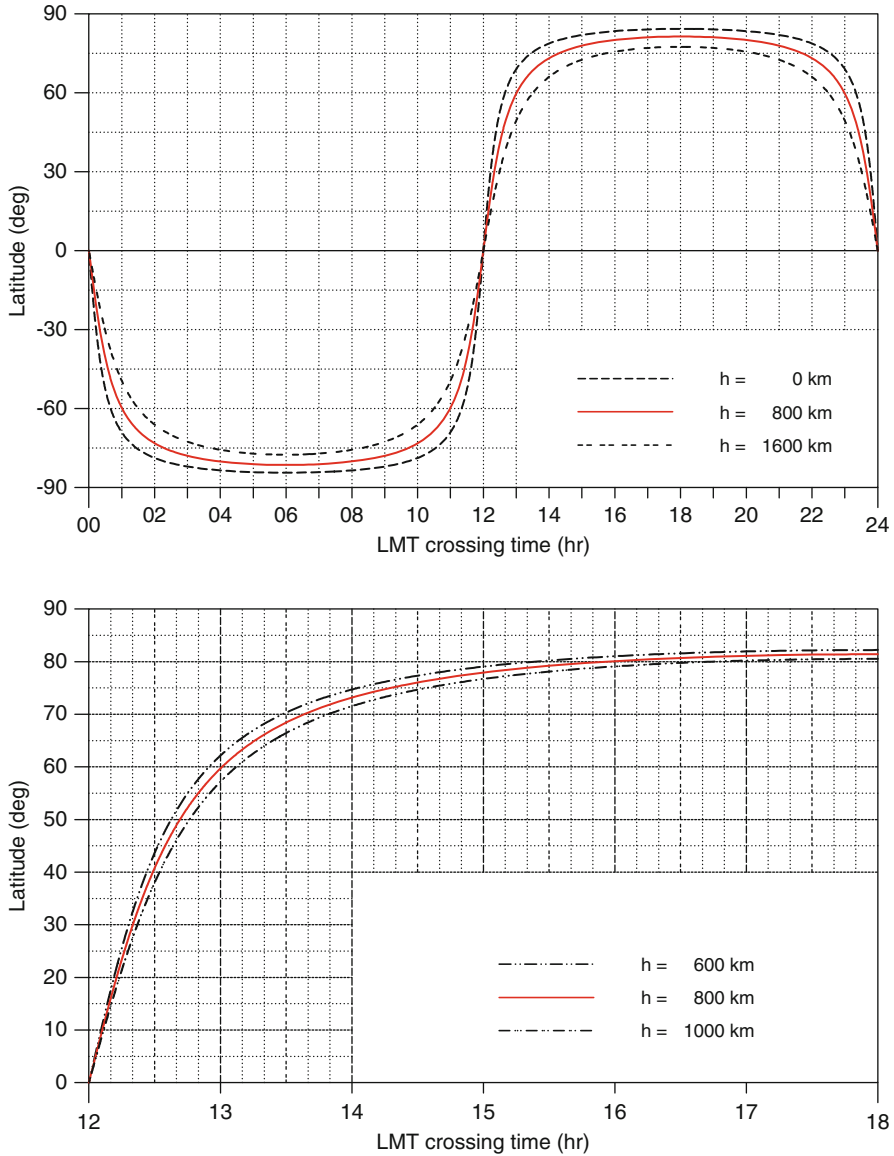


FIG. 10.13 : Graph of  $\psi(\Delta\tau)$ , the relation between the latitude of the point under consideration and the LMT time difference between transit at the ascending node and transit at this latitude, for a Sun-synchronous satellite. Upper: For three values of the altitude,  $h = 800$  km and  $h = 800 \pm 800$  km. Lower: For three values of the altitude,  $h = 800$  km and  $h = 800 \pm 200$  km. This is a magnified view of part of the upper figure.

### Crossing Time at an Arbitrary Latitude

Let  $\tau_{AN}$  and  $\tau_{DN}$  be the crossing times at the ascending and descending nodes, respectively. Then,

$$\tau_{AN} = 12 + \tau_{DN} \pmod{24} .$$

For  $\Delta\tau$ , we take the value defined by (10.9), i.e., between  $-6$  and  $+6$  h. We thereby obtain the two daily crossing times  $\tau_{(A)}$  and  $\tau_{(D)}$  in the ascending and descending parts of the ground track, respectively:

$$\begin{cases} \tau_{(A)} = \tau_{AN} + \Delta\tau , \\ \tau_{(D)} = \tau_{DN} - \Delta\tau = \tau_{AN} + 12 - \Delta\tau . \end{cases} \quad (10.11)$$

At a given latitude, the time difference  $\delta(\psi)$  between two crossings, one in the ascending part and the other in the descending part, is given by

$$\delta(\psi) = \tau_{(A)} - \tau_{(D)} = 12 + 2\Delta\tau . \quad (10.12)$$

We now give some examples of this calculation.

**Example 10.5** Calculate the LMT crossing time at latitude  $15^\circ N$  for a Sun-synchronous satellite at altitude  $h = 800$  km, when the crossing time at the ascending node is 00:00 LMT.

► We have seen that the inclination of the satellite is  $i = 98.6^\circ$  for this altitude. Equation (10.9) yields

$$\Delta\tau = \frac{1}{K} \arcsin\left(\frac{\tan 15}{\tan 98.6}\right) = \frac{1}{15} \arcsin(-0.04052) = \frac{-2.32}{15} \text{ hr} = -9.3 \text{ min} .$$

We thus take  $\Delta\tau = -9$  min, and inserting  $\tau_{AN} = 00:00$  in (10.11), we obtain

$$\begin{aligned} \tau_{(A)} &= \tau_{AN} + \Delta\tau = 24 \text{ h } 0 \text{ min} - 9 \text{ min} = 23:51 , \\ \tau_{(D)} &= \tau_{AN} + 12 - \Delta\tau = 12 \text{ h } 0 \text{ min} + 9 \text{ min} = 12:09 . \end{aligned}$$

The two passages at this latitude thus occur at 23:51 LMT and 12:09 LMT, as can be checked on the upper part of Fig. 10.13. ◀

**Example 10.6** Calculate the LMT crossing time at latitude  $50^\circ$  for the Sun-synchronous satellite SPOT-5, which crosses the ascending node at 22:30 LMT.

► For this satellite and latitude  $50^\circ$ , (10.9) gives  $\Delta\tau = -42$  min. With (10.11) and  $\tau_{AN} = 22:30$ , we will thus have

$$\psi = 50^\circ\text{N} \implies 21:48 \text{ and } 11:12 ,$$

$$\psi = 50^\circ\text{S} \implies 23:12 \text{ and } 09:48 .$$

In the northern hemisphere, the daytime crossing will occur well after 10:30, in fact close to noon, with good solar lighting conditions. In the southern hemisphere, on the other hand, the crossing occurs rather early in the morning and the lighting conditions are not so good. The choice of node, e.g., descending at 10:30 rather than ascending, favours observation of the high latitudes of one hemisphere at the expense of the other. We shall return to this point. ◀

## 10.2.2 Choice of Local Time at the Ascending Node

### Restrictions on the Choice of Crossing Time

The local crossing time at the ascending node is determined by the aims of the mission. It is chosen as a compromise between various constraints which we shall number here from C1 to C5 (where C stands for constraint):

- (C1) To obtain the best solar lighting conditions for the regions observed.
- (C2) To take local meteorological factors into account, e.g., a certain region may be under cloud cover every morning.
- (C3) To reduce the risks of specular reflection (this effect known as glint or Sun glint due to the reflection of sunlight from water surfaces can dazzle the satellite's instruments).
- (C4) To limit periods of solar eclipse.
- (C5) To take into account the crossing time of another Sun-synchronous satellite carrying out the same type of mission.

We shall now discuss the various times chosen according to the type of mission. Figure 10.16 schematises the relationship between constraints and missions.

### Different Choices Depending on Constraints

#### *Remote-Sensing Satellites for Earth Resources*

As already noted, this kind of satellite is always Sun-synchronous.<sup>2</sup> The constraints listed above as (C1) and (C3) are given priority. The local crossing time at the node must be close to noon for (C1), but not too close because of (C3). Moreover, considering the curve  $\psi(\Delta\tau)$ , a shift away from noon yields good solar lighting conditions for high latitudes. Mission designers generally

---

<sup>2</sup>A satellite may carry instruments pertaining to different types of mission. For example, the Russian satellite Resurs-O1-4 carries the Russian imaging device MSU for remote-sensing and the French instrument ScaRaB to study the Earth radiation budget (which can be classified as meteorological). But it is the remote-sensing aspect that determined the choice of crossing time.

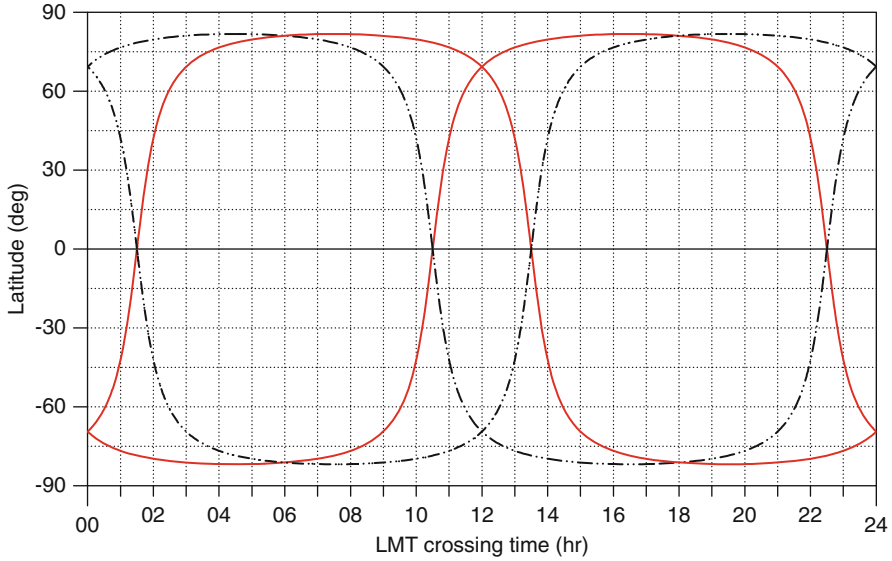


FIG. 10.14 : *Complementarity of Terra and Aqua. LMT crossing time as a function of latitude for the Sun-synchronous EOS satellites, for various values of the LMT ascending node: 10:30 and 22:30 for EOS-AM-1, 01:30 and 13:30 for EOS-PM-1. The continuous curve shows the graph for values corresponding to the crossing time retained in the final project, i.e., 22:30 for EOS-AM-1 and 13:30 for EOS-PM-1 (Terra and Aqua, respectively).*

consider that the optimal time slot for viewing (in local time) lasts for 1 h centered on 11:00 or on 13:00, although this is only a rough guide.

One can thus envisage the following cases, calculated for a satellite at altitude  $h = 800$  km:

- Equatorial crossing at the lower time limit. If the ascending node is at 10:30 ( $\tau_{AN} = 10:30$ ), the latitudes viewed between 10:30 and 11:30 are obtained using (10.10). With  $K = 15$ , the calculation for  $\Delta\tau = 1$  gives

$$\psi = \arctan [(\tan 98.6)(\tan 15)] = -61^\circ ,$$

which corresponds to latitudes lying between  $0^\circ$  and  $61^\circ\text{S}$ . If the descending node occurs at 10:30 ( $\tau_{AN} = 22:30$ ), latitudes viewed during this time interval lie between  $0^\circ$  and  $61^\circ\text{N}$ .

- Equatorial crossing at the upper time limit. If the ascending node occurs at 13:30, latitudes viewed between 12:30 and 13:30 then lie between  $0^\circ$  and  $61^\circ\text{N}$ . If the descending node is at 13:30, latitudes viewed in this time interval lie between  $0^\circ$  and  $61^\circ\text{S}$ .
- Choice of time. Since the noon crossing time at the node is not chosen, to avoid specular reflection, the choice of equatorial crossing time at 10:30 or

13:30 is guided by the choice between northern and southern hemispheres. Naturally, the northern hemisphere is generally favoured, since it encompasses more visible land mass than the other hemisphere, but also because it comprises more nations financing satellite launches.

For satellites observing Earth resources, the choice is thus between the two equatorial crossing times:

$$\tau_{AN} = 22:30 \quad \Longrightarrow \quad \text{descending node } 10:30 ,$$

$$\tau_{AN} = 13:30 \quad \Longrightarrow \quad \text{ascending node } 13:30 .$$

The first is called the morning crossing, and the second the afternoon crossing.

The graphs in Fig. 10.14 explain these choices for the NASA Earth observation satellites originally called EOS-AM-1 and EOS-PM-1. They are in complementary orbits, one with the morning crossing (AM), the other with the afternoon crossing (PM). They have since been renamed Terra and Aqua, respectively. Between local times 10:30 and 13:30 (LMT), the most favourable period for viewing, these two satellites overfly the northern hemisphere, never the southern hemisphere.

The choice between the two possibilities  $\tau_{AN} = 22:30$  or  $\tau_{AN} = 13:30$  is generally made in response to the constraint (C2). In this way, one avoids the rather systematic formation of cloud cover at particular times of the day and in certain well-defined regions. The descending node has been chosen at the end of the morning for most Earth observation satellites. The following list shows the extent to which the choice of 22:30 for the descending node dominates for this kind of satellite. But if Australia were to send up a satellite to study Earth resources, one could be fairly certain that they would choose the ascending node at 10:30!

- Ascending node at 22:30: US satellites Landsat, from -1 to -8, and the following, EO-1 and Terra; the French satellites SPOT, from -1 to -5, SPOT-6 (22:00), Pléiades-1A and -1B; the European satellites ERS-1 and -2, Envisat; the Japanese satellites MOS-1 and -1B, JERS-1, ADEOS-1 and -2, ALOS; all the Indian satellites IRS (except for the oceanographic ones), IRS-1A, -1B, -1C, -1D, -P2, -P3, Resourcesat-1 and -2, Cartosat-1, -2, and -2A, IMS-1 (21:30) and TES; the Russian satellite Resurs-O1-4, the China–Brazil satellites CBERS, -1, -2, and -2B; the Thai satellite THEOS; the Turkish satellite RASAT; the Vietnamese satellite VNRED; the Taiwanese satellite FormoSat-2 (21:30); the Chinese satellites HJ-1A and -1B; the Argentinian satellite SAC-C; the Belgian–European satellite PROBA; and the Israeli satellite EROS-A1. To this list, one should add all the US commercial mapping satellites, Ikonos-2 (22:31), QuickBird-2 (22:27), WorldView-2 (22:50), and GeoEye-1 (22:27) for which the time drifts slightly. The German commercial satellite constellation RapidEye, from -1 to -5, crosses at a slightly different time (23:15).

- Ascending node at 13:30: Aqua and the other satellites of the A-Train (see Fig. 9.22), CloudSat, Calipso, Parosol, Aura, GCOM-W1 (Shizuku); the satellites Suomi-NPP, WorldView-1, Arirang-3; and the 4 French military satellites Hélios-1A, -1B, -2A, and -2B (13:15).
- Ascending node at 10:30: the Korean satellites Arirang-1 and -2; and the British satellites UK-DMC and UK-DMC2.
- Ascending node at 01:30: the Israeli satellite EROS-B; and the Japanese satellite Ibuki (00:50).

Although we have grouped these satellites according to equatorial crossing times, there is a certain dispersion within each group. For example, GeoEye-1 does not cross at 22:30, but rather at 22:27, and Aura does not cross at 13:30, but rather at 13:46. However, as long as the satellite is maintained on orbit, and in particular if it is recurrent, it always crosses at the nominal time, i.e., 22:27 for GeoEye-1 and 13:46 for Aura, to within 1 or 2 min.

### *Meteorological Satellites*

For these satellites which observe meteorological phenomena, the crossing time is not critical, and it can indeed vary significantly from one satellite to the next. Moreover, in most cases, these satellites are not kept at their station, the crossing time being allowed to drift. This drift is quadratic in time, as shown by (10.21) discussed below. For the NOAA satellites, the drift, which can become quite significant, is shown in Fig. 10.15. The DMSP satellites drift in the same way. For the NOAA satellites from TIROS-N and NOAA-6 onwards, the constraint (C5) has been taken into account: for a given region, and with solar illumination, one satellite overflies in the morning and the other in the afternoon.

The organisations NOAA and EUMETSAT set up the IJPS programme (Initial Joint Polar System) to share instruments and coordinate satellites. The programme began with NOAA-18, NOAA-19, and MetOp-A, and will continue with the following NOAA and MetOp-B, then -C. The European satellite operates in the middle of the morning, around 10 h ( $\tau_{AN} = 21:30$ ), the US satellites at the beginning of the morning, around 8 h ( $\tau_{AN} = 19:30$ ) and at the beginning of the afternoon, around 14 h ( $\tau_{AN} = 14:30$ ).

### *Oceanographic Satellites*

When they are not specialised in altimetry, oceanographic satellites are Sun-synchronous. If they do not carry scatterometers, the equatorial crossing is often chosen around noon and midnight, to satisfy constraint (C1): for example,  $\tau_{AN} = 00:00$  for Oceansat-1 and -2,  $\tau_{AN} = 00:20$  for SeaStar.

### *Satellites with High Energy Requirements*

It is important to avoid long breaks in the power supply when satellites carry a radar or other instrument with high energy requirements. The solar

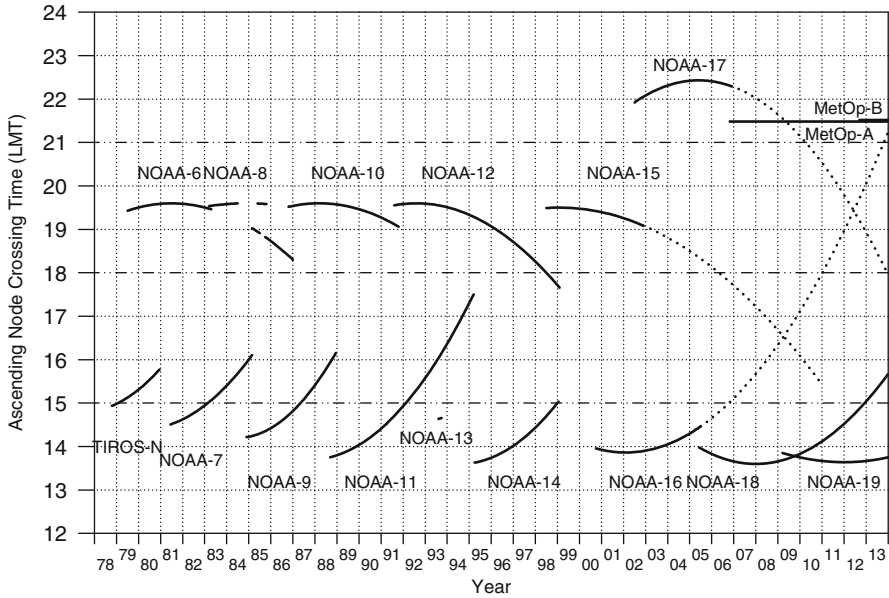


FIG. 10.15 : Drift of ascending node crossing times  $\tau_{AN}$  from 1978 to 2011 for Sun-synchronous meteorological satellites in the POES programme (TIROS-N, NOAA-6 to -19) and MetOp-A (in the IJPS framework). Orbits of satellites in the POES programme are not maintained and hence tend to drift. The time  $\tau_{AN}$  is given for the operating period of each satellite (according to NOAA data). For NOAA-15, -16, and -17,  $\tau_{AN}$  is given by a dotted line when the satellite is a backup. The satellite MetOp-A is maintained in orbit, with  $\tau_{AN} = 21:30$ , to within 2 min (see Example 10.8).

panels must be almost continuously illuminated. To achieve this, the best-suited orbit has normal in the meridian plane, because eclipses are then at their shortest (see later in the chapter). This Sun-synchronous satellite is such that  $\tau_{AN} = 06:00$  or  $18:00$ , and it is called the dawn–dusk orbit. With this orbit there is a clear difference between the two hemispheres: with  $\tau_{AN} = 06:00$ , the northern hemisphere is viewed at night and the southern hemisphere is viewed during the day (between  $06:00$  and  $18:00$ ); with  $\tau_{AN} = 18:00$ , it is exactly the opposite.

Radarsat-1 and -2 are examples, with  $\tau_{AN} = 18:00$ , as shown in Fig. 10.9. The constraint (C4) is given precedence. For the four Italian satellites COSMO-SkyMed-1, -2, -3, and -4, which form a constellation, the crossing times are strictly equal, with  $\tau_{AN} = 06:03$ , while for the German satellite TerraSAR-X,  $\tau_{AN} = 18:00$ , and for the Indian satellite RISat-2,  $\tau_{AN} = 06:00$ .

The same is true for oceanographic satellites using a scatterometer, an instrument measuring the wind speed over the sea. Examples are QuikScat



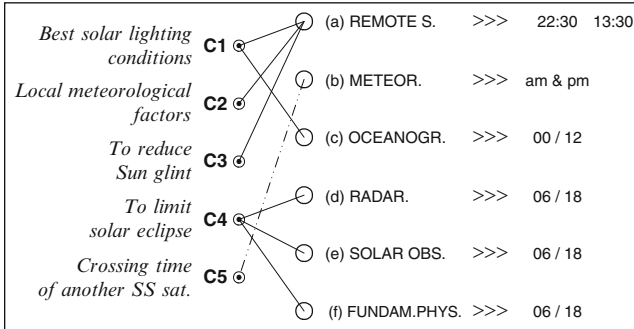


FIG. 10.16 : Choice of ascending node crossing time for Sun-synchronous satellites (equatorial crossing). Schematic view of constraints leading to this choice for various types of mission.

( $\tau_{AN} = 17:55$ ), Coriolis (18:00), HY-2A (18:00), and the future CFOSAT (19:00).

The dawn–dusk orbit is planned for the European projects ADM–Aeolus (Atmospheric Dynamics Mission) and WALES, at low altitude ( $h \approx 400$  km).

#### *Satellites with Orbits Requiring a Specific Configuration Relative to the Sun*

Solar observing satellites, if placed near the Earth, must gain maximum advantage from their view of the day star. By satisfying constraint (C4), only the dawn–dusk orbit can allow such continuous observation. The satellites TRACE ( $\tau_{AN} = 6:00$ ) and Picard ( $\tau_{AN} = 6:00$ ) are on this type of orbit.

#### *Satellites Subject to a Requirement of Limited Temperature Variation*

It is of the utmost importance for satellites carrying out fundamental physics experiments on the equivalence principle that temperature variations should be kept to a minimum. The dawn–dusk orbit satisfies constraint (C4), and this will be the orbit for the satellites  $\mu$ SCOPE and STEP.

The satellite GOCE is in a very low orbit ( $h \sim 250$  km) and should be subject to as little temperature variation as possible. It is thus in a dawn–dusk orbit with  $\tau_{AN} = 18:00$ .

#### *Choices for Other Types of Mission*

The crossing time of the satellite can be determined by the physical nature of the phenomena to be observed. The satellite SMOS (see Fig. 9.21) measures ground humidity. This very delicate measurement is always best when the temperature gradient of the soil is at its minimum, which is the case at 6 h in the morning. If one also requires a roughly constant illumination of the solar panels, it is clearly the dawn–dusk orbit that must be chosen, as in the case of SMOS ( $\tau_{AN} = 6:00$ ). It is also the planned orbit for its US counterpart SMAP.

The dawn–dusk orbit has been chosen for MagSat (Explorer-61, study of the magnetosphere) because the perturbations produced by the Sun on the Earth’s magnetic field, which vary from 1 h to the next, are thereby minimised and rendered constant (Fig. 10.16).

### 10.2.3 Calculating the Drift in Local Crossing Time

The drift in the local crossing time is due mainly to the drift in the inclination  $i$  of the orbital plane. The Lagrange equations show that  $di/dt = 0$  under the effect of the geopotential. However, other gravitational perturbations due to the Sun and Moon, or non-gravitational effects, will cause this slight variation in  $i$ , which is very small at the beginning (a few hundredths of a degree per year), but eventually becomes significant.

The local crossing time  $\tau_{\text{AN}}$  at the ascending node is directly related to the right ascension  $\Omega$  of the ascending node:

$$\tau_{\text{AN}} = 12 + \frac{\Omega - \Omega_{\text{S}}}{K} = 12 + \frac{\Omega_{\text{H}}}{K}, \quad (10.13)$$

where  $\Omega_{\text{S}}$  is the longitude of the direction of the Sun,  $\tau_{\text{AN}}$  is in hours, and  $\Omega$  and  $\Omega_{\text{S}}$  are in degrees ( $K = 15$ ), with  $\Omega_{\text{H}} = \Omega - \Omega_{\text{S}}$ . The drift in the time  $\tau_{\text{AN}}$  is then given by

$$\frac{d\tau_{\text{AN}}}{dt} = \frac{1}{K} \dot{\Omega}_{\text{H}}. \quad (10.14)$$

For a strictly maintained Sun-synchronous satellite,  $\dot{\Omega}_{\text{H}} = 0$  and  $\tau_{\text{AN}}$  is therefore constant.

Whenever  $\dot{\Omega}_{\text{H}} = \dot{\Omega}(a, i) - \dot{\Omega}_{\text{S}}$  is not zero, this is due to the variation of the orbital elements  $a$  and  $i$  relative to the Sun-synchronicity constraints. Recall the expression (7.5) for  $\dot{\Omega}(a, i)$  and the Sun-synchronicity condition (7.102):

$$\dot{\Omega}(a, i) = -K_0 \left( \frac{a}{R} \right)^{-7/2} \cos i,$$

$$\dot{\Omega}_{\text{S}} = -K_0 \left( \frac{a}{R} \right)^{-7/2} \cos i_{\text{HS}}.$$

Calculating the differential of  $\dot{\Omega}(a, i)$  and assuming that  $a$  and  $i$  remain close to their Sun-synchronous values, we obtain

$$d\dot{\Omega} = -\dot{\Omega}_{\text{S}} \left( \frac{7}{2} \frac{da}{a} + \tan i_{\text{HS}} di \right). \quad (10.15)$$

In Example 10.8, it is shown that, over a given interval of time,  $da/a$  is negligible compared with  $di$ . The last relation thus gives

$$\frac{d\dot{\Omega}}{dt} = -\dot{\Omega}_S \tan i_{\text{HS}} \frac{di}{dt} . \quad (10.16)$$

As long as the orbit remains close to the Sun-synchronous position, whence  $\tau_{\text{AN}}$  will remain close to the nominal time  $\tau_0$ , the variation  $di/dt$  is constant. We shall write

$$D_\tau = \left. \frac{di}{dt} \right|_{\tau_0} . \quad (10.17)$$

The sign of this quantity may be positive or negative.

Noting that  $\tan i_{\text{HS}}$  is always negative, (10.16) yields

$$d\dot{\Omega} = +\dot{\Omega}_S |\tan i_{\text{HS}}| D_\tau dt . \quad (10.18)$$

Integrating  $d\dot{\Omega}$  with respect to time with  $\dot{\Omega}(t=0) = 0$ , we then have

$$\dot{\Omega} = +\dot{\Omega}_S |\tan i_{\text{HS}}| D_\tau t , \quad (10.19)$$

and with a second integration,

$$\Omega = \Omega_0 + \frac{1}{2} \dot{\Omega}_S |\tan i_{\text{HS}}| D_\tau t^2 , \quad (10.20)$$

whence the local crossing time is given by

$$\tau_{\text{AN}}(t) = \tau_0 + \ddot{\tau} t^2 . \quad (10.21)$$

The quantity  $\ddot{\tau}$  is generally given in  $\text{min yr}^{-2}$  and it has the same sign as  $D_\tau$  :

$$\ddot{\tau} = \frac{\dot{\Omega}_S}{2K} |\tan i_{\text{HS}}| D_\tau . \quad (10.22)$$

We thus find that  $\tau_{\text{AN}}$  has quadratic time dependence:

$$\begin{aligned} i \text{ increasing: } D_\tau > 0 &\implies \ddot{\tau} > 0 \\ &\implies \tau_{\text{AN}}(t) \text{ parabola concave upwards ,} \\ i \text{ decreasing: } D_\tau < 0 &\implies \ddot{\tau} < 0 \\ &\implies \tau_{\text{AN}}(t) \text{ parabola concave downwards .} \end{aligned}$$

For ADEOS-1,  $\ddot{\tau} = -2.4 \text{ min yr}^{-2}$ , for Aqua,  $\ddot{\tau} = +2.4 \text{ min yr}^{-2}$  (see Example 10.7), and for MetOp-A,  $\ddot{\tau} = -3.9 \text{ min yr}^{-2}$  (see Example 10.8).

**Example 10.7** *Drift in local crossing time for the satellites ADEOS-1 and Aqua.*

► For these two Sun-synchronous satellites, we make use of data provided by the relevant space agencies:

- ADEOS-1. The Japanese space agency NASDA (which has since become JAXA) provides the descending node crossing time  $\tau_{\text{DN}}$ , fixed at  $\tau_{\text{DN}} = 10:30 \pm 0:15$ , and also its predicted drift as time goes by, viz.,

$$\tau_{\text{DN}} = \tau_0 + a\delta + b\delta^2 = 10.6872 + 4.4329 \times 10^{-6}\delta - 5.8434 \times 10^{-10}\delta^2,$$

where  $\tau_{\text{DN}}$  is given in decimal hours and  $\delta$  represents the time elapsed in hours since the time 00:00 on the launch date. As can be seen in Fig. 10.17 (upper curve), the maximum of this quadratic function occurs when

$$\delta = a/2b = 3.793 \times 10^3 \text{ h} \approx 158 \text{ day}.$$

The satellite was launched on 27 August 1996, with  $\tau_{\text{DN}} = 10:41$ . This goes through a maximum  $\tau_{\text{DN}} = 10:42$  after 5 months, then returns to  $\tau_{\text{DN}} = 10:41$  after 10 months. Note the subsequent values:  $\tau_{\text{DN}} = 10:40$  for 12 months,  $\tau_{\text{DN}} = 10:35$  for 24 months, and  $\tau_{\text{DN}} = 10:24$  for 36 months. We reach  $\tau_{\text{DN}} = 10:15$  after 42 months. At this point the orbit must be modified, because  $\tau_{\text{DN}}$  is beginning to change too quickly (but the satellite actually only operated for 10 months). This mission was followed up by ADEOS-2 with the same choice for the local crossing time.

- Aqua. NASA provides the crossing time at the ascending node in decimal hours as  $\tau_{\text{AN}} = 13.525 \text{ h}$  (with the nominal inclination) and  $\tau_{\text{AN}} = 13.565 \text{ h}$  after 365 days. Figure 10.17 (lower curve) reconstructs the time dependence. In practice, the orbit of Aqua, which belongs to the A-Train, is very strictly maintained.



**Example 10.8** *Drift in local crossing time for the MetOp-A satellites.*

► Figure 10.18 shows the time dependence of the ascending node crossing time  $\tau_{\text{AN}}$ , correlated with the corresponding time dependence of the inclination  $i$ . For each change in  $i$ , there is a sudden change in the gradient of  $\tau_{\text{AN}}$ .

We consider two dates between which the changes in  $i$  and  $a$  are close to linear:

19 October 2010	$D = 292$ ,	$h = a - R = 817.518 \text{ km}$ ,	$i = 98.7262^\circ$ ,
25 May 2011	$D = 145$ ,	$h = a - R = 817.439 \text{ km}$ ,	$i = 98.6980^\circ$ ,
Variation	$\Delta D = 218$ ,	$h = a - R = -0.079 \text{ km}$ ,	$i = -0.0282^\circ$ .

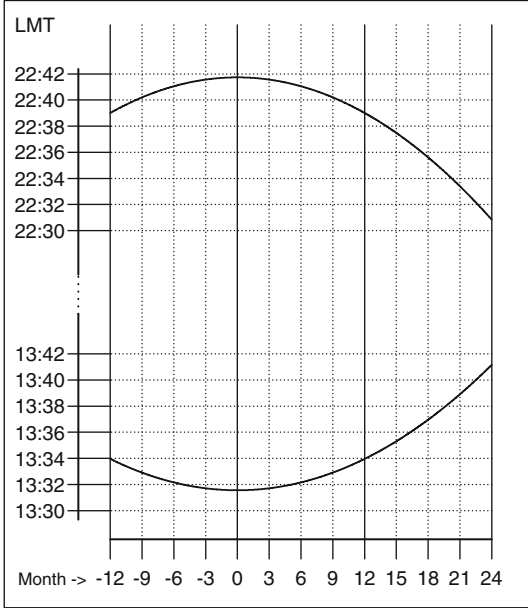


FIG. 10.17 : Time dependence of local crossing time at the ascending node for Sun-synchronous satellites, given in months. The time origin  $t = 0$  is taken when the satellite orbit is exactly at inclination  $i_{HS}$ . Upper: ADEOS-1,  $\tau_{AN}$  around 22:30. Lower: Aqua,  $\tau_{AN}$  around 13:30. The curves are theoretical. ADEOS-1 only operated for 10 months, between month  $-5$  and month  $+5$  on the graph. Aqua is repositioned on its nominal orbit about once a month.

For the quantities in (10.15) and with  $i_{HS} = 98.702^\circ$ , this gives

$$\frac{da}{a} = -\frac{0.079}{6378.1 + 817.5} = -1.0979 \times 10^{-5} \implies \frac{7}{2} \frac{da}{a} = -3.843 \times 10^{-5} ,$$

$$di = -0.0282 \frac{\pi}{180} = -4.9218 \times 10^{-4} \implies \tan i_{HS} di = +321.568 \times 10^{-5} .$$

We see that the influence of  $a$  is 100 times less than the influence of  $i$ , which justifies using (10.16).

We can calculate  $\ddot{\tau}$  with the usual units of  $\text{min yr}^{-2}$ , using (10.22) and expressing  $\dot{\Omega}_S/K$  in  $\text{min yr}^{-1}$  and  $D_\tau$  in  $\text{yr}^{-1}$ , whereupon

$$\dot{\Omega}_S = 1 \text{ revolution per year} \implies \dot{\Omega}_S/K = 1440 \text{ min yr}^{-1} ,$$

$$D_\tau = \frac{-0.0282}{218} \frac{\pi}{180} = -2.2577 \times 10^{-6} \text{ rad day}^{-1} = -8.2463 \times 10^{-4} \text{ rad yr}^{-1} .$$

Equation (10.22) gives

$$\ddot{\tau} = 720 \times |\tan i_{HS}| D_\tau = -720 \times 6.5335 \times 8.2463 \times 10^{-4} = -3.879 \text{ min yr}^{-2} .$$

For the satellite MetOp-A, with  $\ddot{\tau} = -3.9 \text{ min yr}^{-2}$ , the parabola representing  $\tau_{AN}(t)$  is concave downwards. As can be seen from Fig. 10.18, the satellite is repositioned about once every 6 months, and  $\tau_{AN}(t)$  always remains between 21:28 and 21:32, i.e., 21:30 to within 2 min. ◀

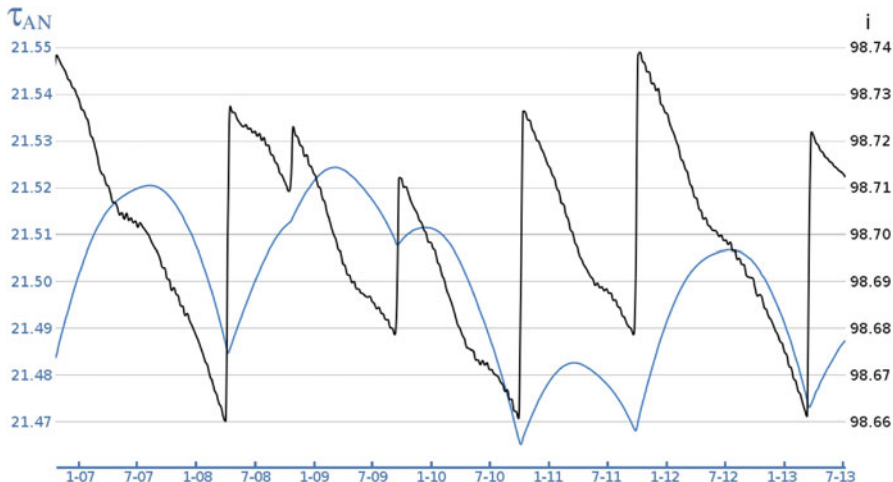


FIG. 10.18 : *Sun-synchronous satellite MetOp-A. Time dependence of the local crossing time at the ascending node  $\tau_{\text{AN}}$  (blue curve) and the inclination  $i$  (black curve), over six and half years. For decreasing  $i$ , the quadratic variation of  $\tau_{\text{AN}}$  is concave downwards.*

## 10.3 Angle Between Orbital Plane and Solar Direction

The angle between the direction of the Sun and the orbital plane of the satellite plays an important role in astronautics, e.g., for the positioning of solar panels. In the specialised literature, this is called the solar angle and it is denoted by  $\beta$ . It varies over the interval  $[-90^\circ, +90^\circ]$ , taking a positive value when the illuminated side is the one containing the normal to the orbital plane. The latter is in turn defined by the satellite motion, in the right-handed trigonometric sense.

### 10.3.1 Position of the Normal to the Orbital Plane

The center of the Earth is denoted by  $O$ , the center of the Sun by  $C$ , the orbital plane by  $\mathcal{P}$ , and the Earth's equatorial plane by  $\mathcal{E}$ . We begin by calculating  $\beta'$ , the angle between the normal  $\mathbf{n}$  to  $\mathcal{P}$  and the direction  $\mathbf{OC}$ , which ranges over the interval  $[0^\circ, 180^\circ]$ , like  $i$ .

A satellite crosses the equator at its ascending node at time  $t = t_0$ , corresponding to local time  $\tau_{\text{AN}}(t_0) = \tau_0$ . We consider this in the frame  $\mathfrak{R}$  centered on  $O$  (see Fig. 10.1). The axis  $Oz$  is the polar axis,  $xOy$  is in  $\mathcal{E}$ , and  $y'Oy$  is identified with the line of nodes (oriented from the descending node to the ascending node). Recall that the hour angle in degrees is obtained from the local crossing time in hours by the relation

$$H_0 = 15(\tau_0 - 12) . \quad (10.23)$$

For a rigorous calculation, the local crossing time should be expressed in LAT, rather than LMT, thereby bringing in the equation of time  $E_T$ .

At another time  $t = t_1$ , with  $\Delta t = t_1 - t_0$ , the center of the Earth  $O$  has revolved around  $C$  with angular speed  $\dot{\Omega}_S$  and the line of nodes has rotated relative to the axes of the frame  $\mathfrak{R}$  at the rate  $\dot{\Omega}$ . The direction of the normal  $\mathbf{n}$  to  $\mathcal{P}$  is specified by:

- the zenith angle  $\zeta_n = i$ , which remains constant, equal to the inclination of the orbit,
- the azimuthal angle  $\alpha_n = \dot{\Omega}\Delta t$ , since the origin of the azimuth is taken on  $Ox$  at  $t = t_0$ .

The direction  $\mathbf{OC}$  of the Sun is specified by:

- the zenith angle  $\zeta_s = 90^\circ - \delta$ , where  $\delta$  is the declination at the given time,
- the azimuthal angle  $\alpha_s = 90^\circ - H_0 + \dot{\Omega}_S\Delta t$ , since  $H_0$  corresponds to the hour angle at  $t = t_0$ .

The Cartesian components of the unit normal vector  $\mathbf{n}$  and the unit vector  $\mathbf{s}$  in the direction  $\mathbf{OC}$  of the Sun are thus given by:

$$\mathbf{n} = \begin{pmatrix} x = \cos(\dot{\Omega}\Delta t) \sin i \\ y = \sin(\dot{\Omega}\Delta t) \sin i \\ z = \cos i \end{pmatrix} , \quad (10.24)$$

$$\mathbf{s} = \begin{pmatrix} x = \sin(H_0 - \dot{\Omega}_S\Delta t) \cos \delta \\ y = \cos(H_0 - \dot{\Omega}_S\Delta t) \cos \delta \\ z = \sin \delta \end{pmatrix} . \quad (10.25)$$

The angle  $\beta'$  is thus determined within its range of possible values.

### 10.3.2 Angle $\beta$

The angle  $\beta = \beta' - 90^\circ$  is obtained from the scalar product  $\mathbf{n} \cdot \mathbf{s}$  by

$$\sin \beta = \sin i \cos \delta \sin [H_0 + (\dot{\Omega} - \dot{\Omega}_S)\Delta t] + \cos i \sin \delta , \quad (10.26)$$

which gives the value of  $\beta$  within its range of definition. For Sun-synchronous satellites, we have  $\dot{\Omega} = \dot{\Omega}_S$  and (10.26) simplifies to

$$\sin \beta = \sin i \cos \delta \sin H_0 + \cos i \sin \delta . \quad (10.27)$$

For non-Sun-synchronous satellites, the hour angle  $H_0$  takes all possible values and  $\sin H_0$  varies between  $-1$  and  $+1$ . The extremal values of  $\sin \beta$  are thus

$$\sin \beta = \pm \sin i \cos \delta + \cos i \sin \delta = \sin(\delta \pm i) . \quad (10.28)$$

The declination  $\delta$  varies over the interval  $[-\varepsilon, +\varepsilon]$ , with obliquity  $\varepsilon = 23.4^\circ$ . The angle  $\beta$  thus varies over the interval

$$\beta \in [-(i + \varepsilon), +(i + \varepsilon)] , \quad (10.29)$$

limited, of course, to the interval of definition of  $\beta$ .

Hence, for Megha-Tropiques,  $i = 20.0^\circ$ ,  $\beta \in [-43.4^\circ, +43.4^\circ]$ ; for ISS,  $i = 51.6^\circ$ ,  $\beta \in [-75.0^\circ, +75.0^\circ]$ ; and for Jason-2,  $i = 66.0^\circ$ ,  $\beta \in [-89.4^\circ, +89.4^\circ]$ .

**Example 10.9** *Time dependence of the solar angle  $\beta$  over 2 years for the Sun-synchronous satellite Calipso and the non-Sun-synchronous satellite Megha-Tropiques.*

► For each of these satellites, we plot the variation of each angle determining the direction of the normal to the orbital plane and the direction of the Sun. These variations are shown graphically in Figs. 10.19 and 10.20:

- Direction of the Sun. The elevation  $\delta = 90^\circ - \zeta_s$  corresponds to the declination. The azimuth  $\alpha_s$  has a cycle of 1 year, and it does not vary exactly linearly with time (the difference being the equation of time  $E_T$ ).
- Direction of the normal to the orbital plane. The zenith angle  $\zeta_n$  remains constant, since the inclination is constant. The main difference between the Sun-synchronous and non-Sun-synchronous satellites is manifested through the variation of the azimuthal angle  $\alpha_n$ . For the Sun-synchronous satellite,  $\alpha_n$  goes round once in 1 year as viewed from  $\mathfrak{R}$ , whereas for the non-Sun-synchronous satellite with fast nodal precession, the cycle is much shorter (and retrograde).
- The angle  $\beta$  between the direction of the Sun and the orbital plane. For Calipso,  $\beta$  varies from  $20^\circ$  to  $35^\circ$ . The general shape of the graph of  $\beta$  as a function of time is heavily influenced by the equation of time. For Megha-Tropiques, the amplitude is much greater, with the angle varying from  $-45^\circ$  to  $+45^\circ$ . In this case, it is occasionally necessary to turn the satellite round so that its solar panels are more effectively illuminated.



## 10.4 Solar Eclipse for Circular Orbits

The satellite undergoes solar eclipse when the Sun is hidden from it by the Earth. During an eclipse,<sup>3</sup> the satellite cools down and its solar panels

---

<sup>3</sup>The name derives from the late Latin *eclipsis*, which itself comes from the Greek ἔκλειψις, εὐζ, meaning “defection.” The word contains the prefix εκ, meaning “outside of” and the verb λείπειν, meaning “to leave.” See the etymological note on the ellipse. The word “ecliptic,” referring to the orbital plane of the Earth around the Sun, is a more recent construction. If an eclipse is to occur, the Moon must cross this plane (a necessary but not sufficient condition).



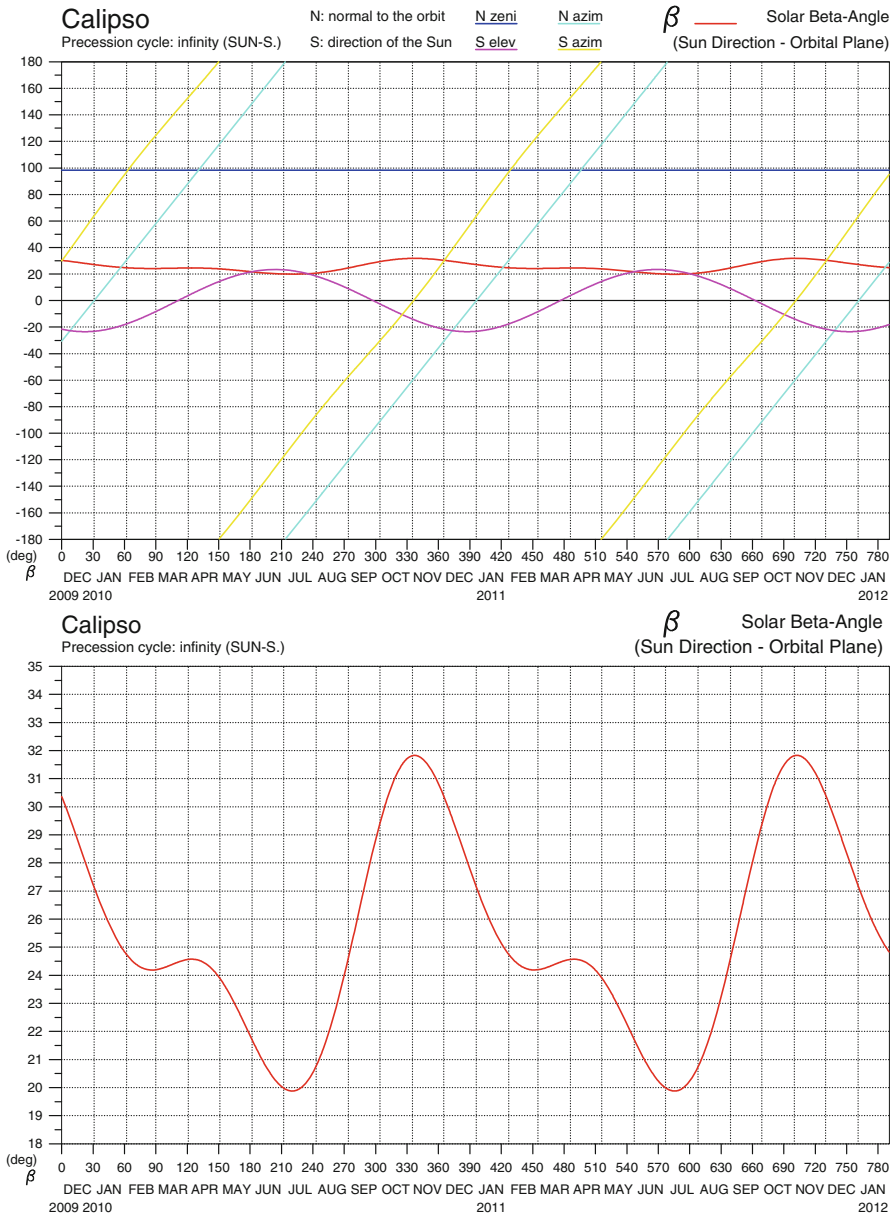


FIG. 10.19 : Upper: Angles relevant to the direction of the Sun and the normal to the orbit. Lower: The angle  $\beta$ . Sun-synchronous satellite Calipso. Ascending node crossing at 13:46:37 (LMT) on 1 January 2010.

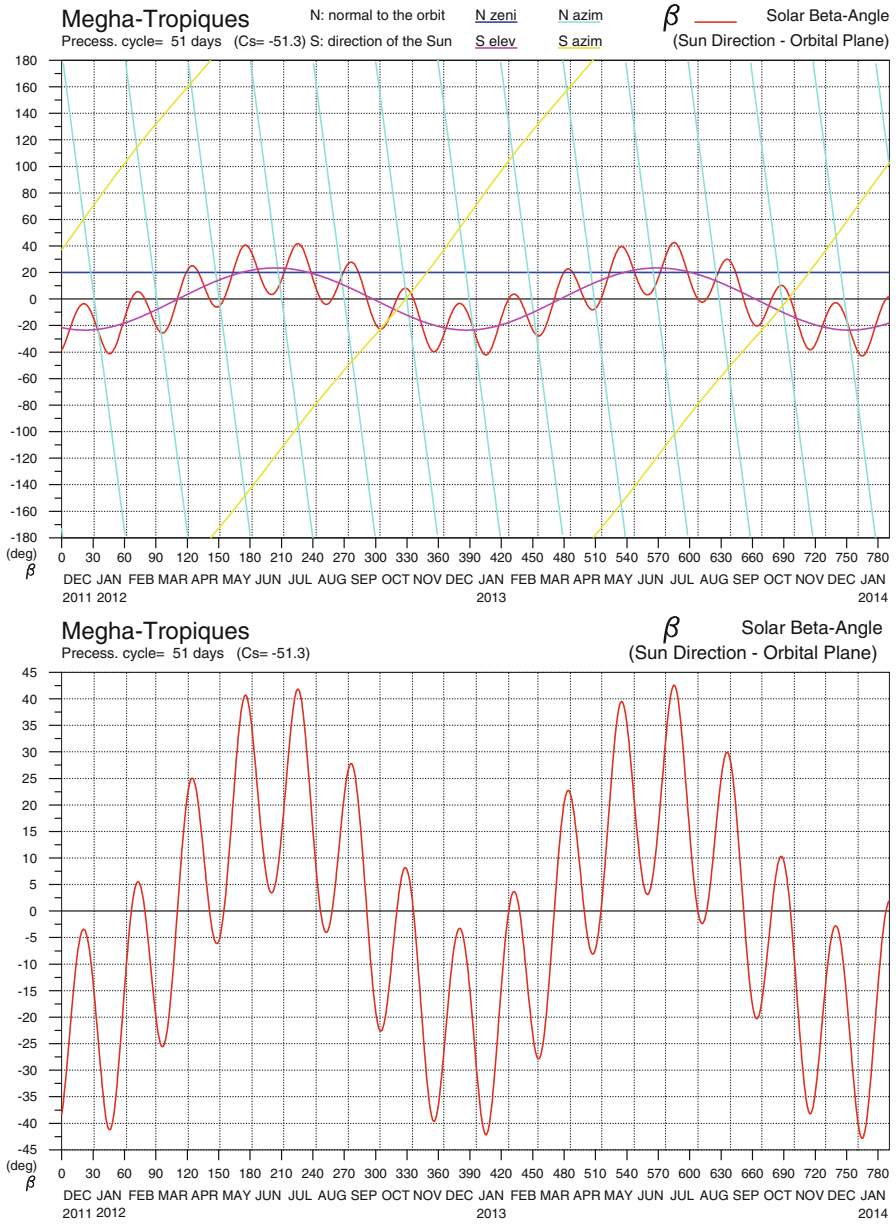


FIG. 10.20 : Angle between the direction of the Sun and the orbital plane. Upper: Angles relevant to the direction of the Sun and the normal to the orbit. Lower: The angle  $\beta$ . Non-Sun-synchronous satellite Megha-Tropiques. Ascending node crossing at 03:44:50 on 1 December 2011.

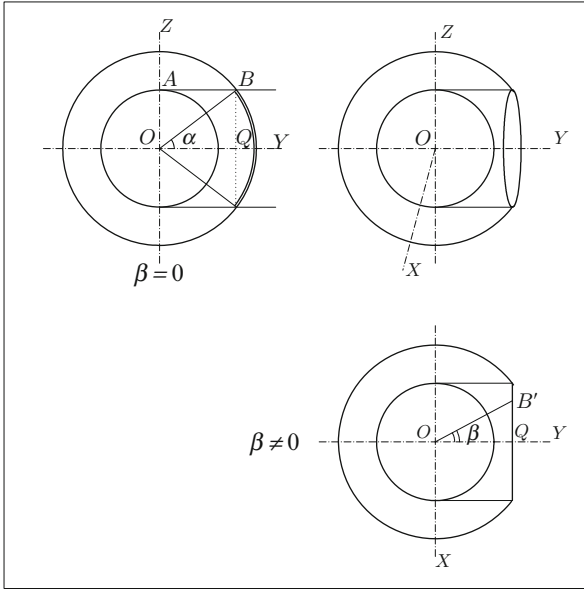


FIG. 10.21 : Determining the duration of the solar eclipse in the case of a circular orbit.  $O$  is the center of the Earth,  $OA$  its radius, and  $OB$  the radius of the orbit. Regarding the frame  $(O; X, Y, Z)$ , the axis  $OY$  is in the direction opposite to the Sun and  $OZ$  is in the orbital plane.

no longer produce electricity. It is useful to know the duration of the eclipse, to know for how long during one revolution the satellite will be deprived of solar light. This problem is particularly important for LEO satellites in near-circular orbits and for geostationary satellites.

### 10.4.1 Duration of Solar Eclipse

If at a given time the direction of the Sun lies in the orbital plane  $\mathcal{P}$  of the satellite, i.e., if  $\beta = 0$  (for the ascending node,  $\tau_{AN} = 00:00$  or  $12:00$ ), it is easy to calculate the proportion of the orbit that lies in shadow. Figure 10.21 (left) shows the circular Earth with center  $O$  and radius  $R$ , and the orbit of the satellite, with radius  $r$  and in the plane  $\mathcal{P}$ . We obtain the angle  $\alpha_0$  (the angle  $\alpha$  when  $\beta = 0$ ) from

$$\sin \alpha_0 = \frac{OA}{OB} = \frac{R}{r} = \frac{1}{\eta},$$

whence we can find the fraction of the orbit in shadow as  $\alpha/\pi$ .

If the direction of the Sun does not lie in the orbital plane, i.e., if  $\beta \neq 0$ , we define an orthonormal frame  $(O; X, Y, Z)$ , centered on  $O$ , and where  $OY$  lies in the antisolar direction. The Earth's shadow defines a cylinder with axis  $OY$  and radius  $R$ . The set of all possible orbits similar to the circular orbit under consideration constitutes a sphere of radius  $r$  centered on  $O$ . The intersection of the sphere and the cylinder gives a circle of radius  $R$ , perpendicular to  $OY$

(see Fig. 10.21). When the satellite crosses this circle it enters and leaves the eclipse.

The angle  $\alpha$  measuring the length of the arc in shadow is given by

$$\cos \alpha = \frac{OB'}{OB}, \quad \cos \beta = \frac{OQ}{OB'},$$

whence

$$\cos \alpha = \frac{\cos \alpha_0}{\cos \beta}. \quad (10.30)$$

If  $T$  is the period and the angles are in radians, we obtain the expression for the duration of the eclipse, denoted by  $\Delta t_e$ , by calculating the quantity  $\mathfrak{U}$ , viz.,

$$\mathfrak{U} = \frac{\sqrt{1 - 1/\eta^2}}{\cos \beta} \implies \begin{cases} \Delta t_e = \frac{T}{\pi} \arccos \mathfrak{U}, & \text{if } \mathfrak{U} < 1, \\ \Delta t_e = 0, & \text{if } \mathfrak{U} \geq 1. \end{cases} \quad (10.31)$$

Given the value of  $\beta$  from (10.26), we can thus obtain  $\Delta t_e$  for any circular orbit. We give two examples in Fig. 10.22 for two non-Sun-synchronous LEO satellites.

Below we examine the case of Sun-synchronous satellites in more detail.

### 10.4.2 Sun-Synchronous LEO Orbit

For a Sun-synchronous satellite in low circular orbit ( $i \sim 100^\circ$ ), the value of  $\sin \beta$ , in (10.27), and hence of  $\Delta t_e$ , depends essentially on  $H_0$ , representing the fixed ascending node crossing time  $\tau_{AN}$  (LMT). Figures 10.23 and 10.24 give the length of the eclipse during each revolution, as the year goes by, for a “standard” Sun-synchronous orbit with  $h = 700$  km. For this orbit, all possible values of  $\tau_{AN}$  from 00:00 to 24:00 are shown, in steps of a quarter of an hour.

For  $\tau_{AN} = 06:00$  (dawn–dusk orbit), we have  $\Delta t_e = 0$  right through the year, except for mid-November to the end of January, with  $\Delta t_e$  going through a maximum of 19 min at the winter solstice. For  $\tau_{AN} = 18:00$  (dawn–dusk orbit), eclipse occurs around the summer solstice (see Fig. 10.28).

For  $\tau_{AN} = 00:00$  or 12:00 (noon–midnight orbit),  $\Delta t_e$  is constant during the year with  $\Delta t_e = 35$  min. When  $\tau_{AN}$  is more than 3 h away from the dawn–dusk orbit, eclipse occurs daily, and always lasts more than 28 min (see Fig. 10.29 upper).

There is a certain disymmetry in the graphs here.<sup>4</sup> It can be put down to the equation of time  $E_T$ , which gives the difference between times in LMT and LAT. The ascending node crossing times are in LMT on the graphs, whereas the eclipse configuration depends on LAT.

---

<sup>4</sup>As an example, consider the most striking case. On 11 February or 1 November, the declination is the same, but the equation of time is very different, not being far from its

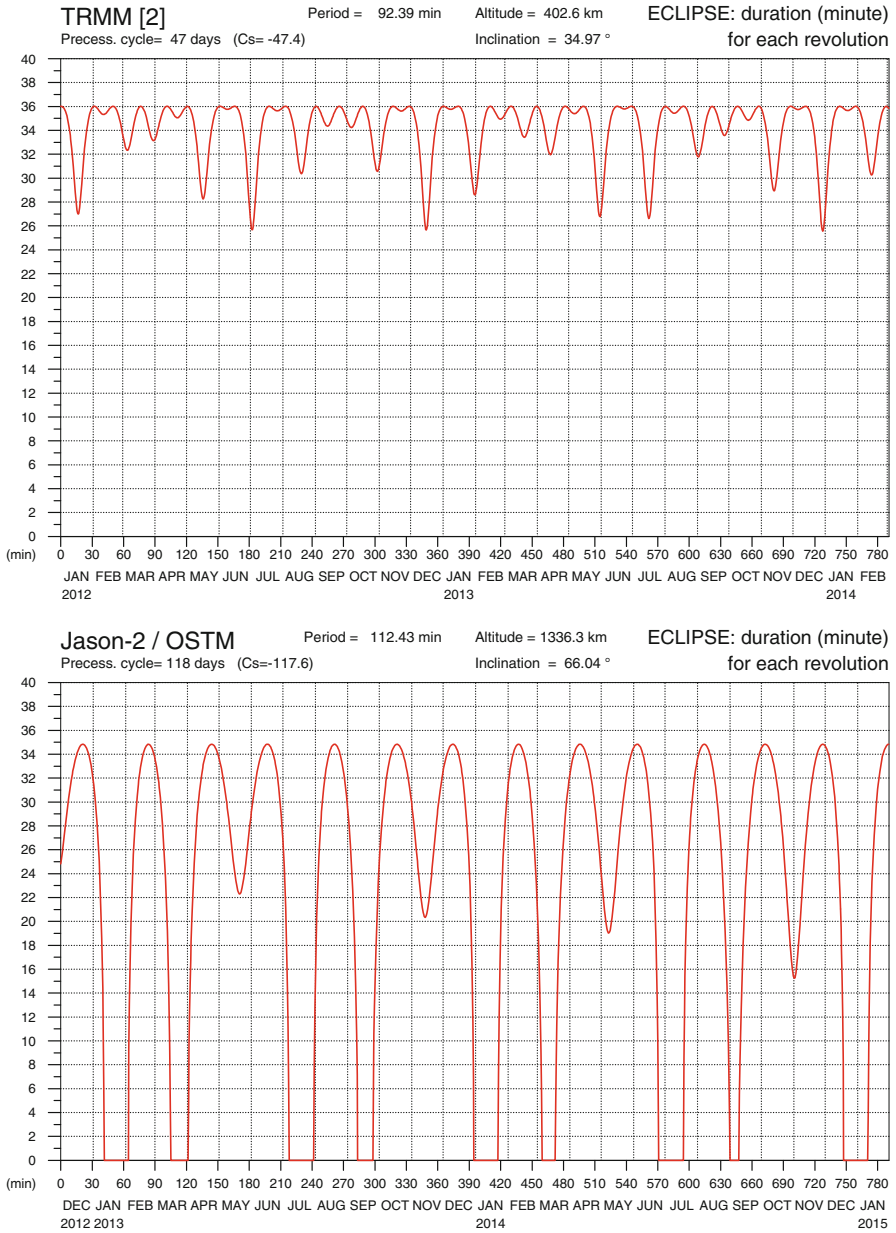


FIG. 10.22 : Duration of solar eclipse in minutes, for each revolution, as a function of the day of the year for non-Sun-synchronous LEO satellites. Upper: TRMM. Lower: Jason-2.

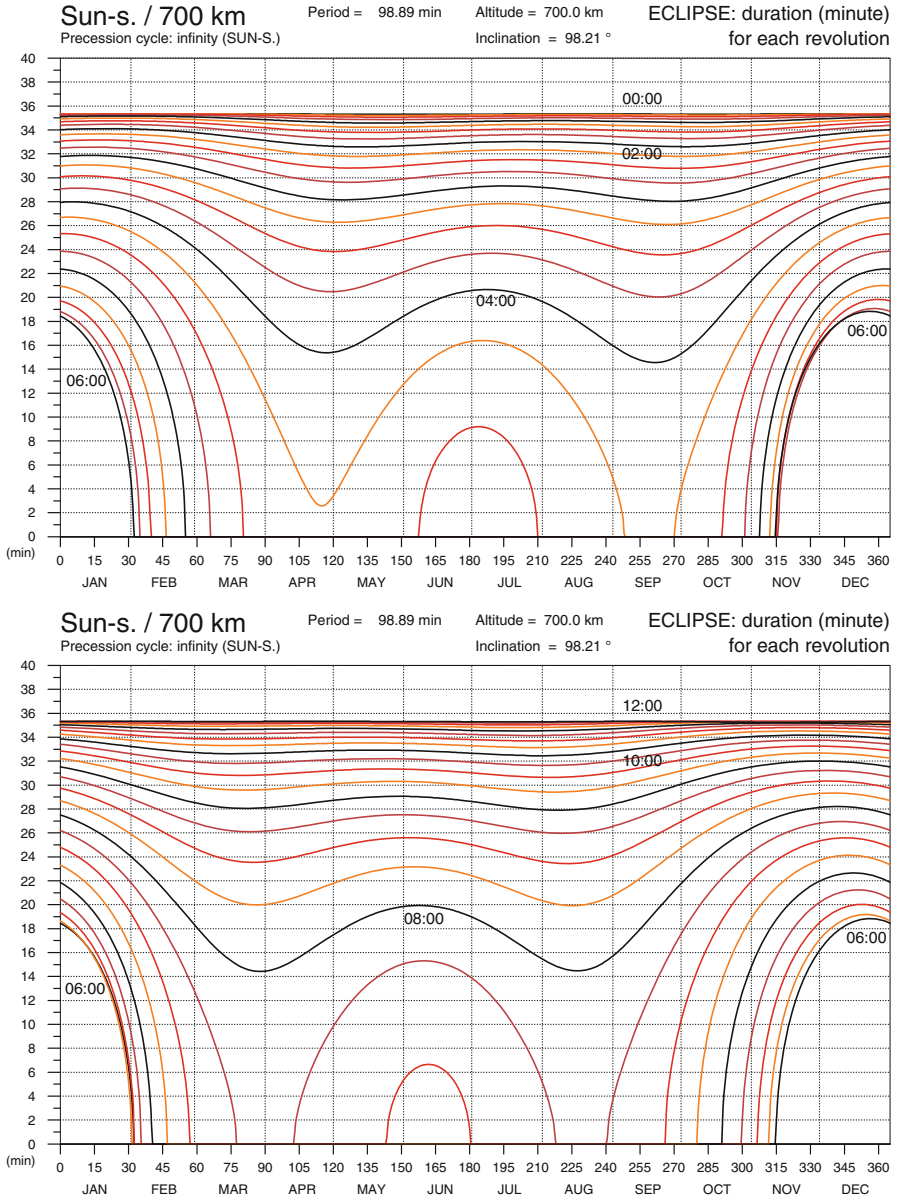


FIG. 10.23 : Duration of solar eclipse in minutes, for each revolution, as a function of the day of the year for Sun-synchronous satellites ( $h = 700$  km), for various ascending node crossing times (LMT) in steps of quarter of an hour. Upper: From 00:00 to 06:00. Lower: From 06:00 to 12:00.

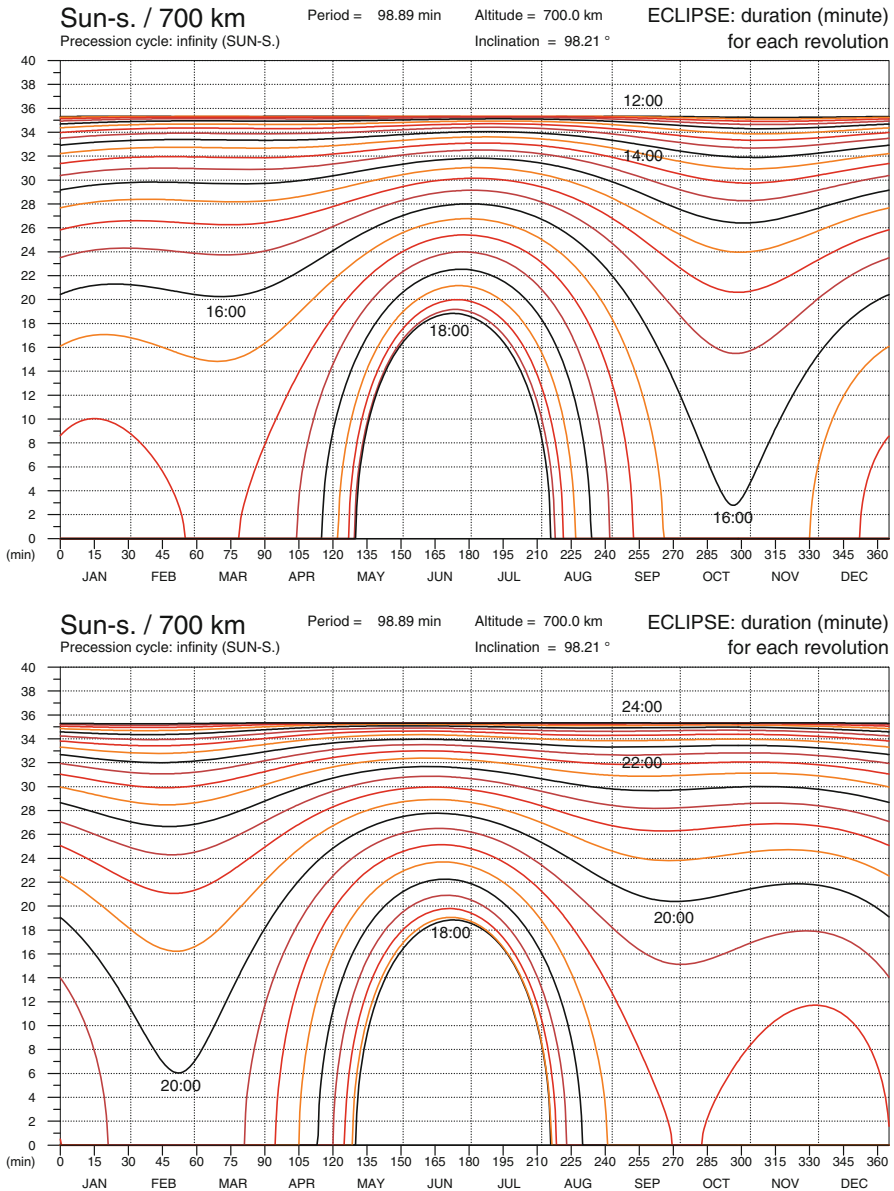


FIG. 10.24 : Duration of solar eclipse in minutes, for each revolution, as a function of the day of the year for Sun-synchronous satellites ( $h = 700$  km), for various ascending node crossing times (LMT) in steps of quarter of an hour. Upper: From 12:00 to 18:00. Lower: From 18:00 to 24:00.

### 10.4.3 Dawn–Dusk Sun-Synchronous LEO Orbit

#### Eclipse Conditions

For Sun-synchronous dawn–dusk orbits, eclipses are critical events. Using the condition (10.31), applied to the dawn–dusk orbit, let us look for the case where eclipse is avoided, for whatever day of the year. The strongest constraint is obtained at one of the two solstices, with  $|\delta| = \varepsilon = 23.44^\circ$ . Under these conditions, when  $\eta$  is varied between 1 and 1.9367, the maximal value for a Sun-synchronous satellite, given by (7.107), the condition on  $\eta$  and  $\beta$  is satisfied when  $\eta$  lies between 1.2181 and 1.5221. Using the altitude, we obtain

$$\text{absence of eclipse} \iff 1\,391 \text{ km} < h < 3\,330 \text{ km} .$$

If the altitude of the satellite is less than 1,391 km, there will be eclipse, because the satellite is not high enough to leave the Earth’s shadow (at least at the solstice). If the altitude is greater than 3,330 km, the orbit is close enough to the equatorial plane ( $i$  tends to  $180^\circ$ ) and the ecliptic to mean that, despite its high altitude, the satellite nevertheless passes through the shadow.

These observations are rather theoretical. In practice, most satellites in dawn–dusk orbit are equipped with radar—with the constraint (C4) considered earlier—and an altitude less than 800 km is then the norm. The eclipse phenomenon is thus inevitable at some point during the year for an LEO satellite.

#### Dates of Eclipse

When there is eclipse, we calculate how long it will last as a function of the date. The results are given in Fig. 10.25 for altitudes between 200 and 1,200 km. The eclipse lasts longer for lower altitudes and reaches its maximal length  $\Delta t_e$  at the solstice (northern winter solstice if  $\tau_{AN} = 06:00$ , northern

---

extremal values:

$$\delta = -14.3^\circ \quad \begin{cases} 11 \text{ February} & E_T = +14 \text{ min} , \\ 1 \text{ November} & E_T = -16 \text{ min} . \end{cases}$$

Consider Fig. 10.24 (upper). On 11 February, the 16:00 curve indicates an eclipse lasting  $\Delta t_e = 21$  min, which corresponds to

$$\text{LAT} = \text{LMT} - E_T = 16:00 - 0:14 = 15:46 .$$

On 1 November, this same value of  $\Delta t_e = 21$  min is obtained with the 15:30 curve, which corresponds to

$$\text{LAT} = \text{LMT} - E_T = 15:30 + 0:16 = 15:46 .$$

At LMT times differing by 30 min, but at the same LAT times, the two dates yield the same length of eclipse.



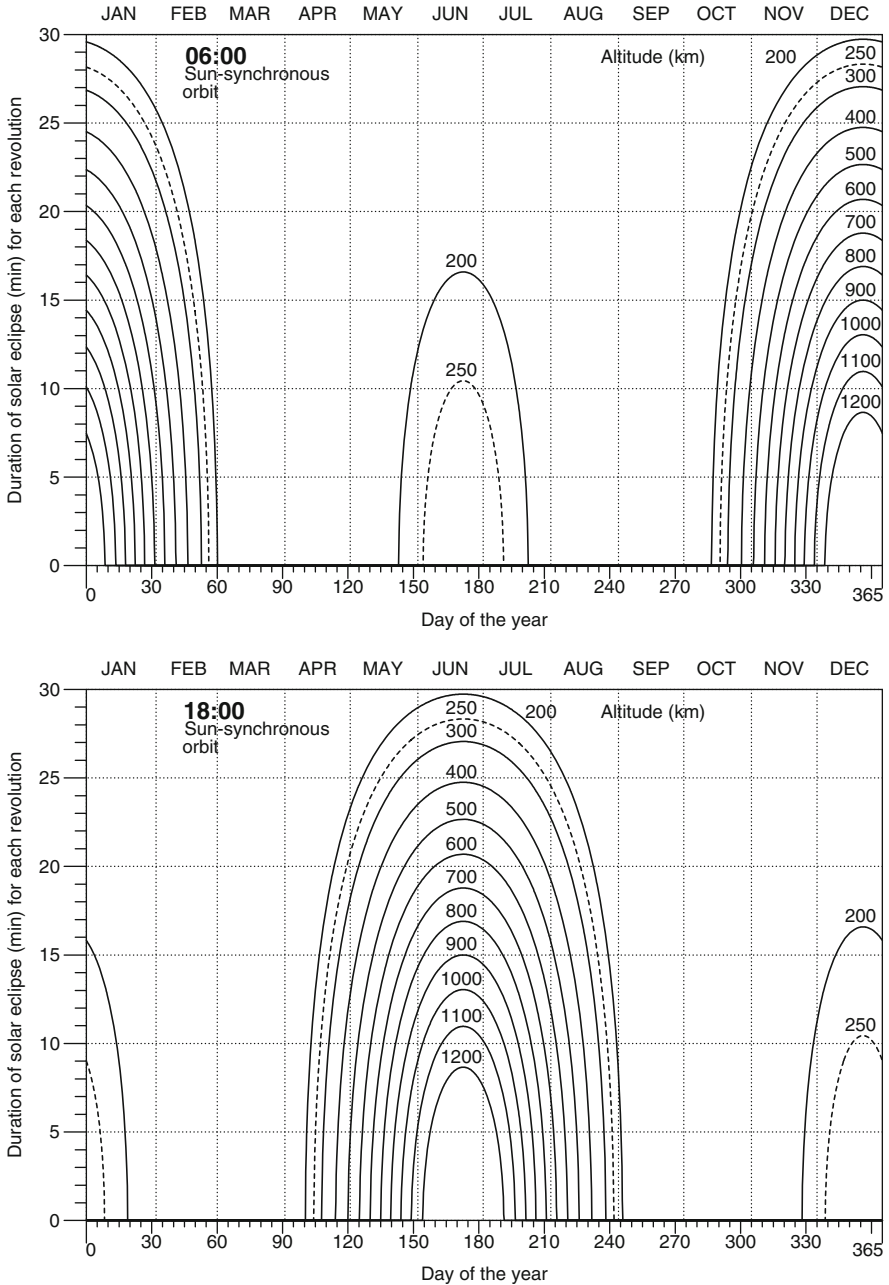


FIG. 10.25 : Duration of solar eclipse in minutes, for each revolution, as a function of the day of the year for dawn-dusk Sun-synchronous satellites, for various altitudes from  $h = 200$  to  $h = 1,200$  km. Ascending node crossing times (LMT): Upper: 06:00. Lower: 18:00.

summer solstice if  $\tau_{AN} = 18:00$ ). For altitudes below 285 km, there is a second, but shorter, period of eclipse at the other solstice (see Example 10.10).

The graphs shown previously for Sun-synchronous satellites are perfectly rigorous. In order to obtain simple and general analytic relations for Sun-synchronous LEO satellites, we establish the following relations by neglecting the equation of time  $E_T$ . So identifying LMT and LAT, we may write

$$06:00 \text{ LMT} \implies \sin H_0 = -1, \quad 18:00 \text{ LMT} \implies \sin H_0 = +1.$$

In (10.27), we then write  $\sin H_0 = \sigma$  with  $\sigma = \pm 1$ , depending on which of the two LMT times we are referring to. This gives

$$\sin \beta = \sin(\delta + \sigma i).$$

Since the satellite is Sun-synchronous ( $i_{HS} > 90^\circ$ ), it is more convenient with regard to the domain of variation of the angles to consider  $j = i_{HS} - 90^\circ$ , rather than  $i_{HS}$ . The last relation then becomes

$$\sin \beta = \cos(\delta + \sigma j).$$

The condition for no eclipse arising from (10.31), viz.,

$$\sqrt{1 - \frac{1}{\eta^2}} > \cos \beta,$$

then becomes

$$\frac{1}{\eta} < \cos(\delta + \sigma j). \quad (10.32)$$

We thus obtain

$$\text{absence of eclipse} \iff |\delta + \sigma j| < \arccos \frac{1}{\eta}. \quad (10.33)$$

The following is an example of this type of calculation.

**Example 10.10** Calculate the eclipse dates for SMOS and GOCE.

► The two European satellites SMOS and GOCE are in Sun-synchronous dawn–dusk orbits:

- **SMOS.** The orbital characteristics of SMOS are  $a = 7\,133.875$  km (whence  $h = 756$  km),  $i_{HS} = 98.44^\circ$ ,  $T_d = 100.06$  min,  $\tau_{AN} = 06:00$ . We thus obtain  $j = 8.44^\circ$ ,  $\sigma = -1$ ,  $1/\eta = 0.8942$ , and  $\arccos(1/\eta) = 26.63^\circ$ . We apply the eclipse condition  $|\delta + \sigma j| > \arccos(1/\eta)$ , for two cases, depending on whether the declination is positive or negative:

if  $\delta > 0$ ,  $\delta - 8.44 > 26.63$ , which is never possible ,

if  $\delta < 0$ ,  $|\delta| + 8.44 > 26.63$ , or  $|\delta| > 18.19^\circ$  .

These negative values of the declination correspond to the eclipse interval [15 November to 28 January]. The maximal length of eclipse occurs at the winter solstice, for  $\delta = -\varepsilon$  :

$$\cos \alpha = \frac{\sin(26.63)}{\sin(31.88)} = 0.8487 , \quad \text{whence } \alpha = 31.93^\circ .$$

The length of the eclipse per revolution is

$$\Delta t_e = T_d \frac{31.93}{180} = 17.75 \approx 18 \text{ min} ,$$

which can be checked from Fig. 10.23 with  $h = 700$  km rather than  $h = 756$  km.

- **GOCE.** The orbital characteristics of this satellite are  $a = 6632.488$  km (whence  $h = 254$  km),  $i_{\text{HS}} = 96.54^\circ$ ,  $T_d = 89.72$  min,  $\tau_{\text{AN}} = 18:00$ . We thus obtain  $j = 6.54^\circ$ ,  $\sigma = +1$ ,  $1/\eta = 0.9617$  and  $\arccos(1/\eta) = 15.92^\circ$ . For positive and negative declinations, we now have:

if  $\delta > 0$ ,  $\delta + 6.54 > 15.92$ , or  $\delta > 9.38^\circ$ ,  
implying the date interval [15 April to 29 August] ,

if  $\delta < 0$ ,  $|\delta| - 6.54 > 15.92$ , or  $|\delta| > 22.46^\circ$ ,  
implying the date interval [6 December to 7 January] .

We may say that there are two eclipse seasons, a long one in the summer and a short one in the winter, as can be clearly seen from Fig. 10.25,  $h = 250$  km (and  $h = 254$  km for GOCE). The maximal length of the summer eclipse occurs at the solstice:

$$\cos \alpha = \frac{\sin(15.92)}{\sin(23.44 + 6.54)} , \quad \text{whence } \alpha = 56.7^\circ , \quad \Delta t_e = 28.26 \approx 28 \text{ min} .$$

The maximal length of the winter eclipse also occurs at the solstice:

$$\cos \alpha = \frac{\sin(15.92)}{\sin(23.44 - 6.54)} , \quad \text{whence } \alpha = 19.3^\circ , \quad \Delta t_e = 9.66 \approx 10 \text{ min} .$$

We can calculate the minimal altitude for which the short eclipse season can be avoided. With  $j = 6.54^\circ$  and with the value  $i_{\text{HS}}$  for GOCE, the condition at the solstice is

$$\arccos \frac{1}{\eta} = 23.44 - 6.54 = 16.90^\circ , \quad \text{whence } \eta = 1.04514 , \quad h = 288 \text{ km} .$$

Now calculating the value of  $i_{\text{HS}}$  for this altitude using (7.105), we obtain the value  $i = 96.63^\circ$  and hence

$$\arccos \frac{1}{\eta} = 23.44 - 6.63 = 16.81^\circ, \quad \text{whence } \eta = 1.04464, \quad h = 285 \text{ km}.$$

A further iteration leads to the same result. If the altitude of the orbit is greater than 285 km, there will be only one eclipse season.



### 10.4.4 MEO Orbit

MEO satellites have a long cycle  $C_S$ , close to 1 year, since they have very small precession rates, e.g., 351 days for Navstar/GPS, 353 days for Glonass, 356 days for Galileo, and 354 days for BeiDou NS. Twice during the cycle (once in the ascending part of the orbit and once in the descending part), the satellite finds itself in an eclipse situation. Eclipses occur for about a month, with a maximal duration of around 60 min.

The date of the eclipse depends on the ascending node crossing time taken as reference. Figure 10.26 (upper) shows the length of the eclipse  $\Delta t_e$  as a function of the date for the Galileo constellation. The figure shows four ascending node crossing times on 1 January, with 6 h spacing, viz.,  $\tau_{\text{AN}} = 00:00, 06:00, 12:00, \text{ and } 18:00$ .

### 10.4.5 GEO Orbit

The situation for GEO satellites can be treated quite generally. We set  $i = 0$  in (10.26) and obtain  $\beta = \delta$ , which is the very definition of the declination  $\delta$ . We then apply the condition (10.31) with  $\eta = \eta_{\text{GS}}$  defined by (7.72).

We may also look at things more specifically. For a geostationary satellite, no shadow is cast by the Earth on the circular orbit as long as the direction of the Sun has an inclination (declination  $\delta$ ) with respect to the equatorial plane greater than the angle with which the satellite views the Earth. Let  $f_0$  be this angle, which is the half-angle at the apex of the observation cone with which the satellite views the Earth and to which we shall return in Chap. 12 [see in particular (12.33)]. The relation  $\sin f_0 = 1/\eta_{\text{GS}}$  gives  $f_0 = 8.7^\circ$ .

There is therefore an eclipse if  $|\delta| < f_0$ . This happens twice a year, around the equinoxes:

$$\text{eclipse for GEO} \iff \begin{cases} [27 \text{ February to } 12 \text{ April}] \\ [1 \text{ September to } 16 \text{ October}] \end{cases}$$

During these two periods of 45 days (from  $D = 58$  to  $D = 102$  and from  $D = 244$  to  $D = 289$ , although dates may vary by 1 day depending on the

year), the longest eclipse occurs at the equinoxes. On that day, it lasts for a time

$$\Delta t_e = \frac{f_0}{\pi} T_0 = \frac{8.7}{180} D_{\text{sid}} = 69.5 \text{ min} \approx 1 \text{ h } 10 \text{ min} . \tag{10.34}$$

The value of  $\Delta t_e$  as a function of the day of the year is shown in Fig. 10.26 (lower).

## 10.5 General Conditions for Solar Eclipse

So far we have calculated the dates and lengths of eclipse and provided analytic formulas in the case of circular orbits. In the general case, for orbits with arbitrary eccentricity, such simple formulas are no longer possible, because too many orbital elements need to be taken into account. However, there is a general method for determining the period of eclipse for any satellite.

### 10.5.1 Establishing General Eclipse Conditions

To calculate the angle  $\beta$ , we chose an arbitrary origin for the axes of the frame  $\mathfrak{R}$ . In order to obtain general eclipse conditions, it is simpler and more logical to choose the direction of the vernal equinox as origin, given that this kind of practical calculation is done using the NORAD elements (where  $\Omega$  is measured from this point  $\gamma$ ).

We thus consider a geocentric pseudo-Galilean frame  $\mathfrak{R}$ , where  $z'Oz$  is the polar axis,  $Oxy$  lies in the Earth's equatorial plane  $\mathcal{E}$ , and  $Ox$  points to the vernal equinox.

#### Position of the Sun

The plane  $\mathcal{E}$  makes an angle  $\varepsilon$ , the obliquity, with the plane of the ecliptic (see Fig. 7.7). Indicating the position of the Sun by the ecliptic longitude  $l$  as defined in (7.46), we obtain the components of the unit vector  $\mathbf{s}$  in the direction of the Sun:

$$\mathbf{s} = \begin{pmatrix} x = \cos l \\ y = \sin l \cos \varepsilon \\ z = \sin l \sin \varepsilon = \sin \delta \end{pmatrix} . \tag{10.35}$$

With (7.62), we obtain the same value  $z$  as in (10.25). For these eclipse calculations, an accuracy of  $0.1^\circ$  in the angles is sufficient, since the apparent diameter of the Sun is  $0.5^\circ$ . We thus take  $\varepsilon = 23.4^\circ$ . For the solar longitude, the relation (7.64), viz.,

$$l = \frac{360}{365}(D - 81) + 1.9 \sin \frac{360}{365}(D - 3) , \tag{10.36}$$

is adequate, where  $D$  is the day of the year, i.e.,  $D = 1, \dots, 365$ .

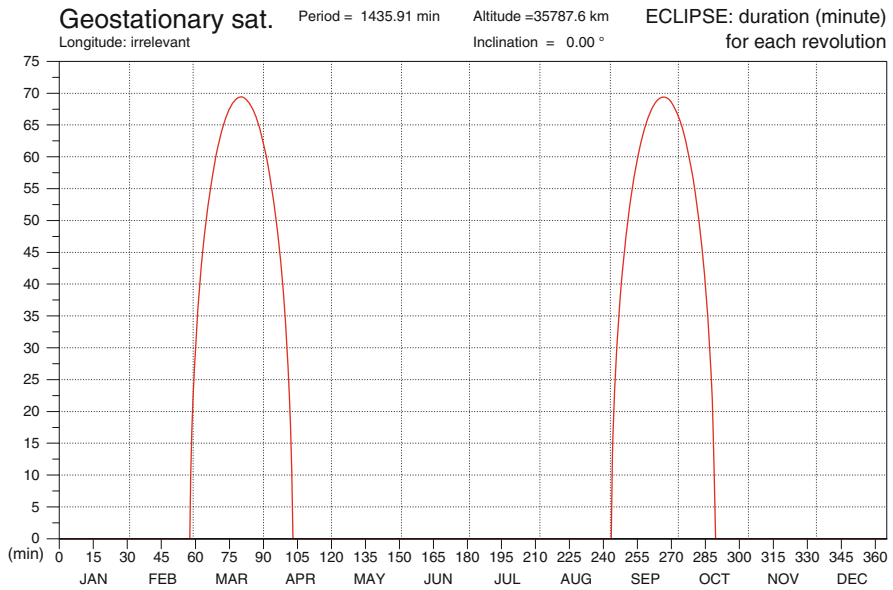
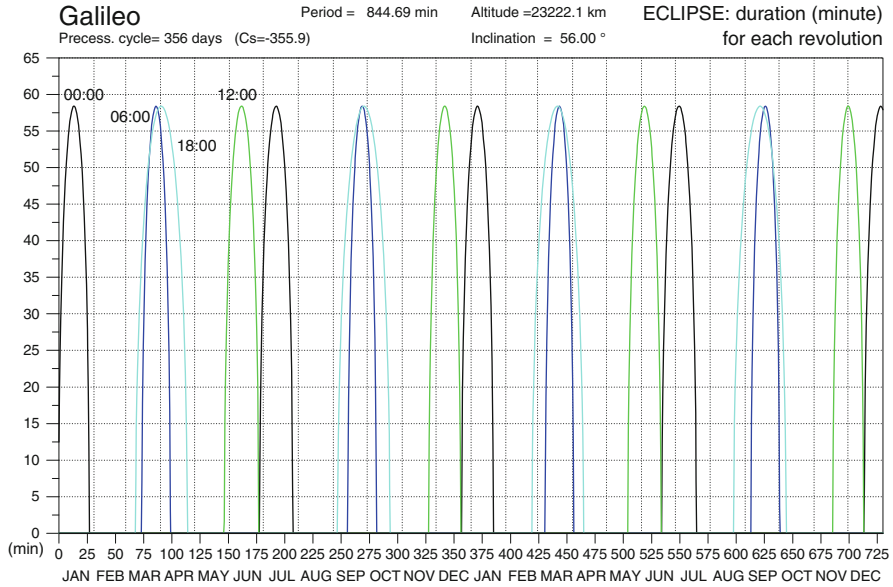


FIG. 10.26 : Length of solar eclipse in minutes as a function of the day of the year. Upper: MEO satellite with four values of the ascending node crossing time (LMT), the initial reference day. Lower: GEO satellite, for any value of the parking longitude.

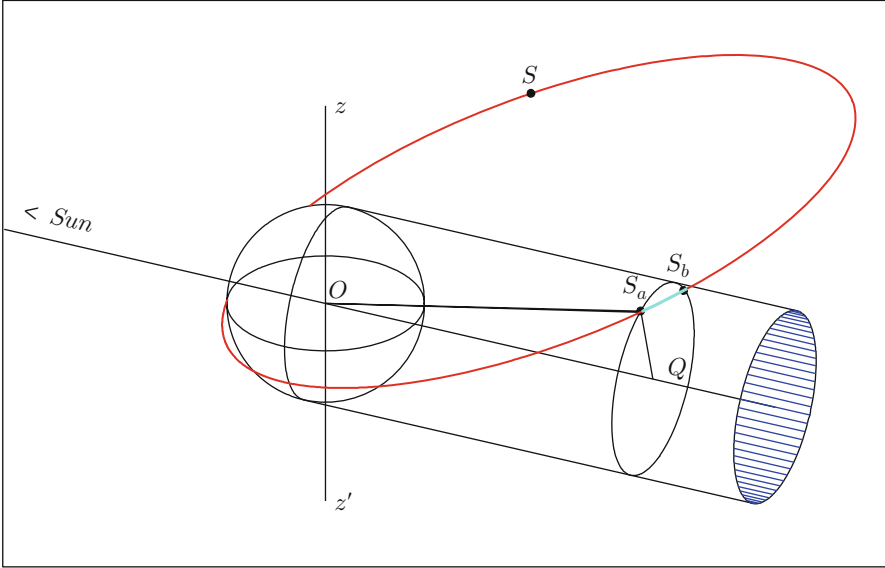


FIG. 10.27 : Geometry of eclipse conditions. The Earth creates a cylinder of shadow with axis in the direction  $OQ$  of the Sun. When the orbit of the satellite  $S$  passes inside the cylinder, in this case between  $S_a$  and  $S_b$ , the satellite undergoes solar eclipse.

**Position of the Satellite**

For the position of the satellite  $S$ , we go back to the specification of its motion in terms of Euler angles, as discussed in Chap. 8, measuring  $\Omega$ , the right ascension of the ascending node, from the vernal equinox. For the unit vector  $\mathbf{e}_r$  in the direction of  $\mathbf{r} = \mathbf{OS}$ , we thus obtain the components given in (8.10):

$$\mathbf{e}_r = \begin{pmatrix} x = \cos \Omega \cos(\omega + v) - \sin \Omega \sin(\omega + v) \cos i \\ y = \sin \Omega \cos(\omega + v) + \cos \Omega \sin(\omega + v) \cos i \\ z = \sin(\omega + v) \sin i \end{pmatrix}. \tag{10.37}$$

Recall that

$$\mathbf{r} = r\mathbf{e}_r, \quad r = \frac{a(1 - e^2)}{1 + e \cos v}.$$

Let  $\chi$  be the angle between the direction of the satellite and the direction opposite to the Sun, with unit vector  $-\mathbf{s}$ . It is determined by the scalar product

$$\cos \chi = -\mathbf{e}_r \cdot \mathbf{s}. \tag{10.38}$$

### Cylinder of Shadow

We treat the Earth as a sphere and the Sun as a point. The planet then produces a cylinder of shadow with axis  $-\mathbf{s}$  and radius  $R$  (equatorial radius). The orbit of the satellite can cut the cylinder of shadow, in which case there will be an eclipse. In Fig. 10.27, the satellite undergoes an eclipse between the positions  $S_a$  and  $S_b$ .

Let  $Q$  be the foot of the perpendicular drawn from  $S_a$  (or  $S_b$ ) to the cylinder axis. In this case, the angle  $\chi$ , then denoted by  $\chi_0$ , represents the angle between the plane of the orbit and the direction of the Sun. This is the solar angle  $\beta$ . The value of  $\chi_0$  is obtained from the relation

$$\sin \chi_0 = \frac{S_a Q}{OS_a} = \frac{R}{r} = \frac{1}{\eta}. \quad (10.39)$$

In this case, we thus have  $\sin \beta = 1/\eta$  when the satellite enters and leaves eclipse.

#### 10.5.2 Criterion for Eclipse

If there is eclipse ( $S$  between  $S_a$  and  $S_b$ ), the angle  $\chi$  is less than  $\chi_0$ . Otherwise there is no eclipse. As the satellite position is given by the true anomaly  $v$ , calculated as a function of time, the method here is to calculate the vectors  $\mathbf{s}$  and  $\mathbf{e}_r$  and the distance  $r$  at each instant of time, then compare  $\chi$  and  $\chi_0$ :

$$\begin{cases} \chi = \arccos(-\mathbf{e}_r \cdot \mathbf{s}), \\ \chi_0 = \arcsin(1/\eta), \end{cases} \implies \begin{cases} \chi < \chi_0 & \iff \text{eclipse,} \\ \chi > \chi_0 & \iff \text{no eclipse.} \end{cases} \quad (10.40)$$

This method requires the use of a propagation software such as *Ixion*. Note that we do not have to calculate  $\beta$  explicitly. Figures 10.28, 10.29, and 10.30 were obtained using this method.



**TerraSAR-X**

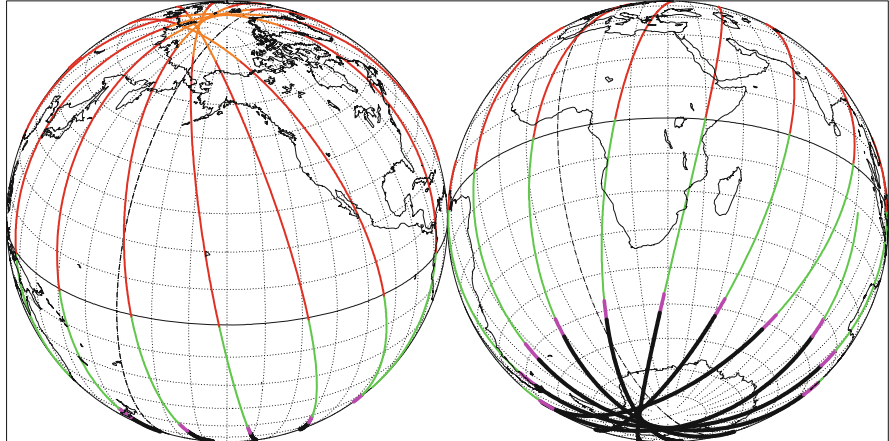
**Orbit - Ground track**

Recurrence = [15; +2; 11] 167

2012 06 22 00:00:00 UTC >>> 720.0 min = 0.50 day

Eclipse and Sun elev. night ECLIPSE night 0 15 30 45 60 75 90

**22 JUN**



Projection: Orthographic

Property: none

⊕ T.:Azimuthal - Graticule: 10°

Pr. centre (r.): 28.0 ° S; 30.0 °E

Aspect: Oblique

{4.2} [-90.0/+118.0/+60.0] [-] EIGEN6C2

Asc. Node: 85.01 ° [18:00 LMT]

[NORAD] Revolution: 27831

[NORAD] 2012 06 21 12:20:20 UTC

*Ιξίων*

MC \* LMD

Ατλας

**TerraSAR-X**

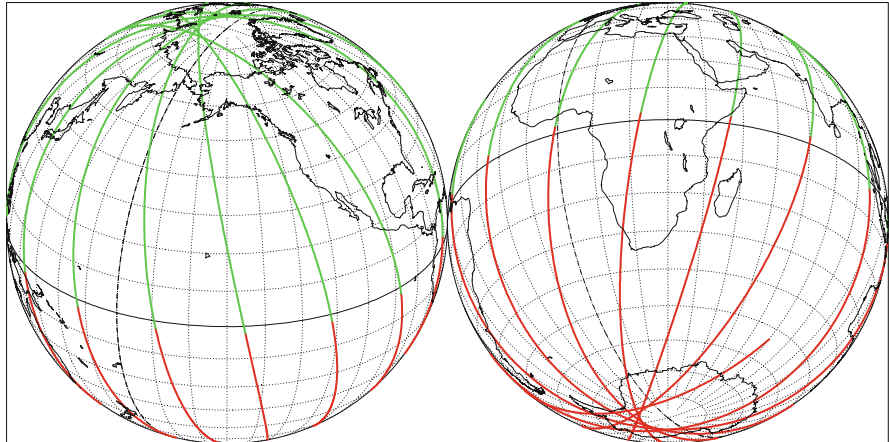
**Orbit - Ground track**

Recurrence = [15; +2; 11] 167

2012 12 22 00:00:00 UTC >>> 720.0 min = 0.50 day

Eclipse and Sun elev. night ECLIPSE night 0 15 30 45 60 75 90

**22 DEC**



Projection: Orthographic

Property: none

⊕ T.:Azimuthal - Graticule: 10°

Pr. centre (r.): 28.0 ° S; 30.0 °E

Aspect: Oblique

{4.2} [-90.0/+118.0/+60.0] [-] EIGEN6C2

Asc. Node: -27.07 ° [18:00 LMT]

[NORAD] Revolution: 30614

[NORAD] 2012 12 21 19:48:43 UTC

*Ιξίων*

MC \* LMD

Ατλας

FIG. 10.28 : Ground track of the Sun-synchronous satellite TerraSAR-X, in dawn-dusk orbit, indicating periods of eclipse. Upper: Summer solstice (eclipse over the Antarctic). Lower: Winter solstice (eclipse free).

**MetOp-B**

Orbit - ref.: Earth

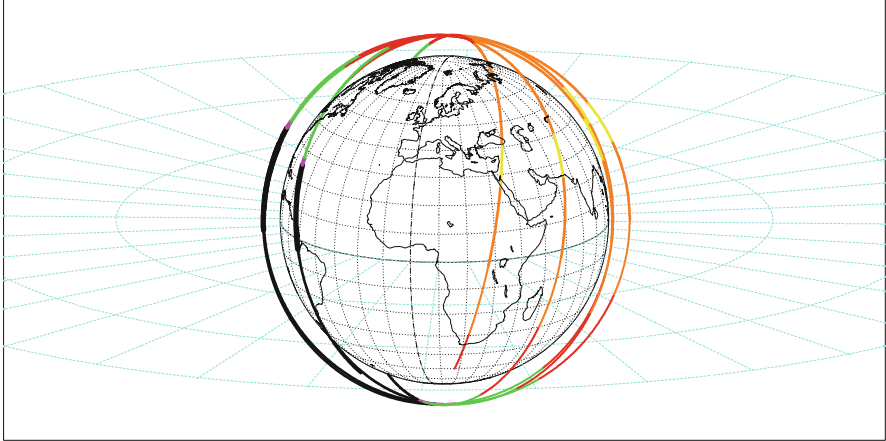
Recurrence = [14; +6; 29] 412

2013 06 01 00:00:00 UTC >>> 480.0 min = 0.33 day

Eclipse and Sun elev.  night ECLIPSE night 0 15 30 45 60 75 90

Altitude = 817.5 km      a = 7195.616 km  
 Incl. / SUN-S. = 98.70 °      e = 0.000170  
 Period = 101.36 min \* rev/day = 14.21  
 Equat. orbital shift = 2820.8 km ( 25.3 °)

01 JUN



Projection: Orthographic      Project. centre: 15.0 ° N; 12.0 ° E      Asc. Node: -86.61 ° [21:32 LMT]      Iξλων  
 Property: none      Aspect: Oblique      [NORAD] Revolution: 3586      MC ★ LMD  
 ⊕ T.:Azimuthal - Graticule: 10°      {4.2} [-90.0/+75.0/+78.0] EIGEN6C2      [NORAD] 2013 05 28 03:18:11 UTC      ΑΤλας

**Akebono (EXOS-D)** < あけぼの >

Orbit - ref.: Earth

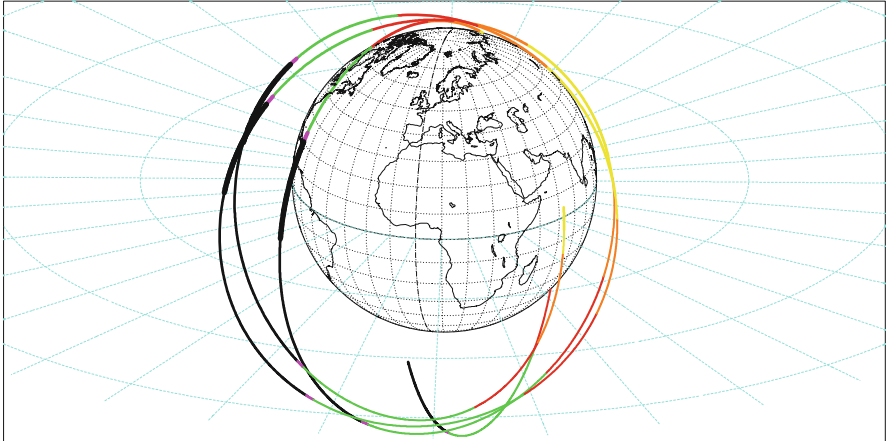
Recurrence ~ [11;-23; 57] 604

2013 06 01 00:00:00 UTC >>> 480.0 min = 0.33 day

Eclipse and Sun elev.  night ECLIPSE night 0 15 30 45 60 75 90

Equiv. altit. = 2342.0 km      a = 8720.158 km  
 Inclination = 75.07 °      e = 0.238666  
 Period = 135.16 min \* rev/day = 10.65  
 h\_a = 4440 km; h\_p = 277 km; arg. perigee: +64.81 °

01 JUN



Projection: Orthographic      Project. centre: 23.0 ° N; 11.0 ° E      [NORAD] 2013 05 28 09:21:42 UTC/R= 74306      Iξλων  
 Property: none      Aspect: Oblique      Asc. Node: 40.87 ° [12:05 LMT]      MC ★ LMD  
 ⊕ T.:Azimuthal - Graticule: 10°      {4.2} [-90.0/+67.0/+79.0] EIGEN6C2      Apogee: -97.43 °      ΑΤλας

FIG. 10.29 : Orbits indicating periods of eclipse. Upper: Sun-synchronous satellite MetOp-B (with  $\tau_{AN} = 21:32$ ). Lower: Non-Sun-synchronous satellite Akebono in elliptical orbit.

**Molniya-3-51** < ΜΟΛΝΙΑ >

Elliptical orbit - Gr. track

Equiv. altit. = 20166.8 km      a = 26544.934 km

CRITICAL Incln. = 63.48 °      e = 0.751163

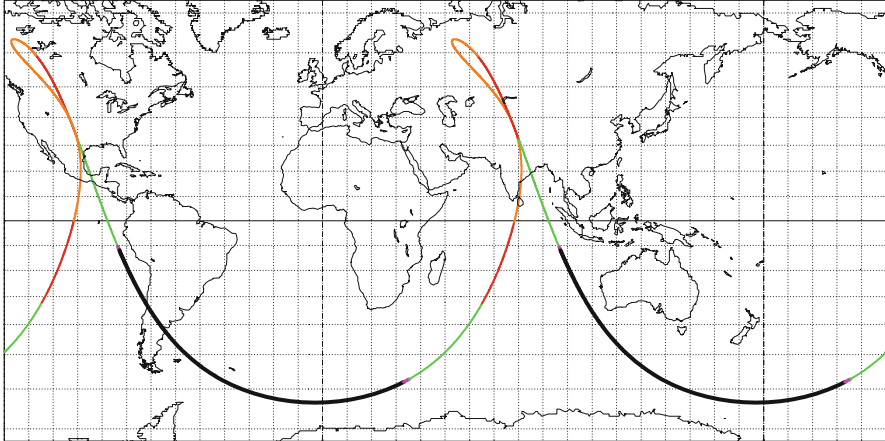
Recurrence = [ 2; +0; 1] 2

Period = 717.40 min \* rev/day = 2.01

2013 06 01 00:00:00 UTC >>> 1440.0 min = 1.00 day

h\_a = 40122 km; h\_p = 243 km; arg. perigee: +254.45 °

Eclipse and Sun elev.      night      ECLIPSE      night      0    15    30    45    60    75    90      **01 JUN**



Projection: Miller

Project. centre: 0.0 ° ; 50.0 °E

[NORAD] 2013 05 21 15:51:08 UTC/R= 8674

Ιξίων

Property: none

Aspect: Direct

Asc. Node: -103.33 ° [08:58 LMT]

MC \* LMD

⊕ T.:Cylindrical - Graticule: 10° [4.2] [+90.0/ +0.0/-140.0] [-] PZ-90

Apogee : 54.07 °

Ατλας

FIG. 10.30 : *Orbital ground track of the satellite Molniya-3-51, indicating periods of eclipse.*

# Chapter 11

## Orbit Relative to the Earth: Recurrence and Altitude

In this chapter, we discuss the position of the satellite orbit relative to the Earth. There are two distinct parts. The first concerns the position of the satellite ground track relative to the Earth, and the second the altitude of the satellite measured from the terrestrial ellipsoid.

### 11.1 Recurrence Constraint

#### 11.1.1 Definition of Recurrence

In observation missions using LEO satellites, one often requires repeated coverage of the Earth, in the sense that the satellite must periodically overfly the same points of the Earth's surface. This means that, for a given point, one is sure to recover geometrically identical observing conditions with this periodicity. Such a recurrence constraint on the mission imposes specific characteristics on the orbital elements.

The recurrence period after which the satellite ground track repeats itself exactly on the Earth's surface is called the recurrence cycle, but also the repeat cycle. This corresponds to the cycle relative to the Earth and we denote its value by  $C_T$ , where the subscript T stands for "terrestrial", just as we denoted the cycle relative to the Sun by  $C_S$  in the last chapter.

When recurrence has been achieved, the ground track of the satellite forms a fixed grid with respect to the Earth, which covers the globe between the highest attained latitudes. One point on the grid (the ascending node is generally chosen) fixes the whole thing. We shall study this recurrence grid below.

The calculational methods developed here to analyse recurrence remain valid even if the satellite has an eccentric orbit. However, in practice, all recurrent LEO satellites are in near-circular orbits. On the other hand, recurrence is not restricted to LEO satellites, but is used for MEO satellites and HEO communications satellites.

### Daily Recurrence Frequency

The precession angle, i.e., the Euler angle  $\alpha_1$  in our notation, plays a key role in the study of recurrence. Using (7.37) and (8.17), we obtain

$$\dot{\alpha}_1 = -(\dot{\Omega}_T - \dot{\Omega}) = -\frac{2\pi}{D_M} \left( 1 + \frac{1-P}{N'_{\text{yr}}} \right), \quad (11.1)$$

$$\alpha_1 = -\frac{n_d}{\kappa}, \quad (11.2)$$

where  $N'_{\text{yr}}$ ,  $D_M$ ,  $P$ , and  $\kappa$  are as defined in Chap. 7.

The daily recurrence frequency defined by (7.43), viz.,

$$\kappa = \frac{\nu}{1 + \frac{1-P}{N'_{\text{yr}}}}, \quad (11.3)$$

allows one to compare the Earth's rotation, the satellite motion, and its nodal precession via the angular speeds. It is close to  $\nu$ , the daily orbital frequency, but it is not the same, except for Sun-synchronous satellites. Indeed only in the latter case do we have  $\kappa = \nu$ , since  $P = 1$ .

#### 11.1.2 Calculating the Recurrence Cycle $C_T$

The intersection of the ascending ground track of the satellite with the equator defines an ascending node of longitude  $\lambda_0$ . If the satellite is recurrent, its ground track will pass precisely through this point  $\lambda_0$  on the equator,  $C_T$  days later. The satellite will have made a whole number of round trips between these two crossings. The number of round trips is denoted by  $N_{T_o}$ , whereas  $C_T$  is an arbitrary real number, unlikely to be an integer. Throughout the rest of this chapter, we shall attach the subscript “o” to whole numbers (integers) entering our calculations.

From the above discussion, we obtain the following relation which gives the length  $\mathbb{L}$  of the time interval between the two crossings at the same ascending node  $\lambda_0$ :

$$\mathbb{L} = C_T D_M = N_{T_o} T_d. \quad (11.4)$$

During this time  $\mathbb{L}$ , the orbital plane makes a whole number of round trips, denoted by  $k_o$ , relative to the frame  $\mathfrak{R}_T$ , since the ground track returns exactly to an earlier position. This yields

$$\mathbb{L}(\dot{\Omega}_T - \dot{\Omega}) = 2\pi k_o . \tag{11.5}$$

Equations (11.4) and (7.43) now imply

$$N_{T_o} T_d \frac{n_d}{\kappa} = 2\pi k_o ,$$

which gives (since  $T_d = 2\pi/n_d$ )

$$\kappa = \frac{N_{T_o}}{k_o} .$$

This relation shows that, for a recurrent satellite, the parameter  $\kappa$  which we have called the daily recurrence frequency is a rational number:

$$\text{recurrent satellite} \iff \kappa \text{ rational} . \tag{11.6}$$

In terms of the daily orbital frequency  $\nu$ , we have

$$C_T D_M = N_{T_o} \frac{D_M}{\nu} ,$$

which implies that the cycle relative to the Earth is

$$C_T = \frac{N_{T_o}}{\nu} . \tag{11.7}$$

The whole number  $k_o$  defined above, which represents a whole number of days, will be denoted by  $C_{T_o}$ . Hence,

$$C_{T_o} = \frac{N_{T_o}}{\kappa} . \tag{11.8}$$

In the general case, we distinguish the recurrence cycle  $C_T$  from the integer recurrence cycle  $C_{T_o}$ . In the special case of Sun-synchronous satellites (and it should be noted that this type of satellite covers most cases of recurrence),  $C_T$  and  $C_{T_o}$  coincide, since in this case  $\kappa = \nu$ . This means that, for a recurrent satellite:

- If it is Sun-synchronous, its ground track always returns to the same point at the same time, i.e., at the end of a whole number of days, and  $C_T$  is an integer.
- If it is not Sun-synchronous, its ground track returns to a given point at different times, and  $C_T$  is not an integer.

### Relationship with Cycle Relative to the Sun

The cycle  $C_S$  relative to the Sun and the cycle  $C_T$  relative to the Earth both depend on the orbital characteristics, but not in a one-to-one manner. The orbital parameters of a satellite can be varied in such a way that, for example,  $C_S$  remains constant while  $C_T$  takes any value we wish.

However, a useful relation can be brought out concerning the difference  $C_T - C_{T_o}$  and the cycle  $C_S$ . From the definitions of  $C_S$ ,  $C_T$ ,  $C_{T_o}$ ,  $P$ , and  $\kappa$ , we may write

$$\frac{\nu}{\kappa} = 1 - \frac{1}{C_S}, \quad (11.9)$$

$$\frac{C_T - C_{T_o}}{C_T} = 1 - \frac{C_{T_o}}{C_T} = 1 - \frac{\nu}{\kappa} = \frac{1}{C_S}.$$

We thus obtain  $C_T$ , given  $C_{T_o}$  and  $C_S$ :

$$C_T = \frac{C_{T_o}}{1 - 1/C_S}. \quad (11.10)$$

For a Sun-synchronous satellite,  $C_T = C_{T_o}$ , since  $C_S$  is infinite.

### 11.1.3 Recurrence Triple

The rational number  $\kappa$ , the daily recurrence frequency, can thus be expressed in the form

$$\kappa = \frac{N_{T_o}}{C_{T_o}}. \quad (11.11)$$

It can be written as the sum of an integer and a positive or negative fractional part with modulus less than  $1/2$ :

$$\kappa = \nu_o + \frac{D_{T_o}}{C_{T_o}}. \quad (11.12)$$

In this expression,  $\nu_o$  is the whole number closest to  $\kappa$  and  $D_{T_o}$  is the unique integer such

$$D_{T_o} = N_{T_o} - \nu_o C_{T_o}. \quad (11.13)$$

Hence,

$$\begin{cases} |D_{T_o}| < \frac{1}{2} C_{T_o}, \\ |D_{T_o}| \text{ and } C_{T_o} \text{ coprime.} \end{cases}$$

We shall call the triple of numbers  $\nu_o$ ,  $D_{T_o}$ , and  $C_{T_o}$  the recurrence triple of the satellite, written

$$[\nu_o, D_{T_o}, C_{T_o}].$$

The recurrence of a satellite orbit can thus be defined equivalently via the recurrence triple or the pair of whole numbers  $N_{T_o}$  and  $C_{T_o}$ .

The value of  $\kappa$  obtained in this way from (11.11) or from (11.12) thus yields  $\nu$  via (11.3), and hence the period or mean motion, after an iterative calculation on  $P$ . The period in minutes is given as a function of  $N_{T_o}$ ,  $C_{T_o}$ , and  $P$  by

$$T_d \text{ (min)} = 1440 \frac{C_{T_o}}{N_{T_o}} \left( 1 + \frac{1-P}{N'_{yr}} \right). \quad (11.14)$$

This iterative calculation involves making a first estimate of  $T$ , which gives  $a$ , and using  $a$  with  $i$  to obtain  $P$ . This in turn gives a new value of  $T$ . The iteration converges rapidly to give a final value for the period.

We provide example calculations below. Naturally, all these calculations are much simpler for a Sun-synchronous satellite, since  $P = 1$ . It is for this reason that we separate the following discussion into two parts, depending on whether the satellite is Sun-synchronous or not.

## 11.2 Recurrence of Sun-Synchronous LEO Satellites

### 11.2.1 Method for Obtaining Recurrence

We have seen that the altitude of a Sun-synchronous satellite in near-circular orbit lies between the theoretical bounds  $h = 0$  and  $h = 5,964$  km, which corresponds to values of the daily orbital frequency of  $\nu = 17.03$  and  $\nu = 6.34$  respectively. In current practice, when  $h$  is situated between 400 and 1,000 km,  $\nu$  varies between 15.5 and 13.8 round trips per day.

For a Sun-synchronous satellite, it is a simple matter to obtain recurrence conditions since  $\nu = \kappa$ . The daily orbital frequency  $\nu = \nu(a)$ , which only depends on  $a$  here, since  $i$  and  $a$  are related, is a rational number which can be written in the form

$$\nu = \nu_o + \frac{D_{T_o}}{C_{T_o}}. \quad (11.15)$$

The satellite ground track repeats every  $C_{T_o}$  days, after  $N_{T_o} = \nu C_{T_o}$  revolutions.

### 11.2.2 Recurrence Module

#### Presentation

We begin with a simple example, considering satellites with frequency  $\nu$  between 14 and 15:

- If the satellite recurrence cycle is 1 day, we have  $\nu = 14$  or 15.



- If it is 2 days, then during this 2 day cycle, it makes  $N_{T_o} = 28, 29$ , or 30 round trips. But if  $N_{T_o} = 28$  or 30, recurrence has already been taken into account by  $C_{T_o} = 1$  day. There thus remains the recurrence  $N_{T_o} = 29$ , represented by the triple  $[14, 1, 2]$ .
- If it is 3 days, then during this 3 day cycle, it makes  $N_{T_o} = 42, 43, 44$ , or 45 revolutions. There remain the recurrences  $N_{T_o} = 43$  or 44, represented by the triples  $[14, +1, 3]$  and  $[15, -1, 3]$ .

And so on and so forth.

### Establishing the Recurrence Module

The recurrence module represents the possible recurrences for an interval  $[\nu_o, \nu_o + 1]$ . For each value of  $C_{T_o}$ , represented on the horizontal axis, we indicate the possible recurrences opposite the corresponding value of  $\nu$  on the vertical axis. If  $C_{T_o}$  is a prime number, all possible values of  $D_{T_o}$  are represented. Otherwise, the only values of  $D_{T_o}$  represented are those such that the numbers  $C_{T_o}$  and  $|D_{T_o}|$  are coprime, i.e., they have no common factors. In its relationship with the prime numbers, this diagram is reminiscent of the sieve of Eratosthenes.<sup>1</sup> Figure 11.1 exemplifies<sup>2</sup> for  $C_{T_o} < 38$ .

If we stack up all these modules for different successive values of  $\nu_o$ , we obtain the recurrence diagram. We replace the scale linear in  $\nu$  by a scale linear in altitude.<sup>3</sup>

### 11.2.3 Recurrence Diagram

The recurrence diagram is designed as an aid to visualising the altitudes leading to different recurrence situations. It is basically a graph in which the altitudes, from lowest to highest, are marked on the ordinate axis and the recurrence cycles (in days) on the abscissa.

<sup>1</sup>*Eratosthenes of Cyrene* (284–192 BC), ὁ Ἐρατοσθένης, οὐς, was a Greek astronomer, mathematician, and geographer. He discovered a systematic method for obtaining the sequence of prime numbers up to any desired value. One writes down the sequence of positive integers, then crosses out the multiples of 2, of 3, of 5, and so on. This method, which sifts the positive integers, keeping only the primes, is known as the sieve of Eratosthenes. His abilities as an astronomer and geographer are revealed by a scientific and relatively accurate measurement of the Earth's radius, in which he measured the shadow cast by a column in Alexandria at noon on a day when he knew that the Sun's rays reached the bottom of the wells in ancient Syene (Assouan), the day of the summer solstice at Syene, under the Tropic of Cancer. He determined the obliquity of the ecliptic and estimated at  $47^\circ 42'$  the arc of the meridian between the two tropics.

<sup>2</sup>Such a graph can also be interpreted by identifying the values of  $D_{T_o}$ . Taking for example  $D_{T_o} = \pm 7$ , this value appears for all values of  $C_{T_o}$  greater than  $2 \times |D_{T_o}| = 14$ , except for  $C_{T_o} = 21, 28, 35$ , etc., that is, multiples of 7.

<sup>3</sup>It is only when we change from  $\nu$  to  $a$  or  $h$  that the type of orbit (inclination, Sun-synchronous or otherwise) becomes relevant. The recurrence module is established without referring to any particular type of satellite and is even independent of the notion of satellite! The only condition is that the phenomenon under consideration should occur uniformly in time.

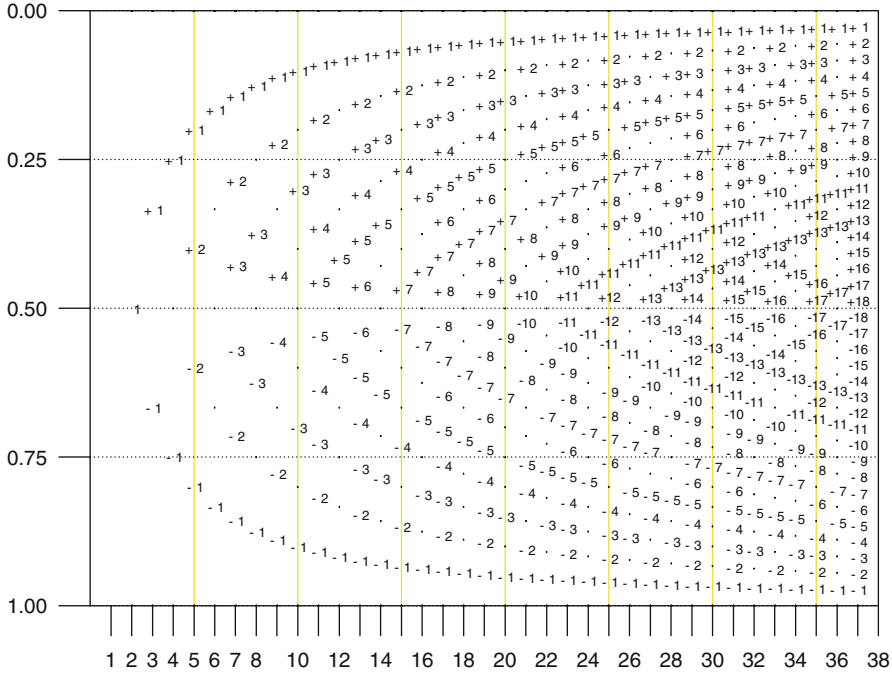


FIG. 11.1 : *Recurrence module*. Vertical axis: *daily frequency (rev/day)*, lying between two integer values  $\nu_o$  and  $\nu_o + 1$ . Horizontal axis: *recurrence cycle (day)*.

For each value of  $\nu_o$ , and for each cycle  $C_{T_o}$ , the quantity  $D_{T_o}$  is varied over its range of possible values and  $\nu$  is obtained from (11.15). This in turn gives the mean motion  $n$  and draconitic period  $T = T_d$ . We thus obtain the altitude and inclination, calculating  $a$  and  $i$  by an iterative method, as in Example 7.3, or Examples 11.1 and 11.2 below.

The value obtained is then marked on the diagram. In Fig. 11.2, these values are marked by small squares. When the value of  $D_{T_o}$  is absent, replaced by a dot, this means that there is strictly speaking no recurrence. In Figs. 11.3, 11.4, and 11.5, the value of  $D_{T_o}$  has been noted explicitly in each case.

The diagram gives an overview of the possibilities for recurrence. For short cycles, we see that these possibilities are limited to a handful of values. Between 450 and 1,000 km, there is only one possible altitude for a 2 day recurrence cycle ( $h = 720$  km for Oceansat-2) and only three possible altitudes for a 3 day cycle. On the other hand, for long cycles, there are more opportunities, especially if  $C_{T_o}$  is a prime number. For  $C_{T_o} = 31$ , there are about 120 possibilities between 0 and 1,200 km, or roughly one available altitude for recurrence every 10 km.

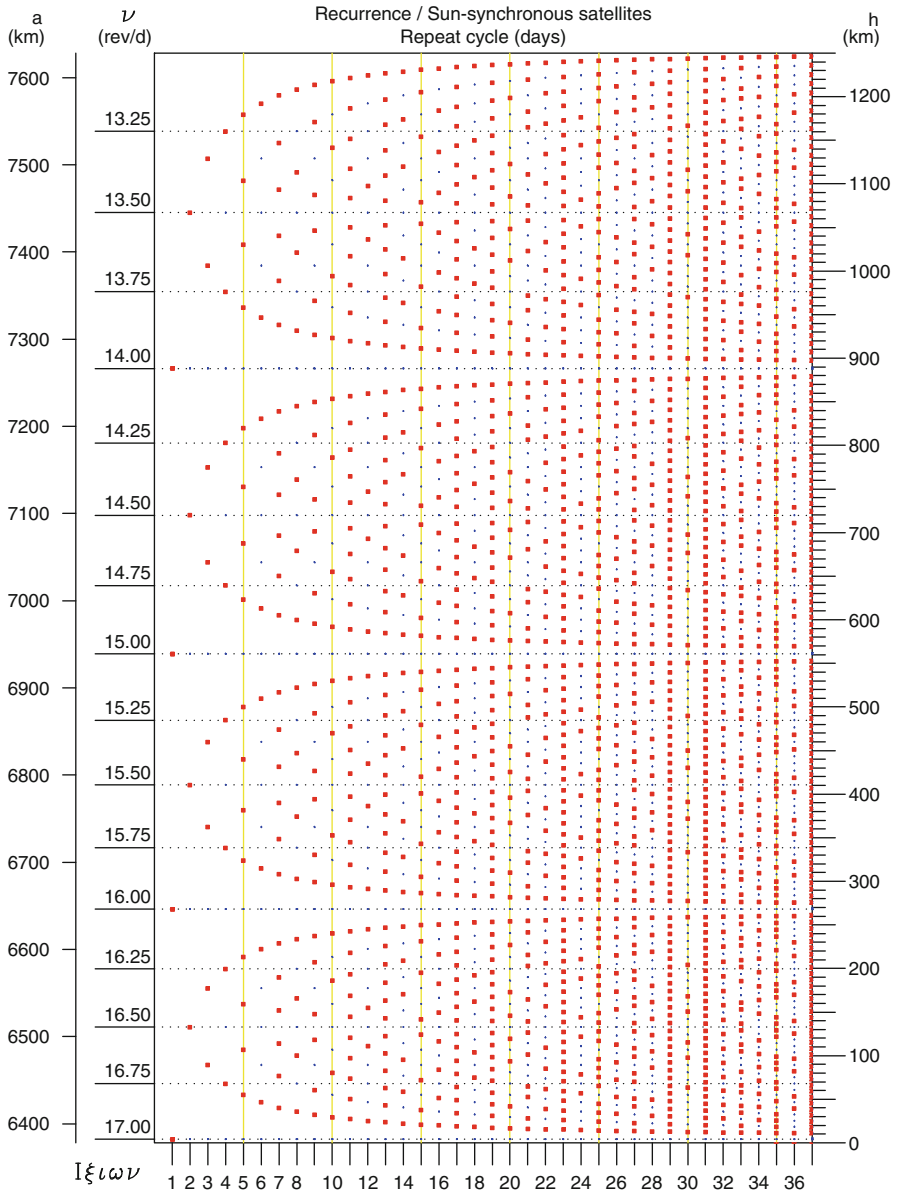


FIG. 11.2 : Recurrence diagram for Sun-synchronous satellites. For altitudes between 0 and 1,250 km, small squares indicate those values of the altitude  $h$  (km) and the semi-major axis  $a$  (km) for which recurrence is possible. Horizontal axis: recurrence cycle (days). Vertical axis: daily frequency  $\nu$  (rev/day).

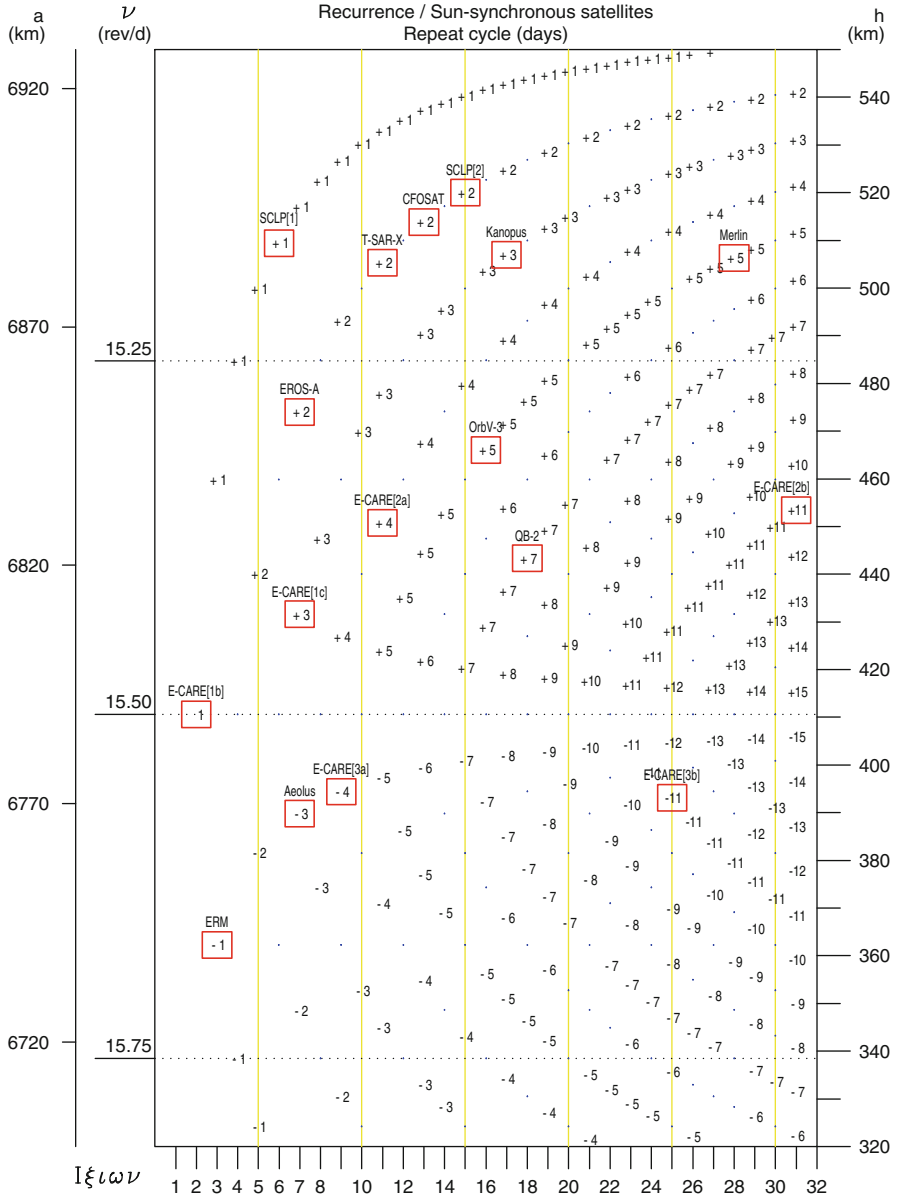


FIG. 11.3 : Recurrence diagram for Sun-synchronous satellites. For altitudes between 320 and 540 km, possible recurrences are indicated by specifying  $D_{T_o}$ . Boxed values correspond to satellites appearing in Tables 11.1 and 11.3. For example, for TerraSAR-X, we have the triple  $[15, +2, 11]$ , whence  $\nu_o = 15$  (the integer closest to  $\nu$ , as ordinate),  $D_{T_o} = +2$  (indicated on the diagram), and  $C_{T_o} = 11$  (abscissa), 11 day cycle.

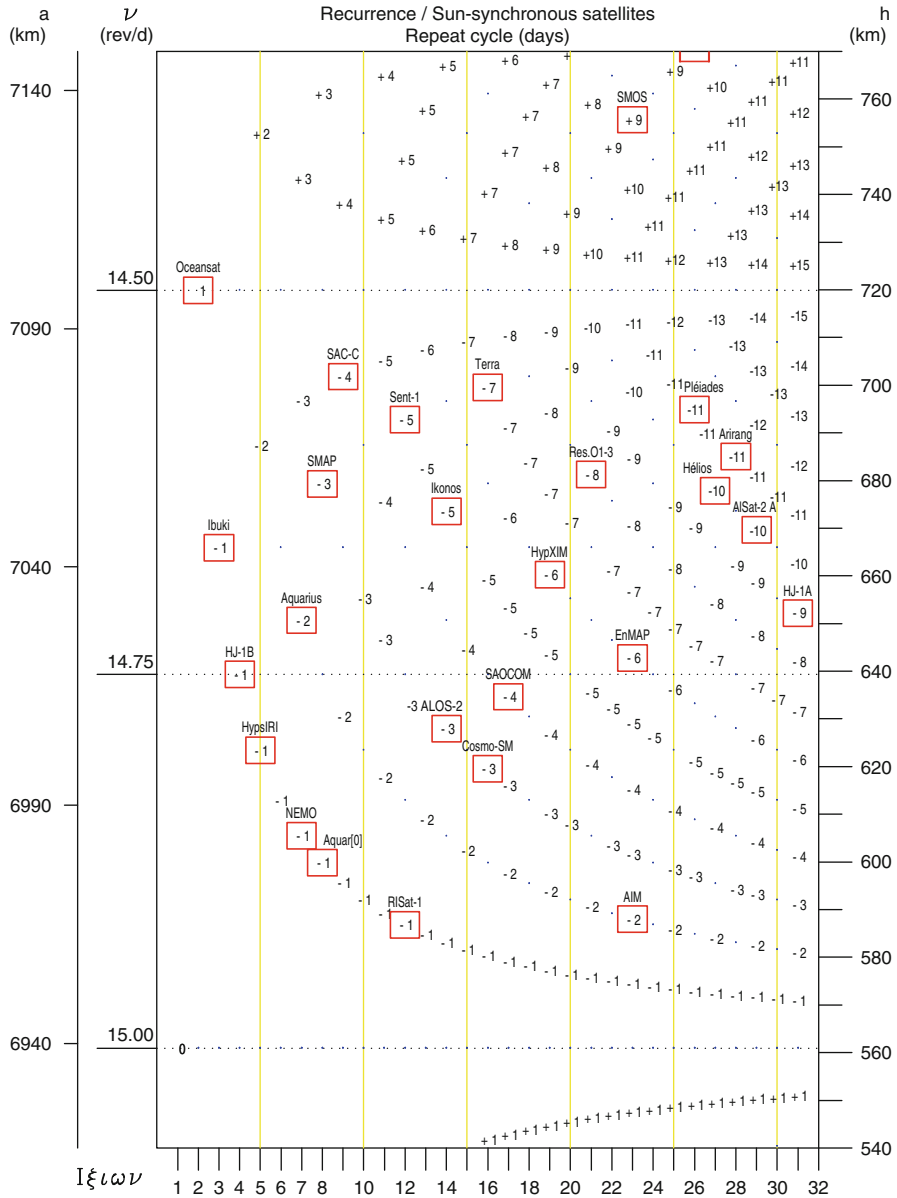


FIG. 11.4: Recurrence diagram for Sun-synchronous satellites. For altitudes between 540 and 760 km, possible recurrences are indicated by specifying  $D_{T_0}$ . Boxed values correspond to satellites appearing in Tables 11.1 and 11.3. For example, for Terra, we have the triple  $[15, -7, 16]$ , whence  $\nu_0 = 15$  (the integer closest to  $\nu$ , as ordinate),  $D_{T_0} = -7$  (indicated on the diagram), and  $C_{T_0} = 16$  (abscissa), 16 day cycle.

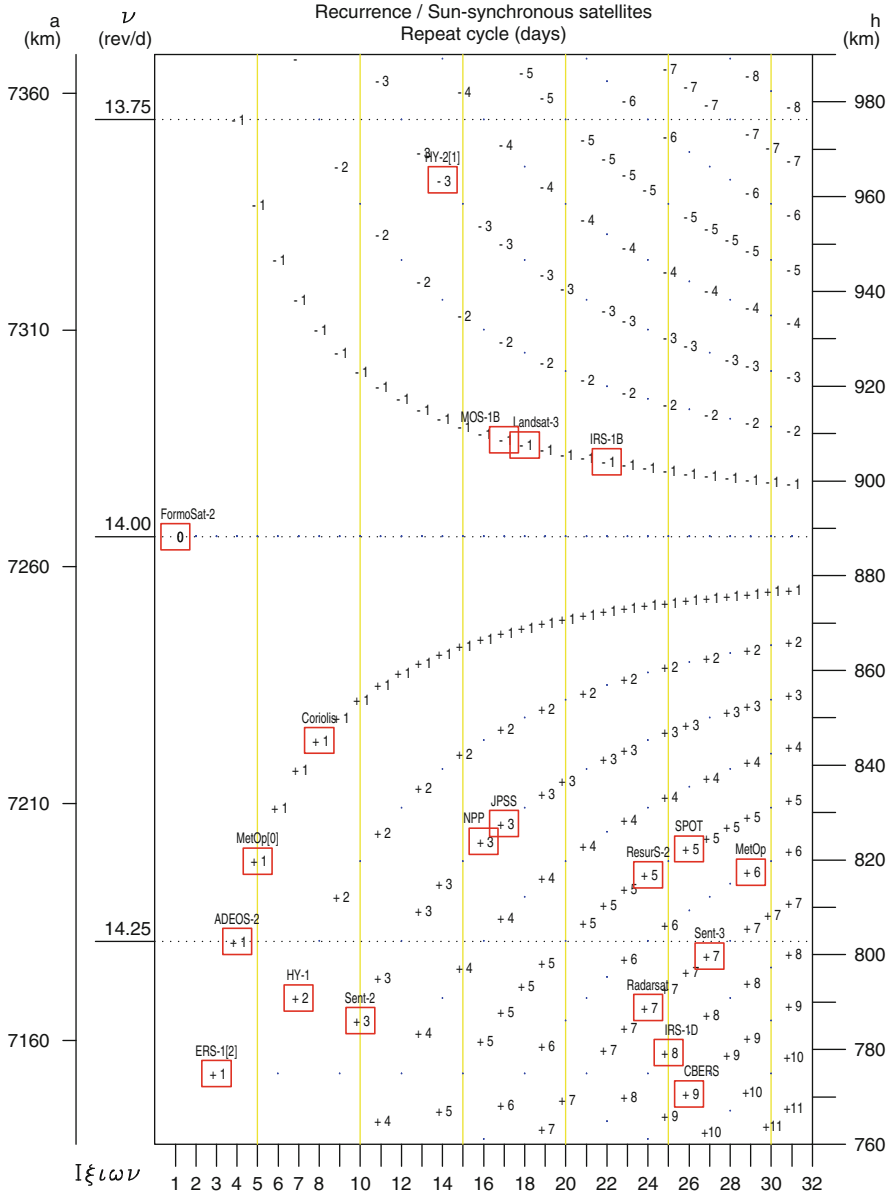


FIG. 11.5 : Recurrence diagram for Sun-synchronous satellites. For altitudes between 760 and 980 km, possible recurrences are indicated by specifying  $D_{T_0}$ . Boxed values correspond to satellites appearing in Tables 11.1 and 11.3. For example, for MetOp-A and -B, we have the triple  $[14, +6, 29]$ , whence  $\nu_0 = 14$  (the integer closest to  $\nu$ , as ordinate),  $D_{T_0} = +6$  (indicated on the diagram), and  $C_{T_0} = 29$  (abscissa), 29 day cycle.

### 11.2.4 Recurrence Defined by the Recurrence Triple

Recurrent Sun-synchronous satellites are defined by the recurrence triple. All Sun-synchronous satellites with the same recurrence triple have the same period, and hence the same values of  $a$  and  $i$ . (They even share the same value of  $e$ , because the orbit is frozen, as we shall see at the end of the chapter.) The recurrence triple thus defines the orbit. We may speak of the SPOT orbit for all satellites having the same recurrence triple as SPOT-1.

Table 11.1 provides an exhaustive list of the recurrence triples of all recurrent Sun-synchronous satellites to our knowledge:

- satellites whose mission has now ended, like Landsat-3,
- satellites still in activity, like Terra,
- satellite projects, like the Sentinel missions,
- satellites belonging to projects that have now been abandoned, like ERM.

Numbers in square brackets, e.g., [1], [2], indicate that the recurrence changes during the mission, while [0] indicates that recurrence was planned but abandoned before launch. For EarthCARE, in Table 11.3 we give all the planned recurrence cycles, which changed over time as the launch date was pushed back.<sup>4</sup>

Figures 11.3, 11.4, and 11.5 show the recurrence diagram over a limited range of altitudes ( $h$  between 320 and 990 km) and cycles ( $C_{T_o}$  from 1 to 31 days). Recurrence possibilities are indicated in each case with  $D_{T_o}$ ,  $C_{T_o}$ , and  $\nu_o$ , deduced from  $\nu$ . Values in use by satellites in Tables 11.1, 11.2, and 11.3 are boxed.

Note that the draconitic period is given in minutes by

$$T_d \text{ (min)} = 1440 \frac{C_{T_o}}{N_{T_o}}, \quad (11.16)$$

which is the adaptation of (11.14) to Sun-synchronous satellites. When the orbit of a Sun-synchronous satellite is defined by its recurrence cycle  $C_{T_o}$  and its approximate altitude, one must determine the recurrence triple, then return to the previous case. The altitude can be used to obtain  $\nu$ , which gives  $\nu_o$ . Once the cycle  $C_{T_o}$  is known, one can deduce  $N_{T_o}$  using an iterative method, then obtain  $D_{T_o}$ .

**Example 11.1** Calculate the characteristics of the SPOT orbit.

---

<sup>4</sup>The European mission ERM (Earth Radiation Mission) was supposed to come into operation around 2006, during a minimum of solar activity, thus allowing a very low altitude orbit. Following an agreement between the ESA and JAXA, ERM was merged with the Japanese project ATMOS-B1 to give EarthCARE. The launch date was postponed and the altitude increased, following the heightened solar activity which reached the culmination of its 11 year cycle in 2012. When the launch date was planned after the solar maximum, a lower altitude was chosen.

Sun-syn sat.	$\nu_0$	$D_{T_0}$	$C_{T_0}$	$N_{T_0}$	$T_d$	$a$	$h$	$i_{HS}$
Landsat-3	14	-1	18	251	103.27	7,285.799	908	99.09
Terra	15	-7	16	233	98.88	7,077.738	700	98.21
OrbView-3	15	+5	16	245	94.04	6,844.207	466	97.30
Ikonos-2	15	-5	14	205	98.34	7,051.765	674	98.11
QuickBird-2	15	+7	18	277	93.57	6,821.490	443	97.21
Coriolis	14	+1	8	113	101.89	7,223.450	845	98.82
AIM	15	-2	23	343	96.56	6,966.149	588	97.76
Aquarius [0]	15	-1	8	119	96.81	6,978.050	600	97.81
Aquar./SAC-D	15	-2	7	103	97.86	7,028.876	651	98.01
NEMO	15	-1	7	104	96.92	6,983.652	606	97.83
Suomi-NPP	14	+3	16	227	101.50	7,202.173	824	98.73
JPSS-1	14	+3	17	241	101.57	7,205.917	828	98.75
HypsIRI	15	-1	5	74	97.30	7,001.653	624	97.90
SCLP [1]	15	+1	6	91	94.95	6,888.104	510	97.46
SCLP [2]	15	+2	15	227	95.09	6,898.237	520	97.50
SMAP	15	-3	8	117	98.46	7,057.515	679	98.13
SPOT-5	14	+5	26	369	101.46	7,200.546	822	98.72
Hélios-2B	15	-10	27	395	98.43	7,056.025	678	98.12
Pléiades-1B	15	-11	26	379	98.79	7,073.059	695	98.19
Merlin	15	+5	28	425	94.87	6,884.494	506	97.45
e-Corce	15	-11	104	1,549	96.68	6,972.027	594	97.79
Envisat	14	+11	35	501	100.60	7,159.496	781	98.55
ERS-1 [2]	14	+1	3	43	100.46	7,153.138	775	98.52
ERS-1 [3]	14	+59	168	2,411	100.34	7,147.192	769	98.50
MetOp-B	14	+6	29	412	101.36	7,195.606	817	98.70
MetOp [0]	14	+1	5	71	101.41	7,197.940	820	98.71
TerraSAR-X	15	+2	11	167	94.85	6,883.512	505	97.45
COSMO-SkyM	15	-3	16	237	97.22	6,997.705	620	97.89
ADM-Aeolus	16	-3	7	109	92.48	6,767.956	390	97.02
EnMAP	15	-6	23	339	97.70	7,020.958	643	97.98
Sentinel-1	15	-5	12	175	98.74	7,070.980	693	98.18
Sentinel-2	14	+3	10	143	100.70	7,164.272	786	98.57
Sentinel-3	14	+7	27	385	100.99	7,177.940	800	98.63
HypXIM	15	-6	19	279	98.06	7,038.490	660	98.05
Z-Earth	15	+39	274	4,149	95.10	6,895.497	517	97.49
MOS-1B	14	-1	17	237	103.29	7,286.941	909	99.10
JERS-1	15	-1	44	659	96.15	6,946.179	568	97.69
ADEOS-1	14	+11	41	585	100.92	7,174.906	797	98.61
ADEOS-2	14	+1	4	57	101.05	7,181.058	803	98.64
ALOS	15	-19	46	671	98.66	7,069.809	692	98.18
ALOS-2	15	-3	14	207	97.39	7,006.172	628	97.92
Ibuki (GOSat)	15	-1	3	44	98.18	7,044.114	666	98.07



Sun-syn sat.	$\nu_o$	$D_{T_o}$	$C_{T_o}$	$N_{T_o}$	$T_d$	$a$	$h$	$i_{HS}$
IRS-1B	14	-1	22	307	103.19	7,282.277	904	99.08
IRS-1D	14	+8	25	358	100.56	7,157.585	779	98.54
Resourcesat-2	14	+5	24	341	101.35	7,195.119	817	98.70
Oceansat-2	14	+1	2	29	99.31	7,098.105	720	98.29
RISat-1 [1]	15	-1	12	179	96.54	6,965.021	587	97.76
RISat-1 [2]	15	-18	119	1,767	96.98	6,986.291	608	97.84
Cartosat-1	15	-21	116	1,719	97.17	6,995.667	618	97.88
Cartosat-2 [1]	15	-1	4	59	97.63	7,017.502	639	97.97
Cartosat-2 [2]	15	-69	310	4,581	97.45	7,008.799	631	97.93
CBERS-2B	14	+9	26	373	100.38	7,148.868	771	98.50
HY-1	14	+2	7	100	100.80	7,169.058	790	98.59
HY-2 [1]	14	-3	14	193	104.46	7,341.734	964	99.34
HY-2 [2]	14	-37	168	2,315	104.50	7,343.852	966	99.35
HJ-1A	15	-9	31	456	97.89	7,030.346	652	98.02
HJ-1B	15	-1	4	59	97.63	7,017.501	639	97.96
CFOSAT	15	+2	13	197	95.03	6,891.997	514	97.48
Resurs-O1-3	15	-8	21	307	98.50	7,059.437	681	98.14
Kanopus-V-1	15	+3	17	258	94.88	6,885.131	507	97.45
Radarsat-2	14	+7	24	343	100.76	7,167.064	789	98.58
SAC-C	15	-4	9	131	98.93	7,079.991	702	98.22
SAOCOM-1A	15	-4	17	251	97.53	7,012.831	635	97.95
Arirang-1	15	-11	28	409	98.58	7,063.280	685	98.15
EROS-A1	15	+2	7	107	94.21	6,852.218	474	97.33
FormoSat-2	14	0	1	14	102.74	7,266.473	888	99.00
AlSat-2A	15	-10	29	425	98.26	7,047.805	670	98.09

TABLE 11.1 : *Orbital characteristics of Sun-synchronous satellites obtained from the recurrence triple  $[\nu_o, D_{T_o}, C_{T_o}]$ , where  $\nu_o$  is the whole number closest to the number of revolutions per day,  $D_{T_o}$  is the whole number equal to  $N_{T_o} - \nu_o C_{T_o}$ ,  $C_{T_o}$  is the recurrence cycle (whole number of days), and  $N_{T_o}$  is the number of revolutions per cycle. The numbers in the triple give the draconitic period  $T_d$  (min) and hence the orbital characteristics: the semi-major axis  $a$  (km), the altitude  $h$  (km) obtained from  $h = a - R$ , and the Sun-synchronous inclination  $i_{HS}$  (deg). The satellites are grouped by nationality in the following order: USA, France and Europe, Japan, India, China, then other. Within each category, they are classified in chronological order.*

► Concerning the orbit of the SPOT satellites, the recurrence triple is [14, 5, 26]. We observe that 5 and 26 are coprime and that 5 is less than 13. For strict recurrence, the draconitic period is held at its exact value given by

$$T_d = 1440 \frac{26}{369} = 101.463 \text{ min.}$$

Type	Satellite on same type of orbit
Landsat-3	Landsat-1, -2
Terra	Landsat-4, -5, -7, -8, EO-1
( <i>Terra</i> →) A-Train	Aqua, Aura, CloudSat, Calipso, Parosol
( <i>Terra</i> →) A-Train	GCOM-W1 (Shizuku), OCO-2
SPOT-5	SPOT-1, -2, -3, -4, THEOS
Pléiades-1B	Pléiades-1A, SPOT-6
Hélios-2B	Hélios-1A, -1B, -2A
Envisat	ERS-1 [1], ERS-2
MetOp-B	MetOp-A
COSMO-SkyMed	HCMM, TerraSAR-L, HypSEO
ADEOS-2	QuikScat
GOSat	EGPM
IRS-1B	IRS-1A
Resourcesat-2	IRS-1C, -P2, -P3, -P6 (Resourcesat-1)
Oceansat-2	Oceansat-1, VEN $\mu$ S
CBERS-2B	CBERS-1, -2

TABLE 11.2 : *Satellites on the same type of orbit as a satellite in Table 11.1.*

Sun-syn sat.	$\nu_o$	$D_{T_o}$	$C_{T_o}$	$N_{T_o}$	$T_d$	$a$	$h$	$i_{HS}$
ERM	16	-1	3	47	91.91	6,740.439	362	96.92
EarthCARE [1a]	16	-4	9	140	92.57	6,772.570	394	97.03
EarthCARE [1b]	15	+1	2	31	92.90	6,788.779	411	97.09
EarthCARE [1c]	15	+3	7	108	92.90	6,809.760	432	97.17
EarthCARE [2a]	15	+4	11	169	93.73	6,828.978	451	97.24
EarthCARE [2b]	15	+11	31	476	93.78	6,831.592	453	97.25
EarthCARE [3a]	16	-4	9	140	92.57	6,772.570	394	97.03
EarthCARE [3b]	16	-11	25	389	92.54	6,771.276	393	97.03

TABLE 11.3 : *As for Table 11.1, but for the project ERM, which became EarthCARE. The altitude increases, then decreases again, depending on the planned launch date (pushed back several times). Possible altitudes depend on the 11 year solar cycle (see Example 11.14).*

To begin with, following the same lines as in Example 7.3, we set  $T_0 = T_d$ , which gives the corresponding Keplerian values:

$$a_0 = 7,206.1 \text{ km} , \quad i_0 = i_{HS} = 98.7^\circ .$$

Using  $a_0$  and  $i_0$ , we then calculate the relative values of the secular variations:

$$\frac{\Delta n}{n_0} = -0.593 \times 10^{-3} , \quad \frac{\dot{\omega}}{n_0} = -0.564 \times 10^{-3} ,$$

which yields a new value  $a_1$  for the semi-major axis:

$$\frac{\Delta a}{a_0} = -\frac{2}{3}1.157 \times 10^{-3}, \quad \Delta a = -5.6 \text{ km},$$

$$a_1 = a_0 + \Delta a = 7,200.5 \text{ km}.$$

The iterative calculation (one step is actually enough) delivers the semi-major axis and the inclination as

$$a = 7,200.546 \text{ km}, \quad i = i_{\text{HS}} = 98.723^\circ.$$

Values given in the CNES documentation concerning SPOT are

$$a = 7,200.547 \text{ km}, \quad i = i_{\text{HS}} = 98.723^\circ,$$

implying an altitude  $h = a - R = 822 \text{ km}$ .

If the secular variations are calculated with the expansion cut off at the term in  $J_2$ , this yields the following values after iteration:

$$a' = 7,200.537 \text{ km}, \quad i = i_{\text{HS}} = 98.70^\circ.$$

Comparing the various values found for the semi-major axis, we thus observe that:

- The term  $a_0 = 7,206.1 \text{ km}$  is obtained from the central term of the Newtonian acceleration (degree 0 of the potential).
- The difference  $|a' - a_0| = 5.6 \text{ km}$  arises from the term of degree 2 (the  $J_2$  term) in the geopotential.
- The difference  $|a - a'| = 10 \text{ m}$  arises from the terms of degree 4 (the  $J_2^2$  and  $J_4$  terms) and higher order in the geopotential.

Concerning the relative orders of magnitude of the values found for the semi-major axis, viz.,

$$|a - a_0| \sim 10^{-3}a_0, \quad |a - a'| \sim 10^{-3}|a - a_0|,$$

we obtain the same values as in Chap. 6 when comparing orders of magnitude of  $J_2$  and 1, then  $J_4$  and  $J_2$ .

These theoretical values can also be compared with the actual values as obtained from the NORAD elements. We select three dates, the first and second, in 2003, being separated by 26 days, and the third being 7 years later, in 2010:

SPOT 5

```
1 27421U 02021A 03040.18015505 .00000155 00000-0 93359-4 0 9661
2 27421 98.7244 116.8304 0000554 58.9354 301.1883 14.20029420 39902
```

SPOT 5

```
1 27421U 02021A 03066.18009415 .00000138 00000-0 85210-4 0 469
2 27421 98.7212 142.4627 0000619 93.4275 266.6981 14.20038040 43590
```

SPOT 5

```
1 27421U 02021A 10005.18145090 .00000277 00000-0 15077-3 0 7284
2 27421 98.7528 81.1934 0001110 114.9171 272.2592 14.20012166397832
```

The orbital elements thereby obtained are as follows:

- Date (1): 9 February 2003, revolution 3,990:  $a = 7,200.542$  km,  $e = 5.54 \times 10^{-5}$ ,  $i = 98.7244^\circ$ ,  $\omega = 58.9354^\circ$ ,  $\lambda_{AN} = 273.1277^\circ$ ,  $\tau_{AN} = 22:31:54$ .
- Date (2): 7 March 2003, revolution 4,359:  $a = 7,200.513$  km,  $e = 6.19 \times 10^{-5}$ ,  $i = 98.7212^\circ$ ,  $\omega = 93.4275^\circ$ ,  $\lambda_{AN} = 273.1552^\circ$ ,  $\tau_{AN} = 22:31:55$ .
- Date (3): 5 January 2010, revolution 39,783:  $a = 7,200.603$  km,  $e = 11.10 \times 10^{-5}$ ,  $i = 98.7528^\circ$ ,  $\omega = 114.9171^\circ$ ,  $\lambda_{AN} = 273.1249^\circ$ ,  $\tau_{AN} = 22:26:08$ .

**Date (1).** With 3,990 revolutions, the satellite completed 10 cycles of 26 days. It had been launched 281 days previously. The orbital parameters are “nominal”.

**Dates (1) and (2).** These dates are separated by a cycle of 369 revolutions, or 26 days. We note a discrepancy for  $\lambda_{AN}$  of  $0.0275^\circ$ , or 3.0 km, less than the tolerance of 5 km for recurrence. The elements  $a$  and  $i$  remain very close to the theoretical values. However,  $e$  is much lower than the value needed to freeze the orbit (see the end of the chapter). Consequently, there is a large variation in  $\omega$  around  $90^\circ$ . The crossing time  $\tau_{AN}$  is assured to within 2 min, which is well below the variations in solar time due to the equation of time.

**Dates (2) and (3).** Between these two dates, there were  $39783 - 4359 = 35424 = 96 \times 369$  revolutions, exactly 96 cycles of 26 days, or 2,496 days. ◀

**Example 11.2** Calculate the orbital characteristics of the Terra orbit.

► For the orbit of satellites in the Terra family (see Table 11.2), the recurrence triple is [15, -7, 16]. The draconitic period is maintained at

$$T_d = 1440 \frac{16}{233} = 98.884 \text{ (min)} .$$

As before, we obtain

$$a_0 = 7,083.4 \text{ km} , \quad i = i_{HS} = 98.2^\circ .$$

We then calculate the relative values of the secular variations:

$$\frac{\Delta n}{n_0} = -0.619 \times 10^{-3} , \quad \frac{\dot{\omega}}{n_0} = -0.591 \times 10^{-3} ,$$

which gives the new value of the semi-major axis as  $a_1 = 7,077.7$  km. By iteration,

$$a = 7,077.738 \text{ km}, \quad i = i_{\text{HS}} = 98.211^\circ.$$

We have seen that, although the value of  $a$  can be accurately determined, the same cannot be said of the altitude, which varies due to the ellipticity of the orbit and the Earth. (We return to this question at the end of the chapter.) If we define the altitude  $h$  as the difference between  $a$  and the equatorial radius  $R$ , the value of  $h$  is well determined. In the case of Terra, we obtain  $h = 700$  km. The NASA documentation gives the value  $h = 705$  km for all satellites in the Terra orbit, the altitude having been determined slightly differently. ◀

**Example 11.3** Calculate the orbital characteristics of the satellite ERS-1, which has had three different recurrence cycles: 35 days, 3 days, and 168 days.

► The ESA satellite ERS-1 was launched on 17 July 1991. It flies at an altitude of about 780 km and its orbit is Sun-synchronous. It initially had a recurrence cycle of 35 days. From 20 December 1993, a slight change of orbit brought the cycle to 3 days, better suited to the study of ice flows during the arctic winter, according to the mission controllers. A further maneuver brought the cycle to 168 days so that it could carry out geodetic observations. The satellite ERS-2, launched on 21 April 1995, carried out a mission in tandem with ERS-1 until 10 March 2000.

We now calculate the triples for each recurrence cycle:

- *Recurrence cycle 1.* 35 day cycle over 501 revolutions:

$$\nu_1 = \frac{501}{35} = 14 + \frac{11}{35} \implies \text{recurrence triple } [14, 11, 35].$$

- *Recurrence cycle 2.* 3 day cycle over 43 revolutions:

$$\nu_2 = \frac{43}{3} = 14 + \frac{1}{3} \implies \text{recurrence triple } [14, 1, 3].$$

- *Recurrence cycle 3.* 168 day cycle over 2,411 revolutions:

$$\nu_3 = \frac{2411}{168} = 14 + \frac{59}{168} \implies \text{recurrence triple } [14, 59, 168].$$

From  $T_d$ , we calculate  $a$  and  $i$  by the above method. The results are given in Table 11.1: ERS-1 recurrence cycle 1 as Envisat, ERS-1 recurrence cycles 2 and 3 as ERS-1 [2] and [3].

Cycle changes were brought about by going from  $\nu_1$  to  $\nu_2$  (obtained by reducing the altitude by 6.358 km), then from  $\nu_2$  to  $\nu_3$  (reducing the altitude by 5.948 km). Very small variations in altitude lead to totally different recurrence cycles, as can be seen very clearly from Fig. 11.2. These variations in altitude are small enough to make them easy to calculate (without carrying

out the above type of iteration), applying the relation for finite increments already used:

$$\frac{\Delta\nu}{\nu} = -\frac{3}{2} \frac{\Delta a}{a}.$$

Setting

$$a_{\text{rec } 1} = 7,159.496 \text{ km},$$

we obtain

$$\Delta\nu = \nu_2 - \nu_1 = \frac{1}{3} - \frac{11}{35}, \quad \frac{\Delta\nu}{\nu_1} = \frac{2}{3 \times 501},$$

$$\Delta a_{\text{rec } 1 \rightarrow \text{rec } 2} = -6.358 \text{ km}.$$

$$\Delta\nu = \nu_3 - \nu_2 = \frac{59}{168} - \frac{1}{3}, \quad \frac{\Delta\nu}{\nu_2} = \frac{3}{56 \times 43},$$

$$\Delta a_{\text{rec } 2 \rightarrow \text{rec } 3} = -5.946 \text{ km}.$$

Note that a recurrence condition based on such a long time scale as  $C_{T_o} = 168$  days is quite exceptional. Values of  $C_{T_o}$  do not generally exceed 45 days.

These three recurrence cycles are reconsidered in Example 11.16 to illustrate the notion of recurrence index. ◀

**Example 11.4** *Analysis of two images obtained by the satellite Envisat in terms of its recurrence cycle.*

► The first is the colour image of the Hawaiian islands shown in Fig. 11.6, a combination of radar images acquired by the ASRA instrument on three different dates:

Day	27 March 2006	↔	16 April 2007	↔	21 January 2008
MJD	53,821	↔	54,206	↔	54,486
Time elapsed	385		280		
Equal to	11 × 35		8 × 35		

The ground track of the satellite crosses exactly the same place. The time elapsed between these images is a multiple of 35 days, corresponding to Envisat's recurrence cycle  $C_T$ . This is easier to check by converting to modified Julian days (MJD) [see (7.67)].

The second is the image of the Yukon delta shown in Fig. 11.7, obtained by combining images in the visible taken by the MODIS instrument at three different dates separated by  $4 \times 35 = 140$  days and 35 days. ◀



FIG. 11.6 : Radar image of Hawaii taken by Envisat. This image, looking north, shows six of the eight main volcanic islands of Hawaii. On the large island, Mauna Kea is visible, the highest point (4,205 m), and further south, Mauna Loa (4,170 m), an active volcano under surveillance. Orbiting radars, like the Advanced Synthetic Aperture Radar instrument (ASAR) on board Envisat, can monitor small changes in land movements. Radar interferometry combines different radar images mathematically. Such images are acquired as close as possible to the same point in space but at different times, in order to build numerical models of land levels. Kilauea is another of the most active volcanoes on Earth, situated in the south of the island in the regions appearing in red and pink. This image was made by combining three shots of the same region acquired by Envisat's ASAR radar on 27 March 2006, 16 April 2007, and 21 January 2008, then associating a different colour code with each. The colours appearing on the combined image result from the changes occurring between the shots. The time elapsed between these shots is a multiple of 35 days, the recurrence cycle of the satellite, as explained in Example 11.4. Credit (image and caption): ESA.

### 11.2.5 One-Day Recurrence Cycle

For LEO satellites (at least, for those which observe the Earth), 1-day recurrence cycles are avoided. Indeed, if such a satellite views exactly the same regions every day, many other places must necessarily be missed out, unless the instruments have a very wide field of view. Those altitudes between 0 and 1,250 km giving a 1-day recurrence cycle appear in the recurrence diagram of



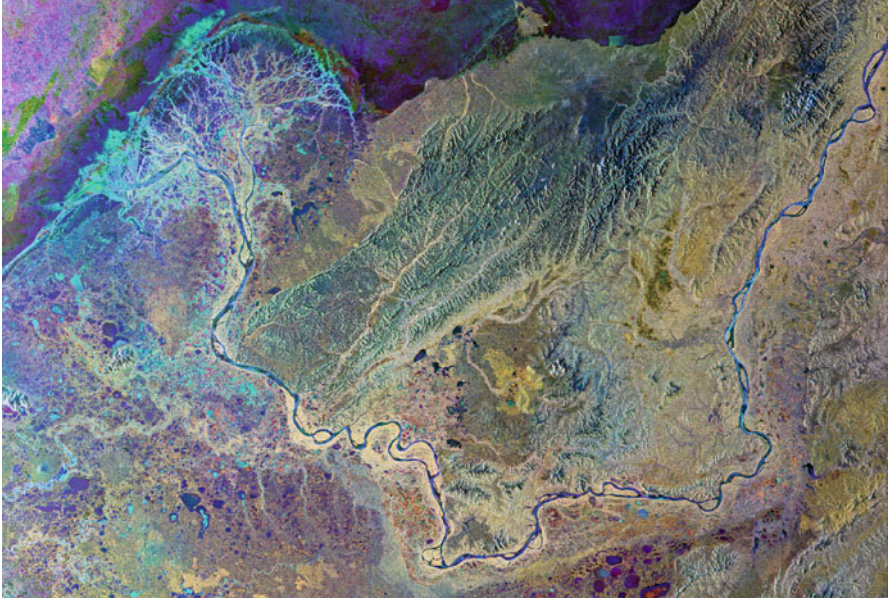


FIG. 11.7: Image of the Yukon delta taken by Envisat (MERIS instrument). This Envisat image features the Yukon delta in Alaska, where the Yukon River fans out into a labyrinth of distributaries, before emptying into the Bering Sea. This image was created by combining three Envisat images (19 November 2009, 8 April 2010, and 13 May 2010) over the same area. The time elapsed between these shots is a multiple of 35 days, the recurrence cycle of the satellite, as explained in Example 11.4. The Medium Resolution Imaging Spectrometer (MERIS) is a programmable, medium-spectral resolution, imaging spectrometer operating in the solar reflective spectral range. VIS-NIR: 15 bands selectable across range 390–1,040 nm. Spatial resolution: ocean  $1,040 \times 1,200$  m, land and coast  $260 \times 300$  m. Credit (image and caption): ESA.

Fig. 11.2 and are also indicated in Table 11.6. The corresponding recurrence triples are of the form  $[\nu_o, 0, 1]$ .

The only case of a Sun-synchronous LEO satellite with 1-day recurrence cycle is Taiwan's FormoSat-2 (launched under the name of Rocsat-2, Republic of China Satellite). The triple  $[14, 0, 1]$  induces a recurrence grid that has been put to very judicious use in connection with the geographic position of Taiwan. We shall return to this point regarding recurrence grids later.



Non-Sun-sync	$\nu_o$	$D_{T_o}$	$C_T$	$N_{T_o}$	$T_d$	$a$	$h$	$i$
Seasat	14	+8	25.07	358	100.85	7,173.367	795	108.00
Geosat [GM]	14	+1	3.01	43	100.76	7,169.140	791	108.10
★ Geosat	14	+6	17.05	244	100.62	7,162.520	784	108.00
★ T/P	13	-3	9.92	127	112.42	7,714.433	1,336	66.04
W-HM	14	-8	20.87	286	105.08	7,371.535	993	78.00
SWOT[1a]	14	-1	2.98	41	104.71	7,354.239	976	78.00
SWOT[1b]	14	-7	21.86	301	104.60	7,348.756	971	78.00
SWOT[2a]	14	+3	21.86	311	101.21	7,188.822	811	78.00
SWOT[2b]	14	+1	21.86	309	101.87	7,220.125	842	78.00
SWOT[2c]	14	-1	21.86	307	102.54	7,251.763	873	78.00
SWOT[2d]	14	-3	21.86	305	103.21	7,283.745	906	78.00
SWOT[2e]	14	-5	21.86	303	103.90	7,316.073	938	78.00
ICESat[c]	15	-1	7.99	119	96.68	6,971.522	593	94.00
ICESat	15	-22	182.75	2,723	96.65	6,970.030	592	94.00
ICESat-2	15	-12	90.88	1,353	96.72	6,973.663	596	94.00
CryoS[c]	14	+1	1.99	29	99.10	7,087.810	710	92.00
CryoSat-2	14	178	368.24	5,344	99.25	7,094.553	716	92.00
UoSAT-12	15	-3	6.92	102	97.73	7,026.467	648	64.50
CoRoT	14	-1	15.96	223	103.04	7,274.323	896	90.00
Megha-Trop.	14	-1	6.87	97	101.93	7,243.679	866	20.00
TRAQ	14	+1	2.96	43	99.17	7,098.043	720	57.00

TABLE 11.4 : *Recurrence triple*  $[\nu_o, D_{T_o}, C_{T_o}]$  and number of revolutions  $N_{T_o}$  per cycle for various non-Sun-synchronous satellites, giving the draconitic period  $T_d$  (min) and orbital characteristics: semi-major axis  $a$ , altitude  $h$  (km), and inclination  $i$  (deg). The cycle in days is  $C_T$  and  $C_{T_o}$  is obtained from (11.13) (it is usually the whole number closest to  $C_T$ ). ★ T/P is the common orbit of TOPEX/Poseidon, Jason-1, and Jason-2. ★ Geosat is the common orbit of Geosat [ERM] and GFO. W-HM: Water-HM. The recurrence cycle for the calibration orbit preceding the main mission is denoted by [c]. Satellites are grouped according to type of mission: oceanographic-altimetric, ice studies, other. Within each category, classification is by chronological order.

## 11.3 Recurrence for Non-Sun-Synchronous LEO Satellites

### 11.3.1 Obtaining the Recurrence Triple

For a non-Sun-synchronous satellite, recurrence is defined by the recurrence cycle  $C_{T_o}$ , in a whole number of days, differing here from the cycle  $C_T$ . To determine the recurrence triple, the altitude and inclination must also be known, with a certain interval of possible variation.

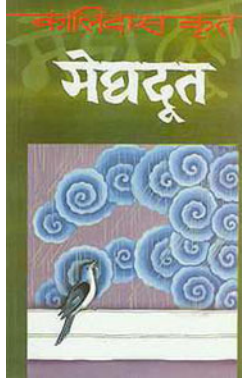


FIG. 11.8 : In Indian culture, the word megha is pregnant with meaning, being associated with a famous poem called Meghaduta, “the cloud messenger”. Its author Kalidasa lived in the north of India in the fifth century and is one of the most famous classical authors of Sanskrit literature. The hero of the poem is exiled for 1 year in the center of India. After 8 months of clear skies, he finally spots a cloud and asks it to carry a message to his wife, who remains at home in the foothills of the Himalayas. He tells the cloud of all the splendid sights awaiting it on the journey to the north. Already highly charged symbolically with the connotations of the word “cloud”, this particular cloud, the messenger, will announce the monsoon.

The daily recurrence frequency is given by (11.3), where  $\nu = \nu(a, i)$  and  $P = P(a, i)$ . We calculate the product  $\kappa C_{T_o}$ , allowing  $a$  and  $i$  to vary until we obtain a whole number, which then represents  $N_{T_o}$ . With this value, we obtain  $\nu_o$ , the integer closest to  $\kappa$ , and by  $N_{T_o} = \nu_o C_{T_o} + D_{T_o}$ , we obtain  $D_{T_o}$ . This gives the recurrence triple  $[\nu_o, D_{T_o}, C_{T_o}]$  and the value of  $C_T$ . Recall that  $C_T$  and  $C_{T_o}$  are given by (11.7) and (11.8).

Table 11.4 gives the main recurrent, non-Sun-synchronous satellites. These are mostly oceanographic satellites (altimetry) or projects to monitor ice cover in the polar regions. In the latter category, there are some very long recurrence cycles, e.g., 183 days for ICESat. This satellite carries just one instrument, a laser altimeter. The cycle guarantees that the satellite will not repeat its ground track before half a year has gone by.

The table also shows future satellites, such as SWOT, or abandoned projects like WatER-HM or TRAQ.

#### Example 11.5 Choice of orbit for Megha-Tropiques.

► In 1994, in order to study meteorological phenomena in the intertropical region, a group of researchers mainly associated with the *Laboratoire de météorologie dynamique* (LMD) of the French national research organisation (CNRS) had the idea of a satellite to be called Tropiques that would follow a circular orbit at a rather high altitude ( $h \sim 1,000$  km) and low inclination ( $i \approx 15^\circ$ ). For economic and political reasons, a collaboration with India trans-

$a$	$P$	$\nu$	$\kappa$	$\kappa C_{T_o}$
7,700.000	-2.1207	12.84404	12.73522	127.3522
7,710.000	-2.1111	12.81908	12.71080	127.1080
7,720.000	-2.1016	12.79419	12.68646	126.8646
7,714.433	-2.1069	12.80803	12.70000	127.0000

TABLE 11.5: *Recurrence triple of TOPEX/Poseidon. Determination of the semi-major axis  $a$ , in km, in terms of the recurrence parameters  $P$ ,  $\nu$ ,  $\kappa$ , and  $C_{T_o}$  (dimensionless).*

$\kappa$	$i = 20$	$i = 65$	$i = 110$	$i = i_{HS}$	$i_{HS}$
	$h$	$h$	$h$	$h$	
16	176.4	214.9	294.6	268.1	96.6
15	478.6	511.6	583.1	561.0	97.7
14	814.4	842.5	906.1	888.3	99.0
13	1,191.1	1,214.5	1,270.6	1,257.1	100.7

TABLE 11.6: *Orbital and recurrence characteristics for satellites with a 1-day recurrence cycle. Non-Sun-synchronous satellites with three different inclinations and result for Sun-synchronous satellites. Altitudes  $h$  are in km and angles  $i$  in degrees. The orbital frequency  $\kappa$  (equal to  $\nu_o$  here) is in rev/day.*

formed this French project into a joint Indian–French venture (ISRO-CNES), and it was renamed Megha-Tropiques, the Sanskrit word *megha* meaning “cloud” (see Fig. 11.8). The inclination of the orbit was changed to  $20^\circ$  so that the Himalayas would be correctly viewed, and the altitude was reduced for technical reasons related to the new instruments it would carry. This choice of altitude, fixed at 817 km, put the satellite at less than 3 km from the altitude for a 1-day recurrence satellite (see Table 11.6). To avoid this situation, which would be unsuitable even for a meteorological satellite, it was decided to impose a 7 day recurrence cycle, to take it away from the altitude range to be avoided. Figure 11.9 (lower) clearly shows the situation here. There were two possibilities:

- the triple  $[14, +1, 7]$ ,  $N_{T_o} = 99$ , with  $h = 764$  km,
- the triple  $[14, -1, 7]$ ,  $N_{T_o} = 97$ , with  $h = 866$  km.

After weighing up the options, the higher altitude was chosen to obtain better sampling. With the triple  $[14, -1, 7]$ , calculation gives  $a = 7,243.700$  km and  $C_T = 6.87$  days (see Table 11.4). ◀

**Example 11.6** *Calculate the recurrence triple and exact altitude for the satellite TOPEX/Poseidon, which has a 10 day cycle and inclination  $i = 66.04^\circ$ . Its altitude is around 1,335 km.*

► The French–US satellite TOPEX/Poseidon comprises the US platform TOPEX (Topography Experiment for Ocean Circulation) and the French altimetric instrument Poseidon, equipped with the DORIS system (*Détermination d’Orbite et Radiopositionnement Intégrés par Satellite*). Poseidon is used to calculate the orbit to within a radial accuracy of 2 cm, whence the mean altitude of the oceans can be measured to the same accuracy. The TOPEX/Poseidon experiment is being continued by Jason-1 then Jason-2, which use exactly the same orbit (the shift in the ground track is discussed below).

To obtain the recurrence characteristics, treating the inclination as fixed at  $i = i_0 = 66.040^\circ$ , we vary  $a$  between 7,700 and 7,720 km (see Table 11.5). By interpolation, we seek the value of  $a$  leading to the integer value  $\kappa C_{T_0} = 127$ . With a further iteration, we obtain the result

$$a = 7,714.433 \text{ km} , \quad i = 66.040^\circ .$$

We calculate the period from these elements:

$$T = 1440 \frac{10}{127} \left( 1 + \frac{1-P}{N_{\text{yr}}} \right) = 1440 \frac{10}{127} \left( 1 + \frac{3.1069}{365.25} \right) = 112.4295 \text{ min} ,$$

$$T_d = 112.4295 \text{ min} , \quad T_a = 112.4184 \text{ min} .$$

The recurrence triple is

$$\kappa = \frac{127}{10} = 13 + \frac{-3}{10} \implies [13, -3, 10] .$$

The reference values communicated by TOPEX/Poseidon are

$$a = 7,714.429 \text{ km} , \quad i = 66.040^\circ .$$

Every 127 revolutions, the satellite repeats its ground track precisely. However, the time elapsed between two passages is not exactly 10 days, but 9.92 days. Indeed,

$$C_T = \frac{127}{\nu} = \frac{127}{12.8080} = 9.9156 \text{ d} = 9 \text{ d } 21 \text{ h } 58 \text{ m } 27 \text{ s} .$$

In 10 days, the satellite thus gains  $2 \text{ h } 01 \text{ m } 33 \text{ s} = 2.043 \text{ h}$  on its local crossing time. After 117.45 days, it has gained  $117.45 \times 0.2043 = 24.00$ , or one whole day, as we have seen in Example 10.1, where  $C_S = -117.45$  corresponds to the cycle relative to the Sun. The relation between  $C_{T_0}$  and  $C_T$  can be obtained directly from (11.10).

Let us now compare these theoretical values with those obtained using NORAD data:

TOPEX/Poseidon

```
1 22076U 92052A 93190.75462958 0.00000008 00000+0 00000-4 0 2807
2 22076 66.0427 282.2676 0008056 266.3864 93.6223 12.80931157 42638
```

## JASON-1

1	26997U	01055A	03288.89652066	-.00000061	00000-0	00000-0	0	1739
2	26997	66.0429	52.6556	0007659	261.4013	98.6134	12.80929092	86743

## JASON-2 (OSTM)

1	33105U	08032A	13157.85878517	-.00000037	00000-0	10349-3	0	6348
2	33105	66.0430	297.7584	0007941	272.1685	245.4026	12.80929165232145	

The corresponding values of the semi-major axis are:

- $a = 7,714.422$  km, for T/P, on 9 July 1993 at 18:06:38 UT.
- $a = 7,714.430$  km, for Jason-1, on 15 October 2003 at 21:30:57 UT.
- $a = 7,714.430$  km, for Jason-2, on 6 June 2013 at 19:47:25 UT.

These results show the very high degree of accuracy with which the satellites of this mission are kept at their station. ◀

### 11.3.2 Recurrence, Altitude, and Inclination

For a non-Sun-synchronous satellite, a given recurrence condition leaves a certain freedom to vary the altitude and inclination. For concreteness, consider a polar satellite, with  $i = 90^\circ$  and recurrence triple  $[14, -1, 17]$ . Calculations then give its altitude as  $h = 894.9$  km. With  $i = 80^\circ$ , the satellite must be brought down to an altitude  $h = 880.9$  km in order to obtain the same recurrence triple, whereas with  $i = 100^\circ$ , it must be moved up to an altitude  $h = 910.2$  km. We see that, in the neighbourhood of  $90^\circ$ , a change of one degree in the inclination implies a change of 1.5 km in the altitude, in order to maintain the same recurrence conditions.

For each triple, we can calculate the value of  $h$  as a function of  $i$ , while the inclination varies from  $0^\circ$  to  $180^\circ$ . The graphs  $h(i)$  are shown in Fig. 11.9 (upper), for all triples  $[14, \pm 1, C_{T_0}]$ , where  $C_{T_0}$  varies between 5 and 17, and also for the triple  $[14, 0, 1]$ . A more restricted range of variations is also shown in the lower part of Fig. 11.9 (lower).

Let us now consider a three-dimensional space with the angle of inclination  $i$  along the  $Ox$  axis, the recurrence cycle  $C_{T_0}$  along the  $Oy$  axis, and the altitude  $h$  along the  $Oz$  axis. We then plot the locus of points for which recurrence occurs. This produces a graph like the one sketched in Fig. 11.10. Examination of the space in the diagram shows that:

- The projection of the curves onto the plane  $xOz$  gives Fig. 11.9 (upper).
- The intersection of the curves with the plane  $yOz$ , for the Sun-synchronous inclination, gives Fig. 11.2 (or Figs. 11.3 or 11.4).

As for Sun-synchronous satellites, 1-day recurrence cycles are not generally favoured for non-Sun-synchronous satellites. The “avoided” altitudes are noted in Table 11.6 for various inclinations.

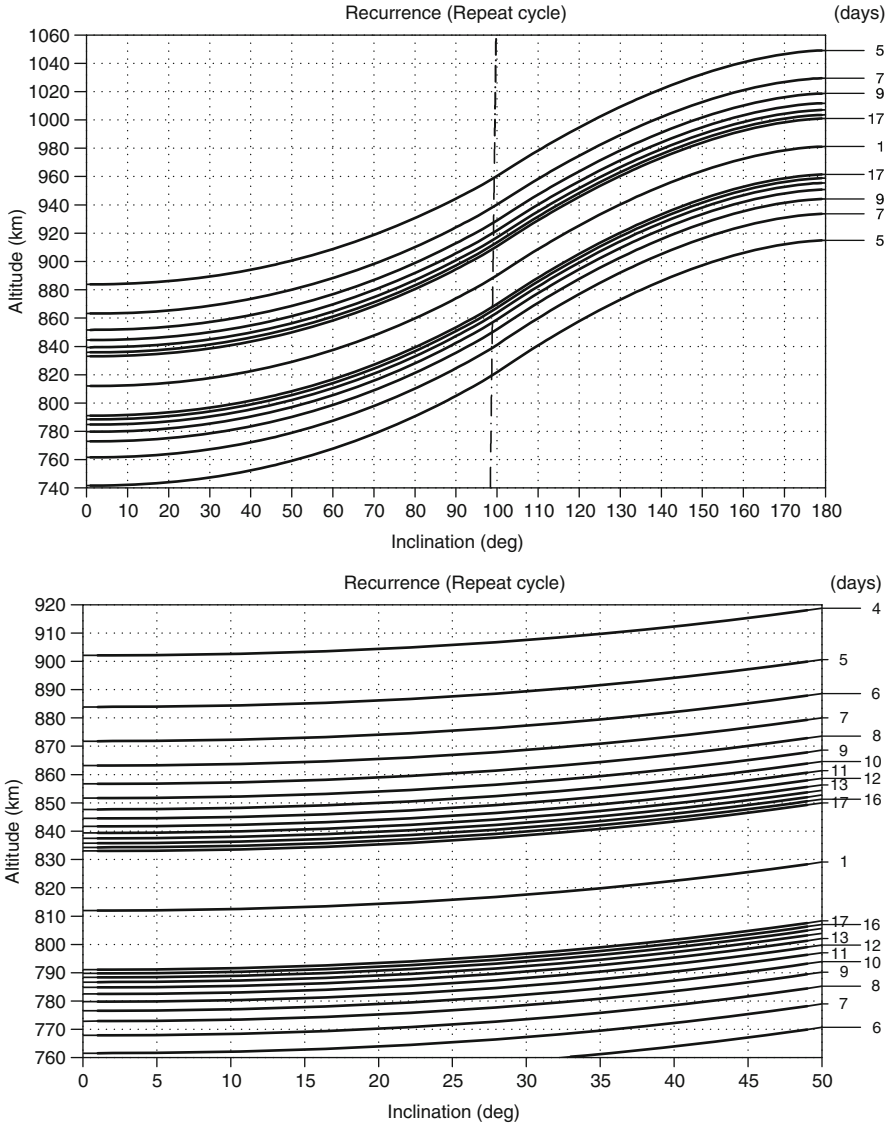


FIG. 11.9: Altitude as a function of inclination for a satellite holding the same recurrence. Upper: recurrence triples  $[14, \pm 1, C_{T_o}]$ , for  $C_{T_o}$  varying from 5 to 17 (in steps of 2) and  $[14, 0, 1]$ . Values corresponding to  $D_{T_o} = -1$  are above the median, representing  $[14, 0, 1]$ , while those corresponding to  $D_{T_o} = +1$  are below it. The dashed line denotes the Sun-synchronous inclination as a function of altitude. Lower: detail from the upper diagram for a restricted range of inclinations, with  $C_{T_o}$  varying from 4 to 17.

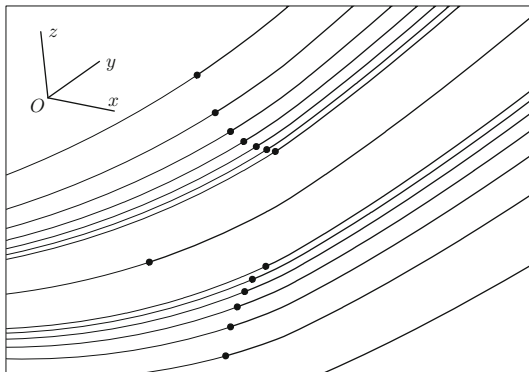


FIG. 11.10 : *Schematic view of the recurrence space. Locus of points at which recurrence occurs. Quantities along axes:  $Ox$  for the inclination  $i$ ,  $Oy$  for the recurrence cycle  $C_{T_0}$ , and  $Oz$  for the altitude  $h$ .*

## 11.4 Recurrence for MEO and HEO Satellites

The possible problems of 1-day recurrence cycles arising for LEO satellites are quite irrelevant for MEO and HEO satellites, for which this type of recurrence is often desirable.

GPS navigation satellites have recurrence properties, as we shall see in Chap. 14. For the US Navstar/GPS system, the recurrence is based on 1 day (2 revolutions per day). For the satellites in the WEST constellation, it is also based on 1 day (3 revolutions per day) (see Table 11.8).

It is also extremely useful for HEO communications satellites to have 1-day recurrence cycles, so that they overfly ground stations (for transmission and reception) once or twice a day with the same viewing geometry, as exemplified by Molniya or Sirius (Tundra orbit). For these orbits, the apogee is fixed following the choice of the critical inclination. Table 11.7 gives the orbital and recurrence characteristics of these HEO satellites.

We have also included planned satellites in the list with existing satellites, and even abandoned projects when the orbit seems interesting and novel. The orbit of Glonass R. E. (Regional Extension) is planned, as the name suggests, for the regional extension of the Glonass system (see Chap. 14).

Although associated with a quite different type of mission, it is interesting to note the recurrence conditions of the satellite Integral, with  $i \sim 63^\circ$ , which makes one revolution in 3 days. This gives the unusual recurrence triple  $[0, 1, 3]$ ,  $N_{T_0} = 1$ .

HEO satellite	$a$	$e$	$i$	$T$	Triple	$N_{T_0}$
Supertundra	42,163.2	0.4230	$i_c$	1,436.03	[1, 0, 1]	1
Tundra	42,163.4	0.2668	$i_c$	1,436.04	[1, 0, 1]	1
Sycomores	42,163.9	0.3458	$i_c$	1,436.07	[1, 0, 1]	1
Glonass R. E.	42,163.3	0.3700	$i_c$	1,436.04	[1, 0, 1]	1
Molniya	26,552.9	0.7500	$i_c$	717.72	[2, 0, 1]	2
Molniya	26,553.6	0.7360	$i_c$	717.75	[2, 0, 1]	2
Molniya	26,554.3	0.7222	$i_c$	717.77	[2, 0, 1]	2
Loopus	29,991.4	0.6000	$i_c$	861.53	[2, -1, 3]	5
FLOWER	22,883.8	0.6558	$i_c$	574.22	[1, +1, 2]	5
VirtualGeo	20,260.2	0.6609	$i_c$	478.36	[3, 0, 1]	3
COBRA	20,260.9	0.6459	$i_c$	478.39	[3, 0, 1]	3
FLOWER CfTM	12,779.4	0.2588	$i_{HS}$	239.64	[6, 0, 1]	6
Ellipso Borealis	10,559.3	0.3463	$i_{HS}$	180.00	[8, 0, 1]	8
Ellipso Borealis	10,472.2	0.3266	$i_{HS}$	177.78	[8, +1, 10]	81
Ellipso Borealis	10,496.9	0.3321	$i_{HS}$	178.41	[8, +1, 14]	113
Ellipso Borealis	10,556.8	0.2357	$i_{HS}$	179.94	[8, 0, 1]	8
EGE	25,556.1	0.6700	$i_c$	717.84	[2, 0, 1]	2
STE-QUEST	32,170.2	0.7802	$\sim i_c$	957.11	[2, -1, 2]	3
Integral	87,704.2	0.7958	$\sim i_c$	4,308.23	[0, +1, 3]	1

TABLE 11.7 : *Orbital and recurrence characteristics for (HEO) Molniya and Tundra satellites, and for other planned satellites. Orbital elements: semi-major axis  $a$  in km, eccentricity  $e$ , and inclination  $i$ . All these satellites are at the critical inclination, either prograde,  $i_c = 63.4^\circ$ , or Sun-synchronous,  $i_{HS} = 116.6^\circ$ . Period  $T$  in minutes.*

MEO satellite	$a$	$h$	$i$	$T$	Triple	$N_{T_0}$
Navstar/GPS	26,560.904	20,183	55.0	717.98	[2, 0, 1]	2
WEST	20,267.139	13,889	75.0	478.63	[3, 0, 1]	3

TABLE 11.8 : *Orbital and recurrence characteristics for the (MEO) navigation satellites Navstar/GPS and those of the WEST constellation on the JOCOS orbit. Distances  $a$  and  $h$  in km, angle  $i$  in degrees, and period  $T$  in minutes. For other navigation satellites, see Table 14.1 in Chap. 14.*



## 11.5 Recurrence Grid

### 11.5.1 Constructing the Recurrence Grid

#### Equatorial Shift

As we saw in Chap. 8, the equatorial shift  $\Delta\lambda_E$  represents the distance between two successive ground tracks (of the same kind, ascending or descending) at the equator. In the following, we consider near-circular satellites in low orbit (LEO), the only ones for which the recurrence grid is relevant. For the quantities already discussed, we have

$$\Delta\lambda_E = -(\dot{\Omega}_T - \dot{\Omega})T_d = -\frac{n_d}{\kappa}T_d = -\frac{2\pi}{\kappa}. \quad (11.17)$$

The equatorial shift is thus very simply related to the daily recurrence frequency  $\kappa$ .

Consider a ground track defining one ascending node as origin, with longitude  $\lambda_0$ . If  $\lambda_1$  is the longitude of the following ascending node, we thus have, by definition of the equatorial shift,

$$\lambda_1 - \lambda_0 = \Delta\lambda_E = -2\pi \frac{C_{T_o}}{N_{T_o}}. \quad (11.18)$$

After  $\nu_o$  revolutions (about 1 day), the ground track cuts the equator at the ascending node with longitude  $\lambda_{\nu_o}$  such that

$$\lambda_{\nu_o} - \lambda_0 = \nu_o \Delta\lambda_E = -2\pi \frac{\nu_o C_{T_o}}{N_{T_o}}.$$

According to (11.12), this can be written in the form

$$\lambda_{\nu_o} - \lambda_0 = -2\pi \left(1 - \frac{D_{T_o}}{N_{T_o}}\right) = -2\pi + 2\pi \frac{D_{T_o}}{N_{T_o}}.$$

Since the longitudes are defined to within  $2\pi$ , we thus have

$$\lambda_{\nu_o} - \lambda_0 = 2\pi \frac{D_{T_o}}{N_{T_o}}. \quad (11.19)$$

If  $D_{T_o}$  is positive, i.e., if  $\nu_o < \kappa$ , we have  $\lambda_{\nu_o} - \lambda_0 > 0$ , whence  $\lambda_{\nu_o}$  lies to the east of  $\lambda_0$ . Indeed, if after  $\nu_o$  revolutions a whole day has not gone by since the crossing at  $\lambda_0$ , the ground track  $\lambda_{\nu_o}$  is indeed to the east of  $\lambda_0$ .

In the opposite situation, if  $D_{T_o}$  is negative, i.e., if  $\nu_o > \kappa$ , a little more than 1 day has gone by and the ground track  $\lambda_{\nu_o}$  is situated west of  $\lambda_0$ , as is clearly shown by the relation  $\lambda_{\nu_o} - \lambda_0 < 0$ .

### 11.5.2 Grid Interval

In the rest of this calculation, we shall denote the day of crossing by a superscript and the number of the crossing in this day by a subscript on the longitude of the ascending node, viz.,

$$\lambda_{\text{crossing}}^{\text{day}} .$$

The origin is denoted by  $\lambda_0^0$ . We consider the case where  $D_{T_o}$  is positive for concreteness. The other case would require us to use  $\nu_o + 1$  rather than  $\nu_o$  and change some of the signs. We thus have, with this notation,

$$\lambda_1^0 - \lambda_0^0 = \Delta\lambda_E .$$

The last ascending node on day 0 is  $\lambda_{\nu_o}^0$ , and the next, which is the first on day 1, is written  $\lambda_1^1$ . Hence,

$$\begin{aligned} \lambda_{\nu_o}^0 - \lambda_0^0 &= \nu_o \Delta\lambda_E \quad [\text{mod } 2\pi] , \\ \lambda_1^1 - \lambda_0^0 &= (\nu_o + 1) \Delta\lambda_E \quad [\text{mod } 2\pi] . \end{aligned}$$

where  $[\text{mod } 2\pi]$  indicates congruence modulo  $2\pi$ .

We now consider the interval  $[\lambda_1^0, \lambda_0^0]$ , which we shall call the base interval, or intertrack interval, counting positively toward the east. We take  $\lambda_1^0$  as origin and set

$$\delta_R = \lambda_0^0 - \lambda_1^0 , \quad \delta_D = \lambda_1^1 - \lambda_1^0 ,$$

where  $\delta_R$  is the interval between ascending nodes for two consecutive revolutions, so that  $\delta_R = -\Delta\lambda_E$ , and  $\delta_D$  is the interval between ascending nodes for 2 consecutive days. The interval  $\delta_R$  is shown in Fig. 11.11a, b, and the interval  $\delta_D$  in Fig. 11.11b, c.

Calling  $\delta$  the grid interval at the equator, defined by

$$\delta = \frac{2\pi}{N_{T_o}} , \tag{11.20}$$

we have the relations

$$\delta_R = C_{T_o} \delta , \quad \delta_D = D_{T_o} \delta .$$

The grid interval<sup>5</sup>  $\delta$ , related in this way to  $\delta_R$  and  $\delta_D$ , is indicated in Fig. 11.11d.

---

<sup>5</sup>For a quick evaluation,  $\delta$  can be obtained from an approximate relation for recurrent satellites of altitude  $h = 900 \pm 300$  km. For these satellites, the daily orbital frequency  $\nu$  lies between 13 and 15. We may thus take  $\nu$  to be equal to 14 and  $N_{T_o}$  equal to  $14C_{T_o}$ . Expressing  $\delta$  in degrees, we then find that

$$\delta \approx \frac{360}{14C_{T_o}} , \quad \text{i.e., } C_{T_o} \delta \approx 25 .$$

We thus see that the product of the grid interval (in degrees) and the recurrence cycle (in days) is roughly equal to 25.

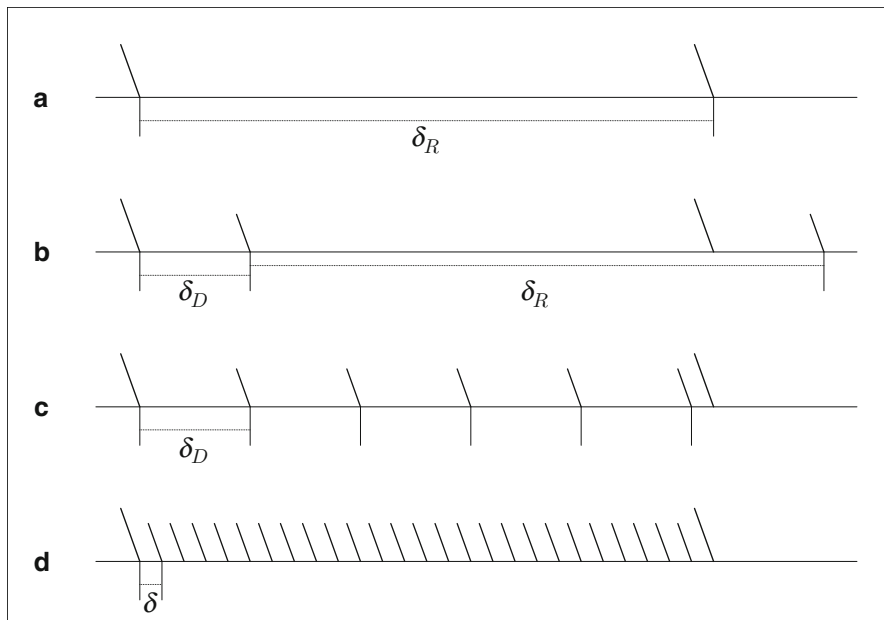


FIG. 11.11 : Constructing the recurrence grid. (a) Two consecutive ground tracks from day 0 determine the base interval  $\Delta\lambda_E$ , denoted here by  $\delta_R$ . These ground tracks are plotted in bold type. (b) One ground track of day 1 passes through the base interval. (c) The ground tracks for the following days 2, 3, ...,  $D$  pass through the base interval. (d) All ground tracks up to day  $C_{T_0} - 1$  define the grid interval. Note that, by “ground track”, we understand the ground track at the ascending node.

In the base interval, we have for the different days:

$$\begin{aligned} \text{for day 1} \quad & \lambda_1^1 - \lambda_1^0 = \delta_D, \\ \text{for day 2} \quad & \lambda_1^2 - \lambda_1^0 = 2\delta_D, \\ \text{for day } D \quad & \lambda_1^D - \lambda_1^0 = D\delta_D. \end{aligned}$$

For day  $D$ , this relation holds if the point  $\lambda_1^D$  lies in the base interval. Otherwise, we subtract a whole number of multiples of  $\delta_R$ , expressing this by congruence relations:

$$\begin{aligned} \lambda_1^D - \lambda_1^0 &= D\delta_D \quad [\text{mod } \delta_R], \\ \lambda_1^D - \lambda_1^0 &= DD_{T_0}\delta \quad [\text{mod } C_{T_0}\delta], \\ \frac{\lambda_1^D - \lambda_1^0}{\delta} &= DD_{T_0} \quad [\text{mod } C_{T_0}]. \end{aligned}$$

We note that the quantity  $(\lambda_1^D - \lambda_1^0)/\delta$  is indeed a whole number. So for a given day, we obtain the position of the ascending node  $\lambda_1^D$  in the base interval, hence also in the recurrence grid.

If  $u(D)$  denotes the position of the ground track on day  $D$  in the base interval, in units of  $\delta$ , i.e.,

$$u(D) = \frac{\lambda_1^D - \lambda_1^0}{\delta}, \tag{11.21}$$

we have the fundamental relation for the recurrence grid:

$$u(D) = DD_{T_0} \pmod{C_{T_0}}. \tag{11.22}$$

The whole number  $u(D)$  can take  $C_{T_0}$  values between 0 and  $C_{T_0} - 1$ .

When we do not wish to favour one bound of the interval rather than the other, we will consider the number  $u^*(D)$  defined by

$$u^*(D) = \min \{u(D), C_{T_0} - u(D)\}, \tag{11.23}$$

which is an integer taking values between 0 and  $C_{T_0}/2$ .

### Using the Recurrence Grid

We now give several examples to show how the recurrence grid is determined and used.

**Example 11.7** Calculate the crossing order in the base interval for the satellites TOPEX/Poseidon and Jason-1 and -2.

► The recurrence triple of these satellites is  $[13, -3, 10]$ , which immediately gives  $N_{T_0} = 127$ . We thus have

$$\delta = \frac{2\pi}{127} = 0.049474 \text{ rad} = 2.8346^\circ = 315.551 \text{ km},$$

and equatorial shift  $\delta_R = 10\delta$ , or  $\delta_R = 28.35^\circ$ . Applying (11.22), we obtain the values of  $u(D)$  for each day of the cycle. We deduce the grid values in the base interval, from  $u = 0$  to  $u = 10$ , noting the value of  $D$  for each  $u$ :

$$\text{from } u = 0 \text{ to } u = 10 \quad \mapsto \quad 0, 3, 6, 9, 2, 5, 8, 1, 4, 7, 10 = 0.$$

Note that  $u^* = 1$  for  $J = 3$  and  $J = 7$ . It is easy to obtain these values graphically, as illustrated in Fig. 11.12. ◀

**Example 11.8** Calculate the crossing order in the base interval for the satellites Landsat-3 and ADEOS-2.

► All recurrent satellites with  $D_{T_0} = \pm 1$  have sequential recurrence grids, i.e., in the base interval, consecutive ground tracks occur in the order of the days. Indeed, in this case, (11.22) implies the simple relation

$$D_{T_0} = +1 \implies u(D) = D, \quad D_{T_0} = -1 \implies u(D) = C_{T_0} - D.$$

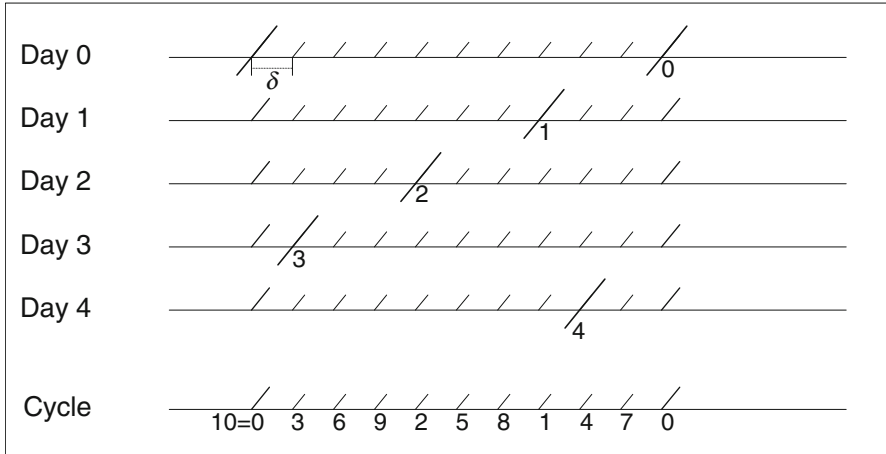


FIG. 11.12: Construction of the recurrence grid for TOPEX/Poseidon (and subsequently Jason-1 and -2). For each day of the cycle ( $D = 0, 1, 2, 3, 4, \dots$ ), the ground track at the equator is marked in the base interval.

There are many satellites like this, as can be seen in Table 11.1. Later on, we shall discover the important consequences of this fact for the ground track during the recurrence cycle. For Landsat-3, with  $D_{T_o} = -1$  for an 18 day cycle, the various ground tracks  $u = 0, 1, 2, 3, \dots, 17, 18$ , occur on days  $D = 18 (= 0), 17, 16, 15, \dots, 1, 0$ . For ADEOS-2, with  $D_{T_o} = +1$  for a 4 day cycle, the various ground tracks  $u = 0, 1, 2, 3, 4$  occur on days  $D = 0, 1, 2, 3, 4$ . ◀

### 11.5.3 Recurrence Subcycle

#### Definition of the Subcycle

Consider a day origin  $D = 0$ . A subcycle  $E_{T_o}$  is then the number of days required for the ground track to pass at a grid interval  $\delta$  from the ascending node origin. This can be formulated as follows:

$$u(E_{T_o}) = \pm 1 \quad [\text{mod } C_{T_o}], \quad (11.24)$$

or by

$$E_{T_o} D_{T_o} = \pm 1 \quad [\text{mod } C_{T_o}], \quad (11.25)$$

or again, bringing in the distance  $u^*$ , by

$$u^*(E_{T_o}) = 1. \quad (11.26)$$

This gives two values for  $E_{T_o}$ . If  $E_{T_o}^*$  is the smallest of the two, we have

$$E_{T_o} = E_{T_o}^* , \quad E_{T_o} = C_{T_o} - E_{T_o}^* .$$

We give several values for the subcycles of satellites discussed earlier.

**Important Note.** Care must be taken not to confuse the two quantities  $D_{T_o}$  and  $E_{T_o}^*$ . For the SPOT satellites, often described in the literature, it happens that  $D_{T_o} = 5$  and  $E_{T_o}^* = 5$ . However, it should not be concluded that  $D_{T_o}$  represents a subcycle, contrary to what is often claimed. It is quite clear in Example 11.9 that, for ADEOS-1, these two quantities are different, since we have  $D_{T_o} = 11$  and  $E_{T_o}^* = 15$ .

**Example 11.9** *Recurrence subcycles for various satellites with environmental missions.*

► Here we calculate  $E_{T_o}^*$  for several satellites:

- For SPOT-5, as for the SPOT-1 to -4 satellites, we obtain  $E_{T_o}^* = 5$ :

$$E_{T_o}^* D_{T_o} = 5 \times 5 = 25 = -1 \pmod{26} .$$

This means that, 5 days before ( $D = -5 \pmod{26} = 21$ ) or 5 days after ( $D = 5$ ) the day origin, the ground track passes at the grid interval from the ground track origin.

- For Terra, as for all the satellites belonging to the A-Train, we obtain  $E_{T_o}^* = 7$ :

$$E_{T_o}^* D_{T_o} = -7 \times 7 = -49 = -1 \pmod{16} .$$

At days  $D = 7$  and  $D = 16 - 7 = 9$ , the satellite is at one grid interval from the ground track origin.

- For ADEOS-1, we have  $E_{T_o}^* = 15$ :

$$E_{T_o}^* D_{T_o} = 15 \times 11 = 165 = +1 \pmod{41} .$$

At days  $D = 15$  and  $D = 41 - 15 = 26$ , the satellite is at one grid interval from the ground track origin.

- For TOPEX/Poseidon,  $E_{T_o}^* = 3$ , whence  $E_{T_o} = 3$  and 7 (see Fig. 11.12).
- For ICESat,  $E_{T_o} = 25$ :

$$E_{T_o}^* D_{T_o} = 25 \times (-22) = -550 = -1 \pmod{183} .$$

The cycle is very long in order to obtain a very short grid interval, viz.,  $\delta = 14.7$  km.



**IRS-1A**

Orbit - Ground track

Recurrence = [14; -1; 22] 307

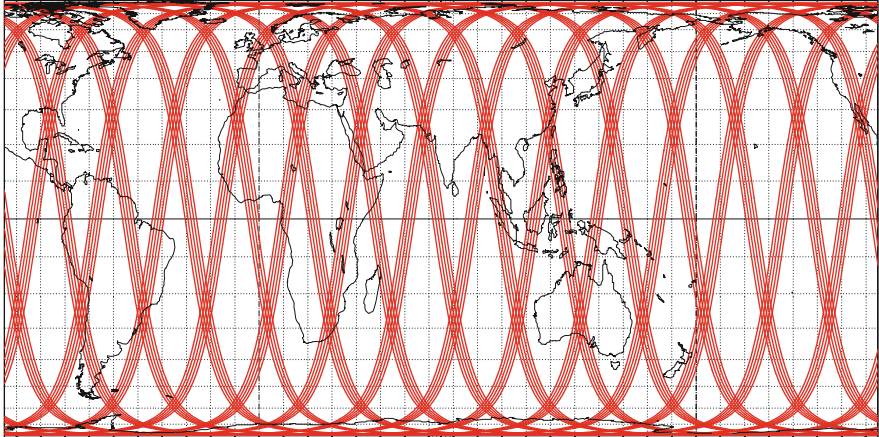
>>>> Time span shown: 5.00 days

Altitude = 904.1 km      a = 7282.275 km

Inclin./SUN-SYNCHRON.= 99.08 °

Period = 103.19 min \* rev/day =13.95

Equat. orbital shift = 2871.8 km ( 25.8 °)



Projection: Behrmann

Project. centre: 0.0 ° ; 75.0 ° E

Asc. Node: 0.00 °

Ιξίων

Property: Equal area

Aspect: Direct

App. inclin. = 103.08 °

MC ★ LMD

⊕ T.:Cylindrical - Graticule: 10°

{4.2} [ +90.0/ +0.0/-165.0] [-] EGM2008

Ατλας

**IRS-P6**

Orbit - Ground track

Recurrence = [14; +5; 24] 341

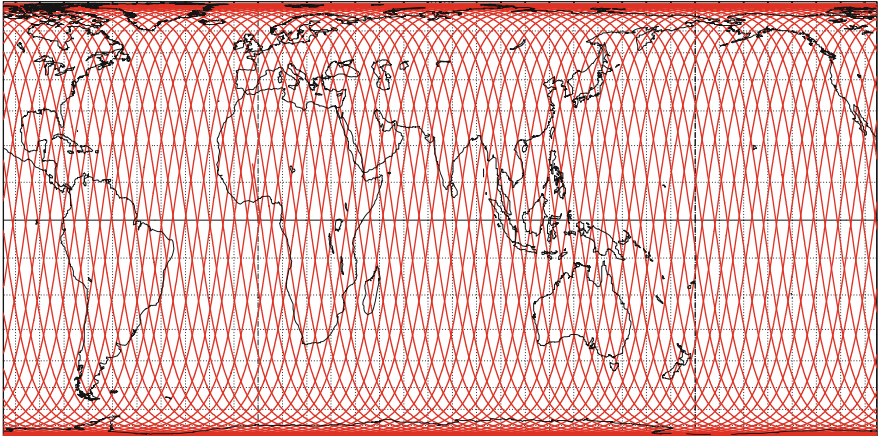
>>>> Time span shown: 5.00 days

Altitude = 817.0 km      a = 7195.118 km

Inclin./SUN-SYNCHRON.= 98.70 °

Period = 101.35 min \* rev/day =14.21

Equat. orbital shift = 2820.5 km ( 25.3 °)



Projection: Behrmann

Project. centre: 0.0 ° ; 75.0 ° E

Asc. Node: 0.00 °

Ιξίων

Property: Equal area

Aspect: Direct

App. inclin. = 102.64 °

MC ★ LMD

⊕ T.:Cylindrical - Graticule: 10°

{4.2} [ +90.0/ +0.0/-165.0] [-] EGM2008

Ατλας

FIG. 11.13 : Ground tracks of IRS-1A and IRS-P2 over 5 days, showing how long it takes to cover the base interval.

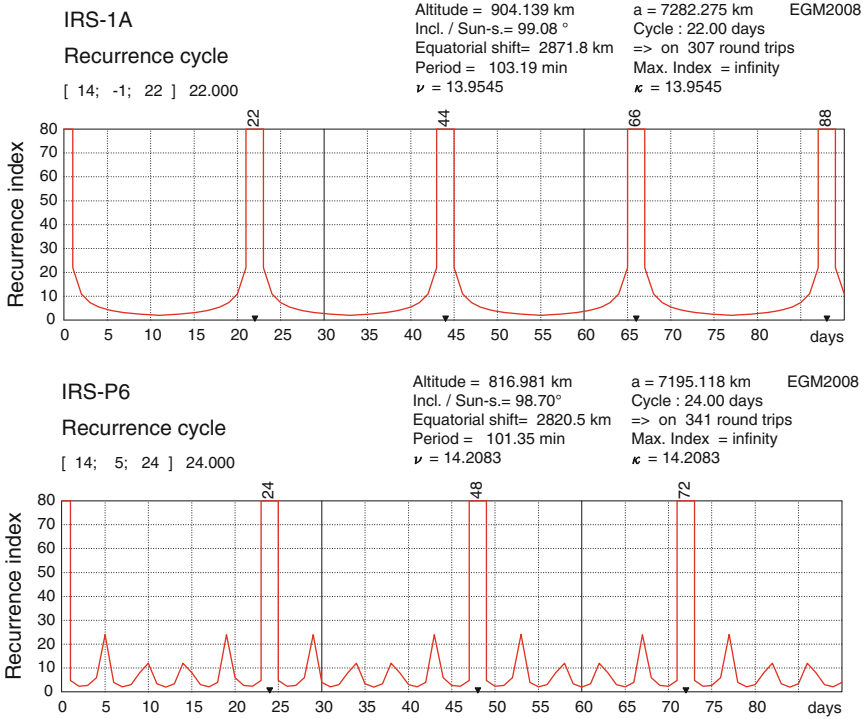


FIG. 11.14 : Recurrence index for two IRS satellites, showing the change of subcycle.

### Time Required to Cover the Base Interval

The main reason for introducing the subcycle is to show how long it takes to cover the base interval. For SPOT-5, the value of the subcycle  $E_{T_o}^* = 5$  indicates that almost the whole of the base interval has been scanned in 5 days. However, for a satellite with  $E_{T_o}^* = 1$ , we see that the ground track remains almost at the same place in the base interval after 1 day and that we need the whole cycle  $C_{T_o}$  (which can be of the order of a month) to cover the whole interval. This situation is generally considered as a drawback, as can be seen from the evolution of certain programmes.

The first Landsat satellites (-1, -2, and -3) had the subcycle  $E_{T_o}^* = 1$ . Then, from Landsat-4, the orbit was changed to obtain  $E_{T_o}^* = 5$ . The same happened with the Indian satellites in the IRS programme: the first IRS (IRS-1A and -1B) were replaced from IRS-P2, with a change of subcycle (but keeping almost the same cycle). This change is very clearly shown in Fig. 11.13, where we have plotted the ground tracks of two IRS satellites over 5 days. For IRS-1A, over this time span, a fraction  $5/22$  or less than one quarter of the interval has been covered. For IRS-P2, the whole interval has been covered. On the ground track of IRS-P2, in the vicinity of the origin ( $\lambda = 0, \varphi = 0$ ), we see the end of the ground track for the fifth day, since in 5 days, this satellite has accomplished



Satellites	Grid	$N_{T_o}$	$\delta$ (deg)	$\delta$ (km)	$\lambda$ origin (deg)
Landsat-1 to -3	WRS-1	251	1.4343	159.7	294.5200
Landsat-4 to -8, Terra	WRS-2	233	1.5451	182.0	295.4000
SPOT-1 to -5	GRS	369	0.9756	108.6	330.4000
ERS-1, 2, Envisat	ERS	501	0.7186	80.0	0.1335
MOS-1, -1B	MWRS	235	1.5190	169.1	326.7500
Oceansat-1, -2	IRSP4G	29	12.4138	1381.9	328.1900
T/P, Jason-1, -2	TPG	127	2.8346	315.5	99.9242

TABLE 11.9 : Characteristics of reference grids for various satellites.  $N_{T_o}$  is the number of revolutions per recurrence cycle,  $\delta$  the grid interval, and  $\lambda$  the longitude origin. Abbreviations: WRS is the Worldwide Reference System, GRS is the Grille de Référence SPOT, ERS is the ERS-SAR Reference System, MWRS is the MOS-1 World Reference System, IRSP4G is the National Remote Sensing Agency (India) IRS-P4 Grid, and TPG is the T/P Grid.

$5 \times 14.208 = 71.04$  round trips. The distance between this ground track and one going through the origin is equal to the interval  $\delta$ , since  $E_{T_o}^* = 5$  for this satellite (Fig. 11.14).

The notion of subcycle is often used for recurrent satellites, since it is rather informative. It tells us that, after a certain number of days representing the subcycle, the ground track passes through almost the same place, where “almost” means within the grid interval  $\delta$ . However, it is just a special case of the notion of recurrence index to be discussed shortly.

### 11.5.4 Reference Grids

For a recurrent satellite, a single point on the ground track completely fixes its ground track on the globe. Earth-observation satellites are maintained on their nominal orbits in order to guarantee the position of their ground tracks to within a few kilometers (generally  $\pm 5$  km, but  $\pm 1$  km for TOPEX/Poseidon and Jason,  $\pm 0.8$  km for ICESat). The SPOT satellites (SPOT-1 to -5), for example, use the same grid, which is fixed by giving an ascending node longitude. Table 11.9 describes the main grids and their characteristics.

**Example 11.10** *Fitting a grid to geographic circumstances: the case of FormoSat-2.*

► FormoSat-2, launched on 20 May 2004 under the name of Rocsat-2, is devoted to the study of Earth resources and meteorology, and in particular, typhoon warnings. Its recurrence triple is [14, 0, 1]. This means that each day, after 14 round trips, it exactly repeats its ground track (see Fig. 11.15 upper). If we examine this grid, we find that the ascending and descending ground tracks cross at latitude  $26.550^\circ$  (see Sect. 11.5.5 on grid points). Now

**FormoSat-2**

**Orbit - Ground track**

Recurrence = [14; +0; 1] 14

2012 10 01 00:00:00 UTC >>> 1440.0 min = 1.00 day

Altitude = 888.3 km

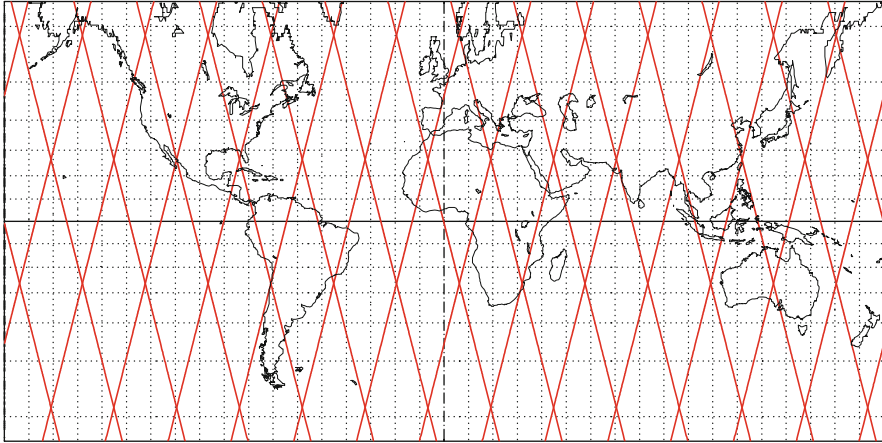
a = 7266.408 km

Incl. / SUN-S. = 98.96 °

e = 0.000186

Period = 102.86 min \* rev/day = 14.00

Equat. orbital shift = 2862.5 km ( 25.7 °)



Proj.: Snyder-Satel.Track/35°

Project centre: 0.0 ° ; 0.0 °

Asc. Node: -103.04 ° [21:45 LMT]

Ιξίων

Property: none [Geoc.L]

Aspect: Direct

[NORAD] Revolution: 42780

MC \* LMD

⊕ T.:Cylindrical - Graticule: 10°

{4.2} [ +0.0/ +0.0/ +0.0] [-] EGM2008

[NORAD] 2012 10 01 04:37:28 UTC

Ατλας

**FormoSat-2**

**Orbit - Ground track**

Recurrence = [14; +0; 1] 14

>>>> Time span shown: 1440.0 min = 1.00 day

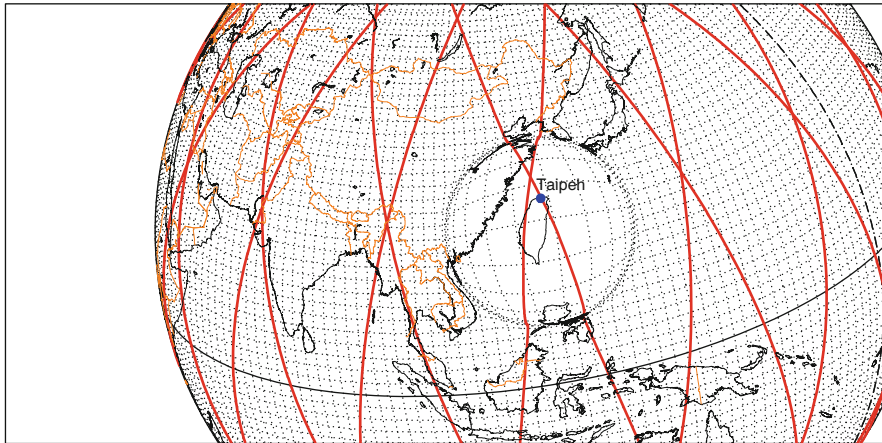
Altitude = 888.3 km

a = 7266.471 km

Inclin./SUN-SYNCHRON.= 99.01 °

Period = 102.86 min \* rev/day = 14.00

Equat. orbital shift = 2862.5 km ( 25.7 °)



Projection: Orthogr. / FishEye

PC: 23.5 ° N;121.2 ° E /ZC: 26.0 ° N;108.0 ° E Asc. Node: 127.63 ° [21:30 LMT]

Ιξίων

Property: none

Aspect: Oblique > zoom : 1.75

MC \* LMD

⊕ T.:Azimuthal - Graticule: 2°

{5.3} [ -90.0/ +66.5/ -31.2] [+10] EGM2008

Ατλας

FIG. 11.15 : Ground track of the Taiwanese satellite FormoSat-2, with 1-day recurrence cycle. Upper: recurrence grid. Lower: magnified view centered on the island of Taiwan, explaining this choice of grid.

the island of Taiwan, formerly Formosa, lies between latitudes  $22^\circ\text{N}$  and  $25^\circ\text{N}$ . The grid can thus be fixed in such a way that the island is crossed twice a day by the (ascending and descending) ground track. The equatorial shift is  $\delta_R = |\Delta\lambda_E| = 360/14 = 25.71^\circ$ . By symmetry considerations, we understand that the longitude of the ground track intersection and the longitude of the ascending node must be separated by a distance equal to one quarter of the equatorial shift. The central longitude of Taiwan is  $\lambda_C = 121.20^\circ\text{E}$ , which implies that the ascending node must have longitude  $\lambda_0$  such that

$$\lambda_0 = \lambda_C + \delta_R/4 = 121.20 + 6.43 = 127.63^\circ\text{E}.$$

Figure 11.15 illustrates this situation, unique for an LEO satellite. ◀

### 11.5.5 Grid Points for Recurrent Satellites

When a satellite is recurrent, its ground track forms a grid fixed on the Earth (the reference grid discussed above). A grid point is any place where two ground tracks intersect, one in the ascending part and the other in the descending part. For satellites with a broad swath, these points are of little interest. However, if the swath happens to be very narrow, or in the case of nadir laser sighting, it is generally extremely useful to know their positions.

At a given latitude, these points are regularly arranged in longitude. As one moves away from the equator, they become more and more closely spaced. We calculate the positions of the grid points using a cartographic method. We saw in Chap. 8, and in particular in Sect. 8.5 on cartographic projections, that the satellite ground track can be represented linearly using a Snyder projection.

Consider therefore the cartographic projection defined by (8.56), with Cartesian coordinates  $x$  as abscissa and  $y$  as ordinate. For clarity, and without loss of generality, we only consider here the quarter ( $x \geq 0, y \geq 0$ ) of the map. The rest can be deduced by symmetry relative to the equator for  $y \leq 0$  and relative to the zero meridian for  $x \leq 0$ . Moreover, we set  $\lambda_{AN} = 0$ . Then,

$$\begin{cases} x = \lambda, \\ y = \mathfrak{F}(\psi), \end{cases} \quad (11.27)$$

with

$$\mathfrak{F}(\psi) = \left| \arcsin \frac{\tan \psi}{\tan i} - \frac{1}{\kappa} \arcsin \frac{\sin \psi}{\sin i} \right|. \quad (11.28)$$

With this cartographic projection, the ground track of the satellite is made up of straight line segments. The recurrence grid looks like a series of identical diamonds lying between the northernmost (geocentric) latitude  $+\psi_m$  and the southernmost (geocentric) latitude  $-\psi_m$ .

We can calculate the maximal value  $y_m$  of  $y$ , when  $\psi = \psi_m$  :

- If  $i < 90^\circ$ ,  $\psi_m = i \implies y_m = 90(1 - 1/\kappa)$  .
- If  $i > 90^\circ$ ,  $\psi_m = 180^\circ - i \implies y_m = 90(1 + 1/\kappa)$  .

This can be summarised by

$$y_m = 90 \left( 1 - \frac{\sigma}{\kappa} \right) , \tag{11.29}$$

where  $\sigma = \text{sign}(\cos i)$ .

**Note.** This method cannot be applied if  $\text{sign}(\cos i)$  and  $\text{sign}(\cos i')$  are not equal, where  $i'$  is the apparent inclination. However, this situation never arises with existing recurrent LEO satellites.

Examples: for Jason-2,  $y_m = 82.9134$ , and for Oceansat-2,  $y_m = 96.2069$ .

During one cycle of  $N_{T_o}$  revolutions in  $C_{T_o}$  days, the satellite crosses a given meridian  $M$  times:

- For a direct orbit,  $i < 90^\circ$ , the satellite and the Earth rotate in the same direction and therefore  $M = N_{T_o} - C_{T_o}$ .
- For a retrograde orbit,  $i > 90^\circ$ , the satellite and the Earth rotate in opposite directions, whence  $M = N_{T_o} + C_{T_o}$ .

The number  $M$  of intersections between the ground track and the given meridian can be summarised by the formula

$$M = N_{T_o} - \sigma C_{T_o} . \tag{11.30}$$

For example, for Jason-2,  $M = 127 - 10 = 117$ , and for Oceansat-2,  $M = 29 + 2 = 31$ .

The length  $L_y$  of the “vertical” diagonal, along the  $y$  axis, of an elementary diamond is expressed as

$$L_y = 4u ,$$

where  $u$  is our measurement unit. The  $M$  intersections produce  $M/2$  diamonds ( $M$  even or odd), which appear clearly in Fig. 11.16 (upper). Along the  $y$  axis, the diamonds cover a total length  $L$  given by

$$L = \frac{M}{2} L_y = 2uM .$$

This distance  $L$  corresponds to the interval  $[-y_m, +y_m]$ , of length  $2y_m$ . We thus deduce that  $u$  is equal to

$$u = \frac{y_m}{M} .$$

**Oceansat-2**

**Orbit - Ground track**

Recurrence = [14; +1; 2] 29

>>>> Time span shown: 2880.0 min = 2.00 days

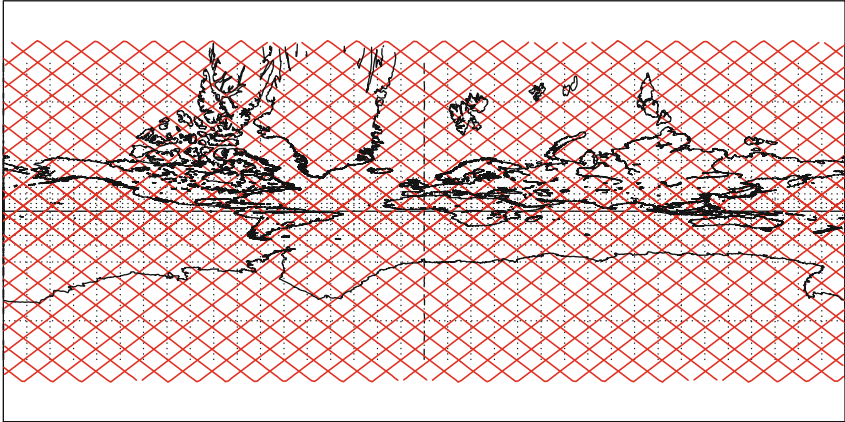
Altitude = 720.0 km

a = 7098.103 km

Inclin./SUN-SYNCHRON.= 98.29 °

Period = 99.31 min \* rev/day=14.50

Equat. orbital shift = 2763.8 km ( 24.8 °)



Proj.: Snyder-Satel.Track/80°  
Property: none [Geoc.L]  
⊕ T.:Cylindrical - Graticule: 10°

Project. centre: 0.0 ° ; 0.0 °  
Aspect: Direct  
{5.3} [ +0.0/ +0.0/ +0.0] [-] EGM96

Asc. Node: -31.81 ° [00:00 LMT]  
App. inclin. = 102.16 °

Iξίων  
MC \* LMD  
Ατλας

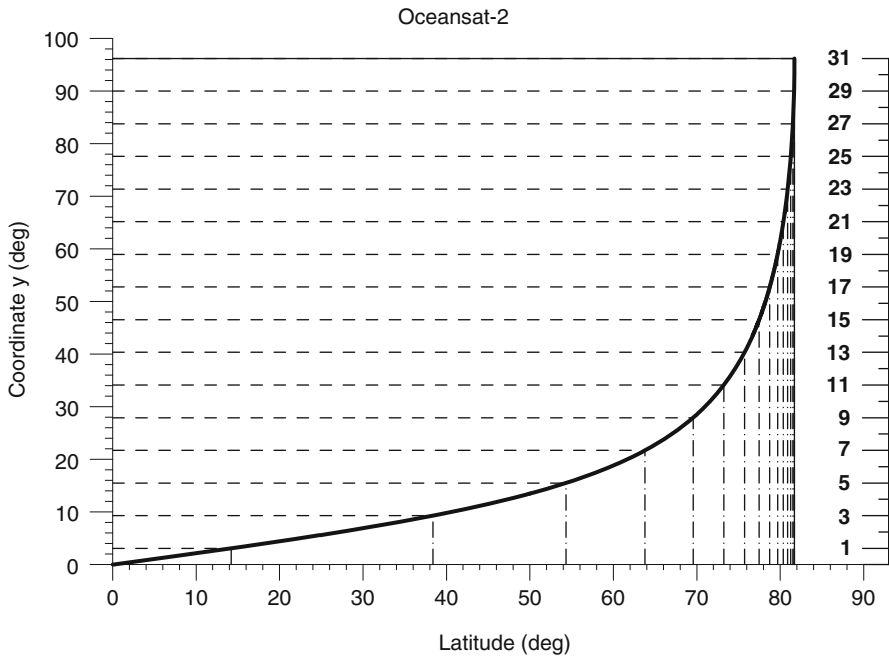


FIG. 11.16 : Upper: ground track of the Sun-synchronous satellite Oceansat-2, with a 2-day recurrence cycle. Adapted Snyder projection. With a little effort, the continents can be made out. Lower: graphical solution of (11.33) giving the (geocentric) latitudes of the grid points.

Considering the expressions for  $M$  and  $y_m$  given above, together with the definition of  $\kappa$ , we obtain

$$\mathbf{u} = \frac{90 - \sigma \frac{C_{T_0}}{N_{T_0}}}{N_{T_0} - \sigma C_{T_0}} ,$$

whence the value of the unit  $\mathbf{u}$  is

$$\mathbf{u} = \frac{90}{N_{T_0}} . \tag{11.31}$$

We now consider the intersections of the ground track with the equator. In one cycle of  $N_{T_0}$  revolutions, there will be  $2N_{T_0}$  intersections. Since these are regularly distributed, there will thus be  $N_{T_0}$  diamond shapes along the  $x$  axis. So if  $L_x$  is the “horizontal” length, along the  $x$  axis, of an elementary diamond, and if we set  $L_x = 4\mathbf{v}$ , we obtain

$$\mathbf{v} = \frac{90}{N_{T_0}} .$$

Then since

$$\mathbf{u} = \mathbf{v} ,$$

we conclude that the units of length along the  $x$  and  $y$  axes are the same. This is a direct consequence of the choice of projection.

Having defined  $\mathbf{u}$  in this way, the ordinates of the grid points are as follows:

$$\begin{cases} M \text{ even} \implies y/\mathbf{u} = 0, 2, 4, 6, \dots, M , \\ M \text{ odd} \implies y/\mathbf{u} = 1, 3, 5, 7, \dots, M . \end{cases} \tag{11.32}$$

Starting from the equator, we number the latitudes of the grid points:

$$\text{grid point } j \iff \begin{cases} \text{ordinate } y_j \iff \text{latitude } \psi_j , \\ y_j = \frac{j}{M} y_m , \\ 0 \leq j \leq M , \quad j \text{ has the parity of } M . \end{cases}$$

Since  $y_j = \mathfrak{F}(\psi_j)$ , we obtain the geocentric latitude  $\psi_j$  by inverting the function  $\mathfrak{F}$ :

$$\psi_j = \mathfrak{F}^{-1}(y_j) . \tag{11.33}$$

The function  $\mathfrak{F}$  is analytic, and  $\mathfrak{F}^{-1}$  can be found numerically.

For each grid point  $j$ , we thus obtain the geocentric latitude  $\psi_j$ , hereafter denoted by  $\psi$ . It corresponds to the geocentric latitude of the satellite or its geocentric ground track  $T$ . From each value of  $\psi$ , we calculate the geodetic latitude  $\varphi$  of the nadir using the method described in Chap. 2 (see Fig. 2.5 and

$j$	Latitude $\varphi$	Latitude $\psi$	Latitude $\varphi_T$
1	26.5500	26.4153	26.5690
3	58.6947	58.5449	58.7160
5	70.8187	70.7139	70.8336
7	76.0404	75.9614	76.0517
9	78.6800	78.6149	78.6892
11	80.1032	80.0460	80.1113
13	80.8230	80.7699	80.8306
15	81.0443	80.9924	81.0517
$M$	Maximal latitude $\psi =$	80.9924	$\lll$
–	180 – inclination =	80.9924	$\lll$

TABLE 11.10: Latitude  $\varphi$  of the grid points for the Sun-synchronous satellite *FormoSat-2*,  $i_{\text{HS}} = 99.0076^\circ$ ,  $C_{T_o} = 1$  day,  $N_{T_o} = 14$ ,  $M = 14 + 1 = 15$ . Grid points are calculated from the geocentric latitude  $\psi$  of the ground track  $T$ , whose geodetic latitude is denoted by  $\varphi_T$ .  $\varphi$  is the geodetic latitude of the nadir, which depends on the altitude. The relation between these latitudes is  $\psi < \varphi < \varphi_T$ .

$j$	Latitude $\varphi$	Latitude $\psi$	Latitude $\varphi_T$
1	14.2803	14.1979	14.2897
3	38.5481	38.3799	38.5673
5	54.4799	54.3166	54.4987
7	63.9408	63.8044	63.9565
9	69.6657	69.5530	69.6787
11	73.3289	73.2338	73.3398
13	75.8021	75.7198	75.8116
15	77.5435	77.4707	77.5519
17	78.8068	78.7410	78.8144
19	79.7402	79.6796	79.7472
21	80.4344	80.3777	80.4409
23	80.9471	80.8934	80.9533
25	81.3157	81.2640	81.3216
27	81.5642	81.5140	81.5700
29	81.7078	81.6585	81.7135
31	81.7548	81.7057	81.7605
$M$	Maximal latitude $\psi =$	81.7057	$\lll$
–	180 – inclination =	81.7057	$\lll$

TABLE 11.11: Latitude  $\varphi$  of grid points for Sun-synchronous satellites *Oceansat-1* and *-2*,  $i_{\text{HS}} = 98.2943^\circ$ ,  $C_{T_o} = 2$  day,  $N_{T_o} = 29$ ,  $M = 29 + 2 = 31$ . For  $\varphi$ ,  $\psi$ , and  $\varphi_T$ , see Table 11.10.

Table 2.4). We have seen that  $\varphi$  depends on the altitude. These values  $\psi$  and  $\varphi$ , and the geodetic latitude  $\varphi_T$  of the ground track are given for each value of  $j$  for two satellites with very short recurrence cycles, namely, FormoSat-2 in Table 11.10 and Oceansat-2 in Table 11.11.

**Example 11.11** Calculate the position of a specific grid point for the ground track of the altimetric satellites TOPEX/Poseidon and Jason-1 and -2.

► From 1960, the USSR began to develop intensive cotton production in Uzbekistan and Kazakhstan. To sustain this, enormous amounts of water were extracted from the two rivers flowing into the Aral Sea, the Syr Darya in the north and the Amu Darya in the south. Water levels in this closed sea began to drop and its area was significantly reduced until, in 1989, it divided into two basins, the Greater Sea, or Big Aral Sea, and the Lesser Sea, or Little Aral Sea (see Fig. 11.17 lower). But draining continued and the Greater Sea itself soon split into two.

Measuring the water levels in the Aral Sea is an interesting application for an altimetric satellite like TOPEX/Poseidon and its successors Jason-1 and -2. Here we calculate the position of a grid point located in the middle of the Aral Sea and denoted by  $A$  in Fig. 11.17 (upper):

- Latitude. The original “historical” sea lies between latitudes  $43.5^\circ\text{N}$  and  $47^\circ\text{N}$ . For T/P,  $C_{T_o} = 10$  day,  $N_{T_o} = 127$ ,  $i = 66.0390^\circ$ , so  $M = 127 - 10 = 117$ . Solving (11.33), we obtain for  $j = 31$  the value  $\psi = \psi_j = 44.5197^\circ$ . We then calculate the geodetic latitude of the nadir, which gives  $\varphi = 44.6785^\circ$ .
- Longitude. The region under consideration lies between longitudes  $58^\circ\text{E}$  and  $62^\circ\text{E}$ . The ascending node fixing the grid is  $\lambda_0 = 99.9242^\circ$ . The unit of length of the diamond is  $\mathbf{v} = 90/127 = 0.7087$ . Since  $M$  is odd, the grid points have longitudes of the form

$$\lambda_k = \lambda_0 + k\mathbf{v} \text{ with } k \text{ odd, between } 0 \text{ and } 4N_{T_o} ,$$

whence

$$\lambda_k = 99.9242 + \frac{90}{127}k \text{ with } k \text{ odd, between } 1 \text{ and } 507 .$$

With  $k = 451$ , we obtain

$$\lambda = 99.9242 + 319.6063 = 59.5305 \quad [\text{mod } 360] .$$

The coordinates of the grid point at the center of the Aral sea, denoted by  $A$  on the map in Fig. 11.17 (upper), are therefore  $44.6785^\circ\text{N}$  and  $59.5305^\circ\text{E}$ .

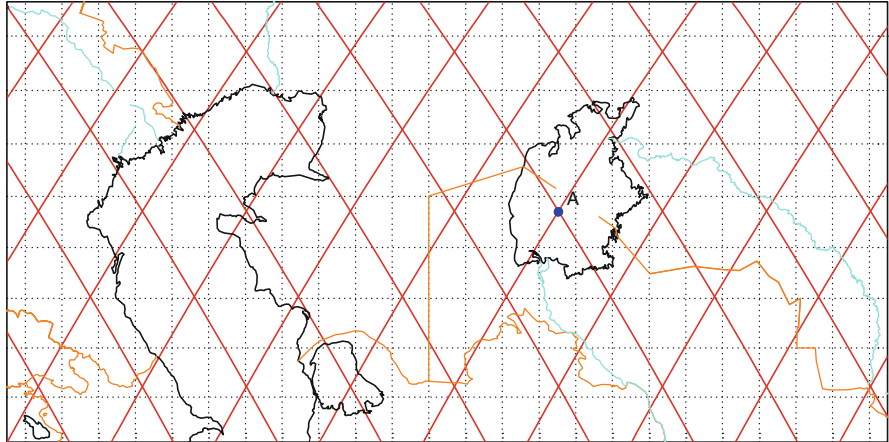




**Jason-2 / OSTM**  
Orbit - Ground track

Recurrence = [13; -3; 10] 127  
>>> Time span shown: 10.00 days

Altitude = 1336.3 km      a = 7714.433 km  
Inclination = 66.04 °  
Period = 112.43 min \* rev/day=12.81  
Equat. orbital shift = 3155.5 km ( 28.3 °)



Projection: Mercator      PC: 0.0 ° ; 0.0 ° /ZC: 44.5 ° N; 56.5 ° E      Asc. Node: 99.92 ° [00:00 LMT]      **Ιξίων**  
Property: Conformal      Aspect: Direct > zoom: 15.00      App. inclin. = 70.29 °      **MC \* LMD**  
⊕ T.:Cylindrical - Graticule: 1°      {5.3} [ +90.0/ +0.0/ -90.0] [-] GRIM5-S1      **Ατλας**

$j$	Latitude $\varphi$	Latitude $\psi$
1	1.9881	1.9771
3	5.9389	5.9062
5	9.8157	9.7624
7	13.5757	13.5033
9	17.1842	17.0947
11	20.6163	20.5118
13	23.8564	23.7390
15	26.8969	26.7689
17	29.7373	29.6006
19	32.3819	32.2383
21	34.8384	34.6895
23	37.1169	36.9641
25	39.2286	39.0730
27	41.1851	41.0277
29	42.9980	42.8396
31	44.6785	44.5197
33	46.2372	46.0785
35	47.6840	47.5258
⋮	⋮	⋮
115	66.1497	66.0321
117	66.1566	66.0390
$M$	Maximal latitude $\psi =$	66.0390
-	Inclination =	66.0390



FIG. 11.17 : Upper: a grid point  $A$ , corresponding to  $j = 31$ , lies in the middle of the Aral Sea. Lower: satellite ground track. Outline of the sea in 1960 and in 2008. Credit: Aviso, CLS, CNES.

## 11.6 Maintaining a Recurrent Satellite on Orbit

In order to keep to its recurrence cycle, the orbit of a recurrent satellite must be accurately maintained. One speaks of orbital maintenance: the orbital elements must be repositioned at the required values whenever necessary. The inclination  $i$  and the eccentricity  $e$  vary little, compared with the semi-major axis  $a$ , which must be watched over very carefully. Here we shall only consider the variation of  $a$ .

The altitude of the satellite tends to drop, mainly due to atmospheric drag and solar radiation pressure. The differential form of Kepler's third law gives

$$dT = \frac{3T}{2a} da .$$

Let  $\Delta a$  be the deviation of the semi-major axis from its nominal value (with  $\Delta a \ll a$ ). The period of the satellite varies by  $\Delta T$ . After one revolution, with period  $T + \Delta T$ , the Earth's rotation leads to a shift  $\Delta \ell$  in the ground track of the satellite at the equator as compared with its nominal ground track. We denote this shift by  $\Delta \ell_1$  for one revolution, and by  $\Delta \ell_D$  for 1 day. Using (8.17) and taking into account nodal precession, we obtain

$$\Delta \ell_1 = -R(\dot{\Omega}_T - \dot{\Omega})\Delta T = -\frac{3}{2}R(\dot{\Omega}_T - \dot{\Omega})T_d \frac{\Delta a}{a} , \quad (11.34)$$

where  $R$  is the equatorial radius. Using (11.17), we then have

$$\Delta \ell_1 = -3\pi R \frac{1}{\kappa} \frac{\Delta a}{a} . \quad (11.35)$$

Note that  $\Delta \ell_1$  and  $\Delta a$  have opposite signs:

- If  $h \uparrow$ , then  $\Delta a > 0 \implies \Delta \ell_1 < 0$ , leading to a westward shift.
- If  $h \downarrow$ , then  $\Delta a < 0 \implies \Delta \ell_1 > 0$ , leading to an eastward shift.

In 1 day, the shift will be

$$\Delta \ell_D = \nu \Delta \ell_1 , \quad (11.36)$$

and with (11.9),

$$\Delta \ell_D = -3\pi R \frac{\nu}{\kappa} \frac{\Delta a}{a} = -3\pi R \frac{\Delta a}{a} \left(1 - \frac{1}{C_S}\right) . \quad (11.37)$$

The daily shift  $\Delta \ell_D$  can be written in the following simplified form, using the reduced distance  $\eta$  and neglecting the term in  $1/C_S$  compared with 1:

$$\Delta \ell_D = -Q\Delta a , \quad \text{where } Q = \frac{3\pi}{\eta} . \quad (11.38)$$

The factor  $Q$ , which we may call the drift coefficient, is thus a dimensionless number by which one must multiply the change in altitude to obtain the daily

shift of the ground track away from its nominal position at the equator. For typical Sun-synchronous LEO satellites with  $\eta \approx 1.11$ , one has

$$Q = 8.5 .$$

For example, if a maneuver raises the satellite by 10 m, the ground track will shift by 85 m every day, provided that  $a$  remains the same after the maneuver.

**Example 11.12** *Orbital maintenance for the altimetric satellite TOPEX-Poseidon.*

► We compare the actual and theoretical positions of the ground track for the satellites TOPEX/Poseidon and Jason-1 and -2.

**Orbital Maintenance Maneuvers.** To ensure that the deviation from the nominal ground track is never greater than 1 km at the equator, the satellite is subjected to orbital maintenance maneuvers (OMM) 2 or 3 times a year. The altitude is thereby raised slightly, by 5–10 m above the nominal altitude, by activating the satellite thrusters for 3–4 s. Figure 11.18 shows the changes  $\Delta\ell$  as time goes by, relating them to changes  $\Delta a$ , over the 7 years of operation of TOPEX/Poseidon. The ground track shifts westward relative to the nominal ground track when the semi-major axis  $a$  decreases.

To calculate the drift of the ground track, we take the example of the third maneuver OMM3 on 30 March 1993. By this maneuver,  $a$  changed from 7,714.426 to 7,714.435 km, thereby increasing by 9 m. Subsequently, for 26 days,  $a$  decreased steadily to 7,714.430, i.e., 4 m above its value at the beginning of the maneuver. We may thus consider an average value of  $\Delta a = 6.5$  m during this period. The numerical data for T/P are  $\eta = 1.2095$ ,  $\kappa = 12.70$ ,  $\nu = 12.81$ , which we use in (11.37) to obtain

$$\Delta\ell_D = -7.86\Delta a = 51.1 \text{ m} .$$

Over 26 days,  $\Delta\ell = 1.33$  km, as can be read off the graph.

**Reference Grid.** In Example 11.6, we calculated  $\lambda_{AN}$  at a given revolution for each of the 3 satellites. We see also from Table 11.9 that the zero longitude of the TPG grid is  $\lambda_0 = 99.9242^\circ$ . The difference between the nominal longitude  $\lambda_{AN}^0$  of the ascending node and  $\lambda_0$  is equal to a whole number of grid intervals  $\delta$ :

$$\lambda_{AN}^0 - \lambda_0 = k \frac{360}{127}, \quad k \text{ integer} .$$

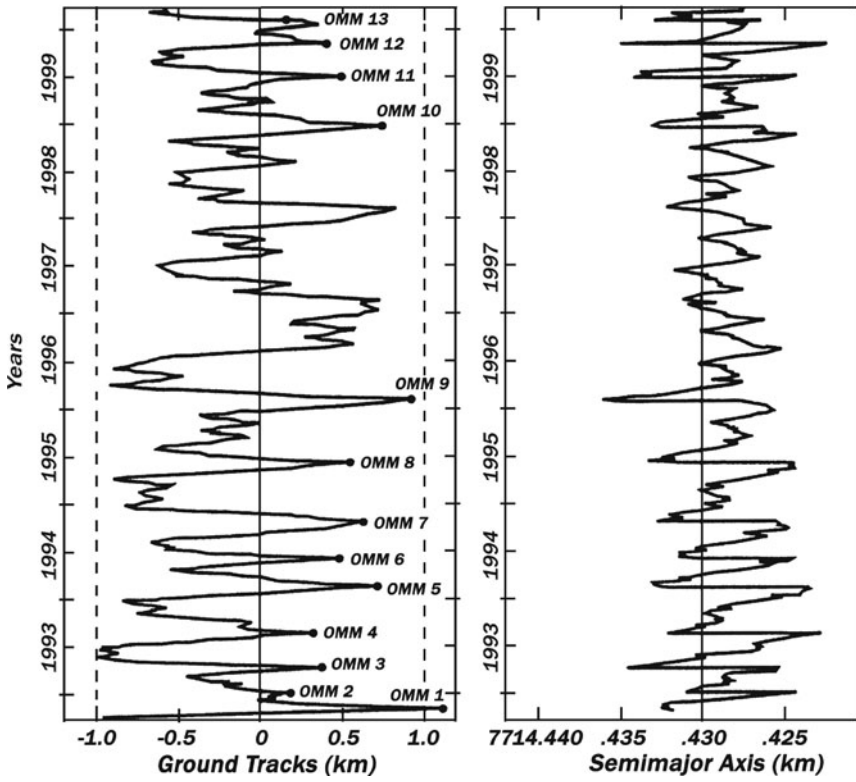
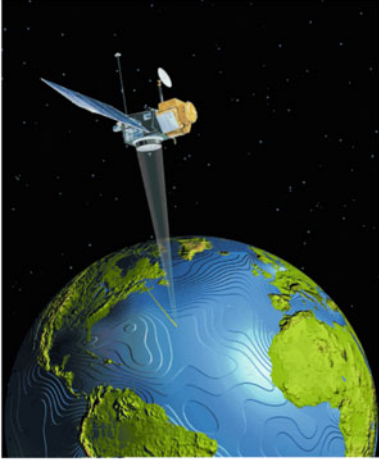


FIG. 11.18 : (continued)

The difference between the actual value  $\lambda_{AN}$  and the nominal value  $\lambda_{AN}^0$  gives the shift in the ground track, and we have  $\Delta\ell = R(\lambda_{AN} - \lambda_{AN}^0)$ :

T/P	Revolution	4263	1993 07 09 18:07 UT ,	
			$\lambda_{AN} - \lambda_{AN}^0 = 82.9247 - 82.9163 = 0.0084$ ,	$\Delta\ell = 0.933$ km .
Jason-1	Revolution	8676	2003 10 15 21:31 UT ,	
			$\lambda_{AN} - \lambda_{AN}^0 = 65.9144 - 65.9085 = 0.0059$ ,	$\Delta\ell = 0.659$ km .
Jason-2	Revolution	23551	2013 07 03 03:16 UT ,	
			$\lambda_{AN} - \lambda_{AN}^0 = 272.8408 - 272.8376 = 0.0032$ ,	$\Delta\ell = 0.357$ km .

**Tandem Mission.** As noted in Chap. 9, when two satellites follow orbits with identical characteristics, this can be used for a tandem mission. When Jason-1 came into operation on 15 August 2002, T/P became a secondary satellite. By shifting T/P to a longitude at the equator exactly equal to  $\delta/2$ , a tandem mission was set up which amounted to working with a recurrence grid that was twice as fine. When Jason-2 became operational on 20 February 2009, it was Jason-1 that became the secondary satellite for the tandem mission, on 20 February 2009, and T/P was withdrawn from service. ◀

## 11.7 Recurrence Index

### 11.7.1 Definition of Recurrence Index

Consider a day origin  $D = 0$  and its base interval, representing the inter-track distance, defined by  $\lambda_1^0$  and  $\lambda_0^0$ , which are separated by the equatorial shift  $\delta_R$ . The ascending node crossing in this interval on a given day  $D$  determines an ascending node of longitude  $\lambda_1^D$ , as discussed above. The distance between  $\lambda_1^D$  and the bounds  $\lambda_1^0$  and  $\lambda_0^0$  will be representative of the recurrence conditions. If the distance to one of the two bounds is zero, this means that the ground track passes once again through a certain point, and we have recurrence with a cycle of  $D$  days, or else  $D$  is a multiple of the cycle. If the distance is small compared with the length of the interval, we may be in a situation with a subcycle.



FIG. 11.18 : Deviations  $\Delta\ell$  from the nominal ground track resulting from deviations  $\Delta a$  from the nominal semi-major axis over the 7 year period of operation of TOPEX/Poseidon (1993–1999). Orbital maintenance maneuvers are denoted by OMM-n at the time of application. At each OMM, the semi-major axis increases suddenly by about 10 m. Credit: Lee-Lueng Fu (JPL/NASA), Anny Cazenave (LEGOS/CNES). Left: Artist's view of T/P. Credit: JPL/NASA.

We set

$$v(D) = \frac{\lambda_1^D - \lambda_0^0}{\delta_R} . \tag{11.39}$$

From (11.21), we then have

$$v(D) = \frac{u(D)}{C_{T_o}} . \tag{11.40}$$

These two equivalent definitions shown that  $v(D)$  is a real number between 0 and 1, representing a relative distance.

Just as we defined  $u^*(D)$  by (11.23), we now define  $v^*(D)$  as the smallest of the two relative distances  $v(D)$  from the ground track to one or other of the bounds, viz.,

$$v^*(D) = \min \left\{ \frac{\lambda_1^0 - \lambda_1^D}{\lambda_1^0 - \lambda_0^0}, \frac{\lambda_1^D - \lambda_0^0}{\lambda_1^0 - \lambda_0^0} \right\} , \tag{11.41}$$

or

$$v^*(D) = \min \{v(D), 1 - v(D)\} = \frac{u^*(D)}{C_{T_o}} , \tag{11.42}$$

whence

$$v^*(D) = D \frac{\delta}{\delta_R} = D \frac{|D_{T_o}|}{C_{T_o}} . \tag{11.43}$$

We shall call this the relative recurrence distance. It lies between 0 and 0.5. We thus have:

- $v^*(D) = 0$ , for a recurrence cycle of  $D$  days,
- $v^*(D) = 1/C_{T_o}$ , for a recurrence subcycle,
- $v^*(D) = 2/C_{T_o}$ , for a ground track passing at  $2\delta$  from a bound,

and so on.

To obtain a function of  $D$  which increases as we approach recurrence conditions, we define the function  $\Phi(D)$  which is simply the reciprocal of  $v^*(D)$ , i.e.,

$$\Phi(D) = \frac{1}{v^*(D)} . \tag{11.44}$$

We shall call this function the recurrence index. It is a dimensionless quantity. We now have

- $\Phi(D) = \infty \implies$  recurrence cycle of  $D$  days ,
- $\Phi(D) = C_{T_o} \implies$  recurrence subcycle for  $D$  ,
- $\Phi(D) = C_{T_o}/2 \implies$  ground track passing  $2\delta$  from a bound ,

- $\Phi(D) = C_{T_o}/3 \implies$  ground track passing  $3\delta$  from a bound ,
- other cases,
- $\Phi(D) > 2$  in every case.

This index provides a useful way of specifying cycles, subcycles, and other quantities related to recurrence for any satellite, whether it is intentionally recurrent or not.

### 11.7.2 Perfect or Imperfect Recurrence

The methods discussed above concern satellites with known recurrence elements. They allow one to find the orbital characteristics from these elements. However, we may encounter another type of problem: given the orbit of a satellite, we may wish to find its recurrence cycle. For this satellite,  $h$  and  $i$  are known, so  $P$  and  $\nu$  are determined, and hence also  $\kappa$ .

The day  $D$  corresponding to the recurrence cycle  $C_{T_o}$  will be such that the product  $\kappa D$  is closest to a whole number. It will therefore be the day giving the highest value of the recurrence index  $\Phi(D)$ , which we shall write  $\Phi_m$ .

Indeed, considering the expression (11.12) for  $\kappa$  as a function of the recurrence triple, the product  $\kappa D$  is

$$\kappa D = D\nu_o + D \frac{D_{T_o}}{C_{T_o}} ,$$

and since  $D\nu_o$  is an integer, we have

$$\text{fractional part of } |\kappa D| = v(D) ,$$

which implies that

$$\text{distance between } |\kappa D| \text{ and the nearest integer} = v^*(D) .$$

If  $\Phi_m$  is infinite, the satellite is recurrent, i.e., perfectly recurrent (and hence probably deliberately recurrent). If  $\Phi_m$  is not infinite, the recurrence is said to be imperfect.

When we seek the recurrence characteristics from the orbital elements, the recurrence may turn out to be imperfect, and in this case, the quantities  $u(D)$  and  $u^*(D)$  are not whole numbers.

### 11.7.3 Applications of the Recurrence Index

We shall now give several example applications to show how the recurrence index is used, where  $\Phi(D)$  is recorded over a period of several months. The keys to the graphs carry the orbital characteristics of the satellite, the values of the cycle, with the maximal recurrence index, which shows whether recurrence is perfect or not, and the two basic quantities in this analysis, namely, the daily orbital frequency  $\nu$  and the daily recurrence frequency  $\kappa$ .

The graphs clearly show the cycles and the subcycles which stand out to varying degrees. It is also very easy to distinguish those satellites that are deliberately recurrent from those with a certain level of recurrence but which have not been intentionally attributed any recurrent behaviour.

**Example 11.13** *Examples of the recurrence index for Sun-synchronous and non-Sun-synchronous satellites.*

- ▶ Unless otherwise mentioned, the satellites are Sun-synchronous and recurrence is intended.
- Change of subcycle leading to more rapid coverage of the base interval. We indicated earlier how, for the Landsat and IRS satellites, a modification of the subcycle  $D_{T_0}$  radically changed the way in which the base interval was covered. For IRS-1A and IRS-P2, shown in Fig. 11.13, the graph of the recurrence index in Fig. 11.14 illustrates this change. For IRS-1A, the ground track moves steadily across the base interval in 22 days. For IRS-P2, the ground track approaches the initial ground track on four occasions during the 24 day cycle, on days  $D = 5, 10, 14,$  and  $19,$  or roughly every 5 days.
- Recurrence index for satellites in the SPOT and Terra families. These two families of remote-sensing satellites include a great many satellites, whose recurrence index is shown in Fig. 11.19. For SPOT, the index has 4 peaks in the 26 day cycle, on days  $D = 5, 10, 16,$  and  $21,$  indicating a passage very close to the initial ground track roughly every 5 days. For Terra, there are two main peaks in the 16 day cycle, for days  $D = 7$  and  $9.$
- Recurrence index for a satellite with very long cycle. The satellite ADEOS-1 has a relatively long recurrence cycle, with  $C_{T_0} = 41$  days. The recurrence index is shown in Fig. 11.20 (upper). Referring to Example 11.9, we see that the two main intermediate peaks, for  $D = 15$  and  $26,$  correspond to  $u^* = 1,$  the next two, for  $D = 11$  and  $30,$  correspond to  $u^* = 2,$  and so on.
- Recurrence index for a non-Sun-synchronous satellite. The non-Sun-synchronous satellite TOPEX/Poseidon has the short recurrence cycle  $C_{T_0} = 10$  days, with two peaks for  $D = 3$  and  $7$  days (see Fig. 11.20 center). We note that  $\kappa$  and  $\nu$  have different values: the cycle takes  $C_T = 9.916$  days. For ICESat, below the subcycle  $D = 25,$  there are two peaks at  $D = 8$  and  $D = 15.$  The base interval is almost swept out in 8 days.
- Recurrence index for a satellite with very long recurrence cycle. Like all satellites engaged in systematically mapping a planet, the recurrence cycle will be very long because the swath of the main instrument will be very narrow. The satellite Z-Earth has a cycle of 274 days, with 4,149 revolutions. It has a subcycle of 7 days over 106 revolutions, which clearly shows on the graph of the recurrence index in Fig. 11.20 (lower). The horizontal axis goes up to 180 days and the maximum at 274 days is not therefore visi-



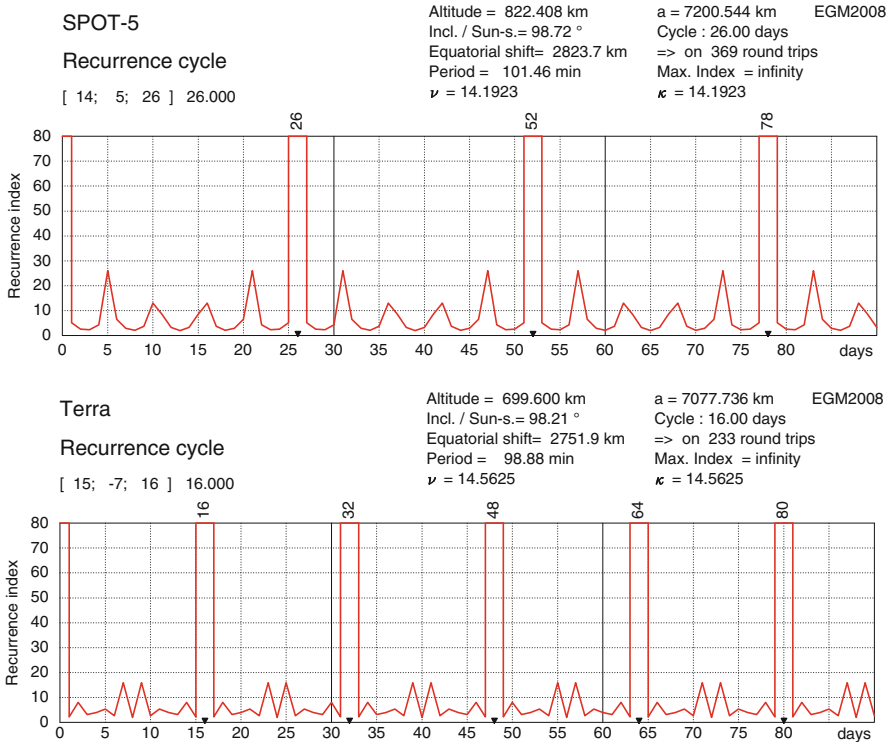


FIG. 11.19 : Recurrence index for satellites in the SPOT and Terra families.

ble. However, the symmetry relative to the abscissa  $C_T/2 = 137$  days is perfectly visible.



### 11.7.4 Recurrence Index and Orbital Characteristics

Recurrence is highly sensitive to changes in inclination and especially altitude. The recurrence index reveals this very clearly. The following three examples show how a change in altitude of a few hundred meters can completely change the recurrence characteristics after a few weeks. Precisely recurrent satellites are moved back onto the nominal orbit as soon as the altitude varies by a fraction of a kilometer. This maneuver is required between one and four times a month.

**Example 11.14** *Recurrence index for the Sun-synchronous satellite Earth-CARE.*

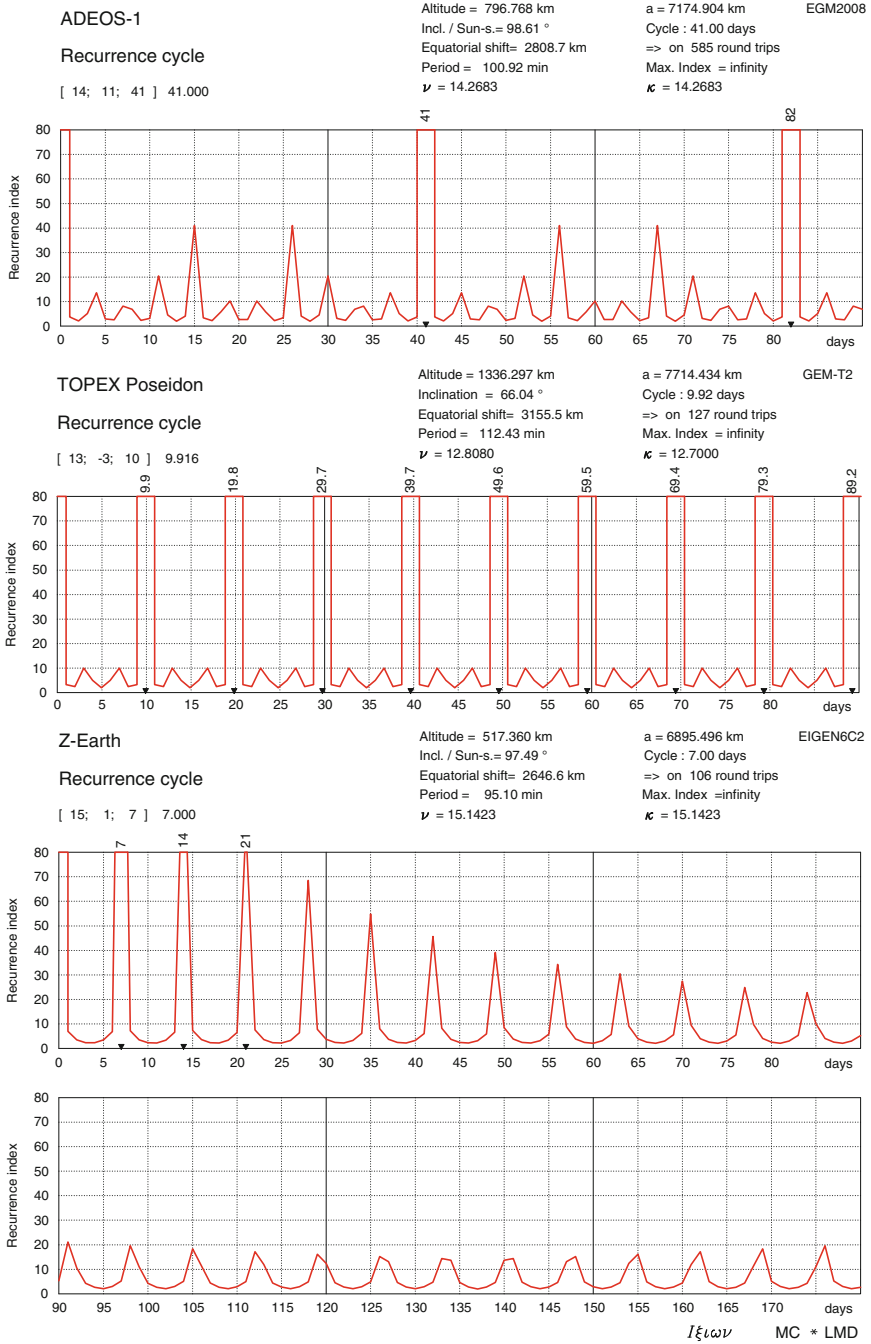


FIG. 11.20 : *Recurrence index for ADEOS-1, TOPEX/Poseidon, and Z-Earth.*

► The satellite EarthCARE will first be launched into the orbit denoted by EarthCARE [3a] in Table 11.3, which is the calibration orbit EarthCARE [cal]. Its altitude will subsequently be reduced by 1.294 km to join the mission orbit EarthCARE, denoted by EarthCARE [3b] in the table.

Figure 11.21 shows how the recurrence cycle goes from 9 days (blue) to 25 days (red) as a result of this change in altitude. ◀

**Example 11.15** *Recurrence index and altitude variations for SPOT-5.*

► Consider a Sun-synchronous satellite of the SPOT-5 type, with recurrence triple [14, 5, 26]. The recurrence index is plotted for various altitudes in Fig. 11.22 (upper) which graphs the function  $\Phi(D, \Delta h)$ . For  $\Delta h = 0$ , i.e., for the value of the altitude giving the required recurrence, we see that the main peaks occur for values of  $D$  that are multiples of  $C_{T_0} = 26$  days. The secondary peaks are clearly visible 5 days before and after the main peak. They become the main peaks for neighbouring altitudes. The recurrence triple [14, 5, 26], for  $\Delta h = 0$ , becomes [14, 4, 21] for  $\Delta h = +0.6$  km and [14, 3, 16] for  $\Delta h = +1.6$  km. Reducing the altitude, this initial recurrence behaviour becomes [14, 6, 31] for  $\Delta h = -0.4$  km, [14, 7, 36] for  $\Delta h = -0.7$  km, [14, 8, 41] for  $\Delta h = -1.0$  km, and so on. ◀

**Example 11.16** *Recurrence index and altitude variations for ERS-1.*

► We return to the Sun-synchronous satellite ERS-1, which has had three different recurrence cycles, as discussed in Example 11.3. The reference altitude will be taken to be the one for Recurrence Cycle 2, the 3 day cycle. This cycle appears for  $\Delta h = 0$  in Fig. 11.22 (lower). If we increase the altitude, with  $\Delta h = +6.358$  km, we obtain Recurrence Cycle 1, the 35 day cycle. If we reduce the altitude, with  $\Delta h = -5.936$  km, we obtain Recurrence Cycle 3, the 168 day cycle. ◀

## 11.8 Altitude Variations

The following analysis of altitude and frozen orbits is valid for any type of orbit, but only proves useful for near-circular LEO orbits. If the orbit is not close to circular, the altitude variations of the satellite during its revolutions are due to the eccentricity of the orbit, compared with which the flattening of the Earth is negligible. For MEO satellites, the altitude is not the relevant quantity. The same is true for GEO satellites, where the altitude is constant in time, since the satellite is stationary.

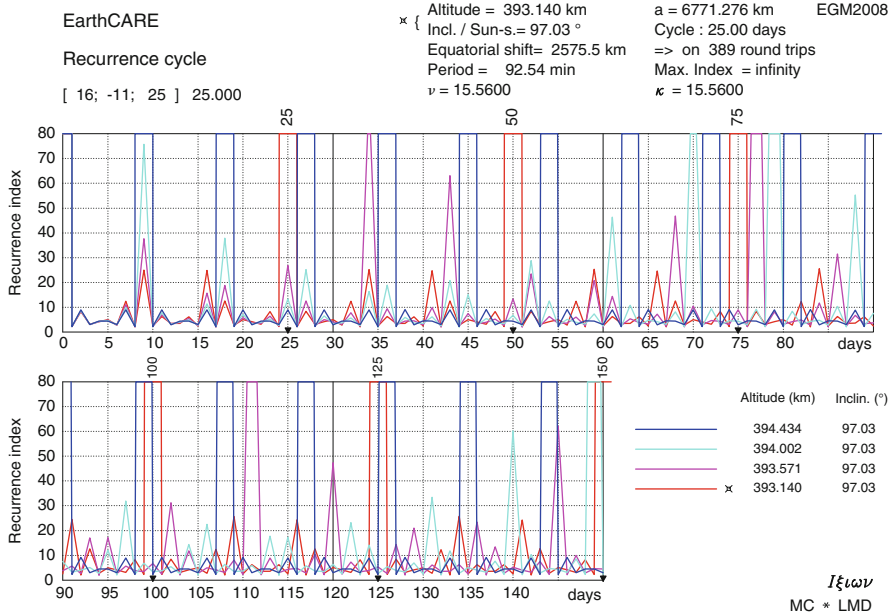


FIG. 11.21 : Recurrence index for EarthCare, with altitude changing from the calibration orbit to the mission orbit.

### 11.8.1 Altitude and Orbital Parameters

As we have seen, the altitude does not constitute a precise way of defining the position of the satellite, and indeed it is not one of the six orbital elements. The so-called near-circular, or even circular, orbit is never strictly circular and the Earth is not exactly spherical.

In previous chapters, devoted to the satellite ground track, the altitude has not been the main subject of discussion. However, it will be important in the following chapters, when we study the way in which the instruments aboard the satellite observe the Earth, i.e., how they “see” it from a certain height.

The altitude of the satellite is found from the difference between the radius vector  $r(a, e, \nu)$  defining the position of the satellite, as given by (4.40) and (4.58), and the Earth radius  $R_T(\psi)$  for the corresponding geocentric latitude  $\psi$ , treating the Earth as an ellipsoid of revolution with flattening  $f$ . This value  $R_T(\psi)$  is given by (1.37), in which  $R_\psi$  represents  $R_T(\psi)$  and where the semi-major axis  $a$  of the ellipse is taken equal to the equatorial radius  $R$ . We note that, with this definition, the altitude does not take into account the relief of the Earth’s surface.

When we work with quantities relating to both the position of the satellite and the terrestrial latitude, calculations are carried out with the geocentric

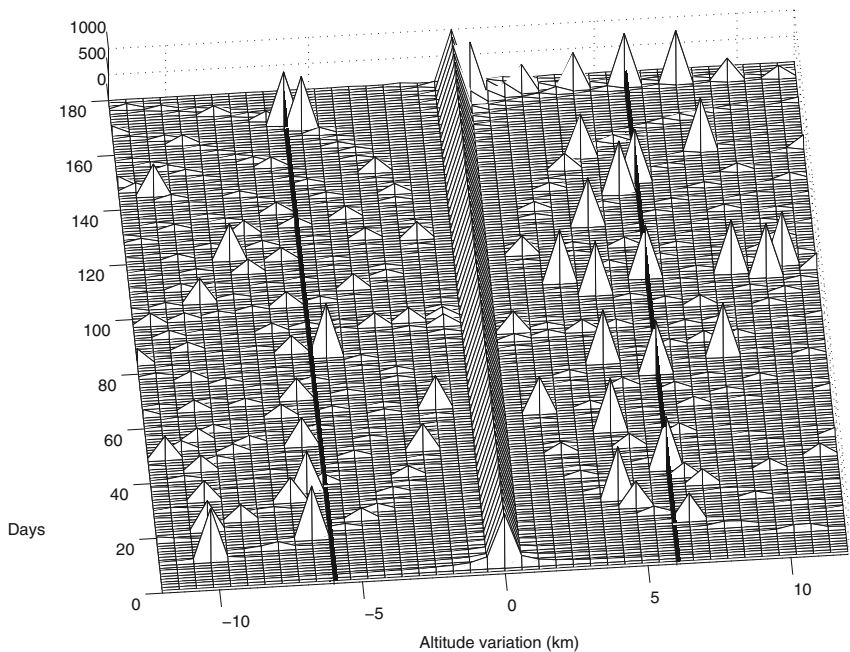
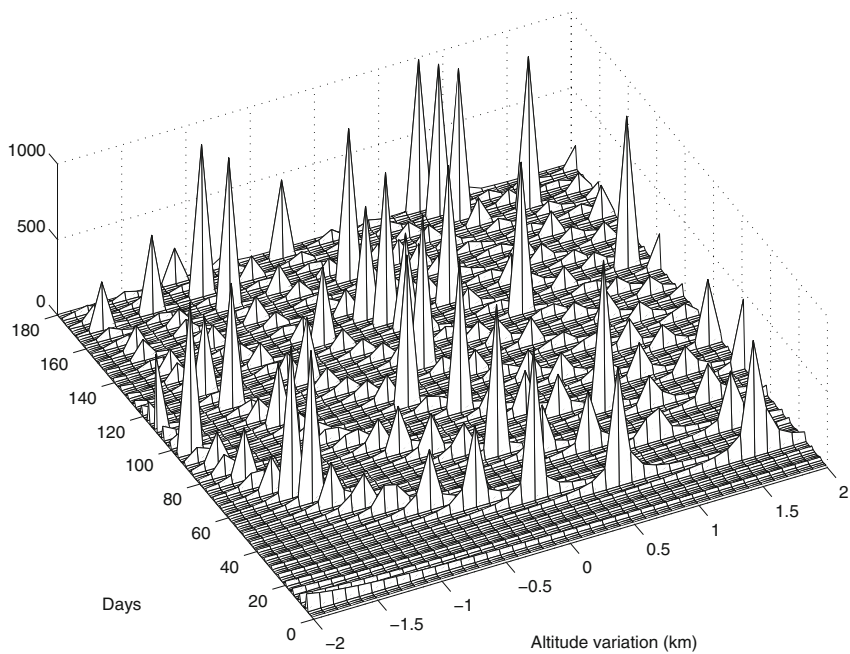


FIG. 11.22 : Recurrence index  $\Phi(J, \Delta h)$  as a function of the day  $D$  and the change in altitude  $\Delta h$ . The value  $\Phi$  infinite is shown as 1,000. Upper: satellite with the characteristics of SPOT-5. Lower: satellite with the characteristics of ERS-1. Explanations are given in Examples 11.15 and 11.16.

latitude  $\psi$ , and the results expressed in terms of the geodetic latitude  $\varphi$ , using (2.4). The altitude studied here is the one we defined as the geocentric altitude in Chap. 2. For LEO satellites, the difference with the geodetic altitude at the nadir is negligible, being just 1 or 2 m [see (2.37)].

We thus write the altitude  $h$  of the satellite in the form

$$h = r(a, e, v) - R_T(\psi) . \tag{11.45}$$

The latitude  $\psi$  is related to  $(i, \omega, v)$  by (6.65) and we obtain  $h$  in the form

$$h = h(a, e, i, \omega, v) . \tag{11.46}$$

The altitude is thus written as a function of five orbital elements. The element  $\Omega$  is not involved, since the terrestrial longitude is irrelevant here. This is the case already discussed in relation to (6.66).

The variation of the altitude is shown schematically in Fig. 11.23. In this figure, the axis  $Ox$  lies in the equatorial plane of the Earth, and the axis  $Oz$  is the polar axis. The difference between the two semi-axes of the ellipse representing the Earth is 21.3 km (see Example 2.1). The trajectory represented is that of a satellite in low, strictly polar orbit, with perigee over the North Pole ( $\omega = 90^\circ$ ). For an eccentricity of the order of  $10^{-3}$ , the distance  $FC$  between the focus  $F$  of the ellipse (center of attraction, center of the Earth) and the center  $C$  of the ellipse, equal to  $ae$ , is of the order of 8 km. The orbit is near-circular.

For a given revolution, we consider in (11.46) the mean values of the orbital elements  $a$ ,  $e$ ,  $i$ , and  $\omega$ . Instead of  $v$ , we have chosen  $\alpha$  to determine the position of the satellite on its orbit. We have already seen in (5.4) that this angle  $\alpha = \omega + v$  specifies the position of the satellite as measured from the ascending node.

The altitude  $h$  is thus expressed in terms of the position on orbit (argument of the latitude)  $\alpha$  by

$$h(\alpha) = r(\alpha) - R_T(\alpha) , \tag{11.47}$$

$$r(\alpha) = r[a, e, v(\omega, \alpha)] = \frac{a(1 - e^2)}{1 + e \cos v} , \tag{11.48}$$

$$R_T(\alpha) = R_T[R, f, \psi(i, \alpha)] = \frac{R}{\sqrt{\cos^2 \psi + \frac{\sin^2 \psi}{(1 - f)^2}}} , \tag{11.49}$$

with

$$v = v(\omega, \alpha) = \alpha - \omega , \quad \psi = \psi(i, \alpha) = \arcsin(\sin i \sin \alpha) .$$

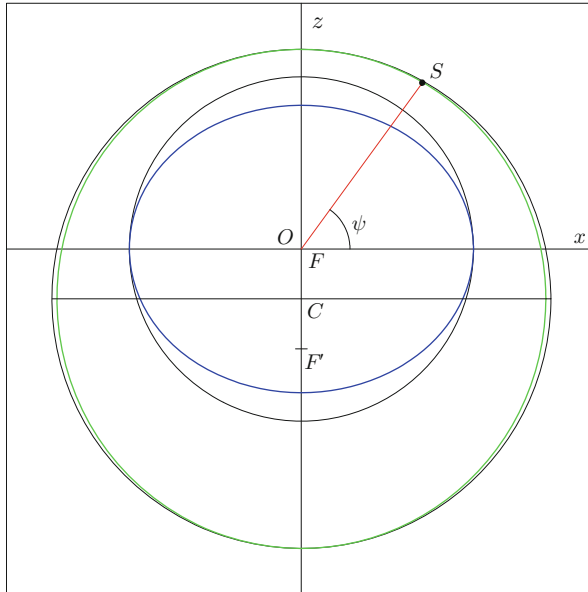


FIG. 11.23 : Schematic representation of the Earth ellipsoid, with center  $O$ , and the elliptical trajectory (polar orbit) of the satellite  $S$ , with center  $C$  and focus  $F$  identified with  $O$ . The principal circles of the ellipses are indicated. The eccentricities used in the figure have been greatly exaggerated compared with the true eccentricities.

## 11.8.2 Altitude During One Revolution

Defining the function  $h(\alpha)$  in this way, we note certain specific values of the altitude:  $h(0)$  at the equator (ascending node),  $h(\omega)$  at the perigee,  $h(\pi)$  at the equator (descending node), and  $h(\omega + \pi)$  at the apogee. The function  $r(\alpha)$  has period  $2\pi$  and amplitude  $ae$ . The function  $R_T(\alpha)$  has period  $\pi$  and its amplitude varies between 21.3 km for polar satellites (value of the product  $Rf$ ) and 0 for equatorial satellites, since in this case,  $R_T(\alpha) = R$  for all  $\alpha$ .

When we give the height of a satellite as a function of the position on orbit, we must specify the revolution, or at least the day, because of the displacement of the perigee.

For the satellites in near-circular orbits that we are concerned with here, the difference between the anomalies  $v$  and  $M$  is very small (see Figs. 4.5 (upper) and 4.6), and we will be able to replace  $\alpha$  by the time  $t$ , using the relation  $\alpha = 2\pi t/T$ .

**Example 11.17** *Altitude during one revolution of four Earth-observation satellites: WorldView-2, RazakSat, RapidEye-5, and Yao Gan-7.*

► The metric orbit elements are practically constant over several days. However, the argument of the perigee  $\omega$  can change quickly (apsidal precession). This is why the day and number of the revolution must be specified. We have used the NORAD data for 6 April 2010. The values of the orbital elements are indicated in the corresponding figure. For each satellite, the graphs are divided into two parts:

- On the lower part, the dashed curve gives

$$r(\alpha) - r(0) ,$$

and the continuous curve gives

$$R_T(\alpha) - R_T(0) .$$

- On the upper part, we have plotted the altitude relative to the altitude at the equator, i.e.,

$$h(\alpha) - h(0) ,$$

which is the difference between the two previous curves.

The altitude at the equator is obtained from

$$h(0) = \frac{a(1 - e^2)}{1 + e \cos \omega} - R .$$

For easier comparison of these variations, all graphs are plotted on the same scale.

**WorldView-2.** This is shown in Fig. 11.24 (upper). This Sun-synchronous satellite has a particularly low eccentricity. The dashed curve representing variations in  $r(\alpha) - r(0)$  is almost flat. Altitude variations arise mainly from variations in the radius of the Earth ellipsoid.

**RazakSat.** This is shown in Fig. 11.24 (lower). For this near-equatorial satellite, the variation in the radius of the Earth ellipsoid is almost zero. In this case, the altitude is only affected by the variation  $r(\alpha) - r(0)$  due to the eccentricity.

**RapidEye-5.** This is shown in Fig. 11.25 (upper). For this Sun-synchronous satellite, the variations in  $r(\alpha)$  and  $R_T(\alpha)$  are of the same order, around 20 km. Consequently,  $h(\alpha)$  varies by about 40 km.

**Yao Gan-7.** This is shown in Fig. 11.25 (lower). This Sun-synchronous satellite has similar curves to the last, with a different position of the perigee. ◀



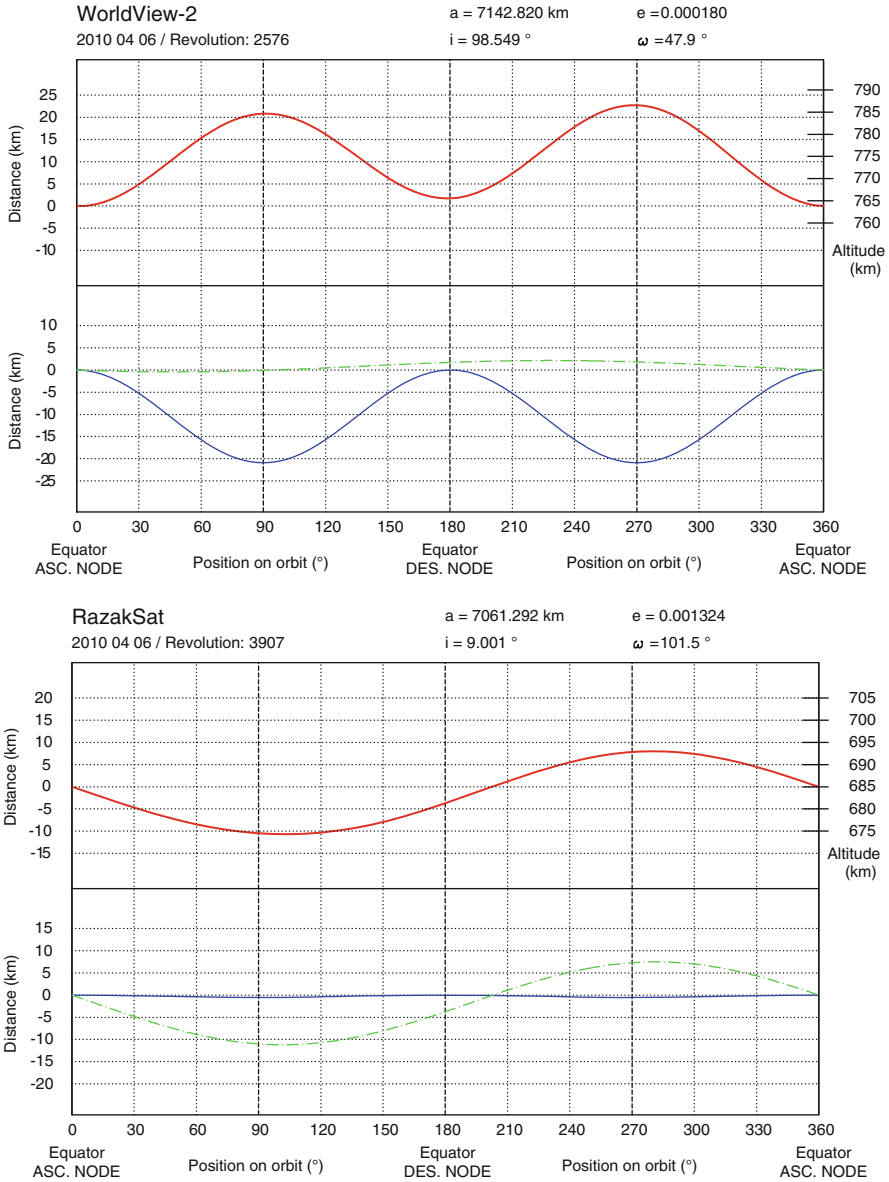


FIG. 11.24 : Altitude of a satellite as a function of position on orbit during one revolution. For more details, see the caption to Fig. 11.28. Upper: WorldView-2. Lower: RazakSat.

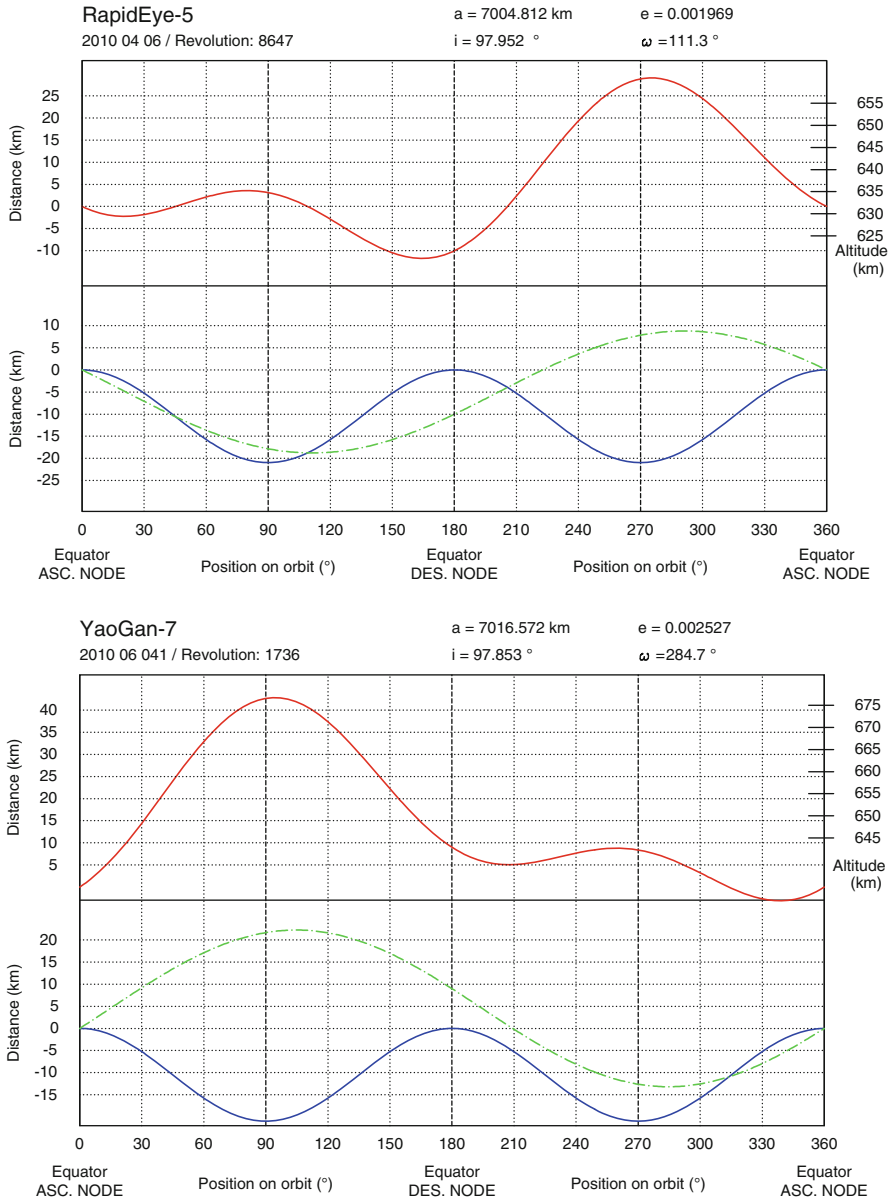


FIG. 11.25: Altitude of a satellite as a function of position on orbit during one revolution. For more details, see the caption to Fig. 11.28. Upper: RapidEye-5. Lower: Yao Gan-7.

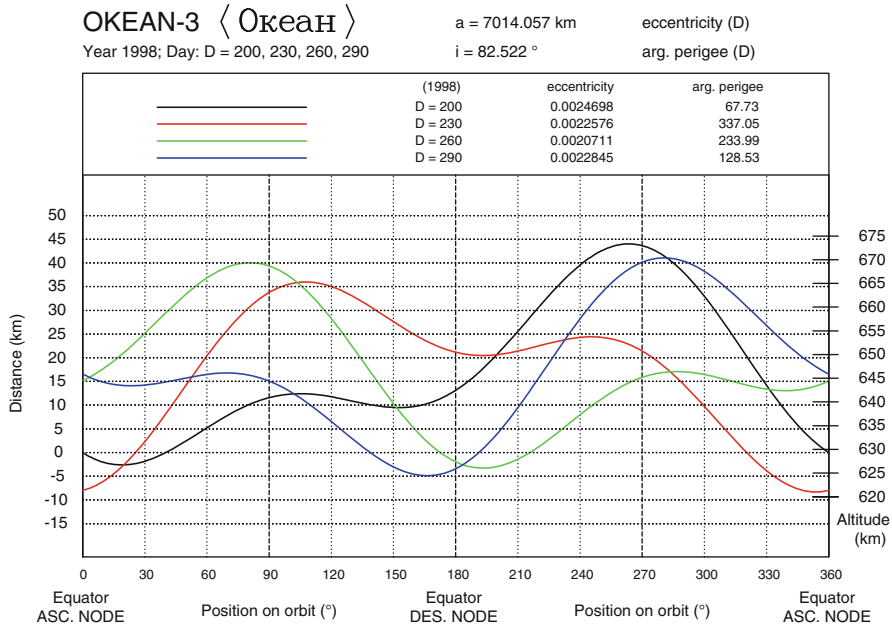


FIG. 11.26 : Altitude of *Okean-3* as a function of position on orbit  $\alpha$ , expressed in degrees. Four revolutions are shown, with an interval of 30 days. On the left, the origin of the distance scale is the equatorial crossing for the day origin ( $D = 200$ ). On the right, the scale indicates altitudes measured from the reference ellipsoid.

### 11.8.3 Variation of the Altitude over a Long Period

If we consider the altitude over a period of several months, the elements  $a$  and  $i$  remain almost constant. The eccentricity  $e$  fluctuates around a central value and the argument of the perigee  $\omega$  undergoes a secular variation to which one must add secondary periodic variations. The form of the altitude variation  $h(\alpha)$  over one revolution depends mainly on the value of  $\omega$  and to a lesser extent on the value of  $e$ , as we shall show in the following example.

**Example 11.18** *Altitude as a function of the position on orbit  $h(\alpha)$  for the satellite Okean-3, on various days of the year 1998.*

► The satellite Okean-01-3, generally called Okean-3, was launched on 4 June 1991. Figure 11.26 shows the altitude  $h(\alpha)$  for 4 days during the year 1998, at intervals of 30 days:  $D = 200$  (19 July),  $D = 230$  (18 August),  $D = 260$  (17 September),  $D = 290$  (17 October). During this 90 day period,  $a$  did not change significantly from  $a = 7,014.051 \text{ km}$ , while  $i$  varied between  $82.521^\circ$  and  $82.523^\circ$ . The eccentricity fluctuated between  $2.07 \times 10^{-3}$  and  $2.47 \times 10^{-3}$ .

For its part, the argument of the perigee varied by  $-90.68^\circ$ ,  $-103.06^\circ$ , and  $-105.46^\circ$  in each of the three 30 day intervals. A small, long-period variation (of the order of a few months) is superposed on the secular variation (proportional to the time) in  $\omega$ . Calculating the mean apsidal precession rate, we find

$$\dot{\omega} = -\frac{360 + 67.73 - 128.53}{90} = -\frac{299.20}{90} = -3.32 \text{ deg/day} .$$

This agrees with the value found with (7.16), which would give  $\dot{\omega} = -3.26$  deg/day. We see how, for  $\omega$ , the periodic variations are superposed on the secular variation. The values of  $e(D)$  and  $\omega(D)$  are indicated in Fig. 11.26. The graphs of  $h(\alpha)$  have been plotted for the 4 days chosen. The left-hand scale takes as origin the altitude at the equatorial crossing for day  $D = 200$ . The right-hand scale indicates the altitude relative to the reference ellipsoid. ◀

## 11.9 Frozen Orbits

### 11.9.1 Definition of a Frozen Orbit

In the expression for  $h$  given by (11.46), we see that the altitude of the satellite relative to its given subsatellite point varies in time, very slightly from one revolution to the next, but quite significantly over a time span of several days, as we saw in Example 11.18. When we require a satellite to be recurrent, with cycle  $C_T$ , the aim is to obtain identical viewing conditions every  $C_T$  days. However, when we arrange for recurrence, it is the ground track which is fixed, not necessarily the altitude.

This may be a drawback for Earth-observation satellites, for which one generally requires the altitude to be constant for a given subsatellite point, from one crossing to the next, in order to compare the images obtained at different dates. We would thus like to arrange for the altitude to depend only on the latitude of the subsatellite point, without variation in time. If such conditions are satisfied, the orbit is said to be frozen.<sup>6</sup> Note that the freezing of an orbit is independent of its recurrence characteristics, but that, in practice, only recurrent satellites (whether Sun-synchronous or otherwise) have frozen orbits.

### 11.9.2 Determining the Frozen Parameters

Consider now the relation (11.46) giving the altitude  $h$  of the satellite above an arbitrary point specified by the position on orbit  $\alpha$ . This altitude,

---

<sup>6</sup>The first publications treating the subject of frozen orbits date back to 1965. They concerned satellites in low orbit around the Moon. The term “frozen orbit” was first used to describe Seasat in 1976.

for this point of geocentric latitude  $\psi$ , will be denoted by  $h_\alpha(t)$ . With (11.46), we see that it varies in time through the osculating, i.e., instantaneous, orbital elements:

$$h_\alpha(t) = h[a(t), e(t), i(t), \omega(t)] . \quad (11.50)$$

We only take into account long period or secular variations here. Short period variations are averaged over one orbital revolution. Under such conditions, as discussed in Chap. 6 and shown schematically in Fig. 6.4, the semi-major axis  $a$  does not change. Equation (6.95) shows that, as long as the inclination is nonzero, the variation in  $i$  is negligible compared with the variation in  $e$ , which is illustrated in Example 6.1.

Equation (11.50), which came from (11.46), thus simplifies to

$$h_\alpha(t) = h[e(t), \omega(t)] . \quad (11.51)$$

Consequently, the two parameters that concern us here,  $e$  and  $\omega$ , undergo a long period variation due to the odd zonal terms, mainly  $J_3$ , while  $\omega$  also undergoes a secular variation due to the even zonal terms, mainly  $J_2$ . Writing down the equations representing  $e$  and  $\omega$ , whose values result from a complete treatment of the Lagrange equations, we must solve

$$\begin{cases} \dot{e} = 0 , \\ \dot{\omega} = 0 , \end{cases}$$

whence  $\dot{e} = de/dt$  and  $\dot{\omega} = d\omega/dt$  are functions of the unknowns  $e$  and  $\omega$ , and to a lesser extent the other orbital elements.

It is a very complex exercise to establish the conditions for a frozen orbit in the general case. Here we shall find them for an expansion up to degree 3. Using the perturbing potential  $\mathcal{R} = \mathcal{R}_2 + \mathcal{R}_3$  calculated in Chap. 6 in the Lagrange equations, we obtain

$$\frac{\dot{e}}{n} = \frac{3}{2(1-e^2)^2} J_3 \left(\frac{R}{a}\right)^3 \left(1 - \frac{5}{4} \sin^2 i\right) \sin i \cos \omega , \quad (11.52)$$

$$\frac{\dot{\omega}}{n} = \frac{3}{(1-e^2)^2} J_2 \left(\frac{R}{a}\right)^2 \left(1 - \frac{5}{4} \sin^2 i\right) \left[1 + \frac{1}{2e(1-e^2)} \frac{J_3}{J_2} \left(\frac{R}{a}\right) \sin i \sin \omega\right] . \quad (11.53)$$

If we neglect  $J_3$  in (11.52) and (11.53), we find  $\dot{e} = 0$  and the relation (6.74), respectively.

### Inclination Close to the Critical Inclination

By the very definition of the critical inclination given in (6.79), the term  $[1 - (5/4) \sin^2 i]$  is zero. We thus have  $\dot{\omega} = 0$  and  $\dot{e} = 0$ . The orbit is frozen, whether the eccentricity is low or high.

For inclinations close to the critical inclination, large oscillations in  $\omega$  are due to the  $J_4$  term (and following) since the contribution from  $J_2$  and  $J_3$  is very small. The expressions (11.52) and (11.53) must be expanded to higher degrees. It can then be shown that, for  $i$  between about  $53^\circ$  and  $74^\circ$  (or between  $106^\circ$  and  $127^\circ$ ), the eccentricity for a frozen orbit varies between 0 and  $30 \times 10^{-3}$ .

### Inclination Far from the Critical Inclination

For inclinations differing significantly from the critical value, i.e., the ranges  $i < 53^\circ$ ,  $74^\circ < i < 106^\circ$ ,  $i > 127^\circ$ , as is usually the case for Sun-synchronous satellites, (11.52) shows that

$$\omega = \pm 90^\circ \implies \dot{e} = 0. \quad (11.54)$$

Substituting this value of  $\omega$ , denoted by  $\omega_F$ , into (11.53), we obtain  $\dot{\omega} = 0$  by setting the expression between square brackets equal to zero, i.e., setting

$$e_F = e(\omega_F) = -\frac{1}{2} \frac{J_3}{J_2} \frac{R}{a} \sin i \sin \omega_F. \quad (11.55)$$

Values for the frozen orbit carry the subscript F. Since this calculation refers to near-circular orbits, we have neglected  $e^2$  compared with 1 in (11.53). We could also use (6.94).

The sign of  $\sin \omega_F$  depends on the sign of  $J_3$  in such a way that the expression for  $e$  comes out positive. For the Earth, with  $J_3$  negative, we take

$$\omega_F = +90^\circ, \quad (11.56)$$

$$e_F = -\frac{J_3}{2J_2} \frac{R}{a} \sin i. \quad (11.57)$$

When the orbit is frozen, the perigee of Sun-synchronous LEO satellites is thus practically over the North Pole.

### Frozen Eccentricity

For the SPOT satellites, (11.57) implies that  $e_F = 1.03 \times 10^{-3}$ . The exact value of the frozen eccentricity is  $e_F = 1.14 \times 10^{-3}$ . For LEO satellites,  $e_F$  is always small, of the order of  $10^{-3}$ , and the orbit is thus near-circular.

Many recurrent satellites, Sun-synchronous or otherwise, have a frozen orbit. For some satellites, it is essential that the parameters  $e$  and  $\omega$  be maintained<sup>7</sup> at the reference values<sup>8</sup>  $e_F$  and  $\omega_F$ .

<sup>7</sup>For example, for the satellite TOPEX/Poseidon, between 1992 and 2002, we may note the following exceedingly narrow ranges of variation for the orbital elements:  $e_F$  from  $0.73 \times 10^{-3}$  to  $0.83 \times 10^{-3}$ ,  $\omega_F$  from  $264^\circ$  to  $270^\circ$ ,  $i$  from  $66.037^\circ$  to  $66.046^\circ$ ,  $a$  from 7,714.422 to 7,714.436 km.

<sup>8</sup>The true values as obtained from the NORAD elements often differ somewhat from the nominal values. In Example 11.1, we note that the true values of the eccentricity of SPOT-5 are well below the nominal values.

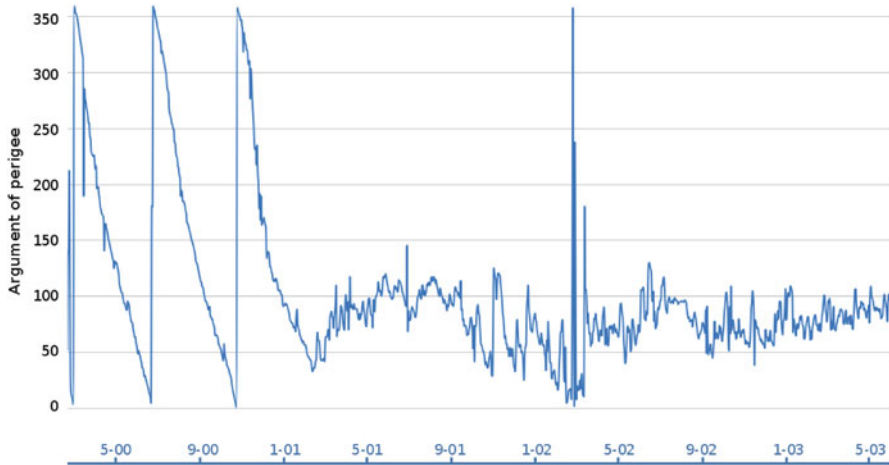


FIG. 11.27 : Variation of the argument of the perigee  $\omega$  of the satellite Terra at different dates. Transition from a revolving to frozen perigee ( $\omega = 90^\circ \pm 20^\circ$ ).

We should also note that some satellites require a non-frozen orbit. To ensure that the perigee does not remain permanently in the vicinity of the North Pole and that the gravitational field is sampled at different altitudes, the geodetic satellite GOCE has variable eccentricity, ranging between 0 and  $4.5 \times 10^{-3}$ . Hence, the altitude varies between 236 and 282 km.

**Example 11.19** *Variation in the position of the perigee for the satellite Terra and transition to a frozen orbit.*

► For the Sun-synchronous satellite Terra, launched on 18 December 1999, the argument of the perigee  $\omega$  had a secular variation between  $0^\circ$  and  $360^\circ$ , occurring at the approximately constant rate of  $\dot{\omega} \approx -3.3^\circ$  per day. However, from 5 February 2001, by varying the eccentricity, the perigee no longer revolves, but sits at the value  $\omega = 90^\circ$ , to within  $20^\circ$  (see Fig. 11.27). ◀

### 11.9.3 Altitude of a Satellite on a Frozen Orbit

In the case of a frozen orbit, where the ellipse representing the satellite trajectory is fixed in the orbital plane, we may calculate the altitude of the satellite as a function of a single variable, e.g.,  $\alpha$ , over a period  $T$ . The altitude variation will then repeat itself identically with period  $T$ . We give here an example calculation of an altitude and altitude variation as a function of position on orbit.

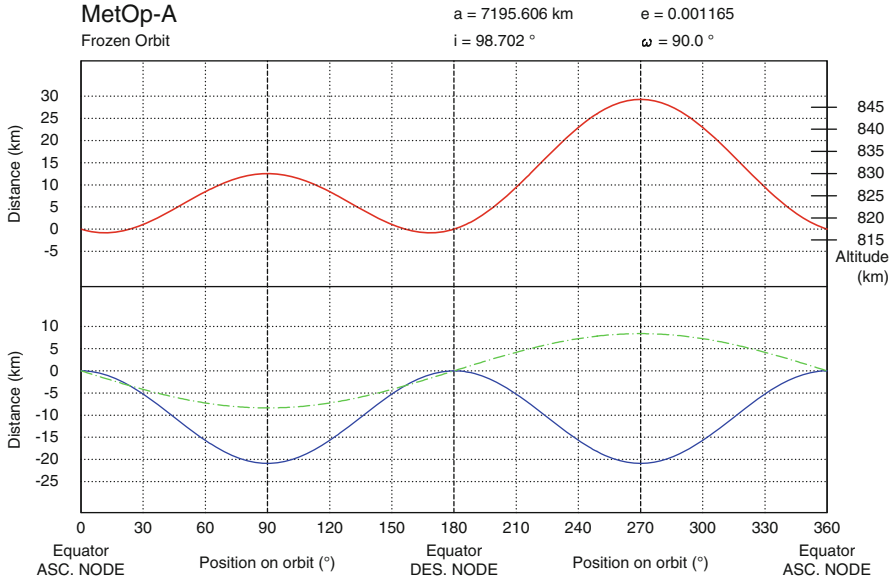


FIG. 11.28 : Altitude of MetOp-A in a frozen orbit. The altitude is given as a function of the position on orbit (argument of latitude)  $\alpha$ , given in degrees. Lower: the difference between the distance  $r(\alpha)$  of the satellite from the center of the Earth and the distance  $r(0)$  at its ascending node crossing is shown by a dashed curve, while the difference between the Earth radius  $R_T(\alpha)$  and the equatorial radius  $R = R_T(0)$  is shown by a continuous curve. Upper: difference between the first and second of the two curves in the lower part of the figure. Left: scale for the differences. Right: scale for the altitudes relative to the reference ellipsoid.

**Example 11.20** Calculate the altitude as a function of the position on orbit for the satellite MetOp-A, which has a recurrent and frozen Sun-synchronous orbit.

► The orbital characteristics of MetOp-A as provided by the ESA are as follows:

- Sun-synchronous inclination.
- Recurrence with 412 revolutions in 29 days.
- Frozen orbit with eccentricity  $e = e_F = 0.0011655$  and  $\omega = \omega_F = 90.0^\circ$ .

The satellite MetOp-B is on the same orbit, and the future MetOp-C should also be.

Using the method presented in Example 11.1, we may calculate the orbital elements from the recurrence triple [14, 6, 29], whence we obtain:

- semi-major axis  $a = 7,195.606$  km,
- Sun-synchronous inclination  $i = i_{HS} = 98.702^\circ$ .



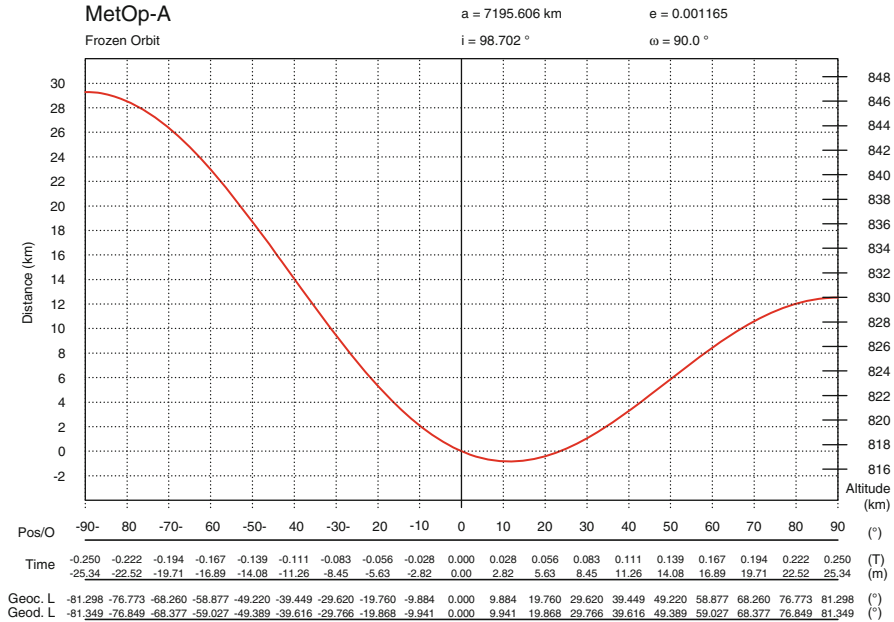


FIG. 11.29 : Altitude of MetOp-A in a frozen orbit. The altitude is given as a function of the position on orbit (Pos/O)  $\alpha$ , given in degrees. The time is given as a fraction of the period and in minutes, with origin at the equatorial crossing (ascending node). The geocentric latitude of the satellite  $\psi$  (Geoc. L) and the geodetic latitude of the nadir  $\varphi$  (Geod. L) are given for each specified value of  $\alpha$ . Close-up of Fig. 11.28.

Given  $a$  and  $e$ , we can calculate  $b$  and  $c$ :

$$c = ae = 8.386 \text{ km}, \quad b = a\sqrt{1 - e^2} = 7,195.601 \text{ km}, \quad a - b = 0.005 \text{ km}.$$

We have already noted that the orbit of a satellite of this kind is a circle shifted by 8 km relative to the center of the Earth (see Example 1.2). The distance  $c$  is proportional to  $e$ , whereas the difference between the semi-axes is a function of  $e^2$ :  $a$  and  $b$  are thus equal to within 5 m.

In Fig. 11.28, distances are expressed as a function of the position on orbit  $\alpha$ . The graph of  $r(\alpha) - r(0)$  shows a difference of  $2ae = 16.772$  km between the radius at apogee  $r_a = r(\omega_F + \pi)$  and the radius at perigee  $r_p = r(\omega_F)$ . Concerning the Earth ellipsoid, the maximum latitude attained, for  $\alpha = \omega_F$ , is  $\psi = \pm\psi_m$ , with  $\psi_m = 180 - i = 81.298^\circ$ , which gives at the perigee

$$R_T[\psi(\omega_F)] = R_T(\psi_m) = R_m = 6,357.240 \text{ km}, \quad R - R_m = 20.897 \text{ km}.$$

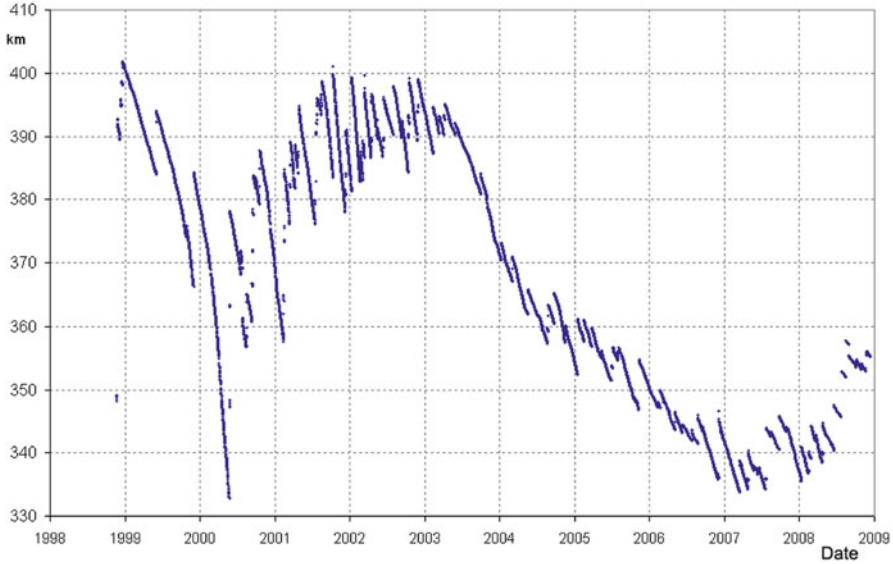


FIG. 11.30 : Altitude of the International Space Station (ISS) at different dates over a little longer than 10 years, from 1998 to 2009. The space station, which is at a relatively low altitude, must be rather frequently raised. Credit: NASA.

We now calculate the values of the altitude for particular points on the orbit (equator, ascending and descending nodes, perigee, and apogee):

$$\begin{aligned}
 \text{Ascending node} \quad h(0) &= a(1 - e^2) - R = 7195.596 - 6378.137 = 817.459 . \\
 \text{Perigee} \quad h(\pi/2) &= a(1 - e) - R_m = 7187.223 - 6357.240 = 829.983 . \\
 \text{Descending node} \quad h(\pi) &= a(1 - e^2) - R = 7195.596 - 6378.137 = 817.459 . \\
 \text{Apogee} \quad h(3\pi/2) &= a(1 + e) - R_m = 7203.989 - 6357.240 \\
 &= 846.749 .
 \end{aligned}$$

$$h(\pi) = h(0) , \quad h(3\pi/2) = h(\pi/2) + 2ae .$$

The minimum altitude is 816.623 km, reached when  $\alpha = 11.5^\circ$  and  $\alpha = 168.5^\circ$ , which corresponds to a latitude of  $11.4^\circ$  ( $\psi = 11.37^\circ$ ,  $\varphi = 11.43^\circ$ ). The maximum altitude is reached at the apogee.

Since the position of the perigee is symmetric with respect to the two nodes for this satellite, the altitude depends only on the latitude  $\varphi$  and we do not have to specify the crossing direction (ascending or descending) of the orbit. In Fig. 11.29, we have indicated the geocentric latitude on the horizontal axis, between its two extreme values  $-\psi_m$  and  $+\psi_m$ , and also the geodetic latitude of the nadir (which takes into account the altitude of the satellite, as explained in Chap. 2). ◀

## 11.10 Altitude and Atmospheric Drag

As we have seen in Chap. 6 when considering non-conservative perturbations, atmospheric drag causes the satellite to drop in altitude. In the examples in this chapter where we have discussed satellite altitude, the effects of drag were not mentioned, either because they were negligible, or because they were frequently compensated, which made them practically imperceptible.

Here we give two examples where the drop in altitude due to drag is significant. In Example 11.21, we show how the orbit of the International Space Station (ISS) is frequently “boosted”, and in Example 11.22, how atmospheric drag can play a fatal role for a spacecraft.

**Example 11.21** *Altitude of the International Space Station (ISS) over the past 11 years.*

► The satellite ISS is in a relatively low LEO orbit and requires frequent energy boosts to remain at a suitable altitude, as can be seen from Fig. 11.30. In this graph supplied by NASA, consider the continuous part of the curve

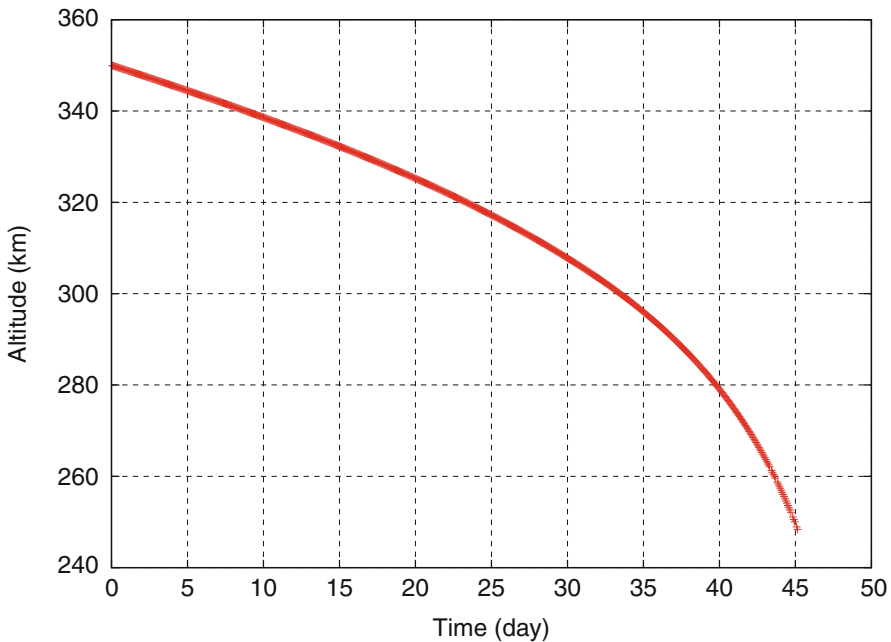


FIG. 11.31 : *Altitude of the satellite in Example 11.22 as a function of time. The altitude drops more and more quickly and the satellite ends by burning up in the lower levels of the atmosphere. Altitude in km, time in days.*

at the beginning of 1999. This linear part indicates that the altitude changed from  $h = 400.0$  km (day  $D = 1$ ) to  $h = 389.9$  km (day  $D = 150$ ), implying a steady drop by 16.1 km over 149 days, or 108 m per day. With  $T = 93$  min, and hence  $\nu = 15.5$ , the drop in altitude per revolution  $\Delta_1 a$  is given by

$$\Delta_1 a = \frac{108}{15.5} = 7.0 \text{ m} .$$

From the general appearance of the graph, we see that this value is representative of the general trend. We use (6.121) with  $a = 6,770$  km to obtain

$$B\rho = \frac{1.11}{a^2} = 2.42 \times 10^{-14} .$$

Using (6.118), we can find the ballistic coefficient  $B$ , taking  $C_d = 2.3$ ,  $S = 600 \text{ m}^2$ ,  $M_s = 250$  tonnes (in 1999, while the mass of the space station went up to 417 tonnes in 2011):

$$C_d = \frac{2.3 \times 600}{2.50 \times 10^5} = 5.5 \times 10^{-3} ,$$

$$\rho = \frac{2.42 \times 10^{-14}}{5.5 \times 10^{-3}} = 4.4 \times 10^{-12} .$$

We thus obtain an average value for the atmospheric density at this altitude (see Table 6.4). ◀

**Example 11.22** *Fall of a low-orbiting satellite ( $h = 350$  km) during a period of maximal solar activity.*

► We consider a satellite in LEO orbit with  $h = 350$  km,  $i = 60^\circ$ , and with ballistic coefficient  $B = 0.0160$  (as for SPOT-4). We choose the scenario of maximal solar activity in the atmospheric model MSIS-90 (see Table 6.4). Under these conditions, the software *Ixion* calculates the change in the orbit in a step by step manner. The drop in altitude  $h = a - R$  is shown in Fig. 11.31. Initially proportional to the time (between  $D = 0$  and 25), the decrease gets faster from  $D = 30$ , and when  $D = 45$ , the satellite reaches an altitude of 250 km. At this point, the craft is doomed to almost immediate disintegration. ◀

# Chapter 12

## View from the Satellite

In the preceding chapters, we have discussed the satellite orbit, position, and ground track. All this can be deduced from the position  $S$  of the satellite as viewed from the center of attraction  $O$ , which is the center of the Earth. The time has come to look at things from a different standpoint: we shall now be concerned with the view from an instrument carried aboard the satellite (see Fig. 12.2). The main difference is that we are now looking at things from the point of view of the satellite  $S$ . As a consequence, this chapter is principally concerned with observation satellites.

### 12.1 Swath of an Instrument

#### 12.1.1 Local Orbital Frame

Up to now the satellite has been treated as a point, or at least, we have considered only the motion of its center of gravity. But as a vehicle, the satellite can also move about its center of inertia. Although this kind of motion is largely irrelevant for the purposes of calculating its trajectory, it is of course crucial when we come to ask what the instruments aboard will be able to view. If we want to produce an image of the Earth, we must not aim at the sky, and conversely!

Manipulation of the angular orientation of the satellite is called attitude control. The attitude of the satellite tends to vary under the action of couples, which may be external, due to radiation pressure or atmospheric drag on solar panels, or internal, due to mechanical motion of the instrument motors. A stabilisation system is thus required to maintain the satellite in the right position relative to the local orbital frame.

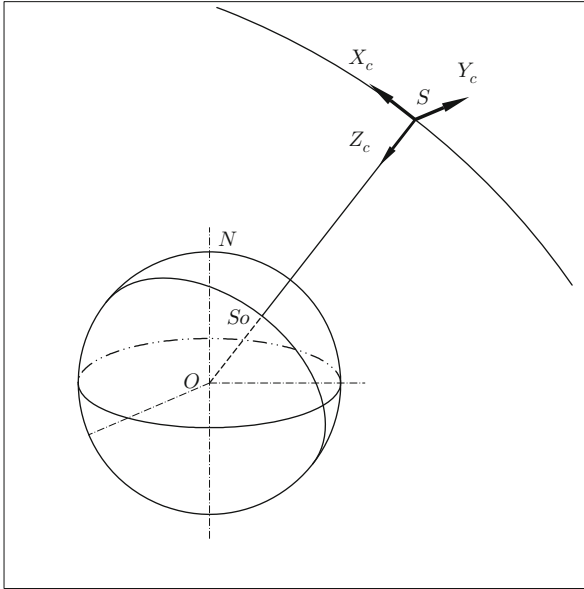


FIG. 12.1 : Cardan frame centered on the satellite  $S$ . The ground track goes through the sub-satellite point  $S_0$ . The axis  $SZ_c$  points toward the center of the Earth and the axis  $SY_c$  is perpendicular to the orbit. If the orbit is circular, the axis  $SX_c$  lies along the velocity vector.

For any point  $S$  on the orbit, this frame is defined by the following three axes, illustrated in Fig. 12.1:

- yaw axis  $SZ_c$ , directed towards the center of the Earth, also called the nadir axis,
- pitch axis  $SY_c$ , directed normally to the orbital plane,
- roll axis  $SX_c$ , lying in the orbital plane and completing a right-handed orthogonal system of axes. This axis lies along the velocity vector of the satellite when the eccentricity is zero.

We shall refer to the axes of the local orbital frame as the Cardan axes, with the appropriate subscript.<sup>1</sup> The angles obtained by rotation relative to these axes are the Cardan angles, defined in Sect. 5.4.

### 12.1.2 Scanning Modes

There are various ways for an instrument to look at the Earth. The sensor can be equipped with a fixed objective relative to the satellite, but in most cases, the sensor is mobile (either itself or through the action of a mirror) along some axis of rotation.

<sup>1</sup>The axes are sometimes taken in a different order, with a different orientation, e.g.,  $SZ_c$  pointing in the opposite direction to the nadir. However, in every case, the triad is right-handed and orthogonal and the direction of the nadir corresponds to one of the axes.



FIG. 12.2 : *Oblique view from the satellite Aqua. Late November 2011 offered mostly cloud-free skies and a compelling view of the entire length of Baja California and the Pacific coast of Mexico. In the midst of the clarity, strong northeasterly winds stirred up dust storms on the mainland and the peninsula. The natural-color images required to make this oblique view were acquired on 27 November 2011, by MODIS (Moderate Resolution Imaging Spectroradiometer) on NASA's Aqua satellite. The Ocean Color Team at NASA Goddard processes images like this to help assess the presence of sediment and plankton in the sea. Dust storms interfere with that processing, as the sandy aerosols block much of the incoming sunlight and the outgoing, reflected light. Credit (image and caption): Norman Kuring, Mike Carlowitz, NASA, Ocean Color Team (NASA Goddard), University of Wisconsin.*

To begin with, we may define three basic scanning modes, when the instrument rotates relative to one of the three Cardan axes. In the first two cases, the instrument axis and the axis of rotation are the same, whereas in the third the instrument axis makes a constant angle with the axis of rotation. These three scanning modes are as follows:

- With rotation about  $SX_c$ , the instrument scans perpendicularly to its displacement. This is orthogonal or cross-track scanning.
- With rotation about  $SY_c$ , the instrument scans along the ground track. This is along-track scanning.
- With rotation about  $SZ_c$ , the instrument scans in conical mode, defined by the half-angle at the apex of the cone, which is the angle between the instrument axis and the axis of rotation.

During observation, the smallest detected element is called a pixel.<sup>2</sup> The set of all such elements viewed on the ground in a single scan is called the swath.

The technical features of the various optical instruments and sensors are not the concern of this book. We shall consider only the geometrical aspects of scanning.

### Scanning Mode for LEO Satellites

An instrument aboard an LEO satellite can use one of the three elementary scanning modes listed above. It can also alternate between the first two, or scan obliquely by a rotation of the instrument about an axis in the plane  $SX_cY_c$ .

In orthogonal scanning, some instruments sweep from side to side across the swath,<sup>3</sup> pixel by pixel as it were. Other instruments simultaneously record all the pixels in one row, and some can even record over several rows at once.<sup>4</sup>

### Scanning Mode for GEO Satellites

Concerning the way images are acquired, for one cannot really say that there is a swath in this case, geostationary satellites fall into two main categories.

For satellites with three-axis stabilisation, such as GOES (from GOES-8) or GOMS, one axis is parallel to the polar axis, one axis points to the center of the Earth, and one axis lies along the satellite's velocity vector. The sensor scans the disk presented by the Earth.

For rotating satellites, such as the METEOSAT, GMS, or FY-2 series, the axis of rotation is parallel to the polar axis. In the case of METEOSAT (first and second generation), the satellite rotates exactly 100 times a minute. A mirror is used to sweep across the Earth's disk. For the satellites METEOSAT-1 to -7 (first generation), this east–west scanning is carried out from south to north at a rate of 2,500 rows in 25 min. From METEOSAT-8 (MSG-1, second generation), 3,712 rows are scanned in 15 min. We note that, with this method, although it gives excellent results, the Earth is only viewed over  $17.4^\circ$  per revolution, i.e., the sensor views the Earth for 4.8 % of the time, spending the other 95.2 % of the time looking into the darkness of space.

---

<sup>2</sup>The word “pixel” was coined in 1969, by contracting *picture* and *element*.

<sup>3</sup>To get some idea, on those satellites which carry it, the instrument known as ScaRaB investigates the radiation budget by scanning every 6 s. The effective part of the scan lasts for 3.18 s. For the remaining 2.82 s, the instrument does a calibration sighting and repositions itself.

<sup>4</sup>Charge-coupled devices (CCD) can acquire a row of pixels (1D-CCD, one dimension) or several rows (2D-CCD, two dimensions). Aboard SPOT-4, the HRVIR instrument uses the so-called push-broom mode with a 1D-CCD. The optical instrument is based on a telescope whose field of view is covered instantaneously by a row of 1,728 detectors, each corresponding to one pixel. In the case of the POLDER instrument, carried aboard ADEOS-1 and -2 and Parasol, the use of 2D-CCDs makes it possible to acquire a set of rows simultaneously, rather than just one.



Whatever method is used, the “swath” of a geostationary satellite will be treated like the cross-track swath of a low-orbiting satellite: for a point  $P$  viewed on Earth, we consider the plane  $SS_0P$  (see Fig. 12.3) and define the angles of sight as for an LEO cross-track swath. We thus define the angle  $S_0SP$  which plays the role of the half-swath angle  $f$  discussed below.

## 12.2 Swath Viewing Geometry

### 12.2.1 Definition of Angles

For the following general relations concerning instrumental swath, we shall treat the Earth as spherical. For more accurate calculations, we use the ellipsoid.

Figure 12.3 shows all angles relevant to the satellite view and swath. The satellite  $S$  is in orbit around the Earth, at distance  $OS = d$  from the center  $O$ . The subsatellite point is denoted by  $S_0$ . Thus  $OS_0 = R$  is the Earth radius and  $SS_0 = h$  the altitude of the satellite. We use the reduced distance

$$\eta = \frac{d}{R} = 1 + \frac{h}{R}, \tag{12.1}$$

i.e., the distance  $SO$  expressed in Earth radii and denoted by  $\eta$ , as already defined in (2.38). For a circular orbit of radius  $a$ , we have  $d = a$ .

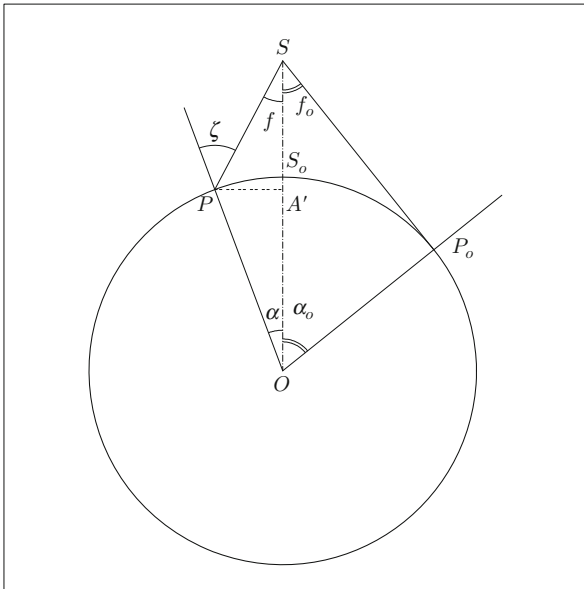


FIG. 12.3 : *Definition of angles relevant to the swath of an instrument aboard a satellite. The satellite is  $S$  and the subsatellite point is  $S_0$ . The instrument looks at points  $P$ , such as the point  $P_0$  on the Earth's limb. The Earth is spherical with center  $O$ .*

At a given instant of time, the angle between the line of sight from the satellite and the nadir<sup>5</sup> is

$$f = (\mathbf{SS}_0, \mathbf{SP}) , \quad (12.2)$$

where  $P$  is the point the instrument is viewing. This angle is called the swath angle or scan angle.

For the point  $P$ , we define the viewing zenith angle<sup>6</sup> by

$$\zeta = (\mathbf{OP}, \mathbf{PS}) . \quad (12.3)$$

This is the angle at which the satellite is seen from the surface, measured from the local vertical. The angle of elevation, or site angle, is the complementary angle of  $\zeta$ , i.e.,  $90^\circ - \zeta$ .

We also use the angle  $\alpha$ , which is the angle at the center of the Earth defined by

$$\alpha = (\mathbf{OS}, \mathbf{OP}) . \quad (12.4)$$

These three angles are related by

$$f + \alpha = \zeta , \quad (12.5)$$

by considering the triangle  $OSP$ . The maximum value of  $f$  is obtained when the target point  $P$  is on the Earth's limb. We denote this point by  $P_0$  and the corresponding angles are given the subscript zero. Considering the triangle  $OSP_0$ , we obtain the relations

$$\sin f_0 = \frac{R}{d} = \frac{R}{R+h} , \quad \alpha_0 = \frac{\pi}{2} - f_0 , \quad \zeta_0 = \frac{\pi}{2} ,$$

or using the reduced distance  $\eta$ ,

$$\sin f_0 = \cos \alpha_0 = \frac{1}{\eta} . \quad (12.6)$$

**Note on Terminology.** The angle  $f$  defined above was called the half-swath angle. When we speak of the swath of an instrument, we generally mean the angle moved through by the instrument at the apex, i.e.,  $2f_M$ , where the angle  $f_M$  is the maximal value reached by  $f$  when the instrument arrives at the limit of its orthogonal scan. The angle at the apex is called the field of view. If  $f_M$  is greater than  $f_0$ , we must obviously take  $f_M = f_0$ . To avoid confusion, we will therefore speak of the maximum possible half-swath to describe  $f_0$  and the maximum instrument half-swath to speak of  $f_M$ .

---

<sup>5</sup>The nadir is the direction given by the vertical, looking downwards, i.e., toward the center of the Earth. The opposite direction is the zenith. The word "nadir" comes from the Arabic *nādir*, from the root of the verb "to look straight at."

<sup>6</sup>In Arabic, *semt er-rās* means "the path of the head." This gives the word "zenith," the point on the sky just above the head. The word "azimuth" comes from *as-semt*, "the path," with assimilation of the article.

### 12.2.2 Relations Between Angles

Let us now establish relations giving one of the angles  $f, \zeta, \alpha$  as a function of one of the other two and the altitude via  $\eta$ . We thus obtain six relations.

**Relations Between  $f$  and  $\zeta$ .** In the triangle  $OSP$ , we have the relation

$$\frac{\sin f}{R} = \frac{\sin \zeta}{d} ,$$

which yields

$$f = f(\zeta, \eta) , \quad \sin f = \frac{1}{\eta} \sin \zeta = \sin f_0 \sin \zeta , \tag{12.7}$$

$$\zeta = \zeta(f, \eta) , \quad \sin \zeta = \eta \sin f = \frac{\sin f}{\sin f_0} . \tag{12.8}$$

**$f$  and  $\zeta$  as Functions of  $\alpha$ .** To obtain  $f$  as a function of  $\alpha$ , consider the triangle  $OSP$  and express the segment  $PA'$  in two different ways (where  $A'$  is the projection of  $P$  on  $OS$ ) to deduce that

$$(d - R \cos \alpha) \tan f = R \sin \alpha .$$

To obtain  $\zeta$  as a function of  $\alpha$ , consider the triangle  $OPA$ , where  $A$  is the intersection of  $OS$  with the line through  $P$  perpendicular to  $OP$ . This yields

$$f = f(\alpha, \eta) , \quad \tan f = \frac{\sin \alpha}{\eta - \cos \alpha} = \frac{\cos \alpha_0 \sin \alpha}{1 - \cos \alpha_0 \cos \alpha} , \tag{12.9}$$

$$\zeta = \zeta(\alpha, \eta) , \quad \tan \zeta = \frac{\sin \alpha}{\cos \alpha - 1/\eta} = \frac{\sin \alpha}{\cos \alpha - \cos \alpha_0} . \tag{12.10}$$

**Expressions for  $\alpha$ .** We immediately obtain the values of  $\alpha$  with (12.5) and the above relations:

$$\alpha = \alpha(f, \eta) , \quad \alpha = -f + \arcsin(\eta \sin f) , \tag{12.11}$$

$$\alpha = \alpha(\zeta, \eta) , \quad \alpha = \zeta - \arcsin\left(\frac{1}{\eta} \sin \zeta\right) . \tag{12.12}$$

### 12.2.3 Ground Swath

The ground half-swath is the distance  $F$  on the Earth's surface between the subsatellite point and the target point at angle  $f$ . The ground swath is then  $2F$ . The maximum ground half-swath is denoted by  $F_0$ . These lengths are given by

$h$	0	350	700	1,050	1,400	2,800
$f_0$	90.0	71.4	64.3	59.2	55.1	44.0
$f$	45.0	45.0	45.0	45.0	45.0	44.0
$\zeta$	45.0	48.2	51.7	55.4	59.6	90.0
$\alpha$	0.0	3.2	6.7	10.4	14.6	46.0
$F_0$	0	2,066	2,861	3,433	3,887	5,118
$F$	0	360	745	1,162	1,623	5,118
$2F$	0	720	1,491	2,324	3,245	10,236

TABLE 12.1 : *Sight angles for a half-swath  $f = 45^\circ$  for an instrument aboard a satellite at various altitudes  $h$ . Cross-track swath. The angles  $f$ ,  $\zeta$ ,  $\alpha$ , and  $f_0$ , defined in this chapter are in degrees. The altitude  $h$  and the distances  $F$  and  $F_0$  are in kilometers.*

$$F = R\alpha, \quad (12.13)$$

$$F_0 = R\alpha_0 = R \arccos \frac{1}{\eta}. \quad (12.14)$$

In Fig. 12.3,  $F$  corresponds to the arc  $S_0P$  and  $F_0$  to the arc  $S_0P_0$ .

**Example 12.1** Calculate the ground swath for an instrument viewing with angle  $f = 45^\circ$ , aboard satellites with different altitudes:  $h = 350, 700, 1,050$  km, etc.

► With  $350/R = 5.487 \times 10^{-2}$ , we calculate  $\eta$  and the angles by the above formulas. The results are given in Table 12.1. We can then compare the swaths of satellites like TRMM ( $h = 350$  km) or Terra ( $h = 700$  km). For satellites with altitude less than 1,000 km, the roundness of the Earth does not account for more than 10% of the value of the ground swath.

The limb is viewed with  $f = 45^\circ$  when  $h = 2,642$  km. Indeed, according to (12.6), we have  $\sqrt{2} = \eta = (R + h)/R$ , and hence  $h = R(\sqrt{2} - 1) = 2,642$  km. We can check from Table 12.1 that, for  $h = 2,800$  km, the swath  $f = f_0$  is less than  $45^\circ$ . ◀

## 12.2.4 Latitudes Viewed and Latitude Overlap

### Viewed Latitude Range

For a satellite of inclination  $i$ , we defined the maximum attained latitude  $\psi_m$  by (8.18). The ground track of the orbit lies within the latitude range

$$[-\psi_m, +\psi_m].$$

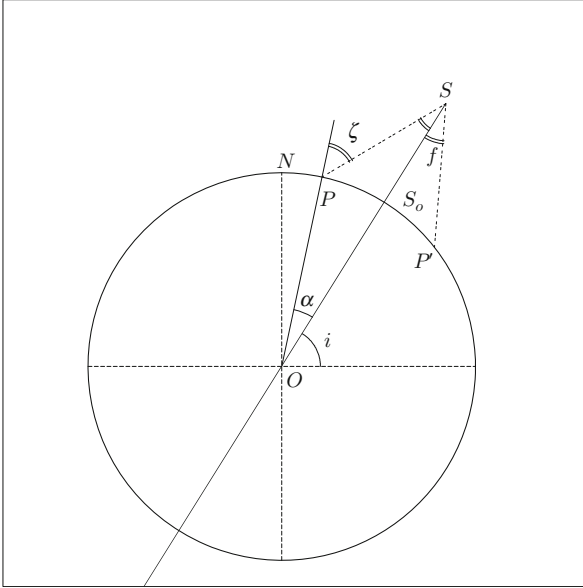


FIG. 12.4 : Swath orthogonal to the ground track of satellite  $S$ , with half-swath  $f$ . The plane of the diagram is the plane perpendicular to the orbit (of inclination  $i$ ) passing through the polar axis  $ON$ , i.e., the plane of the meridian of  $S_0$ . The satellite  $S$  is at its maximum latitude.

Consider the plane perpendicular to the orbit passing through the polar axis, as shown in Fig. 12.4. This is a meridian plane. With cross-track scanning, it is when the satellite crosses this plane that it sees points on the Earth at the extreme latitudes. For an instrument with maximum half-swath  $f_M$ , the swath track lies in the interval

$$[-\psi_v, +\psi_v],$$

where the angle  $\psi_v$  is the maximum latitude viewed, as defined by

$$\psi_v = \begin{cases} \psi_m + \alpha_M, & \text{if } \psi_m + \alpha_M < 90^\circ, \\ 90^\circ, & \text{if } \psi_m + \alpha_M \geq 90^\circ, \end{cases} \tag{12.15}$$

with  $\alpha_M = \alpha_M(f_M, \eta)$  calculated using (12.11).

**Latitude Overlap**

When  $\psi_m + \alpha_M$  is greater than  $90^\circ$ , we say that there is latitude overlap. This overlap concerns latitudes in the ranges:

$$\begin{cases} [+90^\circ, 180^\circ - (\psi_m + \alpha_M)] & \text{in the northern hemisphere,} \\ [-90^\circ, (\psi_m + \alpha_M) - 180^\circ] & \text{in the southern hemisphere.} \end{cases} \tag{12.16}$$

For a satellite with near-circular orbit, if a pole is viewed during a cross-track scan, the two poles are viewed during each revolution.

The geodetic latitude  $\varphi_m$  is then obtained from  $\psi_m$  by the usual relation (2.4).

**Example 12.2** Calculate the maximum viewed latitude and, in the relevant situations, the range of latitudes covered by the ScaRaB ( $f_M = 48.91^\circ$ ) carried by Meteor-3-07, Resurs-O1-4, and Megha-Tropiques.

► For Meteor-3-07,  $i = 82.56^\circ$ ,  $\psi_m = i$ ,  $\eta = 1.187$ , we obtain

$$\psi_m + \alpha = 82.56 + 14.55 = 97.11^\circ .$$

All latitudes are viewed. Moreover, for each hemisphere, there is overlap between the pole and geocentric latitude  $|\psi| = 180 - 97.11 = 82.79^\circ$ , or  $|\varphi| = 82.84^\circ$ .

For Resurs-O1-4,  $i = 99.69^\circ$ ,  $\psi_m = 180 - i = 81.31^\circ$ ,  $\eta = 1.129$ , and we obtain

$$\psi_m + \alpha = 81.31 + 9.40 = 90.71^\circ .$$

All latitudes are viewed. The overlap is very slight, between the pole and latitude  $|\psi| = 89.29^\circ$ , or  $|\varphi| = 89.30^\circ$ , for each hemisphere.

For Megha-Tropiques,  $i = 20.00^\circ$ ,  $\psi_m = i$ ,  $\eta = 1.136$ , and we obtain

$$\psi_m + \alpha = 20.00 + 9.98 = 29.98^\circ , \quad \text{or } \varphi = 30.15^\circ .$$

The latitudes viewed lie in the band  $[30.2^\circ\text{S}, 30.2^\circ\text{N}]$ , which corresponds to the region between the tropics (whence the name of the satellite). ◀

## 12.3 Pixel Distortion

### 12.3.1 Calculating the Distortion Index

We consider an instrument which observes the Earth with cross-track scanning. The axis of rotation of the instrument is perpendicular to the plane defined in Fig. 12.3. While the image is being acquired during the swath, the pixel is distorted in the direction of the swath and normal to it, for purely geometrical reasons. Here we discuss both kinds of distortion.

#### Index $K$ and Relative Distortion of the Pixel in the Swath Direction

Each angular interval  $\delta f$  of the half-swath angle corresponds to a half-swath interval  $\delta F$  on the ground. It is clear that, for a given constant interval, say  $1^\circ$ , the value of  $\delta F$  is smaller at the nadir (for  $f = 0$ ) than when viewing

the limb (for  $f = f_0$ ): the satellite–target distance increases and, furthermore, the roundness of the Earth is relevant here.

The pixel, which depends on the value of the elementary interval  $\delta f$  of the instrument, has size  $\delta F$  in the scanning direction. To find the pixel distortion, we calculate the variation of the ratio  $\delta F/\delta f$  as a function of the position of the target point, which amounts to finding the variation of the ratio  $\delta\alpha/\delta f$  as a function of  $\alpha$ .

Differentiating (12.9), we obtain

$$(1 + \tan^2 f)df = \frac{\eta \cos \alpha - 1}{(\eta - \cos \alpha)^2}d\alpha ,$$

which yields, replacing  $\tan f$  by its value as a function of  $\alpha$ ,

$$\frac{d\alpha}{df} = \frac{\eta^2 - 2\eta \cos \alpha + 1}{\eta \cos \alpha - 1} . \tag{12.17}$$

Considering increments  $\delta f$  and  $\delta\alpha$  small enough to identify them with  $df$  and  $d\alpha$ , we obtain the desired function

$$k(\alpha, \eta) = \frac{\delta\alpha}{\delta f} .$$

To measure the pixel distortion  $K(\alpha, \eta)$ , we set

$$K(\alpha, \eta) = \frac{k(\alpha, \eta)}{k(0, \eta)} ,$$

thereby expressing  $k(\alpha, \eta)$  relative to its value at the nadir. This value is  $k(0, \eta) = \eta - 1$ , which can be checked by calculating  $\delta F$  at the nadir in two different ways (using small angles), from the standpoint of  $S$  or  $O$ , whence  $\delta F = h\delta f = R\delta\alpha$ .

This pixel distortion index is thus

$$K(\alpha, \eta) = \frac{1}{\eta - 1} \frac{\eta^2 - 2\eta \cos \alpha + 1}{\eta \cos \alpha - 1} . \tag{12.18}$$

It thus measures a one-dimensional distortion along the swath for fixed increment  $\delta f$ . (We are not concerned here with scanning in which  $\delta f$  varies with  $f$ .)

### Index $L$ and Relative Distortion of the Pixel Width

The pixel is determined by the intersection of the viewing cone, which is extremely fine, and the sphere of the Earth. The distortion in the width, that is, in the plane defined by Fig. 12.3, depends solely on the length  $SP$ . The index  $L$  representing the corresponding relative distortion is therefore

$$L = \frac{SP}{SP_{\text{nadir}}} = \frac{SP}{SH} .$$

Using the reduced variable  $\eta$ , we obtain

$$L(\alpha, \eta) = \frac{1}{\eta - 1} \sqrt{\eta^2 - 2\eta \cos \alpha + 1}. \quad (12.19)$$

### Index $S$ and Relative Distortion of the Pixel Area

This relative distortion does not depend on the shape of the pixel (diamond, ellipse, etc.). The index  $S$  is the product of the two indices  $K$  and  $L$ , considered in two orthogonal directions:

$$S(\alpha, \eta) = K(\alpha, \eta)L(\alpha, \eta) = \frac{1}{(\eta - 1)^2} \frac{(\eta^2 - 2\eta \cos \alpha + 1)^{3/2}}{\eta \cos \alpha - 1}. \quad (12.20)$$

The maximum value of the angle  $\alpha$  is obtained when viewing the limb and is given by  $\alpha_0 = \arccos(1/\eta)$ . When  $\alpha$  tends to  $\alpha_0$ , the index  $K$ , and hence also  $S$ , tends to infinity. For the index  $L$ , the value is finite, viz.,

$$L(\alpha_0, \eta) = \sqrt{\frac{\eta + 1}{\eta - 1}}.$$

### 12.3.2 Pixel Distortion for LEO Satellites

The indices  $K$ ,  $L$ , and  $S$  are calculated as functions of  $\alpha$ , but the results are generally expressed in terms of the variables  $\zeta$  or  $f$ . The distortion index  $K(f)$  is plotted in Fig. 12.5 (upper) for LEO satellites in near-circular orbit and for altitudes between 200 and 1,400 km, in steps of 200 km. This index becomes large ( $K > 2$ ) when  $f$  reaches roughly two thirds of its maximum value  $f_0$ .

**Example 12.3** Calculate the pixel size and distortion index for the ScaRaB instrument aboard Meteor-3-07 and Resurs-O1-4.

► Two identical ScaRaB instruments are carried aboard the Russian satellites Meteor-3-07 and Resurs-O1-4. Scanning is across the ground track. The maximum instrumental half-scan angle, beyond which the instrument cannot view, is  $f_M = 48.91^\circ$ , implying a field of view of  $97.82^\circ$ . The complete scan comprises 51 pixels, corresponding to 50 increments, which gives a pixel size of

$$\delta f = \frac{2f_M}{50} = 1.956^\circ = 33.146 \text{ milliradians}.$$

Note that this is in fact the effective pixel, while the true pixel is larger to give overlap. At the nadir, this pixel size corresponds to

$$\begin{aligned} \delta F &= 40.8 \text{ km} && \text{for ScaRaB aboard Meteor-3-07,} \\ \delta F &= 27.8 \text{ km} && \text{for ScaRaB aboard Resurs-O1-4.} \end{aligned}$$



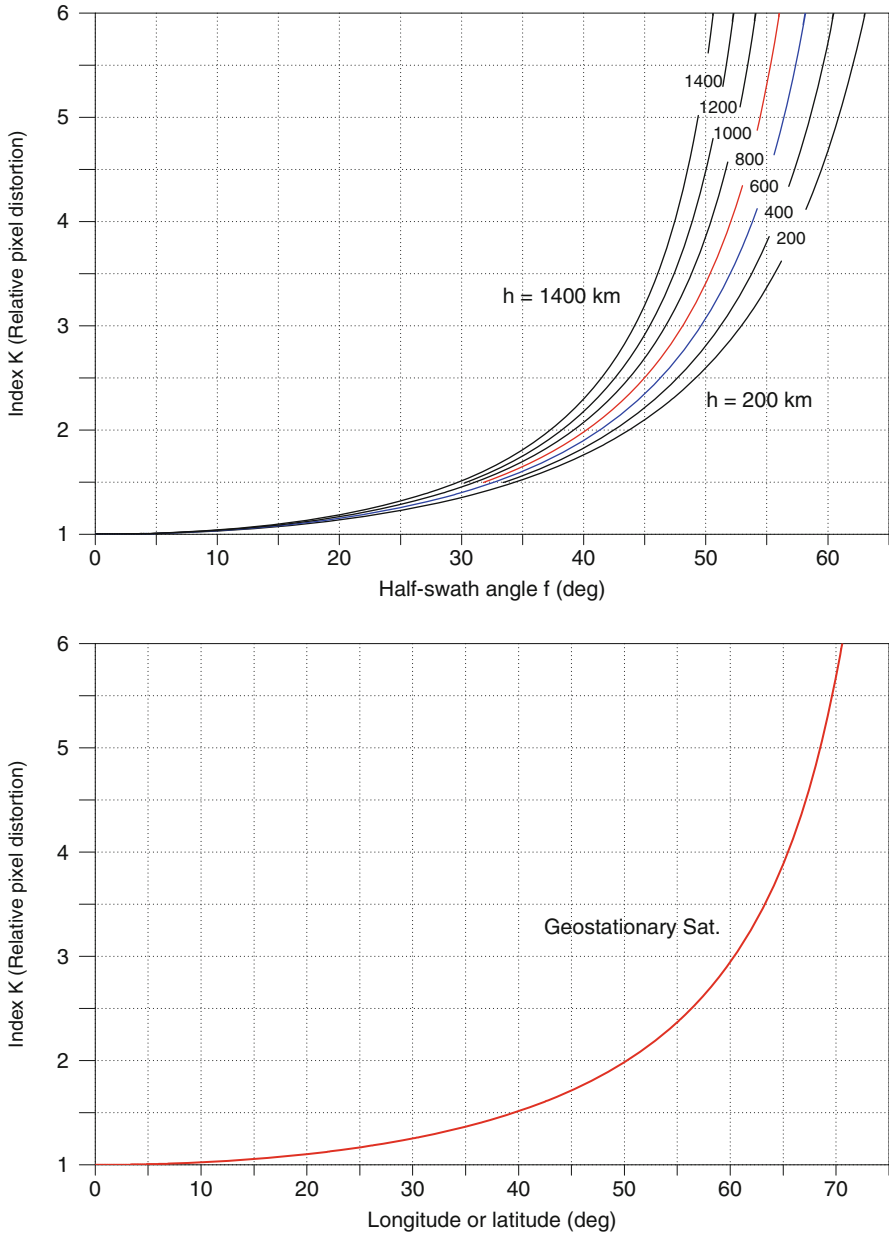


FIG. 12.5: Relative pixel distortion as represented by the index  $K$ , which measures length distortion. Upper: For LEO satellites with altitude  $h = 200\text{--}1,400$  km, in steps of 200 km, as a function of the half-swath angle  $f$ . Lower: For any geostationary satellite, as a function of the angle  $\alpha$ , representing the latitude or longitude from the subsatellite point.

At the limiting value of the scan, the pixel length is  
 $K(f_M) = 4.0 \implies \delta F = 161 \text{ km}$  for ScaRaB aboard Meteor-3-07,  
 $K(f_M) = 3.2 \implies \delta F = 86 \text{ km}$  for ScaRaB aboard Resurs-O1-4.  
 The ground swath is  $2F_M = 3,254 \text{ km}$  for Meteor-3-07, which exceeds the equatorial shift  $\Delta\lambda_E = 3,059 \text{ km}$ . However, for Resurs-O1-4, the ground swath  $2F_M = 2,078 \text{ km}$  is considerably less than the equatorial shift  $\Delta\lambda_E = 2,819 \text{ km}$ . The ScaRaB instrument was originally designed for satellites of type Meteor-3, at an altitude of 1,200 km, the aim being to scan the whole planet in 1 day. To obtain this result aboard satellites like Resurs-O1 at an altitude of 800 km, the instrument would have had to scan up to angles  $f_M = 55^\circ$ , and this would have given a pixel distortion of  $K = 5.3$  (see Fig. 12.8). ◀

**Example 12.4** *Pixel distortion for the ScaRaB instrument aboard Megha-Tropiques.*

► The ScaRaB instrument described in Example 12.3 is also carried aboard the French–Indian satellite Megha-Tropiques. Once again, the swath is cross-track. At the nadir, with an angle of  $33.146 \text{ mrad}$ , the effective size of the pixel (and also the separation between two pixels) is  $865.6 \text{ km}$ . The true pixel, which must overlap neighbouring pixels, is naturally larger. At the nadir, it is diamond shaped with side  $41.60 \text{ km}$ . The diagonals of this diamond have length  $58.82 \text{ km}$ . One of these, called the width, lies along the velocity vector of the satellite, while the other, called the length, is perpendicular, lying along the scan direction.

The pixel is gradually distorted with increasing angle  $f$ . At the limit of the scan, with  $f_M = 48.91^\circ$ , the diagonals have lengths  $99.43$  and  $192.29 \text{ km}$ . The results are given in Fig. 12.6. Figure 12.14 provides a representation of the pixels in situ. ◀

### 12.3.3 Pixel Distortion for GEO Satellites

Although a geostationary satellite sees almost half the Earth's surface, around the edge of the observed disk, the pixel distortion is considerable. The graph of  $K(\alpha)$  in Fig. 12.5 (lower) shows that, for a geostationary satellite, the distortion index exceeds 2 beyond  $50^\circ$ . The angle  $\alpha$  can be replaced by  $|\lambda - \lambda_S|$ , the longitude along the equator, measured from the subsatellite point, or by  $|\psi|$ , the latitude measured along the meridian  $\lambda_S$ . These graphs are clearly going to be the same for all geostationary satellites.

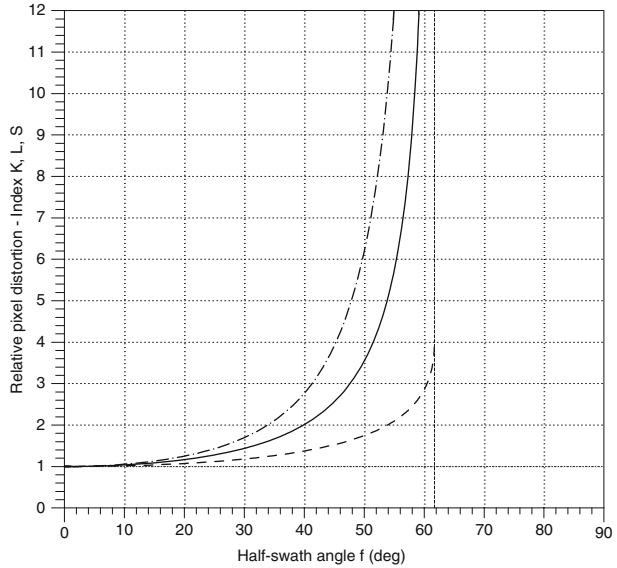
Megha-Tropiques

Altitude = 865.5 km  
 Inclination = 20.00 °  
 Period = 101.93 min  
 Equatorial shift= 2892.0 km  
 $f = (\text{field of view})/2$   
 Maximal half-swath  $f = 61.7^\circ$

Index K (Relative pixel distortion)  
 Index L (Relative width pixel distortion)  
 Index S (Relative area pixel distortion)

$$K \quad L \quad S=K \cdot L$$

$I\xi\omega\nu$   
 MC \* LMD



$f$	$\zeta$	$\alpha$	$K$	$L$	$S$	Length	Width	Area
0.0	0.0	0.0	1.000	1.000	1.000	58.82	58.82	1,729.9
5.0	5.7	0.7	1.009	1.004	1.014	59.37	59.08	1,753.6
10.0	11.4	1.4	1.038	1.018	1.056	61.05	59.85	1,827.1
15.0	17.1	2.1	1.088	1.040	1.132	64.02	61.19	1,958.9
20.0	22.9	2.9	1.165	1.074	1.252	68.55	63.17	2,165.1
25.0	28.7	3.7	1.277	1.120	1.430	75.10	65.89	2,474.3
30.0	34.6	4.6	1.436	1.182	1.698	84.47	69.53	2,936.8
35.0	40.6	5.6	1.667	1.264	2.107	98.03	74.37	3,645.3
40.0	46.9	6.9	2.012	1.375	2.766	118.33	80.87	4,784.4
45.0	53.4	8.4	2.562	1.527	3.911	150.69	89.80	6,765.9
50.0	60.5	10.5	3.542	1.746	6.184	208.32	102.71	10,698.2
55.0	68.5	13.5	5.719	2.098	11.996	336.40	123.38	20,752.6
60.0	79.6	19.6	15.795	2.853	45.070	929.09	167.83	77,965.9
48.9	58.9	10.0	3.269	1.690	2.763	192.29	99.43	9,559.4
61.7	90.0	28.3	$\infty$	3.967	$\infty$	$\infty$	233.35	$\infty$

FIG. 12.6 : Pixel distortion indices for the ScaRaB instrument aboard Megha-Tropiques. The three pixel distortion indices are  $K$ ,  $L$ ,  $S$  (dimensionless). The angles  $f$ ,  $\zeta$ , and  $\alpha$  are in degrees. The length and width dimensions of the ScaRaB pixel are given in km and the area of the diamond-shaped pixel is given in  $\text{km}^2$ . The maximal scan angle is  $f = 48.91^\circ$ . The maximal possible angle (viewing the limb) is  $f_0 = 61.70^\circ$ . See also Fig. 12.14.

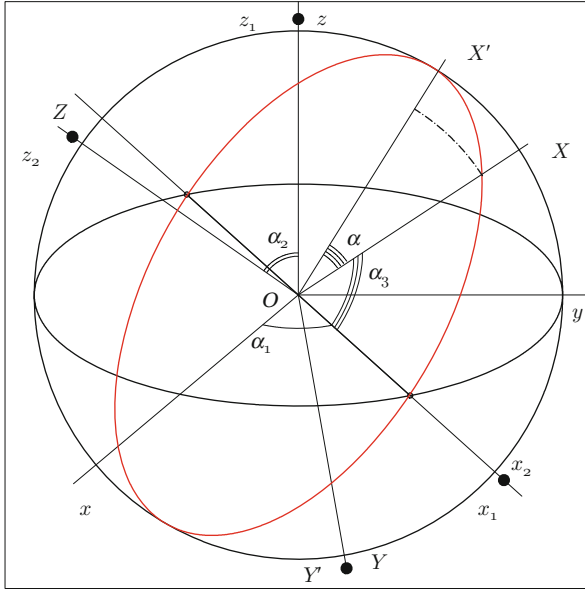


FIG. 12.7 : Rotation through  $\alpha$  corresponding to the swath  $f$  of an instrument aboard the satellite. This figure complements Fig. 8.2. Black dots denote the four axes of rotation. The axis of rotation of the instrument is  $OY$  in the orbital plane  $Ox_2X$ , perpendicular to  $OX$ . The ground track of a half-swath is shown by a dashed curve.

## 12.4 Swath Track for an LEO Satellite

For LEO observation satellites, the two main scanning modes are cross-track and conical. They concern two completely different kinds of instrument. In the case of cross-track scanning instruments, one exploits (although on rare occasions) the possibility of orienting the device differently so that it can view along the track or along some other direction. Here we shall examine these different scanning modes.

### 12.4.1 Cross-track Swath

In order to calculate the coordinates of the points viewed and thus plot the ground track of the cross-track scan, we return to the Euler angles first discussed when determining the subsatellite point on the ground track.

We consider that the scan with instantaneous angle  $f$  from the satellite  $S$  is equivalent to a scan with instantaneous angle  $\alpha$  from the center  $O$  of the Earth. Scanning is in the plane perpendicular to the orbit, passing through  $S$  and  $O$ . Viewed from  $O$ , it is thus a scan with angle  $\alpha$  and axis  $OY$  (parallel to  $SX$  in the orbital plane), where the orthogonal axes  $OXYZ$  were defined previously as in Fig. 8.2.

This rotation has matrix  $P_4$  given by

$$P_4 = \begin{pmatrix} \cos \alpha & 0 & -\sin \alpha \\ 0 & 1 & 0 \\ \sin \alpha & 0 & \cos \alpha \end{pmatrix}. \quad (12.21)$$

If  $(X', Y', Z')$  are the Cartesian coordinates of the target point on the Earth relative to the frame  $\mathfrak{R}(Oxyz)$ , we obtain these new coordinates from

$$\begin{pmatrix} X' \\ Y' \\ Z' \end{pmatrix} = P_4 \begin{pmatrix} X \\ Y \\ Z \end{pmatrix},$$

where the coordinates  $(X, Y, Z)$  of the subsatellite point were obtained using the product of the three rotations defined by (8.8). Figure 12.7 completes Fig. 8.2 with the fourth rotation. Using (8.12) to (8.14), the Cartesian coordinates  $(X', Y', Z')$  can be used to calculate the polar coordinates  $\lambda'$  and  $\psi'$  of the target point.

### Scanning and Ground Track of the Cross-track Swath

When an instrument scans, the scan moves extremely quickly across the ground. For example, the instrument ScaRaB aboard Meteor-3-07 completes one scan in 3.18 s, so that the average speed of the scan on the ground is  $3254/3.18 = 1,024 \text{ km s}^{-1}$ . Compared with the displacement of the subsatellite point along the satellite ground track, which is  $6 \text{ km s}^{-1}$ , each swath track can be treated as instantaneous. For HRVIR aboard SPOT-4, the scan is effectively instantaneous.

The ground track of the orthogonal swath, perpendicular to the orbital plane, thus makes an angle of  $90^\circ - i$  with the equator. However, as we saw previously, the ground track makes an angle  $i'$  with the equator. This is the apparent inclination. In diagrams showing the ground tracks, the normal to the ground track of the swath thus makes an angle  $i - i'$  with the satellite ground track at the equator, given by (8.30). In other words, the ground track of the cross-track swath is not exactly perpendicular to the satellite ground track.

**Note on Cartography.** This angular difference only shows up true to scale on maps plotted with a conformal projection. On the two maps of Fig. 12.8, plotted with the Mercator projection, one can evaluate the angle between the scan and the ground track at the equator and check that this is not a right-angle.

### Equatorial Overlap

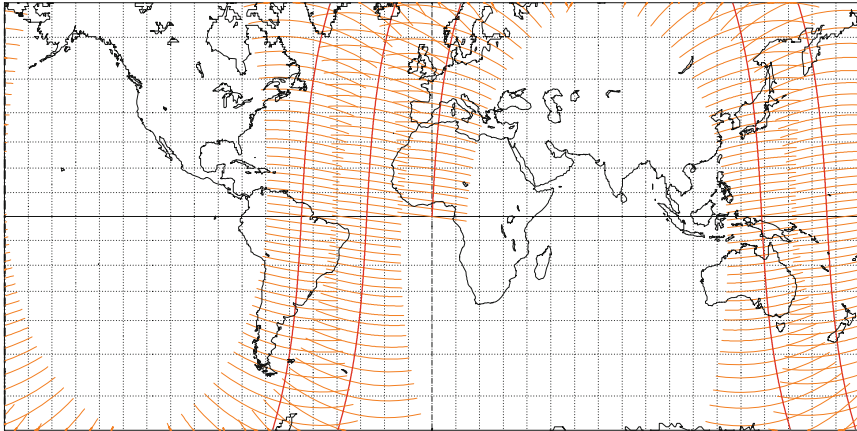
Consider the full swath of an instrument to its viewing limit. Its width on the ground is  $2F_M$ . Let  $L_E$  be the portion of the equator covered by the swath during one crossing by the satellite. To a first approximation,

**Meteor-3-07 / ScaRaB** < Μερεορ >

**Orbit - Ground track**

>>>> Time span shown: 250.0 min = 0.17 day  
 Across track swath (XT mode)

Altitude = 1194.6 km                      a = 7572.704 km  
 Inclination = 82.56 °  
 Period = 109.42 min    \* rev/day =13.16  
 Equat. orbital shift = 3059.5 km ( 27.5 °)  
 \*\* Half-swath: 48.9° => 1622 km [ 1.00 min]



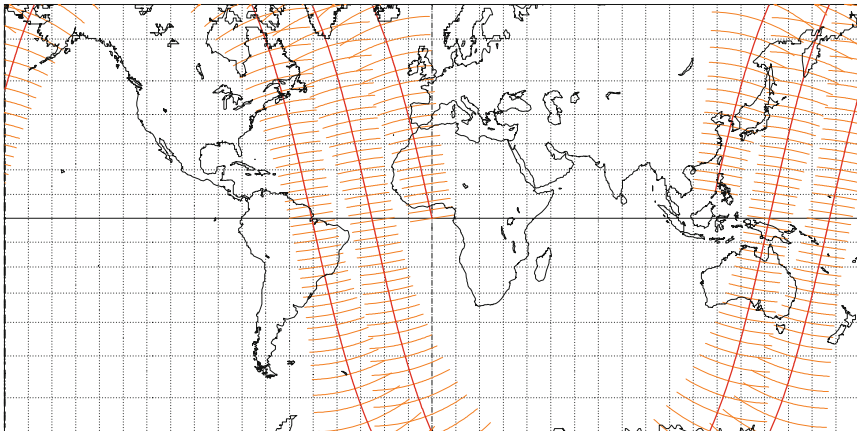
Projection: Mercator                      Project. centre: 0.0 ° ; 0.0 °                      Asc. Node: 0.00 °                      Ιξίωv  
 Property: Conformal                      Aspect: Direct                      Latit. overlap:82.9° <-> 90.0°                      MC ★ LMD  
 ⊕ T.:Cylindrical - Graticule: 10°                      [4.2] [ +0.0/ +0.0/ +0.0] [-]                      PZ-90                      Ατλας

**Resurs-O1-4 / ScaRaB** < Ρεσυρ >

**Orbit - Ground track**

>>>> Time span shown: 250.0 min = 0.17 day  
 Across track swath (XT mode)

Altitude = 814.2 km                      a = 7192.379 km  
 Incl.in./SUN-SYNCHRON.= 98.70 °  
 Period = 101.29 min    \* rev/day =14.22  
 Equat. orbital shift = 2818.9 km ( 25.3 °)  
 \*\* Half-swath: 48.9° => 1034 km [ 1.00 min]



Projection: Mercator                      Project. centre: 0.0 ° ; 0.0 °                      Asc. Node: 0.00 °                      Ιξίωv  
 Property: Conformal                      Aspect: Direct                      Latit. overlap:89.4° <-> 90.0°                      MC ★ LMD  
 ⊕ T.:Cylindrical - Graticule: 10°                      [4.2] [ +0.0/ +0.0/ +0.0] [-]                      PZ-90                      Ατλας

FIG. 12.8 : Ground track of the cross-track scan by ScaRaB carried at different altitudes by the two LEO satellites Meteor-3-07 and Resurs-O1-4.

$$L_E \approx \frac{2F_M}{\sin i} . \tag{12.22}$$

In fact, the ground track is related to the apparent inclination  $i'$  and the swath to the inclination  $i$ , and the exact relation for the orbit and swath ground tracks at the equator is

$$L_E = \frac{2F_M}{\sin i + \cos i \tan(i - i')} = \frac{2F_M}{\sin i} \frac{1}{1 + \frac{\tan \delta i}{\tan i}} . \tag{12.23}$$

Using the value of  $\delta i = i' - i$  given by (8.30), we find

$$L_E = \frac{2F_M}{\sin i} \left( 1 - \frac{\cos i}{\kappa} \right) . \tag{12.24}$$

### Fractional Equatorial Overlap

It is interesting to compare this distance  $L_E$  with the equatorial shift  $D_E$ , as given by (8.27). Both lengths are measured along the equator and their ratio  $Q_E$  thus indicates the fraction of the equator seen by the satellite in 1 day, during the ascending node crossing:

$$Q_E = \frac{L_E}{D_E} = \frac{F_M}{\pi R} \frac{\kappa - \cos i}{\sin i} . \tag{12.25}$$

Introducing the angle at the center  $\alpha_M$  in radians, corresponding to  $F_M$ , we then obtain

$$Q_E = \frac{\alpha_M}{\pi} \frac{\kappa - \cos i}{\sin i} . \tag{12.26}$$

If  $Q_E$  is greater than 1, certain points on the equator are viewed more than once during the ascending node crossing (and likewise, of course, for the descending node crossing).

The average number  $N(\varphi, f)$  of daily crossings, which depends on the latitude  $\varphi$  and the half-swath  $f$ , is

$$N(0, f_M) = 2Q_E . \tag{12.27}$$

We may also calculate the half-swath  $f_Q$  that will yield a predetermined fraction  $Q_E$  of equatorial overlap. We first calculate the corresponding angle  $\alpha_Q$  at the center of the Earth, viz.,

$$\alpha_Q = \pi \frac{\sin i}{\kappa - \cos i} Q_E . \tag{12.28}$$

The value of  $f_Q$  is deduced from  $\alpha_Q$  using (12.9).

**Example 12.5** *Ground track of the swath for the same instrument, ScaRaB, carried aboard three different satellites: Meteor-3-07, Resurs-O1-4, and Megha-Tropiques.*

► ScaraB was originally designed to fly aboard Meteor-3-07. Two instruments with identical geometrical characteristics were then flown aboard Resurs-O1-4 and Megha-Tropiques.

**Meteor-3-07.** This instrument was designed to provide full daily equatorial overlap. To see how to achieve this, we apply (12.28) with  $Q_E = 1$ . For this satellite,  $i = 82.56^\circ$ ,  $\eta = 1.1873$ , and  $\kappa = 13.0986$ . We thus calculate  $\alpha_1$  in degrees:

$$\alpha_1 = 180 \frac{\sin 82.56}{13.0986 - \cos 82.56} = 13.76^\circ ,$$

$$\tan f_1 = \frac{\sin 13.76}{1.1873 - \cos 13.76} = 1.1013 .$$

The half-swath angle is therefore  $f_1 = \arctan(1.1013) = 47.76^\circ$ . The scanning aperture is always chosen very slightly bigger, in this case  $f_M = 48.91^\circ$ . The corresponding value of  $F_M = R\alpha_M$  is obtained by

$$\alpha_M = -f_M + \arcsin(\eta \sin f_M) = -48.910 + 63.488 = 14.578^\circ = 0.2544 \text{ rad} ,$$

$$F_M = 1,622 \text{ km} .$$

Figure 12.8 (upper) shows the swath ground track. For clarity, swaths have been plotted every 60 s, whereas in fact ScaRaB scans every 6 s.

**Resurs-O4-1.** The satellite Resurs-O4-1 is Sun-synchronous and follows a lower orbit:  $\eta = 1.1277$ ,  $i = 98.69^\circ$ ,  $\kappa = \nu = 14.2165$ . With half-swath  $f_M = 48.91^\circ$ , the ground swath is

$$\alpha_M = 48.910 - 58.203 = 9.293^\circ = 0.1622 \text{ rad} , \quad F_M = 1,034 \text{ km} .$$

The fractional equatorial overlap  $Q_E$  is then

$$Q_E = \frac{0.1622}{\pi} \frac{14.2165 - \cos 98.69}{\sin 98.69} = 0.750 .$$

We thus find that  $Q_E$  is less than unity, as can be clearly seen in Fig. 12.8 (lower). For a point on the equator, the daily average number of crossings given by (12.27) is  $N = 1.50$ .

**Megha-Tropiques.** The satellite Megha-Tropiques is in a very slightly inclined orbit:  $\eta = 1.1357$ ,  $i = 20.00^\circ$ ,  $\kappa = 97/7 = 13.8571$ . With  $f_M = 48.91^\circ$ , we obtain

$$\alpha_M = 9.956^\circ , \quad F_M = 1,108 \text{ km} .$$

We thus calculate  $Q_E = 2.08$ , which indicates that the daily average number of crossings at the equator is  $N = 4.16$ . See Fig. 12.15. ◀



## Swath and Mission Constraints

The swath of the main instrument on a satellite and the orbital characteristics of that satellite are related. This is exemplified in Fig. 12.9, which shows that the swath of the VIIRS instrument is such that the Earth is completely scanned every day. This constraint is particularly important if the satellite is recurrent. We shall give here several examples for the very different cases of wide, narrow, and very narrow swaths.

**Example 12.6** *Fulfilling mission requirements with regard to swath and recurrence for Oceansat-1, SPOT-1, and ICESat.*

► These three satellites are in near-polar orbits.

**Oceansat-1.** The Indian satellite Oceansat-1 (IRS-P4) is Sun-synchronous (equatorial crossing at noon and midnight), and recurrent with triple [14, 1, 2], corresponding to a cycle of 29 revolutions over 2 days. The equatorial shift is then

$$\Delta\lambda_E = -\frac{360}{14.5} = -24.83^\circ, \quad D_E = 2,763.8 \text{ km}.$$

The aim of the mission is to view the equator by day every 2 days. To a first approximation (the cross-track swath is practically parallel to the equator), the ground swath  $2F_M$  must be at least equal to half of the equatorial shift, i.e.,

$$\alpha_M = \frac{180}{29} = 6.21^\circ, \quad F_M = \frac{1}{4}D_E = 691 \text{ km}.$$

Equation (12.9) implies that  $f_M = 42.3^\circ$ . The precise calculation using (12.28) with  $Q_E = 0.5$  and  $i = 98.29^\circ$ ,  $\eta = 1.1129$ , and  $\kappa = 29/2 = 14.50$  yields

$$\alpha_M = 90 \frac{\sin 98.29}{14.50 - \cos 98.29} = 6.0816^\circ,$$

and then  $f_M = 41.79^\circ$ . The instrument OCM aboard this satellite has a total swath of 1,420 km, or  $F_M = 710$  km, which is a few kilometers more than the strict minimum swath required. The calculation gives

$$F_M = 710 \text{ km} \implies f_M = 43.0^\circ, \quad Q_E = 0.52.$$

The fractional equatorial overlap is thus slightly above 1/2.

**SPOT-1.** When the SPOT project was under development, the planned altitude was somewhere between 800 and 850 km, low enough to have good resolution, but high enough to avoid atmospheric drag. The instrument HRV carried by SPOT-1 was designed with a field of view of  $8.4^\circ$ , or  $f_M = 4.2^\circ$ .

The aim was that the grid interval  $\delta$  defined by (11.20) should be slightly less than the ground swath.

We can calculate the interval  $\delta \approx 2h \tan f_M \approx 1.06^\circ$ , which implies that the number of round trips during the recurrence cycle is  $N_{T_o} = 360/1.06 \approx 340$ . Then  $\nu$  lies between 14.26 for  $h = 800$  km and 14.11 pour  $h = 850$  km. For the cycle  $C_{T_o} = N_{T_o}/\nu$ , the limiting value is thus  $C_{T_o} = 24$ . During the development stage of the mission, it was also decided that the cycle should be less than 1 month, and this implies that

$$24 \leq C_{T_o} \leq 30 .$$

The recurrence triple will thus have the form  $[14, D_{T_o}, C_{T_o}]$  with  $340 \leq N_{T_o} \leq 427$ . Considerations regarding subcycles then determined the choice of triple  $[14, +5, 26]$ , 369 revolutions.

**ICESat.** The satellite ICESat carries a laser for altimetry. This instrument, known as GLAS, aims at the nadir with an almost “pointlike” field of view, since the pixel measures only 66 m on the ground. Recurrence with the very long cycle of 2,723 round trips in 183 days, implying a grid interval of  $\delta = 15$  km, guarantees that, during the whole cycle, the satellite will never recross its ground track. ◀

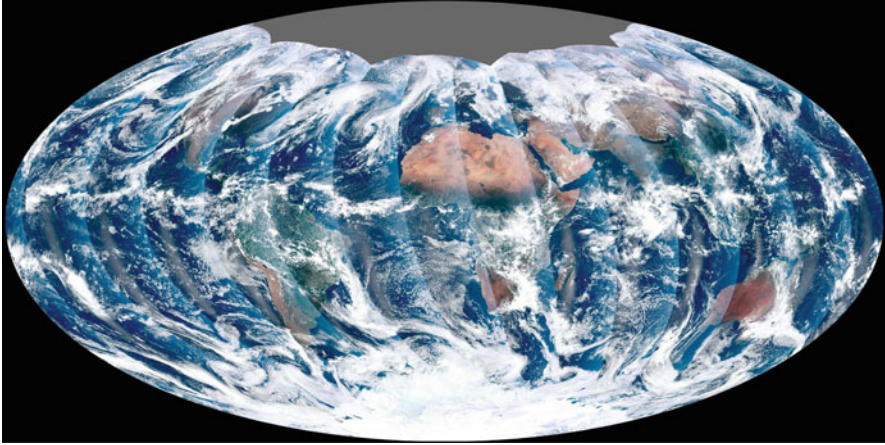
## 12.4.2 Variable-Yaw Swath

Cross-track scanning, or XT mode in the terminology used by NASA, corresponds to a yaw angle of  $0^\circ$ . The yaw angle is measured in a plane perpendicular to the yaw axis, or nadir axis, joining the satellite to the center of the Earth. There are scanning modes along the track, called along-track swath or AT mode, corresponding to a yaw angle of  $90^\circ$ . In this case, the swath does not exactly cover the ground track, for the same reasons that the cross-track swath is not exactly perpendicular to the ground track (see Chap. 8 for the contrast between inclination and apparent inclination, i.e., the angles  $i$  and  $i'$ , or  $j$  and  $j'$ ). By adjusting the yaw angle as a function of the latitude overflow, the ground track can be covered by the swath [see in particular (8.37)]. An application is described in Example 12.7.

Another scanning mode varies the yaw angle continuously, and this is illustrated in Example 12.8.

**Example 12.7** *Difference between along-track (AT-mode) scanning and true along-track (TAT-mode) scanning.*

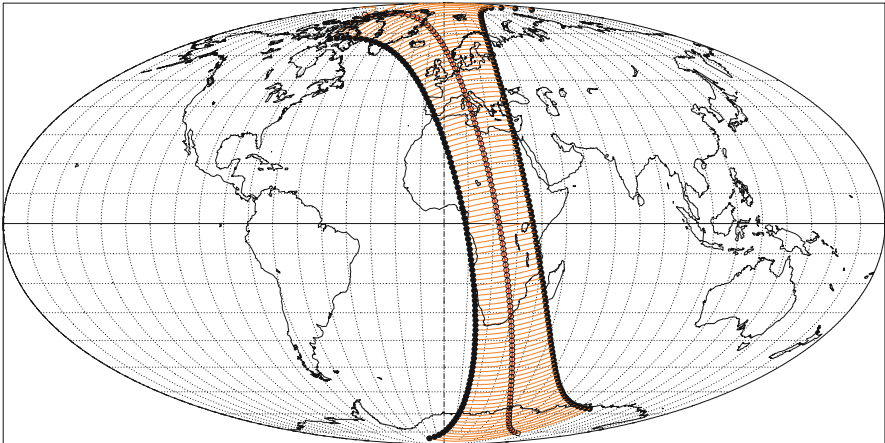
► To study the Earth radiation budget, NASA developed the instrument CERES (Clouds and the Earth’s Radiant Energy System), which has been



**Suomi NPP**  
Orbit - Ground track

Recurrence = [14; +3; 16] 227  
 2011 11 24 11:31:00 UTC >>> 51.0 min = 0.04 day  
 Across track swath (XT mode)

Altitude = 824.0 km      a = 7202.102 km  
 Incl. / SUN-S.= 98.69 °      e = 0.000009  
 Period = 101.50 min \* rev/day =14.19  
 Equat. orbital shift = 2824.7 km ( 25.4 °)  
 \*\* Half-swath: 56.1° => 1500 km [ 0.50 min]



Projection: Mollweide	Project. centre: 0.0 ° ; 0.0 °	Asc. Node: -58.41 ° [13:25 LMT]	Ιξλων
Property: Equal area	Aspect: Direct	[NORAD] Revolution: 374	MC ★ LMD
⊕ T.:Pseudocyl. - Graticule: 10°	4.2 [ +0.0/ +0.0/ +0.0 ] [-]	[NORAD] 2011 11 23 17:18:55 UTC	Ατλας

FIG. 12.9 : Upper: This image from 24 November 2011 is the first complete global image from VIIRS (Visible Infrared Imager Radiometer Suite). This instrument gets a complete view of the Earth every day (375 m/pixel). Note the polar night at high northern latitudes. Credit: NASA, NPP/LPETE. Lower: Ground track of VIIRS aboard Suomi-NPP over a half-revolution, from the South Pole to the North Pole.

**Terra / CERES****Orbit - Ground track**

Recurrence = [15; -7; 16] 233

2004 08 20 02:50:40 UTC &gt;&gt;&gt; 1440.0 min = 1.00 day

Along track swath (AT mode)

Altitude = 699.5 km

a = 7077.675 km

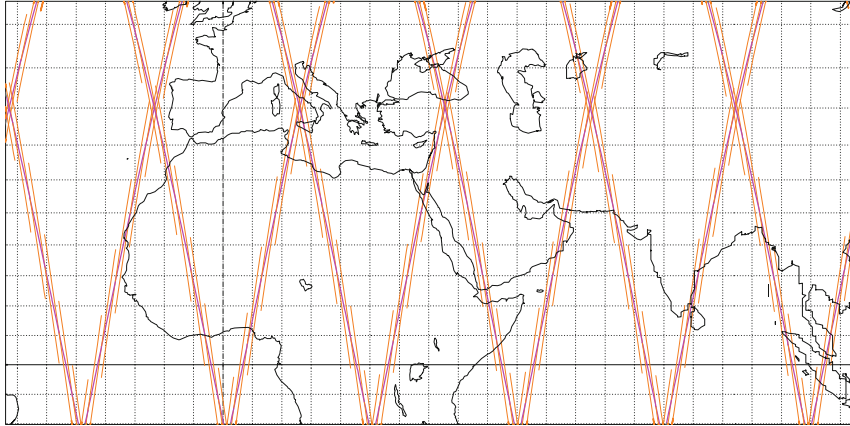
Incl. / SUN-S. = 98.19 °

e = 0.000114

Period = 98.88 min \* rev/day = 14.56

Equat. orbital shift = 2751.9 km ( 24.7 °)

\*\* Half-swath: 61.8° =&gt; 1801 km [ 3.00 min]



Projection: Mercator

PC: 0.0 ° ; 0.0 ° /ZC: 25.0 ° N; 35.0 ° E

Asc. Node: -65.37 ° [22:29 LMT]

Ιξίων

Property: Conformal

Aspect: Direct &gt; zoom : 2.50

[NORAD] Revolution: 24855

MC ★ LMD

⊕ T.:Cylindrical - Graticule: 5°

[4.2] [+90.0/ +0.0/ -90.0] [-] EGM2008

[NORAD] 2004 08 20 02:50:40 UTC

Ατλας

**Terra / CERES****Orbit - Ground track**

Recurrence = [15; -7; 16] 233

2004 08 19 07:04:05 UTC &gt;&gt;&gt; 1440.0 min = 1.00 day

Along track swath - adjusted (AT/PAP mode)

Altitude = 699.5 km

a = 7077.677 km

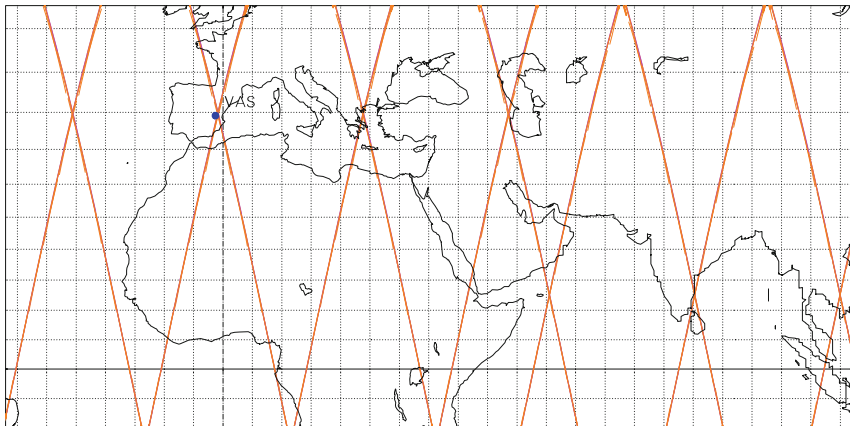
Incl. / SUN-S. = 98.19 °

e = 0.000112

Period = 98.88 min \* rev/day = 14.56

Equat. orbital shift = 2751.9 km ( 24.7 °)

\*\* Half-swath: 61.8° =&gt; 1801 km [ 3.00 min]



Projection: Mercator

PC: 0.0 ° ; 0.0 ° /ZC: 25.0 ° N; 35.0 ° E

Asc. Node: -128.72 ° [22:29 LMT]

Ιξίων

Property: Conformal

Aspect: Direct &gt; zoom : 2.50

[NORAD] Revolution: 24843

MC ★ LMD

⊕ T.:Cylindrical - Graticule: 5°

[4.2] [+90.0/ +0.0/ -90.0] [-] EGM2008

[NORAD] 2004 08 19 07:04:05 UTC

Ατλας

FIG. 12.10: Ground swath of the CERES instrument carried by Terra, with two scanning modes. Upper: Along-track (AT-mode) scanning without yaw adjustment. Lower: Variable-yaw (TAT-mode or AT/PAP-mode) scanning.

carried aboard several satellites.<sup>7</sup> In preliminary studies for the radiometer BBR carried by the satellite EarthCARE, calibration/validation sessions took place in August 2004 at the Valencia Anchor Station (VAS), near Valencia in Spain. The radiometer used was the CERES instrument carried by Terra. Once every cycle of 16 days, the (ascending and descending) ground tracks of the satellite cross on the same day very close to the VAS. Indeed, a grid point can be seen on Fig. 12.10 (lower), very close to the VAS.

In AT mode, the ground swath makes an angle of a few degrees with the satellite ground track. The two tracks do not overlap, as can be seen in Fig. 12.10 (upper). We asked NASA to vary the yaw angle of CERES on 19 August 2004, using the programmable azimuth plane (PAP) scanning mode. In this mode, the yaw angle is determined by (8.37) as a function of the latitude overflow. This gives the value of  $\delta j$ . The result of this modification is clearly apparent in Fig. 12.10 (lower). The ground swath for AT/PAP-mode scanning, also called true along-track (TAT-mode) scanning, exactly covers the ground track of the satellite orbit. ◀

**Example 12.8** *Ground swath of the CERES radiometer carried by the satellite Terra, in cross-track (XT) mode and variable-yaw (RAP) mode.*

► We represent the ground track of the CERES instrument aboard Terra, when the satellite passes over North America, considering two different scanning modes: cross-track (XT-mode) scanning, shown in Fig. 12.11, and variable-yaw (RAP-mode) scanning, shown in Fig. 12.12. The scanning mode known as rotating azimuth plane (RAP) mode consists in making a half-turn in 6 min, then a half-turn back. The swath shown here, every 6 s, corresponds to  $f = 56.1^\circ$ . ◀

### 12.4.3 Conical Swath

Conical swaths are used by microwave radiometers, in particular. In this case, for physical reasons connected with the phenomenon, the target points must be viewed at a constant angle. The maximum half-swath  $f_M$  must therefore be adapted to the altitude of the satellite and also to the angle  $\zeta_M$ .

A conical swath is specified by two angles (see Fig. 12.13), which are in orthogonal planes:

- the half-swath angle  $f_M$  (or viewing zenith angle  $\zeta_M$ ), in a vertical plane,
- the half aperture  $\xi_M$ , in the horizontal plane tangent to the Earth's sphere.

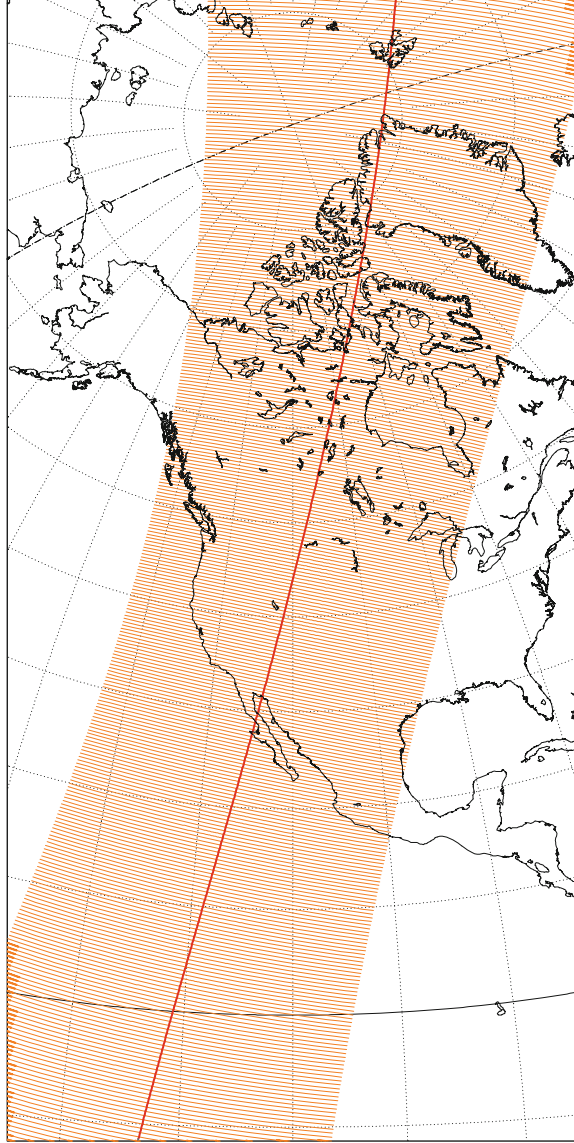
---

<sup>7</sup>There are in fact six versions of this instrument: PFM (Proto Flight Model) aboard TRMM, FM1 and FM2 aboard Terra, FM3 and FM4 aboard Aqua, and FM5 aboard NPP. These instruments FM can operate in cross-track or variable-yaw mode as required.

# Terra / CERES Orbit - Ground track

Altitude = 699.6 km      a = 7077.736 km  
 Incl.in./SUN-SYNCHRON.= 98.21 °  
 Period = 98.88 min \* rev/day = 14.56  
 Equat. orbital shift = 2751.9 km ( 24.7 °)  
 \*\* Half-swath: 61.8° => 1801 km [ 0.10 min]

Recurrence = [15, -7, 16] 233  
 >>>> Time span shown: 99.0 min = 0.07 day  
 Across track swath (XT mode)



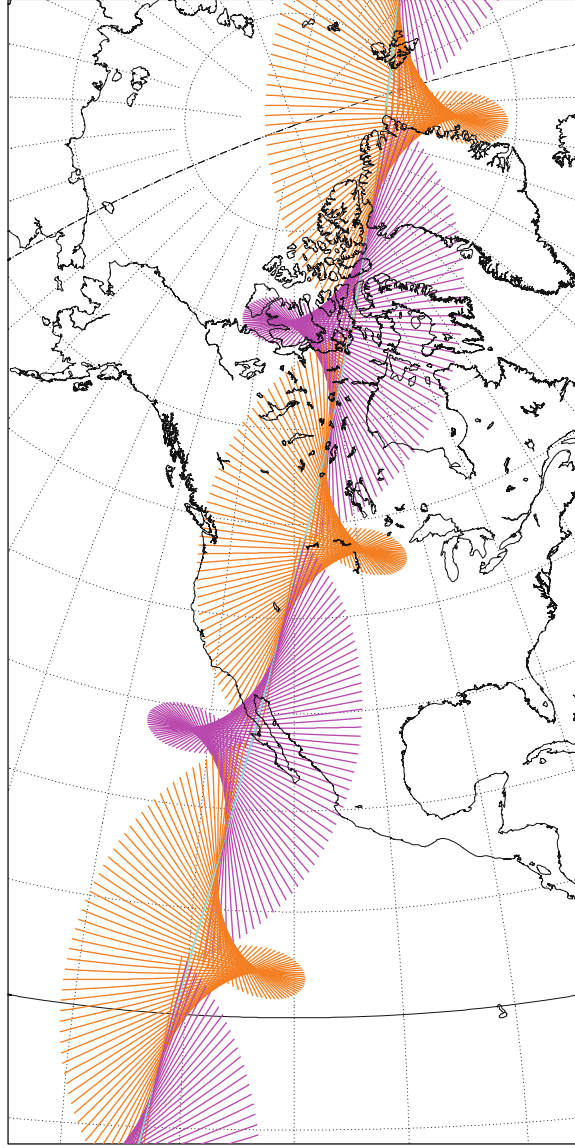
Projection: Guyou      Project centre: 45.0 ° N; 110.0 ° W      Asc. Node: 71.36 ° [22:30 LMT]      IξωωV  
 Property: Conformal      Aspect: Transverse > zoom : 3.50      Latit. overlap: 82.0° <--> 90.0°      MC \* LMD  
 ⊕ T.: [Ellipt. Int.] - Graticule: 10°      [5.3] [-45.0/ -90.0/+110.0] [-] EGM2008      A7λαΣ

FIG. 12.11 : Ground swath of the CERES instrument in XT mode.



**Terra / CERES****Orbit - Ground track**

Altitude = 699.6 km      a = 7077.736 km  
 Incl./SUN-SYNCHRON.= 98.21 °  
 Period = 98.88 min    \* rev/day =14.56  
 Equat. orbital shift = 2751.9 km ( 24.7 °)  
 \*\* Half-swath: 56.1 ° => 1222 km [ 0.10 min]  
 Recurrence = [15; -7; 16] 233  
 >>>> Time span shown: 99.0 min = 0.07 day  
 Alternated variable-yaw swath (RAP mode) [ +12.00 min]



Projection: Guyou      Project centre: 45.0 ° N; 110.0 ° W      Asc. Node: 71.36 ° [22:30 LMT]       $I \xi \omega \nu$   
 Property: Conformal      Aspect: Transverse > zoom :3.50      Swath / Alter. yaw var.      MC \* LMD  
 ⊕ T.: [Ellipt. Int.] - Graticule: 10°      [5.3] [-45.0/-90.0/+110.0] [ ] EGM2008      A7αδ

FIG. 12.12 : Ground swath of the CERES instrument in rotating azimuth plane (RAP) mode.

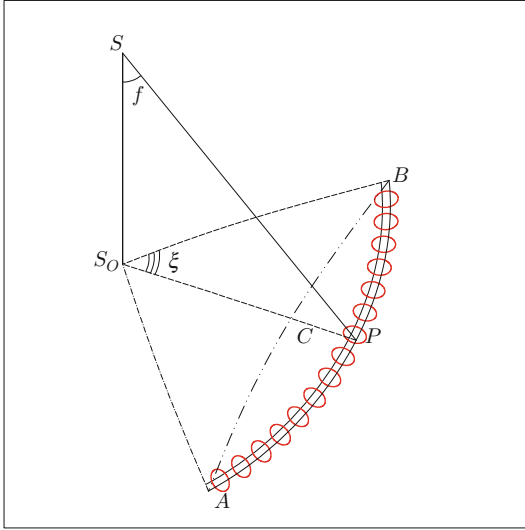


FIG. 12.13 : Schematic view of a conical swath from the satellite  $S$ , with nadir  $S_0$ , half-swath angle  $f$ , and half-aperture  $\xi$ .

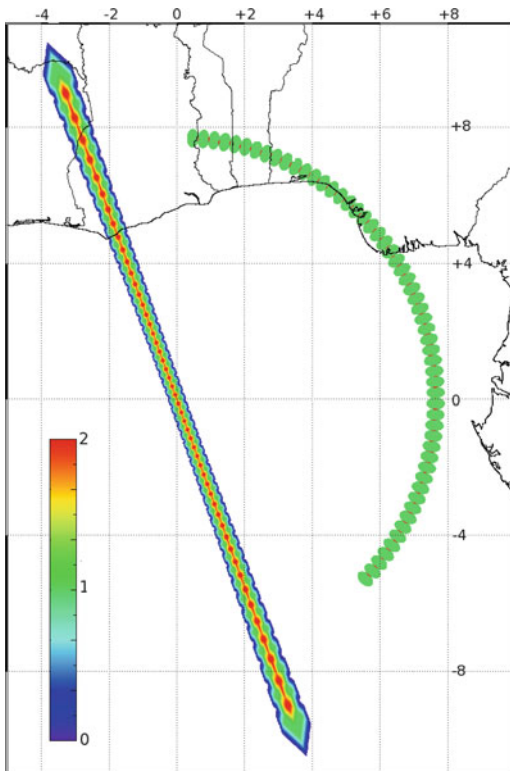


FIG. 12.14 : Cross-track swath (ScaRaB) and conical swath (MADRAS) for two instruments aboard Megha-Tropiques, the satellite being located vertically about the point of longitude  $0^\circ$  and latitude  $0^\circ$ . Each pixel is shown life size with its overlap ratio. Credit: Nicolas Gif, LMD/CNRS. Orbital data Ixion.



The conical swath is generally covered in the forward direction, with  $\xi_M$  of the order of  $60^\circ$ . With  $\xi_M = 90^\circ$ , the conical swath sketches out a half-circle, and with  $\xi_M = 180^\circ$ , a circle. The positions of the points making up the ground track of the conical swath are calculated using a matrix product, with the same kind of calculation as was discussed above for the cross-track swath.

The conical swath is characterised by the radius of the swath circle and by the effective or useful ground swath. The swath circle, centered on  $S_0$ , at the nadir of  $S$ , is generated by the point  $P$  which moves between  $A$  and  $B$ , as shown in Fig. 12.13. Its radius  $\rho_{\text{swath}}$  is thus

$$\rho_{\text{swath}} = R\alpha_M, \tag{12.29}$$

where  $\alpha_M$  is obtained from  $f_M$  or  $\zeta_M$  using (12.11) or (12.12), respectively.

The effective ground swath is the width of the ground swath. If  $F'_M$  is the half-width of the ground track, then  $2F'_M$  is represented by the distance  $AB$ , with midpoint  $C$ . (Note that the point  $C$  is not on the ground track of the swath.) The distance  $F'_M$  is given by the length of the arc  $CB$ , i.e.,  $F'_M = R\alpha'$ , where  $\alpha'$  is the corresponding angle at the center of the Earth (Fig. 12.14).

We obtain  $\alpha'$  from the spherical triangle  $S_0BC$ :

$$\hat{C} = \frac{\pi}{2}, \quad \widehat{S_0} = \xi_M, \quad \widehat{S_0B} = \alpha_M, \quad \widehat{BC} = \alpha'.$$

The sine rule (ST VIII) then gives

$$\sin \alpha' = \sin \alpha_M \sin \xi_M, \tag{12.30}$$

whence the effective half-width of the conical swath is

$$F' = R \arcsin(\sin \alpha_M \sin \xi_M). \tag{12.31}$$

In this result, if  $\xi_M > 90^\circ$ , we take  $\xi_M = 90^\circ$ , since the maximal effective swath is attained for  $\xi = 90^\circ$ .

**Example 12.9** *Swaths of various instruments aboard the satellite Megha-Tropiques.*

► The satellite Megha-Tropiques, flying at altitude  $h = 866$  km, carries three scanning instruments (see Fig. 12.15 upper).

The radiometer ScaRaB scans across track. Its maximal half-swath is  $f_M = 48.91^\circ$ , which corresponds to a maximal zenith angle of  $\zeta_M = 58.78^\circ$ . The ground track, which has width  $2F_M = 2,216$  km, is shown in Fig. 12.15 (lower). For clarity, not all swaths are shown.

The humidity sounder SAPHIR also scans across track:  $f_M = 42.96^\circ$ ,  $\zeta_M = 50.71^\circ$ ,  $2F_M = 1,724$  km (see Fig. 12.16 upper).

The microwave imager MADRAS scans conically, in such a way that points are viewed at an angle  $\zeta = 53.50^\circ$ . The viewing aperture  $\xi_M = 65^\circ$  on either side of the ground track. This determines a swath of effective width 1,702 km, shown in Fig. 12.16 (lower), every 12 s (the actual frequency is higher).



**Megha-Tropiques / ScaRaB**

Orbit - ref.: Earth

Recurrence = [14; -1; 7] 97

>>>> Time span shown: 60.0 min = 0.04 day

Across track swath (XT mode)

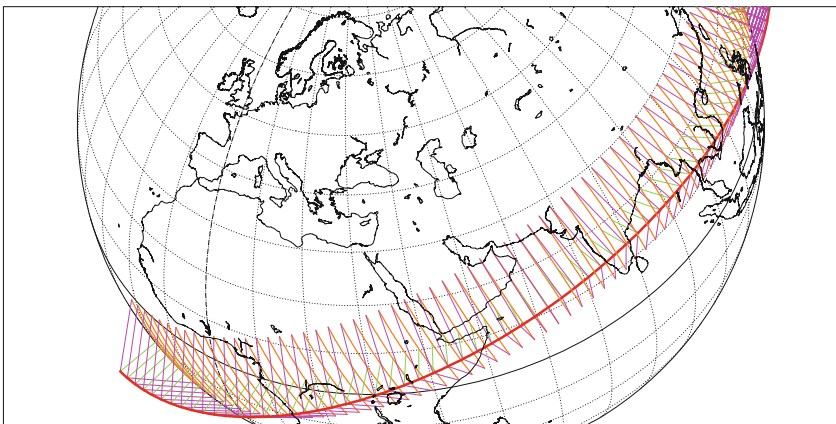
Altitude = 865.5 km                      a = 7243.677 km

Inclination = 20.00 °

Period = 101.93 min    \* rev/day = 14.13

Equat. orbital shift = 2892.0 km ( 26.0 °)

\*\* Half-swath: 48.9° => 1108 km [ 0.75 min]



Projection: Orthographic

Property: none

⊕ T.:Azimuthal - Graticule: 10°

PC: 50.0 ° N; 50.0 ° E / ZC: 35.0 ° N; 45.0 ° E

Aspect: Oblique

§.3[-90.0/ +40.0/ +40.0][ +16] EIGEN-C3

Asc. Node: 12.00 ° [12:00 LMT]

Max. attained latit. = 30.0 °

Ιξίων

MC ★ LMD

Ατλας

FIG. 12.15 : Upper: Satellite *Megha-Tropiques*, with its three instruments *MADRAS*, *Saphir*, and *ScaRaB*. The main innovation of *Megha-Tropiques* is to associate three radiometric instruments able to observe three interrelated components of the dynamic atmospheric system at the same time: water vapour, condensed water (clouds and precipitations), and radiative fluxes. Artist's view. Credit: CNES (Labo Photon—M. Régy). Lower: Cross-track swath of the instrument *ScaRaB* carried by *Megha-Tropiques*.

### Megha-Tropiques / Saphir

#### Orbit - Ground track

Recurrence = [14; -1; 7] 97

>>>> Time span shown: 100.0 min = 0.07 day

Across track swath (XT mode)

Altitude = 865.5 km

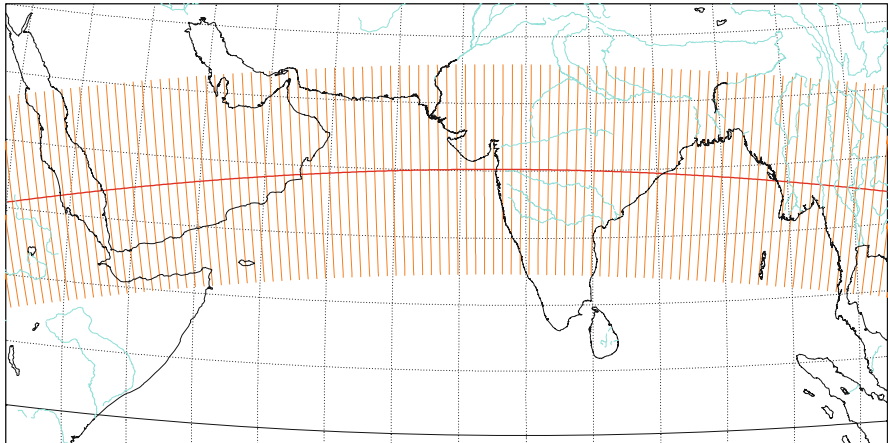
a = 7243.677 km

Inclination = 20.00 °

Period = 101.93 min \* rev/day = 14.13

Equat. orbital shift = 2892.0 km ( 26.0 °)

\*\* Half-swath: 43.0° => 862 km [ 0.20 min]



Projection: Raisz Armadillo

PC: 0.0 ° ; 75.0 °E/ZC: 16.0 ° N; 69.0 ° E

Asc. Node: -10.00 ° [00:00 LMT]

Ιξίων

Property: none

Aspect: Direct > zoom :4.00

Max. attained latit. = 27.8 °

MC ★ LMD

⊕ T.:(various) - Graticule: 5°

{5.3} [+90.0/ +0.0/-165.0] [-] EIGEN6C2

Ατλας

### Megha-Tropiques / MADRAS

#### Orbit - Ground track

Recurrence = [14; -1; 7] 97

>>>> Time span shown: 100.0 min = 0.07 day

Ground track - Conical swath / VZA=53.5°

Altitude = 865.5 km

a = 7243.677 km

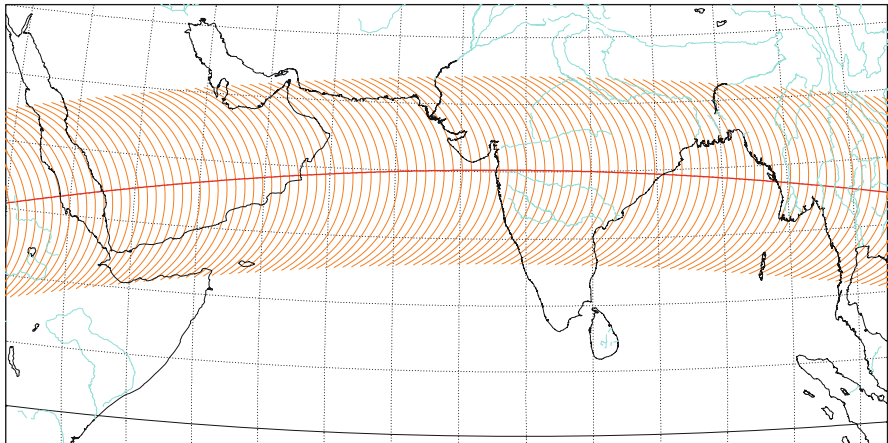
Inclination = 20.00 °

Period = 101.93 min \* rev/day = 14.13

Equat. orbital shift = 2892.0 km ( 26.0 °)

\*\* Half-aperture: 65.0° - Radius/grnd 940 km [ 0.20 min]

\*\* Effect. h-ap.: 42.6 ° => 851 km - Effect. swath: 1703 km



Projection: Raisz Armadillo

PC: 0.0 ° ; 75.0 °E/ZC: 16.0 ° N; 69.0 ° E

Asc. Node: -10.00 ° [00:00 LMT]

Ιξίων

Property: none

Aspect: Direct > zoom :4.00

Max. attained latit. = 27.6 °

MC ★ LMD

⊕ T.:(various) - Graticule: 5°

{5.3} [+90.0/ +0.0/-165.0] [-] EIGEN6C2

Ατλας

FIG. 12.16 : Ground swath of two instruments aboard Megha-Tropiques. Upper: Cross-track swath of Saphir. Lower: Conical swath of MADRAS.

Figure 12.14 indicates the actual ground tracks of the ScaRaB (cross-track) swath and the MADRAS (conical) swath, showing the effective pixels. ◀

**Example 12.10** *Conical ground swath of the radiometer SSM/I aboard the satellite DMSP-5D3 F-18.*

► The instrument SSM/I (Special Sensor Microwave/Imager) is a passive radiometer. Its axis makes a constant angle  $f_M$  with the axis of rotation, the nadir axis  $SZ$ , in such a way that the viewing zenith angle is constant at  $\zeta_M = 53.1^\circ$ . For this satellite at altitude  $h = 848$  km, calculation gives

$$f_M = 44.9^\circ, \quad \rho_{\text{swath}} = R\alpha_M = 913 \text{ km}.$$

Scanning is not through a complete circle of radius  $\rho_{\text{swath}}$ , but over an arc of angle  $2\zeta_M = 102.4^\circ$  on either side of the axis  $SX$  along the velocity vector. For this satellite, scanning is in the forward direction. The effective swath is given by (12.31) as

$$F'_M = 1,417 \text{ km}.$$

Figure 12.17 shows the ground track in steps of 1 min for improved visibility, while the radiometer actually rotates at 31.6 rev/min. During one revolution of the instrument, i.e., 1.9 s, the subsatellite point moves through 12.5 km. Looking at the ground track over 1 day, we see that a large fraction of the Earth's surface is viewed every day. ◀

#### 12.4.4 Ground Track Superposition

There are several reasons why one might wish to superpose the ground tracks of two satellites, for example, for a comparative study of the target-satellite geometry, or for calibration of similar instruments carried aboard two different satellites. Apart from the geometrical superposition of the tracks on the ground, there will also be a temporal constraint: the lapse of time between the crossings of the two satellites at a given point should not exceed 5 min, or 15 min, for example.

**Example 12.11** *Superposition of the ground tracks of the Sun-synchronous satellites MetOp-A and Aqua, during calibration of the instrument IASI.*

► Shortly after the launch of the European satellite MetOp-A, it was decided to compare the results obtained by its instrument IASI with those of a similar instrument aboard the American satellite Aqua. Now it happens that these two Sun-synchronous satellites have very different ascending node crossing

times, viz.,  $\tau_{AN} = 21:30$  for MetOp-A and  $\tau_{AN} = 13:30$  for Aqua. The dihedral angle between the two orbital planes is found by observing that

$$\tau_{AN}(\text{Aqua}) - \tau_{DN}(\text{MetOp-A}) = 13:30 - 09:30 = 04:00 ,$$

which implies an angle of  $4 \times 15^\circ = 60^\circ$ . Figure 10.14 adapted to these two satellites shows that the intersection of the ground tracks at a given time (at the same LMT time at a given place, hence at the same UT time) can only occur at very high latitudes, in the vicinity of  $80^\circ\text{N}$  and  $80^\circ\text{S}$ .

Figure 12.18 gives the result for a time span of 2 days, and tolerance  $\pm 15$  min. For each common ground swath, we note only the central point for greater visibility. With this time tolerance, the superpositions cannot occur for latitudes between  $60^\circ\text{N}$  and  $60^\circ\text{S}$ . ◀

**Example 12.12** *Superposition of the ground tracks of Megha-Tropiques and Terra during calibration of the ScaRaB instrument.*

► ScaRaB and CERES are radiometers yielding measurements of radiative flux. ScaRaB, aboard Megha-Tropiques, has a fixed cross-track (XT mode) scan, while CERES, aboard Terra, can vary its yaw angle and scan in RAP mode, in such a way that the ground swaths of these two instruments coincide and are parallel. For a 51 day validation exercise (this being the length of the cycle  $C_S$  relative to the Sun for Megha-Tropiques), in April and May 2012, we provided NASA with predictions for superpositions (times, places, and yaw angles). Figure 12.19 shows these intersections for the first day, 17 April 2012. ◀

## 12.5 View from a GEO Satellite

In this section, we begin by discussing how the Earth is viewed from a geostationary satellite, taking the Earth to be a sphere. We then examine in more detail the correspondence between the geographic coordinates of the point observed and the associated pixel. In this discussion, the Earth will be treated as an ellipsoid of revolution.

### 12.5.1 Simplified Geometric Conditions

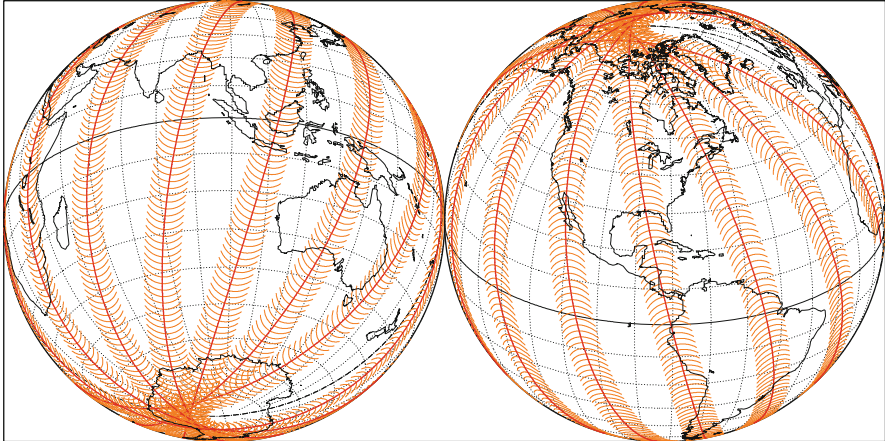
To understand the geometrical conditions under which a GEO satellite views the Earth, it is generally sufficient to treat the planet as spherical, identifying the latitudes  $\varphi$  and  $\psi$ . When the satellite views the Earth, the maximum swath in the sense that we have defined  $f_0$  is

$$f_0 = \arcsin \frac{1}{\eta_{GS}} , \tag{12.32}$$

**DMSP F-13 / SSM/I**  
Orbit - Ground track

>>>> Time span shown: 720.0 min = 0.50 day  
Ground track - Conical swath / VZA=53.1°

Altitude = 848.0 km                      a = 7226.136 km  
Inclin./SUN-SYNCHRON.= 98.83 °  
Period = 102.00 min    \* rev/day =14.12  
Equat. orbital shift = 2838.8 km ( 25.5 °)  
\*\* Half-aperture: 51.0° - Radius/grnd 913 km [ 0.50 min]  
\*\* Effect. h-ap.: 38.6 ° => 709 km - Effect. swath: 1417 km



Projection: Orthographic	Pr. centre (r.): 28.0 ° N; 82.0 ° W	Asc. Node: -4.00 °	<i>Ιξίων</i>
Property: none	Aspect: Oblique	Max. attained latit. = 87.5 °	MC ★ LMD
⊕ T.:Azimuthal - Graticule: 10°	⊕.2{ [-90.0/ +62.0/+172.0] [-] GEM-T2		<i>Ατλας</i>

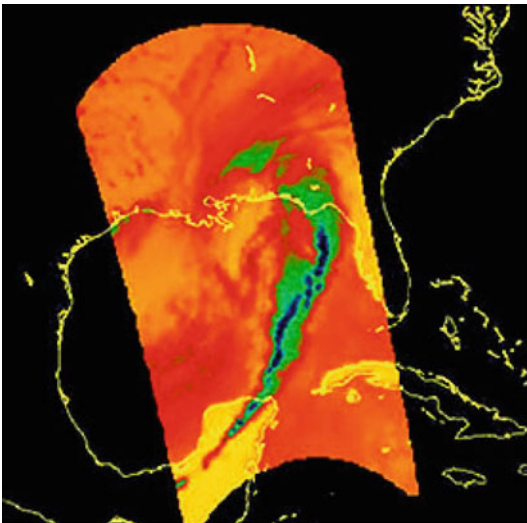


FIG. 12.17 : Meteorological satellite DMSP F-13. Upper: Ground track of the satellite and conical swath of the instrument SSM/I over half a day. Lower: Swath of SSM/I above the Gulf of Mexico. The instrument measures the brightness temperature and can thus distinguish hot and cold clouds. Credit: GSFC NASA.



where the reduced distance  $\eta_{GS}$  is here defined by (7.72). With  $\eta_{GS} = 6.611$ , this gives the numerical value

$$f_0 = 8.700^\circ = 0.1518 \text{ rad} . \tag{12.33}$$

The corresponding angle at the center of the Earth is

$$\alpha_0 = \arccos \frac{1}{\eta_{GS}} = 90^\circ - 8.7^\circ = 81.3^\circ \implies 2F_0 = 18,100 \text{ km} . \tag{12.34}$$

The part of the Earth viewed by a geostationary satellite is called the Earth’s disk, or the slot (see Figs. 12.20 and 12.26).

Let  $\lambda_S$  be the longitude of the satellite  $S$  (the parking longitude or longitude of the subsatellite point). Then the longitudes viewed on the equator by  $S$  lie in the interval

$$[\lambda_S - 81.3^\circ, \lambda_S + 81.3^\circ] .$$

Along the meridian  $\lambda_S$ , the latitudes viewed occupy the same interval of  $81.3^\circ$  on either side of the equator.

For an arbitrary point  $P$  on the Earth, with geographic coordinates  $\lambda$  and  $\varphi$ , we write the distance  $D$  to the subsatellite point  $S_0$  (we mean, of course, the distance on the sphere, measured along a great circle, viz.,  $D = R\alpha$ ) using the spherical triangle  $S_0PP'$ , where  $P'$  is the intersection of the meridian of  $P$  with the equator:

$$\begin{aligned} \cos \widehat{S_0P} &= \cos \widehat{S_0P'} \cos \widehat{PP'} , \\ \cos \alpha &= \cos(\lambda - \lambda_S) \cos \varphi . \end{aligned} \tag{12.35}$$

This corresponds to (ST 1).

The locus of points  $P$  viewed at distance  $D$  from the subsatellite point is thus defined by

$$D = R \frac{\pi}{180} \arccos [\cos(\lambda - \lambda_S) \cos \varphi] , \tag{12.36}$$

where the angles are in degrees. This is the locus of points viewed at the same angle from the satellite, and hence viewed with the same pixel distortion.

The condition for the point  $P$  to be viewed at all is given by (12.6) and (12.35) as

$$\eta_{GS} \cos \varphi \cos(\lambda - \lambda_S) \geq 1 . \tag{12.37}$$

The area  $s$  of the Earth which is viewed, for a given value of the angle  $\alpha$ , is

$$s(\alpha) = 2\pi R^2(1 - \cos \alpha) .$$

The maximal area viewed is thus  $s(\alpha_0)$ , which represents the fraction

$$\frac{s(\alpha_0)}{4\pi R^2} = \frac{1}{2} \left( 1 - \frac{1}{\eta_{GS}} \right) = 0.424 , \tag{12.38}$$

or about 42% of the total area.

### MetOp-A [ & Aqua ]

0 km <-> 1600 km - Locations of overlapping

Altitude = 817.4 km      a = 7195.548 km

Incl. / SUN-S. = 98.67 °      e = 0.000106

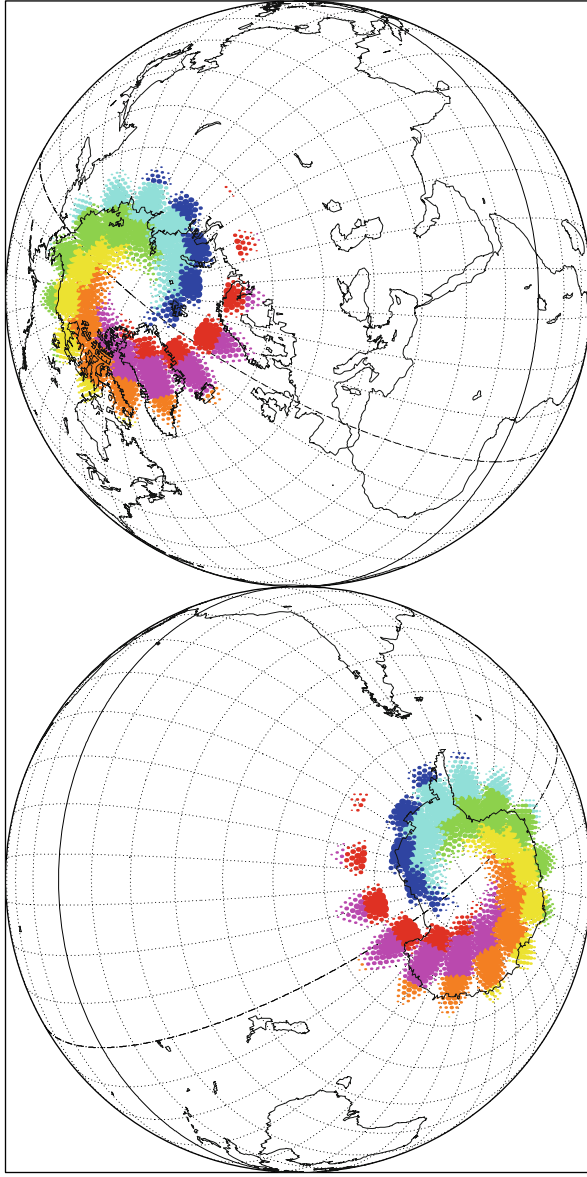
Period = 101.36 min      \* rev/day = 14.21

Recurrence = [14; +6; 29] 412

2008 03 07 00:00:00 UTC >>> 2880.0 min = 2.00 days

<-> [+/- 800 km] MetOp-A      <-> [+/- 800 km] Aqua

Time Difference (min)      -15.0      -10.0      -5.0      0.0      5.0      10.0      15.0      t = 0 <-> MetOp-A



Projection: Orthographic      Pr. centre (r.): 55.0 ° N; 35.0 ° E      Asc. Node: 33.99 ° [21:30 LMT]       $I \xi_{\omega \omega \nu}$

Property: none      Aspect: Oblique      [NORAD] Revolution: 7161      MC ★ L1MID

⊕ T.:Azimuthal - Graticule: 10°      {4.2} [-90.0 / +35.0 / +55.0] [-]      EGM2008      [NORAD] 2008 03 06 19:13:41 UTC      A7λαζ

FIG. 12.18 : Locus of ground track superpositions for MetOp-A and Aqua over 2 days. Calibration of the instrument IASI.

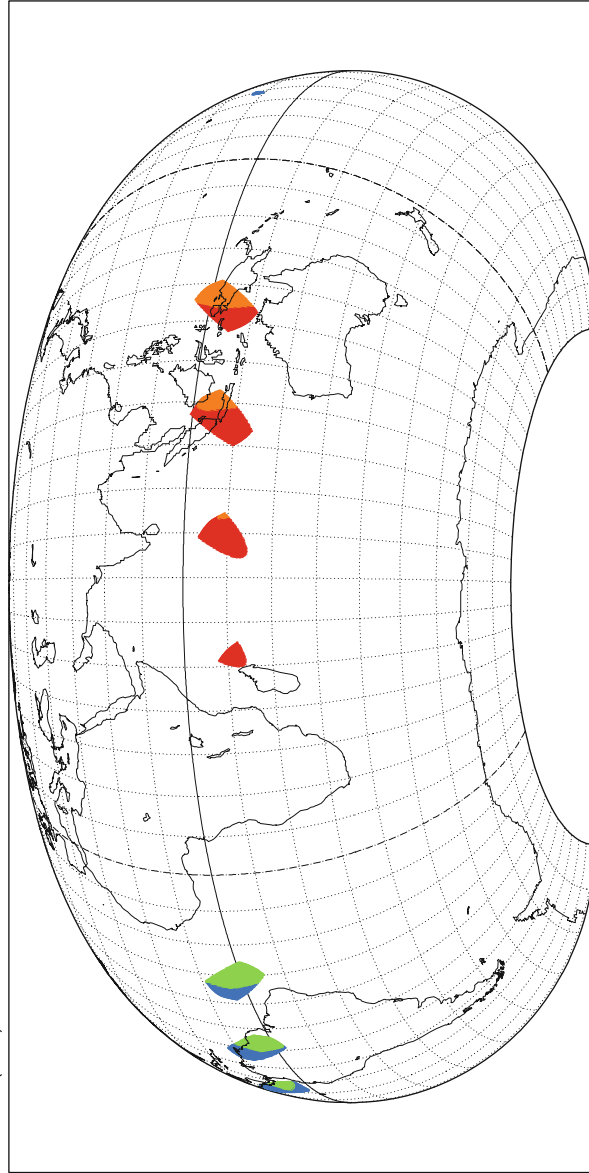


### Megha-Tropiques [ & Terra ]

0 km <-> 1760 km - Locations of overlapping  
 [ +/- 4; 0 min ]  
 Recurrence = [14; -1; 7] 97

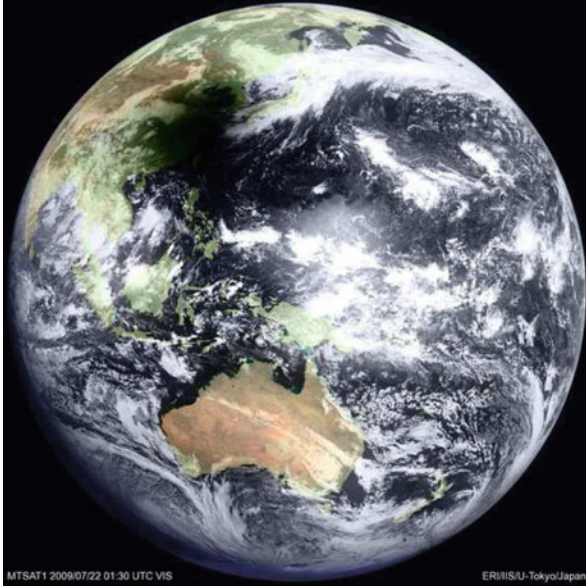
Altitude = 865.5 km      a = 7243.596 km  
 Inclination = 19.98 °      e = 0.001025  
 Period = 101.93 min      \* rev/day = 14.13

2012 04 17 00:00:00 UTC >>> 1440.0 min = 1.00 day <-> [ +/- 1108 km ] Megha-Trop <-> [ +/- 1165 km ] Terra  
 LMT (local) 00 01 02 03 04 05 06 07 08 09 10 11 12 13 14 15 16 17 18 19 20 21 22 23 24 hours



Proj.: Raisz / -19.00°      P.C.: 0.0 ° ; 68.0 ° E / 26.8 ° S; 68.0 ° E      Asc. Node: 147.39 ° [11:37 LMT]       $I \xi \omega \nu$   
 Property: none      Aspect: Direct      [NORAD] Revolution: 2637      MC ★ LMD  
 ⊕ T.: (various) - Graticule: 10°      {4.2} [+90.0/ +0.0/-158.0] [-] EGM2008      [NORAD] 2012 04 16 01:47:39 UTC      A7λ α ζ

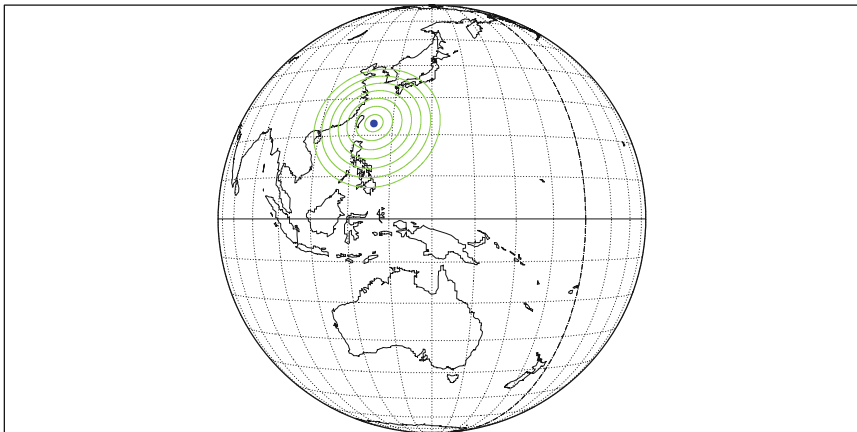
FIG. 12.19 : Locus of ground track superpositions for Megha-Tropiques and Terra over 1 day, on 17 April 2012. Calibration of the ScaRaB instrument. Only daylight superpositions (red or orange) are retained for calibration.



**MTSAT-1R** 〈ひまわり〉

Satellite  
Geostationary

Altitude =35787.6 km                      a<sub>GS</sub> = 42165.785 km  
 Inclination = 0.00 °                      Parking Longit.=140.0 ° E  
 Period = 1435.91 min \* rev/day = 1.00  
 Equat. orbital shift =40072.1 km



Proj.: Perspect.V. h=5.61 R	Project. centre: 0.0 ° ; 140.0 ° E	Geostationary	<i>Ιξίων</i>
Property: none	Aspect: Equatorial		MC ★ LMD
⊕ T.:Azimuthal - Graticule: 10°	{4.2} [-90.0/ +90.0/ -50.0] [-]	EGM2008	Ατλας

FIG. 12.20 : Upper: View of the Earth from MTSAT-1R (Himawari-6), 22 July 2009, 01:30 UT. Total eclipse of the Sun, centered at this precise moment on Taiwan (09:30 local time). Credit: Institute of Industrial Science & Earthquake Research Institute (IISERI), University of Tokyo, Japan. Lower: Reconstitution of the eclipse as seen by MTSAT-1R.

**Example 12.13** Represent the locus of points on the Earth that are equidistant from the subsatellite point of a GEO satellite.

► The distance  $D$  between a point on the Earth seen by the geostationary satellite and the subsatellite point of the same satellite is defined by (12.36). The locus of points on the Earth at the same distance  $D$  has been represented with steps of 500 km in the value of  $D$ , and 250 km in the enlarged maps. We denote these loci by  $\mathcal{L}(D)$ .

**METEOSAT.** In their operational phase, the European satellites METEOSAT are stationed at longitude  $\lambda_S = 0^\circ$ . Figure 12.21 (upper) shows the Earth as it is viewed by the satellite (the Earth's disk or slot). For given  $D$ , the curves  $\mathcal{L}(D)$  are circles, represented by circles on this map, which has a non-conformal but axisymmetric projection, called the perspective projection. The Guyou projection, based on elliptic functions, presents the globe as a rectangle, whilst preserving angles, i.e., it is a conformal projection. The curves  $\mathcal{L}(D)$  are represented in the direct aspect in Fig. 12.21 (lower).

**Feng Yun-2.** The Chinese satellites FY-2A then FY-2B are stationed at longitude  $\lambda_S = 105^\circ\text{E}$ . Figure 12.22 (upper) shows the locus of points  $\mathcal{L}(D)$  viewed from the same angle in an orthographic representation centered on Peking (on the right).

**GOES.** The US satellite GOES-East is stationed at longitude  $\lambda_S = 75^\circ\text{W}$ . This position was previously occupied by the succession of satellites SMS-1, SMS-2, GOES-5, GOES-7, and GOES-8 (partial or total occupation during their operating lifetimes). The Argentinian meteorological office (*Servicio Meteorológico Nacional*) represents data in a stereographic projection centered on the point  $(34.8^\circ\text{S}, 68.6^\circ\text{W})$ , which is located in the middle of the country. We have used this projection in Fig. 12.22 (lower) to represent the locus of points viewed at the same angle. This locus  $\mathcal{L}(D)$  is thus represented by circles here, a property of the stereographic projection. We note that GOES-East and Feng Yun-2 are diametrically opposite one another with respect to the center of the Earth.

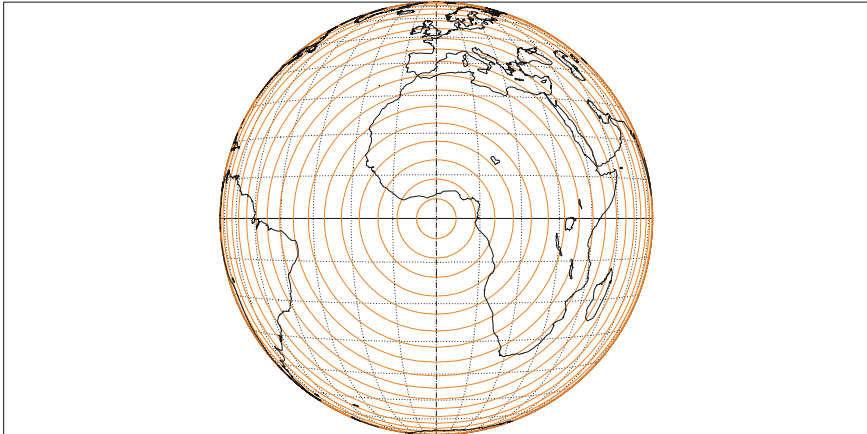
**Elektro-1.** The Russian satellite Elektro-1 (GOMS-1) is stationed at longitude  $\lambda_S = 76^\circ\text{E}$ . We have represented  $\mathcal{L}(D)$  in a transverse Guyou projection centered on Moscow in Fig. 12.23. It is clear why geostationary satellites are not of much interest to Russia.

**Anik-F2.** The Canadian telecommunications satellite Anik-F2 is stationed at longitude  $\lambda_S = 111.1^\circ\text{W}$ . We have represented  $\mathcal{L}(D)$  in a transverse Guyou projection centered on Winnipeg, MB (Canada), in Fig. 12.24. Once again, it is

### METEOSAT

Locus of points  
equidistant  
from the subsatellite point

Altitude = 35787.6 km      a<sub>GS</sub> = 42165.785 km  
 Inclination = 0.00°      Parking Longit. = 0.0°  
 Period = 1435.91 min    \* rev/day = 1.00  
 Equat. orbital shift = -40072.1 km  
 \*\* Half-swath: 8.7° - On ground 9050.2 km [ 500.0 km]

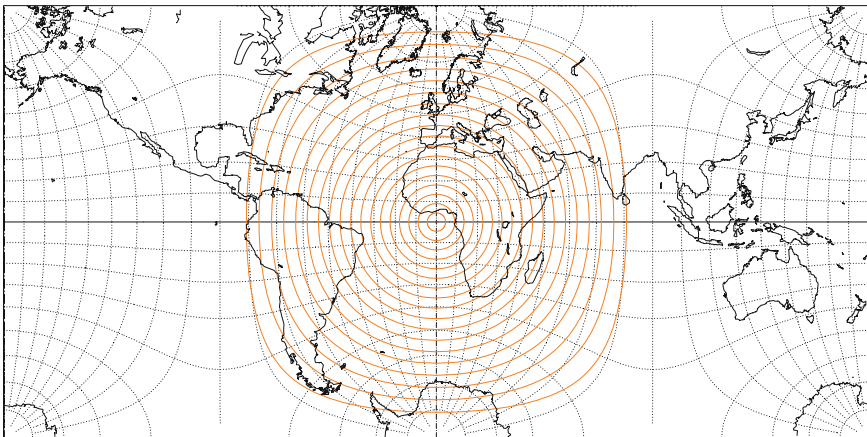


Proj.: Perspect.V. h=5.61 R      Project. centre: 0.0° ; 0.0°      Geostationary      *Ιξίωv*  
 Property: none      Aspect: Equatorial      Max. attained latit. = 81.3°      MC ★ LMD  
 ⊕ T.:Azimuthal - Graticule: 10°    {4.2} [ -90.0/ +90.0/ +90.0] [-] EGM2008      *Ατλας*

### METEOSAT

Locus of points  
equidistant  
from the subsatellite point

Altitude = 35787.6 km      a<sub>GS</sub> = 42165.785 km  
 Inclination = 0.00°      Parking Longit. = 0.0°  
 Period = 1435.91 min    \* rev/day = 1.00  
 Equat. orbital shift = -40072.1 km  
 \*\* Half-swath: 8.7° - On ground 9050.2 km [ 500.0 km]



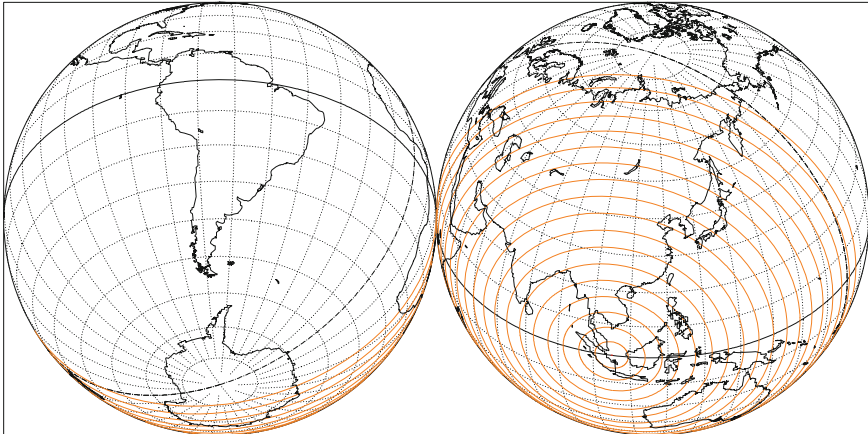
Projection: Guyou      Project. centre: 0.0° ; 0.0°      Geostationary      *Ιξίωv*  
 Property: Conformal      Aspect: Direct      Max. attained latit. = 81.3°      MC ★ LMD  
 ⊕ T.:{Ellipt. Int.} - Graticule: 10°    {4.2} [ +90.0/ +0.0/ -90.0] [-] EGM2008      *Ατλας*

FIG. 12.21 : Locus of points equidistant from the subsatellite point for the geostationary satellite METEOSAT.

### Feng Yun-2 〈風雲二〉

Locus of points  
equidistant  
from the subsatellite point

Altitude = 35787.6 km      a<sub>GS</sub> = 42165.785 km  
 Inclination = 0.00°      Parking Longit. = 105.0° E  
 Period = 1435.91 min \* rev/day = 1.00  
 Equat. orbital shift = 40072.1 km  
 \*\* Half-swath: 8.7° - On ground 9050.2 km [ 500.0 km]



Projection: Orthographic      Pr. centre (r.): 40.0° N; 116.0° E  
 Property: none      Aspect: Oblique  
 ⊕ T.: Azimuthal - Graticule: 10° {4.2} [ -90.0/ +50.0/ -26.0] [-] EGM2008

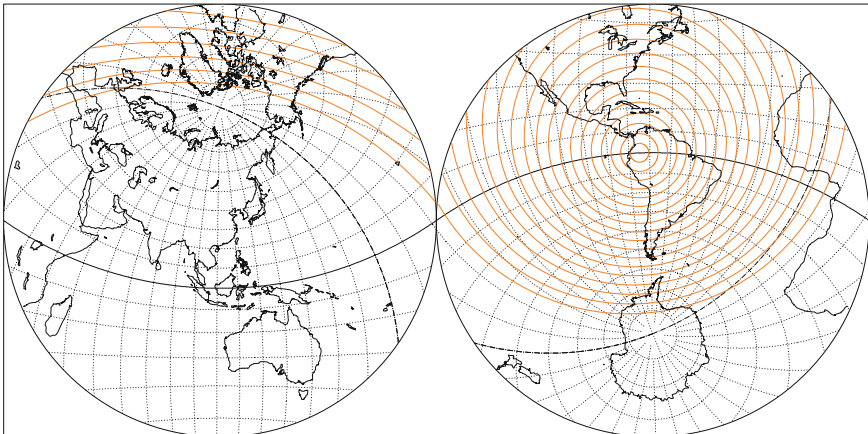
Geostationary  
 Max. attained latit. = 81.3°

Ιξίων  
 MC ★ LMD  
 Ατλας

### GOES-E

Locus of points  
equidistant  
from the subsatellite point

Altitude = 35787.6 km      a<sub>GS</sub> = 42165.785 km  
 Inclination = 0.00°      Parking Longit. = 75.0° W  
 Period = 1435.91 min \* rev/day = 1.00  
 Equat. orbital shift = 40072.1 km  
 \*\* Half-swath: 8.7° - On ground 9050.2 km [ 500.0 km]



Projection: Stereographic      Pr. centre (r.): 34.8° S; 68.6° W  
 Property: Conformal      Aspect: Oblique  
 ⊕ T.: Azimuthal - Graticule: 10° {4.2} [ -90.0/ +124.8/ +158.6] [-] EGM2008

Geostationary  
 Max. attained latit. = 81.3°

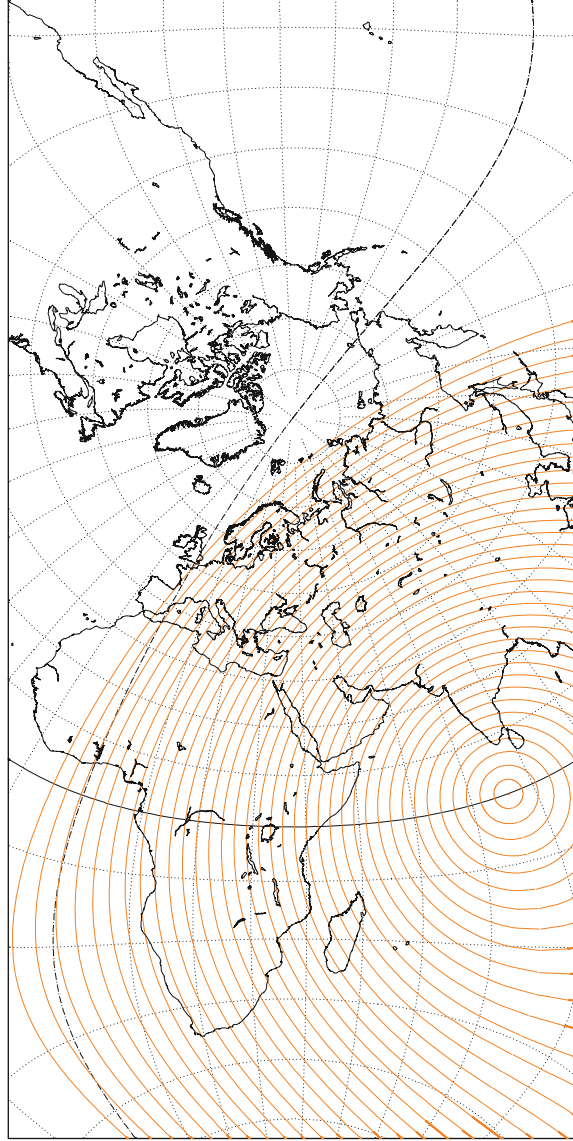
Ιξίων  
 MC ★ LMD  
 Ατλας

FIG. 12.22 : Locus of points equidistant from the subsatellite point for the three satellites GEO, FY-2, and GOES-E.

# GOMS/Elektro < Электро >

Locus of points  
equidistant  
from the subsatellite point

Altitude = 35787.6 km      a<sub>GS</sub> = 42165.785 km  
 Inclination = 0.00°      Parking Longit. = 76.0° E  
 Period = 1435.91 min      \* rev/day = 1.00  
 Equat. orbital shift = 40072.1 km  
 \*\* Half-swath: 8.7° - On ground 9050.2 km [ 250.0 km]



Projection: Guyou      Project. centre: 55.8° N; 37.6° E      Geostationary  
 Property: Conformal      Aspect: Transverse > zoom : 1.60      Max. attained latit. = 81.3°      MC ★ LMD  
 ⊕ T.: [Ellipt. Int.] - Graticule: 10°      (5.3) [-55.8/ -90.0/ -37.6] [-]      EGM2008      ΑΤΛΑΧ

FIG. 12.23 : Locus of points equidistant from the subsatellite point for the Russian GEO satellite Elektro-1. Map centered on Moscow (Russia).

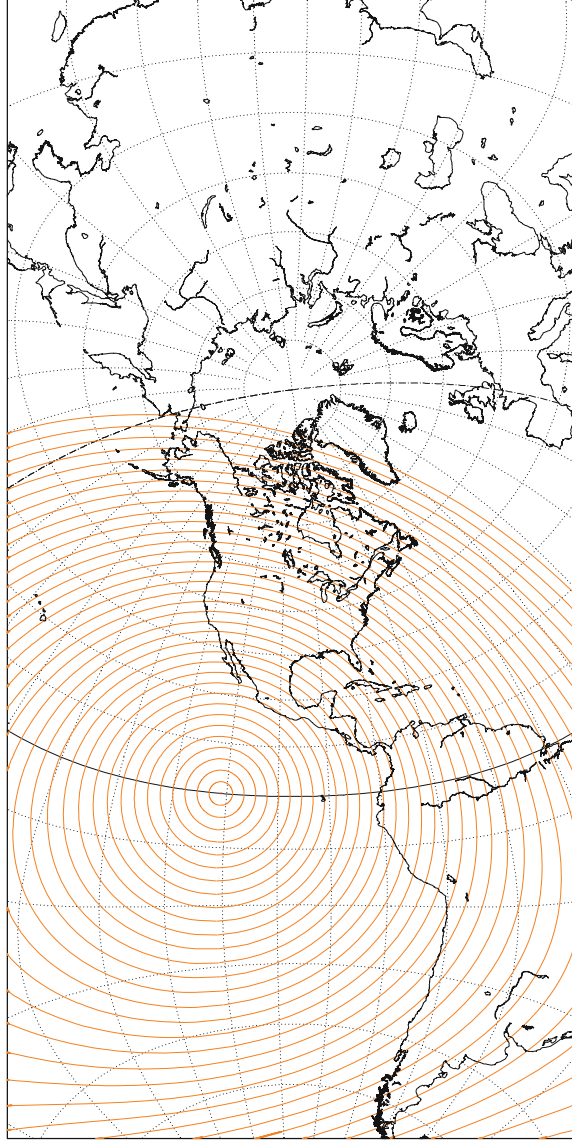


**Anik-F2** (  $\langle \sigma^b \rangle$  )

Locus of points  
equidistant

from the subsatellite point

Altitude = 35787.6 km      a<sub>GS</sub> = 42165.785 km  
 Inclination = 0.00 °      Parking Longit. = 111.1 ° W  
 Period = 1435.91 min      \* rev/day = 1.00  
 Equat. orbital shift = 40072.1 km  
 \*\* Half-swath: 8.7° - On ground 9050.2 km [ 250.0 km]



Projection: Guyou      Project. centre: 49.9 ° N; 97.2 ° W      Geostationary      Iξωων  
 Property: Conformal      Aspect: Transverse > zoom : 1.60      Max. attained latit. = 81.3 °      MC ★ LMD  
 ⊕ T.: [Ellipt. Int.] - Graticule: 10° (5:3) [-49.9/ -90.0/ +97.2] [-]      EGM2008      Ατλας

FIG. 12.24 : Locus of points equidistant from the subsatellite point for the Canadian GEO satellite Anik-F2. Map centered on Winnipeg, MB (Canada).

clear that the position of the geostationary orbit is not particularly favourable for Canada. ◀

### 12.5.2 Precise Correspondence Between Pixels and Geographic Coordinates

Let  $O$  be the center of the Earth and  $R$  its equatorial radius. We consider the following geocentric orthonormal frame:  $Oz$  is the polar axis,  $xOy$  is the equatorial plane, and  $Ox$  passes through  $S$ , the position of the GEO satellite. The parking longitude of the satellite is  $\lambda_S$ . A point  $P$  on the Earth's surface is specified by its geographical coordinates, i.e., the longitude  $\lambda$  and the geodetic latitude  $\varphi$ .

The Cartesian coordinates of the points  $S$  and  $P$  are thus

$$\mathbf{OS} = \begin{pmatrix} r = \eta_{\text{GS}}R \\ 0 \\ 0 \end{pmatrix}, \quad \mathbf{OP} = \begin{pmatrix} x = \mathcal{N} \cos \varphi \cos(\lambda - \lambda_S) \\ y = \mathcal{N} \cos \varphi \sin(\lambda - \lambda_S) \\ z = \mathcal{N}(1 - e^2) \sin \varphi \end{pmatrix}, \quad (12.39)$$

where  $\mathcal{N}$  is the great normal given by

$$\mathcal{N} = \frac{R}{\sqrt{(1 - e^2 \sin^2 \varphi)}},$$

as discussed in Chap. 2 [see (2.15) and (2.12)]. Note in passing that the eccentricity  $e$  appearing here in these expressions relating to geodesy is the eccentricity of the Earth ellipsoid. When we use  $\mathcal{N}$  and  $\varphi$ , the equations are simpler with the eccentricity  $e$  than with the flattening  $f$ .

We consider the plane parallel to  $yOz$  which passes through  $P$ . This plane  $\mathcal{P}$  contains the points  $P$ ,  $P'$ , and  $P''$  (see Fig. 12.25), where  $P'$  is the projection of  $P$  onto the equatorial plane  $xOy$  and  $P''$  is the projection of  $P'$  onto the axis  $Ox$ .

The image of the Earth as viewed from  $S$  is formed in a plane  $\mathcal{I}$  called the image plane, parallel to  $\mathcal{P}$  and located at an arbitrary distance from  $S$ . In  $\mathcal{I}$ , we define a plane coordinate frame with center  $O_i$  at the intersection of  $OS$  with  $\mathcal{I}$ . The axes are  $O_iy_i$ , the intersection of the equatorial plane with  $\mathcal{I}$ , and  $O_iz_i$ , the intersection of the meridian plane  $xOz$  through  $S$  with  $\mathcal{I}$ . Then  $O_iy_i$  is parallel to  $Oy$  and  $O_iz_i$  is parallel to  $Oz$ . A pixel  $Q$  is the image of the point  $P$  on the Earth: it sits at the intersection of  $SP$  with the image plane  $\mathcal{I}$ . The point  $Q$  is specified in  $\mathcal{I}$  by its coordinates  $C$  and  $L$ :

- The coordinate  $C$  (column) is measured along  $O_iy_i$ .
- The coordinate  $L$  (row) is measured along  $O_iz_i$ .

In Fig. 12.25,  $Q''$  is at  $O_i$ ,  $C$  is obtained from  $Q''Q'$ , and  $L$  is obtained from  $Q'Q$ . The coordinates  $C$  and  $L$  have the units of angles.



### Pixel Coordinates as a Function of Geographical Coordinates

The problem here is to establish the mapping  $(\lambda, \varphi) \mapsto (C, L)$ . In fact, it is straightforward to calculate the values of  $C$  and  $L$  in terms of  $\lambda$  and  $\varphi$  by referring everything to  $x$ ,  $y$ , and  $z$ . Consider the triangle  $SP''P'$  in the equatorial plane. This is right-angled at  $P''$  and we have

$$\tan C = \frac{Q''Q'}{Q''S} = \frac{P''P'}{P''S} .$$

Further, the triangle  $SP'P$  is perpendicular to the equatorial plane and right-angled at  $P'$ , and we have

$$\tan L = \frac{Q'Q}{Q'S} = \frac{P'P}{P'S} .$$

We thus obtain

$$\tan C = \frac{y}{r-x} , \quad \tan L = \frac{z}{\sqrt{(r-x)^2 + y^2}} . \tag{12.40}$$

### Visibility Conditions

Let  $\zeta$  be the angle between the normal to the Earth at  $P$ , the local vertical  $\mathbf{Pn}$ , and the direction  $\mathbf{PS}$ . The scalar product  $\mathcal{A}$  specifies the visibility conditions:

$$\mathcal{A} = \mathbf{PS} \cdot \mathbf{Pn} = \|\mathbf{PS}\| \|\mathbf{Pn}\| \cos \zeta . \tag{12.41}$$

If  $\mathcal{A} \geq 0$ , the viewing zenith angle  $\zeta$  lies between  $0^\circ$  and  $90^\circ$  and the point  $P$  is seen by the satellite  $S$ . Otherwise, it is not visible.

By definition,  $\mathbf{Pn}$  lies along the great normal  $\mathcal{N}$ . We can thus deduce its components, and also the components of  $\mathbf{PS}$ :

$$\mathbf{Pn} = \mathcal{N} \begin{pmatrix} \cos \varphi \cos(\lambda - \lambda_S) \\ \cos \varphi \sin(\lambda - \lambda_S) \\ \sin \varphi \end{pmatrix} ,$$

$$\mathbf{PS} = \mathcal{N} \begin{pmatrix} \eta_{GS} R / \mathcal{N} - \cos \varphi \cos(\lambda - \lambda_S) \\ -\cos \varphi \sin(\lambda - \lambda_S) \\ -(1 - e^2) \sin \varphi \end{pmatrix} .$$

Taking the scalar product, the condition  $\mathcal{A} \geq 0$  can be written

$$\eta_{GS} \sqrt{1 - e^2 \sin^2 \varphi} \cos \varphi \cos(\lambda - \lambda_S) + e^2 \sin^2 \varphi \geq 1 . \tag{12.42}$$

In this case,

$$0^\circ \leq \zeta \leq 90^\circ \iff P \text{ visible to } S .$$

Imposing the spherical Earth assumption, i.e., setting  $e = 0$  in (12.42), we obtain (12.37).

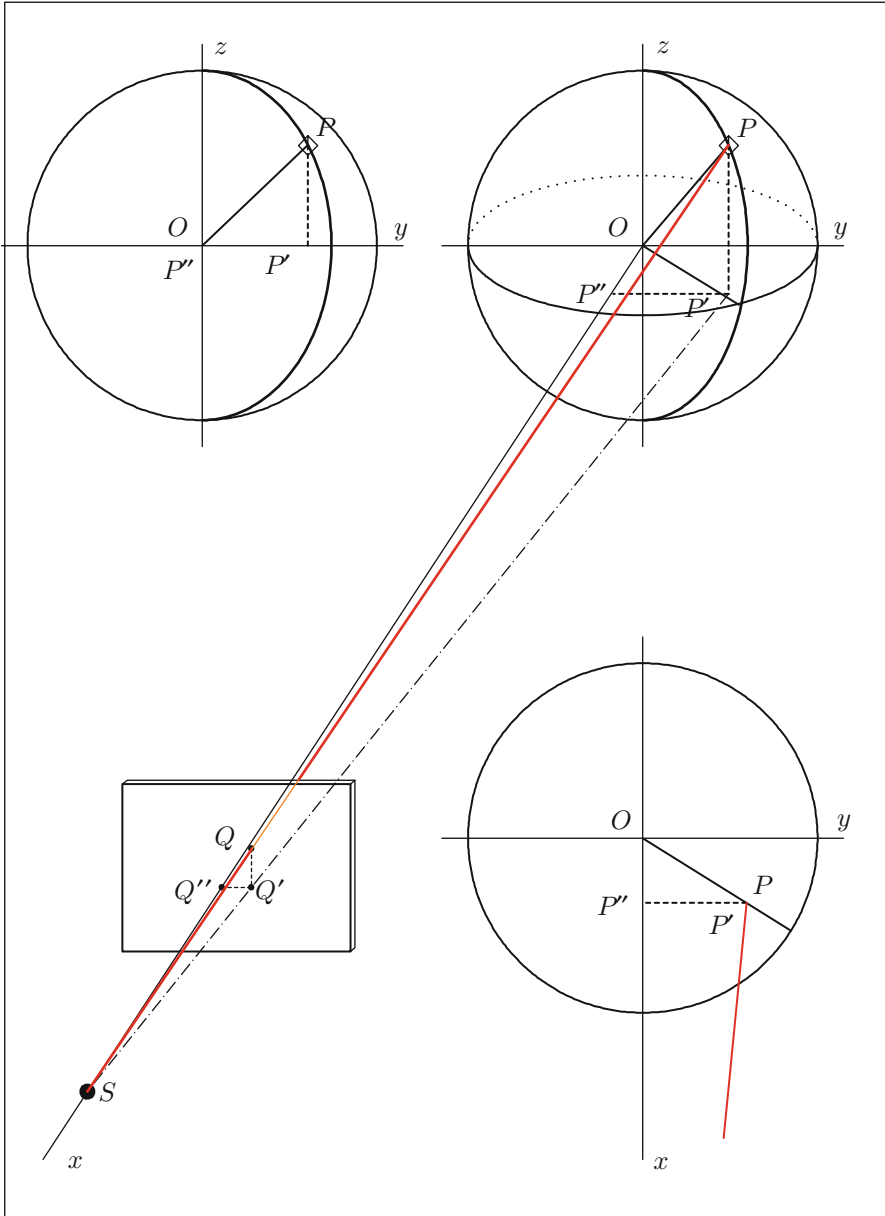


FIG. 12.25 : View of the Earth from a geostationary satellite. Correspondence between pixels and geographical coordinates. The center of the Earth is  $O$  and the satellite is at  $S$ . The observed point (pixel) is denoted by  $P$ . The polar axis is  $Oz$ , the equatorial plane  $xOy$ , and the axis  $Ox$  passes through  $S$ . The points  $Q$ ,  $Q'$ , and  $Q''$  lie in the image plane  $\mathcal{I}$ , parallel to the plane  $\mathcal{P}$ , which contains  $P$ ,  $P'$ , and  $P''$  and is perpendicular to the equatorial plane.

### Geographical Coordinates as a Function of Pixel Coordinates

The problem here is to establish the mapping  $(C, L) \mapsto (\lambda, \varphi)$ . We consider the image plane  $\mathcal{I}$  at an arbitrary distance  $l_0$  from  $S$ . Let  $ul_0$  and  $vl_0$  be the coordinates of the point  $Q$  in the plane  $\mathcal{I}$ , with axes  $O_iy_i$  and  $O_iz_i$  specified above:

$$Q''Q' = ul_0, \quad Q'Q = vl_0.$$

In a frame centered on  $S$ , obtained by translating the frame centered on  $O$  along the axis  $Ox$ , the coordinates of  $Q$  are

$$\mathbf{SQ} = l_0 \begin{pmatrix} -1 \\ u \\ v \end{pmatrix},$$

where  $u$  and  $v$  are dimensionless quantities.

Considering the triangles discussed previously, we obtain  $C$  and  $L$  as a function of  $u$  and  $v$ :

$$\tan C = \frac{Q''Q}{Q''S} = \frac{u}{1}, \quad \tan L = \frac{Q'Q}{Q'S} = \frac{v}{\sqrt{1+u^2}}.$$

Given  $L$  and  $C$ , we can thus find  $u$  and  $v$  from

$$u = \tan C, \quad v = \tan L \sqrt{1 + \tan^2 C}. \tag{12.43}$$

We can slide the plane  $\mathcal{I}$  parallel to itself so that it coincides with the plane  $\mathcal{P}$ , with the axes  $O_iy_i$  and  $O_iz_i$  parallel to the axes  $Oy$  and  $Oz$ . To do this, we multiply the vector  $\mathbf{SQ}$  by a positive scalar  $k$  such that  $k\mathbf{SQ} = \mathbf{SP}$ . Setting  $K = kl_0$ , this amounts to finding the distance  $K$  such that

$$K \begin{pmatrix} -1 \\ u \\ v \end{pmatrix} = \begin{pmatrix} x - r \\ y \\ z \end{pmatrix} \implies \begin{pmatrix} x = r - K \\ y = uK \\ z = vK \end{pmatrix}.$$

To do this, we express the fact that the point  $Q$  coincides with  $P$ , hence lies on the Earth ellipsoid:

$$x^2 + y^2 + \frac{z^2}{1 - e^2} = R^2.$$

Substituting the values of the Cartesian coordinates, we obtain a quadratic equation for  $K$ :

$$wK^2 - 2rK + (r^2 - R^2) = 0, \tag{12.44}$$

where

$$w = 1 + u^2 + \frac{v^2}{1 - e^2}. \tag{12.45}$$

For geostationary satellites, we can define the dimensionless auxiliary quantity  $\varrho$  by

$$\varrho = 1 - \frac{1}{\eta_{\text{GS}}^2} = 0.977119. \quad (12.46)$$

The visibility condition stipulates a positive value for the discriminant of the quadratic in (12.44):

$$w\varrho < 1. \quad (12.47)$$

The locus of points such that  $w\varrho = 1$  corresponds to the boundary of the Earth's disk as seen from the satellite (zero discriminant).

If the point  $P$  is seen by  $S$ , (12.44) gives two solutions: the smallest, the one we keep here, corresponds to the point  $P$  on the viewed face of the Earth, while the other solution corresponds to a point  $P$  that would be visible on the other face if the Earth were transparent.

The required value of  $K$  is therefore the distance

$$K = \frac{1 - \sqrt{1 - w\varrho}}{w} r. \quad (12.48)$$

We thus obtain  $x = r - K$ ,  $y = uK$  et  $z = vK$ , and referring to the definition (12.39) of the vector  $\mathbf{OP}$  in terms of geodetic coordinates, this gives

$$\tan(\lambda - \lambda_{\text{S}}) = \frac{y}{x}, \quad \tan \varphi = \frac{z}{(1 - e^2)\sqrt{x^2 + y^2}}.$$

Finally then, the pixel coordinates  $L$  and  $C$  (row and column) can be used to calculate  $u$  and  $v$ , then  $w$ , and hence obtain  $K$ . With  $K$ , we can calculate  $x$ ,  $y$ ,  $z$  and obtain the geodetic coordinates  $\lambda$  and  $\varphi$ .

**Example 12.14** *Conversion between pixel and geographic coordinates for the METEOSAT satellites.*

► Here we consider the METEOSAT satellites in operating position, stationed on the Greenwich meridian ( $\lambda_{\text{S}} = 0^\circ$ ). Their image is characterised by  $N$ , the number of rows and columns, and  $\Phi$ , the field of view (FOV). We distinguish first generation satellites, viz., METEOSAT-1 to -7, from second, viz., MSG-1, -2, -3, and -4, corresponding to METEOSAT-8 and following (see Figs. 12.26 and 12.27).

With the pixel coordinates  $L$  and  $C$  in degrees, we obtain the corresponding row number  $P_{\text{R}}$  and column number  $P_{\text{C}}$ . Columns are numbered from right to left, rows from bottom to top. As the satellite is parked at longitude  $0^\circ$ , Europe is visible at the top of the image. Rows are acquired from bottom to top, i.e., from south to north, so that Europe benefits from the most recent

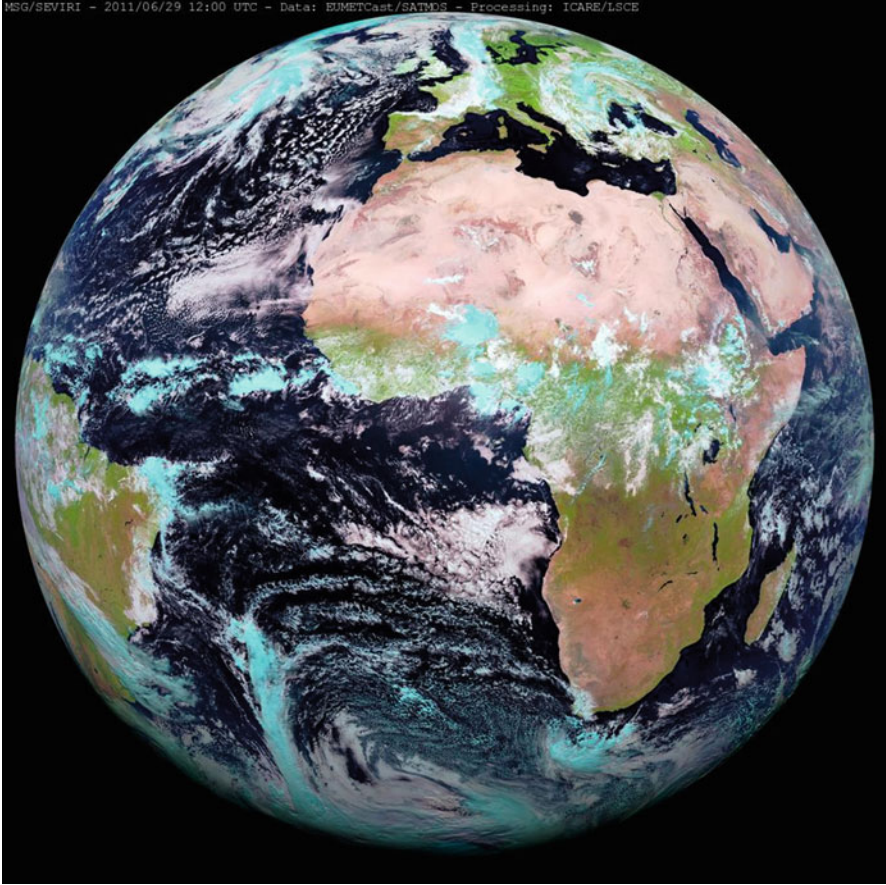


FIG. 12.26 : Image obtained by composite processing using several channels of the imager SEVIRI, on 29 June 2011 at 12:00 UT. METEOSAT-9 (MSG-2), stationed at longitude  $0.0^\circ$ . Credit: SATMOS, Icare (Lille).

observational data (the full scan for an image is 25 min for first generation METEOSAT and 15 min for MSG).

We now establish the mapping  $(C, L) \mapsto (P_R, P_C)$ . We obtain the pixel numbers using the function INT which transforms a real number to its integer part, viz.,

$$\text{if } C \geq 0 : P_C = \frac{N}{2} - \text{INT} \left( C \frac{N}{\Phi} \right) , \quad \text{if } C < 0 : P_C = \frac{N}{2} - \text{INT} \left( C \frac{N}{\Phi} \right) + 1 ,$$

$$\text{if } L \geq 0 : P_R = \frac{N}{2} + \text{INT} \left( L \frac{N}{\Phi} \right) + 1 , \quad \text{if } L < 0 : P_R = \frac{N}{2} + \text{INT} \left( L \frac{N}{\Phi} \right) .$$

Satellite	Rows and columns $N$	Field of view $\Phi$
METEOSAT-1 to -7	2,500	$18.00^\circ$
MSG	3,712	$18.00^\circ$

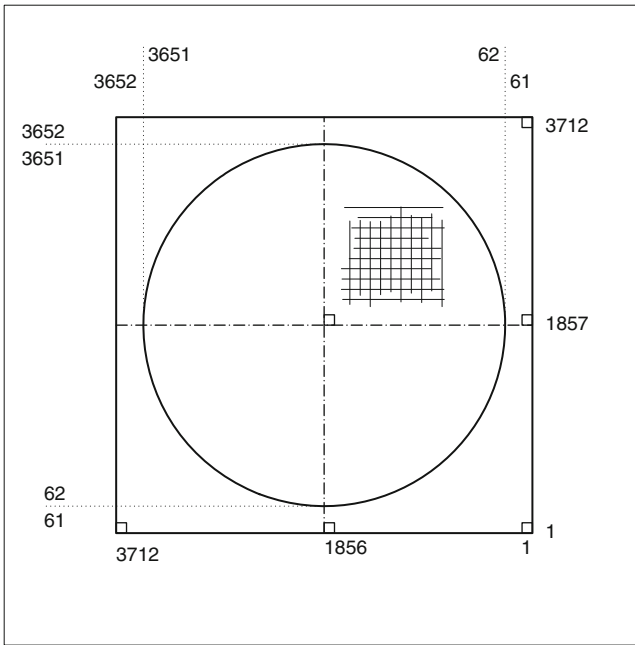


FIG. 12.27 : Schematic view of the Earth from a geostationary MSG satellite. The whole frame represents the field of view and the disk represents the visible disk of the Earth. Columns are numbered from 1 to 3,712, from right to left. Rows are numbered from 1 to 3,712, from bottom to top.

Concerning the mapping  $(P_C, P_R) \mapsto (C, L)$ , once we know  $P_C$  and  $P_R$ , we can obtain  $C$  and  $L$ , and this allows us to obtain the geographic coordinates of the point  $P$ :

$$C = - \left( P_C - \frac{N+1}{2} \right) \frac{\Phi}{N}, \quad L = - \left( P_R - \frac{N+1}{2} \right) \frac{\Phi}{N}.$$

**Application.** Satellite METEOSAT-9 (MSG-2), with  $N = 3,712$ ,  $\Phi = 18.00^\circ$ .

$(\lambda, \varphi) \mapsto (P_C, P_R)$ :

- Place:  $\varphi = 30^\circ$ ,  $\lambda = 30^\circ \mapsto P_C = 984$ ,  $P_R = 2,854$ ,  $\zeta = 47.83^\circ$ .
- Niamey:  $\varphi = 13.53^\circ$ ,  $\lambda = 2.08^\circ \mapsto P_C = 1,783$ ,  $P_R = 2,343$ ,  $\zeta = 16.07^\circ$ .
- Paris:  $\varphi = 48.87^\circ$ ,  $\lambda = 2.33^\circ \mapsto P_C = 1,803$ ,  $P_R = 3,337$ ,  $\zeta = 56.09^\circ$ .

- Moscow:  $\varphi = 55.70^\circ$ ,  $\lambda = 37.55^\circ \mapsto P_C = 1,197$ ,  $P_R = 3,422$ ,  $\zeta = 71.69^\circ$ .
- Oslo:  $\varphi = 59.93^\circ$ ,  $\lambda = 10.75^\circ \mapsto P_C = 1,676$ ,  $P_R = 3,510$ ,  $\zeta = 68.58^\circ$ .

$(P_C, P_R) \mapsto (\lambda, \varphi)$ :

- $P_C = 1,000$ ,  $P_R = 1,000 \mapsto \varphi = -25.19^\circ$ ,  $\lambda = 27.77^\circ$ ,  $\zeta = 42.67^\circ$ .
- $P_C = 1,000$ ,  $P_R = 2,000 \mapsto \varphi = 4.01^\circ$ ,  $\lambda = 24.53^\circ$ ,  $\zeta = 29.05^\circ$ .
- $P_C = 2,000$ ,  $P_R = 1,000 \mapsto \varphi = -24.63^\circ$ ,  $\lambda = -4.37^\circ$ ,  $\zeta = 29.20^\circ$ .
- $P_C = 2,000$ ,  $P_R = 2,000 \mapsto \varphi = 3.94^\circ$ ,  $\lambda = -3.92^\circ$ ,  $\zeta = 6.54^\circ$ .
- $P_C = 3,000$ ,  $P_R = 3,000 \mapsto \varphi = 36.48^\circ$ ,  $\lambda = -46.97^\circ$ ,  $\zeta = 64.55^\circ$ .



## Chapter 13

# Spatiotemporal and Angular Sampling

Once again, we shall change our point of view! From an arbitrary point  $P$  on the Earth, we now note the time and angular conditions of our view of the satellite  $S$ . This is the opposite problem to determining the ground track of the swath: we must now establish the satellite sampling for a given instrument. We shall also determine, for this point  $P$ , the direction of the Sun at the instant of time when  $P$  is viewed by the satellite.

### Basic Principles of Sampling

To obtain the sampling, our method consists in noting all the intersections of the ground swath with a given meridian, called the reference meridian. This method, which underlies the sampling function of the *Ixion* software, can then be used to make various comparisons and produce statistics depending on the latitude of the target point.

For each point viewed, called the target and denoted by  $P$ , we determine, in terms of the satellite position  $S$ , the time at which it is seen and the direction  $PS$ , which is called the line of sight. This straight line is defined by the angles of the spherical coordinate system: the zenith angle, also called the viewing zenith angle (VZA), and the azimuth angle, or viewing azimuth angle:

- For cross-track scanning, the zenith angle varies between  $0^\circ$  and a maximum value  $\zeta_M$ .
- For conical scanning, the zenith angle has a fixed value, e.g.,  $\zeta = 53^\circ$ .

We call this the overpass of the satellite  $S$  at the point  $P$ . We can then refer to the overpass time, and the overpass zenith and azimuth angles.

Temporal sampling is achieved when we know the overpass times in the sense mentioned above for any point, for a given satellite and instrument, over



a certain period of time, e.g., 1 month. Insofar as this temporal sampling is carried out for every point on Earth, we often speak of spatiotemporal sampling. When we speak of angular sampling, we mean a record of the viewing angles for each overpass. When the word “sampling” is used without further specification, we are generally referring to both sets of data. Sampling data is supplemented by stating the conditions of solar illumination, i.e., angles determining the position of the Sun for each target point  $P$ .

## 13.1 Satellite–Target Direction

When calculating viewing angles, the Earth is only treated as an ellipsoid in one case, namely when establishing the correspondence between pixel and geographic coordinates, as we did in the last chapter, where we require an accuracy to within one pixel. But for the present kind of angle calculation, where we rarely require greater accuracy than one degree, we may consider the Earth as spherical and identify the latitudes  $\varphi$  and  $\psi$ . When calculating the viewing zenith angle, for example, this amounts to defining this angle by  $\zeta = (\mathbf{OP}, \mathbf{PS})$  as in Eq. (12.3) (see Fig. 12.3), whereas the strict definition is  $\zeta = (\mathbf{Pn}, \mathbf{PS})$  as in (12.41), where  $\mathbf{Pn}$  is the normal to the ellipsoid at  $P$ , i.e., the local vertical.

### 13.1.1 Line-of-Sight Direction of the Satellite

#### Calculating Angles

Figure 13.1 shows the subsatellite point  $S_0$ , which is the intersection of  $OS$  with the Earth (center  $O$ ). The swath plane  $\mathcal{F}$  is the plane  $OS_0SP$ , orthogonal to the direction of displacement of the satellite  $S$ . The velocity vector defines a right-handed orientation in  $\mathcal{F}$ .

At each time, we know the position  $S$  of the satellite. The position  $P$  of the target is given by the characteristics of the swath. For example, in the case of a cross-track swath,  $f$  gives  $\alpha$  and we may then use (12.21) to obtain the rotation matrix  $P_4$ . The geocentric coordinates of  $S$  or  $S_0$  are denoted by the longitude  $\lambda_S$  and the latitude  $\psi_S$ , and the geocentric coordinates of the pixel  $P$  by  $\lambda$  and  $\psi$ . The two angles specifying the direction  $\mathbf{PS}$  are the zenith and azimuth angles, which belong to the spherical coordinate system centered on  $P$ , with the local horizontal plane  $\mathcal{H}$ . This plane, perpendicular to  $\mathbf{OP}$ , is the tangent plane to the sphere at  $P$ .

**Zenith Angle.** The viewing zenith angle  $\zeta$  is defined by

$$\zeta = (\mathbf{OP}, \mathbf{PS}), \quad (13.1)$$

measured in the positive sense for the orientation defined by the satellite, with the straight line  $\mathbf{OP}$  (the local vertical) as origin, as discussed in relation to

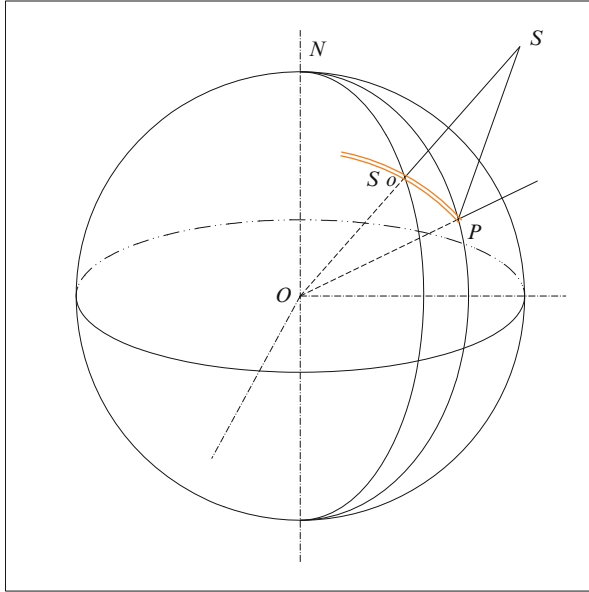


FIG. 13.1 : Directions relating to the swath of an instrument aboard a satellite (XT mode). The Earth is shown with center  $O$ , as is the North Pole  $N$  and the equator. The satellite  $S$ , with subsatellite point  $S_0$ , views the point  $P$  in a swath  $S_0P$  (doubled curve). This swath lies in the plane  $OS_0P$ , called the swath plane  $\mathcal{F}$ , orthogonal to the direction of displacement of the satellite  $S$ . Figure 12.3 shows the angles in the plane  $\mathcal{F}$ .

Fig. 12.3. The angle  $\alpha$  is obtained by spherical trigonometry, using (6.169) [see (6.172) in Example 6.5], or simply from the scalar product  $OP \cdot OS$  :

$$\cos \alpha = \sin \psi \sin \psi_S + \cos \psi \cos \psi_S \cos(\lambda - \lambda_S) . \tag{13.2}$$

The zenith angle  $\zeta$  can be calculated<sup>1</sup> immediately from the angle  $\alpha$  using (12.10). One can also calculate  $\zeta$  directly using the scalar product  $OP \cdot PS$ , or more accurately, using the scalar product  $Pn \cdot PS$ , as explained above.

**Azimuth Angle.** The azimuth angle  $\chi$  is defined in the local horizontal plane  $\mathcal{H}$ . The local vertical confers an orientation on  $\mathcal{H}$ . The angle  $\chi$  is then measured in the positive sense for this orientation, taking the north as origin.

<sup>1</sup>As the swath plane  $\mathcal{F}$  is oriented,  $\zeta$  can take positive or negative values. Indeed,  $\zeta$  varies in the interval  $[-\pi/2, +\pi/2]$ . Insofar as the azimuth angle  $\chi$  is well defined (see below) throughout the whole plane, it would suffice to define  $\zeta$  in the interval  $[0, +\pi/2]$ . However, this redundancy allows one to say whether the satellite is in the ascending or descending stretch of the orbit. One then assigns the sign of  $\zeta$  to  $f$  and  $\alpha$ .

It is the dihedral angle between the swath plane  $\mathcal{F}$  ( $OPSS_0$ ) and the meridian plane  $OPN$  of  $P$ , denoted by  $\mathcal{M}$ :

$$\chi = \text{dihedral angle } \{\mathcal{M}, \mathcal{F}\}, \quad (13.3)$$

that is, the angle in  $\mathcal{H}$  between the ground swath and the meridian at  $P$ . The angle  $\chi$  is called the viewing or line-of-sight azimuth.

To calculate the angle  $\chi$ , we consider the spherical triangle  $NPS_0$ , shown in Fig. 13.1. The three known elements of the triangle are two sides (two arcs) and an angle, the dihedral angle between the two meridian planes through  $P$  and  $S_0$ :

$$\widehat{NS}_0 = \frac{\pi}{2} - \psi_S, \quad \widehat{NP} = \frac{\pi}{2} - \psi, \quad \widehat{N} = \lambda - \lambda_S.$$

We seek the angle  $\chi$ , which is the angle of the spherical triangle at  $P$ . Using (ST X), we obtain

$$\cot \widehat{NS}_0 \sin \widehat{NP} = \cos \widehat{NP} \cos N + \sin N \cot P,$$

or in the present case,

$$\tan \psi_S \cos \psi = \sin \psi \cos(\lambda - \lambda_S) + \frac{\sin(\lambda - \lambda_S)}{\tan \chi},$$

and finally,

$$\tan \chi = \frac{\sin(\lambda - \lambda_S) \cos \psi_S}{\cos \psi \sin \psi_S - \sin \psi \cos \psi_S \cos(\lambda - \lambda_S)}. \quad (13.4)$$

By definition, the image under arctan is an angle in the interval  $[-\pi/2, +\pi/2]$ . To obtain the angle  $\chi$  between  $PS_0$  and the north in the interval  $(-\pi, +\pi]$ , we note that  $\chi$  has the same sign as  $\lambda - \lambda_S$ . We thus deduce that:

- If  $\tan \chi$  has the same sign as  $\lambda - \lambda_S$ , we have  $\chi = \arctan(\tan \chi)$ .
- Otherwise,  $\chi = \arctan(\tan \chi) + \pi \pmod{2\pi}$ .

**Note.** The altitude of the satellite does not appear in the relation giving the azimuth angle  $\chi$ , whereas it obviously must in the determination of the viewing zenith angle  $\zeta$ .

**Example 13.1** Calculate the azimuth angle when the target point and the satellite lie on the same geographic parallel.

► When  $\psi_S = \psi$ , Eq. (13.4) becomes

$$\cot \chi = \sin \psi \tan \frac{\lambda - \lambda_S}{2}.$$

We take the following points:  $P$  ( $45^\circ\text{N}$ ,  $10^\circ\text{W}$ ) and  $S_0$  ( $45^\circ\text{N}$ ,  $20^\circ\text{E}$ ). With the above relation, we obtain  $\tan \chi = -5.278$ , whence  $\arctan(-5.278) = -79.3^\circ$ . With  $\lambda - \lambda_S < 0$ , we have  $\chi = -79.3^\circ$ .

We observe that the direction  $\mathbf{PS}_0$  is not at right-angles to the north. This direction is taken on the arc of the great circle passing through  $P$  and  $S_0$ . As the chosen parallel is situated in the northern hemisphere, this arc is north of the parallel, making an angle of  $10.7^\circ$  with the parallel at  $P$ . The angle is negative ( $S_0$  is east of  $P$ ). If we swap  $P$  and  $S_0$ , the angle  $\chi$  is positive.

If we choose points in the southern hemisphere, such as  $P$  ( $45^\circ\text{S}$ ,  $10^\circ\text{W}$ ) and  $S_0$  ( $45^\circ\text{S}$ ,  $20^\circ\text{E}$ ), we obtain  $\tan \chi = +5.278$ , whence  $\arctan(+5.278) = +79.3^\circ$  and  $\chi = 79.3^\circ - 180^\circ = -100.7^\circ$ . The north is still taken as the origin. ◀

### Polar Viewing Conditions

For a circular orbit, if the pole is attained by the swath, it always sees the satellite with the same zenith angle. A prograde satellite, oriented in the direction of its displacement, always sees the North Pole to its left and the South Pole to its right. Conversely, a retrograde satellite (hence any Sun-synchronous satellite) always sees the South Pole to its left and the North Pole to its right. With the sign conventions mentioned above,  $\zeta$  is positive in the case when a prograde satellite is viewed from the North Pole.

When viewing from the pole, the angles  $\alpha$  and  $i$  are complementary (i.e., the sum of the angles is a right-angle), as can be seen from Fig. 12.4. Equations (12.9) and (12.10) thus become

$$\tan f_{(\text{NP})} = \frac{\cos i}{\eta - \sin i}, \quad \tan \zeta_{(\text{NP})} = \frac{\cos i}{\sin i - 1/\eta}, \quad (13.5)$$

where the subscript (NP) indicates that the point under consideration is the North Pole. The signs of  $\zeta_{(\text{NP})}$  and  $f_{(\text{NP})}$  are given by the sign of  $\cos i$ .

For the South Pole, with subscript (SP), we find the negatives of these values, viz.,

$$f_{(\text{SP})} = -f_{(\text{NP})}, \quad \zeta_{(\text{SP})} = -\zeta_{(\text{NP})}. \quad (13.6)$$

If a satellite in circular orbit is to observe the pole during a revolution, and hence see both poles in each revolution, the half-swath  $f$  of its instrument must be greater than the threshold value  $f_P$ :

$$\text{pole viewed} \iff |f| \geq |f_P| \quad \text{with} \quad f_P = \arctan\left(\frac{\cos i}{\eta - \sin i}\right). \quad (13.7)$$

### 13.1.2 Geostationary Satellites

Although the scanning mode is different, geostationary satellites can be treated using the general relations with the substitutions  $\eta = \eta_{\text{GS}} = 6.611$ ,  $\psi_{\text{S}} = 0$ , taking  $\lambda_{\text{S}}$  to be the parking longitude. As we have already seen, for the level of accuracy required in determining viewing angles, the Earth can be treated as spherical, whence we may identify  $\varphi$  and  $\psi$ .

For the zenith angle, we first calculate  $\alpha$  using (12.35). We then obtain  $\zeta$  from (12.10), which becomes here

$$\tan \zeta = \frac{\sin \alpha}{\cos \alpha - 1/\eta_{\text{GS}}} . \quad (13.8)$$

For the angle  $\chi$ , (13.4) yields

$$\tan \chi = -\frac{\tan(\lambda - \lambda_{\text{S}})}{\sin \psi} . \quad (13.9)$$

The two graphs in Fig. 13.2 give the viewing angles  $\zeta$  and  $|\chi|$  as a function of the latitude  $|\psi|$  and the longitude difference  $|\lambda - \lambda_{\text{S}}|$ . Figure 13.2 (upper) representing the values of  $\zeta$  should be compared with Fig. 12.21, which shows the values of  $\alpha$  (locus of points equidistant from the subsatellite point for the geostationary satellite) as a function of the latitude and the longitude difference.

**Example 13.2** Calculate the viewing (or line-of-sight) directions of the satellite METEOSAT-9 from Paris and of FY-2C from Sydney.

► **METEOSAT-9 ( $\lambda_{\text{S}} = 0^\circ$ ).** Viewing from Paris ( $48^\circ 52' \text{N}$ ,  $2^\circ 20' \text{E}$ ), with  $\lambda_{\text{S}} = 0^\circ$ ,  $\lambda = +2.33^\circ$ ,  $\varphi = +48.87^\circ$ , we obtain

$$\alpha = 48.91^\circ , \quad \zeta = 56.1^\circ , \quad \arctan(\tan \chi) = -3.1^\circ , \quad \chi = 176.9 .$$

The line of sight thus has zenith angle  $56^\circ$  (or elevation angle  $34^\circ$ ) and azimuth angle  $177^\circ$  with the north (or  $3^\circ$  with the south, directed slightly westward).

**FY-2C ( $\lambda_{\text{S}} = 105^\circ \text{E}$ ).** Viewing from Sydney ( $33^\circ 55' \text{S}$ ,  $151^\circ 10' \text{E}$ ), with  $\lambda_{\text{S}} = +105^\circ$ ,  $\lambda = +151.17^\circ$ ,  $\varphi = -33.92^\circ$ , we obtain

$$\alpha = 54.92^\circ , \quad \zeta = 62.6^\circ , \quad \arctan(\tan \chi) = 61.8^\circ , \quad \chi = 61.8 .$$

The line of sight thus has zenith angle  $63^\circ$  (or elevation angle  $27^\circ$ ) and azimuth angle  $62^\circ$  with the north. With  $|\varphi| = 34^\circ$  and  $|\lambda - \lambda_{\text{S}}| = 46^\circ$ , we recover the calculated values of  $\zeta$  and  $\chi$  in Fig. 13.2. ◀

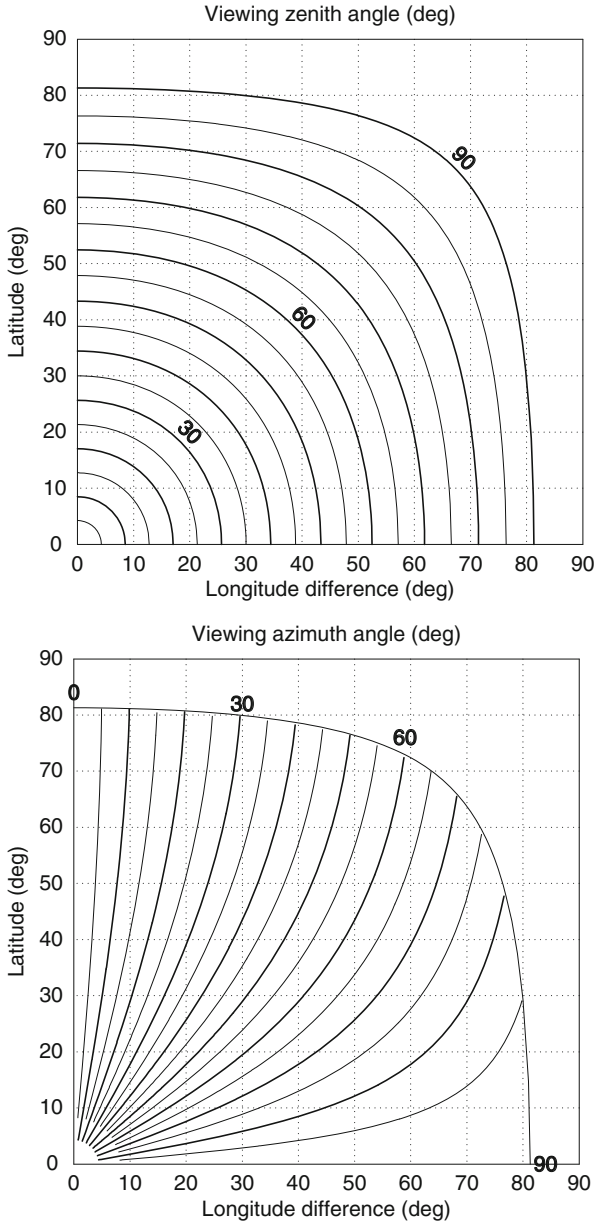


FIG. 13.2 : Viewing angles for the target–satellite direction when the satellite is geostationary, as a function of the latitude  $|\psi|$  and the longitude difference  $|\lambda - \lambda_S|$ . All angles are in degrees. Upper:  $|\zeta|$ . Lower:  $|\chi|$ .

### 13.1.3 Local View and Sky Plots

Local view diagrams, also known as sky plots, show the position of the satellite and its motion over time as seen in the sky at the given location. By “sky”, we understand here the celestial half-sphere centered on the observer at this location. In the terrestrial frame  $\mathfrak{R}_T$  centered on the center of the Earth  $O$ , the position of the satellite  $S$  is specified by the vector  $OS$ . Its Cartesian components are given as a function of time by (8.10), but in which  $\Omega$  is replaced, as explained in Chap. 8, by the Euler angle  $\alpha_1$  defined by (8.17).

In this same frame, the point  $P$  considered as the observation point is defined by the vector  $OP$ . The geographic coordinates of  $P$ , the geodetic latitude  $\varphi$ , the longitude  $\lambda$ , and the altitude above the reference ellipsoid, can be used to obtain the Cartesian coordinates using (2.29).

The local view thus consists in representing the vector  $PS$ . To obtain a representation on a half-sphere, we express the direction of  $PS$  in terms of the two viewing angles, i.e., the viewing zenith angle  $\zeta$  and the viewing azimuth angle  $\chi$ , as calculated above.

Sky plots indicate the trajectories on a grid of polar coordinates. This grid represents the projection of the celestial half-sphere onto the local horizontal plane. There are several ways of doing this projection (orthogonal, linear, stereographic, perspective, and so on). For the stereographic projection presented here, the grid looks like a set of concentric circles and radii.

Each point on the diagram corresponds to a specific direction. The azimuth taken from the north is represented as-is. The zenith angle determines the position in this direction: at the center for  $\zeta = 0^\circ$ , on the edge of the diagram for  $\zeta = 90^\circ$ , and in-between for intermediate values of  $\zeta$ , in accordance with the rules of the stereographic projection.

The zenith angle  $\zeta$  is sometimes replaced by its complement  $h_v = 90^\circ - \zeta$ , called the elevation angle or viewing elevation. When there is no risk of confusion with other symbols used elsewhere, it can be denoted by  $h$  and just called the elevation. The outer circle of the diagram corresponds to the circle of visibility:  $h = 0^\circ$  (or  $\zeta = 90^\circ$ ) if the horizon is perfectly clear,  $h = 5^\circ$  or  $10^\circ$ , or  $20^\circ$ , etc., if specific reception conditions must be ensured. Obstacles such as buildings, trees, etc., which block direct viewing of the satellite at the given location, can also be outlined on the diagram with a suitable projection.

**Example 13.3** *Sky plot for the Bangalore ground station of the Oceansat-2 satellite in India.*

► The Indian oceanographic satellites Oceansat-1 and -2 are Sun-synchronous and recurrent with a very short cycle  $C_T = 2$  days. If the sky plot is established over 2 days, it will remain valid both for the ground track and the time until the end of the satellite’s active life. Figure 13.3 (upper) shows the ground track of the satellite over 2 days, noting the circle of visibility ( $h = 5^\circ$ ) for the

**Oceansat-2**

Orbit - Ground track

Recurrence = [14; +1; 2] 29

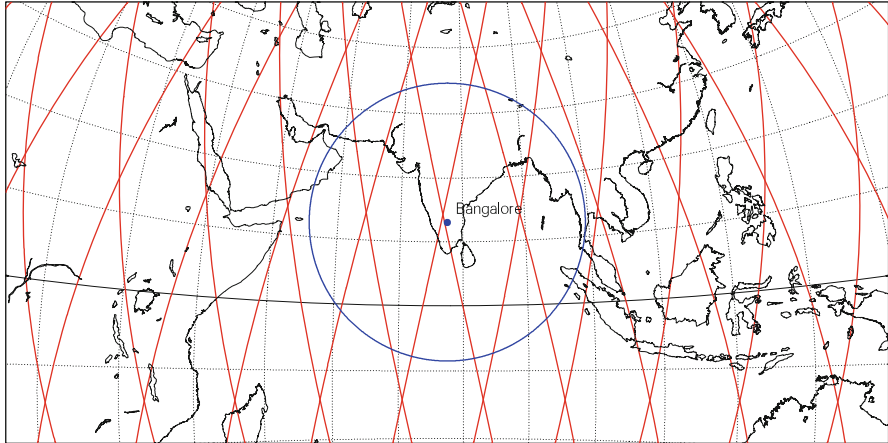
>>>> Time span shown: 2880.0 min = 2.00 days

Altitude = 720.0 km a = 7098.103 km

Inclin./SUN-SYNCHRON.= 98.29 °

Period = 99.31 min \* rev/day =14.50

**Visibility circle for h = 5°**



Projection: Stereographic Project. centre: 13.0 ° N; 77.5 °E Asc. Node: -31.81 ° [00:00 LMT] Ιξίωv  
 Property: Conformal Aspect: Oblique > zoom : 3.30 MC \* LMD  
 ⊕ T.:Azimuthal - Graticule: 10° {5.3} [-90.0/ +77.0/ +12.5] [-] EGM2008 Ατλας

**Oceansat-2**

Orbit - Ground track

Recurrence = [14; +1; 2] 29

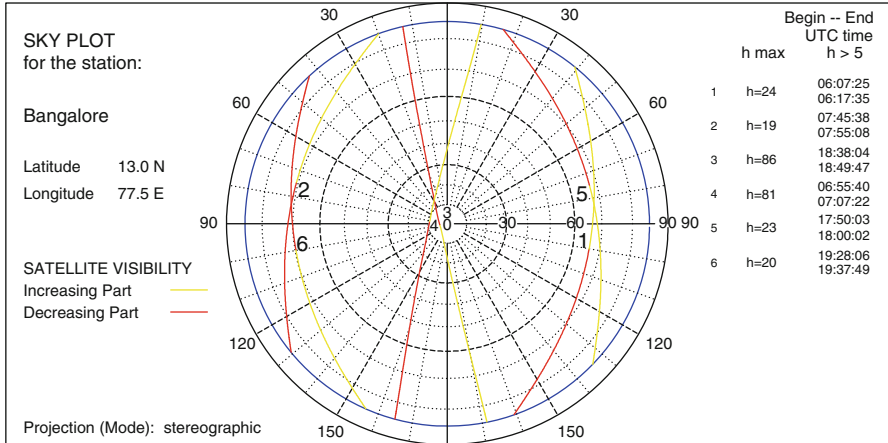
>>>> Time span shown: 2880.0 min = 2.00 days

Altitude = 720.0 km a = 7098.103 km

Inclin./SUN-SYNCHRON.= 98.29 °

Period = 99.31 min \* rev/day =14.50

Equat. orbital shift = 2763.8 km ( 24.8 °)



Circle: Viewing Zenith Angle [0°, +90°] Asc. Node: -31.81 ° [00:00 LMT] Ιξίωv  
 Radius: Azimut - Origin: North MC \* LMD

FIG. 13.3 : Ground track of Oceansat-2 over 2 days (its recurrence cycle). Upper: Map showing the ground track and circle of visibility centered on Bangalore. Lower: Sky plot for Bangalore, KT, India.



$D$	$n$	$R$	Beginning	Middle	End	Duration	$\zeta_m$	$\chi_m$	$d_m$
1	1	3	06:07:25	06:12:30	06:17:35	00:10:10	66	-100	1,215
1	2	4	07:45:38	07:50:22	07:55:08	00:09:30	71	75	1,410
1	3	11	18:38:04	18:43:55	18:49:47	00:11:43	4	106	44
2	4	18	06:55:40	07:01:31	07:07:22	00:11:42	9	82	105
2	5	25	17:50:03	17:55:02	18:00:02	00:09:59	67	-75	1,264
2	6	26	19:28:06	19:32:56	19:37:49	00:09:43	70	100	1,364
3	7	32	06:07:25	06:12:30	06:17:35	00:10:10	66	-100	1,215

TABLE 13.1 : *Overpasses of the satellite Oceansat-2 for the Bangalore ground station: beginning, middle, end, and duration of overpass in UTC (hh:mm:ss). Minimal viewing elevation:  $h = 5^\circ$ . Day  $D$ , number of overpass  $n$  during the revolution  $R$ . Closest overpass of the satellite to the station during a revolution: the angles  $\zeta_m$  and  $\chi_m$  are in degrees and the distance  $d_m$  between station and ground track in kilometers. Bangalore (Karnataka), India:  $\varphi = 13.034^\circ N$  ( $\psi = 12.950^\circ$ ),  $\lambda = 77.511^\circ E$ .*

Bangalore receiving station in India. Each curve within this circle indicates that the satellite overflies with viewing elevation greater than  $5^\circ$  in the skies of Bangalore. Six overpasses are noted over 2 days.

The sky plot in Fig. 13.3 (lower) does indeed show these six overpasses. Two of them, numbered 3 and 4, are very close to the local vertical at the ground station. The beginning, middle, and end of each overpass is noted in Table 13.1. After a cycle of 29 revolutions over 2 days, the satellite exactly repeats its original ground track, and at the same time: the conditions of the overpass during revolution 32 (day 3) are strictly identical to those of revolution 3 (day 1). ◀

**Example 13.4** *Sky plots for HEO communications satellites.*

► Figure 13.4 shows sky plots for two communications satellites, Meridian-6 and Sirius-3, with periods of revolution of a half and one sidereal day, respectively. They follow HEO orbits, the first being Molniya and the second Tundra. They are both recurrent, implying that the diagrams remain unchanged over time, provided that the satellite orbits are maintained. Only the visibility time moves forward by 3 min 56 s every day, corresponding to the difference between the mean and sidereal days discussed in connection with (7.27) in Chap. 7. ◀

### 13.1.4 Visibility Window for LEO Satellites

The time interval over which a satellite  $S$  is visible from a given point  $P$  on the Earth is called the duration of visibility or visibility window of  $S$  by  $P$ . This notion is important for data reception and also when dealing

**Meridian-6** (Меридиан)

Elliptical orbit - Gr. track

Recurrence = [ 2; +0; 1] 2

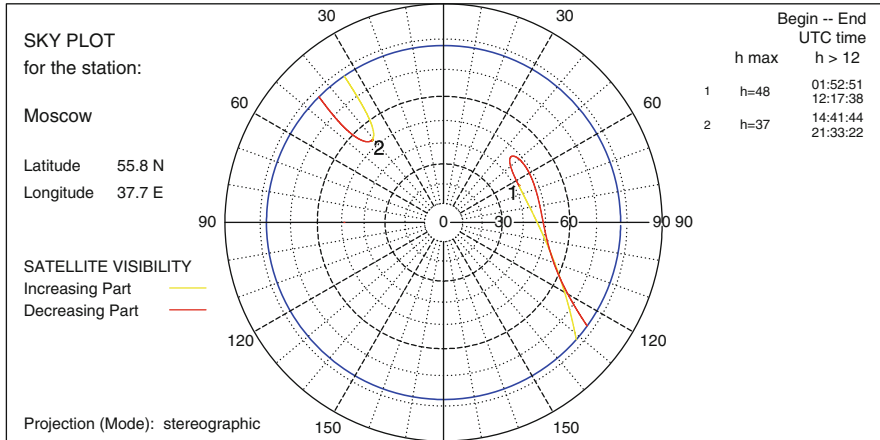
2012 12 15 00:00:00 UTC >>> 1440.0 min = 1.00 day

Equiv. altit. = 20176.0 km a = 26554.180 km

CRITICAL Incl. = 62.81 ° e = 0.721379

Period = 717.76 min \* rev/day = 2.01

h\_a = 39346 km; h\_p = 1034 km; arg. perigee: +295.03 °



Circle: Viewing Zenith Angle [0°, +90°]  
Radius: Azimut - Origin: North

[NORAD] 2012 12 13 13:50:21 UTC//R= 58 Iξων  
Asc. Node: -114.44 ° [06:13 LMT] MC ★ LMD  
Apogee : -64.36 °

**Sirius-3**

Elliptical orbit - Gr. track

Recurrence = [ 1; +0; 1] 1

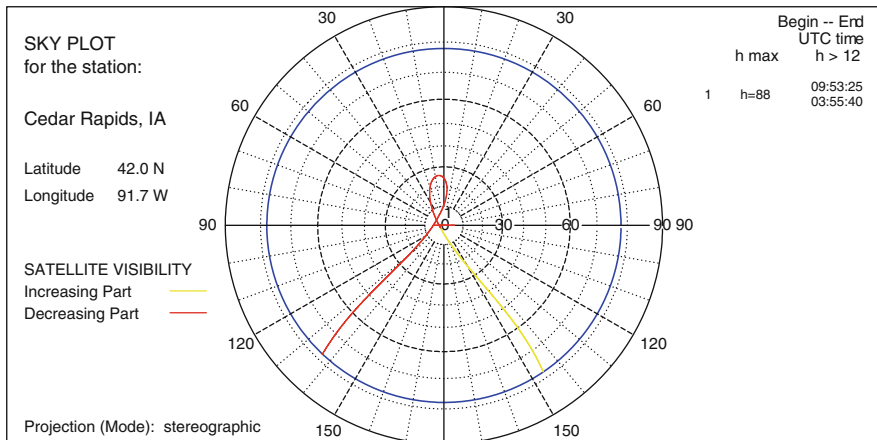
2013 06 15 06:00:00 UTC >>> 1440.0 min = 1.00 day

Equiv. altit. = 35787.3 km a = 42165.453 km

CRITICAL Incl. = 64.42 ° e = 0.267035

Period = 1436.15 min \* rev/day = 1.00

h\_a = 47064 km; h\_p = 24545 km; arg. perigee: +269.84 °



Circle: Viewing Zenith Angle [0°, +90°]  
Radius: Azimut - Origin: North

[NORAD] 2013 06 13 11:09:29 UTC//R= 4592 Iξων  
Asc. Node: -66.01 ° [06:45 LMT] MC ★ LMD  
Apogee : 83.53 °

FIG. 13.4 : Sky plots for two HEO communications satellites over 1 day. Upper: Meridian-6 in Molniya orbit, for Moscow, Russia. Lower: Sirius-3 in Tundra orbit for Cedar Rapids, IA, USA.

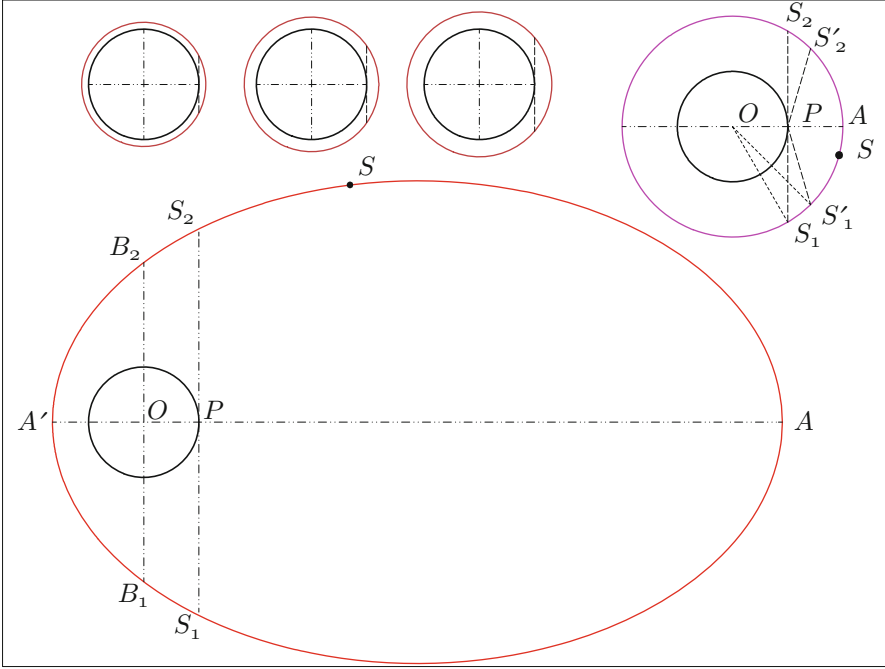


FIG. 13.5 : Schematic view of the Earth and satellite trajectories. The Earth and the orbits represented are on the same scale. Upper: Circular orbit. Examples: LEO,  $h = 800, 1,400, \text{ and } 2,000 \text{ km}$ , and orbit  $h = R$ , with indication of the points used in the text. Lower: HEO orbit, period  $T \approx 24 \text{ h}$ ,  $e = 0.75$ , indicating the points used.

with satellite constellations. With an orbitographic software, the duration of visibility is obtained directly from sky plots, as we have just seen. Below we shall show how this kind of tool can be used to calculate the visibility window from geometric considerations, provided that one makes certain simplifying approximations.

For LEO satellites in circular orbits, the duration of visibility is of the order of quarter of an hour and one can therefore identify the frames  $\mathfrak{R}$  and  $\mathfrak{R}_T$ .

**Satellite Passes Vertically over Observation Point**

We consider the situation where the satellite  $S$  passes vertically over  $P$ , the observation point on the Earth’s surface. The orbit of  $S$ , whose plane contains  $P$ , is shown schematically in Fig. 13.5 (upper). The satellite  $S$  is visible from  $P$  as long as it remains above the local horizon of  $P$ , represented by the straight line  $S_1PS_2$ , hence on the circular arc  $S_1AS_2$ . The angle  $\alpha = (OP, OS_1)$  can be found immediately from

$$\cos \alpha = \frac{R}{R + h} = \frac{R}{a} = \frac{1}{\eta}, \tag{13.10}$$

where  $\eta$  is the reduced distance. The period of the satellite is taken to be the Keplerian period  $T_0$ . The duration of visibility  $\Theta$  is therefore

$$\Theta = \frac{\alpha}{\pi} T_0 . \tag{13.11}$$

In order to take observing conditions into account, let us fix a maximal viewing zenith angle. The angle  $\alpha$  at the center of the Earth is given as a function of  $\zeta$  and the reduced distance  $\eta$  [see (12.12)], which we denote here by  $\alpha(\zeta)$ :

$$\alpha(\zeta) = \zeta - \arcsin\left(\frac{1}{\eta} \sin \zeta\right) . \tag{13.12}$$

It can be checked that  $\alpha(\pi/2) = \arccos(1/\eta)$ .

Denoting the limiting angle by  $\zeta_1$ , visibility therefore lasts for a time

$$\Theta = \frac{\alpha(\zeta_1)}{\pi} T_0 . \tag{13.13}$$

### Satellite Does Not Pass Vertically over Observation Point

When  $S$  crosses the sky at  $P$ , the viewing zenith angle goes through a minimum  $\zeta_v$ , which was zero in the situation just discussed. On the horizontal plane tangent at  $P$  to the terrestrial sphere of radius  $R$ , the distance between  $P$  and the closest point of the ground track is

$$d_v = R \tan \alpha(\zeta_v) .$$

Taking into account  $\zeta_1$ , the radius of the circle of visibility is given by

$$d_1 = R \tan \alpha(\zeta_1) .$$

Visibility thus lasts for a time proportional to the lengths of the ground tracks within the circle of visibility, since the satellite speed is uniform, treating the ground tracks as straight over this interval.

Let  $\Theta(\zeta_1, \zeta_v)$  be the duration  $\Theta$  expressed as a function of the two variables  $\zeta_1$  and  $\zeta_v$  via  $\alpha_1 = \alpha(\zeta_1)$  and  $\alpha_v = \alpha(\zeta_v)$ . With the angles  $(\zeta_1, \zeta_v)$  taken in this order, we obtain

$$\frac{\Theta(\zeta_1, \zeta_v)}{\Theta(\zeta_1, 0)} = \frac{\sqrt{d_1^2 - d_v^2}}{d_1} = \sqrt{1 - \frac{\tan^2 \alpha(\zeta_v)}{\tan^2 \alpha(\zeta_1)}} .$$

Clearly, the condition  $\zeta_v < \zeta_1$  must be respected. The visibility window for circular LEO satellites is thus given quite generally by

$$\Theta(\zeta_1, \zeta_v) = \sqrt{1 - \frac{\tan^2 \alpha(\zeta_v)}{\tan^2 \alpha(\zeta_1)}} \frac{\alpha(\zeta_1)}{\pi} T_0 . \tag{13.14}$$

**Example 13.5** Calculate the duration of visibility for three LEO satellite families: the Transit constellation and the SPOT and Oceansat satellites.

► In each example, we consider a different limiting visibility angle.

**Transit.** All the satellites in the Transit constellation (the first global satellite positioning system) follow a strictly polar circular orbit at an altitude of around  $h = 1,100$  km, whence  $\eta = 1.1725$ ,  $T_0 = 107.4$  min. By fixing a viewing elevation above  $10^\circ$ , or  $\zeta_1 = 80^\circ$ , (13.12) then (13.13) imply

$$\alpha(\zeta_1) = \alpha(80) = 80 - \arcsin \frac{0.9848}{1.1725} = 80 - 57.13 = 22.87^\circ ,$$

$$\Theta = \Theta(80, 0) = \frac{22.87}{180} 107.4 = 13.6 \text{ min} .$$

**SPOT.** For SPOT-5 and all the SPOT satellites, we have  $h = 822$  km,  $\eta = 1.1289$ ,  $T_0 = 101.4$  min. It follows that, for viewing all the way to the horizon,  $\zeta_1 = 90^\circ$ :

$$\alpha = \arccos(1/1.1289) = 27.6^\circ , \quad \Theta = \Theta(90, 0) = \frac{27.6}{180} 101.4 = 15.6 \text{ min} .$$

**Oceansat.** For Oceansat-1 and -2, we have  $h = 720$  km,  $\eta = 1.1129$ , and  $T_0 = 99.3$  min. It follows that, for viewing all the way to the horizon,

$$\alpha = \arccos(1/1.1129) = 26.03^\circ , \quad \Theta(90, 0) = \frac{26.03}{180} 99.3 = 14.36 \text{ min} .$$

With the Oceansat satellites, the conditions are as in the diagram of Fig. 13.3 and Table 13.1. The limit of the viewing zenith angle is  $\zeta_1 = 85^\circ$  ( $h > 5^\circ$  on the diagram). Hence,

$$\alpha(\zeta_1) = 85.00 - 63.53 = 21.47^\circ , \quad \Theta(85, 0) = \frac{21.47}{180} 99.3 = 11.84 \text{ min} .$$

Consider the ground tracks numbered 3 and 6 on the diagram:

- Track 3:  $h = 86^\circ$  or  $\zeta_v = 4^\circ$ . The satellite is almost vertically above the observation point and

$$\alpha(\zeta_1) = 0.406^\circ .$$

Applying (13.14) with this value:

$$\begin{aligned} \Theta(85, 4) &= \sqrt{1 - 0.018^2} \Theta(85, 0) = 0.9998 \Theta(85, 0) \\ &\approx \Theta(85, 0) = 11.84 \text{ min} , \end{aligned}$$

which corresponds to 11:50, to be compared with the exact value of 11:43.

- Track 6:  $h = 20^\circ$  or  $\zeta_v = 70^\circ$ . The satellite is rather low on the horizon, with

$$\alpha(\zeta_1) = 12.396^\circ ,$$

$$\begin{aligned} \Theta(85, 70) &= \sqrt{1 - 0.5589^2} \Theta(85, 0) = 0.8293 \Theta(85, 0) \\ &= 0.8293 \times 11.84 = 9.83 \text{ min} , \end{aligned}$$

which corresponds to 9:49, to be compared with the exact value of 9:43.

We may conclude that the approximate formula (13.14) gives perfectly adequate results. ◀

### 13.1.5 Visibility Window for HEO Satellites

In order to study a highly eccentric elliptical orbit, of HEO type and with eccentricity  $e$ , we consider the most favourable situation, where the point  $P$  is the subsatellite point when the satellite overflies the apogee  $A$ , as shown schematically in Fig. 13.5 (lower). The satellite  $S$  is visible from  $P$  as long as it is on the elliptical arc  $S_1AS_2$ . Given the approximations we have made, the local horizon  $S_1PS_2$  can be replaced by the parallel  $B_1OB_2$  passing through the center of the Earth  $O$ . We then evaluate the duration of visibility as the time taken by the satellite  $S$  to cover the elliptical arc  $B_1AB_2$ .

At a given time, the position of  $S$  is specified relative to the perigee  $A'$  by the true anomaly  $v = (OA', OS)$ . The mean anomaly  $M$  of the point  $B_1$  is calculated from (4.59) with  $v = \pi/2$ , whence

$$M(B_1) = 2 \arctan \sqrt{\frac{1-e}{1+e}} - e\sqrt{1-e^2} . \tag{13.15}$$

We thus obtain the visibility duration as a function of the period, viz.,

$$\Theta = \left[ 1 - \frac{M(B_1)}{\pi} \right] T_0 . \tag{13.16}$$

**Example 13.6** Calculate the visibility window for the Molniya, Tundra, and Supertundra orbits.

- We examine here the three main types of HEO orbit.

**Molniya.** For a Molniya type HEO satellite, we have  $e = 0.736$  and  $T_0 = 718$  min. From (13.15) and (13.16), we obtain

$$M(B_1) = 0.7437 - 0.4983 = 0.2454 \text{ rad} = 14.1^\circ , \quad 1 - \frac{14.1}{180} = 0.92 .$$

**Molniya** ( **Μολνιγια** )

Elliptical orbit - Gr. track

Recurrence = [ 2; +0; 1] 2

>>>> Time span shown: 1440.0 min = 1.00 day

TIME MARKER

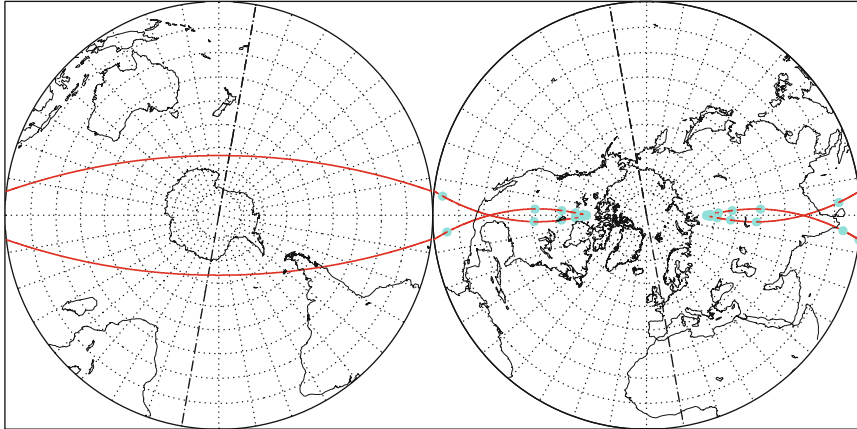
Equiv. altit. = 20174.7 km      a = 26552.863 km

CRITICAL Incln. = 63.42 °      e = 0.750000

Period = 717.72 min      \* rev/day = 2.01

h\_a = 40089 km; h\_p = 260 km; arg. perigee: +270.00 °

Time marker: one point every 60.0 minutes



Projection: Breusing Harmonic Pr. centre (r.): 90.0 ° N; 0.0 °

Property: none      Aspect: Polar

⊕ T.:Azimuthal - Graticule: 10° {4.2} [ +0.0/ +0.0/ +10.0] [-] EGM2008

Longitude / Initialisation:

Asc. Node: 73.47 °

Apogee : 80.00 °

Ιξίων

MC ★ LMD

Ατλας

**Supertundra**

Elliptical orbit - Gr. track

Recurrence = [ 1; +0; 1] 1

>>>> Time span shown: 1440.0 min = 1.00 day

TIME MARKER

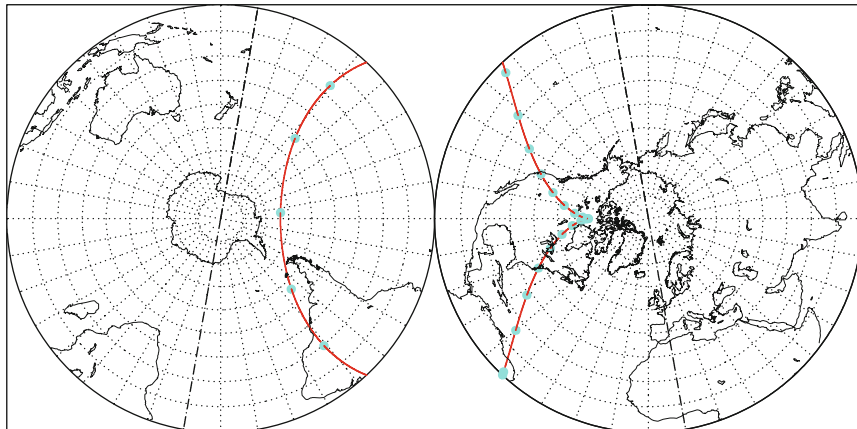
Equiv. altit. = 35785.1 km      a = 42163.199 km

CRITICAL Incln. = 63.43 °      e = 0.423000

Period = 1436.03 min      \* rev/day = 1.00

h\_a = 53620 km; h\_p = 17950 km; arg. perigee: +270.00 °

Time marker: one point every 60.0 minutes



Projection: Breusing Harmonic Pr. centre (r.): 90.0 ° N; 0.0 °

Property: none      Aspect: Polar

⊕ T.:Azimuthal - Graticule: 10° {4.2} [ +0.0/ +0.0/ +10.0] [-] EGM2008

Longitude / Initialisation:

Asc. Node: -53.02 °

Apogee : -100.00 °

Ιξίων

MC ★ LMD

Ατλας

FIG. 13.6 : Ground tracks for two HEO communications satellites HEO over 1 day. The position of the satellite is indicated every hour. Upper: Satellite in a Molniya orbit (2 rev/day). Lower: Satellite in a Tundra orbit (1 rev/day).

During one revolution, the satellite thus spends 92 % of the time in going from  $B_1$  to  $B_2$  via  $A$  (and hence 8 % of the time in going from  $B_2$  to  $B_1$  via  $A'$ ). This corresponds to  $\Theta = 11$  h for a period of 12 h. If we impose a minimum viewing zenith angle  $\zeta \sim 70^\circ$  and if  $P$  is not exactly the subsatellite point of  $A$ , we find that visibility lasts for about 8 h. This property is illustrated here in Fig. 13.6 (upper) and in Chap. 9 by Fig. 9.28.

**Supertundra.** For a Supertundra type HEO satellite, we have  $e = 0.423$  and  $T_0 = 1,436$  min, whence

$$M(B_1) = 1.1340 - 0.3832 = 0.7508 \text{ rad} = 43.0^\circ, \quad 1 - \frac{43.0}{180} = 0.76.$$

This represents a visibility window of 18 h over a period of 24 h. Imposing the restrictions considered above, one nevertheless exceeds a duration of 12 h (see Fig. 13.6 lower).

**Tundra.** For a Tundra type HEO satellite HEO like Sirius-1 to -3, we have  $e = 0.268$  and, as for Supertundra,  $T_0 = 1,436$  min, whence

$$M(B_1) = 1.2995 - 0.2582 = 1.0413 \text{ rad} = 59.7^\circ, \quad 1 - \frac{59.7}{180} = 0.67.$$

This represents a visibility window of 16 h over a period of 24 h. ◀

## 13.2 Target–Sun Direction

### 13.2.1 Solar Line of Sight

For an arbitrary point  $P$  on the Earth’s surface, with coordinates  $\lambda$  and  $\psi$ , we have already defined the local horizontal plane  $\mathcal{H}$ . In this section, quantities carrying the subscript  $s$  refer to the direction of the Sun. We now calculate the spherical coordinates  $\chi_s$  and  $\zeta_s$  of the direction  $PS_s$ ,  $S_s$  representing the position of the Sun.

To do this, we consider the celestial sphere with center  $O$ , relative to the point considered, as shown in Fig. 13.7. The direction of the zenith is  $OZ$ , normal to the horizontal plane  $\mathcal{H}$  represented by the horizon circle at that location. The direction of the celestial north pole is  $ON$ , normal to the equatorial plane  $\mathcal{E}$  represented by the celestial equator. The half-great circle passing through  $N$  and  $Z$  is the geographic meridian  $\mathcal{M}$  at the place in question. This is the plane of Fig. 13.7. The angle between the two straight lines  $OZ$  and  $ON$ , or the dihedral angle  $(\mathcal{H}, \mathcal{E})$ , is equal to the colatitude of the place, i.e., the complementary angle of the latitude  $\psi$ :

$$(OZ, ON) = \frac{\pi}{2} - \psi. \tag{13.17}$$



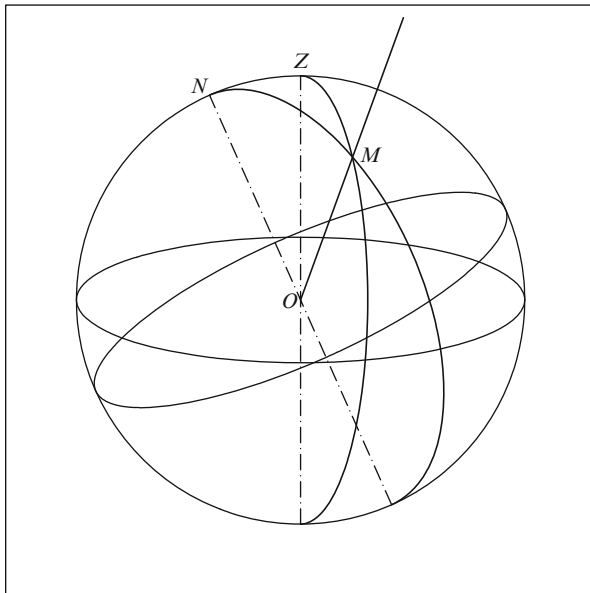


FIG. 13.7 : *Celestial sphere relative to a given point on Earth. The axis  $OZ$  is the local vertical, normal to the local horizontal plane  $\mathcal{H}$ . The axis  $ON$  is the celestial polar axis, normal to the celestial equatorial plane  $\mathcal{E}$ . The straight line  $OM$  represents an arbitrary direction from the point in question.*

Consider now an arbitrary direction  $OM$ . The half-great circle through  $Z$  and  $M$  is the vertical of  $M$ . The half-great circle through  $N$  and  $M$  is the celestial meridian of  $M$ . When describing the direction of the Sun, we consider  $M$  at the intersection of  $OS_s$  with the celestial sphere. This direction  $OM$  can be specified relative to  $\mathcal{E}$  using celestial equatorial coordinates, i.e., the right ascension  $\alpha$  (or the hour angle  $H$ ) and the declination  $\delta$ . Relative to  $\mathcal{H}$ , in local horizontal coordinates, it is specified by the azimuth  $\chi_s$  and the zenith angle  $\zeta_s$ .

We shall express the horizontal coordinates as a function of the time (via  $H$ ), the date (via  $\delta$ ), and the geographical position of the point  $P$  (via  $\psi$ ). In the spherical triangle  $NZM$ , the sides are given by

$$\widehat{NZ} = \frac{\pi}{2} - \psi, \quad \widehat{ZM} = \zeta_s, \quad \widehat{NM} = \frac{\pi}{2} - \delta,$$

and the angles are

$$\widehat{N} = H, \quad \widehat{Z} = \pi - \chi_s, \quad \widehat{M},$$

noting that the angle  $M$ , the angle at the body, is not used here. Concerning the azimuth angles, the origin is taken when the point  $M$  lies in the meridian plane  $\mathcal{M}$ . The azimuth  $\chi_s$ , like  $\chi$ , is measured relative to the northerly direction.

The horizontal coordinates are expressed in terms of the equatorial coordinates and the latitude in the form  $(\chi_s, \zeta_s) = f(H, \delta, \psi)$  by the relations

$$\cos \zeta_s = \sin \psi \sin \delta + \cos \psi \cos \delta \cos H , \tag{13.18}$$

$$\sin \zeta_s \sin \chi_s = \cos \delta \sin H , \tag{13.19}$$

$$\sin \zeta_s \cos \chi_s = -\cos \psi \sin \delta + \sin \psi \cos \delta \cos H . \tag{13.20}$$

The reader is referred to Sect. 6.13 on spherical trigonometry, where the triangle  $ABC$  corresponds here to the triangle  $NZM$ . The above three relations are the fundamental relations of spherical trigonometry, sometimes known as Gauss’ relations.

Equation (13.18) gives  $\zeta_s$ , an angle in the interval  $[0, \pi/2]$ . Substituting its value into (13.19) or (13.20) yields the azimuth  $\chi_s$  in  $[0, \pi]$ . The value of  $\chi_s$ , which lies in  $(-\pi, \pi]$  is then given by comparing with the sign of  $H$ :  $\chi_s$  and  $H$  have the same sign (negative in the morning, positive in the afternoon, with  $H = 0$  at noon).

Equation (13.19) or (13.20) yield  $\zeta_s$  in the full interval  $[-\pi/2, +\pi/2]$ . We can thus determine whether it is daytime (the Sun above the local horizon, with  $\zeta_s \geq 0$ ) or nighttime (the Sun is below the local horizon, with  $\zeta_s \leq 0$ ). In some cases, it is preferable to use the solar elevation  $h_s$  rather than  $\zeta_s$ . These two angles are complementary.

**Example 13.7** Calculate the position of the Sun on 10 July 1998, at 06:30 UT, at the Baikonur space base in Kazakhstan.

► In Example 7.4, we calculated that the instant of time 06:30 UT corresponded on this date with 10:58 LAT. Naturally, one must use the local apparent time in this situation. We thus have for the hour angle

$$H = 10 \text{ h } 58 \text{ m} - 12 \text{ h } 00 \text{ min} = -1 \text{ h } 02 \text{ m} ,$$

whence  $H = -62/4 = -15.5^\circ$ . Regarding the other quantities,

$$\delta(D = 10 \text{ July}) = 22.3^\circ , \quad \varphi = 45^\circ 38' \text{N} ,$$

whence  $\psi = 45.5^\circ$ . Equation (13.18) gives  $\cos \zeta_s = 0.8947$ , whereupon  $\zeta_s = 26.5^\circ$ , implying a solar elevation  $h_s = 63.5^\circ$ . Regarding the azimuth, (13.20) implies that  $\cos \chi_s = 0.8329$ , and since  $H$  is negative,  $\chi_s = -33.6^\circ$ . The straight line  $PS_s$  thus points eastward (this is before apparent noon, i.e., 12:00 LAT). ◀

## 13.2.2 Sunrise, Sunset, and Apparent Noon

### Sunrise and Sunset

The obliquity  $\varepsilon$  is used to define circles on the Earth's surface (small circles called parallels) at certain significant latitudes: the polar circles, which are the Arctic Circle at  $\psi = 90^\circ - \varepsilon = 66^\circ 34'N$  and the Antarctic Circle at  $\psi = 66^\circ 34'S$ , and the tropics, which are the Tropic of Cancer at  $\psi = \varepsilon = 23^\circ 26'N$ , and the Tropic of Capricorn at  $\psi = 23^\circ 26'S$ .

Between the tropics, the Sun passes through the zenith at noon on those 2 days of the year when the declination is equal to the latitude. With  $\delta = \psi$  and  $H = 0$ , (13.18) then gives  $\cos \zeta_s = 1$ , whence  $\zeta_s = 0$  or  $h_s = 90^\circ$ . Beyond the polar circles, there are days when the Sun never rises, and others when it never sets.

To study the sunrise and sunset in the general case, we write (13.18) in the form

$$\cos \zeta_s = \sin h_s = \cos \delta \cos \psi (\cos H - T), \quad (13.21)$$

with

$$T = -\tan \delta \tan \psi.$$

The case of the poles can be treated immediately. Equation (13.18) shows that, for any  $H$ , we have  $h_s = \delta$ . Having dealt with this case, we see that solution of  $\sin h_s = 0$  is equivalent to solution of  $\cos H = T$ . We consider two cases, depending on whether  $|T|$  is greater than or less than 1.

**The Case  $|T| > 1$ .** If  $|T| > 1$ , i.e.,  $|\psi| + |\delta| > 90^\circ$ , the quantity  $\sin h_s$  cannot be zero for any  $H$ . In this case, there is no sunset or sunrise:

- If  $T$  is negative,  $T < -1$ , i.e.,  $|\psi + \delta| > 90^\circ$ , and

$$\sin h_s > 0 \iff h_s > 0.$$

The Sun spends the whole day above the horizon. This is the polar day.

- If  $T$  is positive,  $T > +1$ , i.e.,  $|\psi - \delta| < 90^\circ$ , and

$$\sin h_s < 0 \iff h_s < 0.$$

The Sun spends the whole day below the horizon. This is the polar night.

**The Case  $|T| \leq 1$ .** If  $|T| \leq 1$ , i.e.,  $|\psi| + |\delta| < 90^\circ$ , (13.21) has two roots:

$$\sin h_s = 0 \iff \cos H = T,$$

determining two opposite values of  $H$ , denoted by  $H_{\text{rise}}$  and  $H_{\text{set}}$ :

$$\begin{cases} H_{\text{set}} = \arccos(-\tan \delta \tan \psi), \\ H_{\text{rise}} = -H_{\text{set}}. \end{cases}$$

With  $\zeta_s = 90^\circ$  in (13.20), we obtain the corresponding azimuth values:

$$\begin{cases} \chi_{s_{\text{set}}} = \arccos\left(-\frac{\sin \delta}{\cos \psi}\right), \\ \chi_{s_{\text{rise}}} = -\chi_{s_{\text{set}}}. \end{cases}$$

We note the following special cases:

- At the equator ( $\psi = 0$ ), we have, for the whole year,

$$H_{\text{set}} = 90^\circ, \quad \chi_{s_{\text{set}}} = 90^\circ - \delta.$$

- At the equinoxes ( $\delta = 0$ ), we have, for the whole Earth,

$$H_{\text{set}} = 90^\circ, \quad \chi_{s_{\text{set}}} = 90^\circ.$$

Recall that  $H_{\text{set}} = 90^\circ$  corresponds to sunrise at 06:00 LAT and sunset at 18:00 LAT.

**Note.** In these calculations, we have not taken into account atmospheric refraction. For medium latitudes ( $|\psi| < 55^\circ$ ), and on average over the year, refraction brings the sunrise forward by about 3 min and delays the sunset by the same amount.

### Apparent Noon

Apparent noon, or 12:00 LAT, corresponds to  $H = 0$ . In all the monthly tables showing overpass time at the end of the chapter, where LMT is shown on the abscissa, we thus have

$$\text{noon LMT} = \text{noon LAT} + E_T,$$

where  $E_T$  is the equation of time discussed in Chap. 7 [see (7.58) and (7.60)].

In these monthly tables, i.e., Figs. 13.12 and 13.13, and also 13.16, 13.17, 13.18, and 13.19, the dashed curve shows the times (LMT) of the sunrise, sunset, and apparent solar noon, for the relevant location and during the whole month.

## 13.3 Sun–Target–Satellite Configuration

### Scattering Angle

#### 13.3.1 Angles Describing the Sun–Target–Satellite Configuration

For any point  $P$ , the directions of the Sun and satellite at a given time are defined by the four angles  $\chi$ ,  $\zeta$ ,  $\chi_s$ , and  $\zeta_s$ . When studying certain physical phenomena, such as radiation phenomena or those related to questions of

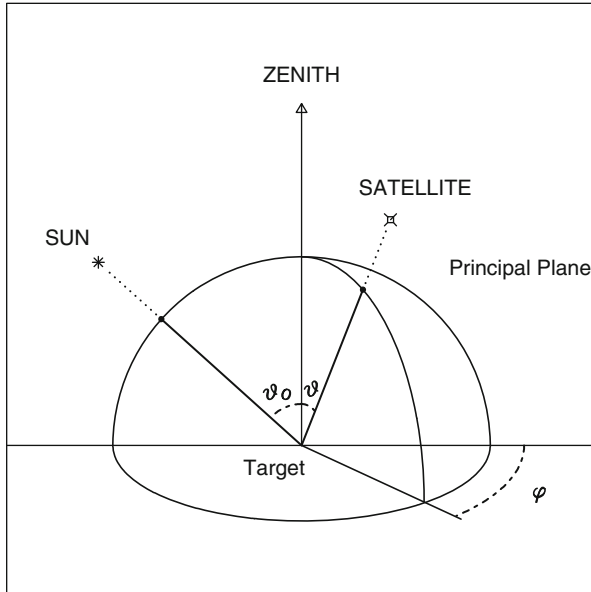


FIG. 13.8 : Angles used to describe the geometric configuration of the Sun, target, and satellite.

remote sensing, it is useful to know that three angles are in fact sufficient to characterise the geometry of the Sun–target–satellite configuration. These are the two zenith angles and the relative azimuth. Using the standard relations here, we set

$$\begin{cases} \theta_0 = \zeta_s , \\ \theta = |\zeta| , \\ \phi_A = \chi_s - \chi + \pi \pmod{2\pi} . \end{cases}$$

Defined in this way, the relative azimuth is zero when the directions are opposite and it is equal to  $\pi$  when the Sun and the satellite are on the same side with respect to the target point (see Fig. 13.8). Most of the phenomena studied are symmetrical with respect to the principal plane, which is the plane spanned by the direction of the Sun and the vertical at the target point. We then consider the relative azimuth in the interval  $[0, \pi]$ . For reasons of clarity, we use  $\phi_A$  to denote the relative azimuth defined in  $[0, 2\pi]$  and  $\phi_B$  to denote the one defined in  $[0, \pi]$ , with

$$\phi_B = \phi_A \text{ if } \phi_A \leq \pi , \quad \phi_B = 2\pi - \phi_A \text{ if } \phi_A > \pi .$$

In radiation studies, when we speak of the relative azimuth without further specification, we are referring to  $\phi_B$ , written  $\phi$ .

The scattering angle is the angle between the two directions denoted here by  $PS$  and  $PS_s$ . This angle  $\gamma$  takes values in the interval  $[0, \pi]$ . Its value is

found as for  $\alpha$  with (13.2). Using the above notation,

$$\cos \gamma = \cos \theta_0 \cos \theta - \sin \theta_0 \sin \theta \cos \phi . \quad (13.22)$$

### 13.3.2 Specular Reflection (Sun Glint)

We speak of specular<sup>2</sup> reflection when rays of sunlight, after reflecting on a surface, end up in the satellite’s onboard detector. This specular reflection, often called Sun glint, can cause irreversible damage to instrumentation, but even if it does not, radiometric measurements can suffer seriously by not taking this phenomenon into account.

Sun glint occurs when the reflecting surface is a liquid surface, like the sea, or even a lake or wetland. The glare from Sun glint gives an idea of the state of the surface, from calm sea (narrow region of glare with intense reflection) to rough waters (broad region with more diffuse reflection). One can thus detect regions polluted by oil slicks, as can be seen from Figs. 13.9 and 13.10.

#### Conditions for Specular Reflection

Strictly speaking, reflection occurs when:

- the directions  $\mathbf{PS}$  and  $\mathbf{PS}_s$  lie in the same plane, on either side of the normal at  $P$ :

$$\chi - \chi_s = \pi \pmod{2\pi}, \quad \text{i.e., } \phi = 0 ,$$

- the angles of incidence are equal:

$$|\zeta| = \zeta_s , \quad \text{i.e., } \theta = \theta_0 .$$

We call  $\mathbf{PS}'_s$  the reflected solar ray. Its direction is given by the zenith angle  $\zeta_s$  and azimuth angle  $\chi_s + \pi$ . If  $\gamma'$  is the angle between  $\mathbf{PS}'_s$  and  $\mathbf{PS}$ , we obtain its value by a similar calculation to the one leading to  $\gamma$ , whereupon

$$\cos \gamma' = \cos \theta_0 \cos \theta + \sin \theta_0 \sin \theta \cos \phi . \quad (13.23)$$

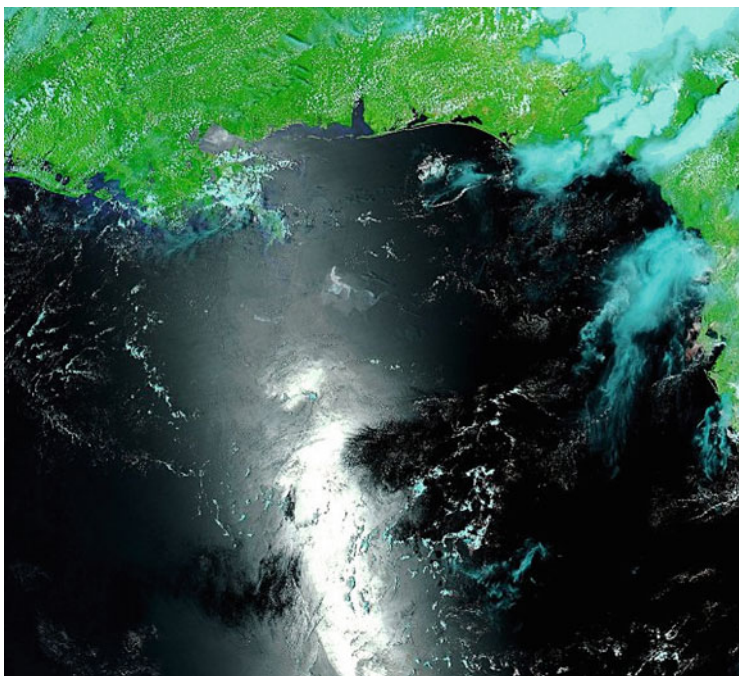
We fix some angle  $\gamma'_0$  which specifies the limit of the effect. We then have the condition

$$\gamma' < \gamma'_0 \quad \iff \quad \text{specular reflection possible .}$$

The two rays  $\mathbf{PS}$  and  $\mathbf{PS}'_s$  then lie inside a cone of half-aperture  $\gamma'_0/2$ . To give an order of magnitude, the angle  $\gamma'_0$  generally takes values between 12° and 20°, depending on the situation.

---

<sup>2</sup>This adjective, borrowed from Middle French, comes from the Latin *specularis*, adjective derived from *speculum*, meaning “mirror”. This word is itself derived from the verb *specere*, meaning “to look” (spectacle), which is associated with the Indo-European root *\*spek-*, “to observe”. The word *spy* also derives from this root.



### Aqua / MODIS

Orbit - Ground track - Sunlight [ Cone:H-apert: 8.0° ]

Altitude = 699.5 km

a = 7077.668 km

2010 07 11 21:00:00 UTC >>> 1440.0 min = 1.00 day

Incl. / SUN-S.= 98.19 °

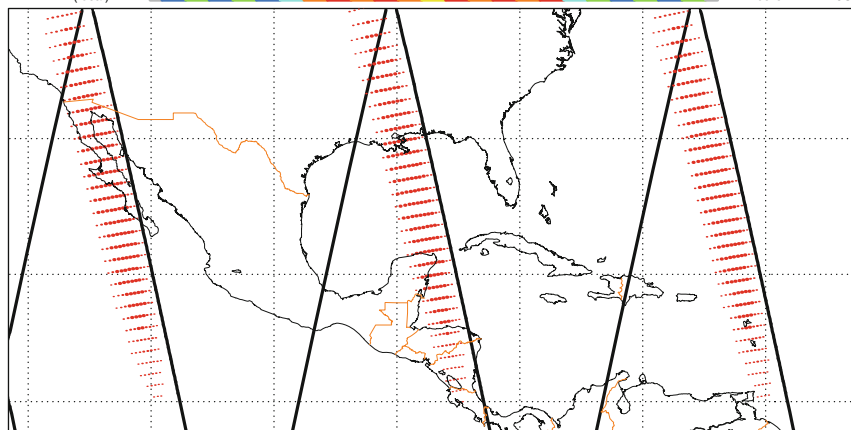
e = 0.000188

Across track swath (XT mode)

Period = 98.88 min \* rev/day =14.56

\*\* Half-swath: 55.2° [ 2.5] - On ground 1165.0 km [ 0.50 min]

LMT (local) 00 01 02 03 04 05 06 07 08 09 10 11 12 13 14 15 16 17 18 19 20 21 22 23 24 hours 12 JUL



Projection: Mercator

PC: 0.0 ° ; 0.0 ° /ZC: 24.0 ° N; 87.0 ° W

Asc. Node: 127.77 ° [13:36 LMT]

Property: Conformal

Aspect: Direct > zoom : 5.20

[NORAD] Revolution: 43541

⊕ T.:Cylindrical - Graticule: 10°

{5.3} [+90.0/ +0.0/ -90.0] [-] EGM2008

[NORAD] 2010 07 11 05:05:22 UTC

Ιξίων  
MC ★ LMD  
Ατλας

FIG. 13.9 : *Specular reflection*. Upper: Image by MODIS carried aboard the satellite Aqua on 12 July 2010. Gulf of Mexico. Specular reflection of sunlight is modified by the presence of oil slicks. Credit: NASA/GSFC, MODIS RR. Lower: Ground track of the satellite Aqua, simulating specular reflection for MODIS. Ixion software initialised by updated NORAD elements. See also Fig. 13.10.

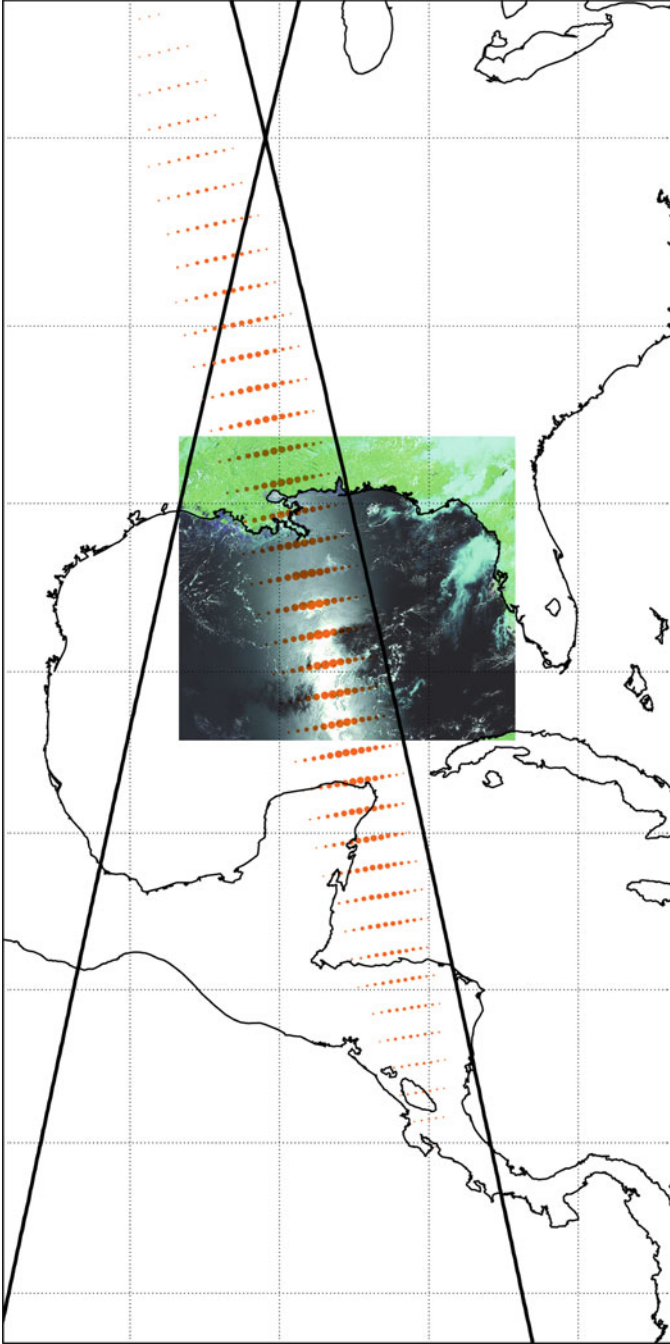


FIG. 13.10 : *Specular reflection in the Gulf of Mexico as seen by the satellite Aqua on 12 July 2010. Image obtained by superposing Fig. 13.9 upper and lower.*



**Example 13.8** *Specular reflection detected by the instrument MODIS aboard the satellite Aqua.*

► The Moderate Resolution Imaging Spectroradiometer (MODIS) is a multi-spectral imager with a pixel of the order of 500 m at the nadir. Its swath is broad enough ( $f_M = 55.2^\circ$ , i.e.,  $2F_M = 2,330$  km on the ground) to observe all points on the Earth every day or every 2 days ( $Q_E = 0.847$ ). NASA uses it aboard the EOS satellites Terra and Aqua for environmental surveillance. On 20 April 2010, the explosion of the Deepwater Horizon oil platform in the Gulf of Mexico led to an oil spill lasting several months which turned out to be the biggest such disaster ever seen in the USA.

Figure 13.9 (upper) is an image of this region taken on 12 July 2010 by Aqua/MODIS. At the top of the image, one can make out the Mississippi delta, and in the center, Mobile Bay, and on the right, the coast of Florida. This provides a perfect example of sun glint. Moreover, the oil slick renders the water surface smoother and intensifies specular reflection.

Figure 13.9 (lower) represents the ground track of Aqua, centering on this region, for the same day. Regions of potential specular reflection are indicated (it can only occur on the sea). This shows that the phenomenon is very significant in the Gulf of Mexico. Figure 13.10 has been obtained by superposing the two last images.

Let us consider the geometric aspects of this phenomenon. Table 13.2 gives all the angles relevant to the Sun–target–satellite configuration on 10–12 July 2010. The target is located at the center of the sun glint, in the pixel with coordinates  $30^\circ\text{N}$  and  $90^\circ\text{W}$ , which corresponds to New Orleans, at the mouth of the Mississippi. Since the table was established for the CERES instrument, we will not take into account the swaths  $f > 55.2^\circ$  for MODIS.

On 12 July, for overpass  $n = 37$ , at 13:08 LMT, the zenith angles are practically equal ( $\zeta = 19^\circ$  and  $\zeta_s = 16^\circ$ ), while the relative azimuth is small ( $\phi_A = 14^\circ$ ). Equation (13.23) gives  $\gamma' = 5^\circ$ , which implies that there will be specular reflection, since the angular bound is  $\gamma' < 16^\circ$  here (cone of half-aperture  $8^\circ$ ).

A little further on, Fig. 13.12 indicates all the cases of specular reflection during the month of July 2010, for New Orleans, with Aqua/MODIS, viz., 3, 12, 19, and 28 July, shortly after 13:00 LMT. With Terra/MODIS, for the same location, see Fig. 13.13: the same phenomenon occurs likewise on 2, 9, 18, and 25 July, at around 11:00 LMT. ◀

**Example 13.9** *Specular reflection detected by the instrument MADRAS aboard the satellite Megha-tropiques.*

► For the conical swath of the MADRAS instrument aboard Megha-Tropiques, and for each observed pixel, we calculate the geometric conditions for specular reflection to occur. If there is no specular reflection, the viewed pixel is indi-

$n$	$D$	LMT	$f$	$\zeta$	$\chi$	$\zeta_s$	$\chi_s$	$\phi_A$	$\gamma$	$\gamma'$
29	10	00:42	-61.6	-77	-90	-	-	-	-	-
30	10	02:21	+39.2	+45	+77	-	-	-	-	-
31	10	13:20	-6.7	-8	+99	19	110	191	11	26
32	11	01:26	-44.8	-51	-96	-	-	-	-	-
33	11	03:03	+60.3	+75	+72	-	-	-	-	-
34	11	12:25	+56.0	+67	-74	9	148	42	74	60
35	11	14:03	-54.3	-64	+94	28	99	185	37	92
36	12	02:08	+23.4	+26	+79	-	-	-	-	-
37	12	13:08	+17.3	+19	-79	16	115	14	35	5
86	28	02:08	+23.4	+26	+79	-	-	-	-	-
87	28	13:08	+17.3	+19	-79	18	124	23	36	7

TABLE 13.2 : Angles used to describe the geometry of the satellite–target–Sun configuration in the case of an across-track swath. Location: New Orleans,  $30.0^\circ N$ ,  $90.0^\circ W$ . Satellite: Aqua. Instrument: CERES  $f_M = 61.8^\circ$ ,  $\zeta_M = 78.0^\circ$ . Initialisation: Date 2010 07 12 20:38:35 UT. Table for July 2010. Number of the overpass in the month is  $n$ , on day  $D$  of the month. Overpass time LMT. Angles  $f$ ,  $\zeta$ ,  $\chi$ ,  $\zeta_s$ ,  $\chi_s$ ,  $\phi_A$ ,  $\gamma$ ,  $\gamma'$ , as defined in the text, given in degrees. Sun glint condition  $\gamma' < 16^\circ$  (fulfilled on  $D = 12$  and  $D = 28$  in this table). Missing values, denoted by a dash, indicate night-time overpass. The values in the table can also be found in Fig. 13.12. Total number of overpasses during the month: 97. Comparing data for 12 and 28 July reveals the 16 day recurrence cycle.

cated on the map by a small black dot. Otherwise, the pixel is represented by a coloured point (depending on the time in LMT) whose size is proportional to the intensity of the Sun glint effect (which increases when the angle  $\gamma'$  tends to 0). If the observed surface is a rather calm sea, and if the geometric conditions for specular reflection are fulfilled, there will be Sun glint (see Fig. 13.11). ◀

## 13.4 Monthly Sampling Tables

For an arbitrary point on the Earth, the monthly sampling tables allow one to visualise all the overpasses of a given satellite, carrying an instrument with well-specified swath. These tables are extremely useful, as much for the preparation of missions as for the exploitation of data transmitted by the satellite. We now give a series of examples.

**Example 13.10** *Monthly sampling tables for a wide swath instrument aboard the Sun-synchronous satellites Terra and Aqua, for a point with latitude  $30^\circ N$ .*

### Megha-Tropiques / MADRAS

Orbit - Ground track - Sun glint [ Cone:H-apert: 9.0° ]

>>>> Time span shown: 102.0 min = 0.07 day

Ground track - Conical swath / VZA=53.5°

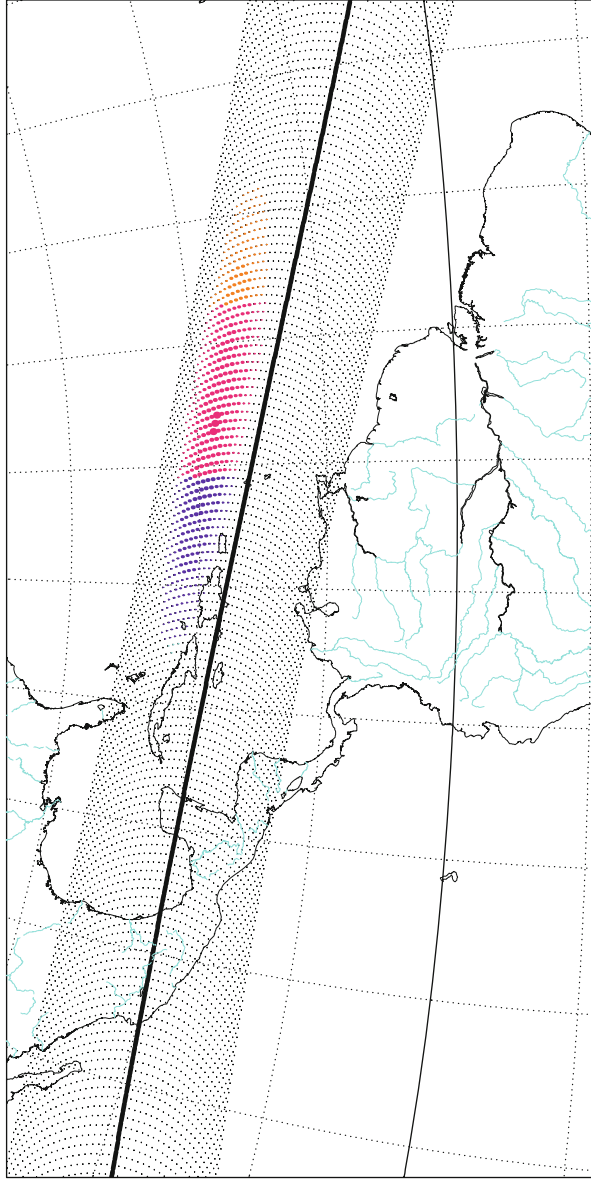
Altitude = 865.5 km

Inclination = 20.00 °

Period = 101.93 min \* rev/day =14.13

\*\* Half-aperture: 65.0° - Radius/grnd 940 km [ 0.40 min]

LMT (local) 00 01 02 03 04 05 06 07 08 09 10 11 12 13 14 15 16 17 18 19 20 21 22 23 24 hours 20 JUL



Projection: Guyou  
 Property: Conformal  
 ⊕ T.: [Ellipt. Int.] - Graticule: 10°  
 PC: 20.0 ° N; 65.0 ° W/ZC: 12.0 ° N; 70.0 ° W Asc. Node: -180.00 ° [00:00 LMT]  
 Aspect: Oblique > zoom : 4.60  
 { 5.3 } [ +90.0/ -25.0 ] [ EIGEN6C2  
 $I \xi_{\omega} \nu$   
 MC \* LMD  
 A T λ α ς

FIG. 13.11 : Detection of specular reflection.

► The CERES instrument scans across track. It has a half-swath  $f_M = 61.8^\circ$  so that  $\zeta_M = 78.0^\circ$ . The overlap fraction is  $Q_E = 1.35$  when the instrument is aboard a satellite on a Terra-type orbit.

**Aqua/CERES.** For the satellite Aqua, we consider the following initial conditions (provided by NORAD):

$$2010\ 07\ 12\ 20:38:35.423\ \text{UT}, \quad \lambda_{AN} = 254.4722^\circ \ (\tau_{AN} = 13:36\ \text{LMT}) .$$

We calculate the sampling for the point  $P$  with coordinates  $30.0^\circ\text{N}$  and  $90.0^\circ\text{W}$  (New Orleans), in order to establish Sun glint conditions as discussed above. The monthly table is drawn up for July, from  $D = 1$  (corresponding to the date 2010 07 01) to  $D = 31$ . For each overpass, we calculate the overpass time (UT then LMT) and the angles specifying the satellite–target–Sun configuration. The results for several consecutive overpasses are shown in Table 13.2. The values for the whole month (31 days, whatever the month) are represented in the monthly sampling table in Fig. 13.12. In this table, the LMT times are given from 0 to 24 on the abscissa axis and the days from 1 to 31 on the ordinate axis. Each point (triangle with apex at the top or the bottom) corresponds to an overpass, dashes (long or short) refer to the target–satellite direction, and small circles (white or black) refer to the target–Sun direction. Dot-dashed lines indicate the times of sunrise and sunset, as well as the local apparent noon, while the slight difference between LAT noon and LMT noon illustrates the equation of time [see (7.58) and (7.60)].

Note that, for this latitude, on almost every day, there are almost three overpasses per day (97 overpasses in 31 days), of which one or two occur during the day (between 12:00 and 14:00 LMT) and two or one during the night (between 1 and 3 o'clock), alternately.

The recurrence cycle  $C_{T_o} = 16$  days is clearly visible. On days  $D$  and  $D + 16$ , we find the same values of  $\zeta$  and  $\chi$ . Moreover, since the satellite is Sun-synchronous, we also find the same values of the LMT time.

Specular reflection ( $\gamma' < 16^\circ$ ) occurs on 3 and 19 ( $= 3 + 16$ ) and also on 12 and 28 ( $= 12 + 16$ ). The Sun glint of 12 July was discussed in Example 13.8 and illustrated in Figs. 13.9 and 13.10.

**Terra/CERES.** For the satellite Terra, on the same orbit as Aqua, we have used contemporaneous NORAD initial data. We calculate the sampling with an identical CERES instrument to the one aboard Aqua (cross-track scanning). The monthly table in Fig. 13.13 for this same point  $P$ , with coordinates  $30.0^\circ\text{N}$  and  $90.0^\circ\text{W}$ , shows a sampling that can be described as “symmetrical” with respect to the one for Aqua. We find three overpasses per day, during the day (between 10 and 12 o'clock LMT) and the night (between 21:00 and 23:00), alternately.

**Average Number of Overpasses per Day.** For a given meridian, Fig. 13.14 shows the average number  $N(\psi, f_M)$  of overpasses per day as a function of the latitude  $\psi$ , from the North Pole to the South Pole, for the CERES instrument

aboard Aqua (or Terra). For the maximum half-swath  $f_M = 61.8^\circ$  of this instrument (continuous curve), the graph of  $N(\psi, f_M)$  shows an almost flat minimum around the equator, then increases towards the poles. Beyond  $\psi = 82^\circ$ , each point is viewed on each revolution of the satellite. In the same figure, we have plotted the graphs of  $N(\psi, f)$  with dotted, dashed, and dot-dashed curves for  $f = 3f_M/4$ ,  $f = f_M/2$ , and  $f = f_M/4$ . Using (12.27), we may check that  $N(0, f_M) = 2Q_E = 2.71$ . ◀

**Example 13.11** *Asymmetry between the northern and southern hemispheres regarding the overpass time of a Sun-synchronous satellite.*

► The instrument known as *Végétation*, or Vegetation Monitoring Instrument (VMI), is an imager with cross-track swath,  $f_M = 50.5^\circ$ , carried aboard the recurrent ( $C_{T_o} = 26$  day) and Sun-synchronous ( $\tau_{AN} = 22:30$ ) satellite SPOT-4. Figure 13.15 is a monthly table with the days of the month on the horizontal axis and latitudes on the vertical axis. We consider a given time slot and note overpass times with triangles and angles  $\zeta$  with line segments. The time slot was of 2.5 h on either side of noon. This is the most favourable period for image acquisition. It is easy to see why the northern hemisphere has the advantage over the southern, through the choice of  $\tau_{AN}$  (in this respect, see Fig. 10.14 and explanations concerning preferences for  $\tau_{AN}$ ). The recurrence cycle of 26 is clearly visible, as is the 5 day subcycle. ◀

**Example 13.12** *Monthly sampling tables for an instrument with medium swath aboard a near-polar satellite (MetOp-A), for locations at various latitudes.*

► The IASI (*Interféromètre atmosphérique de sondage infrarouge*) is a Michelson interferometer measuring the spectral distribution of atmospheric radiation. Its cross-track swath can be described as medium amplitude (between broad and narrow), with  $f_M = 48.3^\circ$ , whence  $\zeta_M = 57.4^\circ$  and  $Q_E = 0.73$ . It is currently operating aboard MetOp-A and MetOp-B and is also planned for MetOp-C.

The satellite MetOp-A is recurrent ( $C_{T_o} = 29$  day) and Sun-synchronous ( $\tau_{AN} = 21:30$ ). We consider the NORAD initial data  $\lambda_{AN} = 266.3619^\circ = 93.64^\circ\text{W}$  at 03:43:01.457 UT (whence  $\tau_{AN} = 21:28$  LMT), on 1 April 2013, and establish the monthly sampling tables for the meridian  $\lambda_{AN}$ :

- On the equator (see Fig. 13.16), there is roughly one overpass and a half every day for this instrument (45 overpasses in 31 days):

$$N(0, f_M) = 2Q_E = 1.46 .$$

The satellite passes through the zenith for  $D = 1$  (initial data) and again for  $D = 30$ , showing that the cycle is indeed 29 days. The 5 day recurrence subcycle is also clearly visible.

# 30 ° N MONTHLY TABLE

\*\*\* Singlint [ ConeHApert: 8.0° ]  
 OVERPASSES ( n = 97 )  
 OF SATELLITE S [ EGM2008 ]  
 FOR POINT P  
 - Latitude : 30.0 ° N  
 - Longitude : 90.0 ° W  
 For P: UTC = LMT + 06h 00m  
 FIELD OF VIEW : 123.6 °

(1) P-S DIRECTION  
 (2) Δ ASC    ▼ DES  
 Right-handed system  
 - Zenith angle (in plane orthog. to track), (1)  
 - Azimuth (in local horiz. plane) / North, (2)  
 SUN  
 ● Zen.    ○ Azi.

**ORBIT**  
 Altitude = 699.5 km  
 Inclination = 98.19 °  
 Equatorial shift= 2751.9 km  
 Period = 98.88 min  
 Mean mot. = 14.56 rev/day  
**SCANNING**  
 Half-swath = 61.8 °  
 Maximal zenith angle = 78.0 °  
 H-swath (ground) = 1801.1 Km  
 Equatorial overlap = 1.335  
 Max. attained latit = 90.0 °  
 Latit. overlap: 82.0° ↔ 90.0°

$I\xi\omega\omega'$   
 MC ★ LMD

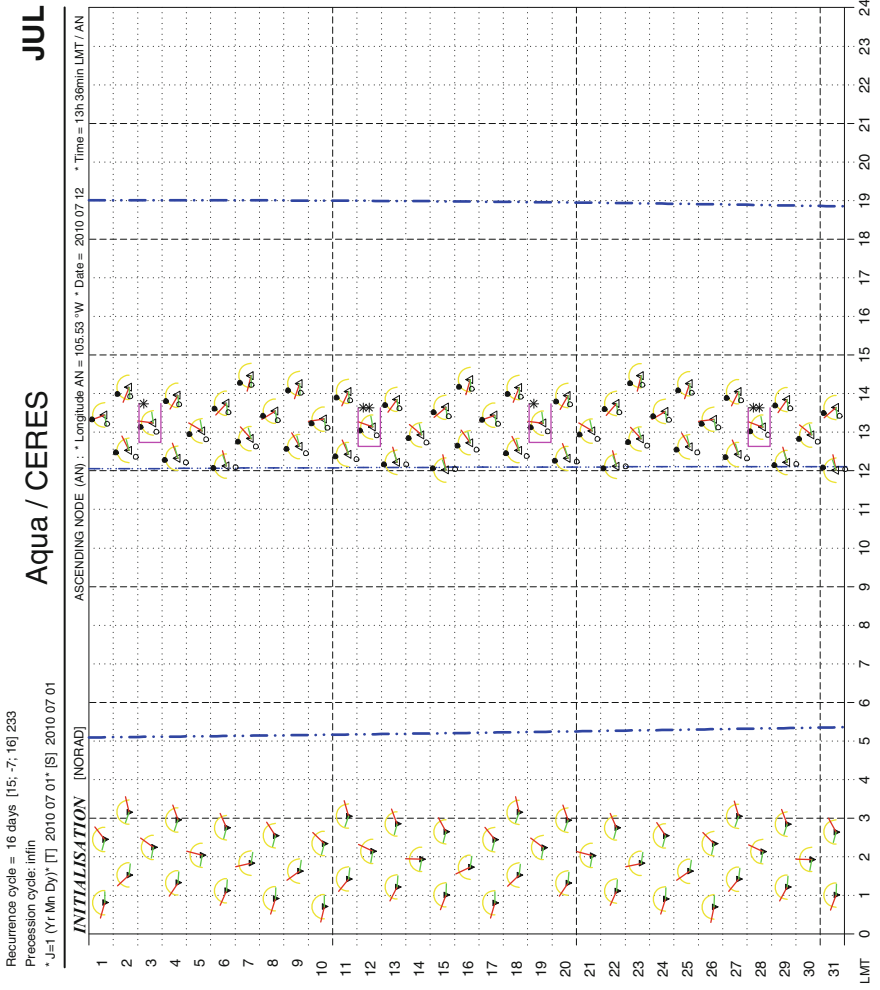
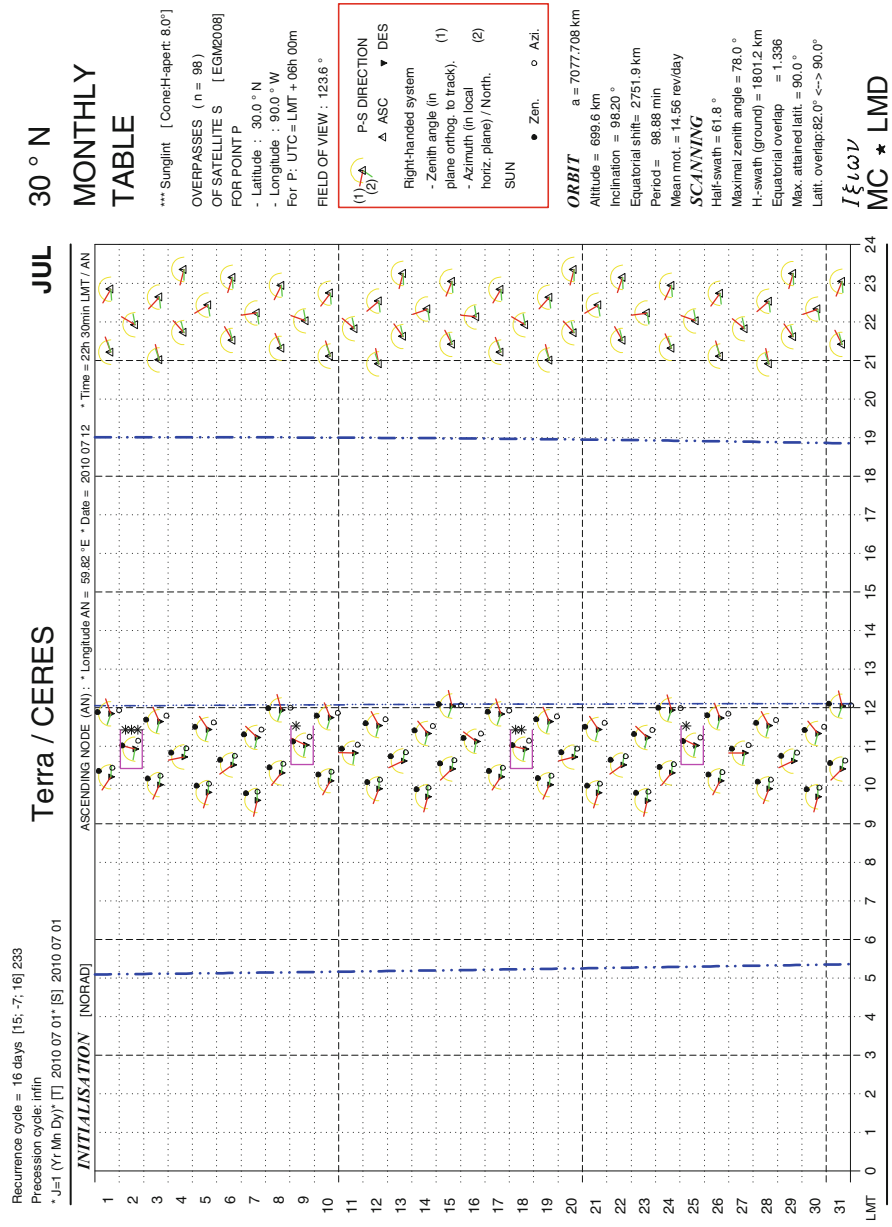


FIG. 13.12 : Monthly table for July. Satellite Aqua, Instrument CERES. Overpass times with indication of Sun glint, for New Orleans, LA.



**JUL**

**Terra / CERES**

Recurrence cycle = 16 days [15; -7; 16] 233

Precession cycle: infini

\*J=1 (Yr: Mn: Dy) [ T ] 2010 07 01\* [ S ] 2010 07 01

ASCENDING NODE (AN) : \* Longitude AN = 59.82° E \* Date = 2010 07 12 \* Time = 22h 30min LMT / AN

INITIALISATION [ NORAD ]

LMT 0 1 2 3 4 5 6 7 8 9 10 11 12 13 14 15 16 17 18 19 20 21 22 23 24

FIG. 13.13 : Monthly table for July. Satellite Terra, Instrument CERES. Overpass times with indication of Sun glint, for New Orleans, LA.

Statistics

MONTHLY TABLE

[T]: Track  
 OVERPASSES OF SATELLITES [EGM2008]  
 FOR POINT P  
 AS FUNCTION OF THE LATITUDE.  
 - Longitude : 90.0 ° W  
 For P: UTC = LMT + 06h 00m  
 FIELD OF VIEW : 123.6 °

STATISTICS ON OVERPASSES  
 Tol. Total Overpasses  
 Mean Overpass/Day  
 Day1 Number of Days  
 with at least 1 Overpass

ORBIT  
 Altitude = 7077.668 km  
 Inclination = 699.5 km  
 Equatorial shift = 2751.9 km  
 Period = 98.88 min  
 Mean mol. = 14.56 rev/day

SCANNING  
 Half-swath = 61.8 °  
 Maximum zenith angle = 78.0 °  
 H-swath (ground) = 1801.1 km  
 Equatorial overlap = 1.335  
 Max. attained latt. = 90.0 °  
 Latt. overlap 82.0° <-> 90.0°

$I\xi\omega\lambda$   
 MC ★ LMD

Aqua / CERES

ASCENDING NODE (AN): Longitude AN = 105.53 °W \* Date = 2010.0712 \* Time = 13h 36min LMT / AN  
 f = 15.5° f = 30.9° f = 46.4° f = 61.8°

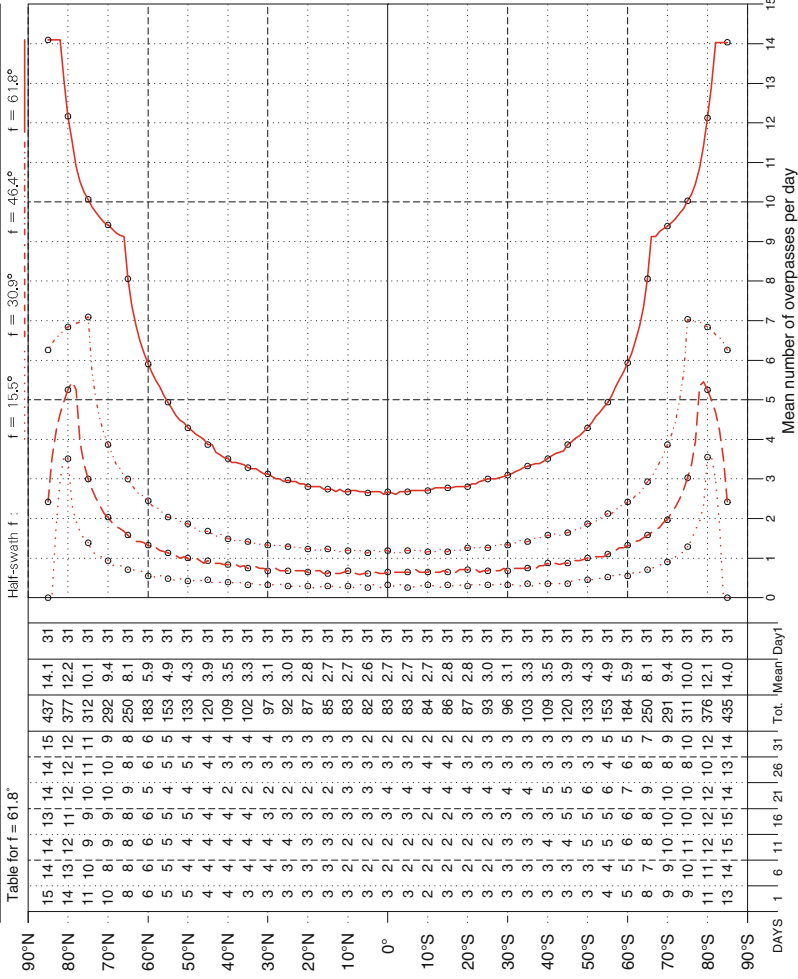


FIG. 13.14 : Monthly table for Aqua. Overpass statistics.



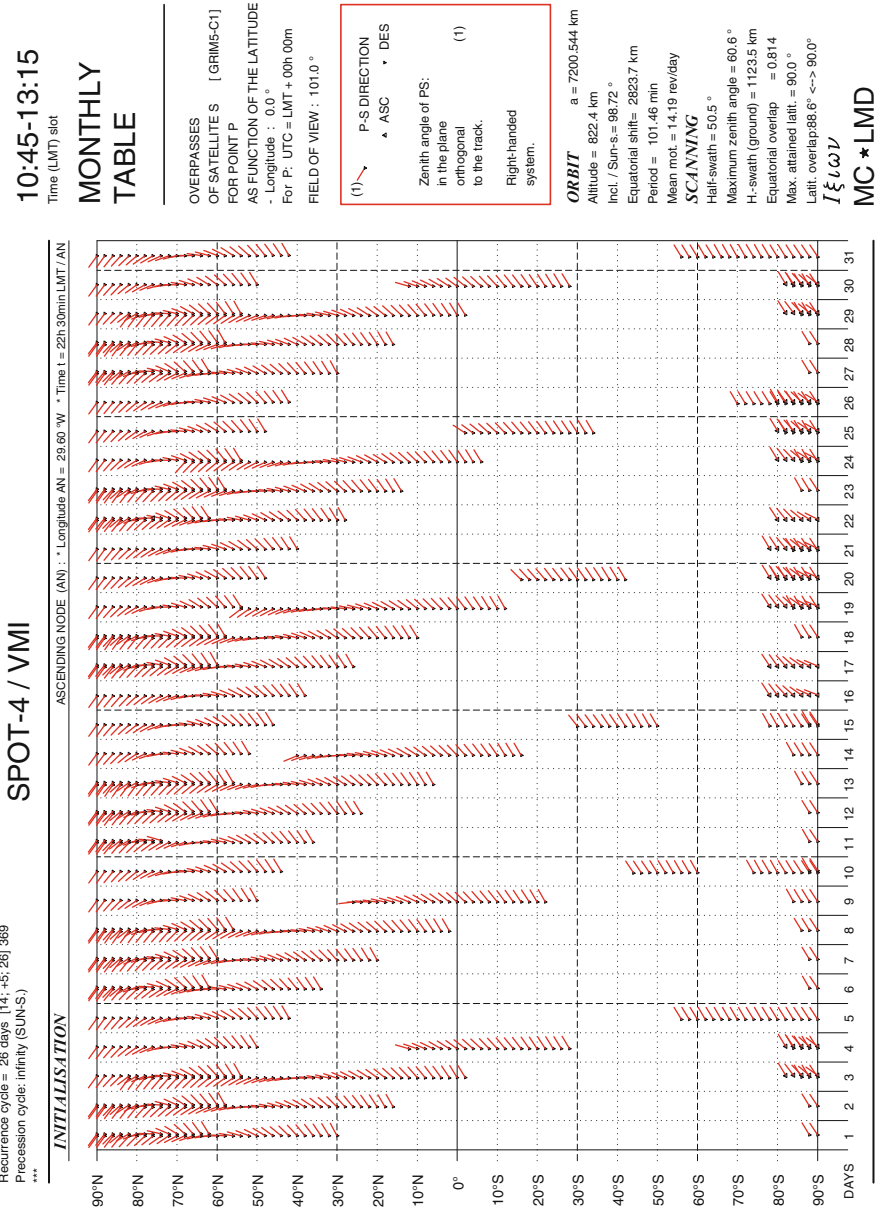


FIG. 13.15 : Monthly table for SPOT-4. Overpasses in time slot, with viewing angle.

- For high latitudes, such as  $\psi = 70^\circ$  (see Fig. 13.17), there are slightly fewer than six daily overpasses (162 overpasses in 31 days), occurring in two batches of three consecutive overpasses.



**Example 13.13** *Monthly sampling tables for an instrument with medium swath aboard a low-inclination satellite (Megha-Tropiques) over two consecutive months.*

► The satellite Megha-Tropiques has inclination  $20^\circ$ . We consider the NO-RAD initial data:  $\tau_{AN} = 11:18$  (LMT) on the date 2013 06 01 and  $\tau_{AN} = 21:05$  (LMT) on the date 2013 07 01. The ScaRaB instrument has a swath of medium amplitude, with  $f_M = 48.9^\circ$ , whence  $\zeta_M = 58.9^\circ$  and  $Q_E = 2.09$ . We consider overpasses for the point  $P$  with geographic coordinates  $\lambda = 75^\circ$ ,  $\psi = 12^\circ\text{N}$ . For such a latitude, with this satellite/instrument configuration, there are more than six overpasses per day during consecutive revolutions:

- Looking at the monthly tables for June and July in Figs. 13.18 and 13.19, we see the influence of nodal precession on the overpass times ( $D = 31$  for June corresponds to  $D = 1$  for July). The value of  $\dot{\Omega}$  calculated above induces a cycle relative to the Sun equal to  $C_S = -51.3$  days. This means that the overpass time moves forward by 28 min on average from 1 day to the next, or by 14 h a month. After 51 days, we return to the same overpass times.
- Figure 13.20 shows the average number  $N(\psi, f_M)$  of overpasses per day as a function of the latitude  $\psi$  and the half-swath  $f_M$ . We have replaced the ScaRaB instrument aboard Megha-Tropiques by an instrument viewing from limb to limb and called here FOV max (maximal field of view). For the maximal half-swath  $f_M = f_0 = 61.7^\circ$  (continuous curve), the graph  $N(\psi, f_0)$  has a flat maximum around the equator. We are then in a situation that may prove useful (and novel): between  $8^\circ\text{N}$  and  $8^\circ\text{S}$ , every point is viewed during each revolution, i.e., 13.1 times a day. On the same figure, we have plotted the graphs of  $N(\psi, f)$  (dotted, dashed, and dot-dashed curves) for  $f = 3f_M/4$  (a value that corresponds roughly to that of ScaRaB),  $f = f_M/2$ , and  $f = f_M/4$ . The slightly shaky aspect of the graphs comes from the fact that the recurrence cycle is short, being just 7 days.

**Note.** As the nodal period  $T_d$  is equal to 101.93 min, the number of round trips per day is  $\nu = 14.1$ . Since the satellite orbits in the prograde sense, i.e., the same sense as the Earth, it only crosses a meridian  $\nu - 1$  times a day. The average daily frequency of intersection of the meridian is thus equal to 13.1 here (if the satellite had inclination  $i = 160^\circ$ , it would cross the meridian 15.1 times a day). The period  $T'$  obtained from this frequency represents the synodic period of the satellite and the Earth. ◀

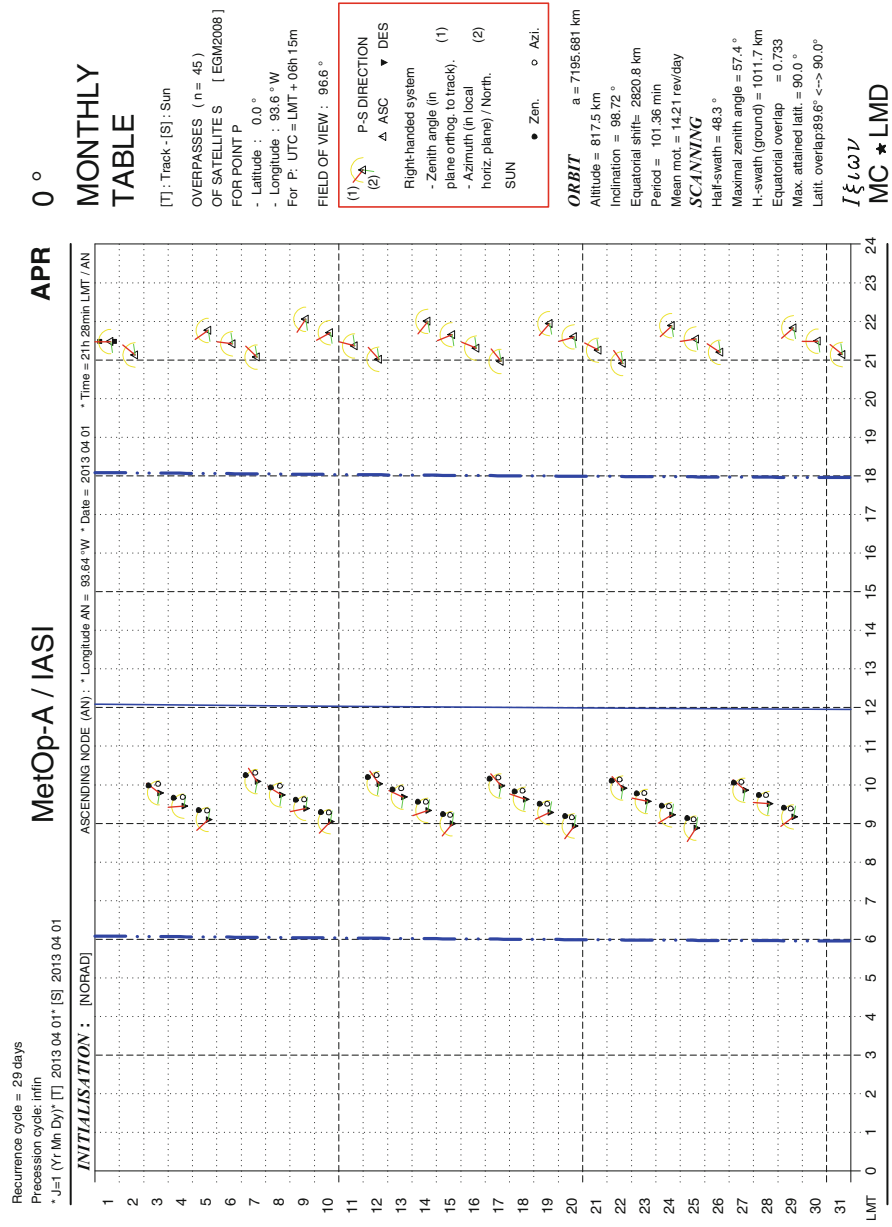
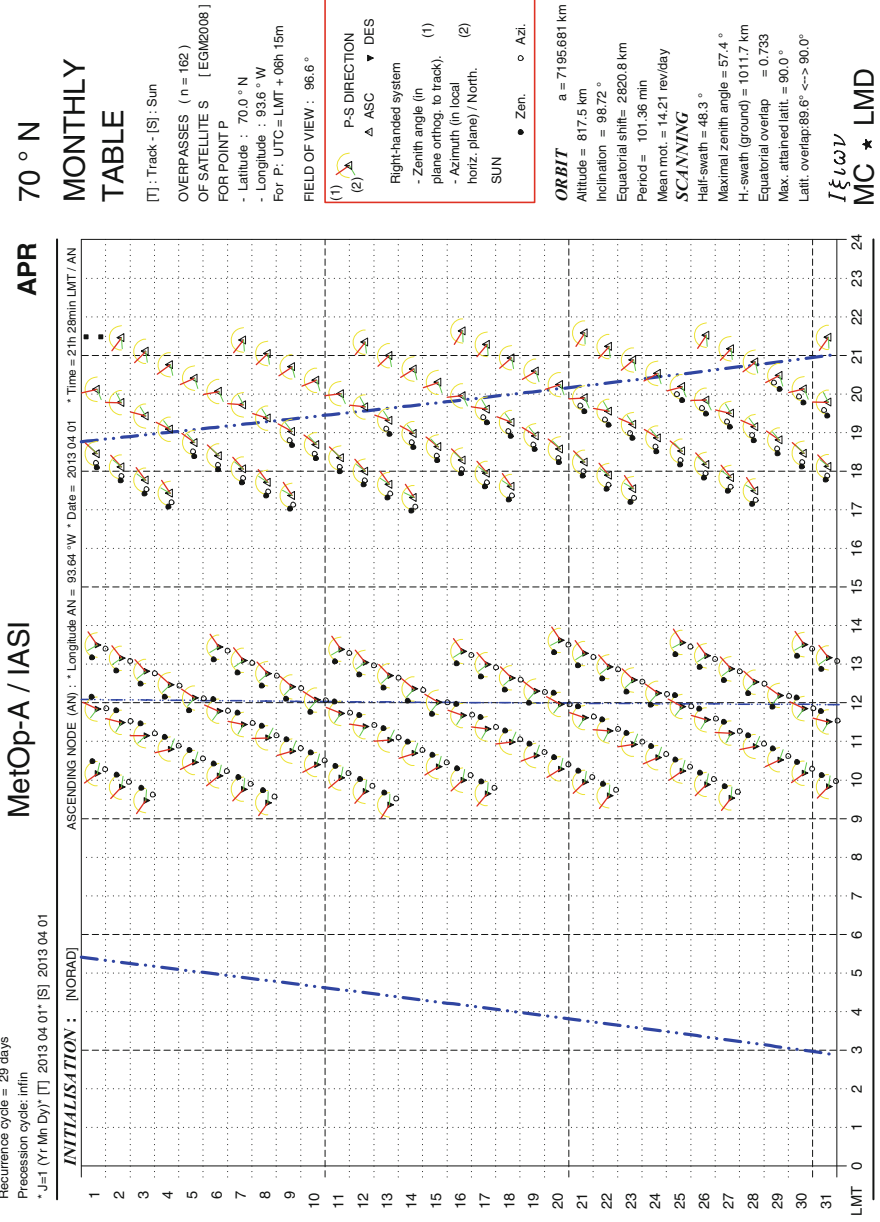


FIG. 13.16: Monthly table for April. Satellite MetOp-A Instrument IASI. Overpass times and angular geometry for Equator.



**APR**

**MetOp-A / IASI**

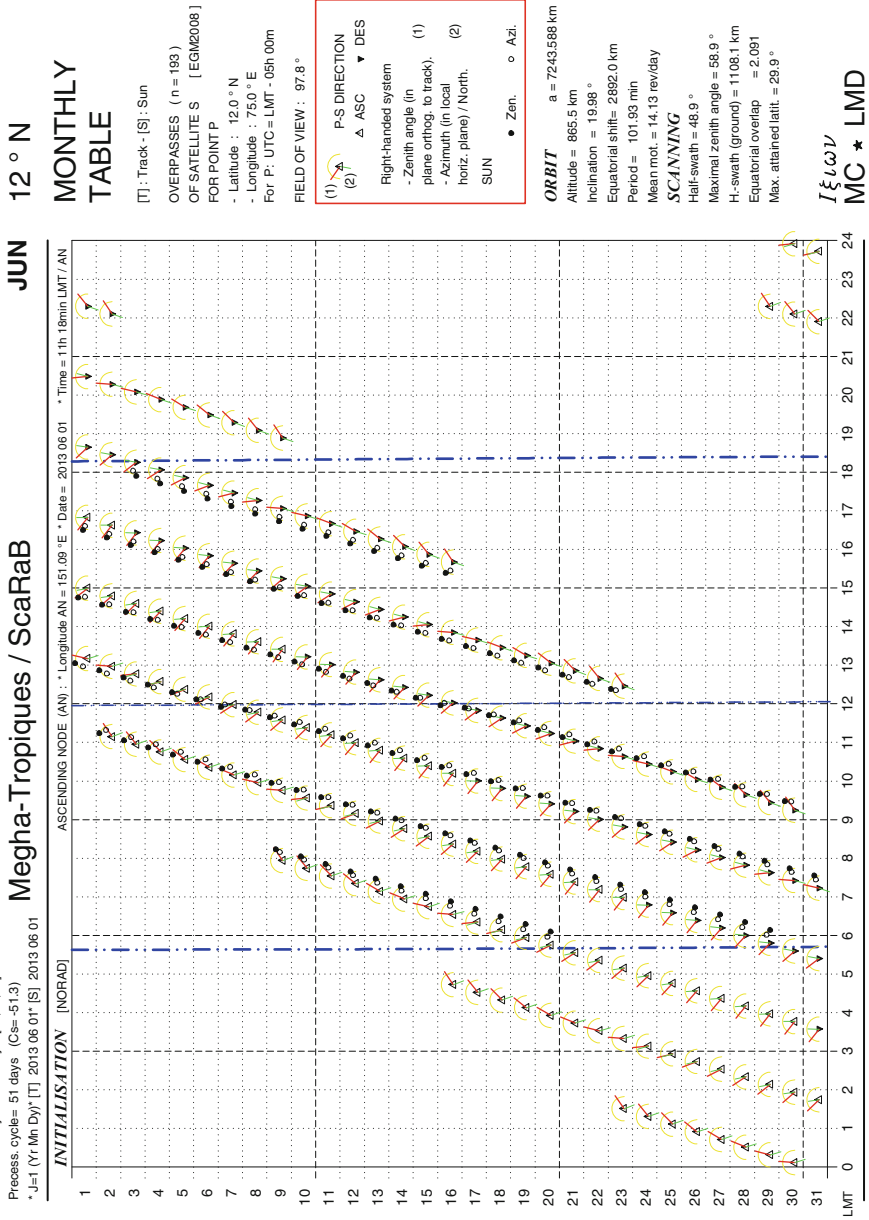
Recurrence cycle = 28 days  
Precession cycle: infin  
\* J=1 (Yr, Mo, Dy) \* [T] 2013 04 01 \* [S] 2013 04 01

INITIALISATION : [NORAD]

ASCENDING NODE (AN) : \* Longitude AN = 93.64° W \* Date = 2013 04 01 \* Time = 21h 28min LMT / AN

LMT 0 1 2 3 4 5 6 7 8 9 10 11 12 13 14 15 16 17 18 19 20 21 22 23 24

FIG. 13.17: Monthly table for April. Satellite MetOp-A, Instrument IASI. Overpass times and angular geometry for 70° N latitude.



**JUN**

**Megha-Tropiques / ScaRaB**

Recurrence cycle = 7 days [14; -1; 7] 97

Process cycle = 51 days (Cs = -51.3)

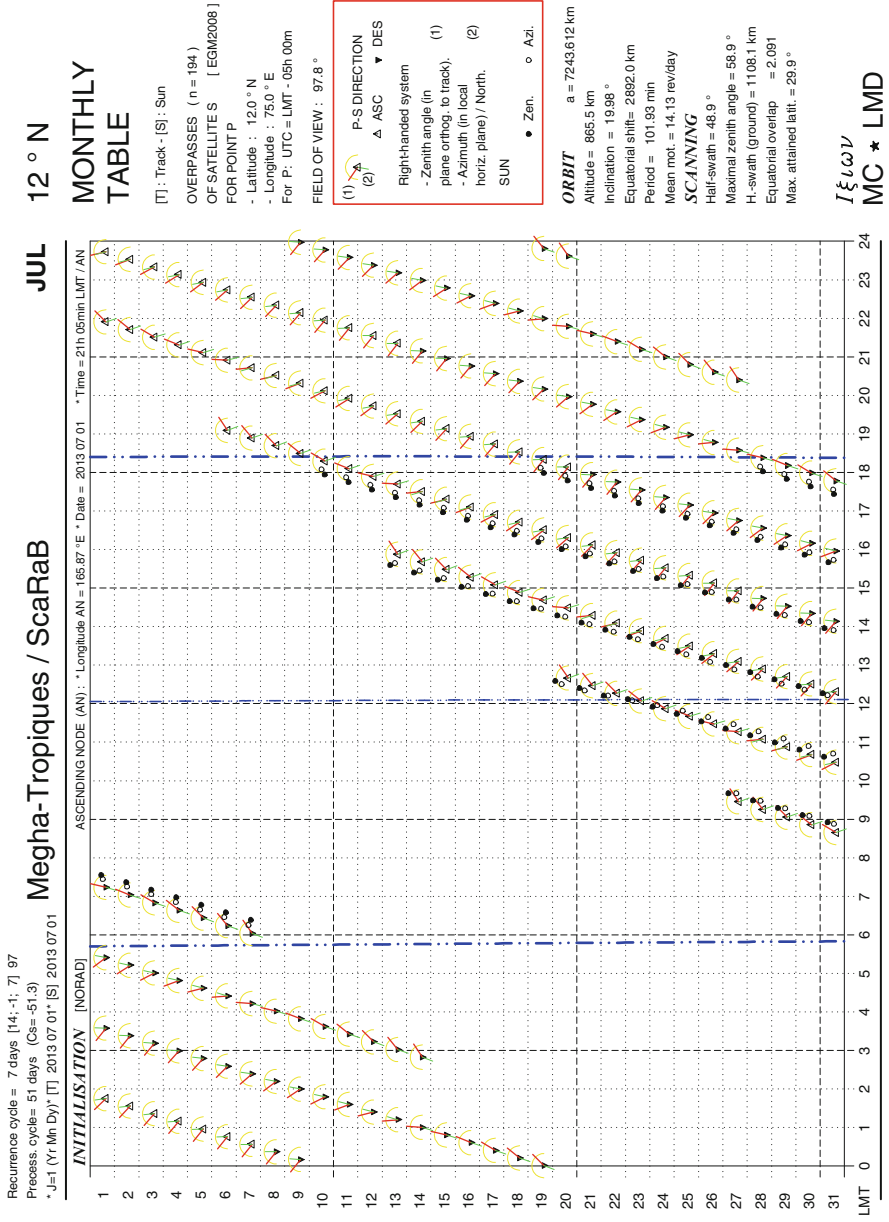
\*J=1 (Yr Mn Dy) [T] 2013 06 01\* [S] 2013 06 01

ASCENDING NODE (AN) - Longitude AN = 151.09° E - Date = 2013.06.01 - Time = 11h 18min LMT / AN

INITIALISATION [NORAD]

LMT 0 1 2 3 4 5 6 7 8 9 10 11 12 13 14 15 16 17 18 19 20 21 22 23 24

FIG. 13.18: Monthly table for June. Satellite MT, Instrument ScaRaB. Overpass times and angular geometry for 12° N latitude.



**Megha-Tropiques / ScaRaB**

Recurrence cycle = 7 days [14; -1; 7] 97  
Process cycle = 51 days (Cs = -51,3)  
\*J=1 (Yr Mn Dy) [T] 2013 07 01\* [S] 2013 07 01

**JUL**

ASCENDING NODE (AN) : \* Longitude AN = 165.87° E \* Date = 2013 07 01 \* Time = 21h 05min LMT / AN

FIG. 13.19 : Monthly table for July. Satellite MT, Instrument ScaRaB. Overpass times and angular geometry for 12° N latitude.

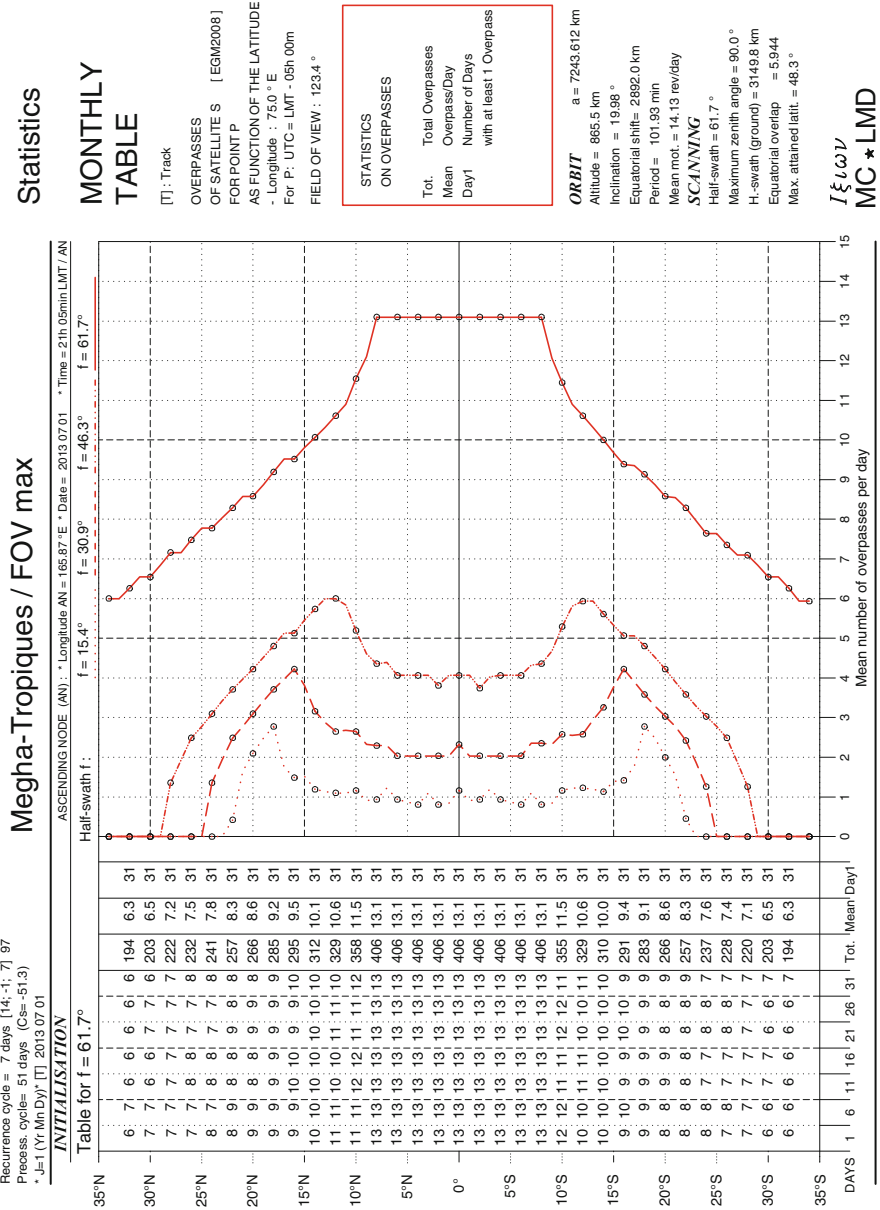


FIG. 13.20 : Monthly table for Megha-Tropiques. Overpass statistics.

# Chapter 14

## Global Positioning Systems (GPS)

### 14.1 Basic Principle of GPS

Positioning by GPS is based on a very simple principle. However, a very high level of technological knowhow is required to make it work. In fact, almost every field of modern physics is involved in some way. This satellite-based system requires:

- very accurate knowledge of satellite positions,
- very accurate clocks aboard each satellite.

The satellites send an electromagnetic signal and the user has a receiver equipped with a clock. (We shall see that this clock does not need to be particularly accurate.) Recall that an electromagnetic signal travels in vacuum at the speed of light  $c$ , and thus travels 30 cm in 1 ns (or  $10^{-9}$  s):

$$0.3 \text{ m} \longleftrightarrow 1 \text{ ns}.$$

#### 14.1.1 Positioning in the Ideal Case

The position of the satellites  $S_i$  is known at each instant of time. The position  $P$  of the receiver is unknown. We begin by considering the ideal case:

1. The satellite  $S_1$  sends a signal at time  $t_1$  and it is received at  $P$  at time  $t'_1$ . The receiver  $P$ , using its clock which measures  $t'_1$  and the message sent



by  $S_1$  at time  $t_1$ , obtains the time  $\Delta t_1 = t'_1 - t_1$ , which corresponds to the distance  $r_1 = \|\mathbf{S}_1\mathbf{P}\|$ :

$$c\Delta t_1 = \|\mathbf{S}_1\mathbf{P}\|. \quad (14.1)$$

The point  $P$  is thus located on the sphere  $\Sigma_1$  of radius  $r_1$  centered on  $S_1$ .

2. Likewise, the satellite  $S_2$  sends a signal, and by measuring the time interval  $\Delta t_2$ , this tells us that  $P$  lies on the sphere  $\Sigma_2$  of radius  $r_2$  centered on  $S_2$ . The point  $P$  is thus on the intersection of the spheres  $\Sigma_1$  and  $\Sigma_2$ , which is a circle.

3. With the satellite  $S_3$ , we obtain a third sphere  $\Sigma_3$ , whose intersection with  $(\Sigma_1 \cap \Sigma_2)$  gives just two points  $P'$  and  $P''$ . One of these two points is therefore  $P$ . The ambiguity between  $P'$  and  $P''$  is easily removed, because one of these two points will be situated in a quite impossible location to be identified with  $P$ , e.g., at an altitude of 35,000 km.

In this ideal case, three satellites therefore suffice to locate  $P$ . However, to achieve this, the clock at  $P$  would have to have the same quality as those carried aboard the satellites, and this would be impossible because such clocks are cumbersome and very expensive. A fourth satellite is thus needed to make up for the inaccuracy of this clock.

### 14.1.2 Positioning in Real Situations

There are two main differences with the ideal case just considered:

- The clock at  $P$  is not perfect and there is a synchronisation error.
- To reach  $P$ , the wave emitted by the satellite must cross the Earth's atmosphere, and this slows the signal down.

Let us just reconsider the logic here. The Cartesian coordinates of  $P$  denoted by  $x$ ,  $y$ , and  $z$ , are unknown. The coordinates  $x_i$ ,  $y_i$ , and  $z_i$ , of the satellite  $S_i$  are known, and the index  $i$  takes values from 1 to  $n$ , since we consider  $n$  satellites. We denote the unit vector in the direction  $\mathbf{S}_i\mathbf{P}$  by  $\mathbf{e}_i$  and set  $r_i = \|\mathbf{S}_i\mathbf{P}\|$ . Then

$$\mathbf{S}_i\mathbf{P} = \begin{pmatrix} x - x_i \\ y - y_i \\ z - z_i \end{pmatrix}, \quad \mathbf{e}_i = \begin{pmatrix} a_{i1} = (x - x_i)/r_i \\ a_{i2} = (y - y_i)/r_i \\ a_{i3} = (z - z_i)/r_i \end{pmatrix}. \quad (14.2)$$

Equation (14.1) for the ideal case becomes

$$c\Delta t_i = \|\mathbf{S}_i\mathbf{P}\| + c\delta t + c \sum_{k=1}^3 \delta_{k,i}t \quad (14.3)$$

in the real case, where we make the following explanatory remarks:

- The synchronisation error  $\delta t$  of the receiver’s clock, which may be positive or negative, is independent of the given satellite and leads to an error in the distance called the clock bias. This is given by

$$b = c\delta t . \tag{14.4}$$

- The time delays  $\delta_{k,i}$  depend on the satellite  $S_i$  and the index  $k$  distinguishes three different effects:
  - $\delta_{1,i}t$  in crossing the ionosphere,
  - $\delta_{2,i}t$  in crossing the troposphere,
  - $\delta_{3,i}t$  due to effects of special and general relativity.

We shall see below how it is possible to measure  $\delta_{1,i}$ , evaluate  $\delta_{2,i}$ , and calculate  $\delta_{3,i}$ , the weak point of the correction being  $\delta_{2,i}$ . But for the moment, we shall take these quantities as being determined.

Finally, we rewrite (14.3) with known values on the left and unknowns on the right:

$$c\Delta t_i - c \sum_{k=1}^3 \delta_{k,i}t = r_i + b . \tag{14.5}$$

The term on the left, a sum of known (measured or evaluated) quantities, is called the pseudo-distance or pseudo-range and it is denoted by  $\rho_i$ . The prefix “pseudo” is justified by the fact that  $\rho_i$  is not equal to the actual distance  $r_i$ , whose value is required, but rather to  $r_i$  plus the (positive or negative) clock bias. For the satellite  $S_i$ , we thus have

$$\rho_i = r_i + b = \sqrt{(x - x_i)^2 + (y - y_i)^2 + (z - z_i)^2} + b . \tag{14.6}$$

With four satellites, we obtain four equations, sufficient to solve for the four unknowns  $x$ ,  $y$ ,  $z$ , and  $b$ .

**Solution for Four Satellites**

A standard method for solving four equations in four unknowns is to linearise the equations. To do this, one must know an approximate position for  $P$ , denoted here by  $\bar{P}$ , with coordinates  $\bar{x}$ ,  $\bar{y}$ , and  $\bar{z}$ , and also an approximate value for the bias  $\bar{b}$ . Then,

$$x = \bar{x} + dx , \quad y = \bar{y} + dy , \quad z = \bar{z} + dz , \quad b = \bar{b} + db ,$$

which yields  $\rho_i = \bar{\rho}_i + d\rho_i$ . We obtain  $d\rho_i$  by differentiating  $\rho_i$ :

$$d\rho_i = dr_i + db .$$

For the distance,

$$dr_i = \frac{\partial r_i}{\partial x} dx + \frac{\partial r_i}{\partial y} dy + \frac{\partial r_i}{\partial z} dz .$$

Applied to the point  $\bar{P}$ , this gives

$$dr_i = \frac{(\bar{x} - x_i)dx + (\bar{y} - y_i)dy + (\bar{z} - z_i)dz}{\sqrt{(\bar{x} - x_i)^2 + (\bar{y} - y_i)^2 + (\bar{z} - z_i)^2}} ,$$

which can also be written

$$dr_i = a_{i1}dx + a_{i2}dy + a_{i3}dz ,$$

where the coefficients  $a_{ij}$ ,  $j = 1, 2, 3$  are the direction cosines of the given direction, i.e., from the satellite  $S_i$  to the point  $\bar{P}$  [see (14.2)].

We consider the corresponding finite increments: the four pseudo-ranges  $\delta\rho_i$  represent the measured quantities, while  $\delta x$ ,  $\delta y$ ,  $\delta z$ , and  $\delta b$  are now the four unknowns. The system of four linear equations in four unknowns is then, for  $i = 1-4$ ,

$$\delta\rho_i = a_{i1}\delta x + a_{i2}\delta y + a_{i3}\delta z + \delta b .$$

In matrix form, this becomes

$$\begin{pmatrix} \delta\rho_1 \\ \delta\rho_2 \\ \delta\rho_3 \\ \delta\rho_4 \end{pmatrix} = \begin{pmatrix} a_{11} & a_{12} & a_{13} & 1 \\ a_{21} & a_{22} & a_{23} & 1 \\ a_{31} & a_{32} & a_{33} & 1 \\ a_{41} & a_{42} & a_{43} & 1 \end{pmatrix} \times \begin{pmatrix} \delta x \\ \delta y \\ \delta z \\ \delta b \end{pmatrix} , \quad (14.7)$$

where the direction cosines are written as follows:

$$a_{i1} = \frac{\bar{x} - x_i}{\bar{\rho}_i - \bar{b}} , \quad a_{i2} = \frac{\bar{y} - y_i}{\bar{\rho}_i - \bar{b}} , \quad a_{i3} = \frac{\bar{z} - z_i}{\bar{\rho}_i - \bar{b}} .$$

This can be written in an equivalent compact notation:

- The vector  $\delta\mathbf{R}$  contains the elements  $\delta\rho_i$ .
- The vector  $\delta\mathbf{X}$  contains the unknowns  $\delta x$ ,  $\delta y$ ,  $\delta z$ , and  $\delta b$ .
- The  $4 \times 4$  matrix  $\mathcal{A}$  contains the elements  $a_{ij}$ .

With this, we have simply

$$\delta\mathbf{R} = \mathcal{A}\delta\mathbf{X} . \quad (14.8)$$

We then calculate the inverse of the matrix  $\mathcal{A}$  and use it to obtain the required result:

$$\delta\mathbf{X} = \mathcal{A}^{-1}\delta\mathbf{R} . \quad (14.9)$$

In practice,  $\bar{P}$  is taken to be the previous value of  $P$ . To initialise, we choose an approximate value of  $P$  and refine the result by successive iteration, varying  $\bar{x}$ ,  $\bar{y}$ ,  $\bar{z}$ , and  $\bar{b}$  so as to minimise  $\|\delta\mathbf{X}\|$ .

**Solution for  $n$  Satellites**

The satellites have orbits such that, apart from certain special cases, any point  $P$  can see about ten GPS satellites at any given time. We then have a system of  $n$  equations (with  $n > 4$ ) available to determine the four unknowns of the vector  $\delta\mathbf{R}$ . The matrix equation (14.7) thus becomes

$$\begin{pmatrix} \delta\rho_1 \\ \delta\rho_2 \\ \vdots \\ \delta\rho_j \\ \vdots \\ \delta\rho_n \end{pmatrix} = \begin{pmatrix} a_{11} & a_{12} & a_{13} & 1 \\ a_{21} & a_{22} & a_{23} & 1 \\ \vdots & \vdots & \vdots & \vdots \\ a_{j1} & a_{j2} & a_{j3} & 1 \\ \vdots & \vdots & \vdots & \vdots \\ a_{n1} & a_{n2} & a_{n3} & 1 \end{pmatrix} \times \begin{pmatrix} \delta x \\ \delta y \\ \delta z \\ \delta b \end{pmatrix}. \tag{14.10}$$

With the previous notation, this can be written

$$\delta\mathbf{R} = \mathcal{A}\delta\mathbf{X}.$$

However, in this case, we cannot obtain  $\delta\mathbf{X}$  directly, because the matrix  $\mathcal{A}$  is not square. In fact the system is overdetermined, because there are more equations than unknowns.

We use the transpose  ${}^T\mathcal{A}$  of  $\mathcal{A}$  to obtain the result

$$\delta\mathbf{X} = [{}^T\mathcal{A}\mathcal{A}]^{-1} {}^T\mathcal{A}\delta\mathbf{R}. \tag{14.11}$$

The solution obtained is the best approximation in the sense of least squares to the solution of (14.10). Using this approach, we consider all the equations to be equivalent. A more refined method, better suited to the problem, is to weight each equation, giving greater weight to satellites viewed with maximal elevation. (The weight is roughly proportional to the cosine of the viewing zenith angle.) But the best suited approach for this kind of problem uses algorithms like Kalman filters.

**GPS Time Base**

Solution of (14.10) by (14.11) yields the desired coordinates of the point  $P$ , but also  $\delta b$ , whence we may determine the clock bias and reset the receiver’s clock relative to the atomic clocks carried by the satellite constellation. The user thus has access to a highly accurate clock and we thereby obtain an excellent time base, common to the whole planet.

**Phase Measurement**

On the wave carrying the signal, with wavelength of the order of 20 cm, the phase of the signal received by the receiver is compared with the phase of the signal emitted by the satellite. We shall not enter into further details on this technique, which considerably improves positioning accuracy (see Table 14.3).

### 14.1.3 Determining User Velocity

Since the position of  $P$  is known at each instant of time (the GPS signal is sent every millisecond), it would be possible to calculate the instantaneous velocity from the definition  $\Delta l/\Delta t$ , but this is not the method actually used, because uncertainties in the position would generate too much error in the velocity. It is better to use the Doppler effect, which can provide much more accurate results. Since the velocity of the satellite is known, the modification of the received signal can be used to obtain the receiver velocity to high accuracy. However, the position of  $P$  must first be determined before carrying out the velocity calculation.

The velocity of the point  $P$  (the user) is denoted by  $\mathbf{U}$  and that of the satellite  $S_i$  by  $\mathbf{V}_i$ , whence

$$\mathbf{U} = \begin{pmatrix} \dot{x} \\ \dot{y} \\ \dot{z} \end{pmatrix}, \quad \mathbf{V}_i = \begin{pmatrix} \dot{x}_i \\ \dot{y}_i \\ \dot{z}_i \end{pmatrix}. \quad (14.12)$$

The satellite  $S_i$  emits a signal at frequency  $f_{0i}$  which is received by  $P$  at frequency  $f_{Ri}$ . The relative change in frequency due to the Doppler effect is equal to the ratio of the relative velocity projected onto the line of propagation of the signal to the velocity of propagation of the signal, which is of course  $c$ , the velocity of light:

$$\frac{f_{0i} - f_{Ri}}{f_{0i}} = \frac{\mathbf{V}_i^{\text{rel}} \cdot \mathbf{e}_i}{c}, \quad (14.13)$$

where  $\mathbf{V}_i^{\text{rel}} = \mathbf{V}_i - \mathbf{U}$  is the relative velocity and  $\mathbf{e}_i$  is the unit vector defined by (14.2).

The clock of the receiver  $P$  generally undergoes an unknown drift, leading to a corresponding drift in the received frequency  $f_{Ri}$ . We have

$$f_{Ri} = f_i \left( 1 + \frac{\dot{b}}{c} \right), \quad (14.14)$$

where  $f_i$  is the frequency measured by the receiver and  $\dot{b}/c$  is dimensionless, being the ratio of two velocities. We thus have

$$c \frac{f_{0i} - f_i(1 + \dot{b}/c)}{f_{0i}} = \mathbf{V}_i \cdot \mathbf{e}_i - \mathbf{U} \cdot \mathbf{e}_i.$$

This is rewritten in such a way that:

- the known quantities  $f_i$  (measured), and  $f_{0i}$  and  $\mathbf{V}_i$  (communicated by the satellite  $S_i$ ) appear on the left,
- the four unknowns  $\dot{b}$  and the three components of  $\mathbf{U}$  appear on the right.

Setting  $\Phi_i = f_i/f_{0i}$ , we obtain

$$c(\Phi_i - 1) + \mathbf{V}_i \cdot \mathbf{e}_i = \mathbf{U} \cdot \mathbf{e}_i - \Phi_i \dot{b}. \tag{14.15}$$

To simplify the notation, we introduce the term  $w_i$  which may be considered as a pseudo-velocity:

$$w_i = a_{i1}\dot{x}_i + a_{i2}\dot{y}_i + a_{i3}\dot{z}_i + c(\Phi_i - 1), \tag{14.16}$$

and then write (14.15) in the form

$$w_i = a_{i1}\dot{x} + a_{i2}\dot{y} + a_{i3}\dot{z} - \Phi_i \dot{b}. \tag{14.17}$$

The term  $\Phi_i$  is very close<sup>1</sup> to unity. In the definition (14.16) of  $w_i$ , the term  $c(\Phi_i - 1)$  is the hallmark of the Doppler effect, but in (14.17),  $\Phi_i \dot{b}$  can be replaced by  $\dot{b}$  and this equation becomes

$$w_i = a_{i1}\dot{x} + a_{i2}\dot{y} + a_{i3}\dot{z} - \dot{b}. \tag{14.18}$$

To begin with we assume that there are four satellites, the minimum for determining velocities. We then obtain the matrix equation

$$\begin{pmatrix} w_1 \\ w_2 \\ w_3 \\ w_4 \end{pmatrix} = \begin{pmatrix} a_{11} & a_{12} & a_{13} & 1 \\ a_{21} & a_{22} & a_{23} & 1 \\ a_{31} & a_{32} & a_{33} & 1 \\ a_{41} & a_{42} & a_{43} & 1 \end{pmatrix} \times \begin{pmatrix} \dot{x} \\ \dot{y} \\ \dot{z} \\ -\dot{b} \end{pmatrix}. \tag{14.19}$$

The  $4 \times 4$  matrix is the same as the matrix  $\mathcal{A}$  in (14.7). Indeed, (14.19) is obtained by differentiating (14.7) with respect to time while fixing the direction cosines.

In view of a more compact notation, we define:

- the vector  $\mathbf{W}$  whose components are the pseudo-velocities  $w_i$ ,
- the vector  $\dot{\mathbf{X}}$  whose components are the unknowns  $\dot{x}$ ,  $\dot{y}$ ,  $\dot{z}$ , and  $\dot{b}$ , and which can be considered to correspond to  $d(\delta\mathbf{X})/dt$ ,
- the  $4 \times 4$  matrix  $\mathcal{A}$ .

Then we may write

$$\mathbf{W} = \mathcal{A}\dot{\mathbf{X}}. \tag{14.20}$$

Since the inverse of  $\mathcal{A}$  has already been found in the position determination, we obtain

$$\dot{\mathbf{X}} = \mathcal{A}^{-1}\mathbf{W}. \tag{14.21}$$

With more than four satellites, as for the position calculation, we use  ${}^T\mathcal{A}$  or the Kalman filter method.

---

<sup>1</sup>The velocity of a Navstar/GPS satellite is 3.9 km/s in a Galilean frame. In a terrestrial frame, the relative velocity  $\|\mathbf{V}_i^{\text{rel}}\|$  is of this order, whence we find  $V_i^{\text{rel}}/c \sim 10^{-5}$ .

## 14.1.4 Perturbation of Signal and Measurement

### Effects Due to the Ionosphere

The ionosphere is a region of the atmosphere located roughly between altitudes 60 and 800 km. Gases there are highly ionised under the effects of solar radiation. The pressure varies between 2 and  $10^{-6}$  Pa depending on the altitude. The ionosphere is a dispersive medium, meaning that the speed of propagation of an electromagnetic wave will depend on its frequency. To measure the perturbation on the signal due to the ionosphere,  $S_i$  transmits a dual frequency wave, i.e., at two different frequencies  $f'$  and  $f''$ . The time difference for the two frequencies to arrive can be used to calculate the ionospheric contribution  $\delta_{1,i}t$  to the signal delay.<sup>2</sup>

### Effects Due to the Troposphere

The troposphere is the region of the atmosphere directly enveloping the Earth's surface, in which weather phenomena take place, e.g., wind, cloud, rain, and so on. It contains about 80 % of the mass of the atmosphere and its upper bound is the tropopause, at which the temperature variation reverses. The altitude of the tropopause is about 8 km at the poles and 16 km at the equator, and varies with the season.

This is a non-dispersive medium. The signal is delayed by crossing the troposphere, and of course the distance travelled depends on the viewing con-

---

<sup>2</sup>Let  $\rho'_i$  and  $\rho''_i$  be the pseudo-ranges measured for the frequencies  $f'$  and  $f''$ , respectively, and let  $r_i$  be the geometric distance between the satellite  $S_i$  and the receiver  $P$ :

$$\rho'_i = r_i + \delta r'_i + \Delta r_i, \quad \rho''_i = r_i + \delta r''_i + \Delta r_i,$$

where  $\Delta r_i$  is the sum of the delays due to causes other than the ionosphere and where  $\delta r'_i$  and  $\delta r''_i$  are the delays due to crossing the ionosphere, which depend on the frequency. (These are generally between 1 and 40 m, depending on the time, the day, the location, and the viewing configurations.) It can be shown that these discrepancies  $\delta r_i$  are proportional to  $f^{-2}$ . Therefore,

$$\delta r'_i = \frac{A_i}{f'^2}, \quad \delta r''_i = \frac{A_i}{f''^2},$$

whence

$$\delta r''_i = \left( \frac{f'}{f''} \right)^2 \delta r'_i.$$

By measuring  $\rho'_i$  and  $\rho''_i$ , and using the known ratio of the frequencies,  $\delta r'_i$  can be determined from

$$\rho'_i - \rho''_i = \delta r'_i - \delta r''_i = \delta r'_i \left[ 1 - \left( \frac{f'}{f''} \right)^2 \right], \quad \delta r'_i = \frac{\rho'_i - \rho''_i}{1 - (f'/f'')^2},$$

so that, with our notation,  $\delta r'_i = c\delta_{1,i}t$ .

figuration, i.e., whether the satellite is low or high above the horizon. The time difference that we have denoted by  $\delta_{2,i}t$  is divided into two parts, one for the dry atmosphere and the other for water vapour. The contribution of the dry atmosphere can be quite well modelled, but the wet atmosphere is another matter, proving very complex to evaluate, since it depends on local meteorological phenomena. We shall see later that it is the differential GPS that best deals with this source of error.

### Relativistic Effects

In an appendix at the end of the chapter (see Sect. 14.11), we explain how relativistic effects can be taken into account. Even though the theoretical concepts may be complex, they are perfectly understood and the inherent corrections can be made with great accuracy. There is almost no error in the term  $\delta_{3,i}t$ .

## 14.1.5 Geometric Considerations and Measurement Accuracy

The fundamental situations involved in satellite positioning can be understood from elementary considerations of geometry, the subject of this section.

### Clock Correction

As we saw earlier, the user's clock is of average quality. This leads to what we called clock bias in (14.4), which is fully determined by the system of equations in (14.7) or (14.10). Here we discuss a simple and clever illustration of how clock bias can be reduced. We consider a simplified situation where the receiver  $P$  is on a spherical Earth. Three satellites  $S_i$  are visible to  $P$ . Each sphere of center  $S_i$  intersects the Earth's sphere in a circle.

Figure 14.1 shows three possible situations regarding clock synchronisation:

- If the receiver clock is perfectly synchronised with the satellite clock, the three circles intersect exactly at  $P$ .
- If the receiver clock is slow, the receiver underestimates the distances  $r_i$  and the circles form a concave triangle containing  $P$ .
- If the receiver clock is fast, the receiver overestimates the distances  $r_i$  and the circles form a convex triangle containing  $P$ .

Given that the three circles should meet at  $P$ , the clock discrepancy is corrected in such a way as to minimise the error triangle.

### Viewing Geometry and Accuracy

The basic principle of GPS exploits the intersection of spheres. A simplified geometrical study can give an insight into the accuracy of horizontal and vertical positioning.

We consider two spheres centered on  $S_1$  and  $S_2$ , represented here by two circles whose intersection determines  $P$  (see Fig. 14.2). Each circle is shown



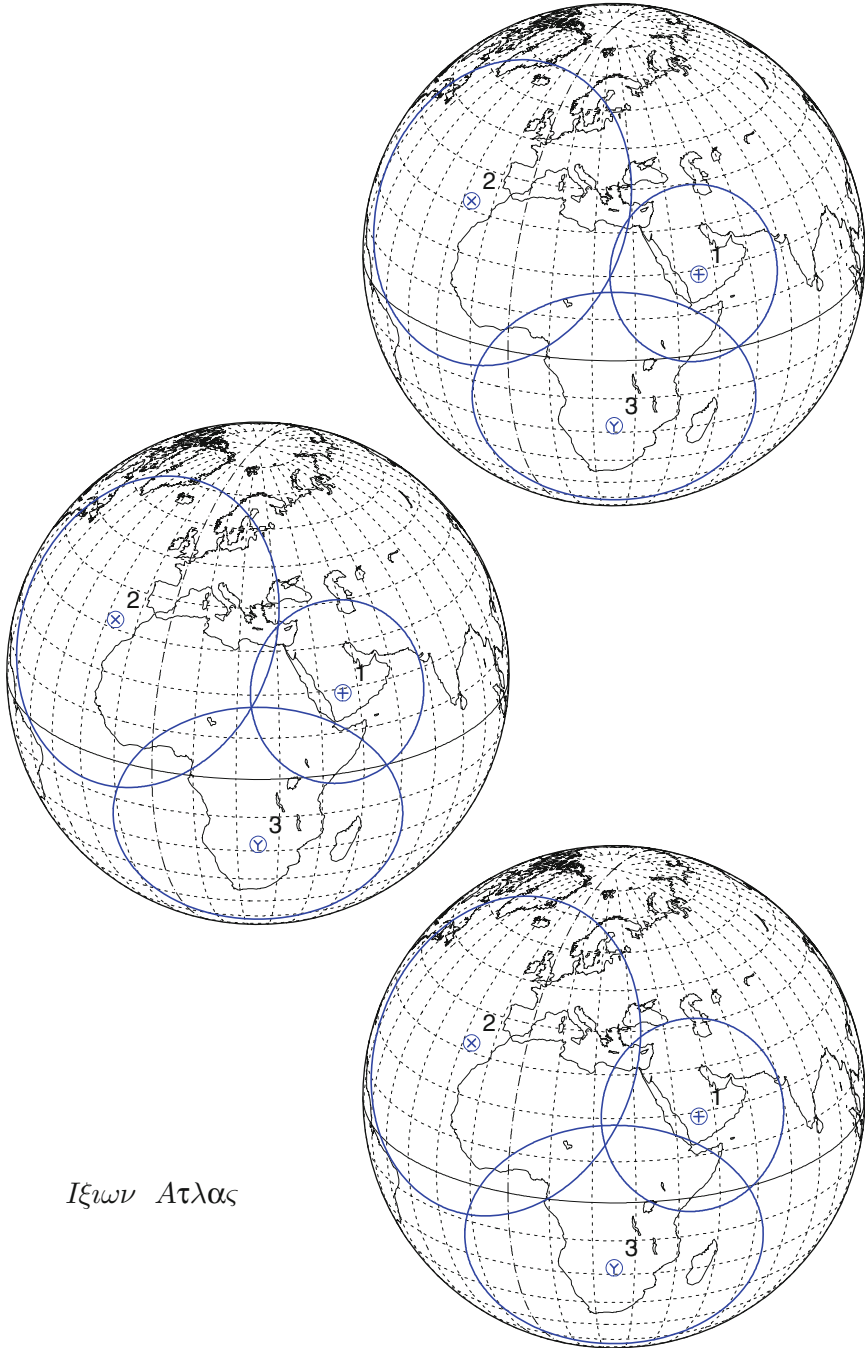


FIG. 14.1: Localisation of the receiver  $P$  by intersecting circles in various cases. Upper: Clock at  $P$  is slow relative to the satellite clock. Center: Clocks are perfectly synchronised. Lower: Clock at  $P$  is fast relative to satellite clock.

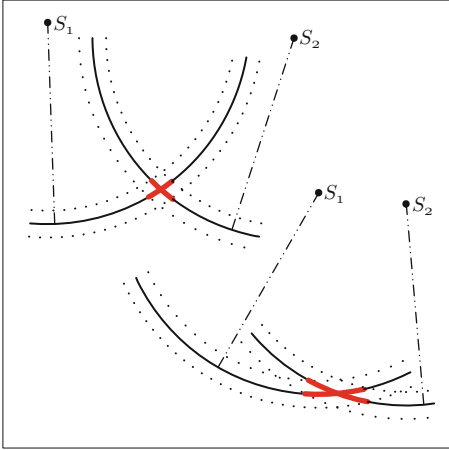


FIG. 14.2 : *Determining the point  $P$  by the intersection of two circles. Left: With a high level of accuracy. Right: With a low level of accuracy.*

with its margin of error. In the situation on the left, where the intersection is obtained by two arcs that are almost orthogonal, the margin of error is quite small. However, in the situation on the right, where the intersection is obtained by two arcs that are almost parallel, the margin of error is rather large.

When we determine a point on the Earth’s surface, in the local horizontal plane, we generally find ourselves in the first of these two situations (Fig. 14.2 left), where  $S_1$ ,  $S_2$ , and the spheres are represented projected onto the local horizontal plane. But to determine the altitude of a point, we are generally in the second situation (Fig. 14.2 right), where the elements of the figure are projected in a local vertical plane. For this reason, altitude determinations tend to be less accurate than horizontal position determinations.

### 14.1.6 Position on Earth and Geographic Coordinates

Solving (14.10) yields the position of the point  $P$  in Cartesian coordinates. To transform to geographic coordinates, i.e., longitude, latitude, and altitude, the main difficulty comes from the fact that the Earth is a geoid. Here we consider the case where the Earth is treated as an ellipsoid and calculate the geodetic coordinates.

The point  $P$  is at altitude  $h$  above the reference ellipsoid. The geodetic latitude of  $P$  is given by the direction  $PH$  (angle of  $PH$  with the equatorial plane), where  $H$  is the foot of the normal to the ellipsoid at  $P$ . With the notation in Fig. 14.3, the geodetic height (or geodetic altitude) of  $P$  is  $h = HP$ . It is obtained from the intersection of the ellipsoid with the grand normal  $\mathcal{N} = PI$ , rather than with  $PO$ .

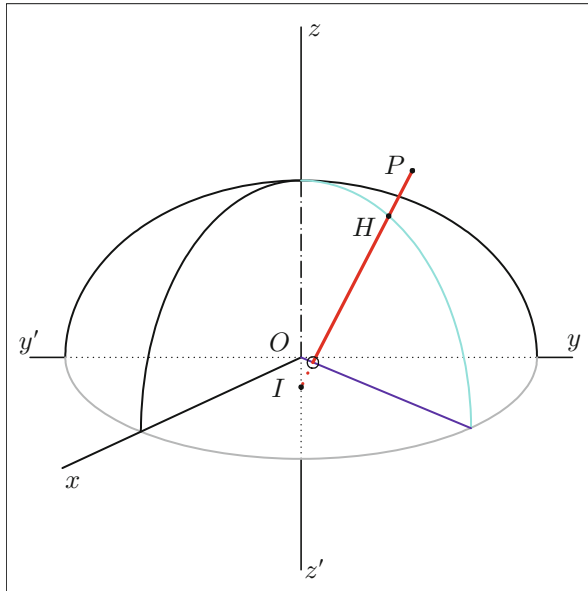


FIG. 14.3 : Geodetic altitude (or height)  $h = HP$  of the point  $P$  above the reference ellipsoid. The length  $IH$  is the great normal  $N$ ,  $z'z$  the polar axis, and  $xOy$  the equatorial plane.

The method for obtaining  $h$  and the latitude  $\varphi$ , iterative or otherwise, was discussed in detail in Chap. 2 (see Fig. 2.5 and Table 2.4). Since the longitude can be obtained directly from (2.30), the point  $P$  is thereafter determined by its local geodetic coordinates  $(\lambda, \varphi, h)$ .

### 14.1.7 Differential GPS (DGPS)

Differential GPS (DGPS) makes use of base stations. Figure 14.4 illustrates the main idea. Consider a base station at point  $A$  whose geographic position  $\mathbf{X}_0$  is known to great accuracy by conventional geodesy. A GPS receiver is placed at  $A$ , whence the position of its antenna is known to within a millimeter. The position of  $A$  is then measured by GPS and the result denoted by  $\mathbf{X}_{\text{GPS}}$ . The difference of position is then

$$\delta_0 \mathbf{X} = \mathbf{X}_{\text{GPS}} - \mathbf{X}_0 . \quad (14.22)$$

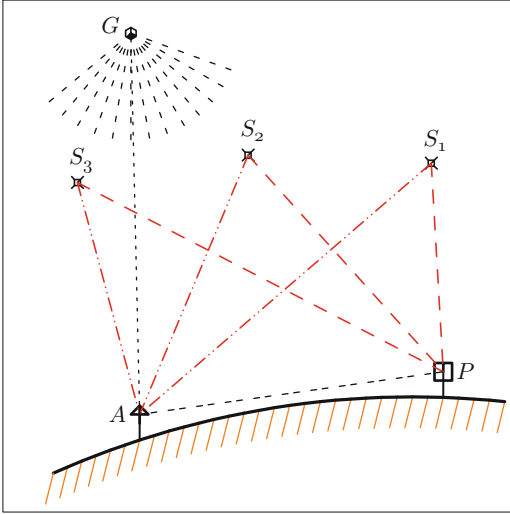


FIG. 14.4 : *Differential GPS.* The base station  $A$  and the receiver  $P$  receive the GPS signal of the satellites  $S_i$ . The position correction is sent from  $A$  to  $P$ . In the case of the so-called augmentation systems, it is sent to the geostationary satellite  $G$ .

It will not generally be zero, because there is a certain error in the GPS position estimate. From what was said above, the only cause of this error  $\delta_0 \mathbf{X}$  will be inaccurate modelling of the signal as it crosses the troposphere.<sup>3</sup>

Weather conditions are considered to be roughly the same over a radius of about a 100 km. The base station  $A$  sends the correction  $\delta_0 \mathbf{X}$  by radio to the receivers  $P$  which take it into account to refine their position. The maximal distance  $AP$  is of the order of a few hundred kilometers. This method, called DGPS, can significantly improve accuracy.

When DGPS had just begun, the base stations were installed in coastal lighthouses. Later they were set up in airports and generalised to other sites.<sup>4</sup> A further development of DGPS are the so-called augmentation systems: corrections are transmitted to a geostationary satellite which retransmits them over wide areas. We shall discuss these WAAS systems when we have described the various GPS satellite constellations.

<sup>3</sup>When the “civilian” GPS signal was downgraded to deliberately limit positioning accuracy, DGPS provided a way to get around this jamming. Accuracy could be improved from 100 to 22 m.

<sup>4</sup>In the USA, the NDGPS (Nationwide DGPS) uses a 100 or so base stations and covers almost the whole territory. The following system HA-NDGPS (High Accuracy NDGPS) should provide submeter positioning accuracy, i.e., of the order of a few decimeters. The system known as RTK (Real Time Kinetic) requires a costly base station to be set up close to the operating center, but provides accuracies of the order of 10 cm.

## 14.2 Navstar/GPS

The system known as Navigation Satellite Time and Ranging/Global Positioning System (Navstar/GPS) was set up by the US government under the direction of the Department of Defense (DoD). The original idea was to rebuild a global positioning system on the basis of new principles, going beyond the system provided by Transit, which had reached its limits.<sup>5</sup> Positioning by Doppler effect was abandoned in favour of triangulation, as exposed above. Such a radical improvement was made possible by the enormous progress in construction of ultra-precise clocks.

### 14.2.1 Setting up the System

#### Main Dates

The first studies date back to the 1960s, and the system was finally developed in the 1970s with launch of the first experimental satellites<sup>6</sup> when the DoD took over the US Navy's Timation system.

From 1978, the GPS system<sup>7</sup> gradually began to take shape with the satellites of Block I, which were research and development satellites. The Block II satellites were functional and operational on the characteristic orbit of the Navstar/GPS satellites from 1989.

---

<sup>5</sup>Navstar is run by the US Air Force, while Transit was managed by the US Navy.

<sup>6</sup>The two experimental Time Navigation (Timation) satellites were part of a trial by the US Navy to find an alternative to Transit. These satellites followed a very specific orbit, with  $h = 900$  km,  $i = 70.0^\circ$ : Timation-1, launched on 31 May 1967, Timation-2, on 30 September 1969. The two Navstar Technology Satellites (NTS) of the US Air Force followed MEO orbits which prefigured the Navstar orbit: NTS-1 (or Timation-3, OPS/7518, P73-3), launched on 14 July 1974,  $h = 13,610$  km,  $i = 125.2^\circ$ , NTS-2 (P76-4), launched on 23 June 1977 on a neighbouring orbit to the one adopted for the first GPS missions, with  $h = 20,186$  km,  $i = 63.9^\circ$ . NTS-2 is discussed further in the appendix of Sect. 14.11.

<sup>7</sup>List of Navstar/GPS satellites:

- The 11 satellites of Block I, on the circular orbit  $h = 20,020$  km,  $i = 63.0^\circ$ , from Navstar-1 (GPS-1, OPS/5111), launched on 22 February 1978, to Navstar-11 (GPS-11, USA-10) on 9 October 1985.
- The 28 satellites of Block II and II-A,  $h = 20,020$  km,  $i = 55.0^\circ$ , from Navstar-2-1 (GPS-14, USA-35), launched on 14 February 1989, to Navstar-2A-19 (GPS-38, USA-135) on 6 November 1997.
- The 21 satellites of Block II-R and II-RM, on the same orbit, from Navstar-2R-2 (GPS-43, USA-132), launched on 23 July 1997, to Navstar-2R-21 (GPS-50, USA-206, Navstar-2RM-8) on 17 August 2009.
- The 12 satellites of Block II-F, from Navstar-2F-1 (GPS-62, USA-213), launched on 28 May 2010, to Navstar-2F-12, for after 2015.
- The eight satellites of Block III-A, still on the same orbit, from Navstar-3A-1 to Navstar-3A-8, from 2014.

Block II: A (advanced), R (replenishment), RM (R modernized), F (follow-on).

On 17 July 1995, the constellation of 24 satellites (only Block II) was complete and the system declared operational (full operational capability FOC). It had been 21 years since the launch of NTS-1 and it had taken more than 30 years of research and ingenuity to go from the idea of a global positioning system to a fully operational satellite implementation.

Another important date was 2 May 2000. It was on this day that US President Bill Clinton decided to suppress the deliberate strategic downgrading of the signal. Standard accuracy went from 100 to 22 m.

Position determinations by GPS are continually being refined thanks to technological improvements, such as more powerful signals and better corrections for atmospheric perturbations, but also due to progress in signal processing.

### Segments of the System

The positioning system has three segments:

- the space segment, comprising the satellite constellation,
- the control segment, consisting of control and monitor stations,
- the user segment, representing all military and civilian users.

#### 14.2.2 Space Segment

The Navstar/GPS constellation is made up of 24 satellites, in 6 planes of 4 satellites each. Any point on the Earth is able to view 4 to 8 satellites at the same time, and up to 11 in some cases, with a minimal viewing elevation of  $15^\circ$ .

Each satellite in Block II carries atomic clocks<sup>8</sup> (relative accuracy  $10^{-13}$  to  $10^{-14}$ ) and of course computers, transmitter–receivers, and all the necessary equipment. The nominal lifetime of the satellite is 10 years.

With a fundamental frequency  $f_0$  equal to

$$f_0 = 10.23 \text{ MHz}, \quad (14.23)$$

the emitter generates two waves in the L band, denoted by L1 and L2, with frequencies:

$$L1 = 154f_0 = 1,575.42 \text{ MHz} \quad (\text{wavelength } 19.03 \text{ cm}),$$

$$L2 = 120f_0 = 1,227.60 \text{ MHz} \quad (\text{wavelength } 24.42 \text{ cm}).$$

---

<sup>8</sup>The satellites of Block II and IIA are equipped with two cesium and two rubidium clocks, and the satellites of Block IIR with three rubidium clocks.

For the satellites in Block IIF and following, a third frequency is emitted:

$$L5 = 115f_0 = 1,176.45 \text{ MHz} \quad (\text{wavelength } 25.48 \text{ cm}).$$

The transmitted message, in addition to the time, provides the ephemeris of the satellite, i.e., the Keplerian elements of the satellite and their derivatives as a function of time, together with auxiliary data.

Several pseudo-random codes known as PRN (pseudo-random noise) are transmitted. The two main codes are the coarse acquisition (C/A) code and the precision (P) code. The C/A code is accessible to the general public, while the P code was originally reserved for authorised, i.e., military users, but became available to all as of May 2000.

The Navstar/GPS satellites carry an order number  $n$  in the form GPS- $n$ . However, the satellite is identified in the constellation by the PRN numbering (from 1 to 32 for Block II).

### Orbit

All the Navstar/GPS (Block II) satellites follow a near-circular MEO orbit, inclined at  $55.0^\circ$  (see Fig. 14.5). The satellites are recurrent with 1-day cycle and make exactly two revolutions in each sidereal day (see Table 14.1 and 14.2, and Fig. 14.7). The altitude is 20,183 km. We also have

$$a = 26,560.906 \text{ km}, \quad \eta = 4.16437, \quad n = 1.4585 \times 10^{-4} \text{ rad s}^{-1}.$$

For this kind of orbit the ratio of the perturbation due to  $J_2$  and the central acceleration is very small, because the altitude is high (see Fig. 6.1). In fact it is less than  $10^{-4}$  (to be compared with  $10^{-3}$  for an LEO orbit). The precession rates are, in degrees per day:

- Nodal precession rate  $\dot{\Omega} = -0.039$ .
- Apsidal precession rate  $\dot{\omega} = +0.022$ , since  $i$  is close to  $i_C$ .
- Variation of the mean motion  $\Delta n = -4.4 \times 10^{-4}$ , since  $i$  is very close to  $54.7^\circ$ , the inclination for which  $\Delta n$  is zero [see (6.75)].

The cycle relative to the Sun is  $C_S = -351.4$  days for this orbit. Recall that, if  $\dot{\Omega}$  is zero, the cycle is equal to 1 year ( $C_S = -365.2$  days). Twice a year, the satellite suffers an eclipse (see Chap. 10 and in particular Fig. 10.26 upper).

### Constellation

The six planes of satellites, denoted by capital letters  $A, B, C, D, E$ , and  $F$ , are regularly spaced in a geocentric pseudo-Galilean frame, separated by  $60^\circ$  of longitude to within a few degrees (see Fig. 14.6 lower and Example 14.1). In any given plane, the four satellites are not regularly spaced (see Fig. 14.8).

**Example 14.1** *Ground track of the orbits of two Navstar/GPS satellites following one another in the same orbital plane.*

**Navstar/GPS [PRN 05]**

Orbit (Celestial ref.) [Galilean]

2011 02 01 14:25:42 UTC >>> 1440.0 min = 1.00 day

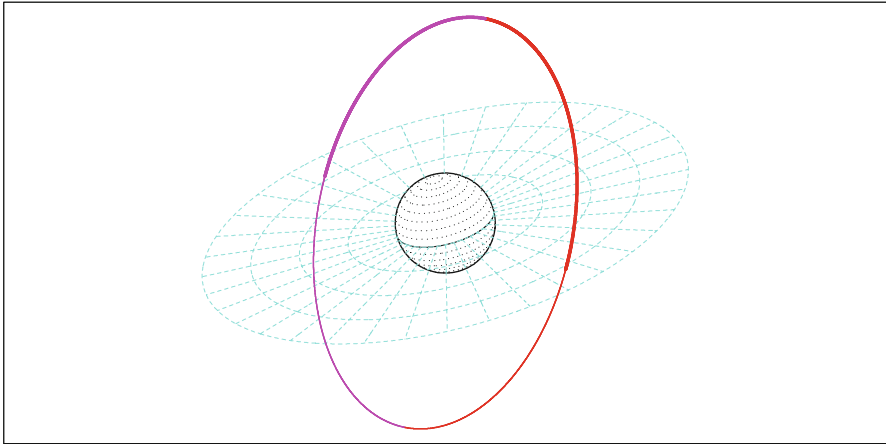
Altitude =20181.5 km

Inclination = 54.74 °

Period = 717.92 min \* rev/day = 2.01 \* Week = 1621

a =26559.604 km

e = 0.002246



Projection: Orthographic

Property: none

⊕ T.:Azimuthal - Graticule: 10°

Project. centre: 25.0 ° N; 124.0 ° W

Aspect: Oblique

{-} [-90.0/ +65.0/-146.0] [ +15] EGM2008

Asc. Node: -93.96 ° [08:10 LMT]

[NORAD] Revolution: 1075

[NORAD] 2011 02 01 14:25:42 UTC

Ιξίων

MC \* LMD

Ατλας

**Navstar/GPS [PRN 05]**

Orbit - ref.: Earth

Recurrence = [ 2; +0; 1 ] 2

2011 02 01 14:25:42 UTC >>> 1440.0 min = 1.00 day

Altitude =20181.5 km

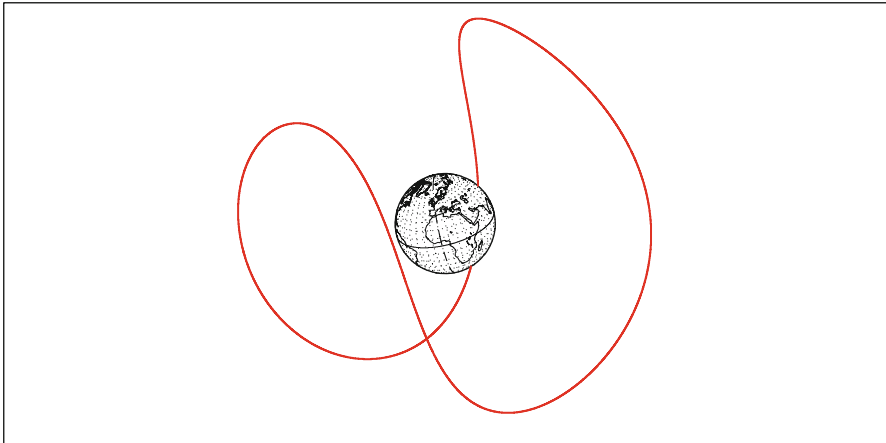
Inclination = 54.74 °

Period = 717.92 min \* rev/day = 2.01 \* Week = 1621

Equat. orbital shift =20036.6 km ( 180.0 °)

a =26559.604 km

e = 0.002246



Projection: Orthographic

Property: none

⊕ T.:Azimuthal - Graticule: 10°

Project. centre: 25.0 ° N; 10.0 ° E

Aspect: Oblique

{4.2} [-90.0/ +65.0/ +80.0] [ +15] EGM2008

Asc. Node: -93.96 ° [08:10 LMT]

[NORAD] Revolution: 1075

[NORAD] 2011 02 01 14:25:42 UTC

Ιξίων

MC \* LMD

Ατλας

FIG. 14.5 : Orbit of a Navstar/GPS satellite. Navstar-2RM-8 [PRN 05] (Navstar-2R-21, GPS-50, USA-206), on 1 February 2011. Upper: Pseudo-Galilean frame fixed relative to the stars. Lower: Terrestrial frame.



MEO satellite	$a$	$h$	$i$	$T_d$	Phase triple	$N_{T_o}$
Navstar	26,560.906	20,183	55.0	717.98	[2, 0, 1]	2
Glonass	25,507.602	19,130	64.8	675.73	[2, +1, 8]	17
Galileo	29,600.268	23,222	56.0	844.69	[2, -3, 10]	17
BeiDou NS	27,905.750	21,528	56.3	773.20	[2, -1, 7]	13
Navstar (I)	26,559.969	20,182	63.0	717.97	[2, 0, 1]	2
Galileo [0]	29,993.691	23,616	56.0	861.58	[2, -1, 3]	5

TABLE 14.1 : *Orbit and recurrence characteristics for MEO navigation satellites. Distances  $a$  and  $h$  in km, angle  $i$  in degrees, draconitic period  $T_d$  in minutes.*

► We consider the first two satellites in plane  $A$  of the GPS constellation, i.e., Navstar-2A-21 [PRN 09] in Slot (1) and Navstar-2RM-2 [PRN 31] in Slot (2). Their NORAD elements are:

GPS BIIA-21 [PRN 09]

```
1 22700U 93042A 11032.82501832 -.00000085 00000-0 10000-3 0 1300
2 22700 56.3096 12.7579 0167604 89.2355 272.6858 2.00562849128903
```

GPS BIIRM-2 [PRN 31]

```
1 29486U 06042A 11030.97501051 -.00000076 00000-0 10000-3 0 1422
2 29486 56.0928 14.5537 0080766 301.2847 57.9187 2.00575401 31902
```

The elements 12.7579 and 14.5537, giving  $\Omega$  (in the pseudo-Galilean frame with origin at the vernal equinox) for [PRN 09] and [PRN 31], respectively, show that these two satellites are almost in the same orbital plane (with a difference of only  $1.8^\circ$ ). Note that the GPS controllers do not attempt to maintain the satellites strictly in one of the six specified orbital planes. What matters is that the position of each satellite should be determined to very high accuracy.

Calculating the ascending nodes of each satellite, we find:

[PRN 09] UT time: 2011 02 01 19:48:01 ,  $\lambda_{AN} = 55.9^\circ\text{W}$  ,  
 [PRN 31] UT time: 2011 02 01 23:20:06 ,  $\lambda_{AN} = 106.3^\circ\text{W}$  .

The satellite [PRN 31] follows about 3 h 30 min behind [PRN 09] and this shifts the ground track by about  $50^\circ$  westward (see Fig. 14.6 upper). ◀

### 14.2.3 Control Segment

The nerve center of GPS is near Colorado Springs, CO, USA, in the Schriever Air Force Base. This is the master control station (MCS). The con-

**Navstar/GPS [PRN 09] [& 31]**

Orbit - Ground track

Recurrence = [ 2; +0; 1] 2

2011 02 01 00:00:00 UTC >>> 1440.0 min = 1.00 day

Altitude =20182.2 km

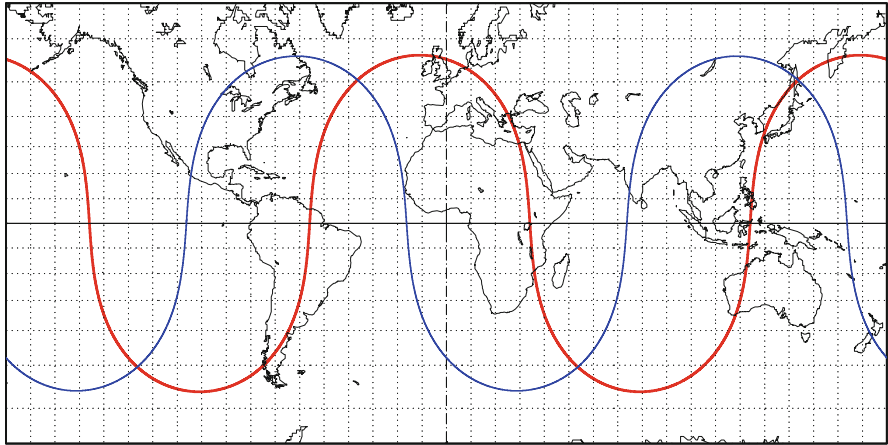
Inclination = 56.31 °

Period = 717.96 min \* rev/day = 2.01 \* Week = 1621

Equat. orbital shift =20037.6 km

a =26560.354 km

e = 0.016764



Projection: Mercator Project. centre: 0.0 ° ; 0.0 ° Asc. Node: 124.09 ° [16:15 LMT] **Ιξίων**  
 Property: Conformal Aspect: Direct [NORAD] Revolution: 12885 **MC \* LMD**  
 ⊕ T.:Cylindrical - Graticule: 10° {4.2} [ +0.0/ +0.0/ +0.0] [-] WGS84 [NORAD] 2011 01 30 07:58:13 UTC **Ατλας**

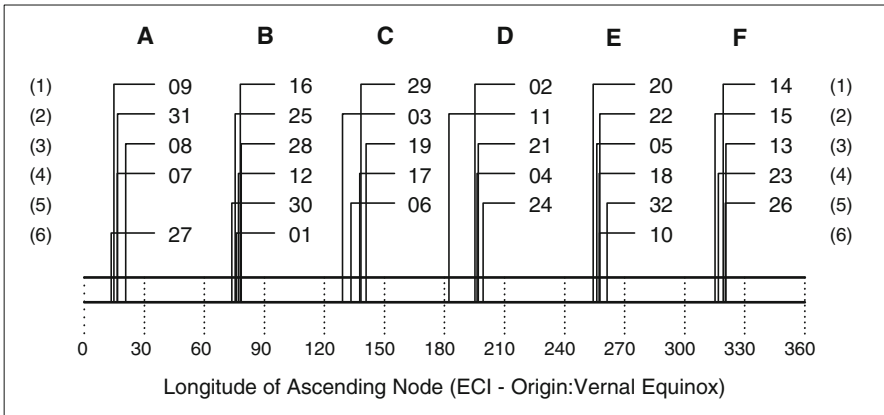


FIG. 14.6 : Upper: Ground track of the satellite Navstar-2A-21 [PRN 09] (bold red curve) superposed on the ground track of Navstar-2RM-2 [PRN 31] (normal blue curve), over 1 day, 1 February 2011. Lower: Position of the ascending node of each Navstar/GPS satellite on 1 February 2011 in a pseudo-Galilean frame fixed relative to the stars and centered on the Earth, with longitude origin at the vernal equinox. The 32 satellites of Block II are identified by the PRN number, from 01 to 32. Planes are indicated by the letters A to F and the position, or slot, by numbers from (1) to (6). The two satellites whose ground tracks are shown in the upper part of the figure are in positions 1 and 2 of plane A.

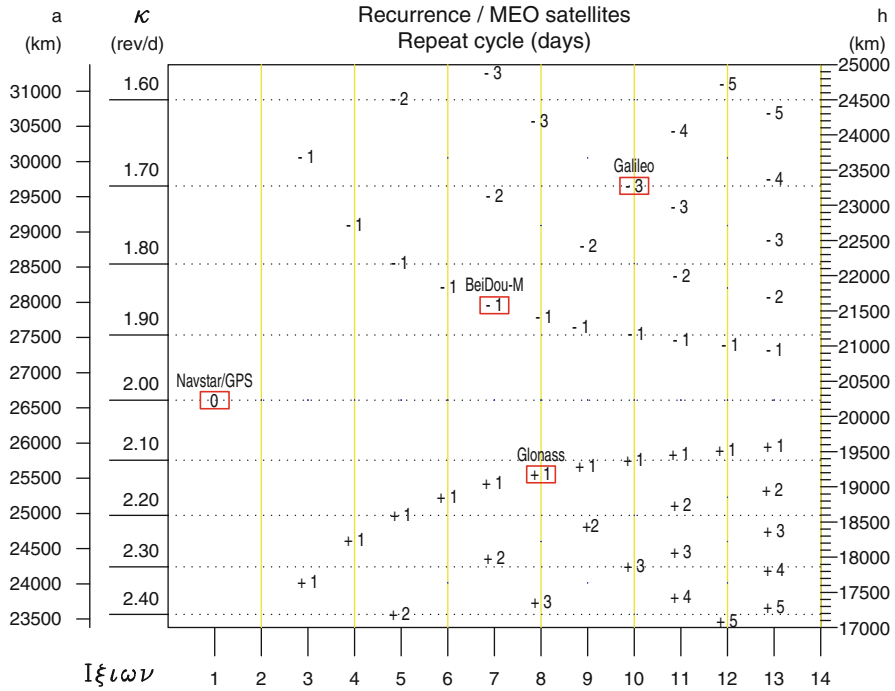


FIG. 14.7: Recurrence diagram for the four constellations of navigation satellites. Possible recurrence cycles are denoted by  $D_{T_o}$ . Boxed values correspond to existing satellites appearing in Table 14.1. For example, for Glonass, we have the recurrence triple  $[2, +1, 8]$ , or  $\nu_o = 2$  (integer closest to  $\kappa$ , ordinate),  $D_{T_o} = +1$  (indicated on the diagram), and  $C_{T_o} = 8$  (8 day cycle, abscissa). The orbits of the four types of satellite have slightly different inclinations so the diagram has been drawn for an average inclination.

trol segment comprises five ground-based monitor stations<sup>9</sup>: Colorado Springs (MCS), Hawaii (HAW), and three stations located on the tiny islands of Ascen-

<sup>9</sup>Colorado Springs has a monitor station as well as the master station. The other four monitor stations are on islands, distributed more or less equidistantly along the equator. Three of these stations, the ground antennas, are not on US territory and the American government has negotiated unassailable agreements to maintain their control of these highly strategic installations:

- Ascension, a small volcanic island in the middle of the Atlantic, is a British Overseas Territory (Saint Helena, Ascension, Tristan da Cunha). The USA set up an airport and a large military base.
- Diego Garcia, an atoll in the Chagos Archipelago, is another British territory, belonging to the British Indian Ocean Territory (BIOT). The US army leased the island in 1966 on an extendible 50 year lease, the condition being that the island be cleared of all its inhabitants at the outset. The British government duly deported 1,600 Chagossians to Mauritius and the Seychelles.

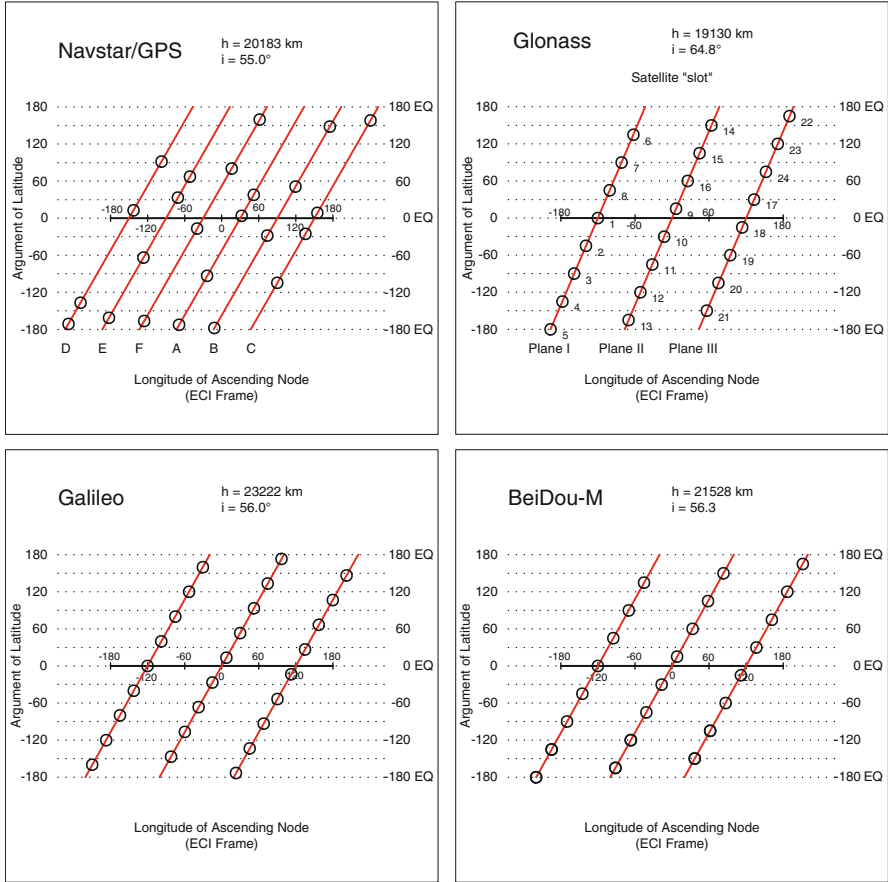


FIG. 14.8 : Satellite constellation showing orbital planes. In each plane, the satellite has been indicated with the angle of its position on orbit (circular arc from the ascending node to the satellite). EQ equator. For Glonass, the official number of each satellite, from 1 to 24, has been indicated, together with the numbers of the orbital planes.

sion (ASC), Diego Garcia (DIG), and Kwajalein (KWJ), outside US territory (see Fig. 14.9). Each station can monitor up to 11 satellites at the same time. These stations receive the GPS signals and transmit the data to the MCS.

- Kwajalein is an atoll which, like Bikini with its explosive reputation, belongs to the Republic of the Marshall Islands (RMI). This tiny country, formally independent since 1986, has a “free alliance” with the USA, which guarantees security and defence.
- Hawaii is the only station on American territory, since this group of islands became the fiftieth state of the United States in 1959.

**Navstar/GPS**

Orbit - Ground track

Recurrence = [ 2; +0; 1] 2

>>>> Time span shown: 1440.0 min = 1.00 day

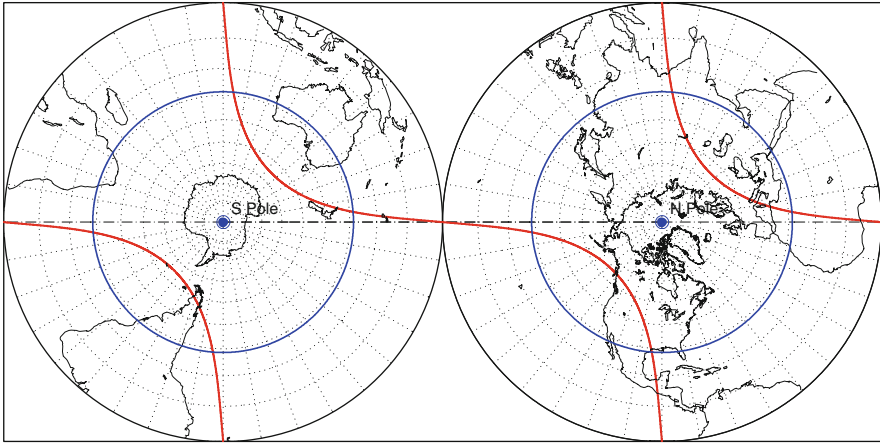
Altitude =20182.8 km

a =26560.906 km

Inclination = 55.00 °

Period = 717.98 min \* rev/day = 2.01

**Visibility circle for h = 15°**



Projection: Stereographic

Pr. centre (r.): 90.0 ° N; 90.0 ° W

Asc. Node: 0.00 °

Ιξίων

Property: Conformal

Aspect: Direct

App. inclin. = 84.87 °

MC \* LMD

⊕ T.:Azimuthal - Graticule: 10° [4.2] [-90.0/ +0.0/-180.0] [-] WGS84

Ατλας

**Navstar/GPS**

Orbit - Ground track

Recurrence = [ 2; +0; 1] 2

>>>> Time span shown: 1440.0 min = 1.00 day

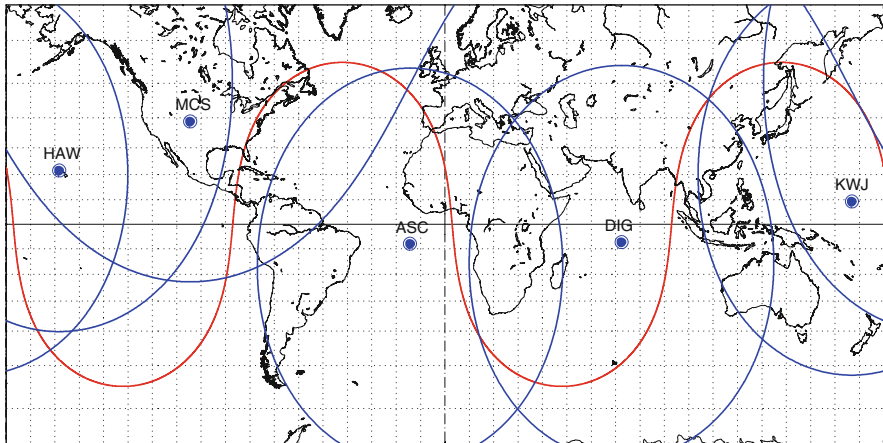
Altitude =20182.8 km

a =26560.906 km

Inclination = 55.00 °

Period = 717.98 min \* rev/day = 2.01

**Visibility circle for h = 15°**



Projection: Mercator

Project. centre: 0.0 ° ; 0.0 °

Asc. Node: -87.04 ° [00:00 LMT]

Ιξίων

Property: Conformal

Aspect: Direct

App. inclin. = 84.87 °

MC \* LMD

⊕ T.:Cylindrical - Graticule: 10° [5.3] [+90.0/ +0.0/-90.0] [-] WGS84

Ατλας

FIG. 14.9 : Ground track of a Navstar/GPS satellite. Upper: Polar projection with circle of visibility ( $h = 15^\circ$ ) for the poles. Lower: Equatorial projection. Location of the five control stations of the Navstar/GPS system, each enclosed within its circle of visibility ( $h > 15^\circ$ ). The orbital ground track of Navstar-2R-8 [PRN 16] (GPS-56, USA-166) has been superposed.

System	Navstar/GPS	Glonass	Galileo	BeiDou NS
$N$	6	3	3	3
$M$	4	8	9	8
Separation	Irregular	$360/8 = 45^\circ$	$360/9 = 40^\circ$	$360/8 = 45^\circ$
$R$	6	3	3	3
Total	30	27	30	27
$T_d$ [sidereal day]	1/2	8/17	10/17	7/13
$T_d$ [decimal hour]	11.9663	11.2622	14.0781	12.8867
$T_d$ [h m s]	11 57 59	11 15 44	14 04 41	12 53 12
$ C_S $ [d]	351	353	356	354
Geodetic system	WGS84	PZ-90.02	GTRF	CGS-2000
$a$ [m]	6,378,137	6,378,136	6,378,137	6,378,137
$1/f = 298.257 \dots$	$\dots 223,563$	$\dots 839,303$	$\dots 222,101$	$\dots 222,101$

TABLE 14.2 : *The four satellite navigation constellations.  $N$  number of planes.  $M$  number of satellites per plane. The separation between satellites in the same plane is given in degrees.  $R$  number of backup satellites. The total refers to the total number of satellites, i.e.,  $N \times M + R$ . The draconitic period  $T_d$  is given in sidereal days, decimal hours, and hours, minutes, and seconds [h m s].  $|C_S|$  is the cycle relative to the Sun.  $a$  is the semi-major axis of the reference Earth ellipsoid in meters and  $1/f$  is the reciprocal flattening of the ellipsoid .*

At the master control station, the satellite ephemerides and clock parameters are calculated and sent to the three ground antennas, transmission stations in Ascension, Diego Garcia, and Kwajalein, which send the data on to the Navstar satellites.

### 14.2.4 User Segment

This term covers the full range of users. Receivers can be highly sophisticated, but in general they are cheap devices available to the general public at ever decreasing prices. GPS can be used dynamically (while in motion) or statically (for a topographic network).

In geophysics, two GPS receiving stations are placed at two points on the Earth a few thousand kilometers apart. With professional equipment, reception continues for months, and high performance statistical methods of signal processing allow one to measure movements of the tectonic plates of the order of just a few millimeters a year (see the appendix in Sect. 14.10 at the end of this chapter). In this case, a precise ephemeris product is used: satellite orbits are given to an accuracy of 5 cm and 0.1 ns. This data is supplied with a 2 week delay.

Type	Restriction	Measurement	Duration	Accuracy
GPS: instantaneous	None	$\rho_i$	Second	10–100 m
GPS: averaged	None	$\langle \rho_i \rangle$	Hour	2–20 m
DGPS: instantaneous	Base < 500 km	$\rho_i$	Second	1–5 m
DGPS: averaged + PO	None	$\langle \rho_i \rangle$ , phase	Day	1 mm to 1 cm

TABLE 14.3 : Positioning accuracy for different methods. Instantaneous pseudo-range measurements are denoted by  $\rho_i$ , and averages by  $\langle \rho_i \rangle$ . PO precise orbits.

## Accuracy

Table 14.3 summarises the accuracies that can be achieved for various uses of the GPS system.

### 14.2.5 Local View

The sky plots discussed in Chap. 13 inform as to the satellite overpasses at a given location. In the next example, we consider the overpasses of the Navstar/GPS satellites for Paris at a given time.

**Example 14.2** *Local view of all Navstar/GPS satellites visible above  $10^\circ$  from Paris on 1 February 2011, at noon UT (12:00 UT).*

► Figure 14.10 (upper) shows all GPS satellites visible at 12:00 UT, together with their ground tracks over 2 h. There are eight satellites visible: two of them, PRN 14 and 19, disappear very quickly, but six of them, PRN 11, 17, 20, 23, 24, and 32, remain visible for at least the two following hours. The little table included in the figure indicates the presence of the satellites every half-hour.

Figure 14.10 (lower) shows the circle of visibility  $h = 10^\circ$  for Paris (which is boat-shaped with the Mercator projection used here), together with the orbital ground track of the satellite Navstar-2R-4 [PRN 20] over 2 h. This satellite passes roughly overhead for this location. We have also superposed the ground tracks of Navstar-2RM-1 [PRN 17] to the west and Navstar-2RM-11 [PRN 19] at the southernmost point of visibility (leaving just after 12:00). ◀

### 14.2.6 Navstar/GPS and Other Systems

It would be misleading to present the four systems—Navstar/GPS, Glonass, Galileo, BeiDou NS—on an equal footing. We should be quite clear that the GPS system was conceived, developed, realised, and improved at the initiative

**Navstar/GPS**

**Ground track**

Recurrence = [ 2; +0; 1] 2

2011 02 01 12:00:00 TUC >>> 120.0 min = 2 hours

Altitude =20183 km

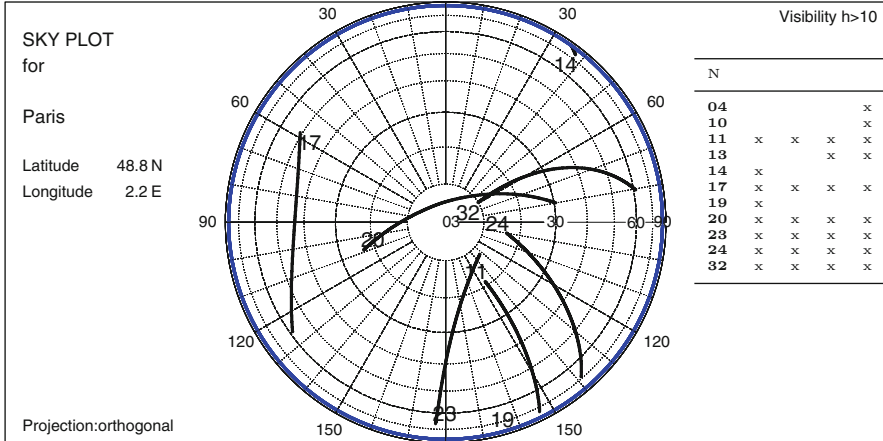
Inclination = 55.0 °

Period = 717.98 min \* Révol./j.= 2.01

PRN -> Navstar satellite

a =26560.906 km

e = 0.004266



Circle: Zenith view angle [0° , +90°]  
Radius: Azimut taken from the north

NORAD TLE

[NORAD] 2011 02 01 12:00:00 -> 14:00:00 TUC MC \* LMD

Ιξίωv

**Navstar/GPS [20] & [17][19]**

**Orbit - Ground track**

Recurrence = [ 2; +0; 1] 2

2011 02 01 12:00:00 UTC >>> 120.0 min = 2 hours

Altitude =20183.0 km

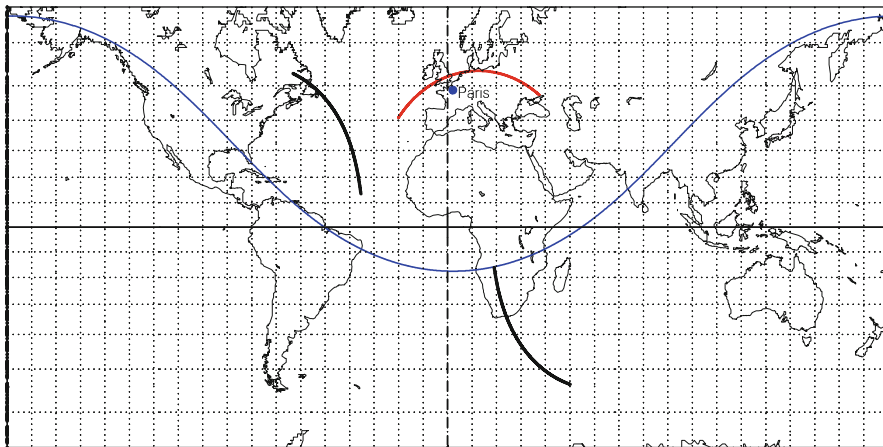
Inclination = 53.54°

Period = 717.98 min \* rev/day = 2.01 \* Week = 1621

Visibility circle for h = 10°

a =26561.141 km

e = 0.004445



Projection: Mercator Project.centre: 0.0° ; 0.0°  
Property: Conformal Aspect: Direct  
⊕ T.:Cylindrical - Graticule: 10° [4.2] [ +90.0/ +0.0/ -90.0] [-] WGS84

Asc. Node: 147.61° [08:01 LMT] Ιξίωv  
[NORAD] Revolution: 7867 MC \* LMD  
[NORAD] 2011 02 01 22:10:26 UTC Ατλας

FIG. 14.10 : Upper: Sky plot of Navstar/GPS satellites for Paris. The ground track is shown over 2h from 1 February 2011, at 12:00 UT. Lower: Ground track of the satellite GPS [PRN 20], over the same period. Superposition of [PRN 17] and [PRN 19] ground tracks.



and under the control of the US Department of Defense. The other systems, either planned or under development merely reproduce the same idea.

A complete positioning system involving dozens of satellites represents a huge investment and requires a technologically advanced industrial base. After the USA, Russia set up its system Glonass. Europe and China, with Galileo and Compass, respectively, will have their own independent systems, even though several of these four systems will be perfectly compatible. We shall see that other systems under way or planned, such as Japan's QZSS, will supplement the existing GPS system locally and cannot therefore be considered as global systems in their own right. China's Beidou-1 is a somewhat special case, to which we shall return later on.

This profusion of systems, most still under development, has led to a proliferation of terminology. Rather than GPS, the generic term Global Navigation Satellite System (GNSS) is now preferred to refer to these positioning systems. However, as long as the American Navstar/GPS system is the only one to be widely used, we shall continue to speak of GPS rather than GNSS in this context.

## 14.3 Glonass

Glonass, also written GLONASS or GloNaSS, is a Russian acronym for *Global'naya Navigatsionnaya Sputnikovaya Sistema*, meaning “planetary system—global—for satellite-assisted navigation”. It was first developed by the USSR from 1976, for military purposes. The first Uragan satellites were launched in 1982 and the system was declared operational on 24 September 1993.

After the collapse of the Soviet Union, the positioning system was not initially Russia's main concern, and Glonass no longer functioned correctly due to a lack of satellites, with only six to eight satellites still working in the constellation. But from 2003, the Russian government made Glonass a priority and several new generation satellites were placed in orbit, making it once again operational.

### 14.3.1 The Three Segments

The space segment<sup>10</sup> is a constellation of 24 satellites (3 planes<sup>10</sup> of 8 regularly spaced satellites). Each satellite is equipped with cesium clocks (stability  $10^{-13}$ ) and emits a signal with two frequencies which differ slightly

---

<sup>10</sup>List of Glonass satellites:

- The first 50 experimental then first generation satellites, from Uragan-1 (Kosmos-1413), launched on 12 October 1982, to Uragan-50 (Kosmos-2206), on 30 July 1992.
- The 37 satellites of the Glonass series, from Glonass-773 (Uragan-51, Kosmos-2234), launched on 17 February 1993, to Glonass-798 (Uragan-87, Kosmos-2417), on 25 December 2005.

from one satellite to the next, centered around  $G1 = 1,609$  MHz and  $G2 = 1,252$  MHz. The new generation Glonass-K satellites emit a third frequency,  $G3 = 1,205$  MHz.

The Glonass orbit is rather similar to that of Navstar/GPS (see Table 14.1). It is a bit lower, at  $h = 19,130$  km, but with the higher inclination  $i = 64.8^\circ$  giving better coverage of high latitudes. The recurrence is 17 revolutions in 8 days (compared with 16 revolutions in 8 days for Navstar), giving a period of 11 h 16 min (see Fig. 14.11).

The precession rates are very small, for the same reasons as for Navstar. In degrees per day, they are

$$\dot{\Omega} = -0.034, \quad \dot{\omega} = -0.004, \quad \Delta n = -0.018.$$

The geodetic reference system is the Russian one<sup>11</sup> PZ-90.02 (*Parametri Zemli*, also written PE-90, Parameter of Earth).

The control segment comprises around ten stations. The master station, Krasnoznamensk, is in the western suburbs of Moscow. At the present time, there are about ten monitor states located throughout the territory of ex-USSR, but mostly Russia. However, the Russian government is hoping to set up similar stations in Cuba, South America, and Australia. The accuracies obtained by Glonass alone are less good than those obtained by Navstar, but the Russian authorities have promised to improve the system. The two systems are compatible.

### 14.3.2 Local View and Visibility Table

We select an arbitrary point  $P$  on the Earth and specify the visibility conditions for the satellites. A viewing elevation of at least  $10^\circ$  or  $15^\circ$  is generally imposed. For a given day, we record in a table all the time windows during which  $P$  is seen by a given satellite. The calculation is repeated for each satellite in the constellation to obtain the visibility table.

**Example 14.3** *Visibility table for all satellites in the Glonass constellation as viewed from Moscow on 1 March 2013. Likewise when viewing from the North Pole and the Equator.*

- 
- The satellites of the Glonass-M series, from Glonass-711 (Uragan-M1, Kosmos-2382), launched on 1 December 2001, then Glonass-736 to -738 (Uragan-M27 to -M29, Kosmos-2644 to -2466), launched on 2 September 2010.
  - The satellites of the new Glonass-K series, beginning with Glonass-K1-11 (Uragan-K1-1, Kosmos-2471).

<sup>11</sup>The Russian word *zemli* means “the Earth”. It comes from the Indo-European root \**ghyōm*, \**ghemō(n)*, of the same meaning, which also gives the Latin word *humus*, *i*, meaning “earth” or “soil”. The Latin *homō*, *hominis* comes from the same root. For example, the French word “homme” literally means “born of the earth”.

**Glonass ( ΓΛΙΟΗΑC C )**

Orbit - Ground track

Recurrence = [ 2; +1; 8] 17

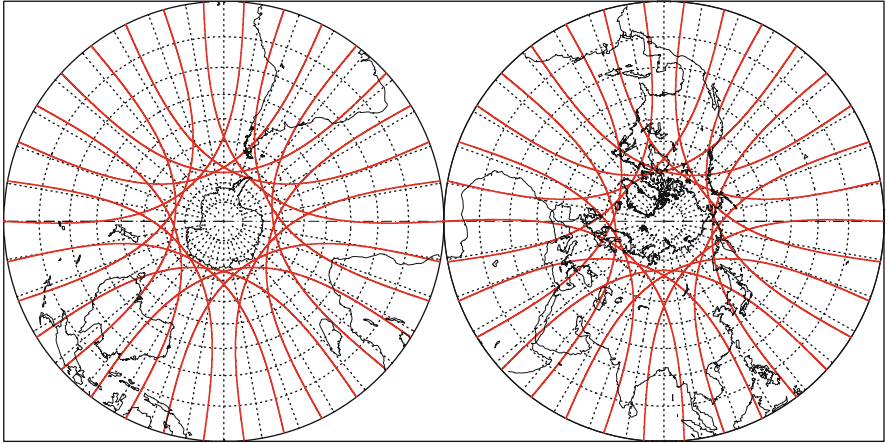
>>>> Time span shown: 8.00 days

Altitude = 19129.5 km      a = 25507.602 km

Inclination = 64.80 °

Period = 675.73 min \* rev/day = 2.13

Equat. orbital shift = 18858.8 km ( 169.4 °)



Projection: Stereographic    Pr. centre (r): 90.0 ° N; 90.0 ° E  
 Property: Conformal      Aspect: Direct  
 ⊕ T.: Azimuthal - Graticule: 10° 4.2 [ -90.0/ +0.0/ +0.0 ] [-] EIGEN6C2

Asc. Node: 0.00 °  
 App. inclin. = 92.84 °

*Ιξίων*  
 MC \* LMD  
*Ατλας*

**Glonass ( ΓΛΙΟΗΑC C )**

Orbit - Ground track

Recurrence = [ 2; +1; 8] 17

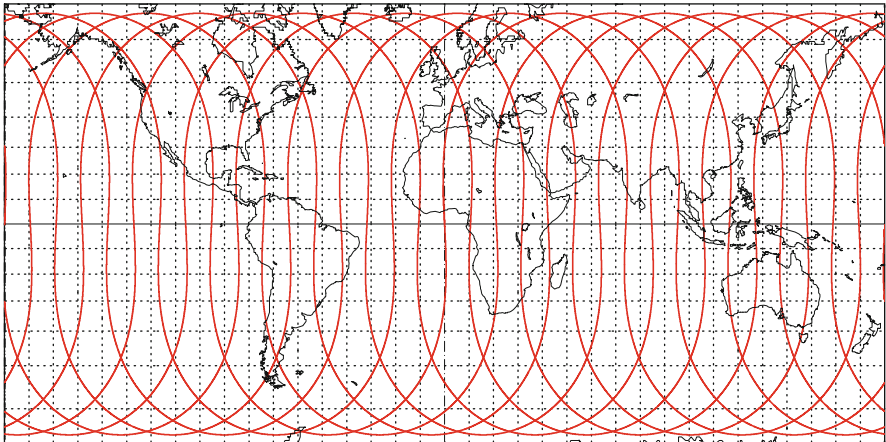
>>>> Time span shown: 8.00 days

Altitude = 19129.5 km      a = 25507.602 km

Inclination = 64.80 °

Period = 675.73 min \* rev/day = 2.13

Equat. orbital shift = 18858.8 km ( 169.4 °)



Projection: Mercator      Project. centre: 0.0 ° ; 0.0 °  
 Property: Conformal      Aspect: Direct  
 ⊕ T.: Cylindrical - Graticule: 10° 4.2 [ +0.0/ +0.0/ +0.0 ] [-] EIGEN6C2

Asc. Node: 0.00 °  
 App. inclin. = 92.84 °

*Ιξίων*  
 MC \* LMD  
*Ατλας*

FIG. 14.11 : Ground track of a Glonass satellite over one recurrence cycle (17 revolutions in 8 days).

► For Moscow (56°N and 38°E), the visibility table is established for the whole Glonass constellation on 1 March 2013, from 0 to 24 h UT (see Fig. 14.12 upper). The minimum viewing elevation is fixed at 15°.

The satellites are numbered from 1 to 24 (see Fig 14.8). Since they are regularly distributed in each plane, the overpasses are also perfectly regular, with a time lapse of about 2 h from one satellite to the next. In the case shown here, the point  $P$  is continually visible to five to seven satellites. Figure 14.12 (lower) shows the ground track of a Glonass satellite over a recurrence cycle, with visibility circle centered on the point  $P$ .

Visibility tables are also established for  $h > 15^\circ$  at a point at the North Pole (see Fig. 14.13 upper) and at a point on the equator (see Fig. 14.13 lower). ◀

## 14.4 Galileo

### 14.4.1 A European Project

In contrast to the American, Russian, and Chinese systems, the European navigation system remains entirely civilian. Galileo was finally chosen in 1999, after much hesitation. Germany and Italy were much in favour, while the United Kingdom considered it an unnecessary expense, since the American GPS was already doing the same job, and it was free! At the time it was hoped that the system would be up and running by 2008.

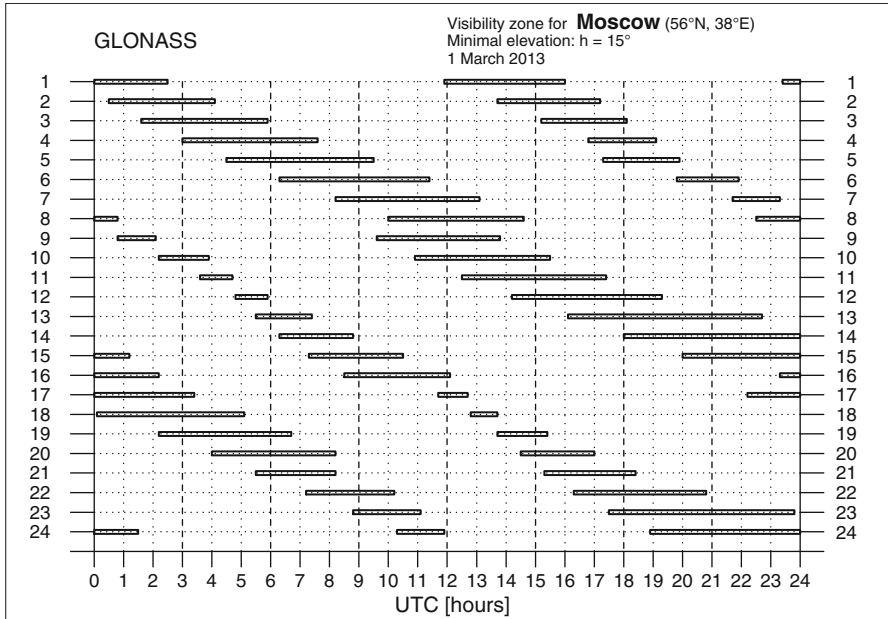
The project is financed by the European Union (EU) and the European Space Agency (ESA), itself financed by the member countries of the EU. The programme soon got behind schedule, in particular thanks to disagreements between Germany and Italy. Without going into the details, which would be more appropriate in a book about political economy than a work on orbitography, let us say that the only clear consensus was for the name: Galileo. It stands as a fine tribute to a visionary and courageous thinker.

After launching two test satellites,<sup>12</sup> the Galileo system is gradually coming into being, with four IOV (in-orbit validation) satellites<sup>13</sup> in 2013, to begin the constellation.

---

<sup>12</sup>Launch dates: GIOVE-A on 28 December 2005 and GIOVE-B on 27 April 2008. These satellites, placed on the Galileo orbit, serve to test the clocks and emitted signal, as well as occupying the frequency bands from an administrative point of view in the eyes of the relevant international organisations. Originally named GSTB-v2A and -v2B (Galileo System Test Bed Version 2), they were renamed GIOVE (Galileo In-Orbit Validation Element). Jupiter is *Giove* in Italian, and this is therefore an affectionate allusion to Galileo, who discovered the four largest moons of this planet.

<sup>13</sup>Launch dates: Galileo-IOV-1 and -2 on 21 October 2011, Galileo-IOV-3 and -4 on 12 October 2012.



**Glonass** ( ГЛОНАСС )

Orbit - Ground track

Recurrence = [ 2; +1; 8 ] 17

>>>> Time span shown: 8.00 days

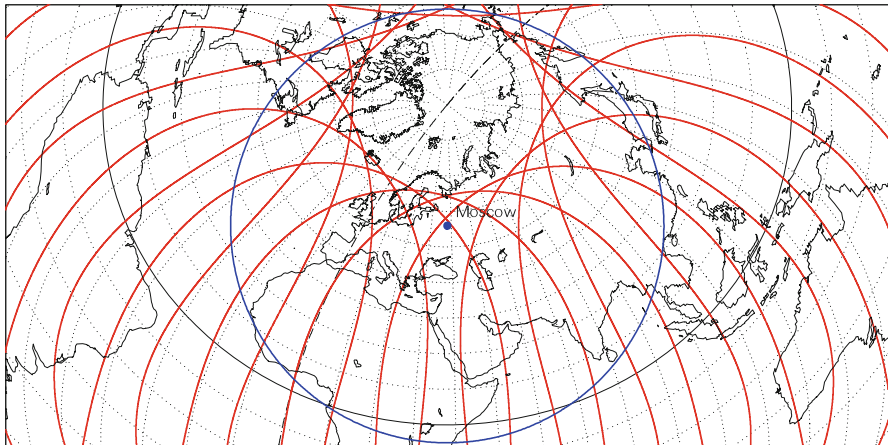
Altitude = 19129.5 km

$a = 25507.602$  km

Inclination =  $64.80^\circ$

Period = 675.73 min \* rev/day = 2.13

Visibility circle for  $h = 15^\circ$



Projection: Postel

Project. centre: 56.0° N; 38.0° E

Asc. Node: 0.00°

Property: none

Aspect: Oblique > zoom : 2.90

⊕ T.:Azimuthal - Graticule: 10° [4.2] [-90.0/+34.0/+52.0] [-] EIGEN6C2

Ιξίων  
MC \* LMD  
Ατλας

FIG. 14.12 : Upper: Visibility table ( $h > 15^\circ$ ) for the 24 Glonass satellites when viewing from Moscow on 1 March 2013. For the satellite numbers, from 1 to 24, see Fig. 14.8. Lower: Ground track of a Glonass satellite over 8 days, with visibility circle ( $h > 15^\circ$ ) centered on Moscow.

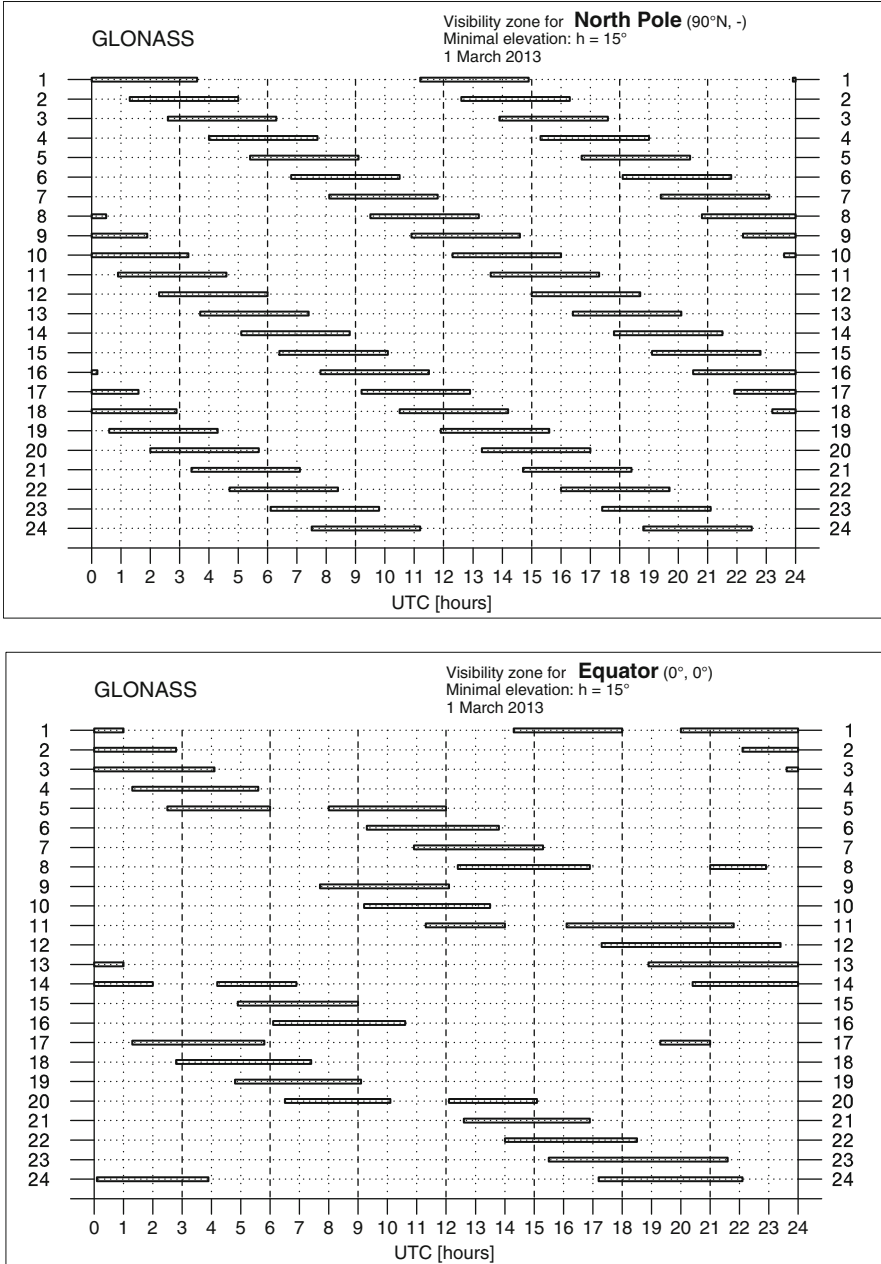


FIG. 14.13 : Visibility tables ( $h > 15^\circ$ ) for the 24 Glonass satellites on 1 March 2013. Upper: For a point at the North Pole. Lower: For a point on the equator (longitude  $0^\circ$ ). For the satellite numbers, from 1 to 24, see Fig. 14.8.

### 14.4.2 The Three Segments

The space segment comprises a constellation of 27 satellites (3 planes of 9 regularly spaced). Each satellite is equipped with a rubidium clock (drift  $5 \times 10^{-13}$  s over 100 s), backed up by a hydrogen maser (drift  $10^{-14}$  s over 3 h). The signal comprises three frequencies: E1 = 1,575.420 MHz, E6 = 1,278.750 MHz, and E5 = 1,191.795 MHz.

The Galileo orbit<sup>14</sup> is 3,000 km above the Navstar orbit, at  $h = 23,222$  km, with almost the same inclination, at  $i = 56^\circ$  (see Table 14.1). The recurrence is 17 revolutions in 10 days (20 revolutions in 10 days for Navstar), giving a period of 14 h 05 min (see Fig. 14.14).

The precession rates are very low. In degrees per day,

$$\dot{\Omega} = -0.026, \quad \dot{\omega} = +0.013, \quad \Delta n = -0.001.$$

The geodetic reference system is the Galileo Terrestrial Reference Frame (GTRF), very close to WGS84, since the two systems are adjusted to the International TRF (ITRF).

The control segment comprises many stations around the globe, and this is where the French presence in La Réunion, Nouméa (New Caledonia), Papeete (French Polynesia), and Kourou (French Guiana) has proved extremely useful. The two master stations are in Oberpfaffenhofen (in Bavaria, 20 km west of Munich) and Fucino (in the Abruzzi region of Italy, 130 km east of Rome).

Regarding the user segment, two different regimes are planned. One is free, like the GPS today, and the other paying. The accuracy promised for the free service is quite outstanding, and one wonders what advantage there will be in the paying service!

## 14.5 BeiDou NS

Like the three other navigation systems already discussed, the Chinese system<sup>15</sup> BeiDou NS turns around a constellation of MEO satellites. They were

---

<sup>14</sup>Originally, a recurrence cycle of five revolutions in 3 days was adopted. This corresponds to the orbit denoted by Galileo [0] in Table 14.1. But this orbit was abandoned because the 5:3 recurrence creates resonance effects with the Earth's gravitational field. In addition, the effects of the Sun and Moon create major instabilities in the Galileo constellation.

<sup>15</sup>*Bei Dou* is the Chinese name for the constellation *Ursa Major*, the Great Bear. In fact, in Chinese astronomy, there are 28 constellations, and they do not correspond exactly to the constellations of Western astronomy, which features many more than this. *Bei* means "north" and *Dou* is an instrument for measuring grain that looks like a large scoop, just as this constellation is sometimes referred to as the Saucepan or the Big Dipper, owing to its shape. Note that the Beidou satellites were also called Big Dipper at the beginning. The word "compass" comes from the Old French (fourteenth century) *compas*, from the verb *compasser*, meaning "to measure out in strides". This in turn derives from the Latin verb composed of *cum*, "with", and *passus*, "stride". The English noun took its present meaning in the fifteenth century. A single idea brings together the Great Bear, which provides an

**Galileo**

**Orbit - Ground track**

Recurrence = [ 2; -3; 10 ] 17

>>>> Time span shown: 10.00 days

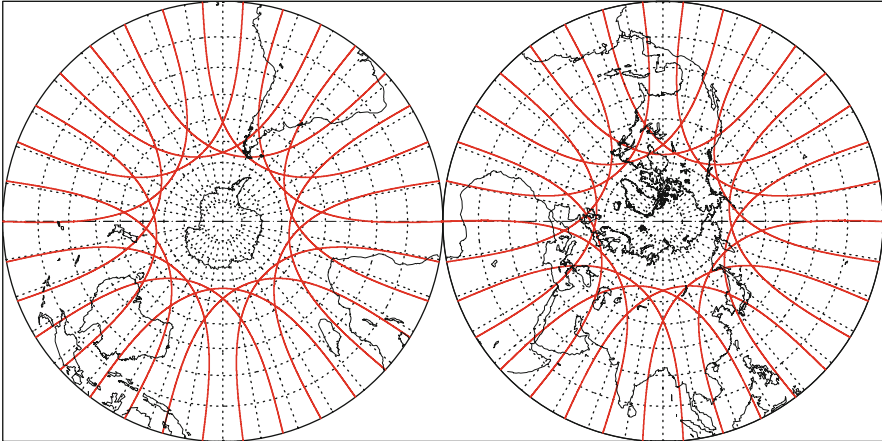
Altitude =23222.1 km

a =29600.268 km

Inclination = 56.00 °

Period = 844.69 min \* rev/day = 1.70

Equat. orbital shift =23573.5 km



Projection: Stereographic

Pr. centre (r): 90.0 ° N; 90.0 ° E

Asc. Node: 0.00 °

*Ιξίων*

Property: Conformal

Aspect: Direct

App. inclin. = 92.01 °

MC \* LMD

⊕ T.:Azimuthal - Graticule: 10° ½.2[ -90.0/ +0.0/ +0.0 ] [-] EIGEN6C2

*Ατλας*

**Galileo**

**Orbit - Ground track**

Recurrence = [ 2; -3; 10 ] 17

>>>> Time span shown: 10.00 days

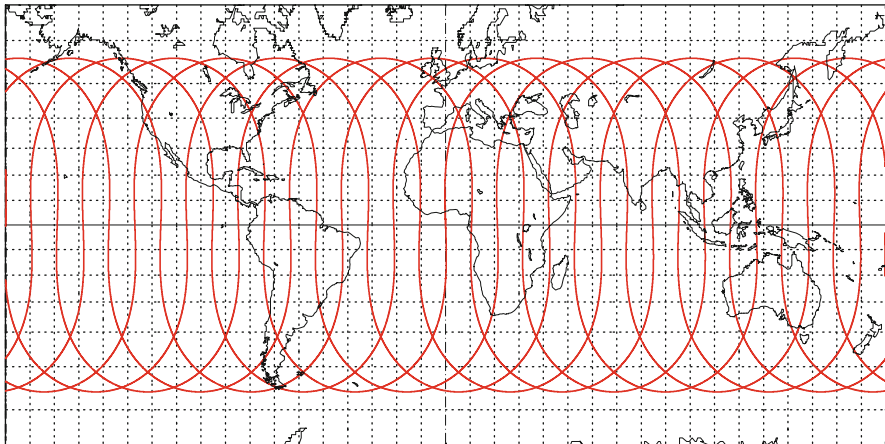
Altitude =23222.1 km

a =29600.268 km

Inclination = 56.00 °

Period = 844.69 min \* rev/day = 1.70

Equat. orbital shift =23573.5 km



Projection: Mercator

Project. centre: 0.0 ° ; 0.0 °

Asc. Node: 0.00 °

*Ιξίων*

Property: Conformal

Aspect: Direct

App. inclin. = 92.01 °

MC \* LMD

⊕ T.:Cylindrical - Graticule: 10° ½.2[ +0.0/ +0.0/ +0.0 ] [-] EIGEN6C2

*Ατλας*

FIG. 14.14 : Ground track of a Galileo satellite over one recurrence cycle (17 revolutions in 10 days).



**BeiDou NS**

**Orbit - Ground track**

Recurrence = [ 2; -1; 7] 13

>>>> Time span shown: 7.00 days

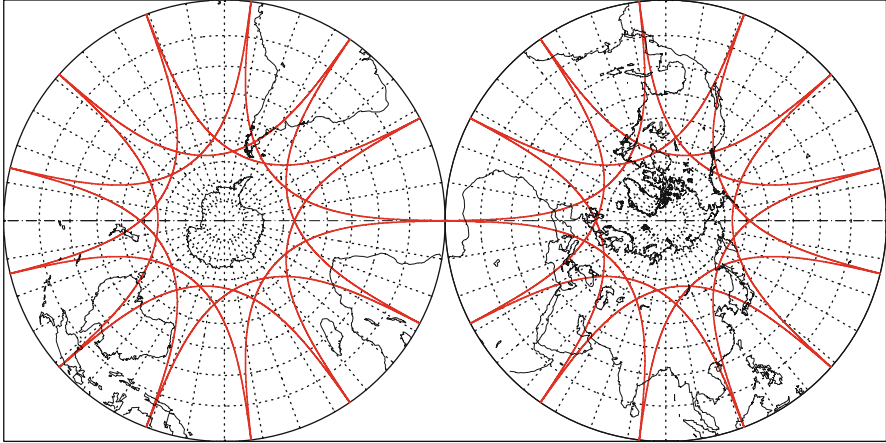
Altitude =21527.6 km

a =27905.750 km

Inclination = 56.30 °

Period = 773.20 min \* rev/day = 1.86

Equat. orbital shift =21578.9 km



Projection: Stereographic

Pr. centre (r): 90.0 ° N; 90.0 ° E

Asc. Node: 0.00 °

*Ιξίων*

Property: Conformal

Aspect: Direct

App. inclin. = 88.87 °

MC ★ LMD

⊕ T.:Azimuthal - Graticule: 10° 4.2[-90.0/ +0.0/ +0.0] [-] EIGEN6C2

*Ατλας*

**BeiDou NS**

**Orbit - Ground track**

Recurrence = [ 2; -1; 7] 13

>>>> Time span shown: 7.00 days

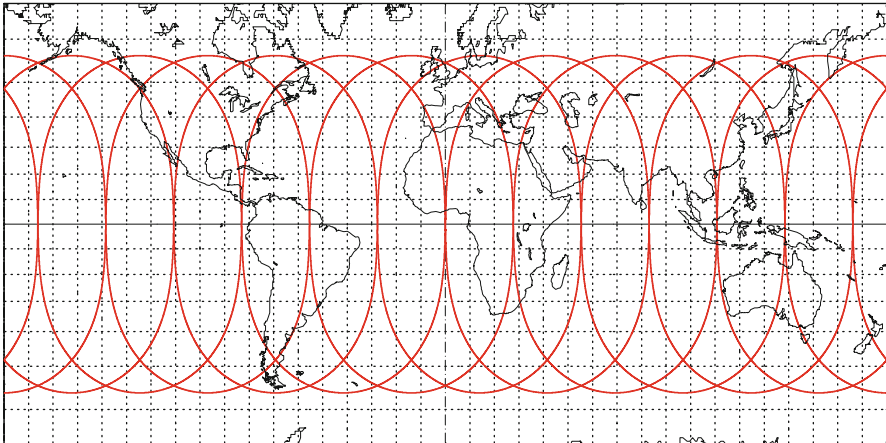
Altitude =21527.6 km

a =27905.750 km

Inclination = 56.30 °

Period = 773.20 min \* rev/day = 1.86

Equat. orbital shift =21578.9 km



Projection: Mercator

Project. centre: 0.0 ° ; 0.0 °

Asc. Node: 0.00 °

*Ιξίων*

Property: Conformal

Aspect: Direct

App. inclin. = 88.87 °

MC ★ LMD

⊕ T.:Cylindrical - Graticule: 10° 4.2[ +0.0/ +0.0/ +0.0] [-] EIGEN6C2

*Ατλας*

FIG. 14.15 : Ground track of a BeiDou NS satellite over one recurrence cycle (13 revolutions in 7 days).

originally called Beidou-2, testimony to the technological inheritance from Beidou-1, a first shot at a positioning system based upon two geostationary satellites. We shall return to that later. It then changed its name to Compass or Compass Navigation Satellite System (CNSS). In December 2012, it became officially known as BeiDou NS or BeiDou Navigation Satellite System (BDNS; Fig. 14.15).

### 14.5.1 The Three Segments

The MEO part of the space segment, BeiDou-M (with M for MEO), comprises a constellation<sup>16</sup> of 24 MEO satellites (3 planes of 8 regularly spaced satellites). Each satellite is equipped with a rubidium clock. The signal is emitted at three frequencies: E2 = 1,561.07 MHz, E6 = 1,268.52 MHz, and E5B = 1,207.14 MHz.

The orbit is very similar to that of Navstar/GPS, with altitude  $h = 21,528$  km and inclination  $i = 56.3^\circ$ . The recurrence cycle is 13 revolutions in 7 days (14 revolutions in 7 days for Navstar), whence a period of 12 h 58 min (see Fig. 14.16 upper). Precession rates are very small, for the same reason as for Navstar. The values are, in degrees per day,

$$\dot{\Omega} = -0.031, \quad \dot{\omega} = +0.015, \quad \Delta n = -0.002.$$

The MEO constellation is supplemented by two further systems<sup>17</sup> (see Fig. 14.16 lower):

- BeiDou-G: five GEO satellites parked at longitudes  $58.75^\circ\text{E}$ ,  $80.0^\circ$ ,  $110.5^\circ$ ,  $140.0^\circ$ , and  $160.0^\circ$ .
- BeiDou-I: three satellites on an inclined geosynchronous satellite orbit (IGSO). This is circular with inclination  $i = 55^\circ$ . They are regularly spaced on the same orbit with ascending node at longitude  $118^\circ\text{E}$ .

The geodetic reference system is CGS-2000 (China Geodetic System), almost identical to ITRF. The control segment comprises one central station and three monitoring stations. For the user, the accuracy is claimed to be on a par with Navstar.

---

easy way to identify the Pole Star in *Ursa Minor* (the Little Bear), and the compass, an instrument used for orientation. That was before the advent of GPS, of course!

<sup>16</sup>Launch dates: Beidou-2-M1 (Compass-M1) on 13 April 2007, Beidou-2-M3 and -M4 on 29 April 2012, Beidou-2-M2 and -M5 on 18 September 2012.

<sup>17</sup>Launch dates for BeiDou-G (Compass-G): Beidou-2-G1 on 16 January 2010, Beidou-2-G2 on 14 April 2009, Beidou-2-G3 on 2 June 2010, Beidou-2-G4 on 31 October 2010, Beidou-2-G5 on 24 February 2012, Beidou-2-G6 on 25 October 2012. Launch dates for BeiDou-I (Compass-I): Beidou-2-I1 on 31 July 2010, Beidou-2-I2 on 17 December 2010, Beidou-2-I3 on 9 April 2011, Beidou-2-I4 on 26 July 2011, Beidou-2-I5 on 1 December 2011. These satellites Beidou-2- $I_n$  are also denoted by Beidou-2-IGSO- $n$ .

### 14.5.2 Beidou-1 Experimental System

The Beidou-1 positioning system, sometimes called the Beidou Navigation Test System (BNTS), is an experimental system. Also known as the Double Star Positioning System (DSPS), it uses two geostationary satellites and requires the user to possess a transmitter–receiver. It has been running since 2003.

It works in the following way. The control station emits a signal with a time signature to the user  $P$  via two satellites  $S_1$  and  $S_2$ , as shown schematically in Fig. 14.17. When the user receives the first signal, from  $S_1$  say, he transmits it to  $C$  via the two satellites.

The control station can thus measure the two time intervals  $\Delta t_1$  and  $\Delta t_2$  corresponding to the two paths:

$$\begin{aligned} C \rightarrow S_1 \rightarrow P \rightarrow S_1 \rightarrow C &\implies c\Delta t_1 = 2d_1 + 2r_1, \\ C \rightarrow S_1 \rightarrow P \rightarrow S_2 \rightarrow C &\implies c\Delta t_2 = d_1 + r_1 + d_2 + r_2, \end{aligned}$$

where  $r_i = \|\mathbf{S}_i\mathbf{P}\|$  and  $d_i = \|\mathbf{S}_i\mathbf{C}\|$ ,  $i = 1, 2$ . The two distances  $d_i$  are known, as is the transponder response time, which we ignore in this simplified discussion. The required values are  $r_1$  and  $r_2$  :

$$\begin{cases} r_1 = \frac{c}{2}\Delta t_1 - d_1, \\ r_2 = \frac{c}{2}(2\Delta t_2 - \Delta t_1) - d_2. \end{cases}$$

The required point is at the intersection of the two spheres  $\Sigma_i$ , centered on the equatorial plane, with centers  $S_i$  and radii  $r_i$ . This intersection takes the form of a circle lying in a plane perpendicular to the equator. Then the intersection of  $\Sigma_1 \cap \Sigma_2$  with the Earth ellipsoid gives two points, one in the northern hemisphere and one in the southern hemisphere. The one in the northern hemisphere corresponds to the position of the Chinese user. A further constraint is thus that the altitude of the point  $P$  must be known:

- If  $P$  is on the ground, the control station  $C$  knows the altitude of  $P$  because it has a very accurate numerical terrain model (NTM) at its disposal for the Chinese territory, with a graticule of one arcsec.
- If  $P$  is in the air, the user must determine his altitude using a barometer, for example, and send this information to  $C$ .

Once the position of  $P$  has been determined, the station  $C$  transmits the result to  $P$ . To the four journeys between the Earth and a geostationary satellite to determine the position, one must therefore add two others for the transmission of the result, making a total of 6, which takes 0.8 s in all.

**BeiDou NS**

**Orbit - Ground track**

Recurrence = [ 2; -1; 7 ] 13

>>>> Time span shown: 7.00 days

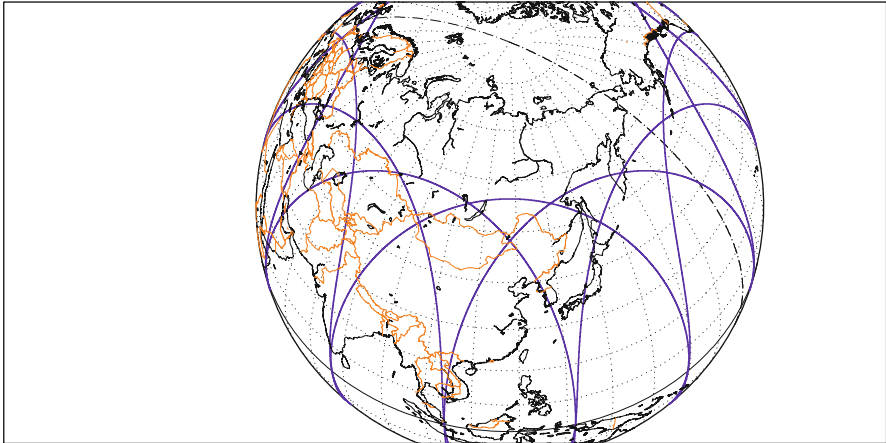
Altitude =21527.6 km

a =27905.750 km

Inclination = 56.30 °

Period = 773.20 min \* rev/day = 1.86

Equat. orbital shift =21578.9 km



Proj.: Perspect.V. h=5.61 R

Property: none

⊕ T.:Azimuthal - Graticule: 10°

PC: 55.0 ° N;118.0 ° E /ZC: 50.0 ° N; 98.0 ° E Asc. Node: -62.00 ° [00:00 LMT]

Aspect: Oblique > zoom : 1.15

§5.3{ -90.0/ +35.0/ -28.0 } [-] EIGEN6C2

Ιξίων  
MC ★ LMD  
Ατλας

**BeiDou NS [I + G]**

**Orbit - Ground track**

Recurrence = [ 1; +0; 1 ] 1

>>>> Time span shown: 1440.0 min = 1.00 day

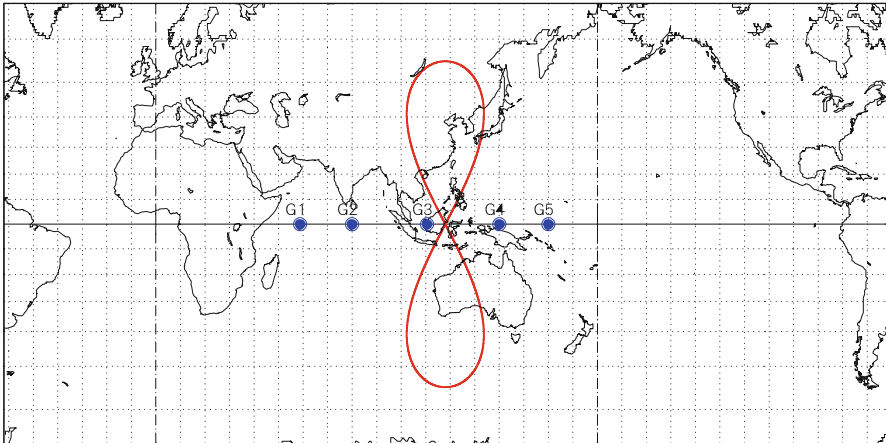
Altitude =35786.4 km

a =42164.496 km

Inclination = 55.00 °

Period = 1436.07 min \* rev/day = 1.00

Equat. orbital shift =40075.9 km



Projection: Mercator

Property: Conformal

⊕ T.:Cylindrical - Graticule: 10°

Project. centre: 0.0 ° ; 118.0 ° E

Aspect: Direct

§4.2{ +90.0/ +0.0/+152.0 } [-] EIGEN6C2

Asc. Node: 118.00 ° [00:00 LMT]

App. inclin. = 117.50 °

Ιξίων  
MC ★ LMD  
Ατλας

FIG. 14.16 : Compass system. Upper: BeiDou-M. Ground track of the orbit over 7 days, viewed from the northernmost point of the BeiDou-I orbit. Lower: BeiDou-I and BeiDou-G. Ground track of the IGSO (geosynchronous) orbit of the three BeiDou-I satellites and positions of the five GEO (geostationary) satellites.

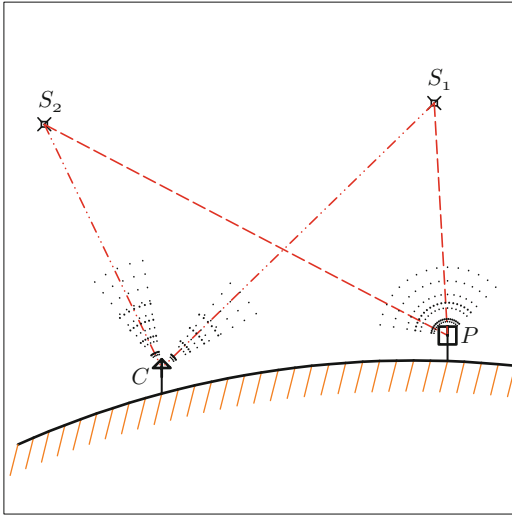


FIG. 14.17: *The Beidou-1 system. A user  $P$  picks up a signal emitted by the control station  $C$  and transmits it to  $C$  via the two geostationary satellites  $S_1$  and  $S_2$ . The signals are analysed by  $C$ , the position of  $P$  is calculated, and the result is sent on to  $P$ .*

The geodetic reference system<sup>18</sup> for Beidou-1 is Beijing-1954. The space segment<sup>19</sup> consists of two geostationary satellites, Beidou-1A and -1B, parked at  $80.0^\circ\text{E}$  and  $140.0^\circ\text{E}$ . A backup satellite is parked at  $110.5^\circ\text{E}$ . The control segment comprises the central station and three monitor stations, all in China.

The user segment consists of a somewhat bulky transmitter–receiver. Coverage is rather limited:

$$\text{latitude} \quad \updownarrow \quad \begin{matrix} 55^\circ\text{N} \\ 5^\circ\text{N} \end{matrix}, \quad \text{longitude} \quad \begin{matrix} 70^\circ\text{E} & 140^\circ\text{E} \\ \leftarrow & \rightarrow \end{matrix}$$

Accuracy is around 100 m. Using the third satellite in a differential method, one could hope to achieve 20 m. This accuracy is immediately lost when the receiver is in movement. As soon as the speed exceeds a few meters per second, the system becomes inaccurate, even unusable. The system also has limited capacity: 540,000 users per hour, with a maximum of 150 users at any given time.

The Beidou-1 positioning system has some advantages over Navstar/GPS:

- It uses two satellites rather than a constellation of at least 24.
- The clocks do not need to be ultra-precise. They need only be stable, since they measure a time difference.

<sup>18</sup>It is surprising to find that Beidou-1 uses such an antiquated reference system. And it is older than its name would suggest, since it is in fact a carbon copy of the Soviet model Krasovsky-1940.

<sup>19</sup>Launch dates: Beidou-1A (BNTS-1A, DFH-51) on 30 October 2000, Beidou-1B (BNTS-1B, DFH-52) on 20 December 2000, Beidou-1C (BNTS-1C, DFH-56) on 24 May 2003.

It is thus a relatively cheap system that can be set up quite quickly. It also has many disadvantages:

- It only gives regional coverage, although this may be considered adequate by Chinese users.
- Accuracy is rather limited, being only around 100 m in standard mode.
- The user terminal is bulky and expensive.
- The number of users is limited.

For the Chinese authorities, the disadvantages outweigh the advantages since, even though they seemed to be satisfied with the Beidou-1 experimental system, they nevertheless decided to set up Beidou-2 (which become Compass, then BDNS) along the lines of the Navstar system, i.e., using a constellation of MEO satellites.

## 14.6 Augmentation Systems

As discussed above, differential GPS (DGPS) exploits the transmission to users of the correction detected by the control station. Rather than sending the information by terrestrial radio relay, it is transmitted directly to a geostationary satellite which broadcasts it back to Earth. The extra satellite thus introduced then provides an augmentation system. These systems, referred to as satellite-based augmentation systems (SBAS), can lead to significant improvements:

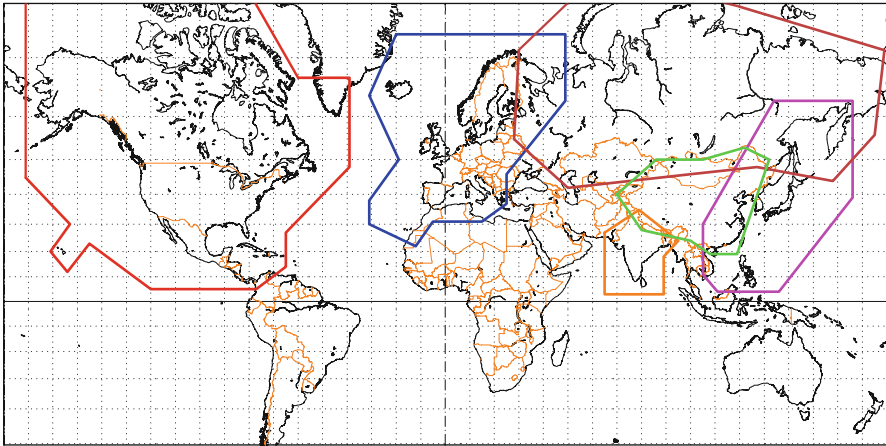
- To begin with, by broadcasting corrections, they extend DGPS quality to many more users.
- Furthermore, they are equipped with GPS clocks and emit a type L1 signal specified by its PRN code, which adds pseudo-range measurements to those obtained by the MEO satellites of the GPS constellation itself.
- Finally, by analysing a whole set of data, these systems provide what is known as an integrity service. Integrity is the guarantee that the signals can be trusted, a necessary condition for GPS use by civil aviation authorities.

The regions covered by the various augmentation systems are shown in Fig. 14.18 (upper) and a list of contributing satellites is given in Table 14.4:

- The Wide Area Augmentation System (WAAS) was developed by the aviation authorities in the USA. It is based upon three or four GEO satellites. Coverage extends over the whole of North America, since the absorption of the Canadian CWAAS, and also Hawaii.
- The American Wide Area GPS Enhancement (WAGE) system run by the US Army (DoD) is only accessible to the military.

Projection: Mercator PC: 0.0° ; 0.0° /ZC: 30.0° N; 0.0°  
 Property: Conformal Aspect: Direct  
 ⊕ T.:Cylindrical - Graticule: 10° {5.3} [+90.0/ +0.0/ -90.0] [-]

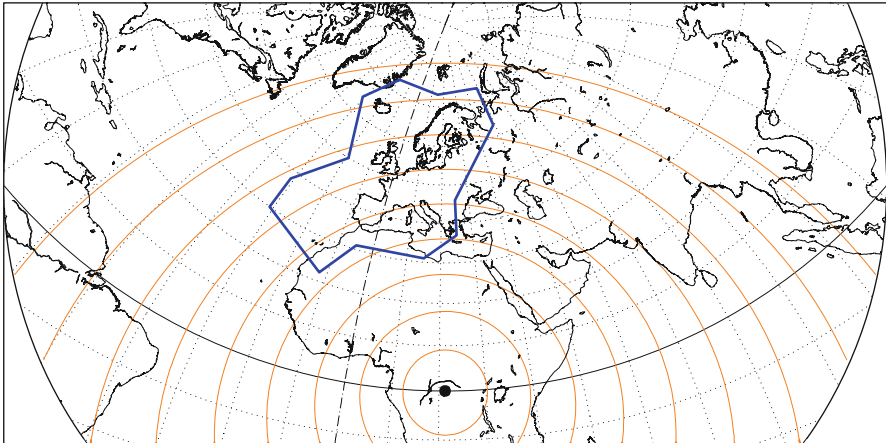
Ιξίων  
 MC★LMD  
 Ατλας



**Artemis**

Locus of points  
 equidistant  
 from the subsatellite point

Altitude = 35787.6 km a<sub>GS</sub> = 42165.785 km  
 Inclination = 0.00° Parking Longit. = 21.3° E  
 Period = 1435.91 min \* rev/day = 1.00  
 Equat. orbital shift = 40072.1 km  
 \*\* Half-swath: 8.7° - On ground 9050.2 km [ 1000.0 km]



Projection: Stereographic PC: 50.0° N; 21.3° E /ZC: 40.0° N; 21.3° E  
 Property: Conformal Aspect: Oblique > zoom : 2.00  
 ⊕ T.:Azimuthal - Graticule: 10° {5.3} [-90.0/ +40.0/ +68.7] [-] GM2008

Geostationary Ιξίων  
 Max. attained latit. = 81.3° MC★LMD  
 Ατλας

FIG. 14.18 : Regional augmentation systems. Upper: Different areas: WAAS (North America), EGNOS (Europe), GAGAN (India), MSAS (Japan), SNAS (China), SDCM (Russia). Lower: European region EGNOS and representation of distances from the subsatellite point to the geostationary satellite Artemis.

System	Satellite/SBAS	PRN	Longitude	
WAAS	Inmarsat/AMR	133	97.7° W	Parking
–	Intelsat/CRW	135	133.0° W	Parking
–	Telesat/CRE	138	107.3° W	Parking
EGNOS	Inmarsat/AOR-E	120	15.5° W	Parking
–	Artemis	124	21.4° E	Parking
–	Inmarsat/IOR-W	126	24.7° E	Parking
GAGAN	GSAT-8	127	55.1° E	Parking
–	GSAT-10	128	83.0° E	Parking
SDCM	Luch-5A	140	94.8° E	Parking
–	Luch-5B	125	15.8° W	Parking
MSAS	MTSAT-1R	129	140.0° E	Parking
–	MTSAT-2	137	145.0° E	Parking
–	QZS-1	183	140.0° E	Apogee

TABLE 14.4 : Satellites used for the augmentation systems, with PRN number and parking longitude for the GEO or apogee for QZSS, as of July 2013. AOR Atlantic Ocean Region, IOR Indian Ocean Region.

- The company John Deere, world leader in agricultural machinery, has developed a private system for its customers by the name of StarFire (accuracy 10 cm), using an Inmarsat satellite.
- The European Geostationary Navigation Overlay Service (EGNOS) uses three GEO satellites and covers Europe, the Atlantic from Iceland to the Azores and the Canary Islands, and also the northern part of North Africa, as shown in Fig. 14.18 (lower).
- The Indian GPS Aided GEO Augmented Navigation System (GAGAN)<sup>20</sup> uses two GEO satellites and covers continental India and its two archipelagos.
- The Japanese Multi-functional Satellite Augmentation System (MSAS) is run by the Japanese meteorological office and ministry of transport. It uses two tso satellites and the QZSS system (see below). The system is limited to Japan.
- The Russian System for Differential Correction and Monitoring (SDCM) is based on three Luch satellites.
- The planned Chinese system will be called Satellite Navigation Augmentation System (SNAS).

<sup>20</sup>This is an acronym with a particularly successful double meaning, since *gagan* means “sky” in Sanskrit.



## 14.7 Regional Systems

Here we discuss two regional systems that are not equivalent: the Indian IRNSS is an autonomous system, while the Japanese QZSS serves only to improve Navstar/GPS positioning in the major Japanese cities.

### 14.7.1 IRNSS

India will develop a navigation system based on GEO and GSO satellites, i.e., geostationary and geosynchronous with inclination. It will thus be regional, since there is no hope of global coverage without MEO satellites. The India Regional Navigation Satellite System (IRNSS) is thus based on seven satellites, three of which are GEO and four GSO, all equipped with rubidium clocks emitting a signal at two frequencies:  $L5 = 1,176.45$  MHz and  $S = 2,492.08$  MHz. It will use the geodetic reference system WGS84.

The three GEO satellites are placed at separations of around  $50^\circ$  in longitude, in fact, at parking longitudes  $34.0^\circ\text{E}$ ,  $83.0^\circ\text{E}$ , and  $131.5^\circ\text{E}$ . The four GSO satellites are placed on two circular geosynchronous orbits with inclination  $i = 29^\circ$ . The longitude of the ascending node is  $55.0^\circ\text{E}$  for one and  $111.0^\circ\text{E}$  for the other (see Fig. 14.19 upper).

The expected accuracy is 20 m over a main region lying between latitudes  $40^\circ\text{N}$  and  $40^\circ\text{S}$  and longitudes  $40^\circ\text{E}$  and  $140^\circ\text{E}$ .

### 14.7.2 QZSS

The Japanese space agency JAXA has come up with an interesting orbit, reminiscent of the Tundra orbit but less eccentric, and with a lower inclination than the critical one.<sup>21</sup> It is a geosynchronous orbit, with  $i = 40^\circ$  and apogee over Tokyo. So not only does the satellite remain for longer over Japan, but it is almost vertically above the large Japanese cities, i.e., at the zenith (see Fig. 14.20), whence the name Quasi-Zenith Satellite System (QZSS).

This constellation should contain three regularly spaced satellites QZS-1, -2, and -3. The first,<sup>22</sup> QZS-1, is already operational. Its ground track is shown in Fig. 14.19 (lower). Each satellite remains visible for about 11 h a day, under the difficult visibility conditions imposed by  $h > 60^\circ$ . Figure 14.21 gives a good idea as to why the Navstar/GPS constellation is not particularly effective under such conditions, since there are rarely more than two or three of these satellites in view. The satellites of the QZSS constellation will supply the fourth, or even the fifth satellite required for adequate positioning.

---

<sup>21</sup>The apsidal precession rate is nevertheless very low, viz.,  $\dot{\omega} = -0.01025^\circ/\text{day}$ , or less than  $4^\circ$  per year, which is easy to compensate.

<sup>22</sup>Launch date: QZS-1 on 11 September 2010. QZS-1 also has the Japanese name *Michibiki*, meaning “guide”.

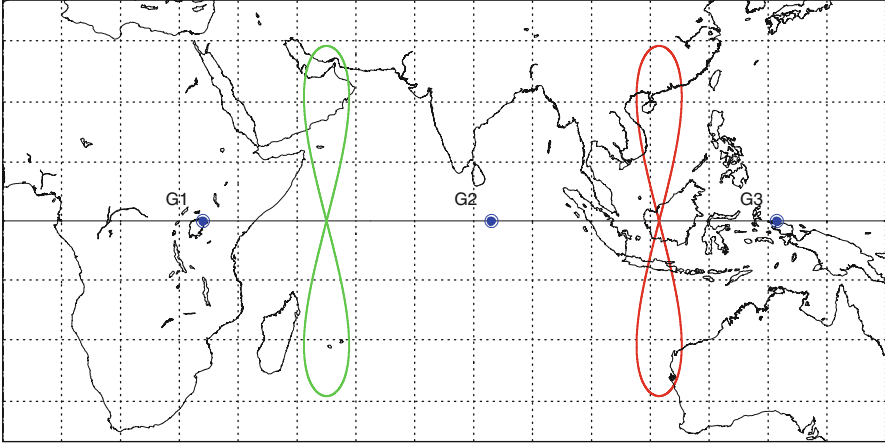
**IRNSS/GSO**

Orbit - Ground track

Recurrence = [ 1; +0; 1] 1

>>>> Time span shown: 1440.0 min = 1.00 day

Altitude = 35787.3 km      a = 42165.410 km  
 Inclination = 29.00 °  
 Period = 1436.02 min \* rev/day = 1.00  
 Equat. orbital shift = 40075.0 km



Proj.: Miller II      PC: 0.0 ° ; 0.0 ° /ZC: 0.0 ° ; 75.0 ° E      Asc. Node: 111.50 ° [00:00 LMT]      *Ιξίων*  
 Property: none      Aspect: Direct > zoom : 2.40      App. inclin. = 104.50 °      MC \* LMD  
 ⊕ T.:Cylindrical - Graticule: 10° {5.3} [+90.0/ +0.0/ -90.0] [-] EIGEN6C2      *Ατλας*

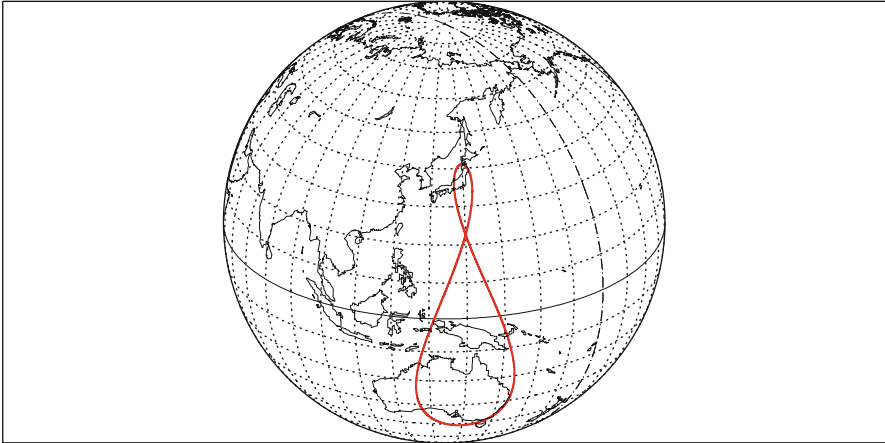
**QZS-1 〈みちびき〉**

Elliptical orbit - Gr. track

Recurrence = [ 1; +0; 1] 1

>>>> Time span shown: 1440.0 min = 1.00 day

Equiv. altit. = 35785.8 km      a = 42163.941 km  
 Inclination = 40.91 °      e = 0.075053  
 Period = 1435.99 min \* rev/day = 1.00  
 h\_a = 38950 km; h\_p = 32621 km; arg. perigee: +270.00 °



Projection: Orthographic      Project. centre: 26.0 ° N; 134.0 ° E      Longitude / Initialisation:      *Ιξίων*  
 Property: none      Aspect: Oblique      Asc. Node: 148.59°      MC \* LMD  
 ⊕ T.:Azimuthal - Graticule: 10° {4.2} [-90.0/ +64.0/ -44.0] [-] EGM2008      Apogee : 140.00°      *Ατλας*

FIG. 14.19 : Upper: IRNSS. Ground track of two GSO (geosynchronous) orbits of the IRNSS-GSO satellites and positions of the three GEO (geostationary) satellites. Lower: Ground track of the geosynchronous orbits of three QZSS satellites.

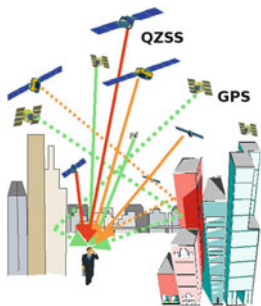


FIG. 14.20 : In the “urban canyons”, to use the beautiful term employed by urban planners, when one finds oneself stuck between two Tokyo skyscrapers, it is not so easy to pick up the GPS signal. Either it does not get there at all, or worse, it does get there but via several routes between the walls of the buildings, and the position calculation is subsequently thrown out. Credit: JAXA.

The reference geodetic system is the Japan Geodetic System (JGS), very close to ITRF. The ground segment consists of the master control station (MCS) at Tsukuba, 60 km north of Tokyo, and nine monitor stations in Japan and overseas, the furthest being in Bangalore to the west, Hawaii to the east, and Canberra to the south.

## 14.8 Non-positioning Uses of GPS

### 14.8.1 Radio Occultation

The occultation of radio waves by the atmosphere was tested on the atmosphere of Mars in 1965 by the Jet Propulsion Laboratory (JPL) using the US probe Mariner-4, and subsequently on the atmosphere of Venus in 1967 using Mariner-5. Then in 1994, the GPS signal was used to sound the Earth’s own atmosphere, by placing a receiver on low-orbiting satellites.

The signal is emitted by the navigation satellite  $S$  and received by the LEO satellite  $L$ . The path  $SL$  (see Fig. 14.22) is a straight line when outside the atmosphere, but is deflected when it crosses it. This deflection through an angle  $\alpha$  (several tenths of a degree) depends on the refractive index of the air, which is mainly a function of the local values of temperature, pressure, density, and water vapour content. In this way, one measures an integrated value over the whole path  $SL$  of length  $ab$ . Using an inversion technique such as Abel inversion, one can then deduce temperature profiles to an accuracy of 0.1–0.5 K, as well as profiles of pressure and other atmospheric parameters.

Situations known as opposition, when the Earth passes between an LEO satellite ( $\nu_1 \sim 14$ ) and a GPS satellite ( $\nu_2 = 2$ ) occur roughly  $\nu_1 - \nu_2 = 12$  times a day, and one can therefore expect 24 occultations. With 24 Navstar/GPS satellites, this means around 500 occultations per day, implying 15,000 per month and per LEO satellite.

The first suitably equipped LEO satellites were the three geodesy satellites CHAMP and GRACE-A and -B, then Ørsted, SAC-C, and MetOp-A and -B. The constellation COSMIC, comprising six satellites FormoSat-3, from

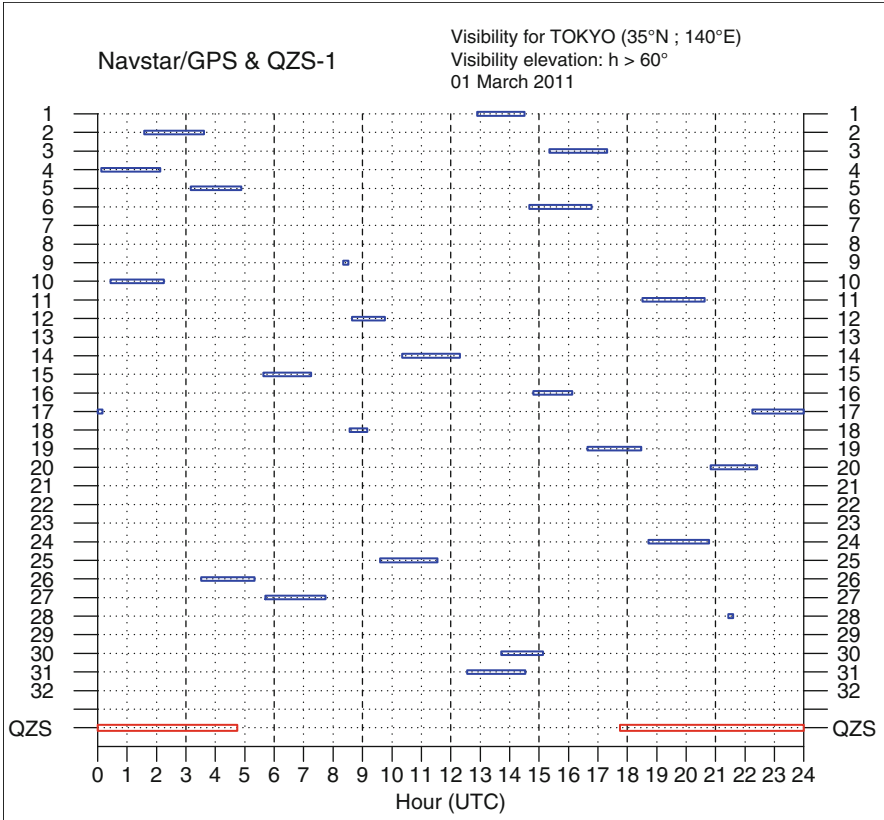


FIG. 14.21 : Visibility table of the 32 Navstar/GPS satellites and the satellite QZS-1, for Tokyo on 1 March 2011. Visibility elevation:  $h > 60^\circ$ . With such a constraint on visibility, corresponding to the situation in the center of the large Japanese conurbations, the Navstar/GPS constellation does not provide sufficient coverage. From the table, we see that most of the time only two or three Navstar/GPS satellites are visible, below the minimal threshold of four. The QZSS satellites (for the time being, only QZS-1) will make a significant contribution here.

-3A to -3F, is the first mission entirely dedicated to radio occultation (see Fig. 14.23 upper). The planned European mission ACE+ (which takes up from the WATS and ACE missions) is of the same type, with four LEO satellites,  $i \sim 90^\circ$ , equipped with GPS receivers. All these satellites are in near-polar orbits. For better sampling of the tropical region, a receiver called Radio Occultation Sounder for the Atmosphere (ROSA) is carried aboard Megha-Tropiques (see Figs. 14.23 lower and 14.24).

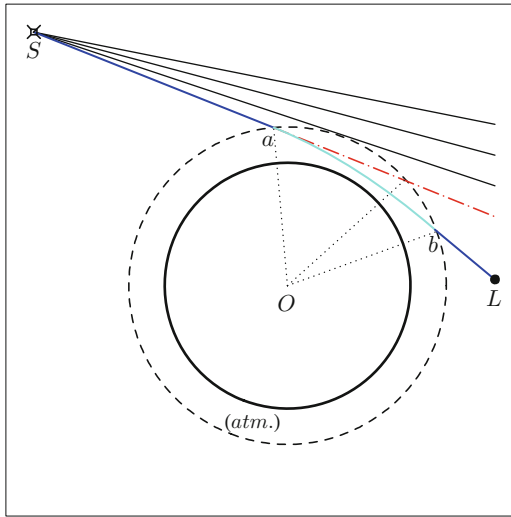


FIG. 14.22 : Schematic view of signal emitted by a GPS satellite  $S$ . The signal received by the LEO satellite  $L$  is deflected as it crosses the atmosphere from  $a$  to  $b$ . The angle of deflection  $\alpha$  is defined by  $\alpha = (\mathbf{S}a, \mathbf{b}L)$ .

## 14.8.2 Studying the Troposphere via the Base Stations

A permanent base station of the DGPS system sends a position correction, denoted by  $\delta_0 \mathbf{X}$  in (14.22), then just throws it away! But meteorological offices recover these binned corrections, because they contain information about the integrated water vapour content in the region of the troposphere traversed by the signal above the station at a given instant of time. This information is supplied continually and almost in real time, and can be assimilated with other physical data to set up weather forecasting models.

## 14.8.3 Other Applications

The applications of GPS now extend beyond just positioning to some quite unexpected areas. Here is an example from the world of finance. At the present time, many transactions on the stock exchange are decided by computers. Among the latest services are the so-called flash orders, which allow certain clients (or rather, their computers) to consult orders on certain stocks a fraction of a second before their competitors. This microsecond insider trading can be exposed by attaching a GPS “time marker” during the transaction.

# 14.9 Historical Note: The First Systems

## 14.9.1 Transit

The Transit navigation programme began with a discovery by American researchers at Johns Hopkins university (JHU/APL) in 1957: the orbit of

### FormoSat-3F/COSMIC

0 km <-> 75 km - Radio Occultation with Navstar/GPS

Altitude = 791.7 km      a = 7169.792 km

Inclination = 72.02 °

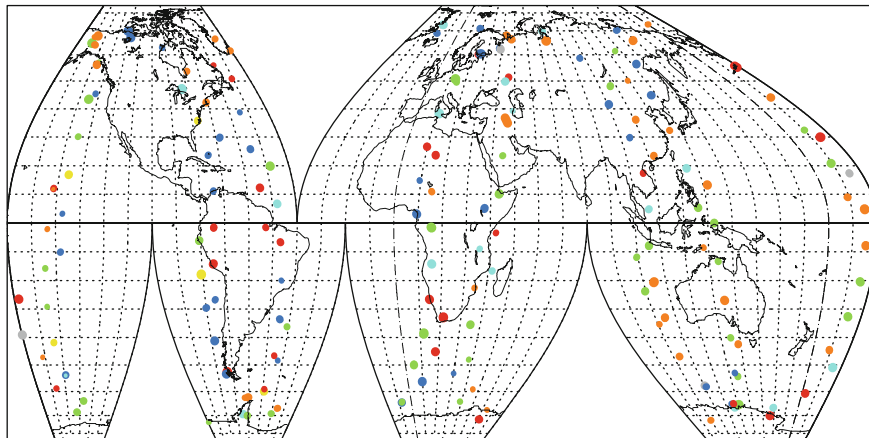
>>>> Time span shown: 7.00 days

Period = 100.78 min \* rev/day = 14.29

Total number of occultations: 172

Equat. orbital shift = 2828.2 km ( 25.4 °)

LMT (local)      00 01 02 03 04 05 06 07 08 09 10 11 12 13 14 15 16 17 18 19 20 21 22 23 24      hours



Projection: McBryde-Thomas sin      Project. centre: 0.0 ° ; 20.0 °E  
 Property: Equal area      Aspect: Direct [interrupted]  
 ⊕ T.:Pseudocyl. - Graticule: 10°      {4.2} [ +0.0/ +0.0/-20.0] [-] EGM2008

Asc. Node: -13.00 ° [00:00 LMT]  
 App. inclin. = 75.95 °

Ιξίων  
 MC ★ LMD  
 Ατλας

### Megha-Tropiques

0 km <-> 150 km - Radio Occultation with Navstar/GPS

Altitude = 865.5 km      a = 7243.677 km

Inclination = 20.00 °

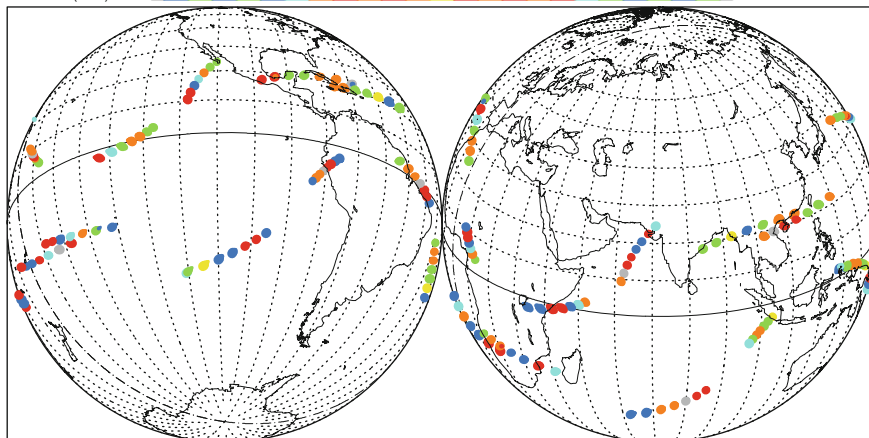
>>>> Time span shown: 7.00 days

Period = 101.93 min \* rev/day = 14.13

Total number of occultations: 170

Equat. orbital shift = 2892.0 km ( 26.0 °)

LMT (local)      00 01 02 03 04 05 06 07 08 09 10 11 12 13 14 15 16 17 18 19 20 21 22 23 24      hours



Projection: Orthographic      Pr. centre (r.): 25.0 ° N; 72.0 °E  
 Property: none      Aspect: Oblique  
 ⊕ T.:Azimuthal - Graticule: 10°      {4.2} [-90.0/ +65.0/ +18.0] [-] EGM2008

Asc. Node: -11.11 ° [00:00 LMT]

Ιξίων  
 MC ★ LMD  
 Ατλας

FIG. 14.23 : Locus of radio occultation between an LEO satellite and a Navstar/GPS satellite [PRN 16] over a time lapse of 7 days. Upper: Sun-synchronous satellite FormoSat-3/COSMIC, atmosphere crossed between 0 and 75 km. Lower: Low inclination satellite Megha-Tropiques, atmosphere crossed between 0 and 150 km.

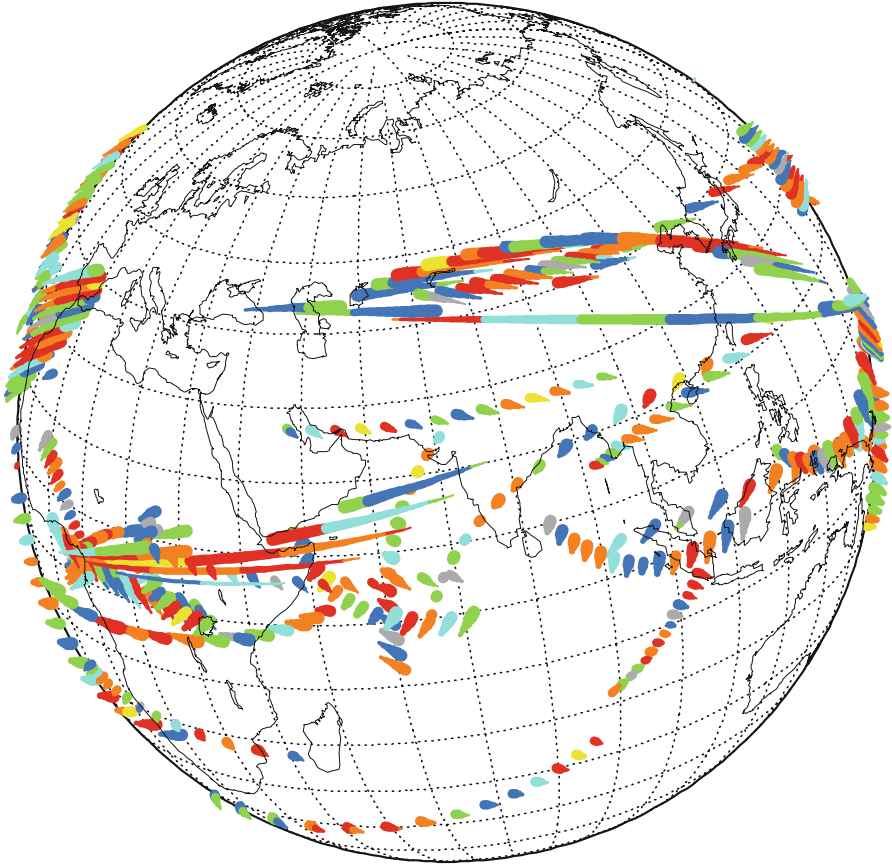


FIG. 14.24 : Locus of radio occultation between Megha-Tropiques and a Navstar/GPS satellite [PRN 16] over 14 days. Atmosphere crossed between 0 and 150 km. For the full caption, see Fig. 14.23 (lower).

the satellite Sputnik-1 could be very accurately determined by measuring the Doppler effect on radio frequencies. They then based their navigation principle on the opposite problem, i.e., if one knows the satellite position very accurately, one can use the Doppler effect to deduce the position of the receiver.

The US Navy, which was currently setting up the Polaris submarine missile launcher programme, took up this idea and developed the first global positioning system under the name of US Navy Navigation Satellite System (NNSS) or Transit. After sending up several experimental satellites in the 1960s, the system became operational in 1964 with the so-called NSS 30 constellation.

This comprised<sup>23</sup> satellites in circular polar orbit at altitude 1,000 km. The position of the receiver was calculated from successive measurements of the Doppler–Fizeau effect on the signal sent by the Transit satellite. This was only possible while the satellite was visible, i.e., at most 15 min per revolution (see Example 13.5). With six satellites, the user could see a satellite every 100 min at the equator, but every 35 min at high latitudes.

The user had to know his altitude, not precisely determined by this method, and it was important that he should not be moving too quickly. Under these conditions, position accuracy was 20 m. For a stationary observer with measurements over several days, accuracy could be brought down to 5 m.

The Transit system began in 1964 for military use, but was opened to the general public from 1967. Receivers cost around 1,000 US dollars and there were up to 80,000 users, mainly involved in maritime activities. It was officially closed down on 31 December 1996, after 32 years of service.

## 14.9.2 The Soviet System

The USSR was a long way behind the USA in the field of positioning systems. It was not until 1974 that they developed a system<sup>24</sup> called Parus that closely resembled Transit, then a civilian system called Tsikada, and

---

<sup>23</sup>The Transit satellites fall into five categories:

- The five experimental satellites, from Transit-1B, launched on 13 April 1960, to Transit-4A, launched on 29 June 1961, on similar orbits, with  $i = 66.7^\circ$ ,  $h_p = 625$  km,  $h_a = 1,080$  km.
- The ten prototype satellites in strictly polar orbit, from Transit-5A-1 on 18 December 1962 to Transit-5C-1 (OPS/4412) on 4 June 1964, with  $i = 90.0^\circ$ ,  $h = 1,100$  km. Transit-5B-1, launched on 28 September 1963, was the first satellite actually used by the US Navy.
- The 24 operational satellites in the Oscar series (O for “operational”), from Transit-O-1 (or NSS-30010, OPS/5798) on 6 October 1964 to Transit-O-25 (NSS-30250, NIMS-25, SOOS-4A) and Transit-O-31 (NSS-30310, NIMS-31, SOOS-4B), launched on 25 August 1988. The satellite Transit-O-13 (NSS-30130, OPS/7218) operated from September 1967 to January 1989.
- The three Triad satellites of the Transit Improvement Program (TIP): Triad-1 (or TIP-1), launched on 2 September 1972, Triad-2 (TIP-2), on 11 October 1975, and Triad-3 (TIP-3), on 1 September 1976, still on strictly polar orbits. These demonstrated the feasibility of the drag-free technique.
- The three Nova satellites, launched in this order: Nova-1 (NSS-30480) on 15 May 1981, Nova-3 (NSS-30500) on 12 October 1984, and Nova-2 (NSS-30490) on 16 June 1988, all on strictly polar orbits, with  $i = 90.0^\circ$ ,  $h = 1,180$  km.

Even after the end of the Transit programme, certain satellites of the Navy Ionospheric Monitoring System (NIMS) continued to operate, providing data on signal transmission through the ionosphere which could be used by the Navstar/GPS system.

<sup>24</sup>The Soviet system can be divided into three families of satellites:

- The 99 military satellites Parus (*parus* means “sail”), or Tsikada-M (M for “military”), from Parus-1 (Kosmos-700), launched on 26 December 1974, to Parus-99 (Kosmos 2463), on 27 April 2010.





FIG. 14.25 : *GPS beacon belonging to the network of the Corinth Rift Laboratory, near Galaxidi, Fokida, Greece, September 2012. Studying the region of high seismic activity in the Gulf of Corinth. Photo M.C.*

finally Nadezhda. This system was widely used from 1990 by the Russian merchant navy. It could localise boats to within 100 m. Russia closed down this operation in May 2007.

## 14.10 Appendix: GPS and Tectonic Plates

Inside the Earth, the radioactivity of certain rocks produces heat by nuclear decay. The upper regions of the mantle come up to the surface in a convective phenomenon to form the Earth's crust. As it cools, this magma becomes brittle and forms plates of thickness 10–100 km. The surface of the globe is thus made up of a set of these very large plates. For example, the MORVEL model (2011) is based on a set of 25 plates.

The plates move relative to one another. This is known as plate tectonic motion.<sup>25</sup> When these plates rub up against each other, it produces continental drift, which leads to earthquakes and volcanic activity.

- 
- Around 40 Tsikada satellites (this is the insect, the cicada), from Kosmos-883, launched on 15 December 1976, to Kosmos-2315, on 5 July 1995, on slightly elliptical near-polar orbits,  $i = 83^\circ$ ,  $h_p = 960$  km,  $h_a = 1,020$  km.
  - The 8 Nadezhda satellites (the word means “hope”), from Kosmos-1383 on 29 June 1982, then Nadezhda-1 on 4 July 1989 to Nadezhda-7 (Nadezhda-M-1) on 26 September 2002.

<sup>25</sup>The word “tectonic” was coined in Germany in 1850 from the Greek *tekton*, ὁ τέκτων, ονος, meaning “carpenter”. This Indo-European root \**tek*, “to produce”, appears in the Greek *technê*, ἡ τέχνη, ης, “handicraft” (giving “technical”) and the Latin *textor*, *oris*, “weaver”, *textus*, *us*, “tissue”, then “text”. This root is also found textually in the scientific formatting software  $\text{\TeX}$ , created by D. Knuth, and its successor  $\text{\LaTeX}$ .

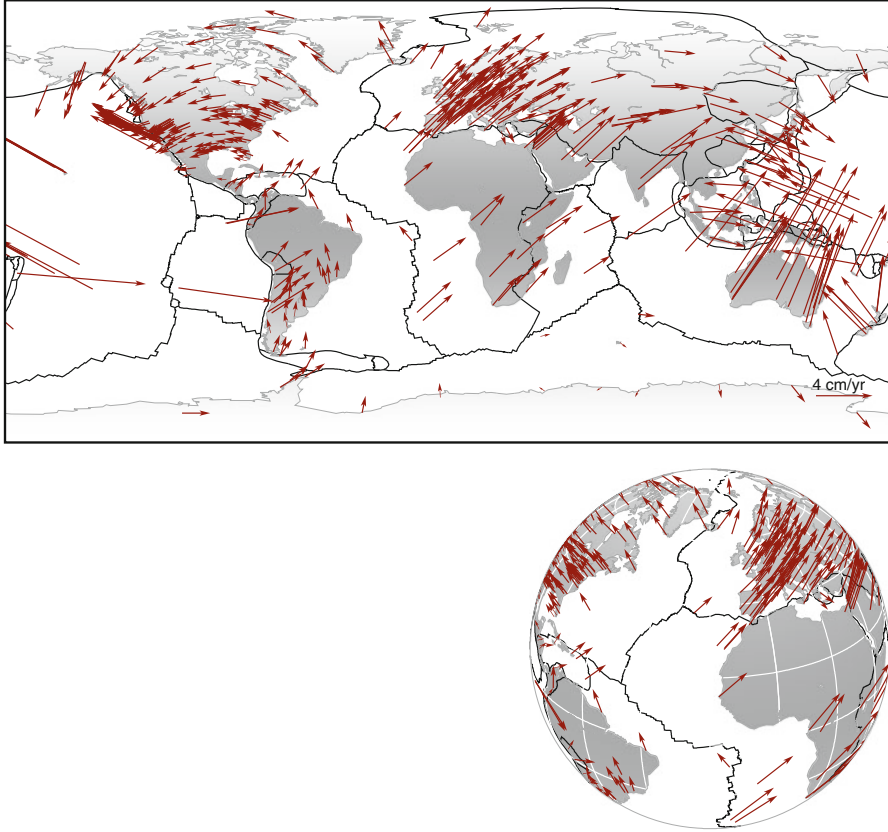


FIG. 14.26 : *Velocity field of horizontal displacements of the tectonic plates as published in the ITRF2008 definition document. Upper: Plane representation. The scale is indicated on the map. Lower: Orthographic representation centered on the Atlantic. These values were obtained mainly from fixed GPS beacons. Document provided by the authors: Zuheir Altamimi (LAREG/IGN), Xavier Collilieux (LAREG/IGN), Laurent Métivier (IPGP), Paris.*

In 1915, the German geophysicist Alfred Wegener had already developed his idea of continental drift on the basis of geographic, geological, and palaeontological considerations. Then from the 1970s, it became possible to corroborate the theory of tectonic plates with the help of geophysical measurements exhibiting changes in the orientation of the Earth's magnetic field in the ocean floor. It even became possible to estimate displacement rates.

But since 1992, these plate displacements have been measured directly using GPS. The technique of very long baseline interferometry (VLBI) and other techniques mentioned in Chap. 3 in the context of the ITRF, can be used

to obtain displacement rates to the same accuracy, but it is much simpler to set up a GPS beacon than a VLBI antenna.

At the present time, there are hundreds of GPS beacons distributed around the globe (many of them in California, for detailed surveillance of the San Andreas fault, and in Japan). On 1 January 2011, there were 6,000 beacons (see Fig. 14.25). Their absolute position is measured in the most accurate GPS mode. The displacement of each beacon can then be ascertained in latitude and longitude, and in the vertical by suitable statistical processing. The result is a map showing the displacements of the tectonic plates, as exemplified in Fig. 14.26.

Satellites over 20,000km away can thus measure absolute displacements of a few millimeters per year at the surface of the Earth. This is surely one of the most extraordinary scientific achievements of GPS.

## 14.11 Appendix: GPS and Relativity

### 14.11.1 Presentation

*Written in collaboration with Florent Deleflie.*

The relevance of the relativity theories to GPS was exhaustively and authoritatively investigated by Ashby right from the beginning, when this navigation system was first conceived. In this appendix,<sup>26</sup> we will not be adding anything fundamentally new to Ashby's work. Our aim is to make a didactic presentation of these relativistic corrections, to highlight the different orders of magnitude, and to demonstrate the effects or lack of effect of the latitude on certain corrections. For the latter point, we shall refer to Chaps. 2, 3, and 6.

These relativistic corrections are determined by understanding the behaviour of the clocks held by the emitter and the receiver, since they constitute the very basis of this navigation system. The setting here is thus the spacetime of Einstein's theories of relativity.

### 14.11.2 Proper Time Difference

A clock is a device for counting the periods of some repetitive phenomenon. The time scale associated with the clock is a measure of the extent to which the repetitive phenomenon has progressed (one tick of the clock corresponds to each instant on the time scale), allowing one to define a unit of time such as the second. A proper time interval is measured by counting a certain number of periods in the frame in which the clock is at rest. In a frame in which the clock is moving, this same number of periods defines a time interval called improper time.

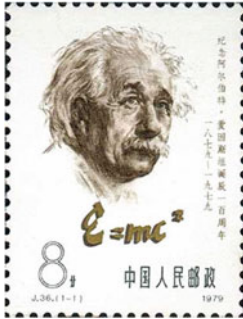
One part of the proper time difference results from the difference of speeds of the satellite and the receiver, and the other part comes from the difference in gravitational potential between the satellite and the receiver. The first effect, due to the speed difference, thus relates to the special theory of relativity (SR), while the second, due to the geopotential, is a term specifically predicted by the general theory of relativity (GR). The latitude of the receiver is relevant to both, due to the fact that the Earth is rotating and the fact that it is not spherical. We shall show that, when the two effects are added together, the latitude is no longer relevant.

### Special Relativity and Time Dilation

In the context of special relativity, Einstein's theory (Fig. 14.27) stipulates that the speed of light  $c$  is the same in every frame. This implies that two frames with relative speed  $V$  have time scales related by the Lorentz factor:

---

<sup>26</sup>We wish to thank Pierre Sagnou, Stephen Lyle, and Richard Kerner for helpful discussions.

FIG. 14.27 : *Albert Einstein.*

$$\Delta t_{\text{improper}} = \frac{1}{\sqrt{1 - (V/c)^2}} \Delta t_{\text{proper}} . \quad (14.24)$$

Let  $\Delta t'$  be the interval of time of 1 s for a body moving with velocity  $\mathbf{V}$  relative to an Earth-centered inertial (ECI) frame  $\mathfrak{R}$ , as defined in Chap. 3, i.e., the time interval between two ticks of the moving clock. The time interval of 1 s for the stationary body in  $\mathfrak{R}$  is denoted by  $\Delta t$ , i.e., the time interval between two ticks of the stationary clock. The Lorentz factor relates these two quantities. Expanding to first order the expression in (14.24), we have

$$\Delta t' \approx \left( 1 + \frac{V^2}{2c^2} \right) \Delta t . \quad (14.25)$$

Note that  $\Delta t' > \Delta t$ , implying that a moving clock always runs more slowly than a clock at rest.

The relative time variation  $\Theta_i^{\text{SR}}$  for a body  $i$ , moving at speed  $V_i$ , is given in special relativity by

$$\Theta_i^{\text{SR}} = \frac{\Delta t' - \Delta t}{\Delta t} = \frac{V_i^2}{2c^2} . \quad (14.26)$$

**(1) Satellite (SR).** Consider a satellite moving at velocity  $\mathbf{V}$  relative to an inertial frame  $\mathfrak{R}$ . Insofar as its orbital motion around the Earth can be treated as uniform (GPS satellite orbits are near-circular), the magnitude of its velocity will be constant and (14.24), which involves  $V^2$ , can be applied. We first consider the case where the orbit with semi-major axis is circular. In this case, (4.52) implies

$$\Theta_{\text{sat}}^{\text{SR}} = \frac{\mu}{c^2} \frac{1}{2a} . \quad (14.27)$$

**(2) Earth (SR).** The receiver clock is carried along by the Earth's rotation and is also in motion relative to  $\mathfrak{R}$ . We consider a clock at arbitrary geocentric latitude  $\psi$ , stationary relative to the Earth. As in Chap. 3,  $\varpi$  denotes the angular speed of the Earth's rotation. For an Earth treated as an ellipsoid of

revolution, with equatorial radius  $R$ , the dependence of the Earth radius  $R_\psi$  on  $\psi$  is given by (1.37). With the approximation given by (1.39), the speed  $V_\oplus(\psi)$  of a point of latitude  $\psi$  at the Earth's surface can be written

$$V_\oplus(\psi) = R_\psi \varpi \cos \psi \approx R \varpi (1 - f \sin^2 \psi) \cos \psi ,$$

and the relative variation due to the Earth's rotation with respect to  $\mathfrak{R}$  is thus

$$\Theta_\oplus^{\text{SR}} = \frac{V_\oplus^2}{2c^2} \approx \frac{\mu}{2Rc^2} m_a \cos^2 \psi (1 - 2f \sin^2 \psi) ,$$

using the dimensionless quantity  $m_a$  defined by (3.34). Since the quantities  $m_a$  and  $f$  are very small, the product  $m_a f$  can be neglected in a first order calculation, and the last formula simplifies to

$$\Theta_\oplus^{\text{SR}} \approx \frac{\mu}{2Rc^2} m_a \cos^2 \psi . \tag{14.28}$$

**(3) Satellite/Earth (SR).** To compare the clock aboard the satellite with the clock “aboard” the Earth, we write down the relative difference  $\Theta^{\text{SR}}$ , viz.,

$$\Theta^{\text{SR}} = \left. \frac{\Delta t'_{\text{sat}} - \Delta t'_\oplus}{\Delta t} \right|_{\text{SR}} = \left. \frac{\Delta t' - \Delta t}{\Delta t} \right|_{\text{sat}}^{\text{SR}} - \left. \frac{\Delta t' - \Delta t}{\Delta t} \right|_{\oplus}^{\text{SR}} .$$

The total effect due to time dilation is therefore the difference between the two values found previously:

$$\Theta^{\text{SR}} = \Theta_{\text{sat}}^{\text{SR}} - \Theta_\oplus^{\text{SR}} , \tag{14.29}$$

which gives in the present case

$$\Theta^{\text{SR}} = \frac{\mu}{2R c^2} \left( \frac{R}{a} - m_a \cos^2 \psi \right) . \tag{14.30}$$

This correction is always positive: the second for the satellite is always longer than the second for the receiver. This is a classic example of time dilation.

**General Relativity and Gravitational Blueshift**

We now consider the effects due to the gravitational potential as predicted by Einstein's general theory of relativity. The relation between proper and improper time is given by the Schwarzschild metric:

$$\Delta t_{\text{improper}} = \frac{1}{\sqrt{1 - (2U/c^2)}} \Delta t_{\text{proper}} , \tag{14.31}$$

where  $U$  is the gravitational potential. Expanding (14.31) to first order, we obtain

$$\Delta t' \approx \left( 1 + \frac{U}{c^2} \right) \Delta t . \tag{14.32}$$

Note that  $\Delta t' > \Delta t$ , implying that a clock runs all the more slowly as the gravitational potential increases.

The relative time variation  $\Theta_i^{\text{GR}}$  for a body  $i$ , subject to a gravitational potential  $U_i$ , is given in general relativity by

$$\Theta_i^{\text{GR}} = \frac{\Delta t' - \Delta t}{\Delta t} = \frac{U_i}{c^2}. \quad (14.33)$$

**(1) Satellite (GR).** For the satellite in circular orbit of radius  $a$ , the potential is

$$U = \frac{\mu}{a},$$

whence  $\Theta_{\text{sat}}^{\text{GR}}$  is given by

$$\Theta_{\text{sat}}^{\text{GR}} = \frac{\mu}{c^2} \frac{1}{a}. \quad (14.34)$$

**(2) Earth (GR).** For a point at the geocentric latitude  $\psi$  on the Earth's surface, assumed ellipsoidal again, the potential is given by (3.27) as

$$U_{\oplus}(\psi) = \frac{\mu}{R_{\psi}} \left[ 1 - J_2 \left( \frac{R}{R_{\psi}} \right)^2 \frac{3 \sin^2 \psi - 1}{2} \right].$$

Note that, in an inertial frame  $\mathfrak{R}$ , the surface of the ellipsoid (or geoid) is not an equipotential surface since the potential  $U_{\oplus}(\psi)$  depends on  $\psi$ .

Expressing  $R_{\psi}$  and neglecting terms in  $J_2 f$ , we deduce that

$$U_{\oplus}(\psi) = \frac{\mu}{R} \left[ 1 + \frac{1}{2} J_2 (1 - 3 \sin^2 \psi) + f \sin^2 \psi \right],$$

and we thus obtain

$$\Theta_{\oplus}^{\text{GR}} = \frac{\mu}{Rc^2} \left[ 1 + \frac{1}{2} J_2 + \sin^2 \psi \left( f - \frac{3}{2} J_2 \right) \right]. \quad (14.35)$$

**(3) Satellite/Earth (GR).** The relative time difference between the satellite and the Earth is therefore given by an expression analogous to (14.29) as

$$\begin{aligned} \Theta^{\text{GR}} &= \Theta_{\text{sat}}^{\text{GR}} - \Theta_{\oplus}^{\text{GR}} \\ &= \frac{\mu}{Rc^2} \left[ \frac{R}{a} - 1 - \frac{1}{2} J_2 - \sin^2 \psi \left( f - \frac{3}{2} J_2 \right) \right]. \end{aligned} \quad (14.36)$$

This is known as the Einstein effect or gravitational blueshift.<sup>27</sup>

---

<sup>27</sup>One also speaks of gravitational redshift, which simply reflects a change of perspective, swapping the emitter and the receiver.

### Sum of the Two Effects: Net Secular Effect

We now add together the two contributions, denoting the total by  $\Theta_1$  :

$$\Theta_1 = \Theta^{\text{SR}} + \Theta^{\text{GR}} ,$$

whereupon we obtain

$$\begin{aligned} \Theta_1 &= \frac{\mu}{Rc^2} \left[ \frac{3R}{2a} - \frac{1}{2}m_a \cos^2 \psi - 1 - \frac{1}{2}J_2 - \sin^2 \psi \left( f - \frac{3}{2}J_2 \right) \right] \\ &= \frac{\mu}{Rc^2} \left[ \frac{3R}{2a} - 1 - \frac{m_a + J_2}{2} - \sin^2 \psi \left( f - \frac{3J_2 + m_a}{2} \right) \right] . \end{aligned} \quad (14.37)$$

We now apply Clairaut's first relation (3.33), viz.,

$$J_2 = \frac{2}{3}f - \frac{1}{3}m_a ,$$

whence it transpires that the term in  $\sin^2 \psi$  in (14.37) cancels out. This means that the sum of the two relativistic corrections is in fact *independent of the latitude of the receiver*. Equation (14.37) can then be written

$$\Theta_1 = \frac{\mu}{Rc^2} \left( \frac{3R}{2a} - 1 - \frac{J_2 + m_a}{2} \right) . \quad (14.38)$$

This quantity is referred to in the literature as the net secular effect.

It is interesting to express  $\Theta_1$  in two parts:  $\Theta_{\text{sat}}$  concerning the satellite and  $\Theta_{\oplus}$  concerning the Earth. Equation (14.38) becomes

$$\Theta_1 = \Theta_{\text{sat}} - \Theta_{\oplus} , \quad (14.39)$$

with

$$\Theta_{\text{sat}} = \Theta_{\text{sat}}^{\text{SR}} + \Theta_{\text{sat}}^{\text{GR}} = \frac{3}{2} \frac{\mu}{ac^2} , \quad (14.40)$$

$$\Theta_{\oplus} = \Theta_{\oplus}^{\text{SR}} + \Theta_{\oplus}^{\text{GR}} = \frac{\mu}{Rc^2} \left( 1 + \frac{J_2 + m_a}{2} \right) . \quad (14.41)$$

In order to go further, expanding the potential to a higher degree, the calculations would become much more complex because other coefficients characterising the topography would have to be included to take into account the fact that the shape of the Earth is no longer treated as an ellipsoid of revolution, and this would make the expression for the centrifugal potential much more complex. This would nevertheless lead to a similar form for the results, although of course incorporating further coefficients such as  $J_4$ ,  $J_n$ , and so on, given that the surface of the rotating Earth remains an equipotential surface. We conclude that, on the geoid, the total relativistic correction is independent of the latitude.



## Numerical Application

**(1) Satellite: Calculation of  $\Theta_{\text{sat}}$ .** The dimensionless quantity  $\Theta_{\text{sat}}$  given by (14.40) is calculated for each satellite, depending on the value of  $a$ , and indicated in Table 14.6. For a Navstar/GPS satellite,

$$\Theta_{\text{sat}} = 2.50464 \times 10^{-10} . \quad (14.42)$$

**(2) Earth: Calculation of  $\Theta_{\oplus}$ .** The dimensionless quantity  $\Theta_{\oplus}$  given by (14.41) breaks down into three terms:

$$\begin{aligned} \frac{\mu}{Rc^2} &= 6.953485651 \times 10^{-10} , \\ \frac{\mu}{Rc^2} \frac{J_2}{2} &= 3.764014052 \times 10^{-13} , \\ \frac{\mu}{Rc^2} \frac{m_a}{2} &= \frac{\varpi^2 R^2}{2c^2} = 1.203436640 \times 10^{-12} , \end{aligned}$$

with total

$$\Theta_{\oplus(J_2)} = 6.969284031 \times 10^{-10} . \quad (14.43)$$

If we add the contribution from geopotential terms<sup>28</sup> up to  $J_{10}$  (the contribution from  $J_4$  to  $J_{10}$  is  $6.391 \times 10^{-16}$ ), it has the value

$$\Theta_{\oplus(J_{10})} = 6.969289401 \times 10^{-10} , \quad (14.44)$$

and up to  $J_{24}$ ,

$$\Theta_{\oplus(J_{24})} = 6.969290044 \times 10^{-10} . \quad (14.45)$$

This should be compared with

$$L_G = 6.969290134 \times 10^{-10} , \quad (14.46)$$

which is the value recommended by the International Astronomical Union (IAU) when calculating the terrestrial time (TT) scale,<sup>29</sup> as explained in

<sup>28</sup>Setting  $\psi = 0$  in the expansion of the geopotential [see (3.45)], we obtain

$$U_{\oplus} = \frac{\mu}{R} \left[ 1 - \left( -\frac{1}{2}J_2 + \frac{3}{8}J_4 - \frac{5}{16}J_6 + \frac{35}{128}J_8 - \frac{63}{256}J_{10} \right) \right] .$$

<sup>29</sup>The coordinated time in the geocentric spacetime system (TCG, *Temps coordonnée géocentrique*) differs from terrestrial time (TT) by a secular term:

$$\text{TCG} - \text{TT} = \Theta_{\oplus} \times \Delta D \times 86,400 \text{ s} ,$$

where  $\Delta D$  is the number of days elapsed since the date chosen as origin [see (6.147)].

Sect. 6.10 on astronomical constants, where  $L_G$  is the quantity denoted here by  $\Theta_{\oplus}$ .

**(3) Satellite/Earth: Calculation of Proper Time Differences.** Applying (14.39), we obtain the factor  $\Theta_1$  which characterises the relative time difference, with the numerical values given by (14.42) and (14.45) or (14.46):

$$\Theta_1 = +2.5046 \times 10^{-10} - 6.9693 \times 10^{-10} = -4.4647 \times 10^{-10} . \quad (14.47)$$

Over 1 day, the net secular effect is found to be

$$\delta t_1 = (\Delta t' - \Delta t)|_{1 \text{ day}} = -4.4647 \times 10^{-10} \times 86,400 = -38.574 \mu\text{s} . \quad (14.48)$$

This difference of 38.574  $\mu\text{s}$  per day in the propagation time of the signal corresponds to a distance of

$$\delta \ell = c \times \delta t_1 = 11.6 \text{ km per day} . \quad (14.49)$$

Clearly, if these relativistic corrections were not taken into account,<sup>30</sup> there would be errors of several hundred meters every hour. Table 14.6 summarises these numerical results for the four types of navigation satellites (GNSS).

**(4) Note on Satellite Altitudes.** The quantity  $\Theta_1$  given by (14.38), which represents the sum total of all these effects, vanishes for a certain value  $a_1$  of the orbital radius equal to roughly  $3R/2$ . More precisely,

$$a_1 = \frac{3}{2} \left( 1 + \frac{J_2 + m_a}{2} \right)^{-1} R \approx \frac{3}{2} \left( 1 - \frac{J_2 + m_a}{2} \right) R ,$$

or an altitude  $h_1$  given by

$$h_1 = a_1 - R = \left[ 1 - \frac{3(J_2 + m_a)}{2} \right] \frac{R}{2} = 0.4966R = 3,167 \text{ km} . \quad (14.50)$$

---

<sup>30</sup>Neil Ashby tells the following story:

At the time of launch of the NTS-2 GPS-precursor satellite (23 June 1977), which contained the first cesium atomic clock to be placed in orbit, there were some who doubted that relativistic effects were real effects that had to be accounted for. A frequency synthesizer was built into the satellite clock system so that after launch, if in fact the rate of a clock in its final orbit were predicted by general relativity, then the synthesizer could be turned on, bringing the clock to the coordinate rate necessary for operation. After one of the cesium atomic clocks was turned on in NTS-2, it was operated for about 20 days to measure its clock rate before turning on the synthesizer. The frequency measured during that period was +442.4 parts in  $10^{12}$  compared to the ground, while relativity theory predicted +446.47 parts in  $10^{12}$ . The discrepancy was only about four parts in  $10^{12}$ , well within the accuracy capabilities of the orbiting clock.

The orbit of NTS-2 was described in section “Main Dates”.

$u = \mu/Rc^2$	Special relativity	General relativity	Total
Satellite	$(R/a)/2 = 0.120066$	$R/a = 0.240133$	0.360199
Earth [E]	$m_a/2 = 0.001731$	$1 + J_2/2 = 1.000541$	1.002272
Earth [P]	$0 = 0.000000$	$1 - f + J_2 = 1.002272$	1.002272
Satellite/Earth [E]	0.118335	-0.760408	-0.642073
Satellite/Earth [P]	0.120066	-0.762139	-0.642073

TABLE 14.5 : Values arising when calculating the relativistic corrections for the satellite Navstar/GPS. Abbreviations: [E] = equator, [P] = pole. Units used here are  $u = \mu/Rc^2$ . To obtain the value of  $\Theta_i^j$ , the values in the table should be multiplied by  $\mu/Rc^2 = 6.95348565 \times 10^{-9}$ .

Note that:

- If  $h < h_1$ , the special relativistic effect dominates and  $\Theta_1 > 0$ .
- If  $h > h_1$ , and this goes for the GPS satellites, the general relativistic effects dominate and  $\Theta_1 < 0$ .

### Summary of Corrections

Table 14.5 summarises the values of the quantities  $\Theta_i^j$ :

$$\text{Satellite in } \mathfrak{R} \implies \Theta_{\text{sat}}^{\text{SR}} + \Theta_{\text{sat}}^{\text{GR}} = \Theta_{\text{sat}}$$

$$\text{Earth in } \mathfrak{R} \implies \Theta_{\oplus}^{\text{SR}} + \Theta_{\oplus}^{\text{GR}} = \Theta_{\oplus}$$

$$\text{Satellite relative to the Earth} \implies \Theta^{\text{SR}} + \Theta^{\text{GR}} = \Theta_{\text{sat}} - \Theta_{\oplus} = \Theta_1 .$$

Taking out the factor  $\mu/Rc^2$  used as unit in Table 14.5 and for the remarks below makes it easier to interpret the results and leads to the following conclusions:

- The main term is  $\Theta_{\oplus}^{\text{GR}} \approx 1$ , general relativistic term for the Earth.
- The terms concerning the satellite,  $\Theta_{\text{sat}}^{\text{SR}} \approx 0.1$  and  $\Theta_{\text{sat}}^{\text{GR}} \approx 0.2$ , give a sum equal to around one third of the main term  $\Theta_{\oplus}^{\text{GR}}$ .
- The term  $\Theta_{\oplus}^{\text{SR}}$  is negligible in a first approximation.

We find the value calculated in (14.38) with

$$\begin{aligned} \Theta_1 &= -0.642073 \frac{\mu}{Rc^2} = -0.642073 \times 6.95348565 \times 10^{-9} \\ &= -4.4647 \times 10^{-10} . \end{aligned} \tag{14.51}$$

### Corrections for GPS

The overall relativistic effect referred to as the net secular effect corresponds to a relative clock variation whose value, given by (14.38), is calculated

using (14.47) or (14.51) for Navstar/GPS. The Navstar/GPS documentation indicates a correction

$$\Theta_1^{\text{GPS}} = -4.464733 \times 10^{-10} .$$

This correction is made directly by the satellite, by modifying the nominal frequency emitted by its clock. While the basic frequency of the GPS signal is given as [see (14.23)]

$$f_0 = 10.23 \text{ MHz} ,$$

the frequency  $f_0^{\text{em}}$  actually emitted is

$$\begin{aligned} f_0^{\text{em}} &= 10.23 \times (1 + \Theta_1^{\text{GPS}}) \\ &= 10.23 \times (1 - 4.464733 \times 10^{-10}) \\ &= 10.2299999954326 \text{ MHz} . \end{aligned} \tag{14.52}$$

With this value, the signal received on Earth by the receiver has the same frequency as if the satellite clock were situated on the geoid.

### 14.11.3 Effect Due to Orbital Eccentricity

The main idea here is to study the effects of variations in speed induced by the eccentricity  $e$  of the orbit, which is typically of the order of  $10^{-3}$  for GNSS satellites. This implies a change in the speed and the potential in the previous equations, replacing  $a$  by  $r$ . We thus consider the value of  $\Theta_1$  as given by (14.38), depending on whether  $e$  is zero (denoted by  $\Theta_{2c}$  for a circular orbit, and corresponding exactly to  $\Theta_1$ ) or not (denoted by  $\Theta_{2e}$  for an eccentric orbit). The difference between  $\Theta_{2e}$  and  $\Theta_{2c}$  then measures the effect on the relative time difference due to  $e$ . With (4.39), we obtain

$$\Theta_2 = \left. \frac{\Delta t' - \Delta t}{\Delta t} \right|^{ecc} = \Theta_{2e} - \Theta_{2c} = \frac{2\mu}{c^2} \left( \frac{1}{r} - \frac{1}{a} \right) . \tag{14.53}$$

We see that  $\Theta_2$  varies over an orbital period from a minimal value at the apogee to a maximal value at the perigee, depending on the value of  $r$ .

Using the eccentric anomaly  $E$  defined in (4.64), we find that (14.53) becomes

$$\Theta_2 = 2 \frac{\mu}{c^2} \frac{1}{a} \frac{e \cos E}{1 - e \cos E} . \tag{14.54}$$

This relative difference will show up during one revolution as a gain or loss of time, with extrema at the apogee and perigee. Appealing to (4.79), which relates  $E$  and  $M$ , we integrate (14.54) with respect to time to obtain a quantity with units of time:

$$\begin{aligned}\Delta t_{\text{ecc}}(t) &= \frac{2\mu}{c^2 a} \int \frac{e \cos E}{1 - e \cos E} (1 - e \cos E) \sqrt{\frac{a^3}{\mu}} dE \\ &= 2 \frac{\sqrt{\mu a}}{c^2} e \sin E .\end{aligned}\tag{14.55}$$

The integration constant is set to zero (it can be included in the clock offsets, which disappear after applying the Kalman filter). During one revolution, the time difference will therefore vary between the extreme values of  $\Delta t_{\text{ecc}}$ , denoted by  $-\delta t_2^{\text{max}}$  and  $+\delta t_2^{\text{max}}$ , where

$$\delta t_2^{\text{max}} = 2 \frac{\sqrt{\mu a}}{c^2} e .\tag{14.56}$$

With (4.68), we note that (14.55) can be written in the form

$$\Delta t_{\text{ecc}}(t) = \frac{2r\dot{r}}{c^2} .\tag{14.57}$$

### Numerical Application

For Navstar/GPS, we obtain

$$\delta t_2^{\text{max}} = 2.2897 \times 10^{-6} e .\tag{14.58}$$

If we take  $10^{-3}$  as a realistic value for the eccentricity,<sup>31</sup> for a GNSS satellite, we find

$$\delta t_2^{\text{max}} = 2.29 \text{ ns} .$$

This is very small compared with the previous effects. It corresponds to a maximal positioning error broadcast by the satellite of the order of a few meters (depending on the exact value of  $e$ ) (see Table 14.6).

### Corrections for GPS

This second effect, due to the geometry of the ellipse (residual periodic effect) is of the order of a few nanoseconds, but varies during a revolution in a way that depends on the orbital elements  $a, e, E$  of the satellite. The correction is transmitted by each satellite ( $e$  differing from one satellite to another). The correction is applied by the receiver.

---

<sup>31</sup>Ever since N. Ashby took  $e = 0.02$  as an example, which gives  $\Delta t = 46$  ns, all documents treating this question have reproduced this result of 46 ns. We note that the eccentricity  $e$  never reaches such a value for navigation satellites placed in orbit since the historic period of the first Navstar/GPS satellite launches.

	Units	Navstar/GPS	Glonass	Galileo	BeiDou NS
$a$	km	26,560.9	25,507.6	29,600.3	27,905.8
$e$	–	$\approx 0.0060$	$\approx 0.0005$	$\approx 0.0005$	$\approx 0.0005$
$V$	km/s	3.873891	3.953066	3.669620	3.779393
$T$	min	717.978	675.735	844.685	773.200
$R/a$	–	0.2401326	0.2500485	0.2154754	0.2285595
$\Theta_{\text{sat}}$	$10^{-10}$	2.50464	2.60806	2.24746	2.38393
$\Theta_{\oplus}$	$10^{-10}$	6.96929	6.96929	6.96929	6.96929
$\Theta_1$	$10^{-10}$	-4.46465	-4.36123	-4.72183	-4.58536
$\delta\ell$	km	11.6	11.3	12.3	11.9
$\delta t_1$	ns	-38,574.6	-37,681.0	-40,796.6	-39,617.4
$\delta t_2^{\text{max}}$	ns	13.7	1.1	1.2	1.2
$\delta t_3^{\text{max}}$	ns	133.4	127.8	149.6	140.6

TABLE 14.6 : Comparison of relativistic effects for the four types of navigation satellite (GNSS).  $a$  semi-major axis of the orbit,  $e$  eccentricity,  $V$  average speed of satellite,  $T$  nodal (draconitic) period,  $R$  equatorial radius.  $\Theta_i$  relative value of the difference between the proper time (in the ECI frame  $\mathfrak{R}$ ) and improper time.  $\Theta_{\text{sat}}$  is the value of  $\Theta_i$  for the satellite (relative to  $\mathfrak{R}$ ), defined by (14.40), and  $\Theta_{\oplus}$  is the value of  $\Theta_i$  for the Earth (relative to  $\mathfrak{R}$ ), the same for all satellites, defined by (14.41) and calculated using (14.45), defined by the IAU by (14.46) or (6.147).  $\Theta_1 = \Theta_{\text{sat}} - \Theta_{\oplus}$ , defined by (14.38) and calculated using (14.47).  $\delta\ell$  maximal daily error, distance defined by (14.49).  $\delta t_1$  daily proper-improper time difference, defined by (14.48).  $\delta t_2^{\text{max}}$  maximal proper-improper time difference, defined by (14.56) for each revolution of the satellite, relating to the orbital geometry and calculated here for the eccentricity indicated in the row for  $e$ .  $\delta t_3^{\text{max}}$  absolute value of the maximal proper-improper time difference for each revolution of the satellite, due to the Sagnac effect and defined by (14.64). Units are given in the first column. A dash indicates dimensionless quantities.

### 14.11.4 Sagnac Effect

The Sagnac effect arises from the non-inertial nature of the frame in which the receiver is at rest. Consider a receiver located at a point  $A$  of the Earth at time  $t_1$ , the instant of emission of the signal by the satellite  $S$ . The signal reaches the receiver at some time  $t_2$ , when it is located at a different point  $A'$  of the inertial frame  $\mathfrak{R}$  ( $A \neq A'$ ), as shown in Fig. 14.28. During the time lapse  $t_2 - t_1$ , the receiver has been displaced through  $\mathbf{AA}'$ .

A geometric approach can be used to calculate the time difference due to the Sagnac effect:

$$\Delta t|_{\text{Sagnac}} = \frac{\mathbf{SA} \cdot (\varpi \mathbf{e}_z \wedge \mathbf{OA})}{c^2}, \tag{14.59}$$

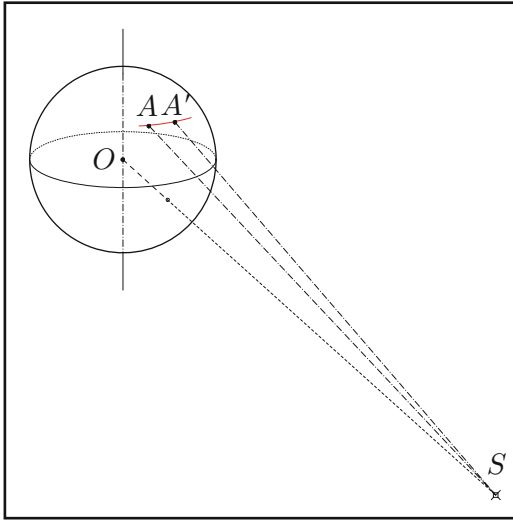


FIG. 14.28 : Earth/satellite geometry involved in the Sagnac effect. Satellite  $S$ , center of the Earth  $O$ . The point  $A$  has moved to  $A'$  in an inertial frame during the time taken for the signal to be transmitted from  $S$  to  $A$ .

where  $\varpi \mathbf{e}_z$  is the angular velocity of the Earth's rotation. We note that the Sagnac effect is zero if the satellite is in the meridian of the point  $A$ , with  $\mathbf{AA}'$  pointing to the east. Its sign depends on the relative direction of the satellite as viewed from the receiver. It is positive before entering the meridian plane containing the satellite (hence to the west), then negative.

Equation (14.59) is then written in the form

$$\Delta t|_{\text{Sagnac}} = 2 \frac{\varpi}{c^2} \mathbf{e}_z \cdot \mathbf{T}, \quad (14.60)$$

where

$$\mathbf{T} = \frac{1}{2} \mathbf{OA} \wedge \mathbf{SA},$$

with  $\mathbf{T}$  the directional area of the triangle  $SOA$ .

For the Earth, we define the quantity  $\mathcal{S}_{\oplus}$  by

$$\mathcal{S}_{\oplus} = 2 \frac{\varpi}{c^2} = 1.62271 \times 10^{-21} \text{ s m}^{-2} = 1.62271 \times 10^{-6} \text{ ns km}^{-2}, \quad (14.61)$$

and then

$$\Delta t|_{\text{Sagnac}} = \mathcal{S}_{\oplus} \mathbf{e}_z \cdot \mathbf{T}. \quad (14.62)$$

The Sagnac effect is given by the scalar product of the vector  $\mathcal{S}_{\oplus} \mathbf{e}_z$  along the polar axis and the vector  $\mathbf{T}$  normal to the surface (directional area), which delivers the projected area of this triangle in the equatorial plane multiplied by the coefficient  $\mathcal{S}_{\oplus}$ .

The maximal value  $\delta t_3^{\max}$  of the Sagnac effect can be evaluated. It corresponds to the maximal possible area of the projection of the triangle  $SOA$ . This situation arises when  $S$  lies in the equatorial plane of the Earth and  $A$  appears at the limb for  $S$ . The triangle  $SOA$  is then right-angled at  $A$ , with  $a = OS$  and  $R = OA$ , whence

$$T_{\max} = \|\mathbf{T}\|_{\max} = \frac{1}{2}R\sqrt{a^2 - R^2} ,$$

and

$$\delta t_3^{\max} = \mathcal{S}_{\oplus} \times T_{\max} . \tag{14.63}$$

### Numerical Application

For a Navstar/GPS satellite,  $T_{\max} = 8.221 \times 10^7 \text{ km}^2$ , which gives the maximal value of the Sagnac effect as

$$\delta t_3^{\max} = 1.62271 \times 10^{-6} \times 8.221 \times 10^7 = 133.4 \text{ ns} . \tag{14.64}$$

See Table 14.6.

### Corrections for GPS

This third effect is due to the geometry of the Earth–satellite configuration. The correction is therefore necessarily applied by the receiver.

#### 14.11.5 Conclusion

Relativistic effects can be classified into three categories:

- **Time Dilation.** A transported clock, in this case on the satellite, runs more slowly than one at rest on the Earth, in this case, the receiver clock. This effect is solely a function of the satellite velocity.
- **Blueshift Effect.** The transported clock runs faster than the one on the Earth. This effect is solely a function of the satellite altitude.
- **Sagnac Effect.** The transported clock runs more slowly or faster than the one on the Earth. This effect depends on the relative position of the satellite and the terrestrial meridian of the receiver.

Several other effects are mentioned in the literature as relevant in the orbits of artificial satellites, including geodesic precession, the Lense–Thirring effect, and the Schwarzschild correction. The Shapiro effect is another phenomenon affecting the transmission of the signal. Taken together, all these effects modify the propagation time by a few picoseconds per day.



# Chapter 15

## Satellites of Mars

### 15.1 Presenting the Planet Mars

#### 15.1.1 Mars and Space Exploration

If we compare the Earth with its two neighbours, it has something in common with Venus on the next orbit in toward the Sun, and that is its size. However, it is with the next planet out, moving away from the Sun, that the Earth has most affinity, because two fundamental parameters, namely, the length of day and the obliquity, have very similar values for these two planets.

Like the Earth, Mars exhibits climatic phenomena, with winter and summer, sandstorms, and permanent ice at the poles. These seasonal phenomena have long been observed by astronomers, as can be seen from the drawings by Huygens in 1672. The atmosphere of Mars (to which we shall return shortly) is in fact rather transparent in the visible, while this is not at all the case for Venus.<sup>1</sup> The fact that Mars is further away from the Sun, about 1.5 astronomical units further away than the Earth, means that it is much colder (the greenhouse effect due to the atmosphere is much less pronounced), and the year is almost twice as long.

The planet has been observed since ancient times. It doubtless owes its association with the god of war to its red colour: Ares for the Greeks<sup>2</sup> (ὁ Ἄρης, εὠς, giving the prefix *areo-* for attributes pertaining to this planet), and Mars for the Romans. Later, telescopic observation revealed some detail on its surface and it was suggested that Martians had been digging canals.

---

<sup>1</sup>On Venus, with a very dense atmosphere and extreme greenhouse effect, temperatures are always very high, both day and night, whatever the season or the latitude. The atmosphere is moving, always in the same direction, following the rotation of the planet in a motion known as super-rotation. The winds are very strong at high altitudes, but much less so near the surface.

<sup>2</sup>*Ares* literally means “warrior, male”, from the Indo-European root \**ar*, meaning “to take, destroy, cause something to perish”.

In the twentieth century, more precise telescopic observations were improved still further by data from probes at the beginning of the space age.

### Space Exploration: The USSR and Russia

In October 1960, the USSR attempted to send two probes (sometimes called Marsnik-1 and -2), just 3 years after the first Sputnik, to overfly Mars. However, they exploded at launch. (In fact it is not clear whether there were one or two probes.) All 14 subsequent probes failed, either at launch or later by loss of contact: Sputnik-29, Mars-1 (which was the first probe to approach Mars, but silent) and Sputnik-31 in 1962, Zond-2 and -3 in 1965, two probes without clearly attributed names (Mars-1969-A and -B) in 1969, Kosmos-419, Mars-2 and -3 in 1971, Mars-4, -5, -6, and -7 in 1973. Note that Mars-2 crashed, but it was the first manmade object to touch Mars, while Mars-3 and Mars-6 seem to have soft-landed, but contact was lost after a few seconds. Attempts resumed 15 years later, with Phobos-1 and -2, launched in July 1988. The mission was to observe the moon Phobos from an orbit around Mars. The probe Phobos-2 came very close to Phobos, then stopped transmitting. The USSR clocked up 17.5 failures out of 18 attempts!

Mars was a forbidden planet for the Soviets and it remained so for the Russians. The mission Mars-96 ended in the Pacific on 16 November 1996, the day of its launch. The same happened in 2011 with the very ambitious mission Phobos-Grunt. The probe was supposed to go into a near-circular equatorial orbit around Mars, thereby approaching Phobos on its orbit, land on it (hence the mission name *grunt*, which means “ground” in Russian), make observations, take samples, and finally return to Earth! The departure was planned for November 2011, with the return to Earth in 2014. But unfortunately, launched on 8 November 2011, the probe remained blocked in Earth orbit and ended up like its predecessor in the Pacific. So Russia’s Mars exploration has seen two failures in two attempts!

### Space Exploration: The USA

The United States launched Mariner-3 and -4 in November 1964. The first probe was lost, but Mariner-4 overflew Mars and sent back the first photographs (21 in all) on 14 July 1965. Launched in February and March 1969, the probes Mariner-6 and -7 overflew the Red Planet and provided a great many photographs. And launched in May 1971 (like Mariner-8, lost at launch), the probe Mariner-9 was the first to go into orbit around the planet ( $h_p = 1,650$  km,  $h_a = 17,100$  km,  $T \approx 12$  h) on 14 November 1971. Up until 27 October 1972, it sent back 7,329 photographs which completely changed our understanding of Mars.

The two probes Viking-1 and -2, launched in August and September 1975, also successfully accomplished their missions (see Fig. 15.1 upper left). For each probe, there was an orbiter and a lander. The landers transmitted data concerning the Martian atmosphere and surface over several Martian years.

The next probe, 17 years after Viking, was the first not to be sent in tandem. This was Mars Observer, launched on 25 September 1992, lost as it was being placed in orbit around Mars.

The probe known as Mars Global Surveyor (MGS), launched on 7 November 1996, took with it many of the instruments designed for the previous mission. It went into orbit around Mars after a 10 month journey to reach its destination at 14 light-minutes from the Earth (Mars orbit insertion MOI). The orbit of MGS was made circular by aerobraking (or air braking).<sup>3</sup> It was also the first Sun-synchronous Martian orbit. The instrument MOLA provided a very accurate topographical study of Mars whose results will be used here. The camera MOC took photographs with a resolution of a few meters on the ground (see Fig. 15.1 lower left).

Launched on 4 December 1996, the probe Mars Pathfinder made an opportune soft-landing on 4 July 1997 and released the microrover Sojourner, which subsequently investigated the immediate vicinity of the landing site.

The orbiter and lander of the Mars Surveyor-98 programme both failed. Concerning the orbiter, the probe Mars Climate Orbiter, launched on 11 December 1998, was lost due to an erroneous correction to its trajectory on 23 September 1999, as it approached Mars. As for the lander, Mars Polar Lander (MPL), launched on 3 January 1999, it went silent on 3 December 1999, just as it arrived on Mars. Contact was lost with the probe and the two Deep Space-2 penetrators.

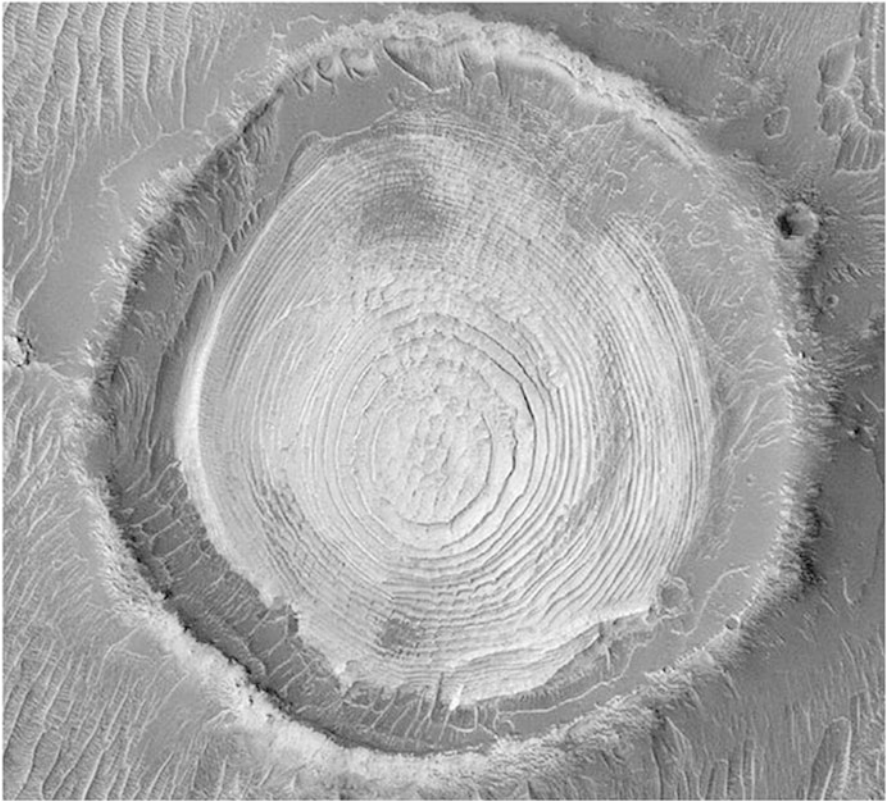
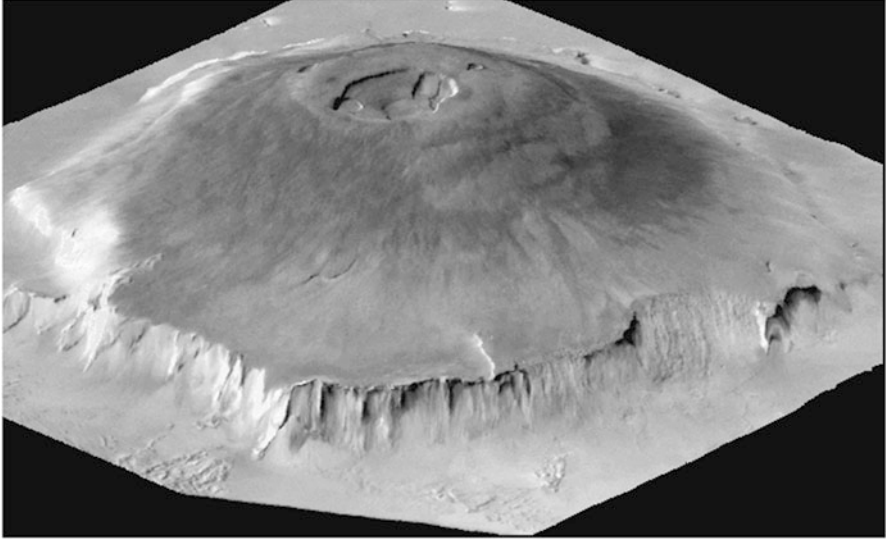
The probe Mars Odyssey was launched on 7 April 2001 and reached Mars on 24 October. The orbit was made circular by aerobraking and became Sun-synchronous and operational on 30 January 2002. Mars Odyssey (2001, a space odyssey to Mars!) mapped the distribution of chemical elements and minerals on the Martian surface. It revealed the presence of large amounts of water ice just a few centimeters beneath the surface in regions of high latitude (above 55°N and 55°S, see Figs. 15.14 and 15.16).

The two American probes known as Mars Exploration Rovers, MER-A and -B, which left on 10 June and 8 July 2003, arrived on 4 and 25 January 2004, dropping the two rovers Spirit and Opportunity, each weighing in

---

<sup>3</sup>The probe, whose motion is mainly governed by the planetary attraction, goes into a highly eccentric orbit with one focus at the center of the planet. To obtain a circular orbit, one uses the drag of the planetary atmosphere on the spacecraft. The satellite loses energy, mainly at the periastron, since this is where it moves most quickly and there is the most atmosphere. The apoastron is thus reduced upon each revolution. This maneuver is known as aerobraking. It has the disadvantage of being very slow. In fact it takes several months. However, it is very economical in terms of energy. Since it does not require use of retro rockets, there is no need to carry propellant. And it is well known that it costs a great deal of propellant to take on extra propellant.

This technique was used for the three US missions in Sun-synchronous orbit: MGS over 850 revolutions (and hence as many periastron passages), Mars Odyssey over 300 revolutions, and MRO over 425 revolutions. The first experiments with aerobraking were made by Magellan around Venus, at the end of its mission in 1993, with a view to testing the technique (see Chap. 16).



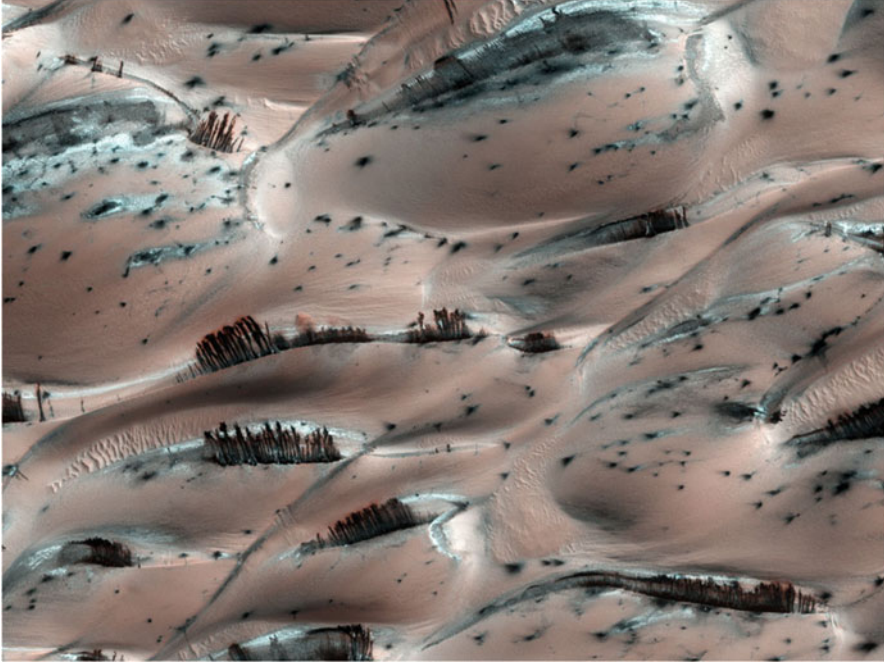


FIG. 15.1: *The images on these two pages show the improving accuracy of pictures of Mars. Upper left: The volcano Olympus Mons. Image reconstructed numerically from images obtained by the Viking orbiter. Altitudes are multiplied by a factor of 10. Credit: JPL/NASA. Lower left: Crater of diameter 2.3 km in the Schiaparelli Basin. With the light coming from the left, the central layer seems to lie above the others. The crater may have been filled with water in the remote Martian past. However, another hypothesis is that these layers may have formed from deposits of sand carried by the wind, as in a stratified dune. Image taken on 3 June 2003 by the camera MOC aboard the MGS. Credit: Malin Space Science Systems (MOC), MGS, JPL/NASA. Upper right: Sand cascades. These are not rows of poplar trees planted in the Sahara! In the spring, near the Martian North Pole, the Sun's rays sublime a thin layer of carbon dioxide snow ( $\text{CO}_2$ ) which covers the dunes. These rays pass through the transparent ice and heat it from the base. The carbon dioxide ice then sublimates, producing geysers which drag up the underlying black sand. When it falls back onto the surrounding ice, the relatively hot sand grains on the carbon dioxide ice are as though in levitation in a phenomenon known as calefaction. They tumble down the slightest slope in a cascade, leaving parallel dark tracks behind them. This image was photographed using the HiRISE camera aboard MRO (25 cm/pixel, field covered 1 km) in April 2008. Credit: HiRISE, MRO, LPL (University of Arizona), NASA.*



at around 180 kg. Designed to operate for a few months, both vehicles significantly exceeded expectations, exploring plains, craters, and hills. Spirit ceased to function on 30 March 2008 after having travelled 7 km, while Opportunity, successfully avoiding damaging intake of sand from the dunes and other pitfalls, has gone on to cover a distance of 37 km in 9 years. In 2013, Opportunity is exploring the flanks of the great crater Endeavour with its diameter of 22 km, and will continue its route southward.

The probe Mars Reconnaissance Orbiter (MRO) was launched on 12 August 2005 and arrived on 11 March 2006. Its orbit was circularised by aerobraking and took its definitive Sun-synchronous, near-circular form with  $h \sim 300$  km. The camera HiRISE took extremely accurate photos [see Figs. 15.1 (upper right) and 15.33]. The mission brought much to our understanding of the role played by water in Mars' past, not to mention the climate in general.

In 2007, the mission known as Phoenix saw part of the MPL and MSP'01 missions rise from the ashes. Launched on 4 August 2007, the probe landed in the high northern latitudes of the planet, on 25 May 2008, placing a lander at a latitude of  $68^\circ\text{N}$ . Phoenix arrived at the end of spring (solar longitude  $L_S = 76^\circ$ , explained below) and operated until 2 November 2008 ( $L_S = 151^\circ$ ), before the end of the northern Martian summer. Phoenix confirmed the presence of water ice in the Martian ground at this location, using its mechanical arm equipped with a spade to uncover the ice beneath a few centimeters of sand. In 2010, the probe MRO formed an image of the Phoenix site. It was observed that the station, which had spent several months under the carbon dioxide ice, had lost a solar panel and was covered with dust.

The mission known as Mars Science Laboratory (MSL) includes a rover, devoted to geology and climatology. Launched on 26 November 2011, the probe arrived on Mars on 6 August 2012 and deployed<sup>4</sup> the rover with great accuracy (2 km error in distance and 1 s in time) at the chosen site.<sup>5</sup> This six-wheeled exploration vehicle called Curiosity has the size of a small car and a mass of 890 kg. It runs on a radioisotope thermoelectric generator (4.8 kg of plutonium dioxide,  $\text{PuO}_2$ , enriched with plutonium 238) which should ensure a lifetime of at least one Martian year, and probably much longer.<sup>6</sup> After a year of operation, the scientific results have already been spectacular.

---

<sup>4</sup>The method selected for the final descent through the atmosphere and release of the rover was new and highly technical (some said, very acrobatic and risky), using a retro rocket and parachute for the last part of the maneuver.

<sup>5</sup>Of 30 sites proposed in 2006, only 4 were shortlisted. Then in July 2011, Gale Crater was finally selected, at an altitude of  $-4.5$  km. The images provided by MRO were used to specify the exact landing site.

<sup>6</sup>The solar energy available on Mars was judged inadequate for this experiment. In fact, the solar constant on Earth is  $C_0^{\text{Earth}} = 1,367 \text{ W m}^{-2}$  (outside the atmosphere). If  $a_S = 1.524 \text{ a.u.}$  is the semi-major axis of the Mars orbit, we find that the solar constant on Mars (outside the atmosphere) is

$$C_0^{\text{Mars}} = C_0^{\text{Earth}} a_S^{-2} = 592 \text{ W m}^{-2} .$$

The Mars Atmosphere and Volatile Evolution (MAVEN) mission is dedicated to the study of the upper Martian atmosphere and its interaction with the solar wind, to understand how Mars may have lost most of its primordial atmosphere. Launch is expected between 18 November and 7 December 2013, with orbit insertion on 16 September 2014. The final orbit, inclined at  $75^\circ$  and elliptical with  $e = 0.46$ , will have a low periastron at  $h_p = 150$  km, with five deep-dip overpasses planned at 125 km.

### Space Exploration: Europe and Other Nations

Europe has had only one mission, but it has been an enormous success. The ESA probe Mars Express, launched on 2 June 2003, went into orbit on 25 December.<sup>7</sup> The seven instruments aboard have perfectly fulfilled their many missions of accurate photography and studies of minerals, the atmosphere, and the interaction of the solar wind with the planet (see Fig. 15.20). Ten years on, Mars Express is still sending back data.

Concerning the ExoMars-TGO programme, the ESA and NASA had planned to join forces. In fact, ExoMars had been envisaged by the ESA and the Trace Gas Orbiter (TGO) by NASA. However, NASA withdrew from the project after committing itself to the programme. At the present time, the ESA project is being carried out in collaboration with the Russian space agency Roskosmos. In 2016, the TGO probe will drop a 600 kg lander before going into orbit, and in 2018, the ESA rover Exomars should be soft-landed using a system that has been largely developed by the Russian team.

For the TGO, launch is planned for January 2016, with orbital insertion on 19 October 2016. The orbit will be circularised by aerobraking, with  $h = 400$  km,  $i = 74^\circ$ . The choice of inclination results from a compromise: high enough to be able to view the poles, but low enough to allow rapid local time sampling,<sup>8</sup> thanks to a high nodal precession rate (see Example 15.2).

Japan hoped to place its probe Nozomi (hope) in orbit, but failed.<sup>9</sup> In November 2013, India will launch the probe Mangalyaan (*Mangala* is the name for the planet Mars in Sanskrit, and *yaan* means “vessel”). This should go into a highly eccentric orbit around Mars, with  $h_p = 372$  km,  $h_a = 80,000$  km.

---

Taking into account the eccentricity  $e = 0.0934$  of the orbit, the Martian value of the constant lies between a minimum at aphelion of  $C_0^{\text{Mars}} [a_S(1 + e)]^{-2}$  and a maximum at perihelion of  $C_0^{\text{Mars}} [a_S(1 - e)]^{-2}$ , implying a variation between 495 and 720  $\text{W m}^{-2}$ .

<sup>7</sup>Unfortunately, the lander Beagle-2 remained silent. The name Beagle given to this ground laboratory can be understood from the note on Darwin.

<sup>8</sup>This increases the occurrences of sunrise and sunset, and by observing these, the atmospheric composition can be sounded in some detail.

<sup>9</sup>Launched on 3 July 1998, the Planet-B probe (Nozomi) was supposed to reach Mars on 11 October 1999, with the help of a Moon–Earth–Moon gravity assist maneuver. However, this maneuver was not perfectly successful and the probe went into a heliocentric orbit. There was still a chance that it could reach Mars in January 2004, 4 years behind schedule, but this too was a failure.

## Launch Dates

These missions are launched at intervals of slightly more than 2 years (26 months). Naturally, the trip from Earth to Mars is undertaken when the conditions required for the journey are as short as possible, and the most economical in terms of fuel. This happens when the two planets are in opposition, i.e., when the Sun, Earth, and Mars are aligned, in that order. The time interval between oppositions corresponds to the synodic period. With the values of the periods given in Table 15.1,  $T = 1$  for the Earth and  $T_1 = 1.88$  for Mars (unit: Earth sidereal year), the synodic period  $T'$  is obtained from (8.44):

$$\frac{1}{T'} = \frac{1}{1} - \frac{1}{1.88} = \frac{0.88}{1.88} \implies T' = \frac{1.88}{0.88} = 2.135,$$

and hence,

$$T' = 2.135 \text{ yr} = 780 \text{ d} \approx 2 \text{ yr } 2 \text{ m}. \quad (15.1)$$

An approximate value is sufficient here, since the orbits of Earth and Mars are not exactly concentric. We calculate more precisely that the interval between two oppositions varies from 764 days (oppositions close to the aphelion of Mars) to 810 days (oppositions close to the perihelion of Mars) owing to the eccentricity of the orbit.

### 15.1.2 Geography of Mars

#### Topography

When discussing the Earth, we have shown maps of our beautiful planet without specific indications. However, the geographical features of Mars are much less familiar to the great majority of Earthlings. And what might those features be in any case? On Mars, there is no division into land and sea, but different regions do appear with differing degrees of lightness and darkness through the telescope, depending on the albedo of the given terrain. The maps presented here are topographical charts bearing no relation to the albedo. The outlines are thus contours of constant altitude, plotted from data obtained by the MOLA instrument aboard MGS, and processed by the MOLA/NASA Science Team.

As on Earth, the zero meridian is chosen arbitrarily. It passes through the small crater<sup>10</sup> Airy-0, in homage to the “creator” of the Greenwich meridian.<sup>11</sup>

<sup>10</sup>In his 1877 map of Mars, the Italian astronomer Schiaparelli measured longitudes from a meridian passing through a region which he considered characteristic and easily identifiable, called *Sinus Meridiani* by Camille Flammarion. When Mariner-9 mapped Mars in 1972, with a resolution of 1 km, a more precisely defined point had to be chosen in this region. The choice of this small impact crater was made by the Mariner-9 Team. It is 500 m across and located in the crater Airy. The coordinates of Airy-0 are 5.2°S, 0.0°E.

<sup>11</sup>*George Biddell Airy* (1801–1892) was a British astronomer who studied diffraction rings from the standpoint of astronomy, physics, and mathematics. As the seventh director of the



Quantity	Symbol	Unit	Mars	Earth
Gravitational constant	$\mu = GM$	$\text{m}^3 \text{s}^{-2}$	4.2828369 $10^{13}$	3.9860044 $10^{14}$
Equatorial radius	$R$	km	3,397.000	6,378.137
Flattening	$1/f$	–	154.40915	298.25766
Equatorial circumference	$L_{\text{P/equat}}$	km	21,343.980	40,075.012
Meridian circumference	$L_{\text{M}}$	km	21,274.922	40,007.860
Acceleration (equatorial)	$g$	$\text{m s}^{-2}$	3.7052	9.7803
Acceleration ( $45^\circ$ )	$g$	$\text{m s}^{-2}$	3.7214	9.8061
Acceleration (pole)	$g$	$\text{ms}^{-2}$	3.7376	9.8321
Gravitational potential	$J_2 \times 10^6$	–	1,955.4513	1,082.6267
Gravitational potential	$J_3 \times 10^6$	–	+31.4559	–2.5327
Gravitational potential	$J_4 \times 10^6$	–	–15.3694	–1.6196
Ratio (frozen orbit)	$J_3/J_2 \times 10^3$	–	+16.0863	–2.3394
Semi-major axis	$a$	a.u.	1.52366	1.00000
Period of revolution				
sidereal	$N_{\text{sid}}$	day	686.9800	365.2564
tropical	$N_{\text{tro}}$	day	686.9725	365.2422
anomalistic	$N_{\text{ano}}$	day	686.9951	365.2496
Angular speed	$\dot{\Omega}_{\text{T}} \times 10^5$	$\text{rad s}^{-1}$	7.088218	7.292115
	$\dot{\Omega}_{\text{T}}$	$^\circ \text{d}^{-1}$	350.891983	360.985559
Period of rotation				
sidereal	$D_{\text{sid}}$	h	24.622962	23.934471
		s	88,642.663	86,164.090
mean solar day	$D_{\text{M}}$	h	24.6598	24.0000
		s	88,775.245	86,400.000
Inclination/ecliptic	$i$	deg	1.8496	–
Obliquity	$\varepsilon$	deg	25.19	23.44
Eccentricity	$e$	–	0.0930	0.01671

TABLE 15.1: *Geodetic and astronomical data for Mars and the Earth. For the units, a dash means dimensionless.*

The zero level of altitude was chosen in an even more arbitrary manner than on Earth. Today, it is defined as the gravitational equipotential surface whose mean value at the equator is equal to the mean radius determined by MOLA, which implies an elevation of 2 km above the old zero level.

---

Royal Observatory at Greenwich, from 1835 to 1881, he considerably increased the importance of the institution when he established the meridian by means of a transit telescope in 1850 and persuaded the whole country to adopt the local mean solar time at Greenwich (GMT). In 1884, the Greenwich meridian was recognised internationally.

The topographic map in Figs. 15.2 and 15.3 shows a very clear difference of altitude between the northern and southern hemispheres. The huge impact basin Hellas<sup>12</sup> in the southern hemisphere is the site of the lowest point on Mars, some 7,825 m below the zero level. Near the equator, Olympus Mons (21,183 m) is the highest mountain in the Solar System<sup>13</sup> (see Fig. 15.1 upper left). To the south-east of Olympus Mons is the Tharsis region, known as the Tharsis Bulge, with its alignment of three volcanoes (14–18 km high), and a little further east is the great scar of Valles Marineris.<sup>14</sup> The poles are covered by the ice caps.<sup>15</sup>

Geologically, the southern hemisphere, above the mean land level, is covered with large craters and composed of ancient landscapes, while the northern hemisphere, several kilometers below the mean land level, features wide plains under a layer of lava. In the equatorial region, the Tharsis Bulge is a vast plateau at high altitude.

The caption to Fig. 15.2 indicates the locations of successful Mars missions. They are situated in low-altitude regions which provide sufficient atmospheric thickness to allow for aerobraking with parachutes.

### Note on Latitudes

Here on Earth, the historical determination of the latitude using the local vertical led us to distinguish geographical and geocentric latitude. On Mars, the precise determination of the latitude dates back only to the space age, and in principle we consider only the latitude determined by satellites, which is the geocentric, or perhaps we should say planetocentric or areocentric latitude.

---

<sup>12</sup>At the end of the nineteenth century, names were attributed on the basis of an Earthly design. Certain dark areas seemed to evoke the shape of the Mediterranean, whereupon Greece or the Gulf of Syrtis were placed there. Naturally, north and south were swapped, an artefact of telescopic vision! The astronomer Giovanni Schiaparelli may be considered as the father of the current Martian nomenclature, thanks to intensive observations he carried out from 1877. He borrowed names from ancient history and classical mythology. The International Astronomical Union (IAU) unified the various appellations. They comprise two Latin nouns, a generic noun such as *mons* for “mount”, and a proper noun such as *Olympus*. This gives names like Olympus Mons, Mare Tyrrhenum, and Hellas Planitia. Valles Marineris is the valley discovered by Mariner-9.

<sup>13</sup>This volcano has a circular base with diameter 650 km. It has a very distinct caldera, 40 km wide and 4 km deep. There is a difference of height of 23 km, since its base is at an altitude of about –2,000 m. It is now inactive, like all Martian volcanoes, but the small number of impacts on its surface indicate that it was active in the geologically recent past. The volume of Olympus Mons is about a hundred times greater than the biggest terrestrial volcano. Eruptions of fluid lava have created an enormous volcanic shield over very long geological periods. This volcano, like the three others of the Tharsis region, has remained in the same position with respect to the source of the magma. This great stability tends to prove that tectonic activity is low or non-existent on Mars.

<sup>14</sup>The Mariner valleys constitute a system of several parallel canyons, about 5,000 km long. The greatest of them is 6 km deep over a width of about 200 km.

<sup>15</sup>The two poles are covered by a polar deposit of radius several hundred kilometers. These are undoubtedly made up of sediments and water ice. The whole thing is then covered over with a permanent cap of water ice in the case of the North Pole and frozen carbon dioxide (CO<sub>2</sub>) at the South Pole. On top of this, a carbon dioxide ice layer condenses seasonally, in the Martian winter, to sublime in summer.

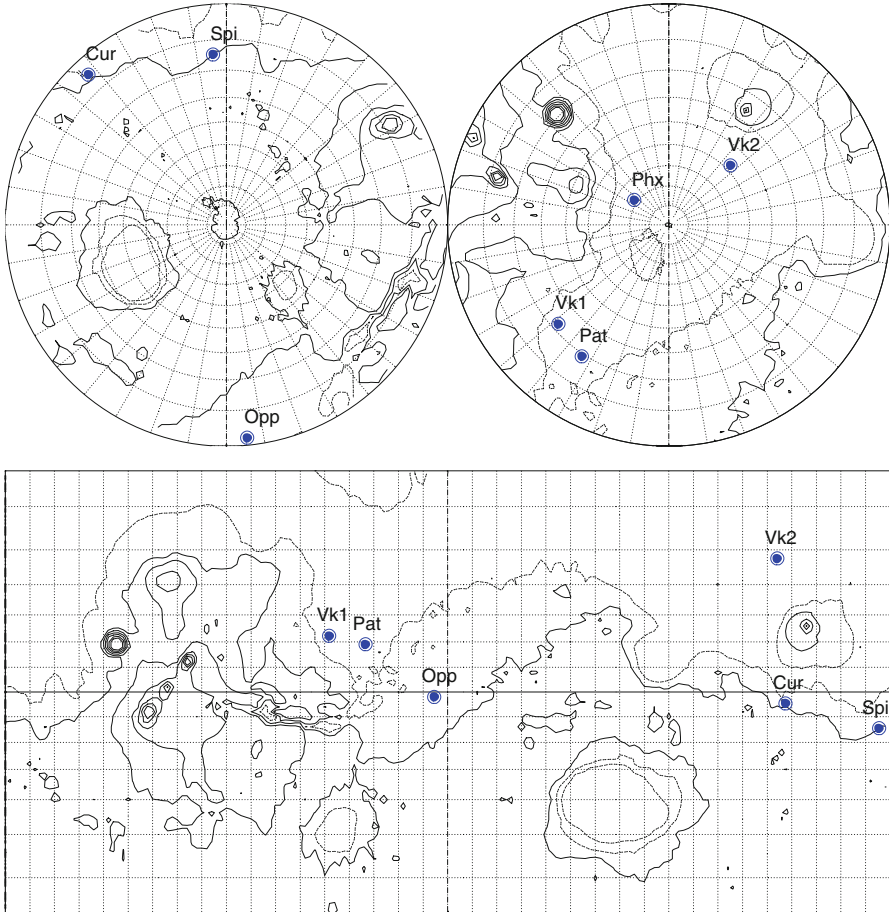


FIG. 15.2 : Topographical chart of the planet Mars, compiled from data gathered by the MOLA instrument aboard MGS (processed by the MOLA/NASA Science Team). Contours: steps of 2.5 km. Altitude 0 in bold, negative altitudes dashed. MOLA data is used here in a downgraded mode, with grid  $2^\circ$  for greater clarity. Geodetic grid: graticule  $10^\circ$  in latitude and longitude. Upper: Polar stereographic projection (North Pole on the right and South Pole on the left). Lower: Equatorial Mercator projection. The highest point is Olympus Mons ( $18^\circ$  N,  $225^\circ$  E). To the south-east is the Tharsis Bulge, a high region encompassing a line of three volcanoes: Ascraeus Mons ( $12^\circ$  N,  $254^\circ$  E), Pavonis Mons ( $0^\circ$ ,  $247^\circ$  E), and Arsia Mons ( $9^\circ$  S,  $239^\circ$  E). It is bordered by Valles Marineris, stretching from  $5^\circ$  S,  $265^\circ$  E to  $15^\circ$  S,  $310^\circ$  E. To the north of this region is Alba Patera ( $42^\circ$  N,  $252^\circ$  E). The main impact basins are Hellas ( $45^\circ$  S,  $70^\circ$  E), Argyre ( $50^\circ$  S,  $320^\circ$  E), Isidis ( $12^\circ$  N,  $88^\circ$  E), and Utopia ( $45^\circ$  N,  $110^\circ$  E). Locations of successful missions: Viking-1 ( $22.48^\circ$  N,  $312.06^\circ$  E), Viking-2 ( $47.97^\circ$  N,  $134.29^\circ$  E), Pathfinder ( $19.17^\circ$  N,  $326.79^\circ$  E), MER-A/Spirit ( $14.57^\circ$  S,  $175.47^\circ$  E), MER-B/Opportunity ( $1.95^\circ$  S,  $354.47^\circ$  E), Phoenix ( $68.21^\circ$  N,  $234.25^\circ$  E), and MSL/Curiosity ( $4.59^\circ$  S,  $137.44^\circ$  E).

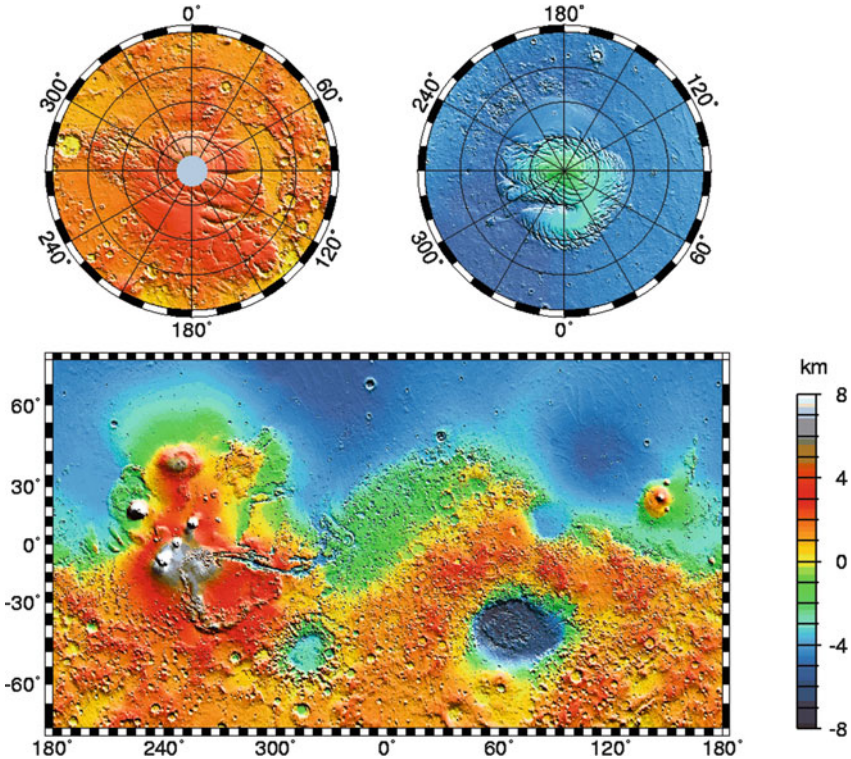


FIG. 15.3: Using MOLA data through October of 2000, the Science Team produced this very high resolution topographic shaded relief map of Mars. The map has a resolution  $0.125^\circ$  and is shown as a Mercator projection to latitude  $70^\circ$  north and south. The polar regions are shown in stereographic projection with the North Pole on the right and the South Pole on the left. Credit: MOLA/NASA Science Team.

However, in the (magnificent) maps of Mars drawn up by the US Geological Survey (USGS), there is a choice between two different grids, depending on whether one is using areocentric (planetocentric) latitudes or areographic (planetographic) latitudes. The difference between the two is maximal for  $45^\circ$  N or S, where it is equal to  $\delta\varphi = 0.337^\circ$ , which corresponds to 20.0 km on the ground [see (2.4) and (2.5)]. In this chapter, we shall use only areocentric latitudes for Mars.

### Martian Atmosphere

The space missions brought us our first real insight into the atmosphere of Mars, first with the radio occultations of Mariner-4 and Mariner-9, then with the landers Viking-1 and -2.

The main components of the atmosphere are, in mole fractions: carbon dioxide  $\text{CO}_2$  (0.95), dinitrogen  $\text{N}_2$  (0.03), argon A (0.02), water  $\text{H}_2\text{O}$

(< 0.0005). The average pressure at the surface is 6 hPa. Due to the condensation of carbon dioxide gas at the polar caps, the atmospheric pressure varies by up to 30% with the seasons. There are thus seasons on Mars, and an atmospheric circulation similar to the circulation on Earth (generally with one large Hadley cell). There are also depressions and anticyclones, hurricanes and tornadoes, and the atmosphere is full of dust. Storms are frequent and in some cases global, enveloping the whole planet in an orange veil.

The Mars missions have greatly refined our scientific understanding and have been used to develop general circulation models (MGCM for NASA, GCM for the LMD in Europe). Conversely, by improving these models, future missions can be better prepared, especially those making use of aerobraking.

## 15.2 Geodetic and Astronomical Quantities

### 15.2.1 Geodetic Data

To study the true (perturbed) motion of a satellite, geodetic characteristics of the planet must be brought into consideration, in particular, higher terms in the expansion of the attractive potential. To characterise specific orbits, e.g., stationary or Sun-synchronous, and study instrument sampling, astronomical features such as the periods of planetary motions, eccentricity, and obliquity are required.

Table 15.1 provides geodetic<sup>16</sup> and astronomical data for Mars, comparing them with the same data for the Earth. Table 15.2 shows how the evaluation of the gravitational constant  $\mu$  has evolved, from the first estimated values obtained following the discovery of Phobos and Deimos to the Goddard Martian Model (GMM) which makes use of MGS observations. The latest models are GMM-3, also called MGM1025 (degree 80 and order 80), see Table 15.3, and JGM85F01, also called MGS85F (degree 85 and order 85).<sup>17</sup>

---

<sup>16</sup>When Mars replaces the Earth as attractive center, we sometimes use the prefix “areo” instead of “geo”, but certain terms such as “geophysics”, “geodesy”, and “geography” are generally retained for all planets. There are exceptions, however.

<sup>17</sup>The Mars Global Surveyor Gravity Science Team at JPL under the direction of William L. Sjogren provides details which give a good idea of the methods used to set up geopotential models. MGS85F is a  $85 \times 85$  spherical harmonic model derived from radio tracking of: Mariner 9 (1971-11-14 to 1972-04-14), Viking Orbiter 1 (1976-06-21 to 1978-11-18), Viking Orbiter 2 (1977-03-02 to 1978-07-25), MGS Science Phasing Orbit 1 and 2 (SPO1 and SPO2) (1998-03-28 to 1998-09-23), MGS Gravity Calibration Orbit (GCO) (1999-02-02 to 1999-03-29), MGS Mapping (MAP) (1999-03-29 to 2001-08-14). The radio tracking data blocks consist of: Mariner 9 with 47,597 observations; Viking Orbiter 1 with 67,545 observations; Viking Orbiter 2 with 70,677 observations; SPO1 and SPO2 at 177 km periapsis with 134,072 observations; GCO at 370 km periapsis with 145,777 observations; MAP at 370 km periapsis with 2,102,977 observations.

Method	Year	$\mu$ (km <sup>3</sup> s <sup>-2</sup> )	Error
Phobos, Deimos (Hall)	1878	42,900	$\pm 70$
Mariner-4	1969	42,828.32	$\pm 0.13$
Mariner-6	1970	42,828.22	$\pm 1.83$
Mariner-9	1973	42,828.35	$\pm 0.55$
MGS/GMM-1	1993	42,828.3580	$\pm 0.0512$
MGS/GMM-2B	2000	42,828.371901	$\pm 0.000074$
MGS/GMM-3 [MGM1025]	2001	42,828.369774	$\pm 0.000060$
MGS+/JGM85F01	2002	42,828.376383	–

TABLE 15.2 : Measured areocentric gravitational constant  $\mu = GM$  and estimated error. Historical evolution with method used and year.

Zonal coefficient	Other coefficients (C)	Other coefficients (S)
$C_{20}^*$ –874.504415509	$C_{22}^*$ –84.585751018	$S_{22}^*$ 48.905551076
$C_{30}^*$ –11.889205542	$C_{31}^*$ 3.800729164	$S_{31}^*$ 25.155150744
$C_{40}^*$ 5.123138995	$C_{32}^*$ –15.933741664	$S_{32}^*$ 8.353919240
$C_{50}^*$ –1.724618348	$C_{33}^*$ 35.023491712	$S_{33}^*$ 25.551471727
$C_{60}^*$ 1.344241356		

TABLE 15.3 : The model GMM-3 (known as MGM1025). Normalised zonal coefficients  $C_{l0}^*$  and other normalised coefficients  $C_{lm}^*$  and  $S_{lm}^*$ . All values should be multiplied by  $10^{-6}$ . Note also that  $C_{00}^* = 1$  and the coefficients  $S_{00}^*$ ,  $C_{10}^*$ ,  $S_{10}^*$ ,  $C_{11}^*$ , and  $S_{11}^*$  are zero.

## Different Radii of the Ellipsoid

Figure 15.4 shows the radii of the ellipsoid at different latitudes, as we did for the Earth ellipsoid in Chap. 2 (see Fig. 2.3). Note the ranges of variation from the equator to the pole (all monotonic in  $[0, \pi/2]$ ):

- The radius of curvature  $\rho$  varies between 3,353.143 and 3,419.143 km.
- The great normal  $\mathcal{N}$  varies between 3,397.000 and 3,419.143 km.
- The radius of the ellipse  $R_\psi$  varies between 3,397.000 and 3,375.000 km.

## 15.2.2 Astronomical Data

To carry out this study for Mars, we repeat the calculations made for the Earth, without change of notation. For example, the angular speed of Mars in its orbit around the Sun and in its rotation about the polar axis will be denoted by  $\dot{\Omega}_S$  and  $\dot{\Omega}_T$ , respectively. In place of (7.21) and (7.26), we obtain

$$\dot{\Omega}_S = 0.5240384^\circ \text{d}^{-1}, \quad (15.2)$$

$$\dot{\Omega}_T = 350.89198266^\circ \text{d}^{-1}. \quad (15.3)$$

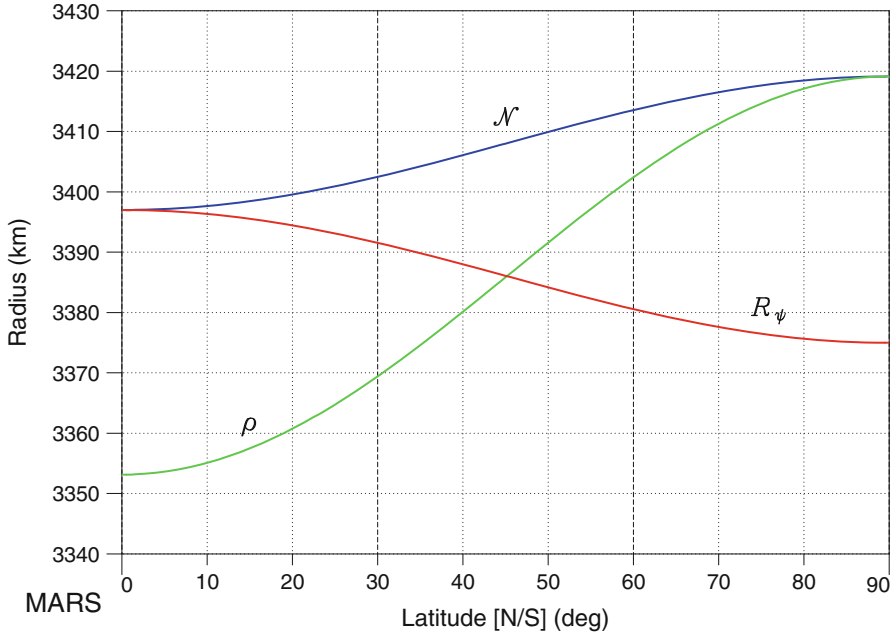


FIG. 15.4 : Different radii of the Mars ellipsoid: radius of curvature  $\rho$  in the meridian plane, the great normal  $\mathcal{N}$ , and the radius of the ellipsoid  $R_\psi$ .

The word “day” refers to the unit of time equal to 86,400 s. As the mean day on Earth lasts 1 day, it is better to find another name for the Martian day. The mean solar day on Mars is traditionally called a sol. We then have

$$\begin{aligned} D_M &= 1 \text{ sol} = 1.02749127 \text{ day} \\ &= 24 \text{ h } 37 \text{ m } 22.663 \text{ s}. \end{aligned} \quad (15.4)$$

It is useful to express the tropical year in sols, since it concerns the recurrence of the seasons and also the sidereal year:

$$N_{\text{tro}} = 668.5921 \text{ sol}, \quad N_{\text{sid}} = 668.5991 \text{ sol}. \quad (15.5)$$

### 15.2.3 Areocentric Longitude and Martian Day

#### True Anomaly and Mean Anomaly

To determine a given day on Mars, i.e., specify the position of the planet on its heliocentric orbit, we do not use the day of the month, and even less so a saint on the calendar, as on Earth. We consider the ecliptic longitude  $l$ , defined in ecliptic coordinates in Chap. 7. It only differs from the true anomaly



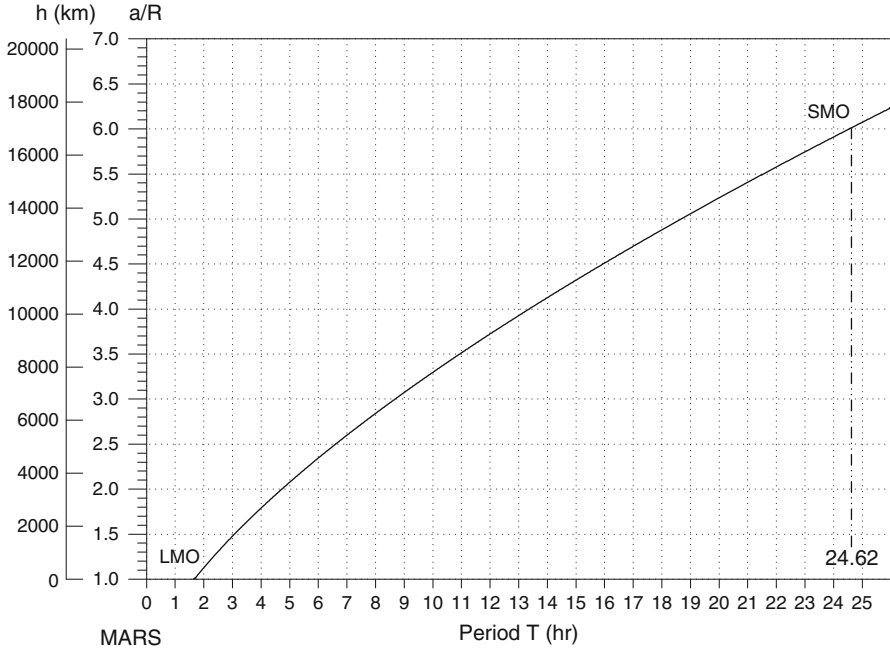


FIG. 15.5 : Relation between period and altitude.

$v$  by choice of origin. The origin for  $l$  is the vernal equinox<sup>18</sup> and for Mars it is traditional to denote this angle  $l$  by  $L_S$ . It is called the areocentric solar longitude, or areocentric longitude for short.

Hence, on Mars, the “date”  $L_S$  is specified by the true anomaly with the spring equinox as origin, whereas on Earth, it is specified by the mean anomaly with 1 January as origin. The true anomaly  $v$  has its origin at the perihelion (periastron). The solar longitude of the perihelion  $L_{Sp}$  is

$$L_{Sp} = 251.0^\circ . \quad (15.6)$$

The mean anomaly  $M$  also has its origin at the perihelion, and we shall denote it by  $M_S$  when the origin is at the vernal equinox. Its value at the perihelion

<sup>18</sup>The orbit of Mars is itself subject to a precession of the equinoxes. This motion is slower than it is for the Earth, being  $7''.51$  per Earth year, or one round trip in 173 kyr (kilo year). For Mars, only the Sun contributes to this precession, whereas on Earth, not only is the Sun’s effect greater, but one must add the even more significant contribution due to the Moon, as we have already seen. The perihelion is also subject to apsidal precessional motion in a prograde direction. The combination of the two motions specifies the climatic precession, which has a cycle of about 55 kyr. There is a fundamental difference between the theory of paleoclimates on the Earth and on Mars. In the case of the Earth, the inclination remains in a narrow range (obliquity between  $22^\circ$  and  $25^\circ$ ), while it varies significantly and chaotically on Mars, between  $0^\circ$  and  $60^\circ$  (between  $15^\circ$  and  $45^\circ$  over the last 10 million years).



is then denoted by  $M_{\text{Sp}}$ . We have the relations

$$v = L_S - L_{\text{Sp}} , \quad (15.7)$$

$$M = M_S - M_{\text{Sp}} . \quad (15.8)$$

Recall that the mean anomaly  $M$  is obtained from the true anomaly  $v$  analytically, but that the converse problem of obtaining the true anomaly  $v$  from the mean anomaly  $M$  requires us to solve the Kepler problem:

$$\begin{aligned} v \longmapsto M : \quad M &= M(v) \quad \text{by (4.59)} , \\ M \longmapsto v : \quad v &= v(E) , \quad E = E(M) \quad \text{by iteration (4.85)} . \end{aligned}$$

To calculate  $M_{\text{Sp}}$ , we first determine the true anomaly  $v_\gamma$  at the vernal equinox, noting that this is not of course the same point  $\gamma$  as for the spring equinox on Earth:

$$v_\gamma = L_{S\gamma} - L_{\text{Sp}} = 0 - L_{\text{Sp}} = 360 - 251.0 = 109.0 \quad [\text{mod } 360] , \quad (15.9)$$

where  $L_{S\gamma}$  is the areocentric longitude of the vernal equinox, which is zero by definition of  $L_S$ .

From (4.59), we obtain the mean anomaly  $M_\gamma$  of the vernal equinox analytically:

$$M_\gamma = M(v_\gamma) = M(109.00) = 98.66 \quad [\text{mod } 360] . \quad (15.10)$$

Then, changing origin, we determine  $M_{\text{Sp}}$  from

$$M_{\text{Sp}} = M_{S\gamma} - M(v_\gamma) = 0 - M(v_\gamma) = 360 - 98.66 = 261.34 \quad [\text{mod } 360] , \quad (15.11)$$

where  $M_{S\gamma}$  is the value of  $M_S$  at the vernal equinox, which is zero by definition of  $M_S$ .

Conversely, starting with  $M_{\text{Sp}} = 98.66^\circ$ , we obtain  $v = 109.00^\circ$  by solving the Kepler problem (see Example 4.4).

To be more precise, note that the perihelion has a slow precessional motion relative to the vernal equinox. This is called climatic precession [see in particular (6.142)], with a cycle of around 55 kyr (where 1 kyr = 1,000 year). The longitude  $L_S$  of the perihelion thus varies slightly over time. If  $A$  is the year number in the Gregorian calendar, then  $L_{\text{Sp}}$  is given in degrees by

$$L_{\text{Sp}} = 250.999 + 0.00645(A - 2000) . \quad (15.12)$$

Calculating  $M_{\text{Sp}}$ , we find

$$M_{\text{Sp}} = 261.342 + 0.00677(A - 2000) . \quad (15.13)$$

For example, for the year 2014,  $L_{\text{Sp}} = 251.09^\circ$  and  $M_{\text{Sp}} = 261.44^\circ$ .

## Relation Between Longitude and Day

**Day Obtained from the Areocentric Longitude.** The day  $D$  (zero at the vernal equinox) is obtained from the mean anomaly by

$$D = \frac{N_{\text{tro}}}{360} M_S . \quad (15.14)$$

We obtain the day in days ( $D_d$ ) or in sols ( $D_s$ ) depending on whether  $N_{\text{tro}}$  is expressed in days or in sols. In the following, we will give the Martian days in sols. Using the relations between angles discussed above and the relation (4.59), we obtain  $D_s$  from  $L_S$  by

$$D_s = D_{\text{sp}} + \frac{N_{\text{tro}}}{360} \left[ 2 \arctan \left( \sqrt{\frac{1-e}{1+e}} \tan \frac{L_S - L_{\text{Sp}}}{2} \right) - \frac{180}{\pi} \frac{e \sqrt{1-e^2} \sin(L_S - L_{\text{Sp}})}{1 + e \cos(L_S - L_{\text{Sp}})} \right] \pmod{N_{\text{tro}}} , \quad (15.15)$$

where

$$\frac{N_{\text{tro}}}{360} = 1.85720 , \quad D_{\text{sp}} = \frac{N_{\text{tro}}}{360} M_{\text{sp}} = 485.36 . \quad (15.16)$$

The values of the angles and days<sup>19</sup> are given in Table 15.4 and Fig. 15.6.

The table also shows the reduced distance  $r/a$ , the distance to the Sun divided by the semi-major axis of the orbit, and the eccentric anomaly  $E$ , which are related by (4.64), together with the quantity

$$E_{\text{CS}} = L_S - M_S , \quad (15.17)$$

comparable with the equation of center  $E_C = v - M$ , defined in Chap. 4 by (4.90). The two angular differences  $E_{\text{CS}}$  and  $E_C$  only differ by a constant:  $E_{\text{CS}}$  vanishes at the vernal equinox and  $E_C$  at the perihelion.

The extreme values of  $E_{\text{CS}}$  are:

- maximum  $E_{\text{CS}} = +0.35^\circ$  for  $L_S = 94.01 + L_{\text{Sp}} = 344.99^\circ$ ,
- minimum  $E_{\text{CS}} = -21.05^\circ$  for  $L_S = 259.99 + L_{\text{Sp}} - 360 = 156.97^\circ$ .

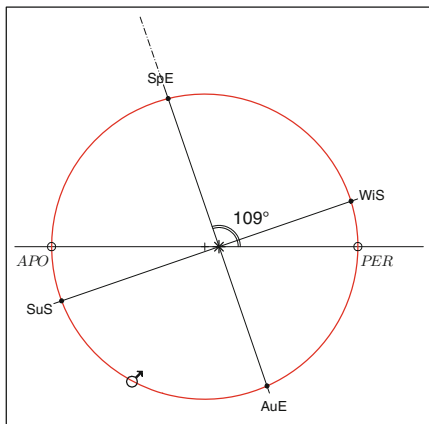
The amplitude of the variation is  $(21.05 + 0.35)/2 = 10.70^\circ$ . According to (4.98), this value, expressed in radians as  $(\pi/180)10.70 = 0.1868$ , corresponds to twice the eccentricity  $e = 0.0934$  of the orbit of Mars.

**Areocentric Longitude Obtained from the Day.** Knowing the day  $D_s$ , we can calculate the difference with the day of passage at perigee. This difference  $D_s - D_{\text{sp}}$  gives the difference in mean anomaly  $M_S - M_{\text{Sp}}$ . By iteration

<sup>19</sup>Concerning the calculation of  $D_s$  using (15.15), the object in square brackets must be expressed in degrees, since it multiplies  $N_{\text{tro}}/360$ . Note also that, since  $L_S = 0$  implies  $D_s = 0$ , the value of  $D_{\text{sp}}$  can be found from (15.15) without using (15.16).

$L_S$ (deg)	$M_S$ (deg)	$E_{CS}$ (deg)	$D_d$ (day)	$D_s$ (sol)	$v$ (deg)	$E$ (deg)	$M$ (deg)	$r/a$
0.0	0.0	0.0	0.0	0.0	109.0	103.9	98.7	1.0224
10.0	10.7	-0.7	20.4	19.8	119.0	114.2	109.3	1.0383
20.0	21.7	-1.7	41.3	40.2	129.0	124.7	120.3	1.0532
30.0	32.9	-2.9	62.9	61.2	139.0	135.4	131.6	1.0665
40.0	44.5	-4.5	84.9	82.6	149.0	146.1	143.2	1.0776
50.0	56.2	-6.2	107.3	104.5	159.0	157.0	154.9	1.0860
60.0	68.2	-8.2	130.1	126.6	169.0	167.9	166.8	1.0913
70.0	80.1	-10.1	152.9	148.8	179.0	178.9	178.8	1.0934
80.0	92.1	-12.1	175.8	171.1	189.0	189.9	190.8	1.0920
90.0	104.1	-14.1	198.6	193.3	199.0	200.8	202.8	1.0873
100.0	115.9	-15.9	221.1	215.2	209.0	211.7	214.5	1.0794
110.0	127.5	-17.5	243.2	236.7	219.0	222.5	226.1	1.0688
120.0	138.8	-18.8	264.9	257.8	229.0	233.2	237.5	1.0560
130.0	149.8	-19.8	285.9	278.3	239.0	243.7	248.5	1.0413
140.0	160.6	-20.6	306.4	298.2	249.0	254.1	259.3	1.0256
150.0	171.0	-21.0	326.3	317.5	259.0	264.3	269.7	1.0092
160.0	181.0	-21.0	345.5	336.2	269.0	274.4	279.7	0.9929
170.0	190.8	-20.8	364.1	354.3	279.0	284.3	289.5	0.9770
180.0	200.2	-20.2	382.1	371.8	289.0	294.0	298.9	0.9620
190.0	209.4	-19.4	399.6	388.9	299.0	303.6	308.1	0.9483
200.0	218.3	-18.3	416.6	405.4	309.0	313.1	317.0	0.9362
210.0	227.0	-17.0	433.2	421.6	319.0	322.4	325.7	0.9260
220.0	235.5	-15.5	449.5	437.4	329.0	331.7	334.2	0.9178
230.0	243.9	-13.9	465.5	453.0	339.0	340.9	342.6	0.9118
240.0	252.2	-12.2	481.4	468.5	349.0	350.0	350.9	0.9080
250.0	260.5	-10.5	497.1	483.8	359.0	359.1	359.2	0.9066
260.0	268.8	-8.8	512.9	499.2	9.0	8.2	7.5	0.9076
270.0	277.1	-7.1	528.7	514.6	19.0	17.3	15.8	0.9108
280.0	285.5	-5.5	544.7	530.1	29.0	26.5	24.1	0.9164
290.0	294.0	-4.0	560.9	545.9	39.0	35.8	32.6	0.9242
300.0	302.6	-2.6	577.5	562.0	49.0	45.1	41.3	0.9341
310.0	311.5	-1.5	594.4	578.5	59.0	54.5	50.2	0.9458
320.0	320.6	-0.6	611.8	595.4	69.0	64.1	59.3	0.9592
330.0	330.0	0.0	629.7	612.9	79.0	73.8	68.7	0.9740
340.0	339.7	0.3	648.2	630.8	89.0	83.7	78.3	0.9897
350.0	349.7	0.3	667.3	649.4	99.0	93.7	88.3	1.0060
360.0	360.0	0.0	687.0	668.6	109.0	103.9	98.7	1.0224

TABLE 15.4 : Correspondence between areocentric longitude  $L_S$  and the day (expressed in days or in sols). The passage at periastron occurs for  $L_S = L_{Sp} = 251.0^\circ$ , and at apoastron for  $L_S = L_{Sa} = L_{Sp} - 180 = 71.0^\circ$  (minimum and maximum of the reduced distance  $r/a$ , respectively). The areocentric longitude  $L_S$ , the mean anomaly  $M_S$ , and hence the days  $D$ , have their origin at the vernal equinox. The anomalies  $v$ ,  $E$ , and  $M$  have their origin at the perihelion passage. The difference  $L_S - M_S$  is the equation of center  $E_{CS}$ .



	$L_S$	$v$	$M$	$D_s$
SpE	0	109.0	98.7	0
SuS	90	199.0	202.8	193.3
AuE	180	289.0	298.9	371.8
WiS	270	19.0	15.8	514.6
PER	251.0	0.0	0.0	485.3
APO	71.0	180.0	180.0	151.0

FIG. 15.6 : Orbit of Mars around the Sun (to scale). Relative position of the perihelion PER and the northern spring equinox SpE. The straight lines SpE–AuE between the spring and autumn equinoxes and SuS–WiS between the summer and winter solstices are orthogonal. Abbreviations  $L_S, v, M, D_s$  are explained in the text.

(Kepler's problem), we obtain the true anomaly  $v$ , and this in turn gives the areocentric longitude  $L_S = v + L_{Sp}$ .

**Note. Relation with the Date on Earth.** To find the longitude  $L_S$  from the date expressed in the form  $D = (\text{year month day hour})$ , it is convenient to begin by transforming the date  $D$  into a Julian date denoted by  $JD$ . We calculate the difference with a date  $JD_0$ , known as the time of passage of Mars at the vernal equinox. We can take

$$D = 31 \text{ July } 2013 \quad \mapsto \quad JD_0 = 2,456,505.1 \quad \implies \quad L_S = 0.$$

This difference gives

$$D_d = JD - JD_0 \quad [\text{mod } N_{\text{tro}}].$$

All these quantities are in Earth days.

We can go from  $D_d$  to  $D_s$  (in sol) using the coefficient given by (15.4) and we obtain  $L_S$  as indicated above.

**Example 15.1** Calculate the solar areocentric longitude for the date 20 December 2012 at 20:12.

► The date  $D = 2012 \text{ } 12 \text{ } 20 \text{ } 20:12$  gives  $JD = 2,456,282.3$ . Taking the zero value  $JD_0$  discussed above, we obtain

$$D_d = JD - JD_0 = -222.1 \quad [\text{mod } 686.97] = 464.2.$$

We obtain  $M_S$  from (15.14):

$$M_S = 360 \times \frac{D_d}{N_{\text{tro}(d)}} = 360 \times \frac{464.2}{686.97} = 243.3 .$$

whence

$$M = M_S - M_{S_p} = 243.3 - 261.4 = 341.8 \quad [\text{mod } 360] .$$

Then  $M$  gives  $v$  by solving the Kepler problem. We find  $v = 338.1$ . We subsequently obtain the solar longitude  $L_S$  from

$$L_S = v + L_{S_p} = 338.1 + 251.1 = 229.2 \quad [\text{mod } 360] ,$$

as required. ◀

### Definition of the Seasons

A season is the length of time corresponding to an interval of solar longitude equal to  $90^\circ$ , starting from the vernal equinox. The seasons are named as on Earth, e.g., the northern spring or southern autumn corresponds to  $L_S$  between  $0^\circ$  and  $90^\circ$ , etc. On Mars, the lengths of the seasons are not the same as on Earth, but the differences in their lengths are greater than on Earth: 193sols for the spring, 143sols for the autumn. The precise length of the seasons is given in the table associated with Fig. 15.7.

It is sometimes useful to define the month in the same way, by an interval of  $30^\circ$  in the solar longitude, starting from the vernal equinox. (No name is attributed to these months, apart from the bounding values of  $L_S$ .) Table 15.4 can be used to calculate the length of these months. The shortest ( $L_S$ :  $240\text{--}270^\circ$ ) lasts 46.1sols, while the longest ( $L_S$ :  $60\text{--}90^\circ$ ) lasts 66.7sols, i.e., 45% longer. These correspond to the passages at perihelion and aphelion, respectively, illustrating Kepler's second law. The passage at perihelion occurs at the end of the northern autumn.

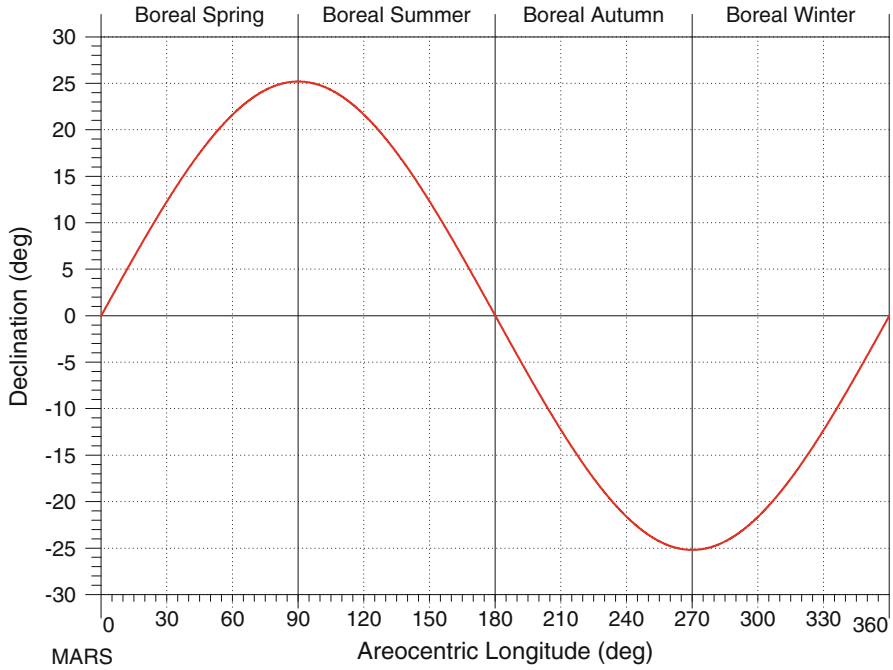
The exact equivalent on Earth of this division into 12 months is the partitioning of the year into 12 signs of the zodiac.<sup>20</sup> This note should in no way be interpreted as an advertisement for astrology!

### 15.2.4 Declination

When considering the Sun and the Earth in Chap. 7 [see Fig. 7.10 and (7.62)], we have already calculated the declination, expressing it as a function of the solar longitude. With the notation used there, we can write

$$\sin \delta = \sin L_S \sin \varepsilon . \quad (15.18)$$

<sup>20</sup>For the Earth, the shortest of these signs ( $l$ :  $270\text{--}300^\circ$ ) is the one containing the passage at perihelion ( $l = 282^\circ$ ), which lasts 29.45 days. The longest ( $l$ :  $90\text{--}120^\circ$ ) lasts 31.45 days, i.e., 7% longer.



$L_S$ [deg]	$D$ [sol]	$\delta$ [deg]	$\delta$	Beginning of season	Length of season
0.0	0.0	0.00	$\delta = 0$	Spring equinox	
24.1	48.7	10.00			
55.3	11.21	200.0			13.39
90.0	193.3	25.19	$\delta = \varepsilon$	Summer solstice	
126.5	271.2	20.00			
19.55	37.82	100.0			16.87
180.0	371.8	0.00	$\delta = 0$	Autumn equinox	
204.1	412.1	-10.00			
233.5	458.4	-00.02			17.24
270.0	514.6	-25.19	$\delta = -\varepsilon$	Winter solstice	
306.5	572.7	-20.00			
335.9	623.4	-00.01			10.45
360.0	668.6	0.00	$\delta = 0$	Spring equinox	

FIG. 15.7 : Graph of the declination  $\delta$  as a function of the areocentric solar longitude  $L_S$ . Table: Particular values of  $\delta$ , with corresponding values of  $L_S$  in degrees and the date  $D$  in sol. The obliquity of Mars is  $\varepsilon = 25.19^\circ$ . Note the unequal lengths of the seasons (in sols). The seasons indicated are those in the northern hemisphere.

The declination is thus very simply obtained as a function of  $L_S$  :

$$\delta = \arcsin(0.42562 \sin L_S) . \quad (15.19)$$

The graph of the function is plotted in Fig. 15.7, which also shows key values of the declination.

Calculations to find the sunrise and sunset are strictly identical to those for the Earth, provided, that we continue to ignore atmospheric refraction. We also define specific parallels on Mars: polar circles ( $64^\circ 49' \text{N}$  and  $\text{S}$ ) and tropics ( $25^\circ 11' \text{N}$  and  $\text{S}$ ), at slightly different values to their terrestrial counterparts.

### 15.2.5 Equation of Time

In Chap. 7, we discussed the definition of the equation of time  $E_T$ , the sum of the equation of center  $E_C$  and the reduction to the equator  $E_R$ . To express the equation of center  $E_C = v - M$ , let us return to (4.96) and (4.97). Stopping at the first order, we can replace  $E$  by  $v$  in the argument of the sine to obtain

$$\begin{cases} v - E \approx e \sin v , \\ E - M \approx e \sin v , \end{cases} \quad (15.20)$$

which gives

$$v - M \approx 2e \sin v , \quad (15.21)$$

whence (15.7) implies that

$$E_C \approx 2e \sin(L_S - L_{Sp}) . \quad (15.22)$$

The expression for the reduction to the equator  $E_R = \alpha - l$  defined by (7.52) is obtained directly from (7.51). Using the areocentric solar longitude, this gives

$$E_R \approx -\tan^2 \frac{\varepsilon}{2} \sin 2L_S . \quad (15.23)$$

The equation of time is then

$$E_T = 2e \sin(L_S - L_{Sp}) - \tan^2 \frac{\varepsilon}{2} \sin 2L_S . \quad (15.24)$$

To express  $E_T$  in minutes, we convert radians into minutes of time:  $2\pi$  rad is equivalent to 1 sol, or 1,479.6 min. Expressing  $L_S$  in degrees, we end up with

$$E_T [\text{min}] = 43.92 \sin(L_S - 251) - 11.74 \sin 2L_S . \quad (15.25)$$

The graph of the function  $E_T$  is plotted in Fig. 15.8, with the graphs for  $E_C$  and  $E_R$ . Significant values of the equation of time are given in the associated tables.

Of course, as on the Earth,  $E_C$  has an annual period and  $E_R$  a period of half the length. However, on Mars, the amplitude of  $E_C$  is four times the amplitude of  $E_R$ , and  $E_T$  reaches large values (with a maximum of 53 min). Recall here that  $E_T = \text{LMT} - \text{LAT}$ .

**Expressions for the Declination and the Equation of Time.** To end this section, note that the expressions for the declination and the equation of time are simpler for Mars than they are for the Earth. This happens because, for Mars, we use  $L_S$  as the variable, which amounts to using the true anomaly, specifying the position of the Sun directly. For the Earth, we use the day, related to the mean anomaly, which is only indirectly related to the position of the Sun.

## 15.3 Satellite in Real Orbit

### 15.3.1 Satellite in Keplerian Orbit

It is no simple matter to put a satellite in orbit around Mars. However, when the probe, launched from Earth, is captured by the Martian gravitational attraction, and if it is captured without simply crashing into the surface of the planet, in other words, once Mars has become the attractive center of the satellite's orbit, its motion can be determined in exactly the same way as all the motions we have been discussing up to now with the Earth as the central attracting body. In order to study the Keplerian motion of a given satellite, with semi-major axis  $a$ , we need only replace the geocentric gravitational constant  $\mu = GM_{\text{Earth}}$  by the areocentric gravitational constant  $\mu = GM_{\text{Mars}}$ , as given in Table 15.1.

Given the radius of the planet, we use (5.5) and (5.6) to define the periods  $T_0$  and  $T_{0(h=0)}$ . This yields

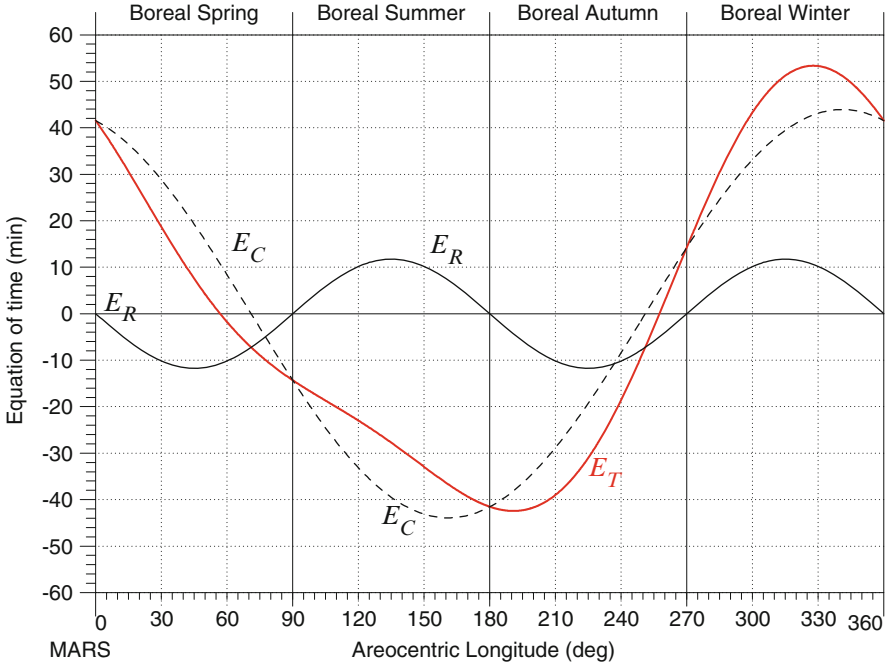
$$T_{0(h=0)} = 100.15 \text{ min} , \quad (15.26)$$

and  $T_0$  is obtained as a function of  $\eta = a/R$  or  $h = a - R$  using (5.8). We have indicated certain orbits (LMO and SMO) on the graph of this function in Fig. 15.5. Their significance will be discussed below. This figure could be compared with Fig. 5.2.

### 15.3.2 Perturbative Accelerations

The only difference in the calculation of the Keplerian orbit for the Earth and for Mars is the value of  $\mu$ , as noted above. For the true orbit, perturbing terms must be taken into account, and these are of the same kind for Mars





$L_s$ [deg]	$D$ [sol]	$E_T$ [min]
0	0	+41.52
2	4	+40.00
28	57	+20.00
57	120	0.00
110	237	-20.00
173	360	-40.00
191	391	-42.43
207	417	-40.00
238	465	-20.00
257	495	0.00
275	522	+20.00
296	556	+40.00
328	609	+53.36
360	669	+41.52

FIG. 15.8 : Graph of the equation of time  $E_T$ , sum of the equation of center  $E_C$  and the reduction to the equator  $E_R$ , as a function of the areocentric solar longitude  $L_s$ . Table: Particular values of  $E_T$ , with corresponding values of  $L_s$  in degrees, and of the date  $D$  in sols. Minutes (min) used for  $E_T$ ,  $E_C$ , and  $E_R$  are minutes of 60 s (1 sol = 1,479.6 min).

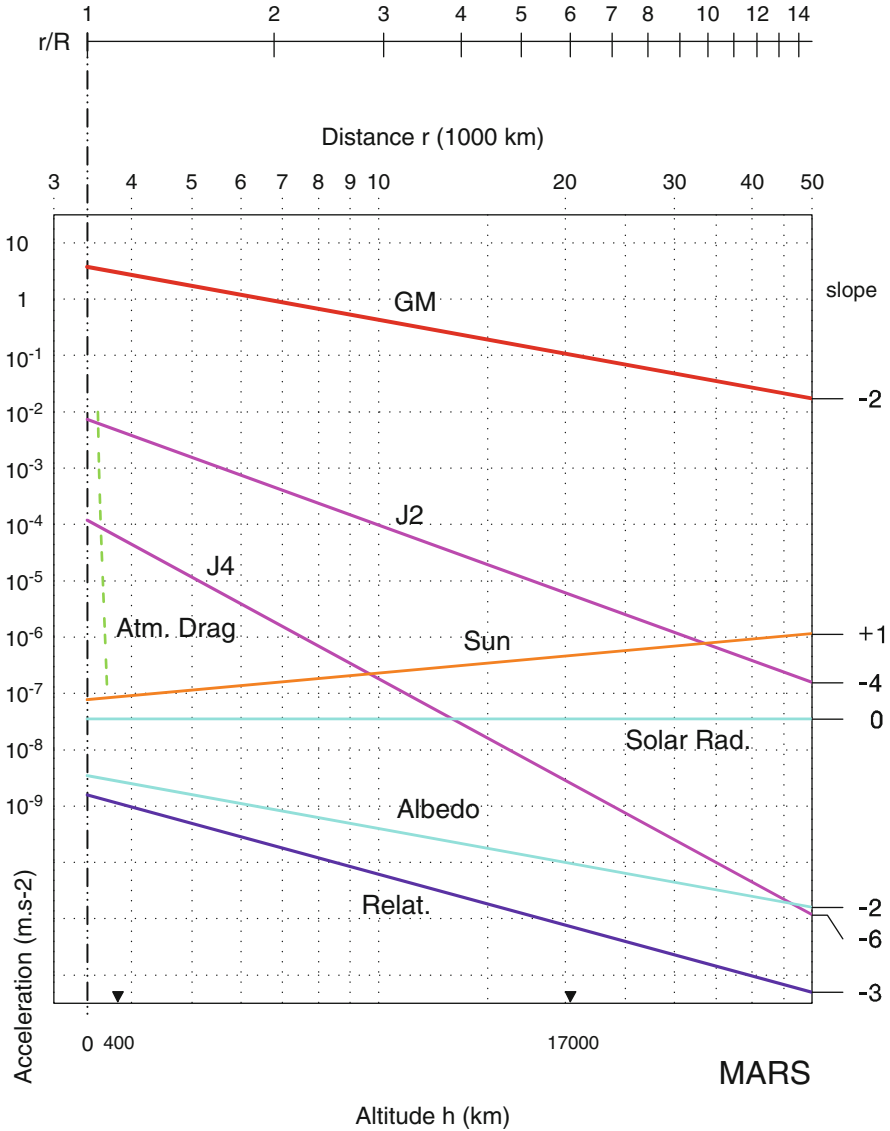


FIG. 15.9 : Central and perturbative accelerations as a function of the distance  $r$  of the satellite from the center of Mars. Log-log scale. In the range of variation considered, the curves are approximately straight lines and their slope is indicated. The altitudes of two types of satellite have also been noted.

as for Earth. Figure 15.9 shows the various accelerations affecting the motion as a function of the distance  $r$  from the satellite to the center of the planet. This corresponds to Fig. 6.1 for the Earth. The notation for the accelerations is the same as in Table 6.1.

**Conservative Forces**

The central acceleration  $\gamma_{CCC}$  has slope  $p = -2$  on a log–log scale. Likewise, the acceleration due to the term in  $J_2$  and those due to the following terms  $J_4, J_6$ , and so on, follow the same pattern as their counterparts for the Earth, i.e.,  $p = -4$  for  $\gamma_{CCN.J2}$ ,  $p = -6$  for  $\gamma_{CCN.J4}$ , etc. At the origin  $h = 0$ , numerical values are

$$\gamma_{CCC}(R) = g(R) = g_0 = 3.73 \text{ m s}^{-2} ,$$

$$\gamma_{CCN.J2}(R) = 7.4 \times 10^{-3} \text{ m s}^{-2} , \quad \gamma_{CCN.J4}(R) = 1.2 \times 10^{-4} \text{ m s}^{-2} .$$

The lunisolar attraction on a terrestrial satellite is simply replaced here by the solar attraction, which is weaker than on Earth. As for the Earth, its value is obtained from (6.151). The slope of the curve is  $p = +1$  and its value at the origin is

$$\gamma_{CS}(R) = 2 \frac{\mu_S}{a_S^3} R = 8 \times 10^{-8} \text{ m s}^{-2} ,$$

where  $a_S$  is the semi-major axis of the heliocentric orbit of Mars.

Tidal effects on the satellite are due to land tides caused by the Sun, which are much less marked than on Earth. The relativistic effect  $\gamma_{CR}$ , with slope  $p = -3$ , is calculated in the same way as for the Earth.

**Dissipative Forces**

Solar radiation pressure is only half the value on Mars as compared with the Earth (term going as  $a_S^{-2}$ ). The albedo effect depends on the region overflown. The albedo of Mars is rather low (mean value 0.22). The effect of drag due to the Martian atmosphere is less than on Earth for the same reduced altitude, because the atmosphere on Mars is less dense and the thermosphere is cooler.

**Note on Atmospheric Drag**

Atmospheric models have been made for Mars, such as the Mars Climate Database (MCD) made by the *Laboratoire de Météorologie Dynamique* (LMD, Paris), which gives the atmospheric density in the form discussed in Chap. 6, with the relation (6.112):

$$\rho_i(h, \tau_{LMT}, D, \psi) , \quad i = 1, 2, \dots, n , \tag{15.27}$$

where the subscript  $i$  runs over a multitude of different scenarios, such as typical year, global storm, etc.

The drag force, modifications of the orbital elements, or  $\Delta V$  are calculated in the same way as for the Earth. The simplified relation (6.129) giving  $\Delta V$  for eccentric orbits is particularly relevant for Mars, where aerobraking has been used for several missions and will no doubt be used again in the future. It applies whenever the eccentricity is greater than some limiting value, calculating using (6.131).

If we set the condition  $\Delta t_{\text{eff}}/T < 0.1$ , with  $H = 8 \text{ km}$ ,  $a = 4,000 \text{ km}$ , we obtain the constant

$$e > 0.03 \iff \text{equation (6.129) is applicable .}$$

### 15.3.3 Secular Variation of Orbital Elements

We use the theory of perturbations to determine the evolution of the six orbital elements of the satellite. We showed in Chap. 6 that the three metric elements  $a$ ,  $e$ , and  $i$  remained constant, ignoring short- and long-period periodic variations. The secular variation of the angular elements is given by (7.1) or (7.4) for  $\dot{\Omega}$ , (7.2) or (7.13) for  $\dot{\omega}$ , and (7.3) for  $\dot{M}$ , as a function of the inclination  $i$  and the semi-major axis  $a$  of the orbit.

The periodic variations can be expressed with the help of the coefficient  $K_0$  defined by (7.7). For Mars, this coefficient can be expressed as follows, depending on the units used:

$$K_0 = 3.07484 \times 10^{-6} \text{ rad s}^{-1} , \quad (15.28)$$

$$K_0 = 15.222^\circ \text{ day}^{-1} , \quad (15.29)$$

$$K_0 = 15.640^\circ \text{ sol}^{-1} , \quad (15.30)$$

$$K_0 = 29.047 \text{ rev}(\text{Martian yr})^{-1} . \quad (15.31)$$

For given values of  $i$  and  $a$ , the precession rates are higher on Mars than on Earth because of the value of the  $J_2$  term, which is twice as great.

The unit for calculations is rad/s, but in graphs showing these quantities as a function of the inclination, we have used units of deg/sol. The nodal precession rate  $\dot{\Omega}$  shown in Fig. 15.10 (upper) has a maximum of  $15.6^\circ \text{ sol}^{-1}$  for  $a = R$  and  $i = 0^\circ$  or  $180^\circ$ . Under the same conditions, the apsidal precession rate  $\dot{\omega}$  shown in Fig. 15.10 (lower) has a maximal value of  $31.2^\circ \text{ sol}^{-1}$ . The value of the critical inclination is independent of the attracting planet.

**Example 15.2** Calculate the nodal precession rate for the satellite ExoMars-TGO.

► The satellite ExoMars-TGO has a circular orbit with  $h = 400 \text{ km}$  and inclination  $i = 74^\circ$  (see Fig. 15.21 lower). We find  $a = 3,788 \text{ km}$ ,  $\eta = a/R = 1.11512$ . Applying (7.4), we obtain

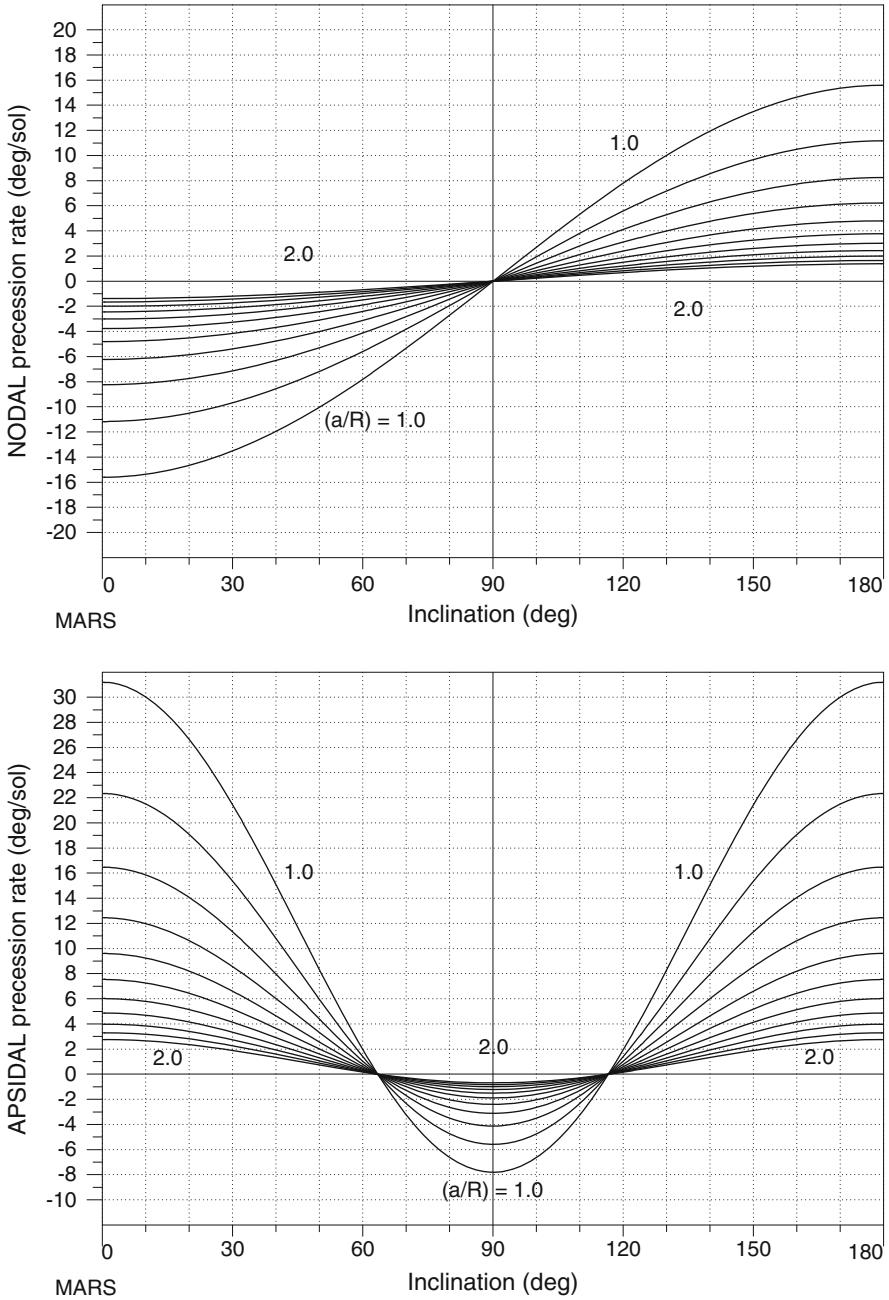


FIG. 15.10 : Precession rate for a circular or near-circular orbit in degrees per sol as a function of the inclination  $i$  for various values of the reduced distance, from  $a/R = 1.0$  to  $a/R = 2.0$ , in steps of  $0.1$ . Upper: Nodal precession rate  $\dot{\Omega}$ . Lower: Apical precession rate  $\dot{\omega}$ . Note that the value of the critical inclination is independent of the attractive source.

$$\dot{\Omega} = -5.6951 \times 10^{-7} \text{ rad s}^{-1} .$$

Converting units, this means that  $\dot{\Omega} = -2.90^\circ \text{sol}^{-1}$ . We can also obtain the result from Fig. 15.10 (upper), where we read off the value directly. Applying (10.2), we obtain  $C_S = -104.8$  for the cycle relative to the Sun, which means that, every 105 sols, we find the same local overpass time. The 24 local hours are thus sampled more than six times every Martian year. Recurrence characteristics, Table 15.8. ◀

**Example 15.3** Calculate the nodal and apsidal precession rates for the satellite MAVEN.

► The orbital characteristics of MAVEN are as follows:

$$a = 6,578 \text{ km} , \quad e = 0.4608 , \quad i = 75^\circ .$$

This satellite is thus in an elliptical orbit with rather low periastron given by  $h_p = 150 \text{ km}$  (see Fig. 15.21 upper). The nodal precession will thus sweep through all local times. Precession rates are calculated using the general formulas (7.15) and (7.16). For the nodal precession rate, we find  $\dot{\Omega} = -0.825^\circ/\text{sol}$ , which gives a (retrograde) cycle relative to the Sun of 306 sols. For the apsidal precession rate, we find  $\dot{\omega} = -0.639^\circ/\text{sol}$ , so the periastron makes one round trip (in the retrograde sense) in 436 sols, or 1.5 round trips per Martian year. ◀

## 15.4 Different Orbits

The classification criteria are the same as for terrestrial satellites. The orbit can be prograde or retrograde. It can be Sun-synchronous, recurrent, or frozen, or none of these. In terms of altitude, we speak of high orbits for areostationary satellites, or stationary Mars orbit (SMO), while a low orbit is one flying below 800 km, a low Mars orbit (LMO). Here we shall be interested in the two types of orbit discussed in Chap. 7, i.e., planetosynchronous and Sun-synchronous.

### 15.4.1 Areosynchronous Satellite

#### Areostationary Satellite

We define an areosynchronous satellite by  $n = \dot{\Omega}_T$ , and an areostationary satellite by adjoining the condition  $i = 0$ . Considering the mean Keplerian motion, we obtain

$$a_0^3 = \frac{\mu}{\dot{\Omega}_T^2} = 8.524274 \times 10^{21} ,$$

$$a_0 = 20,427.694 \text{ km} , \quad h_0 = 17,031 \text{ km} .$$

Bringing the  $J_2$  term into the calculation of the period, we obtain the value  $a_1$ , which is slightly bigger than  $a_0$ . In the case of a stationary satellite for Mars, the perturbing acceleration due to the term in  $J_2$  is 13 times greater than that due to the Sun, as can be seen from Fig. 15.9. Recall that this is not so for a terrestrial stationary satellite, where the lunisolar perturbation is greater than that due to  $J_2$ . We shall take this value  $a_1$  to be the one for an areostationary satellite, denoting it by  $a_{\text{GS}}$  :

$$a_{\text{GS}} = 20,428.500 \text{ km} , \quad h_{\text{GS}} = 17,031.5 \text{ km} , \quad (15.32)$$

$$\eta_{\text{GS}} = \frac{a_{\text{GS}}}{R} = 6.014 . \quad (15.33)$$

The value of  $\eta_{\text{GS}}$  for the Earth given by (7.72) is close to the value found for Mars, because the same is true of the diurnal rotation periods and mean densities of these two planets.

The possibility of placing satellites in areostationary orbits is currently under study, e.g., the satellite MARSat (Mars Areostationary Relay Satellite).

### Stationkeeping

The orbit of the geostationary satellite changes as time goes by:

- The semi-major axis  $a$  is modified by the effects of tesseral terms in the geopotential, which are much greater than for the Earth.
- The eccentricity  $e$  is modified by the effects of solar radiation pressure, much less significant than for the Earth.
- The inclination  $i$  is modified mainly by the action of the Sun, since the plane of the ecliptic in which the apparent Sun moves is tilted at  $25^\circ$  to the plane of the (Martian equatorial) orbit.

The two moons of Mars, also in the equatorial plane, are too small to perturb the motion of such a satellite.

### Longitudinal Acceleration

Here we consider the evolution of  $a$  in more detail. As we saw in Chap. 7, this phenomenon is caused mainly by the tesseral harmonic  $P_{22}$ . Indeed, we calculated this drift (through its longitudinal acceleration), first by expanding the geopotential up to second order, then continuing up to third order. The values of the tesseral coefficients  $C_{22}$ ,  $S_{22}$ ,  $C_{3l}$ , and  $S_{3l}$ , much greater than for the Earth, indicate that the shape of the Martian equator is not circular, and that the planet has a certain triaxiality, i.e., the ellipsoid of revolution is somewhat extended along an axis perpendicular to the axis of rotation (see Table 15.3).

**Expansion of the Geopotential to Order Two.** The longitudinal acceleration is given by (7.85). Using the Mars model MGM1025, we obtain

$$J_{22} = 63.0691 \times 10^{-6}, \quad \lambda_{22} = -15.02^\circ,$$

and

$$\ddot{\lambda} = \mathcal{A} \sin 2(\lambda - \lambda_{22}), \quad (15.34)$$

with

$$\frac{\dot{\Omega}_T}{\eta_{GS}} = \frac{7.088 \times 10^{-5}}{6.014} = 1.1786 \times 10^{-5} \text{ rad s}^{-1},$$

$$\begin{aligned} \mathcal{A} &= 18 \left( \frac{\dot{\Omega}_T}{\eta_{GS}} \right)^2 J_{22} = 18 \times 1.3891 \times 10^{-10} \times 63.0691 \times 10^{-6} \\ &= 157.6965 \times 10^{-15} \text{ rad s}^{-2}. \end{aligned} \quad (15.35)$$

For the coefficient  $\mathcal{A}$  in degrees per sol per sol,

$$\mathcal{A} = 157.6965 \times 10^{-15} \times \frac{180}{\pi} \times (88642.7)^2 = 70.992 \times 10^{-3} \text{ deg sol}^{-2}. \quad (15.36)$$

**Expansion of the Geopotential to Order Three.** The required values are  $J_{31} = 27.4791 \times 10^{-6}$ ,  $J_{33} = 6.0455 \times 10^{-6}$ , and for the longitudes,  $\lambda_{31} = 81.41^\circ$  and  $\lambda_{33} = 12.04^\circ$ .

The acceleration is given by (7.92). Putting in the numbers gives

$$\ddot{\lambda} = \mathcal{A} \left[ \sin 2(\lambda - \lambda_{22}) - 0.0180 \sin(\lambda - \lambda_{31}) + 0.1190 \sin 3(\lambda - \lambda_{33}) \right]. \quad (15.37)$$

The graph of  $\ddot{\lambda}(\lambda)$  in Fig. 15.11 gives the longitudinal acceleration  $\ddot{\lambda}$  as a function of the longitude  $\lambda$ . Since longitudes are measured positively toward the east, we thus have

$$\ddot{\lambda} > 0 \implies \text{eastward displacement}, \quad \ddot{\lambda} < 0 \implies \text{westward displacement}.$$

The solutions of  $\ddot{\lambda} = 0$  are the four longitudes on the graph where  $\ddot{\lambda}(\lambda)$  intersects the horizontal axis. The two stable points are on the downward sloping parts of the curves, and the unstable points on the upward sloping parts. The values are indicated in Fig. 15.11.

The four equilibrium longitudes obtained for Mars are unbelievably close to the terrestrial values. This is purely accidental, since the zero meridian for these two planets is in each case entirely arbitrary and is in no way related to the details of the geopotential.

Equation (15.37) shows that it is the degree 2 harmonic which carries most weight. The four longitudes obtained solely from  $\lambda_{22}$ , namely,

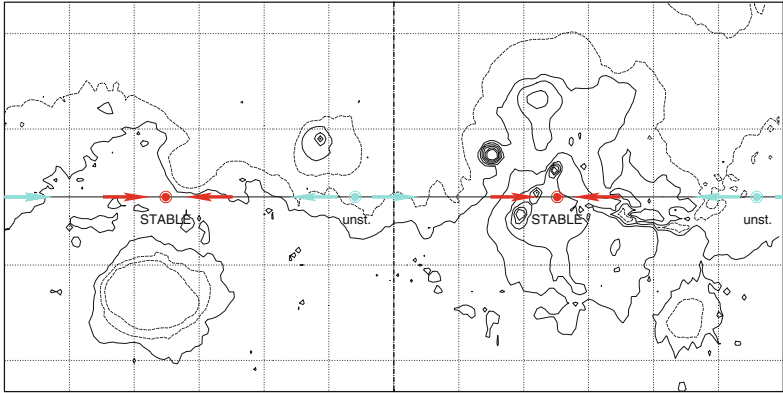
$$\lambda = \lambda_{22} + k 90^\circ, \quad k = 1, 2, 3, 4,$$



**[MARS] AREOSTATIONARY**

Satellite  
Areostationary

Altitude = 17034.0 km      a<sub>GS</sub> = 20430.990 km  
 Inclination = 0.00°      ParkL: 180° W <-> 180° E  
 Period = 1477.11 min \* rev/sol = 1.00  
 Equat. orbital shift = 21341.8 km



Projection: Mercator      Project. centre: 0.0° ; 180.0° W      Areostationary  
 Property: Conformal      Aspect: Direct      MC \* LMD  
 ♂ T.:Cylindrical - Graticule: 30° [3.5] [+90.0/ +0.0/ +90.0] [-] MGM1025 *MOLA Topogr. / h / 2.5km /* ΑΤΛΑΣ

**AREOSTATIONARY**

Longitudinal Acceleration

a<sub>GS</sub> = 20430.990 km      Gravitat. Model: MGM1025  
 Inclination = 0.00°

Stable Point ... 74.6° E  
 Stable Point ... 104.4° W

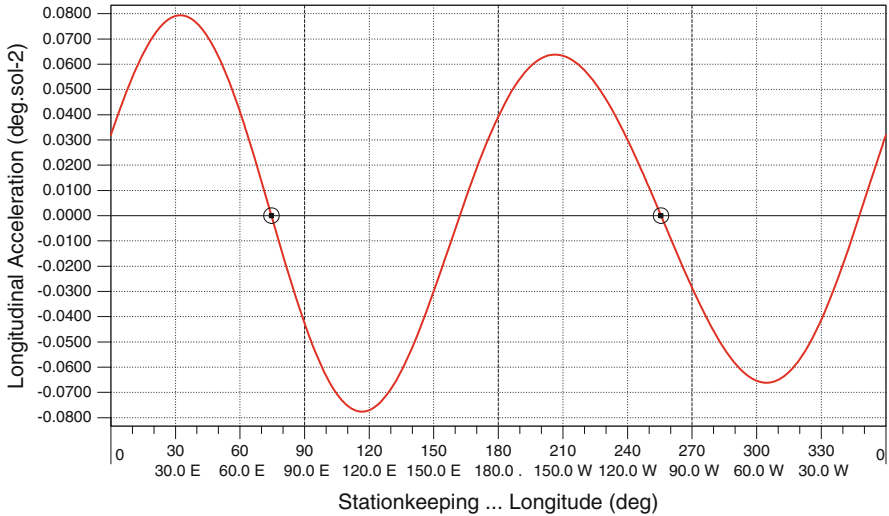


FIG. 15.11 : Longitudinal acceleration for an areostationary satellite as a function of the longitude. Zero values of the acceleration determine equilibrium points:  $\lambda = 74.587^\circ = 74^\circ 35' E$  and  $\lambda = 255.557^\circ = 104^\circ 27' W$  for the stable equilibrium points, indicated by a circle, and  $\lambda = 162.065^\circ = 162^\circ 39' E$  and  $\lambda = 347.741^\circ = 12^\circ 15' W$  for the unstable equilibrium points. The satellite is subject only to orbital perturbations due to the geopotential (model MGM1025). Upper: Map indicating positions of stable and unstable points.

or  $75^\circ$ ,  $165^\circ$ ,  $255^\circ$ , and  $345^\circ$  are very close to the four longitudes obtained from (15.37) by going up to order 3, namely,  $75^\circ$ ,  $162^\circ$ ,  $256^\circ$ , and  $348^\circ$ . The contribution from the other terms becomes negligible from order 4 onwards, since a further multiplicative coefficient  $1/\eta_{\text{GS}}$ , or 0.17, is brought in for each new order.

## 15.4.2 Sun-Synchronous Satellite

### Sun-Synchronicity Constant

For Sun-synchronous satellites, we have seen that the condition  $\dot{\Omega}(a, i) = \dot{\Omega}_{\text{S}}$  must be satisfied. We begin by calculating the constant of Sun-synchronicity using (7.98). For Mars, this gives

$$k_{\text{h}} = 29.0403 . \quad (15.38)$$

This is three times the value for the Earth, because  $J_2$  is greater for Mars, and in addition, the planet moves more slowly around the Sun.

### Sun-Synchronous Satellite: Circular Orbit

From (7.104) or (7.105), we thus obtain the relation between the inclination and the altitude.<sup>21</sup> Figure 15.12 (upper) shows the altitude as a function of the inclination for a Sun-synchronous satellite, which is necessarily retrograde.

The minimal value of  $i_{\text{HS}}$ , denoted by  $i_{\text{HS min}}$  (or  $i_{\text{m}}$ ), is obtained for a (fictitious) satellite revolving at ground level ( $\eta = 1$  or  $h = 0$ ):

$$i_{\text{HS min}} = i_{\text{m}} = \arccos\left(-\frac{1}{k_{\text{h}}}\right) = \arccos(-0.0344) = 92.0^\circ .$$

The maximal value of  $h$  is obtained for  $i = 180^\circ$ :

$$\eta_{\text{HS max}} = \frac{a}{R} = k_{\text{h}}^{2/7} = 2.6182 ,$$

$$a_{\text{HS max}} = 8,892 \text{ km} , \quad h_{\text{HS max}} = 5,496 \text{ km} .$$

It is not therefore possible to place a Sun-synchronous satellite in circular orbit at an altitude greater than 5,500 km (roughly the same bounding altitude as on Earth).

The US satellites MGS, Mars Odyssey, and MRO are on Sun-synchronous orbits.

---

<sup>21</sup> As for the Earth, there is a slight difference in the value of  $i_{\text{HS}}$  depending on the degree to which the planetary potential is expanded. For  $h = 400 \text{ km}$ ,  $i_{\text{HS}}(J_4) = 92.991^\circ$  and  $i_{\text{HS}}(J_2) = 92.914^\circ$ , i.e., a difference of  $0.077^\circ$ .

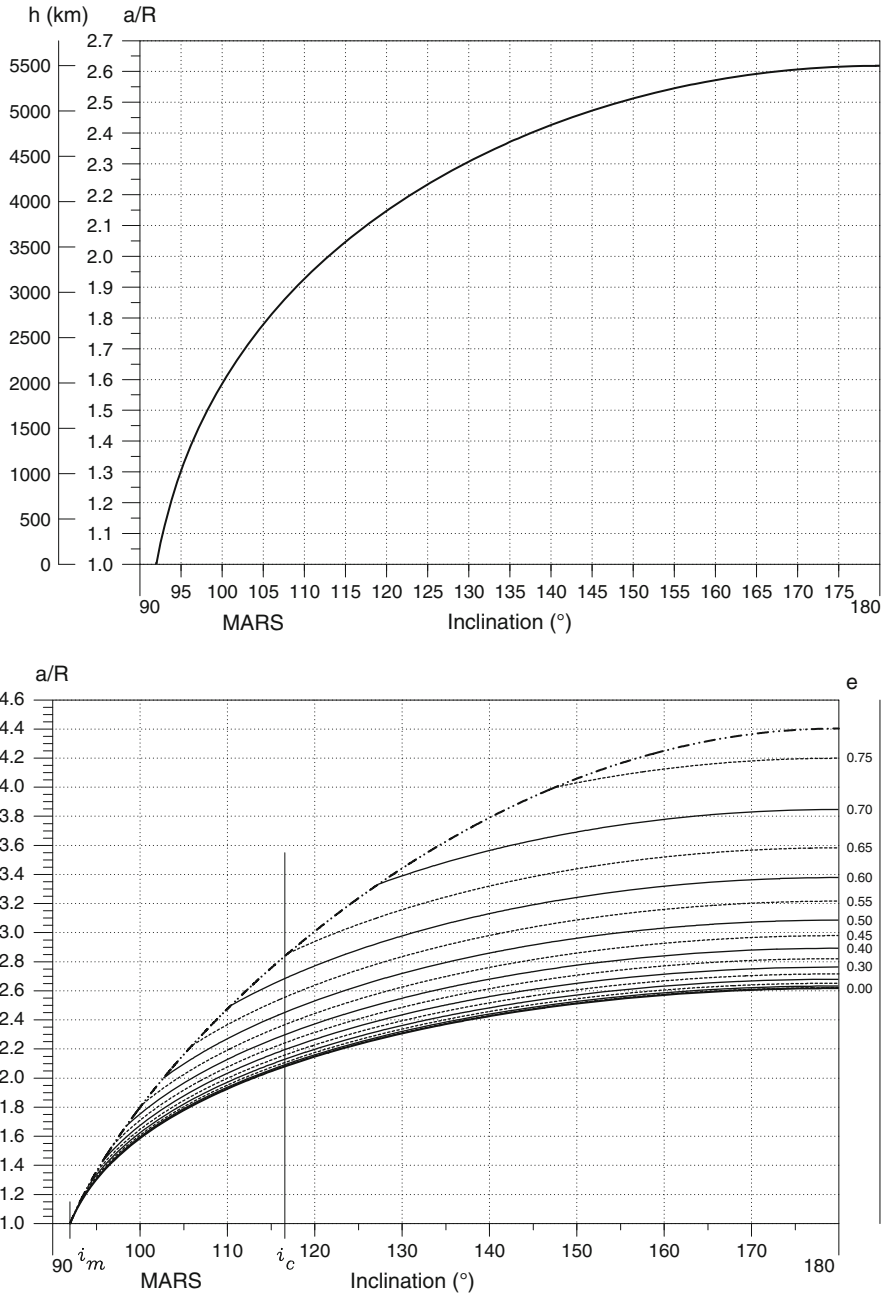


FIG. 15.12: Altitude of a Sun-synchronous satellite as a function of the angle of inclination for Sun-synchronous satellites. The whole possible range is shown. Upper: Satellite in circular orbit. Lower: Satellite in orbit with eccentricity  $e$ . See caption to Fig. 7.15.

## Sun-Synchronous Satellite: Elliptical Case

Calculations for an elliptical Sun-synchronous orbit are done in exactly the same way as for the Earth, using the fundamental relation (7.112), within a limiting eccentricity  $e_1$  for each value of  $\eta_1$  [see (7.114)]. On Mars, the possible range of eccentricities is greater than for the Earth (see Fig. 15.12 lower). For  $i = 180^\circ$ , the reduced distance  $a/R$  ranges from  $\eta = 2.6182$  for  $e = 0$  to  $\eta = \eta_1 = 4.4032$  for  $e = e_1 = 0.7729$ .

When the orbit is eccentric, one must add to the Sun-synchronicity condition the constraint that the periastron should not drift on the orbit. One must therefore choose the critical inclination given by (6.79), which necessarily implies the value  $i = 116.6^\circ$ . For this inclination, the reduced distance varies between  $\eta = 2.069$  for  $e = 0$  and  $\eta = 2.847$  for the maximal eccentricity  $e_1 = 0.649$  (see Example 15.9).



*Throughout the remainder of this chapter, we shall adopt precisely the same presentation for Martian satellites as we did for terrestrial ones. Each Martian section will be a carbon copy of the terrestrial one.*



## 15.5 Ground Track of a Satellite

✠ **Chapter 8.** The representation of the ground track gives fundamentally similar results for terrestrial and Martian satellites. Even the Snyder projection (where the ground track appears as a straight line) can be applied directly using the frequency  $\kappa$ . The only difference with the Earth is that we do not yet have any equivalent of the NORAD TLE for Mars!

### 15.5.1 Representing the Ground Track

The ground track of an LMO satellite has the same general appearance as the ground track of an LEO satellite. Example 15.4 brings out this similarity. For satellites in circular orbit, the equation of the ground track takes the form (8.47) when the time is eliminated, using a suitable value of  $\kappa$ . For operational Sun-synchronous satellites (see Table 15.6) for which  $\kappa = \nu$ , we have

$$\begin{aligned}\kappa &= 13 - 233/550 = 6717/550 = 12.212727, & \text{for MGS,} \\ \kappa &= 12 + 15/32 = 399/32 = 12.468750, & \text{for ODY (Mars Odyssey),} \\ \kappa &= 13 + 65/349 = 4602/349 = 13.186246, & \text{for MRO.}\end{aligned}$$

**[MARS]** Mars Global Surveyor  
Orbit - Ground track

Recurrence = [13;-233;550]6917

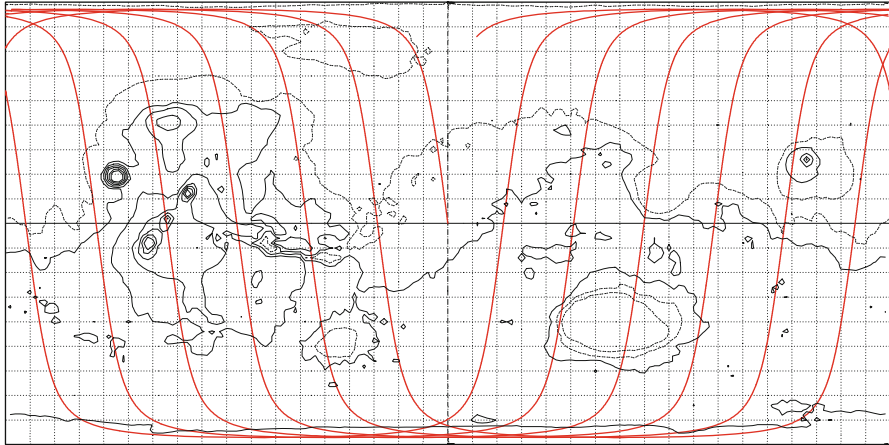
>>>> Time span shown: 739.8 min = 0.50 sol

Altitude = 378.1 km                      a = 3775.088 km

Inclin./SUN-SYNCHRON.= 92.90 °

Period = 117.64 min \* rev/sol = 12.58

Equat. orbital shift = 1697.1 km ( 28.6 °)



Proj.: Plate-carrée	Project. centre: 0.0 ° ; 0.0 °	Asc. Node: 0.00 °	Ιξίων
Property: none	Aspect: Direct	App. inclin. = 97.42 °	MC * LMD
♁ T.:Cylindrical - Graticule: 10°	{3.5} [ +0.0/ +0.0/ +0.0] [-]	MGM1025 <i>MOLA Topogr. / h / 2.5km /</i>	Ατλας

**"Equivalent" MGS**  
Orbit - Ground track

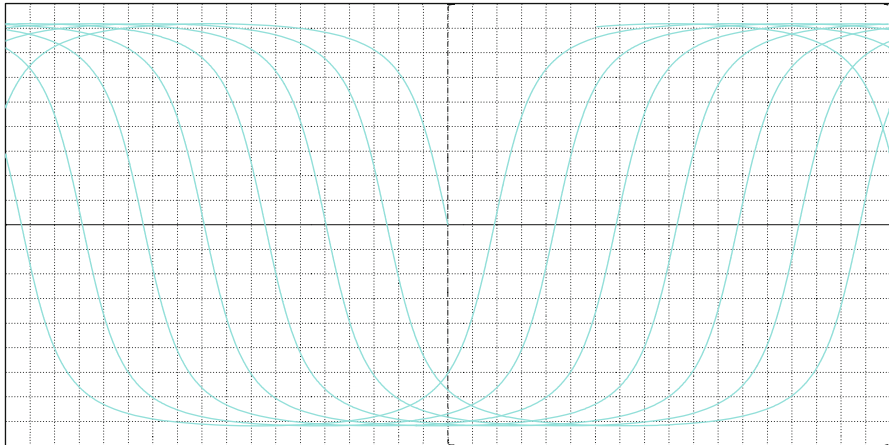
>>>> Time span shown: 720.0 min = 0.50 day

Altitude = 711.6 km                      a = 7089.752 km

Inclin./SUN-SYNCHRON.= 98.26 °

Period = 99.14 min \* rev/day = 14.53

Equat. orbital shift = 2758.9 km ( 24.8 °)



Proj.: Plate-carrée	Project. centre: 0.0 ° ; 0.0 °	Asc. Node: 0.00 °	Ιξίων
Property: none	Aspect: Direct	App. inclin. = 102.12 °	MC * LMD
♁ T.:Cylindrical - Graticule: 10°	{-} [ +0.0/ +0.0/ +0.0] [-]	EGM96	Ατλας

FIG. 15.13 : Upper: Ground track of the Sun-synchronous satellite MGS over half a sol. Lower: Ground track of the fictitious Sun-synchronous satellite equivalent to MGS but with Earth as the attracting body.

**Example 15.4** *Comparison between the ground track of Mars Global Surveyor (MGS), in a near-circular Sun-synchronous orbit around Mars at an altitude of 379 km, with the ground track of a fictitious terrestrial satellite at the same reduced altitude, also on a Sun-synchronous orbit.*

► The reduced distance  $\eta$  is the same for both satellites.

**MGS.** During its topographical phase, MGS followed a Sun-synchronous orbit with  $h = 379$  km. We calculate the reduced distance as

$$\eta = \frac{a}{R} = \frac{3775.1}{3196.2} = 1.1116 .$$

We obtain the inclination of the Sun-synchronous satellite MGS using (7.105):

$$i_{\text{HS}} = \arccos \left( -\frac{1.1116^{2/7}}{29.0403} \right) = 92.03^\circ .$$

Expanding beyond the  $J_2$  term for the nodal precession rate, we obtain

$$i_{\text{HS}} = 92.93^\circ .$$

The ground track of the satellite thus lies between the geocentric latitudes  $87.07^\circ\text{N}$  and  $87.07^\circ\text{S}$ . It is shown in Fig. 15.13 (upper) over half a Martian day (half a sol). With 12.6 round trips per sol, the equatorial shift is  $29^\circ$ .

**Equivalent MGS.** To compare the orbits and ground tracks on Mars and on Earth, we calculate the characteristics of a terrestrial satellite at the same reduced altitude, i.e., the same reduced distance from the attractive center of the planet, and hence the same value for  $\eta$ . We call this fictitious satellite the equivalent MGS for the Earth. With  $\eta = 1.1116$ , we obtain  $a = \eta \times 6378 = 7,090$  km, or  $h = 712$  km.

We deduce the inclination to be

$$i_{\text{HS}} = 98.26^\circ .$$

The ground track of the satellite lies between  $81.74^\circ\text{N}$  and  $81.74^\circ\text{S}$ . It is shown in Fig. 15.13 (lower). With 14.5 round trips per day, the equatorial shift is  $25^\circ$ . We note here the main difference:

- The inclination of the Sun-synchronous Martian satellite is more polar, i.e.,  $k_{\text{h}}$  is greater for Mars than for the Earth.
- The equatorial shift is a little greater for the Martian satellite, because its period is longer, since Mars has a lower mean density than Earth [see (16.3)].

◀

**Example 15.5** *Orbit and ground track of Mars Express over a cycle of 4 sols.*

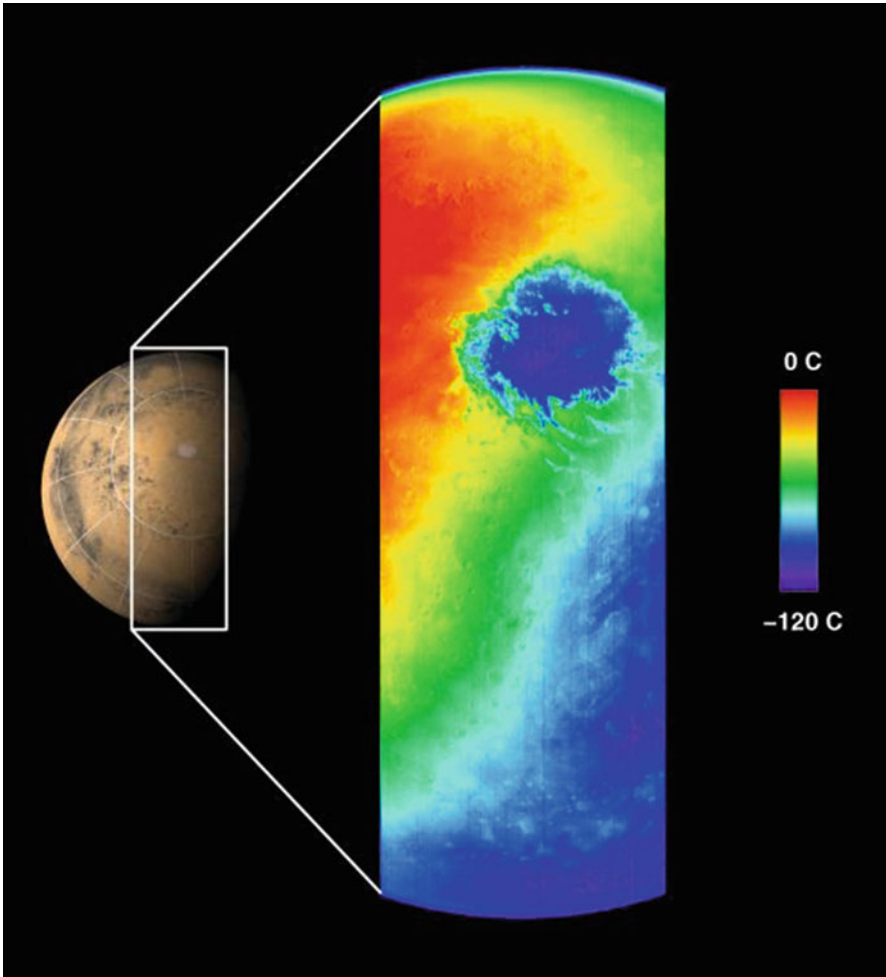


FIG. 15.14 : Infrared image of the Martian South Pole, taken using THEMIS aboard Mars Odyssey on 31 October 2001. The satellite's orbit has not yet been circularised and the image coincides with the ninth revolution, at an altitude of 22,000 km. It is late austral spring in the Martian southern hemisphere ( $L_S = 263^\circ$ ). The extremely cold circular feature shown in blue is the Martian south polar carbon dioxide ice cap at a temperature of about  $-120^\circ\text{C}$ . The cap is more than 900 km in diameter at this time and will continue to shrink as austral summer progresses. The cold region in the lower right portion of the image shows the nighttime temperatures of Mars. The warmest regions occur near local noontime. The thin blue crescent along the upper limb of the planet is the Martian atmosphere. This image covers a length of over 6,500 km spanning the planet from limb to limb, with a resolution of approximately 5.5 km per pixel. Odyssey's infrared camera is planned to have a resolution of 100 m per pixel from its mapping orbit. Credit (image and caption): NASA, JPL, Arizona State University.



**[MARS] Mars Odyssey**  
Orbit - Ground track

Recurrence = [12;+15; 32] 399

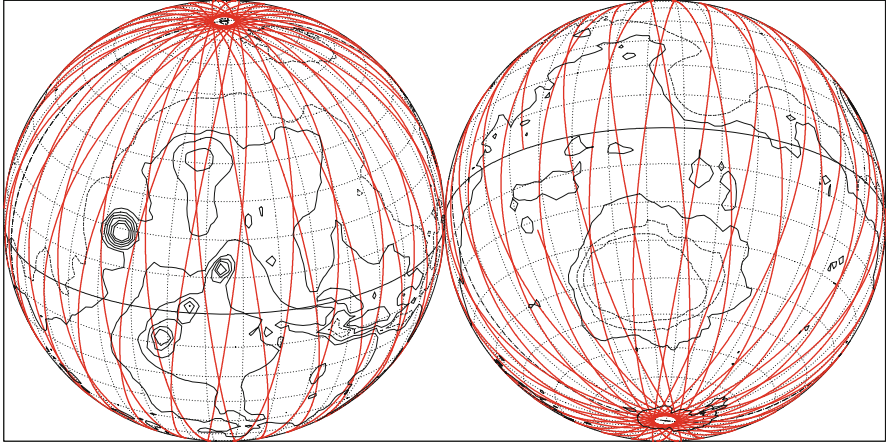
>>>> Time span shown: 2959.1 min = 2.00 sols

Altitude = 399.8 km                      a = 3796.847 km

Inclin./SUN-SYNCHRON.= 92.96 °

Period = 118.66 min \* rev/sol = 12.47

Equat. orbital shift = 1711.7 km ( 28.9 °)



Projection: Orthographic      Pr. centre (r.): 25.0 ° S; 75.0 °E  
Property: none                  Aspect: Oblique  
♁ T.:Azimuthal - Graticule: 10° {3.5} [-90.0/+115.0/+15.0] [-] MGM1025

Asc. Node: 35.00 ° [04:00 LMT]      Iξλων  
MC ★ LMD  
MOLA Topogr. / h / 2.5km /      ΑΤΛαας

**[MARS] Mars Odyssey**  
Orbit - Ground track

Recurrence = [12;+15; 32] 399

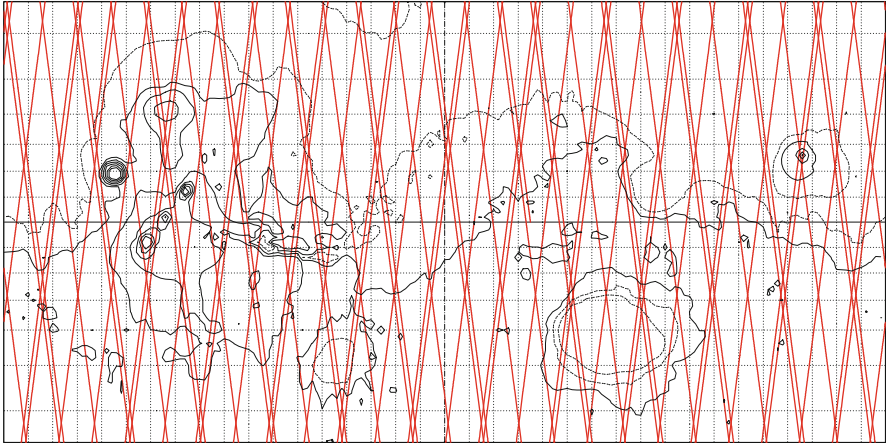
>>>> Time span shown: 4438.6 min = 3.00 sols

Altitude = 399.8 km                      a = 3796.847 km

Inclin./SUN-SYNCHRON.= 92.96 °

Period = 118.66 min \* rev/sol = 12.47

Equat. orbital shift = 1711.7 km ( 28.9 °)



Proj.: Snyder-Satel.Track/30°      Project. centre: 0.0 ° ; 0.0 °  
Property: none [Geoc.L]              Aspect: Direct  
♁ T.:Cylindrical - Graticule: 10° {3.5} [+0.0/ +0.0/ +0.0] [-] MGM1025

Asc. Node: 35.00 ° [04:00 LMT]      Iξλων  
App. inclin. = 97.52 °                  MC ★ LMD  
MOLA Topogr. / h / 2.5km /              ΑΤΛαας

FIG. 15.15 : Orbital ground track of the Sun-synchronous satellite Mars Odyssey. Upper: Over 2 sols. Lower: Over 3 sols (to show the 2-sol subcycle).



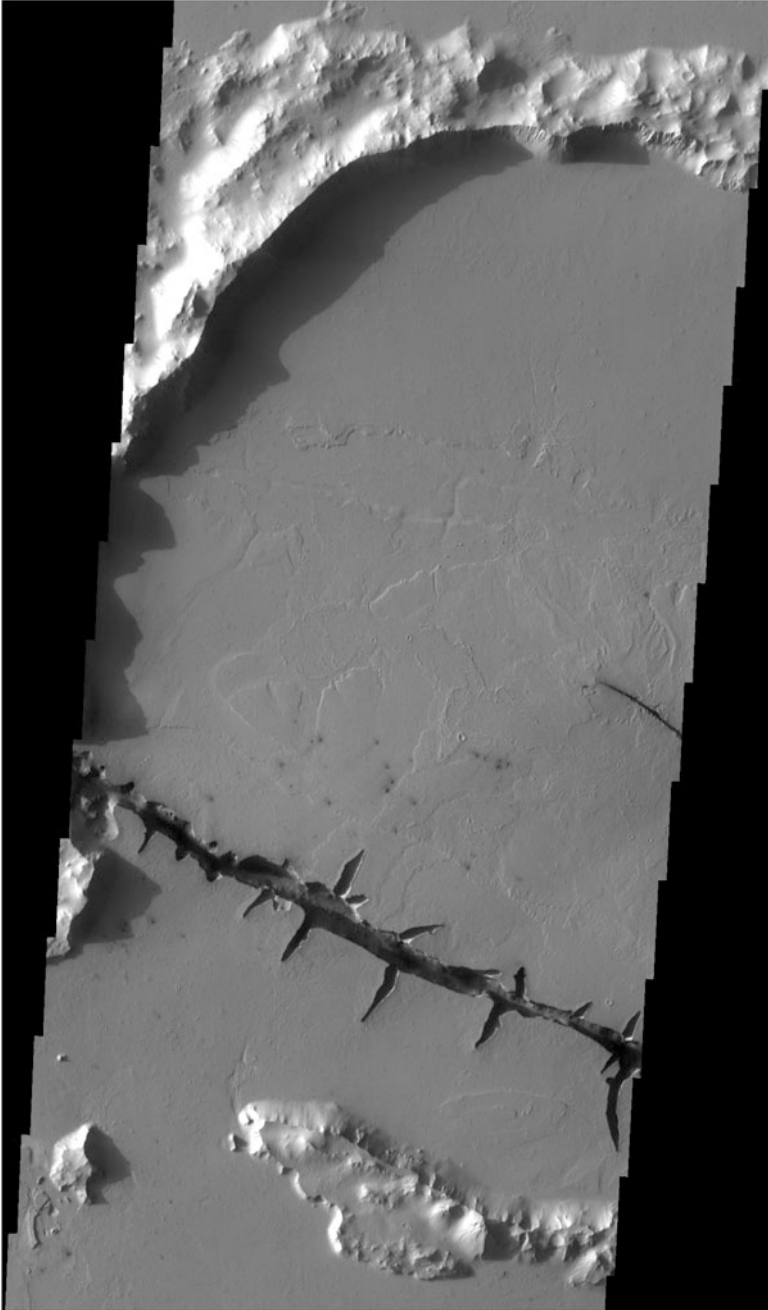


FIG. 15.16 : Geological fracture inside a crater. The circular form of the crater is visible. Image acquired by VIS/THEMIS aboard the satellite Mars Odyssey at time  $D = 2004\ 12\ 13\ 05:20$ . Revolution 13300. Center of image: Latitude = 7.3388, longitude = 161.372. Resolution = 0.018258 km/pixel (pixel size  $18 \times 18$  m). Width of swath 25 km. See Example 15.14. Credit: NASA, JPL, ASU.

**[MARS] Mars Express [G3-u]**

Orbit - ref.: Mars

Recurrence = [ 3; +1; 4] 13

&gt;&gt;&gt;&gt; Time span shown: 5918.1 min = 4.00 sols

Equiv. altit. = 5906.7 km

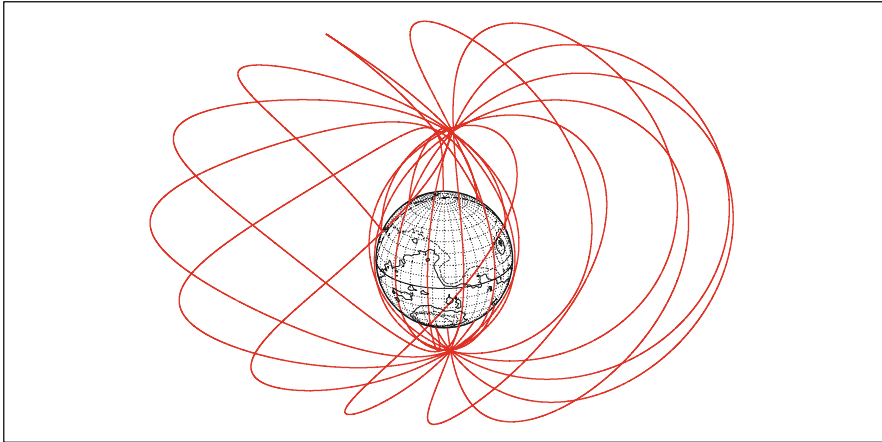
a = 9303.744 km

Inclination = 86.35 °

e = 0.606911

Period = 454.49 min \* rev/sol = 3.26

h\_a = 11553 km; h\_p = 260 km; arg.periapsis: +345.08 °



Projection: Orthographic

Project. centre: 25.0 ° N; 80.0 ° E

Asc. Node: -127.07 °

Ιξίων

Property: none

Aspect: Oblique

Apoapsis : -2.52 °

MC \* LMD

♁ T.:Azimuthal - Graticule: 10° {3.5} [-90.0/ +65.0/ +10.0] [-] MGM1025

MOLA Topogr. / h / 2.5km /

Ατλας

**[MARS] Mars Express [G3-u]**

Gr.tr. ( H &lt; 4000 km ) [ H : geodetic altitude ]

Recurrence = [ 3; +1; 4] 13

&gt;&gt;&gt;&gt; Time span shown: 5918.1 min = 4.00 sols

Equiv. altit. = 5906.7 km

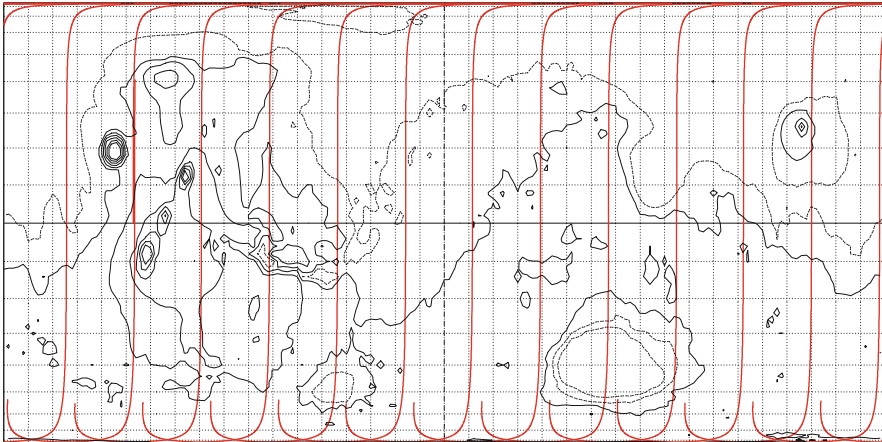
a = 9303.744 km

Inclination = 86.35 °

e = 0.606911

Period = 454.49 min \* rev/sol = 3.26

h\_a = 11553 km; h\_p = 260 km; arg.periapsis: +345.08 °



Projection: Behrmann

Project. centre: 0.0 ° ; 0.0 °

Asc. Node: -127.07 °

Ιξίων

Property: Equal area

Aspect: Direct

Apoapsis : -2.52 °

MC \* LMD

♁ T.:Cylindrical - Graticule: 10° {3.5} [+0.0/ +0.0/ +0.0] [-] MGM1025

MOLA Topogr. / h / 2.5km /

Ατλας

FIG. 15.17 : Upper: Orbit of the satellite Mars Express (orbit G3-u) over 4 sols, from 9 January 2004 ( $L_S = 330^\circ$ ). Lower: Ground track of this orbit, shown only when the altitude of the satellite is lower than 4,000 km.

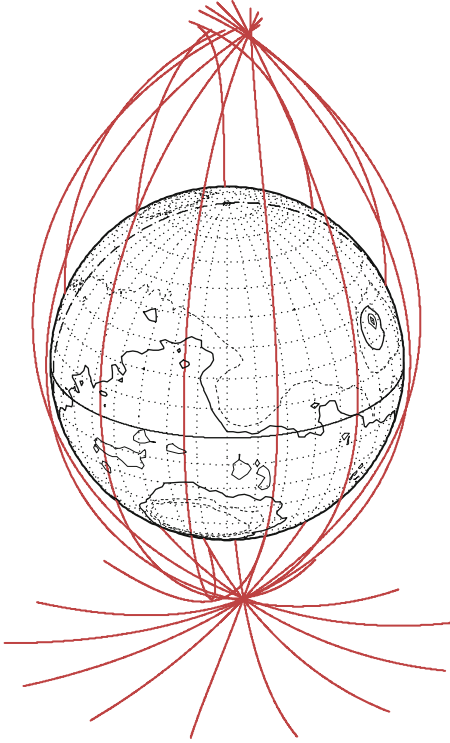


FIG. 15.18 : Orbit of the satellite Mars Express when it has altitude below 4,000 km, over a cycle of 4 sols, from 9 January 2004 ( $L_S = 330^\circ$ ). Type of orbit: 3G-u. This is a synthesis of Fig. 15.17.

► Mars Express has a highly eccentric orbit. Its near-polar inclination is a long way from the critical inclination. This leads to an apsidal precession rate of  $\dot{\omega} = -0.557^\circ$  per sol, corresponding to exactly one round trip of the pericenter in one Martian year. The representations given here concern the orbit type known as 3G-u (see Table 15.7). The period represented begins on 9 January 2004 ( $L_S = 330^\circ$ ) and lasts for one cycle of 4 sols. The orbit shown in Fig. 15.17 (upper) is plotted in a frame moving with the planet. Its ground track, shown in Fig. 15.17 (lower) is only plotted if the altitude of the satellite is less than 4,000 km. Above this altitude, observation of the planet is not accurate enough. Figure 15.18 shows the representation limited to  $h < 4,000$  km for the orbit itself, in a synthesis of the two parts of Fig. 15.17. See also Fig. 15.19. ◀

### 15.5.2 Apparent Inclination

The apparent inclination is calculated using (8.29) or (8.30).

**Example 15.6** Calculate the apparent inclination for the operational Sun-synchronous satellites.

$h$ (km)	$a$ (km)	$\nu$ (rev/s)	$T_0$ (min)	$T_0$ (sol)	$V$	$V_0$	$w_E$ 0	$w_E$ 90	$\mathcal{T}$
0	3,396	14.77	100.15	0.068	3.55	3.55	3.31	3.56	g
100	3,496	14.14	104.61	0.071	3.50	3.40	3.16	3.41	O
200	3,596	13.56	109.13	0.074	3.45	3.26	3.02	3.27	O
300	3,696	13.01	113.71	0.077	3.40	3.13	2.89	3.14	O
400	3,796	12.50	118.36	0.080	3.36	3.00	2.76	3.01	O
500	3,896	12.02	123.06	0.083	3.32	2.89	2.65	2.90	O
600	3,996	11.57	127.83	0.086	3.27	2.78	2.54	2.79	O
700	4,096	11.15	132.66	0.090	3.23	2.68	2.44	2.69	O
4,450	7,846	4.21	351.68	0.238	2.34	1.01	0.77	1.04	C
5,983	9,379	3.22	459.63	0.311	2.14	0.77	0.53		$\Phi$
17,031	20,427	1.00	1,477.38	0.999	1.45	0.24	0.00		S
20,063	23,459	0.81	1,818.16	1.229	1.35	0.20	-0.04		$\Delta$

TABLE 15.5 : *Velocity of the satellite and its ground track, and relative velocity of the ground track for various satellites in circular (Keplerian) orbit. For each satellite, the table gives the altitude  $h$  (in km) and the length of the semi-major axis  $a$ , or the distance to the center of Mars (in km), the daily frequency  $\nu$  (in revs per sol), the Keplerian period  $T_0$  (in minutes and in sols), the velocities  $V$ ,  $V_0$ ,  $w_E$  (for two values of the angle  $i$ ,  $0^\circ$ ,  $90^\circ$ ), already defined. Satellite type  $\mathcal{T}$ : g (ground level), O (for observation), C (for communications), S (areostationary, or SMO). Natural satellites:  $\Phi$  (Phobos),  $\Delta$  (Deimos).*

► Having determined the Sun-synchronous inclination, we use the values of  $\kappa$  given earlier to calculate  $\delta i$  using (8.30):

- For MGS,  $i_{\text{HS}} = 92.90^\circ$ ,  $\delta i = 4.52^\circ \implies i' = 97.42^\circ$ .
- For ODY,  $i_{\text{HS}} = 92.96^\circ$ ,  $\delta i = 4.56^\circ \implies i' = 97.52^\circ$ .
- For MRO,  $i_{\text{HS}} = 92.60^\circ$ ,  $\delta i = 4.32^\circ \implies i' = 96.92^\circ$ .

The difference of inclination  $\delta i$  is roughly  $4^\circ$ , of the same order as for terrestrial satellites. ◀

### 15.5.3 Velocity of Satellite and Ground Track in Circular Orbit

For a circular orbit, we calculate the velocity of the satellite and its ground track using (8.38)–(8.42). Recall that the velocities  $V$  (satellite) and  $V_0$  (ground track) are defined in the Galilean frame  $\mathfrak{R}$ , and the velocities  $w_E$  in the Martian frame  $\mathfrak{R}_T$ . The velocities  $w_E$  are said to be relative because they represent the velocity of the ground track relative to the planet. The results are given in Table 15.5. If we compare a terrestrial satellite with a Martian one at the same relative altitude, we find that the periods are roughly the



FIG. 15.19 : *Oblique view of Coprates Chasma, the eastern part of Valles Marineris. The canyon is 8 km deep. Image acquired by the High Resolution Stereo Camera (HRSC) aboard Mars Express, on 28 May 2005. Credit: ESA, DLR, FU Berlin (G. Neukum).*

same, but the velocities of the Martian satellites are only half the value, as is obvious from the equations. For the areostationary satellite, it can be checked that the relative velocity  $w_E(0)$  is zero. Note also that  $T_0 = D_{\text{sid}}$ , which is slightly different from  $D_M = 1$  sol.

The two moons of Mars are also recorded in Table 15.5, with  $\Phi$  for Phobos and  $\Delta$  for Deimos. These will be discussed further below.

## 15.6 Orbit Relative to the Sun: Crossing Times and Eclipse

✂ **Chapter 10.** To study the ground track in relation to the Sun, and in particular, local crossing times, we apply the methods discussed for the terrestrial satellite to the Martian case. We need only make the following remarks:

- The length of the mean day on Mars is the sol.
- The second is still the unit of time, wherever we are located, and the minute is equal to 60 s.

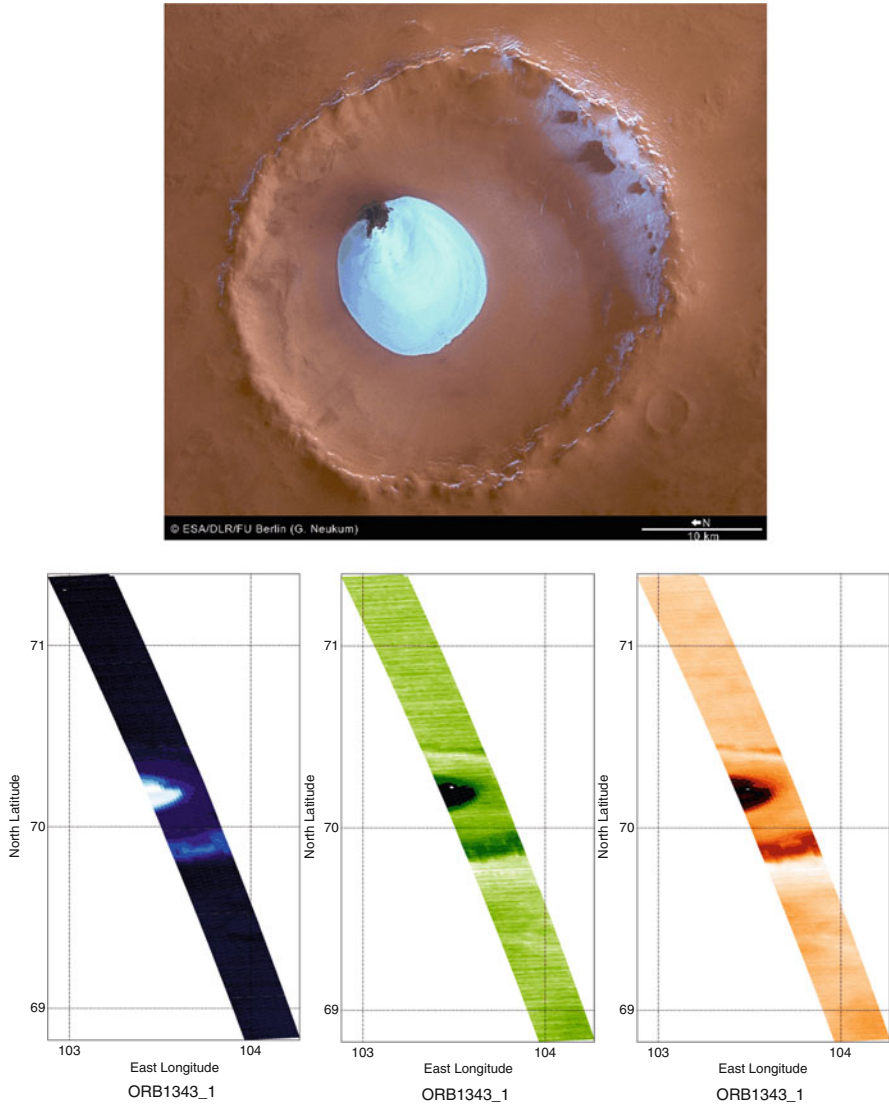


FIG. 15.20: Image of a crater in the Vastitas Borealis plains (center  $70^{\circ} 12' N$ ,  $103^{\circ} 25' E$ ), observed simultaneously by the HRSC (the whole crater) and the OMEGA instrument (three coloured bands), both aboard Mars Express, during revolution 1343. The HRSC image was obtained with a resolution of 15 m per pixel. The crater has diameter 35 km and depth 2 km. Chromatic analysis (blue, green, and red channels) confirms that the colour of the center of the crater is indeed bluish. It contains a deposit of water ice that is both surprising and aesthetic. This has a strong signature in the blue owing to the scattering properties of water ice. Credit: ESA, DLR, FU Berlin (G. Neukum). Credit: caption and document for chromatic analysis courtesy of Aymeric Spiga, LMD/CNRS.



**[MARS] MAVEN**

Orbit - ref.: Mars

Recurrence = [13;+65;349] 4602

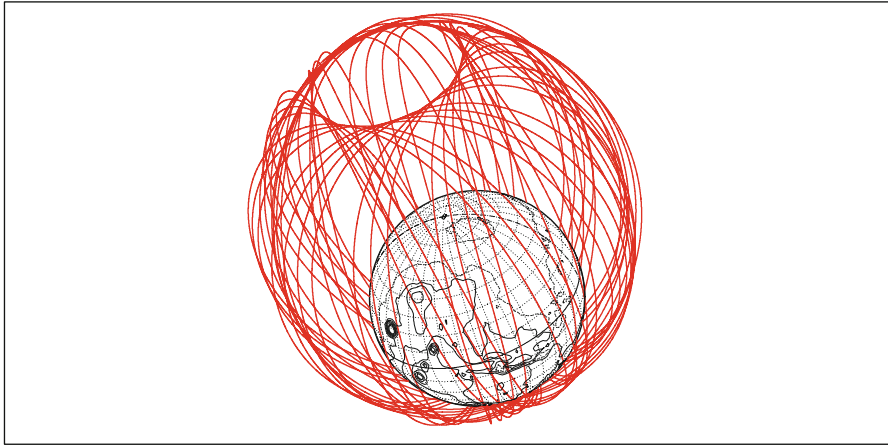
>>>> Time span shown: 7.00 sols

Equiv. altit. = 3181.0 km      a = 6578.000 km

Inclination = 75.00 °      e = 0.460778

Period = 270.20 min \* rev/sol = 5.48

h\_a = 6212 km; h\_p = 150 km; arg.periapsis: +270.00 °



Projection: Orthographic      Project. centre: 35.0 ° N; 71.0 ° W      Asc. Node: 0.00 °      *Ιξίων*  
 Property: none      Aspect: Oblique      Apoapsis: 64.24 °      MC ★ LMD  
 ♂ T.:Azimuthal - Graticule: 10° [3.5] [-90.0/+55.0/+161.0] [+22] MGM1025      *ΜΟΛΑ Topogr. / h / 2.5km /*      *Ατλας*

**[MARS] ExoMars/TGO**

Orbit - Ground track

Recurrence = [12;+92;227] 2816

>>>> Time span shown: 5918.1 min = 4.00 sols

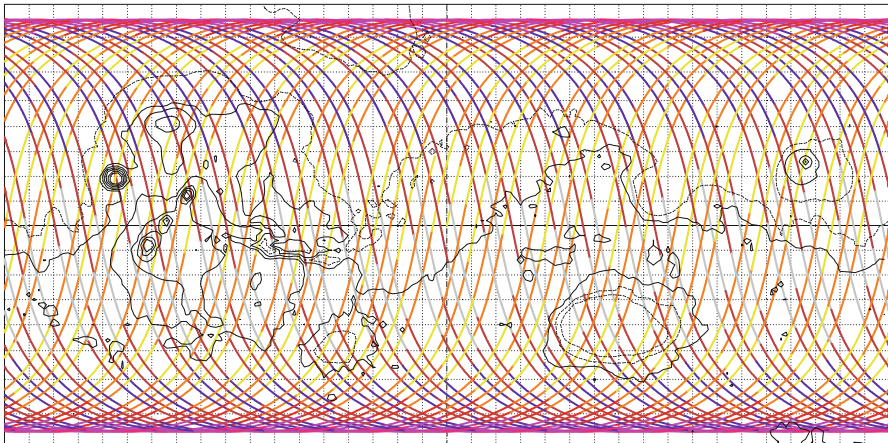
Altitude = 391.1 km      a = 3788.060 km

Inclination = 74.04 °

Period = 118.17 min \* rev/sol = 12.52

Equat. orbital shift = 1720.9 km ( 29.0 °)

LMT (local)    00 01 02 03 04 05 06 07 08 09 10 11 12 13 14 15 16 17 18 19 20 21 22 23 24    1 hr = 1 sol/24



Projection: Arden-Close      Project. centre: 0.0 ° ; 0.0 °      Asc. Node: 0.00 ° [12:00 LMT]      *Ιξίων*  
 Property: none      Aspect: Direct      App. inclin. = 78.57 °      MC ★ LMD  
 ♂ T.:Cylindrical - Graticule: 10° [3.5] [+0.0/ +0.0/ +0.0] [-] MGM1025      *ΜΟΛΑ Topogr. / h / 2.5km /*      *Ατλας*

FIG. 15.21 : Upper: Orbit of the satellite MAVEN over 7 sols. Lower: Orbital ground track of ExoMars-TGO over 4 sols.

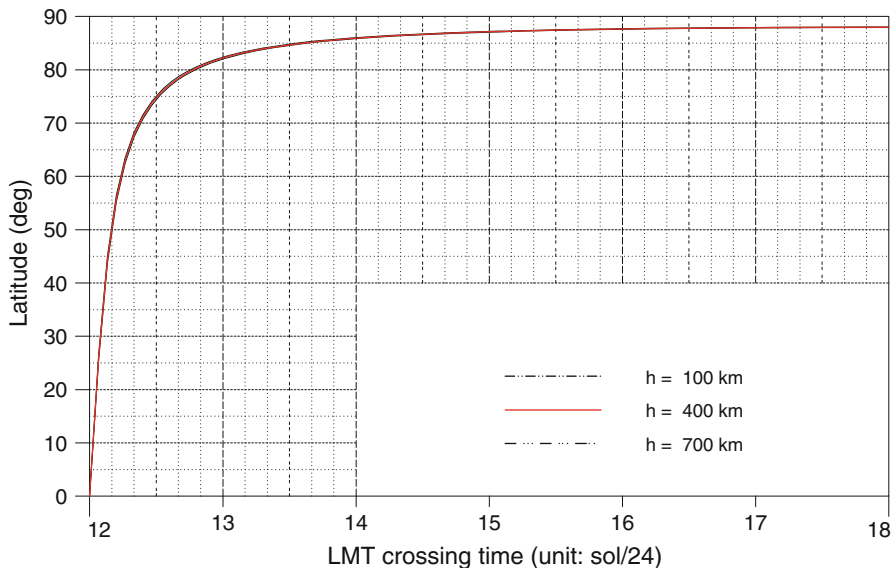


FIG. 15.22 : Graph of  $\psi(\Delta\tau)$ : relation between the latitude of the point under consideration and the LMT time difference between the ascending node crossing and overpass at this latitude for a Sun-synchronous satellite, for altitudes  $h = 400$  km and  $h = (400 \pm 200)$  km (curves almost superposed). Compare with Fig. 10.13.

- But for hours, a word of warning is in order. It is usual to indicate the LMT overpass time as for the Earth, e.g., 22:30 LMT. In this case, the overpass occurs 22.5 h after midnight, where the hour is here the fraction  $1/24$  of a sol. To avoid confusion, we shall avoid using the word “hour” when speaking of Mars, but use instead “sol/24”.

The quantity  $P$ , in round trips per (Martian) year, is used to calculate the cycle  $C_S$ , in sols, from (10.2) to (10.4).

### 15.6.1 Overpass Time for a Sun-Synchronous Satellite

For Sun-synchronous satellites, the overpass time is obtained as a function of the latitude using (10.9). The value of the coefficient to adjust for units is the same as on Earth: if times are in sol/24 and angles in degrees,  $K = 15$ , since 1 sol corresponds to  $360^\circ$ .

The graph of the curve giving the latitude  $\psi$  as a function of  $\Delta\tau = \tau - \tau_{AN}$  is shown in Fig. 15.22. Comparing with Fig. 10.13 (lower), the equivalent for the Earth, we see that on Mars there is no significant change with altitude for a satellite in low orbit: this is due to the high value of the constant of Sun-synchronicity  $k_h$ .



Overpass times are chosen for Sun-synchronous satellites on Mars<sup>22</sup> on the basis of roughly the same considerations as on Earth. To obtain useful lighting conditions, one requires the satellite to cross the equator about 2 h before or after midday. In order to benefit from a maximal illumination of the solar panels, a dawn–dusk orbit is favoured. See Figs. 15.23 and 15.24.

## 15.6.2 Eclipse Conditions

The angle between the orbital plane and the direction of the Sun, called the  $\beta$  angle, is calculated in exactly the same way as for the Earth. It can be used to obtain the period and length of eclipse.

Solar eclipse is a highly critical phenomenon for a Martian satellite. One reason is that the solar constant is only half the value on Earth. Another is that electrical energy storage requires accumulators that considerably increase the mass of the probe to be placed in orbit.

### Dawn–Dusk LMO Orbit

We consider a Sun-synchronous dawn–dusk low-orbiting satellite, with  $\tau_{AN} = 06:00$  or  $18:00$ . Equation (7.103) is satisfied when  $\eta$  lies between 1.1354 and 2.2930, which gives, in terms of the altitude,

$$\text{no eclipse} \iff 460 \text{ km} < h < 4,391 \text{ km} .$$

The altitude range without eclipse is much broader than on Earth. This is explained by the fact that the Martian Sun-synchronous orbit is more polar than the equivalent terrestrial orbit for the same relative altitude (and this in turn is due to the higher value of  $k_h$ ).

The satellite InterMarsNet, in a Sun-synchronous dawn–dusk orbit with  $h = 612$  km, would have escaped eclipse. The communications satellite Mars Telecomm Orbiter (MTO), at altitude  $h = 4,450$  km, Sun-synchronous with  $i_{HS} = 130.2^\circ$ , would have suffered very little eclipse in a dawn–dusk orbit<sup>23</sup> 06:00 or 18:00. With  $h = 4,391$  km,  $i_{HS} = 128.9^\circ$ , there is no eclipse for this type of orbit.

Figure 15.25 shows the length of solar eclipse over one revolution for various low altitudes as a function of the declination, and Fig. 15.26 (upper) the same as a function of the areocentric solar longitude, which can be related to the date.

<sup>22</sup>At the beginning of a mission, a dawn–dusk orbit is generally used. Indeed, the transfer of a space probe from Earth to Mars is made along a trajectory which is tangential to the orbit of Mars, as viewed in the heliocentric frame, at the time of insertion, when the probe becomes a satellite of Mars. The satellite orbit is then perpendicular to the Sun–Mars direction, and is therefore a dawn–dusk orbit. The same reasoning would apply to a satellite of Venus.

<sup>23</sup>With the planned configuration, eclipse would occur on 395 sols per Martian year, with a daily maximum of 47 min.

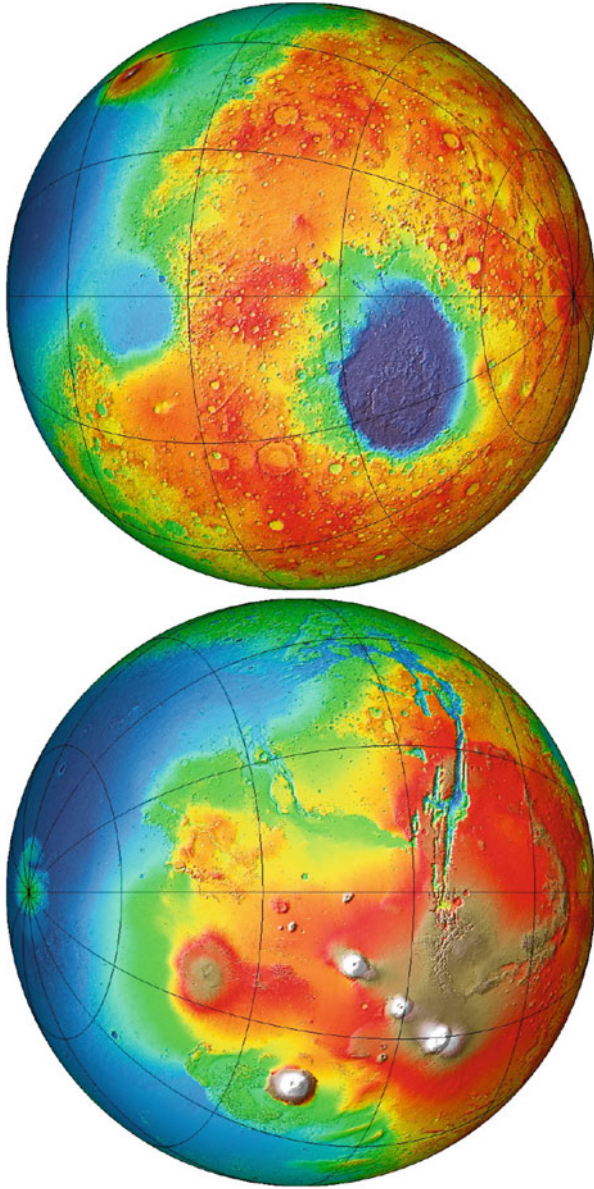


FIG. 15.23 : *Shaded topographic map of Mars based on MOLA data. Credit: MOLA Team, NASA, JPL.*

**[MARS] Mars Reconnaissance Orb.**  
**Orbit - Ground track**

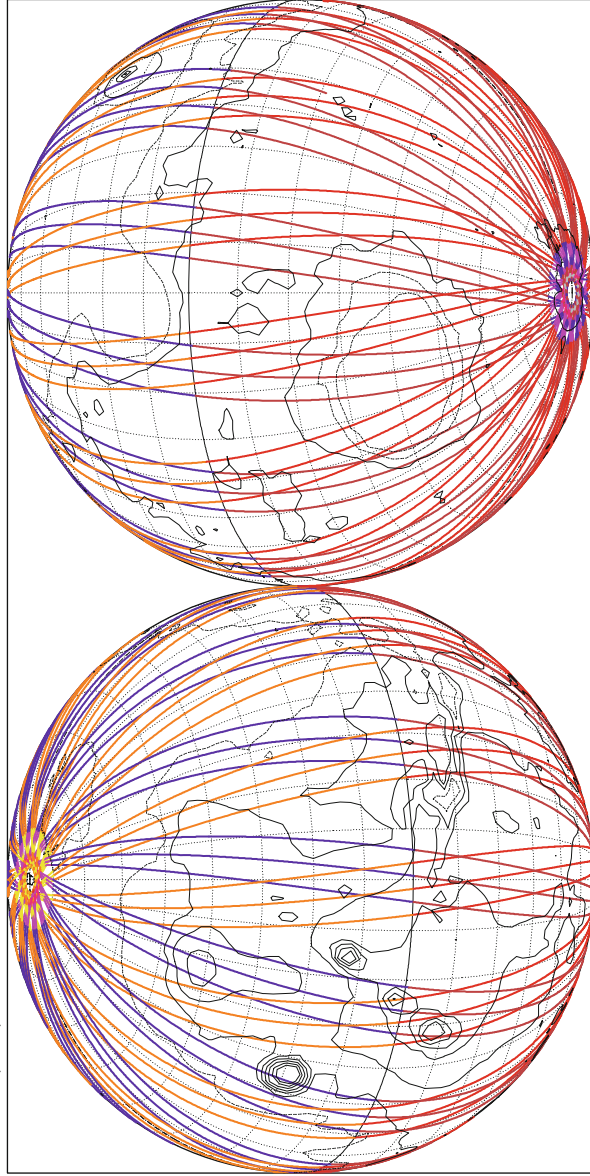
Altitude = 260.4 km      a = 3657.387 km

Inclin./SUN-SYNCHRON.= 92.60°

Period = 112.20 min \* rev/sol = 13.19

Equat. orbital shift = 1618.6 km ( 27.3°)

Recurrence = [13,+65;349] 4602  
 >>> Time span shown: 4438.6 min = 3.00 sols  
 >>> LMT (local) 00 01 02 03 04 05 06 07 08 09 10 11 12 13 14 15 16 17 18 19 20 21 22 23 24      1 hr = 1 sol/24



Projection: Orthographic      Pr. centre (r.): 22.5° S; 90.0° E      Asc. Node: -42.30° [15:30 LMT]       $I\xi_{\omega\nu}$   
 Property: none      Aspect: Oblique       $\text{MC} \star \text{LMD}$   
 ♂ T.:Azimuthal - Graticule: 10° {3.5}[-90.0/+112.5/ +0.0] [-] MGM1025       $\text{MOLA Topogr.} / h / 2.5\text{km} /$        $A\tau\lambda\alpha\zeta$

FIG. 15.24 : Mars Reconnaissance Orbiter (MRO) has a Sun-synchronous orbit: the ascending node crossing time (here  $\tau_{AN} = 15:30$  LMT) depends only on the latitude. Its ground track is shown over 3 sols. The oblique orthographic projection used here is the same as for the Martian topography in Fig. 15.23.

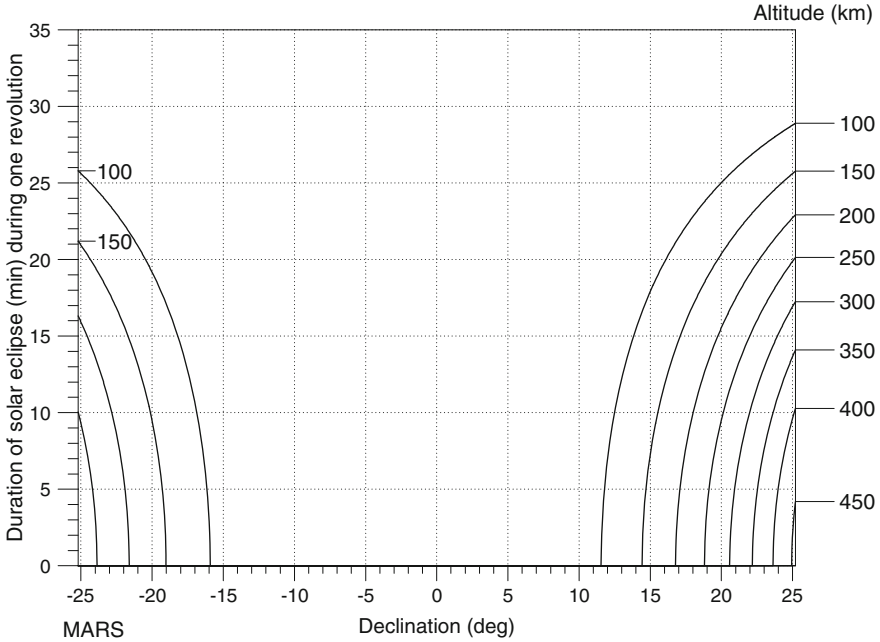


FIG. 15.25 : Sun-synchronous dawn-dusk satellite. Length of solar eclipse in minutes over one revolution for the given altitude as a function of the declination. Graphs established for  $\tau_{AN} = 18:00$ . For  $\tau_{AN} = 06:00$ , consider the minus of the declination.

**SMO Orbit**

For an areostationary satellite, using the value of  $f_0$  obtained below using (15.40), there is an eclipse if  $|\delta| < f_0$ . This happens twice a year, when the areocentric solar longitude is close to that of the equinoxes, with a longitude difference<sup>24</sup> less than  $\Delta L_S = 23^\circ$  :

$$\text{eclipse for SMO} \iff [L_S: 337 - 23], [L_S: 157 - 203]$$

The maximum eclipse is calculated using (10.34). This gives

<sup>24</sup>The value of this bounding difference  $\Delta L_S$  is straightforwardly calculated. Equation (15.18) relates  $\delta$  and  $L_S$ . The condition  $\delta = f_0$  yields

$$\sin \Delta L_S = \frac{\sin f_0}{\sin \epsilon} .$$

Expressing  $f_0$  in terms of the reduced distance, we obtain

$$\Delta L_S = \arcsin \frac{1}{\eta_{GS} \sin \epsilon} = \arcsin \frac{1}{2.560} = 22.99^\circ ,$$

which leads to  $\Delta L_S = 23^\circ$ .

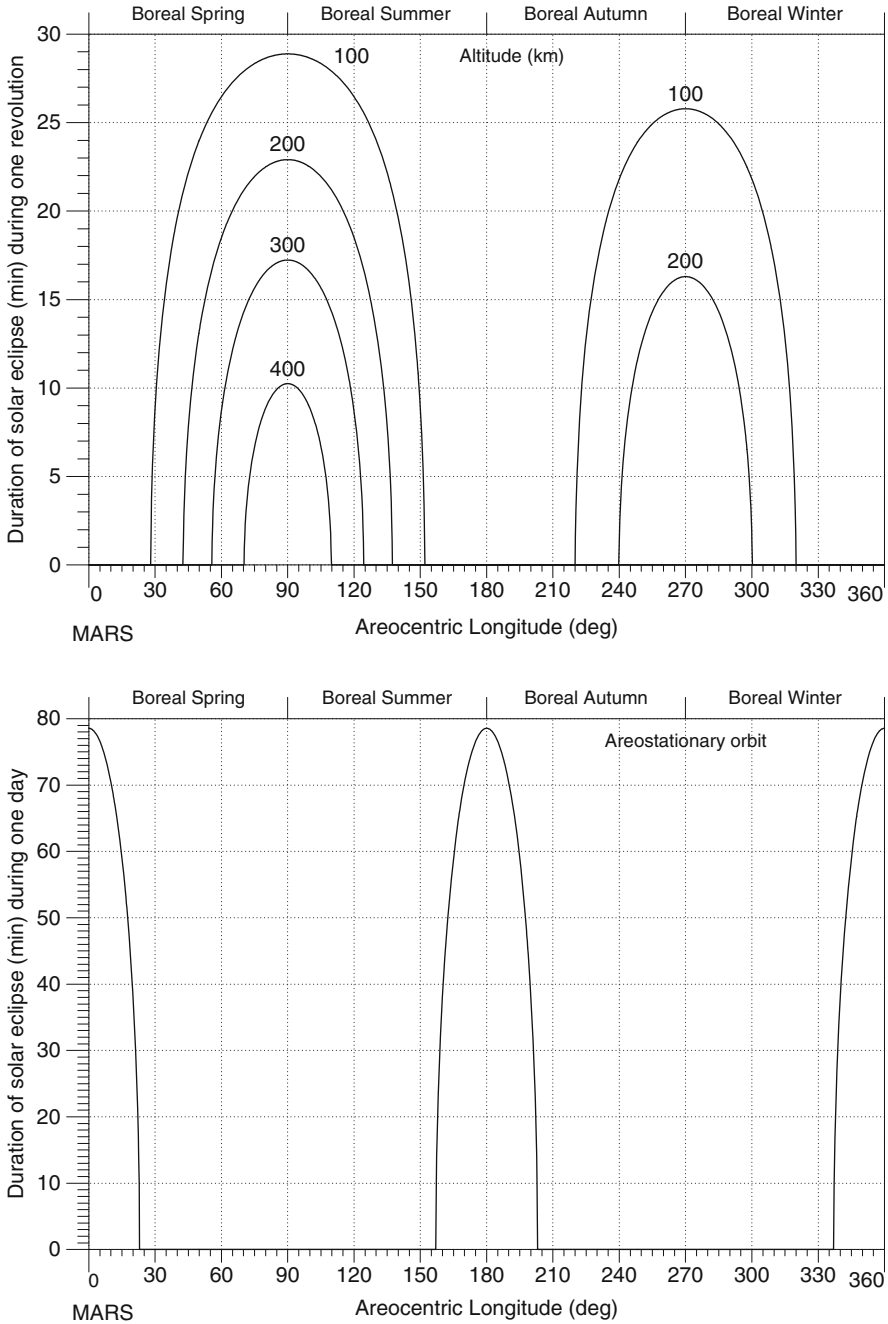


FIG. 15.26 : Length of solar eclipse in minutes as a function of the areocentric solar longitude. Upper: Sun-synchronous dawn-dusk satellite. Length of eclipse over one revolution for the given altitude. Graphs established for  $\tau_{AN} = 18:00$ . For  $\tau_{AN} = 06:00$ , consider the minus of the declination. Lower: Areostationary satellite. Length of eclipse over 1 sol.

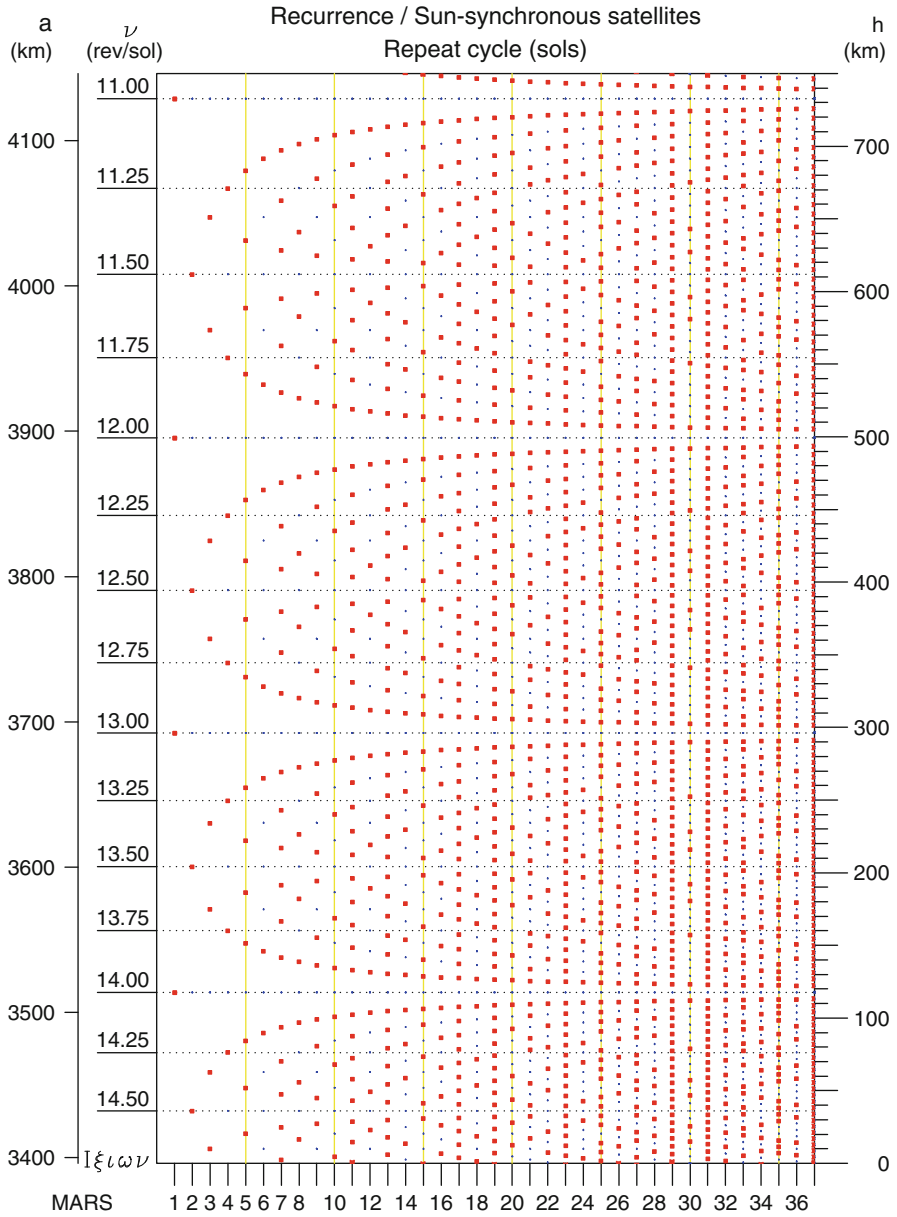


FIG. 15.27 : Recurrence diagram for Sun-synchronous satellites. For altitudes between 0 and 750 km, small squares indicate values of the altitude  $h$  (and the semi-major axis  $a$ ) for which recurrence is possible. The abscissa records the value of the recurrence cycle in sols. The daily frequency  $\nu$  is in round trips per sol.

Sun-sync. sat.	$\nu_o$	$D_{T_o}$	$C_{T_o}$	$N_{T_o}$	$T_d$	$a$	$h$	$i_{HS}$
MGS	13	-233	550	6,917	117.64	3,775.088	379	92.90
Mars Odyssey	12	+15	32	399	118.66	3,796.847	401	92.96
MRO	13	+65	349	4,602	112.20	3,657.386	260	92.60
Mars Observer	13	-1	3	38	116.80	3,757.095	361	92.89
Mars Observer	13	-3	7	88	117.69	3,776.107	380	92.94
InterMarsNet	12	-1	2	23	128.65	4,007.867	612	93.61

TABLE 15.6 : *Orbital and recurrence characteristics for Sun-synchronous satellites obtained from the phase triple  $[\nu_o, D_{T_o}, C_{T_o}]$ . For the full caption, see Table 11.1. Orbits of operational satellites MGS, Mars Odyssey, and MRO and planned orbits for Mars Observer (recurrence over 3 and 7 sols), which failed insertion, and InterMarsNet, which was abandoned.*

$$\Delta t_{e0} = \frac{9.6}{180} D_{\text{sid}} = 78.8 \text{ min} . \quad (15.39)$$

Figure 15.26 (lower) graphs the length of solar eclipse over 1 sol.

## 15.7 Orbit Relative to Mars: Recurrence and Altitude

✧ **Chapter 11.** When we consider the question of recurrence on Mars, we encounter the same advantages and constraints as we have already seen on Earth. Everything discussed in Chap. 11 applies equally to Mars, provided of course that we use sols instead of days.

### 15.7.1 Recurrence

#### Recurrence for Sun-Synchronous Satellites

We have just seen that the altitude of a Martian Sun-synchronous satellite lies between the theoretical bounds  $h = 0$  and  $h = 5,496$  km, which corresponds to the values  $\nu = 14.73$  and  $\nu = 3.49$  of the daily orbital frequency, respectively. The altitudes chosen for Sun-synchronous satellites in missions under development or already carried out are generally less than 600 km.

The recurrence diagram in Fig. 15.27 allows one to visualise the altitudes leading to different recurrence configurations on Mars. This diagram is the counterpart of Fig. 11.2 for the Earth. Recurrent satellites on Mars are shown in Table 15.6 and Fig. 15.28. Given the recurrence triple (which is in principle maintained throughout the mission), one can accurately determine the characteristics of the orbit.

**Example 15.7** *Calculate the orbital characteristics of the satellites Mars Global Surveyor, Mars Odyssey, and Mars Reconnaissance Orbiter.*

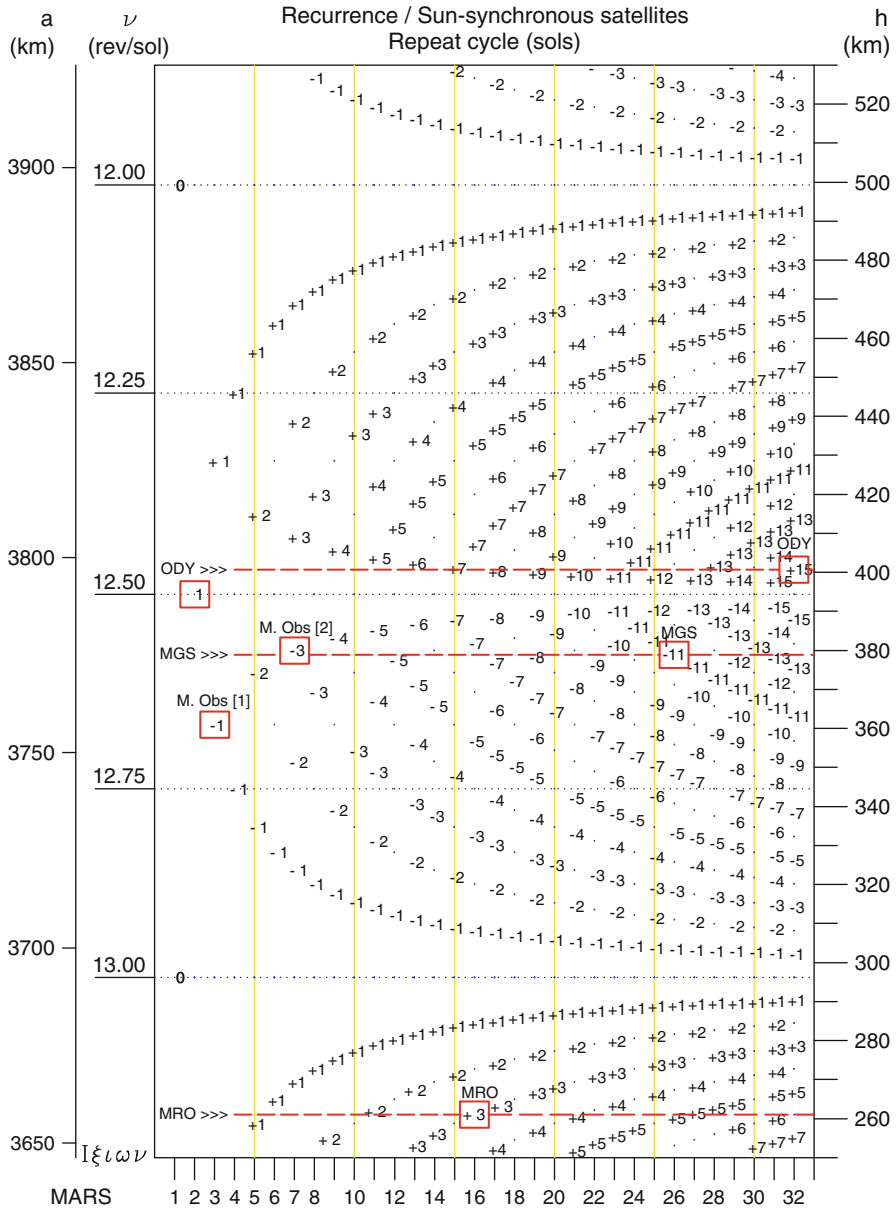


FIG. 15.28 : Recurrence diagram for Sun-synchronous satellites. For altitudes between 250 and 530 km, the possible recurrence cycles are indicated by the value of  $D_{T_0}$ . Boxed values correspond to the exact recurrence cycles appearing in Table 15.6, or to approximate, but shorter cycles determined in Example 15.7. For example, for Mars Odyssey (ODY), we have the triple  $[12, +1, 2]$ , or  $\nu_0 = 12$  (the integer closest to  $\nu$ , as ordinate),  $D_{T_0} = +1$  (indicated on the diagram), and  $C_{T_0} = 2$  (as abscissa).



► All three satellites are Sun-synchronous.

**Mars Global Surveyor (MGS).** The probe Mars Global Surveyor (MGS) left its heliocentric cruise on 12 September 1997 for a highly eccentric areo-centric orbit with  $h_p = 258$  km,  $h_a = 54,021$  km,  $e = 0.88$ ,  $T = 45$  h, known as Mars orbit insertion (MOI). The aerobraking maneuver lasted for 16 months, during which many scientific measurements were carried out, in particular on the magnetic field. The solar panels did not deploy correctly, extending the time required for aerobraking. In February 1999, the final orbit was near-circular, Sun-synchronous, recurrent, and frozen. The satellite MGS then entered its mapping phase. The Mars Orbiter Laser Altimeter (MOLA) then began to make very precise topographic measurements of the planet.

With recurrence maintained at 6,917 revolutions in 550 sols, the draconitic period is given by

$$T_d = \frac{550}{6917} \text{ sol} = 117.64 \text{ min} .$$

To begin with, we set  $T_0 = T_d$ , and thereby deduce the inclination and radius  $a_0 = 3,781$  km of the Keplerian orbit. We calculate the rate of secular variation of the angle elements. We deduce the anomalistic period  $T_a = 117.5090$  min, then the values of the semi-major axis and the inclination, viz.,

$$a = 3,775.088 \text{ km} , \quad i = i_{\text{HS}} = 92.90^\circ .$$

**Mars Odyssey.** The probe Mars Odyssey reached Mars on 24 October 2001 and went into a high and highly eccentric Martian orbit ( $T \approx 18.6$  h). Aerobraking eventually led on 30 January 2002 to a Sun-synchronous ( $\tau_{\text{AN}} = 04:30$ ) circular orbit close to 400 km ( $T \approx 2$  h), with the satellite ground track repeating every 2 days. The recurrence diagram in Fig. 15.27 shows that, at this altitude, a recurrence cycle over 2 sols corresponds to the triple  $[12, 1, 2]$ ,  $\nu = 12.5$ , with 25 revolutions per cycle. The draconitic period is therefore

$$T_d = \frac{2}{25} \text{ sol} = 118.36 \text{ min} ,$$

and the various intervals discussed in Chap. 11 are  $\delta = 360/25 = 14.4^\circ$ ,  $\delta_D = \delta$ ,  $\delta_R = 2\delta$ . By iterative calculation, we obtain the semi-major axis  $a = 3,790.496$  km and the inclination  $i = i_{\text{HS}} = 92.95^\circ$ . In fact, during the science part of the mission, for each 2-sol repeat cycle, the ground track shifts a small amount (53 km) at the equator (see Fig. 15.15). This shift by  $0.9^\circ$ , denoted here by  $\delta'$ , can be considered as the grid interval of a longer cycle. After  $\delta'/\delta = 0.9/14.4 = 16$  cycles of 2 sols, the ground track has thus shifted by an interval  $\delta$ , which means that, after 16 cycles of 25 revolutions, the satellite, with this new recurrence characteristic, has made one revolution less, i.e., 399 revolutions in 32 sols. The recurrence triple is then  $[12, 15, 32]$ . The draconitic period is

$$T_d = \frac{32}{399} \text{ sol} = 118.66 \text{ min} ,$$

and we recover the grid interval  $\delta = 360/399 = 0.9^\circ$ . We then obtain

$$a = 3,796.847 \text{ km} , \quad i = i_{\text{HS}} = 92.96^\circ .$$

It should be noted that the satellite Mars Odyssey is not strictly Sun-synchronous, since its LMT crossing time varied continuously from 03:23 to 05:20 during the 917 (Earth) days of the science mission, then from 05:20 to 06:50 during the 800 following days.

**Mars Reconnaissance Orbiter (MRO).** The probe Mars Reconnaissance Orbiter (MRO) came under the control of the Martian gravitational field on 11 March 2006, entering a highly elliptic polar orbit with  $h_p = 426 \text{ km}$ ,  $h_a = 44,500 \text{ km}$ ,  $\omega = 270^\circ$ , and period  $T = 35 \text{ h}$ . After 5 months of aerobraking (over 445 revolutions), the orbit of the MRO was near-circular. NASA gave the following indications:  $h_p = 255 \text{ km}$ ,  $h_a = 320 \text{ km}$ , frozen Sun-synchronous orbit with recurrence over 349 sols, with 4,602 revolutions.

To obtain the latitude of the apsides and calculate the radius  $R_\psi$  of the planet at this location, using (1.37) or (1.39), we carry out an approximate calculation of  $i_{\text{HS}}$ . With  $i = 93^\circ$ , we may take  $R_\psi = R_p = 3,630 \text{ km}$  (polar radius). We deduce that

$$r_p = R_p + 255 = 3,630 \text{ km} , \quad r_a = R_p + 320 = 3,695 \text{ km} \implies a = 3,662.5 \text{ km} .$$

We obtain  $e = 8.87 \times 10^{-3}$ , which corresponds to the frozen eccentricity  $e_F$ . Equation (11.55), with  $\omega_F = -90^\circ$  and  $i_{\text{HS}} = 92.7^\circ$ , yields  $e_F = 7.7 \times 10^{-3}$ . The draconitic period is

$$T_d = \frac{349}{4602} \text{ sol} = 120.20 \text{ min} ,$$

which implies that  $\kappa = \nu = 13.1862$ . The orbital elements can be found from the values of  $e_F$  and  $\kappa$ , with the result

$$a = 3,657.4 \text{ km} , \quad e = 0.00887 , \quad i = i_{\text{HS}} = 92.60^\circ , \quad \omega = \omega_F = 270^\circ .$$

Mission control indicates a recurrence cycle of 16 sols. With this subcycle, a small shift of 30.6 km is observed at the equator over 211 revolutions, between the tracks at 16 sol intervals. ◀

**Example 15.8** Calculate the orbital characteristics of InterMarsNet.

► The InterMarsNet mission was a European project in collaboration with the United States. This project, planned for 2003, was abandoned in 1996 and more or less replaced by Mars Express, for launch in 2003. We have

included it here as an example because of its interesting orbit, which is Sun-synchronous, dawn–dusk, with 2-sol recurrence, frozen and eclipse-free. With a recurrence of 23 revolutions in 2 sols, we obtain

$$T_d = \frac{2}{23} \text{ sol} = 128.66 \text{ min} .$$

Calculation yields  $a = 4,007.867 \text{ km}$  and inclination  $i_{\text{HS}} = 93.61^\circ$ . ◀

**Example 15.9** *Calculate the characteristics of a Sun-synchronous satellite with 1-sol recurrence and critical inclination.*

► Preliminary orbital studies for the Russian satellite Mars-96 considered an orbit that would have been Sun-synchronous and also have had the critical inclination. We re-examine this idea here, but adding the further constraint that the satellite should be 1-day recurrent, an interesting configuration for links with ground bases. We have calculated the following orbital characteristics, with three different recurrence cycles, considering eccentricities  $e = 0.30$ ,  $e = 0.45$ , and  $e = 0.60$ :

$$\begin{aligned} e = 0.30, & \quad a = 6,993.892 \text{ km}, & \quad i = 116.6, & \quad \text{phase triple } [5, 0, 1], \\ & \quad h_p = 1,499 \text{ km}, & \quad h_a = 5,695 \text{ km}, & \quad T = 296.01 \text{ min (5 rev/day)}, \\ e = 0.45, & \quad a = 8,113.554 \text{ km}, & \quad i = 116.6, & \quad \text{phase triple } [4, 0, 1], \\ & \quad h_p = 1,065 \text{ km}, & \quad h_a = 8,368 \text{ km}, & \quad T = 369.86 \text{ min (4 rev/day)}, \\ e = 0.60, & \quad a = 9,827.020 \text{ km}, & \quad i = 116.6, & \quad \text{phase triple } [3, 0, 1], \\ & \quad h_p = 533 \text{ km}, & \quad h_a = 12,326 \text{ km}, & \quad T = 493.01 \text{ min (3 rev/day)}. \end{aligned}$$

The satellite Ellipso Borealis has this type of orbit around the Earth. ◀

### Recurrence for a Non-Sun-Synchronous Satellite

Mars Express is in a recurrent non-Sun-synchronous elliptical orbit, with several recurrence cycles during the mission.

**Example 15.10** *Characteristics of the various orbits of Mars Express, depending on its recurrence.*

► The European satellite Mars Express, launched from Baikonur on 2 June 2003, arrived on Mars on 25 December and went into a highly eccentric near-polar insertion orbit (known as MOI), with  $i = 86.35^\circ$ . This was quickly transformed into a recurrent elliptical orbit characterised by 13 revolutions in 4 sols (the so-called 3G-u orbit), then by 11 revolutions in 3 sol (the 3G-b orbit). It remained in 3G-u from the beginning of January to 2 May 2004 (revolutions 1–372), then went into 3G-b, where it remained from 6 May up until the end of the main mission, on 11 November 2007 (revolutions 386–4,955).

MEx	$a$	$e$	$T$	Triple, $N_{T_o}$	$h_p$	$h_a$
13:4 [G3-u]	9,318.9	0.60691	455.24	[3, +1, 4] 13	266	11,578
11:3 [G3-b]	8,597.5	0.56973	403.51	[4, -1, 3] 11	302	10,099
18:5	8,703.2	0.56974	410.98	[4, -2, 5] 18	347	10,266
25:7	8,750.2	0.57041	414.27	[4, -3, 7] 25	362	10,344

TABLE 15.7: *Orbital and recurrence characteristics for Mars Express. Semi-major axis  $a$ , altitudes  $h_p$  and  $h_a$  in km at periastron and apastron, and period  $T$  in minutes. For these orbits, with eccentricity  $e$ , the inclination is  $i = 86.35^\circ$ .  $N_{T_o}$  is the number of revolutions in the cycle.*

ExoMars-TGO	$a$	$e$	$T$	Triple, $N_{T_o}$	$i$
	3,788.060	0.0068	118.17	[12, +92, 227] 2816	74.04

TABLE 15.8: *Orbital and recurrence characteristics for ExoMars-TGO. For more details, see the caption to Table 15.7.*

Subsequently, with a slight increase in the semi-major axis  $a$ , MEx moved to a recurrence of 18 revolutions in 5 sols (the 18:5 orbit), from 16 December 2007 to 11 January 2009 (revolution 5,082–6,458), then to a recurrence of 25 revolutions in 7 sols (the 25:7 orbit). The thinking behind these changes was to optimise scientific observations and maintain the periastron on the daylight side for as long as possible, since high resolution observations are made there.

The characteristics of the orbits are given in Table 15.7. As for Mars Odyssey, the orbits are not strictly recurrent. For G3-u, with  $\delta = 360/13 = 27.70^\circ$ ,  $\delta_R = 4\delta = 110.77^\circ$ , the ground track shifts by  $\delta' = 1.09^\circ$  after each cycle of 4 sols. ◀

## Satellites with 1-Day Recurrence

As on Earth, low-orbiting (LMO) satellites around Mars should in principle avoid 1-day recurrence cycles. For example, a Sun-synchronous satellite at altitude  $h = 500$  km would find itself in this situation, as is clear from the recurrence diagram. Every day it would pass over the same ground track, unable to observe other regions. Table 15.9 lists altitudes leading to such recurrence, for Sun-synchronous and non-Sun-synchronous satellites.

$\kappa$	$i = 20$	$i = 65$	$i = 110$	$i = i_{\text{HS}}$	
	$h$	$h$	$h$	$h$	$i_{\text{HS}}$
14	48.6	81.2	146.0	117.6	92.3
13	237.0	263.8	321.0	296.2	92.7
12	449.0	470.6	520.6	499.2	93.3
11	690.5	707.4	750.7	732.6	94.0

TABLE 15.9: *Orbital and recurrence characteristics for satellites with 1-sol recurrence cycles. Non-Sun-synchronous satellites with three different inclinations and comparison with Sun-synchronous satellites. Altitudes  $h$  in km, angles  $i$  in degrees. Daily orbital frequency  $\kappa$ , equal here to  $\nu_0$  in round trips per sol.*

### Grid Points for Recurrent Satellites

The latitudes of grid points are calculated from the function  $\mathfrak{F}(\psi)$  defined by (11.28). There is no difference with a terrestrial satellite, except that, for Sun-synchronous satellites, the inclination  $i_{\text{HS}}$  depends on the planet.<sup>25</sup>

### Recurrence Index

The recurrence index indicates cycles and subcycles. For satellites with very long recurrence cycle, such as MGS or MRO, the index carries much information.

**Example 15.11** *Recurrence index for the very long cycle Sun-synchronous satellites MGS and MRO.*

► These two satellites have near-circular Sun-synchronous orbits.

**MGS.** The recurrence cycle is very long, viz.,  $C_{T_o} = 550$  sol over 6917 revolutions (see Fig. 15.29 upper). The graph in the figure has a secondary peak for 7 sol (over 88 revolutions), and significant peaks for 26 sol (over 327 revolutions), ..., and 144 sol (over 1,811 revolutions). The MGS/JPL nomenclature distinguishes three cycles: the repeat cycle (7 sol), the mapping cycle (26 sol), and the super cycle (550 sol). The instrument MOLA aboard MGS is a laser,<sup>26</sup> which of course has an extremely narrow beam. The very long cycle thus leads to a very small ground track interval,<sup>27</sup> ensuring complete coverage

<sup>25</sup>For the satellite Mars Odyssey, with a 2-sol recurrence cycle and using the notation of Chap. 11, we obtain the following results. For  $d = 1, 3, 5, 7, \dots, M_{T_o} = 27$ , the geocentric latitudes are  $\psi = 26.6, 62.9, 76.0, 80.9, \dots, \psi_m = 87.1 = 180 - i_{\text{HS}}$  (see Fig. 15.15 lower).

<sup>26</sup>On Earth, where cycles  $C_{T_o}$  rarely exceed 40 days, altimetric satellites like ICESat equipped with lasers also have a very long cycle.

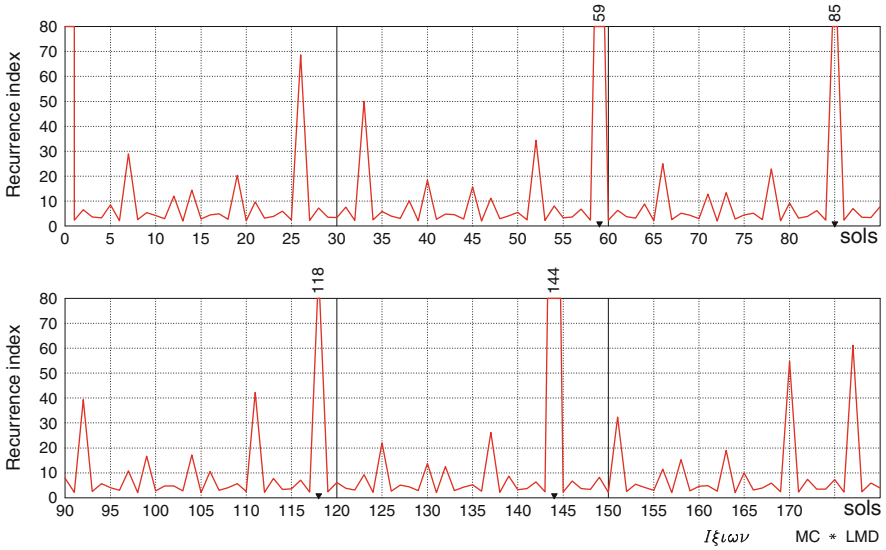
<sup>27</sup>The beam angle of the MOLA laser is  $2f = 0.85$  mrad (or 3 arcsec), which gives a spot on the ground of width  $\Delta = 2fh = 320$  m. With  $N_{T_o} = 6,917$ , the ground track

**Mars Global Surveyor**  
**Recurrence cycle**

[ 13; -61; 144 ] 144.000

Altitude = 378.088 km  
 Incl. / Sun-s. = 92.90 °  
 Equatorial shift = 1697.1 km  
 Period = 117.64 min  
 $\nu = 12.5764$

a = 3775.088 km  
 Cycle : 144.00 sols  
 => on 1811 round trips  
 Max. Index = infinity  
 $\kappa = 12.5764$



**Mars Reconnaissance Orbiter**  
**Recurrence cycle**

[ 13; 19; 102 ] 102.000

Altitude = 260.387 km  
 Incl. / Sun-s. = 92.60 °  
 Equatorial shift = 1618.6 km  
 Period = 112.20 min  
 $\nu = 13.1862$

a = 3657.387 km  
 Cycle : 102.00 sols  
 => on 1345 round trips  
 Max. Index = infinity  
 $\kappa = 13.1862$

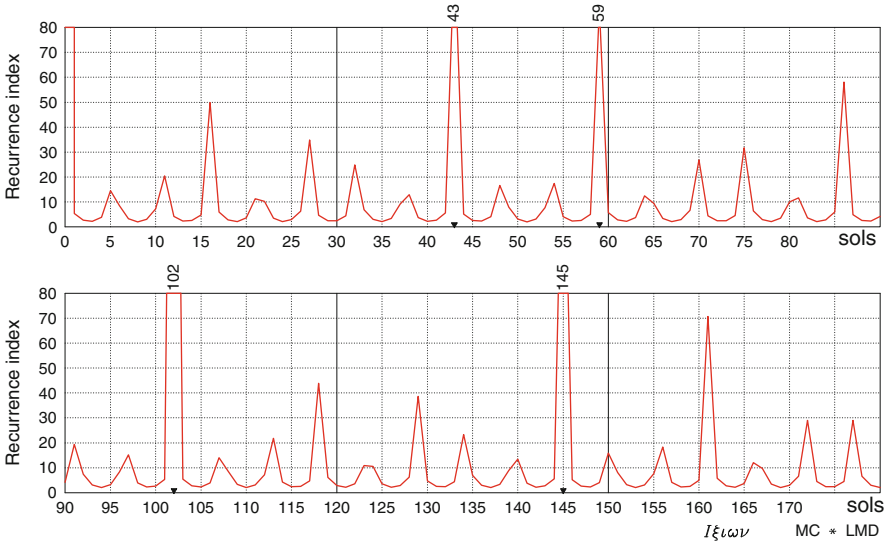


FIG. 15.29 : *Recurrence index.* The recurrence indicated in each caption corresponds to a cycle shorter than 200 sol. Upper: MGS. Lower: MRO.

of the planet, apart from a small disk centered on the poles, which has been dealt with by changing the orientation of the satellite.

**MRO.** The recurrence cycle is slightly shorter than the one for MGS, with  $C_{T_0} = 349$  sol over 4,602 revolutions (see Fig. 15.29 lower). The graph in the figure has a significant peak for 102 sol (over 1,345 revolutions) and secondary peaks for 5 sol (over 66 revolutions), 11 sol (over 145 revolutions), and 16 sol (over 211 revolutions). This last subcycle corresponds to the recurrence triple  $[13, +3, 16]$  211 (see Fig. 15.28). ◀

### 15.7.2 Altitude

Recall that we define the altitude of a satellite as a function of the angle  $\alpha$  giving the position on orbit (see Chap. 11). This altitude  $h(\alpha)$ , expressed in (11.47), is obtained as the difference between the distance  $r(\alpha)$  to the center of the planet (the center of attraction) and the radius  $R_T(\alpha)$  of the reference ellipsoid (the distance of the subsatellite point on the ellipsoid from the center of the planet). Here we consider the geocentric altitude (height).

Frozen orbits are less circular than on Earth, for two reasons:

- The flattening of Mars is more pronounced.
- The frozen eccentricity  $e_F$  given by (11.57) is greater, because the ratio  $|J_3/J_2|$  is equal to  $18.363 \times 10^{-3}$  for Mars, whereas it is  $2.339 \times 10^{-3}$  for the Earth.

We also note that, since  $J_3$  and  $\sin \omega_F$  must have opposite signs, the position of the frozen periastron is given by  $\omega_F = 270^\circ$  for recurrent Sun-synchronous satellites. The periastron of the frozen Sun-synchronous orbit is practically over the South Pole.

**Example 15.12** *Altitude of the satellite MGS during the topographic phase and the satellite MRO during the first scientific phase.*

- ▶ These two satellites have frozen orbits.

**MGS.** The variation in altitude of the satellite MGS is shown in Fig. 15.30 (upper) over one period as a function of the position on orbit  $\alpha$ . The values of the orbital elements provided by NASA are those for a given revolution (indicated in the figure) during its topographical phase. As the orbit is maintained and frozen, we may consider that the variation  $h(\alpha)$  does not change

---

interval  $\delta$  (expressed as a length) is  $\delta = 2\pi R/6917 = 3.085$  km. At the equator, we thus have  $\Delta/\delta \approx 1/10$ .

from one revolution to another. We note that the position  $\omega_F$  of the frozen periastron is at  $7^\circ$  from the ideal position. If we calculate the frozen eccentricity using (11.57) with the orbital elements provided in Table 15.6, we find  $e_F = 8.25 \times 10^{-3}$ . This result is close to the true value for the revolution under consideration, viz.,  $e_F = 8.87 \times 10^{-3}$ .

**MRO.** The variation in altitude of the satellite MRO is shown in Fig. 15.30 (lower) over one period as a function of the position on orbit  $\alpha$ , during the first Martian year after it was placed in orbit (the primary science phase). The altitude depends only on the latitude, regardless of whether the orbit is in its ascending or descending part. In the caption to Fig. 15.34 and Example 15.16, we indicate the altitude communicated by JPL/NASA, viz.,  $h = 297.5$  km. Using (6.64) with  $\psi = 42.2^\circ$  and  $i = 92.6^\circ$ , we obtain

$$\sin \alpha = \frac{\sin 42.2}{\sin 92.6}, \quad \alpha = 44.3^\circ.$$

This is indeed the value given by the graph.

For MRO and MGS, the altitude profiles are very similar, with practically identical values of  $e_F$  and  $\omega_F$ . ◀

## 15.8 View from the Satellite

✧ **Chapter 12.** All the concepts discussed in Chap. 12 apply equally to a Martian satellite. Adaptation to the present case will be particularly simple since we used the variable  $\eta$ , which is the reduced distance  $a/R$ .

### 15.8.1 Viewing Configuration and Pixel Distortion

For an LMO satellite in circular orbit, the pixel distortion index  $K$  is shown in Fig. 15.31 for various altitudes. For an SMO satellite, in high stationary orbit, the curve  $K(\alpha)$  is almost the same as the one for a GEO satellite on Earth, shown in Fig. 12.5 (lower). We obtain  $K = 2$  for  $\alpha = 49^\circ$ ,  $K = 3$  for  $\alpha = 59^\circ$ , instead of  $\alpha = 50^\circ$  and  $\alpha = 61^\circ$ , respectively, for the terrestrial satellite. This similarity between the curves  $K(\alpha)$  is due to the very similar values of  $\eta_{GS}$ .

### 15.8.2 Swath Track for an LMO Satellite

Possible scanning modes are the same for instruments aboard terrestrial and Martian satellites. Here we consider the ground track of an across-track swath.

**Example 15.13** *Swath track of the Mambo instrument aboard Premier.*



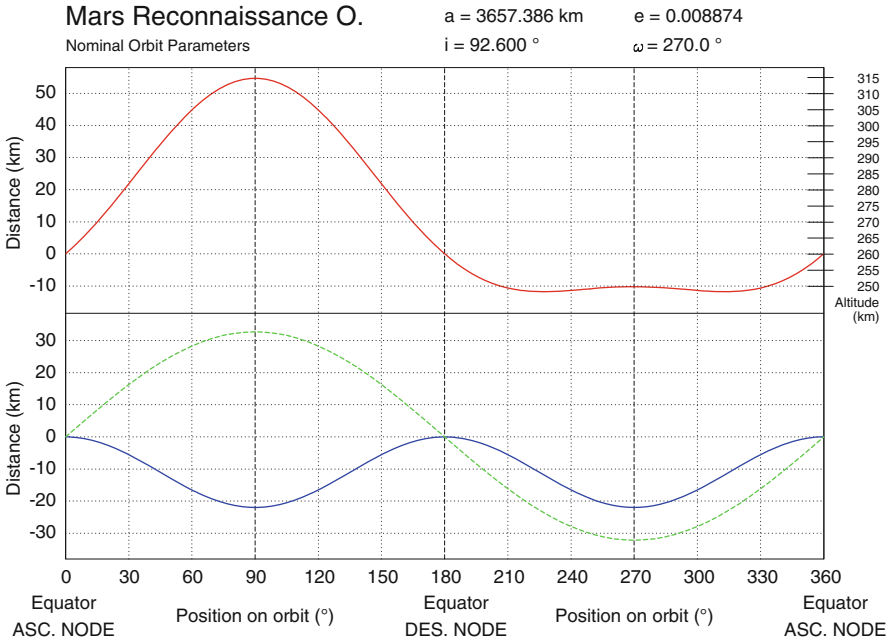
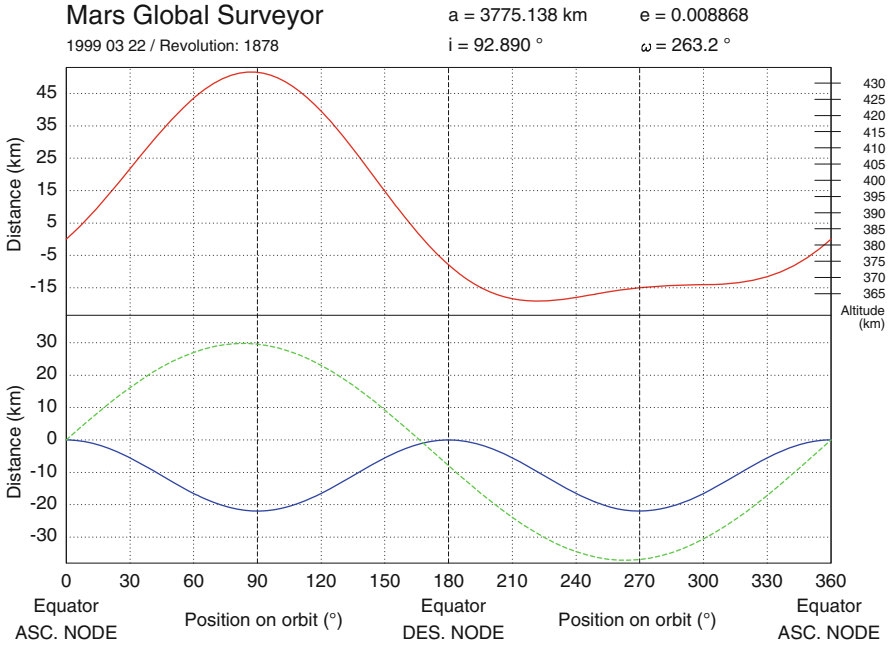


FIG. 15.30 : Altitudes of the satellites MGS and MRO. For a detailed caption, see Fig. 11.28.

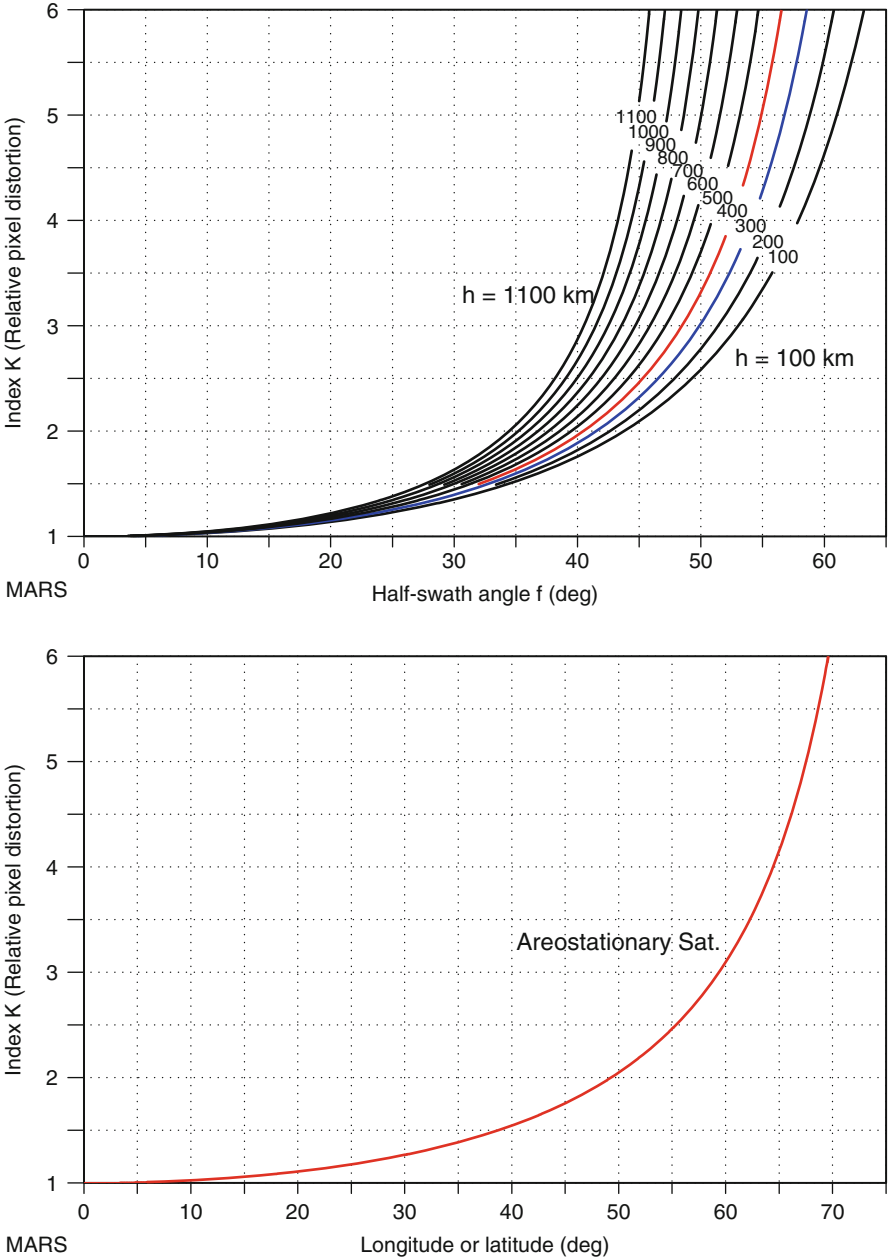


FIG. 15.31 : Pixel distortion index. Length distortion index  $K$ . Upper: For LMO satellites with altitude  $h = 100-1,100$  km, in steps of 100 km, as a function of the half-swath angle  $f$ . Lower: For any stationary satellite, as a function of the angle  $\alpha$ , representing the latitude or longitude from the subsatellite point.

► The Mars Atmosphere Microwave Brightness Observer (Mambo) instrument proposed for the satellite Premier MO-07 views the limit of its cross-track scan, alternately left and right, each minute. In the representation of the track shown in Fig. 15.32 (upper), black dots mark the place viewed at the limiting point, while small circles indicate the nadir of the satellite (the subsatellite point).

The French mission Premier (*Programme de Retour d'Échantillons Martiens et Installation d'Expériences en Réseau*) was cancelled in 2003. This was to prepare the very ambitious French–American mission Mars Sample Return (MSR), which is still on the cards, but postponed indefinitely. ◀

### 15.8.3 Image Acquisition and Apparent Inclination

Image acquisition by an instrument with narrow cross-track swath aboard an LMO satellite provides a good illustration of the difference between inclination and apparent inclination.

**Example 15.14** *Remarks concerning the orientation of images acquired by VIS aboard Mars Odyssey and HiRISE aboard MRO.*

► Among the many instruments carried by Mars satellites, there is always a high-definition camera in the visible range of the spectrum: MOC for MGS, THEMIS/VIS for Mars Odyssey, HiRISE for MRO, and HRSC for Mars Express. These ever higher performance cameras can distinguish decimetric details that can transform our understanding of the geomorphology and geology of the Red Planet. Here we shall examine image acquisition from an orbitographic standpoint. We have chosen two images. In each case, north is at the top of the image.

**Mars Odyssey.** Figure 15.16 was acquired by THEMIS/VIS aboard Mars Odyssey, with  $\tau_{AN} = 04:00$ . The Mars Odyssey Thermal Emission Imaging System (THEMIS) comprises several instruments, including a visible wavelength camera THEMIS/VIS. The image was taken during daytime on the descending part of the orbit (retrograde since Sun-synchronous). The image is acquired in blocks constituting a sawtooth pattern on the image. Each block is acquired instantaneously, hence perpendicularly to the orbital plane. The edge of each block has inclination  $i$ . The general line of the edge follows the satellite ground track. It thus has inclination  $i'$ , the apparent inclination. Measuring these angles on the image, we find

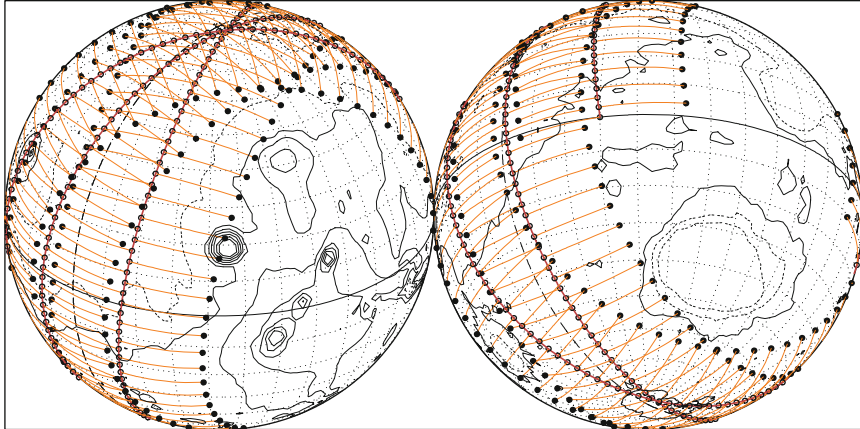
$$i = 93.0^\circ, \quad i' = 97.5^\circ,$$

which agrees with the values calculated in Example 15.6.

**[MARS] Premier MO-07 / Mambo**  
Orbit - Ground track

>>>> Time span shown: 295.9 min = 0.20 sol  
Across track swath (XT mode)

Altitude = 350.0 km                      a = 3747.000 km  
Inclin./SUN-SYNCHRON.= 92.83 °  
Period = 116.34 min \* rev/sol = 12.72  
Equat. orbital shift = 1678.2 km ( 28.3 °)  
\*\* Half-swath: 65.0° => 1397 km [ 1.00 min]

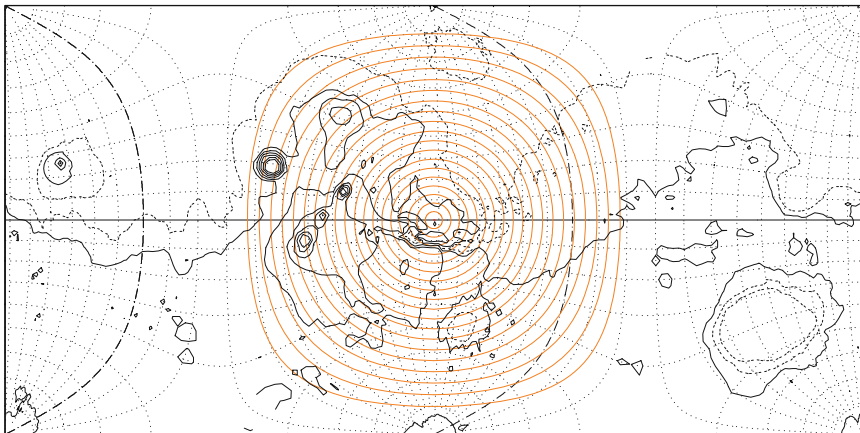


Projection: Orthographic	Pr. centre (r.): 28.0 ° S; 43.0 ° E	Asc. Node: 30.00 ° [16:00 LMT]	Ιξίων
Property: none	Aspect: Oblique	Latit. overlap: 69.3° <-> 90.0°	MC ★ LMD
♁ T.:Azimuthal - Graticule: 10°	{3.5} [-90.0/+118.0/+47.0] [-] MGM1025	MOLA Topogr. / h / 2.5km /	Ατλας

**[MARS] Areostationary**

Locus of points  
equidistant  
from the subsatellite point

Altitude = 17034.0 km                      a<sub>GS</sub> = 20430.990 km  
Inclination = 0.00 °                      Parking Longit. = 62.5 ° W  
Period = 1477.11 min \* rev/sol = 1.00  
Equat. orbital shift = 21341.8 km  
\*\* Half-swath: 9.6° - On ground 4768.5 km [ 250.0 km]



Projection: Guyou	Project. centre: 0.0 ° ; 62.5 ° W	Areostationary	Ιξίων
Property: Conformal	Aspect: Direct	Max. attained latit. = 80.4 °	MC ★ LMD
♁ T.: [Ellipt. Int.] - Graticule: 10°	{3.5} [+90.0/ +0.0/ -27.5] [-] MGM1025	MOLA Topogr. / h / 2.5km /	Ατλας

FIG. 15.32 : Upper: Orbital ground track of the satellite Premier and ground swath of the Mambo instrument. Lower: Locus of points equidistant from the subsatellite point for an areostationary (SMO) satellite.

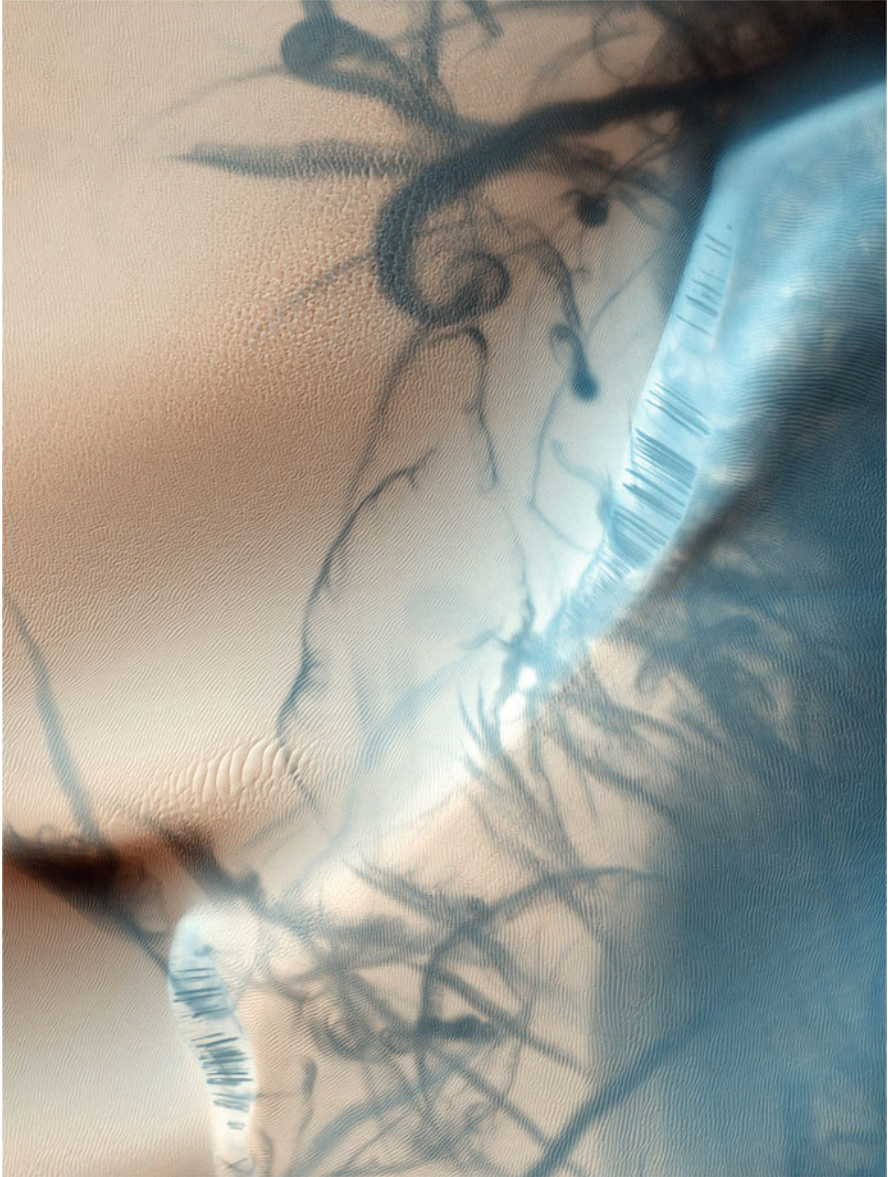


FIG. 15.33 : “Tattoos” on Mars. This image, acquired by HiRISE aboard MRO, should be compared with Fig. 15.1. These dark stains on the bright sand are produced by swirls of dust called dust devils, of the kind that can be encountered on Earth in most arid regions, such as Arizona. These whirlwinds lift the dust lying in a thin red layer on the dunes. The dark sand beneath has larger grains and is not lifted up. On Mars, such dust devils can be as much as 8 km high. Credit: HiRISE, MRO, LPL, University of Arizona, NASA.

**Mars Reconnaissance Orbiter.** Figure 15.34 was acquired by HiRISE aboard MRO, with  $\tau_{AN} = 15:30$ . The High Resolution Imaging Science Experiment (HiRISE) is a high-resolution camera. The image was acquired during daytime, at 15:21 LMT, in the ascending part of the orbit (retrograde since Sun-synchronous). Images are built up continuously, row by row, and the edges of the image follow the satellite ground track. They thus make an angle  $i'$  with the edge of the frame. We measure

$$i' = 97.5^\circ .$$

This can be compared with the value calculated in Example 15.6. ◀

### 15.8.4 View from an SMO Satellite

When an areostationary (SMO) satellite views Mars, the maximal swath in the sense that we have defined  $f_0$  is given by (12.32). With the value of  $\eta_{GS}$  defined by (15.33), we obtain

$$f_0 = \arcsin \frac{1}{6.016} = 9.569^\circ = 0.1670 \text{ rad} . \quad (15.40)$$

The corresponding angle at the center of Mars is

$$\alpha_0 = 90^\circ - 9.6^\circ = 80.4^\circ \implies 2F_0 = 9,535 \text{ km} . \quad (15.41)$$

If  $\lambda_S$  is the longitude of the satellite S (parking longitude or longitude of the subsatellite point), the longitudes viewed by S on the equator lie in the interval

$$[\lambda_S - 80.4^\circ, \lambda_S + 80.4^\circ] ,$$

and depending on the meridian  $\lambda_S$ , latitudes are viewed over the same interval of  $80.4^\circ$  on either side of the equator.

The fraction of the planetary surface viewed by the areostationary satellite, calculated using (12.38), is in this case 0.417 (or about 42 %, as for the Earth).

**Example 15.15** *Locus of points on Mars at an equal distance from the subsatellite point for an areostationary satellite.*

► As in Example 12.13, we plot the locus  $\mathcal{L}(D)$ . The distance  $D$  defined by (12.36) represents here the great circle distance between a point on Mars viewed by the areostationary satellite and the subsatellite point of this same satellite (see Fig. 15.32 lower).  $D$  varies in steps of 250 km. The subsatellite point chosen in this example corresponds to the position originally proposed for the equatorial NetLander of the Premier mission. ◀



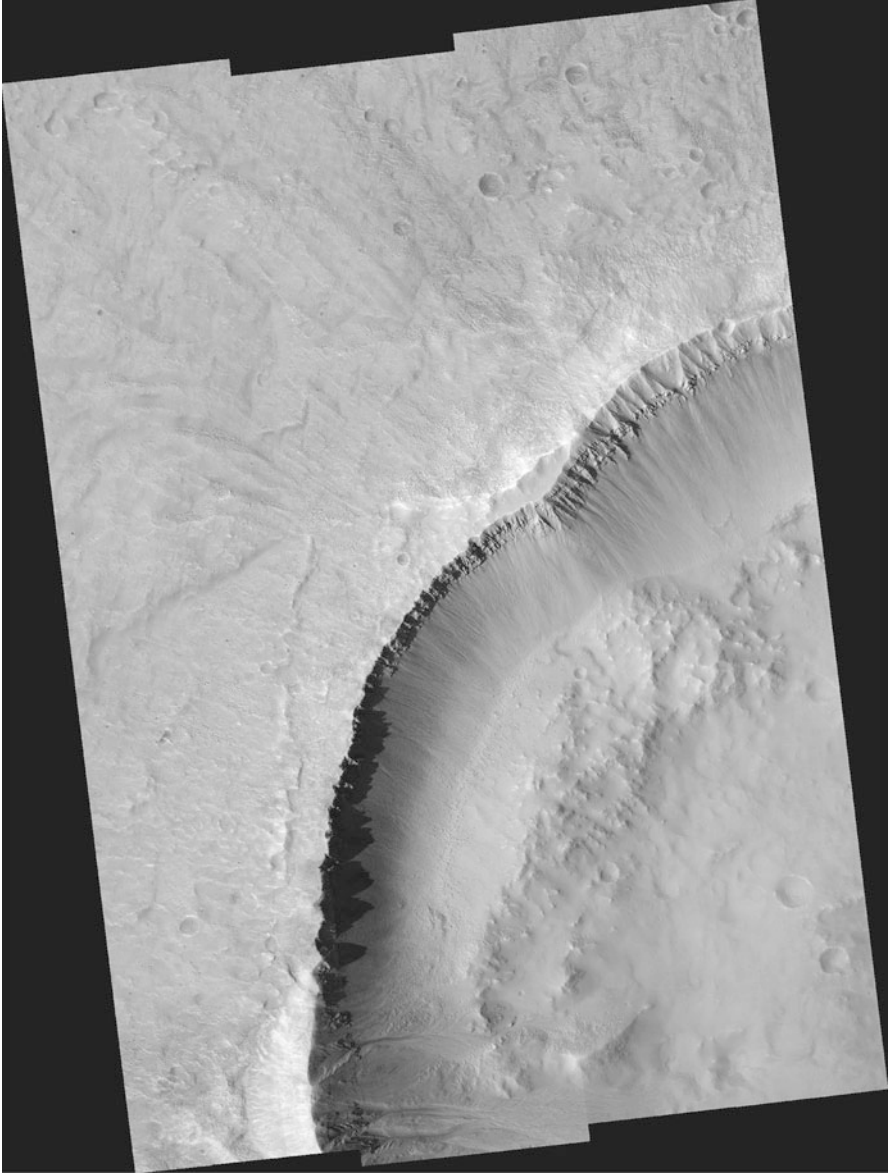


FIG. 15.34 : Gully formation. Image acquired by HiRISE aboard MRO on 12 November 2006. Center of image  $42.2^{\circ}$  N,  $312.0^{\circ}$  E ( $= 48.0^{\circ}$  W). North is at the top. Local time 15:21 LMT, solar elevation  $41^{\circ}$  ( $\theta_0 = 49^{\circ}$ ). Solar areocentric longitude  $L_S = 134.4^{\circ}$  (northern summer). See Fig. 15.35 and Example 15.16. Pixel size 29.8 cm. Altitude of satellite  $h = 297.5$  km. See Example 15.14. Credit: JPL, University of Arizona, NASA.

## 15.9 Spatiotemporal and Angular Sampling

✦ **Chapter 13.** All the concepts discussed in Chap. 13 can be adapted to a satellite of Mars. However, we should note one point that will not be discussed here. When setting up a Mars mission, one must take into account the Sun–target–satellite–Earth configuration. Indeed, while the eyes of the satellite may be turned toward Mars, its ears must be oriented toward the Earth, from whence come its instructions, and so must its mouth, in order to transmit back data.

### 15.9.1 Examples of Sampling

Here we describe an example of temporal and angular sampling in the context of our discussion of the Sun–target–satellite configuration.

**Example 15.16** *Sampling table and statistical table for the wide-field instrument MARCI aboard MRO.*

► We consider the central point of the image shown in Fig. 15.34, which has coordinates  $42.2^\circ\text{N}$  and  $312.0^\circ\text{E}$ . The image was acquired by HiRISE aboard MRO on 12 November 2006, at 15:21 LMT. The altitude of the satellite is  $h = 297.5$  km. The ascending node has characteristics  $\lambda_{\text{AN}} = -42.436^\circ$ ,  $\tau_{\text{AN}} = 15:30$ . The solar areocentric longitude for this date ( $D = 2006$  11 12) was  $L_S = 134.4^\circ$ , which corresponds to sol 287. On Mars, this is in the middle of the northern summer.

**31-Sol or “Monthly” Table.** Carried aboard MRO, the Mars Color Imager (MARCI) is a wide swath instrument with a field of view of  $180^\circ$ , corresponding to an effective field of  $136.5^\circ$  on the ground. It monitors the Martian weather, including storms, clouds, and evolution of the ice caps.

In the table shown in Fig. 15.35, we have indicated:

- On the horizontal axis, LMT “hours”, which are in fact  $1/24$  of a sol, as discussed earlier.
- On the vertical axis, sols from  $D = 1$  for sol 287 ( $L_S = 134^\circ$ ) to  $D = 31$  for sol 318 ( $L_S = 150^\circ$ ).

With regard to dates on Earth, this time interval corresponds to the period from 12 November to 14 December 2006. Sunrise, sunset, and apparent (LAT) noon are shown by dash-dotted lines. Note the significant difference between noon LMT and noon LAT, representing the equation of time.<sup>28</sup> Each overpass

<sup>28</sup>For  $L_S$  between  $134^\circ$  and  $150^\circ$ , we can read off the equation of time in Fig. 15.8, with the result  $E_T \approx -30$  min, which we may write  $-0:30$ . Then, recalling that  $\text{LMT} = \text{LAT} + E_T$ , we have for apparent solar noon,  $\text{LMT} = 12:00 - 0:30 = 11:30$ . In the sampling table,



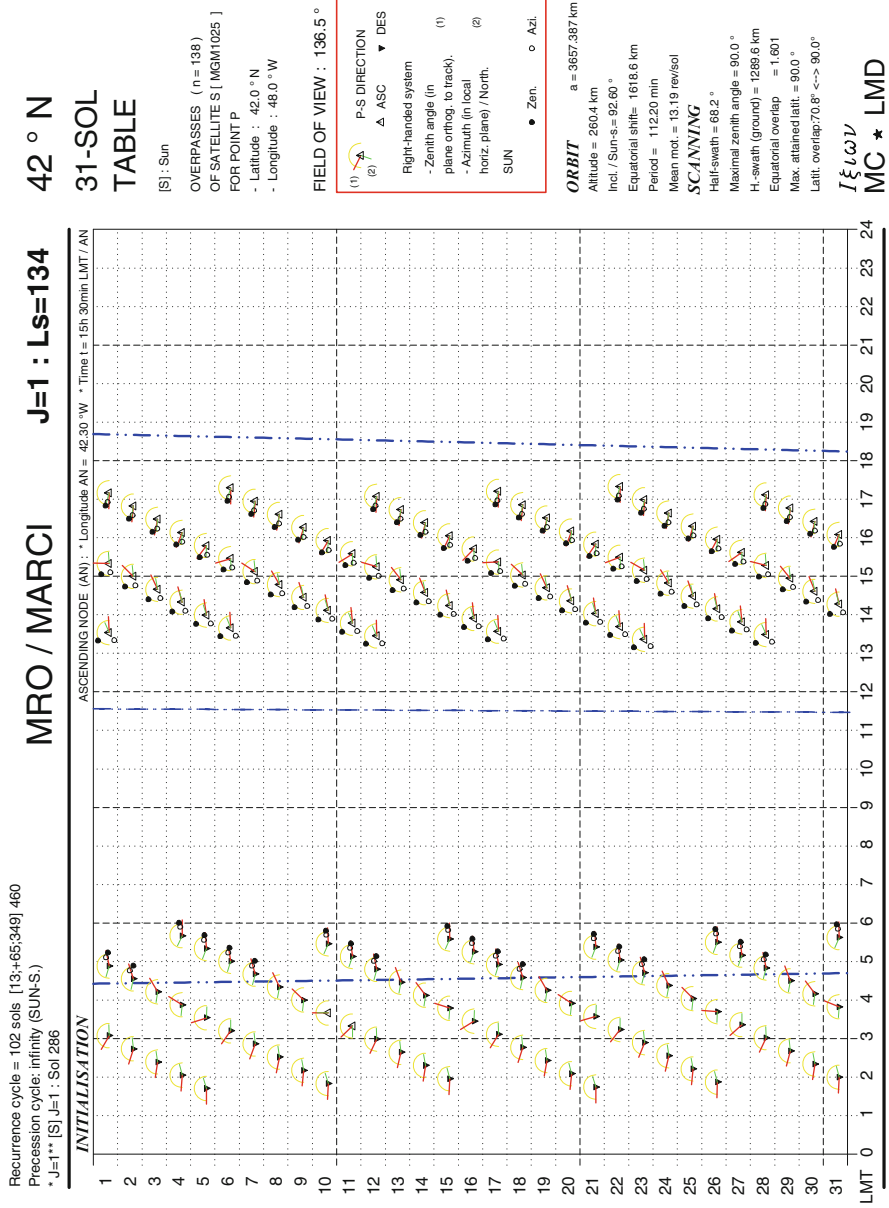


FIG. 15.35 : Thirty-one-sol table of overpass times.

of the satellite under the required viewing conditions is indicated by a triangle (see explanations in Example 13.11). We observe that half of the overpasses occur during the day (in the afternoon) and the other half at night (or very early in the morning).

The overpass at the relevant point occurs on sol  $D = 1$ , at 15:21. The vertical line shows that the satellite passes exactly vertically above the relevant point. Almost the same configuration is repeated for  $D = 17$ , after a subcycle of 16 sols (see Example 15.11).

**Statistics over 31 sols.** We consider points of different latitudes on the meridian passing through the chosen point. This is the meridian  $\lambda = 312.0^\circ$ , or  $\lambda = 48^\circ\text{W}$ . Figure 15.36 is established with:

- On the horizontal axis, the solar zenith angle from  $0^\circ$  (zenith) to  $90^\circ$  (sunrise or sunset).
- On the vertical axis, latitudes from  $+90^\circ$  (North Pole) to  $-90^\circ$  (South Pole).

We calculate the overpasses at these different latitudes for the points along the selected meridian. These overpasses are indicated by dots of various colours depending on the value of the viewing zenith angle. The places overflowed are never viewed with the Sun at the zenith ( $\zeta_s$  is always greater than  $32^\circ$ ) because the overpass time of this Sun-synchronous satellite is in the middle of the afternoon.

**Note.** For the dates considered here, the declination varies from  $+17^\circ$  to  $+12^\circ$ . The many daytime overpasses marked on this graph for latitudes close to the North Pole are due to the polar day being particularly long. Conversely, for places situated beyond latitude  $88^\circ\text{S}$ , it is the polar night. ◀

## 15.9.2 Sun Glint

But is there really cause to consider Sun glint on Mars? The reader may find that we are going a bit too far in our parallel between Mars and the Earth. For where are the lakes and oceans that might cause specular reflection?

Certainly, the phenomenon is much less common than on Earth, but it does happen sometimes. The image in Fig. 15.37 provides an example, acquired by MGS. In mid-February 1998, while MGS was in its aerobraking phase, it found itself in a configuration where the Sun, the satellite, and the center of

---

the line indicating noon LAT does indeed pass through 11:30 LMT. (More precisely, from  $12:00 - 0:28 = 11:32$  LMT for  $D = 1$  to  $12:00 - 0:33 = 11:27$  LMT for  $D = 31$ .)

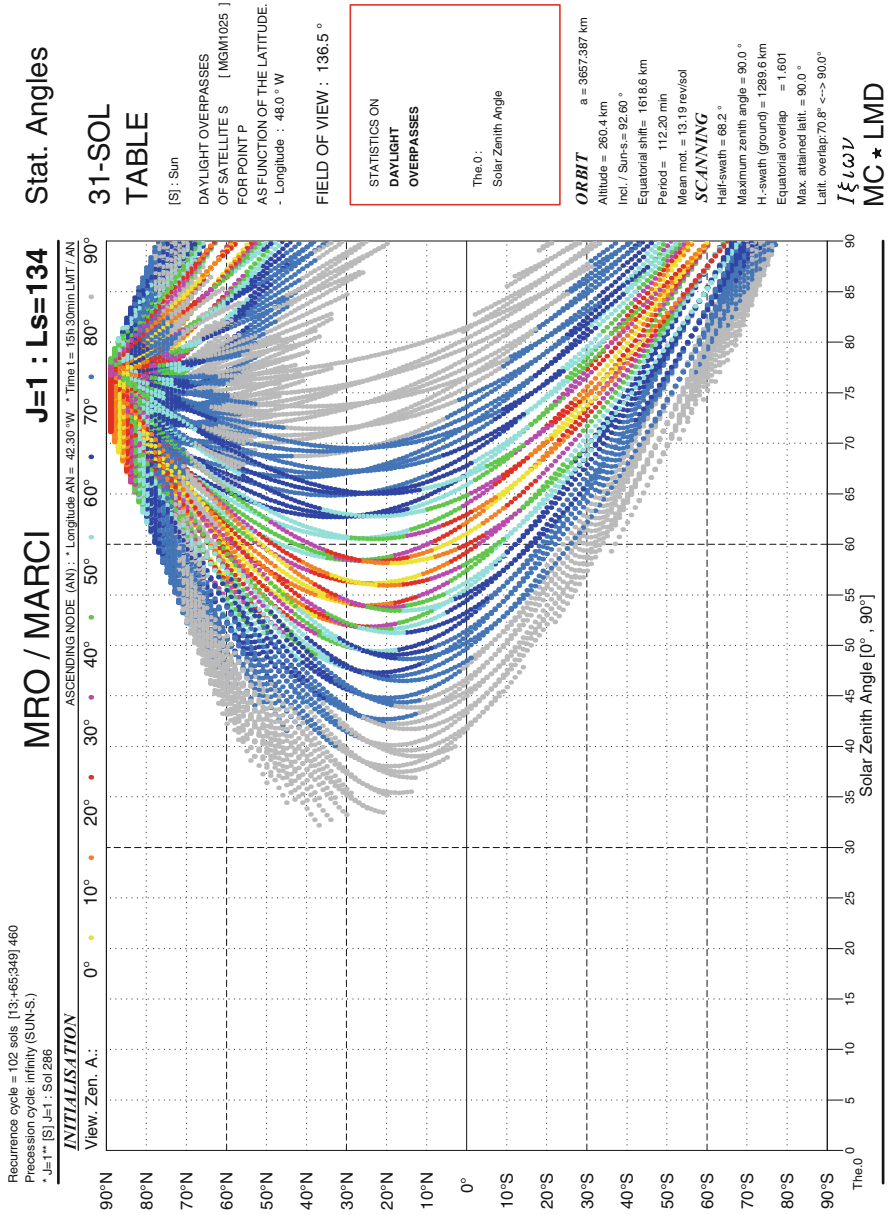


FIG. 15.36 : Thirty-one-sol table. Solar angles as a function of latitude, indicating the viewing zenith angle, for all places on a given meridian.



FIG. 15.37 : *Specular reflection, or Sun glint, on Mars. The Sun, the satellite MGS, and the center of Mars are aligned. Image obtained on 18 February 1998 by the MOC camera in low resolution mode, carried aboard MGS (revolution 136). The point  $P$  is the center of the image, viz.,  $21.0^\circ S$ ,  $4.1^\circ W$ , and  $D = 1998\ 02\ 18 \Rightarrow L_S = 277^\circ \Rightarrow$  declination  $\delta = -24^\circ$ . The latitude of  $P$  is  $\psi = -21^\circ$ . The dark region above the center of the image is Sinus Meridiani. The image was acquired with a wide field of view over half a revolution, from pole to pole. It was then reprojected depending on the latitude and longitude of each observed point, which explains the oval appearance of the object. Credit: MSSS (MOC), MGS, JPL/NASA.*

Mars were aligned at one specific instant of time during each revolution. This geometric configuration corresponds to a situation where specular reflection can occur. Setting  $\theta_0 \approx 0$ ,  $\theta \approx 0$ , and an arbitrary value of  $\phi$  in (13.23), we do indeed obtain  $\gamma' = 0$ .

On Mars, the possibility of Sun glint depends on the physical properties of the surface, e.g., stone, sand, dust, and also on the physical properties of the atmosphere, which may contain aerosols.

## 15.10 Natural Satellites

### 15.10.1 Phobos and Deimos

Mars has two natural satellites, discovered in August 1877 by A. Hall.<sup>29</sup> They have circular, equatorial orbits ( $i$  is about  $1^\circ$ ). Their small size, of the order of 10 km, and their lumpy shape make them look like large rocks. Like the Moon or other natural satellites, they always turn the same face towards their planet.

The largest, Phobos ( $a = 9,379$  km,  $i = 1.07^\circ$ ,  $T = 0.3189$  day), with  $\eta = 2.76$ , is well below the areostationary orbit.<sup>30</sup> The second moon, Deimos ( $a = 23,459$  km,  $i = 1.79^\circ$ ,  $T = 1.2624$  day), with  $\eta = 6.91$ , is slightly higher.

One consequence of tidal effects is that the distance between the planet and its moon varies slightly in time. If the satellite is beyond the synchronous orbit, it moves away. If it is within, it moves closer until it breaks under tidal forces when it reaches the so-called Roche limit, to be discussed in the next chapter [see (16.14)].

The Lagrange points  $L_1$  and  $L_2$  of the Mars–Phobos system have been calculated in Example 6.4.

### 15.10.2 Space Exploration

The Soviet probe Phobos-2 made a novel attempt to approach the moon Phobos. In an equatorial orbit for 2 months from 29 January 1989, the probe gradually moved towards Phobos. When it was only 50 m from the surface of Phobos, on 27 March, it ceased to transmit, just as it was about to launch its landing modules.

---

<sup>29</sup>Hall named them after the two male offspring of Ares and Aphrodite. They had the same weak points as their father: Phobos, ὁ Φόβος, ου, “fear”, Deimos, ὁ Δεῖμος, ου, “dread”. Hall’s source was two lines from the Iliad, Book XV:

ὦς φάτο, καὶ ῥ’ ἵππους κέλετο Δεῖμόν τε Φόβον τε  
 ζευγνύμεν, αὐτὸς δ’ ἔντε ἔδύσετο παμφανόωντα.  
 Ὀμήρου, *Ἰλιάδα*, O (119–120)

In the translation by Ian Johnston:

Then he [Ares] told Terror and Flight to harness his horses,  
 while he dressed himself in his glittering armour.

<sup>30</sup>Phobos is one of the rare known examples of a natural satellite whose orbital angular speed is greater than the angular speed of the planet about its own axis: it is thus below the planetostationary orbit. Until certain discoveries made by Voyager-1 and 2, it was the only natural satellite known to have this property. For a Martian observer, Phobos rises in the west and sets in the east. Seen from Phobos, Mars covers roughly half of the sky. Indeed, the planet is viewed from the apex of a cone with angle  $2f_0 = 2 \arcsin(1/\eta) = 42^\circ$ .

The mission Phobos-Grunt, already mentioned at the beginning of this chapter, was lost due to a failure just after launch.<sup>31</sup> Mars Express flew close by Phobos on several occasions as it followed its elliptical, near-polar orbit, and was able to produce images and help in selecting a landing site (see Fig. 15.38).

### 15.10.3 View and Sampling

Phobos can only be viewed from those points on Mars with latitude less than  $|\psi| = \psi_v = 69.8^\circ$ . Indeed, according to (12.15),

$$\psi_v = i + \arccos \frac{1}{\eta} = 1.07 + 68.77 = 69.84^\circ .$$

The “sampling” of a natural satellite is represented by its synodic period. This period  $T'$  is obtained using (8.44):

$$\frac{1}{T'} = \frac{1}{1.027} - \frac{1}{0.319} = -2.161 \text{ day}^{-1} ,$$

which gives  $T' = -0.463$  day or  $-0.451$  sol. The negative sign of the synodic period indicates that the relative motion occurs in the retrograde direction.

Concerning Deimos, which is rather close to the areostationary orbit, only those points close to the poles cannot view it. Indeed, we now have

$$\psi_v = i + \arccos \frac{1}{\eta} = 1.79 + 81.68 = 83.47^\circ .$$

The synodic period is calculated from

$$\frac{1}{T'} = \frac{1}{1.027} - \frac{1}{1.262} = +0.1811 \text{ day}^{-1} ,$$

which gives  $T' = +5.52$  day or  $+5.37$  sol.

---

<sup>31</sup>It is worth mentioning the very interesting strategy chosen here. In the first stage, the probe was to enter Martian orbit in September 2012, then circularise with  $h_p = 5,800$  km and  $h_a = 6,000$  km. From this “phobosynchronous” orbit, the satellite would have softlanded on Phobos in April 2013, staying until August. In the final stage, it was to return to Earth with a piece of Phobos, in fact a sample of around 200 g.

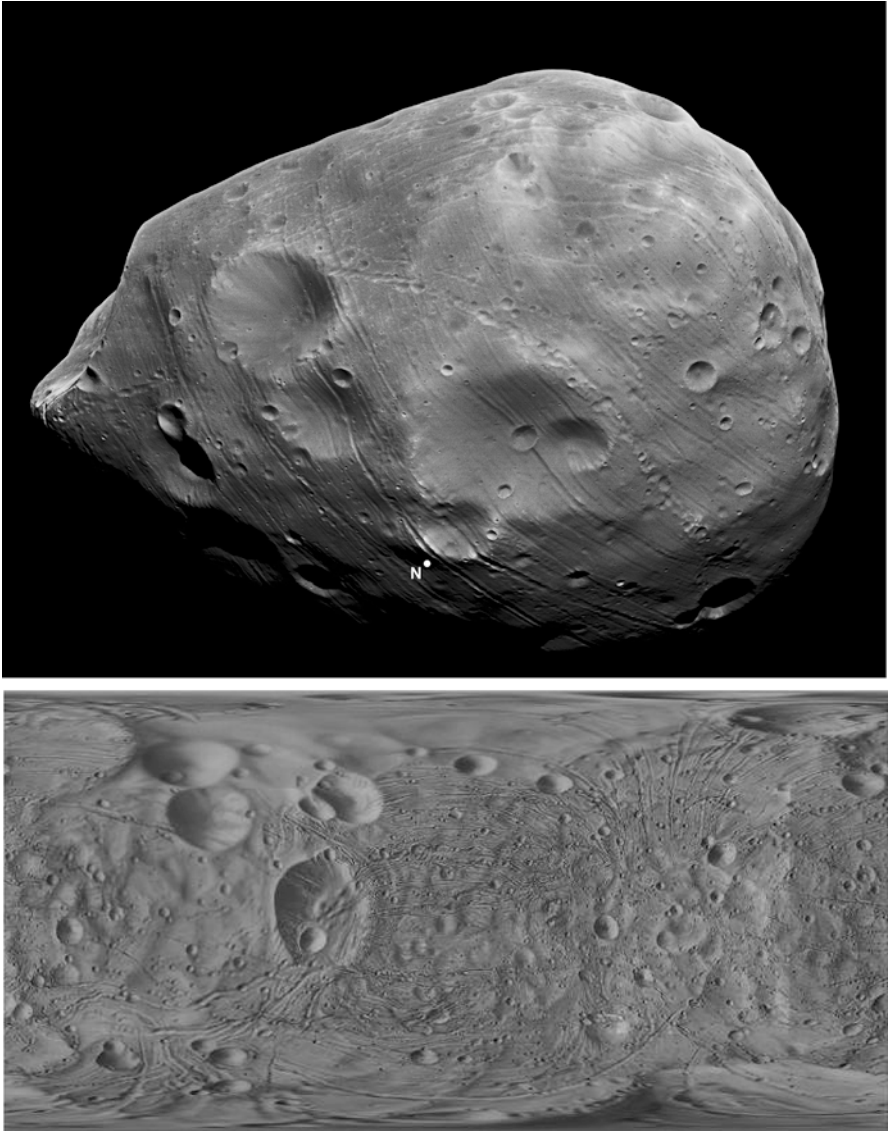


FIG. 15.38 : *Phobos*. Upper: Image acquired on 3 March 2010 by the High Resolution Stereo Camera (HRSC) aboard *Mars Express* during a flyby at 67 km from *Phobos*. N is the North Pole. Credit: ESA, DLR, FU Berlin (G. Neukum). Lower: Photographic map of *Phobos*, using a plate-carrée projection, obtained from *Mars Express* images, supplemented by images from other missions. Credit: ESA.

## 15.11 Historical Note: Kepler and the Planet Mars

### 15.11.1 Calculating the Period of Revolution

As we saw in Chap. 4 (see Fig. 4.13), the subtitle of *Astronomia Nova* was *On the motions of Mars, according to the observations of Tycho Brahe* (see Fig. 15.39). The quality of the measurements made by Tycho Brahe is well known, and all the more astonishing in that they were made with the naked eye. However, the astuteness of Kepler's interpretation was equally impressive. Page 131 of *Astronomia Nova*, reproduced in Fig. 15.40, illustrates this.

Kepler would choose a position of Mars on its orbit and note the time of observation. Then, for each revolution, he noted the time of passage at this same point, *ad idem fixarum punctum* (line 13 of p. 131), to deduce the length of the Martian year. The first passage noted<sup>32</sup> is (lines 10 and 11 of p. 131)

anno MDXC D. v Martii vesperi H. vii M. x ,

which is the year 1590, or day (D. = *die*) 5 of the month of March (*Martii*), in the evening (*vesperi*), at hour (H. = *hora*) 7, and at minute (M. = *minuta*) 10.

Three other passages are then noted. The dates have been transcribed into the modern notation in Table 15.10. Transforming these times<sup>33</sup> into Julian dates (JD), it is easy to calculate the lapse of time between them and thus obtain the period of revolution, which represents the length of the Martian sidereal year.<sup>34</sup>

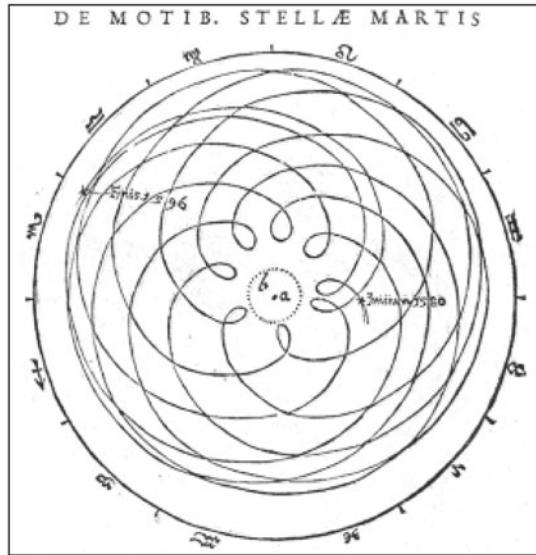
For this method of calculation, based on four observations at intervals of one Martian sidereal year, the reader is also referred to Fig. 1.9. The average of the three values serves to make the comparison:

<sup>32</sup>The attentive reader will note that we have corrected a typing error by Kepler. Instead of MDXCX, which means nothing as a Roman numeral, one should read MDXC for 1590.

<sup>33</sup>We assume that these are the LMT times at Uraniborg, where Tycho Brahe had his observatory. It is located at 55°55'N and 12°45'E on the island of Ven, which now belongs to Sweden. We deduce that UT = LMT (Ven) – 51 min. Another issue is whether Kepler used the Gregorian or the Julian calendar. Defined in 1582, the Gregorian calendar was applied from 1583 by the German Catholic states, but not until 1700 in Denmark and the German Protestant states. The answer can be found from Kepler himself. In just one instance, he specifies an observation date with the day of the week, namely, Saturday 8 November 1597. In the “new” calendar, this day is a Saturday, while in the “old” one it is a Wednesday. Kepler was thus using the Gregorian calendar. Note that these issues of local time and calendar are of no importance when calculating the period, which is based on differences between dates. They are only relevant to the calculation of  $L_S$ .

<sup>34</sup>On a drawing with the note *Copernici* on p. 131 of *Astronomia Nova*, Kepler plotted with a continuous curve the circle  $\delta\gamma$  with center  $\alpha$ , representing the circular trajectory of the Earth as defined by Copernicus. He then plotted with a dotted curve the trajectory of the Earth as he had calculated it. The Sun  $\beta$  is not exactly at the center, indicating the eccentricity of the Earth orbit. The position of the Earth indicated by  $\theta$  corresponds to the 1590 observation, while  $\eta$  corresponds to 1592,  $\varepsilon$  to 1593, and  $\zeta$  to 1594. On the orbit of Mars, the position  $\chi$  of the planet is fixed for these four dates.





Tempus	Locus	Solis a Terra distantia	Marsis a Sole distantia	Marsis aequantia in elliptica	Locus computatus	Locus observatus	Differētia	Latitudo
1582. 23 Nove. H. 16. 0	11.41 ♀	98748	158852	0.42.11	26.40. 0	26.38.30	1.30 +	Bor
26 Dece. H. 8. 30	15. 4 ♀	98226	162104	16. 7.18	17.44.19	17.40.30	3.39 +	4. 49
30 Dece. H. 8. 10	19. 9 ♀	98252	162443	17.56.32	16. 6.20	16. 0.30	5.50 +	4. 5
1583. 26 Janua. H. 6. 15	16.33	98624	164421	0. 6.24	8.17.57	8.20.30	2.33 -	1. 53
1584. 21 Dece. H. 14. 0	10.16 ♀	98207	164907	3.51.45	1.14.34	1.13.30	1. 4 +	3.31
1585. 24 Janua. H. 9. 0	14.53	98295	166210	18.47. 8	24. 3.58	24. 7.30	3.32 -	4. 31
4 Febr. H. 6.40	26.10	98830	166400	23.33.41	19.43.52	19.47. 0	3. 8 -	4.28
12 Mart. H. 10.30	2.16 ♀	99858	166170	9.23.14	11.43.31	11.46. 0	2.29 -	3.22
1587. 25 Janua. H. 17. 0	16. 1	98611	166232	8.13.40	4.41.50	4.42. 0	0.12 -	3.26
4 Mart. H. 13.24	24. 0 X	99595	164737	24.56.50	26.24.41	26.25.40	0.59 -	3.38
10 Mart. H. 11.30	29.52 X	99785	164382	27.35.54	24. 5.55	24. 5.55	0. 0	3.29
21 April. H. 9.30	10.48 ♀	102102	161027	16.44.51	15.49.50	15.48.20	1.30 +	1.48
1589. 8 Mart. H. 16.24	28.36 X	99736	161000	16.55.14	12.14. 7	12.16.50	2.43 -	2. 4
13 April. H. 11.15	5.38 ♀	100810	157141	4. 1.50	4.45. 0	4.43.20	1.40 +	1.10
15 April. H. 12. 5	5.56 ♀	100866	156900	5. 1.41	3.58.57	3.58.20	0.37 +	1. 4
6 Maji. H. 11.20	25.49 ♀	101266	144226	15.30.26	27. 8.17	27. 7.20	0.57 +	0. 7
1591. 13 Maji. H. 14. 0	2.10	101467	147891	12. 7.38 ♀	2.15.36 ♀	2.20. 0 ♀	4.24 -	Aust.
6 Junii H. 12.20	24.59	101769	144981	25.38.48 ♀	27.11.45 ♀	27.15. 0 ♀	3.15 -	1. 31
10 Junii H. 11.50	28.47	101789	144526	27.56.49 ♀	25.57.57 ♀	26. 2.36 ♀	4.39 -	3. 85
28 Junii H. 10.24	15.51	101770	142608	8.29.22 ♀	21. 4.21 ♀	21.10. 0 ♀	5.39 -	4. 45
1593. 21 Julii H. 14. 0	8.26	101498	138376	20. 1.38	17.43.14 X	17.45.45 X	2.31 -	5.46
22 Aug. H. 12.20	9.11 ♀	100761	138463	10.15.25 X	13. 9.39 X	13.10.15 X	0.26 -	6. 7
29 Aug. H. 10.20	11.54 ♀	100562	138682	14.37.15 X	11.11.41 X	11.14. 0 X	2.19 -	5.52
3 Octo. H. 8. 0	20.15 ♀	99500	140697	6.19.39 ♀	7.49.54 X	7.50.10 X	0.16 -	3.17
1595. 17 Sept. H. 16.45	4.18 ♀	99990	143222	22.49.19 ♀	26. 5.45 ♀	26. 7.11 ♀	1.27 -	1. 41
27 Octo. H. 12.20	13.59 ♀	98851	147890	15.35.38 ♀	18.50.46 ♀	18.51.15 ♀	0.29 -	0. 6
3 Nove. H. 12. 0	21. 2 ♀	98694	148773	19.26.33 ♀	16.18.33 ♀	16.18.30 ♀	0. 3 +	0. 17
18 Dece. H. 8. 0	6.43 ♀	98200	154539	13. 2.29	11.39. 1 ♀	11.40. 0 ♀	0.59 -	1. 40

Distantiae igitur methodo capitis huius inquirite ex observati hic positus, probantur infra. Loca vero apparentia, quando Mars motu eccentrico Cancro veritate prodibunt circiter 4 tripulis anteriora, in ♀ & ♀ per totidem promotiora. Neque veniunt hi erroruli ex distantis vitiosis, non enim essent in contrariis plagis quidem sed contrarie qualitates. Exultimo illos conciliari posse mutatione apogei per gradum unum, quod per observata B. A. H. facili licet. Nihil tamen definitio in prelois. Refertur enim & huius apogei & totius hypotheticos correctio in 'GEVS TABVLARVM'.

FIG. 15.39 : Extracts from *Astronomia Nova*. Upper: Page 4. Trajectory of Mars in a geocentric frame, showing the retrograde motion of the orbit. Observations by Tycho Brahe between 1580 and 1596. The beginning and end of the observations are indicated. Lower: Page 309. Example of a measurement table and calculations carried out by Kepler.

Jam postquam femel hujus rei periculum fecimus, audacia subvecti porro liberiores esse in hoc campo incipiemus. Nam conquiram tria vel quotcunque loca vifa MARTIS, Planeta semper eodem eccentrici loco versante: & ex iis lege triangulorum inquiram totidem punctorum epicycli vel orbis annui distantias a puncto æqualitatis motus. Ac cum ex tribus punctis circulus describatur, ex trinis igitur hujusmodi observationibus situm circuli, ejusque augium, quod prius ex præsupposito usurpaveram, & eccentricitatem a puncto æqualitatis inquiram. Quod si quarta observatio accedet, ea erit loco probationis.

CAP.  
XXIV.

PRIMUM tempus esto anno MDXCX D. V Martii vesperi H. VII M. X eo quod tunc ☉ latitudine pene caruit, ne quis impertinenti suspitione ob hujus implicationem in percipienda demonstratione impediat. Respondent momenta hæc, quibus ☉ ad idem fixarum punctum redit: A. MDXCII D. XXI Jan. H. VI M. XLI: A. MDXCIII D. VIII Dec. H. VI. M. XII: A. MDXCIV D. XXVI Octob. H. V M. XLIV. Estq; longitudo

Martis primo tempore ex TYCHONIS restitutione.  $\overset{\circ}{i}$ . 4. 38. 50: sequentibus temporib. toties per  $\overset{\circ}{i}$ . 36 auctior. Hic enim est motus præcessionis congruens tempori periodico unius restitutionis MARTIS Cumq; TYCHO apogæum ponat in  $23\frac{1}{2}^{\circ}$  ♋, æquatio ejus erit  $11. 14. 55$ : propterea longitudo coæquata anno MDXC  $\overset{\circ}{i}$ . 15. 53. 45.

Eodem vero tempore & commutatio seu differentia medii motus SOLIS a medio Martis colligitur  $10. 18. 19. 56$ : coæquata seu differentia inter medium SOLIS & MARTIS coæquatum eccentricum  $10. 7. 51$ .

PRIMUM hæc in forma COPERNICANA ut simpliciori ad sensum proponemus.

Sit a punctum æqualitatis circuitus terre, qui putetur esse circulus  $\delta\gamma$  ex a. descriptus: Et sit Sol in partes  $\beta$ , ut a  $\beta$  linca apogæi

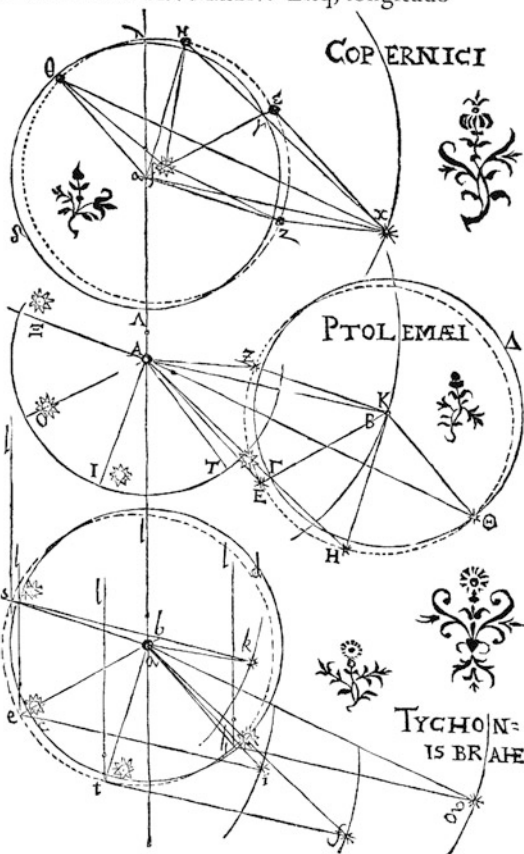


FIG. 15.40 : Astronomia Nova, p. 131. Determining the period of revolution of Mars, i.e., the Martian year.

Date	Time	Julian date (JD)	$\Rightarrow$ difference (d)	$L_S$ (deg)
1590 5 March	19:10	2,301,859.26319	–	316.252
1592 21 January	18:41	2,302,546.24306	686.97987	316.359
1593 8 December	18:12	2,303,233.22292	686.97986	316.357
1595 26 October	17:44	2,303,920.20347	686.98055	316.364

TABLE 15.10 : *Transcription of p. 131 of Astronomia Nova, with calculations using the data. Solar longitude  $L_S$ .*

Quantity	Formula	Earth	Mars
Aphelion	$a(1 + e)$	101,796	166,510
Perihelion	$a(1 - e)$	98,204	138,173
Total	$2a$	200,000	304,683
Difference	$2ae$	3,592	28,337
Semi-major axis	$a$	100,000	152,342
Focal length	$ae$	1,796	14,169
Eccentricity	$e$	0.01796	0.09301

TABLE 15.11 : *Results of Kepler’s calculations. The unit of distance chosen by Kepler was 100,000 for the semi-major axis  $a$  of the Earth orbit.*

Planet	Quantity	Kepler	Current value	Relative error (%)
Mars	Inclination/ecliptic (deg)	1.8420	1.8496	0.4
Mars	Semi-major axis (a.u.)	1.52342	1.52366	0.016
Mars	Eccentricity	0.09301	0.09341	0.4
Terre	Eccentricity	0.01796	0.01671	7.5

TABLE 15.12 : *Results of Kepler’s calculations. Comparison with current values and relative error in percent.*

Kepler’s calculations    686.9801    or 686 d 23 h 31 m 20 s ,  
 Sidereal year            686.9800    or 686 d 23 h 31 m 12 s .

The “fixed point” on the Mars orbit is determined with remarkable accuracy:

$$L_S = 316.358 \pm 0.006^\circ .$$

Kepler’s error in the length of the sidereal year is just 8 s over 687 days, i.e., a relative error of  $10^{-7}$ . In any case, Kepler could not have done better, since his minimal time measurement was the minute. Mechanical clocks date back to the fourteenth century, but truly accurate time measurement began with Huygens in 1673. As far as observation with optical instruments is concerned, this did not get underway until Galileo arrived on the scene in 1610.

### 15.11.2 Other Calculations for the Earth and Mars

The way Kepler used Tycho Brahe's measurements was crucial in valorising them. To begin with, he placed them in a Copernican context, but in addition to this, he brought a wealth of mathematical knowhow. He even improved their accuracy by rigorously accounting for the precession of the equinoxes (*Astronomia Nova*, p. 131) and atmospheric refraction (*Astronomia Nova*, p. 73).

We end this historical note with a few other remarkable results due to Kepler, published in *Astronomia Nova*.

**Inclination.** For the inclination of Mars relative to the ecliptic plane (*Astronomia Nova*, p. 79), Kepler noted that the details of the calculation were very delicate. He obtained the value

$$i = 1^\circ 50\frac{1}{2} \text{ min}$$

in his notation, or  $i = 1.842^\circ$  in decimal degrees.

**Eccentricity and Semi-major Axis.** Kepler calculated the eccentricity of the Earth (*Astronomia Nova*, p. 136) and Mars (*Astronomia Nova*, p. 265), as well as the semi-major axis of the Mars orbit. He attributed 100,000 to the semi-major axis of the Earth orbit (these are thus arbitrary units). The results are shown in Table 15.11 and compared with current values in Table 15.12.

## Chapter 16

# Satellites of Other Celestial Bodies

The princes leave first. Locks are checked.  
Chains are fastened. The clamour of men is  
silent now. Doors once open wide are closed.  
The gods and goddesses of the land have re-  
tired to the skies. They no longer pronounce  
sentence, judge no more.

The night adorns its veil.

The palace is still, the wheat fields hushed.  
The traveller invokes a god; he who awaits  
trial seeks sleep in vain. That most equitable  
of judges, Shamash [the Sun], has entered  
his apartments. Bright stars, divinities of the  
great night, be present at my side.

*Hymn to the Night.*

**Babylon**, circa 2000 BC

Clay tablet, Louvre Museum AO 6769

From the original translation by

Antoine Cavaigneaux.

In the country of clear skies, the cradle of the written word, Mesopotamia and Egypt, the nights were kind to stargazers. Most of the stars were fixed to constellations, while others moved around the zodiac. There was Sirius, and there was Venus. All these mysteries were recorded on clay or papyrus, in the vain hope of divination, works of astrology, bound together with superstition and religion. Far removed from any scientific goal, but nevertheless a beginning. For science begins with observation!

Several centuries later, the astronomers of Greece were influenced by the Babylonians. The sky was still clear, and in their own writing, they were the first to make the formal distinction between stars and planets.<sup>1</sup>



In the present chapter, we shall examine the motion of a satellite around another celestial body, but more concisely than we have done for the Earth and Mars. The chapter is divided into two parts, each following practically the same plan. There is a clear separation between Part A, which concerns the satellites of planets, and Part B, which deals with satellites of natural satellites. In the second part, to avoid confusion, a natural satellite or moon of a planet will be referred to by the term “natural satellite,” and the term “satellite” will be reserved for an artificial or technological satellite.

## *A – Satellite of a Planet*

### 16.1 Planets of the Solar System

#### 16.1.1 Presenting the Planets

The planets of the Solar System gravitate around its central star, the Sun. They fall into two categories: the telluric planets and the giant planets.<sup>2</sup> The telluric planets<sup>3</sup> are the four planets closest to the Sun: Mercury, Venus, Earth, and Mars. They are rather similar to one another in size and composition (iron and siliceous rocks). The giant planets are more remote: Jupiter, Saturn,

---

<sup>1</sup>The word “planet” comes from the Latin *planeta*, itself taken from the Greek *πλάνητες*, plural of *ὁ πλάνης, ητος*, which means “traveller” or “wanderer.” This word derives from the root meaning “to wander, to stray from the path.” Indeed, the Greek astronomers distinguished moving bodies (the planets, *πλάνητες ἀστέρες*) from fixed bodies (the stars, *ἀστέρες*). The Indo-European root \*ster, “star,” reappears in the Greek *ὁ ἀστήρ, τέρος* and in several branches: Germanic (with star, *Stern, ster, stjerne, stārna, stjerner, stjrnū*), Celtic, and Indo-Aryan (with *sitara* in Hindi, *sétaré* in Persian). The variant \*stel gave rise to *stella* in Latin, and from there to the words we find in the Latin languages (*stella, estrela, stea, étoile*)

<sup>2</sup>One also finds the terms “terrestrial” and “Jovian,” the latter being a reference to Jupiter, from the Latin *Jupiter, Jovis*. Up until the Middle Ages, in the days of the geocentric astronomy in which the roles of the Sun and Earth were swapped over, the planets between the Earth and the Sun (the Moon, Mercury, Venus) were known as the inferior planets, while those considered to lie beyond the Sun (Mars, Jupiter, and Saturn) were referred to as the superior planets.

<sup>3</sup>In Latin, *Terra, æ* (f.) means “the Earth,” but *Tellus, uris* (f.) is a poetic name for the Earth goddess, or Mother Earth, “the fertility goddess of crop and cattle” (Horace).

Uranus, and Neptune. They are much bigger than the telluric planets and have totally different compositions (mainly hydrogen and helium). The radius of the giant planets is determined as being the radius of an isobaric surface (at 1 bar). It is not possible to define a ground level or obtain any geographic representation of these planets.

The asteroid belt gravitates between these two groups. The first asteroid, Ceres, was discovered by G. Piazzi<sup>4</sup> at the beginning of the nineteenth century. The asteroid belt is composed of thousands of rocky bodies, sometimes with quite strange shapes.<sup>5</sup> Beyond the giant planets lie a small planet, Pluto, and the asteroids of the Kuiper Belt.<sup>6</sup> Still further out lies the Oort cloud,<sup>7</sup> a mysterious world of comets.<sup>8</sup> Since 2006, Pluto has been classified<sup>9</sup> with the Kuiper planetoids in the category of trans-Neptunian objects.

---

<sup>4</sup>Father *Giuseppe Piazzi* (1746–1826) was an Italian astronomer. He produced a very accurate catalogue of more than seven thousand stars. It was on 1 January 1801, while he was compiling his catalogue, that he discovered the first asteroid, which he called Ceres, the patron saint of Sicily. Having identified the position of this new planet, he had to take a break from his observations at his observatory in Palermo due to bad weather. But when he went back to them later, his Ceres had disappeared. It was the young Gauss who, using methods he had just developed himself, succeeded in tracking it down using the information provided by Piazzi. Within 7 years, three other asteroids had been located by H. Olbers. It was Gauss who showed that they all belonged to the same belt by determining the orbital elements.

<sup>5</sup>Most of these asteroids belong to the Main Belt, between Mars and Jupiter, but some actually lie on the orbit of Jupiter (the Trojan asteroids mentioned in Sect. 6.12), while others cross the trajectory of Mars and even the Earth orbit (near-Earth asteroids). Asteroids are numbered according to the order of their discovery, starting with 1-Ceres, which is also the largest. On 1 January 2000, there were 7,722 (see Fig. 6.9). Since then, an automatic system called Lincoln Near Earth Asteroid Research (Linear) set up by the Lincoln Laboratory at MIT has been in operation. Thousands of asteroids are discovered every year, including some 320,000 in 2012, although there has been a certain decline over the past few years.

<sup>6</sup>*Gerard Kuiper* (1905–1973) was an American astronomer of Dutch extraction. He discovered the atmosphere of Titan (1945) and showed that it was made up of methane. He also showed that the atmosphere of Mars was mainly composed of carbon dioxide (1947). He hypothesised that the Solar System was encircled by an asteroid belt, of which Pluto was a representative. Since 1992, hundreds of trans-Neptunian objects have been discovered, some with a diameter of several hundred kilometers. They form what is now called the Kuiper Belt or Kuiper–Edgeworth Belt.

<sup>7</sup>*Jan Hendrik Oort* (1900–1992) was a Dutch astronomer. From his studies of a great many very long-period comets with orbits well outside the plane of the ecliptic, he deduced in 1950 that one should find, beyond the orbit of Neptune and the Kuiper Belt (which lie largely within the ecliptic), a ball-shaped rather than ring-shaped “cloud,” made up of small celestial bodies, which could be considered as a kind of cometary reservoir. The diameter of this so-called Oort cloud would be some  $10^5$  astronomical units, or one light-year. Gravitational perturbations, even very weak effects, would cause these comets to move either towards the center of the Solar System, or out towards other stars.

<sup>8</sup>The word “comet” comes from Latin, borrowed directly from the Greek *comētēs*, κομήτης, where it means “long-haired,” from the Greek ἡ κόμη, ης, “hair.”

<sup>9</sup>Many planets of the size of Pluto have been found in the Kuiper Belt since the 1990s. It thus became urgent to react in some way. Keeping Pluto as a planet meant accepting hundreds of others. On 24 August 2006, in its 26th General Assembly in Prague, the



The two telluric planets furthest from the Sun both have their own natural satellites: the Earth has one, the impressive Moon, while Mars has two minuscule followers. The giant planets each have a whole series of moons, some of which are larger than Mercury or Pluto.

Mercury, Venus, Mars, Jupiter, and Saturn have been known since ancient times<sup>10</sup> (the Earth itself has not been considered a planet for such a long time), and have inherited in English and most European languages the names of the main divinities in the Roman pantheon.<sup>11</sup> The same custom applied to planets discovered later: Uranus by W. Herschel in 1781, Neptune by J.G. Galle on 23 September 1846, using the celebrated calculations by Le Verrier (see Chap. 6), and Pluto by C.W. Tombaugh on 18 February 1930.

As soon as astronomers had switched to a heliocentric view of the Solar System, they were struck by the regularity or harmony (to use the term employed by Kepler) of this system. The orbits<sup>12</sup> of the first eight planets all lie,

---

International Astronomical Union (IAU) decided to establish a strict definition of what might constitute a planet. The following three criteria were thus laid down:

- It must be in orbit around the Sun.
- It must have almost spherical shape (implying that the body's own gravity has dominated over internal cohesive forces, and one has hydrostatic equilibrium).
- It must have cleared out its own orbit (implying the elimination of any body that might move in the neighbourhood of its orbit).

The Sun is then left with eight planets. Bodies that only satisfy the first two criteria are called dwarf planets. These include Pluto and Ceres.

<sup>10</sup>Including the Moon and Sun in this list, we obtain the seven “planets” giving the days of the week in Roman times: *Saturnus*, *Sol*, *Luna*, *Mars*, *Mercurius*, *Jupiter*, and *Venus*. In the early days of Christianity, the religious authorities were intent on wiping out any reference to Roman or Olympian gods. They thus imposed the *sabbat* on Saturn, while the Lord (*Dominus*) took the place of the Sun, in the Romance languages. But for the other days, they only succeeded in Portuguese and Greek (where Monday is the second day, and so on). In the Germanic languages, the original Roman system remains intact, sometimes fully visible, as in Sunday or Monday, sometimes less obvious, e.g., Friday refers to Fregga, which has the same root as friend and, like Venus, was the goddess of love.

<sup>11</sup>The planet with the shortest period is associated with Mercury (Hermes in Greek): always in motion, appearing and disappearing in quick leaps and bounds during the seasons, it is indeed well represented by the messenger of the gods. The next, the brightest and most beautiful, is Venus (Aphrodite), goddess of love. Then, red as blood, her belligerent companion Mars (Ares), god of war, followed by Jupiter (Zeus), the master of Olympus, plenitude incarnated by a planet, benevolence in person. Beyond him, with his characteristic slow gait and pale countenance, Saturn, father of Jupiter. The old man recalls the idea of time through a Greek play on words between his name (*Kronos*, ὁ Κρόνος, οὐ, from the verb *κράνω*, “to accomplish, to achieve,” with Indo-European root \**kra*, like the Latin *creare*, “to create,” from whence came Ceres, the Roman goddess of growth and the word “cereal,” etc.) and the word for time (*chronos*, ὁ χρόνος, οὐ).

<sup>12</sup>As an example of the kind of regularity they sought, one should mention Bode's law, also called the Titius–Bode law. This was an empirical relation, discovered in 1766 by the German astronomer J.D. Tietz (whose name is Latinised to Titius), then formulated and established as a law by his colleague Bode in 1778. It can be formulated as follows. Let  $a_S$  be the semi-major axis of the planet's orbit, expressed in astronomical units. The relation gives  $a_S$  for the six planets known at the time:

$$a_S = 0.4 + 0.3 \times 2^n ,$$



to within a few degrees, in the same plane, known as the ecliptic. The motion, along almost circular orbits, is always in the same direction, i.e., anticlockwise as viewed from above the north pole of the Sun. In most cases, the planets also rotate in this direction about their own axes, and their natural satellites orbit them in this direction too. Moreover, the fact that this direction is also the direction of rotation of the Sun itself has long suggested that there is a connection with the formation of the Solar System, as proposed in Laplace's theory in *Exposition du système du monde*, in 1796.

### Atmosphere of the Telluric Bodies

Apart from the Earth, two of the telluric planets have an atmosphere:

- Venus with its gases heated to high temperatures by the greenhouse effect [average pressure and temperature at ground level: 90 bar, 750 K; composition: carbon dioxide gas  $\text{CO}_2$  (96 %), nitrogen  $\text{N}_2$  (3 %)].
- Mars with its rarefied gases [average pressure and temperature at ground level: less than  $10^{-2}$  bar, about 250 K; composition: carbon dioxide gas  $\text{CO}_2$  (95 %), nitrogen  $\text{N}_2$  (3 %)].

Two natural satellites of other planets also carry an atmosphere:

- Titan, the largest natural satellite of Saturn [average pressure and temperature at ground level: 1.5 bar, 90 K; composition: nitrogen  $\text{N}_2$  (98 %), methane  $\text{CH}_4$  (2 %)].
- Triton, the largest natural satellite of Neptune [average pressure and temperature at ground level: around  $10^{-5}$  bar (1.5 Pa), 40 K; composition: nitrogen  $\text{N}_2$  (99 %)].

An atmosphere was detected around Pluto by stellar occultation in 1985 [average pressure and temperature at ground level: a few  $\mu\text{bar}$  ( $\approx 0.5$  Pa), 43 K; composition: nitrogen  $\text{N}_2$  (99 %)].

---

where  $n = -\infty$  for Mercury,  $n = 0$  for Venus,  $n = 1$  for the Earth,  $n = 2$  for Mars,  $n = 4$  for Jupiter, and  $n = 5$  for Saturn. These values can be compared with the values of  $a_S$  in Table 16.2. It appears that the result is not so bad. However, we do not have here the accuracy of measurement that forms the basis for astronomy! This law, which is not strictly a law in the scientific sense of the term, has raised much controversy. Is it purely fortuitous? Does it reflect the action of physical forces during the formation of the Solar System? Does it reveal the action of some gravitational phenomenon after the formation of the planets? Today, astronomers have a preference for the first of these three hypotheses, but one cannot deny at least one point in favour of this "law": it has played an important role in the historical development of astronomy. It was while looking for the planet  $n = 6$ , shortly after the formulation by Bode, that Herschel found Uranus. Then, assuming that the body perturbing Uranus was in the orbit  $n = 7$ , Le Verrier was able to calculate the position of Neptune. His own account shows this beyond doubt, and Adams had used the same arguments. The most surprising thing is that the least good agreement between the "law" and measurement is precisely for the case of Neptune! Many astronomers had sought to fill the space at  $n = 3$ , until Piazzi discovered a first asteroid in the space between Mars and Jupiter.

## 16.1.2 Space Exploration of the Planets

One of the main motivations for space exploration today is the desire to find traces of life, something usually associated with the presence of water in the liquid state. This explains in part projects to investigate Mars, or indeed, Europa, a Galilean moon of Jupiter, discussed further below. Another motivation is sometimes the study of the atmosphere in the case of both telluric and giant planets.

At the beginning of space exploration beyond the confines of the Earth, the aims were different: there was thirst for knowledge about the various bodies making up the Solar System, driven by the quest for technological and ideological ascension by the two superpowers of the day, as will be seen from the brief chronology below. The main dates for this exploration are summarised in Table 16.1. We indicate the year marking the beginning of the various types of mission.

### The Moon and Nearby Planets

In 1959, the probe Luna-1 achieved the first lunar flyby in January, Luna-2 landed on the Moon in September, and Luna-3 sent the first photos of the dark side of the Moon back to the USSR from its October flyby (see Fig. 16.31). In 1966, Luna-9 made the first soft landing in January, and Luna-10 was the first lunar satellite in March. The United States had their revenge with the astronauts of Apollo 11 on 20 July 1969 (see Fig. 16.32).

After the Moon, the next target was Venus: for the United States, successful flybys were operated by Mariner-2 in December 1962, Mariner-5 in November 1967, and the two probes Pioneer Venus-1 (or Pioneer Venus Orbiter, or Pioneer-12) and Pioneer Venus-2 (or Pioneer Venus Probe Bus, or Pioneer-13) in December 1978; for the USSR, missions were carried out successfully by Venera-4 in October 1967, and Venera-5 and -6 in May 1969 with atmospheric capsules, while the first soft landing was made by Venera-7 on 15 December 1970, followed by other successful missions Venera-8 to -16, in perfect contrast to their Mars programme! Finally, the Soviets produced Vega-1 and -2 in June 1985, releasing balloons and a landing module. As the atmosphere of Venus is very opaque, it was mapped by radar, from 1990 to 1994, by the American probe Magellan, launched on 4 May 1989 by the shuttle Atlantis (STS-30) and placed in orbit around the planet on 10 August 1990. Before it, three probes had carried out measurements in orbit: Pioneer Venus-1 from 1979 to 1992 and Venera-15 and -16 from 1983 to 1986.

The probe Mariner-10 accomplished the first mission to two planets: launched on 3 November 1973, it flew by Venus on 5 February 1974, then proceeded to three encounters with Mercury,<sup>13</sup> on 29 March 1974, 21 September

---

<sup>13</sup>The overpasses were separated by 176 days. The probe had been placed in an eccentric heliocentric orbit with exactly twice the period  $T_1$  of Mercury ( $T = 88$  day). In this case, the synodic period is  $T' = 2T = T_1 = 176$  day (see Sect. 16.4.1).

Object	Observation	Flyby	Landing	Orbit	Sample	$n$
Moon	$\mathcal{A}$	1959	1959	1966	1969	64
Mercury	$\mathcal{A}$	1974		2011		2
Venus	$\mathcal{A}$	1962	1966	1975		24
Earth	–	1957	1961	1957	–	$N$
Mars	$\mathcal{A}$	1965	1971	1971	(202x)	32
Jupiter	$\mathcal{A}$	1973		1995		7
Saturn	$\mathcal{A}$	1973		2004		4
Uranus	1781	1986				1
Neptune	1842	1989				1
Asteroids	1801	1991	2000	2000	2010	9
Pluto	1930	2015				1
Comets	$\mathcal{A}$	1985	(2014)	(2014)	2006	14

TABLE 16.1 : *Exploration of the Solar System. Dates (Gregorian year or  $\mathcal{A}$ , since ancient times) marking the beginning of the following events: observation from Earth, flyby of celestial body, landing on object, orbit around object, and sample return. Dates in brackets refer to the year when projects should be achieved, with  $x$  representing a number between 0 and 9. The number  $n$  is the number of missions, successful or otherwise, launched prior to 2012. Note that a mission may fly by several bodies, e.g., Galileo counts for Jupiter, asteroid, and comet. For the Earth,  $N$  represents thousands of missions.*

1974, and 16 March 1975. The Venus flyby was the first use of a gravity-assist maneuver.<sup>14</sup>

<sup>14</sup>To model the trajectory of a probe from the Earth to Venus, for example, we use the idea of patched conics. As long as the probe is in the sphere of influence of the Earth or of Venus, its motion is described by a conic section with the relevant planet at the focus (in motion relative to the Sun). Between the two, the motion is heliocentric, described by a conic section whose focus (the Sun) is fixed. The three conics are then patched together. However, to go from the Earth to a non-neighbouring planet (other than Venus or Mars), one can fly close by some intermediate planet. To model the trajectory from the Earth to Mercury under these conditions, one must patch together five conic sections. The third corresponds to a flight close by Venus (generally a branch of a hyperbola). The velocity relative to Venus has the same magnitude when it enters and when it leaves the sphere of influence, but the direction is significantly changed. This is called gravitational deflection. In this way the vectorial velocity relative to the Sun can be greatly modified without energy expenditure. To reach Mercury, the speed must be reduced. To reach Jupiter or the more remote planets, the speed is increased. This kind of maneuver is called a gravitational slingshot. It is used quite systematically for long-distance journeys. The probe Ulysses, launched on 6 October 1990 to study the Sun, thereby reached a speed of 125 km/s (or 450,000 km/h). Using a Jupiter swing-by, it left the plane of the ecliptic to overfly the south pole of the Sun in 1994, then the north pole in 1995. Further examples are given below for the Galileo and Cassini probes.

## Asteroid Belt

After Mars, discussed in the last chapter, we come to the asteroid belt. On its way to Jupiter, the Galileo probe made the first flybys as it crossed the Main Belt: 951-Gaspra and 243-Ida (measuring  $R \sim 20$  km). A natural satellite of 243-Ida was even found, and given the name Dactyl. It is almost spherical, with  $R \approx 0.7$  km. The Near Earth Asteroid Rendezvous (NEAR) mission, launched on 17 February 1996, observed 253-Mathilde on 27 June 1997, before flirting with Eros on St Valentine's day 2000. We shall investigate its orbit shortly. Likewise, we shall return to the various orbits of Dawn, a NASA probe launched in 2007 to visit 4-Vesta and 1-Ceres, the brightest and the biggest of the asteroids, respectively, from 2011.

The Japanese probe<sup>15</sup> Muses-C, renamed Hayabusa (“falcon”), launched in 2003 in the direction of 25143-Itokawa, succeeded in returning some dust samples from the asteroid to Earth,<sup>16</sup> overcoming a string of incidents on the way.

## Giant Planets

**Jupiter.** Jupiter was first overflown on 1 December 1973 by Pioneer-10, launched on 3 March 1972, then on 1 December 1974 by Pioneer-11, launched on 6 April 1973. The latter went on to visit Saturn, flying past on 1 September 1979.

It was the Voyager probes, making full use of the gravity-assist technique, that finally revolutionised our knowledge of the outer planets. NASA took advantage of an exceptional alignment of the planets from Jupiter to Neptune at the beginning of the 1980s to accomplish with these two probes what became known as the Grand Tour. Such a favourable configuration only occurs about once every 180 years.

Voyager-1, launched on 5 September 1977, flew past Jupiter on 5 March 1979 and Saturn on 12 November 1980, before making a closer investigation of Titan. Voyager-2 was the subject of a remarkable round of gravitational billiards: launched on 20 August 1977, it overflew Jupiter on 9 July 1979, Saturn on 26 August 1981, Uranus on 24 January 1986, and Neptune on 24 August 1989, sending back many photos of great quality. These four probes, Pioneer-10 and -11, Voyager-1 and 2, are currently on their way out of the Solar System.

---

<sup>15</sup>Launched on 9 May 2003, the probe arrived in the vicinity of Itokawa on 12 September 2005 and flew close to the asteroid for some 2 years, coming near enough to take samples. On 18 October 2007, it left for the Earth, arriving on 13 June 2010. Before burning up in the atmosphere, the probe released a capsule which was recovered in the Australian desert. On 16 November 2010, the Japanese space agency JAXA announced that the samples they obtained were of extra-terrestrial origin.

<sup>16</sup>Itokawa is an asteroid belonging to the Apollo family, which crosses the orbit of Mars. It was discovered by Linear on 26 September 1998. It looks like a bent cylinder with diameter 200 m and length 500 m.

The probe Galileo, launched<sup>17</sup> in 1989, was placed in orbit around Jupiter in December 1995 to study the giant planet and its four large Galilean moons.<sup>18</sup> Although originally programmed to last 2 years, the mission of the Galileo orbiter actually went on for 8 years. The mission discovered the winds and storms on Jupiter, volcanic activity on Io, possible oceans under the surfaces of Europa and Callisto, and the magnetic field of Ganymede. When the fuel reserves (hydrazine) had almost run out, the probe was sent into Jupiter to remove all risk of collision with Europa, which might have contaminated it with elements of terrestrial life. On the way from the Earth to Jupiter, Galileo photographed several asteroids. And on the way from the Earth to Pluto, the probe New Horizons, discussed below, tested its instruments by photographing Jupiter and its moons (see Fig. 16.1).

**Saturn.** The US probe Cassini<sup>19</sup> was launched on 15 October 1997 to study the Saturn system. Using four gravity-assist maneuvers,<sup>20</sup> it went into orbit around Saturn on 1 July 2004. On 25 December 2004, the European module Huygens<sup>21</sup> separated from Cassini, and 3 weeks later, on 14 January 2005, made a spectacular descent on Titan with the help of a parachute. Originally,

---

<sup>17</sup>The VEEGA trajectory is a Venus–Earth–Earth gravity assist. We give the date (year month day) for each planet overflown: launch 1989 10 18, by the Atlantis shuttle STS-34. Venus flyby: 1990 02 10. Earth flyby 1: 1990 12 08. Earth flyby 2: 1992 12 08. Jupiter Orbit Insertion (JOI): 1995 12 07.

<sup>18</sup>These four natural satellites were discovered in 1610 by Galileo, an event which had important scientific and philosophical consequences. He first gave them the Latin name *Medicea sidera*, which can be translated as “Medician stars,” in homage to the Medici family, the Grand Dukes of Tuscany. Already a leader in many fields, Galileo was also skilled in the exercise of getting himself sponsorship! However, the appellation was eventually dropped. The four moons were named later by other astronomers, after the four beautiful conquests of Zeus, Io, Europa, Ganymede, and Callisto. But spot the boy! Note: solution below.

<sup>19</sup>It was named after Giovanni Domenico Cassini (see the note on Cassini I), who discovered the four natural satellites of Saturn between 1671 and 1684, and the separation between rings A and B, which is known as the Cassini division. Concerning the rings, Galileo had observed in 1610 that Saturn appeared to have two “ears,” which he considered to be moons. However, a few years later, they were no longer visible to him. Huygens realised that they were looking at a ring, which was visible at various inclinations. But it was Cassini who first saw two concentric rings A and B. Other rings were subsequently discovered, and they are currently labelled with letters up to G. Cassini put forward the hypothesis, since confirmed, that the rings were made up of a multitude of small bodies gravitating on very close orbits.

<sup>20</sup>The VVEJGA trajectory is a Venus–Venus–Earth–Jupiter gravity assist. For each planet overflown, we give the date (year month day) and the speeds in km/s in the form [before, after]. Speeds are given in a heliocentric frame: Launch: 1997 10 15. Venus flyby: 1998 04 26 [37.2, 40.9]. Venus flyby: 1999 06 24 [39.2, 42.3]. Earth flyby: 1999 08 18 [35.0, 39.1]. Jupiter flyby: 2000 12 30 [11.6, 13.7]. Saturn orbit insertion (SOI): 2004 07 01.

<sup>21</sup>*Christiaan Huygens* (1629–1695) was a Dutch physicist, mathematician, and astronomer. In addition to his great treatises on probability, dynamics (definition of the centrifugal force), mechanics, e.g., *Horologium oscillatorium* (1673), optics, e.g., *Treatise on Light* (1690), he also wrote fundamental works on astronomy. By eliminating chromatic aberration, he improved the refracting telescope (Huygen’s eyepiece), and with this enhancement, made fundamental discoveries in astronomy. For example, he discovered Saturn’s moon Titan and the rings, as well as the rotation of Mars.

Cassini's mission was to consist in 74 revolutions around Saturn over 4 years, with 52 close encounters with the various moons of Saturn and 45 Titan flybys (see Fig. 16.2). Given the success of this mission, NASA has extended it until 2017. See the mission programme in Fig. 16.25 (upper).

### Trans-Neptunian Objects and Comets

The US probe New Horizons was launched in January 2006 to explore Pluto and the Kuiper Belt,<sup>22</sup> aiming to fly past Pluto in July 2015.

Halley's comet, the most famous of all comets, was approached by six probes in March 1986: ISEE-3 renamed ICE for this mission, Vega-1 and -2 (Soviet probes, *Ve* for *Venera*, *Ga* for *Galleia*, "Venus" and "Halley" in Russian), Giotto (a European probe<sup>23</sup> which flew by at just 600 km from the cometary nucleus), and Sakigake and Suisei (Japanese probes, whose names mean "scout" and "comet" in Japanese) (Fig. 16.3).

The Comet Nucleus Tour (CONTOUR) probe, launched on 3 July 2002, ceased to function shortly afterwards. It was to investigate short-period comets like P/Encke, whose orbit never goes beyond the orbit of Jupiter.

Rosetta<sup>24</sup> is an ESA Cornerstone Mission. The probe was launched on 2 March 2004 and must follow a complex route,<sup>25</sup> going into orbit around the comet<sup>26</sup> 67P/Churyumov–Gerasimenko in May 2014. In November 2014, the Philae module should softland on the cometary nucleus and travel with it until it reaches its perihelion in December 2015.

---

Invited to France by Colbert in 1665, he was one of the founders of the French Academy of Sciences. However, after 20 years in Paris, he returned to the Hague, sickened by the intolerance shown by Catholics toward Protestants. He himself had a "mechanistic" view of the Universe, rejecting the existence of gods and the supposed immortality of the soul: "I believe that two plus two makes four."

<sup>22</sup>So as not to spend too long over its tremendous journey, the probe was given a very fast send-off. Just 9 h after launch on 19 January 2006, it was already in orbit around the Moon. It flew past Jupiter on 28 February 2007, only a little more than a year after its departure. This was a Jovian gravity-assist (JGA) trajectory. It should encounter Pluto on 14 July 2015, at 11:47 UT, flying at an altitude of 13,695 km, and with a speed of 13.78 km/s, then Charon at 12:01 UT. Subsequently, New Horizons will explore at least one planetoid in the Kuiper Belt. This mission replaces the Pluto–Kuiper Express, abandoned in 2000.

<sup>23</sup>In his painting *The Adoration of the Magi*, of 1304, the Italian artist Giotto represented a huge comet. This might well be Halley's comet, which went by in 1301.

<sup>24</sup>The Rosetta stone carries an inscription in three languages, used by Champollion to decipher the hieroglyphs of ancient Egypt in 1822. Rosetta is the English name of a village in the Nile Delta with the Arab name *Rachid*. This was where the stone was found. The ESA chose this name for its Cornerstone Mission because it hopes the results of this mission will enlighten us about the formation of the Solar System.

<sup>25</sup>There have been several gravity-assist maneuvers: Earth (March 2005), Mars (March 2007), Earth (November 2007), and Earth (November 2009).

<sup>26</sup>The launch was initially planned for January 2003, so that Rosetta could meet up with comet 46P/Wirtanen 10 years later.

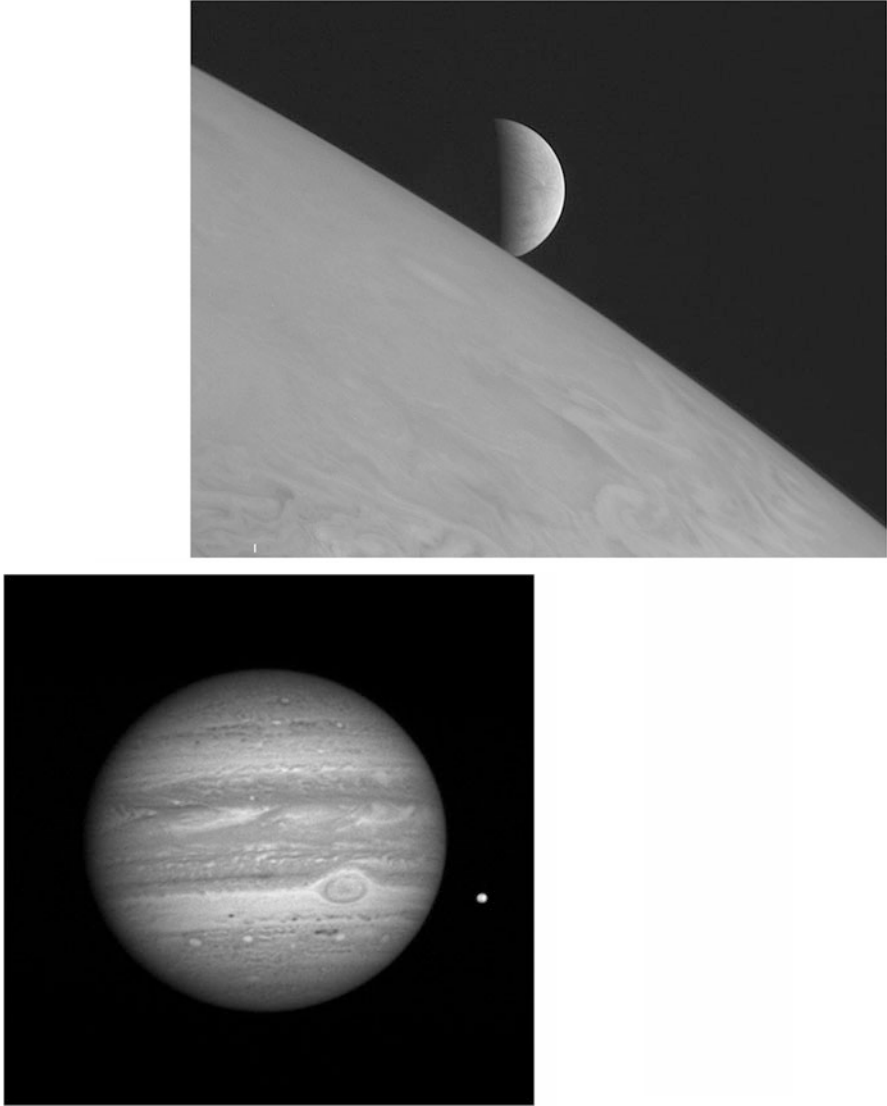


FIG. 16.1 : Images acquired by the probe *New Horizons* on the way to *Pluto*. Upper: *Europa* appears just above *Jupiter*. The image is centered on the point of *Europa* with geographic coordinates  $5^{\circ} S$ ,  $6^{\circ} W$  and has been turned upside-down so that south is at the top. Instrument *LORRI*. Image taken at a distance of 3 million km from *Europa* and 2.3 million km from *Jupiter*, on 28 February 2007, 11:48 UT, at the time of closest approach to *Jupiter*. Lower: *Jupiter*'s Great Red Spot is visible, discovered by *Galileo*. The moon next to the giant planet is *Io*. Image taken at a distance of 81 million km on 8 January 2007. Credit: NASA, Johns Hopkins University/Applied Physics Laboratory, Southwest Research Institute.

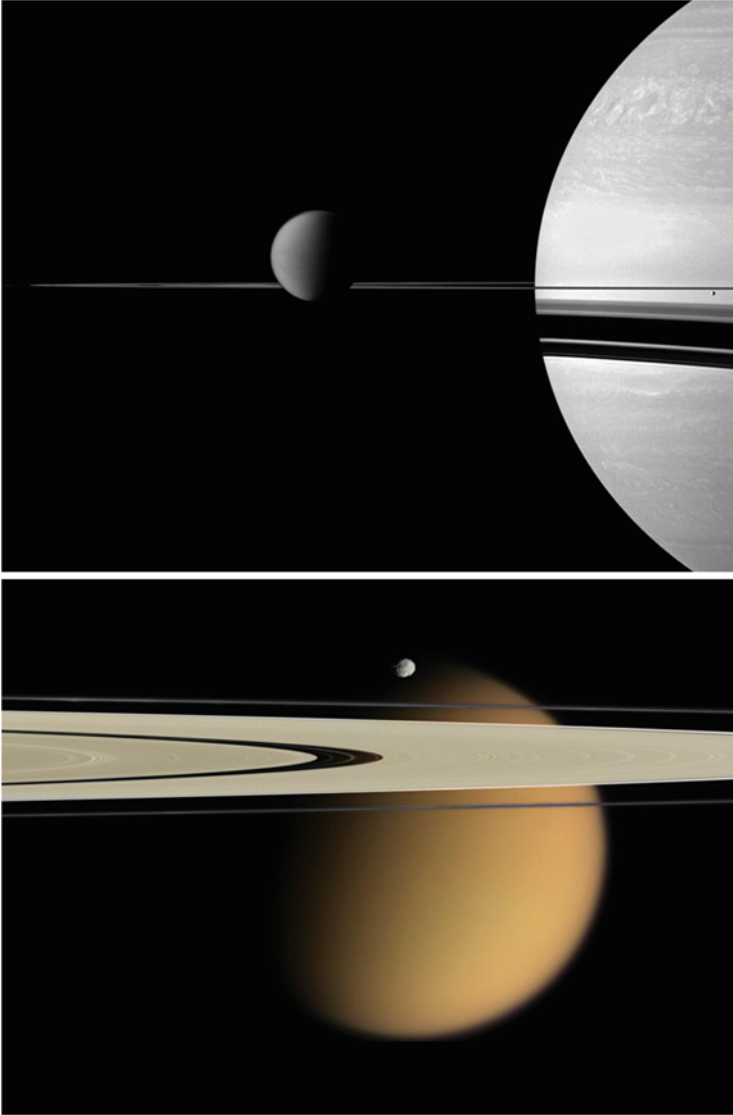


FIG. 16.2 : Images acquired by the Cassini probe. Upper: The probe is in the equatorial plane of Saturn. Titan sits in the middle of the image. The rings have a thickness of around 1 km and their shadow is projected with differing degrees of darkness on Saturn's globe. On the right, just below the rings, one can make out a small point. This is Enceladus. January 2011. Lower: View of Saturn's rings A and F, together with the moon Epimetheus. In the background, Titan is shrouded in its atmosphere. Approximate distance 667,000 km from Epimetheus (4 km/pixel), 1,800,000 km from Titan (11 km/pixel). 28 April 2006. Credit: Cassini Imaging Team, SSI, JPL, ESA, NASA.



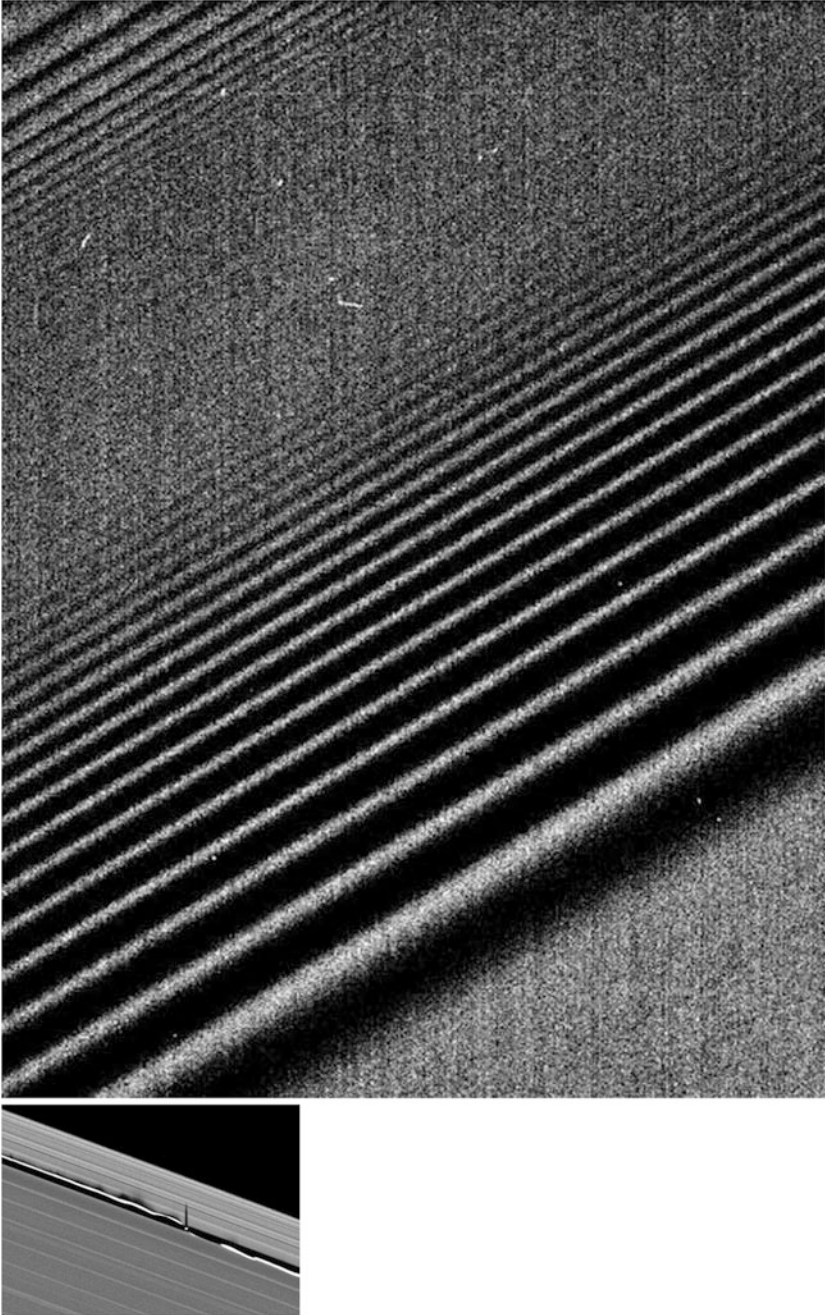


FIG. 16.3 : *These density waves are caused by the presence of small moons close to the rings. Image taken at the end of June 2004 by the Cassini probe. The whole scene pictured is about 220 km across. Left: The shepherd moon Daphnis in the Keeler division (ring A) creates waves that were clearly visible in light at grazing incidence in December 2010. Credit: Cassini Imaging Team, SSI, JPL, ESA, NASA.*

NASA's Stardust and Genesis missions were in situ explorations with sample return.<sup>27</sup>

NASA's Deep Impact mission was launched toward comet 9P/Tempel on 12 January 2005, arriving on 4 July 2005. The probe released an impactor to produce a crater on the comet, causing it to throw out some of its inner material. The impact was observed by the probe itself and by ground-based observatories. Renamed Epoxi, the probe was then redirected to comet 103P/Hartley 2, flying past on 4 November 2010.

## 16.2 Geodetic and Astronomical Quantities for Planets

### 16.2.1 Geodetic and Astronomical Data

Table 16.2a gives the two basic quantities associated with each planet, its constant of central attraction  $\mu$  and its equatorial radius  $R$ , which allow one to calculate the following quantities:

- The acceleration due to gravity  $g_0$  on the surface of the planet, from (6.6).
- The escape velocity  $V_e$ , from (4.34).
- The period  $T_{0(h=0)}$  of a satellite in circular Keplerian orbit at zero altitude, from (5.6), to which we shall return shortly.
- The density  $d$ , that is, the mass per unit volume of the body relative to that of water ( $\rho_{\text{water}} = 10^3 \text{ kg m}^{-3}$ , density  $d_{\text{water}} = 1$ ).

Table 16.2b gives basic astronomical quantities concerning the orbit of the planet around the Sun, including the semi-major axis  $a_S$  and the sidereal period  $N_{\text{sid}}$ .

Ignoring perturbations, Kepler's third law takes the very simple form

$$[N_{\text{sid}} (\text{yr})]^2 = [a_S (\text{a.u.})]^3, \quad (16.1)$$

with the chosen units.

---

<sup>27</sup>Stardust was launched on 7 February 1999 and collected interstellar dust in 2002, then particles from comet Wild-2 on 2 January 2004, before returning a capsule to the Utah desert on 15 January 2006. Its heliocentric orbit took it out beyond the orbit of Mars. Genesis collected particles from the solar wind. This probe was launched on 8 August 2001, with Lissajous orbit insertion (LOI) on 16 November 2001, remaining for more than 2 years at the Lagrange point  $L_1$  (halo orbit). From 3 December 2001 to 1 April 2004, it exposed its collectors to the solar wind to pick up particles from the Sun. It then started back to Earth by means of an astonishing loop-the-loop orbit, arriving as planned above the Utah desert on 10 September 2004. Everything worked exactly as planned until a few seconds before landing: the parachutes were installed upside-down and the capsule crashed into the sand. However, part of its sample was recovered without contamination. Its highly original orbit is described in Chap. 6 in the discussion of Lagrange points (see Table 6.9).

We have also calculated the radius  $\rho_\Sigma$  of the sphere of influence and indicated the characteristics of the planetary orbit, i.e.,  $e$ ,  $i$ , and  $\varepsilon$ , quantities which are not directly necessary in this study, but which allow one to compare the orbits of different planets. For example, we see that the orbit of Pluto is highly eccentric and that the rotation of Venus is retrograde ( $\varepsilon > 90^\circ$ ), etc.

To study the true motion and characterise special orbits, we use the geodetic and astronomical quantities given in Table 16.2c and d. The masses of the planets are usually expressed by the ratio of the mass of the Sun to the mass of the planet (see Table 16.3).

### Different Radii of the Ellipsoid for the Giant Planets

For each giant planet, the ranges of variation from the equator to the pole, for the different radii of the ellipsoid, are given in Table 16.4. Figure 16.4 shows the radii of the ellipsoid at different latitudes, for Jupiter and Saturn, as we did for the Earth ellipsoid in Chap. 2 (see Fig. 2.3) and the Mars ellipsoid in Chap. 15 (see Fig. 15.4).

### 16.2.2 Satellite in Keplerian Orbit

As already discussed, when a satellite is in orbit (semi-major axis  $a$ ) around a planet, the period  $T_0$  of its Keplerian motion is given by (5.5). We can also calculate the period  $T_{0(h=0)}$  of a fictitious satellite at zero altitude. Considering the mean mass per unit volume  $\rho$  of the planet, we have  $\mu = \rho_o V G$ , where  $V$  is the volume of the planet, assumed spherical. Using (5.6), we then obtain

$$T_{0(h=0)} = \sqrt{\frac{3\pi}{G}} \frac{1}{\sqrt{\rho_o}} = 3.7584 \times 10^5 \rho_o^{-1/2}. \quad (16.2)$$

This shows that the Keplerian period  $T_{0(h=0)}$  can be expressed solely in terms of the mean density of the attractive body. As the Earth is the densest planet in the Solar System, the period  $T_{0(h=0)}$  is the shortest. Conversely, the longest period is for a satellite orbiting around Saturn.

Using the mean density  $d$  relative to water and expressing the period in minutes, we obtain

$$T_{0(h=0)} \text{ (min)} \approx 198 d^{-1/2}. \quad (16.3)$$

The Keplerian period for a semi-major axis  $a$  can then be written

$$T_0(\eta) \text{ (min)} \approx 198 \sqrt{\frac{\eta^3}{d}}, \quad (16.4)$$

for reduced distance  $\eta = a/R$ . Figure 16.5 graphs the dependence of  $T_0/T_{0(h=0)}$  on  $\eta = a/R$ .

(a)						
Planet	$\mu = GM$ ( $\text{m}^3 \text{s}^{-2}$ )	$R$ (km)	$g_0$ ( $\text{m s}^{-2}$ )	$V_e$ ( $\text{km s}^{-1}$ )	$xT_0(h=0)$ (min)	$d$
Mercury	$2.203208 \times 10^{13}$	2,439.7	3.70	4.25	85 .02	5.44
Venus	$3.248586 \times 10^{14}$	6,051.8	8.87	10.36	86 .50	5.27
Earth	$3.986004 \times 10^{14}$	6,378.1	9.80	11.18	84 .49	5.52
Mars	$4.282837 \times 10^{13}$	3,397.0	3.71	5.02	100 .15	3.94
Jupiter	$1.266865 \times 10^{17}$	71,492.0	24.79	59.53	177 .85	1.34
Saturn	$3.794063 \times 10^{16}$	60,268.0	10.45	35.48	251 .54	0.69
Uranus	$5.794549 \times 10^{15}$	25,559.0	8.87	21.29	177 .76	1.29
Neptune	$6.836540 \times 10^{15}$	24,764.0	11.15	23.50	156 .08	1.64
Pluto	$8.261000 \times 10^{11}$	1,195.0	0.58	1.18	150 .51	1.73
(b)						
Planet	$a_S$ (a.u.)	$N_{\text{sid}}$ (yr)	$e$ n.d.	$i$ (deg)	$\epsilon$ (deg)	$\rho_S/R$ n.d.
Mercury	0.38709831	0.241	0.20563	7.00	2.0	40
Venus	0.72332982	0.615	0.00677	3.39	177.4	89
Earth	1.00000102	1.000	0.01671	0.00	23.4	126
Mars	1.52367934	1.881	0.09341	1.85	25.2	148
Jupiter	5.20260321	11.862	0.04839	1.31	3.1	587
Saturn	9.55490919	29.456	0.05415	2.49	26.7	788
Uranus	19.21844606	84.019	0.04717	0.77	97.9	1,763
Neptune	30.11038687	164.767	0.00859	1.78	28.8	3,045
Pluto	39.54470589	247.689	0.24881	17.14	122.0	2,244
(c)						
Planet	$D_{\text{sid}}$ (h)	$\eta_{\text{GS}}$ n.d.	$a_{\text{GS}}$ (km)	$h_{\text{GS}}$ (km)	Planeto- synchronous	
Mercury	1,407.509400	99.555	242,885	240,446	Impossible	
Venus	5,832.443616	253.900	1,536,551	1,530,499	Impossible	
Earth	23.934471	6.611	42,164	35,786	Achieved	
Mars	24.622962	6.015	20,428	17,031	Planned	
Jupiter	9.924912	2.238	160,009	88,517	Possible	
Saturn	10.656222	1.863	112,271	52,003	Possible	
Uranus	17.240	3.235	82,689	57,130	Possible	
Neptune	16.110	3.372	83,514	58,750	Possible	
Pluto	153.293352	15.515	18,540	17,345	–	

(d)							
Planet	$N_{\text{sid}}$ (day)	$J_2$ ( $10^{-6}$ )	$J_3$ ( $10^{-6}$ )	$J_4$ ( $10^{-6}$ )	$k_h$ n.d.	$\eta_m$ n.d.	Sun-synchronous
Mercury	87.969	60	0	0	0.13	<1	Impossible
Venus	224.701	6	1	0	0.03	<1	Impossible
Earth	365.256	1,083	-3	-2	10.11	1.94	Achieved
Mars	686.980	1,955	31	-15	29.04	2.62	Achieved
Jupiter	4,332.59	14,736	1	-587	775.46	6.69	Polar
Saturn	10,759.2	16,298	0	-915	1,505.78	8.09	Polar
Uranus	30,688.5	3,339	0	-32	1,245.12	7.66	Polar
Neptune	60,182.3	3,410	0	-35	2,840.11	9.70	Polar
Pluto	90,469.7	0	-	-	0.00	-	-

TABLE 16.2 : *The eight planets of the Solar System. The dwarf planet Pluto has been included for comparison. (a) Geodetic characteristics. Geodetic data: planetocentric gravitational attraction  $\mu$ , equatorial radius  $R$  of planet. Derived quantities: central acceleration  $g_0$  at ground level, escape velocity  $V_e$ , period  $T_{0(h=0)}$  of a satellite in Keplerian orbit at ground level, mean density  $d$ . (b) Astronomical characteristics. Data relating to planetary orbit: semi-major axis  $a_S$ , sidereal period of revolution  $N_{\text{sid}}$ , eccentricity  $e$ , inclination  $i$  with respect to the ecliptic. Data relating to rotation of the planet: obliquity  $\varepsilon$ . Sphere of influence  $\rho_\Sigma/R$ . (c) Planetosynchronicity. Astronomical data: period of rotation  $D_{\text{sid}}$ . Derived quantities: reduced distance  $\eta_{\text{GS}}$  for the orbit of a stationary satellite (whence  $a_{\text{GS}}$  and  $h_{\text{GS}}$ ). The distance  $\eta_{\text{GS}}$  should be compared with  $\rho_\Sigma/R$ . (d) Sun-synchronicity. Astronomical data: period of revolution  $N_{\text{sid}}$ . Geodetic data: terms  $J_2$ ,  $J_3$ , and  $J_4$  in the expansion of the gravitational potential (values to be multiplied by  $10^{-6}$ ). Derived quantities: constant of Sun-synchronicity  $k_h$ , maximal value of the reduced distance  $\eta_{\text{HSmax}}$ , denoted here by  $\eta_m$ , for a Sun-synchronous satellite.*

Mercury	6,023,600.
Venus	408,523.71
Earth + Moon	328,900.561400
Mars	3,098,708.
Jupiter	1,047.3486
Saturn	3,497.898
Uranus	22,902.98
Neptune	19,412.24
Pluto	135,200,000.

TABLE 16.3 : *Planetary mass values, expressed in reciprocal solar masses. JPL Development Ephemeris DE 405 (recommended for IERS standards).*

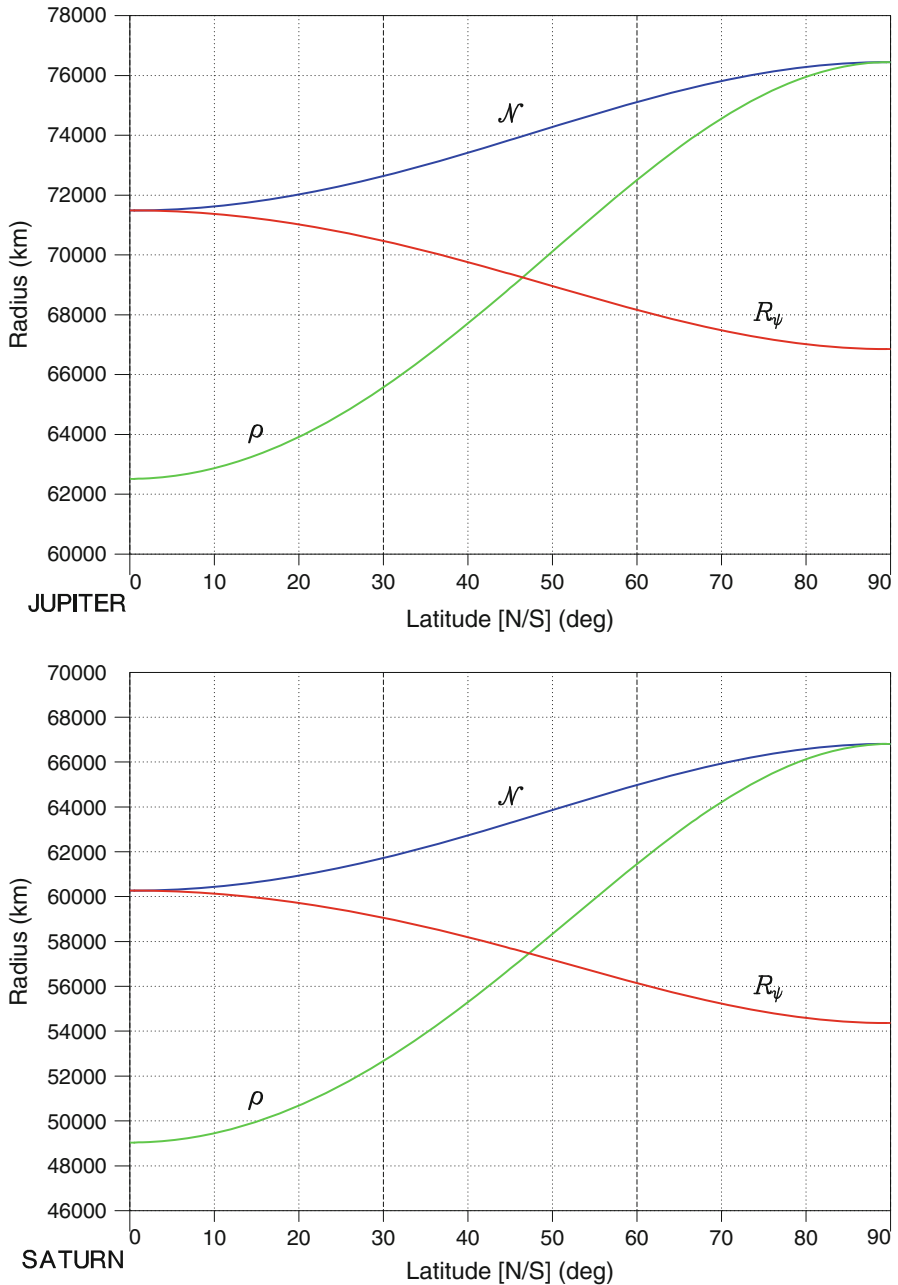


FIG. 16.4 : Different radii of the ellipsoid: radius of curvature  $\rho$  in the meridian plane, the great normal  $\mathcal{N}$ , and the radius of the ellipsoid  $R_\psi$ . Upper: Jupiter. Lower: Saturn.

Quantity		Jupiter	Saturn	Uranus	Neptune
Flattening	$f$	0.06487	0.09796	0.02293	0.01708
Rad. curvature	$\rho(\text{Equ.})$	62,517	49,038	24,400	23,925
–	$\rho(\text{Pole})$	76,452	66,813	26,159	25,194
Great normal	$\mathcal{N}(\text{Equ.})$	71,492	60,268	25,559	24,764
–	$\mathcal{N}(\text{Pole})$	76,452	66,813	26,159	25,194
Rad. ellipsoid	$R_\psi(\text{Equ.})$	71,492	60,268	25,559	24,764
–	$R_\psi(\text{Pole})$	66,854	54,364	24,973	24,341

TABLE 16.4 : Ranges of variation from the equator to the pole for the radii of the ellipsoid, for the giant planets. Radius of curvature  $\rho$  in the meridian plane, great normal  $\mathcal{N}$ , and radius of the ellipsoid  $R_\psi$ . Distances in km.

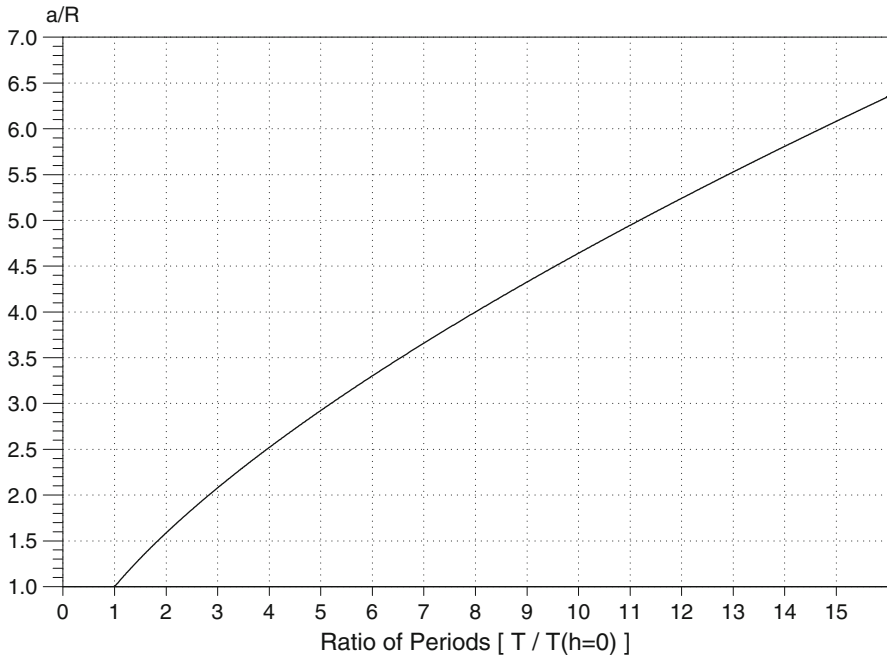


FIG. 16.5 : Keplerian period as a function of altitude. In this graph, the abscissa is the reduced period, i.e., the ratio of the period of the satellite to the period of a satellite at zero altitude, and the ordinate is the reduced distance  $\eta = a/R$ , i.e., the ratio of the semi-major axis of the orbit to the radius of the planet.

### 16.2.3 Geographical Maps

Only the telluric planets can be mapped in the sense that we can produce a geographical map of the surface. The mappable area, calculated on the ellipsoid and expressed in millions of  $\text{km}^2$ , has the following value for each

planet: 75 for Mercury, 460 for Venus, 510 for the Earth (140 for the land masses and 370 for the sea floor), and 143 for Mars. For these four planets, this makes a total of 1,188. We also have 18 for Pluto and 2.6 for the largest of the asteroids (and 0.001125 for 433-Eros). We shall discuss maps of natural satellites shortly.

The geography of Mars (volcanoes, impact basins, etc.) was outlined in the last chapter. We shall not dwell further here on the geography of Venus or the other telluric planets.

In this chapter, we shall use the following maps as background for representing ground tracks or orbits:

- For Venus, the topographical map built up from synthetic aperture radar (SAR) data gathered by Magellan.
- For Eros, the topographical map made from altimetry data gathered by NEAR.

In both cases, contours are plotted at 2 km intervals, with the zero altitude contour in bold face. Those at positive altitudes are represented by continuous curves and those at negative altitudes by dashed curves. For the planets, the zero meridian is chosen arbitrarily (see note on Airy for the Earth and Mars).

## 16.3 Satellite of Planet in Real Orbit

### 16.3.1 Perturbative Accelerations

The sphere of influence discussed in Sect. 6.11 informs us of the distance beyond which one can no longer neglect perturbations due to the Sun. Equation (6.158) gives the values of the radius  $\rho_\Sigma$  for all the planets. The results are displayed in Table 16.2b, where they can usefully be compared with the values in Table 16.2c.

The altitude dependence of the central acceleration and perturbative accelerations has already been plotted for the Earth in Fig. 6.1 and for Mars in Fig. 15.9. To complete the list of telluric planets, we have plotted the same graphs for Mercury and Venus in Fig. 16.6, using the same notation as in Table 6.1 (in which, of course, we replace the terrestrial acceleration by the acceleration due to the relevant planet).

For these two planets, there is no perturbing acceleration due to the terms  $J_n$ ,  $n \geq 3$ , since these terms are almost all zero. The very weak acceleration  $\gamma_{CCN, J_2}$  due to the term in  $J_2$  is soon supplanted (for  $h \sim R$ ) by the perturbing acceleration  $\gamma_{CS}$  due to the solar attraction. For Mercury, the perturbing acceleration  $\gamma_{DP}$  due to solar radiation pressure is still poorly known. For Venus, atmospheric drag causes an acceleration  $\gamma_{DF}$  which can be very large, and depends on the altitude and shape of the satellite. The solar radiation pressure, which leads to the perturbing acceleration denoted by  $\gamma_{DP}$ , impinges



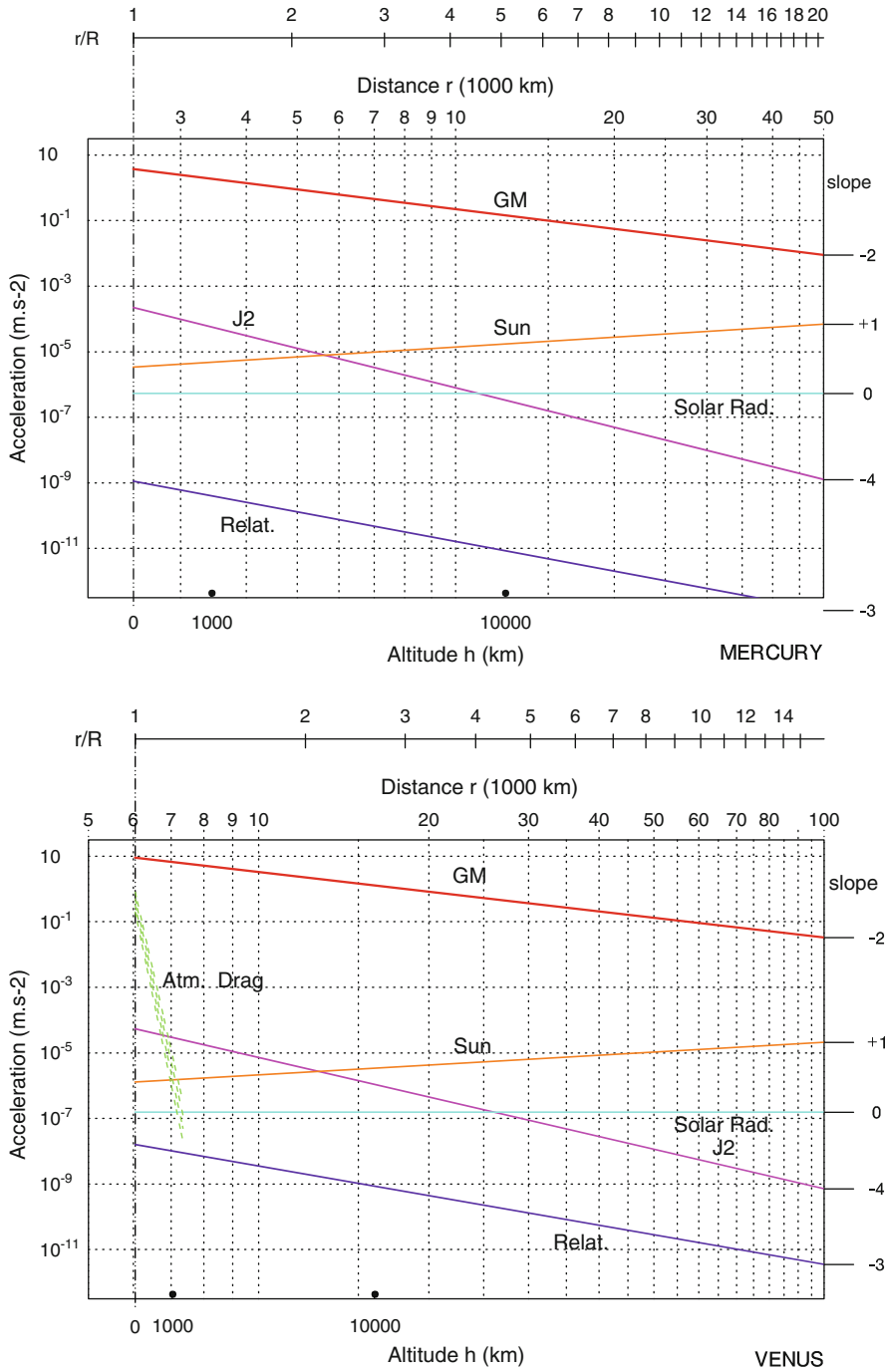


FIG. 16.6 : Accelerations as a function of the distance  $r$  from the satellite to the center of the planet. Log-log scale. Upper: Mercury. Lower: Venus.

on the satellite both directly and indirectly, by the albedo effect, the mean albedo of Venus being very high (0.76).

## 16.3.2 Classification of Satellites

### Rotational Motion of the Planets

The values given in Table 16.2a to d show that the two planets closest to the Sun have very long periods of rotation:  $D_{\text{sid}} = 58.646$  day for Mercury<sup>28</sup> (exactly  $2/3$  of the sidereal period of revolution) and  $D_{\text{sid}} = 243.018$  day for Venus.<sup>29</sup> For these two planets, the day is longer than the year. This is due to the proximity of the Sun.

Moving further out to the Earth and Mars, this period  $D_{\text{sid}}$  is about 1 day, while for the giant planets from Jupiter to Neptune, it is of the order of 10 h.

### Planetosynchronous Satellite

For satellites that are stationary with respect to the planet, we have used (7.69) to calculate the reduced altitude  $\eta_{\text{GS}}$  for a Keplerian orbit in terms of  $D_{\text{sid}}$ . (For the Earth and Mars, the values were calculated for the Keplerian and then the true orbit, in Chaps. 7 and 15.) They are displayed in Table 16.2c.

The results prompt the following remarks:

- For Mercury and Venus, the values of  $\eta_{\text{GS}}$  are so large that this orbit cannot be obtained. The solar perturbative attraction becomes too great for these altitudes, and such an orbit would pass way beyond the sphere of influence of the planet.
- For the Earth and Mars,  $\eta_{\text{GS}}$  is about 6.
- For the giant planets,  $\eta_{\text{GS}}$  is about 2 or 3.

---

<sup>28</sup>According to astronomers, the proximity of the Sun should have led to a 1:1 resonance phenomenon for Mercury, so that it would always present the same face towards the Sun, like the natural satellites and their planets. This was indeed what was thought up until 1965, when radar measurements from the Earth showed that it had a shorter rotation period, of only 59 days. The Italian astrophysicist Giuseppe Colombo showed that this was a very rare case of a 3:2 resonance, i.e., three rotations in two revolutions, due to the high eccentricity of Mercury's orbit.

<sup>29</sup>Venus is the brightest celestial body as seen from Earth, apart from the Sun and the Moon. This is partly because it is surrounded by a very thick layer of cloud. The speed of rotation was only measured in 1962, with the advent of the radar. The clouds have a much faster rotational motion, known as super-rotation. At an altitude of 70 km, the atmosphere makes one round trip in 4 days, corresponding to winds at 100 m/s, in the direction of rotation of the planet.

- For Pluto,<sup>30</sup> the position of the stationary satellite is more complex, but fortunately there is no urgency to carry out such a calculation!

### Sun-Synchronous Satellite

To satisfy the condition (7.95) for a Sun-synchronous orbit, one must have a large  $J_2$  term if the planet is close to the Sun, since its sidereal period of revolution is short. Conversely, a weak  $J_2$  term is required if the planet is remote from the Sun. Now as we have already seen, if the planet is close to the Sun, e.g., Mercury, Venus, its rotation about its own axis is blocked and planetary flattening is very low. This in turn implies that  $J_2$  will be low, or almost zero. We conclude that Sun-synchronicity is impossible.

If a planet is far from the Sun, as in the case of the giant planets, its rapid rotation creates a significant flattening effect and  $J_2$  is consequently large. To counterbalance this effect, the orbit must have a very low value of  $\cos i$ , indeed, practically zero. The orbit is therefore polar, to within a few hundredths of a degree. But we should ask what Sun-synchronicity means for a satellite in orbit around Jupiter, a planet which takes 12 years to go round the Sun, or around Neptune, which takes 165 years!

For the two intermediate planets, the Earth and Mars, this condition can be satisfied. The results for  $k_h$ , the constant of Sun-synchronicity, calculated using (7.98), are given in Table 16.2d, where we have also displayed  $\eta_m$ , the value of the maximal reduced distance  $\eta_{HS \max}$ , obtained for  $i = 180^\circ$ .

### Frozen Orbit

In Chap. 11, we saw that a satellite orbit could be frozen by taking advantage of balancing effects between the various variations in the position of the periastron, i.e., secular and long-period variations. The ratio  $J_3/J_2$  arises when we calculate the frozen eccentricity. For a frozen orbit to be useful, the frozen eccentricity  $e_F$ , which is of the order of  $(1/2)J_3/J_2$ , must be less than 0.01, for beyond this, differences in altitude become too great.

The  $J_3$  term is a zonal term (axial symmetry) expressing the effects of asymmetry between the northern and southern hemispheres. For Mercury and Venus, which are practically spherical,  $J_3$  is zero or very low. For the giant planets,  $J_3$  is zero because the plasticity of these planets only generates even zonal coefficients  $J_{2n}$  (symmetry relative to the equatorial plane, or north-south symmetry).

It follows that the only two planets that can have a satellite in frozen orbit are the Earth and Mars. As regards Sun-synchronous frozen orbits, recall that

---

<sup>30</sup>Pluto is accompanied by Charon, discovered on 2 July 1978 by J.W. Christy. This satellite has such a large relative mass (1/6 of the mass of Pluto) that the Pluto-Charon ensemble can be considered rather as a double planet. The semi-major axis of Charon's circular orbit is  $a_P = 19,460$  km, and it is interesting to note that this value is very close to the value for the planetostationary orbit. We have in fact  $a_P/a_{GS} = 1.05$ .

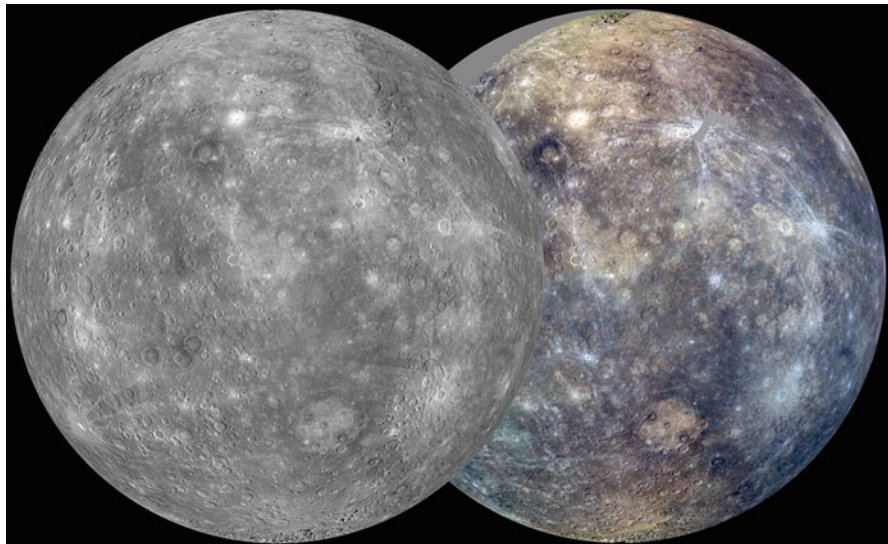


FIG. 16.7 : Map of Mercury obtained by Messenger after 1 day in orbit. On Mercury, a solar day (length of time from noon to noon), or Hermean day, is about 176 Earth days long. And during its first Mercury solar day in orbit, the Messenger spacecraft imaged nearly the entire surface of the planet to generate a global monochrome map at 250 m/pixel resolution and a 1 km/pixel resolution color map. Map centered along the planet's  $75^\circ$  east longitude meridian. Credit (image and caption): NASA, APL/JHU (Johns Hopkins University Applied Physics Laboratory), CIW (Carnegie Institution of Washington).

the argument of the periastron, related to the sign of  $J_3$ , is  $\omega_F = 90^\circ$  for the Earth and  $\omega_F = 270^\circ$  for Mars.

## 16.4 Ground Track for a Satellite of a Planet

The ground track of a satellite over several revolutions is characterised by the equatorial shift, which depends for the main part on the angular speed of rotation of the planet. For the Earth or Mars, the equatorial shift is of the order of  $25^\circ$  for a low-orbiting satellite. For the giant planets, it is two to three times greater. But for Mercury and Venus, which rotate very slowly about their axes, the equatorial shift is very slight.

We shall now discuss in a little more detail the ground tracks of satellites in orbit around Mercury, Venus, and the asteroids Eros, Vesta, and Ceres (Fig. 16.7).

### 16.4.1 Satellites of Mercury

Mercury has only been visited by two probes, Mariner-10 and Messenger. There is also a project called BepiColombo. The abbreviated name of the US Mercury Surface, Space Environment, Geochemistry and Ranging probe, or Messenger, makes reference to the main function of the mythological character Mercury, or Hermes. It was launched in 2004 with no fewer than six gravity-assist maneuvers,<sup>31</sup> and went into a highly eccentric near-polar orbit in 2011. In phase 1, with  $a = 10,136$  km,  $i = 82.5^\circ$ , the periastron was positioned at a latitude of  $60^\circ\text{N}$ , in order to focus attention on the Caloris impact basin. The period was 12 h (see Fig. 16.8 upper). The northernmost point  $\psi = 82.5^\circ$  was overflowed at an altitude between 244 and 640 km. The mission lasted 12 months, i.e., two Mercurian solar days. In phase 2, with  $a = 7,736$  km,  $i = 82.5^\circ$ , the period was reduced to 8 h, and the northernmost point was overflowed at an altitude between 311 and 442 km (see Fig. 16.9).

Note that, for a point on Mercury, the day, i.e., the time elapsed between two noontime passages of the Sun, lasts 176 Earth days. This means that 88 days of night will follow 88 days of daylight. This 176 days corresponds to two revolutions around the Sun. So one Hermean (or Mercurian) day is equal to two Hermean years. This is a consequence of the 3:2 resonance, which means that Mercury does three rotations (relative to an ECI frame, corresponding to 3 Hermean sidereal days) during two revolutions (or 2 Hermean years). Applying (8.44), we obtain the synodic period, which is the Hermean day.

In December 2012, the Messenger team built up the first complete map of Mercury, with a definition of 250 m/pixel. This map, shown in Fig. 16.7, was obtained after one (Hermean) day in orbit.

BepiColombo is a joint mission<sup>32</sup> between Europe and Japan, and should be launched in August 2014 to arrive at its destination in December 2020, after five gravity-assist maneuvers (Earth, Venus twice, and Mercury twice). The probe comprises two orbiters: the Mercury Planetary Orbiter (MPO) run by the ESA and the Mercury Magnetospheric Orbiter (MMO) run by JAXA, both planned to follow highly eccentric polar orbits ( $i = 90^\circ$ ), with perigee at altitude  $h_p = 400$  km. The altitude of the apogee will be  $h_a = 1,500$  km for MPO and  $h_a = 12,000$  km for MMO, so that the period of the latter, viz.,  $T = 560$  min, will be a multiple of the period of the former, viz.,  $T = 140$  min (see Fig. 16.8 lower).

---

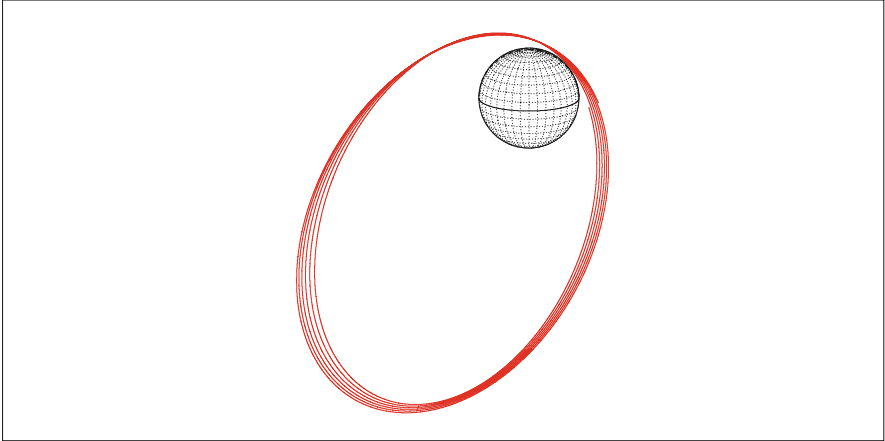
<sup>31</sup>Launched 2004 07 30, Earth flyby (altitude 2,295 km) 2005 07 29, Venus flyby 1 (altitude 3,000 km) 2006 10 23, Venus flyby 2 (altitude 300 km) 2006 10 23, Mercury flyby 1 (altitude 200 km) 2008 01 14, Mercury flyby 2 (altitude 200 km) 2008 10 06, Mercury flyby 3 (altitude 200 km) 2009 09 29, Mercury orbit insertion 2011 03 18.

<sup>32</sup>There were originally two separate projects: the Japanese probe Mercury Orbiter and the European probe BepiColombo Mercury Orbiter, named after the Italian mathematician Giuseppe “Bepi” Colombo (1920–1984), mentioned earlier. The European project included a lander, but this was subsequently deemed too expensive.

### [MERCURY] Messenger [Ph. 1] Orbit - ref.: Mercury

>>>> Time span shown: 4320.0 min = 3.00 days

Equiv. altit. = 7696.5 km      a = 10136.200 km  
 Inclination = 82.50 °      e = 0.729711  
 Period = 719.98 min \* rev/day = 2.00  
 h\_a = 15093 km; h\_p = 300 km; arg.periapsis: +60.87 °

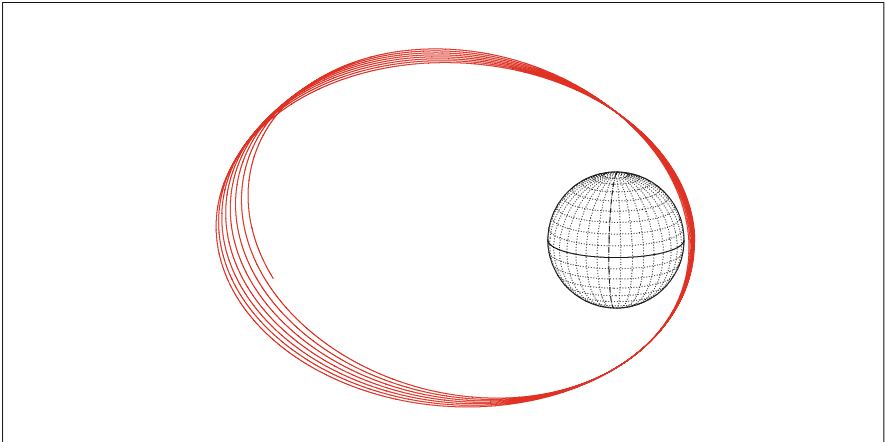


Projection: Orthographic      Project. centre: 15.0 ° N; 90.0 ° E      Longitude / Initialisation:      *Iξων*  
 Property: none      Aspect: Oblique      N.a.: 165.35 ° - Apo.: 0.00 °      MC \* LMD  
 ‡ T.:Azimuthal - Graticule: 10°      {-} [-90.0/ +75.0/ +0.0] [-] IAU91      *Ατλας*

### [MERCURY] MMO BepiColombo Orbit - ref.: Mercury

>>>> Time span shown: 4320.0 min = 3.00 days

Equiv. altit. = 6200.3 km      a = 8640.000 km  
 Inclination = 90.00 °      e = 0.671320  
 Period = 566.61 min \* rev/day = 2.54  
 h\_a = 12001 km; h\_p = 400 km; arg.periapsis: +0.00 °



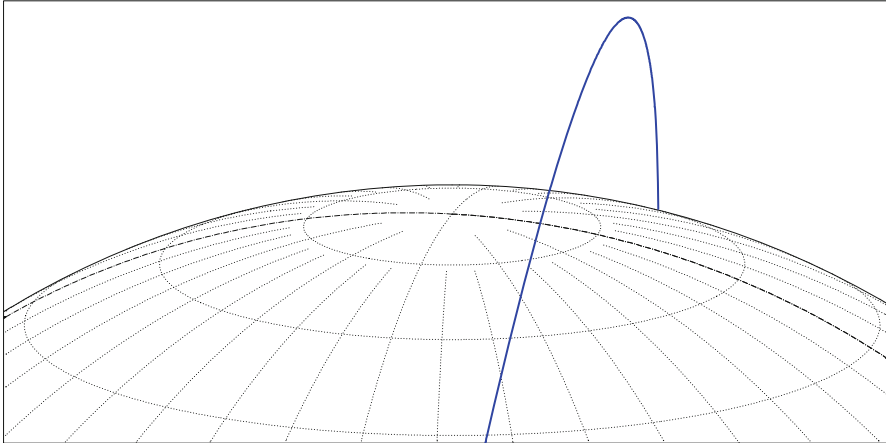
Projection: Orthographic      Project. centre: 15.0 ° N; 6.0 ° E      Longitude / Initialisation:      *Iξων*  
 Property: none      Aspect: Oblique      N.a.: 90.00 ° - Apo.: -91.21 °      MC \* LMD  
 ‡ T.:Azimuthal - Graticule: 10°      {-} [-90.0/ +75.0/ +84.0] [-] IAU91      *Ατλας*

FIG. 16.8 : Orbit of satellite over 3 days, in a frame moving with the planet Mercury. Upper: Messenger [Phase 1]. Lower: BepiColombo MMO.

**[MERCURY] Messenger [Ph. 2]**  
**Orbit - ref.: Mercury**

>>>> Time span shown: 360.0 min = 0.25 day

Equiv. altit. = 5295.9 km      a = 7735.601 km  
 Inclination = 82.50 °      e = 0.635490  
 Period = 480.01 min \* rev/day = 3.00  
 h\_a = 10212 km; h\_p = 380 km; arg.periapsis: +83.37 °



Projection: Orthographic

Property: none

⚡ T.:Azimuthal - Graticule: 10°

PC: 15.0 ° N;102.0 ° E /ZC: 88.0 ° N; 90.0 ° E Longitude / Initialisation:

Aspect: Oblique

⌋ [ -90.0/ +75.0/ -12.0 ] [-] IAU91

N.a.: 96.00 °- Apo.: -34.79 ° MC ★ LMD

Ιξων

Ατλας

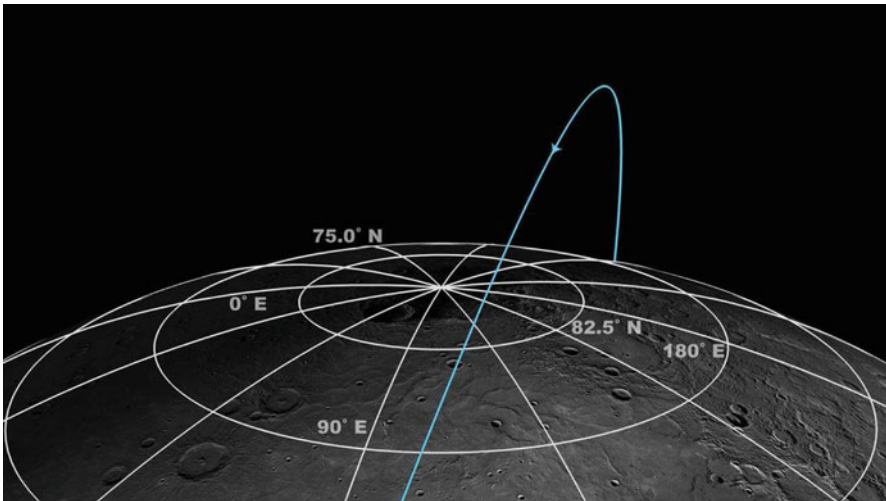


FIG. 16.9 : *Orbit of Messenger (phase 2) in a frame moving with the planet Mercury. Close-up when flying over Mercury's north pole. Upper: Reconstruction of orbital elements using Ixion. Lower: Schematic of Messenger's orbit illustrating some of the challenges to acquiring observations of Mercury's north polar region. Since April 2012, Messenger has been in an 8-h orbit (shown here), and it has been at an altitude between 311 and 442 km at the northernmost point in its trajectory. Credit (image and caption for lower image): NASA, JHU/APL, CIW.*

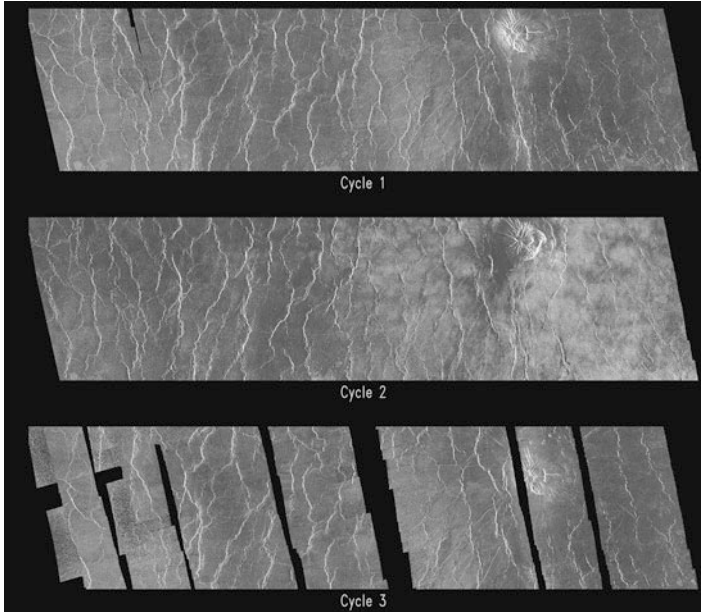


FIG. 16.10 : *Part of Venus (Imdr region) viewed by Magellan's radar during three consecutive cycles (March 1991, November 1991, July 1992). Size: 400 km by 100 km, centered on  $47.5^\circ S$ ,  $226.0^\circ E$ . This set of three Magellan images shows a small volcano. Data quality during portions of cycle 3 was adversely affected by a faulty transmitter aboard the spacecraft, leading to the missing strips in the bottom image. Credit (image and caption): JPL, NASA.*

### 16.4.2 Satellites of Venus

The probe Magellan, named after the sixteenth century Portuguese explorer, was in orbit around Venus from 1990 to 1994. During this time it perfectly accomplished all its missions, the main task being to map the planet (achieved to 98%).

This radar mapping mission consisted of three cycles, each lasting 243 days, during which the Magellan satellite followed an eccentric polar orbit, shown in Fig. 16.14 (upper) with characteristics:

$$\begin{aligned} h_p &= 289.57 \text{ km}, & h_a &= 8,458.5 \text{ km}, & i &= 85.5^\circ, & \omega &= 170^\circ, \\ a &= 10,425.8 \text{ km}, & e &= 0.39176, & T_a &= 195.59 \text{ min} = 3.26 \text{ h}. \end{aligned}$$

The ground track of this orbit has been shown over one revolution in Figs. 16.12 and 16.14. The radar mapping only proceeded for 37.2 min during each revolution, from slightly before to slightly after the passage at perigee.

The length of the cycle of 243 days corresponds to  $D_{\text{sid}}$ , one Venusian sidereal day, the time the planet takes in a Galilean frame to make a complete



round trip relative to the orbit of the satellite, which remains fixed in this frame. Indeed, Venus is almost perfectly spherical ( $J_2 = 4.4098 \times 10^{-6}$ , a very low value) and the orbit of the satellite is near-polar, so precessional motions are almost non-existent. For the orbit defined above, we obtain

$$\dot{\Omega} = -6 \times 10^{-4} \text{ deg/day} , \quad \dot{\omega} = -4 \times 10^{-3} \text{ deg/day} .$$

The three images of the same region shown in Fig. 16.10 were acquired at 8 month intervals, corresponding to the length of the cycle (one Venusian sidereal day), in March 1991, November 1991, and July 1992.

Following the mapping cycles, the satellite was placed in a circular orbit by aerobraking, with  $h = 250$  km, to carry out geodetic studies. It was then sacrificed in a final experiment, known as the windmill experiment. For one and a half months, the solar panels were deployed to transform the satellite into a sort of windmill, transmitting back the parameters of the atmosphere which finally consumed it.

Magellan produced a very accurate map of the planet (see Figs. 16.13 and 16.11). The gravitational potential model of degree and order 21, known as the JPL Venus Gravity Model (JPL-VGM1B), obtained using Doppler radio tracking data from Pioneer Venus Orbiter, has evolved to degree and order 90 thanks to data gathered by Magellan, to give the model MGNP90 (Magellan + PVO, 90th degree and order) (Figs. 16.12, 16.13, and 16.14).<sup>33</sup>

The European probe Venus Express, carrying the same type of instruments as Mars Express, was launched on 9 November 2005. After a 153 day direct trip, it arrived on 11 April 2006 and went into its operational orbit on 18 May of the same year. Venus Express is in a highly eccentric polar orbit, with  $a = 39,176$  km,  $e = 0.839$  ( $h_p = 250$  km,  $h_a = 66,000$  km,  $T = 1,425$  min), and periastron at latitude  $70^\circ\text{N}$  (see Fig. 16.15 upper). This orbit, almost fixed relative to the planet (as happens for all Venusian satellites), will study the atmosphere, which for its part makes a round trip of the planet every 4 days.

The Japanese probe Planet-C (Venus Climate Orbiter or VCO), renamed Akatsuki (“dawn”), was launched on 21 May 2010. An engine problem as it approached Venus on 7 December 2010 prevented it from entering the correct orbit. The Japanese space agency JAXA hold out a slim hope of correcting the error. The planned orbit was highly eccentric and almost equatorial:

$$a = 45,500 \text{ km} , \quad e = 0.8604 , \quad i = 172^\circ ,$$

whence  $h_p = 300$  km and  $h_a = 78,600$  km (see Fig. 16.15 lower).

---

<sup>33</sup>Planetocentric gravitational constant  $\mu$ , in  $\text{km}^3 \text{s}^{-2}$ :  
 $\mu = 324,858.60 \pm 0.05$  for JPL-VGM1B (1990) ,  
 $\mu = 324,858.601 \pm 0.014$  for MGNP90 (1997) .

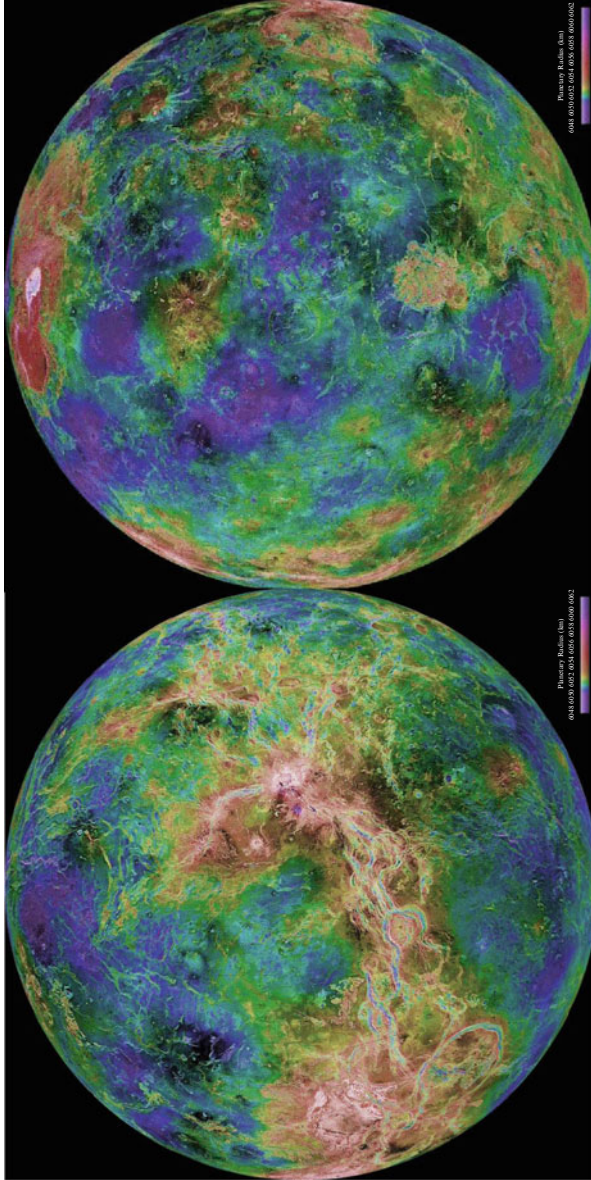
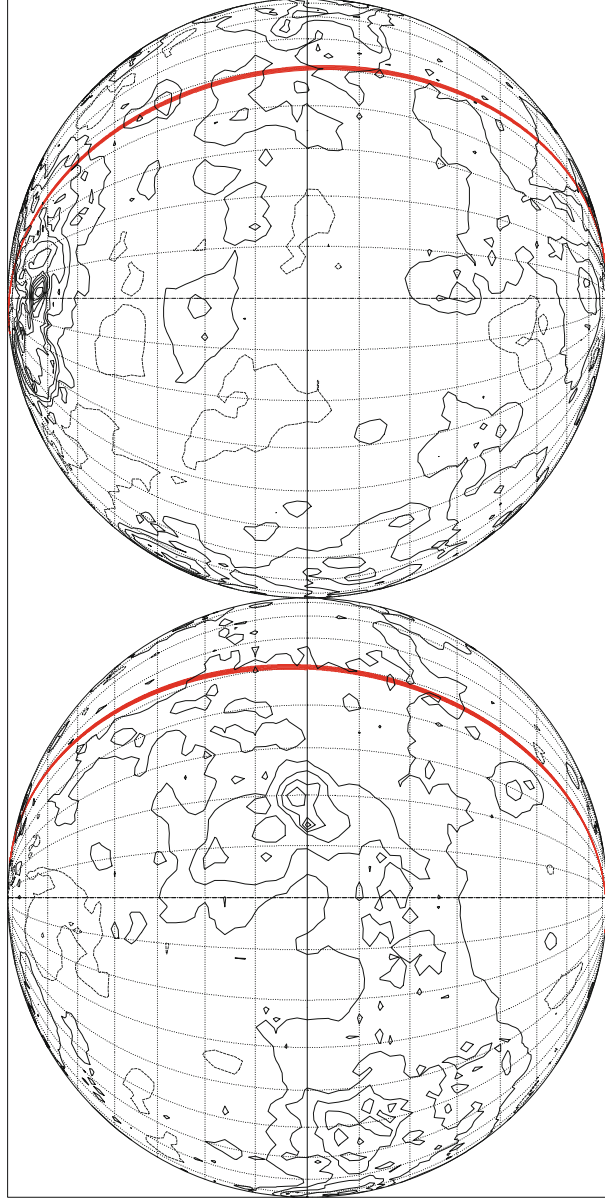


FIG. 16.11 : Topographic map of Venus with colour code: from purple and blue (very low and low altitude) to red and white (high and very high altitude). Equatorial orthographic projection, centered on longitudes of  $0^\circ$  (top) and  $180^\circ$  (bottom). One can make out Maxwell Montes in the Ishtar Terra region, centered on  $64^\circ$  N,  $4^\circ$  E. Credit: Magellan Team, NASA, JPL, MIT, USGS.

**[VENUS] Magellan**  
**Elliptical orbit - Gr. track**

Equiv. altit. = 4374.0 km      a = 10425.835 km  
 Inclination = 85.70°      e = 0.391764  
 Period = 195.59 min      \* rev/day = 7.36  
 h\_a = 8458 km; h\_p = 290 km; arg.periapsis: +170.47°

>>> Time span shown: 1440.0 min = 1.00 day



Projection: Orthographic      Pr. centre (r.): 0.0° ; 0.0°      Longitude / Initialisation:  $I\xi\omega\omega$   
 Property: none      Aspect: Equatorial      N.a.: 130.50° - Apo.: 48.77°      MC ★ LMD  
 ☿ T.:Azimuthal - Graticule: 10°      {3.9} [-90.0/ +90.0/ +90.0] [-]      MGNP60 *Magellan Topogr.* / h / 2km /      A7λας

FIG. 16.12 : Ground track of the satellite Magellan over 1 day. Passage over the Imdr region (see Fig. 16.10). Equatorial orthographic projection, as for the topographic map of Venus in Fig. 16.11.

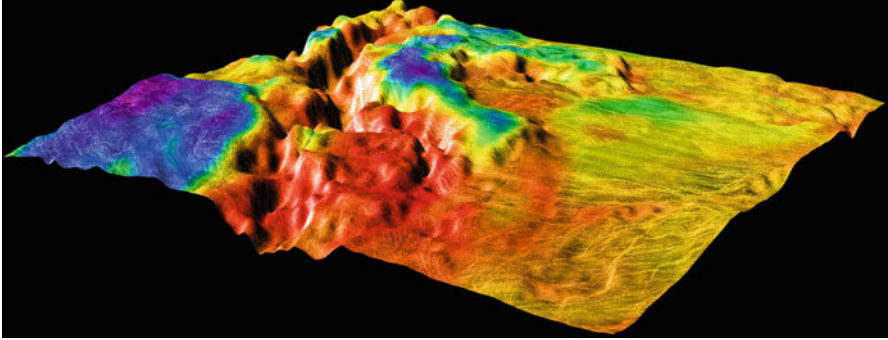


FIG. 16.13 : *Perspective view of Venus, generated by computer from Magellan data and color-coded with emissivity. This image shows the boundary between the lowland plains and characteristic Venusian highland terrain in Onda Regio. Image resolution: 225 m. Size of region shown: 1,125 km E–W and 1,125 km N–S. Vertical exaggeration: 20. Azimuth of viewpoint: 150°. Elevation of viewpoint: 1,200 km. Credit (image and caption): JPL, NASA, USGS.*

#### Example 16.1 *Orbital track of the satellite Magellan.*

► The ground track of the orbit over one Earth day in Fig. 16.12 exhibits no obvious asymmetry, as is often the case for eccentric terrestrial orbits. This is due to the fact that the planet is almost motionless (compared with the satellite motion, even at apoastron) in a Galilean frame. The very slow rotation of the planet about its axis gives a very small equatorial shift of about  $0.20^\circ$ , i.e., about 21 km between two consecutive ground tracks, as can be seen from Fig. 16.14 (lower), for a time lapse of 5 days. In the latter, the Mercator projection used for the map is centered on Maxwell Montes. This great mountain range in Ishtar Terra, the highest in Venus, is 11 km above the mean level of the planet. ◀

### 16.4.3 Satellites of the Asteroid Eros

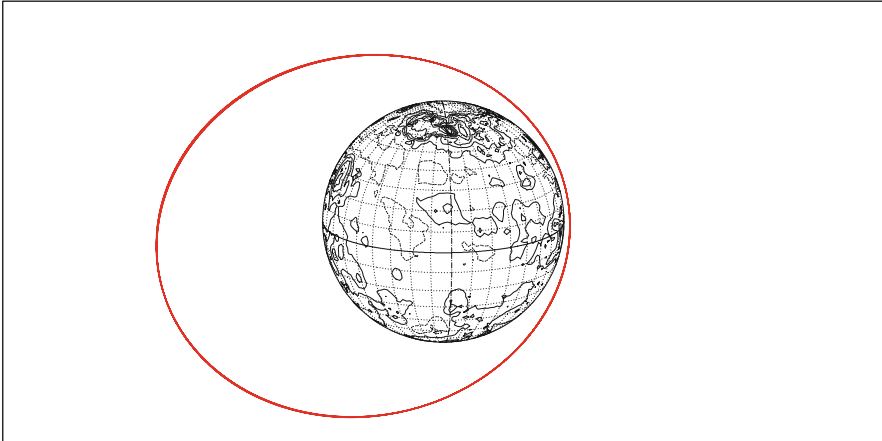
The asteroid 433-Eros, made of siliceous rock, has a rather cylindrical shape.<sup>34</sup> From 14 February 2000, the probe NEAR, since renamed NEAR-Shoemaker, went into orbit to become a satellite of Eros. On an initially eccentric orbit (ellipse with semi-major axis  $a = 365$  km and semi-minor axis  $b = 204$  km,  $i = 36^\circ$ ), the satellite gradually approached Eros by means of

<sup>34</sup>Mean equatorial radius 9.236 km, maximal equatorial radius = 17.452 km, minimum equatorial radius = 3.501 km, North Pole radius 5.338 km, South Pole radius 5.993 km. The radius  $R$  indicated in Table 16.5 is the mean radius.

**[VENUS] Magellan**  
Orbit - ref.: Venus

>>>> Time span shown: 1440.0 min = 1.00 day

Equiv. altit. = 4374.0 km      a = 10425.835 km  
 Inclination = 85.70 °      e = 0.391764  
 Period = 195.59 min \* rev/day = 7.36  
 h\_a = 8458 km; h\_p = 290 km; arg.periapsis: +170.47 °

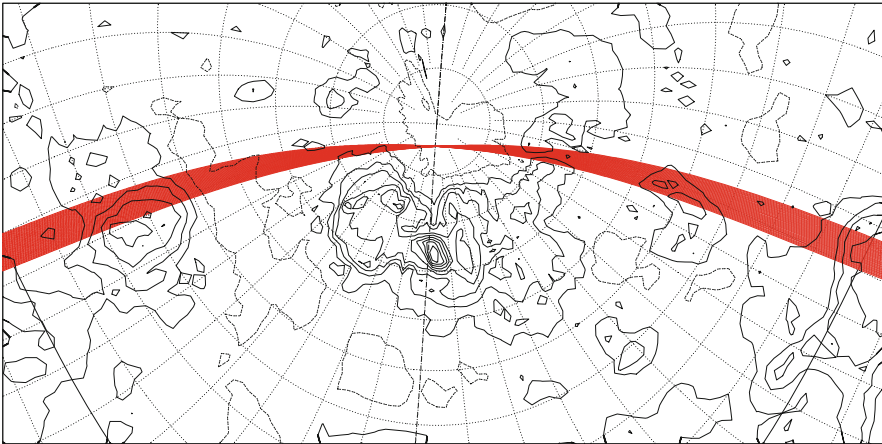


Projection: Orthographic	Project. centre: 15.0 ° N; 4.0 ° W	Longitude / Initialisation:	<i>Ιξίων</i>
Property: none	Aspect: Oblique	N.a.: -90.00 ° - Apo.: 89.27 °	MC ★ LMD
♀ T.:Azimuthal - Graticule: 10°	{3.9}[-90.0/+75.0/+94.0] [-] MGNP60	<i>Magellan Topogr. / h / 2km /</i>	<i>ΑΤΛΑΣ</i>

**[VENUS] Magellan**  
Elliptical orbit - Gr. track

>>>> Time span shown: 5.00 days

Equiv. altit. = 4374.0 km      a = 10425.835 km  
 Inclination = 85.70 °      e = 0.391764  
 Period = 195.59 min \* rev/day = 7.36  
 h\_a = 8458 km; h\_p = 290 km; arg.periapsis: +170.47 °



Projection: Mercator	PC: 64.0 ° N; 4.0 ° E / ZC: 70.0 ° N; 8.0 ° E	Longitude / Initialisation:	<i>Ιξίων</i>
Property: Conformal	Aspect: Oblique > zoom : 1.95	N.a.: -90.00 ° - Apo.: 89.27 °	MC ★ LMD
♀ T.:Cylindrical - Graticule: 10°	{3.9}[+90.0/+64.0/-94.0] [-] MGNP60	<i>Magellan Topogr. / h / 2km /</i>	<i>ΑΤΛΑΣ</i>

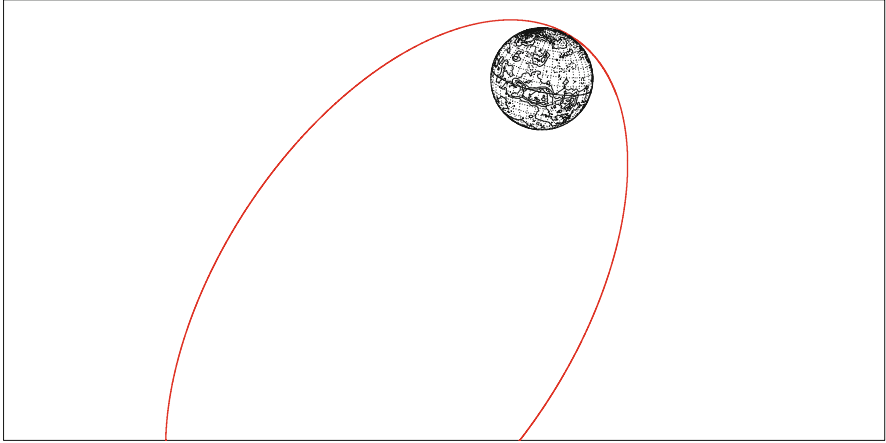
FIG. 16.14 : *Magellan*. Upper: Orbit in a frame moving with Venus, over 1 day. Lower: Ground track of orbit over 5 days. The (oblique Mercator) cartographic projection is centered on Maxwell Montes.

## [VENUS] Venus Express

### Orbit - ref.: Venus

>>>> Time span shown: 1440.0 min = 1.00 day

Equiv. altit. = 33125.0 km      a = 39176.801 km  
 Inclination = 90.00 °      e = 0.839145  
 Period = 1424.71 min \* rev/day = 1.01  
 h\_a = 66000 km; h\_p = 250 km; arg.periapsis: +70.00 °



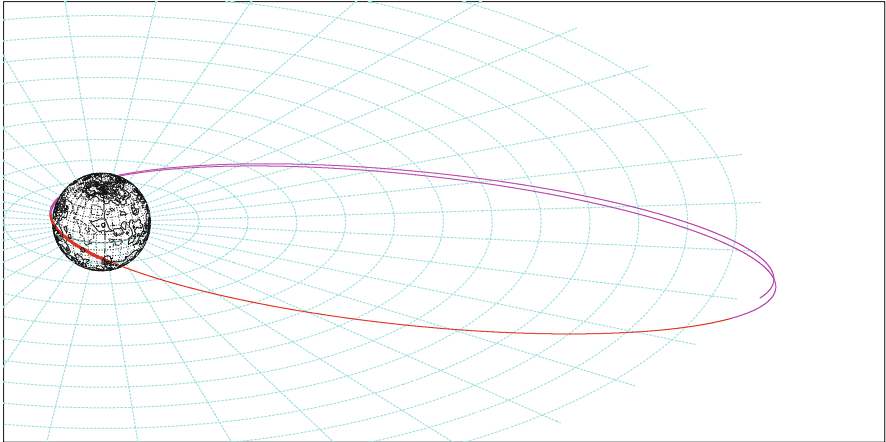
Projection: Orthographic      Project. centre: 15.0 °N; 90.0 °E      Longitude / Initialisation:      *Iξίων*  
 Property: none      Aspect: Oblique      N.a.: -179.28 ° - Apo.: 0.00 °      **MC \* LMD**  
 ♀ T.:Azimuthal - Graticule: 10° {3.9} [-90.0/ +75.0/ +0.0] [-12] MGNP60      *Magellan Topogr. / h / 2km /*      *Ατλας*

## [VENUS] VCO <金星プロジェクト>

### Orbit - ref.: Venus

>>>> Time span shown: 2880.0 min = 2.00 days

Equiv. altit. = 39450.2 km      a = 45502.000 km  
 Inclination = 172.00 °      e = 0.860406  
 Period = 1783.30 min \* rev/day = 0.81  
 h\_a = 78600 km; h\_p = 300 km; arg.periapsis: +90.00 °



Projection: Orthographic      Project. centre: 25.0 °N; 4.0 °W      Longitude / Initialisation:      *Iξίων*  
 Property: none      Aspect: Oblique      N.a.: 0.00 ° - Apo.: 89.11 °      **MC \* LMD**  
 ♀ T.:Azimuthal - Graticule: 10° {3.9} [-90.0/ +65.0/ +94.0] [-] MGNP60      *Magellan Topogr. / h / 2km /*      *Ατλας*

FIG. 16.15 : Upper: Orbit of Venus Express over 1 day. Lower: Orbit of Venus Climate Orbiter (VCO) over 2 days. Both orbits are shown in a frame moving with the planet.



Quantity	Units	Value	Quantity	Units	Value
$\mu = GM$	$\text{m}^3 \text{s}^{-2}$	$4.463 \times 10^5$	$a_S$	a.u.	1.458
$R$	km	7.311	$N_{\text{sid}}$	yr	1.76
$D_1$	km	34.4	$N_{\text{sid}}$	day	643
$D_2, D_3$	km	11.2, 11.2	$e$	–	0.233
$g_0$	$\text{mm s}^{-2}$	2.1 $\leftrightarrow$ 5.5	$i$	deg	10.8
$V_e$	$\text{m s}^{-1}$	3.1 $\leftrightarrow$ 17.2	$D_{\text{sid}}$	h	5.27025
$T_{0(h=0)}$	min	121.18	$\eta_{\text{GS}}$	–	1.895
$d$	–	2.67	$J_2$	$10^{-3}$	116.5
$\rho_\Sigma$	km	308	$J_3$	$10^{-3}$	4.8
$\rho_\Sigma/R$	–	37	$J_4$	$10^{-3}$	–37.5

TABLE 16.5 : Geodetic and astronomical characteristics of the asteroid 433-Eros (results of the NEAR mission). For the meaning of the quantities, see Table 16.2. Dimensions of the asteroid are denoted by  $D_i$ . Note the unusual units used here for  $g_0$  and  $V_e$  and the very high values of the  $J_n$  terms.

maneuvers which alternated elliptical and circular orbits. The near-circular ( $a = 200$  km) near-polar orbit eventually became rather low ( $a = 100$  km) and near-equatorial. On 28 January 2001, the satellite left its approach orbit ( $a = 35$  km,  $i = 180^\circ$ ), and landed on the asteroid, transmitting images up until the final impact.

The characteristics of the asteroid are displayed in Table 16.5 (see also Figs. 16.16 and 16.17). The geodetic data come from the NLR190 (NEAR Laser Rangefinder) model, based on a spherical harmonic expansion to degree and order 24 and 5 million radius measurements collected on day 190 of the year 2000. The  $J_2$ ,  $J_3$ , and  $J_4$  terms are indicated to allow comparison with other planets.<sup>35</sup>

### Example 16.2 Orbital ground track of the satellite NEAR.

► We have represented the orbital ground track of the NEAR probe, which became a satellite of 433-Eros. We have considered two types of orbit, known as OCM-2 and OCM-6. (Successive orbits of NEAR are numbered OCM- $n$ , Orbital Correction Maneuver). In the first case, shown in Fig. 16.18 (upper), the satellite is very high relative to the asteroid, since it takes 10 days to

<sup>35</sup>The normalised coefficients are:

$$C_{20}^* = -0.05210, \quad C_{22}^* = 0.04890, \quad S_{22}^* = 0.13170, \quad C_{30}^* = -0.00180.$$

The coefficients  $J_n$  are introduced using (3.22). The NLR190 model uses spherical harmonics. However, when the body under investigation is so far from spherical, the gravitational potential can be expanded in terms of ellipsoidal harmonics, where the Legendre functions are replaced by the Lamé functions.

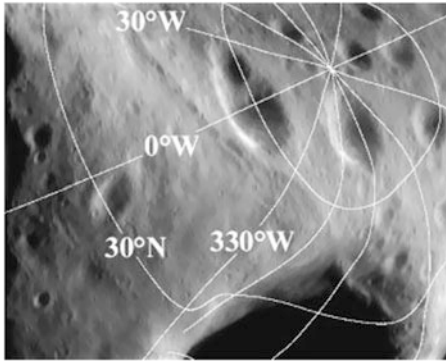


FIG. 16.16 : North polar region of Eros. Image acquired by the probe NEAR-Shoemaker on 31 March 2000, at an altitude of 207 km. The image has been overlain with lines of latitude and longitude, with a graticule of  $30^\circ$ . Latitude is measured in degrees from the equator, and longitude is measured in degrees west of a prime meridian. Credit: NASA, JHU/APL.

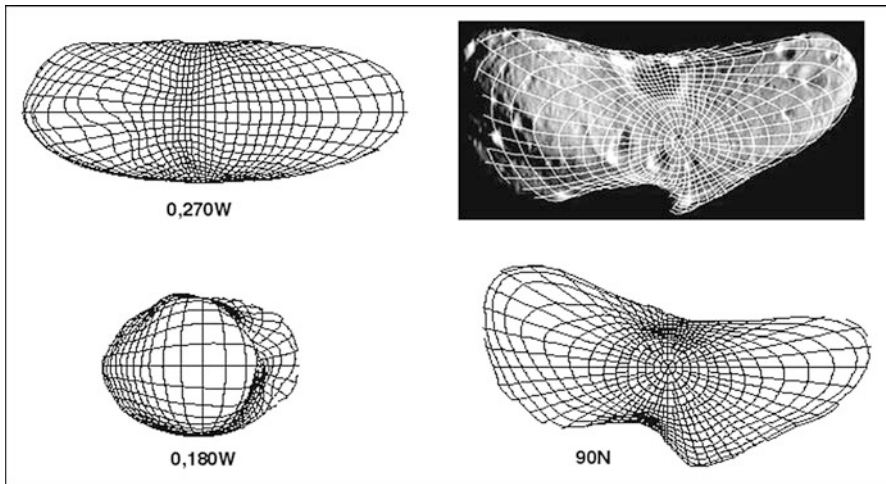


FIG. 16.17 : Different views of Eros. Graticule  $6^\circ$ . Credit: NASA, Johns Hopkins University/Applied Physics Laboratory.

make one round trip. The ground track thus takes 2.5 days to move from the equator to the maximum latitude. In the second case, shown in Fig. 16.18 (lower), the satellite is on a much lower orbit, although it remains above the planetosynchronous orbit. In this second figure, we have used the cartographic projection chosen by the NEAR science team to represent orbital tracks, i.e., the Hammer–Aitoff projection. ◀

#### 16.4.4 Satellites of the Asteroids Vesta and Ceres

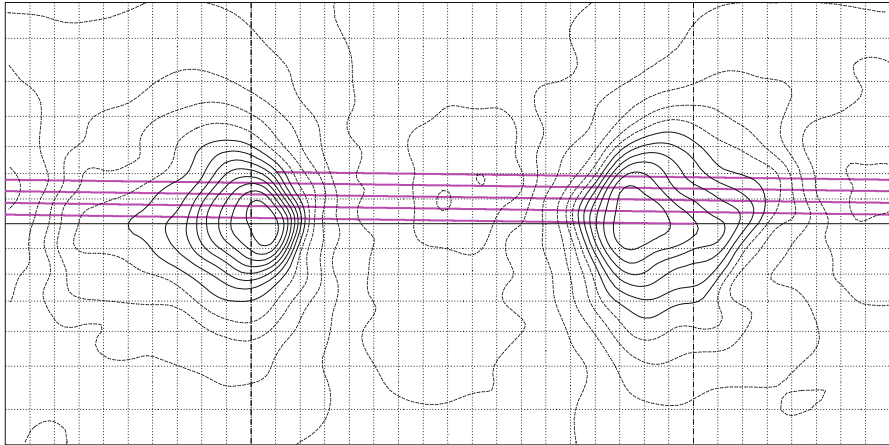
NASA's Dawn mission aims to work toward a better understanding of the “dawn” of the Solar System by exploring the two largest asteroids. The geodetic and astronomical characteristics of 1-Ceres and 4-Vesta are given in



**[433-EROS] NEAR/OCM-2**  
Orbit - Ground track

Altitude = 196.1 km      a = 204.500 km  
Inclination = 37.00°  
Period = 14488.19 min    \* rev/day = 0.10

>>>> Time span shown: 1440.0 min = 1.00 day

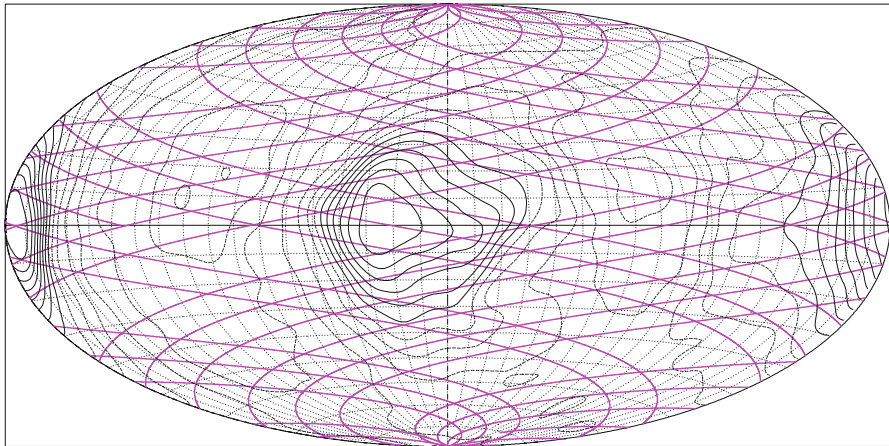


Projection: Mercator      Project. centre: 0.0° ; 100.0° W      Asc. Node: 0.00°      *Ιξίων*  
Property: Conformal      Aspect: Direct      App. inclin. = 179.23°      MC \* LMD  
\* T.:Cylindrical - Graticule: 10° {3.6} [ +90.0/ +0.0/ +10.0] [-] NLR190 NEAR Altim. / h / 2km /      Ατλας

**[433-EROS] NEAR/OCM-6**  
Orbit - Ground track

Altitude = 41.6 km      a = 50.000 km  
Inclination = 90.00°  
Period = 1761.09 min    \* rev/day = 0.82

>>>> Time span shown: 7.00 days



Projection: Hammer-Aitoff      Project. centre: 0.0° ; 0.0°      Asc. Node: -126.00°      *Ιξίων*  
Property: Equal area      Aspect: Direct      App. inclin. = 169.82°      MC \* LMD  
\* T.:Modif. Azim. - Graticule: 10° {3.6} [ +0.0/ +0.0/ +0.0] [-] NLR190 NEAR Altim. /h/2km/      Ατλας

FIG. 16.18 : Orbital ground track of the satellite NEAR: Upper: Over one (Earth) day. Lower: Over 7 days.

Asteroid	$\mu = GM$ ( $\text{m}^3 \text{s}^{-2}$ )	$R$ (km)	$g_0$ ( $\text{m s}^{-2}$ )	$D_i$ (km)	$T_o$ (m)	$d$ –		
Ceres	$6.326004 \times 10^{10}$	480/454	0.26/0.29	960/960/908	138	2.08		
Vesta	$1.781691 \times 10^{10}$	276/227	0.23/0.23	560/544/454	114	3.42		
Asteroid	$a_s$ (a.u.)	$N_{\text{sid}}$ (yr)	$e$	$i$ (deg)	$\varepsilon$ (deg)	$D_{\text{sid}}$ (h)	$\eta_{\text{GS}}$	$\rho_{\Sigma}/R$
Ceres	2.76636	4.603	0.07934	10.586	$\sim 4$	9.075	2.491	2.744
Vesta	2.36158	3.630	0.08890	7.134	$\sim 29$	5.342	1.995	2.454

TABLE 16.6 : Geodetic and astronomical characteristics of the two asteroids 1-Ceres and 4-Vesta. For explanations of the quantities, see Tables 16.2 and 16.5. For  $R$  and  $g_0$ , values at the equator and the pole. Period  $T_o = T_{0(h=0)}$ .

Orbit	$h$ (km)	$a$ (km)	$i$ (deg)	$T_d$ (h)	Rev/day	Rev/ $D_{\text{sid}}$
Vesta SO	2,450	2,726	90	58.92	0.408	0.09
Vesta HAMO	591	867	90	10.68	2.259	0.50
Vesta LAMO	180	456	90	4.20	5.714	1.27
Ceres SO	5,900	6,380	90	111.83	0.215	0.08
Ceres H	1,300	1,780	90	16.50	1.455	0.55
Ceres L	700	1,180	90	8.93	2.693	1.02

TABLE 16.7 : Successive circular orbits adopted by the Dawn mission. Orbital characteristics:  $h$ ,  $a$ ,  $i$ , and  $T_d$ . We have also indicated the number of revolutions per mean day ( $=24$  h) and per sidereal day of the asteroid.

Table 16.6. Dawn was launched on 27 September 2007 and flew past Mars on 17 February 2009 to arrive at Vesta on 21 July 2011. For a year until 25 July 2012, Dawn exploited three successive orbits around Vesta: a survey orbit (SO), a high altitude mapping orbit (HAMO), and a low altitude mapping orbit (LAMO). Increasing its altitude to prepare for departure, Dawn remained for a certain time in the HAMO2 orbit, very close to HAMO. In September 2012, the probe left to pursue its mission to Ceres, which it should finally reach on 1 February 2015. It will follow three orbits: SO, High, and Low, until the end of its mission in July 2015. The orbital characteristics are indicated in Table 16.7.

The first part of the mission, i.e., exploration of Vesta, was extremely successful. The asteroid was studied and mapped with great accuracy (see Fig. 16.19).

### Example 16.3 Orbits of Dawn around Vesta.

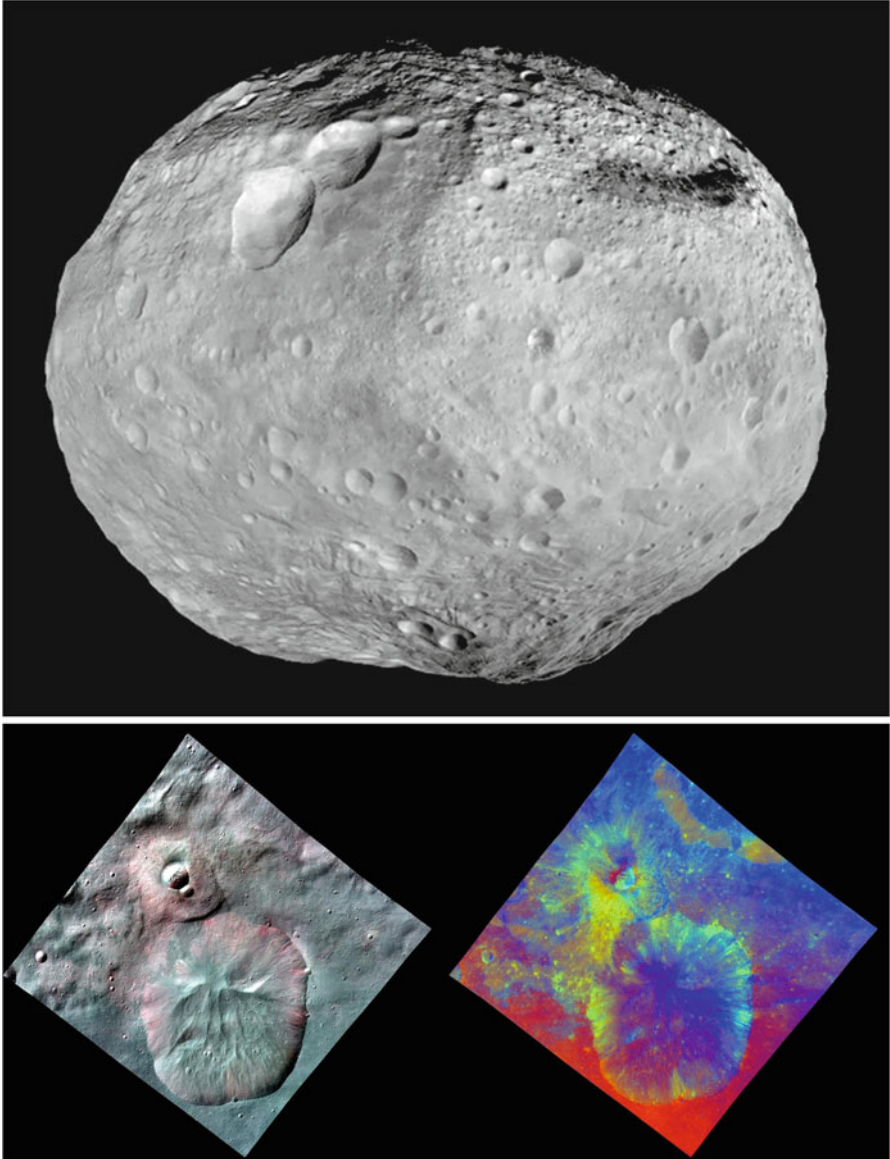


FIG. 16.19 : *The asteroid Vesta, viewed by Dawn. Upper: Overview of Vesta, built up from a mosaic of images. Lower: Images taken by Dawn's framing camera. The far-left image uses near-infrared filters (red 750 nm, green 920 nm, blue 980 nm). The image on the right is an image with colors assigned by scientists, representing different rock or mineral types on Vesta. Credit (image and caption): NASA, JPL, Caltech, UCLA, MPS, DLR (Germany), ASI (Italy).*

### [4-VESTA] Dawn / HAMO Orbit - ref.: 4-Vesta

>>>> Time span shown: 1440.0 min = 1.00 day

Altitude = 591.3 km

$a = 867.287$  km

Inclination =  $90.00^\circ$

Period = 641.04 min \* rev/day = 2.25

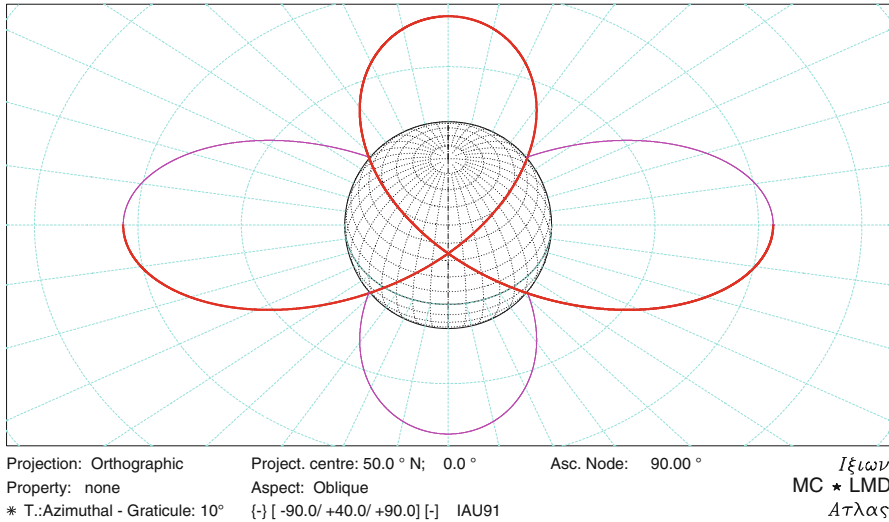


FIG. 16.20 : High altitude mapping (HAMO) orbit of the satellite Dawn around Vesta.

► The orbits considered are circular. When Dawn went in the HAMO orbit with  $a = 867.287$  km, i.e.,  $a - R_e = 591$  km, the nodal period was  $T_d = 641.04$  min, which corresponds to exactly twice Vesta's sidereal day  $D_{\text{sid}} = 320.52$  min. Taking Vesta's sidereal day as time unit, the recurrence triple becomes  $[1, 0, 2]$  1, with the usual notation. This resonance gives an orbit with a strikingly original graphical representation (see Fig. 16.20). Note that, for satellites in orbit around a body as far from spherical as Vesta, with such a large  $J_2$  term, the apsidal precession rate is very high. For Dawn/HAMO,  $\dot{\omega} = -4.7^\circ$  per day and the difference between  $T_d$  and  $T_a = 637.36$  min is considerable.

By increasing the altitude from 591 to 680 km, the period is multiplied by a factor of 1.15 and the satellite thus takes 2.30 sidereal days to make one round trip, whence the shift in the ground tracks (see Fig. 16.21). ◀

#### Example 16.4 Orbits of Dawn around Ceres.

► The H orbit of Dawn around Ceres is similar to the HAMO orbit for Vesta. The probe takes less than 2 sidereal days to make one revolution (see Fig. 16.22 upper). At the end of the mission, Dawn goes into a polar orbit called the L orbit at an altitude of 700 km. The period  $T_d = 8.928$  h is slightly shorter

### [4-VESTA] Dawn / HAMO + Orbit - Ground track

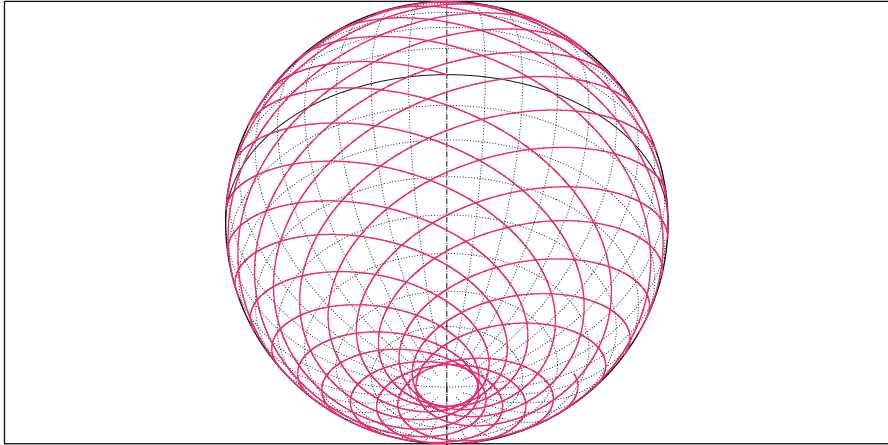
>>>> Time span shown: 6.50 days

Altitude = 680.0 km

a = 956.000 km

Inclination = 98.00 °

Period = 739.80 min \* rev/day = 1.95



Projection: Orthographic

Property: none

\* T.:Azimuthal - Graticule: 10°

Project. centre: 42.0 ° S; 0.0 °

Aspect: Oblique

{ } [ -90.0/+132.0/ +90.0 ] [-] IAU91

Asc. Node: 0.00 °

Ιξίων

MC ★ LMD

Ατλας

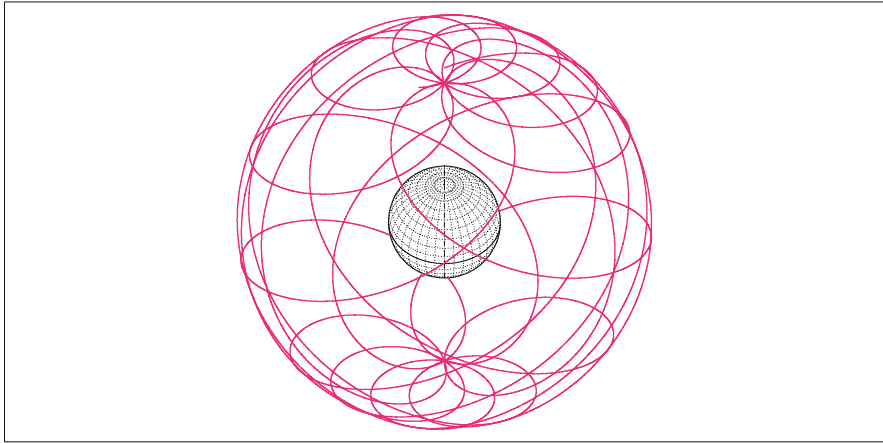


FIG. 16.21 : Ground track of the satellite Dawn. Upper: Reconstruction of the orbital elements by Ixion. The orbit denoted here by HAMO+ is at a slightly higher altitude than the one denoted by HAMO. Lower: The visible and infrared mapping spectrometer aboard NASA's Dawn spacecraft acquired this set of images during the high-altitude mapping orbit phase. Credit (image and caption) for the lower panel: NASA, JPL, Caltech, UCLA, ASI.

**[1-CERES] Dawn / H  
Orbit - ref.: 1-Ceres**

>>>> Time span shown: 5.00 days

Altitude = 1300.0 km      a = 1780.000 km  
 Inclination = 90.00 °  
 Period = 990.39 min \* rev/day = 1.45

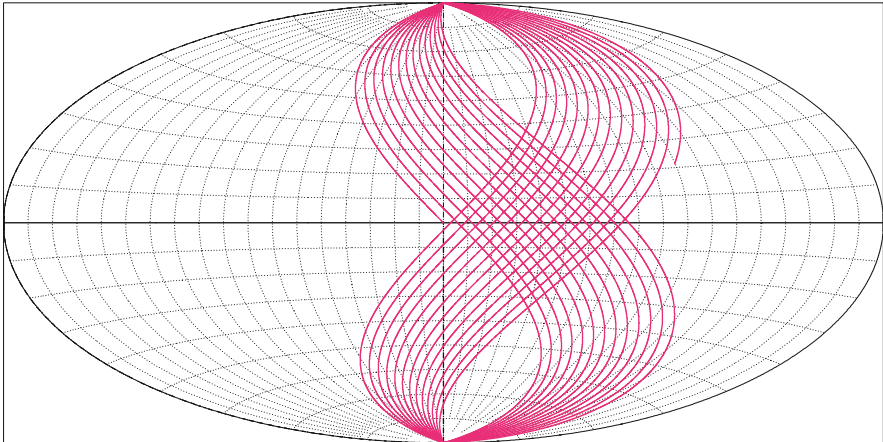


Projection: Orthographic      Project. centre: 48.0 ° N; 0.0 °      Asc. Node: -180.00 °      *Ιξίων*  
 Property: none      Aspect: Oblique      MC \* LMD  
 \* T.:Azimuthal - Graticule: 10°    {} [-90.0/ +42.0/ +90.0] [-] IAU91      Ατλας

**[1-CERES] Dawn / L  
Orbit - Ground track**

>>>> Time span shown: 5.00 days

Altitude = 700.0 km      a = 1180.000 km  
 Inclination = 90.00 °  
 Period = 535.68 min \* rev/day = 2.69  
 Equat. orbital shift = 2967.1 km



Projection: Aitoff      Project. centre: 0.0 ° ; 0.0 °      Asc. Node: 0.00 °      *Ιξίων*  
 Property: none      Aspect: Direct      App. inclin. = 134.53 °      MC \* LMD  
 \* T.:Modif. Azim. - Graticule: 10°    {} [+90.0/ +0.0/ -90.0] [-] IAU91      Ατλας

FIG. 16.22 : *Satellite Dawn around Ceres, over 13.2 sidereal days of Ceres. Upper: H orbit over 7.3 revolutions. Lower: Ground track of L orbit over 13.4 revolutions. The orbit is very close to the synchronous orbit.*



than the length of the sidereal day of Ceres, viz., 9.075 h. The ground track of Dawn thus exhibits a slight shift from one revolution to the next (see Fig. 16.22 lower). ◀

### 16.4.5 Satellites of Giant Planets

The probes in orbit around Jupiter and Saturn cannot really be classified as orbiters. Whereas a satellite around the Earth, Mars, or another telluric planet will revolve for months on end on a virtually unchanging orbit, a probe around Jupiter or Saturn changes orbit upon each revolution. To fly past a given moon, the probe may go from a highly eccentric orbit to a circular one, making frequent use of its thrusters.

#### Jupiter

After 8 years of mission, Galileo had made 34 orbits around Jupiter, each with a period of several weeks.<sup>36</sup> The Juno mission<sup>37</sup> is designed to study the origin and evolution of Jupiter. Once in orbit,<sup>38</sup> the probe should make 32 revolutions over 1 year. Later we shall mention the JUICE mission to Jupiter when discussing exploration of natural satellites.

#### Saturn

The Cassini mission consisted of three main parts. The first, or Prime Mission, from 17 May 2004 to 1 June 2008, made 74 revolutions. Arriving from the Earth, the probe flew past Phoebe on 11 June, before orbit insertion (SOI) on 1 July. It then made 3 Titan flybys, dropping the Huygens module on 14 January 2005. The mission was subsequently devoted primarily to the dynamics of Saturn's atmosphere, occultation by the rings, and the icy moons.

The Extended Mission, up until 11 October 2010, revolution 139, and the Extended Extended Mission up until 18 September 2017, revolution 292, continued to fly past Titan and all the other moons. The dates of these two missions were determined by Saturn's declination. The Extended Mission, renamed Equinox Mission, was centered around the equinox of 11 August 2009, with  $\delta = 0^\circ$ , while the Extended Extended Mission, renamed Solstice Mission, ended shortly after the solstice of 25 May 2017, with  $\delta = 26.7^\circ$  (see

---

<sup>36</sup>Here are some examples with their denomination: G1, flying past Ganymede, 1996 06 27, then G2, past Ganymede again, 1996 09 06, then C3, past Callisto, 1996 11 04, then E4, past Europa, 1996 12 19. Following this, with I for Io and J for Jupiter: J5, E6, G7, G8, C9, C10, E11–19, C20–23, I24–25, G28–29, C30, I31–33, J34.

<sup>37</sup>In Latin and in English, Juno was the wife of Jupiter. The mission is well named, for Juno was interested only in Jupiter and did not even glance at the sublime Io, the regal Europa, the beautiful Callisto, or the young shepherd Ganymede.

<sup>38</sup>Launch 2011 08 05, Earth gravity-assist 2013 10 09, Jupiter orbit insertion (JOI) 2016 08 03.

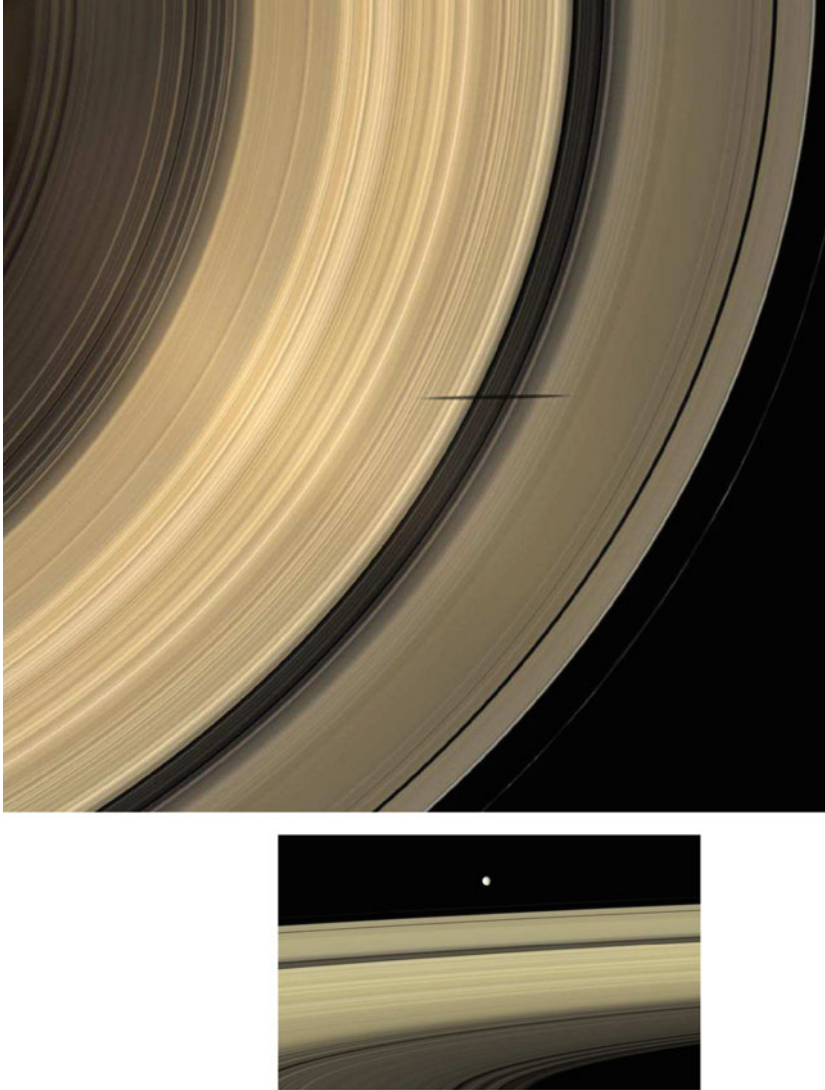


FIG. 16.23 : *Shadow of Mimas on Saturn's rings. The main rings of Saturn are traditionally referred to as C, B, and A, in this order as one moves away from the planet. The natural satellite Mimas is close to the edge of ring A. Upper: The shadow of Mimas appears on the rings, astride the Cassini division. This scene is only possible for a few months before and after the equinox, which only occurs once every 15 years. The date at which the image was taken, viz., 8 April 2009, was close to the equinox of 19 August 2009. The image was acquired by the Cassini Wide-Angle Camera from a distance of 1.1 million km, with a resolution of 64 km/pixel. Lower: The natural satellite Mimas does not move exactly in the plane of the rings ( $i = 1.6^\circ$ ), and this is why one sees its shadow on them. The image acquired by the Cassini Narrow-Angle Camera also reproduces the natural colours. It was taken from a distance of 3.151 million km with a resolution of 19 km/pixel. Credit (images and captions): NASA, JPL, Space Science Institute.*



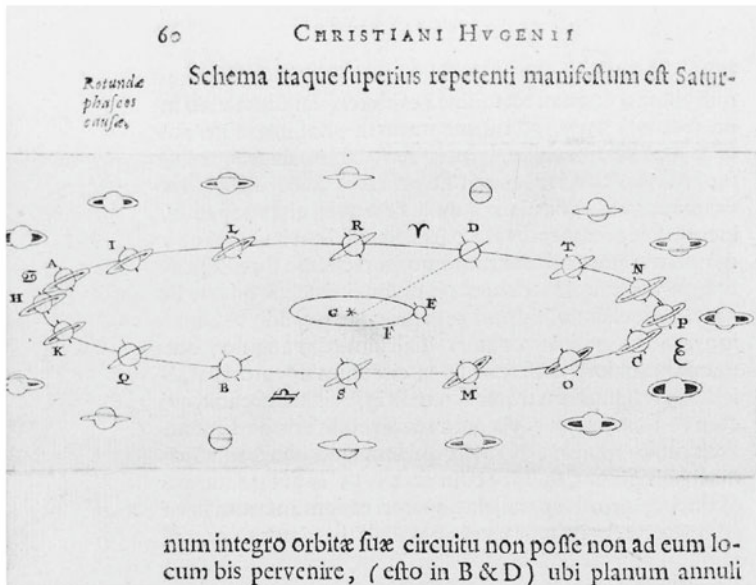
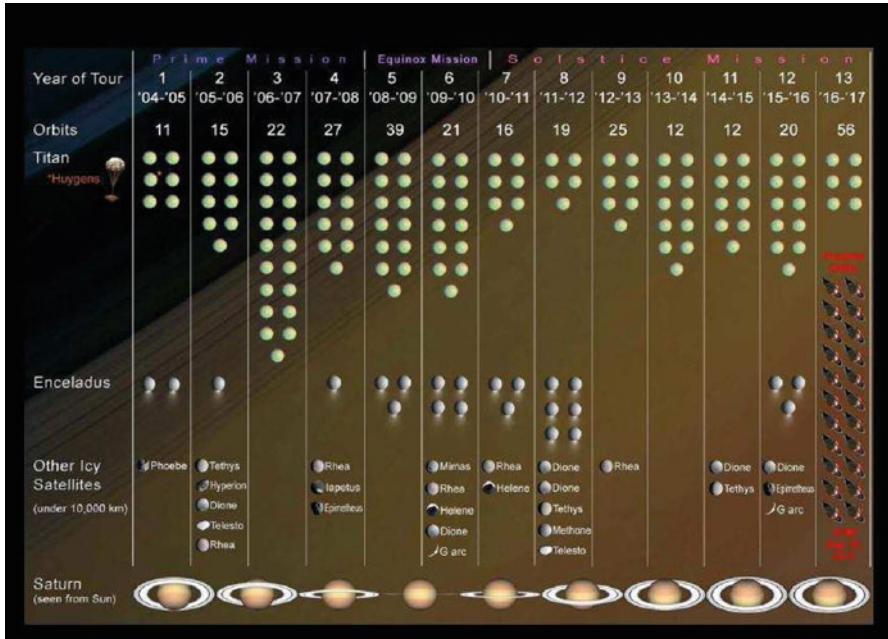


FIG. 16.24 : Upper: Official programme of the Cassini-Huygens mission. Credit: NASA. Lower: Diagram by Huygens, explaining the changing view of Saturn's rings when viewed from the Earth. The solstices occur at A and C, the equinoxes at B and D. Page 60 of Systema Saturnium, sive de causis mirandorum Saturni phaenomenon, Christian Huygens, 1659.



FIG. 16.25 : *Cassini mission. Logos of the Equinox and Solstice missions. Credit: NASA.*

Figs. 16.23, 16.24, and 16.25). The shadow thrown by the rings on the planet during the northern summer solstice is shown in Fig. 16.26.

As soon as it arrived near Saturn, Cassini detected a vertical motion of the rings, as though they were being shaken by waves, shown in Fig. 16.3. Soon afterwards, other shots revealed small, hitherto unknown moons<sup>39</sup> in the rings, which produce these so-called density waves.

The Cassini mission made countless discoveries<sup>40</sup> some of which we present here with the help of the illustrations in Figs. 16.27 and 16.28:

- The honeycomb structure of Hyperion, with a roughly cylindrical shape, about 370 km long and 220 km across.
- The strange bulge of Iapetus (radius  $R = 747$  km), which is in fact a mountain range running strictly along the equator.<sup>41</sup>
- The oversized crater on the surface of Mimas ( $R = 199$  km).
- The tiger stripes of Enceladus ( $R = 252$  km), with their water vapour geysers.<sup>42</sup>

We shall say more about Titan below.

<sup>39</sup>The small natural satellite Daphnis, discovered by this probe in May 2005, has a diameter of just 7 km. It revolves in the Keeler division, 42 km wide, inside ring A. The resulting waves, either in the plane or perpendicular to them, can be made out in the small photo on the left of Fig. 16.3. The motion in the vertical direction is particularly visible in the light at grazing incidence, at a date close to the Saturn equinox.

<sup>40</sup>The moons mentioned here had been discovered long before: Hyperion (also called Saturn VII, or S VII) by C. and G. Bond and W. Lassell in 1848, Iapetus (S VIII) by J.D. Cassini in 1671, and Mimas (S I) and Enceladus (S II) by W. Herschel in 1789. The contribution of the Cassini probe was to provide precise images of each of these moons and to show how very different they are.

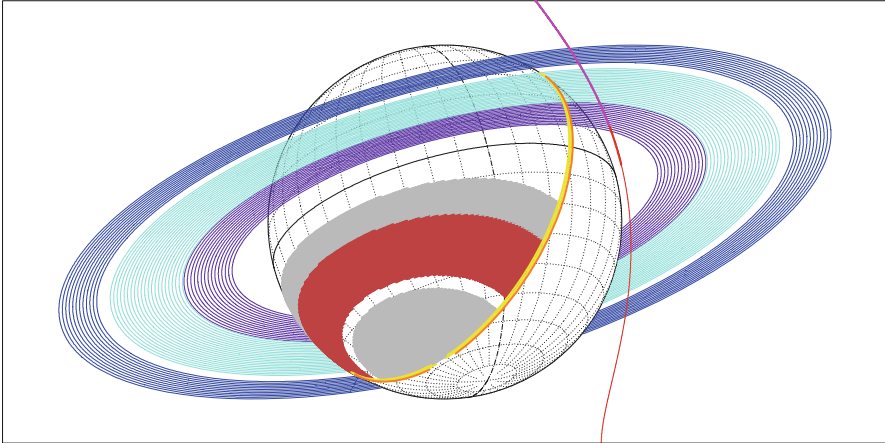
<sup>41</sup>This mountain has a triangular cross-section with base 200 km and height 18 km.

<sup>42</sup>After imaging these geysers, Cassini was programmed to make more frequent flybys of Enceladus. It was discovered that the water from the geysers was mixed with particles of ice and organic compounds. The temperature at the surface of Enceladus is only about 75 K, but higher in the crevices.

**[SATURN]** Cassini Apr.2017  
Orbit - ref.: Saturn

>>>> Time span shown: 150.0 min = 0.10 day

Equiv. altit. = 582478 km      a = 642808.0 km  
CRITICAL Incln. = 64.00 °      e = 0.900823  
Period = 8769.94 min      \* rev/day = 0.16  
h\_a =1161534 km; h\_p = 3422 km; arg.periapsis: +0.00 °



Projection: Orthographic      Project. centre: 22.0 ° S; 20.0 ° W      A.N.: 62.00 °       $\Gamma\xi\omega\nu$   
Property: none      Aspect: Oblique      2017 04 15 /  $\delta=26.7$  /  $\lambda=-58$       MC ★ LMD  
h T.:Azimuthal - Graticule: 10°       $\{ \} [-90.0/+112.0/+110.0] [+15]$  IAU91      KRONOS / Rings       $A\tau\lambda\alpha\varsigma$

FIG. 16.26 : Cassini's trajectory at the end of its mission in April 2017, at the summer solstice. The rings C, B, and A have been represented to scale (in that order as one moves away from Saturn), together with the shadow projected on the planet. The Cassini division is clearly visible.

To accomplish all these flybys, the Cassini probe has a different orbit in each revolution.<sup>43</sup> The eccentricity changes from one orbit to the next, and the inclination varies from  $i = 0^\circ$  to  $i = 75^\circ$ . The periods of the probe around Saturn are of the order of 1–3 weeks.

The next mission to Saturn, TSSM, will be dedicated specifically to the natural satellites of the planet, as we shall see below in the discussion of Titan.

<sup>43</sup>Here are some examples of orbits adopted by Cassini. The apoastron and periastron are given as reduced distances, viz.,  $\eta_a = r_a/R$  and  $\eta_p = r_p/R$ , where  $R$  is the radius of Saturn:

Rev 5:  $i = 0.2^\circ$ ,  $\eta_a = 44.390$ ,  $\eta_p = 3.498$ ,  $T = 20.5$  day, Titan 2005 03 31

Rev 6:  $i = 7.4^\circ$ ,  $\eta_a = 37.956$ ,  $\eta_p = 2.594$ ,  $T = 16.0$  day, Titan 2005 14 16

Rev 49:  $i = 0.5^\circ$ ,  $\eta_a = 69.031$ ,  $\eta_p = 5.351$ ,  $T = 39.7$  day, Titan 2007 08 31  
and Iapetus 2007 09 10

Rev 80:  $i = 74.4^\circ$ ,  $\eta_a = 20.302$ ,  $\eta_p = 3.941$ ,  $T = 7.4$  day, Enceladus 2008 08 11

Rev 248:  $i = 57.8^\circ$ ,  $\eta_a = 23.230$ ,  $\eta_p = 5.578$ ,  $T = 9.6$  day, Titan 2016 11 14

Rev 292:  $i = 61.6^\circ$ ,  $\eta_a = 21.165$ ,  $\eta_p = 10.28$ ,  $T = 6.5$  day, Titan 2017 09 11

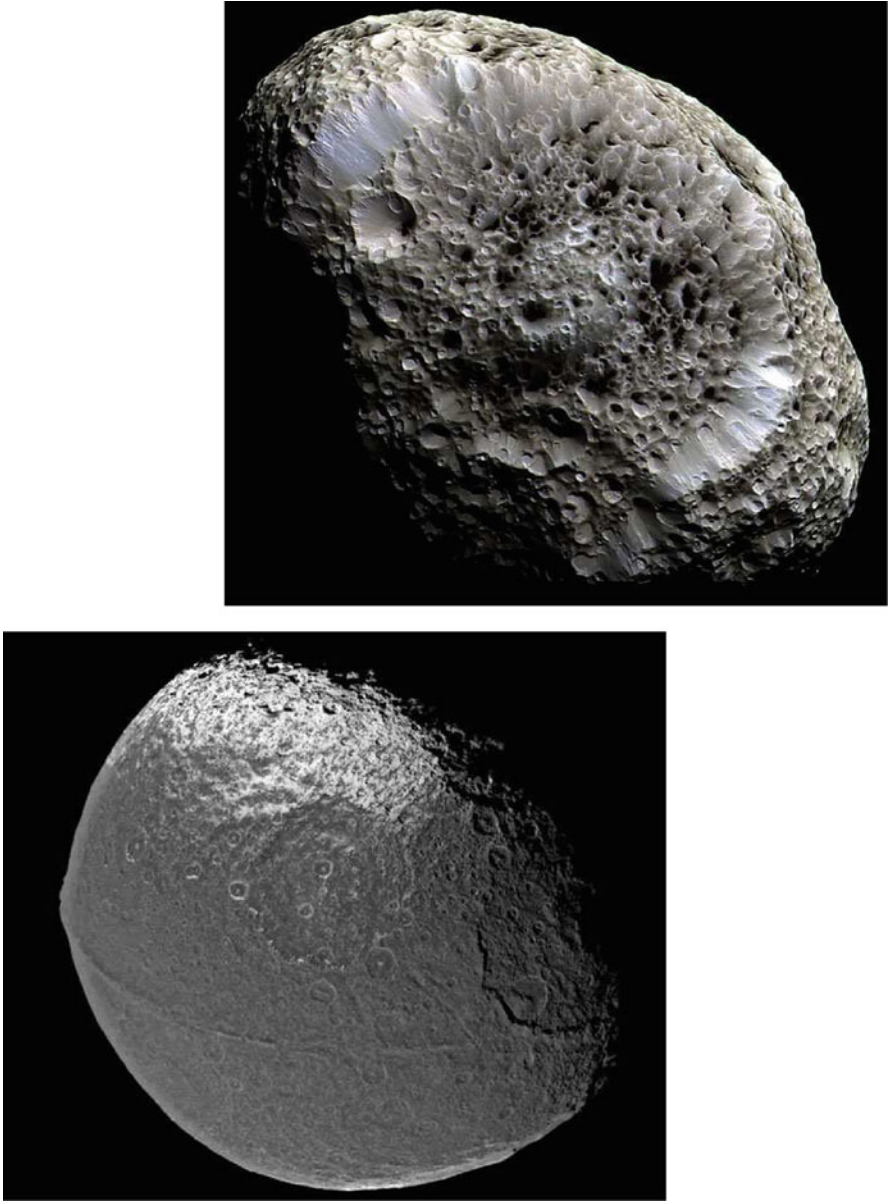


FIG. 16.27 : Two of Saturn's most surprising moons, photographed by Cassini. Upper: Hyperion, with its honeycomb structure and very low density. Its rotation is chaotic, not being blocked in 1:1 resonance with Saturn. Lower: Iapetus, with one very dark region and one very light, has a mountain range 18 km high on its equator. Credit: Cassini Imaging Team, SSI, JPL, ESA, NASA.

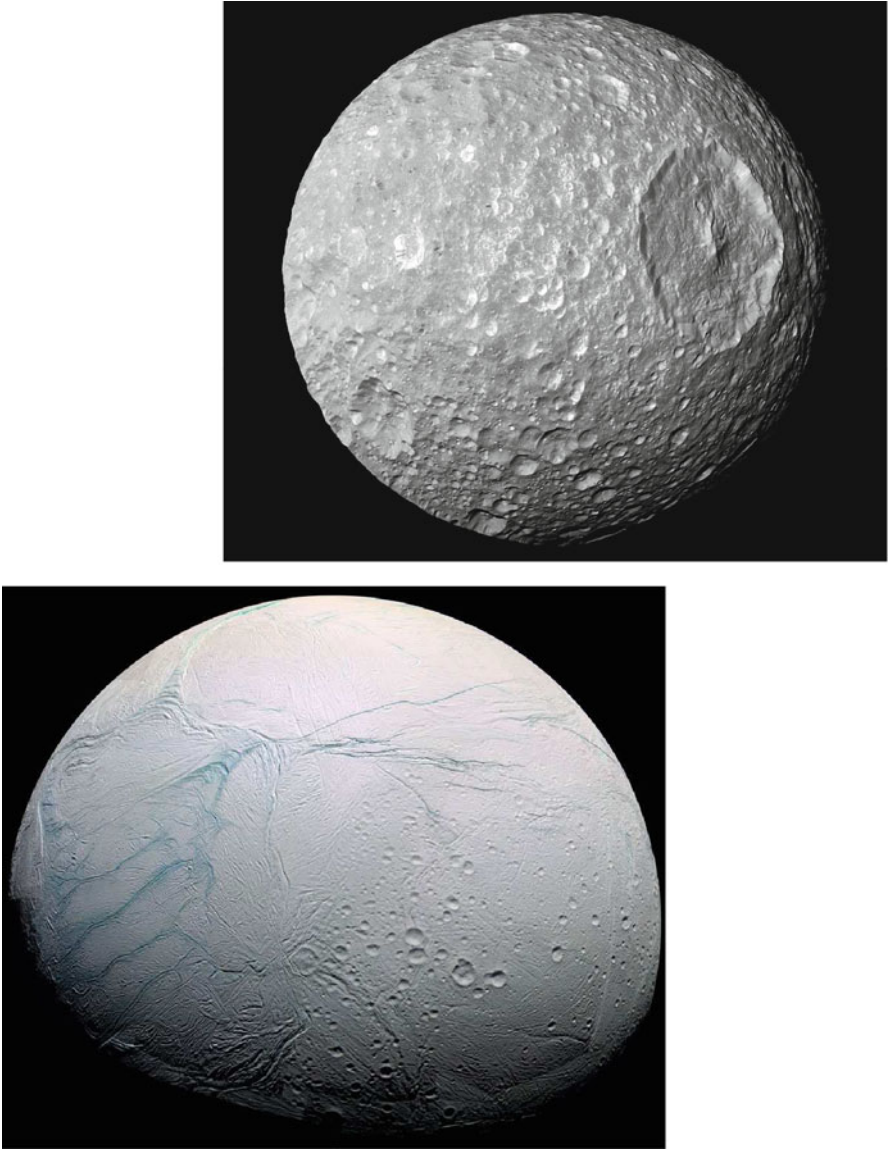


FIG. 16.28 : Two of Saturn's satellites photographed by Cassini. Upper: Mimas. The surface is completely covered by meteorite impact craters. The largest has diameter 130 km (to be compared with the radius of Mimas, just 200 km), and a depth of 10 km, with a central peak rising to 6 km. Lower: Enceladus. Part of the surface is covered with craters, while the other is coated with very clean ice, undoubtedly renewed by regular cryovolcanic activity. The latter is crossed by crevices like tiger stripes, sometimes the scene of water vapour geysers. Enceladus has an albedo close to 1. Credit: Cassini Imaging Team, SSI, JPL, ESA, NASA.



## B – *Satellite of a Natural Satellite*

### 16.5 Natural Satellites in the Solar System

#### 16.5.1 Presentation of the Natural Satellites

In previous chapters, we have discussed the natural satellites of the telluric planets. As far as the giant planets are concerned, the number of known natural satellites literally exploded after 1980, with the contributions of the Voyager missions and the progress made with adaptive optics on Earth-based telescopes. Before this date, we knew of 13 moons for Jupiter, 11 for Saturn, 5 for Uranus, and 2 for Neptune.

Today, the numbers have swollen considerably. Natural satellites are classified into regular and irregular. A moon is regular if it moves in the same direction as the rotation of the planet on a near-circular orbit in the equatorial plane of the planet. Otherwise it is irregular.<sup>44</sup> In 2013, we know of 67 moons (8 regular) for Jupiter, 62 (21 regular) for Saturn, 27 (18 regular) for Uranus, and 13 (6 regular) for Neptune. Concerning Pluto, it gravitates in a binary system with Charon, which has 1/6 of its mass.

Clearly, all the newly discovered moons are much smaller. Some measure only a few tens of kilometers across. As a rule, if a satellite has diameter greater than 400 km, it is rather spherical. If not, it becomes less and less spherical as the size diminishes.

For all natural satellites, the inclination is specified relative to the equatorial plane of the planet. There is one exception, and an important one: our own natural satellite. For the Moon does not gravitate in the equatorial plane of the Earth.<sup>45</sup> In this sense, it should be classified with the irregular natural satellites.

The natural satellites have one very important characteristic: they *all* exhibit synchronous rotation, or 1:1 resonance, i.e., one rotation during one revolution around the planet.<sup>46</sup> They are practically fixed relative to an axis

---

<sup>44</sup>It is thought that the regular satellites were formed at the same time as their host planet. The irregulars would then have a quite different history. A satellite like Nereid with its highly eccentric orbit around Neptune ( $e = 0.75$ ,  $i = 7^\circ$ ) suggests that some irregular moons are probably former asteroids, or trans-Neptunian objects, captured by the gravitational attraction of the host planet.

<sup>45</sup>The Moon has a very complex motion since it is part of a three-body system, comprising the Moon, the Earth, and the Sun ( $\mu/\mu_N = 81.30059$ ). The Moon's eccentric orbit makes an angle of  $5.2^\circ$  with the ecliptic. The inclination of the lunar orbit with respect to the Earth equatorial plane thus varies between  $18.3^\circ$  and  $28.6^\circ$  (see the note on Delaunay).

<sup>46</sup>The only exceptions are two satellites of Saturn, beyond Titan. The most distant, Phoebe, has a retrograde orbit and non-synchronous rotation. The other, Hyperion, trapped between the orbits of Titan and Iapetus, exhibits chaotic rotation.

passing through their center of gravity and the center of the host planet. Like the Moon for the Earth, they always turn the same face towards their planet. This is due to the tidal effect.<sup>47</sup>

## 16.5.2 Space Exploration of Natural Satellites

If we exclude the lunar conquest, discussed at the beginning of the chapter in the more general context of space exploration, there was no specific mission to any of the natural satellites at the beginning of the space age. If a visit was organised, it was always part of a trip to the associated planet.

This situation has changed since the Galileo mission, which made fundamental discoveries about the Galilean moons of Jupiter. And the Cassini–Huygens mission has spent more time observing the moons of Saturn than the host planet itself. Future missions will reinforce this trend, whether to Jupiter, with JUICE, or to Saturn, with TSSM.

# 16.6 Geodetic and Astronomical Quantities for Natural Satellites

## 16.6.1 Geodetic and Astronomical Data

Here we examine several natural satellites in more detail:

- The Moon, because it is our own moon, and has been visited so many times.
- Europa, because it seems there may be liquid water there, and the three other Galilean moons of Jupiter.
- Titan, with its atmosphere, and another satellite of Saturn, Enceladus.
- Triton, satellite of Neptune, which has a thin atmosphere and enigmatic geysers.

Table 16.8 gives the geodetic and astronomical data for these bodies, together with derived quantities.

Even though it does not date from the time of their formation, the blockage of natural satellites so that they always turn the same face toward the host planet is certainly very ancient. It leads to distortion of the moon, to varying degrees. From an ellipsoid of revolution, it is transformed to a triaxial ellipsoid, for which one can define an equatorial radius  $R_x$  along the axis toward the host

---

<sup>47</sup>The planet exerts a tidal force on the natural satellite, much stronger than that exerted by the natural satellite on the planet. Viscous friction inside the natural satellite with its associated dissipation of energy ends up by slowing down the rotation of the natural satellite. When the rotation becomes synchronous, the natural satellite has been deformed into a shape extended in the direction of the planet. This deformation of the Moon in the direction of the Earth is very slight, while that of Phobos towards Mars is enormous, relative to the size of this moon. As soon as the natural satellite finds itself in this 1:1 resonance, it remains trapped in that situation by the restoring couple exerted by the planet.

Satellite	$\mu_N = GM_N$ ( $\text{m}^3 \text{s}^{-2}$ )	$R$ (km)	$g_0$ ( $\text{m s}^{-2}$ )	$V_e$ ( $\text{km s}^{-1}$ )	$T_{0(h=0)}$ (min)	$d$
Moon	$4.9028 \times 10^{12}$	1,737.4	1.62	2.38	108.31	3.34
Io	$5.9599 \times 10^{12}$	1,821.6	1.80	2.56	105.46	3.53
Europa	$3.2027 \times 10^{12}$	1,565.0	1.31	2.02	114.23	2.99
Ganymede	$9.8878 \times 10^{12}$	2,631.2	1.43	2.74	142.14	1.94
Callisto	$7.1793 \times 10^{12}$	2,410.3	1.24	2.44	146.25	1.83
Enceladus	$7.2095 \times 10^9$	252.1	0.11	0.24	159.75	1.61
Titan	$8.9782 \times 10^{12}$	2,575.0	1.35	2.64	144.41	1.88
Triton	$1.4279 \times 10^{12}$	1,352.6	0.78	1.45	137.86	2.06

Satellite	(Satellite) Planet/number	$a_P$ (km)	$\mu/\mu_N$	$\rho_\Sigma$ (km)	$\rho_\Sigma/R$
Moon	Earth I	383,398	81.3	57,433	33.1
Io	Jupiter I	421,671	$2.1256 \times 10^4$	6,820	3.7
Europa	Jupiter II	670,090	$3.9556 \times 10^4$	8,466	5.4
Ganymede	Jupiter III	1,070,339	$1.2812 \times 10^4$	21,196	8.1
Callisto	Jupiter IV	1,882,580	$1.7646 \times 10^4$	32,801	3.6
Enceladus	Saturn II	238,040	$5.2626 \times 10^6$	424	1.7
Titan	Saturn VI	1,221,803	$0.4226 \times 10^4$	37,709	14.6
Triton	Neptune I	354,759	$0.4788 \times 10^4$	10,415	7.7

Satellite	$N_{\text{sid}} = D_{\text{sid}}$ (d)	$e$	$i$ (deg)	$J_2$ $10^{-6}$	$C_{22}$ $10^{-6}$	Area ( $10^6 \text{ km}^2$ )
Moon	27.321661	0.0555	5.16 ECL	203	22	37.9
Io	1.769138	0.0410	0.04 EQU	1,860	559	41.7
Europa	3.551810	0.0090	0.47 EQU	436	132	30.8
Ganymede	7.154553	0.0015	0.20 EQU	128	38	87.0
Callisto	16.689018	0.0070	0.28 EQU	33	10	73.0
Enceladus	1.370218	0.0045	0.02 EQU	2,500	2,500	0.8
Titan	15.945446	0.0291	0.30 EQU	32	11	83.3
Triton	-5.878850	0.0000	156.83 EQU	?	?	23.0

TABLE 16.8: Natural satellites of planets in the Solar System. Geodetic and astronomical quantities. Data and derived quantities are the same as those appearing in Table 16.2. Quantities specific to this table: gravitational constant of the natural satellite  $\mu_N$ , semi-major axis  $a_P$  (planet–natural satellite). The inclination  $i$  is taken relative to the plane of the ecliptic (ECL) or the equatorial plane of the planet (EQU). The rotation of the natural satellite is synchronous:  $D_{\text{sid}} = N_{\text{sid}}$ . For Triton, the orbit is retrograde (minus sign).



planet, another  $R_y$  orthogonal to it, and a polar radius  $R_z$ , each measured from its center. To quantify this distortion of the volume and the mass distribution, we use the harmonic coefficients  $C_{20}$  and  $C_{22}$ , which involve the moments of inertia  $I_x$ ,  $I_y$ , and  $I_z$ , as discussed in Chap. 3. Recall from Table 3.1:

$$C_{20} = \frac{1}{2MR^2}(I_x + I_y - 2I_z), \quad C_{22} = \frac{1}{4MR^2}(I_y - I_x), \quad (16.5)$$

where  $M$  is the total mass and  $R = R_x$ .

For a planet, we have seen that  $C_{20}$  (with the notation  $J_2 = -C_{20}$ ) describes the flattening and  $C_{22}$  is zero, or almost zero. For a natural satellite,  $C_{22}$  is less than  $C_{20}$  but of the same order of magnitude. For a body in hydrostatic equilibrium, i.e., gravitational and pressure forces are balanced, it can be shown that

$$\left| \frac{C_{20}}{C_{22}} \right| = \frac{10}{3}. \quad (16.6)$$

Changes in the trajectory and velocity of probes during flyby can be used to determine these coefficients.

### 16.6.2 Satellite in Keplerian Orbit

Provided its altitude is not too great, in a sense to be defined later, everything happens for the satellite in orbit (semi-major axis  $a$ ) around a natural satellite as if it feels only the attraction of this body. Let  $\mu_N$  be the gravitational constant of this natural satellite, and keep  $\mu$  for the gravitational constant of the corresponding planet. All the formulas derived for the Keplerian orbit can be applied, replacing  $\mu$  by  $\mu_N$ , as in (5.5).

The period of the satellite at altitude 0 is given by (5.6) or (16.3). For example, for the Moon, with  $d = 3.34$ , we obtain for this period

$$T_{0(h=0)} = \frac{198}{\sqrt{3.34}} = 108 \text{ min}.$$

The values of  $T_{0(h=0)}$  are given in Table 16.8 for various natural satellites. Figure 16.5 graphs  $T_0/T_{0(h=0)}$  against  $a/R$ , where  $R$  is of course the radius of the natural satellite.

### 16.6.3 Geographical Maps

Natural satellites of planets can be mapped. The mappable area in millions of  $\text{km}^2$  is indicated in Table 16.8. The total area of the natural satellites is 425, including 232 for Jupiter's four Galilean moons. In this chapter, we shall use the following maps as background to represent the ground track or orbit:

- For the Moon, the topographical map based on laser altimeter data gathered by Clementine. Contours are plotted in 2 km steps, with the same convention for the curves as we used for planetary maps.

- For Europa, we shall not use a map, which would be difficult to read, but several images compiled by Galileo, showing the rather unusual structure of the surface.

We shall not dwell upon the geography of these celestial bodies. Since the first observations of mountains by Galileo, the geography and geology of the Moon have been the subject of extremely detailed studies.

In the case of the natural satellites, the prime meridian is not chosen arbitrarily. The origin for longitudes is taken to be the meridian exactly at the center of the face turned toward the planet.

## 16.7 Satellite of a Natural Satellite in Real Orbit

### 16.7.1 Perturbative Accelerations

For a satellite in orbit around a natural satellite, the sphere of influence identifies the region in which the acceleration due to the mother planet is negligible compared to the central acceleration. To evaluate this, we go back to the formulas in Sect. 6.11, replacing  $\mu_S$  by  $\mu$  and  $\mu$  by  $\mu_N$ , since for the satellite, the planet/Sun system is now replaced by the natural satellite/planet system. Table 16.8 shows the ratios  $\mu/\mu_N$  and the results of the calculation of  $\rho_\Sigma$ . We note that, for Europa,  $\rho_\Sigma$  is very small because its mass is 40,000 less than the mass of Jupiter.

The dependence of the central accelerations and perturbative accelerations on the altitude of the satellite is shown in Fig. 16.29 (upper) for a satellite around the Moon, and in Fig. 16.29 (lower) for a satellite around Europa. The notation for the accelerations is adapted from Table 6.1.

For the central acceleration, (6.6) gives  $\gamma_{CC}(R) = g(R) = g_0$ , which implies a value of  $1.62 \text{ m s}^{-2}$  for the Moon and  $1.31 \text{ m s}^{-2}$  for Europa. The main difference between the cases examined up to now, of satellites around planets, is clearly the presence (and magnitude) of the term  $\gamma_{CC1}$ , the perturbing acceleration due to the central planet.

For a satellite of the Moon close to ground level,  $\gamma_{CCN.J2}$  is greater than  $\gamma_{CC1}$ :

$$\gamma_{CCN.J2}(R) = 32.8 \times 10^{-5} \text{ m s}^{-2}, \quad \gamma_{CC1}(R) = 2.5 \times 10^{-5} \text{ m s}^{-2}.$$

However, above  $h \sim 1,000 \text{ km}$ ,  $\gamma_{CC1}$  soon exceeds  $\gamma_{CCN.J2}$ . For a satellite of Europa,  $\gamma_{CC1}$  is always greater than  $\gamma_{CCN.J2}$ :

$$\gamma_{CCN.J2}(R) = 0.8 \times 10^{-3} \text{ m s}^{-2}, \quad \gamma_{CC1}(R) = 1.3 \times 10^{-3} \text{ m s}^{-2}.$$

Moreover, this term  $\gamma_{CC1}$  increases with altitude (with slope  $p = 1$  on a log-log scale), and when the satellite is at an altitude of about 10,000 km, this

acceleration due to Jupiter is greater than the central acceleration  $\gamma_{\text{CCC}}$  due to Europa. In this case,  $\gamma_{\text{CC1}}$  can no longer be treated as a perturbation, just as the satellite is no longer a satellite of Europa!

Figure 16.29 shows the central and perturbative accelerations for two other Galilean satellites of Jupiter, namely Ganymede and Callisto.

## 16.7.2 Classification of Satellites

### Motion of Natural Satellites

The natural satellites studied here, like the others, all have synchronous rotation, i.e.,

$$D_{\text{sid}} = N_{\text{sid}} ,$$

where the first term is the sidereal period of rotation of the natural satellite about its own axis and the second is the sidereal period of revolution of the natural satellite about the central planet. For the natural satellites considered here, this period ranges from 27 days for the Moon to less than 4 days for Europa, and slightly more than a day for Enceladus. It should be noted that the revolution and hence the rotation of Triton occur in the retrograde direction around Neptune (Fig. 16.30).

### Stationary Satellite

In the example below, we show that it is impossible to place a satellite in stationary orbit around a natural satellite.

**Example 16.5** *Investigate the possibility of placing a satellite in a synchronous orbit, and more specifically, in a stationary orbit, around a natural satellite.*

► A satellite S is in circular orbit with semi-major axis  $a$  around a natural satellite N (with gravitational constant  $\mu_{\text{N}}$ ), which is itself in orbit with semi-major axis  $a_{\text{P}}$  around a planet P (with gravitational constant  $\mu$ ). If the orbit of S is synchronous with N, itself rotating in 1:1 resonance with P, Kepler's third law gives the relation between the mean motions as

$$\frac{\mu}{a_{\text{P}}^3} = \frac{\mu_{\text{N}}}{a^3} .$$

This in turn implies that

$$a_{\text{GS}} = a = \left( \frac{\mu_{\text{N}}}{\mu} \right)^{1/3} a_{\text{P}} , \quad (16.7)$$

where  $a_{\text{GS}}$  is the semi-major axis of the stationary orbit.

We now compare this value with  $\rho_{\Sigma}$ , the radius of the sphere of influence. Adapting (6.158) to the present situation, we obtain

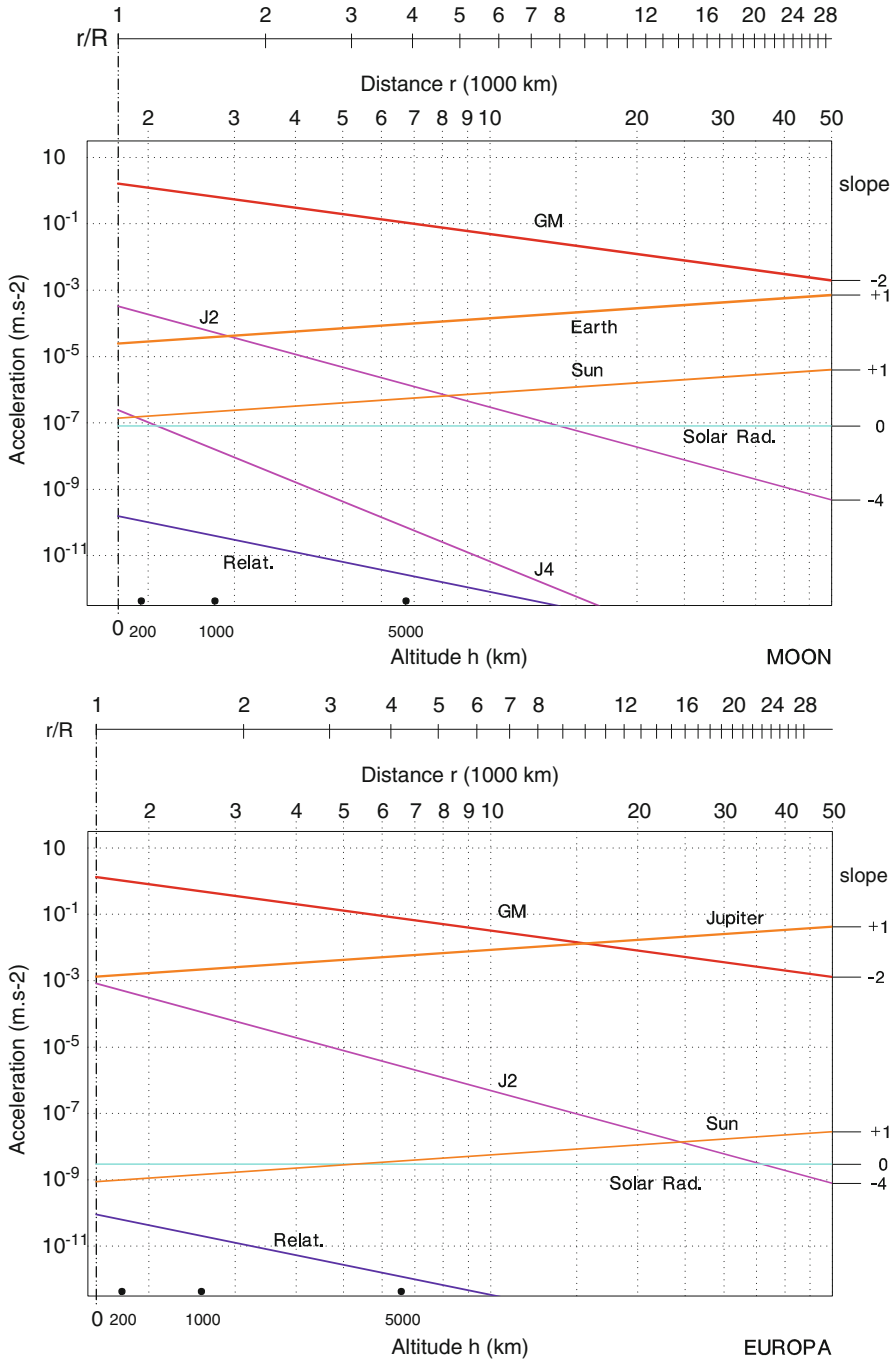


FIG. 16.29: Accelerations as a function of the distance  $r$  of the satellite from the center of the natural satellite. Log-log scale. Upper: Moon. Lower: Europa.

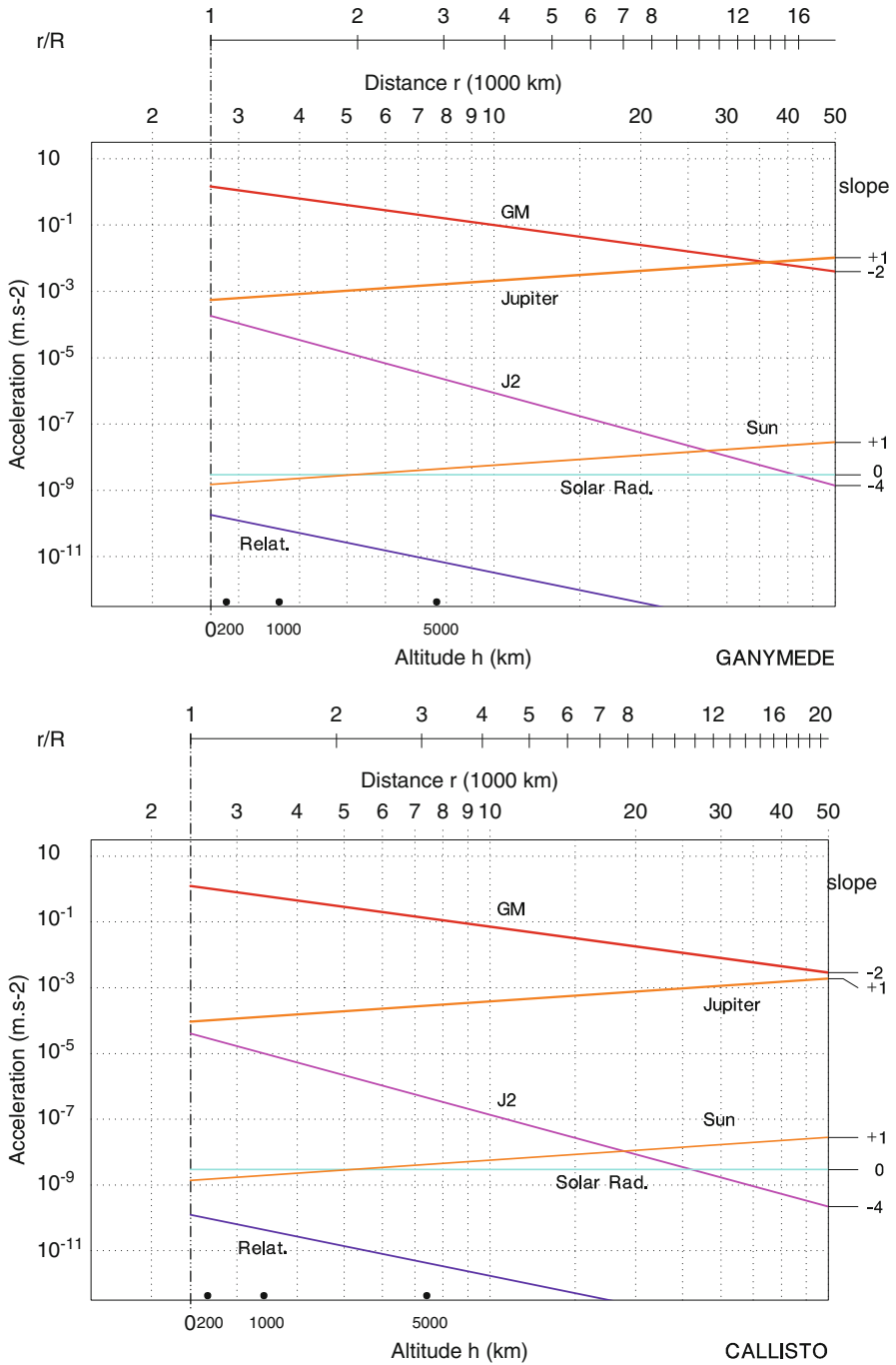


FIG. 16.30: Accelerations as a function of the distance  $r$  of the satellite from the center of the natural satellite. Log-log scale. Upper: Ganymede. Lower: Callisto.

$$\rho_{\Sigma} = 2^{-1/5} \left( \frac{\mu_N}{\mu} \right)^{2/5} a_P . \quad (16.8)$$

The satellite must stay within the sphere of influence, i.e., it must satisfy the inequality

$$a_{GS} < \rho_{\Sigma} . \quad (16.9)$$

Hence, with the values obtained from (16.7) and (16.8),

$$\left( \frac{\mu_N}{\mu} \right)^{5/3} < \frac{1}{2} \left( \frac{\mu_N}{\mu} \right)^2 .$$

Finally,

$$\mu_N > 8\mu . \quad (16.10)$$

But this condition is obviously absurd. A natural satellite cannot have greater mass than the central planet. It is thus impossible to obtain a stationary orbit for a satellite of a natural satellite.<sup>48</sup> ◀

### Sun-Synchronous Satellite

We now study the case of a satellite in Sun-synchronous orbit around a natural satellite. We can calculate the constant of Syn-synchronicity using (7.98). We can also find a relation between  $k_{hN}$  and  $k_{hP}$ , the Sun-synchronicity constants for satellites in orbit around a natural satellite N and around the central planet P, respectively. With the corresponding subscripts, we can write

$$k_{hN} = \frac{3}{2} \frac{T_{\text{sid}}}{T_{0(h=0)N}} J_{2N} , \quad k_{hP} = \frac{3}{2} \frac{T_{\text{sid}}}{T_{0(h=0)P}} J_{2P} .$$

It is important to note that the sidereal period of revolution  $T_{\text{sid}}$  is the same in both cases: the natural satellite N takes the same time as the planet P to accomplish one revolution around the Sun. We obtain

$$\frac{k_{hN}}{k_{hP}} = \frac{J_{2N} T_{0(h=0)P}}{J_{2P} T_{0(h=0)N}} . \quad (16.11)$$

---

<sup>48</sup>In a certain sense, the Lagrange points provide one way of having a stationary position. If a satellite is stationary with respect to a natural satellite, it is also stationary with respect to the planet, because of the synchronous rotation of the natural satellite. This happens when it occupies one of the five Lagrange points. It then remains fixed relative to the natural satellite–planet system. Only the positions  $L_4$  and  $L_5$  are stable. When the satellite is located at  $L_4$  or  $L_5$ , it forms an equilateral triangle with the planet and the natural satellite. In the case of the Moon and Earth, the satellite is thus located some 380,000 km from the natural satellite. Needless to say, this is not much use for an observation satellite. The mission STARS, since abandoned in this form, was envisaged for the  $L_5$  point of the Earth–Moon system, but the aim was not to observe the Moon.

Using (16.2) or (16.3) with the mean densities, we then have

$$\frac{k_{hN}}{k_{hP}} = \sqrt{\frac{d_N}{d_P} \frac{J_{2N}}{J_{2P}}} . \quad (16.12)$$

We now return to the natural satellites investigated here. For the Moon and Europa, the reader is referred to Fig. 16.29, which indicates the different accelerations. For the Moon, the calculation of the Syn-synchronicity constant  $k_h = k_{hN}$  using (16.12) yields

$$k_h = 1.4725 .$$

This in turn implies a minimal inclination of

$$i_{HS \min} = 133^\circ .$$

For a satellite in low orbit around the Moon (LLO, Lunar Low Orbiting), the perturbing acceleration  $\gamma_{CC1}$  due to the Earth is less than the perturbing acceleration  $\gamma_{CCN.J2}$  due to flattening. If the LLO satellite is in Sun-synchronous orbit, the effect of the Earth, which is one tenth the effect due to the  $J_2$  term of the Moon, would soon remove the satellite from this Sun-synchronous orbit, in a matter of a few days.

For Europa, the situation is more radical. The term  $\gamma_{CC1}$  is always greater than  $\gamma_{CCN.J2}$ , even at zero altitude. The perturbation due to Jupiter's gravity is greater than the one due to the flattening of Europa, whatever the altitude of the satellite. There is therefore no hope of obtaining a Sun-synchronous orbit for a satellite around Europa.

### Frozen Orbit

Owing to a lack of accurate data concerning the natural satellites, we can only investigate frozen orbits for satellites around the Moon. In the case of our own natural satellite, the spherical harmonic coefficients of the gravitational potential are well documented (see Table 16.9).

For a satellite in low near-polar orbit (with frozen perigee  $\omega_F = 270^\circ$  since  $J_3 > 0$ ), the frozen eccentricity  $e_F$  can be approximately calculated using (11.57), which gives  $e_F \approx 0.02$ . This is relatively high for a frozen eccentricity. For other inclinations,  $e_F$  can take values between 0.01 and 0.001. These calculations are complicated by the presence of the  $J_7$  term, whose value is rather large here.

## 16.8 Ground Track of a Satellite of a Natural Satellite

### 16.8.1 Satellites of the Moon

After the conquest of the Moon (1959–1972), discussed at the beginning of the chapter in the more general context of space exploration, followed by

$J_2 = 203.236626$	$J_5 = 0.715409$	$J_8 = -9.674866$
$J_3 = 8.475906$	$J_6 = -13.577715$	$J_9 = 15.496033$
$J_4 = -9.591929$	$J_7 = -21.774733$	$J_{10} = 4.267023$

TABLE 16.9 : Values of the coefficients ( $J_n \times 10^6$ ) of the gravitational potential of the Moon in the LPLGM model.

the three Soviet Luna probes (1974–1976), no more probes and orbiters were sent to the Moon for almost two decades (Fig. 16.31 and 16.32).

The Deep Space Probe Science Experiment (DSPSE), known as Clementine, launched on 25 January 1994, went into lunar orbit for 70 days and drew up a very accurate topographic map of the Moon. It had a highly eccentric orbit with  $h_p = 412$  km for the pericenter, or periselene, and  $h_a = 2,940$  km for the apocenter or aposelene. It then failed in its encounter with the asteroid 1620-Geographos. The probe Lunar Prospector, launched on 7 January 1998, went into a near-circular near-polar orbit with  $h = 100$  km, then  $h = 40$  and  $h = 30$  km. It then deliberately impacted the Moon near the South Pole in a controlled crash to look for evidence of water ice, but none was found.

Lunar gravitational potential models first used laser ranging measurements (LLR, Lunar Laser Ranging) carried out by means of reflectors set up on the Moon, then the satellites Lunar Orbiter-1 to -5, Apollo-15 and -16, and Clementine for the models GLGM-1 and 2 (Goddard Lunar Gravity Model). The model known as LPLGM (Lunar Prospector Lunar Gravity Model) also used Lunar Prospector (see Table 16.10).

The European probe SMART-1, launched on 27 September 2003, remained for more than a year, until 2 November 2004, in orbit around the Earth. Then, from 15 November 2004, it revolved around the Moon until it was deliberately crashed on 3 September 2006. The main aim was not so much to study the Moon as to test the newly developed ion drive technology.

In 2007 and 2008, three Asian countries carried out successful missions to the Moon. The Japanese mission Selenological and Engineering Explorer (Selene), renamed Kaguya after the launch on 14 September 2007, comprises a main satellite ( $h = 100$  km) and two auxiliary satellites, Okina (Rstar or Relay Sat,  $h_p = 100$  km,  $h_a = 2,400$  km) and Ouna (Vstar or V RAD Sat,  $h_p = 100$  km,  $h_a = 800$  km). The main satellite was then put in a very low orbit with  $h_p = 20$  km,  $h_a = 50$  km, and subsequently projected onto the lunar surface on 10 June 2009. All these orbits are polar, i.e.,  $i = 90^\circ$ . Japan had already launched the satellite Hiten (Muses-A) in 1990.

The main aim of the Chinese missions Chang'E (the name of a Chinese Moon god) was to map the Moon and prepare manned missions. Chang'E-1, launched on 14 October 2007, went into a circular polar orbit with  $h = 200$  km, crashing into the surface on 1 March 2009, and Chang'E-2, launched on 1 October 2010, went into a circular polar orbit with  $h = 100$  km, then an elliptical orbit with  $h_p = 15$  km,  $h_a = 100$  km.



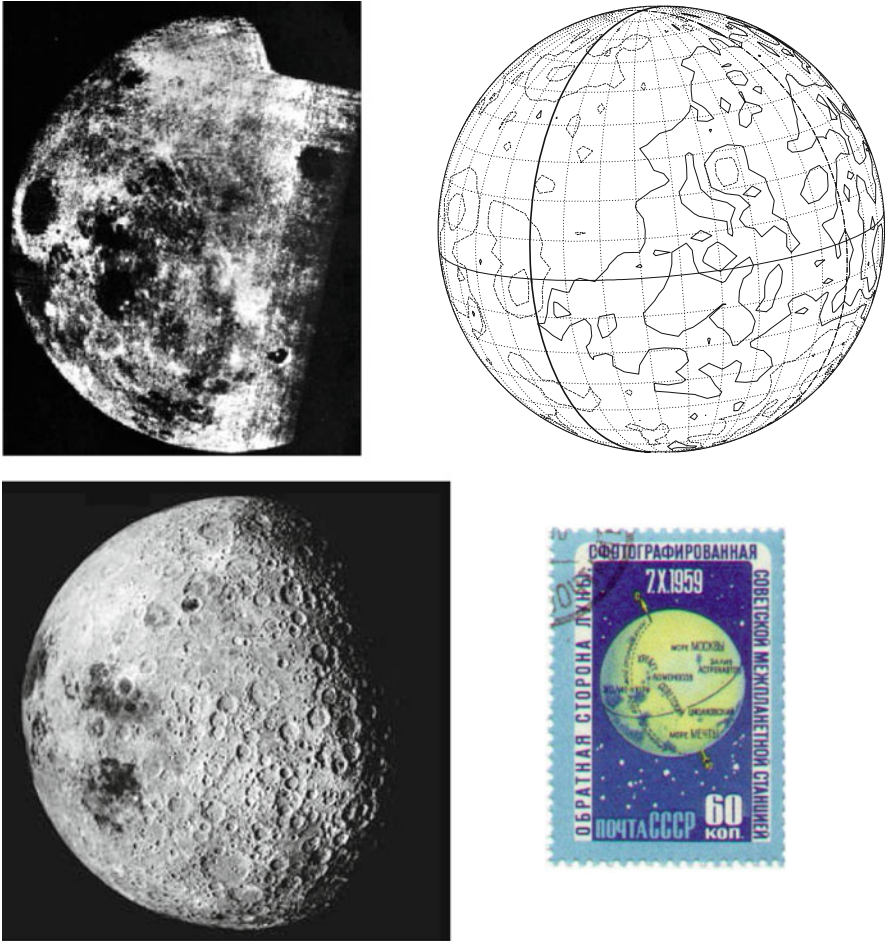


FIG. 16.31 : Images of the hidden face of the Moon. Upper left: Historic photograph taken by Luna-3 on 7 October 1959, during a flyby at altitude 66,000 km. Credit: USSR Academy of Sciences. Upper right: Ixion/Atlas reconstitution of the Moon seen by Luna-3 when the image was taken. The meridian (continuous curve) demarcates the visible face (to the west, on the left) of the hidden face (to the east, on the right). Lower left: View corresponding to the historic photograph, but built up from images obtained by American missions. Credit: NASA.

The Indian satellite Chandrayaan-1 (from *chandra*, meaning “Moon” and *yaan*, meaning “ship”), launched on 22 October 2008, went into circular polar orbit with  $h = 100$  km on 12 November 2008.

Projection: Orthographic Pr. centre (r.): 5.0 ° S; 0.0 °  
 Property: none Aspect: Oblique  
 © T.:Azimuthal - Graticule: 10° 3.5[[-90.0/+95.0/+90.0] [-] Ιξίων  
MC \* LMD  
Ατλας  
Clementine Topogr. /h/2km/

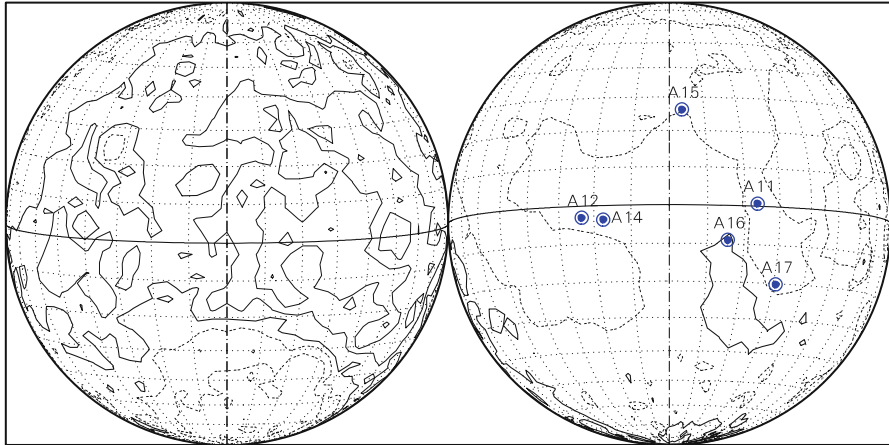


FIG. 16.32 : Landing sites of the 6 Apollo missions. It is no surprise to find that they are all on the visible face of the Moon.

Method used	Year	$\mu$ (km <sup>3</sup> s <sup>-2</sup> )	Error
Laser, LO-4	1980	4,902.799	±0.003
GLGM-1	1993	4,902.8026	±0.0001
GLGM-2	1997	4,902.8029	±0.0002
LPLGM	1999	4,902.80106	±0.00008

TABLE 16.10 : Measured values of the selenocentric gravitational constant  $\mu = GM$  with the estimated error. Historical evolution, mentioning the method used and the year.

American interest in the Moon has been rekindled in the form of their Constellation programme.<sup>49</sup> One part of this vast framework was the Lunar Precursor Robotic (LPR), which led to the launch of the dual mission LRO-LCROSS on 18 June 2009. On 23 June, the Lunar Reconnaissance Orbiter (LRO) went into circular polar orbit with  $h = 50$  km. The aims were mapping and improving the geodetic model (see Figs. 16.33 and 16.36). It carried seven instruments, including the Diviner Lunar Radiometer Experiment (DLRE) to

<sup>49</sup>This programme, launched in 2004 under G.W. Bush, was as ambitious as the Apollo programme at the time of J.F. Kennedy. The aim was to go to the Moon, and from there to Mars. However, this was revised under the Obama presidency. The lunar stage could be dropped and replaced by a manned visit to an asteroid. To be continued.

measure the surface temperature. It identified certain places, such as craters, at the South Pole, that would not have seen sunlight for billions of years, just the kind of places where water ice might be trapped. The surface temperature map of the south polar region shown in Fig. 16.37 (upper) is witness to LRO's near-polar orbit. The data were acquired from September to October 2009, when the temperatures in this region would have been at their maximum. The crater chosen to receive the impact of the Lunar Crater Observation and Sensing Satellite (LCROSS) is indicated with a white circle in the figure. It is one of the coldest points on the Moon (about 40 K, or  $-230^\circ\text{C}$ ). The 3D map of the South Pole in Fig. 16.37 (lower), indicating temperatures, locates the point of impact of LCROSS,<sup>50</sup> which occurred on 9 October 2009. Analysis of the particles thrown up by the impact did indeed reveal the presence of water ice.

The Gravity Recovery and Interior Laboratory (GRAIL) mission is the equivalent for the Moon of GRACE for the Earth, with two satellites, one following the other. Their orbit is circular polar and the distance between GRAIL-A and -B is 175–225 km depending on the different phases of the mission.<sup>51</sup> The altitude  $h = 53$  km at the beginning of the mission went to 23, then 11.5 km. GRAIL enormously improved our understanding of the geopotential and the internal structure of the Moon.

In the following examples, we consider several revolutions of the ground track of Clementine. But in recognition of the great era of lunar exploration, we begin with a thought for Luna-3 and Apollo-15. In all maps of the Moon, we have marked the meridians  $90^\circ\text{E}$  and  $90^\circ\text{W}$  which symbolically divide the visible and hidden faces.

**Example 16.6** *Discovery of the hidden face of the Moon.*



*The Soviet probe Luna-3 was launched on 4 October 1959 and overflew the hidden face of the Moon on 7 October. Unlike its successors, in heliocentric orbit, Luna-3 was in fact a satellite of the Earth, on a highly eccentric orbit, with radius at apogee  $r_a = 469,000$  km and period 16.2 days. (However, it also appears under the entry “space probe” in the index.) Indeed, it burnt up in the Earth atmosphere in April 1960.*

<sup>50</sup>The satellite LCROSS, which remained attached to the last stage of the Centaur rocket, went into a highly eccentric geocentric orbit, overflying the Moon ( $T = 36$  day). After three revolutions, the rocket was detached and crashed into the Moon. The impact was photographed and analysed by LCROSS, which was following it, and which itself ended up crashing into the surface close to the South Pole just 5 min later.

<sup>51</sup>The two satellites GRAIL-A and -B (also named Ebb and Flow, respectively) were launched together on 10 September 2011, then placed separately in lunar orbit on 31 De-

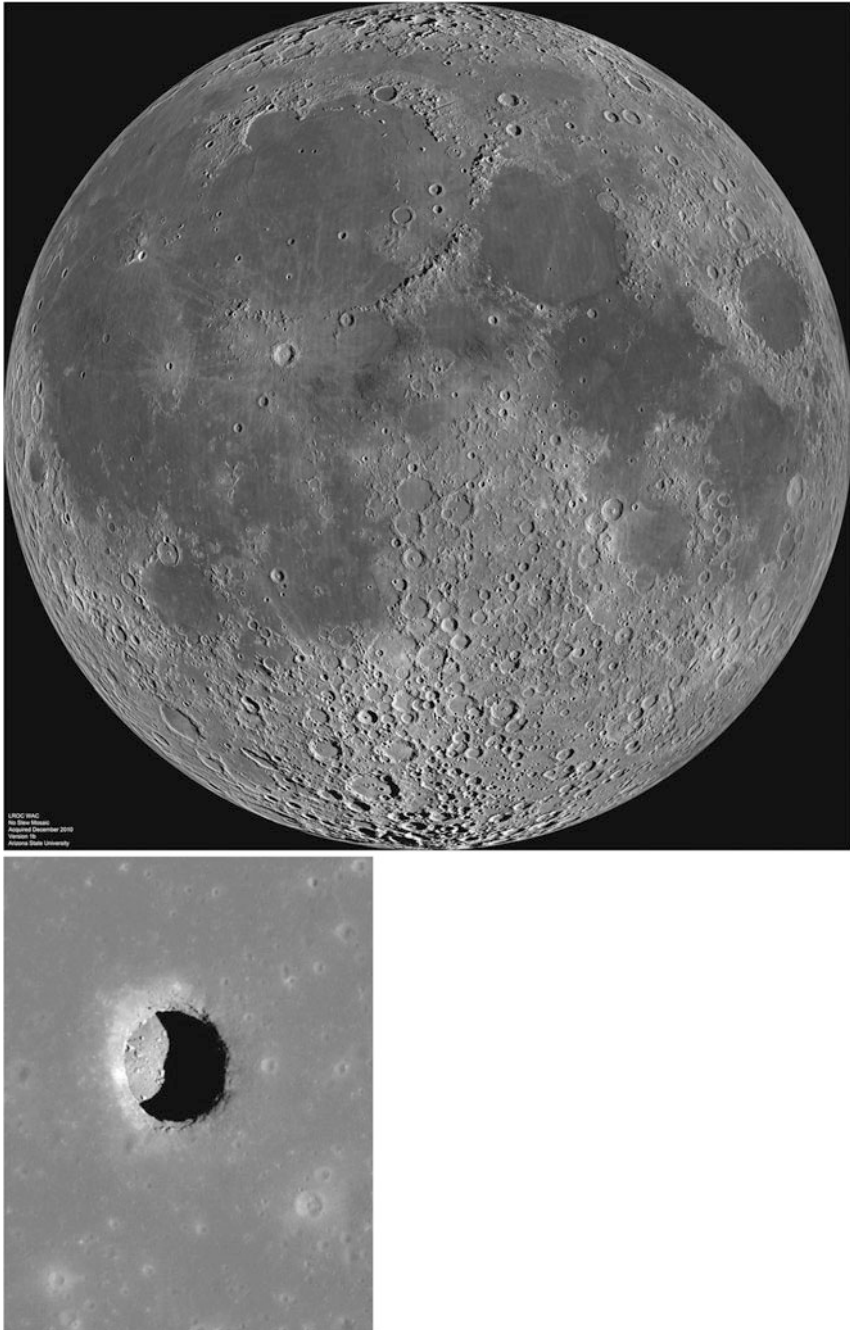


FIG. 16.33 : Image of the hidden face of the Moon, obtained by assembling 1,300 images acquired by the Wide Angle Camera (WAC) aboard the LRO over 2 weeks in mid-December 2010. Left: Detail obtained with the same camera. Chasm of diameter 80 m and depth 100 m (estimated by examining the shadow), located in Mare Tranquillitatis. Credit: NASA, GSFC, Arizona State University.

► The historic photograph of the hidden face is shown in Fig. 16.31. Next to it is a representation of the Moon viewed under the same conditions from a distance of 38 lunar radii. On the left of the photograph and the map is a part of the visible face featuring the dark region of Mare Crisium (centered on  $17.0^{\circ}\text{N}$ ,  $59.1^{\circ}\text{E}$ ).

The hidden face, incompletely photographed by Luna-3, was soon to be better revealed by Zond-3, then fully mapped by the US orbiters (Orbiter-3, -4, Explorer-35, Orbiter-5), as they prepared in 1967 the landing areas for the Apollo programme. It was thus discovered the two faces looked rather different, as can be clearly seen from the map shown in Fig. 16.34 (lower). This difference arises because the lunar crust is thicker on the hidden face than on the visible face, surely a consequence of the tidal effect. The wide basins on the hidden face are not filled with basalts from ancient lava flows, as they are on the visible face. These features have been known as “seas” since ancient times. ◀

**Example 16.7** *Ground track of the Apollo-15 lunar orbiter during its geochemical mapping mission.*

► For the manned Apollo missions to the lunar surface, the capsule remained in lunar orbit with an astronaut aboard (see Fig. 16.34 upper). The other two astronauts in the lunar module (LM) left the capsule to soft land on the Moon. After 1 or 2 days (and six for Apollo-16), they returned to the capsule, which then left its lunar orbit to return to Earth.

During the Apollo-15 mission, the orbiting command module carried out a geochemical mapping experiment, in fact measuring the gamma radiation from the surface, resulting from natural radioactivity of the crust. The ground track of the orbit is shown during this experiment, over 4 days from 1 to 4 August 1971 (see Fig. 16.34 lower). The landing site for this mission was at  $26.10^{\circ}\text{N}$ ,  $3.65^{\circ}\text{E}$ , on the boundary of the maximal attained latitude. The circle of visibility of this point for the satellite is indicated in the figure. As soon as the ground track of the satellite enters this circle, it can be seen from the landing site. The astronauts on the surface did not have long in which to communicate with the orbiter! We see here how little of the surface is scanned in the case of a lunar orbit.

**Note on the Cartography.** The Moon has been shown in Fig. 16.34 (lower) using an interrupted Mollweide projection, in which the central disk represents the visible face. Altitudes are lower than on the hidden face. ◀

---

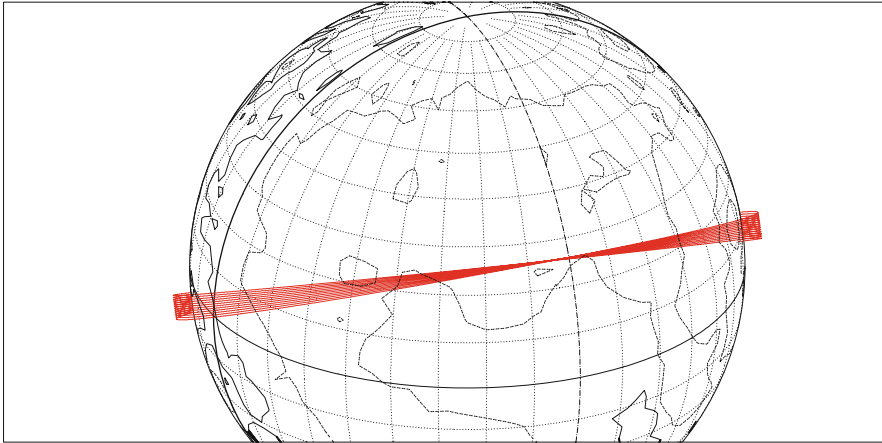
ember 2011 and the following day. The mission ended on 17 December 2012, with a double impact on the Moon.



**[MOON] Apollo-15 (Orbiter)**  
Orbit - ref.: Lune

>>>> Time span shown: 1440.0 min = 1.00 day

Altitude = 113.3 km                      a = 1851.300 km  
Inclination = 154.00 °  
Period = 119.06 min    \* rev/day =12.10  
Equat. orbital shift = 30.2 km ( 1.0 °)

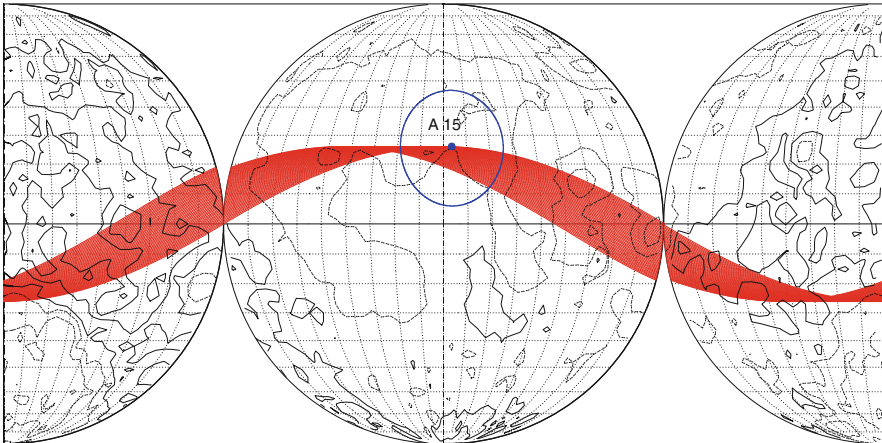


Projection: Orthographic    PC: 26.0 ° N; 24.0 ° W/ZC: 35.0 ° N; 30.0 ° W    Asc. Node: 90.50 °                      *Ιξίων*  
Property: none                      Aspect: Oblique                      MC ★ LMD  
⊞ T.:Azimuthal - Graticule: 10° [3.5] [-90.0/+64.0/+114.0] [-] LPLGM    *Clementine Topogr. / h / 2km / Ατλας*

**[MOON] Apollo-15 (Orbiter)**  
Orbit - Ground track

>>>> Time span shown: 5443.2 min = 3.78 days

Altitude = 113.3 km                      a = 1851.300 km  
Inclination = 154.00 °  
Period = 119.06 min    \* rev/day =12.10  
**Visibility circle for h = 0°**



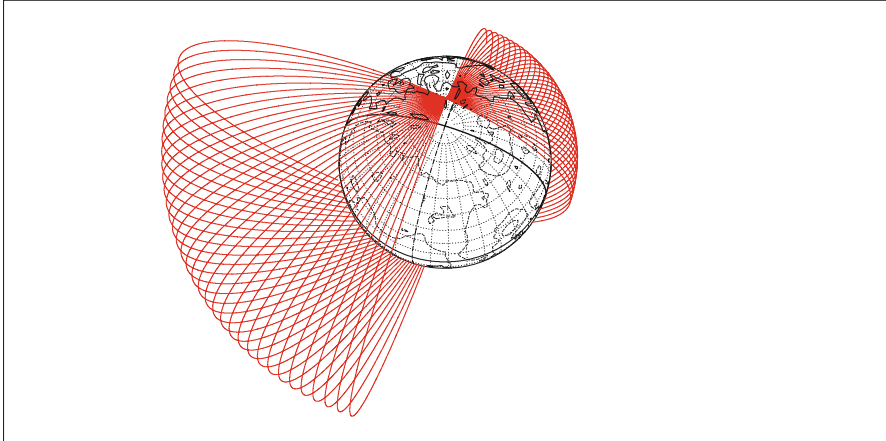
Projection: Mollweide                      Project. centre: 0.0 ° ; 0.0 °                      Asc. Node: 90.50 °                      *Ιξίων*  
Property: Equal area                      Aspect: Direct [interrupted]                      App. inclin. = 154.07 °                      MC ★ LMD  
⊞ T.:Pseudocyl. - Graticule: 10° [3.5] [+90.0/ +0.0/ -90.0] [-] LPLGM    *Clementine Topogr. /h/2km/ Ατλας*

FIG. 16.34 : Upper: Orbit of the lunar satellite Apollo-15 (Orbiter), over 1 day. Lower: Ground track of the orbit over 4 days (geochemical mapping mission), showing the viewing circle for the ground module A15.

**[MOON]** Clementine  
Orbit - ref.: Lune

>>>> Time span shown: 7.00 days

Equiv. altit. = 1675.3 km      a = 3413.300 km  
 Inclination = 91.00 °      e = 0.370300  
 Period = 298.27 min \* rev/day = 4.83  
 h\_a = 2939 km; h\_p = 411 km; arg.periapsis: -12.00 °



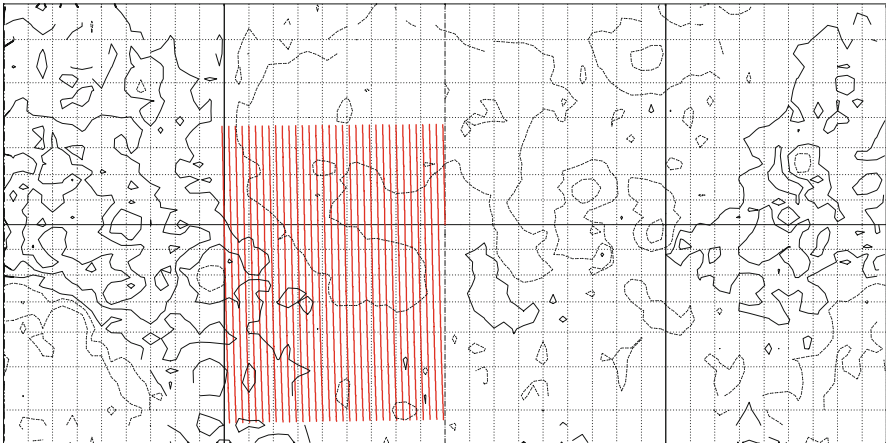
Projection: Orthographic      Project. centre: 70.0 ° N; 18.0 ° E      Longitude / Initialisation:      *Ιξίων*  
 Property: none      Aspect: Oblique      N.a.: 179.80 ° - Apo.: 178.69 °      MC ★ LMD  
 ( T.:Azimuthal - Graticule: 10° {3.5} [-90.0/ +20.0/ +72.0] [-] LPLGM *Clementine Topogr. / h/2km /*      Ατλας

**[MOON]** Clementine

Gr.tr. (H < 640 km) [ H : geodetic altitude ]

>>>> Time span shown: 7.00 days

Equiv. altit. = 1675.3 km      a = 3413.300 km  
 Inclination = 91.00 °      e = 0.370300  
 Period = 298.27 min \* rev/day = 4.83  
 h\_a = 2939 km; h\_p = 411 km; arg.periapsis: -12.00 °



Projection: Mercator      Project. centre: 0.0 ° ; 0.0 °      Longitude / Initialisation:      *Ιξίων*  
 Property: Conformal      Aspect: Direct      N.a.: 0.00 ° - Apo.: -1.11 °      MC ★ LMD  
 ( T.:Cylindrical - Graticule: 10° {3.5} [+90.0/ +0.0/ -90.0] [-] LPLGM *Clementine Topogr. / h / 2km /*      Ατλας

FIG. 16.35 : *Clementine*. Upper: Orbit over 7 days (a quarter of a month). Lower: Ground track for altitudes below 640 km (where the laser altimeter functions correctly).

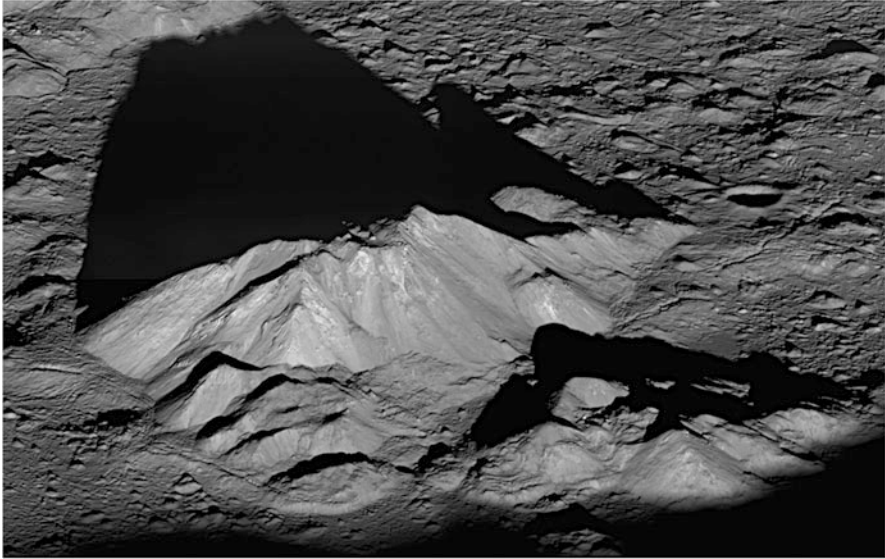


FIG. 16.36 : Image of the central peak of the Tycho crater taken at sunrise on 10 June 2011 by the LRO with a resolution of 1.5 m/pixel. The Tycho crater in the southern hemisphere with its radiating ejecta is one of the most prominent features of the Moon. The crater has a diameter of 85 km, and the central peak a width of 15 km and a height of 2 km above the floor of the crater. Credit: NASA, GSFC, Arizona State University, LRO Team.

**Example 16.8** *Ground track of the satellite Clementine.*

► In its lunar mapping mission, the probe Clementine followed the highly eccentric polar orbit shown in Fig. 16.35 (upper), with pericenter (periselene) at a latitude of  $28^{\circ}\text{S}$  during the first month and  $29^{\circ}\text{N}$  during the second. Indeed, each measurement cycle lasted 1 month, the time required by the satellite to observe the whole of the Moon, since this is in fact the time it required to rotate about its own axis in the Galilean frame. The ground track of the orbit is shown in the two parts of Fig. 16.35 (lower), over 2 days, i.e., 9.5 revolutions ( $T = 5\text{ h}$ ). These are revolutions 103 to 112, on 13 and 14 March 1994 (cycle 1).

Among its instruments, Clementine carried a LIDAR-type laser altimeter (Clementine Laser Image Detection And Ranging) which could only function for altitudes below 640 km. The ground track of the LIDAR is shown over 7 days in Fig. 16.35 (lower). ◀



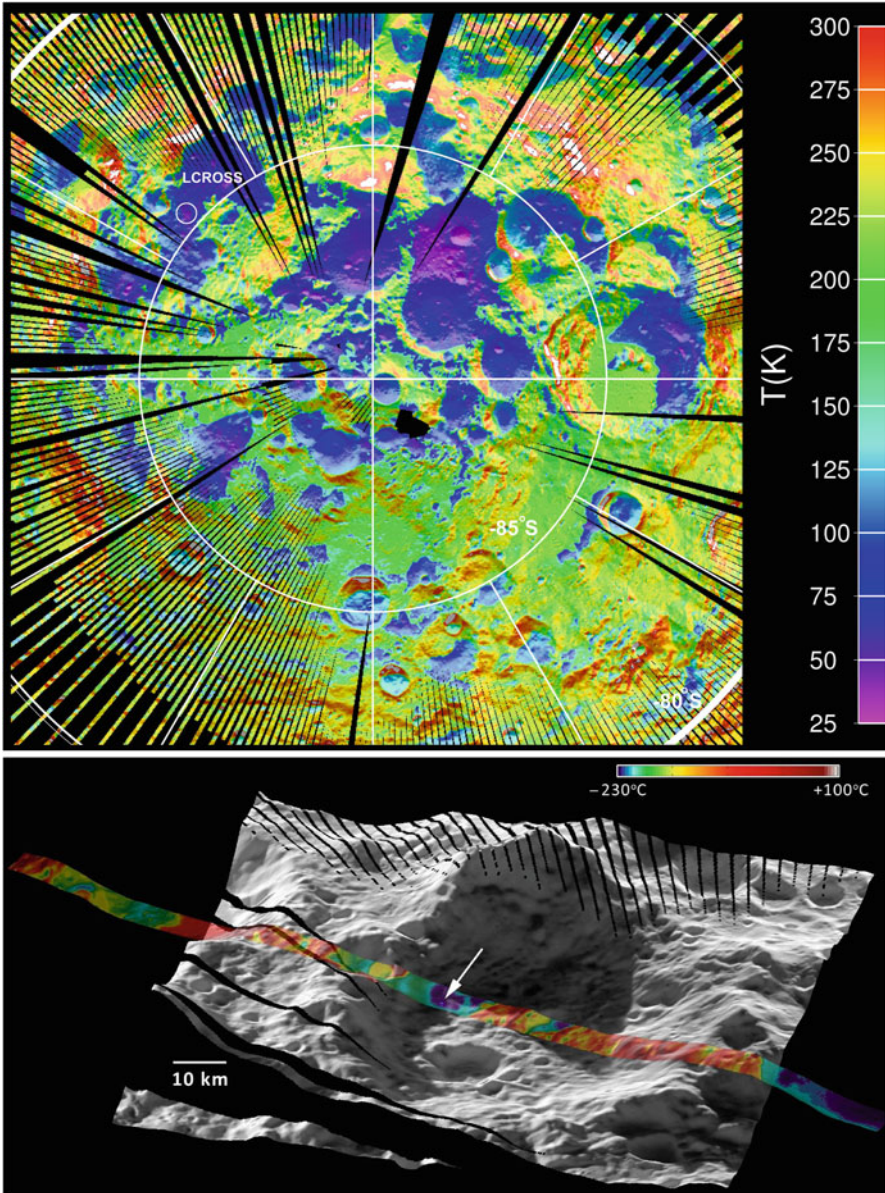


FIG. 16.37 : Upper: *Temperature map of the south polar region of the Moon produced by the LRO.* Lower: *Three-dimensional map of the South Pole, indicating the temperature and location of the LCROSS impact.* Credit: NASA, JPL, UCLA.

## 16.8.2 Satellites of Europa and Ganymede

After Juno, mainly dedicated to Jupiter, the next mission to the giant planet will be JUICE, which will turn its attention to the four Galilean moons. These four large natural satellites of Jupiter each have between half and twice the mass of the Moon. As one moves away from Jupiter, they are Io, Europa, Ganymede, and Callisto. Their motions are related by several resonances.<sup>52</sup> Images of Voyager-1 and -2, refined by those of Galileo, have given us a quite detailed understanding of these satellites (Fig. 16.36).

There are more than 400 frequently erupting volcanoes scattered across Io. This volcanic activity cannot be put down to plate tectonics, but is rather due to the release of heat resulting from the enormous tidal forces produced by Jupiter (Fig. 16.37).

Europa is covered with water ice at temperatures of 110 K at the equator and 50 K at the poles (see Fig. 16.38). Since it appears to have an internal source of heat, undoubtedly due to tidal effects, this suggests that there may be an ocean of liquid water beneath the frozen surface. Hence the enthusiasm of planetary scientists for further exploration!

Ganymede is the largest natural satellite in the Solar System. It has two clearly differentiated types of surface: one is a dark, heavily cratered terrain, the other an icy crust, scarred with grooves. This moon has a magnetosphere. It is thought that there may be a vast ocean of liquid salt water some 150 km below the surface.

Callisto has a rather regular surface, without mountains, and is rather evenly scattered with craters. This moon may also conceal an ocean below the surface.

At the present time, Europa and Ganymede have inspired the most interest for space missions. For example, EJSM-Laplace was a joint NASA–ESA project (EJSM stands for the Europa–Jupiter System Mission, while the mention of Laplace is a homage to the French astronomer), built up from US<sup>53</sup> and European missions that had been planned separately. This mission<sup>54</sup> involved two satellites, the Jupiter Ganymede Orbiter (JGO), developed by the ESA, and the Jupiter Europa Orbiter (JEO), developed by NASA (see Fig. 16.39).

---

<sup>52</sup>There are relations between the mean motions  $n_i$  of the first three Galilean satellites ( $i = 1-3$ ). This is in fact the Laplace resonance:

$$n_1 - 2n_2 = n_2 - 2n_3 = 0.7396 \text{ deg/day} .$$

<sup>53</sup>NASA had gone a long way with the preparatory studies for the Jupiter Icy Moons Orbiter (JIMO), which would have sent an orbiter to circle Europa for 2 months, Ganymede for 4 months, and Callisto for 4 more months. The project was abandoned in 2005.

<sup>54</sup>The journey, following the VEEGA pattern, would have lasted 6 years. After Jovian orbit insertion (JOI), each probe was to fly several times past each of the four Galilean moons before going into orbit around Europa (EOI) in the case of JEO and around Ganymede (GOI) in the case of JGO.

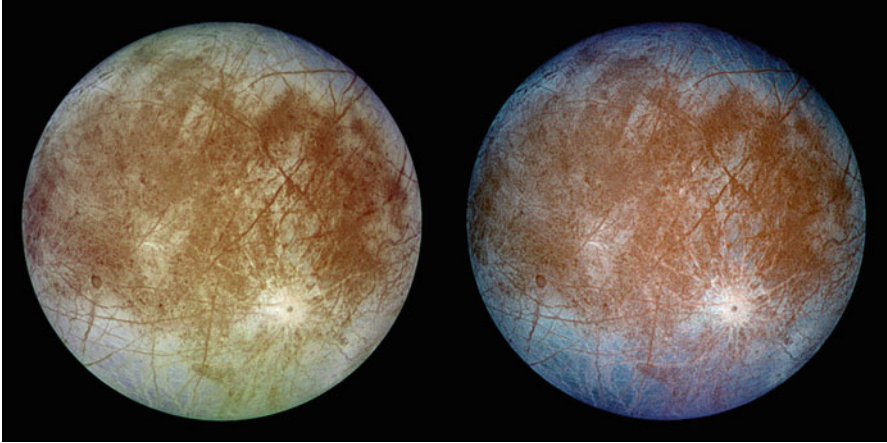


FIG. 16.38 : Two views of the trailing hemisphere of Europa. The left image shows the approximate natural color appearance of Europa. The image on the right is a false-color composite version combining violet, green, and infrared images to enhance color differences in the predominantly water-ice crust of Europa. Dark brown areas represent rocky material. Bright plains in the polar areas are shown in tones of blue. Long, dark lines are fractures in the crust, some of which are more than 3,000 km long. Image taken on 7 September 1996, at a range of 677,000 km, by the camera on board the Galileo spacecraft during its second orbit around Jupiter. Image processed by DLR, Berlin. Credit (image and caption): NASA, JPL, DLR.

When NASA withdrew in April 2011, the ESA transformed EJSM-Laplace/JGO into the Jupiter Icy Moon Explorer (JUICE). After an 8 year journey following the EVEEGA pattern, JUICE will fly by all the Galilean moons except Io, then go into near-polar orbit at  $h = 200$  km around Ganymede (see Fig. 16.40 upper).

### 16.8.3 Satellites of Titan

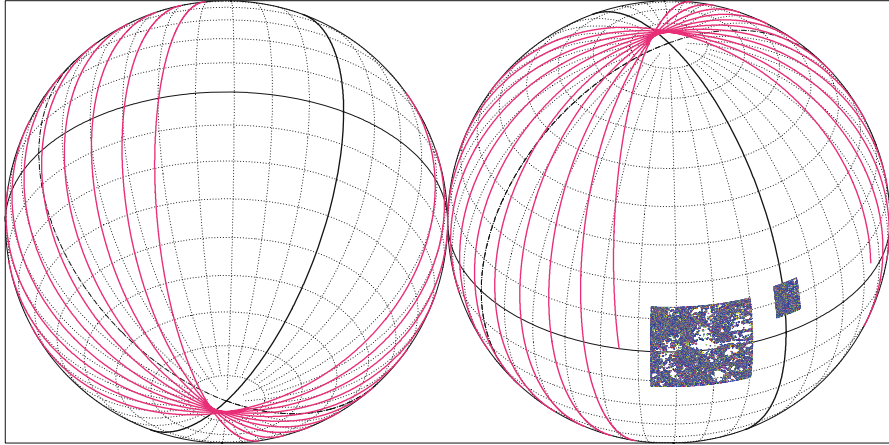
The natural satellite Titan is in equatorial orbit, with a rather high eccentricity, around Saturn. It was discovered by Huygens in 1655 and he gave it the name *Luna Saturni*. In terms of its size and mass, it is the second natural satellite of the Solar System, just after Ganymede. The atmosphere of Titan is 4.5 denser than the atmosphere of the Earth (at ground level, 1.5 bar with absolute temperature only one third of that on Earth). Photochemical reactions abound due to solar UV radiation, leading to the synthesis of an aerosol layer which masks the surface in the visible. Images taken by Voyager-1 do not show the ground, only the cloud cover. The Cassini–Huygens mission has given us a much more detailed view.

The Huygens module was released by the Cassini probe on 14 January 2005, and dropped through the Titan atmosphere, protected by its

**[EUROPA] JEO (EJSM-Laplace)**  
Orbit - Ground track

>>>> Time span shown: 1440.0 min = 1.00 day

Altitude = 200.0 km      a = 1765.000 km  
Inclination = 95.00 °  
Period = 137.28 min \* rev/day = 10.49  
Equat. orbital shift = 263.5 km ( 9.6 °)

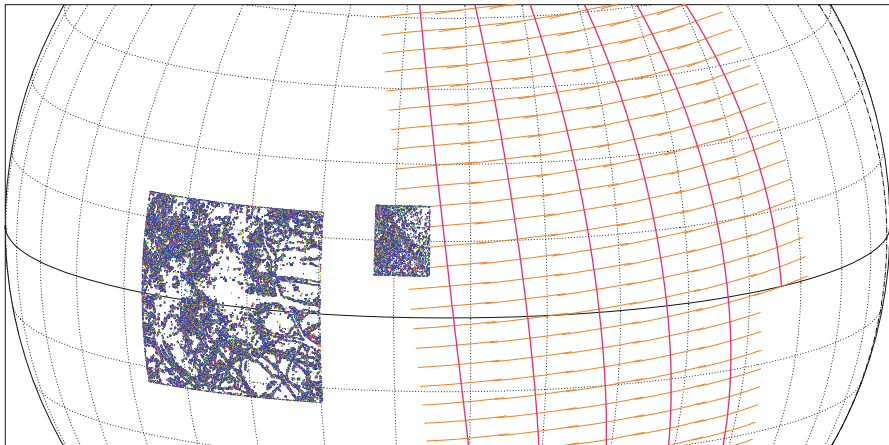


Projection: Orthographic      Pr. centre (r.): 36.0 ° N; 122.0 ° W      Asc. Node: -135.00 °      *Ιξίων*  
Property: none      Aspect: Oblique      MC ★ LMD  
⊞ T.:Azimuthal - Graticule: 10°      {4.7} [-90.0/+54.0/-148.0] [-]      Schub&a *Galileo Images*      Ατλας

**[EUROPA] JEO (EJSM-Laplace)**  
Orbit - Ground track

>>>> Time span shown: 720.0 min = 0.50 day  
Across track swath (XT mode)

Altitude = 200.0 km      a = 1765.000 km  
Inclination = 95.00 °  
Period = 137.28 min \* rev/day = 10.49  
Equat. orbital shift = 263.5 km ( 9.6 °)  
\*\* Half-swath: 35.0° => 144 km [ 1.00 min]



Projection: Orthographic      Project. centre: 12.0 ° N; 83.0 ° W      Asc. Node: -34.00 °      *Ιξίων*  
Property: none      Aspect: Oblique > zoom : 2.00      Latit. overlap: 89.7° <-> 90.0°      MC ★ LMD  
⊞ T.:Azimuthal - Graticule: 10°      {4.7} [-90.0/+78.0/+173.0] [-]      Schub&a *Galileo Images*      Ατλας

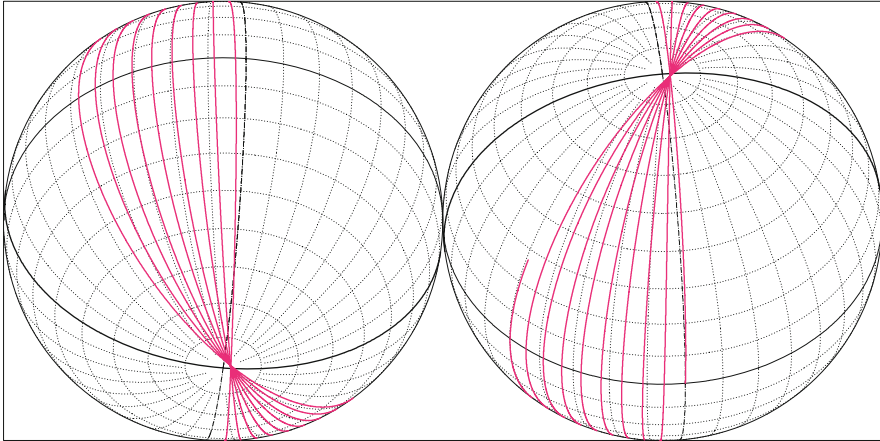
FIG. 16.39 : JEO, a satellite of Europa in the EJSM-Laplace project. Upper: Ground track over 1 day. Lower: Ground track over half a day, with ground track of the cross-track swath.



**[GANYMEDE] JUICE**  
Orbit - Ground track

>>>> Time span shown: 1440.0 min = 1.00 day

Altitude = 200.0 km      a = 2831.200 km  
Inclination = 88.00 °  
Period = 158.67 min \* rev/day = 9.08  
Equat. orbital shift = 254.7 km ( 5.5 °)

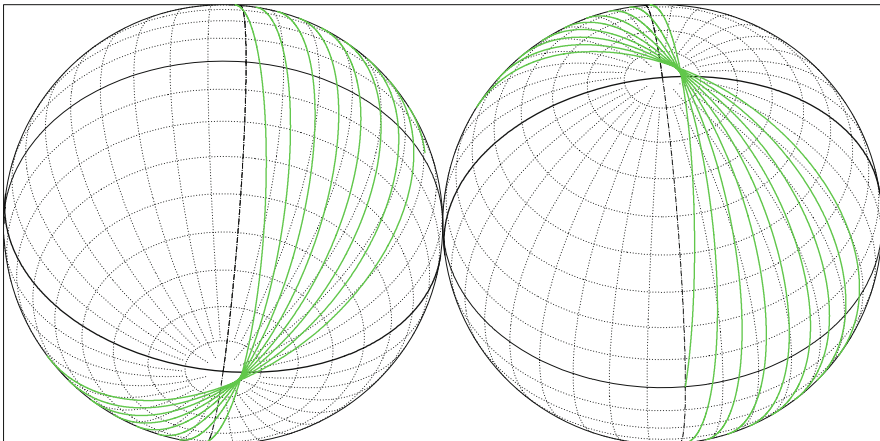


Projection: Orthographic      Pr. centre (r.): 48.0 ° N; 6.0 ° W      Asc. Node: 0.00 °      *Iξων*  
Property: none      Aspect: Oblique      MC ★ LMD  
⊞ T.:Azimuthal - Graticule: 10°      [-] [-90.0/ +42.0/ +96.0] [-] Schub&a      *Ατλας*

**[TRITON] Triton Orbiter**  
Orbit - Ground track

>>>> Time span shown: 1440.0 min = 1.00 day

Altitude = 200.0 km      a = 1552.600 km  
Inclination = 85.00 °  
Period = 169.58 min \* rev/day = 8.49  
Equat. orbital shift = -170.1 km ( -7.2 °)



Projection: Orthographic      Pr. centre (r.): 48.0 ° N; 6.0 ° W      Asc. Node: 0.00 °      *Iξων*  
Property: none      Aspect: Oblique      MC ★ LMD  
⊞ T.:Azimuthal - Graticule: 10°      [-] [-90.0/ +42.0/ +96.0] [-] Rubincam      *Δτλας*

FIG. 16.40 : Ground track of the orbit over 1 day. Upper: JGO, a satellite of Ganymede in the JUICE mission. Lower: Satellite of Triton.

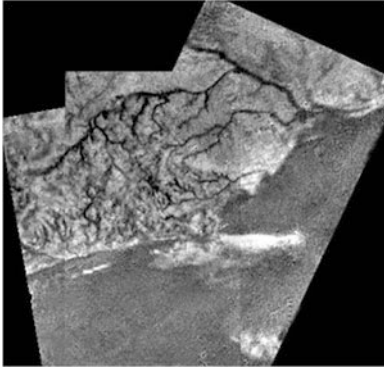


FIG. 16.41: Mosaic of three images acquired by the DISR instrument during the descent of the Huygens module on Titan on 14 January 2005, at an altitude of about 30 km: “Images show a complex network of narrow drainage channels running from brighter highlands to lower, flatter, dark regions. These channels merge into river systems running into lakebeds featuring offshore ‘islands’ and ‘shoals’ remarkably similar to those on Earth.” ESA communication of 21 January 2005. Credit: NASA, JPL, ESA, University of Arizona.

thermal shield. The landing was gentle thanks to its two parachutes, which both deployed correctly. During the 2 h descent, very high quality data and images were sent back, as exemplified in Fig. 16.41, obtained by the Descent Imager Spectral Radiometer (DISR).

The “geography” of Titan, i.e., erosion, river systems, dried-up lakes, coastal scenery, evidence of precipitation, etc., is similar to what we see on Earth, except that water has been replaced by methane ( $\text{CH}_4$ ). This can exist in both liquid or gaseous form on the surface of Titan. When it rains there, what falls is methane, mixed with traces of hydrocarbons. As mentioned at the beginning of this chapter, the Titan atmosphere is mainly composed of nitrogen, but contains 2% methane.

Radar images obtained by the Cassini probe during its many flybys have detected very large lakes of methane or ethane, such as Ontario Lacus,  $72^\circ\text{S}$ ,  $183^\circ\text{W}$ , of length 235 km (temperature 85 K, composition  $\text{CH}_4$  and  $\text{C}_2\text{H}_6$ , light hydrocarbons, and liquid nitrogen  $\text{N}_2$ ). We have already shown examples of specular reflection or Sun glint on the Earth, and even on Mars. Figure 16.42 shows the same effect on Titan, in an image acquired by Cassini, demonstrating the presence of a liquid surface on Titan.

The Cassini–Huygens mission opened the way to further studies of Titan, to the extent that both Europe and the US began to plan their own missions: for the ESA, TandEM (Titan and Enceladus Mission), a Saturn orbiter that would fly past Enceladus, then go into orbit around Titan and release a hot-air balloon into the Titan atmosphere; and for NASA, Titan Explorer, whose orbiter would go into orbit using aerobraking.

In 2009, the two space agencies decided to merge their missions into the Titan Saturn System Mission (TSSM). The orbiter will revolve around Saturn for 2 years, flying past Titan and Enceladus several times, before going into orbit around Titan. The orbiter will then send out two modules: a hot-air balloon that should remain at an altitude of 10 km for 6 months, to study the atmosphere and take accurate photographs of the surface; and a lander that

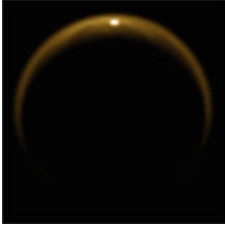


FIG. 16.42 : *First image of specular reflection or Sun glint on Titan, confirming the presence of a liquid surface. Image taken by the VIMS camera of the Cassini probe on 8 July 2009 during its 59th flyby of Titan, at a distance of about 200,000 km. Resolution 100 km/pixel. Credit: University of Arizona, Tucson.*

would soft land in a methane lake. The data collected by the two modules will be transmitted back to Earth via the orbiter. However, at the present time, TSSM would not appear to be a priority.

#### 16.8.4 Satellites of Triton

The natural satellite Triton is in a circular equatorial orbit around Neptune, with eccentricity  $e = 1.57 \times 10^{-5}$ . It was discovered by W. Lassell on 10 October 1846, just 2 weeks after the discovery of Neptune. As already mentioned, the rotation of Triton is synchronous with its revolution, which is retrograde. It is the only large natural satellite to revolve in this direction.

Most of what is known about Triton comes from images transmitted by Voyager-2. As far as it has been observed, these images show a cracked surface, rather like the skin of a melon, and referred to as a cantaloupe terrain (see Fig. 16.43). One can make out geysers of liquid nitrogen with solid nitrogen aerosols, whose plumes rise up to 8 km, attesting to cryovolcanism. Triton's very tenuous atmosphere has been identified using the method of stellar occultation. The inclination of its orbit with respect to the ecliptic creates a sequence of seasons, as on the Earth and Mars.

A mission to Triton would be a difficult undertaking, as it is a long way to Neptune, and it will be some time before we see a satellite in orbit around this icy body. However, Fig. 16.40 (lower) shows the ground track of a hypothetical Triton orbiter! The novelty here is that the shift occurs towards the east. Before bringing this book to a close, we had to find an example of a celestial body in the Solar System which goes round the “wrong” way!

## 16.9 Appendix: The Three Planetocentric Spheres

Three different spheres can be associated with any celestial body, such as a planet P, for example. The first two have already been discussed. Here we outline the third.

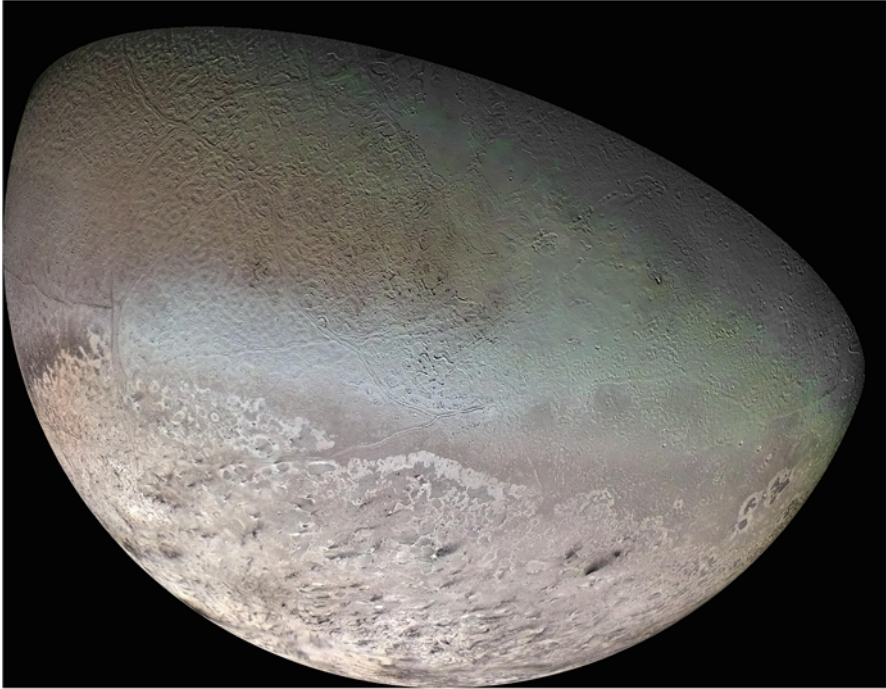


FIG. 16.43 : Triton was photographed on 25 August 1989 by Voyager-2, just after the probe had left Neptune. This image of the southern hemisphere is a mosaic of 12 views acquired from a distance of 530,000 km (pixel 10 km by 10 km). It is night in the northern region. The surface of Triton is extremely cold (37 K in the daytime) and very bright, being mainly composed of nitrogen ice. Credit: JPL, NASA.

## 16.9.1 Presenting the Three Spheres

### Sphere of Influence

The gravitational sphere of influence is defined to be the approximately spherical region centered on the planet P, within which any body is mainly subject to the gravitational attraction of P. It has radius  $\rho_{\Sigma}$  given by (6.158).

### Sphere of the Planetosynchronous Orbit

This is the sphere generated by all the circular orbits for which the revolving body has period equal to the rotational period of P. It has radius  $a_{GS}$  given by (7.69).

### Roche Limit

When a natural satellite N of a planet, characterised by its gravitational constant  $\mu_N$ , its radius  $R_N$ , and its average density  $d_N$ , comes too close to the host planet P, characterised likewise by  $\mu$ ,  $R$ , and  $d_P$ , it will be torn apart by



the action of tidal forces. Indeed, at such distances, these tidal forces will be stronger than the cohesive gravitational forces of the satellite, considered to be in hydrostatic equilibrium.

This limit  $D_R$  corresponds to the region where the differential acceleration defined by (6.151) is equal to the gravitational field of the satellite defined by (6.149):

$$\frac{\mu_N}{R_N^2} = 2R_N \frac{\mu}{D_R^3}. \quad (16.13)$$

We obtain  $D_R$  from this relation by bringing in the masses through  $\mu$  and  $\mu_N$ . A more careful calculation taking into account distortions of the hydrostatic equilibrium leads to a different numerical coefficient. The value generally accepted for this distance, which is known as the Roche limit,<sup>55</sup> is

$$D_R = 2.46 \left( \frac{d_P}{d_N} \right)^{1/3} R. \quad (16.14)$$

## 16.9.2 The Case of the Four Giant Planets

For these planets, the values of  $\mu$ ,  $R$ ,  $\rho_\Sigma$ , and  $a_{GS}$ , together with the average density  $d_P$  denoted here by  $d$ , can be found in Table 16.2. Figure 16.44 shows the planetosynchronous sphere and the Roche limit for the four giant planets of the Solar System. The gravitational sphere of influence has a much greater radius and is not relevant to this discussion, so has been omitted. To facilitate comparison, the radius  $R$  of each planet has been taken equal to unity. The figure also shows the nearby satellites and main (most visible) rings.

The synchronous orbit provides a theoretical separation of the natural satellites into two categories: those closer tend to move toward the planet, while those beyond tend to move away. This very slow displacement is due to tidal forces.<sup>56</sup>

To calculate the Roche limit, we have taken an average of the densities  $d_N$  over all the satellites of the host planet, although strictly speaking, there is a Roche limit for each natural satellite. We obtain:

- For Jupiter,  $D_R/R = 1.92$ , with  $d_N \approx 2.8$ .
- For Saturn,  $D_R/R = 2.18$ , with  $d_N \approx 1.0$ .
- For Uranus,  $D_R/R = 2.34$ , with  $d_N \approx 1.5$ .
- For Neptune,  $D_R/R = 2.73$ , with  $d_N \approx 1.2$ .

<sup>55</sup> *Edouard Roche* (1820–1883) was a French astronomer who devised a cosmogonic theory of the Solar System and studied the internal structure of the Earth. It was his combined understanding of astronomy and geophysics that led him in 1849 to establish an expression for the tidal forces exerted by a host body on its natural satellite.

<sup>56</sup> For example, in the case of the Earth and Moon, the latter is at a distance of  $60R$  from the Earth and  $a_{GS}/R = 6.61$ . The Moon thus moves away from the Earth by about 2 cm per year, as confirmed by laser ranging measurements of the Earth–Moon separation.

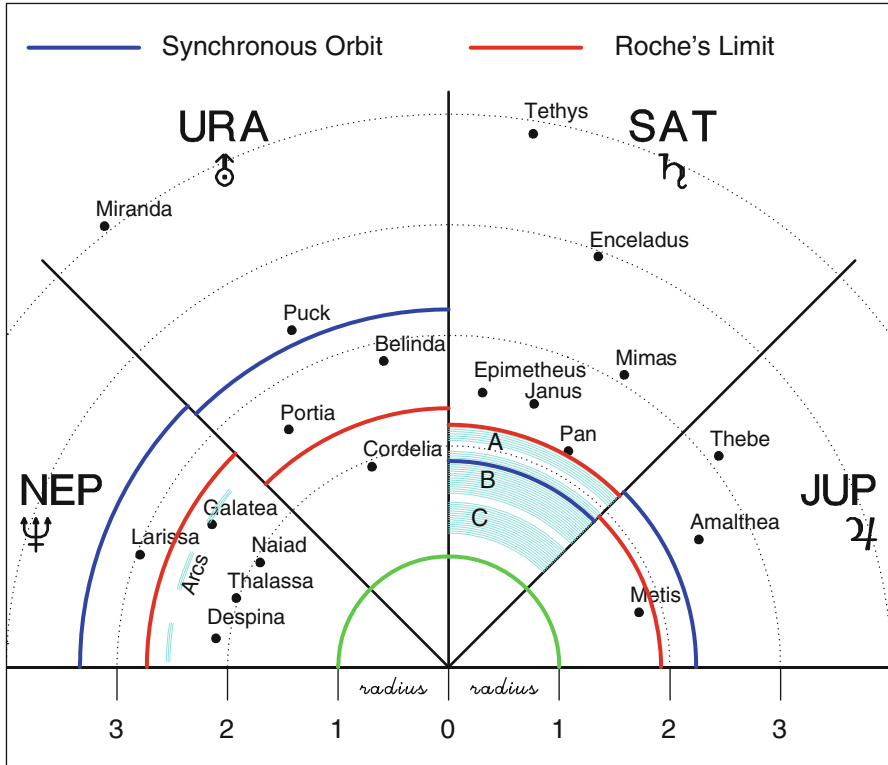


FIG. 16.44 : Positions of the natural satellites of the giant planets in relation to the synchronous sphere and the Roche limit. The radius of each planet is taken as unity.

Here we consider the most visible planetary rings and the closest natural satellites:

- **Jupiter.** Metis revolves slightly within the Roche limit. The internal cohesive forces of this moon are strong enough to prevent it from breaking up. In July 1994, the comet P/Shoemaker-Levy-9 went past Jupiter within the Roche limit and was broken up into about 20 fragments which subsequently crashed into the planet.
- **Saturn.** The rings A, B, and C are inside the Roche limit, which lies just on the outer rim of ring A. It was this observation that encouraged Roche in his calculations. The rings either result from the break-up of natural satellites, or they exist because tidal forces prevented particles at these distances from accreting.
- **Uranus and Neptune.** A few very small satellites, and ring arcs for Neptune, lie within the Roche limit.

Note that the notion of Roche limit is irrelevant to artificial satellites since their structural cohesion is not based on self-gravitation!

## 16.10 Historical Note: Kepler and the Solar System

Even though he may have been preoccupied and inspired by the harmony of the spheres, the music of the planets, and the geometrical beauty of a world contrived by some eminent creator, Kepler, in his *Harmonices Mundi*, remains one of the great minds of astronomy, unbending in the rigour of his calculations.

In Book V, Chap. IV, entitled *In what features relating to the motions of the planets the simple harmonies have been expressed, and that all those which occur in melody are found in heaven*, and in particular, on pp. 192–196, Kepler gives two tables of numerical data. In the first, on p. 193, he gives the “periodic times of the planets” in days and sixtieths of a day. Converted into decimal days, the result is worth comparing with the column for  $N_{\text{sid}}$  [d] of Table 16.2, also given here. The error is less than one hundredth of a day, or quarter of an hour, except for Jupiter, where it is 43 min, not such a large discrepancy in a period of 12 years (Table 16.11).

In the second table, on p. 195, he gives the perihelion and aphelion of each planet, taking 1,000 units for the semi-major axis of the Earth’s orbit. In Table 16.12, we have also included  $a_S$  in a.u. and  $e$ . Once again, it is worth comparing with the columns for  $a_S$  and  $e$  of Table 16.2, repeated here for convenience. There can be no doubt that Kepler was indeed the creator of modern celestial mechanics.

Kepler ends the chapter with these words:

These intervals were sought through the very careful observations of Tycho Brahe, using the method described in *Astronomia Nova – Comments on Mars*, after a painstaking study lasting seventeen years.

The comparison between these two tables led Kepler to his third law.

Planet	Period (d sx) Kepler	Period (decimal day) Kepler	Period (decimal day) Current value
Mercury	87 d 58 sx	87.97	87.97
Venus	224 d 42 sx	224.70	224.70
Earth	365 d 15 sx	365.25	365.26
Mars	686 d 59 sx	686.98	686.98
Jupiter	4,332 d 37 sx	4,332.62	4,332.59
Saturn	10,759 d 12 sx	10,759.20	10,759.20

TABLE 16.11 : *Period of revolution of the planets of the Solar System known to Kepler, in days and sixtieths of a day (d sx), transcribed into decimal days. Values published in Harmonices Mundi, p. 193. Comparison with currently accepted values.*

Planet	Perihelion Kepler	Aphelion Kepler	$a_S$ (a.u.) Kepler	$e$ Kepler	$a_S$ (a.u.) Current	$e$ Current
Mercury	307	470	0.388	0.2098	0.387	0.2056
Venus	719	729	0.724	0.0069	0.723	0.0068
Earth	982	1,018	1.000	0.0180	1.000	0.0167
Mars	1,382	1,665	1.524	0.0929	1.524	0.0934
Jupiter	4,949	5,451	5.200	0.0483	5.201	0.0484
Saturn	8,968	10,052	9.510	0.0570	9.538	0.0542

TABLE 16.12 : *Distance from the Sun of the perihelion and aphelion in the units used by Kepler, corresponding to one thousandth of an astronomical unit, together with the length of the semi-major axis  $a$  and eccentricity  $e$ . Values published in Harmonices Mundi, p. 195. Comparison with currently accepted values.*



FIG. 16.45 : *Kepler: NASA's first mission capable of finding Earth-size and smaller planets around other stars. Logo of the mission. Credit: NASA.*



# Bibliography

Books are classified in sections according to the main themes covered in this work, and arranged chronologically within each section.

## General Mechanics and Geodesy

1. H. Goldstein. *Classical Mechanics*, Addison-Wesley, Cambridge, Mass., 1956
2. L. Landau & E. Lifchitz. *Mechanics (Course of Theoretical Physics)*, Vol. 1, Mir, Moscow, 1966, Butterworth–Heinemann 3rd edn., 1976
3. W.M. Kaula. *Theory of Satellite Geodesy*, Blaisdell Publ., Waltham, Mass., 1966
4. J.-J. Levallois. *Géodésie générale*, Vols. 1, 2, 3, Eyrolles, Paris, 1969, 1970
5. J.-J. Levallois & J. Kovalevsky. *Géodésie générale*, Vol. 4: *Géodésie spatiale*, Eyrolles, Paris, 1970
6. G. Bomford. *Geodesy*, 4th edn., Clarendon Press, Oxford, 1980
7. J.-C. Husson, A. Cazenave, J.-F. Minster (Eds.). *Internal Geophysics and Space*, CNES/Cepadues-Editions, Toulouse, 1985
8. V.I. Arnold. *Mathematical Methods of Classical Mechanics*, Graduate Texts in Mathematics (60), Springer-Verlag, Berlin, 1989
9. W. Torge. *Geodesy*, Walter de Gruyter, Berlin, 1991
10. G. Seeber. *Satellite Geodesy*, Walter de Gruyter, Berlin, 1993
11. E.W. Grafarend, F.W. Krumm, V.S. Schwarze (Eds.). *Geodesy: The Challenge of the 3rd Millennium*, Springer, Berlin, 2003
12. H. Stephani. *Relativity: An Introduction to Special and General Relativity*, Cambridge University Press, Cambridge, 2004
13. G. Schubert (Ed.). *Treatise on Geodesy*, Vol. 3: *Geodesy*, Elsevier, Oxford, 2007
14. D.D. McCarthy, P.K. Seidelmann. *Time: From Earth Rotation to Atomic Physics*, Wiley-VCH, Weinheim, 2009

## Space Mechanics

15. F.R. Moulton. *An Introduction to Celestial Mechanics*, The Macmillan Company, New York, 1902 (Dover Publ., New York, 1970)
16. A. Danjon. *Astronomie générale*, J. & R. Sennac, Paris, 1953
17. D. Brouwer & G.M. Clemence. *Methods of Celestial Mechanics*, Academic Press, New York, 1961

18. H.H. Koelle (Ed.). *Handbook of Astronautical Engineering*, McGraw-Hill, New York, 1961
19. D. King-Hele. *Theory of Satellite Orbits in an Atmosphere*, Butterworths Mathematical Texts, Butterworths & Co. Publ., London, 1964
20. P.R. Escobal. *Method of Orbit Determination*, John Wiley & Sons, New York, 1965
21. Y. Hagihara. *Celestial Mechanics*, Vol. 1: *Dynamical Principles and Transformation Theory*; Vol. 2: *Perturbation Theory*, MIT Press, Cambridge, Mass., 1970, 1972
22. A.E. Roy. *Orbital Motion*, Adam Hilger, Bristol, 1982
23. R.H. Battin. *An Introduction to the Mathematics and Methods of Astrodynamics*, AIAA Education series, Amer. Inst. of Aeronautics and Astronautics, New York, 1987
24. O. Zarrouati. *Trajectoires spatiales*, CNES/Cepadues-Editions, Toulouse, 1987
25. D. Boccaletti & G. Pucacco. *Theory of Orbits*, Vol. 1: *Integrable Systems and Non-Perturbative Methods*; Vol. 2: *Perturbative and Geometrical Methods*, Springer-Verlag, Berlin, 2001
26. V.A. Chobotov (Ed.). *Orbital Mechanics*, 3rd edn., AIAA Education series, Amer. Inst. of Aeronautics and Astronautics, Inc., Reston, 2002
27. G. Beutler. *Methods of Celestial Mechanics*, Springer, Berlin, 2005
28. D.A. Vallado. *Fundamentals of Astrodynamics and Applications*, Space Technology Library, Microcosm Press, Hawthorne, and Springer, New York, 2007
29. G. Xu. *Orbits*, Springer, Berlin, 2010

### Space Missions

30. J.R. Wertz & W.J. Larson (Eds.). *Space Mission Analysis and Design*, Space Technology Library, Kluwer Academic Publishers, Dordrecht, 1991
31. R.J. Gurney, J.L. Foster, C.L. Parkinson (Eds.). *Atlas of Satellite Observations Related to Global Change*, Cambridge University Press, Cambridge & New York, 1993
32. S.Q. Kidder & T.H. Vonder Haar. *Satellite Meteorology. An Introduction*, Academic Press, San Diego, 1995
33. E.D. Kaplan (Ed.). *Understanding GPS. Principles and Applications*, Artech House, Boston and London, 1996
34. M. Courtois (Ed.). *Techniques et technologies des véhicules spatiaux*, Vols. 1, 2, 3, CNES/Cepadues-Editions, Toulouse, 1998
35. O. Montenbruck & E. Gill. *Satellite Orbits: Models, Methods, and Applications*, Springer-Verlag, Berlin, 2000
36. L.-L. Fu & A. Cazenave (Eds.). *Satellite Altimetry and Earth Sciences*, Intern. Geophysics Series, Vol. 69, Academic Press, San Diego, 2001
37. H.J. Kramer. *Observation of the Earth and Its Environment. Survey of Missions and Sensors*, 4th edn., Springer-Verlag, Berlin, 2002
38. P. Fortescue, J. Stark, & G. Swinerd. *Spacecraft Systems Engineering*, 3rd edn., John Wiley & Sons, Chichester, 2003

39. F. Verger, I. Sourbès-Verger, R. Ghirardi. *The Cambridge Encyclopedia of Space: Missions, Applications and Exploration*, Cambridge University Press, Cambridge, 2003
40. N. Ashby. *Relativity in the Global Positioning System*, Living Reviews in Relativity, SAO/NASA Astrophysics Data System, 2003
41. B. Hofmann-Wellenhof, H. Lichtenegger, E. Wasle. *GNSS: Global Navigation Satellite Systems*, Springer, Vienna, New York, Springer-Verlag, Vienna, 2008
42. P.D. Groves. *Principles of GNSS, Inertial, and Multisensor Integrated Navigation Systems*, Artech House, Boston and London, 2008
43. C.W.F. Everitt et al. (Eds.). *Probing the Nature of Gravity. Confronting Theory and Experiment in Space*, Springer & ISSI, New York, 2010

### Planets of the Solar System and Space Missions

44. W.M. Kaula. *An Introduction to Planetary Physics. The Terrestrial Planets*, John Wiley & Sons, New York, 1966
45. Z. Kopal. *The Moon in the Post-Apollo Era*, D. Reidel Publishing Company, Dordrecht & Boston, 1974
46. H.H. Kieffer, B.M. Jakosky, C.W. Snyder, M.S. Matthews (Eds.). *Mars*, The University of Arizona Press, Tucson, 1992
47. D.P. Cruikshank (Ed.). *Neptune and Triton*, The University of Arizona Press, Tucson, 1995
48. S.W. Bougher, D.M. Hunten, R.J. Phillips (Eds.). *Venus II*, The University of Arizona Press, Tucson, 1997
49. C.D. Murray, S.F. Dermott. *Solar System Dynamics*, Cambridge University Press, Cambridge, 1999
50. P.R. Weissman, L.-A. McFadden, T.V. Johnson (Eds.). *Encyclopedia of the Solar System*, Academic Press, San Diego, 1999
51. D. Fischer. *Mission Jupiter. The Spectacular Journey of the Galileo Spacecraft*, Copernicus Books, New York, 2001
52. R. Greeley, R. Batson. *The Compact NASA Atlas of the Solar System*, Cambridge University Press, Cambridge, 2001
53. A. Brahic. *Planètes et satellites. Cinq leçons d'astronomie*, Vuibert, Paris, 2001
54. T. Encrenaz & J.-P. Bibring. *The Solar System*, Springer-Verlag, Berlin, 2004
55. F. Forget, F. Costard, P. Lognonné. *Planet Mars. Story of Another World.*, Springer, Berlin, 2007
56. M.K. Dougherty, L.W. Esposito, S.M. Krimigis (Eds.). *Saturn from Cassini-Huygens*, Springer, Berlin, 2009
57. Bureau des Longitudes – IMCCE. *Introduction aux éphémérides astronomiques. Supplément explicatif à la Connaissance du Temps*, Bureau des Longitudes, EDP-Sciences, Paris, 2013
58. USNO - HMNAO. *The Astronomical Almanach for the Year 2013*, US Gov. Printing Office, Washington, 2013
59. S.E. Urban, P.K. Seidelmann (Eds.). *Explanatory supplement to the Astronomical Almanac*, University Science Books, Herndon, 2013



### History of Celestial Mechanics and Geodesy

60. I. Todhunter. *A History of the Mathematical Theories of Attraction and the Figure of the Earth*. Macmillan and Co., London, 1873
61. G. Veis (Ed.). *The Use of Artificial Satellites for Geodesy*, Proceedings of the First International Symposium on the Use of Artificial Satellites for Geodesy, Washington (April 1962), North-Holland, Amsterdam, 1963
62. J.-J. Levallois. *Mesurer la Terre. 300 ans de géodésie française*, Presses de l'École Nationale des Ponts et Chaussées, Paris, 1988
63. J. Dhombres (Ed.). *Leçons de Mathématiques. L'École Normale de l'an III. Edition annotée des cours de Laplace, Lagrange et Monge*, Dunod, Paris, 1992
64. D. King-Hele. *A Tapestry of Orbits*, Cambridge University Press, Cambridge, 1992
65. W. Andrewes (Ed.). *The Quest for Longitude*, Harvard University, Cambridge, Mass., 1993
66. J.L. Greenberg. *The Problem of the Earth's Shape from Newton to Clairaut*, Cambridge University Press, Cambridge, 1995

### History of Astronomy

67. J.B. Delambre. *Histoire de l'Astronomie Moderne*, M<sup>me</sup> V<sup>e</sup> Courcier, Paris, 1821
68. A. Koestler. *The sleepwalkers: A History of Man's Changing Vision of the Universe*, Hutchinson, London, 1959
69. A. Beer, P. Beer (Eds). *Kepler – Four Hundred Years*, Pergamon Press, Oxford, 1975
70. J. Peyroux. *Astronomie Nouvelle and Harmonie du Monde* (translations of *Astronomia Nova* and *Harmonices Mundi*). Chez le traducteur, Bordeaux, 1979. (*Bibliothèque de la Fondation des Treilles*)
71. J.-R. Roy. *L'Astronomie et son histoire*, Vols. 1, 2, Presses de l'Université du Québec/Éditions Masson, Québec & Paris, 1982
72. J. Blamont. *Le Chiffre et le Songe. Histoire politique de la découverte*, Odile Jacob, Paris, 1993
73. M. Lachièze-Rey & J.-P. Luminet. *Figures du ciel. De l'harmonie des sphères à la conquête spatiale*, Seuil/Bibliothèque nationale de France, Paris, 1998
74. J. Lefort. *La saga des calendriers*, Ed. Belin, Paris, 1998
75. G. Minois. *Dictionnaire des athées, agnostiques, sceptiques et autres mécréants*, Albin Michel, Paris, 2012

### Historical Astronomy

76. J. Kepler. *Astronomia Nova Απιολογητος, sev Physica Coelestis*. Prague, 1609. (*Réserve des livres anciens, École Polytechnique, Palaiseau*)
77. J. Kepler. *Harmonices Mundi*, Prague, 1619. (*Réserve des livres anciens, École Polytechnique, Palaiseau*)
78. J. Picard. *La mesure de la Terre*, Imprimerie royale, Paris, 1671
79. J.L. de Lagrange. *Mécanique analytique*, Chez V<sup>e</sup> Desaint, Paris, 1788
80. P.S. Laplace. *Traité de mécanique céleste*, Chez Duprat, Paris, 1799

- 
81. F. Tisserand. *Traité de mécanique céleste*, Vols. 1, 2, 3, 4, Gauthier-Villars, Paris, 1889, 1891, 1894, 1896

### Mathematics of Cartography

82. D'Avezac. *Coup d'œil historique sur la projection des cartes de géographie*, BGS-Martinet, Paris, 1863
83. A. Germain. *Traité des projections des cartes géographiques*, Arthus Bertrand Editeur, Paris, 1865
84. M.A. Tissot. *Mémoire sur la représentation des surfaces et les projections des cartes géographiques*, Gauthier-Villars, Paris, 1881
85. L. Driencourt, J. Laborde. *Traité des projections cartographiques à l'usage des cartographes et des géodésiens*, Libr. Sc. Hermann, Paris, 1932
86. J.P. Snyder. *Flattening the Earth: Two Thousand Years of Map Projections*, University of Chicago Press, Chicago, 1993
87. J.P. Snyder & P.M. Voxland. *An Album of Map Projections*, U.S. Geological Survey professional paper 1453, Dept. of the Interior, USGPO, Washington, 1994
88. M. Watelet. *Gerard Mercator, cosmographe*, Fonds Mercator-Parisbas, Bruxelles, 1994
89. L.M. Bugayevskiy & J.P. Snyder. *Map Projections. A Reference Manual*, Taylor & Francis, London, 1995
90. J. Lefort. *L'aventure cartographique*, Éd. Belin, Paris, 2004

# Index

- Airy, G., 726  
Apollonius of Perga, 2  
Brahe, T., 144  
Cardan, J., 159  
Cassini (I), J.D., 47  
Cassini (II), J., 47  
Cassini (III), C.F., 47  
Cassini (IV), J.D., 47  
Cavendish, H., 87  
Chandrasekhar, S., 408  
Clairaut, A.C., 75  
Compton, A.H., 408  
Copernicus, N., 142  
Coriolis, G.G., 390  
D'Alembert, J., 60  
Darwin, C., 419  
Delaunay, C., 188  
Eddington, A.S., 419  
Einstein, A., 219  
Eratosthenes, 492  
Euler, L., 159  
Fermi, E., 409  
Galileo, G., 145  
Gauss, C.F., 57  
Halley, E., 215  
Herschel, W., 414  
Hipparchos, 223  
Hubble, E.P., 408  
Huygens, C., 811  
Kepler, J., 144  
    *Astronomia Nova*, 16, 142, 143,  
    799–801, 883  
    *Harmonices Mundi*, 882  
Kuiper, G., 805  
Lagrange, J.L., 174  
    *Mécanique analytique*, 175  
Lalande, J., 216  
Lambert, J.H., 329  
Laplace, P.S., 221  
    *Exposition du système du monde*,  
    222  
    *Mécanique céleste*, 222  
Le Verrier, U., 216  
Legendre, A.M.L., 92  
Maupertuis, P.L.M. de, 48  
Menaechmus, 2  
Mercator, G., 333  
    *Atlas*, 333, 338  
Newton, I., 53  
    *Principia Mathematica*, 146  
Noether, E., 138  
Oort, J.H., 805  
Piazzi, G., 805  
Picard, J.-F., 44  
Planck, M., 415  
Poincaré, H., 221  
Ptolemy, 141  
Ramanujan, S.A., 19  
Roche, E., 879  
Scaliger, J.J., 276  
Tisserand, F., 231  
A-Train, 373, 374, 457, 498, 521  
acceleration  
    Binet's equation, 98  
    central, 96  
    due to weight, 76, 77  
    Newtonian, 99  
    weight, 73  
adjustment angle, 316  
advance of perigee, 170  
advance of perihelion, 170, 217  
aerobraking, 210, 721, 773, 831, 876  
affine transformation, 111  
age of the Universe, 408  
air braking, 721  
albedo effect, 171, 745  
altitude, 256, 339, 504, 542, 781  
    atmospheric drag, 558  
    ellipsoidal, 664  
    ellipsoidal height, 37  
    geocentric, 41, 543  
    geodetic, 37, 38, 43, 543  
    on frozen orbit, 554  
    variation, 542–557  
angle  
    at the body, 630  
    azimuth, 615  
        relative, 634  
        viewing, 614, 620  
    of eccentricity, 13  
    elevation, 566, 620

- half-swath, 566
- hour, 631
- scattering, 633
- sight, 566
- solar  $\beta$ , 465–476
  - Earth, 465
  - Mars, 767
- solar  $\beta'$ , 465
- solar elevation, 631
- swath, 565
- viewing, 614, 620
- viewing zenith, 566
- yaw adjustment, 585
- zenith
  - solar, 634
  - viewing, 614, 620, 634
- angular momentum, 96, 139
  - conservation, 137
- anomalous period, 203
- anomalous year, 261, 270
- anomaly, 107–136, 203, 270, 546, 737
  - anomalía*,  $\alpha$ , 109
  - eccentric, 110, 132, 211, 713, 736
  - mean, 108, 124, 133, 154, 176, 270, 546, 735
  - true, 109, 124, 131, 154, 155, 268, 546, 735
- aphelion, 103, 268, 739, 882
- apoastron, 103
- apocenter, 103
- apogee, 268, 627
- aposelene, 862
- apparent solar day, 272
- apparent solar time, *see* LAT
- apsidal line, 104
- apsidal precession, 170, 203
- apsidal precession rate, 250–251, 254
- apsidal velocity, 104
- apsis, 104, 194
- areal law, 97, 121, 145, 274, 739, 741
- areal speed, 97
- areostationary satellite
  - longitudinal acceleration, 749
  - stationkeeping, 749
- argument of latitude, 154
- argument of perigee, 153, 155, 170, 395, 550
  - frozen, 553
- ascending node, 153
  - longitude, 153
  - right ascension, 153
- asteroids
  - astronomical data, 837, 840
  - geodetic data, 837
  - Linear, 805
  - natural satellite, 810, 834
  - near-Earth, 805
  - space exploration, 834, 838
  - Trojans, 239, 805
- astroid, 3, 21
- astronomical constants, 228, 229
- astronomical unit, 227, 229, 233
- atlas, 333
- atmosphere
  - density, 205
  - models of, 206
  - of Mars, 730
  - of the Earth, 204–212
  - of Titan, 805, 814, 873
  - of Triton, 877
  - of Venus, 824
  - planetary, 807
  - scale factor, 205
- atmospheric drag, 83, 171, 202–212, 344, 745, 824
  - aerobraking, 210
  - ballistic coefficient, 208, 558
  - compensation, 344
  - decreasing altitude, 558
  - Delta V, 208, 745
- atmospheric refraction, 633
- attitude, 161, 561
  - control, 561
- attraction
  - by Earth, 167
  - central, 167
  - differential, 168
  - heliocentric, 232
  - lunisolar, 168
  - planetary, 168
  - planetocentric, 854
- augmentation systems, 691
  - CWAAS, 691
  - EGNOS, 692, 693
  - GAGAN, 693
  - MSAS, 693
  - SDCM, 693
  - SNAS, 693
  - StarFire, 693
  - WAAS, 691, 693
  - WAGE, 691
- azimuth, 566
  - line-of-sight, 616
  - relative, 634
  - solar, 630
  - viewing, 615
- Baker–Nunn camera, 213
- ballistic coefficient, 208, 558
- barycenter, 150
- base interval, 517
- base station for DGPS, 664

- Bernoulli lemniscate, 314  
 BIH, 89  
 Binet's equations, 97  
 BIPM, 89  
 Bode's law, 806
- calendar  
   Gregorian, 798  
   Julian, 798
- canonical variables, 176
- Cardan angles, 160, 161  
   pitch, 160, 161, 562  
   roll, 160, 161, 562  
   yaw, 160, 161, 562
- Cardan axes, 562
- cartographic projection, 329–337  
   Adams, 330  
   Aitoff, 844  
   Arden–Close, 332, 345, 346  
   Armadillo, 331  
   aspect, 330  
   Behrmann, 330  
   Boggs eumorphic, 331  
     interrupted, 440, 441  
   Cassini, 46  
   conformal, 329  
   Craster parabolic, 331  
   equal-area, 329  
   fish eye, 525  
   Gauss, 332  
   Goode homolosine, 331  
   Guyou, 328, 330, 586, 587, 600, 602, 603  
   Hammer–Aitoff, 331, 839  
   Hammer–Wagner, 331  
   interrupted, 331, 440, 441, 699  
   loxodromy, 333  
   McBryde–Thomas, 699  
   Mercator, 330, 332–334, 350, 368, 676  
     transverse, 332  
   Miller, 332, 485  
   Mollweide, 330, 438, 439, 583  
     interrupted, 868  
   orthodromy, 333  
   orthographic, 331, 355, 358, 359, 443, 596, 601  
   perspective view, 331, 367, 600  
   plate-carrée, 331  
   Raisz Armadillo, 331, 446, 447, 597  
   Snyder, 331, 334–336, 758  
   stereographic, 330, 334–338, 349, 601  
   type, 330  
   UTM, 332, 350
- celestial coordinates, 267  
 celestial equatorial coordinates, 266  
 celestial latitude, 267  
 celestial longitude, 267  
 celestial sphere, 266, 629, 630  
 center  
   *centrum*, *i*, 3  
   of curvature, 20  
   ellipse, 3  
   of attraction, 110  
   of mass, 150  
   osculating circle, 20
- central attraction, 202
- century, Julian, 325
- Ceres  
   astronomical data, 840  
   geodetic data, 840  
   space exploration, 840
- chaos theory, 222
- circle of visibility, 620
- civil time, 272
- civil year, 260, 270
- Clairaut's formula, 77, 214, 709
- climate parameter, 225
- clock bias (GPS), 655
- code PRN (GPS), 668
- colatitude, geographic, 629
- colonialism, 334
- comet, 418, 805, 812  
   Churyumov–Gerasimenko, 812  
   Halley, 215, 812  
   Wirtanen, 812
- conic, *see* ellipse
- conic section, 1, 100  
   and energy, 140  
   eccentricity, 7  
   history of, 2, 7  
   parameter, 100  
   patched, 809
- conservation laws, 136
- constellation of satellites  
   ACE (ESA), 697  
   ACE+, 381, 697  
   BeiDou NS, 684  
     orbital planes, 673, 675  
   Beidou-2, 684  
   BeiDou-M, 687  
   Big Dipper, 684  
   CLARREO, 375  
   COBRA, 401  
   Compass, 684  
   COSMO-SkyMed, 378  
   DMC, 384  
   Ellipso Borealis, 298, 401, 515  
   Ellipso Concordia, 401  
   FLOWER, 401  
   FLOWER CFTM, 401  
   FormoSat-3/COSMIC, 363, 697

- FuegoFOC, 383  
 Galileo, 681  
   eclipse, 478  
   orbital planes, 673, 675  
 GlobalStar, 407  
 GlobalStar-2, 407  
 Glonass, 678  
   eclipse, 478  
   orbital planes, 673, 675  
 Gonets-D1, 407  
 GPM, 372  
 ICO, 401  
 Iridium, 407  
 Iridium-Next, 407  
 Loopus, 395  
 Mercury, 428  
 Molniya, 393  
 Nadezhda, 390  
 Navstar/GPS, 84, 666  
   eclipse, 478  
   orbital planes, 671, 673, 675  
 NOSS, 428  
 NSS 30, 701  
 Odyssey, 401  
 Orbcomm, 407  
 Parus, 390, 702  
 QZSS, 694  
 RapidEye, 380  
 Rocsat-3/COSMIC, 363  
 SB-WASS, 428  
 SBIRS-GEO, 426  
 SBIRS-HEO, 426  
 SBIRS-High, 426  
 SBIRS-Low, 426  
 SD-Radio, 290  
 SkyBridge, 407  
 Strela-3, 407  
 SWARM, 381  
 Teledesic, 407  
 Transit, 390, 701  
 Trumpet, 428  
 Tselina, 428  
 Tsikada, 390, 702  
 VIRGO, 395  
 WATS, 697  
 WEST, 401  
 cosmic velocity, 102  
 critical inclination, *see* inclination  
 crossing time, 433  
   afternoon, 455, 456  
   choice of, 454  
   drift, 460  
   morning, 455, 456  
 cryostat, 414  
 cryovolcanism, 851, 877  
  
 cycle  
   recurrence, 487  
   relative to Earth, 487–514, 646, 648  
   relative to planet  
     Mars, 773–779  
     Vesta, 842  
   relative to Sun, 433–449, 746  
   half-cycle, 437  
   repeat, 487  
  
 daily frequency  $\kappa$ , 265  
 daily frequency  $\nu$ , 264  
 daily orbital frequency, 264, 309, 488, 490, 538  
   meridian intersection, 647  
   synodic, 388  
 daily recurrence frequency, 265, 312, 316, 488, 490, 516, 538  
 date, Julian, 325, 738  
 day  
   apparent solar, 272  
   astronomical definition, 261  
   Julian, 274, 325  
   Martian, 733  
   mean, 262, 394, 622  
   mean (sol), 733  
   sidereal, 262, 394, 622  
   stellar, 262  
 declination, 267, 273, 465, 466, 479, 739  
 Delaunay elements, 188  
 Delaunay equations, 188  
 Delta V, 208, 745  
 descending node, 153  
 DGPS, *see* GPS  
 differential attraction, 232  
 divine order, 144, 220, 221, 419  
 DORIS, 91  
 draconitic period, 203, 488  
 draconitic year, 261  
 drag compensation, 82, 83, 344, 421  
 drift coefficient, 534  
 drift, local crossing time, 457, 458, 460  
  
 Earth  
   *Tellus, uris*, 804  
   *Terra, æ*, 804  
   astronomical data, 229, 260, 727, 818  
   atmosphere, 558–559  
   attraction, 167, 809  
   degree of latitude, 34, 49  
   deviation from the vertical, 29  
   disk, 595  
   ellipsoid, 27, 190, 545, 546  
   equatorial radius, 27, 229, 545  
   flattening, 27, 49, 551  
   geodetic data, 69, 229, 727, 818

- geoid, 545
- length of equator, 37
- length of meridian, 37
- limb, 566
- meridian arc length, 34
- motion about polar axis, 261
- motion about Sun, 260
- motion of poles, 89, 263
- natural satellite, *see* Moon
- period of revolution, 260
- period of rotation, 261
- perturbative accelerations, 164–166
- polar radius, 30
- radius, 565
  - equatorial, 86, 543
  - function of latitude, 543, 545
- reference ellipsoid, 25–41
- Earth's disk, 608
- eccentricity, 100, 153, 818, 840, 854
  - angle of, 13
  - conic section, 7
  - ellipse, 4
  - frozen, 553
- eclipse, solar, 464, 466–482, 767
- ecliptic, 267, 466, 807
  - coordinates, 266, 267
  - latitude, 267
  - longitude, 267
- elevation, viewing, 620
- ellipse
  - affine ratio, 13
  - affine transformation, 8
  - affinity, 9
  - angle of eccentricity, 13, 104, 114
  - apsis, 104
  - arc length, 17
  - center, 3
  - conic section, 1
  - Dandelin's theorem, 12
  - definition, 2
  - directrix, 3, 10, 12
  - eccentricity, 3, 13, 14
  - elliptic integral, 18
  - evolute, 20, 22
  - flattening, 13, 14
  - focal distance, 3
  - focus, 3, 21, 545
  - great normal, 31–37
  - history of, 1, 7
  - osculating circle, 20
  - parameter, 6
  - perimeter, 18
  - principal circle, 112
  - properties of, 3
  - radius, 19
  - radius of curvature, 20, 33, 733, 820
  - reflection, 21
  - semi-latus rectum, 6, 200
  - semi-major axis, 3
  - semi-minor axis, 3
  - trajectory, 140
- ellipsoid
  - Earth, 25–41, 66, 71
    - historical reference, 27
    - reference EGM2008, 27
    - reference EGM96, 27
    - reference EIGEN, 27
    - reference GEM-T2, 27
    - reference GRIM5, 27
    - reference GRS80, 27
    - reference WGS72, 27
    - reference WGS84, 27
  - Jupiter, 817, 820, 821
  - Mars, 732
  - Neptune, 817, 821
  - Saturn, 817, 820, 821
  - Uranus, 817, 821
- elliptic integral, 18
- energy conservation, 136
- energy consumption, 282
- equation of center, 124, 268, 271, 274, 736, 741
  - extremum, 124
- equation of time, 267, 270, 300, 433, 465, 466, 470, 633, 741, 790
- equation, *æquatio, nis*, 124
- equator, 26
  - celestial, 629
- equatorial bulge, 223
- equatorial celestial coordinates, 630
- equatorial overlap, 577
  - fractional, 579
- equatorial plane, 152, 153
- equatorial shift, 308, 516, 526, 577
- equinox, 267, 275, 478
  - Mars, 734, 740
  - Saturn, 846, 848
- equipotential surface, 55
- Eros
  - astronomical data, 837
  - geodetic data, 837
  - space exploration, 837
- escape velocity, 102
- ET, 231
- Euler angle, 155, 159, 160, 302, 330, 576
  - nutation, 155, 160, 302
  - precession, 155, 160, 302, 488
  - proper rotation, 155, 160, 302
- evolute of a curve, 20
- exoplanet, search for, 420
- expansion of the Universe, 408

- fictitious satellite  
 equivalent MGS, 755, 756  
 Triton Orbiter, 875, 877  
 zero altitude, 156, 292, 817, 854
- field of view, 566
- finance and GPS, 698
- first integrals, 136
- flattening  
 Earth, 66, 86  
 Giant Planets, 821  
 Mars, 727  
 of gravity, 77  
 planetary, 825
- force  
 conservative, 55  
 dissipative, 56  
 field, 54
- frame  
 Copernican, 53  
 ECEF (EC Earth-fixed), 54  
 ECI (Earth-centered inertial), 54  
 ECSF, 54  
 Galilean, 53  
 ICRF, 54, 89  
 ITRF, 54, 90  
 local orbital, 561  
 planetary, 762  
 pseudo-Galilean, 54  
 terrestrial, 54
- free fall, 421
- frozen orbit, *see* orbit, 781
- fundamental principle of dynamics, 146
- Galilean principle of relativity, 151
- Galilean reference frame, 305, 831
- gamma-ray burst, 426
- Gauss' equations, 203
- Gauss' relations, 242, 631
- Gauss' theorem, 59
- Gaussian gravitational constant, 228
- general relativity, *see* relativity
- geocentric gravitational constant, 229
- geodetic system  
 Beijing-1954, 690  
 CGS-2000, 675  
 GRS-80, 78  
 GTRF, 675, 684  
 ITRF, 684  
 JGS, 696  
 Krasovsky-1940, 690  
 PE-90, 675, 679  
 PZ-90.02, 679  
 WGS84, 78, 675, 684
- geoid, 69, 71, 86, 190, 545
- geopotential, 61–71, 73  
 term in  $J_2$ , 166, 200  
 historical note, 213  
 term in  $J_3$ , 198–200  
 historical note, 214  
 term in  $J_n$ , 166  
 historical note, 215  
 term in  $J_{2n}$ , 198
- geopotential model  
 EGM, 70, 84, 86  
 EGM96, 80  
 EIGEN, 69–71, 86  
 GEM, 70, 84, 86, 88  
 GGM, 84  
 GRIM, 70, 71, 84, 86  
 JGM, 70, 84, 86  
 NWL, 83  
 OSU, 84  
 SAO-SE, 83
- geostationary satellite, 277, 278  
 east–west drift, 280, 281, 283  
 longitudinal acceleration, 283  
 Mars, *see* areostationary satellite  
 north–south drift, 282, 283  
 parking longitude, 277, 288  
 stable and unstable points, 288, 751  
 stationkeeping, 283
- geosynchronicity, 276–290
- GMT, 272
- GNSS, *see* GPS
- GPS  
 base station, 664  
 basic principle, 653  
 clock  
 correction, 661  
 receiver, 657, 705, 711  
 satellite, 653, 667, 705, 710  
 code PRN, 668  
 control station, 673  
 differential (DGPS), 664–665, 676  
 augmentation system, 665  
 HA-NDGPS, 665  
 RTK, 665  
 financial applications, 698  
 non-positioning uses, 696  
 perturbation of signal, 660  
 phase of signal, 657  
 positioning, 92  
 relativistic corrections, 661, 705–717  
 segment  
 control, 670  
 space, 667  
 user, 675  
 tectonic plates, 702  
 time base, 657



- user
  - position, 656
  - velocity, 659
- GRAVES, 322
- gravitation
  - constant of, 56
  - universal law of, 220
- gravitational constant, 56, 87, 147
- geocentric, 60, 87, 88, 742
- heliocentric, 233
- planetocentric, 817, 818, 854
  - 433-Eros, 837
  - Ceres, 840
  - giant planets, 819
  - Mars, 731, 732, 742
  - Mercure, 819
  - Moon, 862, 864
  - Pluto, 819
  - Venus, 819, 831
  - Vesta, 840
- specific, 56
- gravitational deflection, 809
- gravitational potential, 57
  - term in  $C_{lm}$ , 69
  - term in  $J_2$ , 68, 69, 75, 76, 81, 166, 224, 229, 246, 552, 744, 818, 824, 825, 854, 861
    - variation  $dJ_2/dt$ , 85
  - term in  $J_3$ , 79, 552, 553, 781, 818, 825, 861
  - term in  $J_4$ , 69, 79, 250–253
  - term in  $J_6$ , 69
  - term in  $J_n$ , 69, 79, 166, 252, 552, 744, 818
  - term in  $J_{22}$ , 283, 285, 749, 750
  - term in  $J_{2n}$ , 250, 825
  - term in  $J_{31}$ , 286, 750
  - term in  $J_{33}$ , 286, 750
  - term in  $S_{lm}$ , 69
- gravitational sling-shot, 809
- gravity, 60, 72
  - and weight, 60, 74
  - of Earth, 73, 74, 77
- gravity anomalies, 79, 80, 82
- gravity-assist maneuver, 351, 809, 811
- great circle, 26, 241
- Gregorian calendar, 228, 260
- grid interval, 517
- grid points, 524, 526–531
- ground track, 37, 306, 315, 321
  - adjustment angle, 316, 585
  - angle with meridian, 316
  - apparent inclination, 310
  - equation for, 306
  - geocentric, 37, 306
  - geodetic, 37, 306
  - geosynchronous, 313, 314
  - nadir, 37, 38, 40, 306
  - of orbit, 315, 321, 754
    - relative velocity, 317, 762
    - velocity, 762
  - subsattellite point, 37, 38, 40, 306
  - superposition, 592
  - velocity, 317
- gyroscopic approximation, 223
- half-swath
  - ground, 567
  - of instrument, 566
- halo orbit, 239
- Hamiltonian, 177
- harmonic coefficients, 63
  - degree, 63
  - order, 63
  - tesseral, 201
  - zonal, 64, 86
    - non-normalised, 65
    - normalised, 65, 86
- height, ellipsoidal, 37, 664
- heliocentric gravitational constant, 229
- heresy, 145
- horizontal coordinates, 630
- hour angle, 267
- Hubble constant, 408
- hyperbola
  - conic section, 1
  - history of, 7
  - trajectory, 140
- IERS, 89
- inclination, 153, 155, 310, 339
  - apparent, 310–314, 785
  - critical, 194, 250, 255, 298, 395, 515, 552
  - strictly polar, 252
  - Sun-synchronous, 294, 297, 298, 515, 752
    - circular orbit, 753
    - eccentric orbit, 753
  - Sun-synchronous and critical, 401, 754, 777
- inertial mass, 421
- instantaneous pole, 263
- instrument
  - field of view, 566
  - maximum half-swath, 566
  - swath, 564
- interferometry, *see* VLBI
- intertrack interval, 517
- invariability of major axis, 198, 201, 220, 221
- ionosphere, 655

- Julian century, 228  
 Julian date, 276  
     modified, 276  
 Julian day, 274  
 Julian year, 228, 261  
 Jupiter  
     astronomical data, 818, 819  
     ellipsoid, 817, 820, 821  
     geodetic data, 818  
     Great Red Spot, 813  
     natural satellites, 852  
     space exploration, 810, 811
- KAM theory, 222  
 Kaula's method, 201  
 Kepler's equation, 110, 111  
 Kepler's laws, 141, 146, 818, 882  
 Kepler's problem, 107, 115, 118  
 Keplerian elements, 154  
 Keplerian motion, 102, 151, 203, 742, 817  
 Keplerian orbit, 151  
 Keplerian period, 156–159  
 kinetic energy, 139  
 King-Hele method, 202  
 Koskela's theory, 252  
 Kovalevsky's theory, 252  
 Kuiper Belt, 805
- Lagrange bracket, 177  
 Lagrange points, 234–241, 418, 419,  
     860  
 Lagrange's equations, 174  
 lander  
     Curiosity, 724, 729  
     Huygens, 873  
     LM/Apollo-15, 867, 868  
     Mars Pathfinder, 721  
     MER-A and -B, 724  
     MSL, 724  
     NEAR, 837  
     Opportunity, 724, 729  
     Pathfinder, 729  
     Philae, 812  
     Phobos-Grunt, 720  
     Phoenix, 724, 729  
     Spirit, 724, 729  
     TandEM, 876  
     TSSM, 877  
     Viking-1 and -2, 720, 729
- Laplace resonance, 872  
 Laplace vector, 138  
 laser ranging, *see* SLR  
     Moon, 87, 88  
     satellite, 81, 83, 87, 88  
 laser reflector, 81, 87  
 LAT, 272, 433, 470, 790
- latitude  
     areocentric, 728  
     areographic, 728  
     astronomical, 28  
     celestial, 267  
     ecliptic, 267  
     geocentric, 28, 29, 38, 40, 42, 43, 61,  
         72, 728  
     geodetic, 28, 33–35, 38, 40, 42, 43, 72,  
         728  
     geographic, 28, 244, 595, 629, 728,  
         788  
     Mars, 728  
     maximal attained, 306–307, 556, 569  
     maximum viewed, 569  
     of satellite, 61, 189  
     overlap, 569  
     parametric, 28, 29  
     planetocentric, 728  
     planetographic, 728  
     spherical, 26  
 latitudinal drift, 282, 283  
 law of ellipses, 144  
 laws of motion, 53  
 Legendre functions, 93  
     degree, 63  
     order, 63  
 Legendre polynomial, 62, 92  
 lemniscate, 282  
 libration, 234, 239  
 libration points, 234  
 line of nodes, 153  
 line of sight, 613  
     angle, 566  
     to nadir, 566  
 Linear, 805, 810  
 Lissajous curve, 239  
 LLR, 91  
 LMT, 272, 299, 433, 470, 790  
 local apparent time, *see* LAT, 790  
 local mean time, *see* LMT, 299, 790  
 local orbital frame, 561  
 local time, 272, 299  
 local view  
     definition, 620  
     sky plot, 620–622  
 logarithm  
     Mercator projection, 332  
     Napierian, 333  
     politically incorrect, 334  
 longitude  
     areocentric, 734, 737  
     celestial, 267, 734  
     ecliptic, 267, 434  
     geographic, 190, 244, 595, 788  
     of ascending node, 153

- parking, 277, 595, 608, 788
  - stable, 751
  - unstable, 751
- satellite, 595, 608, 788
- solar, 273
- spherical, 26
- subsatellite point, 595, 608, 788
- longitudinal drift, 281–283
- lunisolar attraction, 168, 202
  
- Mars
  - astronomical data, 727, 818, 819
    - historical, 801, 882
  - atmosphere, 719, 730, 807
  - eccentricity of orbit, 15, 16
  - ellipsoid, 732
  - geodetic data, 727, 818
  - geography, 726
  - insertion in orbit, 721
  - latitude, 728
  - map, 768
  - natural satellites, 236, 795
  - perihelion, 737
    - and vernal equinox, 738
  - perturbative accelerations, 742, 744
  - sample return, 720, 785
  - solar angle  $\beta$ , 767
  - solar constant, 724
  - solar longitude, 734
  - space exploration, 720
    - launch dates, 726
  - topography, 726
  - zero altitude, 726
  - zero meridian, 726
- mean anomaly, 154
- mean day, 262
- mean motion, 107
  - correction to, 194
  - Keplerian, 107
  - relative variation, 250, 253
  - resonance, 872
  - true, 194
  - variation, 256
- mean pole, 263
- mean solar time, *see* LMT
- mechanical energy, 139
- Mercator projection, 332
  - Wright, 333
- Mercury
  - astronomical data, 818, 819
  - geodetic data, 818
  - perihelion, 170, 217
  - perturbative accelerations, 823, 824
  - space exploration, 809, 827
- meridian, 26, 261
  - meridies, ei*, 261
- angle with ground track, 316
- celestial, 630
- El Hierro Island, 26
- geographic, 629
- great circle, 26
- Greenwich, 26, 323
- local, 615
- prime, 856
- reference, 613
- zero, 726, 822
- meteorological programme
  - DWSS, 360
  - IJPS, 457, 458
  - JPSS, 360
  - NPOESS, 360
  - POES, 360, 458
- meter, definition, 50–51, 227
- Milankovitch theory, 225, 226
- Milky Way, 329
- Molniya orbit, 104
- momentum conservation, 137
- monotheism, 343
- month
  - definition, 739
  - length, 739
- Moon, 88, 203, 236, 354
  - luna, æ*, 318
  - astronomical data, 854
  - geodetic data, 854
  - Lagrange points, 239
  - libration, 234
  - month, 318
  - perturbative accelerations, 858
  - resonance (1:1), 852
  - seas, 867
  - space exploration, 808
  - Sun-synchronicity, 861
  - velocity, 318
- nadir, 37, 38, 40, 306, 566
- natural satellite, 852–856
  - satelles, itis*, 149
  - Callisto, 854, 872
    - astronomical data, 854
    - geodetic data, 854
    - perturbative accelerations, 859
  - Charon, 812, 825, 852
  - Deimos, 795
  - Dione, 239
  - Enceladus, 814, 815, 848, 849, 851, 854, 873
    - astronomical data, 854
    - geodetic data, 854
  - Epimetheus, 814
  - Europa, 813, 854, 861, 872
    - astronomical data, 854

- geodetic data, 854
- perturbative accelerations, 858
- Galilean, 811, 872
- Ganymede, 854, 872
  - astronomical data, 854
  - geodetic data, 854
  - perturbative accelerations, 859
- Hyperion, 848, 850, 852
- Iapetus, 848–850, 852
- Io, 813, 854, 872
  - astronomical data, 854
  - geodetic data, 854
- irregular, 852
- Metis, 880
- Mimas, 846, 848, 851
- Moon, *see* Moon
- Nereid, 852
- Phobos, 236, 795
- Phoebe, 852
- regular, 852
- satellite of, 856–881
- Tethys, 239
- Titan, 807, 814, 815, 849, 854, 861, 873
  - astronomical data, 854
  - atmosphere, 876
  - geodetic data, 854
- Triton, 807, 854, 861, 877, 878
  - astronomical data, 854
  - atmosphere, 877
  - geodetic data, 854
- nautical mile, 34, 244
- navigation system
  - augmentation, *see* augm. systems
  - BeiDou NS, 684
  - Beidou-1, 688
  - Beidou-2, 684
  - Compass, 684
  - Galileo, 681
  - Glonass, 678
  - IRNSS, 694
  - Nadezhda, 701
  - Navstar/GPS, 666
  - NNSS, 698
  - QZSS, 694
  - regional, 694
  - Transit, 698
  - Tsikada, 701
- Neptune
  - astronomical data, 818, 819
  - discovery, 216
  - ellipsoid, 817, 821
  - geodetic data, 818
  - natural satellites, 807, 852
  - space exploration, 810
- Newton's laws, 53, 146
  - second law, 421
- Newton–Raphson method, 115
- nodal elongation, 154
- nodal period, 203, 488
- nodal precession, 203
- nodal precession rate, 245–250, 252–254, 301
- node, 193
  - ascending, 153
  - descending, 153
- Noether's theorem, 138
- NORAD, 322–327
- nuclear generator, 390
- nutration (angle), 155, 160
- obliquity, 223, 266, 273, 275, 466, 479, 632, 818, 840
- Oort cloud, 805
- opposition, 726
- orbit
  - orbita*,  $\alpha$ , 151
  - areocentric, 773
  - areostationary, 748, 819
  - calibration, 542
  - circular, 245, 317, 624
  - Clarke, 339
  - dawn–dusk, 458, 460, 470, 474, 767
  - equatorial, 279, 339
  - for revolution, 340
  - frozen, 551–557, 781, 825, 861
  - GEO, 339
  - geostationary, 159, 202, 277, 819
  - geosynchronous, 202, 276
  - graveyard, 283
  - halo, 239, 351, 354, 384, 413
  - heliocentric, 351, 773
  - highly eccentric, 627
  - inertial, 252
  - L1LO, 239, 241
  - L2LO, 240, 241
  - LEO, 339
  - loop-the-loop, 816
  - maintenance, 300
  - MEO, 339
  - near-circular, 155, 245, 339
  - near-circular near-equatorial, 155
  - near-equatorial, 155, 279, 339
  - near-polar, 339
  - nodes, 153
  - non-frozen, 554
  - parking, 283
  - petal, 354
  - planetostationary, 819, 824
  - planetosynchronous, 819, 824
  - polar, 252, 436

- prograde, 339
- retrograde, 293, 339, 388, 752
- strictly polar, 252, 339
- Sun-synchronous, 291, 293, 297, 748, 752, 819, 825
- transfer, 340, 368
- type
  - COBRA, 401, 402
  - Ellipso Borealis, 401, 515
  - FLOWER, 401, 515
  - FLOWER CFTM, 401, 515
  - GPS, 515, 670, 672
  - JOCOS, 401, 403, 515
  - Loopus, 395, 400, 515
  - Molniya, 119–121, 126, 202, 393, 396, 515, 622, 623, 627, 628
  - QZS, 694
  - SPOT, 202, 375, 625
  - Supertundra, 290, 395, 515, 627
  - Sycomores, 395, 515
  - Terra, 374, 503
  - Tundra, 290, 395, 515, 622, 623, 627, 628
  - VIRGO, 399
  - VirtualGeo, 395, 399, 515
  - WEST, 401, 403
- xpO (planets)
  - LMO, 748
  - SMO, 748, 786
- xsO (natural satellite)
  - LLO, 861
- xyO
  - ETHO, 414
  - FTO, 340
  - GEO, 340
  - GSO, 340, 694
  - GTO, 340
  - HEO, 340, 393–401, 515, 627
  - IGSO, 340, 687
  - L1LO, 340, 351, 354, 384
  - L2LO, 340, 413, 415
  - LEO, 340
  - MEO, 340, 666
  - NEO, 385
  - THEO, 340
  - VHO, 340
- yOI (insertion)
  - EOI, 872
  - GOI, 872
  - JOI, 811, 845, 872
  - LOI, 816
  - MOI, 720, 721, 724, 725, 773, 777
  - SOI, 811, 845
- orbit determination
  - analytical method, 171
  - numerical method, 171
- orbit extrapolation, 201
- orbital elements, 154, 173, 193, 545
  - adapted, 154
  - angular, 186, 199
  - Delaunay, 188
  - Keplerian, 173
  - long-period variation, 198–201, 552
  - metric, 186, 199
  - NORAD, 154, 265, 322–327, 479, 502
  - osculating, 173, 201, 552
  - periodic variation, 202
  - secular variation, 192, 196–202, 246, 250–253, 552, 746
  - short-period variation, 198, 199
  - TLE, *see* NORAD
- orbital insertion speed, 101
- orbital maintenance, 533
  - maneuver, 534
- orbital period, 203
- orbital plane, 96, 152, 153
  - $\beta$  angle, 464
  - Mars, 767
- orbital resonance, 201
- orthodromic curve, 244
- overpass, 613
  - function of latitude, 645, 652
  - in time slot, 646
  - sampling, 645, 646, 652
  - statistics, 645, 652
- paleoclimate
  - Earth, 225
  - Mars, 734
- paleoclimatology, 226
- parabola
  - conic section, 1
  - history of, 7
  - trajectory, 140
- parallel, 26
  - small circle, 26
- parallel (geographic)
  - local, 616
  - polar circle, 632, 741
  - tropics, 632, 741
- parking longitude, 277
- passive gravitational mass, 421
- periastron, 103, 735
  - frozen, 781
- pericenter, 103
- perigee, 103, 268, 553
  - advance of, 170
  - argument of, 153
  - frozen, 553
- perihelion, 103, 268, 735, 739, 882
  - of Mercury, 170, 217
  - precession of, 170

- period, 106, 203  
   draconitic, 203, 488  
   Keplerian, 106, 742  
   nodal, 203, 488  
   of halo orbit, 239  
   of revolution, 106  
     natural satellite, 857  
     planet, 818  
   of rotation  
     natural satellite, 857  
     planet, 819  
   orbital, 106  
   synodic, 318, 320, 647, 796, 808  
     Earth, 726
- periselenes, 862
- perturbations (Lagrangian method), 171
- perturbative method  
   presentation, 171–179  
   solution (Lagrange), 179–187
- pitch, 562  
   angle, 160
- pixel, 564  
   CCD, 564  
   coordinates, 605, 607  
   distortion, 570  
     area, 572  
     index, 570  
     length, 571  
     width, 571  
   geostationary, 604, 605, 607, 608, 610  
   resolution, 373–386
- planet  
   *planeta*,  $\alpha$ , 804  
   attraction, 809  
   dwarf, 806  
   giant, 804, 852  
   telluric, 804, 852
- planetary frame, 831
- planetocentric sphere, 880
- Platonic solids, 144, 159
- Pluto  
   astronomical data, 818, 819  
   atmosphere, 807  
   geodetic data, 818  
   natural satellite, 812, 825, 852  
   space exploration, 812
- polar, 339  
   circle, 632, 741  
   day, 632  
   motion, 263  
   night, 632  
   viewing geometry, 617
- polhody, 263, 264
- polyhedron, 159  
   regular, 144
- position on orbit (angle), 154, 190, 545, 781  
   constellation GPS, 673, 675
- position vector, 95
- positioning by satellite, *see* GPS
- positioning system  
   DORIS, 91  
   GPS, 92  
   LLR, 91  
   SLR, 90  
   VLBI, 91
- positioning technique, 89
- post-glacial rebound, 85
- potential, 54, 55  
   weight, 72
- potential energy, 139
- potential model  
   433-Eros  
     NLR190, 837  
   Earth  
     model, *see* geopotential model  
   Mars  
     GMM-1, 732  
     GMM-2, 732  
     GMM-3, 732  
     JGM85F01, 731  
     MGM1025, 731, 732  
   Moon  
     GLGM, 864  
     GLGM-1, 862  
     GLGM-2, 862  
     LPLGM, 862, 864  
   Venus  
     JPL-VGM1B, 831  
     MGNP90, 831
- precession, 160  
   *præcessio, nis*, 301  
   angle, 155, 301  
   apsidal, 170, 194, 214, 250–251, 253–255, 550  
   climatic, 225  
   cycle, 435  
   nodal, 193, 213, 245–250, 252, 254, 291, 301  
   of equinoxes, 223, 225, 261, 301, 734  
   rate, 301
- PRN (code), 668  
   GPS, 668, 671  
   SBAS, 693
- proper rotation (angle), 155, 160
- radar  
   emission band, 380  
   missions, 378–388, 506
- radial vector, 128–136  
   average, 129

- radiation pressure, 171, 203, 745
- radio occultation, 363, 696, 698–700, 730
- radius of ellipse, 19
  - geodetic latitude, 32
- receiving station
  - Galileo, 684
  - Glonass, 679
  - Navstar/GPS, 670, 674
- recovery
  - of capsule (film), 386, 387
  - of satellite, 392, 416
- recurrence, 202, 487–542, 581, 773–779
  - and swath, 581
  - avoided, 507, 512, 778
  - cycle, 487–514, 646
  - deliberate, 538
  - diagram, 492
    - Earth, 492–498
    - Mars, 773
  - frequency, 488
  - grid points, 779
  - imperfect, 538
  - index, 536–542, 779
  - module, 491, 493
  - one-day cycle, 201, 507, 512, 514
  - one-sol cycle, 778
  - orbital maintenance, 533–536
  - perfect, 538
  - prime numbers, 492
  - relative distance, 537
  - subcycle, 520, 646
  - triple, 490
- recurrence grid, 487, 516–531
  - interval at equator, 517
  - reference, 524
    - ERS, 524
    - GRS, 524
    - IRSP4G, 524
    - MWRS, 524
    - TPG, 524
    - WRS, 524
- recurrent satellite, 201, 202, 487–542
- redshift, 408
- reduced distance, 40, 156, 565
  - dependence on anomaly, 129, 131–133
- reduction to equator, 269, 741
- reference ellipsoid
  - GRS-80, 78
  - WGS84, 78
- reference frame
  - Galilean, 305
  - terrestrial, 306
- reference system
  - celestial
    - ICRF, 89
    - ICRS, 88
  - terrestrial
    - ITRF, 90
    - ITRS, 89
- relativistic effects, 169, 170, 347, 745
- relativity, 745
  - Einstein's theory, 421–424, 705
    - tests, 421
  - Galilean principle of, 151
  - general, 170, 219, 255, 707
    - Lense–Thirring effect, 170, 347, 717
    - Schwarzschild metric, 707
  - Sagnac effect, 715
  - special, 705
    - Lorentz factor, 705
- resolution, 373–386
- resonance, 824, 827, 853, 872
  - 1:1, 853
  - Laplace, 872
- revolution, 106
- right ascension, 267
  - of ascending node, 153, 155
- Roche limit, 795, 878–880
- roll, 562
  - angle, 160
- rotation
  - blocked, 825
  - chaotic, 852
  - synchronous, 852, 857
- Routh value, 238
- sampling, 613, 790
  - angular, 614
  - monthly tables, 639–647, 790
  - temporal, 613
- satellite
  - satelles, itis*, 149
  - areostationary, 748, 786
    - longitudinal acceleration, 749
    - pixel distortion, 782
    - stationkeeping, 749
    - viewed disk, 788
  - areosynchronous, 748
  - burial, 429
  - fictitious, 156, 292, 755, 756, 817, 854, 875, 877
  - geostationary, 159, 202, 277–290, 318, 391–393, 618
    - Earth's disk, 593–611
  - eclipse, 478–479
    - pixel distortion, 573, 574
    - scanning mode, 564
    - visibility, 605
  - geosynchronous, 202, 276–290, 313
  - LEO scanning mode, 564
  - one-day recurrence, 507

- passenger, 381  
 polar, 252, 436  
 recovered, 392  
 recurrent, 201, 202, 487–542, 773–779  
     one-day cycle, 510, 512  
     one-sol cycle, 779  
 stealthy, 386  
 strictly polar, 252  
 Sun-synchronous, 291–300, 449–460,  
     491–507, 752–754, 773–777  
     eclipse, 470–478, 767  
 tandem mission, 375, 389  
 undetectable, 386  
 velocity, 317  
 visibility, 605, 622–629  
 windmill experiment, 831
- satellite
- (name of satellite)-*n*, 341
- 1957 $\alpha$ , 213  
 1957 $\beta$ , 213  
 1958 $\beta_2$ , 214  
 1959 $\alpha$ , 215  
 1959 $\eta$ , 215  
 1960 $\iota_2$ , 215  
 1961 $\alpha\delta_1$ , 215  
 1961 $v$ , 215  
 1961 $o$ , 215  
 1962 $\alpha\epsilon$ , 215  
 1962 $\beta\mu$ , 215  
 1962 $\beta\nu$ , 215  
 A-1, 343  
 ACE, 239, 241, 354  
 ACE+, 381  
 ACE+-*n*, 697  
 ACE-A, 366  
 ACE-B, 366  
 ACRIMSAT, 389, 416  
 ADE-A, 81  
 ADEOS-1, 383, 456, 462, 499, 521,  
     539, 541, 564  
 ADEOS-2, 383, 456, 497–499, 519,  
     564  
 ADM, 381  
 ADM-Aeolus, 381, 459, 495, 499  
 AEHF-1, 393  
 AEM-1 and -2, 366  
 AEM-3, 348  
 Aeros-1 and -2, 291  
 AFP-731, 387  
 Agila-2, 391  
 Agile, 409  
 AIM, 366, 496, 499  
 Ajisai, 81, 84, 88, 91, 346  
 Akari, 414  
 Akebono, 355, 356, 484  
 Almaz-1, 387  
 Almaz-T-2 and -T-3, 387  
 ALOS, 383, 456, 499  
 ALOS-2, 499  
 AlSat-1, 384  
 AlSat-2A, 496, 500  
 Amos-3, 391  
 Anatolia-1, 392  
 Anik-1, 391  
 Anik-F2, 599, 603  
 ANNA-1B, 81, 215, 344  
 Apollo-11, 91, 428  
 Apollo-14, 91  
 Apollo-15, 91  
 Aqua, 373, 374, 455, 457, 461, 498,  
     563, 592, 596, 636, 637, 639–643,  
     645  
 Aquarius, 496  
 Aquarius/SAC-D, 373, 389  
 ARGOS, 424  
 ARIES-1, 383  
 Arirang-1, 389, 457, 500  
 Arirang-2, 389, 457  
 Arirang-3, 389, 457  
 Arirang-*n*, 496  
 Artemis, 393, 692, 693  
 ASCENDS, 375  
 AsiaSat-1, 392  
 AsiaSat-3 and -3S, 392  
 AsiaSat-5, 391  
 Astérix, 343  
 Astra-1M, 391  
 Astrid-1 and -2, 351  
 Astro-E2, 411  
 Astro-F, 414  
 Astro-G, 416, 417  
 Astron, 411  
 Atlantis, 429, 808, 811  
 Atmosphere-1 and -2, 357  
 ATS-1 to 5, 279  
 ATS-6, 88, 279  
 AUOS-SM-KF, 418  
 AUOS-SM-KI, 418  
 Aura, 373, 374, 457, 498  
 AXAF, 408  
 Azerspace-1, 391  
 Badr-6, 391  
 Badr-B, 382  
 BE-B and C, 81  
 Beacon Explorer-1 and 2, 81  
 BeiDou NS-*n*, 670, 672  
 Beidou-1A, 289, 290, 690  
 Beidou-1B and -1C, 690  
 Beidou-2-G1 to -2-G4, 687  
 Beidou-2-I1 to -2-I5, 687  
 Beidou-2-M1, 687  
 Beidou-2-M2 to -M5, 687



- BeiDou-G-*n*, 689  
 BeiDou-G1 to -G4, 687  
 BeiDou-I-*n*, 689  
 BeiDou-I1 to -I5, 687  
 BeiDou-M-*n*, 689  
 Beijing-1, 384  
 BeppoSAX, 411  
 BilSat-1, 384  
 Bion-11, 425  
 Bion-M1, 425  
 BIRD, 383  
 BNSCSat, 384  
 BNTS-1A to -1C, 690  
 BrazilSat-B4, 391  
 C1 (JPSS), 431  
 C2 (JPSS), 431  
 Calipso, 373, 374, 457, 466, 467, 498  
 Canyon-1 to -7, 428  
 Cartosat-1, 382, 456, 500  
 Cartosat-2, 382, 456, 496, 500  
 Cartosat-2A, 382, 456  
 Cartosat-2B, 382, 384  
 Cartosat-3, 382  
 CBERS-1, 383, 456, 498  
 CBERS-2, 383, 456, 498  
 CBERS-2B, 383, 456, 498, 500  
 CBERS-*n*, 497  
 Celestis-1 to -4, 429  
 Celestis-7, 429  
 CFOSAT, 390, 459, 495, 500  
 CGRO, 409  
 Chalet-1 to -6, 428  
 Challenger, 429  
 CHAMP, 82, 84, 86, 91, 210, 344, 696  
 Chandra, 405, 408, 410, 411  
 China-26, 393  
 ChinaSat-9, 391  
 ChinaStar-1, 391  
 Chollian, 364  
 Choma, 380  
 Choros, 380  
 Chuang Xin-1-02, 383  
 CiS, 430  
 CLARREO, 375  
 CloudSat, 373, 374, 457, 498  
 Cluster, 356  
 Cluster-2, 356  
 COBE, 415  
 COBRA-*n*, 401, 402, 515  
 COBRAS/SAMBA, 415  
 Columbia, 429  
 Compass-G-*n*, 91  
 Compass-G1 to -G4, 687  
 Compass-I-*n*, 91  
 Compass-I1 to -I5, 687  
 Compass-M-*n*, 91  
 Compass-M1, 91, 687  
 Compton, 408, 409  
 COMS-1, 361, 364  
 COMS-*n*, 365  
 Copernicus, 412  
 Coriolis, 390, 459, 497, 499  
 CORONAS-Photon, 418  
 CoRoT, 255, 419, 444, 508  
 COSMIC-FormoSat-3-*n*, 363  
 COSMO-SkyMed-1 to -4, 378, 458, 496, 498, 499  
 Cross-Scale, 357  
 CryoSat, 384  
 CryoSat-2, 91, 92, 384, 508  
 CX-1-02, 383  
 CXO, 411  
 D1-C, 84  
 D1-D, 84  
 Daichi, 383  
 Darwin, 240, 419  
 DE-A and -B, 252  
 Deimos-1, 384  
 DESDynI, 384  
 DFH-1, 343  
 DFH-24, 362  
 DFH-30, 362  
 DFH-31 and -32, 357  
 DFH-38, 354  
 DFH-46, 348, 362  
 DFH-47, 348  
 DFH-50, 383  
 DFH-51 and -52, 690  
 DFH-53, 362  
 DFH-54, 389  
 DFH-55, 383  
 DFH-56, 690  
 DFH-60 and -61, 351  
 DFH-68, 425  
 DFH-70 and -71, 351  
 DFH-78 and -79, 383  
 DFH-80 and -81, 351  
 DFH-90, 383  
 DirectTV-8, 391  
 Discoverer-1, 386  
 Discoverer-14, 386  
 Discoverer-18, 386  
 Discoverer-27, 386  
 Discoverer-34, 215  
 Discoverer-35, 386  
 Discovery, 429  
 DMSP-4A F-1, 362  
 DMSP-4A F-13, 362  
 DMSP-4B F-3, 362  
 DMSP-5A F-1, 362  
 DMSP-5D2 F-8 to F-17, 362  
 DMSP-5D3 F-18, 362, 592, 594

- DMSP-5D3 F-19 and F-20, 362  
 DMSP-*n*, 457  
 DODGE, 424  
 DSCO, 384  
 DSCOVR, 239, 384  
 DSCS-3A3, 393  
 DSCS-3B6, 393  
 DSP-1 and -2, 356  
 DSP-F-21 to -F-23, 426  
 DubaiSat-1, 385  
 DWSS F-1 and DWSS F-2, 362  
 Dynamics Explorer-1 and -2, 252, 351  
 Early Bird (Intelsat-1), 279  
 EarlyBird-1, 385  
 EarthCARE, 366, 372, 495, 498, 501, 540, 543, 582  
 EarthView-01 to -04, 429  
 EarthWatch-1, 385  
 EChO, 419  
 Echo-1, 81, 171, 215, 407  
 Echo-2, 81, 171, 407  
 e-Corce, 380, 499  
 Eddington, 240, 419  
 EGE, 515  
 EGP, 81, 84, 346  
 EGPM, 381, 498  
 EGS-1, 81  
 Einstein, 409  
 EIS-1, 387  
 Elektro-1, 361, 364, 599, 602  
 Elektron-1 to -4, 351  
 Ellipso Borealis, 298, 442, 443  
 Ellipso Borealis-*n*, 291, 401, 515, 777  
 Ellipso Concordia-*n*, 401  
 Endeavour, 429  
 EnMAP, 496, 499  
 Envisat, 91, 92, 381, 456, 498, 499, 505–507, 524  
 EO-1, 374, 379, 456, 498  
 EO-3, 363  
 EOS-AM-1, 374, 455  
 EOS-Aqua, 638  
 EOS-Chem-1, 374  
 EOS-LAM, 384  
 EOS-PM-1, 374, 455  
 EOS-Terra, 638  
 EPE-A to -D, 416  
 EPS-SG-A and -B, 362  
 Equator-S, 354  
 ERBS, 366, 437  
 ERM, 495, 498, 501  
 EROS-A1, 385, 456, 495, 500  
 EROS-B, 385, 457  
 ERS-1, 81, 84, 91, 381, 382, 389, 456, 497–499, 504, 524, 542, 544  
 ERS-2, 81, 84, 91, 381, 389, 456, 498, 524  
 ERTS-1, 331, 374  
 Esafi-1, 391  
 ESSA-1 to -3, 360  
 ESSA-9, 360  
 Essaim-1 to 4, 382  
 ESSP-1 to -5, 374  
 ESSP-6, 373  
 ESSP-7, 375  
 Etalon-1, 84, 88, 91, 344  
 Etalon-2, 84, 88, 91, 344  
 Eutelsat-7A, 391  
 EUVE, 412  
 EXOS-A -B and -C, 356  
 EXOS-D, 355, 356  
 Exosat, 411  
 ExperimentalSat-1 to -3, 383  
 Explorer-1, 342, 343, 351  
 Explorer-6, 360  
 Explorer-7, 360  
 Explorer-11, 409  
 Explorer-12, 215, 416  
 Explorer-14, 416  
 Explorer-15, 416  
 Explorer-19, 81  
 Explorer-22, 81  
 Explorer-26, 416  
 Explorer-27, 81, 88  
 Explorer-29, 81  
 Explorer-30, 416  
 Explorer-34, 351  
 Explorer-36, 81  
 Explorer-37, 416  
 Explorer-38, 415  
 Explorer-44, 416  
 Explorer-48, 409  
 Explorer-49, 415  
 Explorer-50, 351  
 Explorer-57, 412  
 Explorer-58, 366  
 Explorer-59, 239  
 Explorer-60, 366  
 Explorer-61, 348, 460  
 Explorer-62 and -63, 252  
 Explorer-66, 415  
 Explorer-67, 412  
 Explorer-68, 357  
 Explorer-69, 411  
 Explorer-70, 354  
 Explorer-71, 354  
 Explorer-72, 425  
 Explorer-73, 416  
 Explorer-74, 415  
 Explorer-75, 414  
 Explorer-76, 425

- Explorer-77, 412  
Explorer-78, 354  
Explorer-79, 409  
Explorer-80, 415  
Explorer-81, 411  
Explorer-83, 412  
Explorer-84, 409  
Explorer-85 to -89, 357  
Explorer-90, 366  
Explorer-91, 356  
Explorer-92, 414  
EyeSat-1, 382  
FaSat-1, 382  
FAST, 354, 355  
Fermi, 409  
Ferret-2, 428  
FGRST, 409  
FIRST, 414  
Fizeau, 81, 91  
FLOWER CfTM-*n*, 401, 515  
FLOWER-*n*, 401, 515  
FormoSat-2, 383, 456, 497, 500, 507,  
524, 525, 530  
FormoSat-3A, 363, 697  
FormoSat-3F, 363, 697, 699  
FSW-2-3, 387  
FuegoSat, 383  
FUSE, 412  
Fuyo-1, 383  
FY-1A and -1B, 362  
FY-1C, 348, 362  
FY-1D, 362, 389  
FY-2-*n*, 601  
FY-2A, 364, 599  
FY-2B, 364, 599  
FY-2C, 364, 618  
FY-2D, 361, 364  
FY-2E, 361, 364  
FY-3A, 359, 362  
FY-3B, 362  
GACM, 366  
GAIA, 240, 413  
Galaxy-15, 391  
GALEX, 412  
Galileo-*n*, 91, 670, 672, 685, 686  
Garuda-1, 391  
GAUGE, 424  
GCOM-W1, 383, 457, 498  
GEMS, 411  
Genesis, 239–241, 816  
GeoEye-1, 385, 456  
GEOS-1 and -2, 81  
GEOS-3, 81, 84, 88, 389  
Geosat, 81, 84, 389, 508  
Geotail, 354  
GFO, 91, 508  
GFO-1, 389, 407  
GFZ-1, 84, 91, 344  
GIFTS, 363  
GIOVE-A and -B, 91, 681  
GLAST, 409  
GlobalStar-M0-*n*, 407  
GlobalStar-M001, 407  
GlobalStar-M097, 407  
Glonass Regional Extension, 515  
Glonass-711, 678  
Glonass-736 to 738, 678  
Glonass-773, 678  
Glonass-798, 678  
Glonass-*n*, 91, 515, 670, 672, 680,  
682, 683  
Glonass-K1-11, 678  
Glory, 373, 374  
GMS-1 to -5, 364  
GOCE, 83, 85, 86, 210, 344, 459, 476,  
554  
GOES-1, 279, 363  
GOES-2, 363  
GOES-3, 363  
GOES-4, 363  
GOES-5, 363, 599  
GOES-6, 363  
GOES-7, 279, 363, 599  
GOES-8, 279, 363, 564, 599  
GOES-9, 363  
GOES-10, 363  
GOES-11, 363  
GOES-12, 361, 363, 371  
GOES-13, 361, 363  
GOES-14, 361, 363  
GOES-15, 361, 363  
GOES-*n*, 599, 601  
GOES-E, 361  
GOES-W, 361, 365  
GOMS-1, 364, 599, 602  
Gonets-D1-1 to -D1-12, 407  
Gonets-M-1, 407  
GoreSat, 384  
GOSat, 373, 498, 499  
GP-A, 421  
GP-B, 255, 349, 421  
GPS-*n*, *see* Navstar/GPS-*n*  
GRACE-*n*, 86  
GRACE-A, 82, 84, 85, 91, 210, 344,  
347, 350, 374, 696  
GRACE-B, 82, 84, 85, 91, 210, 344,  
347, 350, 374, 696  
Granat, 411  
Gravity Probe B, 255  
GRO, 408  
GSAT-8 and -10, 693  
GSTB-v2A and -v2B, 681

- GTL, 354  
 H2A-LRE, 91  
 Halca, 416, 417  
 Haruka, 416, 417  
 Hay Yang-2A, 389  
 HCMM, 366, 498  
 HealthSat-2, 382  
 HEAO-1 to -3, 409  
 Helios-1 and -2 (heliocentric), 416  
 Hélios-1A, 387, 457, 498  
 Hélios-1B, 387, 457, 498  
 Hélios-2A, 374, 382, 387, 457, 498  
 Hélios-2B, 323, 387, 457, 498, 499  
 Hélios-*n*, 322, 497  
 HellasSat-2, 391  
 Herschel, 240, 241, 414  
 HESSI, 411  
 HETE-2, 409  
 HGS-1, 392  
 HGS-3, 392  
 Himawari-6, 364, 598  
 Himawari-7, 364  
 Hinode, 418  
 Hipparcos, 240, 412  
 Hispasat-1D, 391  
 HJ-1A, 383, 456, 500  
 HJ-1B, 383, 456, 500  
 Homer, 428  
 HSO, 414  
 HST, 408  
 Huan Jing-1A and -1B, 383  
 Hubble, 240, 386, 408, 411, 412, 429  
 HY-1, 497, 500  
 HY-1A and -1B, 389  
 HY-2, 92, 500  
 HY-2A, 91, 389, 459  
 HYDROS, 375  
 HypSEO, 378, 498  
 HypsIRI, 375, 496, 499  
 HypXIM, 499  
 IBEX, 356  
 Ibuki, 366, 373, 457, 496, 499  
 ICE, 812  
 ICESat, 91, 307, 325, 328, 384, 437,  
     508, 521, 524, 539, 582, 779  
 ICESat-2, 384, 508  
 ICO-G1, 401  
 IGS-1A to 8A, 388  
 IGS-1B to 8B, 388  
 IGS-Optical-1 to -5, 388  
 IGS-Radar-1 to -4, 388  
 Ikonos-1, 385  
 Ikonos-2, 385, 456, 496, 499  
 IMAGE, 354  
 IMEWS-2, 426  
 IMP-5, 351  
 IMP-8, 351  
 IMP-F, 351  
 IMP-J, 351  
 IMS-1, 456  
 Inmarsat-*n*, 693  
 Innovation-1, 383  
 INSAT-1A to -1D, 364  
 INSAT-2A and -2B, 364  
 INSAT-2E, 364  
 INSAT-3A, 361, 364  
 INSAT-3E, 361, 364, 391  
 Integral, 406, 409, 514, 515  
 Intelsat-1 F-1, 279  
 Intelsat-702, 424  
 Intelsat-906, 391  
 Intelsat-*n*, 693  
 Interball Aurora, 354  
 Interball Tail, 354  
 Interball-S2-A, 354  
 Interball-S2-X, 354  
 Interbol-1 to -3, 354  
 Interkosmos-12, 357  
 Interkosmos-24, 354, 358  
 Intruder-1, 428  
 IQSY, 416  
 IRAS, 414  
 Iridium-4, 407  
 Iridium-98, 407  
 Iridium-*n*, 407  
 IRIS, 416  
 IRNSS-GEO-*n*, 695  
 IRNSS-GSO-*n*, 695  
 IRS-1A, 382, 456, 498, 522, 523, 539  
 IRS-1B, 382, 456, 497, 498, 500, 523  
 IRS-1C, 382, 456, 498  
 IRS-1D, 382, 456, 498, 500  
 IRS-1E, 382  
 IRS-P2, 382, 456, 498, 522, 523, 539  
 IRS-P3, 382, 456, 498  
 IRS-P4, 382, 389  
 IRS-P5, 382  
 IRS-P6, 382, 497, 498  
 IRS-P7, 382  
 ISEE-1 and -2, 351  
 ISEE-3, 239, 241, 351, 812  
 ISO, 414  
 ISS, 429, 466, 557, 558  
 ItamSat, 382  
 ITOS-1, 360  
 IUE, 412  
 Jason-1, 81, 91, 92, 357, 389, 437,  
     508, 511, 519, 520, 524, 531,  
     532, 534–536  
 Jason-2, 81, 91, 92, 307, 335, 389,  
     437, 441, 466, 471, 508, 511,  
     519, 520, 524, 531, 532, 534–536

- Jason-3, 92, 389  
 JB-3, 383  
 JB-3B and 3C, 383  
 JB5-1 to -3, 383  
 JB6-1 to -4, 383  
 JB7, 383  
 JB8, 383  
 JCSat-12, 391  
 JCSat-RA, 391  
 Jeroboam, 428  
 JERS-1, 383, 456, 499  
 Jian Bing-3, 383  
 Jian Bing-3B and -3C, 383  
 Jikiken, 356  
 JPSS-1, 431, 497, 499  
 JPSS-2, 431  
 Jugnu, 382  
 JWST, 240, 413  
 Ka-Sat, 392  
 Kalpana-1, 361, 364  
 Kanopus-V-1, 425, 500  
 Kanopus-V-2, 425  
 KazSat-1, 391  
 KEO, 430  
 KF1-SJ-4, 354  
 KH-12-1 to -5, 387  
 KH-4A-14, 386  
 KH-7-27, 386  
 Kirari, 393  
 Kitsat-2, 382  
 Kompas, 382  
 KOMPSat-1, -2, and -3, 389  
 KoreaSat-5, 391  
 Koronas-F, 418  
 Koronas-Foton, 418  
 Koronas-I, 418  
 Kosmos-1, 341  
 Kosmos-196, 357  
 Kosmos-389, 428  
 Kosmos-520, 426  
 Kosmos-637, 279  
 Kosmos-700, 702  
 Kosmos-883, 702  
 Kosmos-954, 390  
 Kosmos-1001, 341  
 Kosmos-1127, 380  
 Kosmos-1383, 702  
 Kosmos-1402, 390  
 Kosmos-1413, 678  
 Kosmos-1689, 380  
 Kosmos-1870, 387  
 Kosmos-1939, 380  
 Kosmos-1960, 426  
 Kosmos-1989, 84, 344  
 Kosmos-1990, 380  
 Kosmos-2001, 341  
 Kosmos-2024, 84, 344  
 Kosmos-2054, 341, 393  
 Kosmos-2120, 341  
 Kosmos-2174, 341  
 Kosmos-2206, 678  
 Kosmos-2226, 344  
 Kosmos-2229, 341  
 Kosmos-2234, 678  
 Kosmos-2267, 341  
 Kosmos-2305, 341  
 Kosmos-2315, 702  
 Kosmos-2325, 341  
 Kosmos-2336, 341  
 Kosmos-2348, 341  
 Kosmos-2364, 341  
 Kosmos-2368, 341  
 Kosmos-2376, 341  
 Kosmos-2382, 678  
 Kosmos-2386, 341  
 Kosmos-2396, 341  
 Kosmos-2404, 341  
 Kosmos-2412, 341  
 Kosmos-2417, 341, 678  
 Kosmos-2424, 341  
 Kosmos-2436, 341  
 Kosmos-2440, 426  
 Kosmos-2446, 426  
 Kosmos-2448, 341  
 Kosmos-2458, 341  
 Kosmos-2463, 702  
 Kosmos-2464, 678  
 Kosmos-2465, 678  
 Kosmos-2466, 678  
 Kosmos-2469, 341, 426  
 Kosmos-2471, 678  
 Kosmos-2478, 341  
 Kosmos-2481, 341  
 KRT-25, 416  
 Kua Fu-A, 356  
 Kua Fu-B1 and -B2, 356  
 Kwangmyongsong-3-2, 343  
 Kyokko, 356  
 L5-Mission, 241, 418  
 Lacrosse-1 to -5, 387  
 LAGEOS-1, XII, 81, 82, 84, 88, 91,  
 171, 344, 345, 347, 444, 445  
 LAGEOS-2, 84, 87, 88, 91, 344, 345,  
 347  
 LAGEOS-3, 346, 347  
 Landsat-1, 331, 374, 456, 498, 523  
 Landsat-2, 374, 456, 498, 523  
 Landsat-3, 295, 374, 456, 496, 498,  
 499, 519, 523  
 Landsat-4, 374, 456, 498, 523, 524  
 Landsat-5, 374, 456, 498  
 Landsat-6, 374

- Landsat-7, 374, 456, 498, 524  
 Landsat-8, 295, 335, 374, 456, 498  
 Landsat-*n*, 295  
 LARES, 91, 346, 347  
 LES-5, 393  
 LES-8, 390  
 LES-9, 390, 393  
 LICODY, 83  
 LISA, 424  
 Loopus, 442  
 Loopus-*n*, 400, 515  
 LRE, 344  
 Luch-1, 393  
 Luch-5A and -5B, 693  
 Luch-*n*, 693  
 Luna-3, 392, 865  
 Mabuhay-1, 391  
 MACSat, 385  
 Magion-2, 354  
 Magion-4 and -5, 354  
 MagSat, 291, 348, 460  
 MAP, 415  
 Maroc-Tubsat, 382  
 Mati, 380  
 MeaSat-3, 391  
 Megha-Tropiques, 336, 366, 370, 372,  
     382, 437, 446, 447, 466, 468,  
     508, 509, 570, 574, 575, 579,  
     588–591, 593, 597, 640, 647,  
     650–652, 697, 699, 700  
 Mentor-1 to -5, 428  
 Mercury-1, 428  
 Mercury-2, 428  
 Meridian-1 to -4, 395  
 Meridian-6, 623  
 Merlin, 373, 495, 499  
 Meteor-1-01, 362  
 Meteor-1-27, 362  
 Meteor-2-01, 362  
 Meteor-2-21, 81, 91, 362  
 Meteor-3-01, 362  
 Meteor-3-03 to -3-06, 362  
 Meteor-3-07, 84, 258, 310, 311, 437,  
     439, 570, 572, 577–579  
 Meteor-3M-1, 382, 425  
 Meteor-M-1, 362  
 METEOSAT-1, 279, 363, 564, 608  
 METEOSAT-2, 363  
 METEOSAT-3, 91, 363  
 METEOSAT-4, 363  
 METEOSAT-5, 282, 363  
 METEOSAT-6, 363  
 METEOSAT-7, 361, 363, 564, 608  
 METEOSAT-8, 361, 363, 564, 608  
 METEOSAT-9, 361, 363, 609, 618  
 METEOSAT-10, 361, 363  
 METEOSAT-*n*, 365, 599, 600, 608  
 MetOp-*n*, 497, 642  
 MetOp-A, 15, 362, 457, 458, 461, 462,  
     464, 498, 555–557, 592, 596, 642,  
     648, 649, 696  
 MetOp-B, 362, 457, 498, 499, 555,  
     696  
 MetOp-C, 362, 457  
 METSAT-1, 364  
 Michibiki, 694, 695, 697  
 Microlab-1, 385, 407  
 Microscope, 421  
 μSCOPE, 344, 421, 459  
 Midas-3, 426  
 Midas-4, 215, 408  
 Midas-7, 408  
 Midas-12, 426  
 MIDEX-0, 412  
 MIDEX-1, 354  
 MIDEX-2, 415  
 MIDEX-3, 409  
 MIDEX-5-*n*, 357  
 MIDEX-6, 414  
 Midori, 383  
 Midori-2, 383  
 Minisat-01, 412  
 Mir, 428  
 Misty-1 and -2, 387  
 MMS, 357  
 Molniya-1-01, 393  
 Molniya-1-91, 393  
 Molniya-2-01, 393  
 Molniya-2-17, 393  
 Molniya-3-01, 393  
 Molniya-3-50, 255, 393  
 Molniya-3-51, 393, 485, 628  
 Molniya-3-52, 393  
 Molniya-3-53, 281, 393  
 Molniya-*n*, 120, 126, 170, 202, 255,  
     281, 393–397, 515, 627  
 Momo, 389  
 Momo-1B, 389  
 Monitor-E, 380  
 MOS-1, 389, 456  
 MOS-1B, 389, 456, 497, 499  
 MOST, 419  
 MSG-1, 363, 608  
 MSG-2, 363, 608, 609  
 MSG-3, 363, 608  
 MSG-4, 608  
 MSG-*n*, 608–611  
 MTI, 374, 375  
 MTSAT-1, 364  
 MTSAT-1R, 361, 364, 598, 693  
 MTSAT-2, 361, 364, 693  
 Mugunghwa-5, 391

- Muses-B, 416  
 Nadezhda-1, 702  
 Nadezhda-7, 702  
 Nadezhda-M-1, 702  
 Nahuel-1, 391  
 Nanosat, 382  
 Navstar-1, 666  
 Navstar-11, 666  
 Navstar-2-1, 666  
 Navstar-2A-19, 666  
 Navstar-2A-21, 668, 671  
 Navstar-2F-1, 666  
 Navstar-2F-12, 666  
 Navstar-2R-2, 666  
 Navstar-2R-4, 676  
 Navstar-2R-8, 674  
 Navstar-2R-21, 666, 669  
 Navstar-2RM-1, 676  
 Navstar-2RM-2, 668, 671  
 Navstar-2RM-6, 41  
 Navstar-2RM-8, 669  
 Navstar-2RM-11, 676  
 Navstar-3A-1, 666  
 Navstar-3A-8, 666  
 Navstar/GPS-1, 666  
 Navstar/GPS-11, 666  
 Navstar/GPS-14, 666  
 Navstar/GPS-35, 84, 91  
 Navstar/GPS-36, 84, 91  
 Navstar/GPS-38, 666  
 Navstar/GPS-43, 666  
 Navstar/GPS-50, 666, 669  
 Navstar/GPS-56, 674  
 Navstar/GPS-62, 666  
 Navstar/GPS-*n*, 170, 202, 256, 312, 514, 515, 666, 668, 670, 673, 694, 697  
 Navstar/GPS-PRN-*n*, 669, 671, 676  
 NEMO, 375, 496, 499  
 Newton, 411  
 NFIRE, 426  
 NGSS, 414  
 NGST, 413  
 NigComSat-1R, 391  
 NigeriaSat-1, 384  
 Nilesat-201, 391  
 Nimbus-1, 291, 299, 360  
 Nimbus-2, 360  
 Nimbus-3, 360, 390  
 Nimbus-4 to -7, 360  
 Nimbus-B, 390  
 Nimiq-4, 391  
 NIMS-25, 701  
 NIMS-31, 701  
 NOAA-1 to -5, 360  
 NOAA-6, 360, 457, 458  
 NOAA-7 to -17, 360, 458  
 NOAA-18 and -19, 360, 457, 458  
 Nova-1 and -2, 701  
 Nova-3, 84, 701  
 NPOESS-1, 360, 431  
 NPOESS-2, 431  
 NPOESS-6, 360  
 NPP, 360, 431, 497  
 NROL-2, 387  
 NROL-6, 428  
 NROL-14, 387  
 NROL-19, 428  
 NROL-20, 387  
 NROL-22, 428  
 NROL-26, 428  
 NROL-28, 428  
 NROL-32, 428  
 NROL-34, 428  
 NROL-49, 387  
 NROL-66, 428  
 NSS-30010, 701  
 NSS-30130, 701  
 NSS-30250, 701  
 NSS-30310, 701  
 NSS-30480, 701  
 NSS-30490, 701  
 NSS-30500, 701  
 NTS-1 and -2, 666  
 NuSTAR, 411, 412  
 OAO-1 to -3, 412  
 Ocean-1, 389  
 Oceansat-1, 389, 457, 496, 498, 524, 530, 581, 625  
 Oceansat-2, 389, 457, 493, 496, 498, 500, 528, 530, 621, 625  
 OCO, 373, 374  
 OCO-2, 373, 498  
 Oderacs-2A to -2F, 425  
 Oderacs-A to -F, 425  
 Odin, 366  
 Ofeq-1, 343, 388  
 Ofeq-2 and -3, 388  
 Ofeq-5, 369, 388, 444, 445  
 Ofeq-7, 369, 388  
 Ofeq-9, 388  
 OFO-1, 425  
 OGO-1, 351  
 OGO-2, 351  
 OGO-3, 351  
 OGO-4, 351  
 OGO-5, 351  
 OGO-6, 351  
 Ohsumi, 343  
 Ohzora, 356  
 OICETS, 393, 404, 430  
 Okean-3, 389, 550

- Okean-O, 389  
Okean-O-1, 389  
Okean-O1-1 and -O1-2, 389  
Okean-O1-3, 389, 550  
Okean-O1-4, 389  
Oko-US-K-1, 426  
Oko-US-K-85 to -86, 426  
Oko-US-KMO-1 to -11, 426  
Omid, 343  
Onyx-1 to -5, 387  
OPS/0054, 362  
OPS/1127, 362  
OPS/2222, 428  
OPS/3360, 386  
OPS/3367, 341  
OPS/4412, 701  
OPS/4682, 390  
OPS/5111, 666  
OPS/5798, 701  
OPS/6026, 362  
OPS/6909, 426  
OPS/6911, 426  
OPS/7033, 426  
OPS/7044, 426  
OPS/7218, 701  
OPS/7518, 666  
OPS/8424, 341  
OPS/9454, 428  
OPS/9751, 428  
Optus-D1, 391  
Orbcomm-FM-1 and -2, 385, 407  
Orbcomm-FM-3 to -FM-5, 407  
Orbcomm-FM-41, 407  
Orbcomm-FM-*n*, 407  
Orbcomm-X, 382  
Orbis, 386  
OrbView-1, 385  
OrbView-2, 389  
OrbView-3, 385, 495, 499  
OrbView-4, 385  
Ørsted, 291, 348, 696  
OSCAR-22 (Radio), 382  
OSO-1, 416  
OSO-3, 409  
OSO-7, 409  
OSO-8, 416  
OSTM, 389  
P73-3, 666  
P76-4, 666  
P91-1, 424  
P97-3, 375  
P98-2, 390  
PAGEOS, 81, 171  
PakSat-1, 391, 392  
Palapa-B2 and -B2R, 392  
Palapa-C1, 392  
PanAmSat-1R, 424  
Parasol, 373, 374, 382, 457, 498, 564  
Parus-1, 702  
Parus-99, 702  
PAS-1R, 424  
PAS-22, 392  
PEOLE, 84  
Picard, 418, 459  
Picasso-Cena, 374  
Planck, 240, 241, 415  
PLATO, 419  
Pléiades-1A, 92, 378, 456, 496, 498  
Pléiades-1B, 92, 378, 456, 496, 498, 499  
Polar, 354  
Polar BEAR, 351  
Polaris (TecSAR), 388  
PoSAT-1, 382  
PROBA, 456  
Prognoz-11 and -12, 354  
Prospero, 343  
QuetzSat-1, 391  
QuickBird-1, 385  
QuickBird-2, 385, 456, 495, 499  
QuikScat, 390, 459, 498  
QuikTOMS, 366  
QZS-1, 91, 693–695, 697  
QZS-2 and -3, 694  
QZSS-*n*, 695  
Radarsat-1, 381, 458, 497  
Radarsat-2, 381, 444, 458, 497, 500  
Radcal, 425  
RadioAstron, 91, 416  
Raduga-32, 393  
RAE-A and -B, 415  
RapidEye-1 to -4, 380, 456  
RapidEye-5, 380, 456, 547, 549  
RASAT, 456  
Rascom-QAF-1R, 391  
RazakSat, 385, 547, 548  
RBSP-A and -B, 352, 354  
Reflektor, 382, 425  
Relay-1, 215  
Resource21-01 to -05, 383  
Resourcesat-1, 382, 456  
Resourcesat-2, 382, 456  
Resurs-DK-1, 380  
Resurs-F-1, 380  
Resurs-F-20, 380  
Resurs-F1M-1 and -F1M-2, 380  
Resurs-O1-1 and -O1-2, 380  
Resurs-O1-3, 380, 497, 500  
Resurs-O1-4, 272, 380, 382, 448, 454, 456, 570, 572, 578, 579  
Resurs-R-2 and -R-3, 387  
RHESSI, 411



- Rhythm and Blues, 290  
RISat-1, 382, 496, 500  
RISat-2, 382, 458  
Rock and Roll, 290  
Rocsat-1, 357  
Rocsat-2, 383, 507, 524  
Rocsat-3-*n*, 363  
Rohini, 343  
ROSAT, 411  
Rossi, 411  
RPP, 428  
RS-1, 343  
RSS-1 to -4, 383  
Rumba, 356  
RXTE, 411  
S-15, 409  
S-66a, 81  
SAC-C, 374, 456, 497, 500, 696  
SAC-D/Aquarius, 389, 499  
Safir-2, 382  
SAGE, 366  
Salsa, 356  
Salyut, 428  
Samba, 356  
SAMOS-2, 298  
SAMPEX, 357  
SAOCOM-1A, 380, 496, 500  
SAOCOM-1B, 380  
SAR-Lupe-1 to -5, 387  
SARA, 382  
SARAL, 92, 389  
SAS-2, 409  
SatMex-6, 391  
SAX, 411  
SBIRS-GEO-1 and -2, 426  
SBIRS-HEO-1 and -2, 428  
SBSS-1, 428  
SciSat-1, 366  
SCLP, 384, 495, 499  
SD-Radio-1 to-3, 290  
SDO, 418  
SDS-1, 395  
SDS-7, 395  
Seasat, 81, 389, 508, 551  
SeaStar, 389, 457  
SeatStar, 498  
SECOR-7 to -9, 344  
SEDS-1, 425  
SEDS-2, 425  
Sentinel-1-*n*, 497, 499  
Sentinel-1A to -1C, 381  
Sentinel-2-*n*, 497, 499  
Sentinel-2A to -2C, 381  
Sentinel-3-*n*, 497, 499  
Sentinel-3-A, 92  
Sentinel-3A, 381  
Sentinel-3B and -3C, 381  
Sentinel-4A and -4B, 381  
Sentinel-5, 381  
SES-Sirius-4, 391  
Shi Jian-4, 354  
Shi Jian-5 and -6, 348  
Shi Jian-8, 425  
Shizuku, 383, 457, 498  
Sich-1, 389  
SIM Lite, 413  
Simon-Bolivar-1, 391  
Sirius-1 and -2, 290, 395  
Sirius-3, 290, 395, 623, 628  
Sirius-4 (SES), 391  
Sirius-*n*, 514, 627  
SIRTF, 408, 414  
SJ-4, 354  
SJ-5, 348  
SJ-6A to -6F, 351  
SJ-8, 425  
Skylab, 429  
SMAP, 375, 459, 499  
SMEX-1, 357  
SMEX-2, 354  
SMEX-3, 415  
SMEX-4, 416  
SMEX-5, 414  
SMEX-6, 411  
SMEX-7, 412  
SMEX-9, 366  
SMEX-10, 356  
SMEX-11, 411  
SMEX-12, 416  
SMEX-13, 411  
SMM, 416  
SMOS, 366, 372, 373, 459, 476, 496  
SMS-1, 279, 363, 599  
SMS-2, 279, 363, 599  
SMS-3, 279, 363  
Snapshot, 390  
SNOE, 425  
SOHO, 239–241, 418  
Solar Dynamics Observatory, 418  
Solar-A, 418  
Solar-B, 418  
Solrad-1, 416  
Solrad-7B, 416  
Solrad-9 and -10, 416  
SOOS-4A, 701  
SOOS-4B, 701  
SORCE, 418  
Spektr-R, 416  
Spitzer, 408, 410, 411, 414  
SPOT-1, 375, 456, 498, 524, 581  
SPOT-2, 84, 92, 375, 456, 498  
SPOT-3, 84, 92, 375, 382, 456, 498

- SPOT-4, 92, 375, 378, 393, 456, 498, 564, 642, 646  
SPOT-5, 41, 92, 126, 170, 375, 378, 453, 456, 498, 499, 521, 524, 539, 540, 542, 544, 625  
SPOT-6, 375, 378, 440, 456, 498  
SPOT-7, 375  
SPOT-*n*, 209, 300, 497, 498, 521, 544, 553  
Sputnik-1, 52, 79, 213, 342, 344, 698  
Sputnik-2, 79, 213, 342, 425  
Sputnik-3, 79  
Sputnik-11, 341  
SRMSAT, 382  
SSR-1, 383  
SSR-2, 383  
SST, 408  
ST-3, 391  
Stardust, 816  
Starlette, 81, 82, 84, 91, 208, 344  
STARS, 419, 860  
STE-QUEST, 421–423, 515  
STEDI-1 and -2, 425  
Stella, 81, 84, 91, 344, 382  
STEP, 424, 459  
STEREO-Ahead, 241, 418  
STEREO-Behind, 241, 418  
STRV-1A, 424  
STRV-1B, 353, 424  
STRV-1C, 353, 424  
STRV-1D, 424  
STS-1, 429  
STS-6, 393  
STS-8, 364  
STS-9, 429  
STS-10 (STS-41-B), 392, 429  
STS-11 (STS-41-C), 416  
STS-13 (STS-41-G), 366  
STS-14 (STS-51-A), 392  
STS-25 (STS-51-L), 429  
STS-27, 387  
STS-30, 808  
STS-31, 412  
STS-33, 429  
STS-34, 811  
STS-36, 387  
STS-37, 409  
STS-41, 418  
STS-48, 357  
STS-52, 347  
STS-60, 425  
STS-63, 425  
STS-70, 393  
STS-93, 411  
STS-107, 364, 429  
STS-133, 429  
STS-134, 429  
STS-135, 429  
STS-*n*, 429  
STSS-1 and -2, 426  
Suomi-NPP, 360, 438, 457, 499, 583  
Supertundra-*n*, 398, 515  
SupremeSat-1, 391  
Suzaku, 411  
SWARM-A to -C, 381  
SWAS, 415  
Swift, 409  
SWOT, 389, 508  
Sycomores, 395  
Symphonie-1, 279  
Syncom-1, 278  
Syncom-2, 278, 313, 368  
Syncom-3, 278  
Türksat-3A, 391  
Tachys, 380  
Tan Suo-1 to -3, 383  
TanDEM, 375  
TanDEM-X, 91, 380  
Tango, 356  
TC-1 and -2, 356  
TDF-1, 283  
TDRS-1 and -2, 393  
TDRS-7 to -10, 393  
TechSat-1B, 382  
TecSAR, 388  
Teledat-*n*, 693  
Teledesic-1, 407  
Ten Ce-1 and -2, 356  
Terra, 312, 367, 374, 376–378, 444, 455, 456, 461, 496, 498, 499, 503, 521, 524, 539, 540, 554, 568, 582, 584–587, 593, 597, 639–642, 644  
TerraSAR-L, 380, 498  
TerraSAR-X, 91, 375, 380, 458, 483, 484, 495, 499  
TERRIERS, 425  
TES, 382, 456  
TH-1, 383  
Thaicom-5, 391  
THEMIS-1 to -5, 357  
THEOS, 385, 456, 498  
Thor-6, 391  
3D-Winds, 375  
Tian Hui-1, 383  
Timation-1 to 3, 666  
TIMED, 357  
TIP-1 to -3, 701  
TiPS, 425  
TIROS-1, 360  
TIROS-8, 360  
TIROS-9, 299, 360

- TIROS-10, 299, 360  
 TIROS-N, 360, 457, 458  
 TMC, 430  
 TMSat, 382  
 TOMS-EP, 366  
 TOPEX/Poseidon, 81, 84, 91, 92,  
     169–171, 389, 437, 508, 510,  
     519–521, 524, 531, 532, 534–536,  
     539, 541, 553  
 TRACE, 416, 459  
 Transit-1B, 701  
 Transit-4A, 215, 390, 701  
 Transit-4B, 390  
 Transit-5A-1, 701  
 Transit-5B-1, 390, 701  
 Transit-5B-2, 390  
 Transit-5B-2 and -5B-3, 390  
 Transit-5C-1, 701  
 Transit-*n*, 252, 625  
 Transit-O-1, 701  
 Transit-O-13, 701  
 Transit-O-25, 701  
 Transit-O-31, 701  
 TRAQ, 508  
 Triad-1, 390, 701  
 Triad-2 and -3, 701  
 Triana, 239, 384  
 TRMM, 256, 336, 366, 367, 371, 437,  
     444, 445, 448, 471, 568  
 Trochia, 380  
 Tropiques, 509  
 Trumpet-1 to -3, 428  
 Trumpet-FO-1 and -FO-2, 428  
 TS-1 to -3, 383  
 Tubsat-A, 382  
 Tundra-*n*, 398, 515  
 UARS, 357, 437  
 UK-DMC, 384, 457  
 UK-DMC2, 384, 457  
 UoSAT-12, 508  
 UoSAT-5, 382  
 Uragan-1, 678  
 Uragan-50 et -51, 678  
 Uragan-87, 678  
 Uragan-K1-1, 678  
 Uragan-M1, 678  
 Uragan-M29, 678  
 USA-10, 666  
 USA-21, 395  
 USA-26, 362  
 USA-29, 362  
 USA-34, 387  
 USA-35, 666  
 USA-37, 428  
 USA-53, 387  
 USA-68, 362  
 USA-69, 387  
 USA-73, 362  
 USA-86, 387  
 USA-94, 84  
 USA-100, 84  
 USA-103, 428  
 USA-105, 428  
 USA-106, 362  
 USA-109, 362  
 USA-110, 428  
 USA-112, 428  
 USA-116, 387  
 USA-118, 428  
 USA-129, 387  
 USA-131, 362  
 USA-132, 666  
 USA-133, 387  
 USA-135, 666  
 USA-136, 428  
 USA-139, 428  
 USA-144, 387  
 USA-147, 362  
 USA-152, 387  
 USA-159, 426  
 USA-161, 387  
 USA-166, 674  
 USA-167, 393  
 USA-170, 393  
 USA-171, 428  
 USA-172, 362  
 USA-176, 426  
 USA-182, 387  
 USA-184, 428  
 USA-186, 387  
 USA-191, 362  
 USA-195, 393  
 USA-197, 426  
 USA-200, 428  
 USA-202, 428  
 USA-204, 393  
 USA-206, 666, 669  
 USA-208 and -209, 426  
 USA-210, 362  
 USA-211, 393  
 USA-213, 666  
 USA-214, 393  
 USA-216, 428  
 USA-223, 428  
 USA-224, 387  
 USA-225, 428  
 USA-229, 428  
 USA-230, 426  
 USA-233, 393  
 USA-241, 426  
 Van Allen Probe-A and -B, 352, 354  
 Vanguard-1, 81, 214, 342

- Vanguard-2, 215, 360  
 Vanguard-3, 215  
 VBN-1 and -2, 390  
 VCL, 374  
 Vela-1 and -2, 426  
 Vela-4, 405  
 Vela-9 and -10, 426  
 Vela-11 and -12, 426  
 Venesat-1, 391  
 VEN $\mu$ S, 380, 498  
 VesselSat-1, 382  
 Via-Sat-1, 392  
 Vinasat-2, 391  
 VIRGO-*n*, 395, 399, 515  
 VNRED, 456  
 Vortex-1 to -6, 428  
 Vostok-1, 428  
 VSOP, 416  
 VSOP-2, 416  
 WALES, 459  
 WatER-HM, 389, 508  
 Wespac-1, 91  
 WEST-*n*, 401, 403, 514, 515  
 Westar-6, 392  
 Westford-1, 408  
 Westford-2, 408  
 Westpac-1, 84, 344, 382  
 WGS-1 to -4, 393  
 Wilkinson, 415  
 Wind, 239–241, 354  
 WindSat, 390  
 WIRE, 414  
 WISE, 414  
 WMAP, 240, 241, 415  
 WorldView-1, 385, 457  
 WorldView-2, 385, 456, 547, 548  
 WPLTN-1, 84  
 X-3, 343  
 XMM, 411  
 XTE, 411  
 YahSat-1B, 391  
 Yamal-202, 391  
 Yao Gan-1 to -4, 383  
 Yao Gan-5 and -6, 383, 387  
 Yao Gan-7, 383, 547, 549  
 Yao Gan-8, 383  
 Yao Gan-9A to -9C, 383  
 Yao Gan-10 to -11, 383  
 Yohkoh, 418  
 Z-Earth, 499, 539, 541  
 Zhong Xing-9, 391  
 Zi Yuan-1A and -1B, 383  
 Zi Yuan-2, 383  
 Zi Yuan-2B, 383  
 Zi Yuan-2C, 383  
 ZX-9, 391  
 ZY-1A and -1B, 383  
 ZY-2, 383  
 ZY-2B, 383  
 ZY-2C, 383
- satellite of natural satellite
- Callisto
    - JIMO, 872
  - Europa
    - JEO, 872, 874
    - JIMO, 872
  - Ganymede
    - JGO, 872, 875
    - JIMO, 872
    - JUICE, 873
- Moon
- Apollo-11, 808
  - Apollo-15, 862, 867, 868
  - Apollo-16, 862, 867
  - Apollo-*n*, 864
  - Chandrayaan-1, 863
  - Chang'E-1, 862
  - Chang'E-2, 862
  - Clementine, 856, 862, 869, 870
  - DSPSE, 862
  - Ebb, 865
  - Explorer-35, 867
  - Flow, 865
  - GRAIL-A and -B, 865
  - Hiten, 862
  - Kaguya, 862
  - LCROSS, 865, 871
  - LRO, 91, 865, 866, 870, 871
  - Luna-10, 808
  - Lunar Orbiter-1, 862
  - Lunar Orbiter-4, 864
  - Lunar Orbiter-5, 862
  - Lunar Prospector, 862
  - Muses-A, 862
  - Okina, 862
  - Orbiter-3 to -5, 867
  - Ouna, 862
  - Rstar, 862
  - Selene, 862
  - SMART-1, 862
  - Vstar, 862
  - Zond-3, 867
- Titan
- TandEM, 876
  - Titan Explorer, 876
  - TSSM, 877
- satellite of planet
- asteroid 1-Ceres
    - Dawn, 810, 840, 845
  - asteroid 4-Vesta
    - Dawn, 810, 840–844

- asteroid 433-Eros  
 NEAR, 822, 837, 839  
 NEAR-Shoemaker, 837
- Jupiter  
 Galileo, 811, 845, 856, 873  
 JIMO, 872  
 Juno, 845
- Mars  
 ExoMars, 725  
 ExoMars-TGO, 725, 746, 765, 778  
 InterMarsNet, 767, 773, 774, 776  
 Mariner-9, 720, 726, 728, 732  
 Mars Express, 725, 756, 760, 763,  
 764, 777, 778  
 Mars Global Surveyor, *see* MGS  
 Mars Observer, 773, 774  
 Mars Odyssey, 721, 752, 757, 758,  
 761, 773–775, 785  
 Mars Reconnaissance Orbiter, *see*  
 MRO  
 Mars-96, 777  
 MARSat, 749  
 MAVEN, 725, 748, 765  
 MGS, 721, 726, 729, 732, 752,  
 754–756, 761, 768, 773–775,  
 779–781, 783, 792, 794  
 MRO, 721, 724, 752, 754, 761, 769,  
 773, 774, 776, 779–781, 783, 785,  
 787, 790, 791, 793  
 MTO, 767  
 ODY, *see* Mars Odyssey  
 Phobos-2, 795  
 Phobos-Grunt, 720  
 Premier, 782, 785, 786  
 Trace Gas Orbiter, 725  
 Viking-1 and -2, 720, 730
- Mercury  
 BepiColombo, 827  
 Mercury Orbiter, 827  
 Messenger, 827–829  
 MMO, 827, 828  
 MPO, 827
- Saturn  
 Cassini, 811, 814, 815, 846, 848–851  
 JUICE, 873
- Venus  
 Akatsuki, 831  
 Magellan, 721, 808, 822, 830–835  
 Pioneer Venus Orbiter, 808, 831  
 Planet-C, 831  
 VCO, 831, 836  
 Venera-15, 808  
 Venera-16, 808  
 Venus Climate Orbiter, 831  
 Venus Express, 831, 836
- satellite (programme)  
 8X, 386  
 ACE (ESA), 697  
 ACE+, 697  
 ADEOS, 299, 383  
 Advanced Orion, 428  
 Advanced Vortex, 428  
 AEHF, 393  
 AEM, 366  
 Almaz, 387  
 Apollo, 867  
 Aquacade, 428  
 Archimedes, 290  
 Argon, 386  
 Arkon, 387  
 AsiaSat, 392  
 ATN, 360  
 ATS, 279  
 BeiDou  
 BeiDou-G, 687  
 BeiDou-I, 687  
 BeiDou-M, 687  
 BeiDou NS, 684  
 Beidou-1, 688  
 Beidou-2, 684  
 Big Bird, 386  
 Bion, 425  
 BNTS, 688  
 Canyon, 428  
 CBERS, 383  
 Celestis, 429  
 Chalet, 428  
 Cluster, 356  
 CNSS, 684  
 COBRA, 401  
 Compass, 684  
 Compass-G, 91, 687  
 Compass-I, 91, 687  
 Compass-M, 91, 687  
 COMS, 364  
 Constellation, 864  
 Corona, 386  
 COSMIC, 363, 697  
 COSMO-SkyMed, 378  
 Crystal Kennan, 386  
 DFH, 341  
 DigitalGlobe, 385  
 Discoverer, 386  
 DMC, 384  
 DMSP, 362  
 Dong Fang Hong, 341  
 Dorian, 386  
 Double Star, 688  
 DSCS, 393  
 DSP, 426  
 DSP (Tan Ce), 356

- DSPS, 688  
DWSS, 431  
EarthView, 429  
EarthWatch, 385  
Echelon, 427  
Echo, 407  
Elektro, 364  
Elektron, 351  
Ellipso, 401, 515  
Envisat, 299  
EOGO, 351  
EOS, 299, 374  
EPE, 416  
EPS-SG, 362  
EROS, 385  
ERS, 299, 381  
ESSA, 360  
Essaim, 322  
ESSP, 374  
EXOS, 356  
Explorer, 342, 351, 357, 409  
Feng Yun, 362  
Ferret, 428  
FLOWER, 401  
FLOWER CFTM, 401  
FSW, 387  
FuegoFOC, 383  
FY-1 & -3, 362  
FY-2 & -4, 364  
Galileo, 681  
Gambit, 386  
GCOM, 383  
Geo-1K, 344  
GeoEye, 299, 385  
GEOS, 81  
GGs, 354  
GlobalStar, 407  
GlobalStar-2, 407  
Glonass, 678  
GMS, 364  
GOES, 363  
GOMS, 364  
Gonets-D1, 407  
GPM, 372  
GRAB, 416  
GRACE, 347  
Gravity Probe, 255  
Great Observatories, 408  
GREB, 416  
Hai Yang, 389  
HEAO, 409  
Helios (heliocentric), 416  
Hélios, 299, 322, 387  
Hexagon, 386  
Himawari, 364  
HY, 389  
IGS, 388  
Ikon, 386  
Ikonos, 299, 385  
IMEWS, 426  
Improved Crystal, 386  
INSAT, 364  
Intelsat, 279  
Interball, 354  
Intruder, 428  
IOSA, 428  
Iridium, 407  
Iridium-Next, 407  
IRS, 299, 382  
ISEE, 351  
ISTP, 354  
ITOS, 360  
Jason, 389  
JPSS, 431  
Jumpseat, 428  
Kanopus-V, 425  
KH (Key Hole), 386  
Koronas, 418  
Kosmos, 341  
Kua Fu, 356  
Lacrosse, 387  
Landsat, 299, 374  
Lanyard, 386  
LES, 393  
Luch, 393  
Magion, 354  
Magnum, 428  
Mentor, 428  
Mercury, 428  
Meteor, 362  
METEOSAT, 363, 608  
MetOp, 362  
Midas, 426  
MIDEX, 409  
Milstar, 393  
Misty, 386  
Molniya, 393  
MOS, 389  
MSG, 363, 608  
MTG, 363  
MTSAT, 364  
Nadezhda, 390, 702  
Navstar/GPS, 666  
    Block I, 666  
    Block II, 256, 666  
    Block III, 666  
Nimbus, 360  
NIMS, 701  
NOAA, 360  
NOSS, 428  
Nova, 701  
NPOESS, 360, 431

- NSS 30, 701  
 NTS, 666  
 Oblik, 387  
 Oderacs, 425  
 Ofeq, 388  
 OGO, 351  
 Okean, 389  
 Oko, 426  
 Onyx, 387  
 OPS, 341  
 Orbcomm, 407  
 Orbimage, 385  
 Orbiter, 342  
 OrbView, 385  
 Orion, 428  
 Oscar (Transit), 701  
 OSO, 416  
 Palapa, 392  
 PanAmSat, 279  
 Parus, 390, 702  
 Pléiades-HR, 378, 385  
 POES, 360  
 POGO, 351  
 PRC, 341  
 Priroda, 299  
 Prognoz, 354  
 Prowler, 428  
 QuickBird, 299, 385  
 QZSS, 694  
 Raduga, 393  
 RapidEye, 380  
 RBSP, 354  
 Resource21, 383  
 Resurs, 299  
 Resurs-F, 380  
 Resurs-O, 380  
 Rhyolite, 428  
 SAMOS, 298  
 SAR-Lupe, 387  
 SBIRS, 426  
 SBSS, 428  
 SD-Radio, 290  
 SDS, 395  
 Sentinel, 381  
 Sich, 389  
 SkyBridge, 407  
 SMEX, 409  
 SMS, 279  
 Solrad, 416  
 Space Shuttle, 429  
 SPOT, 299, 375  
 SPRN, 426  
 Sputnik, 342  
 SSF, 428  
 SSR, 383  
 STEREO, 418  
 Strela-3, 407  
 STRV, 424  
 STTW, 393  
 Syncom, 278  
 Tan Ce, 356  
 TDRSS, 393  
 Teledesic, 407  
 TerraSAR, 380  
 THEMIS, 357  
 Timation, 666  
 TIROS, 360  
 TIROS-N, 360  
 TOS, 360  
 Transit, 83, 252, 701  
 Triad, 701  
 Trumpet, 428  
 Tselina, 428  
 Tsikada, 390, 702  
 Tsikada-M, 702  
 Tubsat, 425  
 UNEX, 409  
 UoSAT, 425  
 US-K, 426  
 US-KMO, 426  
 USA, 341  
 Van Allen Probes, 354  
 Vanguard, 342  
 Vela, 426  
 Vela Hotel, 426  
 VIRGO, 395  
 Vortex, 428  
 Watchdog, 426  
 WATS, 697  
 WEST, 401  
 Westford Needles, 408  
 WGS, 393  
 White Cloud, 428  
 WorldView, 299, 385  
 Yantar, 387  
 Zenit, 387  
 Zi Yuan, 383
- Saturn  
   astronomical data, 818, 819  
   diagram by Huygens, 847  
   ellipsoid, 817, 820, 821  
   equinox, 846, 848  
   geodetic data, 818  
   Lagrangian moons, 239  
   natural satellites, 239, 807, 852  
   rings, 811, 814, 846, 847, 849  
     density waves, 815, 848  
     shepherd moon, 815, 848  
   solstice, 848  
   space exploration, 810, 811, 849

- SBAS, *see* augmentation systems
- scanning
- along-track, 563
  - by GEO satellites, 564
  - by LEO satellites, 564
  - conical, 563
  - cross-track, 563
  - Earth's disk, 564
  - mode, 563
    - AT, 582, 584
    - PAP, 582, 584, 585
    - RAP, 582, 585, 587
    - TAT, 582, 584, 585
    - XT, 576, 578, 582, 586, 588, 590, 591, 594
  - orthogonal, 563
  - pixel, 570
  - variable yaw, 582
- scattering angle, 633
- seasons, 274, 741
- beginning, 275
  - definition, 739
  - length, 274, 275, 739, 741
- semi-major axis, 103, 153
- ellipse, 3
- SI units, 227
- sidereal
- day, 262
  - year, 260
- sight to limb, 566, 571
- sky plot, 620–622
- slot, 595
- SLR, 90
- small circle, 26
- software
- Atlas*, VIII, 330, 863
  - Ixion*, VIII, 41, 172, 210, 306, 322, 330, 433, 482, 559, 588, 613, 636, 829, 843, 863
    - Ιξίων, XI
    - Ixion/Web*, XII
- solar angle  $\alpha$ , 434
- solar angle  $\beta$ , 464
- solar eclipse, 454, 464, 466–482, 598
- eclipsis*, 466
    - areostationary orbit, 770
    - dawn–dusk orbit, 470
    - geostationary orbit, 478
- solar elevation, 631
- Solar System, 804–807, 852
- historical data, 882
  - stability, 220–222
- solar time, 272
- solstice, 275, 474
- Mars, 740
  - Saturn, 848
- Somigliana constant, 78
- Somigliana's formula, 78
- space probe
- Akatsuki, 831
  - Apollo-11, 91, 808
  - Apollo-14, 91
  - Apollo-15, 91
  - BepiColombo, 827
  - Cassini, 390
  - Cassini–Huygens, 811, 873
  - Clementine, 870
  - CONTOUR, 812
  - Dawn, 810, 840
  - Deep Impact, 816
  - EJSM-Laplace, 872
  - Epoxi, 816
  - ExoMars-TGO, 725
  - Galileo, 810, 811, 834, 872
  - Genesis, 241, 816
  - Giotto, 812
  - Hayabusa, 810
  - ICE, 351
  - JEO, 872
  - JGO, 872
  - JIMO, 872
  - JUICE, 873
  - Juno, 845
  - Kepler, 420, 882
  - Kosmos-419, 720
  - Luna-1 and -2, 808
  - Luna-3, 808, 863, 865
  - Luna-9 and -10, 808
  - Luna-17, 91
  - Luna-21, 91
  - Magellan, 808, 830
  - Mariner-2, 808
  - Mariner-3, 720
  - Mariner-4, 720, 730, 732
  - Mariner-5, 808
  - Mariner-6, 720, 732
  - Mariner-7, 720
  - Mariner-8, 720
  - Mariner-9, 88, 720, 730, 732
  - Mariner-10, 809, 827
  - Mars Climate Orbiter, 721
  - Mars Exploration Rovers, 724
  - Mars Express, 725
  - Mars Global Surveyor, 721, 775
  - Mars Observer, 721
  - Mars Odyssey, 721, 775
  - Mars Pathfinder, 721
  - Mars Polar Lander, 721
  - Mars Reconnaissance Orbiter, 724, 776
  - Mars Sample Return, 785
  - Mars Science Laboratory, 724



- Mars Surveyor-1998, 721
- Mars Surveyor-2001, 721
- Mars-1 to -7, 720
- Mars-96, 720
- MAVEN, 725
- Mercury Orbiter, 827
- Messenger, 827
- MSL, 724
- MSR, 785
- Muses-C, 810
- NEAR, 810, 834
- New Horizons, 812, 813
- Nozomi, 725
- Phobos-1, 720
- Phobos-2, 720, 795
- Phobos-Grunt, 720
- Pioneer Venus Orbiter, 808
- Pioneer Venus Probe Bus, 808
- Pioneer Venus-1 and -2, 808
- Pioneer-10 and -11, 810
- Pioneer-12 and -13, 808
- Planet-B, 725
- Planet-C, 831
- Pluto–Kuiper Express, 812
- Premier, 785
- Ranger-6 to 9, 88
- Rosetta, 430, 812
- Sakigake, 812
- Solar Orbiter, 419
- Solar Probe Plus, 419
- Sputnik-29, 720
- Sputnik-31, 720
- Stardust, 816
- Suisei, 812
- TandEM, 876
- Titan Explorer, 876
- TPF, 420
- TSSM, 877
- Ulysses, 418, 809
- Vega-1, 808, 812
- Vega-2, 808, 812
- Venera-4 to -7, 808
- Venera-8, 88, 808
- Venera-16, 808
- Venus Express, 831
- Viking-1 and -2, 720
- Voyager-1, 795, 810, 872, 873
- Voyager-2, 795, 810, 872, 877
- Zond-2 and -3, 720
- space shuttle, 429
- space station, 428
- special relativity, *see* relativity
- specular reflection, 454, 635–637, 640
  - Mars, 792, 794
  - Titan, 876, 877
- speed
  - at apsides, 104
  - circular motion, 105
  - dependence on anomaly, 109, 130–136
  - dependence on polar angle, 104
  - dependence on radial vector, 103
- speed of light, 227
- sphere
  - development, 329
  - great circle, 26
  - small circle, 26
- sphere of activity, 233
- sphere of influence, 231–234, 237, 809, 818, 822, 854, 856
- spherical harmonics, 64
  - sectorial, 65
  - tesseral, 65, 201
  - zonal, 65, 195–201
- spherical trigonometry, 241–244
- sponsoring, 811
- stationkeeping, 282, 289, 290, 749
  - drift coefficient, 534
- stellar day, 262
- subsattellite point, 37, 277, 306, 551, 565, 599, 788
- Sun
  - apparent motion, 266–276
  - attraction, 809
  - gravitational constant, 229, 233
  - Lagrange points, 239
  - latitude, 267
  - longitude, 267
  - term in  $J_2$ , 224
- Sun glint, 454, 635–637, 640
  - Mars, 792, 794
  - Titan, 876, 877
- Sun-synchronicity, 291–300, 752
  - circular orbit, 294
  - constant, 291, 752, 825, 860
- sundial, 273
- sunrise, 632
- sunset, 632
- superposition of ground tracks, 592
- swath, 526, 539, 564
  - along-track, 563, 582
  - and recurrence, 581
  - angle, 565, 566
  - conical, 585, 588, 591, 592, 594, 640
  - effective, 592
  - cross-track, 563, 572, 574, 576, 578, 586, 588, 590, 591, 594, 637
  - ground, 567
  - maximal, 566
    - of instrument, 566
  - of instrument, 565
  - variable-yaw, 584, 585, 587

- synod, 318  
 synodic daily frequency, 320  
 synodic period, 318, 320, 647, 796, 808  
     Earth, 726  
 system of units  
     astronomical, 227  
     international (SI), 227
- TAI, 228, 230  
 Tait–Bryan angles, 161  
 tandem mission, 536  
 target, 613  
 TCB, 229, 230  
 TCG, 229, 230, 711  
 TDB, 229, 230  
 tectonic plates, 702  
 three-body problem  
     restricted, 234  
 tidal effect, 795, 853, 879  
     land, 169  
     ocean, 169
- time  
     abbreviations, 89, 229, 272  
     ET, 231  
     GMT, 272, 726  
     LAT, 272, 433, 465, 470  
     LMT, 272, 433, 465, 470  
     TAI, 228  
     TCB, 89, 229, 230  
     TCG, 89, 229, 230, 711  
     TDB, 229, 230  
     terrestrial, 711  
     TT, 228, 230, 711  
     UT, 231, 272  
     UT1, 90, 91, 228  
     UTC, 228  
     time base, 657  
     time scale, 89, 228  
 Titius–Bode law, 806  
 TLE, *see* NORAD  
 train of satellites, *see* A-Train  
 trans-Neptunian objects, 805  
 transit, 419  
 tropical year, 260  
 tropics, 632, 741  
 tropopause, 660  
 troposphere, 655, 660  
 true anomaly, 154  
 true solar time, *see* LAT  
 TT, 228, 230, 711  
 two-body problem, 149
- Uranus  
     astronomical data, 818, 819  
     ellipsoid, 817, 821  
     geodetic data, 818  
     natural satellites, 852  
     space exploration, 810  
 UT, 231, 272  
 UT1, 228, 230  
 UTC, 228, 230
- Van Allen belts, 343, 351, 352  
 velocity  
     Binet’s equation, 98  
     of ground track, 762  
     of satellite, 762
- Venus  
     astronomical data, 818, 819  
     atmosphere, 807, 831  
         super-rotation, 824  
     geodetic data, 818  
     map, 832, 833  
     perturbative accelerations, 823, 824  
     space exploration, 808, 830  
 vernal equinox, 267, 479  
     Mars, 734, 739
- vertical  
     celestial coordinates, 630  
     local, 614
- Vesta  
     astronomical data, 840  
     geodetic data, 840  
     space exploration, 840
- viewing from pole, 617  
 visibility of geostationary satellite, 605  
 VLBI, 91, 415
- WAAS, *see* augmentation system  
 weight, 60, 72, 74  
     and gravity, 60, 74  
     anomalies, 79, 82  
     on Earth, 72, 80  
         at equator, 77  
         at pole, 77
- work, 54
- yaw, 562  
     angle, 160
- year  
     anomalistic, 261, 270, 727  
     civil, 260, 270  
     draconitic, 261  
     Gregorian, 260  
     Julian, 261  
     sidereal, 260, 727  
     tropical, 260, 727
- zenith, 566, 629  
     passage of Sun, 632  
 zodiac, 739